NASA-CR-3251 19840019629

NASA Contractor Report 3251 (Revision 1)

PAN AIR – A Computer Program for Predicting Subsonic or Supersonic Linear Potential Flows About Arbitrary Configurations Using a Higher Order Panel Method

Volume I – Theory Document (Version 3.0)

Michael A. Epton
Alfred E. Magnus

FOR REFERENCE

LIBRARY COPY

APR 0 4 1990

LANGLEY RESEARCH CENTER
LIBRARY NASA
HAMPTON, VIRGINIA

Contract NAS2-12036

FOR EARLY DOMESTIC DISSEMINATION

Because of its significant early commercial potential, this information, which has been developed under a U. S. Government program, is being disseminated within the United States in advance of general publication. This information may be duplicated and used by the recipient with the express limitation that it not be published. Release of this information to other domestic parties by the recipient shall be made subject to these limitations. Foreign release may be made only with prior NASA approval and appropriate export licenses. This legend shall be marked on any reproduction of this information in whole or in part. Date for general release MAR 3 1 1992

NASA Contractor Report 3251 (Revision 1)

PAN AIR – A Computer Program for Predicting Subsonic or Supersonic Linear Potential Flows About Arbitrary Configurations Using a Higher Order Panel Method

Volume I – Theory Document (Version 3.0)

Michael A. Epton
Boeing Computer Services Company
Seattle, Washington

Alfred E. Magnus
Boeing Military Airplane Company
Seattle, Washington

Prepared for
Ames Research Center, and
Langley Research Center
under Contract NAS2-12036

and for the
Air Force Aeronautical Systems Division
Air Force Wright Aeronautical Laboratories
Naval Coastal Systems Center

National Aeronautics and
Space Administration

Ames Research Center
Moffett Field, California 94035

Contents

		Page
List of Figures		xiii
Preface to Version 3.0		xix
1.0	Introduction	1.0-1
2.0	Fundamental Fluid Dynamics	2.0-1
2.1	The Navier-Stokes Equations	2.1-1
2.2	Euler's Equation	2.2-1
2.3	The Unsteady Potential Equation	2.3-1
2.4	The Steady Non-Linear Potential Equation	2.4-1
2.5	The Prandtl-Glauert Equation	2.5-1
3.0	Panel Method Theory	3.0-1
3.1	Coordinate Scaling	3.1-1
3.2	Green's Theorems	3.2-1
3.3	Discretization	3.3-1
3.4	Figures for Section 3	3.4-1
4.0	An Overview of PAN AIR	4.1-1
4.1	Historical Development of Panel Methods	4.1-1
4.2	Summary of PAN AIR Technology	4.2-1
4.2.1	Basis Function Computation	4.2-1
4.2.1.1	Subpanel Splines	4.2-2
4.2.1.2	Outer Splines	4.2-2
4.2.2	Panel Influence Coefficients	4.2-3
4.2.2.1	Near Field PIC's	4.2-3
4.2.2.2	Far Field PIC's	4.2-4
4.2.3	Potential and Velocity Influence Coefficient Assembly	4.2-4
4.2.4	Aerodynamic Influence Coefficient Matrix Construction	4.2-5
4.3	Figures for Section 4	4.3-1
5.0	Elaboration on the Technology in PAN AIR	5.0-1
5.1	Networks and Panels	5.1-1
5.2	Coordinate Transformations	5.2-1
5.3	Network Edge Matching	5.3-1
5.4	Control Points and Boundary Conditions	5.4-1
5.4.1	Control Point Location	5.4-1
5.4.2	Boundary Conditions	5.4-1
5.4.2.1	Impermeability Boundary Conditions	5.4-1
5.4.2.2	Thin Surfaces	5.4-3
5.4.2.3	Thick Configurations	5.4-3
5.4.2.4	Superinclined Surfaces	5.4-4
5.4.2.5	The General Boundary Condition	5.4-5
5.5	Singularity Splines	5.5-1
5.5.1	The Matrices B^S and B^D	5.5-1
5.5.2	Definition of SPSPL	5.5-2
5.5.3	Construction of B Matrices for Continuous Singularity Distributions	5.5-2

5.5.4	Construction of the Discontinuous Source Outer Spline Matrix	5.5-4
5.5.5	Construction of SPSPL	5.5-4
5.6	Influence Coefficients	5.6-1
5.6.1	Computation of Potential and Velocity	5.6-1
5.6.2	Reformulation of the Doublet Velocity Integral	5.6-3
5.6.3	The Far Field Expansion	5.6-4
5.7	The Aerodynamic Influence Coefficient Matrix	5.7-1
5.7.1	Non-Standard Boundary Conditions	5.7-1
5.7.2	Symmetry	5.7-2
5.7.3	Known Singularity Parameters	5.7-7
5.7.4	Multiple Right Hand Sides	5.7-9
5.7.5	Updatability	5.7-9
5.8	Solution of the System of Equations	5.8-1
5.9	Post-Solution Features	5.9-1
5.9.1	Computation of Potential and Velocity	5.9-1
5.9.2	Pressure Computation	5.9-2
5.9.3	Velocity Corrections	5.9-2
5.9.4	Force and Moment Computation	5.9-3
5.9.5	Off-Body Points and Streamlines	5.9-3
5.10	Figures for Section 5	5.10-1
6.0	A Guide to the Appendices	6.0-1
7.0	References	7.0-1
8.0	List of Symbols	8.0-1
	Latin Symbols	8.0-1
	Greek Symbols	8.0-17
	Subscripts	8.0-24
	Superscripts	8.0-25
	Other Symbols	8.0-26
9.0	Engineering Glossary	9.0-1
Appendices		
A.0	Fundamental Fluid Mechanics	A.0-1
A.1	The Small Perturbation Assumptions	A.1-1
A.2	Figures for Appendix A	A.2-1
B.0	The Prandtl-Glauert Equation	B.0-1
B.1	Existence and Uniqueness	B.1-1
B.2	Wakes and Modeling	B.2-1
B.3	Removal of Line Vortex Terms and the Line Source Integration by Parts	B.3-1
B.4	Linear Sources and Quadratic Doublets	B.4-1
B.5	Figures for Appendix B	B.5-1
C.0	The Design Problem	C.0-1
C.1	Linearized Design	C.1-1
C.2	Sequential Design	C.2-1
C.3	Iterative Design	C.3-1
C.4	Stability	C.4-1
C.5	Figures for Appendix C	C.5-1

D.0	Geometry of Networks and Panels	D.0-1
D.1	Networks	D.1-1
D.1.1	Network Types	D.1-1
D.1.2	Wake Networks and the Kutta Condition	D.1-1
D.1.3	Indexing	D.1-2
D.1.4	Collapsing of Network Edges	D.1-3
D.1.5	Additional Network Processing	D.1-3
D.2	Basic Panel Geometry	D.2-1
D.3	Error Checks	D.3-1
D.4	Figures for Appendix D	D.4-1
E.0	Matrices and Coordinates	E.0-1
E.1	Vectors and Dual Vectors	E.1-1
E.2	Metric Matrices, Dual Metrics, and Inner Products	E.2-1
E.3	Coordinate Transformations	E.3-1
E.4	Figures for Appendix E	E.4-1
F.0	Edge Matching	F.0-1
F.1	Continuity Requirements	F.1-1
F.2	Network Abutments	F.2-1
F.3	Automatic Abutment Search	F.3-1
F.4	Doublet Matching Along Abutments	F.4-1
F.5	Abutment Intersections	F.5-1
F.5.1	Graphical Representation of an Abutment Intersection	F.5-2
F.5.2	Modifications to the Abutment Assignment Procedure	F.5-6
F.6	Gap-Filling Panels	F.6-1
F.7	Figures for Appendix F	F.7-1
G.0	Control Point Locations	G.0-1
G.1	Figures for Appendix G	G.1-1
H.0	Boundary Conditions and Onset Flows	H.0-1
H.1	Standard Forms for Boundary Conditions	H.1-1
H.1.1	Reduction of User Specified Boundary Conditions to Standard Form	H.1-1
H.1.2	Classification of Control Points	H.1-3
H.1.3	Boundary Condition Symmetry Types for Networks Lying in a Plane of Symmetry	H.1-4
H.2	Boundary Condition Overrides and Boundary Condition Selection	H.2-1
H.2.1	Superinclined Panel Override	H.2-3
H.2.2	Boundary Condition Selection	H.2-4
H.2.3	Degenerate Boundary Conditions	H.2-6
H.2.4	Doublet Matching, Velocity Jump Matching and Source Matching Boundary Conditions	H.2-7
H.2.5	Closure Boundary Conditions	H.2-11
H.2.6	User Boundary Condition Hierarchy	H.2-13
H.2.7	The Complete Boundary Condition Hierarchy	H.2-14
H.3	Onset Flows	H.3-1
H.4	Figures for Appendix H	H.4-1

I.0 Singularity Splines I.0-1
I.1 Outer Splines I.1-1
I.1.1 Source Splines for Analysis Networks I.1-2
I.1.1.1 Source Spline Vectors for Continuous Splines I.1-2
I.1.1.2 Neighboring Singularity Parameters I.1-2
I.1.1.3 Computation of a Local Coordinate System I.1-2
I.1.1.4 The Bilinear Fit at Panel Corner Points I.1-4
I.1.1.5 Discontinuous Source Analysis Splines I.1-5
I.1.2 Doublet Spline Vectors for Analysis Networks, Doublet Forward Weighted Splines I.1-7
I.1.2.1 The Quadratic Least Squares Fit for Panel Corners or Panel Edge Midpoints I.1-8
I.1.2.2 Neighboring Points for Least Squares Fit I.1-10
I.1.2.3 Construction of a Local Coordinate System I.1-11
I.1.2.4 Weights for the Least Squares Fit I.1-12
I.1.2.5 Edge Splines for Non-Smooth Abutments I.1-12
I.1.2.6 Edge Splines for Smooth Abutments I.1-17
I.1.3 Doublet Spline Vectors for Wake Networks I.1-19
I.1.4 Source Splines for Design Networks I.1-19
I.1.4.1 Source Design 1 I.1-19
I.1.4.2 Source Design 2, Discontinuous Source Splines I.1-19
I.1.4.3 Source Design 2, Continuous Source Splines I.1-20
I.1.5 Doublet Splines for Design Networks I.1-21
I.2 Subpanel Splines I.2-1
I.2.1 Basis Functions for Interpolation on Triangles I.2-1
I.2.2 Source Subpanel Splines I.2-4
I.2.3 Doublet Subpanel Splines I.2-5
I.2.3.1 Considerations of Continuity I.2-7
I.2.3.2 The Definition of "Kappa" Quantities I.2-8
I.2.3.3 Computation of the Nontrivial Kappa Quantities I.2-9
I.3 Full Panel and Half Panel Splines I.3-1
I.3.1 Full Panel Spline Matrices I.3-1
I.3.2 Half Panel Spline Matrices I.3-8
I.4 Panel Moment Matrices I.4-1
I.4.1 Far Field Moments I.4-1
I.4.2 Post Processing Panel Moments I.4-2
I.4.3 Evaluation of Elementary Flat Panel Moments I.4-6
I.5 Constrained Least Squares I.5-1
I.5.1 Definition of the Problem I.5-1
I.5.2 Elimination of the Weights I.5-1
I.5.3 The Case of No Exact Constraints I.5-2
I.5.4 Reduction of the General Case I.5-3
I.6 Figures for Appendix I I.6-1

J.0 Panel Influence Coefficient Calculation J.1-1
J.1 Introduction and Notation J.1-1
J.1.1 Definitions J.1-1
J.1.2 Summary J.1-2
J.1.2.1 Near Field Versus Far Field J.1-2
J.1.2.2 The Domain of Dependence J.1-3
J.1.2.3 Near Field and Intermediate Field PIC Calculation J.1-3
J.1.2.4 Far Field PIC's J.1-6
J.1.3 Integration Techniques J.1-7
J.1.4 Notation J.1-8
J.2 The Distance Algorithm J.2-1
J.2.1 The Far Field Criterion J.2-1
J.2.2 The Intermediate Field Criterion J.2-3
J.3 Supersonic Influence Test J.3-1
J.3.1 Definition of D_p J.3-1
J.3.2 A Zero Influence Test J.3-1
J.3.3 Panels Wholly Within the Mach Cone J.3-4
J.3.4 The Influence Test for a Subpanel J.3-4
J.3.4.1 The Point of Closest Approach J.3-5
J.3.4.2 The Winding Number Test J.3-7
J.3.4.3 Half Panels and Projected Panels J.3-8
J.4 Cylindrical Coordinates J.4-1
J.4.1 Fundamental Results J.4-1
J.4.2 The Mach Disk J.4-2
J.4.3 The Case of the Mach Disk Lying Within the Panel J.4-2
J.4.4 Arbitrary Intersection of the Mach Disk With the Panel J.4-3
J.4.4.1 Corner Points J.4-4
J.4.4.2 The Phase Function J.4-4
J.4.4.3 Edges and the Mach Disk J.4-7
J.4.4.4 Edge Tangents and Normals J.4-7
J.4.4.5 The Function P(ø) J.4-10
J.5 Hyperbolic Coordinates J.5-1
J.5.1 Fundamental Results J.5-1
J.5.2 Subsonic Edges J.5-8
J.5.3 Supersonic Edges J.5-12
J.5.4 Computation of the Integrals J.5-16
J.6 The Panel Integral Matrices J.6-1
J.6.1 Preliminaries J.6-2
J.6.1.1 Transformation Rules J.6-2
J.6.1.2 Transformation of the Integrals J.6-3
J.6.1.3 Singularity Strength Coefficients J.6-5
J.6.1.4 Uniform Formulas for Local Variables J.6-6
J.6.1.5 Differentiation Formulas J.6-9
J.6.2 Source Potential and Velocity J.6-10
J.6.2.1 Source Potential J.6-10
J.6.2.2 Tangential Source Velocity J.6-12
J.6.2.3 Normal Source Velocity J.6-13
J.6.3 Doublet Potential and Velocity J.6-15
J.6.3.1 Doublet Potential J.6-15
J.6.3.2 Tangential Doublet Velocity J.6-16
J.6.3.3 Normal Doublet Velocity J.6-18

	J.6.4	Reduction to Fundamental Integrals	J.6-19
		J.6.4.1 Definition of the Integrals	J.6-20
		J.6.4.2 Source Potential and Velocity	J.6-20
		J.6.4.3 Doublet Potential and Velocity	J.6-23
	J.6.5	The Fundamental Integrals in Terms of Panel and Edge Functions	J.6-25
		J.6.5.1 Computation of a	J.6-25
		J.6.5.2 Computation of b	J.6-27
		J.6.5.3 Computation of $\vec{a}$	J.6-28
		J.6.5.4 Computation of $\vec{b}$	J.6-28
		J.6.5.5 Computation of B	J.6-29
		J.6.5.6 Computation of F	J.6-30
		J.6.5.7 Computation of H	J.6-33
	J.6.6	The Origin Shift	J.6-35
	J.6.7	Finite Parts of Integrals	J.6-41
		J.6.7.1 Definition of a Finite Part	J.6-41
		J.6.7.2 Properties of a Finite Part	J.6-41
		J.6.7.3 Finite Parts and the Integral Equation	J.6-42
		J.6.7.4 Finite Parts and PIC Computation	J.6-42
		J.6.7.5 Summary of Finite Part Integrals	J.6-43
J.7	Edge and Panel Functions		J.7-1
	J.7.1	Expressions for Edge and Panel Functions	J.7-1
		J.7.1.1 Subsonic Flow	J.7-1
		J.7.1.2 Subsonic Edges of Subinclined Panels in Supersonic Flow	J.7-2
		J.7.1.3 Supersonic Edges of Subinclined Panels	J.7-3
		J.7.1.4 Superinclined Panels	J.7-3
		J.7.1.5 Uniform Formulas	J.7-4
	J.7.2	Computation of Edge and Panel Function Arguments in Reference Coordinates	J.7-4
		J.7.2.1 Computation of h	J.7-5
		J.7.2.2 Computation of v	J.7-5
		J.7.2.3 Computation of a	J.7-7
		J.7.2.4 Computation of g	J.7-8
J.8	Rationalization Formulas		J.8-1
	J.8.1	Edge Functions	J.8-1
		J.8.1.1 Non-Sonic Edges	J.8-2
		J.8.1.2 Nearly Sonic Edges	J.8-6
		J.8.1.3 Essentially Sonic Edges	J.8-10
	J.8.2	Panel Function Computation	J.8-12
		J.8.2.1 The Standard Rationalization	J.8-12
		J.8.2.2 A Special Rationalization	J.8-18
J.9	Far Field PIC's		J.9-1
J.10	Line Vortex PIC's		J.10-1
	J.10.1	Computation of $\vec{v}_D^*$	J.10-1
J.11	Singular Behavior of Integrals		J.11-1
	J.11.1	Discontinuous Source Strength	J.11-1
	J.11.2	Discontinuous Doublet Strength	J.11-5
		J.11.2.1 Doublet Potential	J.11-5
		J.11.2.2 Doublet Velocity	J.11-5
	J.11.3	Discontinuities in Doublet Gradient	J.11-6

J.11.4 Singularities of the Panel Function J.11-8
J.11.4.1 The Plane h = 0 J.11-8
J.11.4.2 Discontinuities Due to C_Θ J.11-10
J.11.4.3 Discontinuities in $J_k(\psi)$ J.11-12
J.11.4.4 Summary of Panel Function Behavior J.11-14
J.11.5 Singularities of the Edge Function J.11-15
J.11.5.1 Supersonic Edges J.11-15
J.11.5.2 Subsonic Edges J.11-16
J.11.5.3 Subsonic Nearly Sonic Edges J.11-17
J.11.5.4 Supersonic Nearly Sonic Edges J.11-19
J.11.5.5 Essentially Sonic Edges J.11-19
J.11.6 Singularities in Subsonic Flow J.11-19
J.11.6.1 Discontinuous Source Strength J.11-19
J.11.6.2 Discontinuous Doublet Strength J.11-20
J.11.6.3 Discontinuous Doublet Gradient J.11-22
J.11.7 Discontinuous Source Strength in Supersonic Flow J.11-22
J.11.7.1 Source Potential J.11-22
J.11.7.2 Source Velocity J.11-23
J.11.8 Discontinuous Doublet Strength in Supersonic Flow J.11-23
J.11.9 Discontinuous Doublet Gradient in Supersonic Flow J.11-24
J.12 Figures for Appendix J J.12-1

K.0 AIC Matrix Assembly K.0-1
K.1 Generation of AIC's in the Absence of Symmetry K.1-1
K.1.1 Transformation of a General Boundary Condition into an AIC Row (No Symmetry) K.1-1
K.1.2 Transformation of a Matching Boundary Condition into an AIC Row (No Symmetry) K.1-4
K.1.3 Transformation of a Closure Boundary Condition into an AIC Row (No Symmetry) K.1-6
K.2 Symmetry K.2-1
K.2.1 Admissable Planes of Symmetry K.2-1
K.3 Problem Formulation for One Plane of Symmetry K.3-1
K.4 Problem Formulation for Two Planes of Symmetry K.4-1
K.5 Evaluation of ΦIC's and VIC's When Symmetry is Present K.5-1
K.5.1 One Plane of Symmetry K.5-1
K.5.2 Two Planes of Symmetry K.5-8
K.6 Generation of AIC's when Symmetry is Present K.6-1
K.6.1 General Boundary Conditions K.6-3
K.6.2 Matching Boundary Conditions K.6-5
K.6.2.1 The Form of Doublet Matching Conditions K.6-5
K.6.2.2 The Imposition of Doublet Matching Conditions K.6-8
K.6.2.3 Source Matching K.6-9
K.6.2.4 Velocity Jump Matching K.6-9
K.6.3 Closure Boundary Conditions K.6-12
K.6.4 Degenerate Boundary Conditions K.6-15
K.7 The IC Update Capability K.7-1
K.8 Figures for Appendix K K.8-1

L.0	The Constraint Matrix	L.0-1
	L.1 Calculation of Constraint Vectors	L.1-1
	L.2 The Solution of a Linear System of Equations	L.2-1
	L.3 Desymmetrization of Singularity Parameters	L.3-1
	L.4 Figures for Appendix L	L.4-1
M.0	Computation of the Minimal Data Set	M.0-1
	M.1 Recovery of the Singularity Parameters	M.1-1
	M.2 Singularity Strength Calculation	M.2-1
	M.3 Computation of Potential and Normal Mass Flux	M.3-1
	M.4 Figures for Appendix M	M.4-1
N.0	Surface and Wake Flow Properties	N.0-1
	N.1 Velocity Computation	N.1-1
	N.2 Pressure Formulas	N.2-1
	N.2.1 Preliminary Results	N.2-1
	N.2.2 Constant Density Flow	N.2-2
	N.2.3 Compressible Flow	N.2-3
	N.2.4 Limitations of the Formula	N.2-4
	N.2.4.1 The Vacuum Pressure Coefficient	N.2-5
	N.2.4.2 The Critical Speed	N.2-5
	N.2.4.3 The Pressure Coefficient at the Critical Speed	N.2-7
	N.2.5 The Isentropic Formula Under Simplifying Assumptions	N.2-7
	N.2.5.1 Second Order Theory	N.2-8
	N.2.5.2 The Second Order Theory under Additional Assumptions	N.2-10
	N.3 Velocity Corrections	N.3-1
	N.3.1 The First Velocity Correction	N.3-1
	N.3.2 The Second Velocity Correction	N.3-2
	N.4 Onset Flow Calculations	N.4-1
	N.4.1 Bernoulli's Equation	N.4-1
	N.4.2 Pressure Formulas	N.4-2
	N.4.3 Simplifying Assumptions	N.4-4
	N.4.4 Velocity Corrections	N.4-6
	N.5 Associated Data	N.5-1
O.0	Forces and Moments	O.0-1
	O.1 Basic Formulas	O.1-1
	O.2 Integration Procedure	O.2-1
	O.3 Leading and Side Edge Force	O.3-1
	O.3.1 Linearized Three-Dimensional Theory	O.3-1
	O.3.2 Application in PAN AIR	O.3-1
	O.3.3 Edge Force Verification	O.3-3
	O.4 Coordinate Transformations	O.4-1
	O.5 Added Mass Coefficients	O.5-1
	O.5.1 Formulation of Added Mass Coefficients	O.5-1
	O.5.2 Integration Procedures	O.5-2
	O.5.3 Orthogonal Transformation	O.5-3
	O.5.4 Translation	O.5-4
	O.5.5 Symmetric Configurations	O.5-4
	O.6 Figures for Appendix O	O.6-1

P.0 Flow Properties at Off-body Points and Streamline Calculation P.0-1
P.1 Evaluation of Potential and Velocity at Off-Body Points P.1-1
P.2 Streamline Calculation P.2-1
P.2.1 The Integration of Streamlines P.2-2

This page has been left blank intentionally

List of Figures

Figures are placed at the end of each numbered section or appendix		Page
Section 3		
3.1	Region V of space with boundary S	3.4-1
3.2	A surface S dividing regions V_1 and V_2	3.4-1
3.3	A surface S which does not divide space into 2 separate regions	3.4-2
3.4	Basis function for constant strength panels	3.4-2
Section 4		
4.1	Historical overview of panel methods	4.3-1
4.2	Division of panel into subpanels	4.3-2
4.3	Panel and far field control point	4.3-2
Section 5		
5.1	Network geometry	5.10-1
5.2	Decomposition of panel into 5 planar regions	5.10-1
5.3	Definition of compressibility directions in terms of angles of attack and sideslip	5.10-2
5.4	Superinclined surface, r = -1	5.10-2
5.5	Subinclined and Mach-inclined surfaces	5.10-3
5.6	Gap between leading edge of wing and body	5.10-3
5.7	Example of abutment intersection	5.10-4
5.8	Control point locations	5.10-4
5.9	Thin wing boundary conditions	5.10-5
5.10	Two solutions for potential in enclosed volume	5.10-5
5.11	Thick wing boundary conditions	5.10-6
5.12	Boundary conditions on superinclined surfaces	5.10-6
5.13	Singularity parameter locations	5.10-7
5.14	Singularity parameters in the neighborhood of the panel	5.10-8
5.15	Neighboring source parameters for a panel corner point	5.10-9
5.16	Neighboring doublet parameters for a panel corner point	5.10-9
5.17	Neighboring doublet parameters for a panel edge midpoint	5.10-10
5.18	Panel points and midpoints	5.10-10
5.19	Opposite orientations of adjacent networks	5.10-11
5.20	Configuration and image	5.10-11
5.21	Pressure coefficient rules	5.10-12
5.22	Surfaces of integration for leading edge force	5.10-12
Appendix A		
A.1	Thin wing at small angle of attack	A.2-1
A.2	Blunt object at small Mach number	A.2-1
A.3	Small perturbation "engine-on" case	A.2-2

Appendix B

B.1	An exterior boundary value problem	B.5-1
B.2	A region of finite volume	B.5-1
B.3	Specification of normal flow on both sides of a surface	B.5-2
B.4	A superinclined surface	B.5-2
B.5	A boundary value problem with no unique solution	B.5-3
B.6	The domain of dependence	B.5-3
B.7	A permeable surface inclined to the freestream	B.5-4
B.8	A region which fails to be simply connected	B.5-4
B.9	Airplane and wake	B.5-5
B.10	Leading edge vortices from a highly swept wing	B.5-6
B.11	Panel edge on a network edge	B.5-7
B.12	Two adjacent panel edges	B.5-7
B.13	Three adjacent panels	B.5-8
B.14	Intersection of 3 surfaces (cross-section)	B.5-8
B.15	Region of integration in neighborhood of P	B.5-9

Appendix C

C.1	Design boundary conditions on a thin configuration	C.5-1
C.2	Indexing of network points	C.5-1
C.3	A panel	C.5-2
C.4	Design boundary conditions for a thick wing	C.5-2
C.5	A constant doublet strength spline	C.5-3
C.6	Stability for constant doublet spline	C.5-3
C.7	Quadratically varying doublet spline	C.5-4
C.8	A single interval	C.5-4
C.9	Stability for a quadratic doublet spline	C.5-5
C.10	Instability of analysis spline with design boundary conditions	C.5-6
C.11	A doublet spline for design problems	C.5-7
C.12	Stability for design boundary conditions	C.5-7

Appendix D

D.1	Locations of source singularity parameters	D.4-1
D.2	Doublet analysis and design singularity parameter locations	D.4-2
D.3	Doublet wake singularity parameter locations	D.4-3
D.4	Network and panel indexing	D.4-4
D.5	Network with an edge to be collapsed by the program	D.4-4
D.6	Network with revised geometry	D.4-5
D.7	Panelling of delta wing	D.4-5
D.8	A panel	D.4-6
D.9	A subpanel	D.4-6
D.10	Definition of skewness parameters	D.4-7
D.11	Impermissible network (two adjacent collapsed edges)	D.4-8

Appendix E

E.1	Surface S in compressibility and scaled coordinates	E.4-1
E.2	Illustration of the transformation law for $\hat{n}\ dS$	E.4-2
E.3	Definition of the compressibility vector $\hat{c}_0$ in terms of α_c and β_c	E.4-2

Appendix F

F.1	Impermissible network intersection (in cross-section)	F.7-1
F.2	Leading edge vortex (in cross-section)	F.7-1
F.3	Simulation of a vortex core by a line vortex	F.7-2
F.4	Multiple pairwise abutments involving the same edges	F.7-2
F.5	Each network edge is a refinement of the other	F.7-3
F.6	Edge 1 is a refinement of edge 2	F.7-3
F.7	Control points on a supersonic leading edge are used for doublet matching	F.7-4
F.8a	Six network wing with wakes	F.7-5
F.8b	Doublet distribution arising from specification of μ at trailing edge	F.7-5
F.9	One edge is not precisely a refinement of the other	F.7-6
F.10	An abutment intersection with 4 abutments	F.7-6
F.11	An abutment intersection with 6 abutments	F.7-7
F.12	Another abutment intersection with 4 abutments	F.7-8
F.13	Directed graphs corresponding to three abutment intersections	F.7-9
F.14	Defoliation and matching condition assignment for the graph of Fig. F13b	F.7-10
F.15	A corner point for which $A_1 = A_2$, giving rise to a self-loop	F.7-11
F.16	An extra control point at the end of a smooth abutment	F.7-11
F.17	An abutment intersection in which both the initial and terminal ends of an abutment participate in an abutment intersection	F.7-12
F.18	Gap-filling panel	F.7-13
F.19	Gap-filling panels on an abutment with 3 network edges	F.7-13

Appendix G

G.1	Control point locations	G.1-1
G.2	Division of network edge into two abutments	G.1-1
G.3	Control point recession vectors	G.1-2
G.4	Recession of corner control points when subpanel is triangular	G.1-2
G.5	Abutment with 3 network edges (cross-section)	G.1-3
G.6	Hypothetical locations of a control point	G.1-3

Appendix H

H.1	Summary of the separate cases that must be handled during boundary condition selection	H.4-1
H.2	Boundary condition locations for source networks	H.4-2
H.3	Boundary condition locations for doublet networks	H.4-3
H.4a	Degenerate boundary conditions for configurations with one plane of symmetry	H.4-5
H.4b	Degenerate boundary conditions for configurations with two planes of symmetry	H.4-6
H.5a	The velocity jump matching condition at a thin trailing edge (vorticity matching)	H.4-7
H.5b	The velocity jump matching condition at a thick trailing edge (vorticity matching)	H.4-7
H.6	Types of abutment intersections at which source matching is a reasonable boundary condition	H.4-8

H.7	Columns of panels illustrated by cross-hatching	H.4-9
H.8	Design of upper surface of thick wing	H.4-9
H.9	Pattern of streamlines on imposition of a closure boundary condition	H.4-10
H.10	User boundary condition hierarchy	H.4-11
H.11	User boundary condition hierarchy for control points lying in a plane of symmetry	H.4-12
H.12	Possible boundary condition hierarchies for edge an edge control point in a plane of symmetry, closure is present	H.4-13
H.13	Boundary condition hierarchies for edge and corner control points in a plane of symmetry (no closure)	H.4-15
H.14	Total internal stagnation	H.4-16
H.15	Onset flow, not parallel to compressibility direction	H.4-16
H.16	Propeller slipstream	H.4-17
H.17	Airplane undergoing small rolling motion	H.4-17

Appendix I

1.1a	Panel source parameter locations	I.6-1
1.1b	Panel doublet parameter locations	I.6-1
1.1c	Panel singularity parameter locations for a nine-panel network	I.6-2
1.2	Neighboring source parameters for analysis network	I.6-3
I.3	Location of global source parameters used in the construction of the discontinuous source analysis spline	I.6-4
I.4	Location of source parameter points for the special case construction of discontinuous source analysis splines	I.6-5
I.5	Thin wing with curved planform	I.6-6
I.6a	Neighboring points for least squares fit (P_0 away from network edge)	I.6-7
I.6b	Neighboring points for least squares fit (P_0 near network edge)	I.6-8
I.6c	Neighboring points for least squares fit (P_0 near a smooth abutment)	I.6-9
I.7	Basis vectors for local coordinate system for spline vector construction	I.6-10
I.8	Projections to tangent plane of points on curved surface	I.6-10
I.9a	Unequal spacing in a non-smooth abutment (second edge is a refinement of the first)	I.6-11
I.9b	Identification of points on a network edge	I.6-11
I.10	Differentiable 2-D quadratic spline	I.6-12
I.11a	Neighboring singularity parameters for points P_0 on a smooth abutment	I.6-13
I.11b	Parameterization of an abutment	I.6-14
I.11c	Panel edge on a coarse network	I.6-14
I.12	Computation of panel edge midpoint source strengths for discontinuous SD2 source splines	I.6-15
I.13	Computation of panel corner spline vectors for continuous SD2 source splines	I.6-16
I.14a	Neighboring point for least squares fit (P_0 on a doublet design network)	I.6-17
I.14b	Edge of a doublet design network	I.6-17
I.15	Panel defining points and subpanel local coordinates systems	I.6-18

I.16	Definition of Q_j and Q_k given Q_i	I.6-19
I.17	Interpolation conditions that define basis functions L_i	I.6-19
I.18	Definition of quadratic basis functions $B_i(Q)$, $B_i(Q)$	I.6-20
I.19	Panel with points requiring definition of μ marked with symbols $\bullet$, o, $\square$, x	I.6-21
I.20	A panel in skewed coordinates viewed from above	I.6-22
I.21	The isoparametric representation of a panel	I.6-23
I.22a	Division of a panel into T_2 and T_4 when $d(\vec{P}_1,\vec{P}_3) < d(\vec{P}_2,\vec{P}_2)$	I.6-24
I.22b	Division of a panel into T_1 and T_3 when $d(\vec{P}_2,\vec{P}_4) \leq d(\vec{P}_1,\vec{P}_3)$	I.6-24

Appendix J

J.1	Domain of dependence	J.12-1
J.2	Superinclined panel partially within D_p without corners in D_p	J.12-1
J.3	Notation used frequently in Appendix J	J.12-2
J.4	Two region approximations to panel	J.12-3
J.5	Region in which intermediate field PIC is not performed	J.12-4
J.6	Splitting a panel into half panels	J.12-4
J.7	$(\tilde{X},\tilde{Y})$ coordinate system	J.12-5
J.8	Subsonic and supersonic edges	J.12-5
J.9	Point of closest approach	J.12-6
J.10	Subinclined and superinclined panel	J.12-6
J.11	P* lies in the interior of the subpanel	J.12-7
J.12	Region of integration $\Sigma' \cap C_h$ for a typical subpanel	J.12-7
J.13	$P_k^{\pm}$, $Q_k^{\pm}$ when $C_h \subset {}'\Sigma$	J.12-8
J.14	Edge numbering for various panel configurations	J.12-8
J.15	Phase angle ϕ' exceeds π	J.12-9
J.16	Coordinate systems in the (ξ', η') plane	J.12-9
J.17	Determining if an edge of Σ' is an edge of $\Sigma' \cap C_h$	J.12-10
J.18	Definition of $P(\phi)$, the upper limit of integration for ρ	J.12-11
J.19	Region of integration for superinclined panel	J.12-12
J.20	Transformation to (s,t) variables and region of integration	J.12-13
J.21	Numbering of edges of $\Sigma' \cap H_h$	J.12-13
J.22	A region Σ' with edge E, oriented tangent $\vec{t}$ and outward edge normal n	J.12-14
J.23	An edge E and its image E in the s - t coordinate (subsonic edge)	J.12-14
J.24	An edge E and its image E in the s - t coordinate (supersonic edge)	J.12-15
J.25a	Region of integration for subinclined panel	J.12-16
J.25b	Region of integration for subinclined panel	J.12-17
J.26	Polygon Σ'_ε approximating $\Sigma' \cap D_p$	J.12-18
J.27	Illustration of supersonic, nearly sonic edges on which v changes sign	J.12-19
J.28	An example of a superinclined panel with $g^2 = h^2 - a^2 \approx 0$	J.12-19
J.29	Evaluating v on the boundary of D_p: the various special cases	J.12-20
J.30	The value of J' for some special configurations	J.12-21

J.31 Region with nearly sonic edge J.12-22
J.32 Potential lines of discontinuity in J^+ J.12-22
J.33 Panel corners on Mach lines J.12-23
J.34 A point lies on the extension of an edge (subsonic flow) J.12-24
J.35 A point lies on the extension of an edge (supersonic flow) J.12-24
J.36 Edge barely intersects D_p J.12-25
J.37a The Mach wedge in cross-section J.12-25
J.37b Mach wedge behind supersonic panel edge J.12-26
J.38 Subsonic nearly sonic edge J.12-27
J.39 The distances h, v, a, g, and R in subsonic flow J.12-28

Appendix K

K.1 Reflection of point ($\vec{p}$) in a plane of symmetry K.8-1
K.2 Reflections of a point $\vec{p}$ in 2 planes of symmetry K.8-2
K.3 A configuration with one plane of geometric symmetry K.8-3
K.4 A configuration with two planes of geometric symmetry K.8-4
K.5 Comparison of AIC formula obtained from using (K.3.28), (K.3.46), with (K.5.28-31) when $\vec{p} \in S_1$ K.8-5
K.6 Four cases of an abutment lying on a plane of symmetry K.8-6
K.7 Doublet matching for $\hat{\phi}^S$ at a plane of symmetry K.8-8
K.8 Velocity jump matching on a network lying on a plane of symmetry K.8-9
K.9 Extra singularity parameter and control point dependent on existence of updateable network K.8-10

Appendix L

L.1 Order of Transformation Application for the case n=5 L.4-1
L.2 Diagram describing the Application of T_{ij} to various subarrays of the working array $A = [A_{ij};\ i,j=1(1)5]$ L.4-2

Appendix M

M.1 Neighboring control points for potential spline computation M.4-1

Appendix O

O.1 Effect of leading edge force O.6-1
O.2 Leading edge force on a three-dimensional thin wing O.6-1
O.3 Definition of $x_{n,1}$ and $x_{n,2}$ O.6-2
O.4 Edge force correction factors O.6-3
O.5 Comparison of leading edge suction predicted by PAN AIR with theoretical results O.6-4
O.6 Comparison of drag predicted by PAN AIR with theory for a delta wing in supersonic flow O.6-5

1.0 Introduction

PAN AIR (an abbreviation for "panel aerodynamics") is a system of computer programs designed to analyze subsonic or supersonic inviscid flows about arbitrary configurations. It is one of a sequence of computer programs developed over the past two decades which fall in the category of "panel methods." Generally speaking, a panel method is a program which solves a linear partial differential equation numerically by approximating the configuration surface by a set of panels on which unknown "singularity strengths" are defined, imposing boundary conditions at a discrete set of points, such as panel centers, and thereby generating a system of linear equations relating the unknown singularity strengths. The equations are then solved to obtain the singularity strengths, which, once known, provide complete information about the flow.

PAN AIR differs from earlier panel methods in that it is a "higher order" panel method; that is, the singularity strengths are not constant on each panel. This is necessitated by the more stringent requirements of supersonic flow problems. Numerical solution of the differential equation for supersonic flow, the wave equation, is far more sensitive to the numerical idiosyncracies of a panel method than is the solution of Laplace's equation, which governs subsonic flow. The potential for numerical error is greatly reduced by requiring the doublet singularity strength to be continuous.

It is this "higher order" attribute which, in turn, allows PAN AIR to be used to analyze flow about arbitrary configurations. The A-230 program (Reference 1.1), for instance, can only analyze flow about thick objects such as bodies and thick wings, while the Woodward program (Reference 1.2) can only deal with "linearized" configurations, in which a wing is represented by its mean surface. So, PAN AIR can handle the simple configurations considered in preliminary design, and at the same time serve as an "analytical wind tunnel" for the analysis of flow about detailed, complex configurations.

The basic Version 3.0 PAN AIR capabilities include:

(a) the ability to handle, within the limitations of linear potential flow theory, completely arbitrary configurations, using either exact or linearized boundary conditions,

(b) the ability to handle asymmetric configurations as well as those with one or two planes of symmetry,

(c) the ability to handle symmetric configurations in either symmetric or asymmetric flow,

(d) the ability to superimpose an incremental velocity on the freestream, either locally or globally, in order to simulate effects such as a rotational motion, differing angles of attack for different portions of a configuration, or a propeller slipstream,

(e) the ability to calculate pressures, forces and moments using a variety of pressure formulas (such as isentropic, linear, etc.), including the forces and moments due to momentum flux through the surface,

(f) the ability to calculate leading edge and side edge thrust forces and moments for thin configurations,

(g) the ability to perform non-iterative design of a configuration, a process in which a desired pressure or tangential velocity distribution is specified. The program then determines the "residual" normal flow through the surface required to obtain the desired pressure distribution, and

(h) the ability to calculate streamlines and to evaluate flow properties at user specified off body points.

This document has been structured to provide an overview of the theory of potential flow in general and PAN AIR in particular, with detailed mathematical formulations reserved for the appendices. Section 2 contains a brief discussion of fluid dynamics, outlining without proofs the steps from the Navier-Stokes equations to the linear differential equation solved by PAN AIR. Section 3 discusses the general theory of panel methods without discussing PAN AIR in particular. Section 4 is an overview of PAN AIR as it compares to older panel methods. Section 5 is devoted specifically to PAN AIR.

A complete discussion of the theory of potential flow and PAN AIR will be given in the appendices.

This document is not intended to be a textbook on fluid dynamics, and thus detailed derivations which are available in standard texts will not be repeated here; rather, the appropriate reference will be given. The standard potential theory and fluid mechanics references we will use are the works of Kellogg (1.3), Liepmann and Roshko (1.4) and Ward (1.5). Those appendices dealing with items of theory unique to PAN AIR will be more thorough, however, referring to outside sources only for standard discussions of topics such as linear algebra, graph theory and numerical analysis. There will be a correspondence between appendices and portions of the actual computer code, with each appendix either supplying background information or discussing the theory behind a module or part of a module of PAN AIR.

A glossary containing the definition of technical terms is contained in this document. When a term first appears, it will be given in quotes, and briefly defined. The glossary will give a more detailed definition if necessary.

The authors wish to thank Kathleen Christianson, Michele Sorensen, and Valerie Spura for their efforts in typing this document and Forrester Johnson for his assistance in its preparation.

2.0 Fundamental Fluid Dynamics

In this section, we will outline the process by which one arrives at a second order linear partial differential equation, called the Prandtl-Glauert equation, which describes steady, irrotational, inviscid flow in a perfect fluid. Our starting point is the Navier-Stokes equations, which describe flow in a fluid under very general circumstances. The assumption that viscosity can be neglected permits the Navier-Stokes equations to be replaced by a simpler system of equations including a "continuity equation," a "momentum equation," two "energy equations," and "Euler's equation." The further assumptions of "irrotationality" and "isentropic flow" lead to the "unsteady potential equation." The assumption of steady flow leads to the "steady non-linear potential equation." Finally, the "small perturbation assumption" leads to the "Prandtl-Glauert equation." The remainder of this document will deal with the numerical solution of the latter equation.

2.1 The Navier-Stokes Equations

The basic equations describing the flow of a viscous compressible, heat-conducting fluid are the Navier-Stokes equations. These are:

(a) The equation of continuity,

$$\frac{\partial \rho}{\partial t} + \nabla \cdot (\rho \vec{V}) = \frac{\partial \rho}{\partial t} + \sum_{i=1}^{3} \frac{\partial(\rho V_i)}{\partial x_i} = 0 \qquad (2.1.1)$$

where $\nabla = \left(\frac{\partial}{\partial x_1}, \frac{\partial}{\partial x_2}, \frac{\partial}{\partial x_3}\right)$ is the gradient operator with respect to the location vector $\vec{x} = (x_1, x_2, x_3)$, and where we have used the conventional index notation as an alternate to $\vec{x} = (x, y, z)$. In addition, t is time, $\rho(\vec{x},t)$ is the density, and $\vec{V}(\vec{x},t)$ is the total velocity, with $\vec{V} = (V_1, V_2, V_3)$.

(b) The momentum equation

$$\frac{\partial}{\partial t}(\rho V_j) + \sum_{i=1}^{3} \frac{\partial}{\partial x_i}(\rho V_i V_j) = \frac{-\partial p}{\partial x_j} + \sum_{i=1}^{3} \frac{\partial}{\partial x_i} \tau_{ji} + \rho f_j$$

$$(j = 1,2,3) \qquad (2.1.2)$$

where τ_{ij} is the deviatoric portion of the "stress tensor" which vanishes for a frictionless fluid, $\vec{f}(\vec{x},t)$ is an external body force per unit mass exerted on the fluid, and $p(\vec{x},t)$ is the pressure.

(c) The energy equation

$$\frac{\partial}{\partial t}\left(\rho e + \frac{1}{2}\rho|\vec{V}|^2 + p\right) + \sum_{i=1}^{3} \frac{\partial}{\partial x_i}\left[\left(\rho e + \frac{1}{2}\rho|\vec{V}|^2 + p\right) V_i\right]$$

$$= \frac{\partial p}{\partial t} + \sum_{i,m} \frac{\partial}{\partial x_i}\left(\tau_{im} V_m + k \frac{\partial T}{\partial x_i}\right) + \rho \sum_i f_i V_i \qquad (2.1.3)$$

where $e(\vec{x},t)$ is the "internal energy" of the fluid, k is the coefficient of heat conductivity for the fluid, and $T(\vec{x},t)$ is the temperature.

(d) The equation of state

$$f(\rho, p, T) = 0 \qquad (2.1.4)$$

where the function f depends on the type of fluid. For a perfect gas, (2.1.4) can be written as

$$p = \rho RT \qquad (2.1.5)$$

where R is a constant.

The equations in this section are derived in Liepmann and Roshko (1.4), section 13.13.

2.2 Euler's Equation

The Navier-Stokes equations can be simplified by the neglect of viscosity, which is equivalent to setting the deviatoric stress tensor $\tau_{ij} = 0$. Combining the momentum and continuity equations, we obtain

$$\rho \frac{dV_j}{dt} = - \frac{\partial p}{\partial x_j} + \rho f_j \qquad j = 1,2,3 \qquad (2.2.1)$$

where the usual convective derivative operator is defined,

$$\frac{d}{dt} = \frac{\partial}{\partial t} + \sum_i V_i \frac{\partial}{\partial x_i}$$

Equation (2.2.1) is called Euler's equation. We can obtain a full system of equations including (2.2.1) as follows (see Liepmann and Roshko (1.4), p. 188, for details).

The continuity and energy equations can be reduced to two energy equations:

$$\rho \frac{d}{dt} (\frac{1}{2} |\vec{V}|^2) = -\vec{V} \cdot \nabla p + \rho \vec{V} \cdot \vec{f} \qquad (2.2.2)$$

and the rate of increase of heat per unit mass is given by

$$q = \frac{1}{\rho} \nabla.(k \nabla T) = \frac{d\rho}{dt} + p \frac{d}{dt} (\frac{1}{\rho}) \qquad (2.2.3)$$

In addition, it follows from (2.1.5) and (2.2.3) that a perfect gas obeys the equation

$$\frac{\partial e}{\partial t} = C_v \frac{\partial T}{\partial t} \qquad (2.2.4)$$

where C_v is the specific heat of the gas at constant volume.

2.3 The Unsteady Potential Equation

The equations of section 2.2 can be reduced to a single equation (see ref. 2.1 Landahl, section 1.2, for details) if four further assumptions are made. First we assume "isentropic flow" so that no heat is added to the fluid, and thus

$$q = 0 \tag{2.3.1}$$

Second, we assume irrotationality, that is,

$$\nabla \times \vec{V} = 0 \tag{2.3.2}$$

which is shown in Liepmann and Roshko (p. 196) to be equivalent to the existence of a "potential" function $\Phi(\vec{x},t)$ such that

$$\nabla \Phi = \vec{V} \tag{2.3.3}$$

Third, we assume the existence of a freestream potential Φ_∞, whose gradient is the uniform velocity $\vec{V}_\infty$ attained at points sufficiently distant from the disturbance being analyzed, and thus write

$$\phi = \Phi - \Phi_\infty \tag{2.3.4}$$

and

$$\vec{V} = (u,v,w) = \nabla \Phi = \nabla \Phi_\infty + \nabla \phi = \vec{V}_\infty + \nabla \phi \tag{2.3.5}$$

The quantities ϕ and $\vec{v}$ are called the perturbation potential and velocity, respectively. For convenience, we assume the freestream $\vec{V}_\infty$ is aligned in the x direction and has magnitude 1.

Fourth, we assume that

$$|\vec{v}| \ll a_\infty \tag{2.3.6}$$

everywhere, where a_∞ is the freestream speed of sound. Equation (2.3.6) is generally called a small perturbation assumption, but the reader is warned that other "small perturbation" assumptions exist in the literature and in this document.

Based on these four assumptions, one can obtain (denoting differentiation by subscripts) the unsteady potential equation (writing M_∞ for $|V_\infty| / a_\infty$):

$$\begin{aligned}
&(1-M_\infty^2)\phi_{xx} + \phi_{yy} + \phi_{zz} - 2M_\infty^2 \phi_{xt} - M_\infty^2 \phi_{tt} \\
&= M_\infty^2 \Big[\tfrac{1}{2}(\gamma - 1)(2u + 2\phi_t + |\vec{v}|^2)\nabla^2\phi \\
&\quad + (2u + u^2)\phi_{xx} + v^2 \phi_{yy} + 2vw\,\phi_{yz} + w^2 \phi_{zz} \\
&\quad + 2(1 + u)(v\,\phi_{xy} + w\,\phi_{xz}) + 2(uu_t + vv_t + ww_t)\Big]
\end{aligned} \tag{2.3.7}$$

where γ is the ratio of specific heats

2.4 The Steady Non-Linear Potential Equation

If we assume the flow conditions do not change with time, we can eliminate the time derivative terms in (2.3.7), obtaining (see Landahl, (2.1))

$$
\begin{aligned}
&(1 - M_\infty^2)\, \phi_{xx} + \phi_{xx} + \phi_{zz} \\
&= M_\infty^2 \Big[\tfrac{1}{2} (\gamma-1)\, (2u + |\vec{v}|^2)\, \nabla^2 \phi \\
&\quad + (2u + u^2)\, \phi_{xx} + v^2\, \phi_{yy} + 2vw\, \phi_{yz} + w^2\, \phi_{zz} \\
&\quad + 2(1 + u)(v\, \phi_{xy} + w\phi_{xz}) \Big]
\end{aligned}
\tag{2.4.1}
$$

where γ is the ratio of specific heats.

Equation (2.4.1) is often called the "small perturbation transonic equation" because it holds at transonic speeds (that is, for $M_\infty \approx 1$) under the assumption (2.3.6). Of course, the assumptions of steady, inviscid, irrotational, and isentropic flow must also hold.

2.5 The Prandtl-Glauert Equation

So far, each reduction of the Navier-Stokes equations to a simpler form has been based on precisely defined assumptions. But the conditions under which (2.4.1) reduces to a linear differential equation are not so precisely defined.

If $M_\infty = 0$, (2.4.1) reduces to Laplace's equation,

$$\nabla^2 \phi = 0 \tag{2.5.1}$$

a linear partial differential equation. If $M_\infty \neq 0$, (2.4.1) reduces to a linear differential equation provided additional assumptions are made.

Suppose

$$M_\infty^2 \, |\vec{v}| \ll 1 - M_\infty^2 \tag{2.5.2}$$

and

$$M_\infty^2 \, |\vec{v}| \ll 1 \tag{2.5.3}$$

which, like (2.3.6), are called small perturbation assumptions. Under those assumptions, the steady non-linear potential equation reduces (see Appendix A) to the Prandtl-Glauert equation:

$$(1 - M_\infty^2)\, \phi_{xx} + \phi_{yy} + \phi_{zz} = 0 \tag{2.5.4}$$

Equations (2.5.2) and (2.5.3) should be considered carefully by any user of PAN AIR, since they best indicate when PAN AIR will provide a reasonable analysis of the flow about a configuration. Equation (2.5.2) clearly cannot be satisfied for $M_\infty \approx 1$, and thus the Prandtl-Glauert equation does not describe "transonic" flow. Equation (2.5.3) does not hold for $M_\infty \gg 1$, and so (2.5.4) does not describe "hypersonic" flow.

But there is no precise answer to the question: for what range of Mach numbers does (2.5.4) describe the flow For a thick configuration, or one at a high angle of attack, the perturbation quantities u, v, and w tend to be large, and thus (2.5.2) and (2.5.3) only hold for a narrow range of Mach numbers. For a very slender configuration, at a small angle of attack, (2.5.3) and (2.5.4) hold for a much wider range of Mach numbers. But deciding whether (2.5.4) is a "reasonable" approximation for a particular configuration and a particular Mach number may be very difficult, and depend greatly on one's definition of "reasonable."

The remainder of this document will deal with the solution of the Prandtl-Glauert equation. Using Green's theorem, (2.5.4) is used to derive an integral representation formula where the integrals extend over the configuration surface. Additional assumptions are then brought to bear in order to obtain an integral equation on the configuration surface. The integral equation is then solved by a "discretization" process: the configuration surface is divided into panels, "boundary conditions" are imposed at a discrete set of points, and a system of linear equations is generated. The system of equations is solved, and data of aerodynamic interest is calculated from that solution.

3.0 Panel Method Theory

In this section, we outline the process by which the Prandtl-Glauert equation

$$(1 - M_\infty^2)\, \phi_{xx} + \phi_{yy} + \phi_{zz} = 0 \qquad (3.0.1)$$

is converted to an integral equation, and the way in which a general panel method solves that integral equation.

In section 3.1 we describe the Prandtl-Glauert scale transformation by which equation (3.0.1) is converted to either Laplace's equation ($M_\infty < 1$) or the wave equation ($M_\infty > 1$). In section 3.2 we state Green's third identity which provides a representation formula for ϕ in the subsonic case ($M_\infty < 1$). (The corresponding representation formula for the supersonic case is given in Ward, ref. (1.5)). For the subsonic case, a simple problem is then formulated showing how the integral representation formula leads to an integral equation. Finally, in section 3.3 we describe the discretization process by which a panel method solves the resulting integral equation.

3.1 Coordinate Scaling

Equation (3.0.1) is further simplified by performing a scaling of the coordinate system. If we define the flow type indicator s by

$$s = \text{sign}\,(1 - M_\infty{}^2) \tag{3.1.1}$$

and the compressibility scale factor β by

$$\beta = \sqrt{s\,(1 - M_\infty{}^2)} \tag{3.1.2}$$

then the scaled coordinates we require are given by

$$\begin{aligned} \bar{x} &= x \\ \bar{y} &= \beta\, y \\ \bar{z} &= \beta\, z \end{aligned} \tag{3.1.3}$$

In this new, scaled coordinate system, (3.0.1) can be written

$$s\,\phi_{\bar{x}\bar{x}} + \phi_{\bar{y}\bar{y}} + \phi_{\bar{z}\bar{z}} = 0 \tag{3.1.4}$$

But equation (3.1.4) is just the same as (3.0.1) with $M_\infty = 0$ or $M_\infty = \sqrt{2}$. Thus, the subsonic case reduces to the $M_\infty = 0$ case while the supersonic case reduces to the $M_\infty = \sqrt{2}$ case. Equation (3.1.4) is called Laplace's equation if $s = 1$, and the wave equation if $s = -1$. These equations occur in other branches of physics (for instance, Laplace's equation occurs in electrostatics), and thus PAN AIR potentially has applications in fields other than fluid mechanics.

For the rest of section 3, we will assume $M_\infty = 0$ (note, incidentally, that this does not mean $|\vec{V}_\infty| = 0$; rather, $|\vec{V}_\infty| = 1$ and the freestream speed of sound a_∞ is infinite). A similar discussion, for the case $M_\infty = \sqrt{2}$, is given in Ward (1.5). The integral representation formula (3.2.7) which results may be generalized to arbitrary subsonic and supersonic Mach numbers, as discussed by Ward in sections 2.8 and 2.10.

3.2 Green's Theorems

There are a number of theorems, all of them slightly different formulations of the same result, known as Green's theorem or theorems. It is one of these results, often known as Green's third identity (see Kellogg, p. 219) which allows us to obtain an integral representation formula for a function ϕ satisfying Laplace's equation. The most fundamental version of these theorems is also known as the "divergence theorem," or Gauss' Theorem, which states that if $\vec{F}(\vec{x})$ is a "well-behaved" function (that is, continuously differentiable) on a "nice" region V in space with boundary S (see figure 3.1), then

$$\iiint_V \nabla \cdot \vec{F} \, dV = \iint_S \hat{n} \cdot \vec{F} \, dS \tag{3.2.1}$$

where $\hat{n}(\vec{x})$ is an outward-pointing unit normal to the surface. This theorem is discussed on p. 39 of Kellogg.

Green's third identity follows from (3.2.1). We need some notation to state this result, however. Let U be a twice continuously differentiable function in a region V of space. Let P be a point in V, S the boundary of V, Q an arbitrary point of integration on S, and $R = |\vec{P} - \vec{Q}|$. Then

$$\begin{aligned} U(P) = & -\frac{1}{4\pi} \iiint_V \frac{\nabla^2 U}{R} \, dV_Q \\ & - \frac{1}{4\pi} \iint_S \frac{\hat{n} \cdot \nabla U}{R} \, dS_Q \\ & + \frac{1}{4\pi} \iint_S U \, \hat{n} \cdot \nabla \frac{1}{R} \, dS_Q \end{aligned} \tag{3.2.2}$$

This result is derived in Chapter VIII of Kellogg, where opposite signs appear because Kellogg's normal points inward. Also,

$$\nabla^2 = \nabla \cdot \nabla = \sum_{i=1}^{3} \frac{\partial^2}{\partial x_i^2} \tag{3.2.2a}$$

A number of results follow by substituting into (3.2.2) a function ϕ satisfying Laplace's equation

$$\nabla^2 \phi = 0 \tag{3.2.3}$$

First, letting P approach S we find that ϕ is finite as we approach S. Thus, ϕ is an integrable function over S. Next, let V be a region consisting of all of space except for a surface S, which is thus the boundary of V. We illustrate two such cases. In figure 3.2, S is a closed surface, and thus V is divided into two regions: V_1, the "interior" of S, and V_2, the "exterior." In figure 3.3, S is not closed, and thus V consists of a single region. Let us define the "upper" surface of S as the surface bounding that portion of V into which n points, where $\hat{n}$ is the outward-pointing normal for a closed surface, and may be chosen arbitrarily otherwise. Let us write ϕ_U and ϕ_L to denote the limiting values of ϕ at a point on S, approaching from above and below. Then (see p. 221 of Kellogg)

$$\phi(P) = -\frac{1}{4\pi} \iint_S \left[\frac{\hat{n} \cdot (\nabla \phi_U - \nabla \phi_L)}{R} - (\phi_U - \phi_L)\hat{n} \cdot \nabla \frac{1}{R} \right] dS_Q \tag{3.2.4}$$

Equation (3.2.4) is the fundamental integral representation formula which a panel method uses to obtain a solution to the potential flow problem. When combined with appropriate "boundary conditions" (see below), the formula (3.2.4) can be manipulated to yield an integral equation (of Fredholm type) on the singularity surface S. A panel method then obtains an approximate solution of this integral equation by means of the numerical method of collocation. Two functions defined on S are generally introduced because of their importance in the manipulation of (3.2.4). The first is the "source strength," defined by

$$\sigma(Q) = \hat{n} \cdot \left[\nabla \phi_U(Q) - \nabla \phi_L(Q) \right] \tag{3.2.5}$$

and the second is the "doublet strength," defined by

$$\mu(Q) = \phi_U(Q) - \phi_L(Q) \tag{3.2.6}$$

These quantities are often called "singularity strengths," because they measure the singular behavior of ϕ on S. Using these quantities, (3.2.4) becomes

$$\phi(P) = -\frac{1}{4\pi} \iint_S \left[\frac{\sigma}{R} - \mu\, \hat{n} \cdot \nabla \frac{1}{R} \right] dS \tag{3.2.7}$$

As mentioned above, equation (3.2.7) must be supplemented with boundary conditions in order to obtain the integral equation that is solved by PAN AIR. Generally, these boundary conditions are equations relating ϕ, σ, μ and their derivatives on S. The specification of boundary conditions in conjunction with (3.2.7) amounts to a formulation of a "boundary value problem." This problem in turn is called "well-posed" if it has a unique solution, and "ill-posed" otherwise. A typical example of a set of boundary conditions leading to boundary value problem formulation might be (see figure 3.2)

$$\phi_L = 0 \tag{3.2.8}$$

combined with

$$\nabla \phi_U \cdot \hat{n} = b$$
$$= - \vec{V}_\infty \cdot \hat{n}, \text{ say} \tag{3.2.9}$$

It can be shown (see Appendix B) that the combination of (3.2.7) with the specification of the boundary conditions (3.2.8) and (3.2.9) on the configuration in figure 3.2 is a well-posed boundary value problem. We will discuss ill-posed and well-posed boundary value problems further in section 4 and Appendix B of this document; see also Appendix A of the PAN AIR User's Manual.

In fact, the boundary conditions (3.2.8) and (3.2.9) constitute the "Morino formulation" of the potential flow problem (cf. ref. (4.6)). Referring again to figure (3.2), we see that the boundary condition (3.2.8) implies that $\phi = 0$ for all points interior to V_1. This follows from the general uniqueness result for solutions of Laplace's equation with Dirichlet boundary conditions (cf. Kellogg). Consequently we find that

$$\nabla \phi_L \cdot \hat{n} = 0 \tag{3.2.10}$$

Substituting this and (3.2.9) into (3.2.5) yields for σ,

$$\sigma = - \vec{V}_\infty \cdot \hat{n} \tag{3.2.11}$$

Note as well that ϕ_U is equal to the doublet strength μ; for, combining (3.2.6) and (3.2.8) we get

$$\mu = \phi_U - \phi_L = \phi_U - 0 = \phi_U \tag{3.2.12}$$

We can now obtain the integral equation mentioned above. Evaluating equation (3.2.7) on the upper surface of S, we obtain after using (3.2.11) and (3.2.12)

$$\mu(P) - \frac{1}{4\pi} \left(\iint_S \mu \, \hat{n} \cdot \nabla \frac{1}{R} \, dS \right)_U = \frac{1}{4\pi} \iint_S \frac{\vec{V}_\infty \cdot \hat{n}}{R} \, dS \tag{3.2.13}$$

When proper care is taken to evaluate the integral appearing on the left hand side on the upper surface of S, this equation is the integral equation for $\mu(Q)$ that is solved by PAN AIR, given the Morino formulation of the boundary value problem.

3.3 Discretization

We now outline the discretization process by which a panel method solves the integral equation obtained by combining (3.2.7) with a properly posed set of boundary conditions. In point of fact we will not actually describe the integral equation formulation of the potential flow problem. Rather, we shall describe in an operational way the process by which PAN AIR transforms a specific boundary condition imposed at a particular point into a constraint relation imposed on a set of singularity parameters. This point of view is consistent with the actual operation of PAN AIR, in which the problem formulation is implicitly left as a task to the user.

The general idea of this discretization process consists of two parts. First, finite dimensional approximate representation formulas are developed for the singularity functions $\sigma(Q)$, $\mu(Q)$ which express these functions as linear combinations of known basis functions $s_i(Q)$, $m_i(Q)$ with unknown coefficients λ_i, $i=1, \ldots, N$. The set $\{\lambda_i\}_{i=1}^{N}$ is called the set of singularity parameters. In the second part, a set of equations determining the unknown coefficients λ_i is obtained by imposing the boundary conditions specified by the program user at selected points, called "control points" or collocation points. By imposing a total of N conditions of this sort using N control point/boundary condition combinations, we obtain a system of N constraint relations involving the N unknown singularity parameters $\{\lambda_i\}_{i=1}^{N}$. Solving this system of equations yields values for λ_i, completely determining the functions σ and μ by virtue of the finite dimensional representation formulae (see equations (3.3.1) and (3.3.2) below). Then, by virtue of the integral representation formula (3.2.7), the potential function $\phi(P)$ is determined for all points P, solving the problem. We now amplify somewhat the details of this two part discretization process.

The first part of the discretization process consists of the development of finite dimensional representations for σ and μ. One begins by approximating the singularity surface S by a collection of "panels." Next a collection of points is chosen (for example, all panel centers), and the values of σ and μ at these points are identified as the unknown singularity parameters, λ_i. Approximate distributions $\sigma(Q)$ and $\mu(Q)$ are then developed by assuming that the values λ_i are known and applying a combination of linear least squares fitting techniques and polynomial interpolation processes to extend the discrete values of $\{\lambda_i\}_{i=1}^{N}$ to all points on the surface S. One obtains by this method the representations for σ and μ,

$$\sigma(Q) = \sum_{i=1}^{N} \lambda_i \, s_i(Q) \tag{3.3.1}$$

$$\mu(Q) = \sum_{i=1}^{N} \lambda_i \, m_i(Q) \tag{3.3.2}$$

Here, the functions $s_i(Q)$ and $m_i(Q)$, called the source and doublet basis functions, describe the source and doublet distributions obtained by setting $\lambda_i = 1$ and $\lambda_j = 0$ for all $j \neq i$. Of course if λ_i is a <u>doublet</u> parameter the corresponding source basis function s_i is identically zero. Similarly if λ_i is a source parameter, $m_i(Q) \equiv 0$. (The simplest sort of basis functions, frequently employed in "constant strength" panel methods, are obtained by extending the value λ_i over its associated panel. A basis function for such a method is illustrated by figure 3.4).

Having described the finite dimensional representation formulae for $\sigma(Q)$ and $\mu(Q)$, (3.3.1-2), we now show how a particular boundary condition imposed at a control point is transformed into a linear constraint relation imposed on $\{\lambda_i\}_{i=1}^{N}$. In order that this process by made quite clear, we consider the case of boundary condition (3.2.8) imposed at P:

$$\phi_L(P) = 0 \tag{3.3.3}$$

Upon substituting the representations (3.3.1-2) into the integral representation formula (3.2.7), one obtains the expression for $\phi_L(P)$ (note the evaluation at $P-\varepsilon n$, a point just below P)

$$\phi_L(P) = \left[-\frac{1}{4\pi} \iint_S \frac{1}{R} \sum_{i=1}^{N} \lambda_i s_i(Q) \, dS_Q \right]_{\vec{P}-\varepsilon\hat{n}}$$

$$+ \left[\frac{1}{4\pi} \iint_S \hat{n} \cdot \nabla(1/R) \sum_{i=1}^{N} \lambda_i m_i(Q) \, dS \right]_{\vec{P}-\varepsilon\hat{n}} \tag{3.3.4}$$

We identify the coefficient of λ_i in this equation the i-th component of a row vector ΦIC_L:

$$\llcorner \Phi IC_L(P) \lrcorner_i = -\frac{1}{4\pi} \iint_S (s_i/R)\, dS_Q + \frac{1}{4\pi} \iint_S \hat{n} \cdot \nabla(1/R)\, m_i\, dS_Q \tag{3.3.5}$$

Combining (3.3.4) with (3.3.5), we have expressed $\phi_L(P)$ as a linear combination of $\{\lambda_i\}_{i=1}^{N}$:

$$\phi_L(P) = \llcorner \Phi IC_L(P) \lrcorner \vec{\lambda} \tag{3.3.6}$$

Finally, imposing the boundary condition (3.3.3) leads to the "AIC constraint equation:"

$$\llcorner \Phi IC_L(P) \lrcorner \vec{\lambda} = 0 \tag{3.3.7}$$

Now we impose boundary conditions (which are not necessarily the same form as equation (3.3.3)) at all the control points in the configuration, obtaining as many boundary conditions as there are singularity parameters. Each boundary condition generates one linear equation, and thus we have a system of N equations in the N variables $\lambda_i, \ldots, \lambda_N$:

$$[AIC]\, \vec{\lambda} = b \tag{3.3.8}$$

where b is a vector of "constraints" (the entry of b corresponding to the boundary condition equation (3.3.7) is zero). Each row of the square matrix [AIC] is a row vector of a form similar to $\llcorner \Phi IC_L(P) \lrcorner$ for some control point P.

Once the AIC equation (3.3.8) has been formulated, it is solved for the values λ_i by means of standard linear algebra techniques. With these values known, $\sigma(Q)$ and $\mu(Q)$ are known by virtue of equation (3.3.1-2). The potential at a point can be computed by evaluating equation (3.2.7), the representation formula for ϕ. The velocity can be computed by evaluating the gradient of equation (3.2.7). Once the velocity is known, the pressure and pressure coefficients can be obtained from standard formulas (see figure (5.21) below).

In section 5 below, we will describe the PAN AIR discretization process more fully. In particular, we will describe the process of transforming a general boundary condition into an AIC constraint relation of the form (3.3.7). For even more detail, the reader is referred to appendix K.

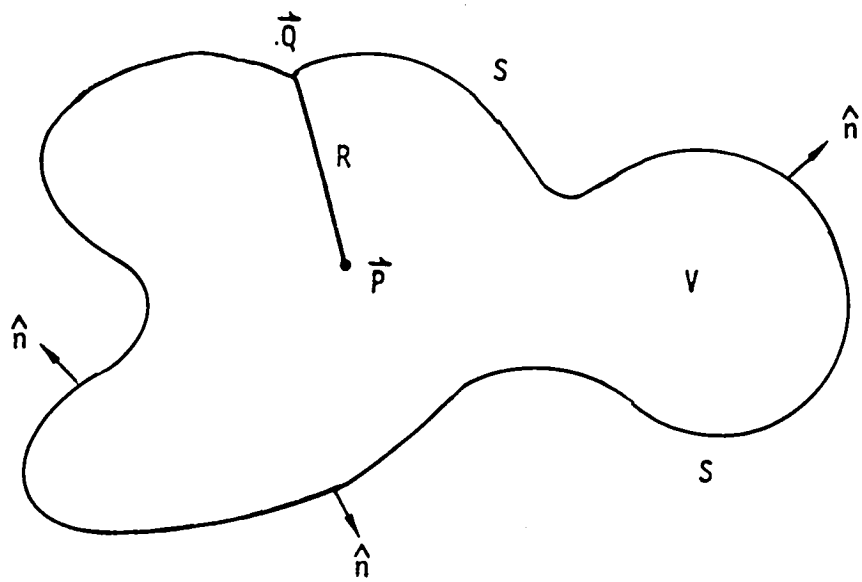

Figure 3.1 - Region V of space with boundary S

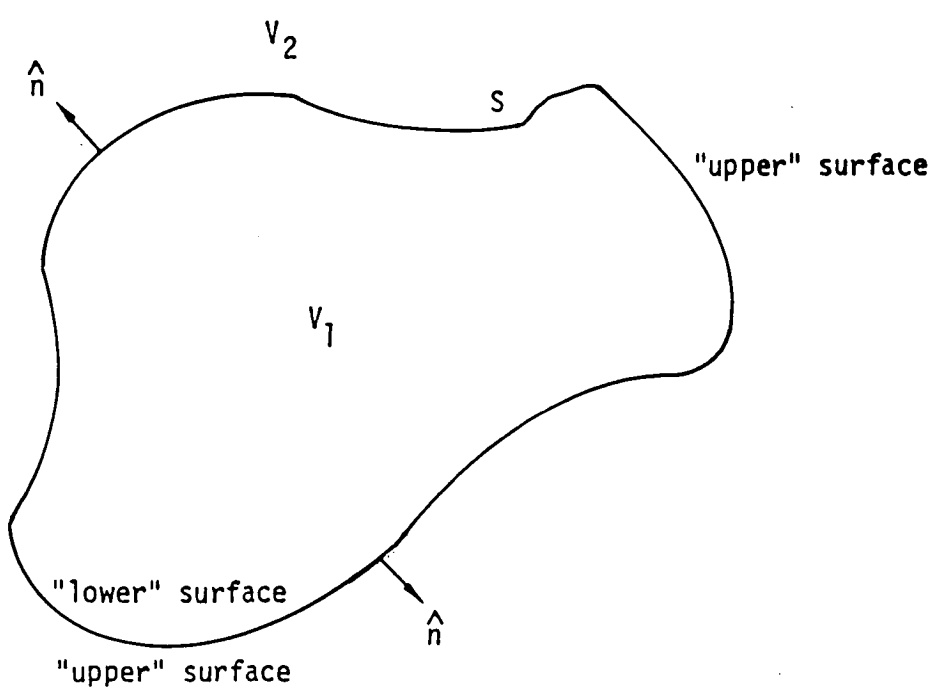

Figure 3.2 - A surface S dividing regions V_1 and V_2

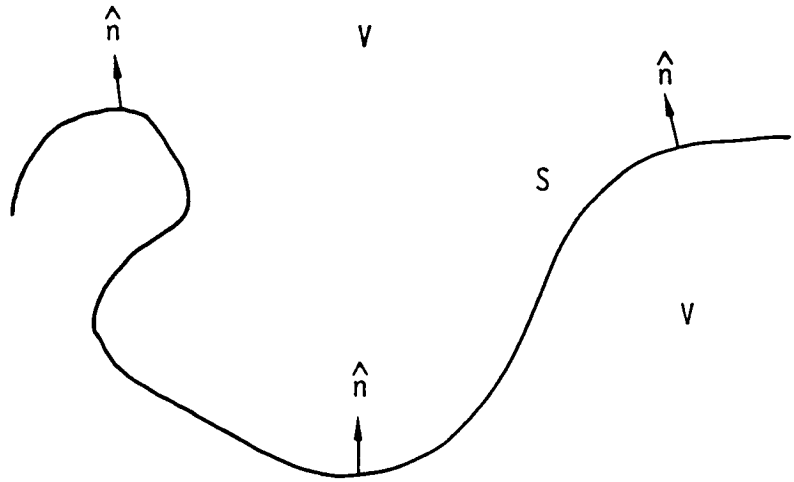

Figure 3.3 - A surface S which does not divide space into 2 separate regions

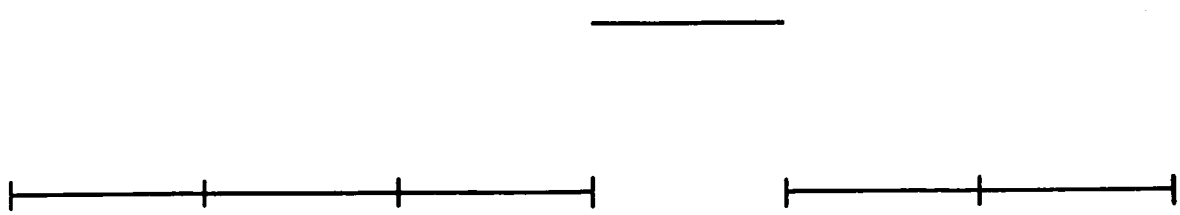

Figure 3.4 - Basis function for constant strength panels

4.0 An Overview of PAN AIR

4.1 Historical Development of Panel Methods

In this section, we will discuss the features which distinguish PAN AIR from earlier, less complex, panel methods. These features are (a) "continuous geometry," (b) linear source and quadratic doublet variation, and (c) continuity of doublet strength. We will explain how these features make PAN AIR more accurate and reliable than previous methods, and discuss briefly the manner in which these items are implemented in PAN AIR.

Virtually every panel method approximates the configuration geometry with panels whose planform is a quadrilateral. Thus, if the panels themselves are planar, only a small class of configurations (such as cylinders and flat wings) can be described without gaps being left between panels. These gaps tend to be very small, except for highly twisted surfaces. In subsonic flow, the gaps cause little numerical error, but in supersonic flow the cumulative effect of the gaps is serious, not because of "leakage" of flow through the gaps, but because the doublet strength jumps abruptly from a non-zero value to zero at a panel edge which does not exactly meet the adjacent edge. In PAN AIR, gaps are closed by means of "piecewise flat" panels, that is, panels which are comprised of several planar regions.

Some panel methods use "curved" panels, generally paraboloidal in shape. These approximate the configuration surface far more accurately in regions of high curvature such as the leading edge of a wing, but necessarily have gaps, even though small ones. Thus they are excellent for the analysis of subsonic flow, but not for supersonic flow.

As we stated earlier, PAN AIR employs a linear source variation and a quadratic doublet variation. That is, the basis function b_i corresponding to a source parameter is locally linear, while the basis function corresponding to a doublet parameter is locally quadratic. This contrasts with earlier, simpler programs in which the doublet and source variations were locally constant.

The reasons behind the "higher order" singularity distributions in PAN AIR are discussed in detail in Appendix B.4. Briefly, they are as follows. Consider a control point on a panel, and assume the source and doublet distributions in the immediate neighborhood of the control point are polynomials. Then we show in Appendix B.4 that a source distribution locally of the form

$$\sigma(\xi, \eta) = \sum_{N=1}^{\infty} \sum_{i=0}^{2N} a_{iN}^{S} \xi^{i} \eta^{2N-i} \tag{4.1.1}$$

or a doublet distribution

$$\mu(\xi, \eta) = \sum_{N=1}^{\infty} \sum_{i=1}^{2N+1} a_{iN}^{D} \xi^{i} \eta^{2N+1-i} \tag{4.1.2}$$

does not induce any perturbation velocity locally. That is, even terms in the polynomial source distribution and odd terms in the doublet distribution do not generate a local perturbation velocity. So, since we have concluded that constant source and doublet strengths are insufficient, the next reasonable higher order approximation to use is linear source strength and quadratic doublet strength.

Another reason for using a higher order doublet distribution is to provide a continuous doublet distribution; that is, each of the basis functions m_i is constructed so that it is continuous everywhere. (Obviously, a locally constant function cannot be continuous.) A continuous doublet strength, once again, is much more important in supersonic than in subsonic flow. This is due to the failure of disturbances caused by doublet discontinuities to diminish with distance in supersonic flow as they do in subsonic flow. A detailed description of the behavior of these disturbances is given in Appendix J.11.

In addition, experimental evidence (references (4.5), (4.8), (4.9)) indicates that exact surface analysis is not feasible in supersonic flow without doublet continuity. The requirement of doublet continuity results in the spline complexity discussed in section 5.

In figure 4.1, we compare some panel methods of the last two decades. The list is by no means complete, with inclusion in the list generally reserved for methods containing innovations, whether or not the method enjoyed any great success.

Of the other panel methods described in figure 4.1, the one which most closely resembles PAN AIR is that of Ehlers et al. That program was written to demonstrate the technological feasibility of a panel code which was capable of analyzing arbitrary configurations in supersonic flow. The development of that program took place with the intention of eventually constructing production software (that is, PAN AIR) based on the same principles, and thus that program is generally referred to as the PAN AIR "pilot code."

4.2 Summary of PAN AIR Technology

We now outline the method by which PAN AIR computes a row of the aerodynamic influence coefficient matrix. There are four basic steps. First, the basis functions must be computed. That is, the locally linear or locally quadratic variation on every panel must be precisely defined for each basis function (see section 4.2.1). Next, for each panel, the perturbation that the panel induces on the potential and velocity at each control point, in terms of the singularity parameters, must be computed (see section 4.2.2 for details). Next (see section 4.2.3) these perturbation influences must be summed over all panels, to give a "potential influence coefficient" row vector ($\llcorner \Phi IC(P) \lrcorner$) and a "velocity influence coefficient" matrix [VIC(P)] with the properties

$$\phi_A(P) = \sum_{j=1}^{N} \llcorner \Phi IC(P) \lrcorner_j \lambda_j = \llcorner \Phi IC(P) \lrcorner \vec{\lambda} \tag{4.2.1}$$

$$(\vec{v}_A(P))_i = \sum_{j=1}^{N} [VIC(P)]_{ij} \lambda_j = ([VIC(P)] \vec{\lambda})_i \qquad i = 1,2,3 \tag{4.2.2}$$

That is, the jth columns of $\llcorner \Phi IC(P) \lrcorner$ and [VIC(P)] give the dependence of the potential and velocity at P on the j-th singularity parameter. The subscript A indicates that the average of upper and lower surface potential and velocity are to be computed. Note that upper and lower surface potential and velocity are different, their difference being defined by the source and doublet strength (cf. (3.2.5-6)).

Finally, a fairly general boundary condition of the form

$$a_A \vec{v}_A \cdot n + c_A \phi_A + \vec{t}_A \cdot \vec{v}_A = b \tag{4.2.3}$$

(where $\vec{t}$ is a user-defined tangent vector) leads to a row $\llcorner AIC(P) \lrcorner$ of [AIC] as follows:

$$\llcorner AIC(P) \lrcorner = c_A \llcorner \Phi IC(P) \lrcorner + (a_A \hat{n} + \vec{t}_A)^T [VIC(P)] \tag{4.2.4}$$

More general boundary conditions than this are handled by PAN AIR, but we defer their full treatment until later (see sections 5.4.2.5, 5.6 and 5.7 below).

4.2.1 Basis Function Computation

The computation of the basis functions is one of the more complex portions of PAN AIR. To be precise, we do not directly compute basis functions, but rather, for each region on which the source and doublet strengths are defined by a single polynomial, we compute matrices which describe the coefficients of these polynomial distributions as linear combinations of the singularity parameters in the neighborhood of the panel. A column of such a matrix defines the coefficients of a basis function on a subpanel.

These matrices are called "spline" matrices, and are computed in two steps as described in the following two subsections.

4.2.1.1 Subpanel Splines

The first step is the computation of a "sub-panel spline" (SPSPL) matrix. Each panel is divided into eight triangular regions called "subpanels", as indicated in figure 4.2. The source subpanel spline matrices are 3x5 matrices $SPSPL^S$ giving the three coefficients σ_0, σ_ξ, σ_η of a linearly varying source strength (a linear function in two variables has three coefficients) in terms of five "panel source parameters," $\sigma_1, \ldots, \sigma_4, \sigma_9$, that is, the values of source strength at five points on the panel:

$$\begin{Bmatrix} \sigma_0 \\ \sigma_\xi \\ \sigma_\eta \end{Bmatrix} = [SPSPL^S] \begin{Bmatrix} \sigma_1 \\ \vdots \\ \sigma_4 \\ \sigma_9 \end{Bmatrix} \tag{4.2.5a}$$

where σ is defined in terms of local coordinates by

$$\sigma(\xi, \eta) = \sigma_0 + \sigma_\xi \xi + \sigma_\eta \eta \tag{4.2.5b}$$

Similarly, the (6x9) doublet subpanel spline matrices give the six coefficients of a quadratically varying doublet strength on the region in terms of nine "panel doublet parameters:"

$$\begin{Bmatrix} \mu_0 \\ \vdots \\ \mu_{\eta\eta} \end{Bmatrix} = [SPSPL^D] \begin{Bmatrix} \mu_1 \\ \vdots \\ \mu_9 \end{Bmatrix} \tag{4.2.6}$$

where

$$\mu(\xi,\eta) = \mu_0 + \mu_\xi \xi + \mu_\eta \eta + \frac{1}{2} \mu_{\xi\xi} \xi^2 + \mu_{\xi\eta} \xi\eta + \frac{1}{2} \mu_{\eta\eta} \eta^2 . \tag{4.2.7}$$

4.2.1.2 Outer Splines

Next, in the second step, the five panel source parameters and nine panel doublet parameters are described, as linear combinations of singularity parameters in the neighborhood of the panel, by "outer spline" matrices B^S $(5xk_S)$ and B^D $(9xk_D)$ where k_S and k_D are the number of source and doublet singularity parameters in the neighborhood of the panel for which the dependence is non-zero:

$$\begin{Bmatrix} \sigma_1 \\ \vdots \\ \sigma_4 \\ \sigma_9 \end{Bmatrix} = [B^S] \begin{Bmatrix} \lambda_1^S \\ \vdots \\ \lambda_{k_S}^S \end{Bmatrix} \tag{4.2.8}$$

$$\begin{Bmatrix} \mu_1 \\ \vdots \\ \mu_9 \end{Bmatrix} = [B^D] \begin{Bmatrix} \lambda_1^D \\ \vdots \\ \lambda_{k_D}^D \end{Bmatrix} \tag{4.2.9}$$

The values k_S and k_D depend on the location of a panel in a network (networks are discussed in section 5.1). In general, k_S is 9 and k_D is 21. In all cases, $k_S + k_D \leq 31$.

4.2.2 Panel Influence Coefficients

The perturbations that a source and doublet distribution on a panel induce at a control point are described by "panel influence coefficient" (PIC) matrices. These matrices include a 4x5 matrix PIC^S and a 4x9 matrix PIC^D which give the potential and velocity at the control point, induced by the panel, in terms of the five panel source parameters and nine panel doublet parameters. That is,

$$\begin{Bmatrix} \phi(P) \\ \hline \vec{v}(P) \end{Bmatrix}_{\substack{\text{perturbation} \\ \text{induced by panel}}} = [PIC^S] \begin{Bmatrix} \sigma_1 \\ \vdots \\ \sigma_4 \\ \sigma_9 \end{Bmatrix} + [PID^D] \begin{Bmatrix} \mu_1 \\ \vdots \\ \mu_9 \end{Bmatrix} \tag{4.2.10}$$

where σ_1 through σ_4, σ_9 and μ_1 through μ_9 are the panel source and doublet parameters.

The method by which the PIC matrices are calculated depends on the distance from the panel to the control point.

4.2.2.1 Near Field PIC's

If the distance is small compared to panel size, a "near field" method is used, and the PIC matrices are computed as a sum of integrals over the eight subpanels. For instance,

$$\lfloor PIC^S_{POTENTIAL} \rfloor^{1x5}$$

$$= -\frac{1}{4\pi} \sum_{i=1}^{8} \iint_{\Delta_i} J_i \frac{1}{R} \lfloor 1 \quad \xi \quad \eta \rfloor \quad d\xi \quad d\eta \quad [SPSPL_i^S]^{3x5} \tag{4.2.11}$$

Here, (ξ, η) are the local coordinates on the i-th subpanel Δ_i, and $SPSPL_i^S$ is the 3x5 source subpanel spline matrix; J_i denotes an area jacobian for the local to reference coordinate transformation. Note that, for a point $Q = (\xi, \eta)$, using (4.2.5a) and (4.2.5b),

$$\sigma(Q) = \lfloor 1 \quad \xi \quad \eta \rfloor \quad [SPSPL_i^S] \begin{Bmatrix} \sigma_1 \\ \vdots \\ \sigma_4 \\ \sigma_9 \end{Bmatrix} \tag{4.2.12}$$

and thus (4.2.11) follows from (3.2.7) and (4.2.10). The integrals in (4.2.11) are evaluated analytically, and can be expressed as logarithms and arctangents of quantities which are determined by the geometric relation between the panel and the control point. In equation (4.2.11) the entries of $[SPSPL_i^S]$ are constants and may be removed from the integral. The application of (3.2.7) and an equation similar to (4.2.12) leads to a similar equation for the row of PIC^D corresponding to the potential. The rows of the PIC matrices corresponding to velocity are computed by using a differentiated version of (3.2.7). The entire subject of PIC computation is discussed in more detail in section 5.6 and Appendix J.

4.2.2.2 Far Field PIC's

If the distance from the panel to the control point is large compared to panel size, a "far field" approximation is used in computing the influence of the panel. This is done by approximating the expression (1/R) by a power series

$$\frac{1}{R} = \frac{1}{R_0} \left(1 + a_1 \frac{\Delta R}{R_0} + a_2 \frac{\Delta R^2}{R_0}\right) \tag{4.2.13}$$

where R_0 and ΔR are illustrated in figure 4.3. This far field evaluation requires considerably less computer time than the near field method (see section 5.6 for further details). To further save computer time, an "intermediate field" method described in section 5.6 is used when the near field method is not necessary and the far field method is inadequate.

4.2.3 Potential and Velocity Influence Coefficient Assembly

The influence of each panel is accumulated to determine the influence of the entire configuration on the control point. Combining equations (4.2.8-10), we see that the products

$$[PIC^S \cdot B^S] \quad \text{and} \quad [PIC^D \cdot B^D]$$

give us the potential and velocity induced by a panel, in terms of the singularity parameters in the neighborhood of the panel. These matrices are then "added" together; that is, entries of distinct PIC matrices which correspond to the same singularity parameter are accumulated, so that the "sum" of expanded PIC matrices (none of which has more than 31 non-zero columns) is the 4xN matrix

$$\begin{bmatrix} \Phi IC(P) \\ \hline VIC(P) \end{bmatrix}$$

Here, N is the total number of singularity parameters.

4.2.4 Aerodynamic Influence Coefficient Matrix Construction

Once the matrices $\llcorner \Phi IC(P) \lrcorner$ and [VIC(P)] have been constructed, the vector $\llcorner AIC(P) \lrcorner$ is easily constructed using equation (4.2.4). The entire process is performed for all the control points in the configuration, and the result is the square matrix [AIC]. Additional details are given in section 5.7.

From here on, the basic structure of PAN AIR is similar to that of other panel methods. The system of linear equations is solved, "post-multiplication" (multiplying $\llcorner \Phi IC \lrcorner$ and [VIC] by the vector $\vec{\lambda}$) is performed, and the resulting potential and velocity values are used to compute pressures.

ORIGINATOR AND METHOD NAME (IF ANY)	YEAR	REF #	PANEL GEOMETRY	SOURCE TYPE	DOUBLET TYPE	BOUNDARY CONDITIONS	RESTRICTIONS	COMMENTS
HESS AND SMITH (DOUGLAS)	1962	4.1	FLAT	CONSTANT	NONE	SPECIFICATION OF NORMAL FLOW	NON-LIFTING WINGS AND BODIES ONLY	
RUBBERT (VORTEX LATTICE)	1964	4.2	FLAT	NONE	CONSTANT	NORMAL FLOW	PLANAR WINGS ONLY	
RUBBERT AND SAARIS (A-230)	1968	1.1	FLAT	CONSTANT	CONSTANT	NORMAL FLOW	NEARLY CONSTANT PANEL DENSITY	
WOODWARD	1968	1.2	FLAT	CONSTANT	LINEAR	NORMAL FLOW	WINGS MUST BE PLANAR	
HESS	1972	4.3	FLAT	CONSTANT	LINEAR	NORMAL FLOW	WINGS AND BODIES ONLY	
ROBERTS AND RUNDLE	1973	4.4	PARABOLOIDAL	QUADRATIC	QUADRATIC	NORMAL FLOW		NUMERICAL INTEGRATION - VERY EXPENSIVE
MERCER, WEBER AND LESFORD	1973	4.5	FLAT	NONE	SMOOTH, CUBIC/ QUADRATIC	NORMAL FLOW IN LEAST SQUARES SENSE	PLANAR WINGS	SUBSONIC AND SUPERSONIC CUBIC SPANWISE, QUADRATIC CHORDWISE
MARINO AND KUO	1974	4.6	CONTINUOUS, HYPERBOLOIDAL	CONSTANT	CONSTANT	POTENTIAL	NO THIN CONFIGURATIONS	
JOHNSON AND RUBBERT	1975	4.7	PARABOLOIDAL	LINEAR	QUADRATIC	NORMAL FLOW		
EHLERS AND RUBBERT (MACH LINE PANELING)	1976	4.8	FLAT	LINEAR	CONTINUOUS QUADRATIC	NORMAL FLOW	PLANAR WINGS, SPECIAL PANELING	SUPERSONIC FLOW
EHLERS ET AL ("PILOT CODE")	1977	4.9	CONTINUOUS, PIECEWISE FLAT	LINEAR	CONTINUOUS QUADRATIC	ARBITRARY IN ϕ, $\nabla\phi$		SUBSONIC AND SUPERSONIC
PAN AIR	1980		CONTINUOUS, PIECEWISE FLAT	LINEAR	CONTINUOUS, QUADRATIC	ARBITRARY IN ϕ, $\nabla\phi$		SUBSONIC AND SUPERSONIC

Figure 4.1 - Historical Overview of Panel Methods

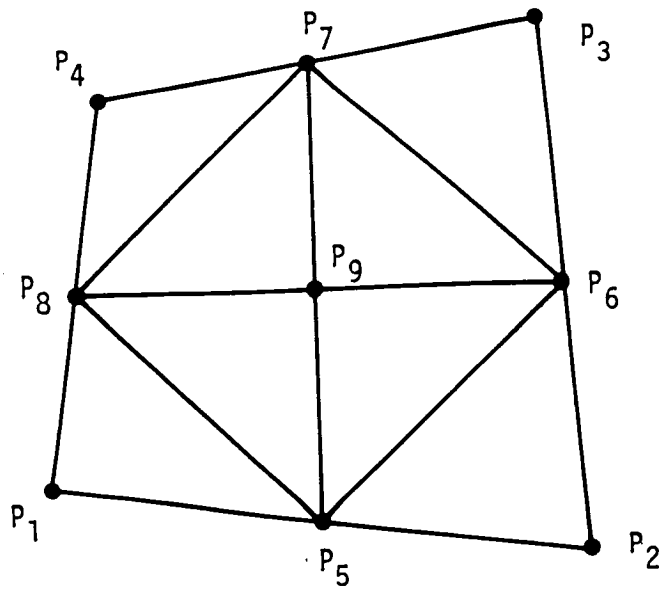

$\sigma_i = \sigma(P_i)$,

$i = 1, 2, 3, 4, 9$

$\mu_i = \mu(P_i)$,

$i = 1, \ldots, 9$

Figure 4.2 - Division of panel into subpanels

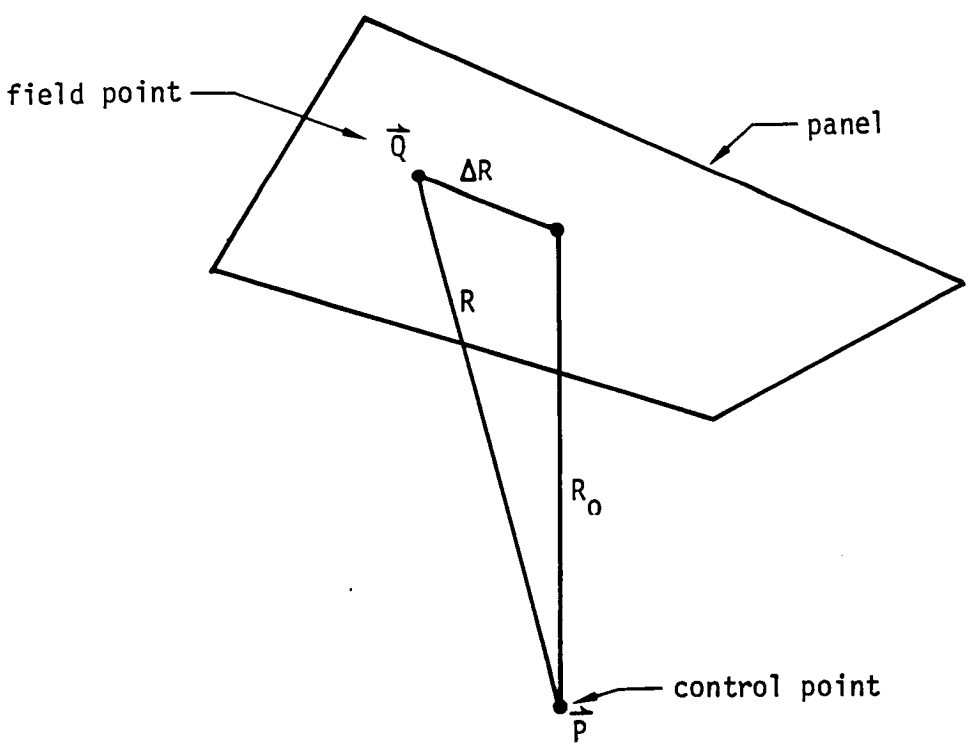

Figure 4.3 - Panel and far field control point

5.0 Elaboration on the Technology in PAN AIR

We now proceed to greater depth in the discussion of the technological details of PAN AIR. In section 5.1 we describe the way in which the program user describes his configuration geometry to PAN AIR using networks of panels. Section 5.2 gives the form of the general integral representation formula for ϕ together with a summary of all of the coordinate transformations used by PAN AIR, while section 5.3 discusses doublet matching along network abutments. The general form of a PAN AIR boundary condition is developed in section 5.4 and this is followed by the treatment of spline matrices in 5.5 and panel influence coefficients (PIC's) in 5.6. The results of sections 5.4, 5.5 and 5.6 are then combined to describe the formation of the aerodynamic influence coefficient matrix (AIC) and right hand side vector (b) in section 5.7. The discussion concludes with some remarks on the solution of the AIC constraint equation (section 5.8) followed by a summary of PAN AIR's post processing features (section 5.9).

5.1 Networks and Panels

The configuration on which boundary conditions are to be imposed is described by a collection of networks of points. Each network consists of (say) N columns of points lying on the configuration surface, where each column has the same number (M,say) of points. By a point, we mean its (x,y,z) coordinates, with each point's coordinates given in the same arbitrary coordinate system. Thus, each network consists of an MxN grid of points in space (see figure 5.1). This grid need not lie in a plane, but it should be sufficiently regular to define a surface which does not intersect itself and on which the surface normal does not change too radically from panel to neighboring panel.

Each network is assigned two "singularity types," describing the manner in which the source and doublet distributions are defined on the portion of the surface defined by the network. A network source type may be "null," "analysis," or "design," while its doublet type may be "null," "analysis," "design," or "wake." The singularity type "null" means that the corresponding singularity distribution is identically zero over the whole network. The singularity type "analysis" is used when the corresponding boundary conditions are the standard ones of zero normal flow, while the singularity type "design" is used when the boundary conditions correspond to specifying a desired pressure distribution on the surface. The doublet type of "wake" is generally used with a source type of null to model a wake surface. A wake is a surface across which a discontinuity in potential exists, while normal flow is continuous; generally a wake is attached to the trailing edge of a lifting surface. The positioning of wakes can be a complicated problem, and is discussed in more detail in the PAN AIR User's and Case Manual.

Note that, unless the source or doublet type is null, all networks are composite networks, that is, both the network's source distribution and its doublet distribution are non-zero. This is in contrast to most earlier panel methods, which required source networks and doublet networks to be entered separately. Generally speaking, all non-wake networks in PAN AIR will be composite networks which directly describe the impermeable object about which one is analyzing the flow. In particular, the "internal lifting system" doublet networks required by the Boeing A-230 program (Ref. 1.1) are not required in PAN AIR. These composite networks allow two boundary conditions, such as the standard boundary conditions of (5.4.28), to be imposed on a surface.

Each network of M rows and N columns of points defines (M-1) rows and (N-1) columns of panels, where a panel is a quadrilateral defined by four network points all lying in two adjacent rows and two adjacent columns of a network. Figure 5.1 illustrates the subdivision of a network into panels. In the example of Figure 5.1, there are five rows and columns of points and four rows and columns of panels.

Now, each panel is defined by its four corner points, but these four points need not lie on a plane. Previous programs using flat panels on arbitrary surfaces have handled this problem by projecting the four corner points onto an "average plane," thus forming a planar quadrilateral panel. The formation of such panels leaves gaps between panel edges, however, since the resulting planar panels do not in fact go through their corresponding corner points.

This discontinuity in geometry is avoided by constructing piecewise flat panels which do in fact contain all four corner points and, in fact, all four panel edges (a panel edge is a line segment connecting adjacent corner points). The decomposition of a panel into five planar regions is illustrated in figure 5.2. It will be shown in Appendix D that the four edge midpoints, which define the vertices of the interior quadrilateral, do in fact lie on a plane. In section 5.5, the interior quadrilateral will be divided into four triangular regions for the purpose of defining source and doublet distributions. Thus the panel will be divided into 8 "subpanels" there, but at least four of them will lie in one plane.

5.2 Coordinate Transformations

Recall (see (3.2.7)) that for $M_\infty = 0$, we wrote the fundamental integral representation formulas as

$$\phi(P) = \frac{1}{4\pi} \iint_S \left[-\frac{\sigma}{R} + \mu\, \hat{n} \cdot \nabla \left(\frac{1}{R}\right) \right] dS \tag{5.2.1}$$

We can easily generalize this equation to arbitrary Mach number. For details, see Ward (Ref. 1.5). Let $P = (x,y,z)$, and the point of integration $Q = (\xi, \eta, \zeta)$. Recall

$$\begin{aligned} s &= \text{sign}\,(1 - M_\infty^2) \\ \beta &= \sqrt{s(1 - M_\infty^2)} \end{aligned} \tag{5.2.2}$$

Now, generalizing the definition of R for $M_\infty \neq 0$, let

$$R = \sqrt{(\xi - x)^2 + s\,\beta^2 (\eta - y)^2 + s\,\beta^2 (\zeta - z)^2} \tag{5.2.3}$$

when the expression under the square root is non-negative. Let R be zero otherwise.

For subsonic flow, let D_p, the "domain of dependence" of the point P, be all of space, while for supersonic flow let it be the set of points Q such that $\xi \leq x$, and the expression under the square root is non-negative. Let $\kappa = 2\pi$ if $s = -1$, $\kappa = 4\pi$ if $s = +1$. Let us define the compressible gradient operator

$$\tilde{\nabla} = \left(s\,\beta^2 \frac{\partial}{\partial \xi}, \frac{\partial}{\partial \eta}, \frac{\partial}{\partial \zeta}\right) = [B]\,\nabla \tag{5.2.4}$$

where the dual metric matrix [B], referred to compressibility coordinates, is given

$$[B] = \begin{bmatrix} s\beta^2 & 0 & 0 \\ 0 & 1 & 0 \\ 0 & 0 & 1 \end{bmatrix} \tag{5.2.5}$$

Let the conormal vector $\tilde{n} = \vec{\nu}$ be defined

$$\tilde{n} = \vec{\nu} = [B]\,\hat{n} \tag{5.2.6}$$

and let σ be given by

$$\sigma = \nabla (\phi_U - \phi_L) \cdot \tilde{n} \tag{5.2.7}$$

a generalization of our previous definition of source strength to arbitrary Mach number. Then we can rewrite (5.2.1) for arbitrary M_∞ as

$$\phi(P) = \frac{1}{\kappa} \iint_{S \cap D_p} [- \frac{\sigma}{R} + \mu \, \hat{n} \cdot \tilde{\nabla} \frac{1}{R}] \, dS \tag{5.2.8}$$

Here, "$S \cap D_p$" means the set of points common to both S and D_p. This is the general form of the integral representation for ϕ, upon which all of PAN AIR is founded.

Now, in order to obtain "panel influence coefficient" matrices, we must perform integrations of the form of (4.2.11). This task is somewhat obscured by the multiplicity of coordinate systems with which we deal. We will now discuss these coordinate systems and describe the transformations among them.

The coordinate system with which this document primarily deals is the "compressibility axis coordinate system." This is the system in which equation

$$(1 - M_\infty^2) \, \phi_{xx} + \phi_{yy} + \phi_{zz} = 0 \tag{5.2.9}$$

is valid.

For $M_\infty \neq 0$, (5.2.9) requires a preferred direction, called the "compressibility direction," which is the direction of $\vec{V}_\infty$. We have assumed so far that this is the x-direction.

A program user, however, may not want to describe the configuration geometry in the compressibility axis coordinate system. PAN AIR permits the user to specify an arbitrary compressibility direction by specifying angles α_c and β_c, angles of attack and sideslip, which describe the compressibility direction with respect to the input (or reference) coordinate system.

If the coordinates of a point are (x,y,z) in the compressibility axis system, and (x_0, y_0, z_0) in the reference axis system, then

$$\begin{Bmatrix} x \\ y \\ z \end{Bmatrix} = [\Gamma_c] \begin{Bmatrix} x_0 \\ y_0 \\ z_0 \end{Bmatrix} \tag{5.2.10}$$

where Γ_c is the coordinate transformation matrix

$$\Gamma_c = \begin{bmatrix} \cos\alpha_c \cos\beta_c & -\sin\beta_c & \sin\alpha_c \cos\beta_c \\ \cos\alpha_c \cdot \sin\beta_c & \cos\beta_c & \sin\alpha_c \sin\beta_c \\ -\sin\alpha_c & 0 & \cos\alpha_c \end{bmatrix} \tag{5.2.11}$$

We show how Γ_c is obtained as a product of a rotation by an angle α_c about the y-axis and a rotation by an angle β_c about the modified z-axis in Appendix E.3. It should be noted that the above sequence of coordinate rotations is equivalent to the opposite sequence of basis vector transformations. That is, the configuration is first rotated about its z-axis by an angle β_c, then about its y-axis by an angle α_c. This transformation is discussed further in the User's Document.

Now, the unit vector in the compressibility direction is given in reference coordinates by

$$c_o = [\Gamma_c]^{-1} \begin{Bmatrix} 1 \\ 0 \\ 0 \end{Bmatrix} \tag{5.2.12}$$

Since Γ_c is an orthogonal matrix,

$$\hat{c}_o = [\Gamma_c]^T \begin{Bmatrix} 1 \\ 0 \\ 0 \end{Bmatrix} = \begin{Bmatrix} \cos\alpha_c \quad \cos\beta_c \\ -\sin\beta_c \\ \sin\alpha_c \quad \cos\beta_c \end{Bmatrix} \tag{5.2.13}$$

The relationship of $\hat{c}_o$ to the reference coordinate system is shown in figure 5.3.

A third coordinate system of importance in PAN AIR is the "local" coordinate system (see Glossary). We want to compute the surface integrals required for PIC calculation as integrals in two variables, and thus we construct a local coordinate system (x',y',z') for each subpanel, in which the subpanel lies in the x'-y' plane.

The transformation from reference to local coordinates is not orthogonal, however, but includes a scaling transformation so that the factor β does not appear in the expression for R. This simplifies the influence coefficient integrals, such as (5.6.9), which must be calculated.

Recall from (5.2.3) that in compressibility coordinates, for a control point P = (x,y,z) and field point (ξ, η, ζ), we have

$$R^2 = (\xi - x)^2 + s\,\beta^2 (\eta - y)^2 + s\,\beta^2 (\zeta - z)^2 \tag{5.2.14}$$

where R is the denominator of the integrand of (5.2.8). In order to describe the appearance of R in local coordinates, we need to introduce the panel inclination indicator r,

$$r = \text{sign}\,(\hat{n} \cdot \tilde{n})$$

$$= (\text{by } (5.2.6))\ \text{sign}\,(\hat{n}^T\,[B]\,\hat{n}) \qquad (5.2.15)$$

$$= \text{sign}\,\{\hat{n}, \hat{n}\}$$

where we define $\{.,.\}$ by saying that for any two vectors X and Y,

$$\{\vec{X},\vec{Y}\} = \vec{X}^T[B]\,\vec{Y} \qquad (5.2.16)$$

The meaning of r can be understood if we work in compressibility coordinates.

Then by (5.2.5) and (5.2.6),

$$r = \text{sign}\,(s\,\beta^2\,n_x^2 + n_y^2 + n_z^2) \qquad (5.2.17)$$

If $s = 1$ (that is, for subsonic flow), we see that the expression in (5.2.17) is positive, and so $r = 1$. If $s = -1$ (supersonic flow), and $\beta = 1$ ($M_\infty = \sqrt{2}$), we see that

$$r = -1 \quad \text{if} \quad n_x^2 > n_y^2 + n_z^2$$

$$r = +1 \quad \text{if} \quad n_x^2 < n_y^2 + n_z^2 \qquad (5.2.18)$$

Recall from section 4.2.1.1 that the PAN AIR panels are comprised of eight triangular subpanels. Each of these flat subpanel surfaces has a unit surface normal n of fixed direction. If n is such that $r = -1$ in equation (5.2.18), the surface normal is inclined at more than 45° to the freestream. But this 45° angle is also that of the "Mach cone" emanating forward from a point P on the subpanel, as illustrated in figure 5.5, and defines the "domain of dependence" of P. In other words, point P is affected only by disturbances (such as those produced by the source and doublet distributions) that originate within this forward Mach cone.

Thus we see that if $r = -1$, no point on the subpanel surface lies in the domain of dependence of any other point on the subpanel, and we call such a surface "superinclined." If $r = +1$, the more upstream points on the subpanel do lie in the domain of dependence of the more downstream points, and such a surface is called subinclined. If $\hat{n}.\tilde{n} = 0$, the more upstream points lie exactly on the boundary of, but never in the interior of, the domain of dependence of more downstream points. Such a surface is called Mach-inclined. We will see shortly that no portion of the panelled configuration is permitted to be Mach-inclined. The above definitions, illustrated in figures 5.4 and 5.5, are equally valid at all supersonic Mach numbers.

Now, for ease of integration, we want the local coordinate system (x',y',z') defined on each subpanel to have the property that if $P = (x',y',z')$, $Q = (\xi', \eta', \zeta')$ then

$$R^2 = r(\xi' - x')^2 + s(\eta' - y')^2 + rs(\zeta' - z')^2 \tag{5.2.19}$$

In this manner, we reduce the denominator of (5.2.8) to one of three standard forms:

(a) Subsonic flow

$$R = \sqrt{(\xi' - x')^2 + (\eta' - y')^2 + (\zeta' - z')^2} \tag{5.2.20}$$

(b) Supersonic flow, subinclined panels

$$R = \sqrt{(\xi' - x')^2 - (\eta' - y')^2 - (\zeta' - z')^2} \tag{5.2.21}$$

(c) Supersonic flow, superinclined panels

$$R = \sqrt{(\zeta' - z')^2 - (\xi' - x')^2 - (\eta' - y')^2} \tag{5.2.22}$$

So, if we can find a local coordinate system in which (5.2.19) holds, we will have succeeded in removing the factors of β from the integrand of (5.2.8). Further, the subpanel always lies in the (ξ', η') plane.

We will compute the reference to local coordinate transformation A, such that

$$[A] \begin{Bmatrix} x_0 \\ y_0 \\ z_0 \end{Bmatrix} = \begin{Bmatrix} x' \\ y' \\ z' \end{Bmatrix} \tag{5.2.23}$$

in Appendix E.3.

We now describe the result computed there. Let $\hat{v}_0$ be a unit vector perpendicular to $\hat{c}_0$ and $\hat{n}_0$, the unit normal to the subpanel, all three of these vectors being expressed in reference coordinates. Let $\hat{u}_0 = \hat{v}_0 \times \hat{n}_0$. Let the metric matrices in reference coordinates be given by

$$[C_0] = s\beta^2 [I] + (1 - s\beta^2) [\hat{c}_0 \hat{c}_0^T] \tag{5.2.24}$$

$$[B_0] = [I] + (s\beta^2 - 1) [\hat{c}_0 \hat{c}_0^T] \tag{5.2.25}$$

Note that the definition (5.2.5) of [B] in the compressibility axis coordinate system is consistent with (5.2.25) since

$$[\hat{c}\ \hat{c}^T] = \begin{bmatrix} 1 & 0 & 0 \\ 0 & 0 & 0 \\ 0 & 0 & 0 \end{bmatrix} \tag{5.2.26}$$

in the compressibility axis coordinate system, in which the compressibility axis coincides with the x axis. Recalling the definition (5.2.16) of $\{\cdot,\cdot\}$, the 3x3 matrix A is found to be given by

$$A = \left[\frac{1}{|\{\hat{n}_o, \hat{n}_o\}|^{1/2}} [C_o]\ \hat{u}_o \ \middle|\ \frac{rs}{\beta} [C_o]\ \hat{v}_o \ \middle|\ \frac{\beta}{|\{\hat{n}_o, \hat{n}_o\}|^{1/2}} \hat{n}_o \right]^T \tag{5.2.27}$$

Several remarks may be made here. First, if $M_\infty = 0$, $\hat{c}_0$ is meaningless, but is given a default value by PAN AIR just so that no special formula is needed to replace (5.2.27). Since all occurrences of $\hat{c}_0$ are multiplied by $(1 - s\,\beta^2) = M_\infty^2$ any value for $\hat{c}_0$ is equally valid if $M_\infty = 0$.

Next, (5.2.27) blows up if $\beta = 0$ or $\{\hat{n}_0, \hat{n}_0\} = 0$. Both of these cases are disallowed in PAN AIR, the case $\beta = 0$ corresponding to transonic flow, $M_\infty = 1$, the case $\{\hat{n}_0, \hat{n}_0\} = 0$ corresponding to a Mach-inclined panel.

5.3 Network Edge Matching

The splines which are discussed in section 5.5 insure that the doublet strength on the configuration is continuous within a network, but do nothing to insure continuity across network edges. The contribution of continuous doublet splines to the goal of increased program reliability would be wasted if the doublet strength were discontinuous at network boundaries.

One solution to the problem of matching doublet strength at network edges (hence called the edge matching problem) is to impose the boundary condition of zero normal flow along the edge. As shown in Appendix J.11, a discontinuity in doublet strength along an edge induces an infinite velocity there. Thus, the requirement that the flow be finite causes the doublet strength to be continuous across the edge. This method has worked successfully (in the earlier versions of the "pilot code," for instance) in many cases. Unfortunately, the method requires that the geometric fit among networks be exact; if there is a gap, say, where networks meet, the boundary condition of zero normal flow will force the doublet strength along the edge to zero.

The requirement that network edges match exactly in a geometric sense is a severe burden on the user of a panel code. Figure 5.6 illustrates the type of panelling frequently used by aerodynamicists at the intersection of the leading edge of a wing and the body of an airplane. The aerodynamicist is usually more interested in detailed wing pressures than detailed body pressures; further, the high curvature of the wing leading edge requires dense panelling for accurate definition. But accurate definition of the leading edge of the wing is incompatible with coarse definition of the body, unless a gap is left between network edges. In figure 5.6, the shaded area represents the gap between the body and the wing.

The most complex portion of the edge matching problem is the determination of those pairs (or larger collections) of network edges along which the doublet strength is to be matched. This determination is performed in two ways: (1) For each network edge, the program searches for other network edges which lie within a user-input tolerance distance of the first network edge. (2) For edges which lie far from each other (compared to the tolerance), but which ideally would be identical, such as those of figure 5.6, there is an option which permits the user to directly specify that doublet matching should occur along the edges.

PAN AIR incorporates two features to insure the matching of doublet strength across network edges. The first feature is that the matching of doublet strength is done directly rather than indirectly. That is, in construction of the AIC matrix, the boundary condition $\mu_1 - \mu_2 = 0$ (assuming μ_1 and μ_2 are the doublet strengths at two opposing points where networks meet) is imposed exactly (rather than approximately by the requirement of zero normal flow). The second feature is that "gap-filling" panels are introduced whenever there are gaps between network edges which do not actually represent gaps in the physical configuration. A doublet distribution is defined on these gap-filling panels in such a manner that continuity of doublet strength is produced everywhere.

Imposing doublet matching exactly, rather than indirectly, requires considerable care. The doublet matching boundary conditions must never be redundant. Redundancy is permissible in the case of zero normal flow boundary conditions because of the rather inexact manner in which these boundary conditions perform doublet matching. (Experimentation has shown however that the partial redundancy of zero normal flow boundary conditions may lead to ill-conditioned matrices.) But when matching of doublet strength is imposed exactly, any redundancy leads to a singular AIC matrix.

Preventing redundancy along a curve where two or more network edges meet (such a curve is called an abutment) is fairly straightforward. The only difficult problem occurs at "abutment intersections," that is, points where several abutments meet (see figure 5.7). The details concerning the imposition of edge matching, the generation of gap-filling panels and the handling of abutment intersections are given in Appendix F.

5.4 Control Points and Boundary Conditions

5.4.1 Control Point Location

Control points are points at which boundary conditions are imposed. Such points are either (1) in the vicinity of a panel center (the point whose coordinates are the average of the panel corner coordinates), (2) in the vicinity of the midpoint of a panel edge which also lies on a network edge, or (3) in the vicinity of a panel corner which lies on a network edge. These points are called center, edge, and corner control points respectively. "Extra" corner control points are located at panel corners which belong to "abutment intersections." Figure 5.7 illustrates a situation which would cause the construction of an extra control point. There, N_1, N_2, and N_3 are three separate networks.

In figure 5.8 we illustrate the control point locations on a network with no extra control points. Note that control points are always receded slightly from a panel edge. This is done because the velocity induced by the doublet distribution on a panel causes an infinite velocity at the panel edge. Thus, for numerical reasons the control point is withdrawn approximately 1/10 of the way toward the center of the panel. The precise method by which control points are receded is described in Appendix G.

5.4.2 Boundary Conditions

Boundary conditions are imposed only at control points. Recall that a boundary condition is a linear equation in ϕ and its derivatives. Since ϕ or its gradient may be discontinuous on the configuration surface, upper and lower surface potential and velocity are different, and so the boundary condition equation may involve "upper surface" and/or "lower surface" terms. The number of boundary conditions imposed at a control point is between zero and two (inclusive), and is determined by the basic principle that the number of boundary conditions must equal the number of singularity parameters. For analysis networks, there are two boundary conditions imposed at every panel center control point, but, since only doublet parameters (and not source parameters) are located on network edges, there is only one boundary condition imposed at panel edge and corner control points.

5.4.2.1 Impermeability Boundary Conditions

For most cases, the boundary condition the user wishes to impose is that there is no flow through the configuration surface. At Mach zero, this is achieved by setting

$$\vec{V} \cdot \hat{n} = 0 \tag{5.4.1}$$

or equivalently,

$$\nabla \phi \cdot \hat{n} = \vec{v} \cdot \hat{n} = - \vec{V}_\infty \cdot \hat{n} \tag{5.4.2}$$

Equation (5.4.2) does not generalize in that form to arbitrary Mach number however. In Appendix H, we see that the appropriate boundary condition for non-linear potential flow (that is, flow satisfying the non-linear potential equation (2.4.1)) is

$$\rho \vec{V} \cdot \hat{n} = 0 \tag{5.4.3}$$

where ρ is the density of the fluid.

In section 1.11 of Ward (1.5), it is shown that, neglecting terms of the same order as those neglected in reducing equation (2.4.1) to the Prandtl-Glauert equation, we have

$$\rho \vec{V} = \rho_\infty \vec{W} \approx \rho_\infty (\tilde{\nabla} \phi + \vec{V}_\infty) \tag{5.4.4}$$

where ρ_∞ is the density at infinity. Note that $\tilde{\nabla} \phi$ rather than $\nabla \phi$ occurs in (5.4.4). Thus the appropriate boundary condition to impose is

$$\rho_\infty (\tilde{\nabla} \phi + \vec{V}_\infty) \cdot \hat{n} = 0 \tag{5.4.5}$$

or

$$\tilde{\nabla} \phi \cdot \hat{n} = -\vec{V}_\infty \cdot \hat{n} \tag{5.4.6}$$

The validity of (5.4.4) can be justified intuitively by recalling that the continuity equation (2.1.1), neglecting the unsteady flow term, is

$$\nabla \cdot (\rho \vec{V}) = 0 \tag{5.4.7}$$

while the Prandtl-Glauert equation

$$s \beta^2 \phi_{xx} + \phi_{yy} + \phi_{zz} = 0 \tag{5.4.8}$$

can be rewritten as

$$\nabla \cdot (\rho_\infty \vec{V}_\infty + \rho_\infty \tilde{\nabla} \phi) = 0 \tag{5.4.9}$$

since ρ_∞ is a constant and

$$\nabla \cdot \vec{V}_\infty = 0$$

So, we see that both the left and right hand sides of (5.4.4) are vector fields whose divergence is zero, that is, they are "conserved quantities."

The expression $(\rho/\rho_\infty) \vec{V}$ (also denoted $\vec{W}$) is called the mass flux, $\tilde{\nabla} \phi + \vec{V}_\infty$ is called the total linearized mass flux, and $\tilde{\nabla} \phi$ (also denoted $\vec{w}$) is called the linearized perturbation mass flux. We will not consider the non-linear mass flux in this section, and thus will drop the modifier "linearized." We will denote the perturbation and total mass flux by $\vec{w}$ and $\vec{W}$ respectively, and call $\vec{w} \cdot \hat{n}$ and $\vec{W} \cdot \hat{n}$ the perturbation and total normal mass flux. Note that as a consequence of the definition (5.2.25) of B_0 and (5.2.4) of $\tilde{\nabla}$ together with the fact the perturbation velocity $\vec{v}$ is given by $\nabla \phi$, we have, in reference coordinates,

$$\vec{w} = \tilde{\nabla} \phi = B_0 \nabla \phi = B_0 \vec{v} \tag{5.4.10}$$

Now, the combination of (5.4.3) and (5.4.4) indicates that to specify impermeability of a surface, we set total normal mass flux equal to zero. This can be done directly or indirectly, as illustrated by the following examples.

5.4.2.2 Thin Surfaces

In the case of the thin wing illustrated in figure 5.9, we clearly require both the upper and lower surfaces to be impermeable, and thus specify

$$\vec{w}_U \cdot \hat{n} = - \vec{V}_\infty \cdot \hat{n}$$
$$\vec{w}_L \cdot \hat{n} = - \vec{V}_\infty \cdot \hat{n} \qquad (5.4.11)$$

But recall from section 5.2 that

$$\sigma = \nabla (\phi_U - \phi_L) \cdot \tilde{n} = \nabla (\phi_U - \phi_L) \cdot [B_o] \hat{n} \qquad (5.4.12)$$

$$= \left\{\nabla (\phi_U - \phi_L)\right\}^T [B_o] \hat{n} = \left\{[B_o] \nabla (\phi_U - \phi_L)\right\}^T \hat{n} \qquad (5.4.13)$$

$$= \tilde{\nabla} (\phi_U - \phi_L) \cdot \hat{n} = \vec{w}_U \cdot \hat{n} - \vec{w}_L \cdot \hat{n} \qquad (5.4.14)$$

Note that these equations reveal

$$\tilde{n} \cdot \vec{v} = \hat{n} \cdot \vec{w} \qquad (5.4.15)$$

This relation will be used later. Combining (5.4.11) and (5.4.14) now yields

$$\sigma = 0 \qquad (5.4.16)$$

so that the thin wing boundary conditions (5.4.11) are equivalent to

$$\vec{w}_U \cdot \hat{n} = -\vec{V}_\infty \cdot \hat{n}$$
$$\sigma = 0 \qquad (5.4.17)$$

Note that we show a wake trailing behind the wing in figure 5.9. A wake is a surface across which a potential jump occurs, even though the surface does not correspond to a solid, physical object. Deciding where to position the wake for a particular configuration is an extremely difficult problem. For many problems, however, any wake position roughly parallel to the freestream and extending downstream from the object being analyzed is adequate. A detailed study of wake positioning is not part of this document.

5.4.2.3 Thick Configurations

For a "thick" wing, that is, a wing for which we panel both the upper and lower surfaces, we cannot simply impose the boundary conditions (5.4.17). This is because imposition of zero normal flow at all points on the interior of a closed surface is an ill-posed boundary value problem since there is no unique solution: if a particular function ϕ satisfies the Prandtl-Glauert equation and the boundary conditions, then adding any constant to ϕ in the interior of the closed surface yields another solution. We illustrate the two possible solutions in figure 5.10.

So, we must specify zero normal flow on the interior of a closed surface in some other manner. There are many possibilities, some of which are discussed in section 5 of the maintenance document. The method illustrated in figure 5.11 has been experimentally shown to be reliable in a wide variety of circumstances. There, the boundary condition $\phi_L = 0$ on the configuration surface ensures (assuming a sufficient density of control points) that ϕ is identically zero in the entire interior region. Such a condition is called "perturbation stagnation" (it is not really stagnation, since the total potential is not constant), since $\nabla \phi$, the perturbation velocity, is zero in the interior region.

Thus we impose the boundary conditions

$$\begin{aligned} \phi_L &= 0 \\ \vec{w}_U \cdot \hat{n} &= -\vec{V}_\infty \cdot \hat{n} \end{aligned} \tag{5.4.18}$$

But $\vec{w}_L = \tilde{\nabla} \phi_L = 0$, so we can replace $\vec{w}_U \cdot \hat{n}$ by $(\vec{w}_U - \vec{w}_L) \cdot \hat{n} = \sigma$, and thus we obtain

$$\begin{aligned} \phi_L &= 0 \\ \sigma &= -\vec{V}_\infty \cdot \hat{n} \end{aligned} \tag{5.4.19}$$

The boundary conditions (5.4.19) for a thick wing, or (5.4.17) for a thin wing are preferable to their equivalents (5.4.18) and (5.4.11) because they directly specify the source strength. This allows the source parameters to be removed from the system of linear equations, thus considerably lowering the cost of solving the equations.

5.4.2.4 Superinclined Surfaces

A final example of the imposition of boundary conditions is shown in figure 5.12. The surface shown perpendicular to the freestream is a superinclined surface; recall from section 5.2 that a surface is superinclined whenever

$$\hat{n} \cdot \tilde{n} < 0 \tag{5.4.20}$$

An important result, which we discuss further in Appendix B, is that boundary conditions of zero normal mass flux must never be placed on the upstream side of a superinclined surface, or else the boundary value problem is ill-posed. This is not really too surprising, since the flow about any impermeable object so blunt as to be superinclined certainly violates the "small perturbation" assumption.

The need for permeable superinclined surfaces does occur, however, nacelle faces being the prime example. The example in figure 5.12 shows the use of boundary conditions on the lower (that is, downstream) surface to induce perturbation stagnation in the interior of the configuration.

5.4.2.5 The General Boundary Condition

The previous three examples do not exhaust the generality of boundary conditions which a PAN AIR user may impose. But we must warn that, while an arbitrary condition on ϕ and its derivatives is permitted, the boundary condition may not yield a well-posed problem. The arbitrary boundary condition can be written

$$\begin{aligned} & a_A \vec{w}_A \cdot \hat{n} + c_A \phi_A + \vec{t}_A \cdot \vec{v}_A \\ & + a_D \sigma + c_D \mu + \vec{t}_D \cdot \nabla\mu = b \end{aligned} \tag{5.4.21}$$

where the subscripts A and D stand for "average" and "difference," that is,

$$\phi_A = \frac{1}{2} (\phi_U + \phi_L) \tag{5.4.22}$$

$$\phi_D = \phi_U - \phi_L = \mu \tag{5.4.23}$$

Comparing to equation (3.2.6), we see that the definition of doublet strength is the same for all Mach numbers. The constants a and c may be arbitrary, while the vectors $\vec{t}$ are tangent to the surface at the control point (as opposed to $\hat{n}$, which is normal to the surface).

To see that (5.4.21) permits an arbitrary combination of upper or lower surface conditions, we solve (5.4.22-23) for ϕ_U and ϕ_L, obtaining

$$\begin{aligned} \phi_U &= \phi_A + \frac{1}{2} \phi_D = \phi_A + \frac{1}{2} \mu \\ \phi_L &= \phi_A - \frac{1}{2} \mu \end{aligned} \tag{5.4.24}$$

Similarly,

$$\begin{aligned} \vec{w}_A \cdot \hat{n} &= \frac{1}{2} (\vec{w}_U \cdot \hat{n} + \vec{w}_L \cdot \hat{n}) \\ \sigma = \vec{w}_D \cdot \hat{n} &= \vec{w}_U \cdot \hat{n} - \vec{w}_L \cdot \hat{n} \end{aligned} \tag{5.4.25}$$

and, solving,

$$\begin{aligned} \vec{w}_U \cdot \hat{n} &= \vec{w}_A \cdot \hat{n} + \frac{1}{2} \sigma \\ \vec{w}_L \cdot \hat{n} &= \vec{w}_A \cdot \hat{n} - \frac{1}{2} \sigma \end{aligned} \tag{5.4.26}$$

Thus the boundary condition pair

$$\phi_L = 0$$
$$\vec{w}_U \cdot \hat{n} = - \vec{V}_\infty \cdot \hat{n} \tag{5.4.27}$$

can be written as

$$\phi_A - \frac{1}{2} \mu = 0$$
$$\vec{w}_A \cdot \hat{n} + \frac{1}{2} \sigma = -\vec{V}_\infty \cdot \hat{n} \tag{5.4.28}$$

Thus, the first equation in (5.4.28) is equivalent to (5.4.21) with

$$c_A = 1$$
$$c_D = - \frac{1}{2}$$
$$a_A = a_D = 0 \tag{5.4.29}$$
$$\vec{t}_A = \vec{t}_D = 0$$
$$b = 0$$

while the second equation corresponds to

$$c_A = c_D = 0$$
$$a_A = 1$$
$$a_D = \frac{1}{2}$$
$$\vec{t}_A = \vec{t}_D = 0 \tag{5.4.30}$$
$$b = -\vec{V}_\infty \cdot \hat{n}$$

For the remainder of this document, we will generally use the boundary condition formulation (5.4.21) since it is used internally in PAN AIR. It should be noted, however, that the program user need not be concerned with this formulation, but may express boundary conditions in the upper and lower form if he wishes. The average and difference formulation is used in PAN AIR in order to separate out the singularity strength (or difference) contribution to the boundary condition, which are computed from the splines. The difference potential and velocity are given in terms of the singularity distributions at a point by the formulae (cf. eqns. (5.4.23) and (B.3.29-31))

$$\phi_D = \mu \tag{5.4.31}$$

$$\vec{v}_D = [\sigma\hat{n} + (\hat{n} \times \nabla \mu) \times \vec{v}]/(\hat{n},\vec{v}) \tag{5.4.32}$$

The average potential and velocity at a point on the surface are given in terms of the complete singularity distribution functions by the formulae (cf. eqns. (5.2.8) and (B.3.28); we use the formula for the velocity field $\vec{v}(\vec{p})$ with the line vortex term removed),

$$\phi_A(\vec{p}) = (1/\kappa)\left[\iint_{S \cap D_p} [-\sigma/R + \mu\, \hat{n}.\, \tilde{\nabla}_q(1/R)]dS_q\right]_{avg} \tag{5.4.33}$$

$$\vec{v}_A(\vec{p}) = (1/\kappa)\left[\iint_{S \cap D_p} [\sigma\ \nabla_q\ (1/R) + (\hat{n} \times \nabla_q\ \mu) \times \tilde{\nabla}_q\ (1/R)]dS_q\right]_{avg} \tag{5.4.34}$$

Note that the subscript "avg" refers to the process of evaluating the average value of the given integral expression above and below the singularity surface S at the point $\vec{p}$. In appendices J.6, J.7 and J.8 it is shown that this average value calculation is a matter of concern only for the subpanel $Q \subset S$ that contains the point $\vec{p}$. For this case, it is shown in appendix J that the average value calculation is accomplished simply by using an average value of the panel integral J to evaluate the influence coefficient matrices [S] and [D] (cf. eqns. (J.6.152) and (J.6.164)). The surface average value calculation for the panel integral J is fully discussed near the end of appendix J.8.

There is one type of user-specified boundary condition, called a closure boundary condition, which is not of the form (5.4.21). This is used in design problems to specify the integral of the normal mass flux over a surface. A detailed description of the use and implementation of closure boundary conditions, discussed briefly in section (5.7.1), will be treated fully in Appendices H.2.5, K.1.3 and K.6.3.

5.5 Singularity Splines

In this section we will discuss without details the construction of spline matrices for analysis and wake networks. The technical details of the spline construction, and all discussion of splines for design networks, will be reserved for Appendix I. In figure 5.13, we illustrate the locations of source parameters on a source analysis network, and the locations of doublet parameters on a doublet analysis or wake network.

Source parameters on analysis networks are located at panel centers only. Doublet parameters on analysis networks are located at panel centers and in addition along network edges as illustrated. The value of a source parameter is always the value of source strength at the parameter location, and similarly for a doublet parameter. The "extra" doublet parameters occur at those points at which an "extra" corner control point was stationed because of edge matching considerations (see figure 5.7). Doublet parameters are required on network edges (while source parameters are not) because of the quadratic variation of the approximation to the doublet strength. A quadratic variation causes rapid changes in doublet strength which make extrapolation of the doublet values from the interior of the network to the edges ill-advised. The source strength approximation is only linear, however. Finally, doublet parameters are only located on the upstream edge of a wake network. The doublet strength on a wake network is defined to be constant in the streamwise direction, and thus doublet parameters are only required on one edge in order to define the doublet strength on the entire network.

5.5.1 The Matrices B^S and B^D

The outer spline matrices define the source strength and doublet strength at certain points on the panel as linear combinations of source and doublet parameters in the neighborhood of the panel. While a single doublet outer spline matrix has been found satisfactory for all purposes, it has been found that two source outer splines matrices are generally required. One of the source outer spline matrices helps define a continuous source distribution used in post processing applications, where it is essential for processing considerations that source strength be a uniquely defined function on a network (cf. sec. 5.5.3). The other source outer spline matrix helps define a discontinuous source distribution used in AIC matrix construction, where it is important that the total source strength on a network be accurately measured by the corresponding integral of the splined source distribution (cf. sec. 5.5.4).

To be precise, consider the panel and network in figure 5.14. A source outer spline matrix B^S is a 5 x 9 matrix which gives the value of source strength at P_1, P_2, P_3, P_4, and P_9 in terms of the source parameters $\{\lambda_i^S, i = 1,\ldots,9\}$ located at the nine panel centers marked by a circle. The matrix B^D is a 9 x 21 matrix giving the values of doublet strength at $P_1\ldots,P_9$ in terms of the doublet parameters $\{\lambda_i^D, i=1,\ldots,21\}$ located at the 21 panel centers marked by an x. Because μ is a continuous locally quadratic function whereas σ is only a locally linear function, μ must be defined at 9 points on a panel by B^D while σ is only defined by 5 points by B^D. The values of σ at the 5 points are called "panel source parameters," while the values of

μ at the 9 points are called "panel doublet parameters."

5.5.2 Definition of SPSPL

The subpanel spline matrices (one source matrix $SPSPL^S$ and one doublet matrix $SPSPL^D$ for each of the eight triangular regions composing the panel) each define the coefficients of the polynomial distribution of singularity strength on the triangular region as a linear combination of the singularity strengths at the panel points P_i mentioned above. Thus, on each triangular region, source and doublet strengths $\sigma(\xi', \eta')$ and $\mu(\xi', \eta')$ are defined in terms of local coordinates (ξ', η'). (Cf. eqn. (5.2.27) for the definition of the local coordinate transformation A. Note that the local coordinates ξ', η' used here include an origin shift as well; i.e. $\vec{\xi}' = A(\vec{x} - \vec{x}_0)$ where $\vec{x}_0$ is the triangle's origin.)

$$\begin{aligned}
\sigma(\xi', \eta') &= \sigma_0 + \sigma_\xi \xi' + \sigma_\eta \eta' \\
\mu(\xi', \eta') &= \mu_0 + \mu_\xi \xi' + \mu_\eta \eta' \\
&\quad + \frac{1}{2}\mu_{\xi\xi} \xi'^2 + \mu_{\xi\eta}\xi'\eta' + \frac{1}{2}\mu_{\eta\eta}\eta'^2
\end{aligned} \tag{5.5.1}$$

where the constants σ_0, σ , σ_η, $\mu_0, \ldots, \mu_{\eta\eta}$ are defined by the subpanel spline matrices:

$$\begin{Bmatrix} \sigma_0 \\ \sigma_\xi \\ \sigma_\eta \end{Bmatrix} = \left[SPSPL^S\right] \begin{Bmatrix} \sigma(P_1) \\ \sigma(P_2) \\ \sigma(P_3) \\ \sigma(P_4) \\ \sigma(P_9) \end{Bmatrix} \tag{5.5.2}$$

and

$$\begin{Bmatrix} \mu_0 \\ \mu_\xi \\ \vdots \\ \mu_{\eta\eta} \end{Bmatrix} = \left[SPSPL^D\right] \begin{Bmatrix} \mu(P_1) \\ \vdots \\ \mu(P_9) \end{Bmatrix} \tag{5.5.3}$$

5.5.3 Construction of B Matrices for Continuous Singularity Distributions

A B matrix associated with a continuous singularity distribution is constructed one row at a time. Each row defines the singularity strength at a panel corner, edge midpoint, or panel center in terms of surrounding singularity parameters. This identical row vector then becomes part of the B matrix of each panel which shares the particular grid point. This insures that the value of the singularity strength is identical as one approaches the grid point from the interior of any of the panels sharing it.

The source strength at a panel corner is obtained from the source singularity parameters located at the centers of the four panels sharing that corner, as illustrated in figure 5.15. The dependence of σ_1 on $\lambda_1, \ldots \lambda_4$ is

determined by a bilinear fit procedure described in Appendix I.1. Essentially, this procedure determines what "bilinear" function (a bilinear function in two variables (ξ,η) is a quadratic function which reduces to a linear function for constant ξ or η)

$$f(\xi, \eta) = a + b\xi + c\eta + d\xi\eta \tag{5.5.4}$$

is determined by the four values λ_i^S, and then sets σ_1 to be the "value" the function takes at that point. By "value", we mean a row vector (a_1,a_2,a_3,a_4) such that

$$\sigma_1 = \llcorner a_1 \; a_2 \; a_3 \; a_4 \lrcorner \begin{Bmatrix} \lambda_1^S \\ \lambda_2^S \\ \lambda_3^S \\ \lambda_4^S \end{Bmatrix} \tag{5.5.5}$$

regardless of the values of the λ_i^S's.

Now, finding the row vector that describes the source strength at a panel center is very simple, since a source parameter is located there. To obtain a matrix B^S for a panel, we assemble the row vectors corresponding to the 5 grid points. Each row vector has length 4, but by adding zeros each row vector expands to length 9. Thus each row vector has one entry from each of the 9 source parameters in the neighborhood of the panel. While only four parameters lie in the neighborhood of a particular corner point, (cf. figure 5.14) nine parameters lie in the neighborhood of at least one of the panel corners. Collecting the five row vectors, we have the 5 x 9 matrix B^S, which was first introduced by equation (4.2.8).

Thus, for the panel in figure 5.14, B^S has the structure

$$B^S = \begin{bmatrix} 0 & * & * & 0 & * & * & 0 & 0 & 0 \\ * & * & 0 & * & * & 0 & 0 & 0 & 0 \\ 0 & 0 & 0 & * & * & 0 & * & * & 0 \\ 0 & 0 & 0 & 0 & * & * & 0 & * & * \\ 0 & 0 & 0 & 0 & * & 0 & 0 & 0 & 0 \end{bmatrix} \tag{5.5.6}$$

where the columns of B^S are arranged according to the integer labels given to the source parameters in figure 5.14. Here, an asterisk denotes some generally non-zero entry.

The outer doublet spline matrix B^D, introduced in equation (4.2.9), is similarly constructed row by row. To obtain the row vector describing μ at a panel corner, a least squares fit is used. As shown in figure 5.16, $\mu(P)$ is obtained by finding the quadratic function $\mu(\xi,\eta)$ which best goes through the 12 values λ_i^D at the 12 doublet parameter locations in the neighborhood of P in a weighted least squares sense (a quadratic function in two variables certainly can not go through 12 values exactly). The computation of the weights is discussed in Appendix I.1.2.4. The quadratic function thus obtained (its 6 coefficients are each row vectors of length 12, since they depend on the λ_i^D) is evaluated at P to obtain $\mu(P)$. This weighted least squares procedure will be described in detail in Appendix I.5.

To obtain a row vector defining μ at a panel edge midpoint, we again use a weighted least squares fit, though this time we only fit to 8 neighboring singularity parameters, as illustrated in figure 5.17. If the grid point lies near the network edge, a special treatment (which is described in Appendix I.1) is used.

5.5.4 Construction of the Discontinuous Source Outer Spline Matrix

The discontinuous source outer spline matrix (cf. appendix I.1.15), is constructed by means of a two stage process. First, a linear source distribution over the whole panel is determined in terms of the panel's neighboring source parameters λ_i^S , $i = 1,\ldots,9$ by means of a weighted least squares procedure. Second, this distribution is evaluated at the five points P_1, P_2, P_3, P_4, P_9 to give the dependency of the five "panel source parameters" upon the neighboring source parameters λ_i^S.

It is the first step of this process that ensures that total source strength is accurately measured. This accuracy is achieved by the combination of the linear fit and the fact that the panel's own source parameter is heavily weighted in the least squares fitting procedure.

It is appropriate to observe here that although the discontinuous source outer spline is not explicitly constrained to be continuous, it is in fact very nearly continuous wherever the configuration is sufficiently finely panelled that the angle between adjacent panel normals is less than, say, 10°.

5.5.5 Construction of SPSPL

Next, let us consider the method by which the subpanel spline matrices use the panel singularity values ($\sigma_1 \ldots \sigma_4$, σ_9, $\mu_1 \ldots \mu_9$) to define singularity distributions within a panel. In referring to the panel illustrated in figure 5.18, we will write σ_i for $\sigma(P_i)$ and μ_i for $\mu(P_i)$.

Recall that σ_1, σ_2, σ_3, σ_4 and σ_9 are defined in terms of neighboring source singularity parameters by the matrix B^S. We then define

$$\sigma_5 = \frac{1}{2}(\sigma_1 + \sigma_2) \quad , \sigma_6 = \frac{1}{2}(\sigma_2 + \sigma_3), \ \sigma_7 = \frac{1}{2}(\sigma_3 + \sigma_4), \text{ and } \sigma_8 = \frac{1}{2}(\sigma_4 + \sigma_1) \quad .$$

We have now defined σ_i at all vertices of all 8 triangular regions, and we now define a linear distribution $\sigma(\xi', \eta')_i$, $i = 1,\ldots,8$ on each triangular region by specifying it to be the unique linear distribution to attain the appropriate values at the 3 vertices of the triangle.

Note that this construction forces σ to vary linearly along the edge of a triangular region, and thus the value of σ at any point along the edge is determined by the values of σ at the two endpoints of the edge. Thus σ is continuous within the panel. Further, since σ at a panel edge midpoint M is the average of the values at the adjacent corners, σ varies as a single linear function on an entire panel edge. Thus σ on a panel edge is determined by its values at the two endpoints, and so, within a network, σ is continuous across panel edges, as long as the continuous source spline is being used. At network edges, σ is not continuous across the network edge.

To determine the doublet distribution on each of the 8 regions, we note first that a quadratic distribution on a triangular region is uniquely defined by its value at the three vertices and the three edge midpoints of the triangle. Thus the doublet distribution on each triangle is determined once we know μ at $P_1,\ldots, P_9$, and $M_1,\ldots, M_{16}$. Now μ at $P_1,\ldots, P_9$ is defined by B^D . We define μ at $M_1,\ldots, M_8$, and $M_{13},\ldots, M_{16}$ by requiring that μ be described by a single quadratic function in one variable on the line segments $P_1P_5P_2$, $P_2P_6P_3$, $P_3P_7P_4$, $P_4P_8P_1$, $P_5P_9P_7$, and $P_6P_9P_8$. Note that a quadratic function on a line is uniquely determined by its values at 3 distinct points. Finally, μ is defined at M_9, M_{10}, M_{11}, M_{12} in such a manner as to minimize the discontinuities in doublet gradient at P_5, P_6, P_7, P_8.

By defining μ at M_i, $i = 1,\ldots, 16$, in this manner, we insure that, within a network, the doublet strength is continuous across triangle boundaries. (Doublet strength matching at network edges is discussed in section 5.3.) In addition, the doublet gradient is continuous at P_9. Also, the doublet strength is continuous across panel edges because the values of μ at the endpoints and midpoints of an edge define the value on the whole segment.

Summarizing, for each triangular region we obtain subpanel spline matrices $SPSPL^S$ and $SPSPL^D$ such that

$$\begin{Bmatrix} \sigma_0 \\ \sigma_\xi \\ \sigma_\eta \end{Bmatrix} = [SPSPL^S] \begin{Bmatrix} \sigma_1 \\ \vdots \\ \sigma_4 \\ \sigma_9 \end{Bmatrix} \tag{5.5.7a}$$

$$\begin{Bmatrix} \mu_o \\ \cdot \\ \cdot \\ \cdot \\ \mu_{\eta\eta} \end{Bmatrix} = [SPSPL^D] \begin{Bmatrix} \mu_1 \\ \cdot \\ \cdot \\ \cdot \\ \mu_9 \end{Bmatrix} \tag{5.5.7b}$$

Furthermore, we have already discussed the construction of outer spline matrices B^S and B^D such that

$$\begin{Bmatrix} \sigma_1 \\ \cdot \\ \cdot \\ \cdot \\ \sigma_4 \\ \sigma_9 \end{Bmatrix} = [B^S] \begin{Bmatrix} \lambda_1^S \\ \cdot \\ \cdot \\ \cdot \\ \lambda_9^S \end{Bmatrix} \tag{5.5.8a}$$

and

$$\begin{Bmatrix} \mu_1 \\ \cdot \\ \cdot \\ \cdot \\ \mu_9 \end{Bmatrix} = [B^D] \begin{Bmatrix} \lambda_1^D \\ \cdot \\ \cdot \\ \cdot \\ \lambda_{21}^D \end{Bmatrix} \tag{5.5.8b}$$

Combining (5.5.7) and (5.5.8), we obtain the source and doublet distributions on a triangular region, in terms of source and doublet parameters, by

$$\begin{Bmatrix} \sigma_o \\ \sigma_\xi \\ \sigma_\eta \end{Bmatrix} = [SPSPL^S]\,[B^S] \begin{Bmatrix} \lambda_1^S \\ \cdot \\ \cdot \\ \cdot \\ \lambda_9^S \end{Bmatrix} \tag{5.5.9a}$$

$$\begin{Bmatrix} \mu_o \\ \cdot \\ \cdot \\ \cdot \\ \mu_{\eta\eta} \end{Bmatrix} = [SPSPL^D]\,[B^D] \begin{Bmatrix} \lambda_1^D \\ \cdot \\ \cdot \\ \cdot \\ \lambda_{21}^D \end{Bmatrix} \tag{5.5.9b}$$

5.6 Influence Coefficients

In order to impose the arbitrary boundary condition given by equation (5.4.21), viz.,

$$a_A \vec{w}_A \cdot \hat{n} + c_A \phi_A + \vec{t}_A \cdot \vec{v}_A + a_D \sigma + c_D \mu + \vec{t}_D \cdot \nabla\mu = b \tag{5.6.1}$$

at a control point, it is necessary to evaluate the left hand side expression as a linear combination of the singularity parameters $\{\lambda_i\}$. To evaluate σ and μ at the control point, we use the subpanel spline and outer spline matrices. For example, if a control point P has local coordinates (ξ', η'), we find, using equations (5.5.1), (5.5.7) and (5.5.8),

$$\sigma(P) = \lfloor 1 \quad \xi' \quad \eta' \rfloor \; [SPSPL^S] \; [B^S] \begin{Bmatrix} \lambda_1^S \\ \cdot \\ \cdot \\ \cdot \\ \lambda_9^S \end{Bmatrix} \tag{5.6.2}$$

and thus the row vector describing $\sigma(P)$ in terms of all the λ_i^S is the expansion of the 1x9 matrix

$$\lfloor 1 \quad \xi' \quad \eta' \rfloor \; [SPSPL^S] \; [B^S]$$

into the corresponding 1xN matrix (where all but 9 values are zero), with an entry for each of the N singularity parameters in the entire configuration. We obtain the row vector describing $\mu(P)$ similarly.

5.6.1 Computation of Potential and Velocity

Next we wish to evaluate ϕ_A and $\vec{v}_A$ at a control point, as a linear combination of all the singularity parameters in the configuration. The row vectors which describe these quantities at a control point are called the potential influence coefficient and velocity influence coefficient matrices, or ϕIC and VIC respectively. The matrices ϕIC and VIC should not be confused with the panel influence coefficient (PIC) matrices, introduced in section 4.2.2, which define the perturbation potential and velocity induced by a panel on a control point. The ϕIC matrix is evaluated by using the basic representation formula, equation (5.2.8)

$$\phi(x,y,z) = -\frac{1}{\kappa} \iint_{S'} \frac{\sigma(Q)}{R} \, dS + \frac{1}{\kappa} \iint_{S'} \mu(Q) \, \hat{n} \cdot \tilde{\nabla}_Q\left(\frac{1}{R}\right) \, dS \tag{5.6.3}$$

(where $S' = S \cap D_P$ is the intersection of the domain of dependence of P with the surface of integration S) while the VIC matrix is calculated using the gradient of equation (5.2.8),

$$\vec{v}(x,y,z) = -\frac{1}{\kappa}\nabla_P \iint_{S'} \frac{\sigma(Q)}{R}\, dS$$

$$+\frac{1}{\kappa}\nabla_P \iint_{S'} \mu(Q)\, \hat{n} \cdot \tilde{\nabla}_Q\left(\frac{1}{R}\right) dS \tag{5.6.4}$$

where $P' = (x,y,z)$, $Q = (\xi,\eta,\zeta)$ is a point on S,

$$\tilde{\nabla}_Q = \begin{Bmatrix} s\beta^2 \;\; \partial/\partial\xi \\ \partial/\partial\eta \\ \partial/\partial\zeta \end{Bmatrix} \qquad \nabla_P = \begin{Bmatrix} \partial/\partial x \\ \partial/\partial y \\ \partial/\partial z \end{Bmatrix} \tag{5.6.5}$$

and

$$R^2 = (\xi - x)^2 + s\,\beta^2\,(\eta - y)^2 + s\beta^2\,(\xi - z)^2 \tag{5.6.6}$$

We perform the integration one triangular region at a time; thus, denoting a subpanel by Δ, with local coordinates (ξ', η'), we have

$$\phi(x,y,z) = \sum_{\Delta} \left\{ -\frac{1}{\kappa} \iint_{\Delta \cap D_P} \frac{\sigma(\xi', \eta')}{R}\, dS\, (\vec{q}(\xi', \eta')) \right.$$

$$\left. +\frac{1}{\kappa} \iint_{\Delta \cap D_P} \mu(\xi', \eta')\; \hat{n} \cdot \tilde{\nabla}_Q\left(\frac{1}{R}\right) dS\, (\vec{q}(\xi', \eta')) \right\} \tag{5.6.7}$$

and a corresponding expression for $\vec{v}(x,y,z)$. Here we substitute for the exact (and unknown) values of σ the row vector in (5.6.2) and a similar row vector for μ.

In practice, the sum over triangular regions is taken as a sum over all panels, and the integral over a panel is taken as a sum of integrals over the 8 triangular regions in the panel. The integral over a single panel describes the perturbation potential and velocity induced at the control point (which does not necessarily lie near the panel) by the panel. Since the singularity distribution on the panel depends on the 5 panel source parameters and the 9 panel doublet parameters, the perturbation potential and velocity induced by the panel can be defined by two "panel influence coefficient" (PIC) matrices, one a 4x5 source matrix, PIC^S, the other a 4x9 doublet matrix PIC^D.

That is,

$$\begin{Bmatrix} \phi(x,y,z) \\ \partial\phi/\partial x(x,y,z) \\ \partial\phi/\partial y(x,y,z) \\ \partial\phi/\partial z(x,y,z) \end{Bmatrix} = [PIC^S] \begin{Bmatrix} \sigma_1 \\ \vdots \\ \sigma_4 \\ \sigma_9 \end{Bmatrix} + [PIC^D] \begin{Bmatrix} \mu_1 \\ \vdots \\ \mu_9 \end{Bmatrix} \tag{5.6.8}$$

Substitution of (5.6.2) into (5.6.7) shows that

$$PIC^S = \sum_{\substack{8 \text{ sub-} \\ \text{panels}}} -\frac{1}{\kappa} \iint_{\Delta_i \cap D_p} \begin{Bmatrix} 1/R \\ \partial/\partial x(1/R) \\ \partial/\partial y(1/R) \\ \partial/\partial z(1/R) \end{Bmatrix}^{4x1} \lfloor 1 \ \xi' \ \eta' \rfloor^{1x3} [SPSPL_i^S]^{3x5} \, dS \tag{5.6.9}$$

Similarly,

$$PIC^D = \sum_{i=1}^{8} \frac{1}{\kappa} \iint_{\Delta_i \cap D_p} \begin{Bmatrix} \hat{n} \cdot \nabla_Q (1/R) \\ \partial/\partial x \ \hat{n} \cdot \nabla_Q (1/R) \\ \partial/\partial y \ \hat{n} \cdot \nabla_Q (1/R) \\ \partial/\partial z \ \hat{n} \cdot \nabla_Q (1/R) \end{Bmatrix}^{4x1} \tag{5.6.10}$$

$$\lfloor 1 \quad \xi' \quad \eta' \quad \frac{1}{2}\xi'^2 \quad \xi'\eta' \quad \frac{1}{2}\eta'^2 \rfloor^{1x6} \quad [SPSPL^D]^{6x9} \quad dS$$

5.6.2 Reformulation of the Doublet Velocity Integral

In Appendix J, we describe the method by which we calculate the matrix PIC^S. The integral PIC^D, however, is evaluated by making use of the continuity of μ. We show in Appendix B.3 that the velocity due to the doublet can be written as

$$\vec{v}(P) = \frac{1}{\kappa} \nabla_P \iint_{S \cap D_p} \mu(Q) \, \hat{n} \cdot \tilde{\nabla}_Q \frac{1}{R} \, dS$$

$$= \frac{1}{\kappa} \iint_{S \cap D_p} (\hat{n} \times \nabla_Q \mu) \times (\tilde{\nabla} \frac{1}{R}) \, dS + \frac{1}{\kappa} \int_{\partial S \cap D_p} \mu \ \tilde{\nabla}_Q \frac{1}{R} \times d\vec{l} \tag{5.6.11}$$

Here, ∂S is the boundary of the surface S. The first integral is called the regular part of the doublet velocity, and the second integral is called the line vortex part. Now, in general, $\mu = 0$ on the boundary of an isolated network edge because the doublet matching boundary conditions in PAN AIR force this to be the case. Further, where two networks meet along a common line,

the doublet strengths in PAN AIR are made equal; thus, if the integration is performed one network at a time, the integral of the line vortex term over the edge of the first network cancels with the corresponding integral over the edge of the second network (see figure 5.19). The integrals similarly cancel when three or more networks meet because of the doublet matching boundary conditions which are imposed (see Appendices B.3, F and K).

Similarly, when we divide S up into subpanels (triangular regions), the line vortex integrals cancel on the subpanel boundaries because the doublet strength is continuous. Thus every contribution to the second integral in (5.6.11) is cancelled by an equal and opposite contribution, provided μ is everywhere continuous. So, if μ is continuous, we see that the doublet velocity may be defined by an integral in the quantity $\hat{n} \times \nabla\mu$, which is generally known as the surface vorticity. For a discussion of surface vorticity, see section 2.8 of Ward.

The assumption that μ is continuous everywhere is in fact violated in only one instance in PAN AIR, namely, on the trailing edge of a wake. The doublet strength there is non-zero, but this edge is so far from the control points at which boundary conditions are imposed that neglect of the line vortex term for this edge results in a negligible error.

There are two reasons for evaluating the regular part of (5.6.11) rather than the complete integral. First, if the boundary of a subpanel (triangular) region of integration contains points $Q = (\xi', \eta', \zeta')$ for which $R = 0$, the line vortex term may be infinite (especially in supersonic flow), where this infinite quantity is cancelled out by an identical infinite integral in the opposite direction. This is unacceptable in a numerical method; even if infinite quantities are avoided, the cancellation of large numbers of opposite sign tends to be inexact, and the final answer may lose many digits of accuracy. In evaluating the regular part of the integral, however, large numbers are generated, with a few exceptions, only when the final answers are large. The singular behavior of these integrals will be discussed further in Appendix J.11.

5.6.3 The Far Field Expansion

The second reason for evaluating only the regular integral is efficiency. When R is small compared to panel size, the integral in (5.6.11) must be evaluated exactly in terms of transcendental functions (logarithms and arc tangents) whose arguments are complicated expressions depending on the geometric relationship of the control point and the panel. To evaluate the first form of equation (5.6.11), that is, the complete integral, requires the computation of a greater number of these expressions than is required by the regular part of (5.6.11), and thus takes longer. Further, if R is large compared to panel size, the integrand can be replaced by a power series in

$$\Delta\vec{Q} = \vec{Q} - \vec{Q}_0 = (\xi' - \xi_0', \eta' - \eta_0', \zeta' - \zeta_0') \qquad (5.6.12)$$

where $\vec{Q}_0 = (\xi_0', \eta_0', \zeta_0')$ is the panel center. This power series has coefficients which only depend on $\vec{Q}_0$ and the control point P, while the terms of the power

series only depend on the panel. Then (see Appendix J.9 for details) the coefficients can be taken out from under the integral, while the integral itself now depends only on the panel and thus need only be evaluated once in the course of the problem, rather than once for every pair of panel and control point. The approximation of the integrand by a power series in $\Delta\vec{Q}$ is called a far field expansion.

Now, applying a gradient operator to 1/R yields with a factor of R^{-3}, and applying a gradient operator to those terms yields terms with the factor R^{-5}. Thus the left hand expansion in (5.6.11) contains terms with R^{-5}, while the regular part only contains terms with R^{-3}. Now, for a fixed value of R, R^{-3} is more accurately expressible as a power series in ΔQ of fixed length than R^{-5} (see below for a justification), and so a far field expansion can be used for smaller values of R if only the regular part of (5.6.11) is evaluated. This is important since the far field expansion is considerably less time-consuming than the exact evaluation of the integral. In practice, PAN AIR will use the far field expansion if R is large compared to the panel diameter for all points Q on the panel. For details, see appendix J.2.

To justify these remarks about accuracy, consider a quantity $\varepsilon \ll 1$. By the binomial theorem

$$(1+\varepsilon)^r = 1 + r\varepsilon + \frac{r(r-1)}{2}\varepsilon^2 + \ldots$$

$$= 1 + \sum_{i=1}^{\infty} \frac{r(r-1)\ldots(r-i)}{(i+1)!} \varepsilon^{i+1} \tag{5.6.13}$$

That is, taking $r = -\frac{3}{2}$ and then $r = -\frac{5}{2}$,

$$(1+\varepsilon)^{-3/2} = 1 - \frac{3}{2}\varepsilon + \frac{15}{8}\varepsilon^2 - \frac{135}{48}\varepsilon^3 + \ldots$$

$$(1+\varepsilon)^{-5/2} = 1 - \frac{5}{2}\varepsilon + \frac{35}{8}\varepsilon^2 - \frac{315}{48}\varepsilon^2 + \ldots \tag{5.6.14}$$

So if we want to approximate $(1+\varepsilon)^{-5/2}$ by a power series with 3 terms (that is, a quadratic expression), the first neglected term has a coefficient of 315/48, which is more than twice the size of the first neglected coefficient if we approximate $(1+\varepsilon)^{-3/2}$. Thus, for a particular value of ε our quadratic approximation to $(1+\varepsilon)^{-3/2}$ is better than our quadratic approximation to $(1+\varepsilon)^{-5/2}$.

5.7 The Aerodynamic Influence Coefficient Matrix

Once the 1xN matrix ØIC and the 3xN matrix VIC (N the total number of singularity parameters in the configuration) have been computed for a control point, it is quite straightforward to impose the boundary condition (5.6.1). The left hand side of (5.6.1) then gives a row of the [AIC] matrix (see equations (4.2.4) and (3.3.8))

$$a_A \{\hat{n}\}^{T\,1x3} [VIC(P)]^{3xN} + c_A \lfloor \Phi IC(P) \rfloor^{1xN} + \{\vec{t}_A\}^{T\,1x3} [VIC(P)]^{3xN}$$

$$+ a_D \lfloor 1 \quad \xi' \quad \eta' \rfloor^{1x3} [SPSPL^S]^{3x5} [B^S]^{5xN}$$

$$+ c_D \lfloor 1 \quad \xi' \quad \eta' \quad \tfrac{1}{2}\xi'^2 \quad \xi'\eta' \quad \tfrac{1}{2}\eta'^2 \rfloor^{1x6} [SPSPL^D]^{6x9} [B^D]^{9xN}$$

$$+ \{\vec{t}_D\}^{T\,1x3} [A^T]^{3x3} \begin{bmatrix} 0 & 1 & 0 & \xi' & \eta' & 0 \\ 0 & 0 & 1 & 0 & \xi' & \eta' \\ 0 & 0 & 0 & 0 & 0 & 0 \end{bmatrix}^{3x6} [SPSPL^D]^{6x9} [B^D]^{9xN} \qquad (5.7.1)$$

In arriving at this result, equation (5.6.2) was used for σ (a similar equation for μ), and we have used the fact that $\tilde{n}.\vec{v}=\hat{n}.\vec{w}$ (see equation (5.4.15)). The control point P has local coordinates (ξ', η'), A is the transformation from reference to local coordinates and B^S and B^D are the outer spline matrices, the overbar signifying that they have been expanded to N columns, with one column of zeros for every singularity parameter on which the panel source or doublet distribution does not depend. We will show in Appendix K that the last term of (5.7.1) is equivalent to $\vec{t}_D \cdot \nabla\mu$; the remaining terms have been discussed previously. Thus, a row of the AIC matrix (corresponding to a boundary condition) can be generated in a completely straightforward manner. Several considerations make the process somewhat less straightforward, however. These are: imposition of boundary conditions which are not of the form (5.6.1), utilization of the existence of one or two planes of configuration symmetry in order to reduce the size of the problem, and elimination of singularity parameters whose values are directly specified by a boundary condition ("known" singularity parameters) from the system of equations.

5.7.1 Non-Standard Boundary Conditions

There are two types of boundary conditions which are not of the form (5.6.1). The first type is a matching boundary condition (see section 5.3, or Appendices K.1.2, K.6.2 for full details). The second type is a closure boundary condition, described in full detail in Appendices K.1.3, K.6.3. To understand how a closure condition arises, observe that a program user may specify a desired pressure distribution on a design network by imposing boundary conditions of the form

$$\vec{t}_U \cdot \vec{v}_U + \vec{t}_L \cdot \vec{v}_L = b \qquad (5.7.2)$$

at panel center control points. When a tangential component of the flow is thus specified over a surface, there are no boundary conditions remaining at panel centers to also require that the normal flow to the surface be zero; but the boundary conditions at a network edge may not yet have been used. At these control points one may specify

$$\iint_{\substack{\text{column or}\\ \text{row of panels}}} \left[a_U \vec{w}_U \cdot \hat{n} + a_L \vec{w}_L \cdot \hat{n} \right] dS = b \qquad (5.7.3)$$

For $a_L = 0 = b$, for instance, equation (5.7.3) requires that the integral of the normal flow over a column (or row) of panels be zero. When the program user then updates the network geometry to approximately impose impermeability of the surface, the position of the trailing edge of the network will not be changed.

This alternate iteration of a potential flow solution with an update of the surface geometry is a method of solving the design problem, in which a user wishes to obtain an impermeable surface with a specified pressure distribution. The closure boundary condition is used, for example, in designing a thick wing, in order to ensure that the trailing edge of the wing remain closed. The design problem is discussed further in Appendix C. The implementation of eqn. (5.7.3) is discussed in appendix (K.1.3) where it is shown how the integral is approximated as a weighted sum over panel centers in a column or row of panels.

5.7.2 Symmetry

While we defer to the appendices all of the detailed technical details associated with the treatment of symmetry, we will describe here at a fairly cursory level how PAN AIR takes advantage of configuration symmetry to reduce the cost of solving the potential flow problem. (For greater detail see especially appendix K and also appendices F.5 and H.)

In the discussion that follows, we will treat in detail the case of a configuration having one plane of configuration symmetry as illustrated in figure 5.20. That part of the configuration surface lying to the right of the plane of symmetry is denoted S^+, its image on the left is denoted S^- and the part of the configuration surface lying on the plane of symmetry P_1 is denoted S_1. The combined surface $S^+ \cup S_1$, which is the geometry input by the user, is called the principal image of the configuration. To simplify the discussion we will further assume the following:

(i) The compressibility axis is aligned with the x-axis of the reference coordinate system.

(ii) The single plane of symmetry coincides with the x-z plane, $\{\vec{p} \mid y = 0\}$

As a consequence of these assumptions the normal to the plane of symmetry is given by $\hat{n}_1^T = (0, 1, 0)$. Further, for any point $\vec{p}^{\,+} \in S^+$, the corresponding point $\vec{p}^{\,-} \in S^-$, the image of S^+, is given by

$$\vec{p}^{-} = [I - 2\hat{n}_1 \hat{n}_1^T]\, \vec{p}^{+} = R_1 \vec{p}^{+} = \begin{bmatrix} 1 & & \\ & -1 & \\ & & 1 \end{bmatrix} \vec{p}^{+} \tag{5.7.4}$$

Notice that we have implicitly given here the definition of R_1, the reflection matrix associated with the plane of symmetry P_1.

Having defined this much of the terminology of symmetry, we can now state the basic principal that motivates our treatment of symmetry. In PAN AIR, symmetry is handled by setting up <u>separate integral equations</u> for the symmetric and antisymmetric parts of ϕ, defined by

$$\begin{aligned} \hat{\phi}^{+}(p) = \hat{\phi}^{S}(p) &= \text{symmetric part of } \phi \\ &= \phi(\vec{p}) + \phi(R_1\vec{p}) \end{aligned} \tag{5.7.5a}$$

$$\begin{aligned} \hat{\phi}^{-}(p) = \hat{\phi}^{A}(p) &= \text{antisymmetric part of } \phi \\ &= \phi(\vec{p}) - \phi(R_1\vec{p}) \end{aligned} \tag{5.7.5b}$$

The integral equations that we obtain for $\hat{\phi}^S$ and $\hat{\phi}^A$ involve only integrals over the principal image of the configuration, $S^{+} \cup S_1$. Thus, each integral equation, when discretized, leads to an AIC equation that is (approximately) half the dimension of an AIC equation for the whole configuration. Since the cost of solving a large, dense AIC equation increases as the cube of its dimension, we find -

$$\begin{aligned} \text{cost of solving 2 AIC equations of size } N/2 &= 2[K(N/2)^3] \\ &= K[N^3/4] \end{aligned}$$

$$\text{cost of solving 1 AIC equation of size } N = KN^3$$

so that symmetry permits us to reduce by a factor of 4 the cost of AIC solution. Further, (and this is actually more significant), symmetry also allows us to reduce by a factor of two the cost of AIC generation. This last fact follows from the observation that of the four influence coefficients defined by:

$$\Phi_I^{Q^+}(\vec{p}) = \Phi_\sigma^{Q^+}(\vec{p}, s_I) + \Phi_\mu^{Q^+}(\vec{p}, m_I)$$

= potential induced at $\vec{p}$ due to the source distribution s_I and the doublet distribution m_I restricted to panel $Q^+ \subset S^+$

$$\Phi_I^{Q^+}(R_1\vec{p})$$

$$\Phi_I^{Q^-}(\vec{p}) \qquad Q^- = \text{image of } Q^+ = \{\vec{q}^- \mid \vec{q}^- = R_1\,\vec{q}^+,\ \vec{q}^+ \in Q^+\}$$

$$\Phi_I^{Q^-}(R_1\vec{p})$$

only the first two need to be computed since

$$\Phi_I^{Q^-}(\vec{p}) = \Phi_I^{Q^+}(R_1\,\vec{p})$$

$$\Phi_I^{Q^-}(R_1\,\vec{p}) = \Phi_I^{Q^+}(\vec{p})$$

We now show how PAN AIR combines the boundary conditions at control points $\vec{p}^+ \in S^+$ and $\vec{p}^-(= R_1\,\vec{p}^+ \in S^-)$ to obtain a boundary condition for each of $\hat{\phi}^S$ and $\hat{\phi}^A$ imposed at $\vec{p}^+$. (See below for the discussion of control points $\vec{p} \in S_1$.)

First we note that corresponding boundary conditions at points $\vec{p}$ and $R_1\vec{p}$ are required by PAN AIR to be connected to one another as follows. (Compare these forms with equation (5.4.21))

$$\vec{p}\ :\quad a_A\,\hat{n}^T(\vec{p})\,B(\vec{v}(\vec{p}))_A + c_A(\phi(\vec{p}))_A + \vec{t}_A^T(v(\vec{p}))_A + a_D\,\sigma(\vec{p}) + c_D\,\mu(\vec{p}) + \vec{t}_D^T\,\nabla\mu(\vec{p}) = b^+ \tag{5.7.6a}$$

$$R_1\vec{p}\ :\quad a_A\,\hat{n}^T(\vec{p})\,R_1\,B(\vec{v}(R_1\vec{p}))_A + c_A(\phi(R_1\vec{p}))_A + \vec{t}_A^T\,R_1(\vec{v}(R_1\vec{p}))_A + a_D\,\sigma(R_1\vec{p}) + c_D\,\mu(R_1\vec{p}) + \vec{t}_D^T\,R_1\,\nabla\mu(R_1\vec{p}) = b^- \tag{5.7.6b}$$

Adding and subtracting these equations while taking account of the following definitions

$$\hat{v}^+(\vec{p}) = \hat{v}^S(\vec{p}) = \vec{v}(\vec{p}) + R_1\,\vec{v}(R_1\vec{p}) \tag{5.7.7a}$$

$$\hat{v}^-(\vec{p}) = \hat{v}^A(\vec{p}) = \vec{v}(\vec{p}) - R_1\,\vec{v}(R_1\vec{p}) \tag{5.7.7b}$$

$$\hat{\sigma}^S(\vec{p}) = \sigma(\vec{p}) + \sigma(R_1\vec{p}) \tag{5.7.8a}$$

$$\hat{\sigma}^A(p) = \sigma(\vec{p}) - \sigma(R_1\vec{p}) \tag{5.7.8b}$$

$$\hat{\mu}^S(\vec{p}) = \mu\ (\vec{p}) + \mu(R_1\vec{p}) \tag{5.7.8c}$$

$$\hat{\mu}^A(\vec{p}) = \mu\ (\vec{p}) + \mu(R_1\vec{p}) \tag{5.7.8d}$$

we obtain after some manipulation

$$\begin{aligned} & a_A\ \hat{n}^T(\vec{p})\ (\hat{v}^S(\vec{p}))_A + c_A(\hat{\phi}^S(\vec{p}))_A + \vec{t}_A^T\ (\hat{v}^S(\vec{p}))_A \\ & + a_D\ \hat{\sigma}^S(\vec{p}) + c_D\ \hat{\mu}^S(p) + \vec{t}_D^T\ \ \nabla\hat{\mu}^S \qquad = b^+ + \bar{b} \end{aligned} \tag{5.7.9a}$$

$$\begin{aligned} & a_A\ \hat{n}^T(\vec{p})\ (\hat{v}^A(\vec{p}))_A + c_A(\hat{\phi}^A(\vec{p}))_A + \vec{t}_A^T\ (\hat{v}^A(\vec{p}))_A \\ & + a_D\ \hat{\sigma}^A(\vec{p}) + c_D\ \hat{\mu}^A(\vec{p}) + \vec{t}_D^T\ \ \nabla\hat{\mu}^A \qquad = b^+ - \bar{b} \end{aligned} \tag{5.7.9b}$$

Now it can be shown that the fundamental representation formulas (5.6.3-4) for ϕ and $\vec{v}$ induce similar representation formulas for $\hat{\phi}^i$ and $\hat{v}^i$ (see equations (K.3.28) and (K.3.46)) having the following properties:

(i) the integrals extend only over the principal image $S^+ \cup S_1$,

(ii) $\hat{\phi}^i$ and $\hat{v}^i$ depend only upon $\hat{\sigma}^i$ and $\hat{\mu}^i$, the corresponding symmetrized singularity distributions.

These observations combined with a close inspection of equations (5.7.9) show that we have decoupled the symmetric and antisymmetric parts of ϕ, at least as far as boundary conditions away from the plane of symmetry are concerned.

When a control point lies on a network which itself lies on a plane of symmetry, it is still possible to obtain a decoupling of the symmetric and antisymmetric potentials, provided the user's boundary conditions satisfy certain restrictions. If the network in question is a source network, the user must specify a nontrivial boundary condition of the form

$$a_D\ \sigma(\vec{p}) + c_A(\phi(\vec{p}))_A + \vec{t}_A^T\ (\vec{v}(\vec{p}))_A = b \qquad \text{(source network, on a plane of symmetry)}$$

This is equivalent to the following condition imposed upon $\hat{\phi}^S$:

$$a_D\ \hat{\sigma}^S(\vec{p}) + c_A(\tfrac{1}{2})(\hat{\phi}^S(\vec{p}))_A + \vec{t}_A^T(\tfrac{1}{2})(\hat{v}^S(\vec{p}))_A = b \tag{5.7.10a}$$

The corresponding condition to be imposed upon $\hat{\phi}^A$ is the degenerate boundary condition,

$$\hat{\sigma}^A(\vec{p}) = 0$$

Notice in equation (5.7.10a) that because a source distribution on S_1 induces a component of ϕ that is symmetric with respect to the plane of symmetry P_1, we make the identification:

$$\sigma \Big|_{S_1} \equiv \hat{\sigma}^S \Big|_{S_1}$$

For doublet networks lying on a plane of symmetry, the user must specify a nontrivial boundary condition of the form

$$a_A \, \hat{n}^T(\vec{p}) \, B(\vec{v}(\vec{p}))_A + c_D \, \mu(\vec{p}) + \vec{t}_D^T \quad \nabla\mu(p) = b \qquad \text{(doublet network on a plane of symmetry)}$$

This is equivalent to the following condition imposed upon $\hat{\phi}^A$:

$$a_A \, \hat{n}^T(\vec{p}) \, (\tfrac{1}{2}) \, B(\hat{v}^A(\vec{p}))_A + c_D \, \hat{\mu}^A(\vec{p}) + \vec{t}_D^T \quad \nabla\hat{\mu}^A(p) = b \qquad (5.7.10b)$$

The corresponding condition to be imposed upon $\hat{\phi}^S$ is the degenerate boundary condition

$$\hat{\mu}^S \, (\vec{p}) = 0$$

Notice that in deriving (5.7.10b) we have made the identification:

$$\mu \Big|_{S_1} = \hat{\mu}^A \Big|_{S_1}$$

because a doublet distribution on S_1 induces a component of potential that is antisymmetric with respect to P_1.

A comment is in order regarding the rather anomalous factors of (1/2) that appear in equations (5.7.10). To see how these factors arise, consider the evaluation of $(\phi(\vec{p}))_A$. Solving equation (5.7.5) for $\phi(\vec{p})$ we obtain

$$\phi(\vec{p}) = \frac{1}{2} [\hat{\phi}^S(\vec{p}) + \hat{\phi}^A(\vec{p})]$$

Averaging the relation above and below $\vec{p}$, which lies on the plane of symmetry we get

$$(\phi(\vec{p}))_A = \tfrac{1}{2}(\hat{\phi}^S(\vec{p}))_A + \tfrac{1}{2}(\hat{\phi}^A(\vec{p}))_A$$

Since the function $\hat{\phi}^A(\vec{p})$ is antisymmetric with respect to the plane of symmetry, $(\hat{\phi}^A(\vec{p}))_A = 0$ (to see this, examine eqn. (5.7.5b) carefully). Thus

$$(\phi(\vec{p}))_A = (\tfrac{1}{2})(\hat{\phi}^S(\vec{p}))_A$$

and the factor of (1/2) appearing here is the same as that appearing in equation (5.7.10a).

All of the results given here for networks lying on a plane of symmetry are worked out in detail in appendix (K.3). Further, in appendices (K.6.2) and (K.6.3) the corresponding decoupling results are worked out for matching and closure boundary conditions.

The treatment of doublet matching when symmetry is present deserves special comment. Whenever doublet matching is performed on an abutment or at an abutment intersection that lies on a plane of symmetry, doublet matching conditions must be selected separately for each symmetry condition. That is, the matching condition overrides must be assigned separately for $\hat{\phi}^A$ and $\hat{\phi}^S$. Thus, it is in the handling of doublet matching that we see most clearly the fact that the discretization in PAN AIR is formulated separately for each symmetry condition.

5.7.3 Known Singularity Parameters

In a variety of cases, the value of a singularity parameter is directly specified. The most common example occurs with impermeable boundary conditions on a thick configuration (equation (5.4.19)), in which case a source parameter is specified directly as

$$\sigma = -\vec{V}_\infty \cdot \hat{n} \tag{5.7.11}$$

If, of the N singularity parameters in the whole configuration, p are directly specified and q are not, we can reorder them so that $(\lambda_1,\ldots,\lambda_p)$ are specified, and thus (assuming no planes of symmetry) the basic system of linear equations can be written as

$$\left[\begin{array}{c|c} [DI]^{p\times p} & 0^{p\times q} \\ \hline [AIC_{KP}]^{q\times p} & [AIC_{UP}]^{q\times q} \end{array}\right] \left\{\begin{array}{c} \lambda_1 \\ \vdots \\ \lambda_p \\ \hline \lambda_{p+1} \\ \vdots \\ \lambda_N \end{array}\right\} = \left\{\begin{array}{c} b_1 \\ \vdots \\ b_p \\ \hline b_{p+1} \\ \vdots \\ b_N \end{array}\right\} \tag{5.7.12}$$

Here, the matrix DI is a diagonal matrix whose entries are the coefficients a_D or c_D in equations of the form

$$a_D\sigma = b \tag{5.7.13}$$

or

$$c_D\mu = b$$

which specify the value of a singularity parameter.

The matrix AIC_{KP} (KP stands for known parameters, UP for unknown parameters) gives the dependence of the boundary condition expressions

$$a_A\vec{w}_A \cdot \hat{n} + c_A\phi_A + \vec{t}_A \cdot \vec{v}_A + a_D\,\sigma + c_D\,\mu + \vec{t}_D \cdot \nabla\mu \tag{5.7.14}$$

on the set of known parameters, while AIC_{UP} gives the dependence of the expressions (5.7.14) on the set of unknown parameters.

As a specific example, consider the case where all the source singularity parameters are specified according to equation (5.7.11). Then, $\lambda_{p+1},\ldots,\lambda_N$ are the unknown doublet singularity parameters, while for $1 \leq j \leq p$, $\lambda_j = \sigma(P_j)$ and $b_j = -\vec{V}_\infty \cdot \hat{n}_j$. Also, $[DI] = [I]$, and $[AIC_{KP}]$ gives the effect of the known source strength singularity parameters on the expression (5.7.14), which, in our example, becomes lower surface potential.

Now, the first p lines of (5.7.12) express the system of equations

$$[DI] \begin{Bmatrix} \lambda_1 \\ \vdots \\ \lambda_p \end{Bmatrix} = \begin{Bmatrix} b_1 \\ \vdots \\ b_p \end{Bmatrix} \tag{5.7.15a}$$

which implies

$$\begin{Bmatrix} \lambda_1 \\ \vdots \\ \lambda_p \end{Bmatrix} = [DI]^{-1} \begin{Bmatrix} b_1 \\ \vdots \\ b_p \end{Bmatrix} \tag{5.7.15b}$$

where $[DI]^{-1}$ is readily computable since $[DI]$ is a diagonal matrix. The remainder of (5.7.12) is

$$[AIC_{KP}] \begin{Bmatrix} \lambda_1 \\ \cdot \\ \cdot \\ \cdot \\ \lambda_p \end{Bmatrix} + [AIC_{UP}] \begin{Bmatrix} \lambda_{p+1} \\ \cdot \\ \cdot \\ \cdot \\ \lambda_N \end{Bmatrix} = \begin{Bmatrix} b_{p+1} \\ \cdot \\ \cdot \\ \cdot \\ b_N \end{Bmatrix} \tag{5.7.16}$$

Substituting (5.7.15b) into (5.7.16), we obtain

$$[AIC_{UP}]^{qxq} \overset{qx1}{\begin{Bmatrix} \lambda_{p+1} \\ \vdots \\ \lambda_N \end{Bmatrix}} = \overset{qx1}{\begin{Bmatrix} b_{p+1} \\ \vdots \\ b_N \end{Bmatrix}} - [AIC_{KP}]^{qxp} [DI^{-1}]^{pxp} \overset{px1}{\begin{Bmatrix} b_1 \\ \vdots \\ b_p \end{Bmatrix}} \tag{5.7.17}$$

We have thus reduced (5.7.12), a system of equations in the N parameters $\lambda_1,\ldots,\lambda_N$ to a system of equations in the q unknown parameters $\lambda_{p+1},\ldots,\lambda_N$.

5.7.4 Multiple Right Hand Sides

So far, we have always considered a system or systems of equations of the general form

$$[AIC]^{nxn} \vec{\lambda}^{nx1} = \vec{b}^{nx1} \tag{5.7.18}$$

But if the AIC matrix does not change, it is very economical to solve (5.7.18) for a sequence of distinct vectors $\vec{b}_i$, obtaining a sequence of solution vectors $\vec{\lambda}_i$.

The ability to solve (5.7.18) for multiple vectors b can be very useful. The uses include analyzing the flow about a configuration at multiple angles of attack or sideslip, evaluating stability derivatives, or analyzing a variety of quasi-steady flows in which the configuration is undergoing a pitching, rolling, or yawing motion. This is especially useful when $M_\infty = 0$, and the small perturbation assumption is not necessary for the Prandtl-Glauert equation to hold. For a further discussion of "right hand side" or "constraint" vectors $\vec{b}$, see Appendix L.

So, in its most general form, (5.7.18) can be written

$$[AIC]^{nxn} [\Lambda]^{nxm} = [B]^{nxm} \tag{5.7.19}$$

where each of the m columns of B is a constraint vector $\vec{b}_i$, and each column of Λ is a solution vector $\vec{\lambda}_i$.

5.7.5 Updatability

Another feature of PAN AIR is that of "updatability." That is, a program user may identify certain networks as being subject to modification. The program then segregates boundary conditions and singularity parameters corresponding to these networks, so that the AIC matrix in (5.7.18) can be partitioned as:

$$[AIC] = \left[\begin{array}{c|c} AIC_{NU} & AIC_{U,1} \\ \hline AIC_{U,2} & AIC_{U,3} \end{array}\right] \tag{5.7.20}$$

Here, the subscripts U and NU stand for updatable and non-updatable.

Now, the matrix AIC_{NU} is stored, and when the program user makes a second run in which updatable networks are modified, the program need only recalculate $AIC_{U,1}$, i = 1, 2, 3, rather than the whole AIC matrix. Here, "modification" may consist of the alteration of the network geometry, or the alteration of the left hand side boundary condition expressions (5.7.14). It is easy to see that AIC_{NU} remains unchanged under a modification of an "updatable" network. For a full discussion, see Appendix K.7.

5.8 Solution of the System of Equations

As we see from (5.7.7), (5.7.8), (5.7.18), and (5.7.19) the program sets up a system or systems of linear equations of the general form

$$[A]^{nxn}\,[X]^{nxm} = [B]^{nxm} \tag{5.8.1}$$

Generally speaking, the matrix A is too large to store in the central memory of a computer at one time. Thus the matrices are stored in block format on a disk, and (5.8.1) is solved with no more than three of these blocks in core at once.

Generally, the matrix A is decomposed as a product of lower triangular and upper triangular matrices

$$[A]^{nxn} = [L]^{nxn}\,[U]^{nxn} \tag{5.8.2}$$

This process frequently involves "in-block pivoting," that is, the interchange of columns within one of the blocks composing A. It can happen that a boundary value problem of aerodynamic interest results in one of the blocks of A which lies on the diagonal being singular, in which case a decomposition of the form (5.8.2) is not possible. Such a case requires the interchange of columns lying in different blocks, a process called "out-of-block pivoting." The out-of-block pivoting process decreases the efficiency of the solution process since additional data must be transferred between disk and core. This process is described in Appendix L.

After the decomposition (5.8.2) the next step is "forward substitution," that is, the system of equations

$$[L]^{nxn}\,[Y]^{nxm} = [B]^{nxm} \tag{5.8.3}$$

is solved for the matrix Y. The final step is "back substitution," in which the system

$$[U]^{nxn}\,[X]^{nxm} = [Y]^{nxm} \tag{5.8.4}$$

is solved for the matrix X.

The solution procedure has two distinct "updatability" features. First, suppose A is an AIC matrix partitioned as in (5.7.20). Then the factorization (5.8.2) is performed on AIC_{NU} first, after which A is factored in its entirety. The factorization of AIC_{NU} is stored, and in a later run in which $AIC_{U,i}$, $i = 1, 2, 3$, are changed, the factorization continues from that point. They may result in a significant saving of time.

The other "updatability" feature is that a program user may request the entire factorization (5.8.2) to be stored, and then at a later time submit additional constraint vectors b. Thus, a user may find that the results for one angle of attack are useful, and thereupon obtain results for additional angles of attack, angles of sideslip, or for stability derivatives, at small additional cost.

5.9 Post-Solution Features

5.9.1 Computation of Potential and Velocity

Once the system or systems of linear equations (5.7.19) have been solved for one or more solution vectors, it remains to translate the vector(s) into quantities of aerodynamic or hydrodynamic interest. The first step is to obtain the values of ϕ_A and $\vec{v}_A$ at control points. Clearly

$$\phi_A = [\phi IC]^{1xN} \vec{\lambda}^{Nx1}$$
$$\vec{v}_A = [VIC]^{3xN} \vec{\lambda}^{Nx1} \tag{5.9.1}$$

but obtaining ϕ_A and $\vec{v}_A$ this way requires the storage of 4N words of data for each control point. Often it is possible to obtain ϕ_A from a boundary condition. For example (recalling $\phi_L = \frac{1}{2}(\phi_U + \phi_L) - \frac{1}{2}(\phi_U - \phi_L) = \phi_A - \frac{1}{2}\mu$), the boundary condition

$$\phi_L = \phi_A - \frac{1}{2}\mu = 0 \tag{5.9.2}$$

is often imposed at control points. Thus,

$$\phi_A = \frac{1}{2}\mu \tag{5.9.3}$$

Since μ at the control point is already available (it is one of the unknown parameters), we can obtain ϕ_A without storing the ϕIC matrix.

Once ϕ_A has been found at every control point, we may make use of the doublet spline matrices to obtain a distribution of ϕ_A on the whole surface. This quadratic distribution may then be differentiated to obtain tangential velocities on the surface. The conormal component of velocity, $\vec{v}_A \cdot \tilde{n} = \vec{w}_A \cdot \vec{n}$, can often be obtained from a boundary condition of the form

$$\vec{w}_A \cdot \hat{n} = -\vec{V}_\infty \cdot \hat{n}$$

Then, all three components of velocity may be obtained from the tangential and conormal components. The details of how we can use boundary conditions and splines to obtain velocities at control points or grid points (panel corner points, centers, or edge midpoints) are given in Appendix M.

The velocities are calculated at control points or grid points in a user-selected reference coordinate system (x_o, y_o, z_o). The formulas for calculating pressures are most easily written in the compressibility coordinate system (x,y,z), in which the freestream direction is the x-direction, so we will describe them in that system, in which we write

$\vec{v} = (u,v,w)$ and $\vec{V}$ (the total velocity) $= (|\vec{V}_\infty| + u,\ v,\ w)$.

5.9.2 Pressure Computation

PAN AIR will calculate the pressure from the velocity according to any of five different pressure coefficient rules. These pressure rules will be derived in Appendix N. We assume we are dealing with a gas or an incompressible liquid. Let γ be the ratio of specific heats. Subject to certain constraints on the range of velocities for which the pressure coefficient rules hold, they are listed in figure 5.21. For an incompressible liquid, the isentropic formula does not apply.

5.9.3 Velocity Corrections

In addition, PAN AIR will calculate two semi-empirical velocity correction formulas. The first is often used in practice in areas such as inlets where the component of the velocity in the freestream direction is less than the freestream. If $u < 0$, we solve the following equation for V'_x:

$$|\vec{V}_\infty| + s\beta^2 u = W_x = V'_x \left[1 + \frac{\gamma - 1}{2} M_\infty^2 \left(1 - |V'_x|^2\right)\right]^{\frac{1}{\gamma - 1}} \tag{5.9.5}$$

The corrected velocity is given

$$\vec{V}' = \begin{Bmatrix} V'_x \\ v \\ w \end{Bmatrix} \tag{5.9.6}$$

This velocity correction, denoted SA1 in the User's Manual, is closely related to the Lieblein-Stockman formula (cf. Reference 5.1).

The second velocity correction formula, denoted SA2 in the User's Manual, is often used in regions of near-stagnation such as the leading edge of a wing. If $u \geq 0$, we set

$$\vec{V}' = \frac{|\vec{V}|}{|\vec{W}|}\ \vec{W} \tag{5.9.7}$$

If $u < 0$, we set

$$\vec{V}' = \frac{\vec{W}}{1 - M_\infty^2\, u} \tag{5.9.8}$$

where the denominator is a first order approximation to ρ/ρ_∞ .

These two correction formulas are essentially empirical. The first has been used successfully only in subsonic flow, while the second has been used successfully in both subsonic and supersonic flow. Successful applications of the second velocity correction are given in reference 4.9 (Ehlers et. al., p. 89 and figure 36) and reference 5.4 (Chen and Tinoco, figure 5).

5.9.4 Force and Moment Computation

PAN AIR will also integrate pressures on a surface to obtain coefficients of force. The formula we use for the force is

$$\vec{F} = - \iint_S \left\{ \frac{\rho \vec{V} \cdot \hat{n}}{|\vec{V}|^2} \vec{V} + p\hat{n} \right\} dS \qquad (5.9.9)$$

where p is the pressure and ρ is the density.

The first term in the integrand, the momentum flux term, is zero for an impermeable surface, but does in fact contribute to the force on a porous surface. The evaluation of this integral is discussed in Appendix O.

PAN AIR also evaluates the moment M about a point. If $\vec{R}_0$ is the point in question, and $\vec{Q}$ is a point on the surface,

$$\vec{M} = - \iint_S \left\{ (\vec{Q} - \vec{R}_0) \times \left(\frac{\rho \vec{V} \cdot \hat{n}}{|V_\infty|^2} \vec{V}\right) + p\,(\vec{Q} - \vec{R}_0) \times \hat{n} \right\} dS \qquad (5.9.10)$$

The derivation of (5.9.9) and (5.9.10) is given in Ashley and Landahl (reference 5.3), section 1-6.

Equation (5.9.9) ignores a contribution to the total force, called the edge force, which occurs for thin configurations. To obtain the force on the configuration illustrated in figure 5.22, we should integrate the expression in (5.9.9) over the combined surface $S_1 \cup S_2$, while in fact we only integrate the expression over S_1. The evaluation of the integral over S_2, the edge force, requires the use of some special extrapolation and correction techniques. The basic idea is to evaluate the limit in the expression for edge force, (cf. ref. 5.2):

$$\text{edge force per unit length} = (\pi/8)\beta_n \left[\lim_{x_n \to 0} (\mu/\sqrt{x_n})\right]^2 \qquad (5.9.11)$$

(here, β_n is an edge normal compressibility factor and x_n is the distance from the edge) by evaluating the expression $(\mu/\sqrt{x_n})$ at panel centers near the edge. A correction factor is then applied to the result to account for some nonuniform convergence effects arising from the fact that PAN AIR does not allow μ to behave like $c\sqrt{x_n}$ in the neighborhood of the leading edge. For more details of the edge force computation, see appendix O.

5.9.5 Off-Body Points and Streamlines

In order to help the program user in visualizing the flow field, PAN AIR provides the capability to calculate potential and velocity at off body points. In addition, this basic capability of evaluating ϕ and $\vec{V}$ at points away from the configuration surface has been combined with an ordinary differential equation solver to provide a streamline tracing capability. In

this section we summarize these capabilities, deferring to appendix P the details of their implementation.

The evaluation of ϕ and $\vec{v}$ at off body points is a straightforward task once the singularity vector $\vec{\lambda}$ has been obtained by solving equation (5.7.18). To see this, simply observe that once $\vec{\lambda}$ is known, the source and doublet distributions are completely determined by equations (3.3.1-2). Once σ and μ are known, ϕ and $\vec{v}$ are given at any point P by the integral representation formulas, equations (5.6.3) and (5.6.4). The evaluation of the integrals appearing in equations (5.6.3) for ϕ and (5.6.4) for $\vec{v}$ is treated in detail in appendix J.

Given the capability of evaluating $\vec{v}$ at an arbitrary point P, the tracing of a streamline is accomplished by numerically solving an ordinary differential equation. To see this let $\vec{P}(t)$ denote the coordinates of a velocity streamline parameterized by t. By the definition of such a streamline, the tangent vector to the streamline given by

$$\text{tangent to streamline } \vec{P}(t) = \frac{d\vec{P}}{dt} \tag{5.9.12}$$

is parallel to the velocity field at $\vec{P}(t)$. Mathematically this implies

$$\frac{d\vec{P}}{dt} = g(t)\ \vec{V}(\vec{P}(t))$$

The apparently arbitrary function g(t) does not affect the shape of the streamline but rather, just modifies its parameterization. By convention we set $g \equiv 1$ in PAN AIR. Thus, given an initial point $\vec{P}_0$ on a velocity streamline, PAN AIR determines a sequence of points on that streamline by solving the following initial value problem:

$$\frac{d\vec{P}}{dt} = \vec{V}(\vec{P}(t)) = \vec{V}_\infty + \vec{v}(\vec{P}(t)) \tag{5.9.13}$$

$$\vec{P}(0) = \vec{P}_0$$

In actual practice, it is usually preferable to compute mass flux streamlines, i.e., streamlines where tangents are parallel to the mass flux vector field $\vec{W}(\vec{P})$. The initial value problem used to define these streamlines is given (cf. equations (5.4.4) and (5.4.10))

$$\frac{d\vec{P}}{dt} = \vec{W}(\vec{P}(t)) = \vec{V}_\infty + B_0\ \vec{v}(\vec{P}(t)) \tag{5.9.14}$$

$$\vec{P}(0) = \vec{P}_0$$

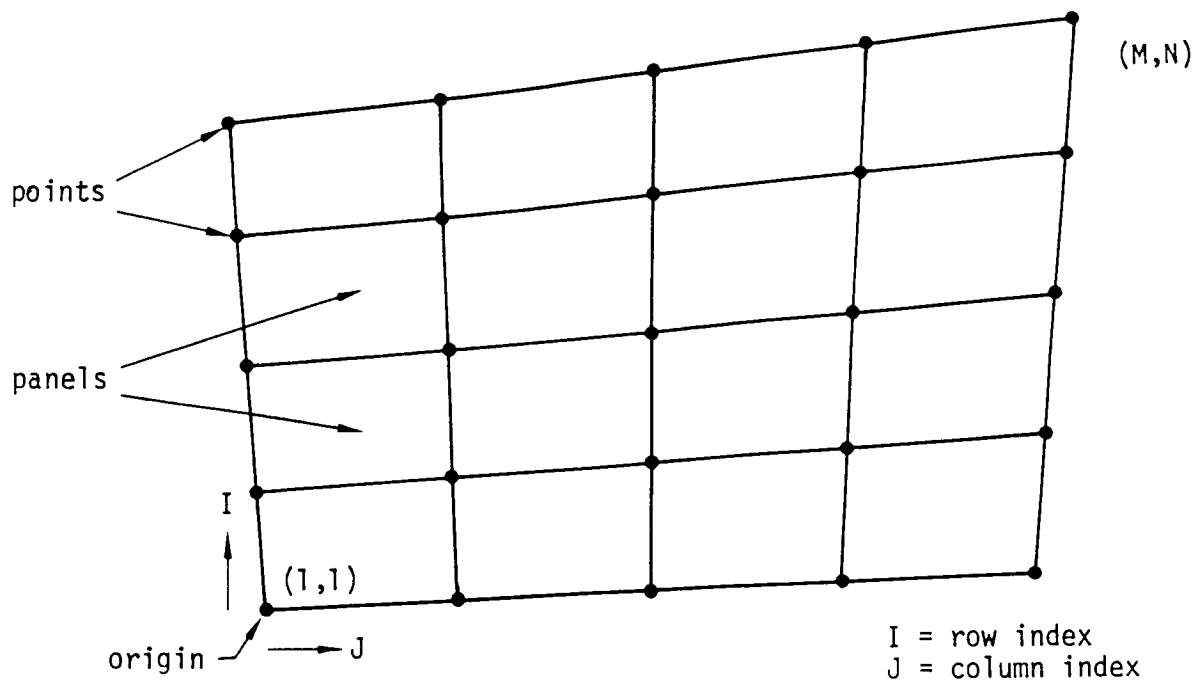

Figure 5.1 Network geometry

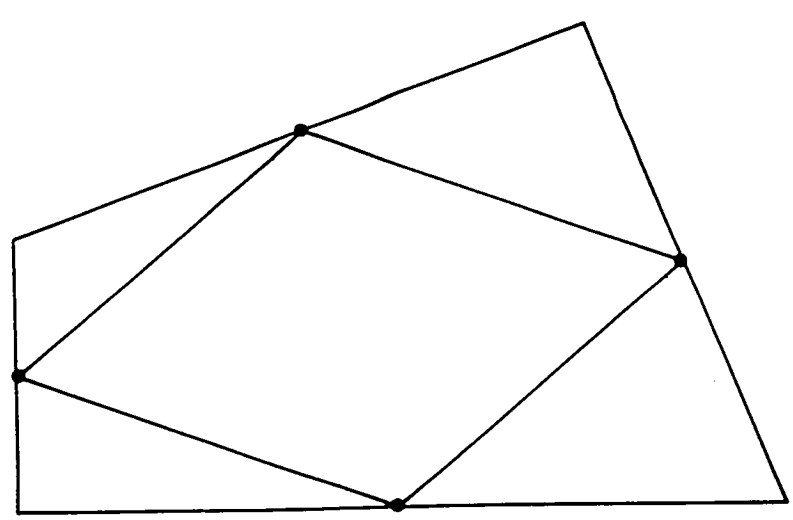

Figure 5.2 Decomposition of panel into 5 planar regions

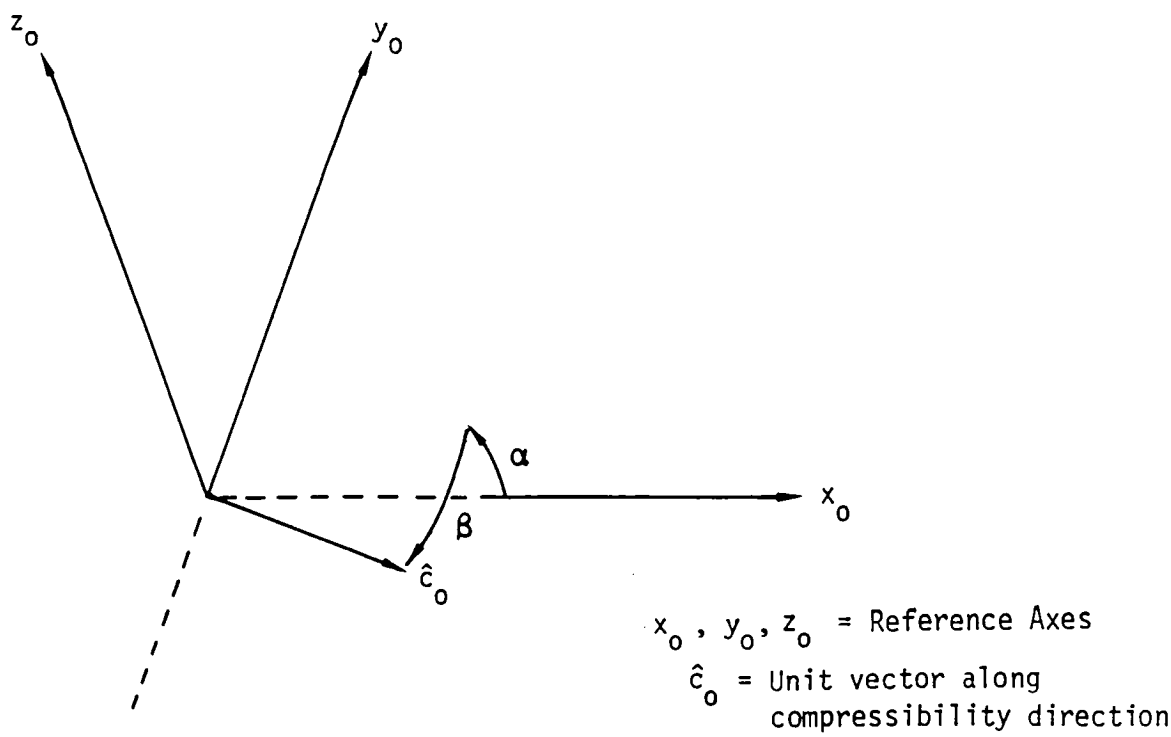

Figure 5.3 - Definition of compressibility directions in terms of angles of attack and sideslip

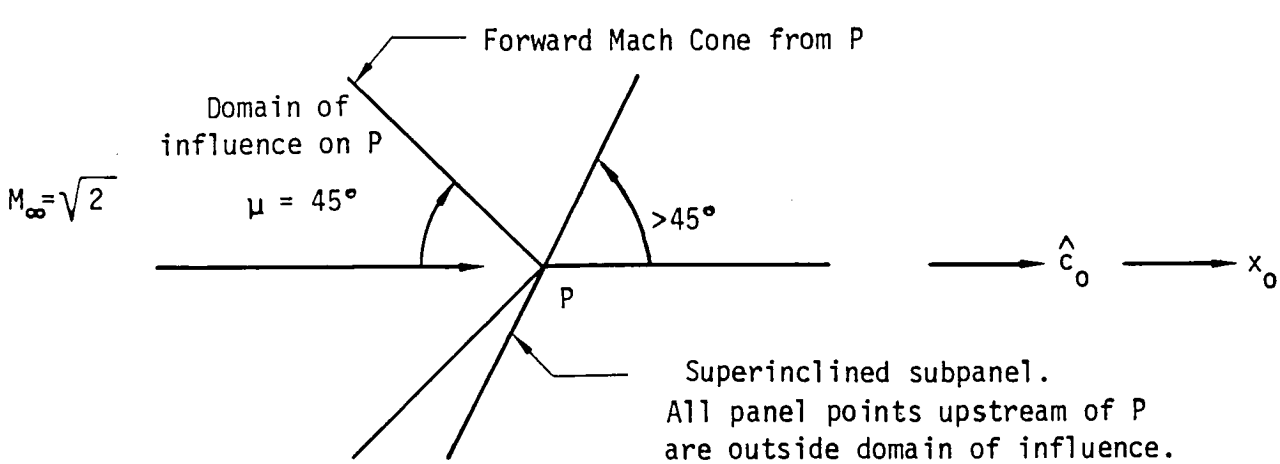

Figure 5.4 - Superinclined Surface, r = -1

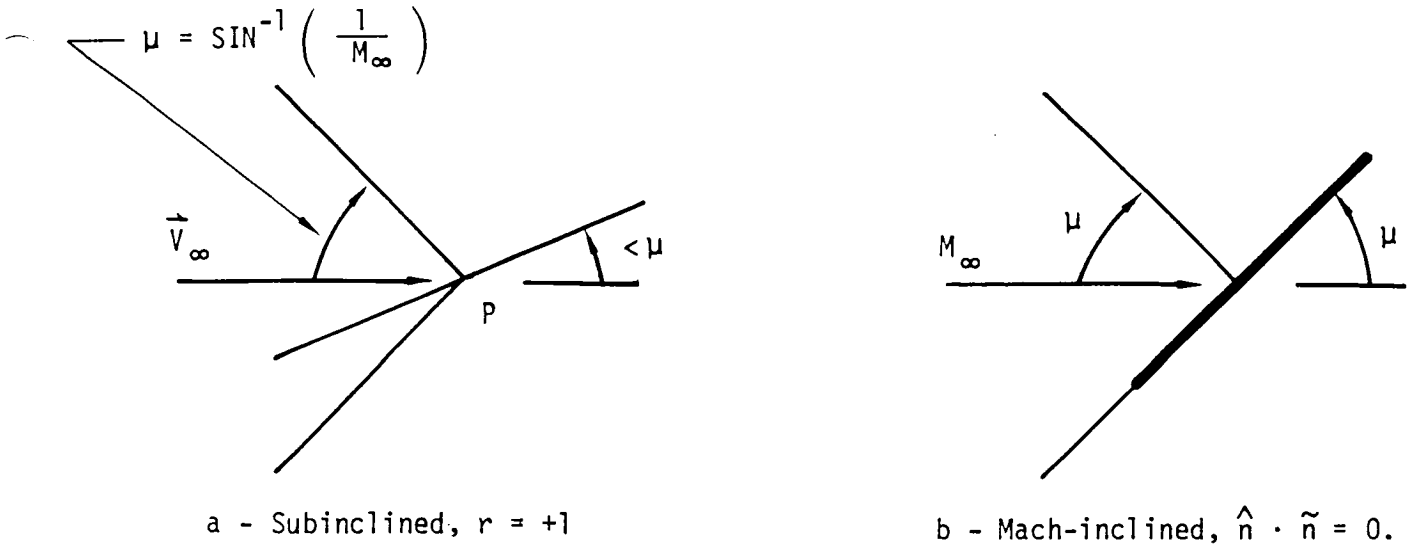

a - Subinclined, $r = +1$

b - Mach-inclined, $\hat{n} \cdot \tilde{n} = 0$.

Figure 5.5 - Subinclined and Mach-inclined surfaces

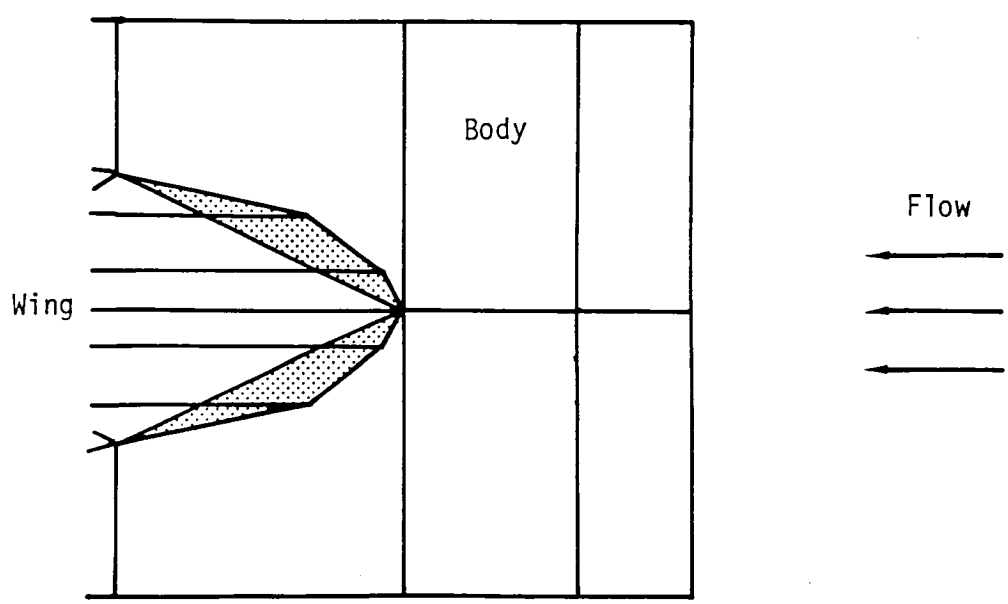

Figure 5.6 - Gap between leading edge of wing and body

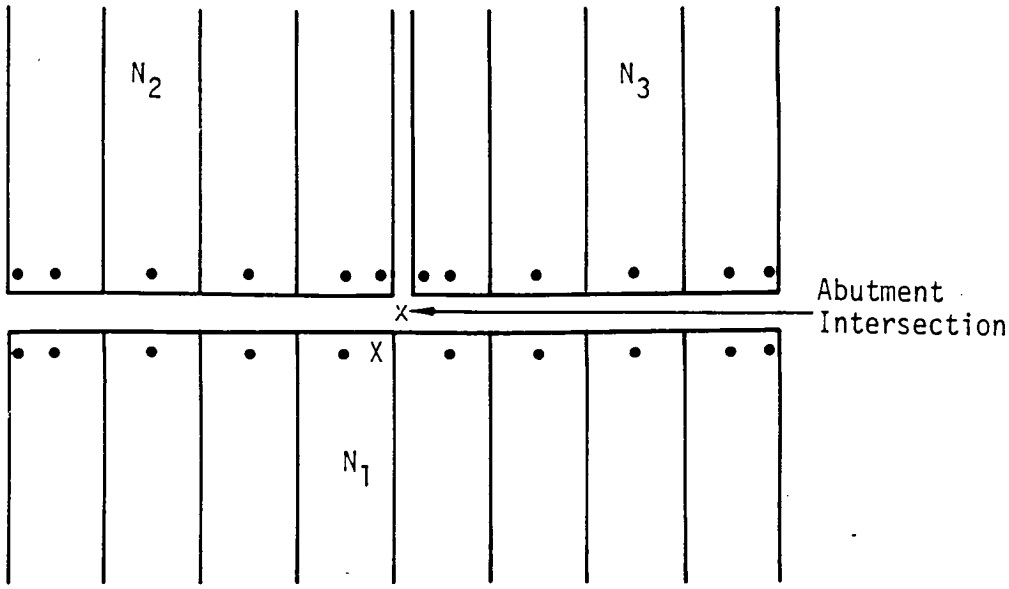

• ordinary edge and corner control points

X extra control point

Figure 5.7 - Example of abutment intersection

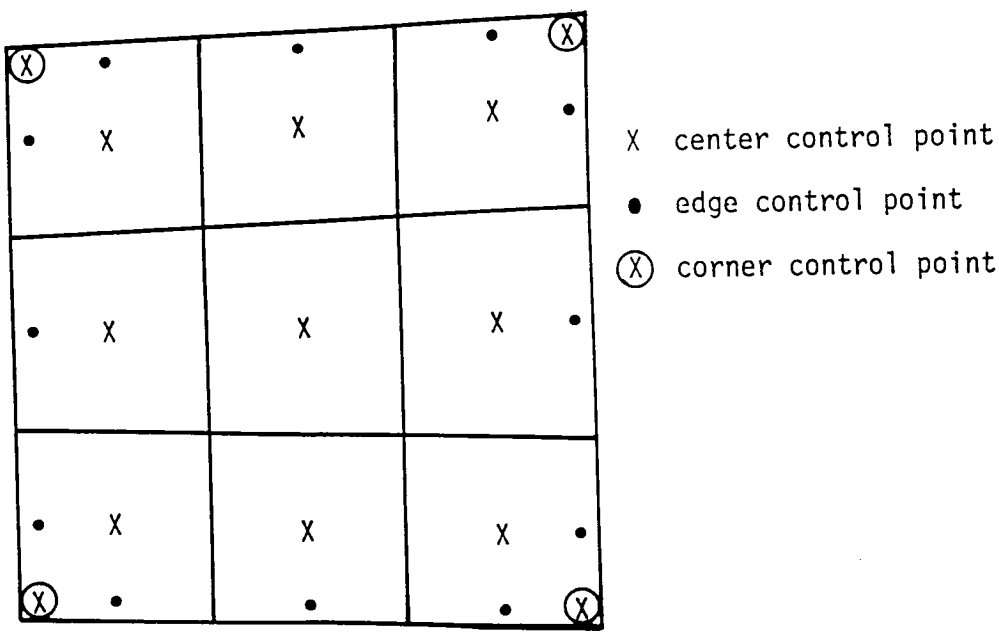

Figure 5.8 - Control point locations

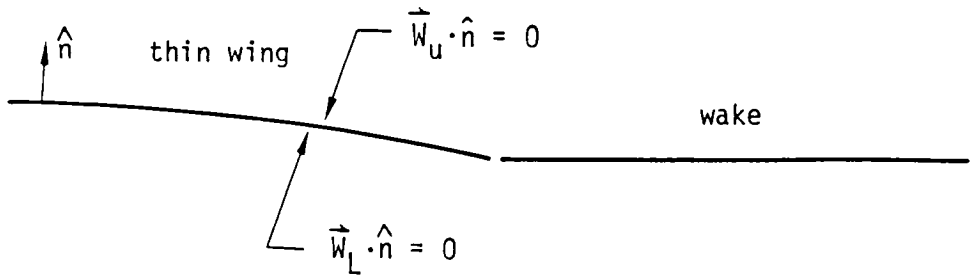

Figure 5.9 - Thin wing boundary conditions

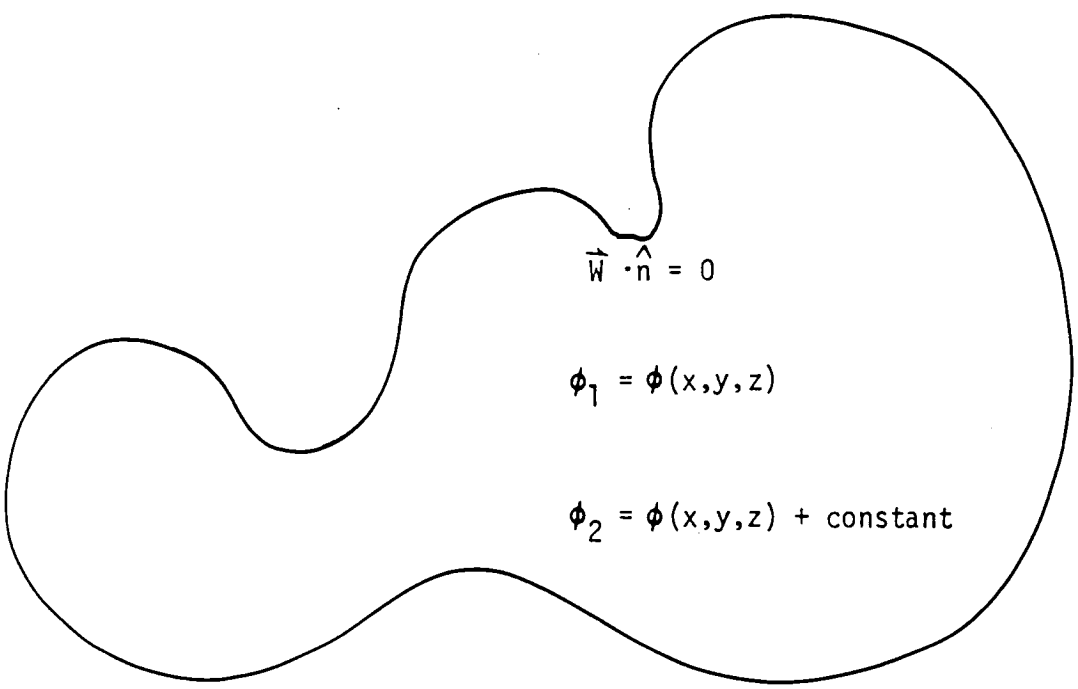

Figure 5.10 - Two solutions for potential in enclosed volume

Figure 5.11 - Thick wing boundary conditions

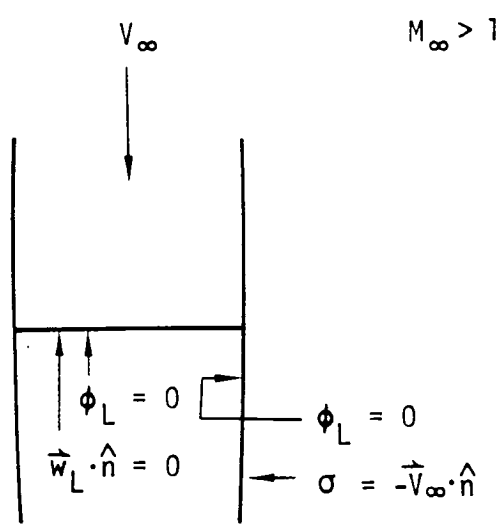

Figure 5.12 - Boundary conditions on superinclined surfaces

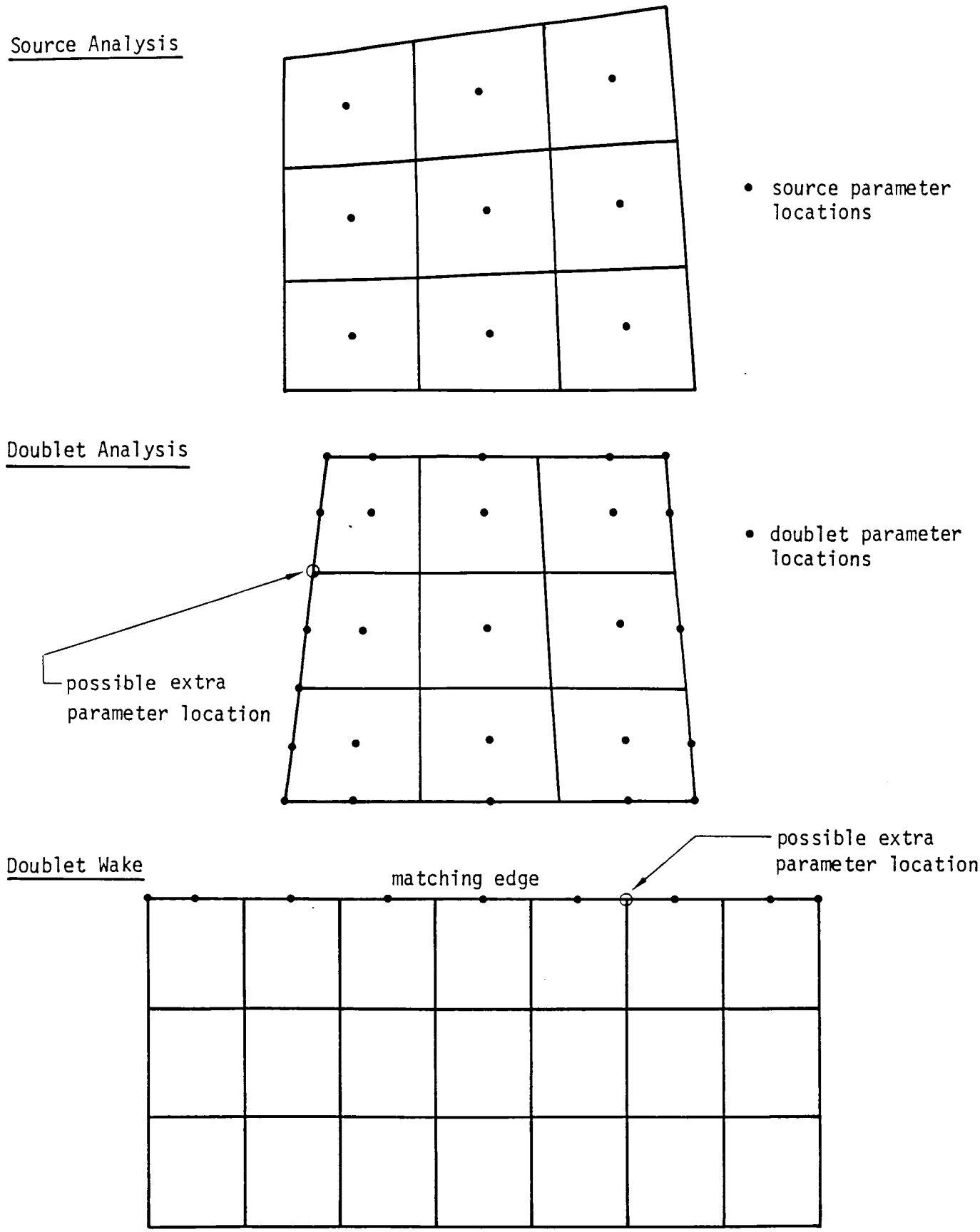

Figure 5.13 - Singularity parameter locations

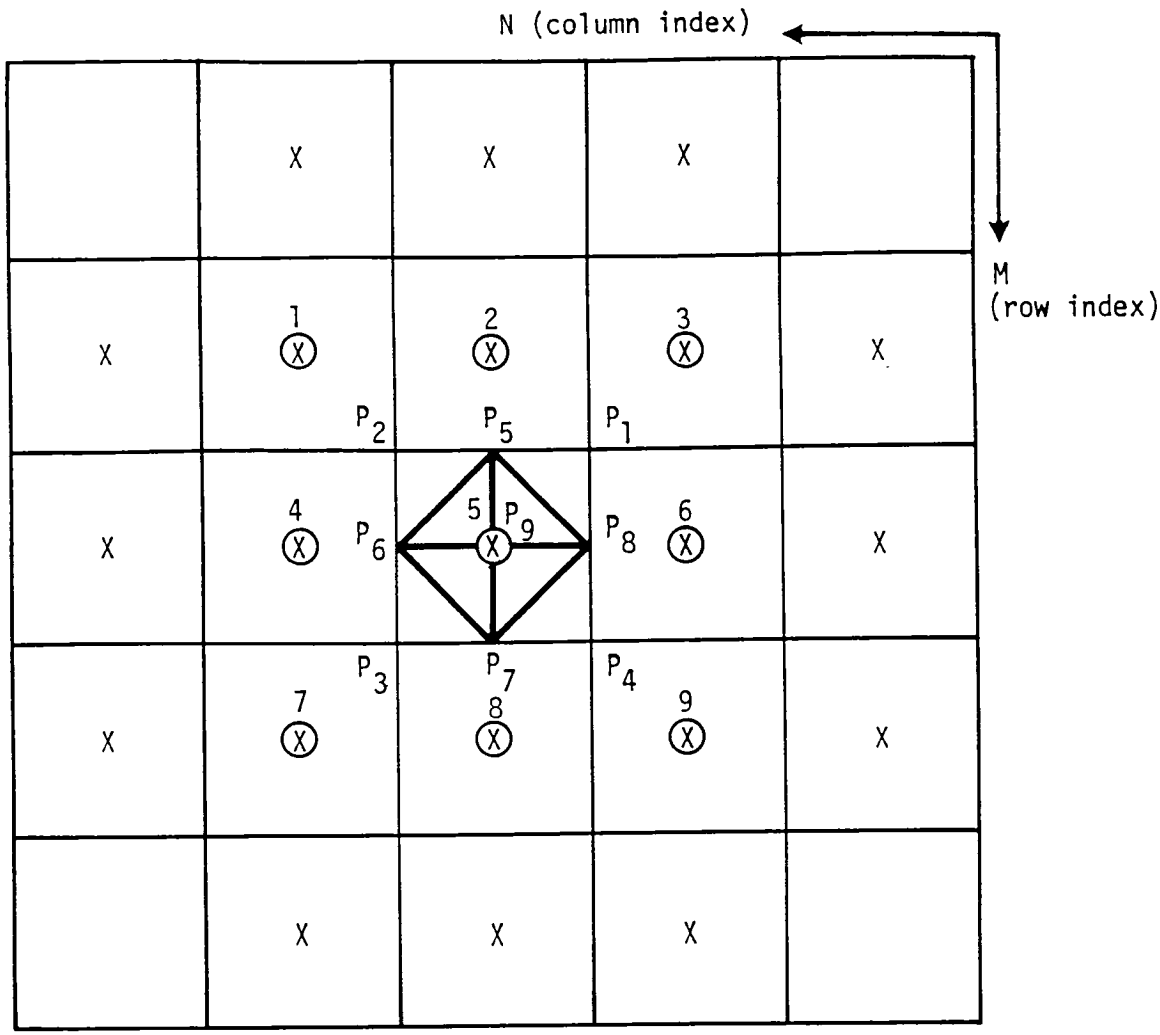

X doublet parameters in the neighborhood of the panel

○ source parameters in the neighborhood of the panel

Figure 5.14 Singularity parameters in the neighborhood of the panel

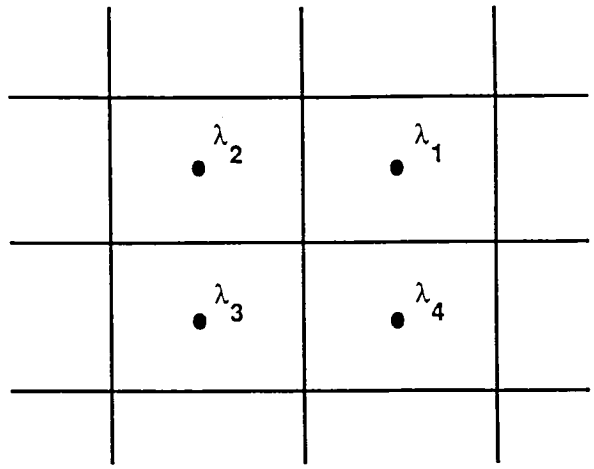

● neighboring source parameter

Figure 5.15 - Neighboring source parameters for a panel corner point

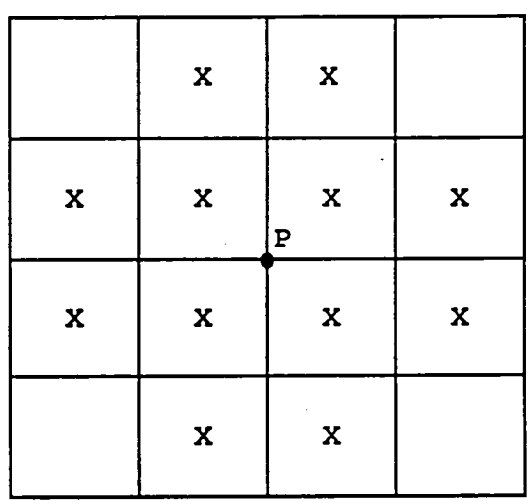

x neighboring doublet parameters

Figure 5.16 - Neighboring doublet parameters for a panel corner point

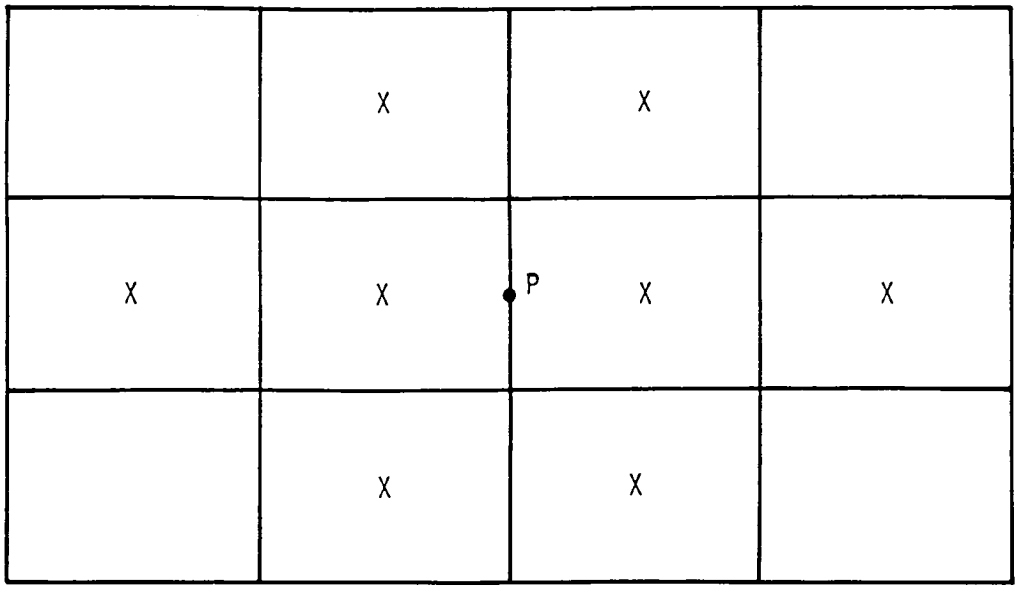

Figure 5.17 - Neighboring doublet parameters for a panel edge midpoint

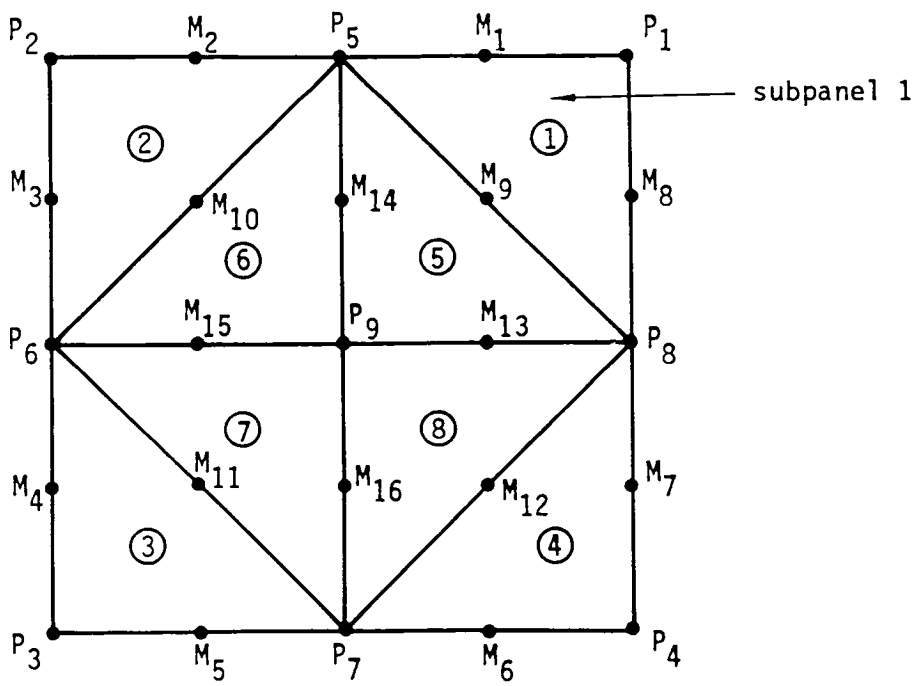

Figure 5.18 - Panel points and midpoints

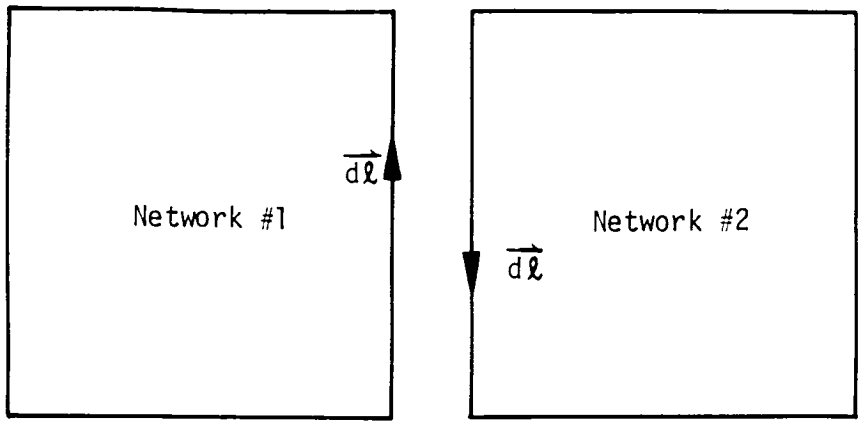

Figure 5.19 - Opposite orientations of adjacent networks

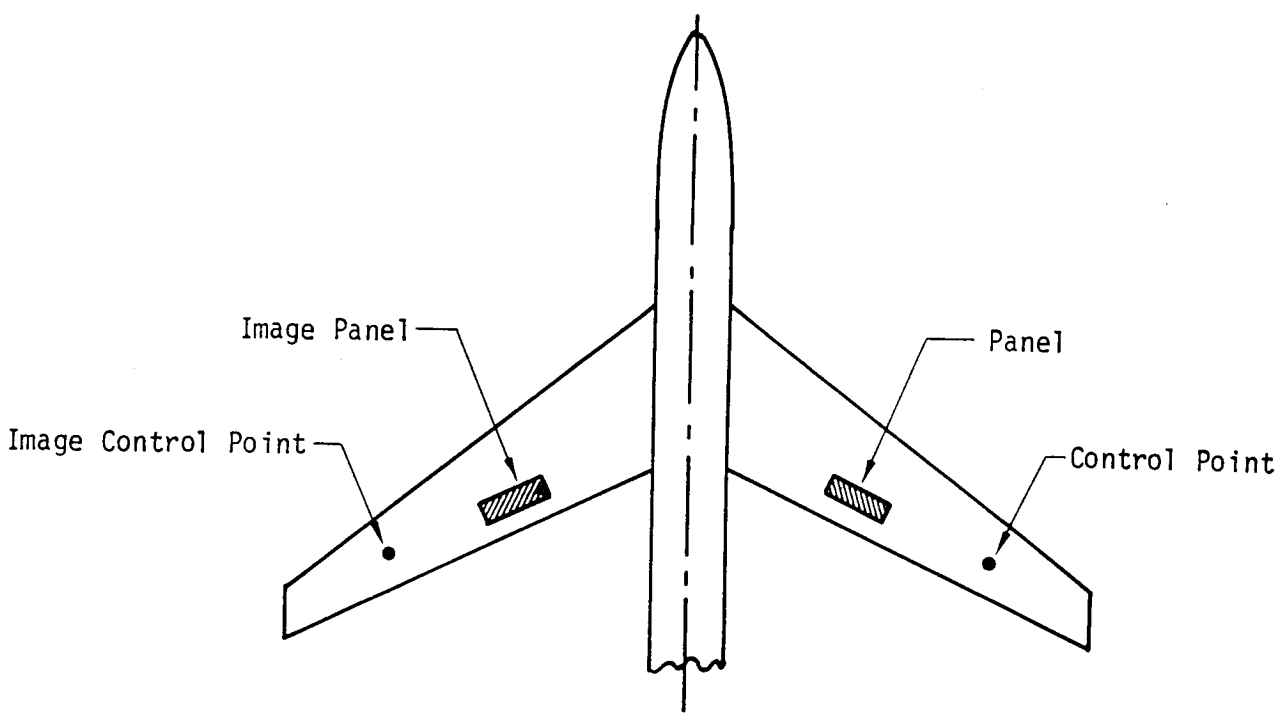

Figure 5.20 - Configuration and image

RULE	C_p
Isentropic	$\frac{2}{\gamma M_\infty^2}\left\{\left[1+\frac{\gamma-1}{2}M_\infty^2\left(1-\frac{\lvert\vec{V}\rvert^2}{\lvert V_\infty\rvert^2}\right)\right]^{\frac{\gamma}{\gamma-1}}-1\right\}$ used if $M_\infty > .01$
Incompressible	$1-\lvert\vec{V}\rvert^2/\lvert V_\infty\rvert^2$ used if $M_\infty \leq .01$
Second Order	$1-\lvert\vec{V}\rvert^2+M_\infty^2u^2$
Slender Body	$-(2u+v^2+w^2)$
Linear	$-2u$
Reduced Second Order	$1-\lvert\vec{V}\rvert^2$

Figure 5.21 - Pressure coefficient rules

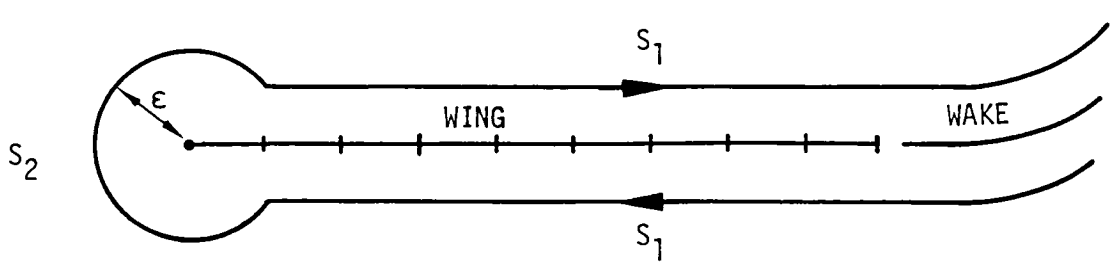

Figure 5.22 - Surfaces of integration for leading edge force

6.0 A Guide to the Appendices

The purpose of the appendices is three-fold:

(a) they give background material, not reflected in the computer code, but explaining why the computer program performs the functions it does,

(b) they describe in considerable detail the functions performed by the program, and

(c) they describe the equations which are actually implemented in the code.

Appendices A through C cover background material exclusively. The remaining appendices are predominantly devoted to the PAN AIR program, but often derivations are supplied to prove or justify the validity of an equation.

Often a conflict may occur between organizing the material according to the structure of the program or organizing it according to subject matter (for instance splines, panels, networks, pressures, etc.) or capability (for instance symmetry, updatability, multiple right hand sides, etc.). This conflict will almost invariably be resolved in favor of organization according to subject matter.

This document will generally discuss only engineering functions within PAN AIR. Specifically, the functions of the Data Input Processor (DIP), which reads and echoes user-input data, and the Print Plot Processor, which prepares files of output data for processing by plotting programs, will be ignored. Also, input/output and other data manipulation functions which are necessary due to core limitations, will, with few exceptions, be ignored. For example, a detailed discussion of the abutment analysis processor in DQG will be contained in the Maintenance Document rather than the Theory Document, since the complexity of this procedure is largely due to data manipulation problems. Finally, there will be no discussion of the "Scientific Data Management System" (SDMS) used by PAN AIR to transfer data between core and disk.

7.0 References

PAN AIR Documents

PAN AIR – A Computer Program for Predicting Subsonic or Supersonic Linear Potential Flows about Arbitrary Configurations using a higher Order Panel Method.

Volume II, User's Manual (Version 1.1) by K. Sidwell, J. E. Bussoletti, and P. K. Baruah, NASA CR-3252, 1981.

Volume IV, Maintenance Document (Version 1.1), by P. K. Baruah et al., NASA CR-3254, 1981.

Other References

1.1 Rubbert, P. E., and Saaris, G. R.: "Review and Evaluation of a Three-Dimensional Lifting Potential Flow Computational Method for Arbitrary Configurations," AIAA Paper 72-188, January 1972.

1.2a Woodward, F. A.: Analysis and Design of Wing-Body Combinations at Subsonic and Supersonic Speeds," Journal of Aircraft, Vol. 5, No. 6,. Nov-Dec 1968, pp. 528-534.

1.2b Woodward, F. A.: "An Improved Method for the Aerodynamic Analysis of Wing-Body-Tail Configurations in Subsonic and Supersonic Flow, Part I – Theory and Application," NASA CR-2228, Part I, 1973.

1.3 Kellogg, O. D.: Foundations of Potential Theory, New York, Dover Publishing Company, 1953.

1.4 Liepmann, H. W., and Roshko, A.: Elements of Gasdynamics, New York, John Wiley and Sons, 1957.

1.5 Ward, G. N.: Linearized Theory of Steady High-Speed Flow, Cambridge University Press, 1955.

2.1 Landahl, M. T.: Unsteady Transonic Flow, Pergamon Press, 1961.

4.1 Hess, J. L., and Smith, A. M. O.: Calculation of Nonlifting Potential Flow About Arbitrary Three-Dimensional Bodies, ES-40622, Douglas Aircraft Company, 1962.

4.2 Rubbert, P. E.: Theoretical Characteristics of Arbitrary Wings by a Non-planar Vortex Lattice Method, D6-9244, The Boeing Company, 1964.

4.3 Hess, J. L.: Calculation of Potential Flow About Arbitrary Three-Dimensional Lifting Bodies, Douglas Report MDC-J5679-01, October 1972.

4.4 Roberts, A., and Rundle, K.: Computation of First Order Compressible Flow About Wing-Body Configurations, S/T MEMO-14173, British Aircraft Corporation, February 1973.

4.5 Mercer, J. E., Weber, J. A., and Lesferd, E. P.: Aerodynamic Influence Coefficient Method Using Singularity Splines, NASA CR-2423, May 1974.

4.6 Morino, L.,and Kuo, Ching-Chiang: "Subsonic Potential Aerodynamics for Complex Configurations: A General Theory," AIAA Journal, Vol. 12, No. 2, pp. 191-197, February 1974.

4.7 Johnson, F. T., and Rubbert, P. E.: "Advanced Panel-Type Influence Coefficient Methods Applied to Subsonic Flow," AIAA Paper 75-50, January 1975.

4.8 Ehlers, F. E., and Rubbert, P. E.: A Mach Line Panel Method for Computing the Linearized Supersonic Flow Over Planar Wings, NASA CR-152126, 1978.

4.9 Ehlers, F. E., Epton, M. A., Johnson, F. T., Magnus, A. E., and Rubbert, P. E.: A Higher Order Panel Method for Linearized Supersonic Flow, NASA CR-3062, 1979.

5.1 Lieblein, S., and Stockman, N. O.: "Compressibility Corrections for Internal Flow Solutions," Journal of Aircraft, Vol. 9, No. 4, pp. 312-313, April 1972.

5.2 Hancock, G. J., and Garner, H. C.: On the Application of Subsonic Linearised Wing Theory to Second-Order Forces and Moments, ARC-R/M-3758, 1975.

5.3 Ashley, H., and Landahl, M.: Aerodynamics of Wings and Bodies, Addison-Wesley, 1965.

5.4 Chen, A. W., and Tinoco, E. N.: "PAN AIR Applications to Aero-Propulsion Integration," Journal of Aircraft, Vol. 21, No. 3, March 1984, pp. 161-167.

B.1 Butter, D. J., Compressibility Corrections Used in Panel Methods, HSA-MAE-R-FDM-0039, British Aircraft Corporation, November 1978.

B.2 Johnson, F. T., Lu, P., Tinoco, E. N., and Epton, M. A.: UTTL: An Improved Panel Method for the Solution of Three-Dimensional Leading Edge Vortex Flows, NASA CR-3278, 1979.

F.1 Jones, R. T., and Cohen, D.: High Speed Wing Theory, No. 6, Princeton Aeronautical Paperbacks, Princeton, N.J., Princeton U. Press, 1960.

F.2 Deo, N.: Graph Theory with Applications to Engineering and Computer Science, Prentice-Hall, 1974.

H.1 Dahlquist, G., and Bjorck, A.: Numerical Methods, Prentice-Hall, 1974.

J.1 Johnson, F. T.: A General Panel Method for the Analysis and Design of Arbitrary Configurations in Incompressible Flows – Boundary Value Problem, NASA CR-3079, 1979.

J.2 Abramowitz, M., and Stegun, I. A. (editors): Handbook of Mathematical Functions, National Bureau of Standards, 1964.

J.3 Robinson, A.: "On Source and Vortex Distributions in the Linearized Theory of Steady Supersonic Flow," Quart. J. Mech. Appl. Math., Vol. I, pp. 408-432, Dec. 1948.

O.1 Medan, R. T.: Aerodynamic Loads Near Cranks Apexes, and Tips of Thin, Lifting Wings in Incompressible Flow, AGARD-CP-204, 1976, No. 18.

O.2 Sidwell, K.: Added Mass Coefficients from the PAN AIR System, NCSC Document D180-24636-1, April 1978.

P.1 Shampine, L. F., and Gordon, M. K.: Computer Solution of Ordinary Differential Equations: The Initial Value Problem, W. H. Freeman, 1975.

8.0

List of Symbols

Latin Symbols

a, a_∞	speed of sound, freestream speed of sound (m/sec)	[2.3]
a_A, a_D	average and difference normal mass flux coeffcients	[5.4.2.5]
a, a_i, a_k	distance (signed) from control point's projection to an edge of Σ (local coordinates)	[J.5]
a, $\vec{a}$	fundamental integrals in PIC computation	[J.6]
a^S_{iN}, a^D_{iN}	generic coefficients in polynomial expansions for source and doublet	[4]
a_i	constant coefficient of L_i, linear basis function on a triangle	[I.2]
A, $\vec{A}$	end point of an edge [cf.: B, M, κ_{AB}]	[I.2.3.2]
A	area [i.e., dA]	
$[A]$, $[A_k]^{4x4}$, A_k	reference (X_o) to local (X') coordinate transformation (A_k = transformation for k-th panel or subpanel, depending on context)	[5.2, E.3]
A_i	i-th abutment in an abutment intersection	[F.5]
$A(G)$	adjacency matrix of a graph G	[F.5]
$[A]$, A	Left hand side (AIC) matrix	[5.8.2]
A_{ij}	submatrix of AIC matrix A	[L.2]
$A^{(i,j)}$	partially reduced AIC matrix, after stage (i,j) of factorization	[L.2]
[AIC], AIC	aerodynamic influence coefficient matrix	[3.3, 5.7]

Variants: (AIC^{ij}_I, AIC entry for λ_I, symmetry condition (i,j), [K.6])

(AIC_{KP}, AIC_{UP}, [5.7.3])

(AIC_{NU}, $AIC_{U,1}$, $AIC_{U,2}$, $AIC_{U,3}$ [5.7.5])

$\hat{A}_i$	Intermediate matrix used in $PSPL^D$ calculation	[I.3.1]
A	a 2x2 hyperbolic skew	[J.5]
b	generic right hand side term for a boundary condition Variants: ($\vec{b}$, vector of right hand side terms, [5.7]) ($\hat{b}^{ij}_{\alpha}$, $\vec{b}$ for symmetry condition (i,j), solution index α, [L.0])	[5.4]
b, $\vec{b}$	fundamental integrals in PIC computation	[J.5]
b_i	ξ-coefficient of L_i, linear basis function on a triangle	[I.2]
B, $\vec{B}$	end point of an edge [cf.: A, M, κ_{AB}]	[I.2.3.2]
[B]	fundamental integrals in PIC matrix	[J.5]
[B]	right hand side matrix containing constraint vectors for multiple solutions	[5.8]
[B]	dual compressibility metric matrix, compressibility axis coordinates Variants: (B, same as [B], [5.2]) (B_o, [B_o], reference coordinates, [5.2]) ($\bar{B}$, [$\bar{B}$], scaled coordinates [E.3]) (B', [B'], local coordinates [E.3])	[5.2]
B^S	source outer spline matrix Variant: ($\overline{B^S}$, extended to all N λ_I, [5.7])	[5.5, I.1]
B^D	doublet outer spline matrix Variant: ($\overline{B^D}$, extended to all N λ_I, [5.7])	[5.5, I.1]
$B_i(Q)$, $B_i'(Q)$	quadratic interpolatary basis functions on a triangle	[I.2]
[BL]	bilinear generalized Vandermonde matrix	[I.1]
$\hat{c}_o$	compressibility axis, reference coordinates Variant: ($\hat{c}$: compressibility axis coordinates [5.2])	[5.2, E.3]

c_A, c_D	average and difference potential coefficients	[5.4.2.5]
$\vec{c}(\tau)$	a curve on the singularity surface S	[K.1]
c_i	n-coefficient of L_i, linear basis function on a triangle	[I.2]
$c_{4,i}$	coefficients of μ_i in evaluation of $\tilde{\mu}(s,t)$ at C_4^*	[I.3]
C_{ij}	mean panel moment integrals	[I.4]
C_v	ratio of specific heats at constant volume	[2.2]
C_p	pressure coefficient Variants: (C_p^{lin}, linear C_p, [H.2.4]) (ΔC_p, pressure jump, $C_{p,upper} - C_{p,lower}$) ($C_{p,vac}$, vacuum value of C_p, [N])	[5.9.2]
$\vec{C}_F$	force coefficient vector	[O.1]
$\vec{C}_M$, $\vec{C}_M'$	moment coefficient vector ($\vec{C}_M'$: referred to an alternate origin)	[O.1]
$C^0(S)$, $C^{-1}(S)$, $C^1(S)$	Continuity classes for functions defined on S	[B.3]
$\vec{C}_4$, $\vec{C}_4^*$	half panel #4 center ($\vec{C}_4$) and corresponding point on the hyperbolic paraboloidal panel ($\vec{C}_4^*$)	[I.3]
C(Q)	a cubic basis function on a triangle	[I.2]
C^i, C_1, C^+, C^-	regions of space when one plane of symmetry is present	[K.3]
C^{ij}, C_1^j, C_2^i	regions of space when two planes of symmetry are present. Variants: (C^{++}, C^{+-} etc., C_1^+, C_1^-, C_2^+, C_2^-)	[K.4]
C_i	i-th corner in an abutment intersection	[F.5]
C_h	Mach disk on a superinclined panel	[J.4]
C_Θ	winding number coefficient for PIC integrals	[J.4]

$[C]$	compressibility metric matrix, compressibility axis coordinates Variants: (C, same as $[C]$, [5.2]) (C_o, $[C_o]$, reference coordinates, [5.2]) ($\bar{C}$, $[\bar{C}]$, scaled coordinates, [E.3]) (C', $[C']$, local coordinates, [E.3])	[5.2]
d	prefix: differential (i.e., $d\vec{\ell}$, dA, dS, etc.)	
$\hat{d}$	design direction	[C.1]
d	distance from a point to a line Examples: $d(\vec{s},E)$ = distance from $\vec{s}$ to edge E $d(\vec{s}, T_i)$ = distance from $\vec{s}$ to edge segment T_i	[F.3]
det	determinant	
D_p	Domain of dependence for control point p	[5.2, J]
$[D]$	Full doublet panel influence matrix, without origin shift. $[D_o]$ (cf. [J.6.6]) includes the origin shift.	[J.6.4.3]
$[D]$	A local coordinate metric matrix	[E.3]
$[DI]$	A diagonal matrix associated with known singularity parameters	[5.7.3]
e	internal energy per unit mass	[2.2]
$\hat{e}_1$, $\hat{e}_2$, $\hat{e}_3$, $\hat{e}_i$	natural unit vectors in R^N	
e_A, e_D, e_U, e_L	average, difference, upper and lower $\hat{n}.\vec{v}$ coefficients for the general boundary condition	[H.1]
E, E_i	a network edge, the i-th network edge in an abutment	[F.3]
E, E_k	a panel or subpanel edge	[I.4, J]
$\tilde{E}$	the image of a panel or subpanel edge under a hyperbolic skew transformation	[J.5]
ΔE	Energy added by incremental onset flow	

$\vec{f}$, f_i	Body force per unit mass, newtons/kg	[2.1]
$f(\rho,p,T)$	Equation of state	[2.1]
f_-, f_o, f_+	Lagrange interpolation functions of the edge variable v, defined on an edge	[J.10]
F	A fundamental integral in the PIC calculation	[J.6]
$\vec{F}$	Total force on the configuration	[5.9]
$\vec{F}$	Generic vector field	[B.3]
FFM_0^D, FFM_1^D	Far field moments used in post processing	[I.4, O.2]
g, g_k	Compressible distance from a control point projection to a panel edge	[J.7, J.8]
$\vec{G}$	Generic vector field	[B.3]
G	a graph	[F.5]
[G]	Intermediate matrix used in constructing the half panel doublet spline matrix	[I.3]
[G]	Transformation from Prandtl-Glauert scaled coordinates to local coordinates	[E.3]
[G]	2x2 local compressible metric matrix, used to define the pseudo inner product <.,.>	[J]
G_j^K	Kernel moments used to calculate Ψ_α	[J.9]
$G_{ij}^{(k)}$	Intermediate quantity in calculation of C_{ij}	[I.4.3]
h	height of the control point above the plane of the panel, local coordinates	[J.4]
h_2	quadratic function fitting 6 data values on a triangle	[I.2]
h_3	cubic function fitting 7 data values on a triangle	[I.2]
H_i	hypothetical location of a control point on the i-th network of an abutment or abutment intersection	[G]
$H_{\alpha\beta}$, $\overline{H}_{i\alpha\beta}$	panel far field moments	[I.4, J.9]

H_α, $\bar{H}_{i\alpha}$	far field estimates of certain panel integrals	[J.9]
H_j^K	Kernel moments for $(1/R^3)$	[J.9]
H_h, $\tilde{H}_h$	Mach hyperbola, before and after application of an edge's skew transformation	[J.5]
H^{ij}	2x2 matrix used for symmetrization of potential ϕ, velocity $\vec{v}$, and boundary conditions	[K.3]
$HPINT^S$, $HPINT^D$	half panel PIC integral matrices	[J.1]
$HPSPL^S$, $HPSPL^D$	half panel spline matrices	[I.3, J.1]
I	row index	
I, I_k	edge function, edge function associated with edge k	[J.7]
$I(\psi)$, $I(\chi)$	edge integrals of functions ψ, χ	[J.7]
$\hat{I}$	rationalized form of I_k, edge function	[J.8]
J	column index	
J, J_k	Jacobian area ratio, dS'/dS_o	[E.3]
J_m	Mean panel jacobian area ratio $dS_m'/dS_{o,m}$	[J.9]
J	hyperbolic paraboloidal panel jacobian matrix, $\partial(\xi,n)/\partial(s,t)$	[I.3]
J	Panel function	[J.4]
$J(\psi)$, $J(\chi)$	Panel integrals of functions ψ, χ	[J.7]
J_k	Edge contribution to panel integral	[J.6]
k	Coefficient of heat conductivity	[2.1]
k	subscript, superscript, index of summation	[K]
k_D, k_S	number of doublet and source singularity parameters (global) in the neighborhood of a panel	[4.2]
k_N^-, k_N^+	previous and next edge number on network N at an abutment intersection	[F.5]
[K]	matrix describing the evaluation of $\tilde{\mu}(s,t)$ at seven points [$HPSPL^D$ calculation]	[I.3]

$\hat{K}$	rationalized quantity used in evaluation of $I(\chi)$	[J.8]
$d\vec{\ell}$	element of arc length	[B.3]
ℓ	subscript, superscript, index of summation	[K]
[L], L	lower triangular matrix factor	[5.8, L]
L_R	reference length	[O]
$L_i(Q)$	basis function for linear interpolation on a triangle	[I.2]
[LSQ]	pseudo inverse for a least squares problem	[I.5]
[LINV]	matrix giving an edge's line vortex contribution to a panel influence coefficient	[J.10]
m_I, m_i	global basis functions for the doublet distribution	[3.3]
$m_{2,i}$	coefficients of μ_i in the evaluation of $\tilde{\mu}(s,t)$at $\vec{M}_2^*$	[I.3]
mod	mod(i,j) = the remainder of i/j	
$\vec{M}_2$, $\vec{M}_2^*$	edge midpoint common to half panel 2 and half panel 4. $\vec{M}_2^*$ is the corresponding point on the hyperbolic paraboloidal panel	[I.3]
$\vec{M}$	total moment (about some specified point) on the configuration (newton-meters)	[5.9]
M_∞, M_ℓ	freestream Mach number, local Mach number	[2.3]
M, $\vec{M}$	midpoint of an edge	[K.2.3.2]
M	number of rows of panel corner points in a network	[5.1]
[M]	matrix giving quadratic doublet coefficients	[J.6]
$\mathcal{m}$	2x2x2 tensor giving cubic doublet coefficients	[J.6]
M	subpanel center	[I.3]
$\hat{n}$	unit normal vector, pointing out of the singularity surface, into the fluid (components: n_x, n_y, n_z)	[3.2]

$\tilde{n}$	conormal vector, also denoted $\vec{\nu}$	[5.2]
$\vec{n}$	edge normal, normalized with pseudo inner product, <.,.>. (Components: n_ξ, n_η)	[J.5]
n_x, n_y, n_z	components of $\hat{n}$, the normal to S	[5.2]
n_ξ, n_η	components of $\vec{n}$, the 2-D edge normal in local coordinates	[J.5]
N	number of columns of panel corner points in a network	[5.1]
N	number of singularity parameters λ_I in a configuration, or in the principal image of the configuration [K]. Sometimes denotes the number of unknown singularity parameters.	[3.3]
N_{ES}	number of network edge segments in a configuration	[F.3]
N	generic upper limit of a sum	
$NCPM_1$, $NCPM_2$	moment matrices used in post processing	[I.4]
p, p_∞	pressure, freestream pressure (newton/m^2)	[2.1]
$\vec{p}$	field point, control point	
$\vec{p}^-$, $\vec{p}^+$	points just below ($\vec{p}^-$) and just above ($\vec{p}^+$) a control point	
p	number of known singularity parameters	[5.7.3]
p	priority used in assignment of matching conditions at an abutment intersection	[F.5]
p_i	size of the i-th partition in the blocking of the AIC matrix	[L.2]
ph	phase function. ph(x,y) = Arg(x+iy)	[J.4]
phh	hyperbolic phase function. phh(x,y) = (1/2)log[(x+y)/(x-y)]	[J.5]
$P(\phi)$	upper limit of integration in cylindrical or hyperbolic cylindrical coordinates	[J.4, J.5]
P	field point or control point (see $\vec{p}$)	[3.2]
$\vec{P}$	vector of coordinates of the point P (see $\vec{p}$)	

$\vec{P}(t)$	streamline parameterized by t	[5.9]
$\vec{P}^*$	a point on the line emanating upstream from a control point and piercing a panel	[J.3]
P_i	panel defining point, $1 \leq i \leq 9$	[5.5]
P_{AI}	the location of an abutment intersection	[F.5]
PIC	panel influence coefficient matrix	[5.6]
$PSPL^S$, $PSPL^D$	source and doublet panel splines	[I.3]
q	heat generation (per unit mass) added to fluid	[2.2]
$\vec{q}$	source point or panel point	[K]
q	edge type indicator, -1 for supersonic, +1 for subsonic edges	[J.5]
$\vec{q}_o$, $\vec{q}_s$, $\vec{q}_t$, $\vec{q}_{st}$	panel center and bilinear coefficients for the hyperbolic paraboloidal panel	[I.3]
$\vec{q}^i$, $\vec{q}^{ij}$	images of a source point or panel point Also: $\vec{q}^+$, $\vec{q}^-$, $\vec{q}^{++}$, $\vec{q}^{+-}$, $\vec{q}^{-+}$, $\vec{q}^{--}$	[K]
$\vec{q}(s,t)$, $\vec{q}_m(s,t)$	hyperbolic paraboloidal (H-P) panel, mean plane H-P panel	[I.3]
Q	source point or panel point	[3.2]
$\vec{Q}$	vector of coordinates of the point Q	
$\Delta\vec{Q}$	panel point deviation from panel center. $\Delta\vec{Q} = \vec{Q} - \vec{Q}_o$	[5.6.3]
$\vec{Q}_o$	panel center, expansion point for far field influence coefficients	[5.6.3]
Q_i, $\vec{Q}_i$	corners of a triangle, i = 1,2,3	[I.2]
Q_i', $\vec{Q}_i'$	triangle edge midpoints. Q_i' is opposite Q_i	[I.2]
$\vec{Q}'$	panel point, local coordinates	[J.9]
Q_k, $\bar{Q}_k$	corner phase functions for evaluation of the panel function J.	[J.8]

Q, Q^+, Q^-	Q = a panel, Q^+ = principal image of a panel, Q^- = reflected image of a panel	[K.5]
r	panel type indicator. $r = \text{sign}\,(\hat{n}\cdot\bar{n})$. (+1, subinclined; -1, superinclined)	[5.2]
R	gas constant, joule/(kg ^{o}K)	[2.1]
R, $R(\vec{p},\vec{q})$	compressible distance between $\vec{p}$ and $\vec{q}$	[5.2]
$\vec{R}$	control point recession vector	[G]
R_o	compressible distance from the control point to the panel center	[4.2.2.2]
R_1, R_2	reflection matrices for the first and second planes of symmetry	[K.2]
R^i, R^+, R^-	reflection matrices associated with various images when one plane of symmetry is present	[K.3]
R^{ij}, R^{++}, R^{+-}, etc.	reflection matrices associated with various images when two planes of symmetry are present	[K.4]
$\vec{R}$	$\vec{Q} - \vec{P}$, vector from field point to source point	
$\Delta\vec{R}$	$\Delta\vec{R} = \vec{R}^+ - \vec{R}^-$ = change in $\vec{R}$ along an edge	[J.3]
$R(\Sigma)$	radius of a panel Σ	[J.3]
$R_x(\alpha)$, $R_y(\alpha)$, $R_z(\alpha)$	rotation matrices of angle α about the x, y and z axes	[E.3]
$R_k(v)$	value of R on edge E_k as a function of v, the edge variable	[J.4]
s	flow type indicator, $\text{sign}(1 - M_\infty^2)$	[3.1]
s_i, s_I	global basis function for the source distribution	[3.3]
s_k	$= \pm 1$, sign of edge orientation relative to an abutment's orientation	[B.3]
s, $\tilde{s}$	first local coordinate before (s) and after ($\tilde{s}$) the application of a hyperbolic skew	[J.5]

$\vec{s}$	a point on a network edge	[F.3]
$\vec{s}$	vector pointing into the network interior	[F.5.2]
ds	differential element of arclength	[I.4]
s,s*	first isoparametric coordinate on a hyperbolic paraboloidal panel	[I.3]
S	the singularity surface across which ϕ and ϕ_n are allowed to jump	[3.2]
∂S	boundary of S	[B.3]
S_1	the component of S lying in the first plane of symmetry	[K.3]
S_2	the component of S lying in the second plane of symmetry	[K.4]
$S_1^{\pm}$, $S_2^{\pm}$, S_1^j, S_2^i	components of S lying in the first or second plane of symmetry (1 or 2) and in the principal (+) or reflected (-) image	[K.4]
$S^{\pm}$, S^+, S^-, S^i	components of S lying away from the symmetry plane and in the principal (+) or reflected (-) image	[K.3]
S^{ij}, S^{++}, S^{+-}, etc.	components of S lying away from either symmetry plane and in the various components of space, C^{++}, C^{+-}, etc.	[K.4]
dS_o	element of surface area in reference coordinates, X_o	[E.3]
dS'	element of surface area in local coordinates, X'	[E.3]
S	a sphere surrounding an abutment intersection point, P_{AI}	[F.5]
$\hat{S}$	a skew symmetric matrix used in constructing $[PSPL^D]$.	[I.3]
[S]	a hyperbolic skew used to build the reference to local coordinate transformation matrix	[E]
[S]	Full source panel influence matrix, without origin shift. $[S_o]$ (cf. [J.6.6]) includes the origin shift.	[J.6.4.3]

S_R	reference surface area	[0.1]
SP^S , SP^D	source and doublet spline vectors	[I.1]
$[SPSPL_i^S]$, $[SPSPL_i^D]$	source and doublet subpanel spline matrices for i-th subpanel	[5.5]
$[SPINT^S]$, $[SPINT^D]$	source and doublet panel influence integrals	[J.1]
t	time, seconds	[2.1]
t	edge parameter	[F.6]
$\vec{t}$	vector tangent to surface	[E.1]
$\vec{t}$	two-dimensional edge tangent	[J.4, J.5]
$\hat{t}$	unit vector tangent to edge	[I.4]
t_ξ, t_η	components of $\vec{t}$, the two dimensional edge tangent	[J.5]
t, $\tilde{t}$	second local coordinate on a panel, before (t) and after ($\tilde{t}$) the application of a hyperbolic skew	[J.5]
$\vec{t}_A$, $\vec{t}_D$	coefficients of the average and difference of the velocity in the standard boundary condition	[5.6]
T	temperature, degrees Kelvin	[2.1]
T_i	edge segment	[F.3]
T	a tree (graph theory concept)	[F.5]
T_k	subpanel k of a standard panel	[I.2]
$[T]$	matrix used for cubic interpolation in the construction of $[HPSPL^D]$	[I.3.2]
T_S, T_D	source and doublet PIC origin shift transformations	[J.6.6]
T	a 2x2x2 tensor of rank 3	[J.6.4.2]
$\lfloor T_4 \rfloor$	the rearrangement of the entries of the 2x2x2 tensor T as a 4-vector	[J.6.4.2]

$T_{i,j}$	the transformation associated with stage (i,j) of the out-of-core factorization	[L.2]
(u,v,w)	components of perturbation velocity in a coordinate system whose x-axis is aligned with the freestream or uniform onset flow	[2.3]
$\hat{u}_o$	unit vector perpendicular to the panel normal normal and the compressibility axis	[5.2]
U, [U]	an upper triangular matrix	[5.8, L.2]
$\vec{U}_\infty$, $\vec{U}_{\infty,\alpha}$	uniform onset flow. $\vec{U}_{\infty,\alpha}$ refers to the uniform onset flow for solution index α	[L.1]
$\vec{U}_o$, $\vec{U}^{ij}_{o,\alpha}$	total onset flow. $\vec{U}^{ij}_{o,\alpha}$ refers to solution index α and symmetry image (i,j)	[L.1]
$\Delta\vec{U}$, $\Delta\vec{U}^{ij}_\alpha$	incremental onset flow (user specified). $\Delta\vec{U}^{ij}_\alpha$ refers to solution index α and symmetry image (i,j)	[L.1]
U	a generic function represented via Green's third identity	[3.2]
$\vec{v}$, v_i	$\vec{v}$ is the perturbation velocity vector having components v_i Variant: $\vec{v}^{ij}$ = velocity in symmetry image (i,j)	[2.3, K.3]
$\hat{v}$, $\hat{v}^{ij}$, $\hat{v}^{SS}$ etc.	Various symmetrized velocity fields $\hat{v}^{+}=\hat{v}^{S}$ = symmetric part of $\vec{v}$ $\hat{v}^{-}=\hat{v}^{A}$ = antisymmetric part of $\vec{v}$ $\hat{v}^{++}=\hat{v}^{SS}$ = $\vec{v}$, symmetrized w.r.t. 1-st and 2nd planes of symmetry $\vec{v}^{+-}=\hat{v}^{SA}$ = symmetric w.r.t. 1-st POS antisymmetric w.r.t 2-nd POS $\hat{v}^{--}=\hat{v}^{AA}$ $\hat{v}^{-+}=\vec{v}^{AS}$	[K.3, K.4]
$\vec{v}_S$, $\vec{v}_D$	source induced component of velocity ($\vec{v}_S$) and doublet induced component of velocity ($\vec{v}_D$)	[B.3, J.1.1]

$\vec{v}_D^*$	regular part of $\vec{v}_D$, excluding the line vortex part	[B.3]
v	local edge coordinate	[J.4, J.5]
$\hat{v}_o$	unit vector perpendicular to $\hat{u}_o$ and $\hat{n}$, used to construct the reference to local coordinate transformation	[5.2]
$\vec{v}_\xi$, $\vec{v}_\eta$, $\vec{v}_\zeta$	basis vectors used to define a local coordinate system for spline vector computation	[I.1]
v_{ij}	matrix entries of an elementary column transformation matrix V	[L.2]
V	a region of space	[3.2]
$\vec{V}$, V_i	total velocity, components of total velocity	[2.1]
$\vec{V}_\infty$	freestream velocity	[3.1, 5.4]
$\vec{V}_\sigma(\vec{p},s)$	source velocity functional giving the source velocity at $\vec{p}$ induced by the source distribution $s(\vec{q})$	[K.4]
$\vec{V}_\mu(\vec{p},m)$	doublet velocity functional giving the doublet velocity at $\vec{p}$ induced by the doublet distribution $m(\vec{q})$	[K.4]
$\vec{V}^{Q\pm}$, $\vec{V}_\sigma^{Q\pm}$, $\vec{V}_\mu^{Q\pm}$	velocity functionals associated with the principal (Q^+) and reflected (Q^-) image of a panel	[5.7, K.5]
$\vec{V}_{1,\sigma}$ $\vec{V}_{1,\mu}$ $\vec{V}_{1,\sigma}^{Q}$ $\vec{V}_{1,\mu}^{Q}$, $\vec{V}_{1,\sigma}^{Q\pm}$, $\vec{V}_{1,\mu}^{Q\pm}$	velocity functionals associated with panels lying in the first plane of symmetry that may be reflected in a second plane of symmetry ($Q^\pm$)	[5.7, K.3, K.5]
$\vec{V}_{2,\sigma}$ $\vec{V}_{2,\mu}$ $\vec{V}_{2,\sigma}^{Q\pm}$ $\vec{V}_{2,\mu}^{Q\pm}$	velocity functionals associated with panels lying in the second plane of symmetry	[5.7, K.4, K.5]
$\vec{V}_\sigma^*$	total source velocity functional (includes integrals over the full principal image of S)	[K.5]

$\vec{V}^*_\mu$	total doublet velocity functional	[K.5]
$\vec{V}(\vec{P}(t))$	total velocity at $\vec{P}(t)$	[5.9.5, P.2]
V_x	total velocity in the compressibility axis direction	[5.9.3]
V_x'	total corrected velocity in the compressibility axis direction	[5.9.3]
V	An elementary transformation used in the factorization of the AIC matrix	[L.2]
V_c	critical speed	[N.2.4.2]
[VIC], $[VIC^i]$ $[VIC^{ij}]$	A velocity influence coefficient matrix [VIC], and various symmetrizations of the velocity influence coefficients	[5.7, K.5]
$\overrightarrow{VIC}^i_I$, $\overrightarrow{VIC}^{ij}_I$	the velocity influence 3-vector corresponding to symmetrized singularity parameter $\hat{\lambda}^i_I$ or $\hat{\lambda}^{ij}_I$	[K.5]
$\vec{w}$, w_i	$\vec{w}$ is the perturbation mass flux vector having components w_i	[5.4]
$\vec{w}_U$, $\vec{w}_L$, $\vec{w}_A$, $\vec{w}_D$	upper, lower, average and difference components of perturbation mass flux	[5.4, H.1]
w_i	a weighting factor used in a least squares fitting procedure	[I.5]
$\vec{W}$, W_i	$\vec{W}$ is the total linearized mass flux vector having components W_i	[5.4]
W_x	x-component of total mass flux $\vec{W}$	[5.9.3]
$\vec{W}(\vec{P}(t))$	total linearized mass flux evaluated at $\vec{P}(t)$	[5.9.5, P.2]
$\vec{W}_1$, $\vec{W}_2$, $\vec{W}_3$	basis vectors for skew coordinate transformation calculation	[J.2]
$\vec{W}_\alpha$	far field vector panel integral	[J.9]
$\lfloor WIC \rfloor$	normal mass flux influence coefficient row vector	
$\vec{x}$	position vector in R^3	[2.1]

x_i, x_1, x_2, x_3	Cartesian coordinates of $\vec{x}$ in R^3	[2.1]
$(x_o\ y_o\ z_o)$	reference coordinates	[5.2]
(x,y,z)	compressibility axis coordinates	[2.3]
$(\bar{x},\bar{y},\bar{z})$	Prandtl-Glauert scaled coordinates	[3.1]
(x',y',z')	local coordinates; several local coordinate systems are used in appendices I and J	[5.2]
x_n	edge normal distance	[5.9.4, 0.3]
$\bar{x}$	the x coordinate after application of a hyperbolic skew	[J.5]
X_o	the reference coordinate system	[E.0]
X	the compressibility axis coordinate system	[E.0]
$\bar{X}$	the Prandtl-Glauert scaled coordinate system	[E.0]
X'	a panel's local coordinate system	[E.0]
$[X]$	a matrix to be computed by solving a system of linear equations	[5.8]
X_k, Y_k	x and y arguments for the phase function (ph(x,y)), used in the calculation of the panel function components J_k	[J.8]
$\bar{y}$	the y coordinate after application of a hyperbolic skew	[J.5]
y_o, y, $\bar{y}$, y'	see, respectively, x_o, x, $\bar{x}$, x'	[2.3, 3.1, 5.2]
$[Y]$	intermediate matrix in the process of solving the AIC equation	[5.8]
Y_k	see X_k	[J.8]
z_o, z, $\bar{z}$, z'	see, respectively, x_o, x, $\bar{x}$, x'	[2.3, 3.1, 5.2]
Z	argument for ϕ_q, the edge integral primitive	[J.8]

Greek Symbols

α	angle of attack, radians	[H.2]
α_c	compressibility axis angle of attack, radians	[5.2, E.0]
α	downstream parameter used in abutment intersection processing	[F.5]
α	solution index	[L.0, L.1]
β	compressibility scale factor, $\lvert 1 - M_\infty^2 \rvert^{1/2}$	[3.1]
β	angle of sideslip, radians	[H.2]
β_c	compressibility axis angle of sideslip, radians	[5.2, E.0]
β_n	edge normal compressibility factor	[5.9.4, O.3]
β, β_α^{ij}	generic right hand side term (β) , right hand side term associated with solution index α, symmetry image (i,j)	[L.0, L.1]
γ	ratio of specific heats of a gas	[2.4]
$\vec{\gamma}$	surface vorticity	[N.5]
$\llcorner\gamma_4\lrcorner$, $\llcorner\gamma_5\lrcorner$	row vectors associated with spline construction	[I.1.5]
Γ	rotation matrix specified by the user	[O.4]
Γ_c	rotation matrix for the reference to compressibility coordinate transformation	[5.2]
δ	quantity used in the calculation of recession vectors	[G.0]
δ_{ij}, δ^{ij}	Kronecker deltas	
Δ_i	i-th subpanel, i=1(1)8	[5.6]
ε	user defined tolerance distance for edge matching	[F.3]
ε	small quantity whose higher powers may be neglected	[5.6.3 et. al.]
ε_{ijk}	the permutation symbol	[B.3]

ζ	third coordinate of a source point, reference coordinates	[5.2]
ζ, ζ'	third local coordinate of a source point	[5.2]
η	second coordinate of a source point, reference coordinates	[5.2]
η, η'	second local coordinate of a source point	[5.2]
$\Delta\eta_k$	change in η along edge k	[I.4]
θ	generic quantity to be matched by a matching condition of the form $\sum s_k \theta_k = 0$, ($\theta = \sigma$, μ or $\vec{t}.\Delta\vec{v}$)	[M.D., Sec. 5]
θIC	influence coefficients associated with a matched quantity θ	[M.D., Sec. 5]
κ, $\varkappa$	4π for subsonic flow, 2π for supersonic flow	[5.2]
κ, $\varkappa$	quantity associated with a quadratic function defined on an edge. Alternatives: $\bar{\kappa}_{58}$, $\bar{\kappa}_{85}$, κ_{AB}	[I.2]
λ_i, λ_I, $\vec{\lambda}$	global singularity parameters (λ_i, λ_I) and the vector containing them ($\vec{\lambda}$)	[3.3, 5.7.4]
λ_I^i, λ_I^{ij}	global singularity parameters associated with symmetry image (i), or (i,j) Alternatives: λ_I^+, λ_I^-, λ_I^S, λ_I^A, λ_I^{SS} etc.	[K, L]
$\vec{\lambda}^i$ $\vec{\lambda}^{ij}$, $\{\lambda^i\}$, $\{\lambda^{ij}\}$	Vectors of global singularity parameters associated with various symmetry images	[K, L]
$\hat{\lambda}_I^i$, $\hat{\lambda}_I^{ij}$, $\hat{\lambda}^i$, $\hat{\lambda}^{ij}$	Symmetrized global singularity parameters and vectors corresponding to λ_I^i, λ_I^{ij}, $\vec{\lambda}^i$, $\vec{\lambda}^{ij}$	[K, L]
$\vec{\lambda}_\alpha^{ij}$, $\{\lambda_\alpha^{ij}\}$	$\vec{\lambda}^{ij}$ for solution index α	[L]
$\hat{\lambda}_\alpha^{ij}$, $\{\hat{\lambda}_\alpha^{ij}\}$	$\hat{\lambda}^{ij}$ for solution index α (symmetrized singularity vectors)	[L]
$\vec{\lambda}_1$, $\vec{\lambda}_2$, $\vec{\lambda}_3$, $\vec{\lambda}_4$	$\vec{\lambda}$ for the four images of the configuration. Equivalent to $\vec{\lambda}^{++}$, $\vec{\lambda}^{-+}$, $\vec{\lambda}^{--}$, $\vec{\lambda}^{+-}$, respectively	[M]

λ_i^S , i=1, ... k_s	global source parameters defining a panel's source distribution. Each λ_i^S corresponds to a column of B^S	[5.5.1]
λ_i^D , i=1, ... k_D	global doublet parameters defining a panel's doublet distribution. Each λ_i^D corresponds to a column of B^D	[5.5.1]
$[\Lambda]$	matrix containing singularity parameter vectors to be determined by solving an AIC equation	[5.7.4]
Λ	sweep angle for the leading edge of a wing	[0.3]
μ, $\mu(\vec{q})$	doublet strength, doublet distribution function	[3.2]
$\mu_o, \mu_\xi, \mu_\eta, \mu_{\xi\xi}, \mu_{\xi\eta}, \mu_{\eta\eta}, \mu_{\xi\xi\xi}, \mu_{\xi\xi\eta}, \mu_{\xi\eta\eta}, \mu_{\eta\eta\eta}$	polynomial coefficients of μ in local coordinates	[5.5]
μ^i, μ^{ij}	the function μ restricted to various symmetry images (i), (i,j) Variants: μ^+, μ^-, etc.	[K.3, K.4]
$\bar{\mu}^i$, $\bar{\mu}^{ij}$	the functions μ^i, μ^{ij} defined with respect to points in the principal image	[K.3, K,4]
$\hat{\mu}_1^A$, $\tilde{\mu}_2^{iA}$, $\tilde{\mu}_1^{Aj}$	the function μ restricted to panels lying in the first or second plane of symmetry	[K.3, K.4]
μ_1, μ_2, ... μ_9	the value of μ at nine canonical points on the panel	[5.5]
$\mu(\xi', \eta')$	doublet distribution function referred to local coordinates	[5.5]
$\vec{\mu}$	the two vector: $\begin{Bmatrix} \mu_\xi \\ \mu_\eta \end{Bmatrix}$	[J.6]
$\tilde{\mu}(s,t)$	the doublet distribution on a hyperbolic paraboloidal panel (isoparametric element) defined in terms of the coordinates of parameter space	[I.3.2]
$\mu_{x,\alpha}$, $\mu_{y,\alpha}$	coefficients of $(\partial\mu/\partial x)$, $(\partial\mu/\partial y)$ used for the far field PIC computation	[J.9]
$\hat{\mu}^i$, $\hat{\mu}^{ij}$	symmetrized doublet distributions	[K.3, K.4]
$\mu_{1,5}$, $\mu_{5,6}$, etc.	$\mu_{1,5}$ refers to the value of μ at the mid-point of the line connecting points 1 and 5 on the panel	[I.2]

μ_-, μ_o, μ_+	value of μ at the beginning, middle and end of some panel edge	[J.10]
$\vec{\nu}$	panel conormal, $\vec{\nu} = B\,\hat{n}$ (See $\tilde{n}$)	[5.2]
$\vec{\nu}$	edge conormal, $\vec{\nu} = G\,\vec{n}$	[J.6]
ξ, ξ'	first local coordinate of a source point	[5.2]
ξ	first coordinate of a source point, reference coordinates	[5.2]
$\Delta\xi_k$	the change in the value of ξ along edge k	[I.4]
π	the ratio of the circumference to the diameter of a circle	[3.2]
ρ	density of the fluid, kg/m^3	[2.1]
ρ_∞	density of fluid in freestream, kg/m^3	[5.9]
ρ	hyperbolic or circular radius of hyperbolic or circular cylindrical coordinates	[J.4, J.5]
$\vec{\rho}$, (ρ_1, ρ_2)	vector from control point projection to source point, local coordinates	[J.4, J.5]
$\vec{\rho}_i^-$, $\vec{\rho}_i^+$	values of $\vec{\rho}$ at beginning and end of edge i	[J.4, J.5]
σ, $\sigma(\vec{q})$	source strength, source distribution function	[3.2]
σ_o, σ_ξ, σ_η, $\sigma_{\xi\xi}$, $\sigma_{\xi\eta}$, $\sigma_{\eta\eta}$	polynomials coefficients of σ in local coordinates	[5.5]
σ^i, σ^{ij}	the function σ restricted to various symmetry images (i), (i,j) Variants: σ^+, σ^-, etc.	[K.3, K.4]
$\bar{\sigma}^i$, $\bar{\sigma}^{ij}$	the functions σ^i, σ^{ij} defined with respect to points in the principal image	[K.3, K.4]
$\hat{\sigma}_1^S$, $\tilde{\sigma}_2^{iS}$, $\tilde{\sigma}_2^{Sj}$	the function σ restricted to panels lying in the first or second plane of symmetry	[K.3, K.4]
σ_1, σ_2, σ_3, σ_4, σ_9	the value of σ at five canonical points on a panel	[5.5]
$\sigma(\xi',\eta')$	source distribution function referred to local coordinates	[5.5]

$\vec{\sigma}$	the two-vector: $\begin{bmatrix} \sigma_\xi \\ \sigma_\eta \end{bmatrix}$	[J.6]
$\hat{\sigma}^i$, $\hat{\sigma}^{ij}$	symmetrized source distributions	[K.3, K.4]
Σ	summation symbol	[2.1]
Σ, Σ_m	panel (Σ), mean panel (Σ_m)	[I.4]
Σ_i	surfaces involved in an abutment	[B.3]
$[\Sigma]$	2x2 matrix, $\begin{bmatrix} \sigma_{\xi\xi} & \sigma_{\xi\xi} \\ \sigma_{\xi\eta} & \sigma_{\eta\eta} \end{bmatrix}$ giving quadratic variation of $\sigma(\xi,\eta)$	[J.6]
τ_{ji}	stress tensor, newtons/m^2	[2.1]
τ	parameter for a line, $\tau \in [0,1]$	[I.4, K.1]
τ	edge normalization parameter. In some contexts, $\tau = \lvert [\hat{t}, \hat{t}] \rvert^{1/2}$, in others $\tau = \lvert \langle \vec{t}, \vec{t} \rangle \rvert^{1/2}$	[J.7, J.10]
τ_k	indicator for sgn (a_k)	[J.8]
ϕ, $\phi(\vec{p})$	perturbation potential function	[2.3]
$\phi^i(\vec{p})$, $\phi^{ij}(\vec{p})$	ϕ restricted to symmetry image (i) or (i,j) Variants: ϕ^+, ϕ^-, ϕ^{++}, ϕ^{+-}, etc.	
$\hat{\phi}^i(\vec{p})$, $\hat{\phi}^{ij}(\vec{p})$	symmetrized perturbation potential functions. Variants: $\hat{\phi}^S$, $\hat{\phi}^A$, $\hat{\phi}^+$, $\hat{\phi}^-$, $\hat{\phi}^{SS}$, $\hat{\phi}^{++}$, etc.	[K.3, K.4]
ϕ_U, ϕ_L, ϕ_A, ϕ_D	upper surface, lower surface, average and difference values of ϕ	[5.4]
ϕ	circular (or hyperbolic) phase	[J.4, J.5]
ϕ_k^-, ϕ_k^+	value of circular (or hyperbolic) phase at the beginning and end of a subpanel edge segment	[J.4, J.5]
ϕ_α, $\llcorner\phi_\alpha\lrcorner$	set of basis functions of local variables (ξ,η) defined on a panel. $\llcorner\phi_\alpha\lrcorner = \llcorner 1, \xi, \eta, \xi^2/2, \ldots \eta^3/6 \lrcorner$	[J.9]
ϕ_q, $\phi_q(Z)$	a form of the edge integral independent of q, the edge type	[J.8]

Φ	total potential	[2.3]
Φ_∞	potential for onset flow	[2.3]
$\Phi_\sigma(\vec{p},s)$	source potential functional giving the source potential at $\vec{p}$ induced by the source distribution $s(\vec{q})$	[K.3]
$\Phi_\mu(\vec{p},m)$	doublet potential functional giving the doublet potential at $\vec{p}$ induced by the doublet distribution $m(\vec{q})$	[K.3]
$\Phi^{Q\pm}$, $\Phi_\sigma^{Q\pm}$, $\Phi_\mu^{Q\pm}$	potential functionals associated with the principal (Q^+) and reflected (Q^-) image of a panel	[5.7, K.5]
$\Phi_{1,\sigma}$ $\Phi_{1,\mu}$ $\Phi_{1,\mu}^{Q}$ $\Phi_{1,\sigma}^{Q}$ $\Phi_{1,\sigma}^{Q\pm}$ $\Phi_{1,\mu}^{Q\pm}$	potential functionals associated with networks and panels lying in the first plane of symmetry that may be reflected in a second plane of symmetry	[5.7, K.3, K.5]
$\Phi_{2,\sigma}$, $\Phi_{2,\mu}$, $\Phi_{2,\sigma}^{Q}$, $\Phi_{2,\mu}^{Q}$, $\Phi_{2,\sigma}^{Q\pm}$, $\Phi_{2,\mu}^{Q\pm}$	potential functionals associated with networks and panels lying in the second plane of symmetry	[5.7, K.4, K.5]
Φ_σ^*	total source potential functional (includes integrals over the full principal image of S)	[K.5]
Φ_μ^*	total doublet potential functional	[K.5]
$\lfloor\Phi IC\rfloor$ $\lfloor\Phi IC^i\rfloor$ $\lfloor\Phi IC^{ij}\rfloor$	a potential influence coefficient row vector (ΦIC) and the various symmetry conditions of this	[5.7, K.5]
ΦIC_I, ΦIC_I^i, ΦIC_I^{ij}	potential influence coefficients associated with singularity parameters λ_I, $\hat{\lambda}_I^i$, $\hat{\lambda}_I^{ij}$	[K.5]
χ	hyperbolic angle	[J.5]
χ	the function $R(\vec{p},\vec{q}) = [\vec{p}-\vec{q},\ \vec{p}-\vec{q}]^{1/2}$	[J.6]
ψ	the fundamental kernel function, $\psi = 1/R$	[J.6]
Ψ_α	far field approximate integral associated with $\iint \psi\ \phi_\alpha\ d\xi\ d\eta$	[J.9]

$\vec{\omega}$, $\vec{\omega}_\alpha$	vectors describing strength and direction of the rotational onset flows	[H.3, L.1]
ω_-, ω_o, ω_+	integrals associated with line vortex influence coefficient generation	[J.10]

Subscripts

A	average of upper and lower
c	denotes compressibility or refers to the compressibility axis
D	difference of upper and lower (upper minus lower)
D	refers to quantities associated with μ, the doublet distribution
i,j,k,l	indices of vectors in R^3, e.g., v_i
i	index of a global singularity parameter, λ_i
I	index of a global singularity parameter, e.g., λ_I
KP	corresponding to known parameters
L	lower surface
NU	non-updatable
S	refers to quantities associated with σ, the source distribution
U	upper surface
U	updatable
UP	corresponding to unknown parameters
v	refers to constant volume quantities (c_v)
x,y,z,ξ,η,ζ	denotes partial differentiation, e.g., U_x, U_y, U_z
α	a solution index
α,β,γ	index subscripts
0	denotes reference coordinates
1,2,3,4	denotes images of real configuration (first image = input)
1	refers to first plane of symmetry
2	refers to a second order quantity, e.g., $C_{p,2}$
2	refers to second plane of symmetry
∞	refers to quantities associated with the far field

Superscripts

A	denotes antisymmetric part, e.g, $\hat{\phi}^A$
D	doublet, quantity pertaining to doublet strength
(i)	pertaining to i-th symmetrized matrix or vector, i = 1,2,3,4 (equivalent to SS, AS, AA, SA respectively)
i,j,k,l	superscripts in the index set {-1,1}, e.g., H^{ij}, H^{kl}
I	input, that is, defined by the user
S	source, quantity pertaining to source strength
S	denotes symmetric part, e.g., $\hat{\phi}^S$
T	matrix transpose
-T	inverse of transpose (same as transpose of inverse)
-	denotes Prandtl Glauert scaled coordinate system, e.g., $\bar{X}$
→	denotes a vector, e.g., $\vec{v}$
′	denotes local coordinate system, e.g., X'
′	image value, e.g., $\vec{p}'$
*	finite part of integral
~	denotes vector modified by application of metric matrix
~	denotes a partially symmetrized quantity, e.g., $\tilde{\sigma}_1^{Sj}$
^	denotes a fully symmetrized quantity
+	alias for +1 in the index set {+1,-1}; also denotes symmetric part or principal image
-	alias for -1 in the index set {+1,-1}; also denotes antisymmetric part or reflected image

Other Symbols

∂	denotes partial differentiation
∂	boundary of a region
∇, $\vec{\nabla}$	gradient operator
$\bar{\nabla}$	compressible gradient operator, see section B.1
∇^2	$= \vec{\nabla}\cdot\vec{\nabla}$ = Laplace operator
∇_p	gradient with respect to location of (control point) P
∇_Q	gradient with respect to location of (integration point) Q
$\vec{\nabla}_2$	gradient operator in two dimensions
∇x	curl operator
$(\ , \ )$	Euclidean inner product
$\{ \quad \}$	denotes a column vector or a three-index tensor
$\{ \ , \ \}$	dual compressible inner product, see equation (E.2.8)
$\llcorner \ \lrcorner$	denotes a row vector
$[\ ]$	denotes a matrix
$[\ ]_{ij}$	(i,j) entry of the matrix
$[\ , \ ]$	compressible inner product, see equation (E.2.4)
$[\ , \ ]_p$	positive definite compressible inner product, see equation (J.2.7)
$< \ , \ >$	pseudo-inner product, see equation (J.6.44)
$\cup$	union of sets of points
$\cap$	intersection of sets of points
$\int$	line integral
$\iint$	surface integral
$<<$	very much less than

$\mid$	qualifier symbol, read "such that." For example, the expression $\{ x \mid f(x) = 0\}$ is read, "the set of values x such that $f(x) = 0$."
∞	refers to far field quantities, e.g., Φ_∞
x	vector cross product operation
:	denotes contraction of two matrices, defined by equation (J.6.37)
:	qualifier symbols, read "such that." See remarks concerning " $\mid$ "
b.c.	boundary condition
c.p.	control point
s.p.	singularity parameter
Δ	used as a prefix, the jump in a quantity across S (e.g., $\Delta\vec{v} = \vec{v}_U - \vec{v}_L$)
det	determinant
$\approx$	approximately equal to

9.0 PAN AIR Engineering Glossary

This glossary defines the most commonly used engineering terms in the PAN AIR Theory and User's Documents. In general, all specialized terms (that is, terms whose meaning in the context of PAN AIR is different from their meaning in common usage) are included, as are standard engineering terms which are used in the PAN AIR engineering documents. Terms which relate to the computing aspects of PAN AIR are defined in a separate glossary, the PAN AIR computing glossary, which is contained in the maintenance document.

The format of the glossary is the following: Each term is followed by a list of principal references and a definition. The references give the section number where the item is discussed, preceded by a T for Theory Document, a U for User's Document, and an S for Summary Document.

ITEM	DEFINITION	REFERENCES
Abutment	A curve where two or more network edges (exactly or approximately) meet.	T-5.3, U-B.3.5
Abutment, empty space	An abutment involving only one network edge, which is thus a free edge.	T-F.2
Abutment intersection	A point where several abutments meet.	T-5.3, T-F.5
Abutments, overlapping	Two distinct user-defined abutments which involve the same portion of some network edge.	Program printout only
Abutments, pairwise	Abutments involving pairs of network edges. They are generated by the program whenever the distance between network edges is less than the tolerance distance.	T-F.2
Abutment parameterization	The assignment of a real number between zero and one to each panel corner or panel edge midpoint in an abutment. Zero is assigned to the starting point, one to the end point.	T-F.6
Abutment, program generated	An abutment generated by the program rather than defined by the user, involving any number of network edges, computed by analyzing pairwise abutments.	T-F.2
Abutment search, automatic	The process by which the program determines the set of all pairwise abutments.	T-F.3
Abutments, user-defined	Any abutment which the program user identifies.	T-F.2
Angle of attack, α	The angle of coordinate rotation about the y-axis; this appears in the coordinate transformation (rotation) matrices.	T-5.2, U-B.2.2
Angle of sideslip, β	The angle of coordinate rotation about the modified z-axis; this appears in coordinate transformation (rotation) matrices. Note: The effect of the orientation of the flow due to the specification of an angle of attack α and an angle of sideslip β corresponds to effect of rotating the configuration through the sideslip angle β, followed by a rotation through the angle of attack α.	T-5.2, U-B.2.2

ITEM	DEFINITION	REFERENCES
Area, reference	A user-defined scaling factor for the force and moment coefficient computation.	T-0.1, U-B.4.3
Axis system	A coordinate system in which the force and moment coefficients are expressed.	U-2.1.7, U-B.2.1
Axis system, body	An arbitrary user-defined coordinate system specified by means of Euler angles.	U-2.1.7, U-B.2.1
Axis system, reference	The reference coordinate system (that system in which user defines the configuration geometry).	U-2.1.7, U-B.2.1
Axis system, stability	The coordinate system conventionally used by stability and control engineers.	U-2.1.7, U-B.2.1
Axis system, wind	The coordinate system whose x-axis is aligned with uniform onset flow.	U-2.1.7, U-B.2.1

ITEM	DEFINITION	REFERENCES
Basis function	A function (of surface coordinates) which expresses the distribution due to a unit value of a single singularity parameter.	T-3.3, T-4.2.1
Boundary condition	A linear equation imposed at points on the configuration. This equation specifies some combination of the velocity potential and its derivatives.	T-2.5, T-3.2, T-3.3, T-4.2, T-5.4, T-H
Boundary surface	A surface, defined by the user, on which boundary conditions are imposed.	U-A.3
Boundary condition, aerodynamic	The specific form of boundary conditions for the aerodynamic problem in PAN AIR.	T-K.3
Boundary condition classes	The result of grouping the boundary conditions into five separate categories.	U-B.3.1
Boundary condition, closure	An equation specifying the total normal mass flux passing through a surface.	U-B.3.5, T-5.4, T-5.7.1, T-K.4
Boundary condition coefficient, average, $(\ )_A$	The average of upper and lower coefficients.	T-5.4, U-B.3.1
Boundary condition coefficient, difference, $(\ )_D$	The difference of upper and lower coefficients.	T-5.4, U-B.3.1
Boundary condition coefficients, upper (lower), $(\ )_U$, $(\ )_L$	Coefficients in the boundary condition equations corresponding to the upper (lower) side of the configuration.	T-5.4, U-B.3.1
Boundary condition, doublet (or edge) matching	A boundary condition specifying continuity of doublet strength across network edges.	T-5.3, T-5.7.1, T-F
Boundary condition hierarchy	An ordering of all admissible boundary conditions defined by the program. When two user-input boundary conditions are supplied and only one needs to be imposed, the program imposes that boundary condition which is higher on the hierarchy.	T-H.2.5

ITEM	DEFINITION	REFERENCES
Boundary condition, non-standard	Either a closure or a doublet matching boundary condition.	T-5.7.1, U-B.3.5
Boundary condition, right-hand-side	The specified value of the linear combination of the potential and its derivatives given by the boundary condition.	T-5.7.4
Boundary value problem	The combination of a partial differential (or integral) equation and boundary condition equations on a surface.	T-3.2, U-A.3
Boundary value problem, analysis	A boundary value problem with boundary conditions specifying the normal component of the velocity or mass flux.	U-3.3, U-B.3.2
Boundary value problem, design	A boundary value problem in which the boundary conditions specify the values of a tangential component of the velocity on a surface.	T-C, U-B.3.3
Boundary value problem, ill-posed	A boundary value problem which does not have a unique solution, or has no solution.	T-5.4, T-B.1, U-A.3
Boundary value problem, well-posed	A boundary value problem which has a unique solution.	U-A.3, T-3.2, T-5.4, T-B.1

ITEM	DEFINITION	REFERENCES
Column index	An integer which, in conjunction with the row index, describes the indicial location of a panel or a panel corner point. When panel corner points are defined by a user, all the points whose column indices are identical are input consecutively.	U-B.1.1, T-5.1
Compressibility direction	The direction of freestream flow in the Prandtl-Glauert equation. It is defined by the input terms "CALPHA" and "CBETA".	T-5.2, U-B.2.1
Compressibility vector	A unit vector in the compressibility direction.	T-5.2
Configuration	The surface (including possible wakes) on which flow boundary conditions are applied or the potential or velocity is discontinuous.	T-5.1
Configuration, image part	That part of a symmetric configuration which is not input by the user.	T-5.7.2, U-2.1.2
Configuration modeling	The process of representing an object, the flow field about which is of physical interest, as a collection of networks of panels on which boundary conditions are applied.	U-3.1, U-B.1, T-B.2, S-2.2
Configuration modeling, exact	The representation of a physical surface with networks of panels describing the exact physical location of the surface.	U-2.1.4, S-3.1.4
Configuration modeling, linearized	The representation of thickness or deflection of a physical surface by means of a mean surface paneling combined with the specification of boundary conditions which simulate the perturbation of the true surface geometry from the paneled surface.	U-2.1.4, S-3.1.4
Configuration, real part	The user-defined (that is, input) part of a symmetric configuration.	T-5.7.2, U-2.1.2
Configuration symmetry	Existence of one or two (perpendicular) planes through which the real part of configuration may be reflected to obtain the complete configuration.	T-5.7.2, U-2.1.2, U-B.2.3, S-3.1.2

ITEM	DEFINITION	REFERENCES
Configuration, thick	A configuration model in which one surface of a network is exposed to a flow field of interest, while the other surface is exposed to a flow field of no physical interest.	U-2.1.2, T-5.4.2.3, S-3.1.3
Configuration, thin	A configuration model in which both sides of a network are exposed to the flow field of interest. An example arises from the modeling of a wing as a single paneled surface.	U-2.1.2, T-5.4.2.2 S-3.1.3
Conormal vector, $\tilde{n}$	The vector obtained by a Mach number - dependent transformation of a unit surface normal vector. In compressibility coordinates, $\tilde{n} = (s\beta^2 n_x, n_y, n_z)$.	T-5.2, T-E.2
Constraint matrix	The right-hand-side term in a multiple system of boundary condition equations, that is, a system of equations with more than one right-hand-side vector.	T-5.7.4, T-L
Constraint number	The right-hand-side term of a single boundary condition equation.	T-3.2
Constraint vector	The right-hand-side term in a system of boundary condition equations with only one right-hand-side vector.	T-3.3, T-5.7.2
Continuity of doublet strength	The condition that a certain alternating sum of doublet strengths along an abutment is zero. This reduces to equality of doublet strengths if two network edges are involved. It permits the elimination of the line vortex term from the integral equation.	T-F
Continuity equation	The equation expressing conservation of mass in a small fluid element.	T-2.1
Control points	The points on a configuration surface at which up to two boundary conditions are applied.	T-3.3, T-5.4, T-G
Control point, center	A control point whose location is receded slightly from a panel center point.	T-G, U-B.3.4
Control point, corner	A control point whose location is receded slightly from a panel corner point at the end of an abutment.	T-G, U-B.3.4

ITEM	DEFINITION	REFERENCES
Control point, edge	A control point whose location is receded slightly from a panel edge midpoint on a network edge.	T-G, U-B.3.4
Control points, extra	Control points introduced by the subdivision of a network edge into more than one abutment.	T-5.4, T-G
Control point recession vector	A vector which defines the difference between the location of the control point and the location of the point from which it is receded.	T-G
Compressible gradient operator,	The gradient operator whose component in the freestream direction has been multiplied by $(1-M^2)$, where M is the freestream Mach number.	T-5.2
Coordinate system, compressibility, (x,y,z)	The coordinate system in which the preferred direction of the Prandtl-Glauert equation is the x-direction.	T-5.2, U-B.2.1
Coordinate system, local, (x', y', z')	A generally non-orthogonal coordinate system used to compute surface integrals for each subpanel, and generally distinct for each subpanel.	T-5.2
Coordinate system, reference, (x_o, y_o, z_o)	An arbitrary rectangular Cartesian coordinate system in which the program user defines the configuration geometry.	T-5.2, U-B.2.1
Coordinate system, scaled, (x,y,z)	The non-orthogonal coordinate system in which the Prandtl-Glauert equation transforms to either Laplace's equation or the wave equation.	T-3.1
Coordinate transformation	A linear transformation, defined by a matrix, which transforms point coordinates from one system to another.	T-E, U-B.2.1
Corrections, velocity	Optional semi-empirical corrections applied to the computed velocity.	U-B.4.1, T-5.9.3, T-N.3
Critical speed	The speed of sound at a particular point in the flow field.	U-B.4.2, T-N.2.4.2

ITEM	DEFINITION	REFERENCES
Data check	A run of PAN AIR in which the validity of the configuration geometry and boundary conditions is checked without a potential flow solution being attempted.	U-2.3.1
Differentiated influence coefficients	Matrices which define the derivative with respect to panel or control point location of the potential and velocity induced by a panel on a control point. (Not currently used in PAN AIR.)	T-C.3
Dirichlet problem	A boundary value problem consisting of the specification of potential on the boundary of a region of finite volume.	U-A.3
Discretization	A numerical method for solving an integral equation by replacing continuous quantities with discrete ones.	T-2.5, T-3.3
Displacement modeling	The representation of viscous effects such as a boundary layer by a perturbation of the boundary conditions (through the definition of a specified flow) or the surface paneling.	U-2.1.4
Design capability	The ability to specify a desired pressure distribution on a surface whose shape is only known approximately, and obtain a relofted surface which more nearly yields the desired pressure distribution.	U-2.2, T-C, S-1.0
Design, iterative	A multi-step design procedure in which the relofting algorithm makes use of "differentiated influence coefficients".	T-C.3
Design, linearized	A one-step design procedure in which a first order approximation to the desired surface is sufficient.	T-C.1
Design, sequential	A multi-step design procedure in which the relofting algorithm makes use of the normal mass flux which the program computes on the paneled surface.	T-C.2
Domain of dependence	The spatial domain in which disturbances are felt at a particular point P. It consists of all of space in subsonic flow and the upstream Mach cone from P in supersonic flow.	T-5.2

ITEM	DEFINITION	REFERENCES
Domain of influence	The domain in which disturbances at a point P are felt. It consists of all of space in subsonic flow, and the downstream Mach cone from P in supersonic flow.	T-Figure 5.4
Doublet distribution	One of the two unknown quantities in the fundamental integral equation.	T-3.2, U-A.2
Doublet matching	See boundary condition, doublet matching.	U-B.3.5
Doublet parameters	Unknown quantities on which the doublet distribution on the configuration depends.	T-5.5
Doublet strength	The value of the doublet distribution at a particular point. It is equal to the size of the jump in velocity potential across the surface.	T-3.1, U-A.2
Drag	The x-component of the force on the configuration in the wind axis system. PAN AIR computes drag on an impermeable surface by integrating the pressure distribution on the surface. The drag computed by PAN AIR does not include viscous effects.	U-2.1.7
Dual vector	A real-valued linear function on a vector space. Dual vectors transform according to equation (E.1.8e) of the Theory Document. Typical dual vectors are the gradient operator and the surface normal. A dual vector is also known as a covariant vector.	T-E.1
Dual vector, almost	A vector transforming according to equation (E.1.12) of the Theory Document.	T-E.1

ITEM	DEFINITION	REFERENCES
Edge conormal	A vector lying in the plane of the panel or subpanel whose "pseudo-inner product" with the edge tangent is zero.	T-J.5.1
Edge function	One of the two basic components (along with the panel function) of the entries of a PIC matrix. It is defined by an integral along a panel or subpanel edge.	T-J.7
Edge force computation	A special computation of forces on the edge of a thin surface, where the small perturbation assumptions may not be valid.	T-5.9.4, T-0.3, U-B.4.3
Edge matching	The problem of imposing appropriate conditions on singularity strength variation across network edges.	T-2.2, U-B.3.5
Edge, nearly sonic	A subpanel or panel edge for which the pseudo-inner product of the edge tangent with itself is approximately zero. Such an edge can only occur in supersonic flow, and is inclined to the flow at approximately the same angle as a Mach cone.	T-J.5.1
Edge, network	That collection of panel edges lying on one extreme of a network and thus not shared by two adjoining panels.	T-D.1, U-B.1.1
Edge normal	A vector lying in the plane of the panel or subpanel and perpendicular to the edge.	T-J.5.1
Edge, panel	A line segment connecting two panel corner points.	T-D.1
Edge, subsonic	A subpanel or panel edge for which the "pseudo-inner product" of the edge tangent with itself is positive.	T-J.5.1
Edge, supersonic	A subpanel or panel edge for which the pseudo-inner product of the edge tangent with itself is negative. Such an edge can only occur in supersonic flow, and is inclined to the flow at a greater angle than the Mach cone.	T-J.5.1
Edge tangent	A unit vector parallel to a panel or subpanel edge.	T-J.5.1

ITEM	DEFINITION	REFERENCES
Energy equation	An equation expressing conservation of energy in a small fluid element.	T-2.1
Entrainment	The phenomenon in which an efflux from a propulsion source absorbs fluid from the surrounding flow as the distance from the configuration increases.	U-2.1.4
Equation of state	An equation relating the pressure, density, and temperature of a fluid.	T-2.1
Euler's equation	A differential equation relating density, velocity, and pressure in a fluid (momentum equation for inviscid fluid without body forces).	T-2.2
Existence of a solution	The problem of determining whether a boundary value problem has at least one solution.	T-B.1, U-A.3
Extension matrix, doublet	A matrix which gives the values of doublet strength at the corners of a subpanel and the "kappa quantities" for its edges in terms of the panel doublet parameters.	T-I.2.2.4
Extension matrix, source	A matrix which gives the values of source strength at the corners of a subpanel in terms of panel source parameters.	T-I.2.1.3

ITEM	DEFINITION	REFERENCES
Far field method	An approximation for the computation of panel influence based upon the distance of the control point from the panel being much greater than distances within panel.	T-4.2.2, T-5.6, T-J.9
Far field moment, subpanel	A matrix or tensor which describes the dependence of a particular integral over a panel on the panel source or doublet parameters.	T-I.4.2.1
Far field moment, basic	Scalars giving the values of certain integrals of polynomial functions over a subpanel.	T-I.4.3
Far field moment, subpanel	A matrix or tensor which describes the dependence of the same integral over a subpanel on the panel singularity parameters.	T-I.4.2.1
Flow symmetry	The existence of one or two (orthogonal) planes of symmetry for the flow field.	T-5.7.2, U-2.1.2, U-B.2.1
Force	For impermeable surfaces, the force is the integral over the surface of the pressure times the surface normal vector. For permeable surfaces, an additional "momentum transfer" term contributes to the force.	U-2.1.7, T-O
Force coefficient	A normalized form of the force vector which removes the force due to the freestream flow and allows for a scaling factor introduced by the user. The force coefficient on an impermeable surface is the integral of the pressure coefficient times the normal vector divided by a user-supplied reference area.	T-O.1, U-B.4.3
Force, edge	See edge force computation.	
Freestream, $\vec{V}_\infty$	The uniform flow which is perturbed by the introduction of a configuration on which boundary conditions are imposed. See also onset flow, uniform, and velocity perturbation.	T-2.3

ITEM	DEFINITION	REFERENCES
Global data	Information (such as symmetry plane locations and the compressibility direction) supplied by the PAN AIR user to describe the configurations as a whole.	U-7
Gradient operator, $\vec{\nabla}$	A vector whose entries are the partial differentiation operation with respect to the coordinate functions.	T-B.3
Grid points	Panel corner points.	T-5.1, U-B.1.1
Grid points, fine or enriched	Rectangular array of points which are corner points, edge midpoints, or center points of quadrilateral (or triangular) panels of a network.	T-5.1, U-B.1.1
Green's theorems	Several relations between spatial integrals and surface integrals. These relations are used to derive the integral equation (B.0.1) of the Theory Document, which PAN AIR solves numerically.	T-3.2

ITEM	DEFINITION	REFERENCES
Influence coefficient	A matrix giving one or more field flow properties as a linear combination of the array of singularity parameters.	T-5.6
Influence coefficient, aerodynamic, AIC	Combination of potential and velocity influence coefficient matrices giving left-hand-side of boundary condition equation as a linear combination of singularity parameters.	T-3.3, T-4.2, T-5.7
Influence coefficient, panel, PIC	Matrix giving perturbations that a source or doublet distribution on a panel induces at a control point.	T-4.2.2, T-5.6, T-J
Influence coefficient, potential, ϕIC	Matrix giving the perturbation velocity potential at network control points as a linear combination of singularity parameters.	T-4.2, T-5.6
Influence coefficient, velocity, VIC	Same for perturbation velocity.	T-4.2, T-5.6
Intermediate field method	Approximation for computation of panel influence; intermediate between near field and far field methods.	T-5.6, T-J.9
Irrotational flow	Property that the curl of the velocity field is zero; assure existence of velocity potential.	Y-2.3

ITEM	DEFINITION	REFERENCES
Jet efflux	A flow emanating from the propulsion unit. A jet efflux may be modeled in PAN AIR by paneling the jet efflux with a wake network.	U-2.1.1
Jet efflux tube	The cylindrical surface surrounding the jet efflux, extending from the configuration to infinity.	U-2.1.1

ITEM	DEFINITION	REFERENCES
Kappa quantity, κ	A quantity defined for a line segment (generally a panel or subpanel edge) on which a quadratic function is defined. The value of the quantity is the value of the function at an endpoint of the segment plus half the gradient of the function dotted into the difference vector between the positions of the two endpoints.	T-I.2.2.2
Kutta condition	The boundary condition imposed at the trailing edge of a lifting surface such as a wing, specifying that the jump in pressure coefficient be zero there.	U-A.2, T-B.2

ITEM	DEFINITION	REFERENCES
Laplace's equation	Fundamental partial differential equation saying that divergence of gradient of a scalar is zero.	T-3.2, U-2
Least squares fit, constrained	The process of fitting a function as well as possible to a set of values at a point on a plane. The values need not be known in advance; the result of the process is a matrix giving the defining coefficients of the function in terms of the unknown values.	T-I.1.2.1, T-I.5.1
Length, reference	A user-input length for the scaling of moment coefficients computed by the program.	T-0.1, U-B.4.3
Line vortex term	The line integral in the expression for velocity at a point in space. This integral vanishes if doublet continuity is maintained everywhere.	T-5.6, T-B.3, U-A.2
Lofting	The revision of the geometry of a surface to more nearly attain a pressure distribution specified in a design run.	T-C.2

ITEM	DEFINITION	REFERENCES
M-direction	The direction of increasing panel row index.	U-7.4, U-B.1.1
Mach angle	The angle formed between the freestream direction and a Mach line.	T-J
Mach cone, upstream	A right circular cone located upstream of a field point, containing domain of dependence of that point, in supersonic flow.	T-5.2
Mach disk	The interior of the circle resulting from the intersection of a Mach cone with a plane perpendicular to its axis.	T-J.4.2
Mach - inclined surface	A surface whose normal is perpendicular to its conormal ($\hat{n} \cdot \tilde{n} = 0$). Such a surface is tangent to a Mach cone.	T-5.2, U-B.1.3
Mach line	A straight line generator of the Mach cone. One of the lines of intersection of the Mach cone with a plane containing the origin point of the cone.	T-J
Mach number	The ratio of the speed of the fluid to the speed of sound.	T-2.3
Mach wedge	The set of all point affected by a disturbance on a supersonic edge. The Mach wedge emanates fownstream from the edge. A point Q lies in the Mach wedge if some point P on the edge lies in the domain of dependence of Q.	T-J.11
Mass flux, linearized perturbation, $\vec{w}$	The vector obtained by applying the compressible gradient operator to the velocity potential, or by scaling the freestream component of the perturbation velocity by $(1-M_\infty{}^2)$. In compressibility coordinates $\vec{w} = (s\beta^2 u, v, w) = \vec{\nabla}\phi$.	T-5.4
Mass flux, total, $\vec{W}$	Produce of local density (normalized by freestream density) and velocity of fluid, $\vec{W} = (\rho/\rho_\infty)\vec{V} = \vec{V} + \vec{w}$.	T-4.5
Matrix decomposition	Expression of a square matrix as product of lower and upper triangular matrices.	T-5.8

ITEM	DEFINITION	REFERENCES
Metric matrices	Matrices which account for compressibility effects. The first metric matrix (denoted B) multiplies the freestream component of a vector by $(1-M_\infty{}^2)$, while the second metric matrix (denoted C) multiplies the component of the vector perpendicular to the freestream by $(1-M_\infty{}^2)$.	T-E.2
Minimal data set	A small amount of data (potential, normal mass flux, source and doublet strength) stored for each solution and each control or grid point in anticipation of post-processing.	T-M, U-2.1.1
Modified data set	A small amount of data (potential, normal mass flux, source and doublet strength) stored for each solution and each control or grid point in anticipation of post-processing.	T-M, U-2.3.4
Modeling	See configuration modeling.	
Modified dual vector	A dual vector whose component in the freestream direction has been sealed by $(1-M_\infty{}^2)$. A modified dual vector is obtained from a dual vector by the application of the first metric matrix.	T-E.2
Modified vector	A vector whose component perpendicular to the freestream has been scaled $(1-M_\infty{}^2)$. A modified vector is obtained from a vector by the application of the second metric matrix.	T-E.2
Moment coefficient, C_m	An angular momentum analog of the force coefficient. The moment coefficient contains a user-supplied scaling factor, and is defined by equation (0.1.3) of the Theory Document.	T-0.1, U-B.4.3
Momentum equation	Equation expressing conservation of linear momentum in a small fluid element.	T-2.1
Multiply connected	A region of space is multiply connected if a closed path can be drawn be in the region which cannot be shrunk to a point. See also "simply connected."	T-B.1, U-A.3

ITEM	DEFINITION	REFERENCES
N-direction	The direction of increasing panel column index.	U-7.4, U-B.1.1
Navier - Stokes equation	Combination of continuity, momentum, and energy equation for a fluid.	T-2.1
Near field method	Computation of a panel influence coefficient matrix by summing over all eight subpanels the influence of each subpanel.	T-J.1
Network	An indically rectangular array of panels corner points; basic unit for defining the geometry of the configuration.	T-5.1, U-B.1.1, T-D.1
Network, analysis	Network with singularity parameter locations as required for analysis boundary conditions.	T-5.1
Network, composite	Network having both source and doublet distributions.	T-5.1
Network, design	Network with singularity parameter locations as required for design boundary conditions.	T-5.1
Network, doublet	Network having a (locally quadratic) doublet distribution.	T-5.1
Network gaps	Gaps due to non-coincidence of network edges.	T-4.1, T-5.3
Network, wake	See wake network.	
Network, source	Network having a (locally linear) source distribution.	T-5.1
Network type, doublet	A description of the function performed by the doublet distribution on the network. Doublet types existing are analysis, design, wake, and null (zero doublet distribution).	T-5.1, T-D
Network type, source	Same for source distribution. Types are analysis, design, and null.	T-5.1, T-D
Network, wake	Network used to model wake surfaces: has continuous normal flow, may have discontinuity in potential across network.	T-5.1, U-B.1.1
Normal vector, unit	See unit normal vector.	

ITEM	DEFINITION	REFERENCES
Onset flow, $\vec{U}$	The user-defined flow field in which the configuration is analyzed. In the simplest case, this is just the uniform freestream flow $\vec{V}_\infty$.	U-B.2, T-H.3, S-3.1.5
Onset flow, local incremental, $\Delta\vec{U}$	A supplementary term added to the onset flow at individual control points to simulate the superposition of a non-uniform effect (such as a slipstream) onto the freestream.	U-B.2, T-H.3
Onset flow, rotational	A supplementary term added to simulate a rolling or pitching motion.	U-B.2, T-H.3
Onset flow, total, $\vec{U}_0$	The sum of all terms in the onset flow.	U-3.2.1
Onset flow, uniform, $\vec{U}_\infty$	An onset flow which is constant over the entire flow field, and is used to simulate a uniform freestream. The uniform onset flow need not be parallel to the freestream direction $\vec{V}_\infty$ on which compressibility effects are based.	U-B.2, T-H.3

ITEM	DEFINITION	REFERENCES
Panel	Part of a network surface, defined by four network defining points which are indicially adjacent.	T-3.3, T-4.1, T-5.1, T-D.1
Panel, almost non-convex	A panel with an interior angle of nearly 180°.	U-B.1.3, T-D.2
Panel aspect ratio	The ratio of the length of a panel to its width.	U-B.1.3, T-D.2
Panel center point	The point whose coordinates are the average of the coordinates of the four panel corner points.	T-D.1
Panel column	A sequence of panels with the same column index. See column index.	U-B.1.1, T-5.1
Panel corner point	One of the grid of points which defines a network. Four of these points (appropriately adjacent in an indicial sense) are sufficient to construct a panel's geometry.	T-D.1
Panel defining points	The corner points, edge midpoints, and center point of a panel.	T-D.2
Panel diameter	Twice the panel radius.	T-D.2
Panel edge midpoint	The midpoint of a segment connecting adjacent panel corner points.	T-D.1
Panel function	One of the two basic components (along with the edge function) of the entries of a PIC matrix. Defines as an integral over a panel or subpanel.	T-J.7
Panel integral matrix	Matrix giving the velocity and/or potential induced at a control point by a panel or subpanel, in terms of the coefficients of the polynomial describing the source or doublet strength on the region.	T-J.6
Panel method	Method for solving potential flow problems, using panel model of surface to reduce integral equation to a system of linear equations.	T-1.0, T-4.1 U-A.2

ITEM	DEFINITION	REFERENCES
Panel, non-convex	A panel containing interior angles exceeding 180°.	U-B.1.3, T-D.2
Panel radius	The distance.	T-D.2
Panel skewness parameters	Real numbers whose magnitude describe the extent to which a panel fails to be a parallelogram.	T-D.2
Panel, subinclined, superinclined, or Mach-inclined	See subinclined, superinclined, or Mach-inclined surface.	
Panel, triangular	A panel two of whose corner points coincide.	U-B.1.1
Parameterization	See abutment parameterization.	T-J.4.4.2
Perturbation	Change to undisturbed flow field or geometry.	T-2.3, T-A.1
Phase function	Function with two arguments equivalent to the FORTRAN function ATAN2 with arguments reversed. Phase (x,y) = arg(x+iy), where arg is the argument of a complex number.	T-J.4.4.2
Post-processing	The computation of pressures, or forces and moments from the minimal data set.	U-2
Potential	See velocity potential.	
Potential flow	Fluid flow characterized by the existence of a velocity potential function, satisfying a particular partial differential equation, whose gradient at a point is the velocity there.	T-2, T-A
Prandtl-Glauert equation	Partial differential equation for compressible flow: divergence of compressible gradient of perturbation velocity potential is zero.	T-2.5, T-A, S-2.0, U-A.1

ITEM	DEFINITION	REFERENCES
Preferred direction	In the solution of the potential flow problem (that is, the construction and solution of the system of linear equation), it is the compressibility direction. In post-processing, it is the user-specified x-direction in which velocity = (u,v,w) for the computation of the pressure coefficient.	T-H.3, U-B.2.1
Pressure, P	Force per unit area.	T-N.1, U-B.4.2
Pressure coefficient, Cp	A normalized expression for pressure which removes the contribution of the freestream flow to the pressure.	T-N.2.1, U-B.4.2
Pressure coefficient, isentropic	A formula for pressure coefficient resulting from certain basic assumptions about the character of the fluid flow.	T-N.2.1, U-B.4.2
Pressure coefficient, linear	A formula for pressure coefficient resulting from the additional assumption that second order terms in perturbation quantities are negligable.	T-N.2.5, U-B.4.2
Pressure coefficient, reduced second order	A formula for pressure coefficient based on the second order assumption and the additional assumption that terms containing the Mach number squared are negligable.	T-N.2.5, U-B.4.2
Pressure coefficient, second order	A formula for the pressure coefficient resulting from the additional assumption that third powers of perturbation quantities are negligable.	T-N.2.4, U-B.4.2
Pressure coefficient, slender body	A formula for pressure coefficient based on the second order assumption and the additional assumption that second order terms in the component of velocity parallel to the freestream are negligable.	T-N.2.5, U-B.4.2
Pressure coefficient, vacuum	The most negative value the isentropic pressure coefficient can attain.	U-B.4.2, T-N.2.4.1
Pseudo-inner product	Modified inner product, one of whose terms in scaled to account for compressibility.	T-J.5.1

ITEM	DEFINITION	REFERENCES
Recession vector	See control point recession vector.	
Refinement of paneling	The paneling along one network edge is a refinement of the paneling along a second network edge on the same abutment if the first edge has a panel corner point wherever the second edge has a panel corner point.	T-I.1.2.5
Region, exterior	Spatial region outside a finite surface.	T-3.2
Region, interior	Spatial region inside a finite surface.	T-3.2
Right-hand-side	See boundary condition, right-hand-side.	
Row index	An integer which, in conjunction with the column index, describes the indical location of a panel or panel corner point. When the panel corner points are input by the user all points with the same column index are input consecutively. For each column of points input by the user, the row index runs consecutively from 1 to the maximum row index.	T-5.1, U-B.1.1

ITEM	DEFINITION	REFERENCES
Shear layer	A surface in the flow field on which the velocity tangential to the surface is discontinuous. A shear layer is modeled in PAN AIR by means of a wake network.	U-2
Simply connected	A region of space in which any path may be shrunk to a point. See also "mulitply connected" and Figure B.8 of the Theory Document.	T-B.1, U-A.3
Singularity parameters	Unknown in system of linear equations constructed by a panel method.	T-3.3
Singularity parameters, unknown	Singularity parameters specified by a single boundary condition equation.	T-5.7.2, T-5.7.3, T-K.2
Singularity parameter, panel	The value of source strength at one of five panel points (corners or center) or the value of doublet strength at the nine panel defining points.	T-I.1, T-I.2
Singularity type	The source of doublet type of network. This may be analysis, design, wake 1 or wake 2 (for doublets only), or null.	U-A.2
Slipstream	The flow field induced by a rotating propeller.	T-H.3
Small perturbation assumptions	Assumptions that certain quantities are small enough that their higher powers may be ignored. The Prandtl-Glauert equation holds for irrotation, isentropic, inviscid flow in which certain small perturbation assumptions have been satisfied.	T-A.1
Solution list	A list of different constraints under which the system of linear equations is to be solved. Typically, a list of solutions might consist of several angles of attack and/or sideslip.	U-7
Solution vector	The vector of unknowns in the system of linear equations.	T-5.7.4
Source distribution	One of two unknown quantities in the fundamental integral equation.	T-3.2, U-A.2

ITEM	DEFINITION	REFERENCES
Source parameters	Known or unknown quantities on which the source distribution on the configuration depends.	T-5.5
Source strength, σ	The value of the source distribution at a particular point. It is equal to the size of its jump in normal mass flux across the surface.	T-3.2, U-A.2
Specified flow, b	The right-hand side term in a boundary equation. That is, some combination of potential and velocity is specified by the equation to equal b.	U-B.3
Spline	The method by which a function on a surface is obtained from the specification of values of the function at a discrete set of points on the surface.	T-I
Spline, edge	The method by which doublet spline vectors are constructed for five grid points on the edge of a network.	T-I.1.2
Spline matrix, outer	A matrix giving values of (five source or nine doublet) panel singularity parameters values in terms of surrounding singularity parameters.	T-I.1
Spline matrix, subpanel (or panel or half panel)	A matrix giving the singularity distribution on subpanel (or panel or half panel) in terms of panel singularity parameters.	T-4.2.1.1, T-5.5, T-I.2, T-I.3.1, T-I.3.2
Spline, two-dimensional	The method by which a function on a line segment is obtained from the specification of values of the function at a discrete set of points on the line segment.	T-C.4
Spline vector	A row vector giving source or doublet strength at a fine grid point in terms of surrounding singularity parameters.	T-I.1
Stability	The property of a spline, in conjunction with a set of boundary conditions, that a perturbation in the boundary conditions at one point causes a disturbance in the solution which decreases rapidly with distance from the point.	T-C.4

ITEM	DEFINITION	REFERENCES
Stagnation to ambient	Flow which is no faster than freestream (ambient) flow, yet not highly perturbed as to have a negative component in the freestream direction. Such a flow may be corrected using the semi-empirical "velocity corrections".	U-B.4.1
Stagnation, perturbation	A point at which the perturbation velocity is zero.	T-5.4.2.3
Stagnation, total	A point at which the total velocity is zero.	T-5.4.2.3
Subinclined surface	A surface for which the inner product of normal and conormal is positive. All surfaces are subinclined in subsonic flow.	U-B.1.1, T-5.2
Subpanel	A flat triangular surface which is the basic unit of the panel analysis in PAN AIR (a panel consists of eight subpanels).	T-4.2.1.1, T-5.1
Subpanel, subinclined, superinclined, or Mach-inclined	See subinclined, superinclined, or Mach-inclined surface.	
Subsonic flow	Flow for which the Mach number is less than one.	T-3.1, U-2.0, S-1.0
Superinclined surface	A surface for which the inner product of normal and conormal is negative. Such a surface is inclined to the freestream at more than the Mach angle.	U-B.1.1, T-5.2
Supersonic flow	Flow for which the Mach number is greater than one.	T-3.1, U-2.0, S-1.0
Surface, lower	The side opposite to the upper surface.	T-5.4, U-A.3.1
Surface, upper	The side of the surface bounding the region into which the unit normal points. An exception is that for post-processing only, upper and lower surfaces are switched by means of the "reverse" option.	T-5.4, U-A.3.1
Symmetry, plane of	A plane such that either the flow or the configuration geometry is left unchanged if reflected in this plane.	U-2.1.2, U-B.2.3, T-K.1

ITEM	DEFINITION	REFERENCES
Tangent vector	A vector perpendicular to the surface normal.	T-5.4
Thick body	See configuration, thick.	
Thin body	See configuration, thin.	
Tolerance distance	A distance supplied by the user. The program searches for network edges which lie closer together than the tolerance distance, and forms pairwise abutments for these edges.	T-F.2, U-3
Total	The sum of a freestream quantity and a perturbation quantity.	U-A.1
Transformation, orthogonal	A length-preserving coordinate transformation.	T-E.3

ITEM	DEFINITION	REFERENCES
Update, IC	The capability allowing reuse of AIC's for some networks when modifying other networks.	T-5.7.5, T-K.6, S-3.3.3, U-2.3.2
Update, solution	Capability of storing AIC's and reusing them later in a new problem in which only the boundary condition constraints have been changed.	U-2.3.2, T-L, T-5.8, S-3.3.2
Unit normal vector, $\hat{n} = (n_x, n_y, n_z)$	A vector of length 1 which is perpendicular to a surface. Its direction is defined as the direction of increasing column index cross the direction of increasing row index.	T-D.2

ITEM	DEFINITION	REFERENCES
Velocity, $\vec{V}$	The time rate of position change of fluid particles.	T-2.1, U-A.1
Velocity computation method	One of two methods of computing the velocity at a point from the minimal data set. The boundary condition method attempts to obtain data from boundary conditions and spline it, while the VIC method obtains the velocity from the product of a velocity influence coefficient matrix with the vector of singularity parameters.	U-2.1.6
Velocity, perturbation, $\vec{v}$	The difference between total velocity and that of the undisturbed fluid.	T-2.3, U-A.1
Velocity potential, $\phi, \vec{\Phi}$	The function whose gradient is the velocity, $\vec{v} = \vec{\nabla}\phi$, $\vec{V} = \vec{\nabla}\Phi$.	T-2.3, U-A.1
Vorticity, surface, $\vec{\gamma}$	The cross product of surface normal vector and doublet gradient, $\vec{\gamma} = \hat{n} \times \vec{\nabla}\mu$.	U-A.2, T-5.6.2

ITEM	DEFINITION	REFERENCES
Wake, physical	A sheet of vorticity shed from the physical configuration.	T-5.1, T-B.2
Wake network	A network used by PAN AIR to model a physical wake. The normal mass flux is continuous on such a network, while the potential and tangential velocity may be discontinuous.	T-5.1, T-B.2
Wave equation	A particular hyperbolic partial differential equation. PAN AIR solves this equation when the Mach number is $\sqrt{2}$.	T-3.1
Wetted surface	A surface is wetted by a region of space of it borders on that region.	U-A.3

A.0 Fundamental Fluid Mechanics

To repeat our warning in section 1, this document is not meant to be a text in basic fluid mechanics (several basic references are listed in section 1). We will not discuss the derivations of the equations which lead to the Prandtl-Glauert equation, nor will we discuss the assumptions of irrotational, inviscid, steady, and isentropic flow which lead to the Prandtl-Glauert equation. We will, however, briefly discuss the "small perturbation" assumptions, since these assumptions pervade both the theory and usage of panel methods, and hence determine the application and validity of the methods to particular problems.

A.1 The Small Perturbation Assumptions

Recall from section 2.3 that we assumed

$$|\vec{v}| \ll |\vec{V}| \ll a_\infty \tag{A.1.1}$$

To be precise, the transonic small perturbation equation is obtained by assuming (in addition to irrotational, inviscid, isentropic flow) that terms of order $|\vec{v}|^2/a^2$ can be ignored. Recall that $\vec{v}(x,y,z)$ is the perturbation of the local velocity from a uniform freestream $\vec{V}_\infty$. Assumption (A.1.1) holds under a wide variety of cases, including

a. a thin wing at small angle of attack (shown in figure A.1) at any Mach number other than approximately 1,
b. a blunt object at small Mach number (see figure A.2)
c. a static airplane configuration with engines on, sucking in air, with local velocities in the inlet duct which are small compared to the speed of sound:

$$|\vec{v}| = |\vec{V}| \lessapprox .2a_\infty \tag{A.1.2}$$

(see figure A.3).

In case (a), both $|\vec{v}| / |\vec{V}|$ and $|\vec{v}| / a_\infty$ are small. In case (b), $|\vec{v}|$ is of the same order as $|\vec{V}_\infty|$, and so we are ignoring terms of size

$$|\vec{v}|^2/a^2 \approx (.1)^2 = .01 \tag{A.1.3}$$

Similarly, in case (c), we ignore terms of size

$$|\vec{v}^2|/a^2 \approx (.2)^2 = .04 \tag{A.1.4}$$

which is still small with respect to one.
But now, let us reconsider case (c), with

$$|\vec{V}|/a_\infty = .7 \tag{A.1.5}$$

In that case, assumption (A.1.1) no longer holds, since we are ignoring terms of order $.7^2 = .49$, which are not small compared to 1.

Thus, the "engine-on" problem does not satisfy the small perturbation transonic equation, let alone the Prandtl-Glauert equation, if the "local Mach number" ($|\vec{V}|/a$) is too large. This does not mean that PAN AIR has no use for such a problem. Its use, however, is restricted to predicting qualitative trends, rather than detailed pressure distributions. Note that as the forward speed of the airplane increases, the perturbation velocity within the duct decreases, and equation (A.1.1) is more nearly satisfied.

Now, let us examine the small perturbation steady transonic equation (assuming $|\vec{V}_\infty| = 1$):

$$(1-M_\infty^2)\,\phi_{xx} + \phi_{yy} + \phi_{zz} = M_\infty^2[1/2\,(\gamma-1)\,(2u + |\vec{v}|^2)\,\nabla^2\phi +$$

$$(2u + u^2)\,\phi_{xx} + v^2\phi_{xy} + 2vw\phi_{yz} + w^2 + w^2\phi_{zz} \qquad \text{(A.1.6)}$$

$$+ 2(1+u)(v\phi_{xy} + w\phi_{xz})]$$

Since $|\vec{v}|^2 = u^2 + v^2 + w^2$, all the terms on the right side of (A.1.6) are quadratic or cubic expressions in the first or second derivatives of ϕ, while the terms on the left hand side are linear expressions in the derivatives of ϕ. So, formally, it is justifiable to drop all the terms on the right, and say that to first order, the Prandtl-Glauert equation

$$(1-M_\infty^2)\,\phi_{xx} + \phi_{yy} + \phi_{zz} = 0 \qquad \text{(A.1.7)}$$

holds (where the freestream direction is the x-direction).

But a formal elimination of all quadratic and cubic terms only has meaning if the terms being ignored are in fact small, compared to the terms which are being retained.

We can rewrite (A.1.6) as

$$[(1-M_\infty^2) + A]\,\phi_{xx} + B\phi_{xy} + C\phi_{xz}$$

$$+ (1+D)\phi_{yy} + E\phi_{yz} + (1+F)\phi_{zz} = 0 \qquad \text{(A.1.8)}$$

where

$$A = -M_\infty^2\,[1/2(\gamma-1)\,(2u+|\vec{v}|^2)+(2u+u^2)]$$

$$B = -2M_\infty^2\,(1+u)v$$

$$C = -2M_\infty^2\,(1+u)w$$

$$D = -M_\infty^2\,[1/2(\gamma-1)\,(2u+|\vec{v}|^2)+v^2] \qquad \text{(A.1.9)}$$

$$E = -2M_\infty^2\,vw$$

$$F = -M_\infty^2\,[1/2(\gamma-1)\,(2u+|\vec{v}|^2+w^2]$$

Now, (A.1.7) holds if the sum of all the ignored terms is small compared to each of the retained terms, that is, if

$$A \ll 1-M_\infty^2$$

$$S = A + B + C + D + E + F \ll 1 \qquad \text{(A.1.10)}$$

Adding the terms in (A.1.9)

$$S \leq M^2 \quad [3/2(\gamma-1)(2|u| + |\vec{v}|^2 + 2u + u^2 + 2|1+u|(|v| + |w|) + v^2 + 2|vw| + w^2] \tag{A.1.11}$$

Now, since the absolute value of a sum is at most the sum of the absolute values,

$$S \leq M^2 \quad [3(\gamma-1)|u| + 3/2(\gamma-1)|\vec{v}|^2 + 2|u| + u^2 + 2|\vec{v}| + 2|w| + 2|uv| + 2|vw| + v^2 + 2|vw| + w^2 \tag{A.1.12}$$

Now, since $|u|$, $|v|$, and $|w|$ are $\leq |\vec{v}|$ and all products of these are $\leq |\vec{v}|^2$, we obtain

$$S \leq M_\infty^2 \quad [(3(\gamma-1)+2+2+2)|\vec{V}| + (3/2(\gamma-1)+1+2+2+1+2+1)|\vec{v}|^2] \tag{A.1.13}$$

or $$S \leq M_\infty^2 \quad [(3+3\gamma)|v| + 15/2 + 3/2\gamma)|\vec{v}|^2] \tag{A.1.14}$$

or $$S \leq M_\infty^2 \quad k(\gamma)[|\vec{v}| + |\vec{v}|^2] \tag{A.1.15}$$

where $$k(\gamma) = \max(3+3\gamma, 15/2 + 3/2\gamma) \tag{A.1.16}$$

depends only on the gas. For diatomic gases, $\gamma = 7/5$, and thus $k(\gamma) = 9.6$.

Thus, we see that (A.1.10) holds if

$$M_\infty^2 \quad k(\gamma)[|\vec{v}| + |\vec{v}|^2] << 1 \tag{A.1.17}$$

and $$M_\infty^2 \quad k(\gamma)[|\vec{v}| + |\vec{v}|^2] << 1 - M_\infty^2 \tag{A.1.18}$$

(since $|A| \leq |S|$).

Recall from section 2.3 that $|\vec{V}_\infty| = 1$; thus $|\vec{v}|$ is the size of the perturbation velocity divided by the freestream speed.

For Mach numbers $< \sqrt{2}$, (A.1.18) is the more restrictive equation, while for $M_\infty > \sqrt{2}$, (A.1.17) is more restrictive. Equations (2.5.2) and (2.5.3) are simplifications of (A.1.17) and (A.1.18), based on a scaling by a factor of $2k(\gamma)$ of what we mean by "very much less than", and based on the assumption

$$|\vec{v}|^2 \leq |\vec{v}| \tag{A.1.19}$$

Equation (A.1.19) holds in virtually all cases of aerodynamic interest, since we have assumed that $|\vec{V}_\infty| = 1$, that is, we are not dealing with the "engine-on" case, in which $|\vec{V}_\infty| = M_\infty = 0$.

From (A.1.17) and (A.1.18), we derive the principle that the more nearly transonic or the more hypersonic the flow becomes, the smaller the perturbations to the free stream must be. Small perturbations, in turn, mean slender objects and small angles of attack. This does not mean, however, that PAN AIR is of no use if the restrictions (A.1.17) or (A.1.18) are violated locally. Experimentation has shown that, for instance, wings with rounded leading edges can be successfully analyzed at Mach numbers such as .7, at which (A.1.17) is thoroughly violated. This is true because the Prandlt-Glauert equation is only violated in a small region of space, and the quality of the solution in other areas is not affected. Further, semi-empirical velocity correction formulas (see section 5.9) are available. Pressures calculated from the correction velocity agree more accurately with those determined by experiments. Thus a fairly accurate approximation to the true flow properties can be obtained in this case despite the violation of the assumptions behind the Prandtl-Glauert equation.

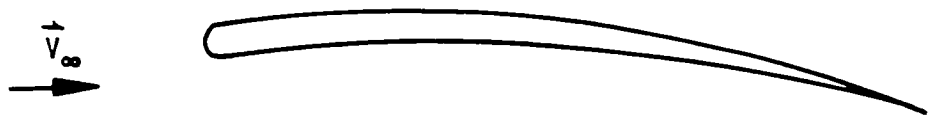

$M_\infty = .1$

or $M_\infty = .9$

or $M_\infty = 3$

Figure A.1 - Thin Wing at small angle of attack

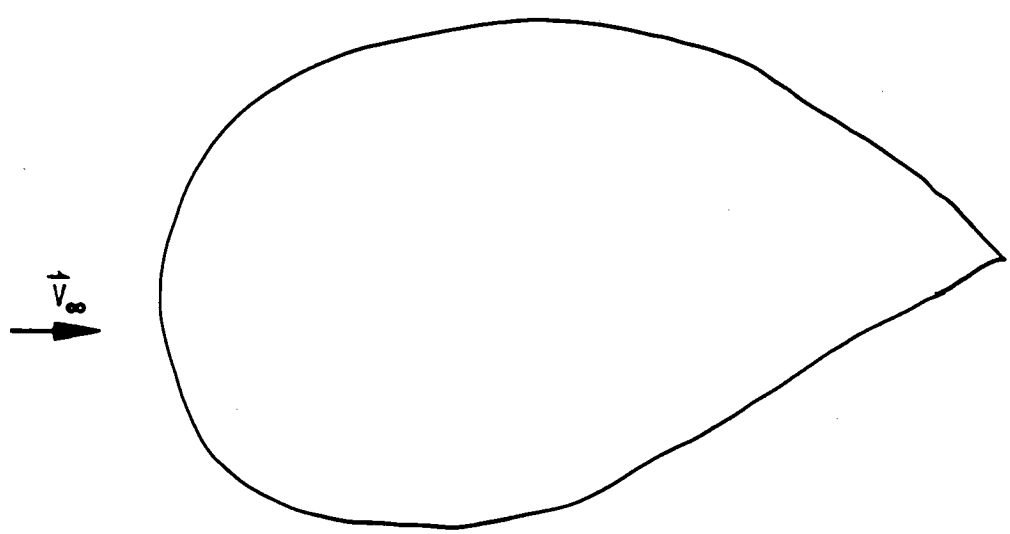

$M_\infty = .1$

Figure A.2 - Blunt object at small Mach number

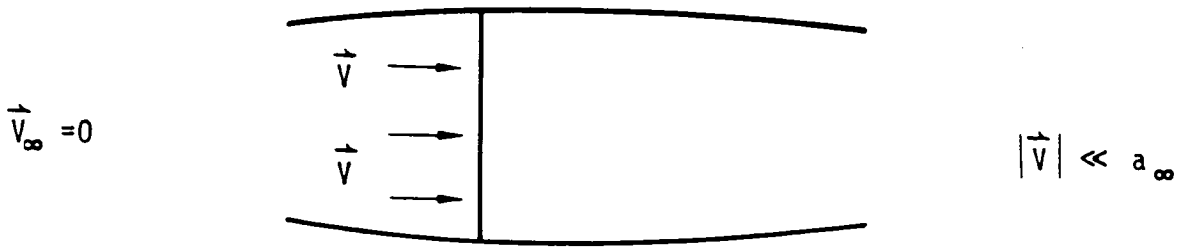

Figure A.3 - Small perturbation "engine-on" case

B.0 The Prandtl-Glauert Equation

In this appendix, we discuss some basic results concerning solutions of the Prandtl-Glauert equation. We make no effort to prove results which are proved in any of the standard references, but we will supply derivations of results which are not available elsewhere.

The basic step in analyzing solutions ϕ (x,y,z) of the Prandtl-Glauert equation is to convert it to the integral equation

$$\phi(x,y,z) = \frac{1}{\kappa} \iint_{S \cap D_p} \left[\frac{-\sigma(Q)}{R} + \mu(Q)\hat{n} \cdot \tilde{\nabla}\left(\frac{1}{R}\right)\right] dS \qquad (B.0.1)$$

where $S \cap D_p$ is the intersection of the configuration surface S with the domain of dependence D_p on the point P=(x,y,z),

$$\begin{aligned}
\sigma &= \tilde{\nabla}(\phi_u - \phi_L) \cdot \hat{n} \\
\hat{n} &= \text{unit surface normal} \\
\mu &= \phi_u - \phi_L \\
Q &= (\xi, \eta, \zeta) \\
R^2 &= (\xi - x)^2 + s\beta^2(\eta - y)^2 + s\beta^2(\zeta - z)^2 \qquad (B.0.2) \\
s &= \text{sign}\,(1 - M_\infty^2) \\
\beta^2 &= |1 - M_\infty^2| \\
\kappa &\begin{cases} = 2\pi \text{ if } s = -1 & \text{and} \\ = 4\pi \text{ if } s = +1 \end{cases} \\
\nabla_Q &= \begin{Bmatrix} s\beta^2\, \partial/\partial\xi \\ \partial/\partial\eta \\ \partial/\partial\zeta \end{Bmatrix}
\end{aligned}$$

The asterisk refers to the fact that for supersonic flow we only take the "finite part" of the integral, a concept defined in section 3.4 of Ward (1.5), and in section J.6.7 of this document.

Equation (B.0.1) is derived for subsonic flow in Ward, Chapter 2, and for supersonic flow in Chapter 3. A more thorough derivation is given for $M_\infty = 0$ in Kellogg (1.3), p. 221, and for $M_\infty > 1$ in Ehlers, et al.(4.9), sections 3.5 and 3.7.

In this appendix, we discuss the concept of a boundary value problem, that is, the combination of (B.0.1) with a set of boundary conditions. In section B.1, we discuss boundary value problems for which existence and uniqueness of a solution have been proved or disproved. In B.2, we discuss the role of wakes in the formulation of a boundary value problem. And finally, in B.3, we show that the gradient of (B.0.1), defining $\vec{v}(x,y,z)$, can be replaced by a different expression which is more readily computable. All of the material in this appendix is "background" material; none of it is reflected in the actual PAN AIR computer code.

We emphasize that Pan Air actually solves the integral equation (B.0.1), with boundary conditions imposed on the true configuration geometry (cf., (3.1.3)) while other panel methods solve the integral equation corresponding to Laplace's equation with zero normal velocity boundary conditions applied on the scaled geometry. These methods can be demonstrated to be equivalent in subsonic flow (cf., Butter,reference B.1), and go under the general name "Gothert's rule".

We note that the two versions of Gothert's rule are equivalent only in subsonic flow. This is because the scaling (3.1.3) in subsonic flow yields an "equivalent incompressible geometry", and at zero Mach number mass flux is identical to velocity. In supersonic flow, on the other hand, application of (3.1.3) yields an "equivalent geometry" corresponding to a Mach number of $\sqrt{2}$. But at this Mach number, velocity and mass flux are not identical; rather, the freestream components of perturbation velocity and mass flux have opposite sign. Thus normal mass flux and normal velocity boundary conditions are inherently different in supersonic flow.

In addition, some European panel methods use yet another method, referred to as Gothert Rule 2, to account for compressibility effects in subsonic flow. In this method, the Prandtl-Glauert equation is solved, with boundary conditions of normal velocity (rather than normal mass flux) applied on the true configuration. This method is not equivalent to either of the two equivalent versions of Gothert's rule described above.

B.1 Existence and Uniqueness

In this section, we give four examples of boundary value problems which are well-posed (that is, for which there exists a unique solution), and two examples of ill-posed boundary value problems. Finally, we discuss two boundary value problems for which excellent numerical results have been obtained, without any actual proof that the problem is well-posed.

The first well-posed problem is the subsonic exterior Neumann problem. A Neumann problem is the specification of normal mass flux on the boundary of a region R. If R is a infinite region with finite boundary as illustrated in figure B.1 or figure B.3, the boundary value problem is called "exterior" since the boundary of R is the "outer" surface of S. The precise formulation of the result (see p. 311 of Kellogg, 1.3) is: The specification of a continuous distribution of $\tilde{n} \cdot \nabla\phi$ on the boundary S of an infinite region R yields a unique distribution of potential ϕ, whose value approaches zero at infinity on R, satisfying the Prandtl-Glauert equation, for $M_\infty < 1$. Kellogg only proves this result for $M_\infty = 0$, but the coordinate scaling (3.1.3) (which reduces the Prandtl-Glauert equation to Laplace's equation in the scaled coordinates) allows one to prove the result for arbitrary subsonic Mach numbers.

The second well-posed boundary value problem is the interior subsonic Dirichlet problem (a Dirichlet problem is the specification of ϕ on a surface). Again, this is shown to be well posed (see Kellogg, p. 311) for $M_\infty = 0$, and is formulated precisely as follows: Let R be a region of finite volume (see figure B.2). Then the specification of a continuous distribution of ϕ on the boundary S of R is a well-posed boundary value problem. Further, if the specification of ϕ is a constant b, then ϕ is identically equal to b in all of R.

The third well posed boundary value problem is discussed in Ward, 1.5, section 4.13, and is formulated as follows. Let S be a finite smooth surface (see figure B.3) which is everywhere inclined behind the Mach angle (such a surface has $\hat{n}\cdot\tilde{n} > 0$, and is called subinclined). The specification of a continuous distribution of $\vec{w}\cdot\hat{n}$ on both sides of S defines a unique value of ϕ in all of space for $M_\infty \neq 1$. For $M_\infty < 1$, this is just a special case of the first boundary value problem discussed above.

The fourth well-posed boundary value problem is illustrated in figure B.4. There, S is a smooth superinclined surface ($\hat{n}\cdot\tilde{n} < 0$, which automatically implies $M_\infty > 1$). Then, the specification of continuous distributions of both $\vec{w}.\hat{n}$ and ϕ on the downstream side of S is a well posed boundary value problem, and once again is discussed by Ward in section 3.2.

Now let us consider two ill-posed boundary value problems. The first is the interior Neumann boundary value problem, that is, the specification of $\vec{w}.\hat{n}$ on the boundary of a region R of finite volume, as illustrated in figure B.5. The proof that no unique solution exists is simple. Suppose a certain function $\phi(x,y)$ were a solution. Then, for any constant ϕ_0, $\phi(x,y,z) + \phi_0$ is also a solution, since $\nabla\phi_0 = 0$ and thus the normal mass flux ($\vec{w} \cdot \hat{n} = \tilde{\nabla}\phi \cdot \hat{n}$) is unchanged. Thus, there cannot exist a unique solution ϕ, and so the problem is ill-posed.

A second example of an ill-posed boundary value problem is the specification of ϕ or $\vec{w}\cdot\hat{n}$ on the upstream side of a superinclined surface. Consider, for instance, the point P in figure B.4. According to the integral equation (B.0.1), $\phi(P)$ is an integral over $S \cap D_p$. But the intersection of S with D_p, the domain of dependence of the point P, is empty. That is, there is no point on S which influences P, since the domain of dependence consists of the interior of a cone pointing upstream from P, as illustrated in figure B.6.

So, $\phi(P) = 0$, regardless of the source or doublet distribution on S. Further, this holds for all points P on the upstream side of S. So, specifying $\phi = b$ or $\vec{w}\cdot\hat{n} = b$ on the upstream surface of S results in infinitely many solutions if $b = 0$, and no solutions if $b = 0$. Thus, no matter what our choice of b, upstream specification is an ill-posed boundary value problem.

This discussion of ill-posed and well-posed boundary value problems is of some interest to the user of PAN AIR because of a basic principle. This principle is that the use of a panel method to solve an ill-posed boundary value problem invariably leads to a system of linear equations whose matrix is singular. Even if the system of equations has infinitely many solutions, the numerical equation solving techniques used by panel methods break down, and none of the solutions can be found.

On the other hand, the lack of a proof that a particular boundary value problem is well-posed should not be an impediment to attempting to find a numerical solution. The prime examples of this are the successes achieved by the "pilot code" in solving the exterior Neumann problem and interior Dirichlet problem for subinclined surfaces in supersonic flow (see figures B.1 and B.2). Specific cases are described in Ehlers, et al., (4.9). A second example is the specification of design boundary conditions, a subject which will be discussed in more detail in Appendix C.

Summarizing, for a thick closed configuration such as that of figure B.2, one is fairly safe (assuming that the surface is subinclined when $M_\infty > 1$) in imposing the boundary conditions

$$\phi_L = 0 \qquad \vec{W}_U \cdot \hat{n} = 0 \tag{B.1.1}$$

which, as pointed out in section 5.4, is equivalent to

$$\phi_L = 0 \qquad \sigma = -\vec{V}_\infty \cdot \hat{n} \tag{B.1.2}$$

Here, the subscripts U and L refer to upper and lower surfaces. For thin configurations such as that in figure B.3, the boundary conditions should be (assuming the surface is subinclined again)

$$\vec{W}_U \cdot \hat{n} = 0 \qquad \vec{W}_L \cdot \hat{n} = 0 \tag{B.1.3}$$

or, equivalently

$$\vec{W}_U \cdot \hat{n} = 0$$
$$\sigma = 0 \tag{B.1.4}$$

For a permeable surface inclined to the freestream, as shown in figure B.7, the boundary conditions for subsonic flow should be

$$\phi_L = 0$$
$$\vec{W}_U \cdot \hat{n} = b \tag{B.1.5}$$

or equivalently

$$\phi_L = 0 \tag{B.1.6}$$
$$\sigma = - \vec{V}_\infty \cdot \hat{n} + b$$

while for supersonic flow they should be

$$\phi_L = 0 \tag{B.1.7}$$
$$\vec{W}_L \cdot \hat{n} = b'$$

B.2 Wakes and Modeling

Up to this point, we have implicitly assumed that the surface S on which non-zero source or doublet distributions are given represents a real phyical object. But for a wide variety of problems of physical interest, it does not suffice to impose boundary conditions of impermeability on the physically existing configuration. The general problem of determining the surface S, and what boundary conditions should be imposed there, is called the modeling problem, and will be discussed here briefly.

The first case of a non-physical surface S arises from one of the hypotheses of Green's Theorem which we ignored when discussing the subject in section 3.2. This hypothesis requires that the region V on which ϕ is defined be "simply connected". That is, there must not be any closed path in V which cannot be shrunk to a point within V. In figure B.8, we illustrate in cross section a region V, whose boundary S is the surface of a nacelle, which fails to be simply connected. The imposition of boundary conditions of impermeability on S once again results in an ill-posed boundary value problem.

The boundary value problem can be made well-posed by the addition of a surface S' which "blocks off" the inlet. The surface S' is not impermeable, however; so the user specifies the total normal mass flux b flowing through the surface. The boundary conditions illustrated in figure B.7 only apply to subsonic flow, though. For supersonic flow, upper surface normal mass flux must not be specified on the superinclined surface S'; instead, the boundary condition

$$\begin{aligned} \vec{W}_L \cdot \hat{n} &= b \\ \phi_L &= 0 \end{aligned} \qquad \text{(B.2.1)}$$

should be imposed.

The second case in which the surface S includes non-phyical surfaces arises not from theoretical but from empirical considerations. These considerations arise from the fact that the assumption of zero viscosity is invalid near the trailing edge of a wing. No matter how small the viscosity of the fluid, the conditions at the trailing edge are considerably different from those of the zero viscosity case. The difference is the following: at zero viscosity, the velocity at the trailing edge of a wing becomes infinite, while at any non-zero viscosity, the velocity is bounded by a fixed number which depends mostly on the wing geometry and Mach number, and is only weakly dependent on the viscosity.

In order to reproduce this effect while using a program which ignores viscous effects, the concept of a wake is introduced. A wake is a surface across which the normal mass flux is continuous, while the potential and the tangential velocity are not. Thus, source strength is zero on a wake, while doublet strength μ is non-zero, and the jump in tangential velocity is $\nabla\mu$. The actual physical situation, namely that the tangential velocity varies very rapidly in a small region of space, is modeled quite well by this type of surface.

In modeling a configuration, wakes are generally inserted in a roughly streamwise direction emanating from the trailing edges of all "lifting surfaces" such as wings, fins, etc. The exact location of the wake generally is not very important. The boundary conditions imposed on the wake, reflecting the physical situation, are generally (though not in PAN AIR):

$$\sigma = 0$$
$$\vec{W}_U \cdot \hat{n} = 0 \qquad \text{(B.2.2)}$$

The flow about lifting surfaces in subsonic flow is known to satisfy a condition called the "Kutta condition", that is, the pressure jump across the surface is zero along the trailing edge. The successful modeling of a potential flow problem generally requires that the Kutta condition be satisfied. In section D.1.1, we describe the boundary conditions that PAN AIR imposes on wake networks. We also outline a justification that these boundary conditions result in the Kutta condition being satisfied.

An illustration of the wake location for a typical wing-body configuration is given in figure B.9. Note that no trailing edge of the wake is shown. In true physics, the wake is dissipated by viscous effects. In terms of solving the Prandtl-Glauert equation, the effect of the far regions of the wake on the configuration is negligeable, and thus the wake can be terminated at any finite point which is reasonably far from the physical configuration. The division of the wake into "wake 1" and "wake 2" networks will be discussed in section D.1.2.

Several major exceptions exist to the assertions that a wake should generally be positioned in a streamwise direction from the trailing edge of a lifting surface, and that the exact position of the wake is generally not important. One is the case of a "leading edge vortex", a phenomenon that occurs at the leading edge of a highly swept wing at large angles of attack as illustrated in figure B.10. In that case, the wake tends to roll up (trailing wakes also roll up, but at so much greater distance from the airplane as to be ignored) as shown, and the exact position of the wake is important in determining the aerodynamic behavior of the configuration. The use of a potential flow program to analyze such a case involves an iterative determination of the wake position, a problem similar to the design problem discussed in Appendix C. Some success in obtaining numerical solutions of this problem has been obtained by the program of Johnson, et al., (B.2).

Another case in which wake positioning is important is the case where the wake from a wing passes near the tail of the airplane. Generally speaking, whenever the flow leaving the trailing edge of a lifting surface passes near another portion of the configuration (or the ground, if ground effect is being studied), the location of the wake is important in analyzing the flow.

B.3 Removal of Line Vortex Terms and the Line Source Integration by Parts

In order to impose boundary conditions involving $\nabla\phi$ (such as $\vec{v}.\tilde{n} = b$), we must evaluate the perturbation velocity at an arbitrary point. Differentiating (B.0.1), we obtain

$$\vec{v}(x,y,z) = \nabla_p\phi = \frac{1}{\kappa}\nabla_p \iint^{*}_{S\cap D_p} \left[\frac{-\sigma(Q)}{R} + \mu(Q)\hat{n} \cdot \tilde{\nabla}_Q\left(\frac{1}{R}\right) \right] dS \qquad (B.3.1)$$

Putting the gradient within the integral, and writing it as ∇_p to emphasize that we are differentiating in (x,y,z) coordinates, we write

$$\vec{v} = \frac{1}{\kappa} \iint^{*}_{S\cap D_p} \left[-\sigma(Q)\, \nabla_p\left(\frac{1}{R}\right) + \mu(Q)\nabla_p\left(\tilde{\nabla}_Q\left(\frac{1}{R}\right) \cdot \hat{n}\right) \right] dS \qquad (B.3.2)$$

Recalling that,

$$\nabla_p = \begin{Bmatrix} \partial/\partial x \\ \partial/\partial y \\ \partial/\partial z \end{Bmatrix} \qquad \tilde{\nabla}_Q = \begin{Bmatrix} s\beta^2\, \partial/\partial\xi \\ \partial/\partial\eta \\ \partial/\partial\zeta \end{Bmatrix}$$

and

$$R^2 = (\xi - x)^2 + s\beta^2 (\eta - y)^2 + s\beta^2(\zeta - z)^2 \qquad (B.3.3)$$

we have

$$\tilde{\nabla}_Q(R) = \left(\frac{s\beta^2(\xi - x)}{R}, \frac{s\beta^2(\eta - y)}{R}, \frac{s\beta^2(\zeta - z)}{R}\right) = \frac{s\beta^2}{R}(\xi - x, \eta - y, \zeta - z) \qquad (B.3.4)$$

and similarly

$$\nabla_p(R) = -\frac{(\xi - x,\ s\beta^2(\eta - y),\ s\beta^2(\zeta - z))}{R} \qquad (B.3.5)$$

Further, by the chain rule,

$$\tilde{\nabla}_Q(R^n) = nR^{n-1}\, \tilde{\nabla}_Q(R) \qquad (B.3.6)$$

$$= s\beta^2 n\, (\xi - x,\ \eta - y,\ \zeta - z)\, R^{n-2} \qquad (B.3.7)$$

and similarly

$$\nabla_p(R^n) = -\, n\, (\xi - x,\ s\beta^2(\eta - y),\ s\beta^2(\zeta - z))\, R^{n-2} \qquad (B.3.8)$$

Thus, the integral expression (B.3.2) for $\vec{v}$ contains the term $\nabla_P \tilde{\nabla}_Q (1/R)$ given by:

$$\nabla_P \tilde{\nabla}_Q (1/R) = \frac{s\beta^2}{R^3} \begin{bmatrix} 1 & & \\ & 1 & \\ & & 1 \end{bmatrix} - \frac{3s\beta^2}{R^5} \begin{bmatrix} (\xi - x) \\ s\beta^2 \; (\eta - y) \\ s\beta^2 \; (\zeta - z) \end{bmatrix} (\xi - x, \; \eta - y, \; \zeta - z)$$

In subsonic flow (s=+1) this expression behaves like $1/R^3$ as $R \to 0$ while in supersonic flow (s=-1) it behaves like $1/R^5$ as $R \to 0$ for points (ξ, η, ζ) lying near the Mach cone and away from (x,y,z):

$$\xi \to x + \beta \sqrt{(\eta - y)^2 + (\zeta - z)^2} \; .$$

This strongly singular behavior of $\nabla_P \tilde{\nabla}_Q (1/R)$ causes substantial numerical difficulty in the subsonic case and, in the supersonic case causes the finite part integral

$$\iint^{*}_{S \cap D_P} \mu \; \nabla_P \tilde{\nabla}_Q (1/R) \cdot \hat{n}(Q) \, dS$$

to be unbounded for piecewise flat surfaces S. Historically in the development of subsonic panel methods, this strongly singular behavior has been used to approximately enforce doublet matching at network edges. However, this approach was never very satisfactory in achieving doublet matching and it was abandoned during the PAN AIR pilot code development when it was realized that it was unworkable for supersonic flows.

In PAN AIR the difficulty of this singular behavior is resolved by performing the line vortex integration by parts on the expression (B.3.2) for $\vec{v}$, thereby separating $\vec{v}$ into its regular part and its singular line vortex part. The regular part of $\vec{v}$ has the virtue that the singularities of its integrand are much less severe than those of equation (B.3.2) and further, that the finite part is nicely bounded for virtually all piecewise flat surfaces S. The singular line vortex part of $\vec{v}$ is then analytically removed from the calculation by enforcing doublet matching conditions of the type discussed in section 5.3 and appendix F.

A side benefit of the line vortex removal arises when we consider the evaluation of "far field" velocity influence coefficients. In this evaluation procedure one is required to use a Taylor series expansion for an inverse power of R. Without line vortex removal one would expand R^{-5} in a power series; with line vortex removal one expands R^{-3}. Because the resulting power series for R^{-3} converges more rapidly than the series for R^{-5}, the far field evaluation procedure is more accurate (for a given order of expansion) when the line vortex terms is removed.

Having given this statement of the fundamental problem, we now set out to discuss its resolution via the line vortex integration by parts. In what follows we will show that equation (B.3.2) implies that

$$\vec{v}(x,y,z) = -\frac{1}{\kappa} \iint^{*}_{S\cap D_p} \sigma(Q)\, \nabla_p\left(\frac{1}{R}\right) dS + \frac{1}{\kappa} \iint^{*}_{S\cap D_p} (\hat{n} \times \nabla_Q \mu) \times \tilde{\nabla}_Q\left(\frac{1}{R}\right) dS \tag{B.3.9}$$

$$+ \frac{1}{\kappa} \int^{*}_{\partial S} \mu\, \tilde{\nabla}_Q\left(\frac{1}{R}\right) \times d\vec{l}$$

where ∂S is the boundary of the surface S.

Before giving the derivation of this result (cf. equations (B.3.19) through (B.3.27)), we first discuss its significance and practical application. We will also shortly show why the line vortex integral (the last term of (B.3.9)) can be ignored. As a matter of terminology, the second term on the right of (B.3.9) is called the regular term of the doublet velocity, while the third term is called the line vortex term.

Now, we perform the integrations in (B.3.9) one panel at a time. Let us consider what is required for the line integrals to vanish. First, consider a panel edge with no adjoining panel edge next to it, for instance, the edge AB in figure B.11. Clearly, if μ identically equals zero on AB, the line integral along AB vanishes. Second, consider two adjacent panels as shown in figure B.12. As a convention, we define $d\vec{l}$ as being in the counterclockwise direction when looking from "above". That is, $d\vec{l} \times \hat{n}$ lies in the plane of the panel and points outward. Then if the doublet strength on the panel Σ_1 is $\mu_1(x,y,z)$, and on Σ_2 it is $\mu_2(x,y,z)$, and if $\mu_1 = \mu_2$ at every point on the edge AB, we have

$$\iint^{*}_{\Sigma_1 \cap AB \cap D_p} \mu\, \nabla_Q(1/R) \times d\vec{l} + \iint^{*}_{\Sigma_2 \cap AB \cap D_p} \mu\, \nabla_Q(1/R) \times d\vec{l} = 0 \tag{B.3.10}$$

since the integrands have identical values with opposite sign due to the opposite directions $d\vec{l}$.

We can generalize (B.3.10) to the case where arbitrarily many panel edges meet (see figure B.13 for an illustration of 3 panels meeting). Let

$$s_i = \text{sign}\,(d\vec{l}_i \cdot (\vec{B} - \vec{A})) \tag{B.3.11}$$

where $d\vec{l}_i$ is the counterclockwise direction on Σ_i.

Then if n = number of panels, and

$$\sum_{i=1}^{n} s_i\, \mu_i = 0 \tag{B.3.12}$$

on the entire edge AB, then

$$\sum_{i=1}^{n} \iint^{*}_{\Sigma_i \cap AB \cap D_p} \left\{ \mu_i \ \nabla Q\left(\frac{1}{R}\right) \times d\vec{l} \right\}_i = 0 \qquad \text{(B.3.13)}$$

Equation (B.3.13) follows from the fact that

$$\sum_{i=1}^{n} \mu_i \ d\vec{l}_i = 0 \qquad \text{(B.3.14)}$$

at all points on AB, which in turn follows from (B.3.11) and (B.3.12). It should be noted that if $n = 1$ or 2, (B.3.12) reduces to our previously derived results. So, if (B.3.12) is satisfied along a particular intersection of panel edges, the line integral in (B.3.9) can be ignored along that edge.

But now we must justify that (B.3.12) is physically reasonable. Consider the three surfaces in figure B.13, illustrated in cross section in figure B.14. Let P_1, P_2, and P_3 be points a small distance apart, as illlustrated illustrated in figure B.14. Let us assume (and this is not a completely trivial assumption) that ϕ is continuous in each of the regions V_1, V_2, and V_3, and bounded by some fixed value in the general vicinity of the intersection line. Writing ϕ_i for $\phi(P_i)$, it is then true that ϕ_i does not change much if P_i is moved slightly. Thus, we can let P_i approach one of the surfaces Σ_j without changing ϕ_i much. In particular, letting P_1 and P_2 approach Σ_1, we see that $\phi_1 - \phi_2 \approx \mu_1$. In fact, in the limit as P_1 and P_2 approach the intersection line,

$$\phi_1 - \phi_2 = \mu_1 \qquad \text{(B.3.15)}$$

Similarly, in the limit as the P_i approach the intersection,

$$\phi_3 - \phi_2 = \mu_2 \qquad \text{(B.3.16)}$$

$$\phi_1 - \phi_3 = \mu_3 \qquad \text{(B.3.17)}$$

Subtracting (B.3.15) from the sum of (B.3.16) and (B.3.17), we obtain

$$0 = -\mu_1 + \mu_2 + \mu_3 \qquad \text{(B.3.18)}$$

which is equivalent to equation (B.3.12).

The previous argument is generalizeable to an intersection of n surfaces. The assumption that ϕ be continuous off the surfaces is valid (and is in fact required for the basic integral representation formula to hold), but the requirement that ϕ be bounded in a neighborhood of the surface is not necessarily valid. It is, however, physically reasonable, since an unbounded potential produces an infinite velocity. So, we will make the assumption within PAN AIR. The mechanism by which (B.3.12) is applied is described in Appendix F. As a result of this assumption, the line vortex term in (B.3.9) may be ignored.

We now return to the proof of the relation (B.3.9). If we denote by $\vec{v}_D$ the part of $\vec{v}$ (cf. equation (B.3.1)) that depends only upon the doublet strength μ, then we have

$$\vec{v}_D(P) = \frac{1}{\kappa} \nabla_p \iint^{*}_{S \cap D_p} \mu(Q)\, \hat{n} \cdot \tilde{\nabla}_Q (1/R)\, dS_Q \tag{B.3.19}$$

If we write Stokes' theorem in the form

$$\int_{\partial S} d\vec{l} \cdot \vec{F} = \iint_S (\hat{n}\, dS \times \nabla) \cdot \vec{F} = \iint_S (\hat{n} \cdot \nabla \times \vec{F}) dS \tag{B.3.20}$$

then it is also clearly true that

$$\int_{\partial S} d\vec{l} \times \vec{G} = \iint_S (\hat{n} dS \times \nabla) \times \vec{G} \tag{B.3.21}$$

Setting $\vec{G} = \mu\, \tilde{\nabla}_Q (1/R)$ we obtain

$$\begin{aligned} \int_{\partial S} d\vec{l} \times [\mu\, \tilde{\nabla}_Q (1/R)] &= \iint_S (\hat{n}\, dS \times \nabla_Q) \times [\mu\, \tilde{\nabla}_Q (1/R)] \\ &= \iint_S (\hat{n}\, dS \times \nabla_Q \mu) \times \tilde{\nabla}_Q (1/R) \\ &+ \iint_S \mu\, (\hat{n}\, dS \times \nabla_Q) \times (\tilde{\nabla}_Q (1/R)) \end{aligned} \tag{B.3.22}$$

Now the integrand in the second term on the right can be expanded using the standard formula for a vector triple product $[(\vec{a} x \vec{b}) x \vec{c} = \vec{b}(\vec{a}.\vec{c}) - \vec{a}(\vec{b}.\vec{c})]$ to give

$$\begin{aligned} \mu\, (\hat{n}\, dS_Q \times \nabla_Q) \times (\tilde{\nabla}_Q (1/R)) &= \mu\, [dS_Q\, (\hat{n} . \tilde{\nabla}_Q)\, \nabla_Q (1/R) \\ &\quad - dS_Q\, \hat{n}\, (\nabla_Q \cdot \tilde{\nabla}_Q) (1/R)] \end{aligned}$$

Using the fact that the kernel function (1/R) satisfies the Prandtl-Glauert equation (cf. equation (5.4.9)),

$$\nabla_Q \cdot \tilde{\nabla}_Q (1/R) = 0 \tag{B.3.23}$$

we may simplify (B.3.22) to obtain

$$\int_{\partial S} d\vec{l} \times [\mu \ \tilde{\nabla}_Q \ (1/R)] = \iint_S (\hat{n} \ dS \times \nabla_Q \ \mu) \times \tilde{\nabla}_Q \ (1/R)$$

$$+ \iint_S \mu \ (\hat{n} \ . \ \tilde{\nabla}_Q) \ \nabla_Q \ (1/R) \ dS_Q \qquad \text{(B.3.24)}$$

Using the fact that $\nabla_Q \ (1/R) = - \nabla_p \ (1/R)$, the second integral on the right is clearly equal to

$$- \nabla_p \iint_S \mu(\hat{n} \ . \tilde{\nabla}_Q) \ (1/R) \ dS_Q$$

Solving for this quantity we obtain

$$\nabla_p \iint_S \mu \ (\hat{n} \ . \ \tilde{\nabla}_Q) \ (1/R) \ dS_Q = \iint_S (\hat{n} \times \nabla_Q \ \mu) \times \tilde{\nabla}_Q \ (1/R) \ dS_Q$$

$$+ \int_{\partial S} \mu \ \tilde{\nabla}_Q \ (1/R) \times d\vec{l}$$

$$\text{(B.3.25)}$$

In the case of supersonic problems, this relation must be interpreted as being true in a distributional sense, with all integrals taken to be finite part integrals. The modified equation reads

$$\nabla_p \iint^{*}_{S \cap D_p} \mu \ (\hat{n} \ . \ \tilde{\nabla}_Q) \ (1/R) \ dS_Q = \iint^{*}_{S \cap D_p} (n \times \nabla_Q \ \mu) \times \tilde{\nabla}_Q \ (1/R) \ dS_Q$$

$$+ \int^{*}_{\partial S \cap D_p} \mu \ \nabla_Q \ (1/R) \times d\vec{l}$$

$$\text{(B.3.26)}$$

The expression on the left is clearly recognizable as $[\kappa \ \vec{v}_D \ (P)]$, where $\vec{v}_D(P)$ was defined by (B.3.19). We find consequently that $\vec{v}_D(P)$ may be split as follows

$$\vec{v}_D(P) = (1/\kappa) \iint^{*}_{S \cap D_p} (\hat{n} \times \nabla_Q \ \mu) \times \tilde{\nabla}_Q \ (1/R) \ dS_Q$$

$$+ (1/\kappa) \iint^{*}_{\partial S \cap D_p} \mu \ \tilde{\nabla}_Q \ (1/R) \times d\vec{l} \qquad \text{(B.3.27)}$$

It is also clear that the substitution of (B.3.27) into (B.3.2) yields the splitting given by equation (B.3.9), completing our derivation of the line vortex integration by parts.

If we assume that the appropriate doublet matching is performed, so that the line vortex term can be dropped, then we may write the following formula for $\vec{v}^*(P)$, the regular part of $\vec{v}(P)$: (compare with equation B.3.9)

$$\vec{v}^*(P) = (1/\kappa) \iint_{S \cap D_p} \sigma(Q) \nabla_Q (1/R)\, dS_Q$$

$$+ (1/\kappa) \iint_{S \cap D_p} (\hat{n} \times \nabla_Q \mu) \times \tilde{\nabla}_Q (1/R)\, dS_Q \qquad \text{(B.3.28)}$$

Now while the evaluation of $\vec{v}^*(P)$ as given by (B.3.28) is a substantially better conditioned process than the evaluation of $\vec{v}(P)$ as given by equation (B.3.2), there still remains a mildly troublesome logarithmic singularity in $\vec{v}^*(P)$. This singularity can be isolated by a further integration by parts called the line source integration by parts. While it is not possible to fully implement this formula in PAN AIR*, we do state and prove it because it helps motivate the velocity jump matching condition used to enforce the Kutta condition.

We begin our derivation of the line source integration by parts by stating the Helmholtz relation for the velocity jump $\Delta\vec{v}$ across a singularity surface S. The formula reads**

$$\Delta\vec{v} = \sigma\, \hat{n}/(\hat{n},\vec{\nu}) + \nabla_t \mu \qquad \text{(B.3.29)}$$

where $\vec{\nu}$, the surface conormal is given by

$$\vec{\nu} = B\, \hat{n} \qquad \text{(B.3.30)}$$

---

* Such an implementation would require a geometry system capable of handling a continuous surface normal, $\hat{n}(Q)$, continuous source strength $\sigma(Q)$ and continuously differential (C^1) doublet strength, $\mu(Q)$.

** A simple proof of the Helmholtz' relation (B.3.29) is accomplished as follows. By virtue of the usual formula for calculating a vector triple product we have,

$$\nabla\phi = [(\hat{n} \times \nabla\phi) \times \vec{\nu} + \hat{n}(\vec{\nu} \cdot \nabla\phi)]/(\hat{n},\vec{\nu})$$

Evaluating this on the upper and lower surface of S, the singularity surface, we form the difference and obtain (footnote continued on following page)

and the tangential gradient operator ∇_t is given by

$$\nabla_t f = (\hat{n} \times \nabla f) \times \vec{v}/(n,\vec{v}) \tag{B.3.31}$$

Applying Stokes' theorem in the form (B.3.21) to the vector field $\vec{G} = B\Delta\vec{v}(1/R)$, we obtain after using Leibniz' rule on the right hand side

$$\int_{\partial S} d\vec{l} \times [B\Delta\vec{v}\,(1/R)] = \iint_S [\hat{n}\, dS \times \nabla(1/R)] \times B\Delta\vec{v} + \iint_S (1/R)\,[(\hat{n}\, dS \times \nabla) \times B\Delta\vec{v}] \tag{B.3.32}$$

Now the first integral appearing on the right hand side of this equation can be shown to be related to $\vec{v}^*$ (cf. (B.3.28)) by the formula

$$\iint_S [\hat{n}dS \times \nabla(1/R)] \times B\Delta\vec{v} = \kappa\,\vec{v}^* - \iint_S (\Delta\vec{v})\,\hat{n} \cdot \tilde{\nabla}(1/R)\, dS \tag{B.3.33}$$

To prove the formula (B.3.33), we simply expand the vector triple product in the integrand appearing on the left to get,

$$[\hat{n} \times \nabla(1/R)] \times B\Delta\vec{v} = \nabla(1/R)\,(\hat{n} \cdot B\Delta\vec{v}) - \hat{n}\,(\nabla(1/R) \cdot B\Delta\vec{v}) \tag{B.3.34}$$

It is easy to show from the formula for $\Delta\vec{v}$, (B.3.29), that

$$\hat{n} \cdot B\Delta\vec{v} = \vec{v} \cdot \Delta\vec{v} = \sigma \tag{B.3.35}$$

and that

(footnote continued from previous page)

$$(\nabla\phi)_U - (\nabla\phi)_L = [(\hat{n} \times \nabla(\phi_U - \phi_L)) \times \vec{v}]/(\hat{n},\vec{v}) + (\vec{v} \cdot \nabla(\phi_U - \phi_L))\hat{n}/(\hat{n},\vec{v})$$

We recognize the left hand side as the jump in perturbation velocity, $\Delta\vec{v}$, while the doublet strength and source strength appear on the right hand side in the forms (cf. equations (3.2.6) and (5.2.7)),

$$\mu = \phi_U - \phi_L$$

$$\sigma = (\vec{v} \cdot \nabla\phi)_U - (\vec{v} \cdot \nabla\phi)_L$$

Using these facts, we obtain finally,

$$\Delta\vec{v} = [(\hat{n} \times \nabla\mu) \times \vec{v}]/(\hat{n},\vec{v}) + \sigma\hat{n}/(\hat{n},\vec{v})$$

reproducing equation (B.3.29).

$$\hat{n} \times \Delta\vec{v} = \hat{n} \times \nabla_t \mu = \hat{n} \times \nabla\mu \tag{B.3.36}$$

As a consequence of this second relation we find in addition

$$\begin{aligned} -\hat{n}\,(\nabla(1/R) \cdot B\Delta\vec{v}) &= -\hat{n}\,(\tilde{\nabla}(1/R) \cdot \Delta\vec{v}) \\ &= (\hat{n} \times \Delta\vec{v}) \times \tilde{\nabla}(1/R) \\ &\quad - \Delta\vec{v}\,(\hat{n} \cdot \tilde{\nabla}(1/R)) \\ &= (\hat{n} \times \nabla\mu) \times \tilde{\nabla}(1/R) - \Delta\vec{v}\,(\hat{n} \cdot \tilde{\nabla}(1/R)) \end{aligned} \tag{B.3.37}$$

Substituting (B.3.35) and (B.3.37) into (B.3.34) we obtain

$$\begin{aligned} [\hat{n} \times \nabla(1/R)] \times B\Delta\vec{v} &= \sigma\,\nabla(1/R) + (\hat{n} \times \nabla\mu) \times \tilde{\nabla}(1/R) \\ &\quad - \Delta\vec{v}\,(\hat{n} \cdot \tilde{\nabla}(1/R)) \end{aligned} \tag{B.3.38}$$

Integrating this expression over S then yields

$$\begin{aligned} \iint_S [\hat{n}\,dS \times \nabla(1/R)] \times B\Delta\vec{v} &= \iint_S [\sigma\,\nabla(1/R) + (\hat{n} \times \nabla\mu) \times \tilde{\nabla}(1/R)]\,dS \\ &\quad - \iint_S \Delta\vec{v}\,\hat{n} \cdot \tilde{\nabla}(1/R)\,dS \end{aligned} \tag{B.3.39}$$

The first integral on the right is clearly equal to $\kappa\,\vec{v}^*$ as defined by (B.3.28). This proves the validity of the formula (B.3.33).

We conclude our derivation by substituting (B.3.33) into (B.3.32) to obtain

$$\begin{aligned} \int_{\partial S} d\vec{l} \times [B\Delta\vec{v}\,(1/R)] &= \kappa\,\vec{v}^* - \iint_S \Delta\vec{v}\,\hat{n} \cdot \tilde{\nabla}(1/R)\,dS \\ &\quad + \iint_S (1/R)\,(\hat{n}\,dS \times \nabla) \times B\Delta\vec{v} \end{aligned}$$

A trivial rearrangement of terms then yields the "line source integration by parts:"

$$\begin{aligned} \vec{v}^* &= -(1/\kappa) \iint_S \frac{(\hat{n} \times \nabla) \times B\Delta\vec{v}}{R}\,dS \\ &\quad + (1/\kappa) \iint_S \Delta\vec{v}\,\hat{n} \cdot \tilde{\nabla}(1/R)\,dS \\ &\quad + (1/\kappa) \int_{\partial S} (d\vec{l} \times B\Delta\vec{v})\,(1/R) \end{aligned} \tag{B.3.40}$$

Note that the last term on the right, which we call a line source term, isolates the logarithmically singular part of $\vec{v}^*$. The condition that must be satisfied in order to drop this term is quite similar to equation (B.3.12),

the analogous condition for dropping the line vortex term. This condition, imposed on the velocity jumps $\Delta\vec{v}_i$ is given

$$\sum_{i=1}^{n} s_i \; \Delta\vec{v}_i = 0 \tag{B.3.41}$$

We remark that this condition cannot generally be imposed in PAN AIR, even along panel boundaries in the interior of a network. The fundamental reason for this is that PAN AIR imposes on the functions $\hat{n}(Q)$, $\sigma(Q)$ and $\mu(Q)$ only the fairly weak continuity requirements

$$\hat{n}(Q) \in C^{-1}(S), \text{ the class of piecewise continuous functions on } S \tag{B.3.42a}$$

$$\sigma(Q) \in C^{-1}(S) \tag{B.3.42b}$$

$$\mu(Q) \in C^{0}(S), \text{ the class of continuous functions on } S \tag{B.3.42c}$$

whereas the satisfaction of condition (B.3.41) in the interior of a network would require

$$\hat{n}(Q) \in C^{0}(S) \tag{B.3.43a}$$

$$\sigma(Q) \in C^{0}(S) \tag{B.3.43b}$$

$$\mu(Q) \in C^{1}(S), \text{ the class of continuously differentiable functions} \tag{B.3.43c}$$

It is the first and last of these requirements (B.3.43a and B.3.43c) that would be most difficult to satisfy, both demanding the services of a C^1 geometry system for the singularity surface S.

Even though it is not generally feasible to impose the velocity jump matching condition (B.3.41) along all subsurface boundaries, it has nevertheless been found useful to impose a condition derived from it along the trailing edge of a lifting surface. This condition, sometimes called the vorticity matching Kutta condition, has the form

$$\vec{t} \cdot \sum_{i=1}^{n} s_i \; \Delta\vec{v}_i = 0 \tag{B.3.44}$$

where the vector $\vec{t}$ lies in the plane of the wake attached to the lifting surface and points downstream in the assumed direction of the convected vorticity. In section (H.2.4) we will show how equation (B.3.44) enforces the matching of upper and lower surface pressure coefficients (linear C_p rule) for standard configurations. It is in the sense that equation (B.3.44) enforces this matching of upper and lower surface values of $C_{p,\,\text{linear}}$ that it is appropriate to call it a "vorticity matching Kutta condition."

A few final remarks are appropriate concerning the line source integration by parts. We begin by adding the line vortex term back in to equation (B.3.40)

to obtain an expression for the perturbation velocity field, $\vec{v} = \nabla_p \phi$:

$$\vec{v} = -(1/\kappa) \iint_S \frac{(\hat{n} \times \nabla) \times B\Delta\vec{v}}{R} dS + (1/\kappa) \iint_S \Delta\vec{v}\, \hat{n} \cdot \tilde{\nabla}_Q (1/R)\, dS$$

$$+ (1/\kappa) \iint_{\partial S} (d\vec{l} \times B\Delta\vec{v})\, (1/R) + (1/\kappa) \iint_{\partial S} \mu\, \nabla_Q (1/R) \times d\vec{l} \tag{B.3.45}$$

First note that the terms on the first line bear a striking resemblance to the source and doublet terms of the standard representation of ϕ,

$$\phi = -(1/\kappa) \iint_S \frac{\Delta[\hat{n} \cdot \tilde{\nabla}\phi]}{R} dS + (1/\kappa) \iint_S \Delta\phi\, n \cdot \tilde{\nabla}_Q (1/R)\, dS$$

In fact it can be shown that the jump in the conormal derivative of $\vec{v}$, $\Delta[(\hat{n}.\tilde{\nabla})\vec{v}]$ satisfies the condition

$$\Delta\, [(\hat{n} \cdot \tilde{\nabla})\vec{v}] = (\hat{n} \times \nabla) \times B\Delta\vec{v}$$

so that the analogy between the two representation formulas is indeed quite close. Of course we would rather expect this to be the case given the fact that $\vec{v} = \nabla_p \phi$ must also satisfy the Prandtl-Glauert equation. What is somewhat surprising about equation (B.3.45) is the appearance of the singular line vortex and line source terms on the second line. The line vortex term must be added in to make $\vec{v}$ irrotational for those doublet distributions that do not satisfy the usual doublet matching conditions. Similarly, the line source terms are required to preserve the conservation of mass condition

$$\tilde{\nabla} \cdot \vec{v} = 0$$

for surface distributions of $\Delta\vec{v}$ that do not satisfy velocity jump matching conditions of the form (B.3.41).

B.4 Linear Sources and Quadratic Doublets

In this section we outline a justification for the use of a linear source strength approximation and a quadratic doublet approximation. For simplicity, we assume $M_\infty = 0$, though the proof is readily extendable to all subsonic Mach numbers. These results cannot be readily generalized to supersonic Mach numbers, however.

Nevertheless, for both supersonic and subsonic flow, we can show that a doublet distribution whose order is one higher than that of the source distribution is reasonable. We do this by considering the jump $\vec{v}_D$ in velocity occuring on a surface. In section N.1, we find

$$\vec{v}_D = \vec{\nabla}\mu + \frac{\sigma}{\hat{n}\cdot\hat{n}}\ \hat{n} \tag{B.4.1}$$

Thus the discontinuity in velocity has the same direct dependence on doublet gradient as on source strength. In addition, we will see in section J.11 that a discontinuity in doublet gradient induces the same singularities in potential and velocity as a singularity in source strength.

For these reasons we conclude that the doublet gradient is the same order of singularity as the source strength. It is thus reasonable to approximate the source strength and the components of the doublet same order of polynomial. Thus the doublet strength should be approximated by a polynomial of one degree higher than the source strength.

We now consider the case of zero Mach number. We consider the perturbation velocity resulting at a point P = 0 due to a source distribution

$$\sigma(\xi,\eta) = \sum_{i+j \leq n} \sigma_{ij}\ \xi^i\eta^j, \quad i \geq 0,\ j \geq 0 \tag{B.4.2a}$$

or a doublet distribution

$$\mu(\xi,\eta) = \sum_{i+j \leq n} \mu_{ij}\xi^i\eta^j \tag{B.4.2b}$$

on the square region S of size $2\epsilon \times 2\epsilon$ about P, illustrated in figure B.15.

Let us first consider the source distribution. By (B.3.1),

$$\vec{v}^S(x,y,z) = \frac{1}{4\pi}\ \nabla_P \iint_S \frac{-\sigma(\xi,\eta)}{\sqrt{(\xi-x)^2 + (\eta-y)^2 + (\zeta-z)^2}}\ d\xi d\eta \tag{B.4.3}$$

Thus,
$$\vec{v}_x\ (P) = \frac{1}{4\pi}\iint_{-\epsilon-\epsilon}^{\epsilon\epsilon} \frac{-\sigma_{ij}\ \xi^{i+1}\ \eta^j}{(\xi^2 + \eta^2)^{3/2}}\ d\xi\ d\eta \tag{B.4.4}$$

$$v_y(P) = \frac{1}{4\pi} \int_{-\varepsilon}^{\varepsilon}\int_{-\varepsilon}^{\varepsilon} \frac{-\sigma_{ij}\, \xi^i \eta^{j+i}}{(\xi^2+\eta^2)^{3/2}}\, d\xi d\eta \tag{B.4.5}$$

and

$$v_z(P) = \lim_{z\to 0} \frac{1}{4\pi} \int_{-\varepsilon}^{\varepsilon}\int_{-\varepsilon}^{\varepsilon} \frac{-\sigma_{ij}\, \xi^i \eta^j (-z)}{(\xi^2+\eta^2+z^2)^{3/2}}\, d\xi d\eta \tag{B.4.6}$$

Now, let us consider (B.4.4) one term at a time; that is, we assume

$$\sigma(\xi,\eta) = \sigma_{ij}\, \xi^i \eta^j \tag{B.4.7}$$

If (i+j) is even, the integrand in (B.4.4) is an "odd" function in ξ or η; that is, its value at (ξ,η) is minus its value at $(-\xi,\eta)$, or minus its value at $(\xi,-\eta)$, and thus the integral over S is zero. Similarly, if (i+j) is even, the integral (B.4.5) corresponding to that term is zero. Finally, let us consider the integral (B.4.6) for a single term.

We have

$$v_z(P) = \lim_{z\to 0} \frac{\sigma_{ij} z}{4\pi} \int_{-\varepsilon}^{\varepsilon}\int_{-\varepsilon}^{\varepsilon} \frac{\xi^i \eta^j}{(\xi^2+\eta^2+z^2)^{3/2}}\, d\xi d\eta \tag{B.4.8}$$

Now,

$$\int_0^{\varepsilon} \frac{\xi}{(\xi^2+\eta^2+z^2)^{3/2}}\, d\xi = \tag{B.4.9}$$

(substituting $u = \xi^2 + \eta^2 + z^2$)

$$\int_{\eta^2+z^2}^{\varepsilon^2+\eta^2+z^2} \left(u^{-3/2}\right) 1/2\, du = \left[-u^{-1/2}\right]\Big|_{\eta^2+Z^2}^{\varepsilon^2+\eta^2+z^2}$$

$$= \frac{1}{(\eta^2+z^2)^{1/2}} - \frac{1}{(\varepsilon^2+\eta^2+z^2)^{1/2}} \tag{B.4.10}$$

When this function is integrated over η, the result is $f(\varepsilon,z) - \log|z|$ where $f(\varepsilon,z)$ is bounded as $z\to 0$. Thus the limit in (B.4.8) is zero, provided $i = 1$. Since ε is small, $\xi^i\eta^j < |\xi|$ so the limit in (B.4.8) is zero whenever $i \geq 1$. Similarly, it is zero whenever $j \geq 1$, so we see that

$$\lim_{z\to 0} \int_{-\varepsilon}^{\varepsilon}\int_{-\varepsilon}^{\varepsilon} \frac{z\, \xi^i \eta^j}{(\xi^2+\eta^2+Z^2)^{3/2}}\, d\xi d\eta = 0 \tag{B.4.11}$$

if $i+j \geq 1$, and in particular, whenever i+j is even and greater than zero.

So, writing

$$\vec{v}^{S}(P)_{ij} = \frac{1}{4\pi} \nabla_P \iint_S \frac{\sigma_{ij}\xi^i\eta^j \, d\xi d\eta}{((\xi-x)^2+(\eta-y)^2+(\zeta-z)^2)^{1/2}} \tag{B.4.12}$$

we have $$\vec{v}^{S}(P)_{ij} = 0 \tag{B.4.13}$$

if i+j is even, and i+j > 0.

Let us now consider the velocity

$$\vec{v}^{D}(P)_{ij} =$$

$$\frac{1}{4\pi} \nabla_P \iint_S \mu_{ij}\xi^i\eta^j \, \hat{n}\cdot\vec{\nabla}_Q \frac{1}{[(\xi-x)^2+(\eta-y)^2+(\zeta-z)^2]^{1/2}} \, d\xi d\eta \tag{B.4.14}$$

induced by a polynomial doublet distribution

$$\mu(\xi,\eta) = \mu_{ij}\xi^i\eta^i \tag{B.4.15}$$

on the region in figure B.15.

Now,

$$\hat{n} = \begin{pmatrix} 0 \\ 0 \\ 1 \end{pmatrix} \tag{B.4.16}$$

and so $$\hat{n}\cdot\nabla_Q = \partial/\partial\zeta \tag{B.4.17}$$

Now,

$$\frac{\partial}{\partial\xi} \frac{1}{[(\xi-x)^2+(\eta-y)^2+(\zeta-z)^2]^{3/2}} =$$

$$-(\zeta-z)/[(\xi-x)^2+(\eta-y)^2+(\zeta-z)^2]^{3/2} \tag{B.4.18}$$

and since $\xi = 0$, x=y=0

$$\vec{v}^{D}(P)_{ij} = \lim_{z\to 0} \frac{1}{4\pi} \mu_{ij} \iint_S \frac{3z\,\xi^i\eta^i}{[\xi^2+\eta^2+z^2]^{3/2}} \begin{pmatrix} +\xi \\ +\eta \\ -z \end{pmatrix} d\xi d\eta$$

$$+ \iint_S \frac{\xi^i\eta^j}{[\xi^2+\eta^2+Z^2]^{3/2}} \begin{pmatrix} 0 \\ 0 \\ 1 \end{pmatrix} d\xi d\eta \tag{B.4.19}$$

For the x and y components of $\vec{v}^D(P)_{ij}$ we see that if i+j is even then the integrand is an odd function, so the integrals are zero. If i + j is odd and greater than 1, then performing an integration similar to (B.4.9) shows that the integrals in (B.4.19) are of the form $f(\varepsilon,z) - \log z$ where $f(\varepsilon,z)$ is bounded as $z \to 0$. Multiplying by z and taking the limit as $z \to 0$ we conclude that

$$\vec{v}^D_x\,(P)_{ij} = \vec{v}^D_y\,(P)_{ij} = 0 \qquad \text{(B.4.20)}$$

if $i + j > 1$.

The z component of $\vec{v}^D(P)_{ij}$ behaves somewhat differently, due to the presence of the second term. Both terms vanish if at least one of i or j is odd, by the usual odd function argument. In addition, the first term is zero if $i + j \geq 3$ by the same reasoning as the last paragraph. The second term,

$$\lim_{z\to 0} \frac{\mu_{ij}}{4\pi} \iint_S \frac{\xi^i \eta^j}{(\xi^2+\eta^2+z^2)^{3/2}}\, d\xi d\eta \quad , \qquad \text{(B.4.21)}$$

does not necessarily vanish if both i and j are even. But it is of order ε^2 if $i + j \geq 4$, and since it vanishes for $i + j = 3$, it seems reasonable to approximate the local doublet distribution by a polynomial with $i + j \leq 2$.

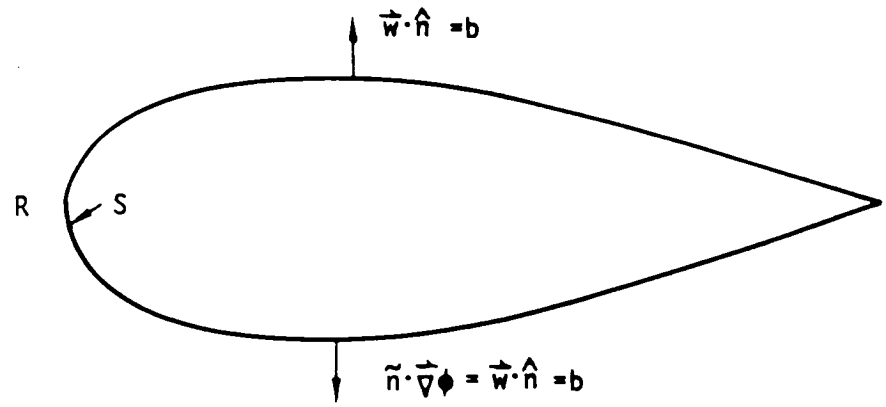

Figure B.1 - An exterior boundary value problem

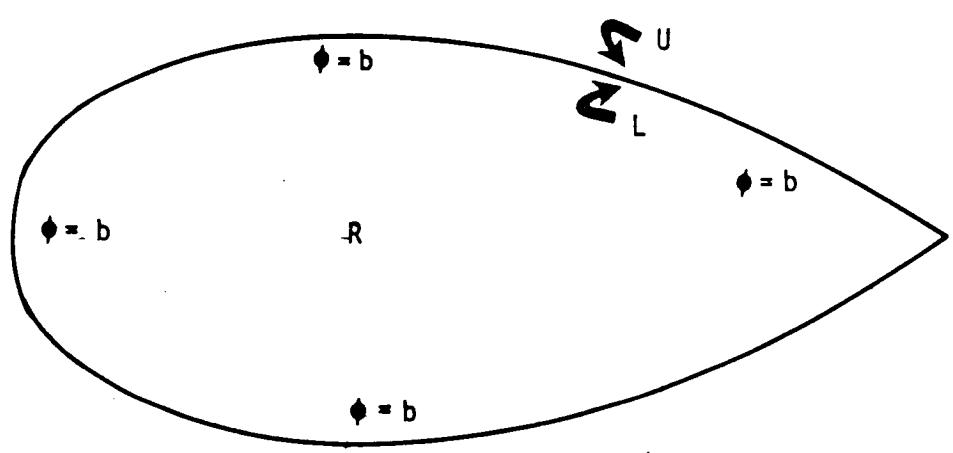

Figure B.2 - A region of finite volume

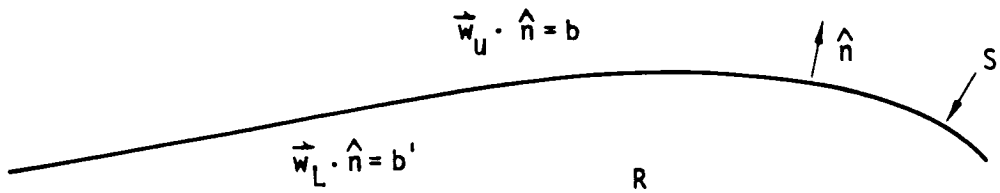

Figure B.3 - Specification of normal flow on both sides of a surface

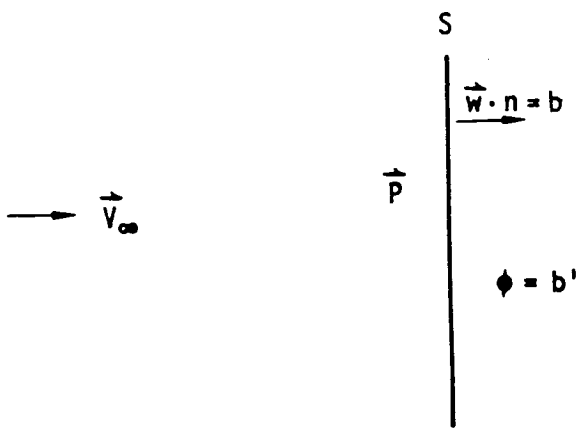

Figure B.4 - A superinclined surface

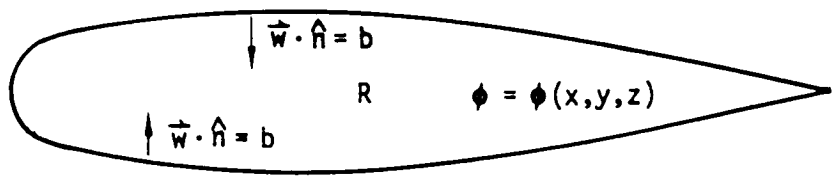

Figure B.5 - A boundary value problem with no unique solution

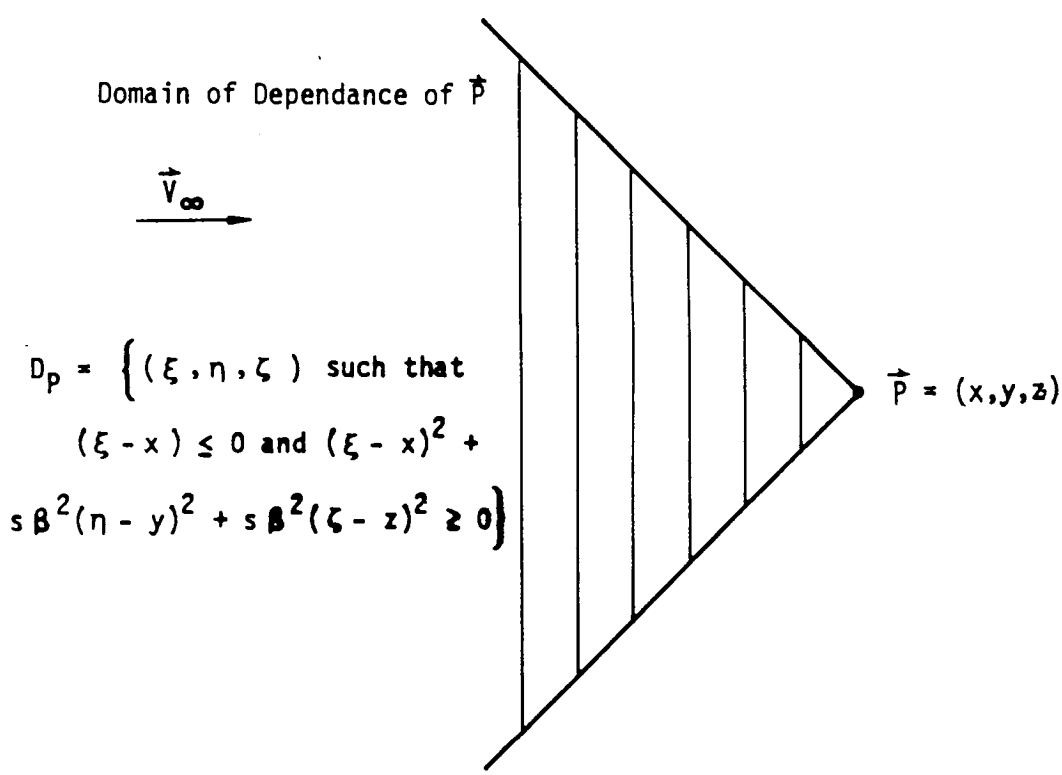

Figure B.6 - The Domain of Dependence

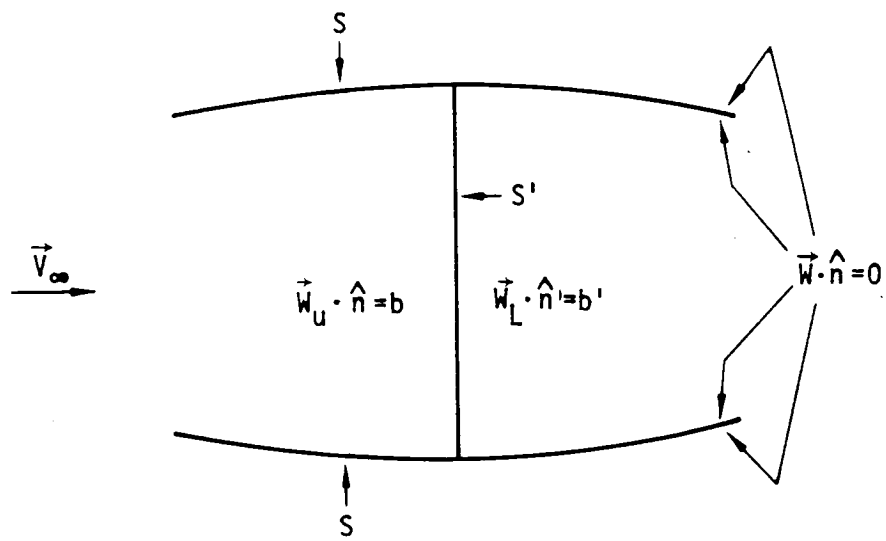

Figure B.7 - A permeable surface inclined to the freestream

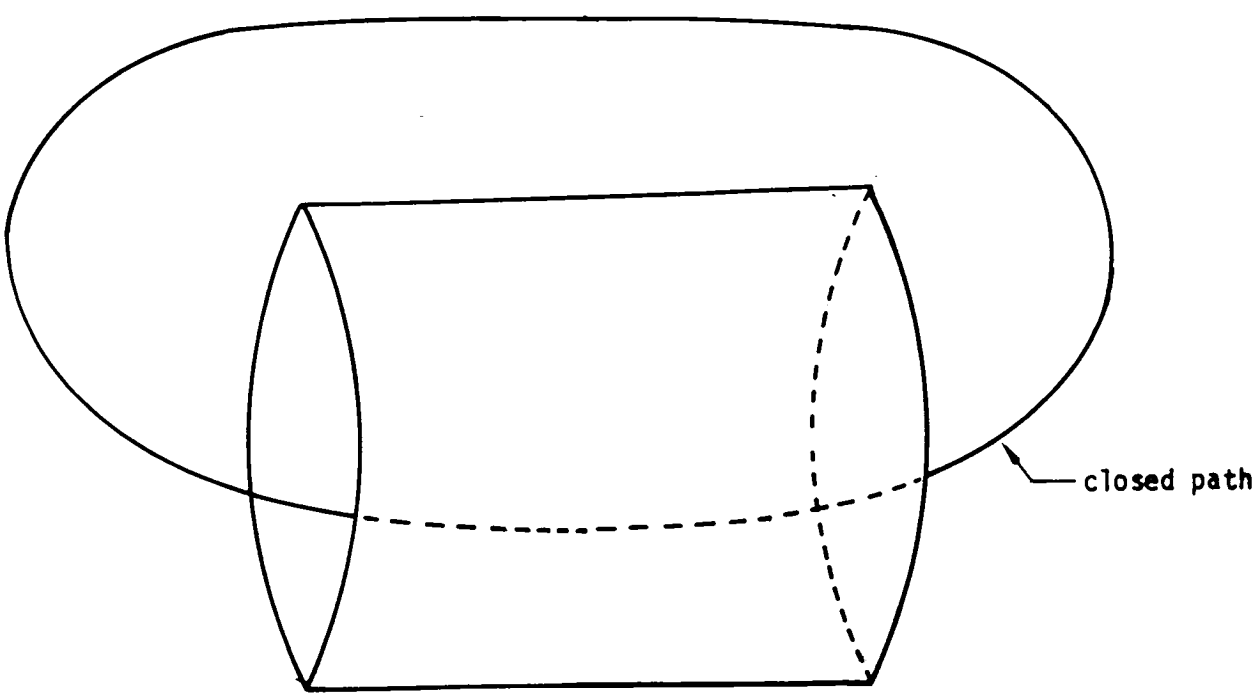

Figure B.8 - A region which fails to be simply connected

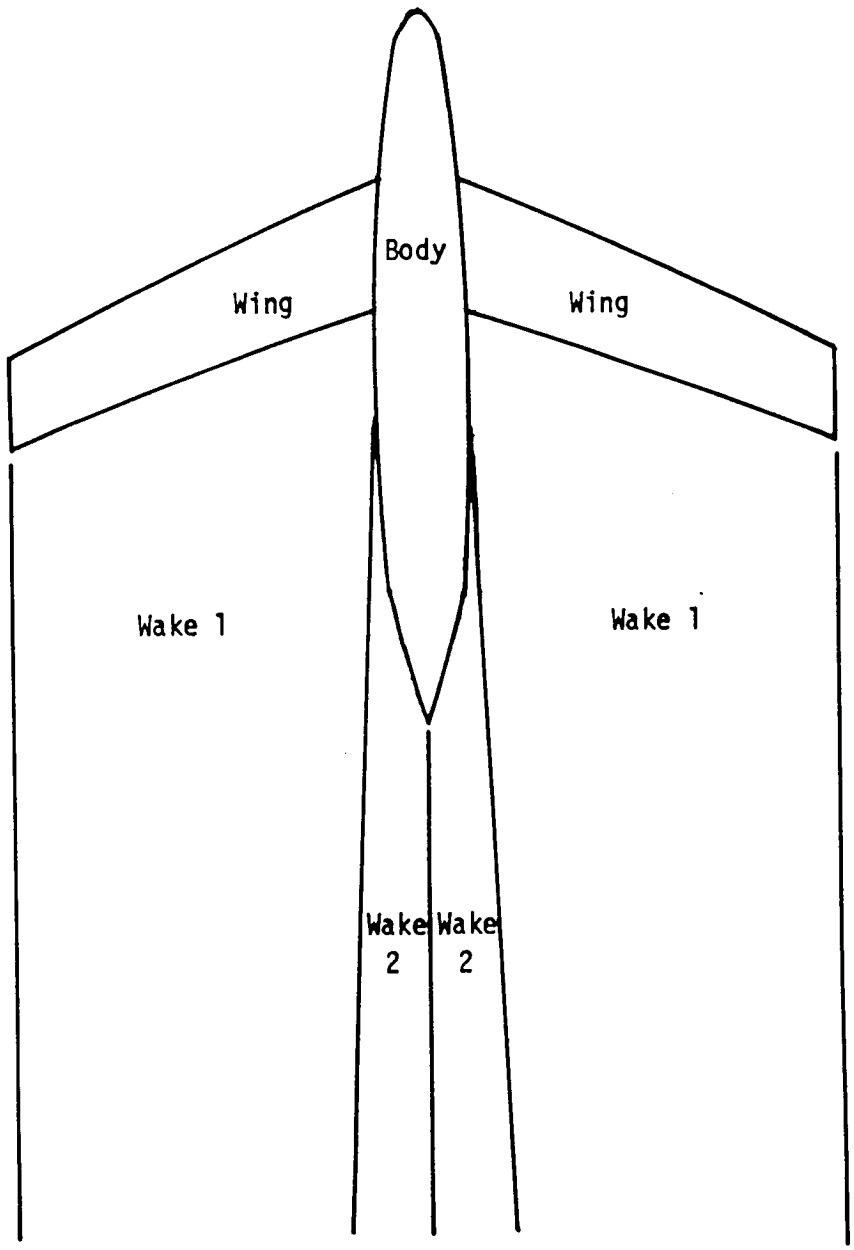

Figure B.9 - Airplane and wake

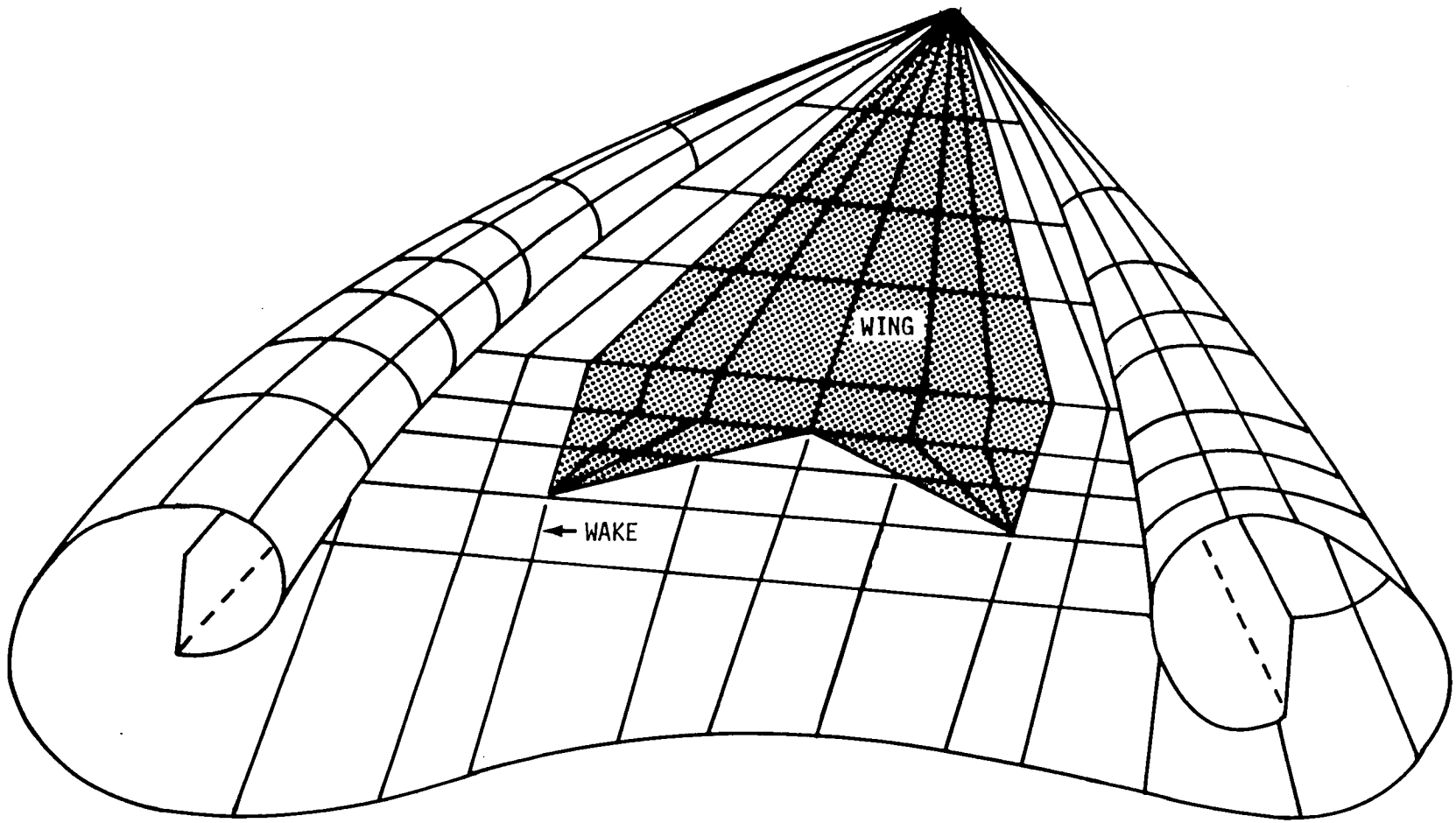

Figure B.10 - Leading edge vortices from a highly swept wing

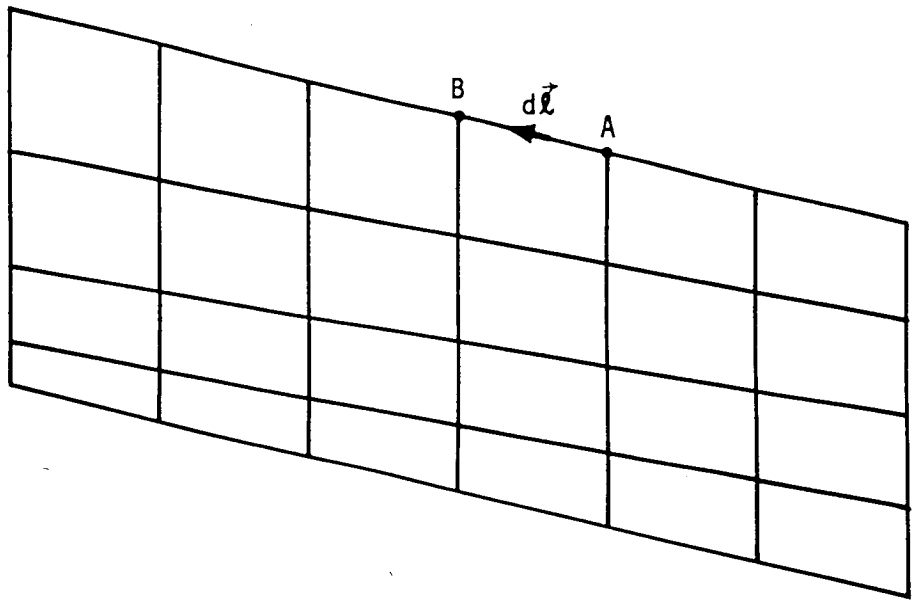

Figure B.11 - Panel edge on a network edge

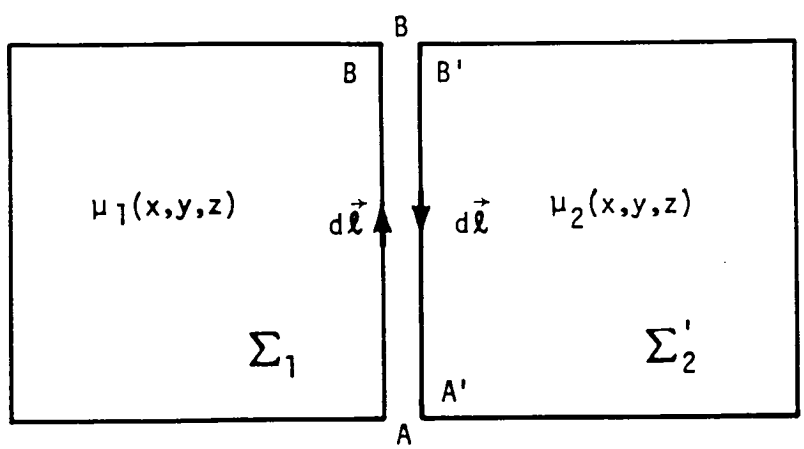

Figure B.12 - Two adjacent panel edges

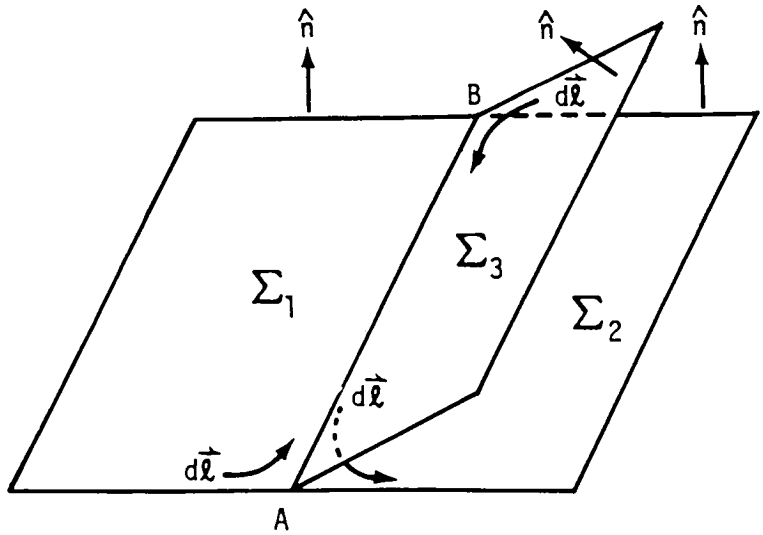

Figure B.13 - Three adjacent panels

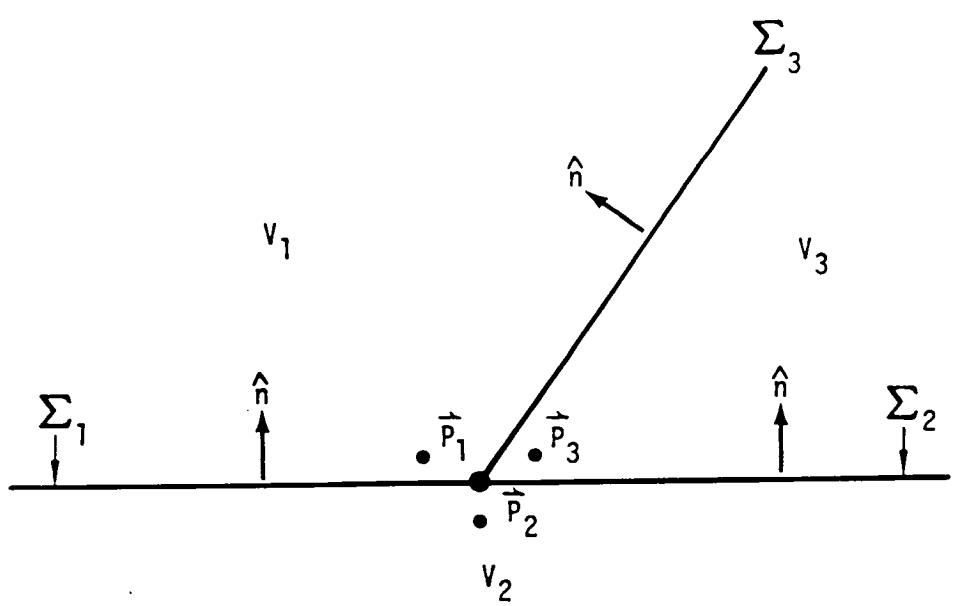

Figure B.14 - Intersection of 3 surfaces (cross-section)

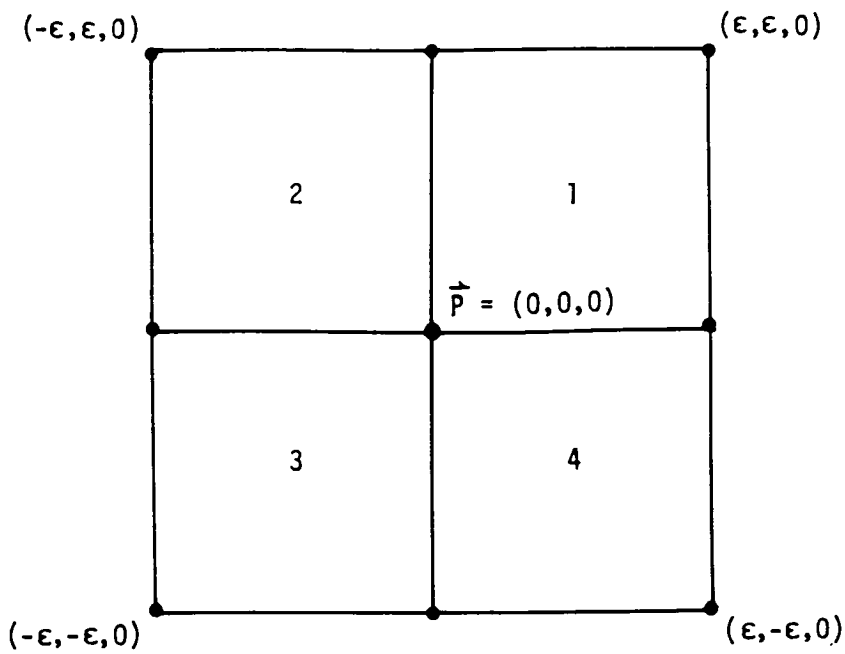

Figure B.15 - Region of integration in neighborhood of $\vec{P}$

C.0 The Design Problem

In the design problem the user attempts to obtain a configuration whose shape is unknown, but is subject to certain constraints. For instance, a wing may be required to have a certain planform, but its camber and thickness distributions may be the subject of the design process. The constraints involved in this case would be (1) that the surface be impermeable, and (2) that particular pressure or tangential velocity distributions be required.

Now, specification of both normal and tangential flow on a surface is an overspecification of boundary conditions, and thus in general there is no one step solution to the design problem. The exception is called "linearized design", in which the user is satisfied with a first order approximation to the solution. This method is discussed in section C.1.

In section C.2, we discuss a somewhat more sophisticated procedure, which we call sequential design. This is a non-automatic iterative procedure in which a single loop in the iteration consists of:

(a) a potential flow analysis (for example, a boundary value problem with impermeability boundary conditions) of the configuration at hand,
(b) a comparison of the pressures computed in (a) with the desired pressure distribution, leading to the specification of tangential velocity boundary conditions,
(c) solution of the potential flow problem for the tangential velocity boundary conditions, and computation of the normal flow through the surface, and
(d) "relofting" of the configuration geometry, using the normal flow data, in order to produce a more nearly impermeable surface.

This procedure can be executed in the first version of PAN AIR, though steps (b) and (d) will have to be performed manually by the program user.

In section C.3, we briefly discuss a still more sophisticated design method, which we simply call "iterative design". This method is distinguished from sequential design in its relofting method.

Finally, in section C.4, we discuss stability problems occuring from the discretization process. These problems generally result when a small perturbation in a boundary condition generates a perturbation in the solution which does not die out with distance. Since the discretization process always results in some numerical error, stability problems can result in a totally incorrect solution.

We do not discuss the imposition of "closure" boundary conditions in this appendix, but rather discuss that subject in section H.2.

C.1 Linearized Design

The basic assumption of linearized design is that

$$C_p = -2u \tag{C.1.1}$$

where C_p is the pressure coefficient at a point, and u is a component of the perturbation velocity

$$\vec{v}\ (x,y,z) = (u,v,w) \tag{C.1.2}$$

Again, we assume $|\vec{V}_\infty| = 1$.
Equation (C.1.1) will be derived in Appendix N. Generally speaking, (C.1.1) is valid only for thin configurations with little camber at small angles of attack, such as the configuration in figure C.1.

Now, the program user wishes to specify a difference in pressure distribution ΔC_{p_S} (x,y,z) on the configuration, where

$$\Delta C_p = C_{p,\ \text{upper}} - C_{p,\ \text{lower}} \tag{C.1.3}$$

Noting that $$u = \vec{v}\cdot\vec{V}_\infty \tag{C.1.4}$$

(since $|\vec{V}_\infty| = 1$) we have

$$\begin{aligned} \Delta C_p &= -2(\vec{v}_U - \vec{v}_L)\cdot\vec{V}_\infty \\ &= -2\vec{\nabla}(\phi_U - \phi_L)\cdot\vec{V}_\infty \\ &= -2\vec{\nabla}\mu\cdot\vec{V}_\infty \end{aligned} \tag{C.1.5}$$

Thus, the boundary condition to impose at (x,y,z) is

$$(-2\vec{V}_\infty)\cdot\vec{\nabla}\mu = \Delta C_{p_S}\ (x,y,z) \tag{C.1.6}$$

which is of the form

$$\vec{t}_D\cdot\vec{\nabla}\mu = b \tag{C.1.7}$$

(see (5.4.21) for the general boundary condition equation).

Now, the boundary value problem described by (C.1.7) is solved numerically, in the course of which the total mass flux at the control points is evaluated. The mass flux is used to reloft the surface as follows. <u>The procedure we describe is not incorporated in version 1.0 of PAN AIR.</u>

The relofting takes place one network at a time (for a brief discussion of networks and panels, see section 5.1). Two edges of the network are left fixed or, if the geometry of the adjacent network has been relofted, these edges are adjusted to close the gap. In figure C.2, these edges are edges 1 and 4.

The remainder of the network is relofted one panel corner point at a time. This is done by alternately relofting columns and rows of corner points. For instance, in the example of figure C.2, first point (2,2) is relofted, then (3,2), etc., then (6,2), then (2,3), then (2,4), and then we move one row and column inward, relofting (3,3),...,(6,3), and then (3,4), and one final time we move one more row and column inward, and then the whole network in figure C.2 has been relofted. Thus a point is relofted only after all the points closer to the network origin (in an indicial sense) have been relofted. We now describe the relofting procedure for a typical point.

The point P_4(see figure C.3) is relofted to a point P_4' as follows. Let $\Delta\vec{P}_4 = \vec{P}_4' - \vec{P}_4$. Then the user chooses a direction $\hat{d}$ for ΔP_4; that is, requires that

$$\Delta\vec{P}_4 = k\hat{d} \tag{C.1.8}$$

One then determines the value of k which minimizes $\vec{W}\cdot\hat{n}'$, where $\hat{n}'$ is the normal of the relofted panel. In Appendix D, we show that

$$\hat{n}' = \frac{(\vec{P}_3-\vec{P}_1) \times (\vec{P}_4'-\vec{P}_2)}{|(\vec{P}_3-\vec{P}_1) \times (\vec{P}_4'-\vec{P}_2)|} \tag{C.1.9}$$

So, we can equally well minimize

$$|\delta\cdot\vec{W}\cdot\hat{n}'| = |\vec{W}\cdot\left\{(\vec{P}_3-\vec{P}_1) \times (\vec{P}_4'-\vec{P}_2)\right\}| \tag{C.1.10}$$

where δ is the denominator of (C.1.9).

Writing $$\vec{P}_4' = \vec{P}_4 + k\hat{d} \tag{C.1.11}$$

we minimize $|f(k)|$, where

$$f(k) = \vec{W}\cdot\left\{(\vec{P}_3-\vec{P}_1) \times (\vec{P}_4-\vec{P}_2)\right\} + k\vec{W}\cdot(\vec{P}_3-\vec{P}_1) \times \hat{d} \tag{C.1.12}$$

which, being linear in k, is zero for

$$k = \frac{-\vec{W}\cdot(\vec{P}_3-\vec{P}_1) \times (\vec{P}_4-\vec{P}_2)}{\vec{W}\cdot\left\{(\vec{P}_3-\vec{P}_1) \times \hat{d}\right\}} \tag{C.1.13}$$

This is well defined providing $\hat{d}$ has been chosen so that it is not parallel to $(\vec{P}_3-\vec{P}_1)$ and provided $\vec{W}$ is not in the plane spanned by $(\vec{P}_3-\vec{P}_1)$ and $\hat{d}$.

So, (C.1.11) defines P_4', and we may continue to the next corner point to be relofted.

In the case of linearized design, we stop here, since we have the best answer we can obtain with the linear pressure formula. The relofted configuration is considered the surface whose distributions of pressure and normal mass flux are the desired ones.

C.2 Sequential Design

In sequential design, the first step is again to supply a guess at the configuration which will yield the desired pressure distribution, and solve the potential flow problem about that configuration with zero normal flow boundary conditions. This results in a pressure distribution $C_p(x,y,z)$. Generally speaking, the second order or isentropic pressure formula would be used to compute this pressure distribution. Now, barring remarkable aerodynamic insight on the part of the user, this pressure distribution will differ from his desired distribution $C_{p_S}(x,y,z)$, but hopefully not by too much. We also compute the preliminary perturbation velocity distribution $\vec{v}(x,y,z)$ resulting from the potential flow solution.

Now, we "linearize" about our previous solution by making the assumption (analogous to (C.1.1)) in that if $C_{p_S}(x,y,z)$ is close to $C_{p_p}(x,y,z)$, then

$$C_{p_S}(x,y,z) - C_{p_p}(x,y,z) = -2\vec{V}_\infty \cdot (\vec{v}_S(x,y,z) - \vec{v}_p(x,y,z)) \qquad \text{(C.2.1)}$$

where $\vec{v}_S$ is the unknown velocity distribution which produces the desired pressure distribution C_{p_S}. Solving for the freestream component of $\vec{v}_S$,

$$\vec{V}_\infty \cdot \vec{v}_S(x,y,z) = \vec{V}_\infty \cdot \vec{v}_p(x,y,z) - 1/2(C_{p_S} - C_{p_p}) \qquad \text{(C.2.2)}$$

Considering the configuration in figure C.4 (in which $C_{p,upper} = \Delta C_p$ since $C_{p,lower} = 0$), equation (C.2.2) shows that we apply the boundary condition

$$\vec{t}_D \cdot \vec{\nabla}\mu = b \qquad \text{(C.2.3)}$$

since

$$\vec{\nabla}\mu = \vec{v}_U - \vec{v}_L = \vec{v}_U \qquad \text{(C.2.4)}$$

where $\vec{t}_D$ is the projection of $\vec{V}_\infty$ to the surface

and

$$b = \vec{V}_\infty \cdot \vec{v}_p(x,y,z) - 1/2(C_{p_S} - C_{p_p}) \qquad \text{(C.2.5)}$$

Now, once the potential flow problem with the boundary conditions has been solved, the relofting is performed just as described in section C.1. Then an analysis case (that is, a potential flow problem with impermeability boundary conditions) is run, and the new pressure and velocity distributions are evaluated, and the next cycle of the procedure continues.

If all goes well, the procedure converges, resulting in a configuration of reasonable shape, with the desired pressure distribution. Unfortunately, if the initial guess does not yield a pressure distribution $C_p(x,y,z)$ close to $C_p(x,y,z)$, the procedure may fail to converge.

C.3 Iterative Design

The procedure we describe briefly in this section is much more accurate and rapidly convergent than sequential design, but also considerably more sophisticated, and not available in PAN AIR. It encompasses two features not found in sequential design. The first one is full automation; the relofting and the formulation of the boundary conditions are performed automatically by the program. The second is a more sophisticated relofting method.

This relofting method involves "differentiated influence coefficients". That is, once the potential flow solution has been performed, and the source and doublet parameters are known, the matrices $\frac{\partial \vec{v}(P_i)}{\partial CP_j}$ are computed for all i and j, where P_i is the ith control point, and CP_j is the jth panel corner point. The matrix $[\partial v/\partial CP_j]$ is a 3x3 matrix, one of which exists for each pair of control point P_i and corner point CP_j, whose k,l entry is $\partial v_k/\partial CP_l$. Given these matrices, standard optimization techniques can be used in order to generate a revised geometry for which $\iint_S W\cdot\hat{n}'\, dS$ is minimized, subject to user-input constraints such as leaving the planform area the same.

We will not discuss this process further here, since PAN AIR does not make use of differentiated influence coefficients, and thus does not perform iterative design. A more detailed discussion of iterative design, for the special case of leading edge vortices, is given in reference (B.2).

C.4 Stability

The problem of stability arises from the inherent numerical error in the discretization process, rather than from the theory of the Prandtl-Glauert equation. It is the splining method (see section 5.5 for a discussion of splines) in combination with the boundary conditions which is called stable or unstable. Precisely, a spline is called unstable if the perturbation of a single boundary condition results in a perturbation in the original solution which does not die out with distance from the point at which the boundary condition is located.

In checking for stability, we may make use of the fact that the sum of solutions of the Prandtl-Glauert equation is again a solution. Thus, the solution to any boundary value problem is a linear combination of individual solutions of cases in which one boundary value is set equal to one and the rest are set to zero. We thus check for stability by observing the singularity distribution which occurs when one boundary value is set to one and the rest to zero. The resulting singularity distribution should rapidly dimimish in magnitude as the distance from the non-zero boundary condition increases. We consider a spline more stable, the more rapidly the singularity distribution diminishes.

The simplest way to illustrate stability is with two-dimensional examples. Thus, a "network" of "panels" consists of a sequence of intervals. For simplicity, all our splines will be doublet splines, though what we discuss will be applicable to source splines as well.

In figure C.5, we illustrate a doublet spline with singularity parameters and control points located at panel centers, and for which the doublet strength on a panel is constant, and equal to the singularity parameter value. In figure C.6, we illustrate the doublet distribution arising from the boundary conditions $\mu = 0$ at all but one control point, $\mu = 1$ at the remaining one. We see that the perturbation induced on the uniformly zero solution by the single non-zero boundary value dies down extremely rapidly; in fact, the perturbation is zero except on the single panel containing the non-zero boundary condition. Thus this spline is very stable. But we know (see Appendix B.4) that locally constant splines are insufficient, so we consider a quadratic spline, as illustrated in figure C.7. Because of the rapid variation a quadratic function may exhibit, control points and singularity parameters are required at the network edges in order to define the singularity strength adequately.

The spline is a piecewise quadratic one, where the quadratic variation is constructed as follows. The value of, for instance, $\mu(P)$ is determined by finding the quadratic function $f(x)$ which goes through Q_2 and Q_3 exactly, and then goes through Q_1 and Q_4 in a least squares sense. Then $\mu(P)$ is given as $f(P)$. The details concerning the method by which we obtain the row vector S of length 4 such that

$$\mu(P) = \lfloor S \rfloor \begin{Bmatrix} \mu(Q_1) \\ \cdot \\ \mu(Q_4) \end{Bmatrix} \tag{C.4.1}$$

are given in Appendix I.5.

Now, once we know μ at every corner point on the network, the quadratic distribution of μ on an interval is that quadratic function which takes on the computed values at the endpoints, and the singularity parameter value at the panel center. Considering the interval in figure C.8, in the local coordinates illustrated there, we have

$$\mu(x) = a+bx+cx^2 \tag{C.4.1}$$

$$\mu(-1) = \mu(P) = a-b+c \tag{C.4.2}$$

$$\mu(0) = \mu(Q) = a \tag{C.4.3}$$

$$\mu(1) = \mu(P') = a+b+c \tag{C.4.4}$$

So, subtracting (C.4.2) from (C.4.4),

$$2b = \mu(P') - \mu(P) \tag{C.4.5}$$

while, adding these equations,

$$2a + 2c = \mu(P) + \mu(P') \tag{C.4.6}$$

$$= 2c + 2\mu(Q) \tag{C.4.7}$$

Thus (by (C.4.3)) we have values for a, b, and c, and so

$$\mu(x) = \mu(Q) + \frac{\mu(P')-\mu(P)}{2} x + \frac{\mu(P)+\mu(P')-2\mu(Q)}{2} x^2 \tag{C.4.8}$$

In figure C.9 , we illustrate the doublet distribution we obtain by setting $\mu = 1$ at one control point, and $\mu = 0$ at the others, given the spline just described. Note that this spline is nearly as stable as that of figure C.6; the disturbance dies down very quickly.

Further, this spline yields a doublet strength which is continuous across panel edges, something which is very important.

But the same spline, with boundary conditions

$$\frac{\partial\mu}{\partial x} = 1 \tag{C.4.9}$$

at the last control point, and

$$\frac{\partial\mu}{\partial x} = 0 \tag{C.4.10}$$

at the others (except $\mu = 0$ at the first control point to insure uniqueness) yields the doublet distribution (solving the boundary value problem numerically) illustrated in figure C.10, which compares unfavorably with the identically zero doublet distribution obtained by replacing the right size of (C.4.9) by zero.

But now, consider the doublet parameter and control point locations illustrated in figure C.11. If we impose the boundary conditions (C.4.9) and (C.4.10), we claim that the resulting doublet distribution is illustrated in

figure C.12. While the doublet distribution in figure (C.10) was obtained numerically, that of figure (C.12) can be obtained theoretically in the following manner.

Consider a distribution $\mu(x) = a+bx+cx^2$ on the interval in figure C.8. Now,

$$\frac{\partial\mu}{\partial x}(Q) = \frac{\partial\mu}{\partial x}(0) = b \tag{C.4.11}$$

and by (C.4.5)

$$b = \frac{\mu(P') - \mu(P)}{2} \tag{C.4.12}$$

Thus,

$$\mu(P') = \mu(P) + 2b = \mu(P) + 2\frac{\partial\mu}{\partial x}(Q) \tag{C.4.13}$$

So, applying (C.4.10) and (C.4.13) to figure C.12 with $P=P_0$, $P' = P_1$, $Q=Q_1$, we obtain

$$\mu(P_1) = 0 \tag{C.4.14}$$

But now that we know $\mu(P_1)$, we apply (C.4.14) to the second intervals, and so

$$\mu(P_2) = 0 \tag{C.4.15}$$

We continue this way, obtaining

$$\mu(P_i) = 0, \; i\leq 6 \tag{C.4.16}$$

$$\mu(P)_7 = \mu(P_6) + 2\frac{\partial\mu}{\partial x}(Q_7) = 2$$

$$\mu(P_6) + 2\frac{\partial\mu}{\partial x}(Q_7) = 2$$

If we now obtain $\mu(Q_i)$ by least squaring to the 4 surrounding P_i, we see

$$\mu(Q_i) = 0, \; i \leq 5 \tag{C.4.17}$$

$$\mu(Q_6) = 0 \tag{C.4.18}$$

$$\mu(Q_7) = 1 \tag{C.4.19}$$

and thus we obtain the doublet distribution of figure C.12.

So, comparing with figure C.10, we see that the imposition of doublet derivative boundary conditions at panel centers requires a different spline than the imposition of boundary conditions defining doublet strength. This situation generalizes to three dimensions, and thus requires different splines for design (that is, doublet gradient) boundary conditions than are used for analysis (that is, normal mass flux) boundary conditions.

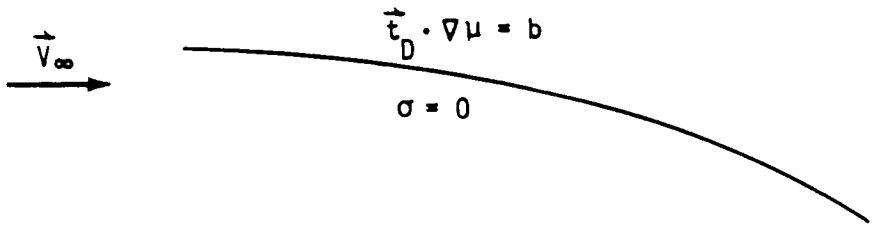

Figure C.1 - Design boundary conditions on a thin configuration

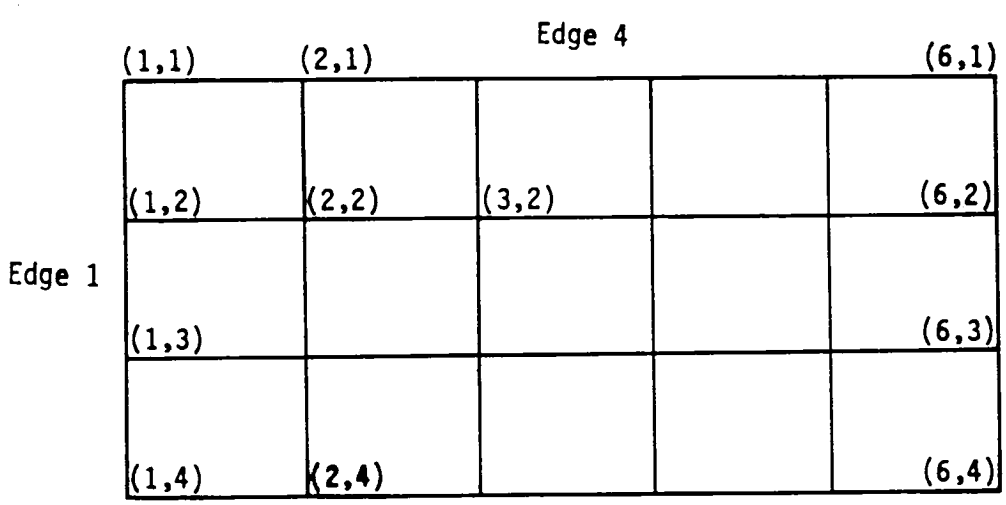

Figure C.2 - Indexing of network points

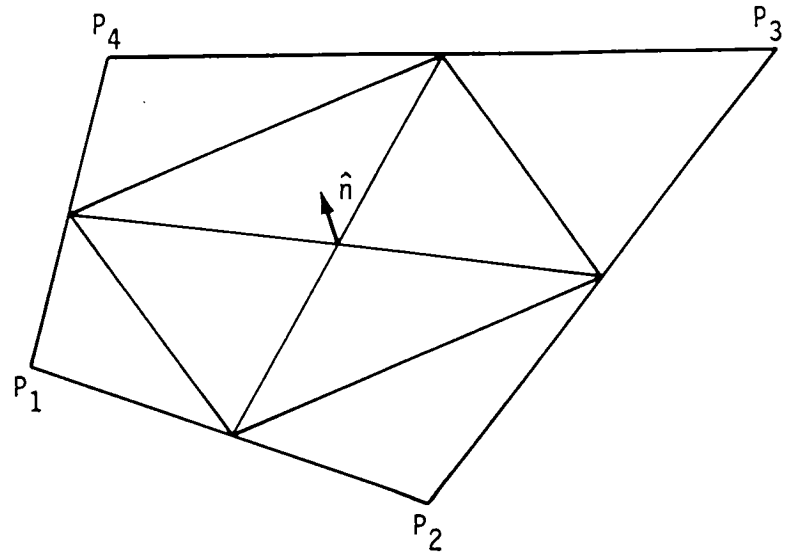

Figure C.3 - A panel

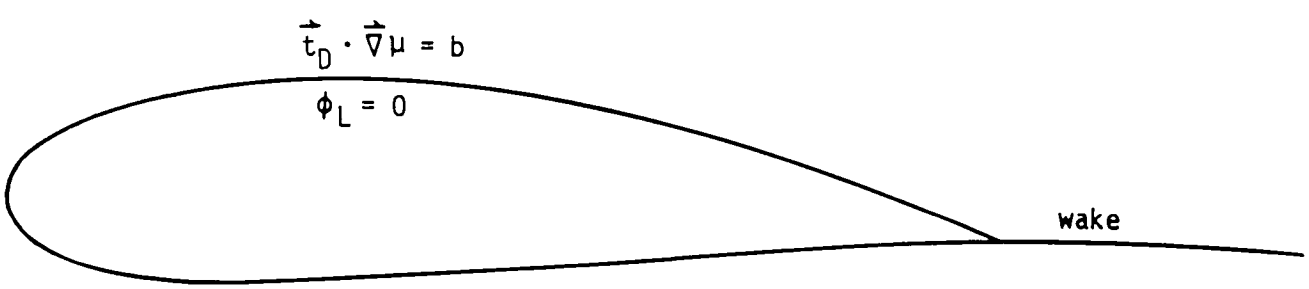

Figure C.4 - Design boundary conditions for a thick wing

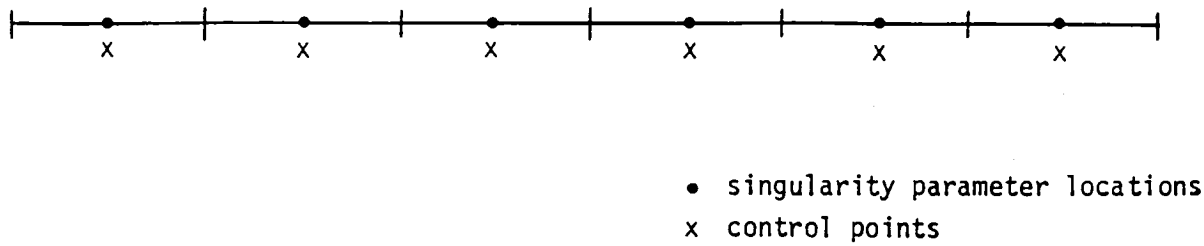

Figure C.5 - A constant doublet strength spline

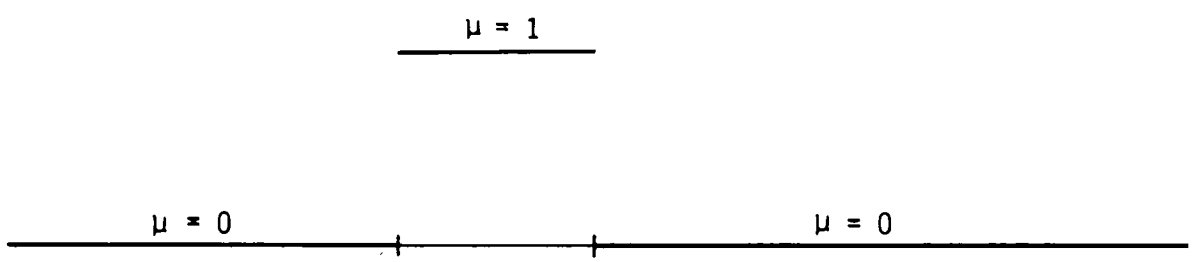

Figure C.6 - Stability for constant doublet spline

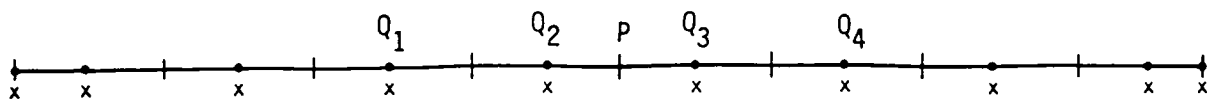

Figure C.7 - Quadratically varying doublet spline

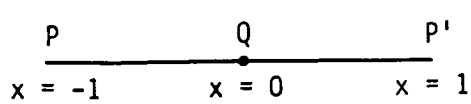

Figure C.8 - A single interval

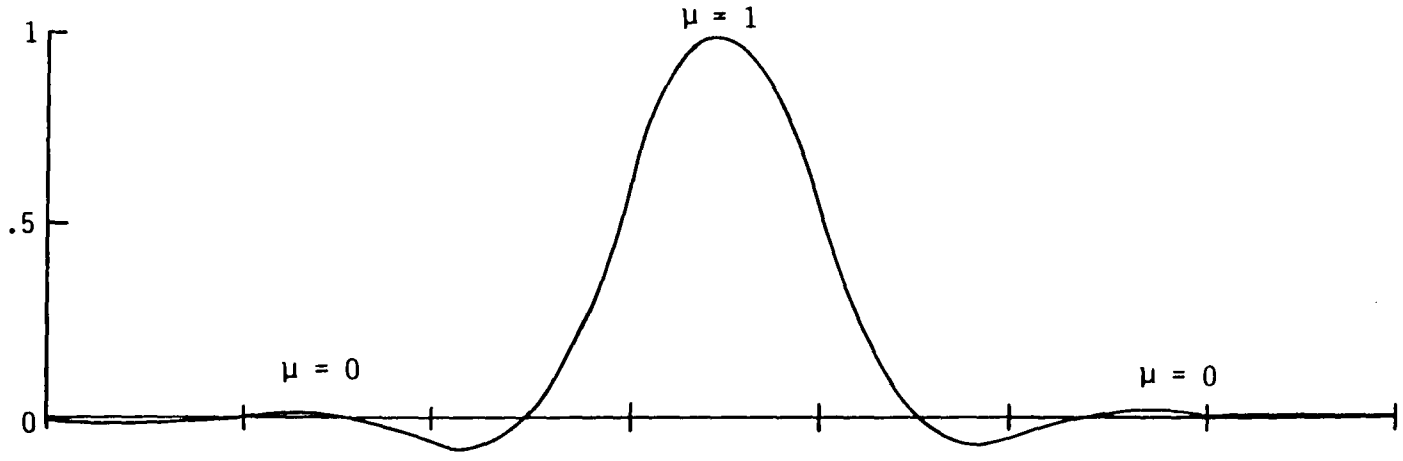

Figure C.9 - Stability for a quadratic doublet spline

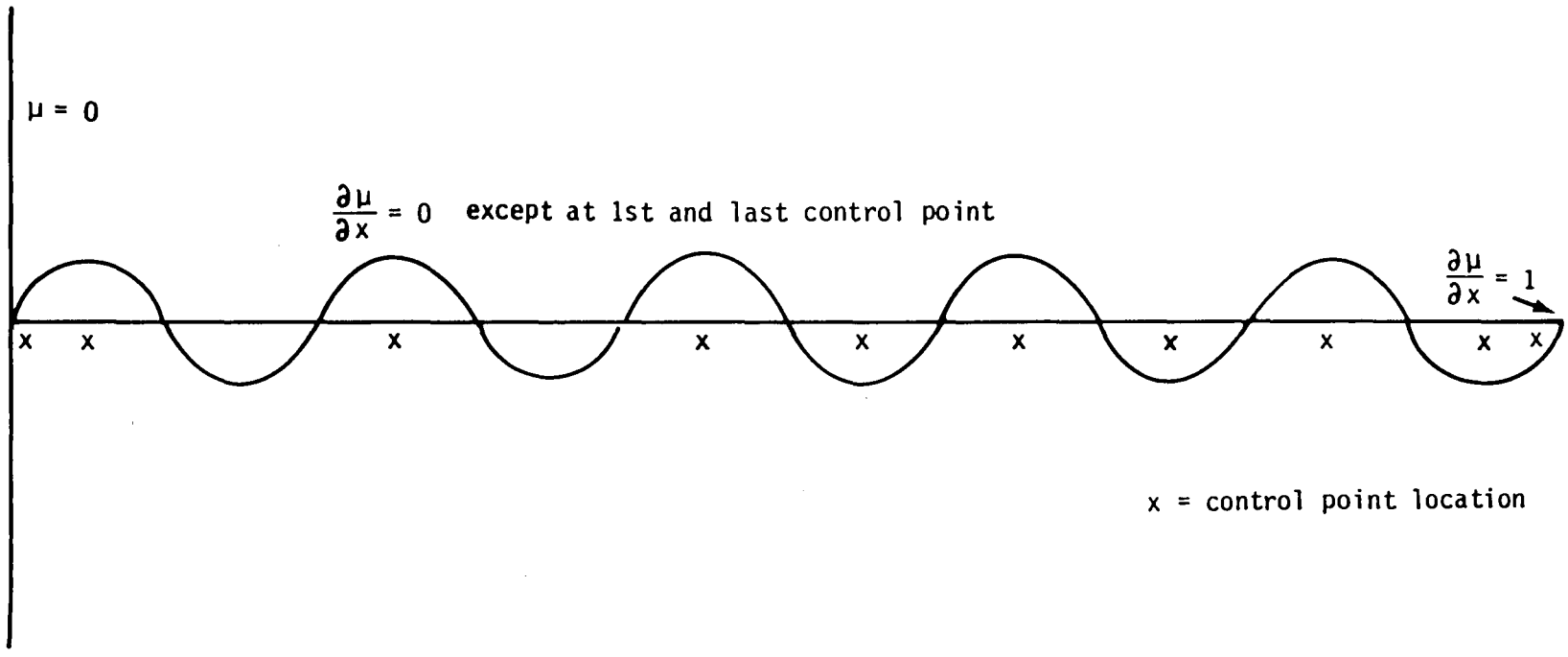

Figure C.10 - Instability of analysis spline with design boundary conditions

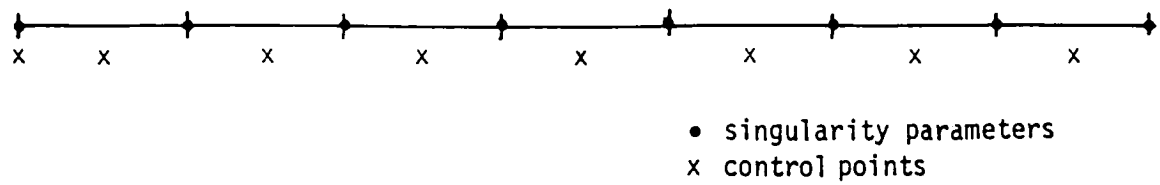

Figure C.11 - A doublet spline for design problems

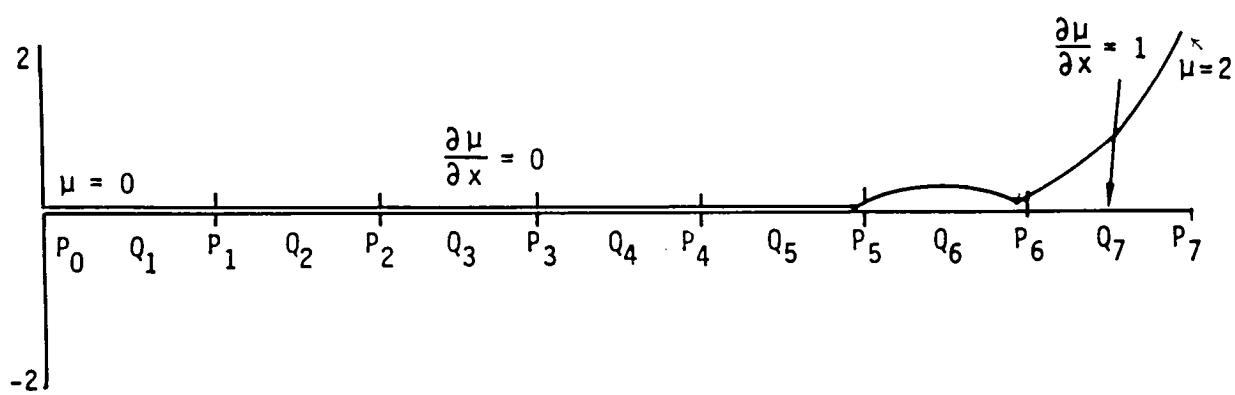

Figure C.12 - Stability for design boundary conditions

D.0 Geometry of Networks and Panels

This appendix will discuss the manner in which PAN AIR handles configuration geometry. In section D.1, we will describe the different types of "networks" by which a program user can describe a portion of the configuration. We will also discuss modifications in the geometry generated by the program under certain circumstances. In section D.2, we will discuss basic panel geometry. In section D.3, we will discuss the geometric error detection methods which discover geometric situations which could cause the program to execute improperly or terminate abnormally.

D.1 Networks

A network is an array (with, say, M rows and N columns) of points in space which define a portion of the configuration geometry. In addition, source and doublet distributions are defined on the network (that is, the network is a "composite" network), with singularity parameter locations and spline methods determined by the network's "source type" and "doublet type".

D.1.1 Network Types

The possible source types are "analysis", "source design 1," "source design 2," and "null", while the doublet types are "analysis", "doublet forward weighted," "design", "wake 1", "wake 2", and "null". Source and doublet analysis networks are used in conjunction with boundary conditions defining impermeability. Design networks are used in conjunction with "design" boundary conditions, that is, those which specify tangential velocity. Note that a "doublet forward weighted" network is really a doublet design network. A network of type "null" is used to denote that the source or doublet strength is zero; one could equally well use an analysis network in conjunction with the uniform boundary condition

$$\sigma = 0$$

or

$$\mu = 0$$

To model a wake, as described in section B.2, one would generally use a doublet wake network in conjunction with a source null network. The boundary conditions, which are only imposed at the wake leading edge, specify the matching of doublet strength on that edge to the doublet strength at the trailing edge of the adjacent wing network(s). In figures D.1 through D.3, we illustrate the singularity parameter locations corresponding to each of these network types.

D.1.2 Wake Networks and the Kutta Condition

Two types of wake networks are available. In wake 1 networks, the doublet strength is variable along the leading edge, and constant in the indicially perpendicular direction. In wake 2 networks, the doublet strength is constant over the entire network. In the example of figure B.9, the wake extending behind the wing would generally be modeled with a wake 1 network, while the portion of the wake extending back from the body would be modeled with a wake 2 network.

The two types of wake networks have distinct purposes. The wake 1 network is PAN AIR's approach to satisfying the Kutta condition (see below), while the purpose of the wake 2 network if to carry over the doublet strength from the wing to the plane of symmetry.

The Kutta condition, which should hold at the trailing edge, is

$$\Delta C_p = 0 \qquad \text{(D.1.1)}$$

where C_p is the pressure coefficient. If the freestream direction is the x direction, and the freestream has unit magnitude, then (cf. (C.1.5)) for a

thin wing, the linear expresssion for ΔC_p is

$$\Delta C_p = -2 \frac{\partial \mu}{\partial x} \tag{D.1.2}$$

Now, the boundary conditions on the wake insure doublet continuity from the thin wing to the wake. In addition, it follows from section J.11 that the zero normal mass flux boundary conditions along the trailing edge of the wing insure the continuity of the x-component of the doublet gradient.

Now, the wake spline is such that the doublet strength is constant in the streamwise direction, that is,

$$\left. \frac{\partial \mu}{\partial x} \right|_{\text{wake}} = 0 \tag{D.1.3}$$

Since the normal mass flux boundary conditions insure matching of the doublet x-derivative, we have, in light of (D.1.2),

$$\left. \Delta C_p \right|_{\text{trailing edge of wing}} = 0 \tag{D.1.4}$$

Thus for a thin wing, the use of a wake 1 network results in the satisfaction of the Kutta condition, using the linear pressure coefficient formula. It is therefore natural to use the wake 1 network to satisfy the Kutta condition for a thick wing. This is done in PAN AIR, even in the absence of a theoretical justification of its validity.

Wake 2 networks have a purpose which is not related to the Kutta condition. In figure B.9, we show a wake 1 network emanating from the wing trailing edge. Now, the body is not a lifting surface, and therefore one would not in general expect a panel method to require a wake emanating from the body. The wake 2 network is required in PAN AIR, however, because in its absence the doublet matching boundry conditions on the wake 1 network would drive the doublet strength to zero along its inboard edge.

Because the doublet strength on the wake is constant, the doublet gradient is zero, and thus the surface vorticity, $\hat{n} \times \nabla\mu$, is zero. This corresponds to the physics of the configuration; that is, the body "sheds" no vorticity.

D.1.3 Indexing

We now discuss the indexing system used internally in PAN AIR. The user specifies an array [CP(I,J)] of panel corner points, where I, $1 \leq I \leq M$, is called the row index, and J, $1 \leq J \leq N$, is called the column index. The upper surface is defined by an upward pointing unit normal $\hat{n}$ whose direction is the vector cross product (direction of increasing column index) x (direction of increasing row index). In figure D.4, we illustrate a network with $\hat{n}$ pointing up from the paper. The network edges are labeled in counterclockwise fashion as shown, and each panel's corner points are similarly labelled in counterclockwise fashion. The point CP(1,1) is called the origin of the

network. Finally, a panel Σ is given a row index and column index equal to the row and column index of the point P_1 on Σ .

Singularity parameters are indexed by a distinct integer for each parameter. For each index, the parameter type (source or doublet) and location are stored, and, conversely, for each location on a network, the program stores the indices of any singularity parameter located there.

D.1.4 Collapsing of Network Edges

Network edges are collapsed when a network of the type illustrated in figure D.5 is defined by the user. The distance shown there is a user-input "tolerance distance" (ε). The short edge of the network in that figure is collapsed as follows: the five panel corner points on that edge are each replaced by the same new point whose coordinates are the averages of the coordinates of the endpoints of the edge. Thus, the revised network has panel corner points as illustrated in figure D.6. The array of points is still a rectangular (MxN) array, except that now the same point occurs five times.

The reason for collapsing a network edge is that the existence of nearly triangular panels (as opposed to exactly triangular panels) such as those in figure D.4 causes nearly singular spline matrices, resulting in significant numerical error. On the other hand, triangular networks (which necessarily have triangular panels) cannot be excluded from consideration because the natural paneling of many surfaces such as delta wings (see figure D.7) requires the use of triangular networks.

A network edge is collapsed whenever the average panel edge length on the network edge is less than the tolerance distance. If, however, the average panel edge length exceeds ε, yet one or more of the panel edges have length less than ε, the program terminates. The edge cannot be left uncollapsed because some of the panels are too nearly triangular, it cannot be collapsed because the user-input geometry would be excessively perturbed, and it cannot be partially collapsed because of the indexing problems which would result when singularity parameter locations are assigned.

D.1.5 Additional Network Processing

Additional processing is performed on the geometry of each network, but will not be discussed here. This processing includes labeling of all but one singularity parameter on a collapsed network edge as "null", and storing data concerning each network edge separately in preparation for the automatic abutment search described in Appendix F.3. Since this data is associated with computing questions rather than engineering questions, this processing will be discussed in section 3 of the maintenance document.

D.2 Basic Panel Geometry

In this section we describe some basic quantities concerning panel geometry.

A panel is uniquely defined by its four corner points P_i, $i=1,\ldots,4$, but for convenience we define nine panel defining points as shown in figure D.8, where $P_5,\ldots,P_8$ are panel edge midpoints, and

$$\vec{P}_9 = \frac{1}{4}\ (\vec{P}_1 + \vec{P}_2 + \vec{P}_3 + \vec{P}_4) \tag{D.2.1}$$

Note that even though P_i, $i=1,\ldots,4$, are arbitrary, P_j, $j=5,\ldots,9$ lie in a plane. The proof comes from noting that by definition an edge midpoint is the average of the endpoints of the edge, and so

$$\begin{aligned}
\vec{P}_5 &= \frac{1}{2}\ (\vec{P}_1 + \vec{P}_2) \\
\vec{P}_6 &= \frac{1}{2}\ (\vec{P}_2 + \vec{P}_3) \\
\vec{P}_7 &= \frac{1}{2}\ (\vec{P}_3 + \vec{P}_4) \\
\vec{P}_8 &= \frac{1}{2}\ (\vec{P}_4 + \vec{P}_1)
\end{aligned} \tag{D.2.2}$$

and so

$$\begin{aligned}
\frac{1}{2}\ (\vec{P}_5 + \vec{P}_7) &= \frac{1}{4}\ (\vec{P}_1 + \vec{P}_2 + \vec{P}_3 + \vec{P}_4) = \vec{P}_9 \\
\frac{1}{2}\ (\vec{P}_6 + \vec{P}_8) &= \frac{1}{4}\ (\vec{P}_2 + \vec{P}_3 + \vec{P}_4 + \vec{P}_1) = \vec{P}_9
\end{aligned} \tag{D.2.3}$$

Thus $P_5,\ldots,P_8$ lie in the plane defined by the line connecting P_5 and P_7, and the line connecting P_6 and P_8.

Thus P_9 is the midpoint of the edge P_5P_7 as well as of the edge P_6P_8, and so P_5,P_9 and P_7 lie on a line, as do P_6,P_9, and P_8. But a basic theorem in geometry states that there exists a plane containing any two intersecting lines, and so $P_5,\ldots,P_9$ lie in that plane, which is called the panel's "average plane".

We define the panel normal $\hat{n}$ as the unit vector normal to the plane containing $P_5,\ldots,P_9$, a vector which is unique provided the plane is unique, that is, provided the set $P_5,\ldots,P_9$ contains at least 3 distinct points. The vector n can be computed in a multitude of ways:

$$\hat{n} = \pm\ \frac{\vec{V} \times \vec{W}}{|V \times W|} \tag{D.2.4}$$

for any linearly independent pair of vectors $\vec{V}$ and $\vec{W}$ lying in the plane. Equation (D.2.4) holds because the cross product of two vectors is perpendicular to each of them; the condition that $\vec{V}$ and $\vec{W}$ be linearly independent (i.e., non-parallel) insures that

$$\vec{V} \times \vec{W} \neq 0 \tag{D.2.5}$$

since

$$\vec{V} \times \vec{W} = |\vec{V}|\ |\vec{W}| \sin\theta \tag{D.2.6}$$

where θ is the angle between $\vec{V}$ and $\vec{W}$. Further, $|\hat{n}| = 1$ as long as the denominator of (D.2.4) is non-zero.

In practice, PAN AIR defines

$$\begin{aligned}
\vec{P}_{10} &= 1/2\ (\vec{P}_5 + \vec{P}_6) \\
\vec{P}_{11} &= 1/2\ (\vec{P}_6 + \vec{P}_7) \\
\vec{P}_{12} &= 1/2\ (\vec{P}_7 + \vec{P}_8) \\
\vec{P}_{13} &= 1/2\ (\vec{P}_8 + \vec{P}_5)
\end{aligned} \tag{D.2.7}$$

and

$$\hat{n} = \frac{(\vec{P}_{10} - \vec{P}_{12}) \times (\vec{P}_{11} - \vec{P}_{13})}{|(P_{10} - P_{12}) \times (P_{11} - P_{13})|} \tag{D.2.8}$$

which insures that $\hat{n}$ points up out of the paper (see figure D.8). The equation (D.2.8) is used in PAN AIR because that formulation would hold even for "curved panels" (not included in version 1.0 of PAN AIR) for which $P_5,\ldots,P_9$ do not lie in a plane.

We now compute $\hat{n}$ by a different method, in order to obtain a result used in section C.1. Applying (D.2.4),

$$\hat{n} = \frac{(\vec{P}_5 - \vec{P}_7) \times (\vec{P}_6 - \vec{P}_8)}{|(P_5 - P_7) \times (P_6 - P_8)|} \tag{D.2.9}$$

and thus, substituting (D.2.2) into (D.2.9),

$$\hat{n} = \frac{1/2(\vec{P}_1 + \vec{P}_2 - \vec{P}_3 - \vec{P}_4) \times 1/2(\vec{P}_2 + \vec{P}_3 - \vec{P}_4 - \vec{P}_1)}{|1/2(P_1 + P_2 - P_3 - P_4) \times 1/2(P_2 + P_3 - P_4 - P_1)|} \tag{D.2.10}$$

The numerator of (D.2.10) is

$$\begin{aligned}
& 1/4\left\{(\vec{P}_1 - \vec{P}_3) + (\vec{P}_2 - \vec{P}_4)\right\} \times \left\{-(\vec{P}_1 - \vec{P}_3) + (\vec{P}_2 - \vec{P}_4)\right\} \\
&= 1/4\left\{(\vec{P}_1 - \vec{P}_3) \times (\vec{P}_2 - \vec{P}_4)\right\} - \left\{(\vec{P}_2 - \vec{P}_4) \times (\vec{P}_1 - \vec{P}_3)\right\} && \text{(D.2.11)} \\
&= 1/2\ (\vec{P}_1 - \vec{P}_3) \times (\vec{P}_2 - \vec{P}_4) && \text{(D.2.12)}
\end{aligned}$$

Substituting this into (D.2.10),

$$\hat{n} = \frac{(\vec{P}_1 - \vec{P}_3) \times (\vec{P}_2 - \vec{P}_4)}{|(P_1 - P_3) \times (P_2 - P_4)|} \tag{D.2.13}$$

a result quoted in section C.1.

Now, $P_1,\ldots,P_4$ need not lie in the plane containing $P_5,\ldots,P_9$. Thus, a panel contains 5 planar regions; the center region which contains four triangular regions as illustrated in figure D.9, and 4 outer regions containing one triangular region each. The triangular regions are called subpanels, and so a panel contains 8 subpanels, which are labeled in figure D.8.

Much of the geometric data for a panel is computed for each subpanel, though this is occasionally redundant. These include: (1) a subpanel origin and reference to local transformation describing a local subpanel coordinate system (see Appendix E), (2) a subpanel unit normal vector and co-normal, (3) the subpanel area, (4) unit edge tangent vectors for the subpanel edges along with their "compressible" norm, (5) subpanel edge normals in local coordinates, (6) a Jacobian factor relating subpanel area in global coordinates to that in local coordinates, and (7) a flag indicating whether the subpanel is subinclined or superinclined.

To obtain the unit normal to the subpanel illustrated in figure D.9, we compute

$$\hat{n} = \frac{(\vec{P}_j - \vec{P}_i) \times (\vec{P}_k - \vec{P}_i)}{|(P_j - P_i \times P_k - P_i)|} \tag{D.2.14}$$

where $\hat{n}$ is not computed if the denominator is less than 10^{-10}. In that case, the subpanel area is set equal to zero, and no subpanel calculations are performed. The area of the subpanel is (from geometry)

$$A = 1/2\ |\vec{P}_j - \vec{P}_i|\ |\vec{P}_k - \vec{P}_i|\ \sin\theta \tag{D.2.15}$$

Combining (D.2.6) and (D.2.15),

$$A = 1/2\ \ |(\vec{P}_j - \vec{P}_i) \times (\vec{P}_k - \vec{P}_i)| \tag{D.2.16}$$

The unit edge tangents are

$$\hat{t} = \frac{\vec{P}_j - \vec{P}_i}{|\vec{P}_j - \vec{P}_i|} \tag{D.2.17}$$

etc. The compressible norm of $\hat{t}$ (see Appendix E for a discussion of this norm) is (by definition)

$$[\hat{t},\hat{t}] = \hat{t}\cdot\hat{t} - M_\infty^2(\hat{c}_o \cdot \hat{t})^2 \tag{D.2.18}$$

The subpanel conormal is defined in compressibility axis coordinates (in which the compressibility direction $c_0 = (1,0,0)$) as

$$\tilde{n} = \begin{pmatrix} s\beta^2 n_x \\ n_y \\ n_z \end{pmatrix} \tag{D.2.19}$$

$$= (s\beta^2-1)\ (\hat{c}_0\cdot\hat{n})\hat{c}_0 + \hat{n} \tag{D.2.20}$$

since

$$n_x = \hat{c}_0\cdot\hat{n} \tag{D.2.21}$$

Thus,

$$\tilde{n} = \hat{n} - M_\infty^2(\hat{c}_0\cdot\hat{n})\hat{c}_0 \tag{D.2.22}$$

The Jacobian factor J is given by

$$J = \frac{\text{Area in reference coordinates}}{\text{Area in local coordinates}} \tag{D.2.23}$$

Its use will be discussed in Appendices I and J.

Finally, the sub-panel is "subinclined" if

$$\hat{n}\cdot\tilde{n} > 0 \tag{D.2.24}$$

and "superinclined" if

$$\hat{n}\cdot\tilde{n} < 0 \tag{D.2.25}$$

If

$$\hat{n}\cdot\tilde{n} \approx 0 \tag{D.2.26}$$

the subpanel is "Mach-inclined", and the program terminates for reasons which will be discussed in Appendix E.

Some items of data computed for each panel are not concerned with just a single subpanel. For instance, all the data computed for the subpanels is also computed for the "projected panel", the projection of the panel to the average plane. In addition, it is computed for the four "half panels", that is, the triangles $P_1P_2P_4$, $P_2P_3P_1$, $P_3P_4P_2$, $P_4P_1P_3$.

These data are needed to compute "intermediate field" influence coefficients, in the computation of which the panel is approximated either by two half panels or by the projected panel. These are used when measuring the influence of the panel on a control point which is sufficiently far not to require the 8-subpanel representation of the panel, but not far enough to permit the far field influence coefficient computation method (see Appendix J.2). All the items are computed for the projected panel or half panels in the same manner as for subpanels. Redundant data is not necessarily computed (e.g., the projected panel is super- or sub-inclined whenever subpanels 5 through 8 are).

Finally, the program calculates, for each panel, its radius, its diameter, and certain skewness parameters. The radius is the distance from the center to the farthest corner point and the diameter is the maximum distance between any two corner points. The skewness parameters result from a non-orthogonal transformation of coordinates after which

$$P_9 = \begin{Bmatrix} 0 \\ 0 \\ 0 \end{Bmatrix}, \quad P_8 = \begin{Bmatrix} 1 \\ 0 \\ 0 \end{Bmatrix}, \quad P_5 = \begin{Bmatrix} 0 \\ 1 \\ 0 \end{Bmatrix}, \quad \hat{n} = \begin{Bmatrix} 0 \\ 0 \\ k \end{Bmatrix}, k > 0 \quad \text{(D.2.27)}$$

We may see from figure D.8 that this is not the standard choice of x and y axes, but it results from having derived the relevant formulas with the panel in figure D.8 rotated by 180°.

We use this coordinate system, which we write (x^*,y^*,z^*) because the interior region bounded by $P_5,\ldots,P_8$ becomes a square, as illustrated in figure D.10. Note that in general (since most panels are not square), this is not an orthogonal coordinate system. The numbers C_{ij}, $j=1,\ldots,4$, $i=1,2$, are called skewness parameters since they are all zero for a panel which is a parallelogram in the original coordinate system as

$$(\vec{P}_1 - \vec{P}_9) = (\vec{P}_5 - \vec{P}_9) + (\vec{P}_8 - \vec{P}_9) \quad \text{(D.2.28)}$$

for a parallelogram.

The doublet subpanel spline matrices are calculated in the (x^*,y^*,z^*) coordinate system, but rather than transform the panel coordinates, we compute the matrices using the skewness parameters (see section I.2 for details).

Computing the skewness parameters is fairly straightforward. Combining

$$\vec{P}_1 = \begin{Bmatrix} 1 + C_{11} \\ 1 + C_{21} \\ z \end{Bmatrix} \quad \text{(D.2.29)}$$

with (D.2.27), (D.2.28) we obtain

$$(\vec{P}_1 - \vec{P}_9) = (1 + C_{11})\,(\vec{P}_8 - \vec{P}_9)$$

$$+ (1 + C_{21})\,(\vec{P}_5 - \vec{P}_9) + \hat{n}\,\frac{z}{k} \quad \text{(D.2.30)}$$

Taking the cross product on the left with (P_8-P_9), and dotting into n, we obtain

$$\left\{(\vec{P}_8-\vec{P}_9)\times(\vec{P}_1-\vec{P}_9)\right\}\cdot n = (1+C_{11})\,0\cdot\hat{n}$$
$$+\,(1+C_{21})\left\{(\vec{P}_8-\vec{P}_9)\times(\vec{P}_5-\vec{P}_9)\right\}\cdot\hat{n}$$
$$+\,\frac{z}{k}\,[(\vec{P}_8-\vec{P}_9)\times\hat{n}]\cdot\hat{n} \qquad \text{(D.2.31)}$$

The final term is zero, and so

$$C_{21} = \frac{\left\{(\vec{P}_8-\vec{P}_9)\times(\vec{P}_1-\vec{P}_9)\right\}\cdot\hat{n}}{(P_8-P_9)\times(P_5-P_9)\cdot\hat{n}} - 1 =$$

$$\frac{\left\{(\vec{P}_8-\vec{P}_9)\times(\vec{P}_1-\vec{P}_9)\right\}\cdot\hat{n}}{(P_8-P_9)\times(P_5-P_9)\cdot\hat{n}} \qquad \text{(D.2.32)}$$

Similarly

$$\left\{(\vec{P}_1-\vec{P}_9)\times(\vec{P}_5-\vec{P}_9)\right\}\cdot\hat{n} = ((1+C_{11})(\vec{P}_8-\vec{P}_9)\times(\vec{P}_5-\vec{P}_9))\cdot\hat{n} \qquad \text{(D.2.33)}$$

and thus

$$C_{11} = \frac{\left\{(\vec{P}_1-\vec{P}_9)\times(\vec{P}_5-\vec{P}_9)\right\}\cdot\hat{n}}{(P_8-P_9)\times(P_5-P_9)\cdot\hat{n}} - 1$$

$$= \frac{\left\{(\vec{P}_1-\vec{P}_8)\times(\vec{P}_5-\vec{P}_9)\right\}\cdot\hat{n}}{\left\{(P_8-P_9)\times(P_5-P_9)\right\}\cdot\hat{n}} \qquad \text{(D.2.34)}$$

Examination of figure D.10 gives us

$$\begin{aligned} C_{12} &= C_{11} \\ C_{22} &= -C_{21} \\ C_{13} &= -C_{11} \\ C_{23} &= -C_{21} \\ C_{14} &= -C_{11} \\ C_{24} &= C_{21} \end{aligned} \qquad \text{(D.2.35)}$$

This concludes the discussion of basic panel geometric quantities.

D.3 Error Checks

In this section, we summarize the basic checks performed by the program to insure that the geometry of the configuration is admissible. These checks are the following:

a. Check if the average panel edge length on a network edge exceeds the tolerance ε, while some panel edge length is less than ε (violation is a fatal error).
b. Check if two adjacent edges of network collapse. This is inadmissible because the calculation of spline matrices would be impossible for panels near both collapsed edges. See figure D.11 for a network in which adjacent edges are collapsed.
c. Check if a panel edge in the network interior has length less than ε. This is inadmissible because of logic problems which would occur in calculating the spline matrices if the edge were collapsed, and numerical inaccuracies occurring from nearly triangular panels.
d. Check the panel aspect ratio. This is the ratio of the furthest distance from the panel center to its boundary over the smallest distance. Large aspect ratios cause numerical error in spline and influence coefficient calculation (this has only been verified experimentally). Aspect ratios over 10^6 are forbidden and those over 100 result in a warning message.
e. A panel or subpanel is essentially Mach inclined. If $\tilde{n} \cdot \tilde{n} < 10^{-4}$ this is a fatal error, and if $< 1/10$ a warning message is printed.
f. The panel is seriously skewed. Warning messages are printed if the panel is non-convex ($1+c_{i1}+c_{i2} < 0$ for some $i = 1,\ldots, 4$), nearly non-convex ($1+c_{i1}+c_{12} > 0$), or triangular while having four distinct vertices ($1+c_{i1}+c_{i2} \approx 0$).
g. A subpanel has zero area when projected to the average plane. If so, a flag is set, no normal or conormal vector is calculated, the subpanel splines are set to zero, etc.

a. Source analysis network

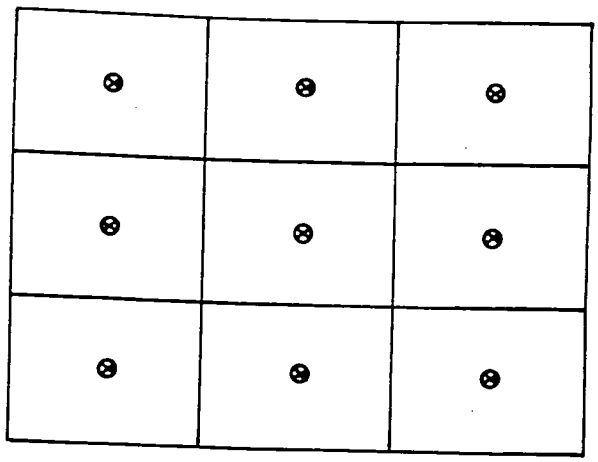

b. Source design 1 network

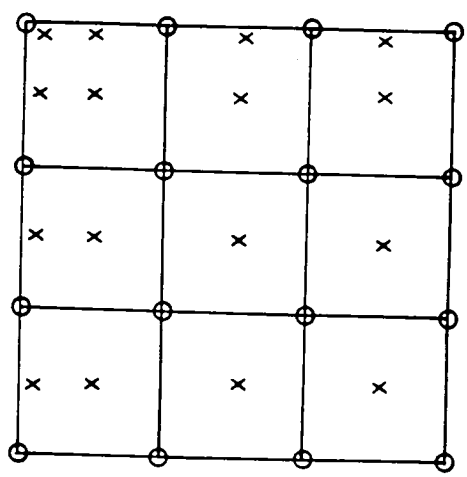

c. Source design 2 network

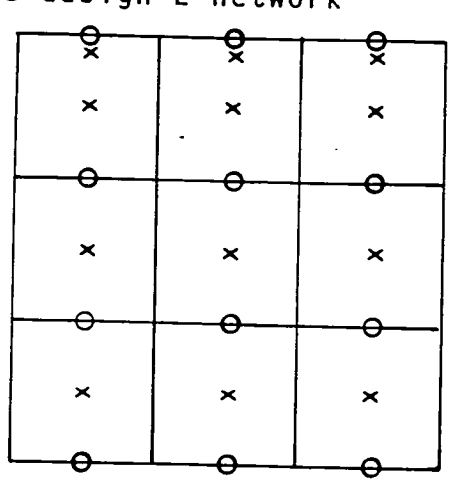

O source parameter locations

× locations of corresponding non-trivial boundary conditions

Figure D.1 - Locations of source singularity parameters

a. Doublet analysis, doublet forward weighted

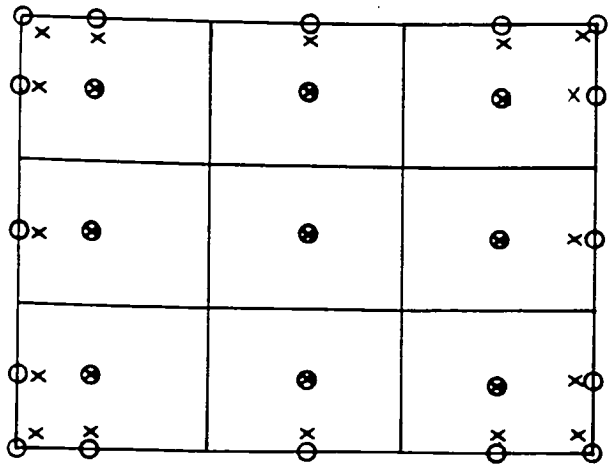

b. Doublet design

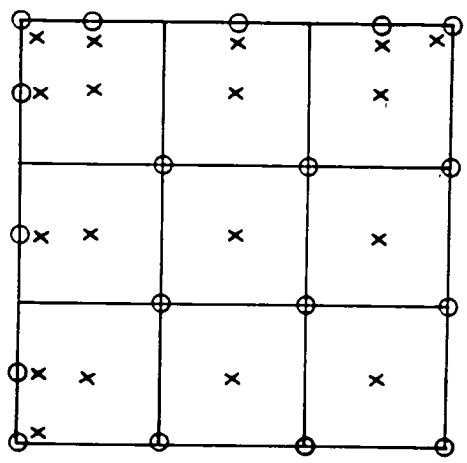

○ doublet parameter locations

× boundary condition locations

Figure D.2 - Doublet analysis and design singularity parameter locations

a. Doublet wake 1

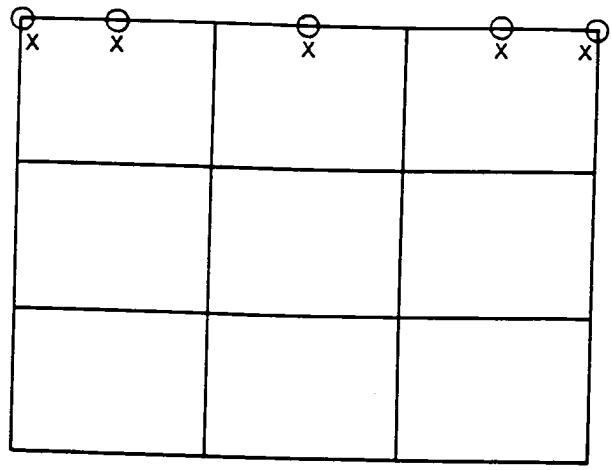

b. Doublet wake 2

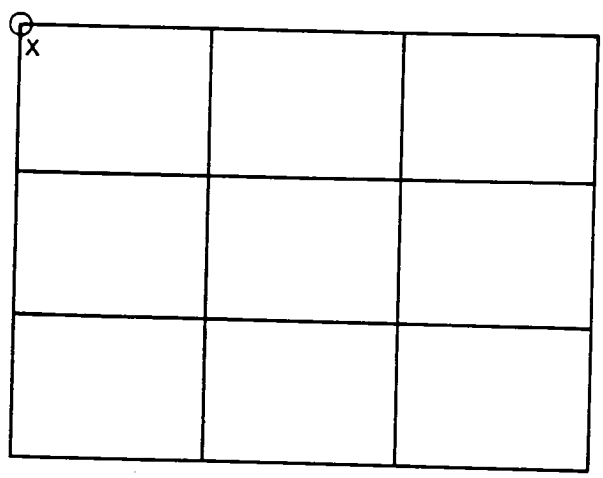

○

x boundary condition locations

Figure D.3 - Doublet wake singularity parameter locations

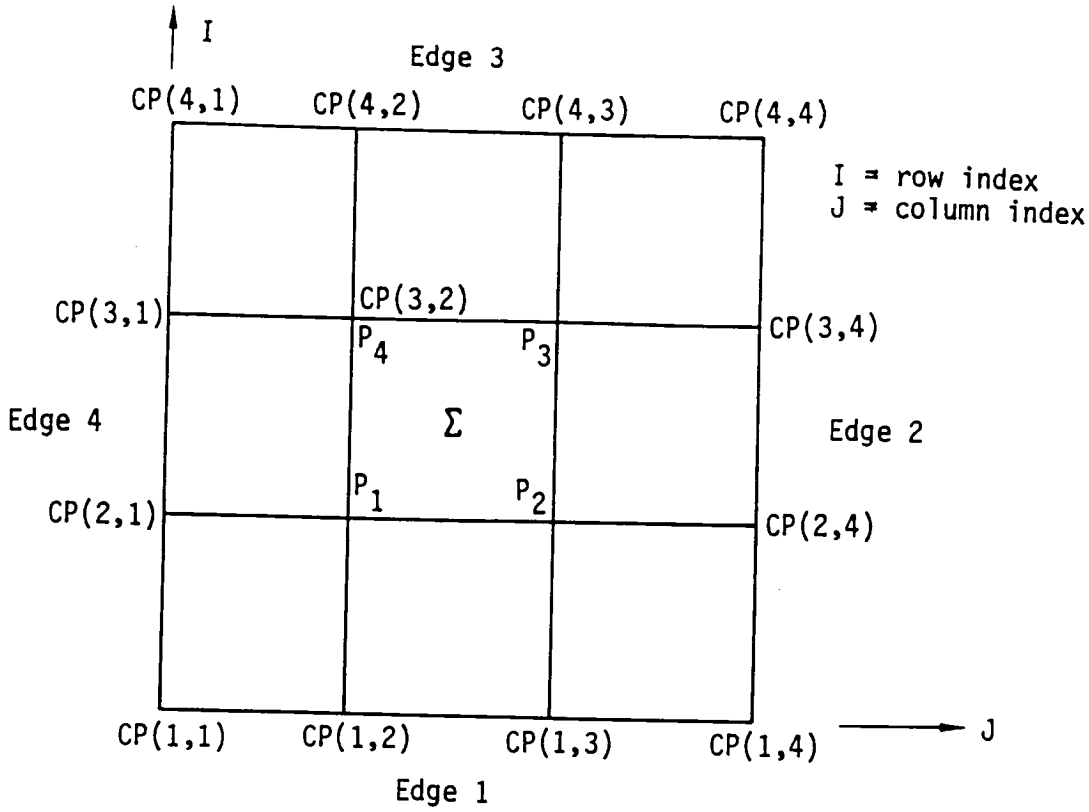

Figure D.4 - Network and panel indexing

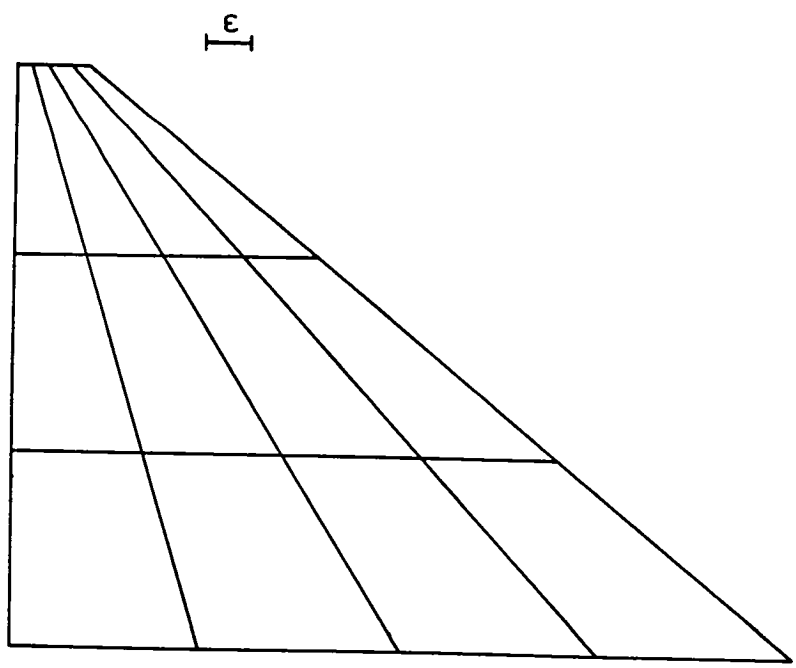

Figure D.5 - Network with an edge to be collapsed by the program

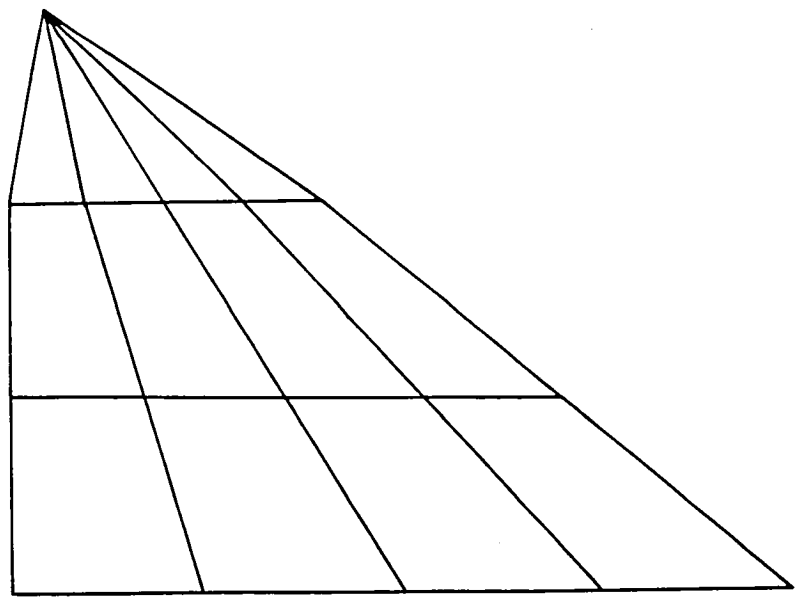

Figure D.6 - Network with revised geometry

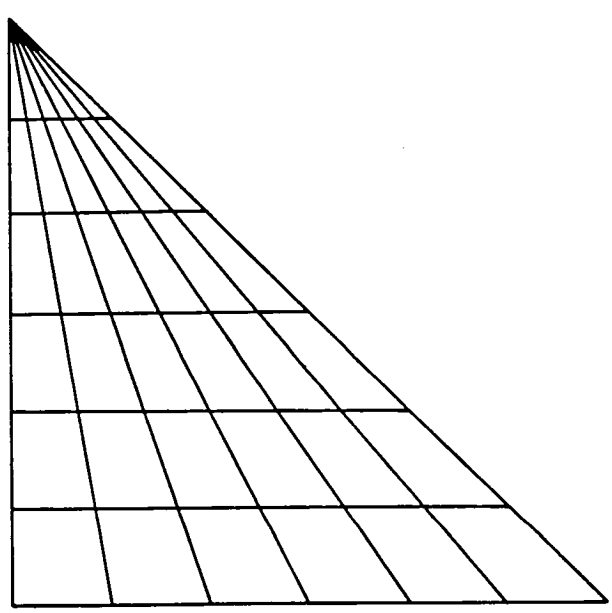

Figure D.7 - Panelling of delta wing

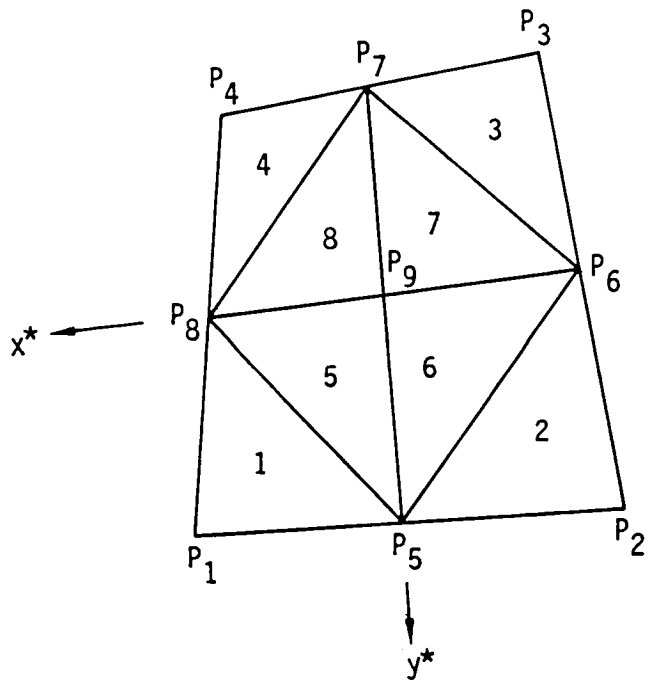

Figure D.8 - A panel

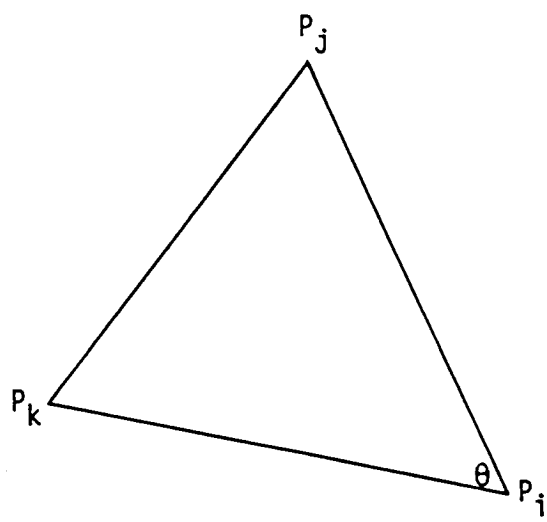

Figure D.9 - A subpanel

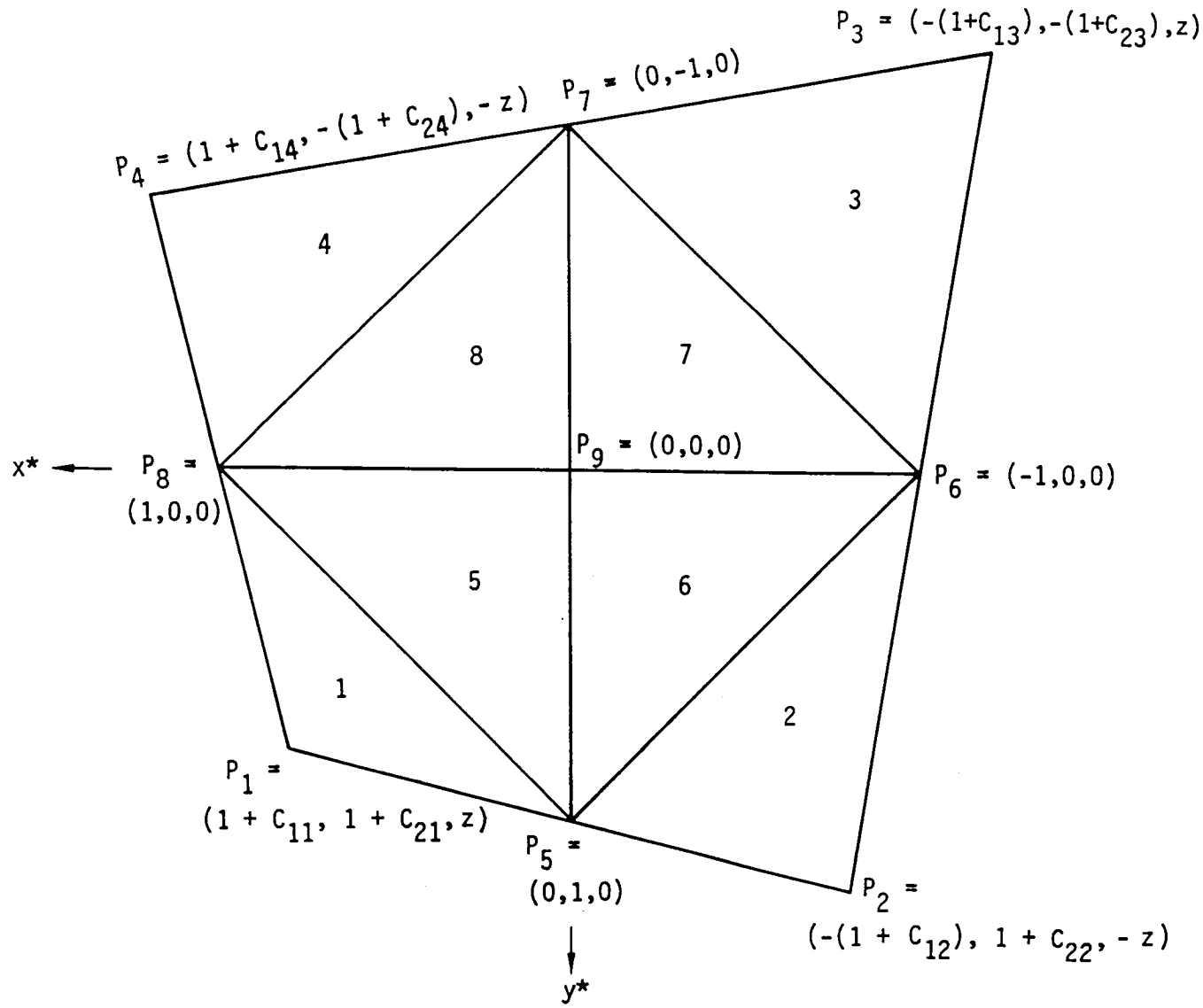

Figure D.10 - Definition of skewness parameters

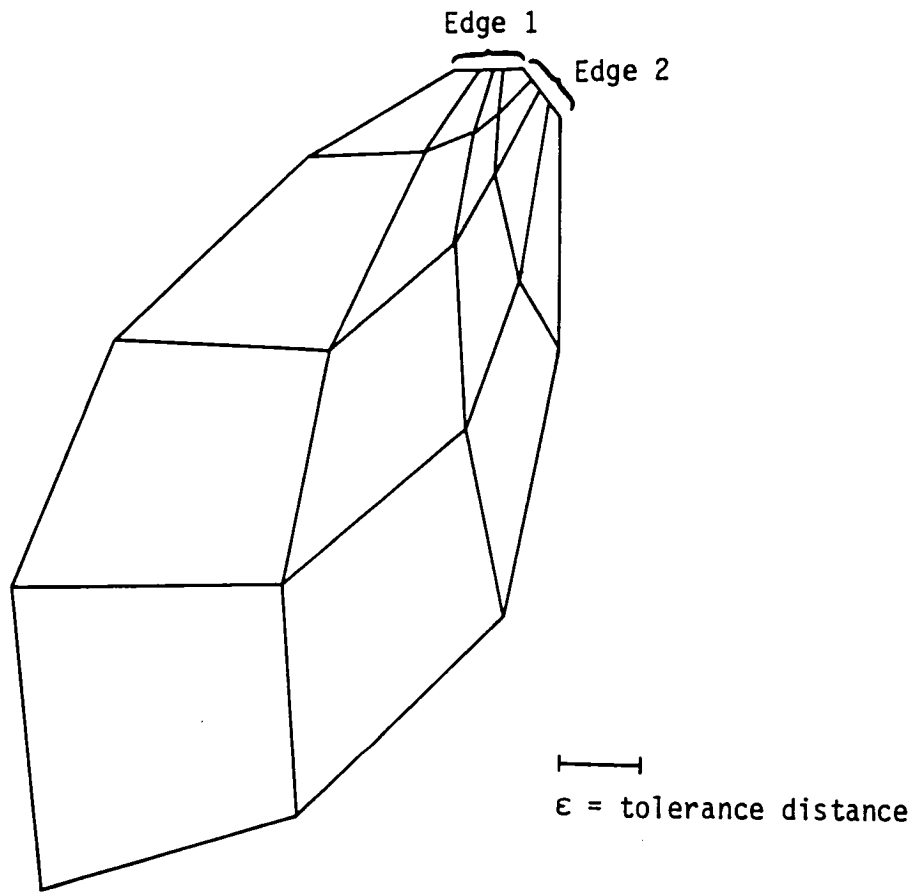

Figure D.11 - Impermissible network (two adjacent collapsed edges)

E.0 Matrices and Coordinates

The material in this appendix is hardly reflected in the PAN AIR code, but rather provides background material on coordinate systems and transformations. This material is referred to in the course of the influence coefficient derivations of Appendix J. In addition, we derive (in section E.3) the expression for the reference to local transformation (see (5.2.27))

$$A = \left[\frac{1}{|\{\hat{n}_0,\hat{n}_0\}|^{1/2}} \quad [C_0]\hat{u}_0 \;\vdots\; \frac{rs}{\beta}[C_0]\hat{v}_0 \;\vdots\; \frac{\beta\,\hat{n}_0}{|\{\hat{n}_0,\hat{n}_0\}|^{1/2}} \right]^T \tag{E.0.1}$$

and for the transformation between orthogonal coordinate systems (see (5.2.11))

$$\Gamma = \begin{bmatrix} \cos\alpha\cos\beta & -\sin\beta & \sin\alpha\cos\beta \\ \cos\alpha\sin\beta & \cos\beta & \sin\alpha\sin\beta \\ -\sin\alpha & 0 & \cos\alpha \end{bmatrix} \tag{E.0.2}$$

Because Γ is a transformation between two orthogonal coordinate systems, it is in fact an orthogonal matrix. That is, its inverse is its transpose, and for all vectors X,Y, the Euclidean inner product is invariant under transformation by :

$$(\Gamma X, \Gamma Y) = (X,Y) \tag{E.0.3}$$

This arises from the fact that Γ is a rotation (see section E.3)

In our application, Γ will be the matrix relating reference coordinates and the compressibility coordinate system, in which the x-axis is the compressibility direction.

The matrix A is less well-behaved, however. This transformation is the product

$$A = GS\Gamma \tag{E.0.4}$$

where we have

$$X_0 \xrightarrow{\Gamma} X \xrightarrow{S} \bar{X} \xrightarrow{G} X' \tag{E.0.5}$$

Here, X_0 is the reference coordinate system defined by the program user, X is the compressibility coordinate system in which the freestream is in the x-direction, $\bar{X}$ is a coordinate system in which the y-and z-axes have been scaled according to (3.1.3), and X' is the local coordinate system in which (5.2.19) holds.

While the matrices Γ and G are orthogonal, the scaling matrix S is not, and so the product matrix A is not orthogonal either. The bulk of the complexity of this appendix arises from this fact. In figure E.1, we illustrate a surface S in the compressibility coordinate system X and its image S' in the local coordinate system X'. We illustrate vectors $\vec{t}$ and $\hat{n}$, tangent and normal to

the surface S respectively, and their images $\bar{t}'$ and $\bar{n}$ in the scaled coordinate system X'.

In section E.1, we consider the properties of vectors and their images under an arbitrary transformation. The reader may find some benefit in verifying

the results of E.1 for a "typical" matrix A, such as a diagonal matrix which is not the identity. In section E.2, we derive the properties of some special inner products. In section E.3, we verify that the matrix (E.0.1) has all the properties we require of a reference-to-local transformation. We do so, in fact, without ever constructing the transformation G of (E.0.5).

E.1 Vectors and Dual Vectors

We consider here the effect of the coordinate transformation $A = [a_{ij}]$

$$A: \quad X_0 \longrightarrow X' \tag{E.1.1}$$

by which a position vector $\vec{x}_0 = \begin{Bmatrix} x_1 \\ x_2 \\ x_3 \end{Bmatrix}$, expressed in the coordinate system X_0, is transformed into an image vector $\vec{x}' = \begin{Bmatrix} x_1' \\ x_2' \\ x_3' \end{Bmatrix}$, expressed in the coordinate system X'. This image vector represents the same physical quantity (such as location) as the original vector, but in a different coordinate system. It is a different vector only in the sense that its entries are distinct from those of $\vec{x}$.

The entries x_i' of the image vector $\vec{x}'$ are given by the formulas

$$x_i' = \sum_{j=1}^{3} a_{ij} \; x_j \quad = \quad \left\{ A \, \vec{x}_0 \right\}_i \qquad i = 1,2,3 \tag{E.1.2}$$

where a_{ij} are the entries of the transformation matrix A. We shall occasionally find it convenient to write this equation using the summation convention for repeated indices, that is, $x_i' = a_{ij} \, x_j$. Examples of other vectors which transform according to the formula (E.1.2) include the vector element of arc length, dl, and surface tangent vectors t:

$$dl_i' = a_{ij} \; dl_j = \left\{ A \vec{dl} \right\}_i \tag{E.1.3}$$

$$t_i' = a_{ij} \; t_j = \left\{ A \vec{t} \right\}_i \tag{E.1.4}$$

Equation (E.1.4) may be interpreted to assert that when $\vec{t}_0$ is a surface tangent to some surface S at some point y_0 in S, then $\vec{t}' = A\vec{t}_0$ will be a surface tangent vector to the image surface S'

$$S' = \left\{ \vec{x}' : \vec{x}' = [A] \, \vec{x}_0 \quad \text{for some } \vec{x}_0 \text{ in } S \right\} \tag{E.1.5}$$

at the image point $\vec{y}' = [A] \, \vec{y}$. Unless [A] is an orthogonal matrix, however, we need not expect that t' will be a unit vector even when t is. However, if $\vec{t} = \hat{t}$ is any unit vector, then we define the corresponding image unit vector by

$$\vec{t}' = A\hat{t} / \, |A\hat{t}| \tag{E.1.6}$$

Thus the transformation rule for unit vectors is somewhat more complicated than the corresponding rule for vectors. In particular, the image of a unit vector as scaled in (E.1.6) is a distinct vector from the original one. Here,

and from now on, we use a $\wedge$ to denote a vector of unit length.

We now turn to a discussion of dual vectors. A dual vector is, by definition, a real-valued linear function on the vector space. Whereas the typical vector was the position vector x_0, the typical dual vector is the unit normal vector n_0 or gradient operator

$$\vec{\nabla} = \begin{Bmatrix} \partial/\partial x \\ \partial/\partial y \\ \partial/\partial z \end{Bmatrix} = \begin{Bmatrix} \partial/\partial x_1 \\ \partial/\partial x_2 \\ \partial/\partial x_3 \end{Bmatrix} \tag{E.1.7a}$$

It should be noted that tensor analysis works generally refer to vectors as "contravariant vectors," and dual vectors as "covariant vectors." Both the normal vector and the gradient operator are linear functions on the vector space in a natural manner through the dot product

$$\vec{\nabla} \cdot \vec{Y} = \sum_i \frac{\partial}{\partial x_i} (Y_i) \tag{E.1.7b}$$

$$\hat{n}_0 \cdot \vec{Y} = \sum_i n_i Y_i \tag{E.1.7c}$$

The transformation rules for dual vectors $\vec{v}_0$ (such as $\vec{\nabla}$ and $\hat{n}_0$) is that the image $\vec{v}'$ in the coordinate system X' satisfies

$$\vec{v}' \cdot \vec{Y}' = \vec{v}_0 \cdot \vec{Y} \tag{E.1.8a}$$

for every vector Y.

Now,

$$\vec{v}' \cdot \vec{Y}' = \vec{v}'^T \vec{Y}' = \vec{v}'^T [A] \vec{Y} \tag{E.1.8b}$$

while

$$\vec{v}_0 \vec{Y} = \vec{v}_0^T \vec{Y} = \vec{v}_0^T [A^{-1} A] \vec{Y} \tag{E.1.8c}$$

Thus, for (E.1.8a) to hold, we require

$$\vec{v}'^T = \vec{v}_0^T [A^{-1}] = \left\{ [A^{-T}] \vec{v}_0 \right\}^T \tag{E.1.8d}$$

or

$$\vec{v}' = [A^{-T}] \vec{v} \tag{E.1.8e}$$

where the superscript $-T$ denotes the inverse of the transpose matrix, which is the same as the transpose of the inverse.

Thus dual vectors transform by A^{-T}, while ordinary vectors transform (cf. (E.1.2)) by A. It should be noted that if A happens to be an orthogonal matrix, $A = A^{-T}$ and is length-preserving, and thus regular vectors, unit

vectors, and dual vectors transform identically.

The gradient operator may also be applied to functions f of position x. We see that if we define ∇' by

$$\nabla' f(\vec{x}') = \frac{\partial}{\partial x_i'} f(\vec{x}') \equiv \frac{\partial}{\partial x_i} f(\vec{x}_0)\Big|_{\vec{x}_0 = A^{-1}\vec{x}'} \tag{E.1.9}$$

we obtain

$$(\nabla' f(x))_i = \frac{\partial f}{\partial x_k} \frac{\partial}{\partial x_i} [A^{-1}]_{kj} x'_j = \frac{\partial f}{\partial x_k} [A^{-1}]_{kj} \delta_{ij} =$$

$$\frac{\partial f}{\partial x_k} [A^{-1}]_{ki} = [A^{-1}]_{ki} \frac{\partial}{\partial x_k} f \tag{E.1.10a}$$

where δ_{ij} is the Kronecker delta:

$$\delta_{ij} = \begin{cases} 1 \text{ if } i = j \\ 0 \text{ if } i \neq j \end{cases} \tag{E.1.10b}$$

We thus obtain

$$\nabla' = A^{-T} \nabla \tag{E.1.11}$$

which is consistent with our transformation rule (E.1.8e) for dual vectors.

Next we see that, whenever w_1 and w_2 are vectors in X_0 then $w_1 \times w_2$ is "almost" a dual vector in the sense that

$$w_1' \times w_2' = (Aw_1) \times (Aw_2) = (\det A) A^{-T} (w_1 \times w_2) \tag{E.1.12}$$

This equation is proved below. Thus, apart from the factor of det A, the cross product of two vectors transforms in the same way as a dual vector. In a similar vein, we note as well that the cross product of two dual vectors, $\vec{v}_1 \times \vec{v}_2$, transforms very much like a vector

$$\vec{v}_1' \times \vec{v}_2' = (A^{-T} \vec{v}_1) \times (A^{-T} \vec{v}_2) = (\det A)^{-1} A (\vec{v}_1 \times \vec{v}_2) \tag{E.1.13}$$

It is appropriate at this time that we give brief proofs of the above assertions. In addition, we will show that $\hat{n}dS$, the surface unit normal times the element of surface area, transforms like an "almost" dual vector, (cf. (E.1.12)).

A vector $\vec{t}$ that is tangent to some surface S at some point x may be regarded as the tangent to some curve $\vec{c}(\tau)$, parametrized by τ and lying completely on S, as that curve passes through the point x. In other words, when $\vec{t}$ is a tangent to S at x_0, there exists a curve $\vec{c}(\tau)$ such that $\vec{c}(\tau)$ lies in S, $x_0 = \vec{c}(\tau_0)$ and

$$\frac{d}{d\tau}\ \vec{c}\,(\tau)\Big|_{\tau\ =\ \tau_0} = \vec{t} \tag{E.1.14}$$

Given this specification of $\vec{t}$, it is easy to see how tangent vectors transform. The image tangent vector $\vec{t}'$ will simply be the tangent to the image curve $\vec{c}'(\tau) = A\,\vec{c}(\tau)$ evaluated at the point

$\vec{x}_0' = \vec{c}'(\tau) = A\,\vec{c}(\tau) = A\vec{x}_0$. Thus

$$\frac{d}{d\tau}\,\vec{c}'(\tau)\Big|_{\tau=\tau_0} = \frac{d}{d\tau}\,A\vec{c}(\tau)\Big|_{\tau=\tau_0} = A\,\frac{d}{d\tau}\,\vec{c}(\tau)\Big|_{\tau=\tau_0} = A\vec{t} = \vec{t}' \tag{E.1.15}$$

as asserted.

Next we prove equation (E.1.12) for vectors v and w. Recall from section B.3 that

$$(\vec{v} \times \vec{w})_r = \varepsilon_{pqr} v_p\, w_q \tag{E.1.16}$$

where ε_{pqr} is defined there. So,

$$(\,A\vec{v}\ \times\ A\vec{w}\,)_r = \varepsilon_{pqr}(A\vec{v})_p\,(A\vec{w})_q = \varepsilon_{pqr}\,A_{pi}\,v_i\,A_{qj}\,w_j \tag{E.1.17}$$

Multiplying by A^T on the left,

$$(A^T\,(A\vec{v} \times A\vec{w}))_s = [A^T]_{sr}\,(A\vec{v} \times A\vec{w})_r = \varepsilon_{pqr}\,A_{pi}\,v_i\,A_{qj}\,w_j \tag{E.1.18}$$

But, generalizing the definition of determinant

$$\det A = \varepsilon_{pqr}\,A_{p1}\,A_{q2}\,A_{r3} \tag{E.1.19}$$

we see

$$\varepsilon_{ijs}\det A = \varepsilon_{pqr}\,A_{pi}\,A_{qj}\,A_{rs} \tag{E.1.20}$$

and thus substituting in (E.1.18),

$$(A^T\,(A\vec{v} \times A\vec{w}))_s = \varepsilon_{ijs}\,(\det A)v_i\,w_j = (\det A)(\vec{v} \times \vec{w})_s \tag{E.1.21}$$

and so

$$A^T(A\vec{v} \times A\vec{w}) = (\det A)\,(\vec{v} \times \vec{w}) \tag{E.1.22}$$

or

$$A\vec{v} \times A\vec{w} = (\det A)[A^T]\,(\vec{v} \times \vec{w}) \tag{E.1.23}$$

which is equivalent to (E.1.12)

Next we examine the transformation law for unnormalized normal vectors n. Such vectors are specified only up to an arbitrary multiplicative constant; their principle characteristic is that they are perpendicular to all tangent vectors. Thus, if $\vec{t}_1$ and $\vec{t}_2$ are two linearly independent tangent vectors, $\vec{n}$ is given by

$$\vec{n} = \alpha\,(\vec{t}_1 \times \vec{t}_2) \tag{E.1.24}$$

where α may be chosen arbitrarily non-zero.

Next, we note that the image $\vec{n}'$ of $\vec{n}$ must be perpendicular to the images $\vec{t}_1'$, $\vec{t}_2'$, of $\vec{t}_1$ and $\vec{t}_2$; thus

$$\vec{n}' = \alpha'(\vec{t}_1' \times \vec{t}_2') \tag{E.1.25}$$

Using equation (E.1.4) we find

$$\vec{n}' = \alpha'\left\{\vec{A}t_1 \times \vec{A}t_2\right\} = \alpha'\,(\det A)\,A^{-T}\left\{\vec{t}_1 \times \vec{t}_2\right\}$$

$$= \frac{\alpha}{\alpha'}\,(\det A)[A^{-T}]\;\vec{n} \tag{E.1.26}$$

Choosing $\alpha' = \dfrac{\alpha}{\det A}$, we obtain the desired results.

Finally we note that $\hat{n}dS$ transforms as in equation (E.1.12). This observation follows immediately from the definitions (see figure (E.2)

$$\hat{n}_0 dS = \vec{dl}_1 \times \vec{dl}_2$$

$$\vec{n}'dS = \vec{dl}_1' \times \vec{dl}_2'$$

$$dl_i' = (Adl)_i \tag{E.1.27}$$

Upon applying equation (E.1.12) we find that

$$\vec{n}'\,dS' = (\det A)\,A^{-T}\,\vec{n}\,dS \tag{E.1.28}$$

We conclude our discussion of vectors and dual vectors with the observation that the Euclidean inner product of a vector $\vec{w}$ with a dual vector $\vec{v}$ is invariant under transformation, that is

$$(\vec{v},\vec{w}) = \vec{v}^T \vec{w} = \vec{v}^T [A^{-1} A] \vec{w} = (A^{-T} \vec{v})^T A\vec{w} = \vec{v}'^T \vec{w}'$$

$$= (\vec{v}',\vec{w}') \qquad \text{(E.1.29)}$$

E.2 Metric Matrices, Dual Metrics and Inner Products

The introduction of metric and dual metric matrices is best motivated by a careful consideration of the Prandtl-Glauert equation (3.0.1) (for the dual metric) and the definition of the function R (5.2.14) (for the metric matrix). First we define the metric matrix C.

Recall from section B.0 that R^2 is given in terms of a control point P and a surface point Q in the compressibility coordinate system (x,y,z) by

$$R^2 = (P_1 - Q_1)^2 - s\beta^2 (P_2 - Q_2)^2 - s\beta^2 (P_3 - Q_3)^2 \tag{E.2.1}$$

This relation may be written in matrix-vector form as

$$R^2 = (\vec{P} - \vec{Q})^T \begin{bmatrix} 1 & 0 & 0 \\ 0 & s\beta^2 & 0 \\ 0 & 0 & s\beta^2 \end{bmatrix} (\vec{P} - \vec{Q}) \tag{E.2.2}$$

This equation motivates us to define the metric matrix C by

$$[C] = \begin{bmatrix} 1 & & \\ & s\beta^2 & \\ & & s\beta^2 \end{bmatrix} \tag{E.2.3}$$

Corresponding to C, we define the compressible inner product $[\vec{w}_1, \vec{w}_2]$ of two vectors $\vec{w}_1$, $\vec{w}_2$ by

$$[\vec{w}_1, \vec{w}_2] = \vec{w}_1^T [C]\vec{w}_2 = (\vec{w}_1, [C]\vec{w}_2) \tag{E.2.4}$$

Turning now to the definition of the dual metric matrix B, we note that the Prandtl-Glauert equation can be written (since $s\beta^2 = 1 - M_\infty^2$)

$$(\partial/\partial x \;\; \partial/\partial y \;\; \partial/\partial z) \begin{bmatrix} s\beta^2 & & \\ & 1 & \\ & & 1 \end{bmatrix} \begin{Bmatrix} \partial/\partial x \\ \partial/\partial y \\ \partial/\partial z \end{Bmatrix} \vec{\nabla}\phi = 0 \tag{E.2.5}$$

In matrix vector form this reads

$$\left\{ \vec{\nabla}^T [B] \; \vec{\nabla} \right\} \phi = 0 \tag{E.2.6}$$

where [B] is defined by (cf. (5.2.5), where reference and compressibility coordinates are assumed to be identical)

$$[B] = \begin{bmatrix} s\beta^2 & & \\ & 1 & \\ & & 1 \end{bmatrix} \tag{E.2.7}$$

Since the operator $\vec{\nabla}$ transforms like a dual vector (cf. (E.1.8e), equation (E.2.6) motivates us to define the dual compressible inner product $\{\vec{v}_1, \vec{v}_2\}$ of two dual vectors by

$$\{\vec{v}_1, \vec{v}_2\} = \vec{v}_1^{\,T} [B] \vec{v}_2 = (\vec{v}_1, [B]\vec{v}_2) \tag{E.2.8}$$

An important relationship between B and C is the identity

$$[B] [C] = s_\beta^2 [I] \tag{E.2.9}$$

When we investigate the transformation rules for [B] and [C] we will find that this relationship is preserved under linear transformations.

Careful examination of equations (E.2.5) and (E.2.8) shows that we may define modified vectors $\tilde{w}$ and modified dual vector $\tilde{v}$ by

$$\tilde{w} = C\vec{w} \qquad \text{(modified vector)} \tag{E.2.10}$$

$$\tilde{v} = B\vec{v} \qquad \text{(modified dual vector)} \tag{E.2.11}$$

With modified vectors defined in this fashion, it is easy to see that the inner product relations (E.2.4) and (E.2.8) can be written

$$[\vec{w}_1, \vec{w}_2] = (\vec{w}_1, \tilde{w}_2) = (\tilde{w}_1, \vec{w}_2) \tag{E.2.12}$$

$$\{\vec{v}_1, \vec{v}_2\} = (\vec{v}_1, \tilde{v}_2) = (\tilde{v}_1, \vec{v}_2) \tag{E.2.13}$$

Two examples of modified dual vectors include the conormal,

$$\tilde{n} = [B] \hat{n} \tag{E.2.14}$$

and the modified gradient operator, $\tilde{\nabla}$, defined by (5.2.4).

We now examine the transformation rules for metrics and dual metrics. When a coordinate transformation of the form (E.1.1) is performed, the metric matrix C and dual metric matrix B in the new coordinate system X' are defined by the invariance requirements that

$$[\vec{w}_1', \vec{w}_2'] = \vec{w}_1'^{\,T} [C'] \vec{w}_2' = [\vec{w}_1, \vec{w}_2] \tag{E.2.15}$$

$$\left\{\vec{v}_1', \vec{v}_2'\right\} = \vec{v}_1'^{\,T} [B'] \vec{v}_2' = \{\vec{v}_1, \vec{v}_2\} \tag{E.2.16}$$

whenever $\vec{w}_i' = A\vec{w}_i$, $\vec{v}_i' = [A^{-T}]\vec{v}_i$. For the metric matrix C', (E.2.15) implied that, for arbitrary vectors $\vec{w}_1$, $\vec{w}_2$

$$\vec{w}_1^T[C]\vec{w}_2 = [\vec{w}_1, \vec{w}_2] = \vec{w}_1'^T[C']\vec{w}_1' = \vec{w}_1^T[A^T C' A]\vec{w}_2 \tag{E.2.17}$$

Consequently we find that

$$C = A^T C' A, \qquad C' = A^{-T} C A^{-1} \tag{E.2.18}$$

Similarly, equation (E.2.16) provides us with the transformation rule

$$B = A^{-1} B' A^{-T}, \qquad B' = ABA^T \tag{E.2.19}$$

It is now an easy matter to verify that the relationship (E.2.9) is preserved under transformation; calculation gives

$$B' C' = (A B A^T)(A^T C A^{-1}) = A(B C)A^{-1} = A(s\beta^2 I) A^{-1} = s\beta^2 I \tag{E.2.20}$$

There is no a priori condition that determines how $\tilde{w}$ transforms, so we make the reasonable requirement that

$$(\tilde{w})' = (\tilde{w}')\sim \tag{E.2.21}$$

Then

$$\tilde{w}' = (w')\sim = C'\vec{w}' = C' A \vec{w} = [C' A C^{-1}]\tilde{w} \tag{E.2.22}$$

From equation (E.2.18) we see that

$$C' A C^{-1} = A^{-T} \tag{E.2.23}$$

so that

$$\tilde{w}' = A^{-T}\tilde{w} \tag{E.2.24}$$

This shows that modified vectors are in fact dual vectors.

Similarly, one may show that modified dual vectors are vectors. That is, assuming, for a dual vector $\vec{v}$, that

$$(\tilde{v})' = (v')\sim \tag{E.2.25}$$

then

$$\tilde{v}' = A\tilde{v} \tag{E.2.26}$$

These observations provided us with an interesting interpretation of equations (E.2.12) and (E.2.13): $[\vec{w}_1, \vec{w}_2]$, which is the compressible product of the vectors w_1 and w_2, is the same as the Euclidean inner product of the vector w_1 and the dual vector w_2 ; similarly $\{\vec{v}_1, \vec{v}_2\}$, the dual compressible inner product of the dual vectors v_1 and v_2 is the Euclidean inner product of $\vec{v}_1$ (a vector) and $\vec{v}_2$ (a dual vector). This observation shows that the invariance properties (E.2.15) and (E.2.16) are closely related to the invariance relation (E.1.29).

E.3 Coordinate Transformations

We recall from section E.0 the reference coordinate system X_0, the compressibility system X, the scaled system X, and the local system X'. In this section, we will determine the properties required by the transformation A: $X_0 \rightarrow X'$, and then show that the matrix (E.0.1) is the unique matrix with these properties.

In general the x-axis of coordinate system X_0 need not line up with the free stream. Thus it is necessary to define a new coordinate system X in which the x-axis is lined up with the free stream axis (that is the x-axis of the Prandtl-Glauert equation (3.0.1)) . This is possible if the user provides the compressibility direction by means of a compressibility vector $\hat{c}_0$.

The PAN AIR program user will specify the compressibility axis by giving an angle of attack α_c and a sideslip angle β_c as shown in fig. E.3. The orientation of the compressibility axis is given by the unit vector (cf. (5.2.12))

$$\hat{c}_0 = \begin{Bmatrix} \cos\alpha_c \cos\beta_c \\ -\sin\beta_c \\ \sin\alpha_c \cos\beta_c \end{Bmatrix} \tag{E.3.1}$$

A free stream oriented coordinate system X must be defined such that the compressibility vector c_0 lies along the x-axis of this new coordinate system. The transformation from X_0 to X may be characterized as an angle of attack rotation of $(-\alpha_c)$ about the y_0 -axis followed by an angle of sideslip rotation of $(-\beta_c)$ about the resulting z axis.
Note that coordinates transform in the opposite manner from basis vectors. Thus if we denote the transformation from X_0 to X by Γ_c so that

$$\Gamma_c: \qquad X_0 \longrightarrow X \tag{E.3.2}$$

we have

$$\Gamma_c = R_z(-\beta_c)\, R_y(-\alpha_c) = \begin{bmatrix} \cos\beta_c & -\sin\beta_c & 0 \\ \sin\beta_c & \cos\beta_c & 0 \\ 0 & 0 & 1 \end{bmatrix} \begin{bmatrix} \cos\alpha_c & 0 & \sin\alpha_c \\ 0 & 1 & 0 \\ -\sin\alpha_c & 0 & \cos\alpha_c \end{bmatrix}$$

$$= \begin{bmatrix} \cos\alpha_c \cos\beta_c & -\sin\beta_c & \sin\alpha_c \cos\beta_c \\ \cos\alpha_c \sin\beta_c & \cos\beta_c & \sin\alpha_c \sin\beta_c \\ -\sin\alpha_c & 0 & \cos\alpha_c \end{bmatrix} \tag{E.3.3}$$

Here R_y and R_z denote rotations about the respective axes.

Thus the compressibility axis in coordinate system X is given by

$$\hat{c} = \Gamma_c \, \hat{c}_o = \begin{Bmatrix} 1 \\ 0 \\ 0 \end{Bmatrix} \tag{E.3.4}$$

which is the desired result.

In fact, if Γ_c is partitioned by rows, we see immediately that the first row of Γ_c is simply $\hat{c}_o^T$ while the remaining two rows are orthogonal to c_o and to one another:

$$\Gamma_c = \begin{Bmatrix} \hat{c}_o^T \\ \hat{s}_o^T \\ \hat{t}_o^T \end{Bmatrix} \tag{E.3.5}$$

In fact, Γ_c is an orthogonal matrix; $\Gamma_c^T \; \Gamma_c = I$

A matrix of the form Γ_c, transforming reference coordinates orthogonally to another user-defined system, is used after the potential flow solution has been obtained.

This axis system X* is defined by an angle of attack α^* and an angle of sideslip β^*, with the transformation $\Gamma^*: X_o \rightarrow X^*$ defined by

$$\Gamma^* = \begin{bmatrix} \cos\alpha^* \cos\beta^* & -\sin\beta^* & \sin\alpha^* \cos\beta^* \\ \cos\alpha^* \sin\beta^* & \cos\beta^* & \sin\alpha^* \sin\beta^* \\ -\sin\alpha^* & 0 & \cos\alpha^* \end{bmatrix} \tag{E.3.6}$$

The angles α^* and β^* are user-supplied, and describe the coordinate system in which the user wishes PAN AIR to calculate forces or moments.

Before we consider the transformation from reference (X_o) to local (X') coordinates, let us consider the transformations (see (E.2.18) and (E.2.19), substituting $_c$ for A)

$$[C_o] = \Gamma_c^T \; C \; \Gamma_c$$

$$[B_o] = \Gamma_c^T \; B \; \Gamma_c \tag{E.3.7}$$

The matrices B_o and C_o have the same properties in reference coordinates that B and C have in compressibility coordinates. That is, equations (E.2.2), (E.2.4), and (E.2.8) hold for B_o and C_o if the vectors in these equations are written in reference coordinates.

Now, from (E.2.3) and (E.2.7)

$$[C] = s\beta^2 \, I + (1-s\beta^2) \, \hat{e}_1 \, \hat{e}_1^T$$

$$[B] = I + (s\beta^2 - 1) \, \hat{e}_1 \, \hat{e}_1^T \qquad \text{(E.3.8)}$$

where $\hat{e}_i$ is the ith column of the identity matrix I.

Now, since $\Gamma_c^{-1} = \Gamma_c^T$ because Γ_c is orthogonal, and

$$\Gamma_c^T \, \hat{e}_1 = \hat{c}_o$$

by (E.3.5),

$$[C_o] = s\beta^2 \, I + (1-s\beta^2) \, \hat{c}_o \, \hat{c}_o^T$$

$$[B_o] = I + (s\beta^2 - 1) \, \hat{c}_o \, \hat{c}_o^T \qquad \text{(E.3.9)}$$

Let us now consider the properties we require of the transformation

$$A: \; X_o \rightarrow X' \qquad \text{(E.3.10)}$$

where X' is the local coordinate system for each subpanel.

The reasons for these requirements are given following (E.3.15).

First, recalling (5.2.19) through (5.2.22), we require, for points p and q, that

$$\begin{aligned} R^2 &= (p'_1 - q'_1)^2 + (p'_2 - q'_2)^2 \\ &\quad + (p'_3 - q'_3)^2 && \text{for subsonic flow} \\ &= (p'_1 - q'_1)^2 - (p'_2 - q'_2)^2 \\ &\quad - (p'_3 - q'_3)^2 && \text{for subinclined panels in supersonic flow} \\ &= -(p'_1 - q'_1)^2 - (p'_2 - q'_2)^2 \\ &\quad + (p'_3 - q'_3)^2 && \text{for superinclined panels.} \end{aligned} \qquad \text{(E.3.11)}$$

Second, we require that on the subpanel on which the X' coordinate system is

defined,

$$z' = 0 \tag{E.3.12}$$

Third, we require that the "upstream" direction be the $x' < 0$ direction for subsonic flow or subinclined panels, (cf. (E.3.13)) and that the upstream direction be preserved for superinclined panels. (cf. (E.3.14)). That is, if the surface normal in reference coordinates is pointing into the flow, then so should the surface normal in local coordinates, and similarly if the normal is pointed with the flow. Precisely, we require

$$(\hat{c}_0, A^{-1} \hat{e}_1) > 0 \tag{E.3.13}$$

in the former case, and

$$\text{sign } (\hat{c}_0, A^{-1} \hat{e}_3) = \text{sign } (\hat{c}_0, \hat{n}_0) \tag{E.3.14}$$

in the latter case. The fourth requirement is

$$\det A > 0 \tag{E.3.15}$$

Before proving that these requirements are satisfied, let us discuss them further. Equation (E.3.11) is necessary in order to obtain reasonable formulas for the influence coefficients, that is, formulas which do not have scaling coefficients all over. The requirement that the subpanel lie in a coordinate plane makes the integrals needed for influence coefficient calculation computable, the $z' = 0$ plane is chosen throughout in order to permit uniform formulas for all three cases. The constraint on the upstream direction makes the notation for the derivation of the influence coefficient formulas simpler. Finally, the requirement that A have positive determinant insures that the local coordinate system will be a right-handed one.

In the remainder of this appendix, we will rigorously prove that the matrix A in (E.0.1) satisfies the requirements. We will not, however, explain where A came from, since we did not arrive at A through a rigorous procedure.

Recall that we claim that

$$A^T = \left[\frac{1}{|\{\hat{n}_0,\hat{n}_0\}|^{1/2}} [C_0] \hat{u}_0 \;\vdots\; \frac{rs}{\beta} [C_0] \hat{v}_0 \;\vdots\; \frac{\beta \hat{n}_0}{|\{\hat{n}_0,\hat{n}_0\}|^{1/2}} \right] \tag{E.3.16a}$$

satisfies the requirements (E.3.11-15), where

$\hat{n}_0$ = unit normal vector

$\hat{v}_0 = (\hat{n}_0 \times \hat{c}_0)/|\hat{n}_0 \times \hat{c}_0|$

$r = \text{sign } \{\hat{n}_0, \hat{n}_0\}$

$$\hat{u}_0 = \hat{v}_0 \times \hat{n}_0 \tag{E.3.16b}$$

The subscript o indicates these vectors are in reference coordinates.

If $\hat{n}_o$ is parallel to $\hat{c}_o$, $\hat{v}_o$ may be chosen arbitrarily as any unit vector perpendicular to them. Since $\hat{u}_o$ and $\hat{v}_o$ are linearly independent vectors orthogonal to $\hat{n}_o$, the second requirement on A, (E.3.12) is equivalent to

$$(A\,\hat{u}_o,\ \hat{e}_3) = 0$$

$$(A\,\hat{v}_o,\ \hat{e}_3) = 0 \qquad \text{(E.3.17)}$$

or $$(\hat{u}_o,\ A^T\,\hat{e}_3) = (\hat{v}_o,\ A^T\,\hat{e}_3) = 0 \qquad \text{(E.3.18)}$$

or $$A^T\,\hat{e}_3 = k\,\hat{n}_o,\quad k \neq 0 \qquad \text{(E.3.19)}$$

But this just says that the third column of A^T should be proportional to $\hat{n}_o$, which is satisfied by the matrix in (E.0.1).

Next, by definition,

$$R^2 = (p_1 - q_1)^2 + s_\beta^2\,(p_2 - q_2)^2 + s_\beta^2\,(p_3 - q_3)^2$$

$$= (\vec{p} - \vec{q})^T \begin{bmatrix} 1 & & \\ & s_\beta^2 & \\ & & s_\beta^2 \end{bmatrix} (\vec{p} - \vec{q}) \qquad \text{(E.3.20)}$$

$$= \left\{\Gamma_c(\vec{p}_o - \vec{q}_o)\right\}^T [C] \quad \Gamma_c(\vec{p}_o - \vec{q}_o)$$

$$= (\vec{p}_o - \vec{q}_o)^T\,[\Gamma_c^T\ \ C\ \ \Gamma_c](\vec{p}_o - \vec{q}_o) \qquad \text{(E.3.21)}$$

= (by (E.2.18))

$$(\vec{p}_o - \vec{q}_o)^T\,[C_o]\ \ (\vec{p}_o - \vec{q}_o) \qquad \text{(E.3.22)}$$

On the other hand, we can unify (E.3.11) by noting that r = -1 if and only if the panel is superinclined, and so (E.3.11) becomes

$$R^2 = \left\{A\,(\vec{p}_o - \vec{q}_o)\right\}^T \begin{bmatrix} r & & \\ & s & \\ & & rs \end{bmatrix} A\,(\vec{p}_o - \vec{q}_o) \qquad \text{(E.3.23)}$$

Combining with (E.3.22), we obtain the requirement on [A]:

$$[A^T] \begin{bmatrix} r & & \\ & s & \\ & & rs \end{bmatrix} [A] = [C_o] \tag{E.3.24}$$

Inverting (E.3.24)

$$A^{-1} \begin{bmatrix} r & & \\ & s & \\ & & rs \end{bmatrix} A^{-T} = [C_o]^{-1} \tag{E.3.25}$$

or

$$\begin{bmatrix} r & & \\ & s & \\ & & rs \end{bmatrix} = [A][C_o]^{-1} [A^T] \tag{E.3.26}$$

But, by (E.3.7), $[C_o]^{-1} = \Gamma_c^T [C^{-1}] \Gamma_c$ (E.3.27)

$$= \Gamma_c^T \begin{bmatrix} 1 & & \\ & 1/s\beta^2 & \\ & & 1/s\beta^2 \end{bmatrix} \Gamma_c \tag{E.3.28}$$

$$= \frac{1}{s\beta^2} \left[\Gamma_c^T \; B \; \Gamma_c \right] = \frac{1}{s\beta^2} B_o \tag{E.3.29}$$

$$= \text{(by E.3.9)} \; \frac{1}{S\beta^2} [I] + \left(1 - \frac{1}{S\beta^2} \right) [\hat{c}_o, \hat{c}_o^T] \tag{E.3.30}$$

Thus, we must show that

$$[D] \equiv A \, C_o^{-1} \, A^T = \frac{1}{s\beta^2} [A \, A^T] + \left(1 - \frac{1}{s\beta^2}\right) [A \, \hat{c}_o \, \hat{c}_o^T \, A^T]$$

$$= \begin{bmatrix} r & & \\ & s & \\ & & rs \end{bmatrix} \tag{E.3.31}$$

Now,

$$[D]_{11} = \frac{1}{|\{\hat{n}_o, \hat{n}_o\}|} \left(\frac{1}{s\beta^2} \hat{u}_o^T [C_o]^T [C_o] \hat{u}_o \right.$$

$$\left. + \left(1 - \frac{1}{s\beta^2}\right) \hat{u}_o^T [C_o]^T \hat{c}_o \hat{c}_o^T [C_o] \hat{u}_o \right) \tag{E.3.32}$$

But from (E.3.9)

$$[C_o^T C_o] = \beta^4 [I] + 2 s\beta^2 (1 - s\beta^2) [\hat{c}_o \hat{c}_o^T]$$

$$+ (1 - s\beta^2)^2 [\hat{c}_o \hat{c}_o^T \hat{c}_o \hat{c}_o^T] \tag{E.3.33}$$

$$= \beta^4 [I] + (2s\beta^2 - 2\beta^4 + 1 - 2s\beta^2 + \beta^4) [\hat{c}_o \hat{c}_o^T] \tag{E.3.34}$$

$$= \beta^4 [I] + (1 - \beta^4) [\hat{c}_o \hat{c}_o^T] \tag{E.3.35}$$

Next,

$$[C_o^T \hat{c}_o \hat{c}_o^T C_o] = [s\beta^2 I \hat{c}_o \hat{c}_o^T s\beta^2 I]$$

$$+ [s\beta^2 I \hat{c}_o \hat{c}_o^T (1 - s\beta^2) \hat{c}_o \hat{c}_o^T]$$

$$+ [(1 - s\beta^2) \hat{c}_o \hat{c}_o^T \hat{c}_o \hat{c}_o^T s\beta^2 I]$$

$$+ [(1 - s\beta^2) \hat{c}_o \hat{c}_o^T \hat{c}_o \hat{c}_o^T (1 - s\beta^2) \hat{c}_o \hat{c}_o^T] \tag{E.3.36}$$

$$= \beta^4 [\hat{c}_o \hat{c}_o^T] + (s\beta^2 - \beta^4) [\hat{c}_o \hat{c}_o^T]$$

$$+ (s\beta^2 - \beta^4) [\hat{c}_o \hat{c}_o^T] + (1 - s\beta^2)^2 [\hat{c}_o \hat{c}_o^T] \tag{E.3.37}$$

$$= [\hat{c}_o \hat{c}_o^T] \tag{E.3.38}$$

So, $\hat{u}_o^T [C_o^T C_o] \hat{u}_o = \beta^4 \hat{u}_o^T \hat{u}_o$

$$+ (1 - \beta^4) \hat{u}_o^T [\hat{c}_o \hat{c}_o^T] \hat{u}_o \tag{E.3.39}$$

$$= \beta^4 + (1 - \beta^4) (\hat{u}_o, \hat{c}_o)^2 \tag{E.3.40}$$

and

$$\hat{u}_o^T [C_o^T] [\hat{c}_o \hat{c}_o^T] [C_o] \hat{u}_o = (\hat{u}_o, \hat{c}_o)^2 \tag{E.3.41}$$

So,

$$[D]_{11} = \frac{1}{|\{\hat{n}_o,\hat{n}_o\}|} \left[\frac{\beta^4}{s\beta^2} + \frac{1-\beta^4}{s\beta^2} (\hat{u}_o, \hat{c}_o)^2 + (1 - \frac{1}{s\beta^2}) (\hat{u}_o, \hat{c}_o)^2\right] \quad \text{(E.3.42)}$$

$$= \frac{1}{|\{\hat{n}_o, \hat{n}_o\}|} [(s\beta^2 + (1 - s\beta^2) (\hat{u}_o, \hat{c}_o)^2] \quad \text{(E.3.43)}$$

Now, for vectors A,B,C,

$$(\vec{A} \times \vec{B})\cdot\vec{C} = \epsilon_{ijk} A_i B_j C_k = \epsilon_{jki} B_j C_k A_i = (\vec{B} \times \vec{C})\cdot\vec{A} \quad \text{(E.3.44)}$$

Thus, applying (E.3.16b),

$$\hat{u}_o\cdot\hat{c}_o = (\hat{v}_o \times \hat{n}_o) \cdot \hat{c}_o = (\hat{n}_o \times \hat{c}_o)\cdot\hat{v}_o$$
$$= (\hat{n}_o \times \hat{c}_o)(\hat{v}_o \cdot \hat{v}_o) = \hat{n}_o \times \hat{c}_o \quad \text{(E.3.45)}$$

Thus

$$\hat{u}_o\cdot\hat{c}_o = |\hat{n}_o \times \hat{c}_o| = \pm \sin\theta \quad \text{(E.3.46)}$$

where θ is the angle between $\hat{n}_o$ and $\hat{c}_o$.

On the other hand by (E.3.9)

$$\hat{n}_o, \hat{n}_o = \hat{n}_o^T B_o \hat{n}_o = \hat{n}_o^T \hat{n}_o + (s\beta_2 - 1) (\hat{n}_o \cdot \hat{c}_o)^2 \quad \text{(E.3.47)}$$

$$= 1 + (s\beta^2 - 1) (\hat{n}_o \cdot \hat{c}_o)^2 = 1 + (s\beta^2 - 1) \cos^2\theta \quad \text{(E.3.48)}$$

since $(\hat{n}_o , \hat{c}_o) = \cos\theta$.

$$\text{So, } D_{11} = \frac{s\beta^2 + (1 - S\beta^2) \sin^2\theta}{r (1 + (s\beta^2 - 1) \cos^2\theta)} \quad \text{(E.3.49a)}$$

(since $r\{\hat{n}_o, \hat{n}_o\} = |\{\hat{n}_o, \hat{n}_o\}|$) (E.3.49b)

$$= \frac{s\beta^2 + (1 - s\beta^2) (1 - \cos^2\theta)}{(1 + (s\beta^2 - 1) \cos^2\theta) r} \quad \text{(E.3.50)}$$

$$= \frac{1 + (1 - s\beta^2)\ (-\cos^2\theta)}{(1 + (s\beta^2 - 1)\cos^2\theta)\ r} = r \tag{E.3.51}$$

Next, let us consider D_{22}. By (E.3.31) and (E.0.1),

$$D_{22} = \frac{1}{s\beta^2}\ \frac{r^2\ s^2}{\beta^2}\ (C_o\ \hat{v}_o)^T\ C_o\ \hat{v}_o$$

$$+ \left(1 - \frac{1}{s\beta^2}\right)\ \frac{r^2\ s^2}{\beta^2}\ (C_o\ \hat{v}_o)^T\ [\hat{c}_o\ \hat{c}_o^T]\ C_o\ V_o \tag{E.3.52}$$

$$= \frac{1}{s\beta^4}\ V_o^T\ C_o^T\ C_o\ V_o + \left(1 - \frac{1}{s\beta^2}\right.\ \frac{1}{\beta^2}\ V_o^T\ [C_o^T\ \hat{c}_o\ \hat{c}_o^T\ C_o]\ V_o \tag{E.3.53}$$

Now, $\hat{c}_o^T\ \hat{v}_o = 0$ (E.3.54)

and applying (E.3.35) we therefore get

$$\frac{1}{s\beta^4}\ \hat{v}_o^T\ [C_o^T\ C_o]\ \hat{v}_o = \frac{1}{s}\ \hat{v}_o^T\ \hat{v}_o = s \tag{E.3.55}$$

Applying (E.3.38) we find that the second term of (E.3.53) vanishes, and thus

$$D_{22} = s \tag{E.3.56}$$

Next (by (E.0.1) and (E.3.31)),

$$D_{33} = \frac{\beta^2}{s\beta^2}\ \frac{\hat{n}_o^T\ \hat{n}_o}{|\{\hat{n}_o, \hat{n}_o\}|} + \left(1 - \frac{1}{s\beta^2}\right)\ \frac{\beta^2}{|\{\hat{n}_o, \hat{n}_o\}|}\ \hat{n}_o^T\ \hat{c}_o\ \hat{c}_o^T\ \hat{n}_o \tag{E.3.57}$$

Using (E.3.48)

$$D_{33} = \frac{s}{|\{\hat{n}_o, \hat{n}_o\}|} + \frac{\beta^2\ (1 - 1/s\beta^2)}{|\{\hat{n}_o, \hat{n}_o\}|}\cos^2\theta \tag{E.3.58}$$

$$= \frac{s + (\beta^2 - s)\cos^2\theta}{|\{\hat{n}_o, \hat{n}_o\}|} = \tag{E.3.59}$$

(by (E.3.48) and (E.3.49a))

$$\frac{s\,(1 + (s\beta^2 - 1)\cos^2\theta)}{r\,(1 + (s\beta^2 - 1)\cos^2\theta)} = rs \tag{E.3.60}$$

Next, we consider D_{12} . By (E.0.1) and (E.3.31),

$$D_{12} = \frac{rs}{s\beta^3\,|\{n_o,n_o\}|^{1/2}} \quad (C_o\,\hat{u}_o)^T \;\; C_o\,\hat{v}_o$$

$$+ \frac{1}{1 - s\beta^2} \quad \frac{rs}{\beta\,|\{n_o,n_o\}|^{1/2}} \quad C_o\,\hat{u}_o\,[\hat{c}_o\,\hat{c}_o^T]\,C_o\,\hat{v}_o \tag{E.3.61}$$

Applying (E.3.35) and (E.3.38), we see that each term contains either $\hat{c}_o^T\,\hat{v}_o$ or $\hat{u}_o^T\,\hat{v}_o$, both of which are zero by (E.3.16b), and thus

$$D_{12} = 0 \tag{E.3.62}$$

Next, D_{13} =

$$\frac{\beta}{|\{\hat{n}_o,\,\hat{n}_o\}|}\;\frac{1}{s\beta^2}\;\hat{u}_o^T\;[C_o^T]\;\hat{n}_o + (1 - \frac{1}{s\beta^2})\;\hat{u}_o^T\,[C_o^T\,\hat{c}_o\,\hat{c}_o^T]\,\hat{n}_o \tag{E.3.63}$$

= (by (E.3.9))

$$\frac{\beta}{|\{n_o,\,n_o\}|}\;\frac{1}{s\beta^2}\;\hat{u}_o^T\;s\beta^2\;\hat{n}_o + \frac{1-s\beta^2}{s\beta^2}\;\hat{u}_o^T\,\hat{c}_o\,\hat{c}_o^T\,\hat{n}_o$$

$$+ (1-\frac{1}{s\beta^2})\;\hat{u}_o^T\;s\beta^2\,\hat{c}_o\,\hat{c}_o^T\,\hat{n}_o$$

$$+ (1-\frac{1}{s\beta^2})\;(1 - s\beta^2)\;\hat{u}_o^T\,\hat{c}_o\;\hat{c}_o^T\,\hat{c}_o\,\hat{c}_o^T\,\hat{n}_o \tag{E.3.64}$$

= (by(E.3.16))

$$\frac{\beta}{|\{n_o, n_o\}|} \left(0 + \frac{1}{s\beta^2} - 1\right)(\hat{u}_o^T \ \hat{c}_o \ \hat{c}_o^T \hat{n}_o)$$

$$+ (s\beta^2 - 1)\ (\hat{u}_o^T \hat{c}_o \hat{c}_o^T \hat{n}_o) + \left(2 - \frac{1}{s\beta^2} - s\beta^2\right)\ (\hat{u}_o^T \hat{c}_o \hat{c}_o^T \hat{n}_o) \tag{E.3.65}$$

$$= \frac{\beta}{|\{n_o, n_o\}|} \cdot 0 = 0 \tag{E.3.66}$$

Finally, D_{23} can be expressed by (E.3.63), changing the factor in front to

$\frac{rs}{|\{n_o,n_o\}|^{1/2}}$, and replacing $\hat{u}_o$ by $\hat{v}_o$. But since we also have

(by (E.3.16))

$$\hat{v}_o^T \hat{n}_o = 0 \tag{E.3.67}$$

we can follow the steps (E.3.63-66) again to obtain

$$D_{23} = 0 \tag{E.3.68}$$

Now, combining the fact that D is symmetric (see(E.3.31)) with (E.3.51), (E.3.56), (E.3.60), (E.3.62), (E.3.66), and (E.3.68), we have

$$[D] = \begin{bmatrix} r & & \\ & s & \\ & & rs \end{bmatrix} \tag{E.3.69}$$

which we have shown is equivalent to (E.3.31) (see the argument from (E.3.20) to (E.3.31)).

So, we have proved that R^2 has the appropriate form in the X' system (E.3.11), and earlier we showed that the subpanel lies in the z' = 0 plane.

To show that the upstream direction transforms correctly, we exhibit A^{-1} first. We claim

$$A^{-1} = r\left[\frac{\hat{u}_o}{|\{n_o,n_o\}|^{1/2}} \ \vdots \ \frac{\hat{v}_o}{\beta} \ \vdots \ \frac{B_o \ \hat{n}_o}{\beta\ |\{n_o,n_o\}|^{1/2}}\right] \tag{E.3.70}$$

Verifying that $[AA^{-1}] = [I]$ is tedious, and uses the same sort of arguments as evaluating D.

First,

$$[AA^{-1}]_{11} = \frac{r}{|\{n_o, n_o\}|} \hat{u}_o^T \; C_o^T \; \hat{u}_o \tag{E.3.71}$$

= (by E.3.9)

$$\frac{r}{|\{n_o, n_o\}|} (s\beta^2 \hat{u}_o^T \hat{u}_o + (1 - s\beta^2) \hat{u}_o^T \hat{c}_o \hat{c}_o^T \hat{u}_o) \tag{E.3.72}$$

= (by (E.3.46), (E.3.48), and (E.3.48a))

$$\frac{r}{r\,(1 + (s\beta^2 - 1) \cos^2 \theta} (s\beta^2 + (1 - s\beta^2) \sin^2 \theta) = 1 \tag{E.3.73}$$

Next,

$$[AA^{-1}]_{22} = \frac{r^2 s}{\beta^2} \hat{v}_o^T C_o^T \hat{v}_o = \tag{E.3.74}$$

= (by (E.3.9))

$$\frac{s}{\beta^2} (s\beta^2 \hat{v}_o^T \hat{v}_o + (1 - s\beta^2) \hat{v}_o^T \hat{c}_o \hat{c}_o^T \hat{v}_o) \tag{E.3.75}$$

= (by (E.3.16)) $\hat{v}_o^T \hat{v}_o = 1$ (E.3.76)

Next,

$$[AA^{-1}]_{33} = \frac{r}{|\{n_o, n_o\}|} \hat{n}_o^T \; B_o \; \hat{n}_o \tag{E.3.77}$$

= (by definition)

$$\frac{r\,\{\hat{n}_o, \hat{n}_o\}}{|\{n_o, n_o\}|} = 1 \tag{E.3.78}$$

by (E.3.49a).

Next,

$$r\beta|\{\hat{n}_o, \hat{n}_o\}|^{1/2} [AA^{-1}]_{12} = \hat{u}_o^T c_o^T \hat{V}_o = \tag{E.3.79}$$

(by (E.3.9), since C_o is its own transpose by (E.3.24))

$$(1 - s\beta^2) \hat{u}_o^T \hat{c}_o \hat{c}_o^T \hat{v}_o + s\beta^2 \hat{u}_o^T \hat{v}_o = 0 \tag{E.3.80}$$

by (E.3.16).

Next, $r\beta|\{\hat{n}_o, \hat{n}_o\}| [AA^{-1}]_{13} = \hat{u}_o^T [C_o B_o] \hat{n}_o$

But from (E.2.20) we see

$$C_o B_o = s\beta^2 I \tag{E.3.81}$$

and thus by (E.3.16),

$$[AA^{-1}]_{13} = 0 \tag{E.3.82}$$

Next,

$$\beta^2 r^2 s|\{\hat{n}_o, \hat{n}_o\}|^{1/2} [AA^{-1}]_{23} = \hat{v}_o^T [C_o^T B_o] \hat{n}_o \tag{E.3.83}$$

Once again applying (E.3.81) and (E.3.16), we obtain

$$[AA^{-1}]_{23} = 0 \tag{E.3.84}$$

Next,

$$\frac{\beta |\{\hat{n}_o, \hat{n}_o\}|^{1/2}}{r^2 s} [AA^{-1}]_{21} = v_o^T C_o u_o = 0 \tag{E.3.85}$$

by (E.3.80).

Next,

$$\frac{r |\{\hat{n}_o, \hat{n}_o\}|}{\beta} [AA^{-1}]_{31} = \hat{n}_o^T \hat{u}_o = 0 \tag{E.3.86}$$

by (E.3.16).

Finally

$$r |\{\hat{n}_o, \hat{n}_o\}|^{1/2} [AA^{-1}]_{32} = \hat{n}_o^T \hat{v}_o = 0 \tag{E.3.87}$$

by (E.3.16).

Thus we have shown that

$$[AA^{-1}] = I \tag{E.3.88}$$

Applying (E.3.70) when $r = +1$,

$$[A^{-1}] \begin{Bmatrix} 1 \\ 0 \\ 0 \end{Bmatrix} = \frac{\hat{u}_o}{|\{\hat{n}_o, \hat{n}_o\}|^{1/2}} \tag{E.3.89}$$

and so

$$\hat{c}_o^T A^{-1} \begin{Bmatrix} 1 \\ 0 \\ 0 \end{Bmatrix} = \frac{(\hat{c}_o, \hat{u}_o)}{|\{\hat{n}_o, \hat{n}_o\}|^{1/2}} = \frac{\hat{n}_o \times \hat{c}_o}{|\{\hat{n}_o, \hat{n}_o\}|^{1/2}} > 0 \tag{E.3.90}$$

This proves (E.3.13). Applying (E.3.70) when $r = -1$,

$$[A^{-1}] \begin{Bmatrix} 0 \\ 0 \\ 1 \end{Bmatrix} = \frac{-[B_o]\hat{n}_o}{\beta|\{\hat{n}_o, \hat{n}_o\}|^{1/2}} \tag{E.3.91}$$

and so

$$\hat{c}_o^T [A^{-1}] \begin{Bmatrix} 0 \\ 0 \\ 1 \end{Bmatrix} = - \frac{\hat{c}_o^T [B_o] \hat{n}_o}{\beta |\{n_o, n_o\}|^{1/2}} = \tag{E.3.92}$$

(by (E.3.9) and (E.3.48))

$$- \frac{1}{\beta |\{\hat{n}_o, \hat{n}_o\}|^{1/2}} (\hat{c}_o^T \hat{n}_o + (s\beta^2 - 1) \hat{c}_o^T \hat{c}_o \hat{c}_o^T \hat{n}_o) \tag{E.3.93}$$

$$= \frac{- s\beta (\hat{c}_o, \hat{n}_o)}{\beta |\{\hat{n}_o, \hat{n}_o\}|^{1/2}} \tag{E.3.94}$$

which has the same sign as $(\hat{c}_o , \hat{n}_o)$ since $s = -1$, thus proving (E.3.14).

Finally, we show that $\det A > 0$.

Applying (E.1.12) to $\hat{u}_o$ and $\hat{v}_o$,

$$A\hat{u}_o \times A\hat{v}_o = (\det A) [A^{-T}] (\hat{u}_o \times \hat{v}_o) = (\det A) [A^{-T}] \hat{n}_o \tag{E.3.95}$$

(by E.3.16).

Applying (E.3.70),

$$A^{-T}\, n_o = \begin{Bmatrix} \dfrac{r}{|\{\hat{n}_o,\hat{n}_o\}|^{1/2}} \quad \hat{u}_o \cdot \hat{u}_o \\ \\ \dfrac{r}{\beta} \quad \hat{v}_o \cdot \hat{n}_o \\ \\ \dfrac{r}{\beta\,|\{\hat{n}_o,\hat{n}_o\}|^{1/2}} \quad \hat{n}_o^T \; B_o \; \hat{n}_o \end{Bmatrix} \tag{E.3.96}$$

$$= \begin{Bmatrix} 0 \\ 0 \\ \dfrac{1}{\beta} \; |\{n_o,n_o\}|^{1/2} \end{Bmatrix} \tag{E.3.97}$$

Now, recalling from (E.3.79) that $\hat{u}_o^T\,[C_o]\,\hat{v}_o = 0$, and applying (E.3.16),

$$[A] \;\; \hat{u}_o = \begin{Bmatrix} \dfrac{\hat{u}_o^T\,[C_o]\,\hat{u}_o}{|\{\hat{n}_o\,,\,\hat{n}_o\}|}\;1/2 \\ 0 \\ 0 \end{Bmatrix} = \begin{Bmatrix} r\,|\{\hat{n}_o\,,\,\hat{n}_o\}|^{1/2} \\ 0 \\ 0 \end{Bmatrix} \tag{E.3.98}$$

by (E.3.71-73).

Next, applying (E.3.16) and (E.3.79),

$$[A]\;\hat{v}_o = \begin{Bmatrix} 0 \\ \dfrac{rs}{\beta} \quad \hat{v}_o^T \;\; [C_o^T] \;\; \hat{v}_o \\ 0 \end{Bmatrix} = \begin{Bmatrix} 0 \\ r\beta \\ 0 \end{Bmatrix} \tag{E.3.99}$$

by (E.3.74-76).

So,

$$A\,\hat{u}_o \times A\,\hat{v}_o = \begin{Bmatrix} 0 \\ 0 \\ \beta\,|\{\hat{n}_o,\hat{n}_o\}|^{1/2} \end{Bmatrix}$$

$$\text{(by (E.3.80))} \quad = \beta^2\,[A^{-T}]\,\hat{n}_0 \tag{E.3.100}$$

Substituting in (E.3.95), we see that

$$\det A = \beta^2 > 0 \tag{E.3.101}$$

This concludes our proof that [A] satisfies (E.3.11-15).

A useful result relating to the area jacobian J for the reference to local transformation matrix can be derived using the results of this section combined with some results from the previous two sections, E.1 and E.2. Using the formula (E.1.28), we form the inner product of the vector $\hat{n}'dS'$ with itself using the metric B'. We obtain:

$$(\hat{n}'dS')^T\,B'(\hat{n}'dS') = (\det A)^2\,(\hat{n}_o dS)\,A^{-1}\,B'\,A^{-T}\,(\hat{n}_o dS) \tag{E.3.102}$$

Now the matrix B' satisfies the equations (cf. (E.2.19) with slight modifications to account for the rotation Γ_c):

$$B_o = A^{-1}\,B'\,A^{-T} \qquad\qquad B' = A\,B_o\,A^T \tag{E.3.103}$$

Using the fact that $\det(A) = \beta^2$, equation (E.3.102) simplifies to read

$$(dS')^2\,(\hat{n}'^T\,B'\,\hat{n}') = \beta^4\,(dS)^2\,\hat{n}_o^{\,T}\,B_o\,\hat{n}_o \tag{E.3.104}$$

Now equation (E.3.31) defining the diagonal matrix D can be combined with the result

$$[B_o]\,[C_o] = s\,\beta^2\,I \tag{E.3.105}$$

which is readily derivable from (E.3.9) to conclude that B' as given by (E.3.103) satisfies:

$$[B'] = [A][B_o][A]^T = [A]\,(s\,\beta^2\,[C_o]^{-1})[A]^T = s\,\beta^2\,[D]$$

$$= \beta^2 \begin{bmatrix} rs & & \\ & 1 & \\ & & r \end{bmatrix} \tag{E.3.106}$$

Combining this with the fact that

$$\hat{n}' = \begin{Bmatrix} 0 \\ 0 \\ 1 \end{Bmatrix} \tag{E.3.107}$$

and recalling the definition of the dual inner product, (E.2.13), we rewrite equation (E.3.104) in the form

$$(dS')^2 \, (r \, \beta^2) = \beta^4 \, (dS)^2 \quad \left\{ \hat{n}_o, \hat{n}_o \right\} \tag{E.3.108}$$

Taking absolute values and rearranging this slightly, we obtain the desired result for the area jacobian:

$$J = \frac{dS}{dS'} = \frac{\text{area in reference coordinates}}{\text{area in local coordinates}}$$

$$= 1/[\beta \quad \left| \left\{ \hat{n}_o, \hat{n}_o \right\} \right|^{1/2}] \tag{E.3.109}$$

Note also that by taking the sign of equation (E.3.108) we obtain,

$$r = \text{sign} \left\{ \hat{n}_o, \hat{n}_o \right\} \tag{E.3.110}$$

reproducing the third of equations (E.3.16b).

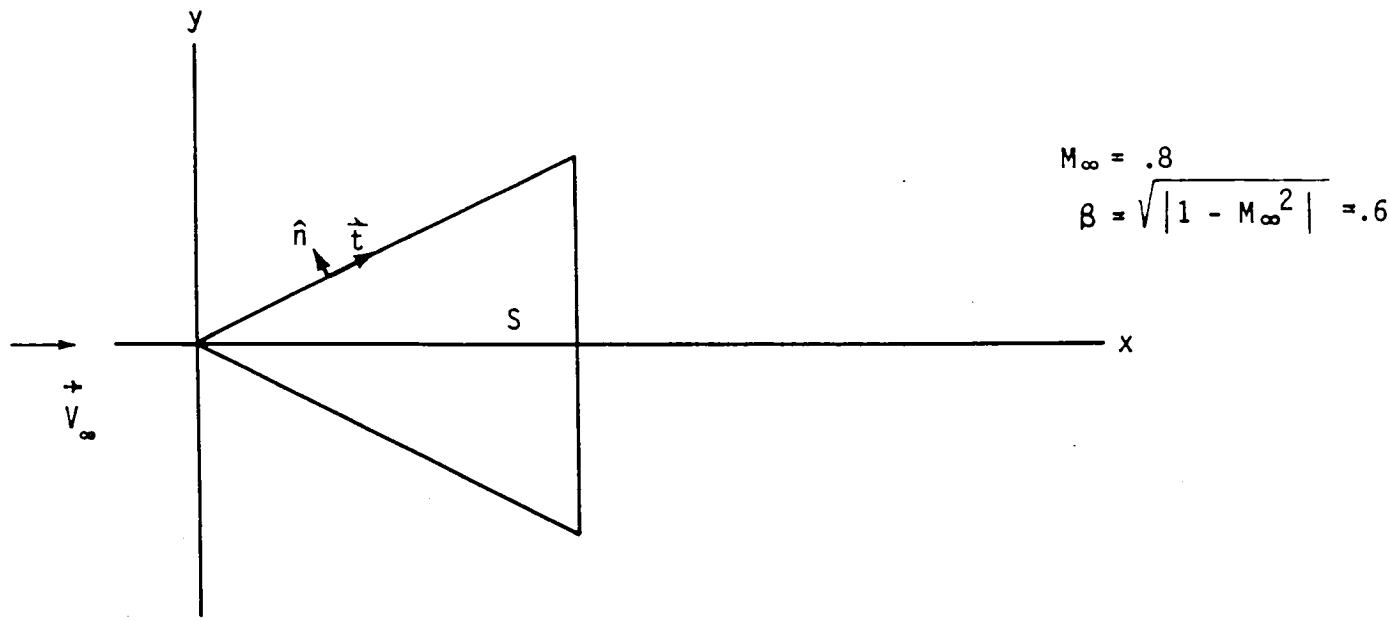

a. Compressibility coordinates

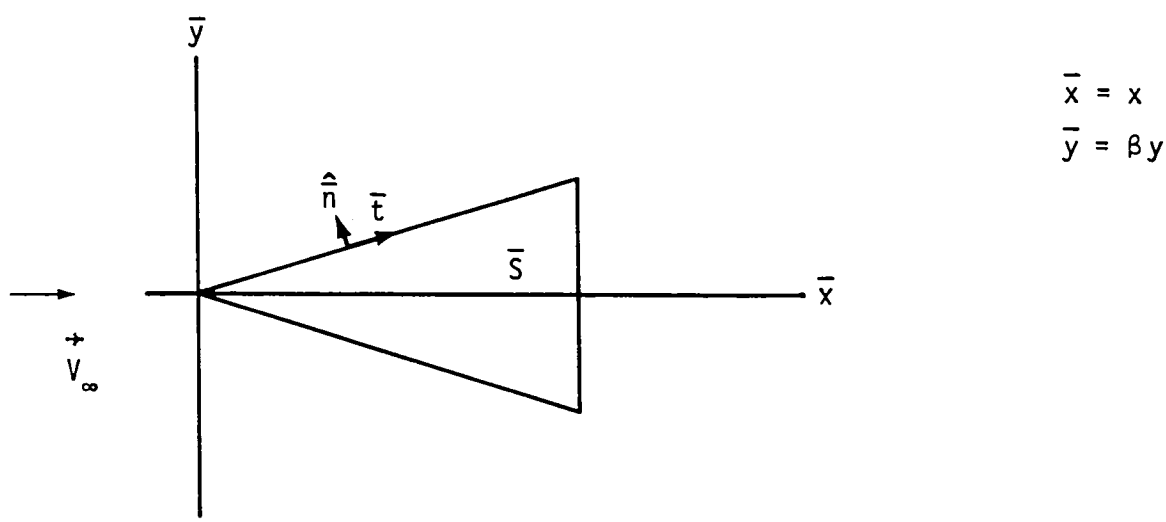

b. Scaled coordinates

Figure E.1 - Surface S in compressibility and scaled coordinates

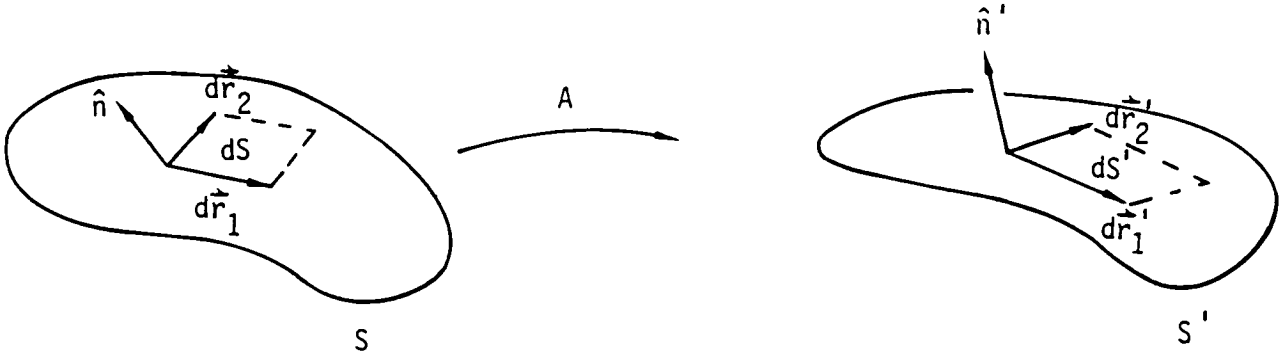

Figure E.2 - Illustration of the transformation law for $\hat{n}$ dS

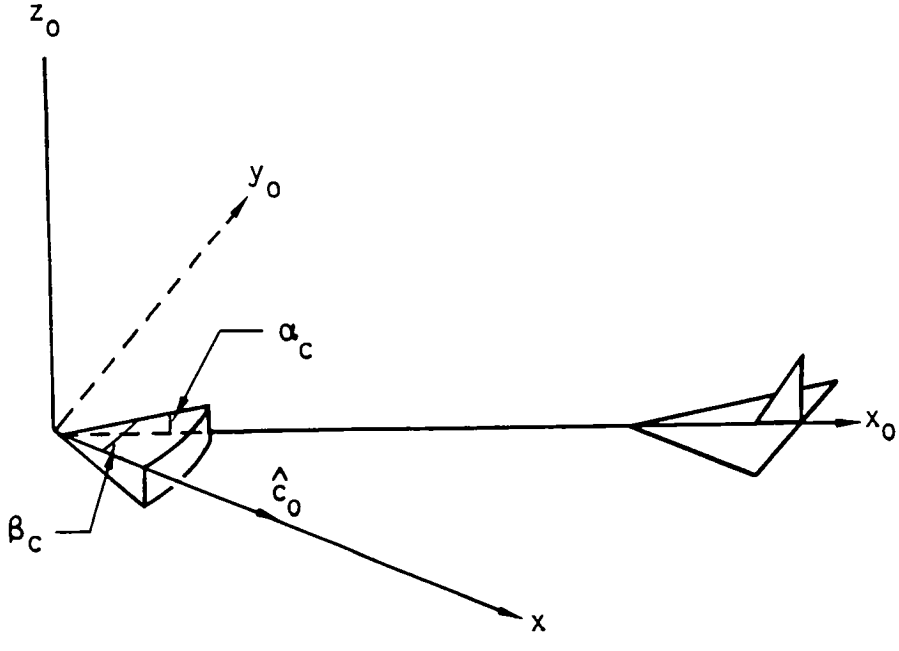

Figure E.3 - Definition of the compressibility vector $\hat{c}_o$ in terms of α_c and β_c

F.0 Edge Matching

In this appendix, we will discuss the process by which the program performs "edge matching", that is, insures "continuity" of doublet strength. In section F.1 we will supply the theoretical background, summarizing section B.3 and discussing a few points not mentioned there. In section F.2, we will discuss the concept of abutments between networks, introducing some of the terminology used within the program. In section F.3, we discuss the process by which the program determines the list of abutments defined by the user-input configuration. In section F.4, we describe the assignment of one edge in the abutment to be the matching edge, and show how this assignment insures doublet matching along the abutment. In section F.5, we discuss the special techniques used by the program to process "abutment intersections", points in space at which abutments meet. In section F.6, we discuss "gap-filling panels," which are added by the program along abutments where gaps between network edges exceed the user-input tolerance distance.

F.1 Continuity Requirements

Recall equation (B.3.12), that along any panel edge we should have

$$\sum_{i=1}^{n} s_i \mu_i = 0 \tag{F.1.1}$$

where n is the number of panel edges meeting, and $s_i = \pm 1$ is determined by the direction of the panel normal. We supplied three distinct types of justification for (F.1.1). First, it is physically reasonable. Second, it has been experimentally shown to be necessary for the analysis of supersonic flow. Third, (F.1.1) can be used to increase the efficiency of the program by allowing the removal of the "line vortex terms."

The imposition of (F.1.1) is effected in one of three ways. Within the interior of the network, it is effected by splines, discussed in Appendix I, which impose the equation

$$\mu_1 - \mu_2 = 0 \tag{F.1.2}$$

along all panel edges. Note that therefore two networks must not meet except along network edges; else, the value of n along the line of intersection would be at least 3, while the spline methods assume n = 2. In figure F.1, we illustrate such an impermissible intersection of networks. Along network edges, boundary conditions (called edge matching boundary conditions) are used to impose (F.1.2). The curve along which network edges meet is called an abutment. If an abutment consists of only two network edges, the user may specify it as a "smooth abutment", in which case a splining method (discussed in Appendix I), is used in place of boundary conditions to impose (F.1.2). This results in fewer boundary conditions, and thus reduces the size of the system of equations to be solved.

The use of smooth abutments is restricted to networks which, together, define a continuously smooth surface. If the surface defined by the networks is not smooth, the doublet gradient at the intersection should in fact be discontinuous, while the smooth abutment specification will make the gradient approximately continuous, resulting in an erroneous solution. For the same reason, a single network should never be used to describe a surface containing a discontinuity of slope.

There is one case in which (F.1.1) does not hold. This case is that of a leading edge vortex (see figure B.10). The true physics of the situation is that the vortex rolls up tighter and tighter (see figure F.2) until it dissipates due to viscous effects. A potential flow program could only simulate the roll-up of the wake by supplying a wake with infinitely many turns in it. This not being practical, wake roll-up can be simulated by replacing the "core" (the region where viscous effects predominate) by a "line vortex" (see figure F.3). Along this network edge, the doublet strength is in fact discontinuous; that is, it is non-zero on the wake, while it is zero in the region of space surrounding the free edge of the wake. The discontinuity of doublet strength means that when the influence of the wake on a control

point is computed, the "line vortex terms" must be added in, that is

$$\int_{\partial s} \mu \quad \tilde{\nabla} \left(\frac{1}{R}\right) \times \vec{dl} \tag{F.1.3}$$

must be computed. We describe the computation of this quantity in appendix J.

The mechanism by which the program user causes the line vortex term (F.1.3) to be added into the influence coefficient matrix is the following. He specifies "no doublet matching" for a particular network edge. The program then insures that the boundary conditions imposed at the control points along the edge are not those of doublet matching (that is, of the form (F.1.1)), and furthermore adds in the line vortex contribution for each panel edge lying along the network edge when measuring the influence of the panel on a control point.

F.2 Network Abutments

PAN AIR deals with a number of distinct data sets called abutments. There are "pairwise abutments", "user-defined abutments", "empty space abutments", and "program-generated abutments". The latter three types of abutments are end products of the procedure which generates a list of all existing network abutments. User-defined abutments are those described by the user, either in order to indicate that they are smooth, or else because the user is not sure that the "automatic abutment search" described in section F.3 will define that abutment. Empty space abutments are those which describe a network edge or portion thereof which does not lie in proximity to any other network edge. Program-generated abutments (those which are neither user-defined nor empty space abutments) are computed in a two step procedure. The first step is the computation of pairwise abutments, each of which lists two network edges or portions thereof which lie in proximity to one another. In the second step, the program distills the list of pairwise abutments into a non-redundant list of program-generated abutments. The latter procedure is described in some detail in the Maintenance Document (see section 4-G), and will not be discussed further here.

F.3 Automatic Abutment Search

In this section we describe the procedure used to identify "pairwise abutments." An edge segment S (the line connecting two adjacent boundary mesh points) is said to form a pairwise abutment with a network edge E provided the end points $\vec{s}_-$ and $\vec{s}_+$ of S satisfy $d(\vec{s}_\pm, E) < \varepsilon$ where ε is some user specified tolerance distance. Here, distance from a point $\vec{s}$ to an edge E is defined in the usual way, $d(\vec{s},E) = \min_{\vec{e}\in E} d(\vec{s},\vec{e})$.

The practical implementation of this definition requires that one know how to compute the distance from a point $\vec{s} = \vec{s}_-$ or $\vec{s}_+$ to an edge E. Let edge E consist of edge segments T_i connecting points $\vec{t}_{i-1}$ and $\vec{t}_i$, $i = 1, 2, \ldots n$. Then $d(\vec{s},E)$ is given by the formula

$$d(\vec{s},E) = \min_{1\le i\le n} d(\vec{s},T_i) \tag{F.3.1}$$

where the distance from a point to a line segment is given by

$$d(\vec{s},T_i) = \begin{cases} |\vec{s} - \vec{t}_{i-1}| & (\vec{s} - \vec{t}_{i-1}, \vec{t}_i - \vec{t}_{i-1}) < 0 \\ |\vec{s} - \vec{t}_i| & (\vec{s} - \vec{t}_i, \vec{t}_i - \vec{t}_{i-1}) > 0 \\ |(\vec{s} - \vec{t}_{i-1}) \times (\vec{t}_i - \vec{t}_{i-1})| \;/\; |\vec{t}_i - \vec{t}_{i-1}| & \text{otherwise} \end{cases} \tag{F.3.2}$$

Having clearly defined the concept of a pairwise abutment of an edge segment with an edge, we now describe what is meant by a pairwise abutment of an "edge portion" with an edge. First, by "edge portion" we mean a subset P of some network edge consisting of <u>contiguous</u> edge segments, $S_k, \ldots S_l, \ldots, S_m$. The edge portion P then, forms a pairwise abutment with E provided each of the edge segments S_l does. If the situation illustrated in figure F.4 occurs, several pairwise abutments of edge portions P, Q, R with edge E will be defined. There are, however, limitations on the permissibility of configurations of the form of figure F.4. These limitations are noted in the User's Manual, sec. B.3.5.

Clearly the process of determining all pairwise abutments requires a large amount of computation for a configuration with many networks. (The amount of work is proportional to N_{ES}^2 where N_{ES} is the number of edge segments in the configuration.) In PAN AIR this computational effort is reduced by avoiding the computation of the distances $d(\vec{s}_\pm, E)$ whenever the edge of which S is a segment is sufficiently far away from E that a pairwise abutment is impossible.

F.4 Doublet Matching Along Abutments

The purpose of doublet matching boundary conditions is to ensure that equation (F.1.1) holds at every point along an abutment, even though a boundary condition of this form is imposed at only a finite number of points. In this section we discuss the enforcement of the doublet matching condition at control points along the interior of the abutment while the enforcement of doublet matching at the ends of an abutment is treated in section F.5.

The ability of a finite number of boundary conditions to cause doublet matching along the full abutment depends directly on the splining techniques used to define the doublet strength along network edges. We discuss this subject in section I.1.2.5, but we will summarize here the results we derive there.

Given any pair of network edges belonging to an abutment, we call the first edge a refinement of the other if, at every point where a panel corner is located on the second edge, a panel corner is also located on the first edge. According to this definition, each network edge in figure F.5 is a refinement of the other, while in figure F.6, edge 1 is a refinement of edge 2.

We show in section I.1.2.5 that if an abutment contains edges $E_1, \ldots, E_n$, and some edge E_k is a refinement of each of the other (n-1) edges of the abutment, then doublet matching can be forced to take place along the entire abutment provided it occurs at the endpoints of the abutments, and at the panel edge midpoints on edge E_k. In practice, precise doublet matching will not occur because PAN AIR uses a "least squares" rather than a differentiable edge spline (see section I.1.2.5). The extent to which doublet matching fails to occur is very small, and has been found experimentally to be negligible.

The program takes into consideration the above results when assigning one edge of an abutment to be the "matching edge", that is, the edge at whose panel edge midpoints doublet matching boundary conditions are imposed. Thus, when no special considerations intervene, the edge with the densest paneling is assigned to be the matching edge. Assuming that the program user has in fact provided one edge in the abutment which is a refinement of all the other edges, then that edge is clearly the most densely paneled edge, and so doublet matching will occur.

Under certain circumstances, the program does not assign the most densely paneled edge in the abutment as the matching edge. The first such case arises from a matching edge of a doublet design or doublet wake network taking part in the abutment.

Unlike doublet analysis networks, design and wake networks are asymmetric; boundary conditions are only imposed along certain edges of these networks, called matching edges, as illustrated in figures D.2 and D.3. When a matching edge of a design or wake network belongs to an abutment, the program assigns it to be the matching edge for the abutment, even if it is not the most densely paneled edge. This is done mostly for convenience; the user is not likely to know what boundary condition to impose at the control points along the matching edge and so the program evades this dilemma by assigning doublet matching boundary conditions there.

The other circumstances under which the most densely paneled edge is not chosen as the matching edge is illustrated in figure F.7. To be specific, whenever the curve defined by an abutment is "supersonic" (that is, no point on the edge is in the domain of dependence of any other point), then that network edge which is a leading edge (that is, upstream of the remainder of the network) is assigned as a matching edge.

The basis for this assignment is largely empirical. Experience with the PAN AIR "pilot code" with the configuration shown in figure F.8a, illustrates the need for imposing doublet matching on the leading supersonic edges of networks in supersonic flow. When doublet matching was imposed along the trailing edges of networks 1, 2, and 3, the solution was completely erratic, while shifting the matching boundary conditions to the leading edges of networks 4, 5, and 6 resulted in a solution which was physically reasonable.

The reasons for the numerical problems resulting from the assignment of matching edges as shown in figure F.8a are not precisely known. It is known, however, that specification of normal mass flux in a two-dimensional, linearized, planar, supersonic flow problem is equivalent to specification of the doublet gradient. We may see this by combining equation (C.1.5), which states that ΔC_p is proportional to $\partial\mu/\partial x$, with equations (11-1) and (11-3) of reference F.1, which states that ΔC_p is proportional to normal mass flux.

Thus for a two-dimensional configuration, the specification of zero normal mass flux at panel center points, in combination with doublet matching at the trailing edge, is equivalent to the situation in figure C.10, with the trailing edge boundary condition becoming specification of μ. But this set of boundary conditions, in conjuction with the doublet analysis spline, does not have a unique solution. We see this by noting that the doublet distribution $\mu_0(x)$ shown in figure F.8b satisfies $\mu = 0$ at the leading and trailing edges, and $\partial\mu/\partial x = 0$ at panel centers. Thus, if some solution $\mu(x)$ exists which satisfies the boundary conditions above, so does $\mu(x) + \alpha\,\mu_0(x)$ for all real numbers α. Thus it is not permissible to specify μ at the trailing edge of a two-dimensional network on which normal mass flux is specified at panel centers.

Of course, the configuration in figure F.8a is not a two-dimensional one. Nevertheless, it seems to have enough resemblance to a two-dimensional configuration that the imposition of doublet strength specification on the trailing edge of networks 1, 2, and 3 is an unstable boundary condition specification for the doublet analysis network spline in use on those networks.

Summarizing, PAN AIR selects the network edge to be used for doublet matching along an abutment according to the following criteria:

(i) Matching edge of a doublet design network
(ii) Matching edge of a doublet wake network
(iii) If neither (i) nor (ii) occur, and the abutment is supersonic, the leading edge of the most "downstream pointing" network is used.
(iv) If none of the above occur, the most densely panelled network edge is selected for matching.

Thus, to insure precise doublet matching, a program user must be sure, for every abutment containing a matching edge of a doublet design or wake network, that this edge is a refinement of all the other network edges. Similarly, if the abutment contains a supersonic edge, the leading edge of the most downstream pointing network must be a refinement of the others. Finally, in all other cases, some edge must be a refinement of all the others (recall that, if two edges have identical paneling, each is a refinement of the other).

If these rules are followed, the edge chosen by the program as the matching edge will in fact always be the most densely paneled one, so precise doublet matching will occur. This does not necessarily mean that minor violations of the rules will be serious. For instance, in figure F.9 (ignoring the gap - filling panels for the moment), the edge of the network A is not quite a refinement of the edge of network B. There is no reason to believe, however, that the doublet discontinuities which result from the small discrepancies in figure F.9 are significant.

Next we must discuss the complications introduced into the above procedure by considerations of symmetry. Fortunately, these are few and simple. First, we must recognize that either all of an abutment lies on a plane of symmetry or else no portion of it lies on a plane of symmetry - an abutment cannot partially abut a plane of symmetry. If a network edge lies on a plane of symmetry along part of its length and then breaks away, PAN AIR will recognize two abutments and place an extra control point at the network course grid point at which the breakaway takes place.

Now when an abutment lies on a plane of symmetry, doublet matching along that abutment takes place automatically whenever the potential is symmetric with respect to that plane of symmetry. Consequently we find in PAN AIR that abutment doublet matching conditions are imposed only on selected symmetry conditions when the abutment lies on a plane of symmetry. These are given:

- If an abutment lies on the 1st plane of symmetry, impose edge matching on $\hat{\phi}^{AS}$, $\hat{\phi}^{AA}$ only.

- If an abutment lies on the 2nd plane of symmetry, impose edge matching on $\hat{\phi}^{SA}$, $\hat{\phi}^{AA}$ only.

- If an abutment lies on both planes of symmetry impose edge matching on $\hat{\phi}^{AA}$ only.

(Remark: The various symmetrized potentials, $\hat{\phi}^{SS}$, $\hat{\phi}^{AS}$, etc., are defined as follows. The superscripts S or A indicate whether the given function is symmetric or antisymmetric in a particular plane of symmetry. The first (second) superscript indicates the function's symmetry property with respect to the first (second) plane of symmetry.)

F.5 Abutment Intersections

Within the interior of an abutment, the equation

$$\sum s_i \mu_i = 0 \tag{F.5.1}$$

can easily be imposed by assigning a particular edge as the matching edge, and imposing (F.5.1) at the panel edge midpoints on this edge.

At abutment intersections, points where two or more abutments meet, (see figure F.10), the choice of points at which to impose (F.5.1) becomes more difficult. Only one matching boundary condition may be imposed at a network corner point (since only one control point is located there), yet the corner point lies at the end of two distinct abutments. We will say that a corner point C is "assigned" to an abutment A if the boundary condition imposed at C is doublet matching across A.

A second complication is the danger of overspecification. Consider the example of the abutment intersection formed by four networks, illustrated in figure F.10. Let us define μ_i to be the doublet strength at the corner of network N_i at this intersection. In order to obtain doublet matching, we require

$$\mu_1 = \mu_2 = \mu_3 = \mu_4 \tag{F.5.2}$$

But these are only three equations. Thus, if we assign corner point C_1 to abutment A_1, C_2 to A_2, and C_3 to A_3, that is, impose the boundary conditions

$$\begin{aligned} &\mu_1 = \mu_2 \text{ at } C_1 \\ &\mu_2 = \mu_3 \text{ at } C_1 \\ \text{and} \quad &\mu_3 = \mu_4 \text{ at } C_3 \end{aligned} \tag{F.5.3}$$

we have satisfied (F.5.2). If we were to assign corner point C_4 to abutment A_4 in addition, the resulting boundary condition

$$\mu_4 = \mu_1 \text{ at } C_1 \tag{F.5.4}$$

would be redundant, since it follows from (F.5.3). If a row of the AIC matrix corresponding to (F.5.4) were generated, the resulting matrix would therefore be singular, since this row would be a linear combination of three rows corresponding to (F.5.3).

Thus overspecification must be avoided if the program is to provide a numerical solution to the potential flow problem. This is straightforward for any reasonable example, but clearly the program must follow a well-defined method which assigns corner points to abutments in such a manner that doublet matching occurs at all abutments while no overspecification occurs. As an example, the abutment intersection in figure F.11 may arise from a realistic

airplane configuration, yet an automatic procedure assigning corner points to abutments is not obvious. In this section, then, we will describe a graph theoretic interpretation of this abutment intersection problem together with the corresponding solution of this problem. This will be accomplished in two phases. In section F.5.1 we will describe the graphical representation of an abutment intersection in the "usual case" together with the corresponding abutment assignment procedure. Following this, in section F.5.2 we will outline those special features supported by PAN AIR that affect abutment assignment together with the modifications to the basic assignment procedure that enable PAN AIR to correctly implement those special features.

F.5.1 Graphical Representation of an Abutment Intersection

In figures F.10, F.11 and F.12 we present diagrams for three examples of abutment intersections. We will denote by P_{AI} (the abutment intersection point), the point at which the various abutments meet. The directed graph G associated with the abutment intersection is constructed as follows.

Let a small sphere S be constructed with P_{AI} as its center. The nodes of G are to be identified with the points at which the various abutments pierce S. The branches of G are to be identified with the lines on S along which the various networks involved in the abutment intersection cut the surface of S. An orientation (direction) for a branch/line is induced in a natural way by the orientation of the network that generates it. To see how this is done, let N be a network that is involved in the abutment intersection and let L_N (= N S) be the line along which N cuts S. Denote by N' the subsurface of N that lies outside of S. Notice that the line L_N is part of the boundary of N'. Now since N' is a subsurface of N, the orientation of N provides an orientation for N'. An orientation for N' in turn provides an orientation (that is, a direction of traversal) for the boundary of N'. This traversal direction is, of course, the usual counterclockwise traversal of the boundary when the network is viewed from above. If then, one traces the boundary of N' in the traversal direction provided by its orientation, part of the trace will move along the line L_N in a unique direction. This direction is the orientation of L_N. If we denote the abutment at the beginning of the line L_N by A_N^- and the abutment at the end by A_N^+ then we say that the branch induced by network N points from node/abutment A_N^- to node/abutment A_N^+.

The procedure given above generates a directed graph G lying on the sphere S. Such a graph can be spread out on a plane simply by puncturing S at some point that does not lie on the graph and then stretching the surface S, with the graph G imbedded in it, out onto a plane.

The graphs generated by the abutment intersections of figures F.10, F.11 and F.12 are drawn in figure F.13.

An alternative (and consistent) interpretation of branch orientation is possible if, as is usually the case, the abutment intersection point P_{AI} coincides with a corner point of network N lying at the last point of edge

k_N^- and at the first point of edge k_N^+(*). When this happens, we denote by A_N^- the abutment in which edge k_N^- participates and by A_N^+ the abutment in which k_N^+ participates. Having done this, we say that branch/network N proceeds from node/abutment A_N^- to node/abutment A_N^+.

Once the directed graph representing an abutment intersection has been constructed, it is quite an easy matter to write down all of the doublet matching conditions of the form (F.5.1) associated with the abutments in the abutment intersection. Given a node/abutment A, we compute the values s_i associated with the doublet matching condition according to the following rules:

$$s_i = \begin{cases} +1 & \text{if branch/network } N_i \text{ is directed away from A} \\ -1 & \text{if branch/network } N_i \text{ is directed toward A} \\ 0 & \text{if branch/network } N_i \text{ is not connected to A} \end{cases} \qquad \text{(F.5.5)}$$

Using these rules, together with the graphs provided by figure F.13, we obtain the following sets of matching conditions

Figure F.10

$$\begin{array}{lllllll} A_1: & +\mu_1 & -\mu_2 & & & & = 0 \\ A_2: & & +\mu_2 & -\mu_3 & & & = 0 \\ A_3: & & & +\mu_3 & -\mu_4 & & = 0 \\ A_4: & -\mu_1 & & & +\mu_4 & & = 0 \end{array} \qquad \text{(F.5.6)}$$

Figure F.11

$$\begin{array}{lllllllll} A_1: & +\mu_1 & -\mu_2 & -\mu_3 & & & & & = 0 \\ A_2: & & & +\mu_3 & -\mu_4 & & -\mu_6 & & = 0 \\ A_3: & & & & \mu_4 & +\mu_5 & & & = 0 \\ A_4: & & & & & & +\mu_6 & -\mu_7 & = 0 \\ A_5: & & +\mu_2 & & & -\mu_5 & & & = 0 \\ A_6: & -\mu_1 & & & & & & +\mu_7 & = 0 \end{array} \qquad \text{(F.5.7)}$$

* Remark: Usually it will happen that $k_N^+ = k^*$ where $k^* = \text{mod}\ (k_N^-, 4) + 1$. However if edge k^* is a collapsed edge of network N, we will have $k_N^+ = \text{mod}\ (k_N^- + 1, 4) + 1$.

Figure F.12

$$
\begin{array}{llllll}
A_1: & \mu_1 & -\mu_2 & +\mu_3 & & = 0 \\
A_2: & & \mu_2 & & & = 0 \\
A_3: & & & -\mu_3 & +\mu_4 & = 0 \\
A_4: & -\mu_1 & & & -\mu_4 & = 0
\end{array}
\tag{F.5.8}
$$

(The reader is urged to verify the correctness of these matching conditions by carefully re-examining the original figures).

The matching conditions given above have been written down in a format such that they can be readily re-expressed in the shorthand form

$$A(G)\,\vec{\mu} = 0 \tag{F.5.9}$$

where $\vec{\mu}$ is the vector of doublet values associated with the branches/networks of the graph and A(G) is called the <u>incidence matrix</u> associated with a directed graph G. For the three graphs given in figure F.13, the incidence matrices are

Fig. F.13a

$$A(G) = \begin{bmatrix} 1 & -1 & 0 & 0 \\ 0 & 1 & -1 & 0 \\ 0 & 0 & 1 & -1 \\ -1 & 0 & 0 & 1 \end{bmatrix} \tag{F.5.10}$$

Fig. F.13b

$$A(G) = \begin{bmatrix} 1 & -1 & -1 & 0 & 0 & 0 & 0 \\ 0 & 0 & 1 & -1 & 0 & -1 & 0 \\ 0 & 0 & 0 & 1 & 1 & 0 & 0 \\ 0 & 0 & 0 & 0 & 0 & 1 & -1 \\ 0 & 1 & 0 & 0 & -1 & 0 & 0 \\ -1 & 0 & 0 & 0 & 0 & 0 & 1 \end{bmatrix} \tag{F.5.11}$$

Fig. F.13c

$$A(G) = \begin{bmatrix} 1 & -1 & 1 & 0 \\ 0 & 1 & 0 & 0 \\ 0 & 0 & -1 & 1 \\ -1 & 0 & 0 & 1 \end{bmatrix} \tag{F.5.12}$$

Having expressed the doublet matching conditions at an abutment intersection in terms of an incidence matrix A(G) for the directed graph G describing the abutment intersection, we are now in a position to avail ourselves of the many powerful results from graph theory. In fact, graph theory not only provides theorems that yield much information about the structure of abutment intersections, it also provides a number of powerful algorithms that, when suitably tailored, generate the doublet-matching boundary condition assignments required by PAN AIR. The standard reference for all graph theoretical results quoted in this appendix will be ref. F.2, N. Deo, "Graph Theory with Applications to Engineering and Computer Science." Throughout the remainder of this appendix, it is assumed that the reader has at least a nodding familiarity with the elements of graph theory.

The first result from graph theory that we shall need is given (cf. THEOREMS 7-2 and 9-6, ref. F.2)

<u>Theorem</u>* Let G be a connected directed graph containing n nodes and having incidence matrix A(G). Then rank(A(G))=n-1. Furthermore, any set of n-1 rows selected from A(G) is a linearly independent set.

This result can be extended to directed graphs G that are not connected by observing that any such graph can be written as the union of connected components. Thus, for a graph G with k components, we write

$$G = \bigcup_{i=1}^{k} G_i \tag{F.5.13}$$

The theorem can now be applied individually to each component G_i. In fact, whenever G is not connected, PAN AIR performs doublet-matching assignments by treating separately each component G_i of G. Consequently, to simplify the discussion, we shall always assume in what follows that the graph G associated with an abutment intersection is a connected graph.

We now turn to the problem of assigning doublet matching conditions (nodes) to replace user specified boundary conditions at control points lying on a network (branch) involved in the abutment intersection. At this point we treat just the simple "usual case" characterized by the following conditions:

(i) the graph G associated with the abutment intersection is connected,

(ii) each branch/network in the graph has a doublet distribution,

* For the reader familiar with electrical circuit theory, this result is equivalent to the result that for a connected circuit with n nodes, the Kirchoff current law provides n relations, any n-1 of which are linearly independent.

(iii) each branch/network in the graph has a control point available for use as a doublet matching control point whose hypothetical location is essentially coincident with the abutment intersection point P_{AI}.

When these assumptions are made, the following procedure ensures that n-1 abutment matching conditions are selected to replace user specified boundary conditions on n-1 networks

A.1 Form a spanning tree T G. T must contain all of G's nodes but have no loops. (Remark: By a theorem of graph theory, T will contain (n-1) branches.)

A.2 Select any node of G(T) and label it as the <u>ground node</u>.

A.3 Defoliate T by removing one branch at a time until all (n-1) branches have been removed. Algebraically, this is accomplished by constructing a sequence of trees $T = T_n \supset T_{n-1} \supset \ldots \supset T_1$ where T_j is obtained from T_{j+1} by finding a node of degree 1 in T_{j+1} (not the ground node), and removing that node and the single branch to which it is attached. As this is done, the doublet matching condition associated with the node is assigned to replace a user boundary condition on the network associated with the branch.

In figure F.14 we illustrate the application of this procedure to the graph given by figure F.13b.

F.5.2 Modifications to the Abutment Assignment Procedure

The many special features supported by PAN AIR, especially those features associated with symmetry, add considerable complication to the basic algorithm for performing doublet matching at abutment intersections. In addition to symmetry, the most significant complicating features are,

(i) an edge of a network may be marked "no doublet edge matching" by the user,

(ii) a network's corner control point may be a "non-matching corner point" in the sense that there is no boundary condition (i.e., AIC row) associated with the corner control point that might be replaced with a doublet matching condition.

This presentation of our response to these complications will consist of three parts. First, we will describe some of the general considerations that must be taken account of. Second, we will outline the numerous ways by which symmetry, "no-doublet edge matching" and "non-matching corner points" affect the properties of networks, corner control points, user boundary conditions, edges, abutments and abutment intersections. Third we will describe the algorithm employed by PAN AIR that produces a consistent set of doublet matching assignments while satisfying the constraints imposed by PAN AIR's special program features.

General Considerations

In addressing the problem of symmetry, we adopt the fundamental point of view of formulating separately the boundary value problems for the various symmetric and antisymmetric parts of the perturbation potential. Thus, when two planes of geometric symmetry are present, our symmetrized potentials ($\hat{\phi}^{SS}$, $\hat{\phi}^{AS}$, $\hat{\phi}^{AA}$, $\hat{\phi}^{SA}$, see appendix K for definitions) will generally be required and a separate boundary value problem will be formulated for each. If an abutment intersection lies away from any plane of symmetry, doublet matching assignments will be the same for all symmetry conditions and indeed will be the same as if no symmetry were present at all. On the other hand, if the abutment intersection point lies on a plane of symmetry, doublet matching assignments will be performed separately for each symmetry condition and it becomes important to know the following facts about the abutment intersection:

- which plane(s) of symmetry the abutment intersection point lies on,
- which plane(s) of symmetry the individual abutments lie on,
- which (if any) plane of symmetry an individual network may lie in. (N.B. A network is said to lie in a plane of symmetry if all its points lie on the plane of symmetry so that the network normal is parallel to the plane of symmetry normal. See appendix H.1.2 for more detail.)

The first of these facts must be known in order to determine which planes of symmetry are active, in the following sense: the first (second) plane of symmetry is said to be active if P_{AI} lies on the first (second) plane of symmetry and the symmetry condition under consideration is either $\hat{\phi}^{SS}$ or $\hat{\phi}^{SA}$ (for the second plane of symmetry: $\hat{\phi}^{SS}$ or $\hat{\phi}^{AS}$). This information is important for two reasons. First, for an abutment lying on an active plane of symmetry, doublet matching is automatically satisfied by virtue of the symmetry properties of the symmetrized potentials. Consequently, a doublet matching condition is never explicitly imposed for an abutment lying on an active plane of symmetry. Second, the doublet distribution on a network lying in an active plane of symmetry is identically zero so that such networks do not participate at all in the assignment of doublet matching conditions.

Other Significant Considerations

Here we outline the ways in which the properties of networks, corner control points, etc. are modified by PAN AIR program features. In addition we will discuss briefly the mechanisms by which modifications take place.

Properties of Networks

- A network may lie in a plane of symmetry. A network will lie in a plane of symmetry if (i) the user explicitly informs PAN AIR of this fact in the program input, or (ii) by examination of the network's mesh points PAN AIR determines that all points on the network are closer than the geometric tolerance distance to a plane of symmetry.

- The program user will assign to each network one of the following network doublet types:

		Matching Condition Default
Doublet Analysis	(DA)	
Doublet Design 1	(DD1)	Edges 1,4
Doublt Forward Weighted	(DFW)	
Doublet Wake 1	(DW1)	Edge 1
Doublet Wake 2	(DW2)	Corner 1
No Doublet	(NOD)	

  Only those networks not marked "no doublet" are of interest when one is analyzing doublet matching at an abutment intersection. In the discussions that follow, it will be assumed that the matching edges and corners for the various network types are given by the list of defaults given above.

- If a network's doublet type is not "no doublet", the user may specify the doublet value at all control points. Even if this specification is $\mu = 0$, such networks are treated differently from "no doublet" networks in the sense that these networks are always involved in doublet matching along abutments and at abutment intersections. In particular, the abutment intersection processing may replace a specified doublet boundary condition with a doublet matching condition. As a consequence, the doublet strength may be slightly nonzero near the boundary of a network for which the user has specified $\mu = 0$.

Properties of Corner Control Points

- A corner control point may be a "matching corner point" in the sense that no user specified boundary condition is available to generate an AIC row that has been reserved for the control point. Thus, the control point must have a doublet matching condition assigned to it. A "matching corner point" is any corner control point of the following types:

  (i) any corner control point lying on the matching edge of a DW1 network. This includes corners 1 and 2 as well as any extra control points along the matching edge.

  (ii) the matching corner control point of a DW2 network

(iii) any corner control point lying on edges 1 and 4, the "doublet matching" edges, of a DD1 network.

- A corner control point may be a "no matching corner point" in the sense that no AIC row has been reserved for any boundary condition associated with that control point. Control points of this type include:

  (i) corner points 3 and 4 of DW1 networks

  (ii) corner points 2, 3 and 4 of DW2 networks

  (iii) corner point 3 of DD1 networks

  (iv) any extra control point on an edge that is marked with either "no doublet edge matching" (a user specification) or "non-matching edge" (edges 2, 3 and 4 of DW1 networks; all edges of DW2 networks and edges 2 and 3 of DD1 networks

  (v) a regular corner control point (that is, one that has an AIC row reserved for it) for which both adjacent edges are marked "no doublet edge matching."

- A corner control point is said to lie on a plane of symmetry if its hypothetical location lies on a plane of symmetry. It is possible for a control point to lie on two planes of symmetry.

- A corner control point is said to lie <u>in</u> a plane of symmetry if it lies on a plane of symmetry and, in addition, the panel normal at the control point is parallel to the plane of symmetry's normal. (In PAN AIR, the only control points that lie in a plane of symmetry are the control points on networks that themselves lie in a plane of symmetry.)

- A corner control point always has associated with it two <u>abutment ends</u>. (Note: In the code of the program DQG, the initial end of an abutment is denoted by (+1) (Abutment index) while the terminal end of an abutment is denoted by (-1) (Abutment index).) The orientation of the network provides an ordering for these abutment ends, e.g. $\langle A_1, A_2 \rangle$, where A_1 and A_2 are abutment end indices. In figure F.15 we illustrate the anomalous situation in which $A_1 = A_2$. In intersection, such a situation gives rise to a <u>self-loop</u>, which is subsequently ignored during the tree construction process. This is possible because the network's splines impose doublet matching at such an abutment end point.

- The single corner control point at the end of a smooth abutment has associated with it two non-smooth abutments as illustrated in figure F.16.

Properties of User Boundary Conditions

- When a doublet matching condition is assigned to a network lying in an inactive plane of symmetry, the doublet matching condition will replace the user specified antisymmetric boundary condition. An antisymmetric boundary condition has the general form

$$a_A(\vec{w}.\hat{n})_A + c_D\ \mu + \vec{t}_D.\nabla\mu = b \qquad \text{(F.5.14)}$$

(Note: A doublet network lying in a plane of symmetry must be assigned an antisymmetric boundary condition of the form given above.)

Properties of Edges

- A network edge may be marked "no doublet edge matching" by the program user. When this is done, the network's doublet strength along that edge will not participate in any doublet matching conditions for the abutment(s) in which that edge is involved.

- A network edge may be marked "closure edge" by the user. If in addition the user has specified that the closure boundary condition override doublet matching, the network's control points will not be used for doublet matching along the interior of the closure edge. It is generally permissible for control points at the ends of a closure edge to be used for doublet matching.

- Certain network edges are implicitly marked "matching edge" by PAN AIR. These include:

  (i) Edge 1 of a DW1 network

  (ii) Edges 1 and 4 of a DD1 network

- Certain network edges are implicitly marked "non-matching edge" by PAN AIR. These include:

  (i) Edges 2, 3 and 4 of a DW1 network

  (ii) All edges of a DW2 network

  (iii) Edges 2 and 3 of a DD1 network

- Every portion of a network edge is involved in exactly one abutment.

Properties of Abutments

- Abutments involving any interior edge of a network are forbidden.

- The initial end of an abutment may participate in an abutment intersection with the terminal end of an abutment. (Figure F.17

illustrates how this situation can arise for a tube panelled as one network.) Since doublet matching must, in general, be imposed at both ends of an abutment it is necessary to distinguish the initial and final ends of an abutment during abutment intersection analysis. As noted above, the scheme used by PAN AIR labels the initial end with (+1) (abutment index) and the terminal end with (-1) (abutment index).

- An abutment may lie on 0, 1 or 2 planes of symmetry. If any portion of an abutment lies on a plane of symmetry, the whole of the abutment lies on that plane of symmetry. If an abutment lies on an active plane of symmetry, doublet matching along that abutment is automatically satisifed by virtue of the symmetry properties of the symmetrized potentials $\hat{\phi}^{ij}$. Thus, doublet matching conditions are never enforced for an abutment lying on an active plane of symmetry.

- Smooth abutments do not explicitly enter into the analysis of an abutment intersection.

Properties of Abutment Intersections

- An abutment intersection may lie on 0, 1 or 2 planes of symmetry.

<u>Selection of Matching Conditions</u>

We now describe the process by which doublet matching assignments are made while carefully taking into account the considerations outlined above.

The basic procedure for performing doublet matching will remain essentially the same as the tree defoliation procedure outlined at the end of section F.5.1. The complete procedure, however, will be significantly more complex at each stage of processing. A summary of the stages of the complete procedure is given -

B.1 Construct the graph G containing just those branches corresponding to networks whose type is not "no doublet" and do not lie in an active plane of symmetry. During this construction process, some relabelling of nodes may be performed to account for the "no doublet edge matching" feature. In addition, branches associated with control points that cannot accept a matching condition (e.g. corners 3 and 4 of a DW1 network) are excluded from G.

B.2 Form a spanning tree for G, $T \subset G$. If G has k components ($G = \bigcup_{i=1}^{k} G_i$), T will have k components, $T = \bigcup_{i=1}^{k} T_i$ (*). In contrast with the earlier algorithm, T is not an arbitrary spanning tree of G, but rather is constructed with careful regard for the properties of the neworks/branches of G.

B.3 Without first selecting a ground node, each component tree T_i is defoliated, the removal of each branch providing an association of a node with a branch. At the end of this process, there will be left one node that is not associated with any branch, and this node becomes the ground node for the tree.

B.4 Finally, the assignments are examined to determine if the requisite doublet matching conditions have in fact been associated with eligible branches. In addition, it is verified that all of those branches that <u>must</u> receive a doublet matching condition have in fact done so.

Several remarks about this algorithm are appropriate before proceeding with its detailed exposition. First, steps B.1 and B.4 are essentially deterministic given the specification of the problem. Steps B.2 and B.3, on the other hand are substantially heuristic, step B.2 being ambiguous with regard to the choice of spanning tree and step B.3 being ambiguous with regard to the defoliation strategy. Although the detailed exposition of the algorithm will resolve most of these ambiguities, the solutions presented should not be regarded as unique. They are, nevertheless, very good.

<u>B.1</u> The detailed description of an abutment intersection includes the following information

- o Symmetry condition, $\hat{\phi}^{SS}$, $\hat{\phi}^{AS}$, $\hat{\phi}^{AA}$ or $\hat{\phi}^{SA}$. [ISYM]**

- o A description of the plane(s) of symmetry that the abutment intersection point lies on. [LABT]

* Note, however, that if some component G_i of G contains only one node, all of its branches being self loops, then $T_i = \phi$. In practice, self loops cause no special difficulty for the doublet matching problem simply because the doublet strength on a network that generates a self loop "matches itself."

** The expressions given in brackets are corresponding FORTRAN variable names for elements of the calling sequence to subroutine ABTINT (PALIB).

For each network/control point/branch N involved in the abutment intersection, the following information is given.

- The abutment ends in which N participates at P_{AI} are given in positive sequence $\langle A_1, A_2 \rangle$. The two edge segments of N that are involved in the abutments A_1, A_2 are denoted E_1, E_2 respectively. Because of the requirement that A_1 and A_2 be given in positive sequence, an oriented traversal of the boundary of N would encounter edge segment E_1 followed immediately by edge segment E_2. [IPQSEG]

- "No doublet edge matching" information is given for each edge segment E_i. [NDMSEG]

- Let $\vec{t}_i$ denote unit vectors drawn along edge segments E_i, pointing away from P_{AI}. Let $\vec{s} = (\vec{t}_1 + \vec{t}_2)/|\vec{t}_1 + \vec{t}_2|$ and $\hat{c}_o$ be the "compressibility axis downstream parameter" α is defined by

  $$\alpha = \vec{s} \cdot \hat{c}_o \qquad \text{(F.5.15)}$$

  This parameter is given for each branch. [CSEG]

- Each branch is classified as follows [KSEG]:

  0, no doublet network.

  2, doublet network, but no corner control point is available to enforce doublet matching.

  3, doublet network with regular corner control point, but at least one of the edges E_i is marked "no doublet edge matching."

  4, doublet network with regular corner control point.

  5, doublet network with "matching" corner control point

- The plane of symmetry <u>in</u> which N lies, if any, is given. [LSEG]

For each abutment-end/node involved in the abutment intersection, the following information is given

- The global abutment-end index [IPNOD]

- a flag indicating which planes of symmetry the abutment end lies on [LNOD]

Given the information outlined above, the graph G is constructed in three stages. First, a graph $G^{(1)}$ is constructed using all those branches in

classes 2, 3, 4 and 5. Second, a graph $G^{(2)}$ is constructed from $G^{(1)}$ by examining each branch of $G^{(1)}$ for "no doublet edge matching" marks on either end of the branch. If such a mark is found, the corresponding branch-end is detached from the node to which it is attached and a new node is created. Third, a graph $G^{(3)}$ is constructed from $G^{(2)}$ by deleting all branches in class 2 and all branches (i.e., control points) lying <u>in</u> an active plane of symmetry. The resulting graph $G^{(3)}$ is the graph G that we seek.

Once the graph $G = G^{(3)}$ has been constructed, all of the nodes in the problem (that is all of the nodes of $G^{(2)}$), are divided into three types:

Node type	Characterization
"preferred ground node" [MNOD = -1]	- an extra node created during the construction of $G^{(2)}$
not a "preferred ground node" [MNOD = 0]	- an ordinary abutment for which matching must be performed
"automatic node" [MNOD = +1]	- a node appearing in $G^{(2)}$ but not in $G^{(3)}$. These nodes of $G^{(2)}$ are characterized by the fact that the only branches attached to them are in class 2. Doublet matching is assumed to occur "automatically" at such nodes.

The node type determines whether or not the corresponding matching condition must be imposed. Basically, matching is imposed only for nodes that are <u>not</u> "preferred ground nodes" (i.e., MNOD = 0).

The last node type, the "automatic node" can arise quite naturally when a configuration includes compound wakes. To see this, consider figure F.10 with all networks taken to be DW1 networks for which edge 1 is the matching edge. When this happens, the node corresponding to abutment A1 will be an "automatic node" since both C_1 = (network N1, corner 3) and C_2 = (network N2, corner 4) are "no matching corner points." In this particular instance, it is easy to see that matching along abutment A1 is already taken care of by a doublet matching condition imposed at some point upstream of the abutment intersection. In practice PAN AIR assumes that this is generally the case and that doublet matching conditions at "automatic nodes" need not be explicitly imposed.

Having classified the nodes of the problem, the number of required matching conditions is computed:

Number of required matching conditions = N_{REQ}

$$= \max\,(N_{-1}+N_0+N_1-1,\ N_0+N_1)$$

where

N_{-1} = number of "preferred ground nodes"

N_0 = number of "not preferred ground nodes"

N_1 = number of "automatic nodes."

This number is used at the end of processing to determine whether or not the assignment procedure was successful. The test is passed if

$$N_1 + N_{ACT} \geq N_{REQ}$$

where N_{ACT} denotes the actual number of matching conditions assigned.

B.2 Without loss of generality, we may suppose that the graph generated in step B.1 is connected. If in fact G is not connected, we simply perform steps B.2, B.3 and B.4 separately on each of G's components.

Any given connected graph will, in general, possess many spanning trees and the problem of determining all of the spanning trees of a particular graph is very difficult (cf. ref. F.2, p. 280). The problem of determining a particular spanning tree is fairly simple, however, and the standard algorithm is given in (ref. F.2, pp 277-279). Basically this algorithm proceeds by considering in some order, each branch of the graph as a candidate for membership in the spanning tree. If a branch causes a closed loop, it is rejected, and if it does not cause a closed loop it is accepted.

It is clear that the spanning tree resulting from this procedure depends crucially upon the order in which branches are examined. In PAN AIR, branches are considered in order of decreasing priority in accordance with the following priority scheme:

$$p = \begin{cases} 3 + \alpha/2 & \text{class 3 branches} \\ 4 + \alpha/2 & \text{class 4 branches} \\ 5 & \text{class 5 branches} \end{cases} \qquad \text{(F.5.16)}$$

Thus, branches with the highest values of p are considered first for potential memebership in the spanning tree. Here, α is the "compressibility axis downstream parameter" defined above by equation (F.5.15).

B.3 In this step of the algorithm, we must select a defoliation scheme for the spanning tree T. If T has n nodes, then there are precisely n distinct defoliation schemes that assign nodes to branches, one corresponding to each choice of ground node in subalgorithm A.3 of section F.5.1. Thus, one possibility that suggests itself is to examine each of the n possible defoliation schemes and determine which one provides the most suitable set of

assignments. It turns out that such a complex procedure is not necessary and that a fairly straightforward modification of subalgorithm A.3 generates a suitable choice of ground node without an exhaustive search(*).

The modified defoliation algorithm proceeds as follows. As before, we set $T_n = T$ and define a sequence of trees $T_n \supset T_{n-1} \supset \ldots \supset T_1$ such that T_j is obtained from T_{j+1} by identifying in T_{j+1} a node of degree 1 and removing that node and the single branch to which it is attached. If there is more than one node of degree 1 available, the choice is made by means of the following prioritization scheme based upon node type ("preferred ground node" or not) and branch class (3,4 or 5):

Node Type	Branch Class: 3 or 4 [KB = 0]	Branch Class: 5 [KB = +1]
"preferred ground node" [MNOD = -1]	2	1
not a "preferred ground node" [MNOD = 0]	3	4

Priority classes for removing a node/branch combination

Given this prioritization scheme, the node/branch combination in the highest priority class is selected for defoliation. In the event that there is more than one node/branch combination in the highest priority class, the one with the lowest value of p (see eqn. (F.5.16) above) is selected if the node is a "preferred ground node" while the highest value of p (cf. equation F.5.16) is selected if the node is not a "preferred ground node."

B.4 The algorithm described above will have achieved a successful set of doublet matching assignments provided the following conditions are satisfied

(i) all "matching corner point" branches (branch class 5) are included in the spanning tree T.

(ii) a "preferred ground node" is never assigned to a class 5 branch (i.e., priority class 1 is never selected.)

(iii) the ground node actually selected for a tree T is a "preferred ground node," if any appear in T.

(*)
Note that a completely exhaustive examination of all possible matching assignments possible for a connected graph G would involve (n . s) separate cases, where n is the number of nodes in G and s is the number of spanning trees.

F.6 Gap-Filling Panels

Whenever a gap whose size is greater than the user-specified tolerance distance occurs between portions of two or more network edges which form an abutment, gap-filling panels are defined. The placement of gap-filling panels is illustrated for an abutment containing two network edges in figure F.9.

We now briefly outline the process by which gap-filling panels are constructed, first considering the case of two network edges. First, each edge in the abutment is "parametrized." That is, each panel corner point on the edge is assigned a real number t between 0 and 1 inclusive, where t is the ratio of two distances. The first distance is the sum of the lengths of the panel edges between the starting point of the abutment and the panel corner point in question, while the second distance is the sum of the lengths of all the panel edges on a network edge. Thus t represents the proportion of the entire edge length which one has traveled in proceding from the start of the abutment to the panel corner point in question. In figure F.9, each panel corner point is given a value t.

Now, suppose the distinct values of t which occur for the two network edges are $t_0, t_1, \ldots, t_n$, where

$$0 = t_0 < t_1 < \ldots < t_n = 1 \qquad \text{(F.6.1)}$$

In the example of figure F.9, n = 9, since there are 11 panel corner points other than the initial points, and the values t = .80 and t = 1.0 occur twice.

Now, up to n gap-filling panels may be constructed to fill the gap in the abutment. For each integer i, $1 < i < n$, the quadrilateral region with corner points lying on the two network edges, with respective parameter values $t = t_{i-1}$ and $t = t_i$ is examined. If t_i is not the parameter value of a corner point (for instance, .30 is not the parameter value of any cornerpoint on network A in figure F.9), linear interpolation between corner points is used to find the point on the panel edge with that parameter value. If three or more of the four edges of this quadrilateral region have length greater than the user-specified tolerance distance ε, a gap-filling panel is defined.

Thus, for the abutment in figure F.6, no gap-filling panels would be defined, since the gap size is uniformly smaller than ε, and so all potential gap-filling panels have two edges of length less than ε. On the other hand, if, in figure F.9, ε were approximately .05 times the abutment length, seven gap-filling panels would be defined, while two potential ones would be discarded because two edges of the panels would be too short. The reason that very small gap-filling panels are never defined is that numerical difficulties could occur in measuring the influence of these panels on control points. It is not known at this time under which circumstances the resulting doublet discontinuity might be significant.

Next, we address the question of how to define the doublet strength on the gap-filling panels so that doublet continuity is attained. The edge splines constructed in appendix I assure that, if one edge is a refinement of the other, then the doublet strength matches at points on the two network edges with the same parameter value t. Thus we want the doublet strength to be constant on the panel along the direction perpendicular to the direction of the abutment.

We illustrate this in figure F.18. The four corner points of the panel are P_i and P_{i+1} on edge A and P_i' and P_{i+1}' on edge B. We then define M_i as the midpoint of the segment $P_i\ P_{i+1}$, and M_i' similarly. Then, since P_i, P_{i+1}, and M_i each has the same parameter value as its primed counterpart, it also has the same doublet strength, namely μ, μ_{i+1}, or μ_i^+ respectively. Thus, we have defined μ at six of the nine panel defining points, and we define μ at the remaining three panel defining points in the natural way.

This defines μ uniquely on the whole panel (see section 5.5). Further, it insures continuity of μ on the whole edge $P_i\ P_{i+1}$ and the whole edge $P'\ P_{i+1}'$, since these two gap-filling panel edges are subsets of ordinary panel edges. Thus the doublet strength on the network edges is defined by a single quadratic function in one variable, and therefore agrees with the doublet strength on the gap-filling panel edge everywhere, since it agrees at three points.

Finally we must consider the case of three or more network edges meeting in an abutment, as illustrated in cross-section in figure F.19. There, network E_0 is the most densely paneled network edge, and so, if the user has followed the paneling rules, it is a refinement of edges E_1 and E_2. We construct gap-filling panels as illustrated in order to fill the gap in the abutment.

It still remains to be decided how to define the doublet strength on the gap filling panels. We want the doublet strength to be continuous across edges E_1 and E_2, while at E_0 we want

$$\mu_0 - \mu(1) - \mu(2) = 0 \tag{F.6.2}$$

where $\mu(i)$ is the doublet strength on the gap-filling panel spanning the gap from E_0 to E_i. On the other hand, the doublet edge splines and matching boundary conditions insure

$$\mu_0 - \mu_1 - \mu_2 = 0 \tag{F.6.3}$$

where μ_i is the doublet strength on edge E_i. Thus the specification

$$\begin{aligned} \mu(1) &= \mu_1 \\ \mu(2) &= \mu_2 \end{aligned} \tag{F.6.4}$$

insures doublet continuity (in the form (F.1.1)) everywhere.

Thus the general procedure used by Pan Air for gap-filling panels in abutments with three or more network edges is:

a. choose the most densely paneled edge (which should be a refinement of all the other network edges),

b. define gap-filling panels in the gap between the finest edge E_0 and each other edge E_i, just as if this were an abutment with only two edges, and

c. define the doublet strength on the gap-filling panels to be equal to the doublet strength on the edge E_i.

Note that this procedure works even if there are only two edges in the abutment. Further, it insures that the equation

$$\sum s_i \mu_i = 0 \qquad \text{(F.6.5)}$$

is imposed along all network edges.

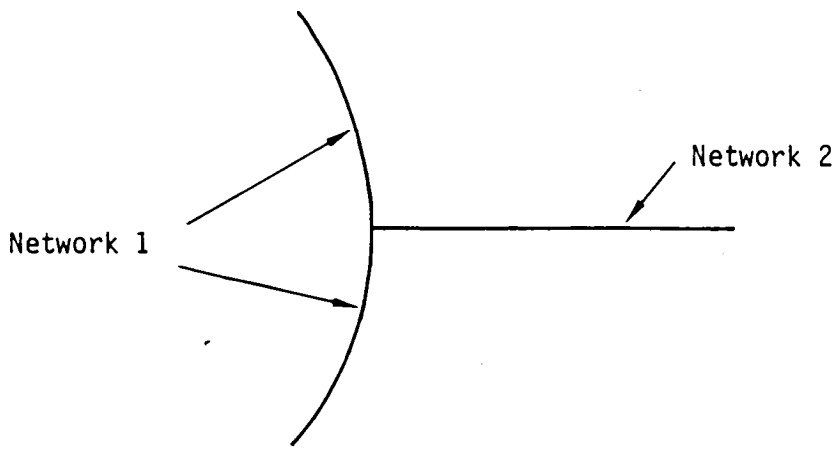

Figure F.1 - Impermissible network intersection
(in cross-section)

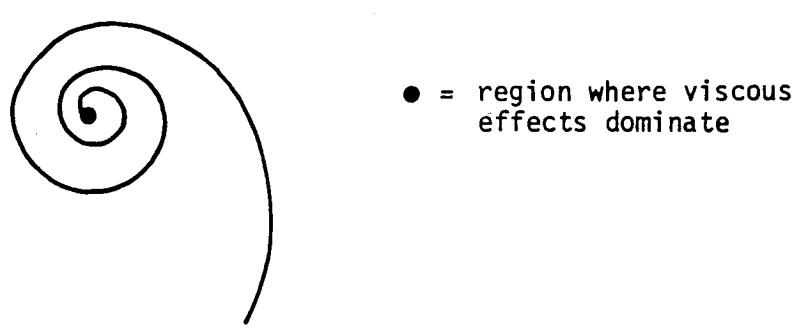

Figure F.2 - Leading edge vortex (in cross-section)

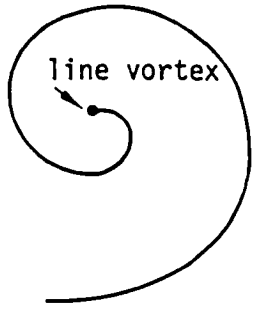

Figure F.3 - Simulation of a vortex core by a line vortex

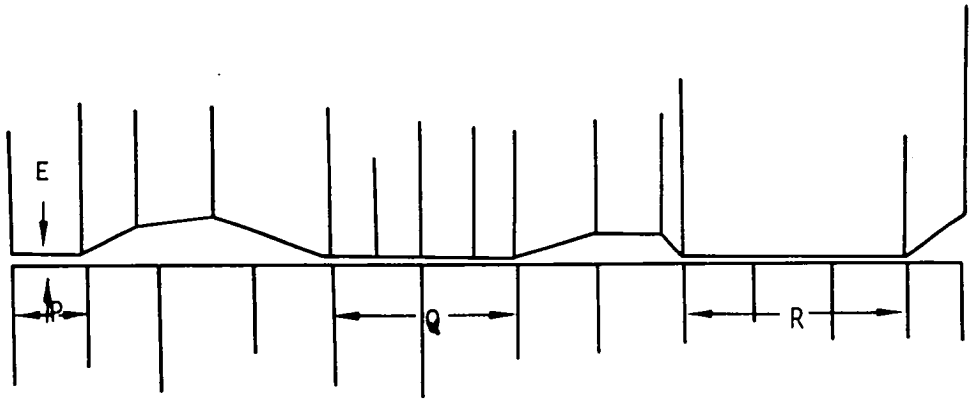

Figure F.4 - Multiple pairwise abutments involving the same edges

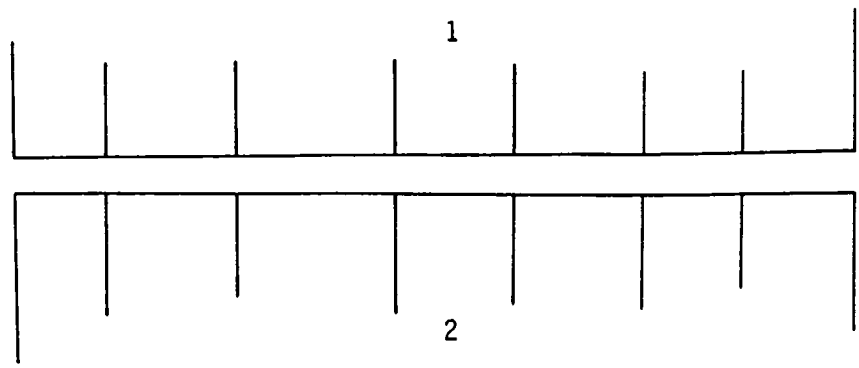

Figure F.5 - Each network edge is a refinement of the other

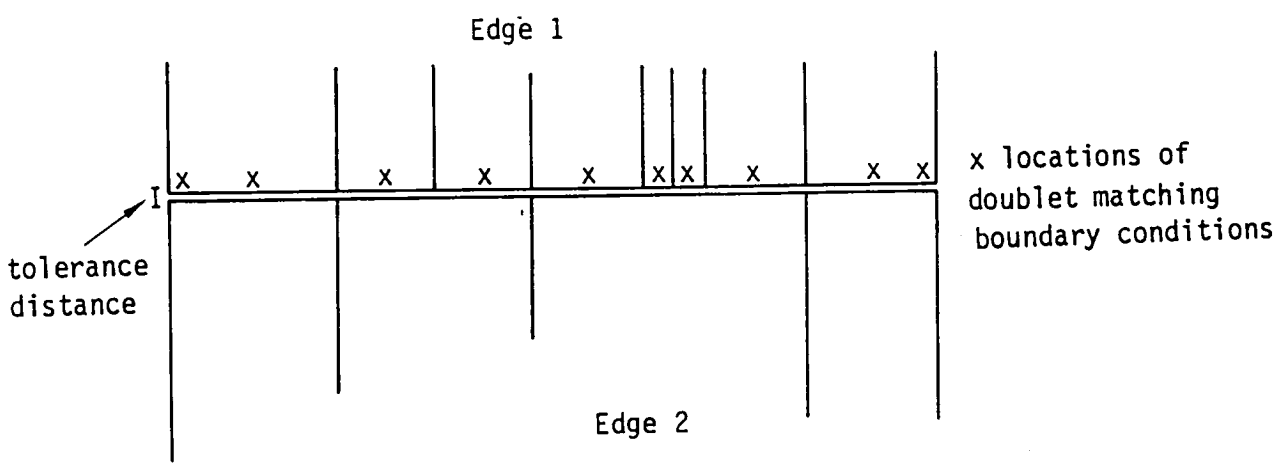

Figure F.6 - Edge 1 is a refinement of edge 2

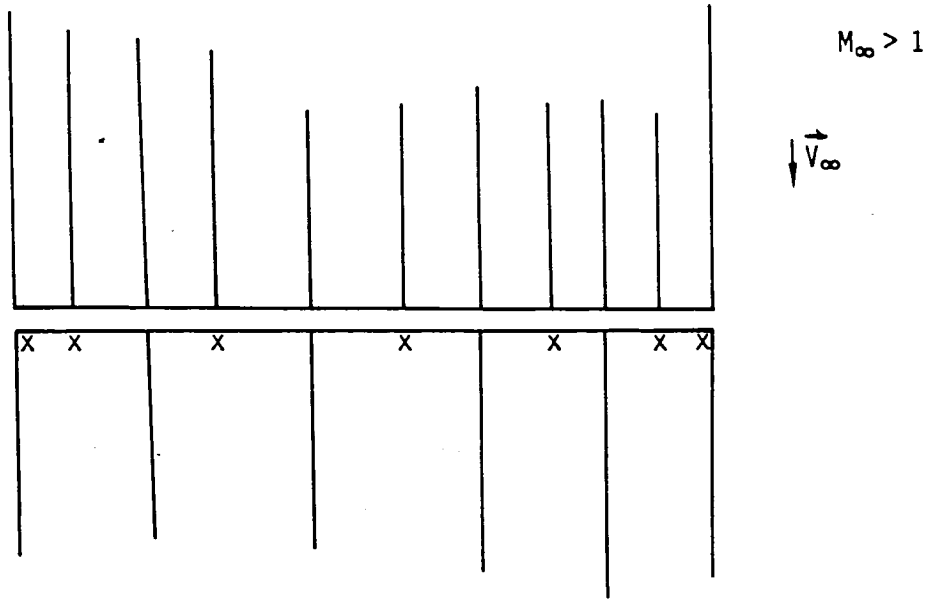

x control points used for doublet matching

Figure F.7 - Control points on a supersonic leading edge are used for doublet matching

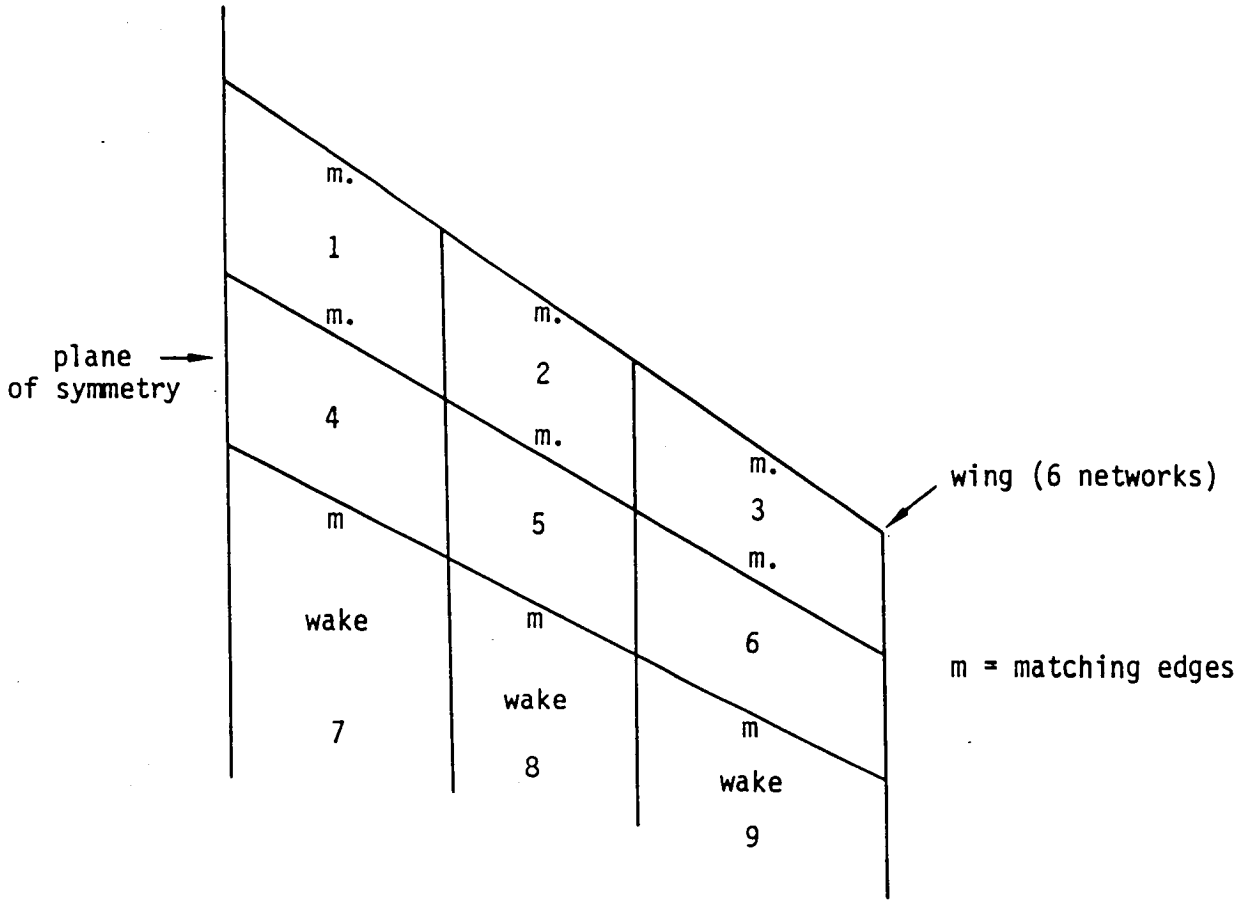

Figure F.8a - Six network wing with wakes

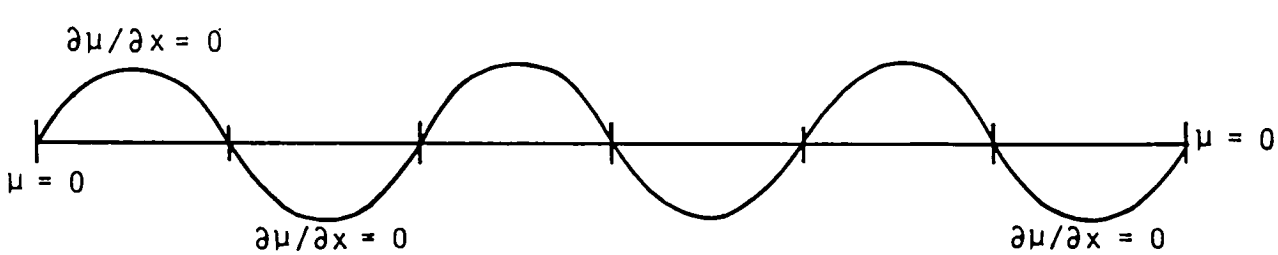

Figure F.8b - Doublet distribution arising from specification of μ at trailing edge

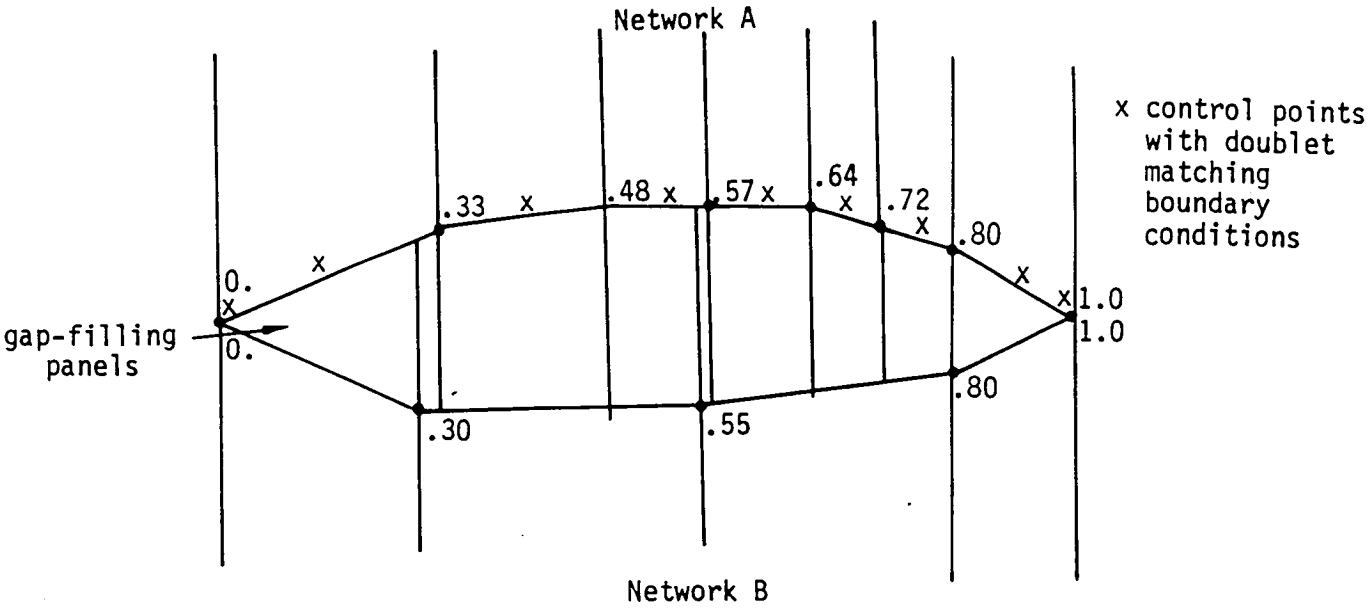

Figure F.9 - One edge is not precisely a refinement of the other

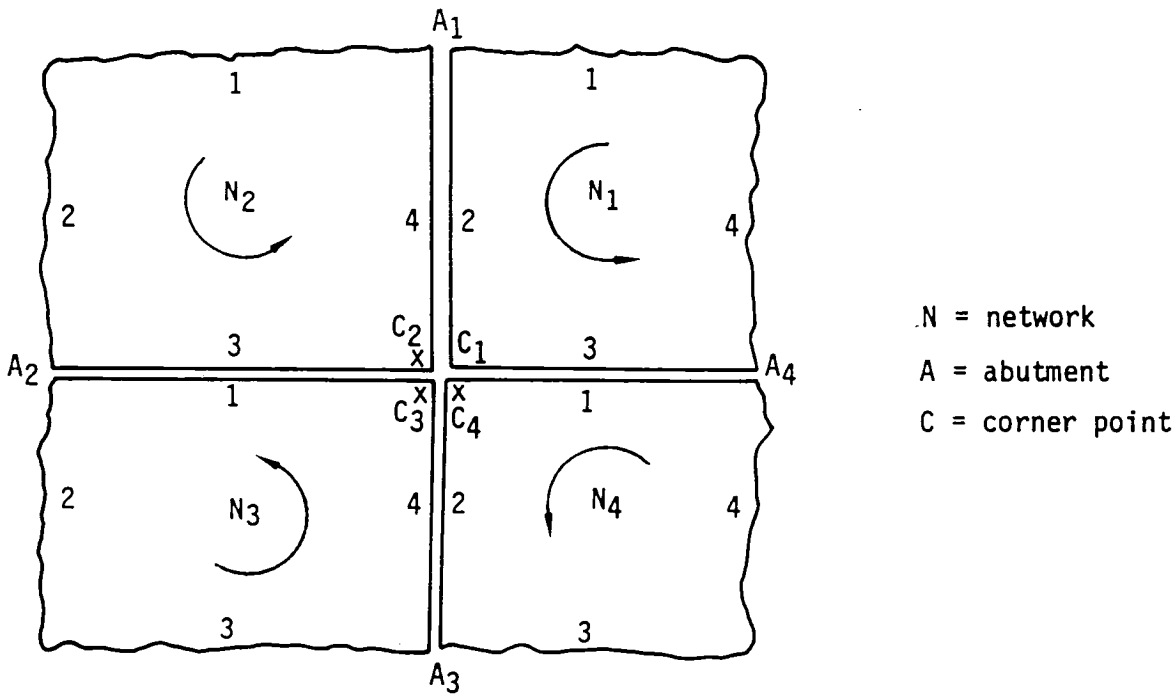

Figure F.10 - An abutment intersection with 4 abutments

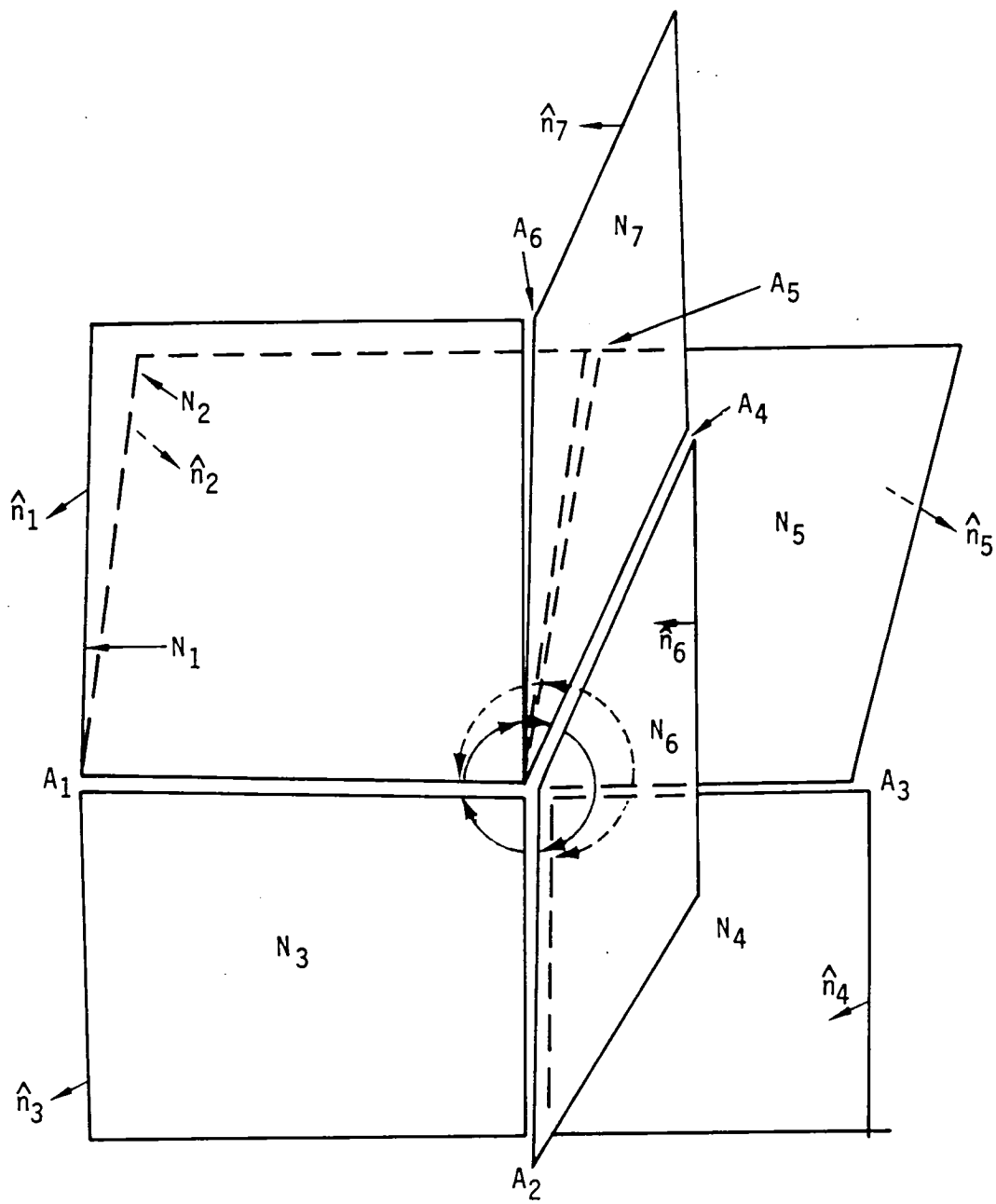

Figure F.11 - An abutment intersection with 6 abutments

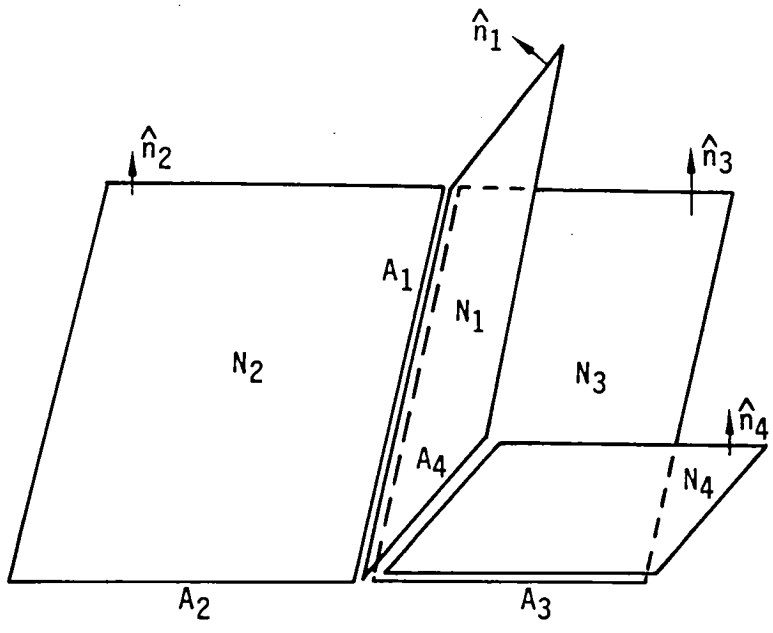

Figure F.12 - Another abutment intersection with 4 abutments

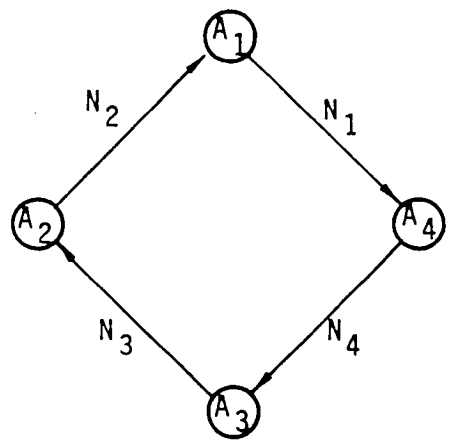

Figure F.13a

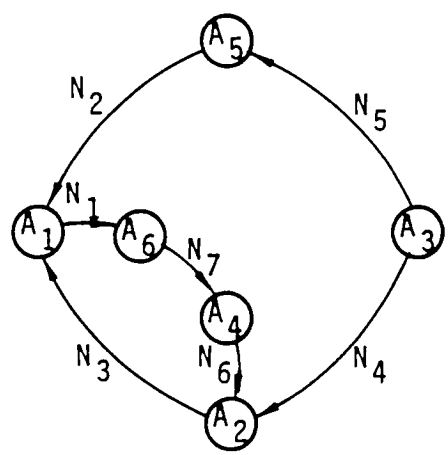

Figure F.13b

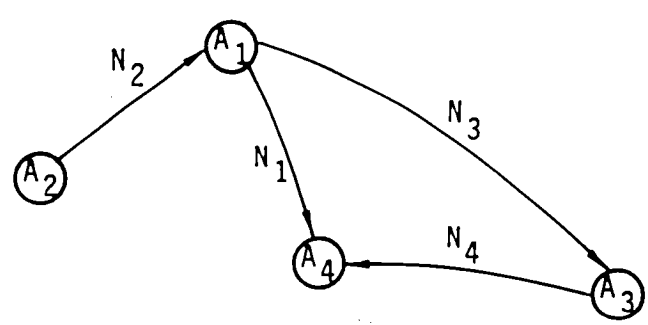

Figure F.13c

Figure F.13- Directed graphs corresponding to three abutment intersections

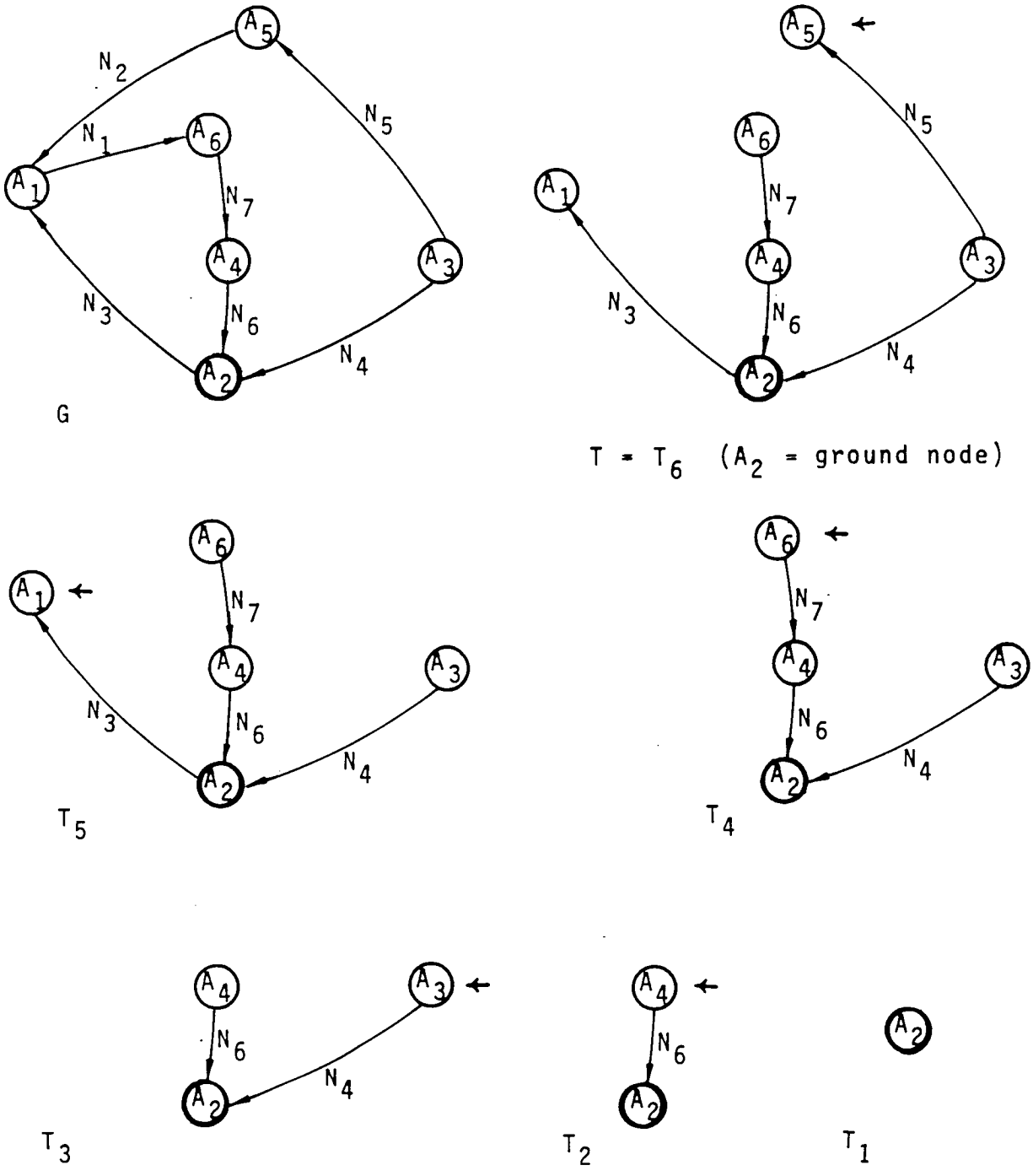

Matching Assignments: $A_5 - N_5$, $A_1 - N_3$, $A_6 - N_7$, $A_3 - N_4$, $A_4 - N_6$

Figure F.14 Defoliation and matching condition assignment for the graph of Figure F.13b

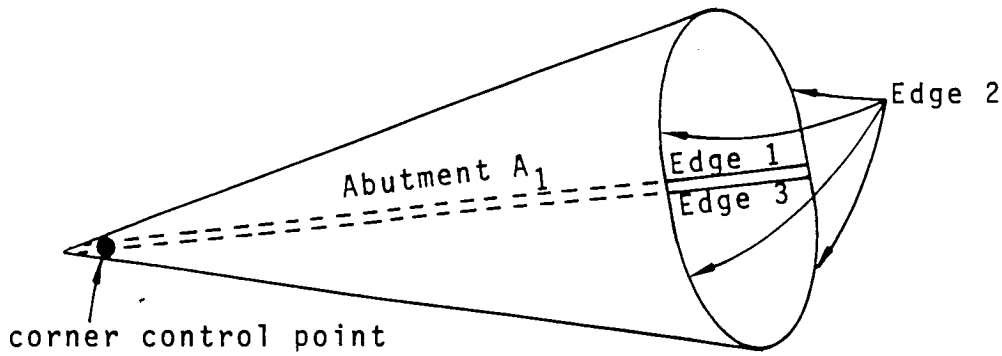

Figure F.15 A corner control point for which $A_1 = A_2$, giving rise to a self loop.

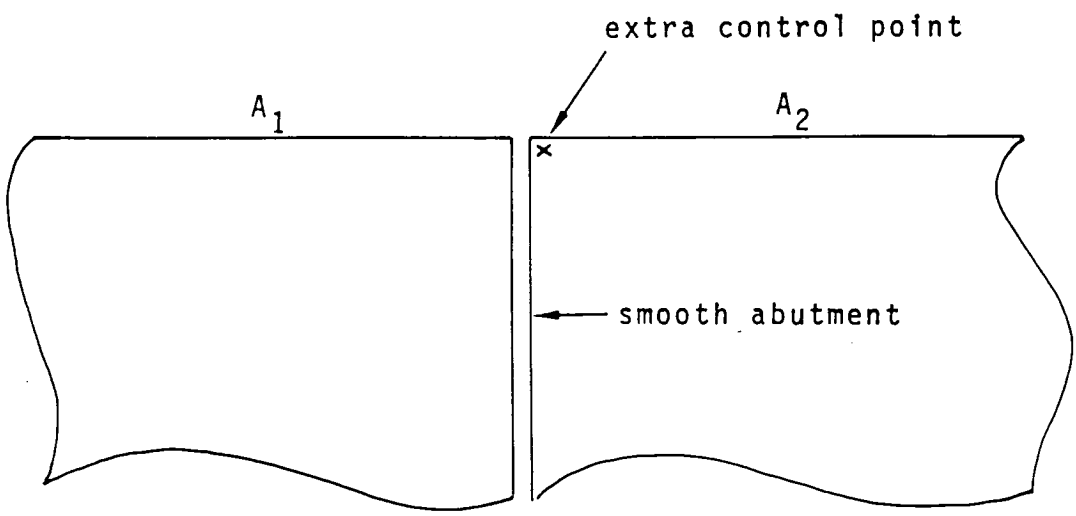

Figure F.16 An extra control point at the end of a smooth abutment.

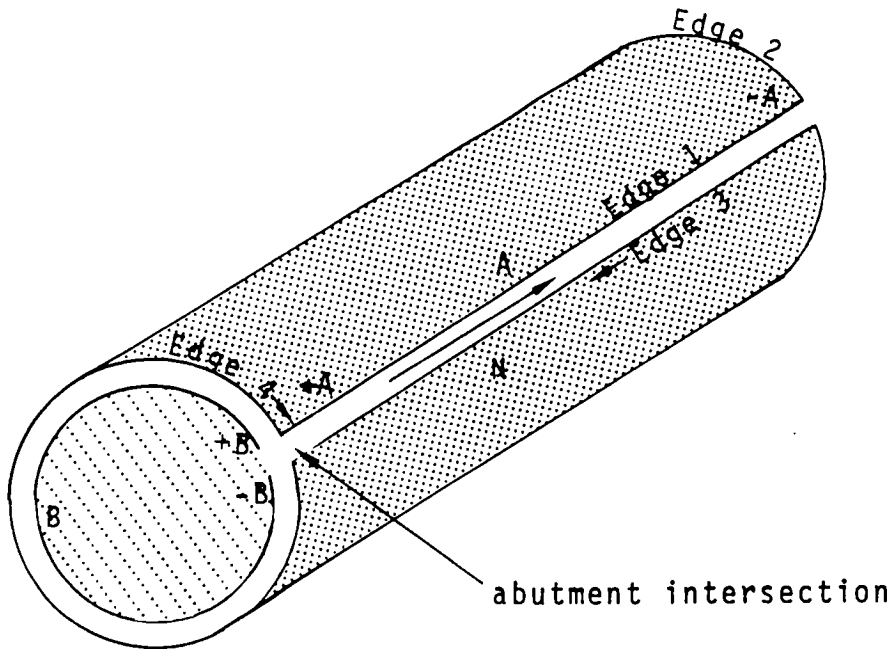

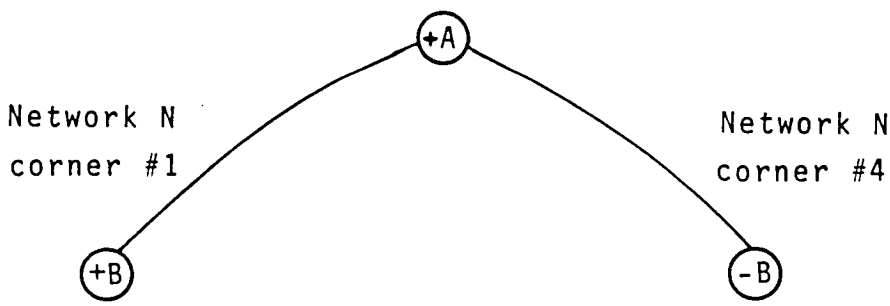

Figure F.17 An abutment intersection in which both the initial and terminal ends of an abutment participate in an abutment intersection

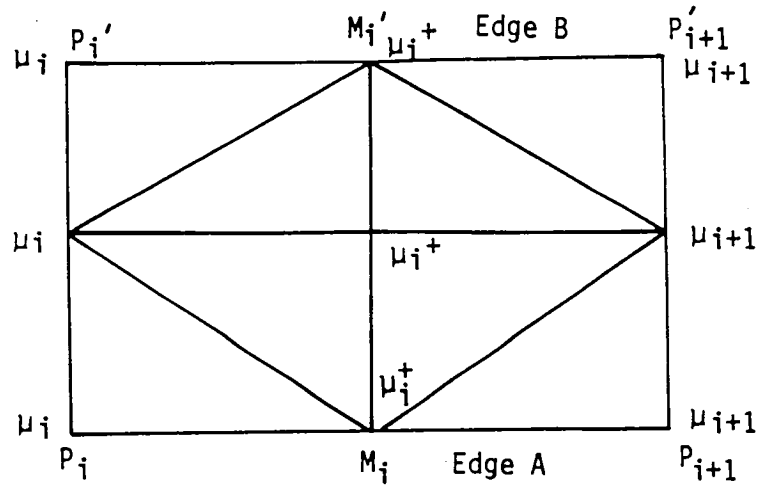

Figure F.18 - Gap-filling panel

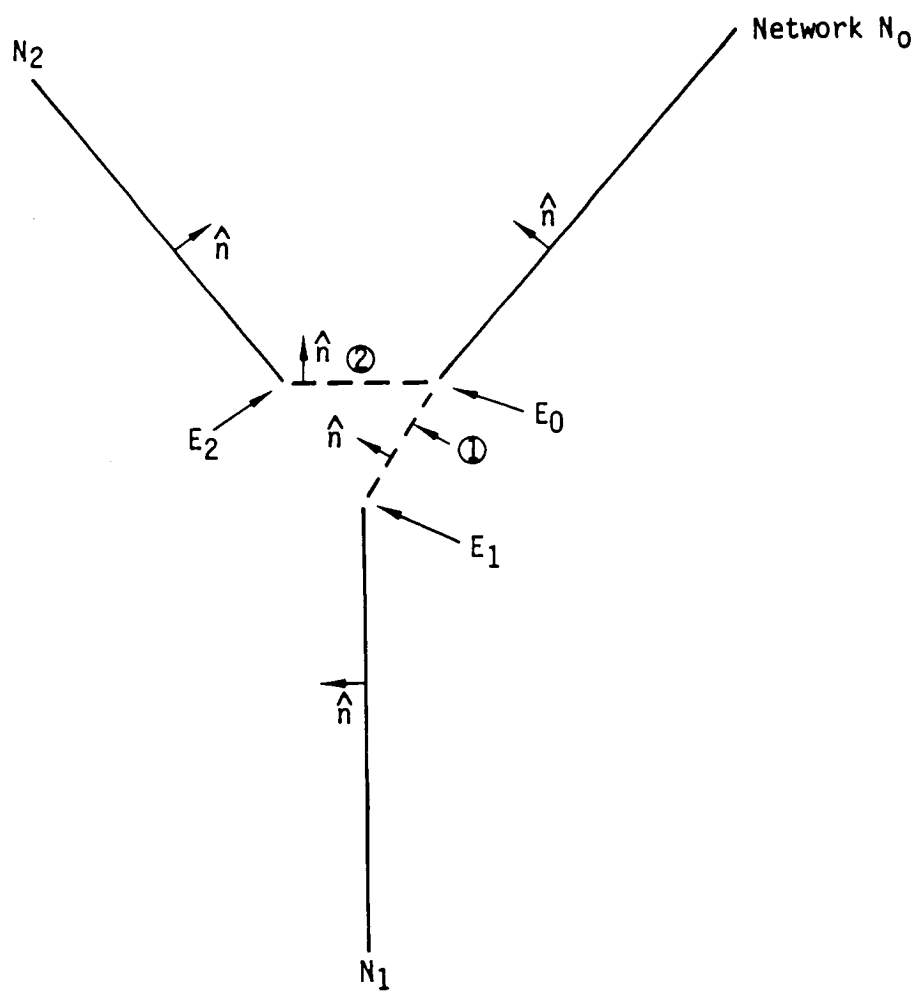

Figure F.19 - Gap-filling panels on an abutment with 3 network edges

G.0 Control Point Locations

In figure G.1 we illustrate the possible location of points on a network, called control points, at which boundary conditions are defined. These locations are independent of the source type or doublet type of the network; however, we will see in Appendix H that meaningful boundary conditions are not necessarily imposed at all control points (for instance, on wake networks, boundary conditions are only imposed along one edge).

Note that controls points are illustrated as being located near, but not directly on, midpoints of panel edges lying on network edges. This is due to the disastrous results which would occur from attempting to measure the velocity or potential at a control point that lies directly on a panel edge (see section J.11). Later in this section we describe the procedure used to recede control points from the panel edge.

When a network edge is divided into distinct portions belonging to separate abutments, as illustrated in figure G.2, an extra control point, in addition to those in figure G.1, is defined. The same data are computed for these control points as for ordinary control points.

In order to determine its location, a control point is placed in one of three categories: panel center control points, edge midpoint control points, and panel corner control points. The latter two categories are only defined along the network perimeter. The control point is defined by prescribing a "hypothetical location" (the center point, edge midpoint, or corner point at which the control point would ideally be located), and a "recession vector" which describes the extent to which the control point is receded into a subpanel from its hypothetical location.

The size of the "recession vector" has been determined experimentally. Basically, it has been chosen as small as possible without causing severe numerical error. We refer to figure G.3 in defining the recession vectors. There, we show an edge control point as P_5 and a corner point at P_1 ; for control points at other points or edge midpoints the procedure is identical.

Panel center control points are only receded very slightly from the center point P_9 since the doublet distribution is differentiable and the source distribution is continuous at P_9 ; as a result (see section J.11) the potential and velocity induced by the singularity distributions are very well behaved at P_9. It is still necessary to recede the control point slightly, however, because influence coefficients can not be computed for a point lying directly on a sub-panel edge, because the calculations yield singular results there. So, we choose the recession vector to be

$$\vec{R} = \frac{(\vec{P}_8 - \vec{P}_9) + (\vec{P}_7 - \vec{P}_9)}{200} \qquad (G.0.1)$$

Edge control points are receded considerably further because of the discontinuities in doublet derivative, surface slope, and source strength which occur at network edges. Thus, for the control point located at P_5, we define its recession vector to be

$$\vec{R} = \delta \left\{ \frac{|\vec{P}_8 - \vec{P}_5|}{|\vec{P}_8 - \vec{P}_5| + |\vec{P}_9 - \vec{P}_5|} (\vec{P}_9 - \vec{P}_5) + \frac{|\vec{P}_9 - \vec{P}_5|}{|\vec{P}_8 - \vec{P}_5| + |\vec{P}_9 - \vec{P}_5|} (\vec{P}_8 - \vec{P}_5) \right\} \tag{G.0.2}$$

where

$$\delta = \begin{cases} \dfrac{\min \{|\vec{P}_8 - \vec{P}_5| , |\vec{P}_9 - \vec{P}_5| , |\vec{P}_1 - \vec{P}_5|\}}{10 \; |P_9 - P_5|} & \text{if} \quad |\vec{P}_1 - \vec{P}_5| > 0 \\ 1/10 & \text{otherwise} \end{cases} \tag{G.0.3}$$

The recession vector $\vec{R}$ bisects the angle between the vectors $(\vec{P}_8 - \vec{P}_5)$ and $(\vec{P}_9 - \vec{P}_5)$. If δ were unity, the head of the recession vector $\vec{R}$ emanating from point $\vec{P}_5$ would lie on the line segment joining points $\vec{P}_8$ and $\vec{P}_9$. If edge 1 is collapsed as in figure G.4, then δ is taken to be a tenth. The recession vector $\vec{R}$ would also be used for any control points located at $\vec{P}_1$ and $\vec{P}_2$ in this case. If edge 1 is not collapsed, then δ will be at most a tenth and possibly less, if the panel is skewed. The recession vectors for other edge midpoint control points are defined analogously, control points whose hypothetical locations are $\vec{P}_6$, $\vec{P}_7$, $\vec{P}_8$ being withdrawn, respectively, into triangles 6, 7, and 8.

For the corner control point located at P_1 which does not lie on a collapsed edge the recession vector is

$$R = \frac{1}{10} \left\{ \frac{|\vec{P}_5 - \vec{P}_1|}{|\vec{P}_8 - \vec{P}_1| + |\vec{P}_5 - \vec{P}_1|} (\vec{P}_8 - \vec{P}_1) + \frac{|\vec{P}_8 - \vec{P}_1|}{|\vec{P}_8 - \vec{P}_1| + |\vec{P}_5 - \vec{P}_1|} (\vec{P}_5 - \vec{P}_1) \right\} \tag{G.0.4}$$

This particular construction provides the recession vector $\vec{R}$ with properties similar to the edge control point recession vector in (G.0.2). Note that the recession vector in (G.0.4) lies in subpanel 1. The recession vectors for other corner control points are handled in a similar fashion.

Some geometric quantities in addition to location and hypothetical location are computed by the program for each control point. One of these is the subpanel on which the control point actually lies. This is needed later (see section J.8) to insure that an average potential and velocity are computed correctly in measuring the influence that the sub-panel on which the control point lies exerts on the control point.

Also, for each edge or corner control point at which a matching boundary condition is imposed, a set of "extra hypothetical locations" and their associated sign is computed. These arise from the matching boundary condition (see section F.1)

$$\sum s_i \mu_i = 0 \qquad (G.0.5)$$

where the μ_i are the values of doublet strength on different networks.

In figure G.5, we illustrate an abutment containing three network edges. Although the control point is receded from the edge, the matching boundary condition involves singularity strengths at the edge; in this example (G.0.5) becomes

$$\sum_{i=0}^{2} s_i \mu(H_i) = 0 \qquad (G.0.6)$$

where H_0 is the (default) hypothetical location of the control point, while H_1 and H_2 are extra hypothetical locations.

In Appendix F we indicate how the signs s_i are computed; here we describe the computation of the extra hypothetical locations. Hypothetical locations are computed one abutment at a time by parametrizing the abutment (see section F.4), a process that assigns to each panel corner point or edge midpoint P on that portion of a network edge belonging to an abutment a real number t(P) between 0 and 1.

In figure G.6, we illustrate an abutment with two network edges. Given the control point and default hypothetical location H_0 , we compute the extra hypothetical location H_1 as follows. Parametrization of the abutment gives us $t(H_0)$, and also assigns a value t to every panel corner point and edge midpoint on the edge of network 1.

By interpolation between these points, we find H_1 as the point satisfying

$$t(H_1) = t(H_0) \qquad (G.0.7)$$

In addition to the coordinates of the extra hypothetical locations, the program determines the panel and subpanel on which each extra hypothetical location lies, so that the doublet strength can be computed there later.

Our discussion of matching boundary conditions has assumed we are dealing with doublet matching. In the case of a source matching boundary condition (which may occur on the edge of a source design network)

$$\sum s_i \sigma_i = 0 \qquad (G.0.8)$$

and extra hypothetical locations and signs are computed as before.

There are two final pieces of geometric data, associated with control points, which we have not yet discussed. These are the normal and conormal of the subpanel on which the control point lies. The normal is needed in post-processing to compute velocity from the potential and the normal mass flux (see Appendix N), while the conormal $\tilde{n}$ is needed to compute the normal mass flux from the velocity influence coefficient matrix by the formula

$$\vec{v} \cdot \tilde{n} = \vec{w} \cdot \hat{n} \tag{G.0.9}$$

The computation of the normal is described in section D.2, while

$$n = [B_0]\, n \tag{G.0.10}$$

where

$$[B_0] = I + (s\beta^2 - 1)\, \hat{c}_0\, \hat{c}_0^T \tag{G.0.11}$$

by equation (E.3.9).

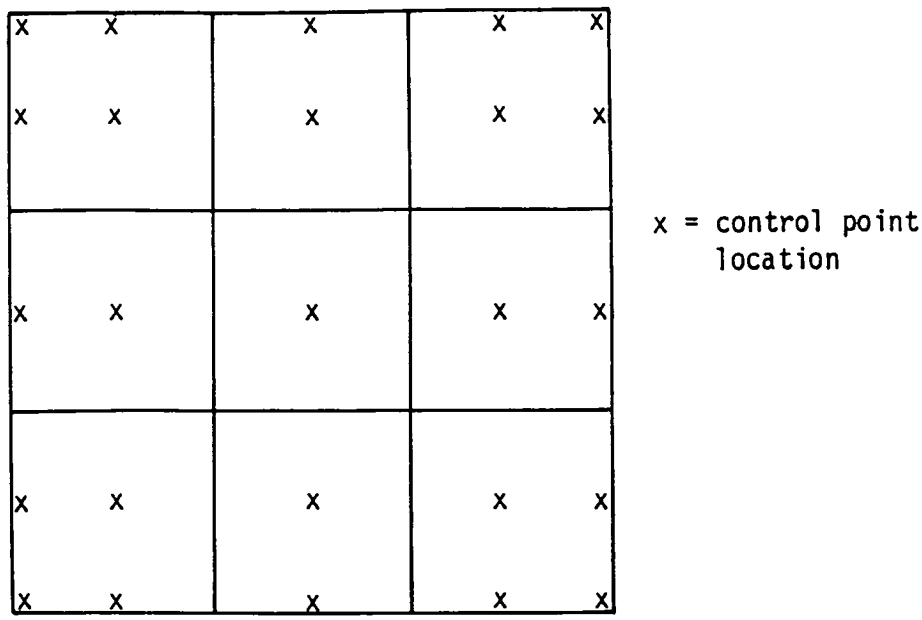

Figure G.1 - Control point locations

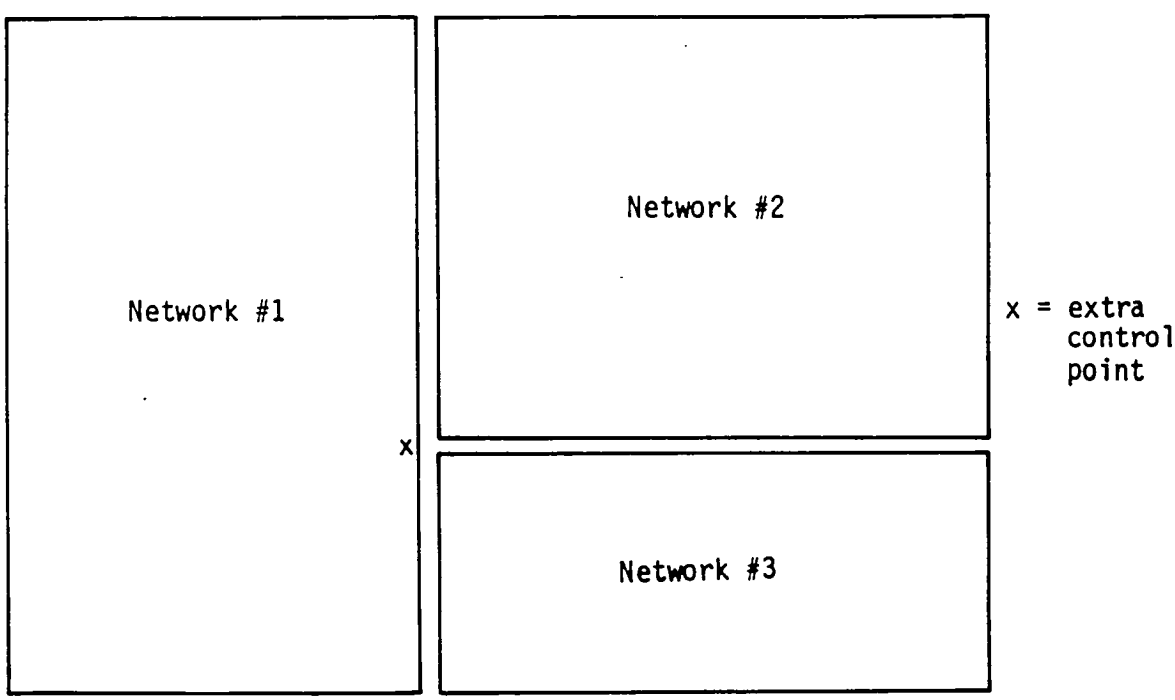

Figure G.2 - Division of network edge into two abutments

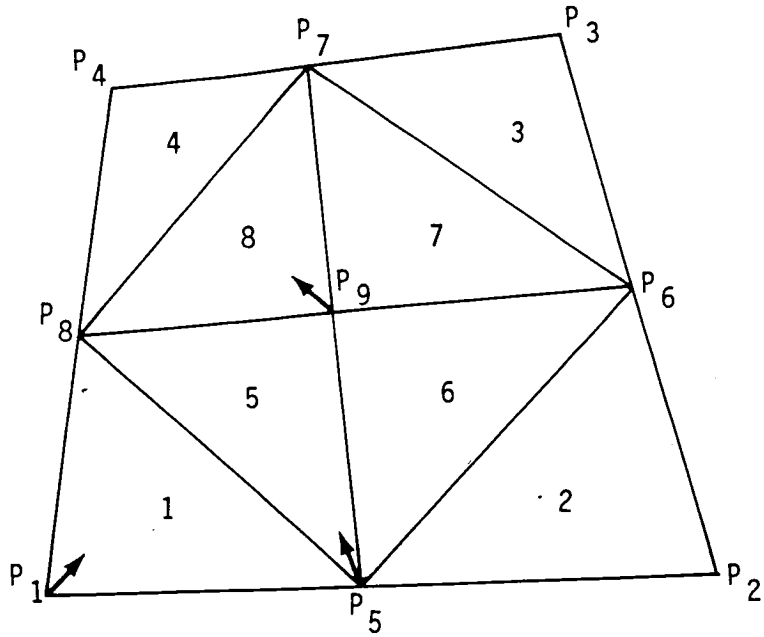

Figure G.3 - Control point recession vectors

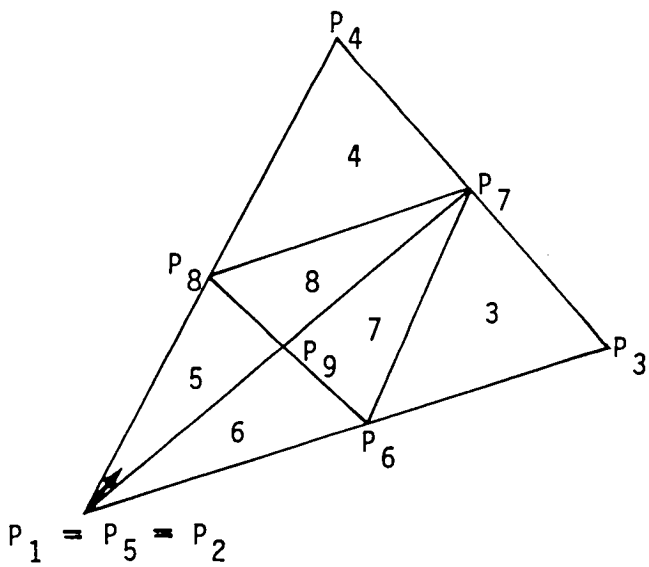

Figure G.4 - Recession of corner control points when subpanel is triangular

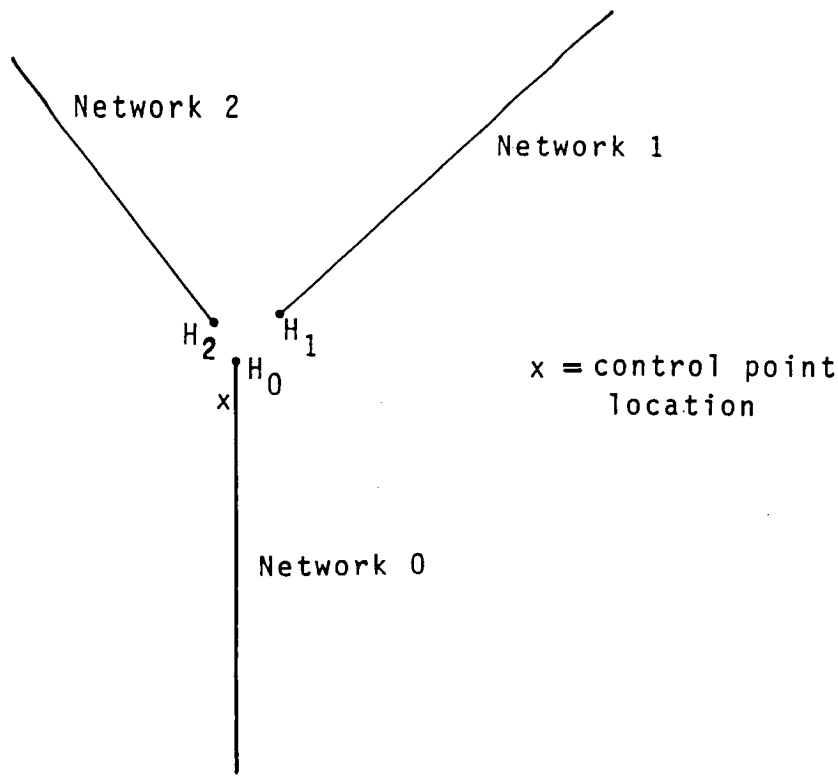

Figure G.5 - Abutment with 3 network edges (cross-section)

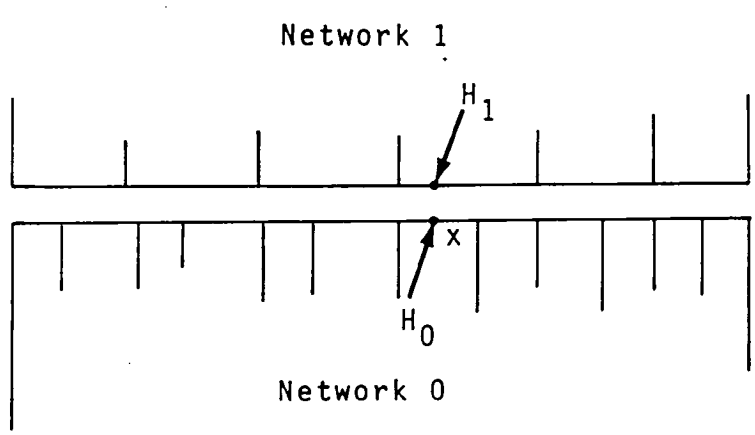

Figure G.6 - Hypothetical locations of a control point

H.0 Boundary Conditions and Onset Flows

In this appendix, we describe the processing of the user-input boundary condition data by the program. The program is not (with one exception) concerned with the nature of the boundary value problem defined by the user (that is, whether or not it is well posed). Under certain circumstances, however, user-specified boundary conditions are over-ridden by the program.

In section H.1, we discuss the standard boundary condition equation,

$$a_A \vec{w}_A \cdot \hat{n} + c_A \phi_A + \vec{t}_A \cdot \vec{v}_A + a_D \sigma + c_D \mu + \vec{t}_D \cdot \nabla \mu = b \qquad \text{(H.0.1)}$$

and describe how the program computes the coefficients of the left hand side of the equation. In section H.2, we discuss program overrides of the user-specified boundary conditions. In section H.3, we discuss the computation of the right hand side of (H.0.1) via onset flows.

H.1 Standard Forms for Boundary Conditions

H.1.1 Reduction of User Specified Boundary Conditions to Standard Form

The program user usually defines two boundary conditions at each control point. Generally this is done on a network-wide basis (especially in defining the left hand side of (H.0.1)), but it may be done on a point-by-point basis. The User's Manual (section 3) explains how to define the boundary condition coefficients; for standard cases it is done automatically by the program. In any case, the user-input boundary condition can be much more general than (H.0.1); it can be of the form (though almost all coefficients would generally be zero);

$$
\begin{aligned}
& a_U^I \vec{w}_U \cdot \hat{n} + c_U^I \phi_U + \vec{t}_U^I \cdot \vec{v}_U + e_U^I \vec{v}_U \cdot \hat{n} \\
+ & a_L^I \vec{w}_L \cdot \hat{n} + c_L^I \phi_L + \vec{t}_L^I \cdot \vec{v}_L + e_L^I \vec{v}_L \cdot \hat{n} \\
+ & a_A^I \vec{w}_A \cdot \hat{n} + c_A^I \phi_A + \vec{t}_A^I \cdot \vec{v}_A + e_A^I \vec{v}_A \cdot \hat{n} \\
+ & a_D^I \sigma + c_D^I \mu + \vec{t}_D^I \cdot \mu + e_D^I \vec{v}_D \cdot \hat{n} = b
\end{aligned}
\tag{H.1.1}
$$

Here, the subscripts U, L, A, D refer to upper, lower, average, and difference, while the superscript I specifies that these are user-input quantities.

Letting X stand for any of the quantities $\vec{w}$, ϕ, or $\vec{v}$, we have, by definition,

$$
\begin{aligned}
X_A &= \frac{1}{2}(X_U + X_L) \\
X_D &= X_U - X_L
\end{aligned}
\tag{H.1.2}
$$

Inverting (H.1.2) we have

$$
\begin{aligned}
X_U &= X_A + \frac{1}{2} X_D \\
X_L &= X_A - \frac{1}{2} X_D
\end{aligned}
\tag{H.1.3}
$$

Thus, $\alpha_U X_U + \alpha_L X_L = (\alpha_U + \alpha_L) X_A + \frac{1}{2}(\alpha_U - \alpha_L) X_D$ (H.1.4)

where α_U and α_L are any real numbers.

Substituting (H.1.4) into (H.1.1), we have

$$(a_U^I + a_L^I + a_A^I)\,\vec{w}_A \cdot \hat{n} + (c_U^I + c_L^I + c_A^I)\,\phi_A$$

$$+ (\vec{t}_U^I + \vec{t}_L^I + \vec{t}_A^I) \cdot \vec{v}_A + (e_U^I + e_L^I + e_A^I)\,\vec{v}_A \cdot \hat{n}$$

$$+ (\tfrac{1}{2}\,a_U^I - \tfrac{1}{2}\,a_L^I + a_D^I)\,\sigma$$

$$+ (\tfrac{1}{2}\,c_U^I - \tfrac{1}{2}\,c_L^I + C_D^I)\,\mu$$

$$+ (\tfrac{1}{2}\,\vec{t}_U^I - \tfrac{1}{2}\,\vec{t}_L^I + \vec{t}_D^I) \cdot \nabla\mu$$

$$+ (\tfrac{1}{2}\,e_U^I - \tfrac{1}{2}\,e_L^I + e_D^I)\,\vec{v}_D \cdot \hat{n} = b \qquad \text{(H.1.5)}$$

Here, we have used the facts that $\sigma = \vec{w}_D \cdot \hat{n}$ and $\mu = \phi_D$. So we have replaced upper and lower flow quantities in (H.1.1) with average and difference quantities. But in order to put the equation in the non-redundant form (H.0.1), we still have to eliminate the normal velocity terms which may be selected by a program user in place of normal mass flux.

Now, we have already shown (see 5.4.16a) that

$$\vec{w} \cdot \hat{n} = \vec{v} \cdot \tilde{n} \qquad \text{(H.1.6)}$$

where $\tilde{n}$ is the co-normal. Now, assuming

$$\hat{n} \cdot \tilde{n} \neq 0 \qquad \text{(H.1.7)}$$

($\hat{n} \cdot \tilde{n} = 0$ is the case of a forbidden "Mach-inclined" panel), we have the identity

$$\hat{n} = \frac{1}{\hat{n} \cdot \tilde{n}}\,\tilde{n} + \tilde{\tau} \qquad \text{(H.1.8)}$$

where

$$\tilde{\tau} = \hat{n} - \frac{1}{\hat{n} \cdot \tilde{n}}\,\tilde{n} \qquad \text{(H.1.9)}$$

Now

$$\hat{n} \cdot \tilde{\tau} = 1 - \frac{\hat{n} \cdot \tilde{n}}{\hat{n} \cdot \tilde{n}} = 0 \qquad \text{(H.1.10)}$$

and so $\tilde{\tau}$ is in fact a tangent vector or zero.
Thus, by (H.1.8),

$$\vec{v} \cdot \hat{n} = \frac{1}{\hat{n} \cdot \tilde{n}}\,\vec{v} \cdot \tilde{n} + \tilde{\tau} \cdot \vec{v} = \frac{1}{\hat{n} \cdot \tilde{n}}\,\vec{w} \cdot \hat{n} + \tilde{\tau} \cdot \vec{v} \qquad \text{(H.1.11)}$$

Substituting (H.1.11) into (H.1.5), we obtain

$$
\begin{aligned}
&(a_U{}^I + a_L{}^I + a_A{}^I + \frac{1}{\hat{n} \cdot \tilde{n}} (e_U{}^I + e_L{}^I + e_A{}^I))\, \vec{w}_A \cdot \hat{n} \\
&+ (c_U{}^I + c_L{}^I + c_A{}^I)\, \phi_A \\
&+ (\vec{t}_U{}^I + \vec{t}_L{}^I + \vec{t}_A{}^I + (e_U{}^I + e_L{}^I + e_A{}^I)\, \tilde{\tau}) \cdot \vec{v}_A \\
&+ (\tfrac{1}{2} a_U{}^I - \tfrac{1}{2} a_L{}^I + a_D{}^I + \frac{1}{\hat{n} \cdot \tilde{n}} (\tfrac{1}{2} e_U{}^I - \tfrac{1}{2} e_L{}^I + e_D{}^I))\, \sigma \\
&+ (\tfrac{1}{2} c_U{}^I - \tfrac{1}{2} c_L{}^I + c_D{}^I)\, \mu \\
&+ (\tfrac{1}{2} \vec{t}_U{}^I - \tfrac{1}{2} \vec{t}_L{}^I + \vec{t}_D{}^I + (\tfrac{1}{2} e_U{}^I - \tfrac{1}{2} e_L{}^I + e_D{}^I)\, \tilde{\tau}) \cdot \nabla \mu = b
\end{aligned}
\tag{H.1.12}
$$

Thus, (H.1.5) is of the form (H.0.1), with

$$
\begin{aligned}
a_A &= a_U{}^I + a_L{}^I + a_A{}^I + \frac{1}{\hat{n} \cdot \tilde{n}} (e_U{}^I + e_L{}^I + e_A{}^I) \\
c_A &= c_U{}^I + c_L{}^I + c_A{}^I \\
t_A &= t_U{}^I + t_L{}^I + t_A{}^I + (e_U{}^I + e_L{}^I + e_A{}^I)\, (\hat{n} - \frac{1}{\hat{n} \cdot \tilde{n}} \tilde{n}) \\
a_D &= \tfrac{1}{2} a_U{}^I - \tfrac{1}{2} a_L{}^I + a_D{}^I + \frac{1}{\hat{n} \cdot \tilde{n}} (\tfrac{1}{2} e_U{}^I - \tfrac{1}{2} e_L{}^I + e_D{}^I) \\
\vec{t}_D &= \tfrac{1}{2} \vec{t}_U{}^I - \tfrac{1}{2} \vec{t}_L{}^I + \vec{t}_D{}^I + (\tfrac{1}{2} e_U{}^I - \tfrac{1}{2} e_L{}^I + e_D{}^I)\, (\hat{n} - \frac{1}{\hat{n} \cdot \tilde{n}} \tilde{n})
\end{aligned}
\tag{H.1.13}
$$

H.1.2 Classification of Control Points

The correct implementation of symmetry in PAN AIR requires that the boundary condition processing in overlays 3 and 4 of DQG recognize some distinctions concerning a control point's position relative to a plane of symmetry. These distinctions, to be defined presently, are that a control point lie:

- Away from a plane of symmetry
- On a plane of symmetry
- In a plane of symmetry

In appendix K we show that when a configuration has two planes of symmetry, these two planes of symmetry are characterized by the specification

$$P_i = \{ \vec{q} \mid (\hat{n}_i, \vec{q} - \vec{p}_0) = 0 \} \qquad \text{(H.1.14)}$$

$$= \text{i-th plane of symmetry}$$

Here, $\vec{p}_0$ is any point lying on the intersection of the two planes of symmetry while $\hat{n}_i$ denotes the unit normals for symmetry plane P_i. The unit normals $\hat{n}_1$, $\hat{n}_2$ satisfy the conditions

$$\hat{n}_1 \cdot \hat{n}_2 = 0$$

$$\hat{n}_i \cdot \hat{c}_0 = 0$$

where $\hat{c}_0$ is the compressibility axis.

With this notation developed, we can now define our concepts. Let $\vec{p}$ be the position vector for the hypothetical location of a control point and let n be the unit normal to the singularity surface at $\vec{p}$. Then, $\vec{p}$ is said to lie <u>away</u> from any plane of symmetry if $\vec{p} \in P_i$, that is, if

$$\text{(away)} \qquad (\vec{p} - \vec{p}_0, \hat{n}_i) \neq 0 \qquad \text{(H.1.15)}$$

Next, $\vec{p}$ is said to lie <u>on</u> P_i if $\vec{p} \in P_i$, that is,

$$(\vec{p} \text{ on } P_i) \qquad (\vec{p} - \vec{p}_0, \hat{n}_i) = 0 \qquad \text{(H.1.16)}$$

Notice that it is possible for $\vec{p}$ to lie on two planes of symmetry. Finally, $\vec{p}$ is said to lie <u>in</u> P_i if $\vec{p} \in P_i$ and in addition $\hat{n}$ is parallel to $\hat{n}_i$. Thus

$$(\vec{p} \text{ in } P_i) \qquad (\vec{p} - \vec{p}_0, \hat{n}_i) = 0, \qquad (\hat{n}, \hat{n}_i) = 1 \qquad \text{(H.1.17)}$$

Because of the extra condition that $\hat{n}$ be parallel to $\hat{n}_i$, it is impossible for a control point to lie <u>in</u> two planes of symmetry.

In practice these distinctions are modified slightly. In the actual implementation of PAN AIR, the only control points that are recognized as lying <u>in</u> a plane of symmetry are those control points in a network such that the <u>whole</u> network lies in a plane of symmetry. If a control point does not lie <u>in</u> a plane of symmetry, the only way by which it will be recognized as lying <u>on</u> a plane of symmetry is if (i) it is a network edge control point and, (ii) <u>the</u> network edge abuts a plane of symmetry. Of course if the network edge abuts both planes of symmetry, the control point will be recognized as lying on both planes of symmetry. Finally, if a control point is not found to lie either on or in a plane of symmetry by these tests, it is said to lie away from the planes of symmetry.

H.1.3 Boundary Condition Symmetry Types for Networks Lying in a Plane of Symmetry

When a user has specified that a configuration has a plane of symmetry, PAN AIR assumes that the boundary condition to be imposed at p' the image of a

control point $\vec{p}$ has the form, (compare with equation (H.0.1))

$$a_A \vec{w}_A (\vec{p}') \cdot R_1 \hat{n} + c_A \phi_A (\vec{p}') + \vec{v}_A (\vec{p}) \cdot R_1 \vec{t}_A$$
$$+ a_D \sigma (\vec{p}') + c_D \mu (\vec{p}') + \nabla \mu (\vec{p}') \cdot R_1 \vec{t}_D = b' \qquad \text{(H.1.18)}$$

where R_1 denotes the usual reflection matrix defined by the normal $\hat{n}_1$ to the plane of symmetry, (cf. Dahlquist, Bjorck, ref. H.1, p. 212)

$$R_1 = I - 2 \hat{n}_1 \hat{n}_1^T.$$

Now when a control point lies in the plane of symmetry, so that $\vec{p}$ is identical with p', the concept of an image control point breaks down and we find that different side conditions must be imposed upon the boundary conditions in order to decompose the original boundary value problem into its symmetric and antisymmetric parts. In appendix K it is shown that a doublet network lying in a plane of symmetry must have an antisymmetric boundary condition of the form:

Antisymmetric Boundary Condition

$$a_A \vec{w}_A (\vec{p}) \cdot \hat{n} + c_D \mu (\vec{p}) + \nabla \mu (\vec{p}) \cdot \vec{t}_D = b \qquad \text{(H.1.19)}$$

while a source network lying in a plane of symmetry must have a symmetric boundary condition of the form:

Symmetric Boundary Condition

$$a_D \sigma (\vec{p}) + c_A \phi_A (\vec{p}) + v_A (\vec{p}) \cdot \vec{t}_A = b \qquad \text{(H.1.20)}$$

These restrictions on the form of boundary conditions for networks lying in a plane of symmetry should be regarded as the proper extension of the restriction (H.1.18) imposed upon boundary conditions at image control points.

H.2 Boundary Condition Overrides and Boundary Condition Selection

We discuss here all of the considerations that lead to the selection of the appropriate boundary conditions to be imposed at a control point. Two basic problems must be addressed.

First, the specification of a boundary condition on the upstream surface of a superinclined panel leads to an ill-posed boundary value problem. Consequently, if by user error or inadvertence this situation should occur, the user specified boundary conditions will be modified by PAN AIR in a prescribed fashion so as to eliminate the difficulty. This modification process, to be described presently, is quite straightforward.

Second, at some control points more boundary conditions may be available for use than are actually required.

This situation may arise in two possible ways:

(i) On a composite network, one typically specifies two boundary conditions at every control point. However, there are always some control points (typically on the boundary of the network) which require only one boundary condition.

(ii) PAN AIR is capable of internally generating boundary conditions that take priority over all user specified boundary conditions. These internally generated boundary conditions include the following

- Degenerate boundary conditions of the form $\hat{\sigma}^A = 0$ or $\hat{\mu}^S = 0$ for networks lying in a plane of symmetry
- Doublet matching conditions
- Velocity jump matching conditions (also known as the vorticity matching Kutta condition)
- Closure conditions
- Source matching conditions

The problem to be addressed, then, is to determine which boundary conditions are to be imposed when more than enough are available. Any response to this problem must address separately the different cases indicated by figure H.1. Thus we must distinguish whether a control point is interior to, on the edge of, or on the corner of a network. Additionally, we must distinguish the cases for which the control point lies away from, on or in a plane of symmetry. Finally, we remark that whenever a control point lies on or in a plane of symmetry, boundary condition assignments must be done separately for each symmetry condition. The reason for this last requirement is that whenever a control point lies on a plane of symmetry, there is the possibility that a degenerate boundary condition is being imposed nearby, and this fact can crucially affect the assignment of matching conditions, depending upon the symmetry condition.

The approach that PAN AIR uses to resolve the dilemma of too many boundary conditions is to define a boundary condition hierarchy. Thus, by defining a

prioritization of the available boundary conditions, PAN AIR is able to select the top one or two in accordance with its needs. This particular resolution of the dilemma should not be regarded as the only possible or even the only reasonable resolution. In fact, we shall see that it is not even adequate and requires some modification when the control point lies in a plane of symmetry. Alternative approaches that could also be used include:

(i) The boundary conditions required by PAN AIR could be tagged "source type" or "doublet type," the basic idea being that "source type" boundary conditions are applied at source boundary condition points while "doublet type" conditions are applied at doublet boundary condition points (see figures D.1, D.2, D.3). In addition, the DQG generated boundary conditions could also be typed in this way. For example, we would define

Degenerate doublet, $\hat{\mu}^S = 0$,	Doublet type
Degenerate source, $\hat{\sigma}^A = 0$,	Source type
Doublet Matching	Doublet type
Source Matching	Source type
Velocity Jump Matching	Doublet type
Closure	Doublet type (if "no doublet matching")
	Source type (if "no source matching")

Finally, the two user specified boundary conditions would be typed, one "source type" and the other "doublet type" (this is the tricky part). Then, during boundary condition assignment, a "doublet type" DQG boundary condition would replace a "doublet type" user boundary condition while a "source type" DQG boundary condition would replace a "source type" user boundary condition.

For this scheme to work, we would have to ensure that a "doublet type" ("source type") DQG boundary condition never be requested unless a "doublet type" ("source type") boundary condition is actually needed at that point. In addition, for class 4 and class 5 boundary conditions, it would almost certainly be necessary to require that the user specify the singularity type of each of his boundary conditions.

(ii) The program could proceed just as it does now in terms of prioritizing internally generated boundary conditions, but impose upon the user the requirement that he assign boundary condition priorities to the boundary conditions that he provides. (Section H.2.7 summarizes PAN AIR's current prioritization of internally generated boundary conditions.)

H.2.1 Superinclined Panel Override

In describing the program override which occurs on superinclined panels, that is, those for which

$$\hat{n} \cdot \tilde{n} < 0 \tag{H.2.1}$$

we will assume for convenience that the "upper" surface of the panel is the "upstream" surface, that is, that

$$\hat{n} \cdot \hat{c}_o < 0 \tag{H.2.2}$$

where $\hat{c}_o$ is the compressibility vector.

This assumption is not made within the program, of course, but is merely used here to simplify the discussion. Under this assumption, any upper surface specification is ill-posed, or very nearly so. Nevertheless, such a boundary condition could accidentally occur if a panel significantly inclined to the freestream becomes superinclined as the Mach number is increased.

We say that an upper surface condition has been specified if all the coefficients of X_L 's are zero, where X_L is defined in (H.1.3), and X stands for $\vec{w} \cdot \hat{n}$, ϕ, or $\vec{v}$. Using (H.1.3), we see that

$$X_A - 1/2\, X_D = X_L \tag{H.2.3}$$

Now, an upper surface boundary specification has occurred if

$$\begin{aligned} a_L &= 0 \\ c_L &= 0 \\ \text{and } \vec{t}_L &= 0 \end{aligned} \tag{H.2.4a}$$

that is, if

$$\begin{aligned} a_A &= 2\, a_D \\ c_A &= 2\, c_D \\ \text{and } \vec{t}_A &= 2\, \vec{t}_D \quad . \end{aligned} \tag{H.2.4b}$$

Whenever (H.2.4) occurs, the boundary condition (H.0.1) is replaced by the revised boundary condition

$$\vec{w}_L \cdot \hat{n} = \vec{w}_A \cdot \hat{n} - 1/2\, \sigma = 0 \tag{H.2.5}$$

or, if this boundary condition has already been specified as the other boundary condition at the control point, (H.0.1) is replaced by

$$\phi_L = 0 \tag{H.2.6}$$

Finally, if the boundary condition (H.0.1) is

$$\sigma = b \tag{H.2.7}$$

the program assumes this to be an indirect upper surface boundary condition associated with interior perturbation stagnation, and thus replaces this with either the boundary condition (H.2.5) or (H.2.6) as appropriate.

Once this override of the user specified boundary conditions has been performed, PAN AIR proceeds with its analysis treating the new boundary conditions exactly as if they had been directly specified by the user.

H.2.2 Boundary Condition Selection

The selection process for boundary conditions consists of four stages:

(i) The number of nontrivial boundary conditions to be imposed at a control point is determined. Denote this number by N_{NTBC}. (If the control point lies in a plane of symmetry, these boundary conditions must also be classified as to symmetry type, symmetric or antisymmetric (cf. section H.1.3). In this case, two numbers are determined, N^S_{NTBC} and N^A_{NTBC}, the number of symmetric and antisymmetric boundary conditions to be imposed.) Figures D.1, D.2 and D.3 describe the locations of nontrivial boundary conditions for the various network types.

(ii) The internally generated boundary conditions to be imposed at a control point are determined. If the control point lies on or in a plane of symmetry, both the number and nature of these boundary conditions may vary from one symmetry condition to another. (For control points lying in a plane of symmetry, these conditions are classified as to symmetry type.)

(iii) The user boundary conditions associated with a control point are determined and then ranked in a hierarchy. (Again, if the control point lies in a plane of symmetry, these boundary conditions must be classified as to symmetry type.)

(iv) Finally a list of all available boundary conditions is constructed. The internally generated boundary conditions are ranked according to the prioritization

1. Degenerate boundary condition
2. Doublet matching/velocity jump matching
3. Closure
4. Source matching

Following these, the list of user specified boundary conditions developed in part (iii) is appended. Then, the first N_{NTBC} boundary conditions (cf. part (i)) are selected for imposition at the control

point. If the combined list contains fewer than N_{NTBC} boundary conditions, the program terminates with an error message.

(If the control point lies in a plane of symmetry, two lists must be prepared, one containing symmetric boundary conditions and the other containing antisymmetric boundary conditions. Letting N^S_{NTBC}, N^A_{NTBC} denote respectively the number of symmetric and antisymmetric boundary conditions to be imposed, we select N^S_{NTBC} boundary conditions from the symmetric list and N^A_{NTBC} boundary conditions from the antisymmetric list. If an insufficient number of boundary conditions of the correct symmetry type is available, the program terminates with an error message.)

When a control point lies away from any plane of symmetry, the above procedure is carried out only once, since the boundary conditions to be imposed are independent of symmetry condition. However, whenever a control point lies on or in a plane of symmetry, the procedure must be repeated for each symmetry condition.

In the remainder of this subsection (H.2.2), we discuss in detail part (i) of the above procedure. Part (ii) is covered in three sections, (H.2.3) on degenerate boundary conditions, (H.2.4) on source and doublet matching conditions and (H.2.5) on closure boundary conditions. Part (iii), the user boundary condition hierarchy, is discussed in section (H.2.6). Part (iv) is discussed in section (H.2.7) where it is shown that there will never be more than two internally generated boundary conditions imposed on a composite network, and never more than one on a source alone or doublet alone network.

Let us now consider the method by which the program determines N_{NTBC}, the number of nontrivial boundary conditions to impose at a control point. Here, the underlying principle is that the number of boundary conditions must equal the number of singularity parameters. But this principle has already been built into the definitions of the various network types, as illustrated by the balance between x's and o's in figures D.1, D.2, and D.3.

Consider then the following procedure. Define N^S_{NTBC} and N^A_{NTBC} by

$$N^S_{NTBC} = \begin{cases} 1 & \text{if the control point location is a boundary condition location for the network's source type} \\ 0 & \text{otherwise} \end{cases} \tag{H.2.8a}$$

$$N^A_{NTBC} = \begin{cases} 1 & \text{if the control point location is a boundary condition location for the network's doublet type} \\ 0 & \text{otherwise} \end{cases} \tag{H.2.8b}$$

For the purposes of this computation, the boundary condition location points are given by figure H.2 for source networks and figure H.3 for doublet networks. The total number of nontrivial boundary conditions is the sum of these two counts,

$$N_{NTBC} = N^S_{NTBC} + N^A_{NTBC}. \tag{H.2.9}$$

Notice that this procedure also provides us with the numbers N^S_{NTBC} and N^A_{NTBC} of symmetric and antisymmetric boundary conditions to be imposed at control points lying in a plane of symmetry.

If a control point is an "extra" control point, the procedure given above must be modified slightly. Here we set $N^S_{NTBC} = 0$ always, and define N^A_{NTBC} by: (extra control point case)

$$N^A_{NTBC} = \begin{cases} 1 & \text{if the extra control point lies on a doublet analysis or doublet forward weighted network or else on a matching edge of a doublet wake 1 or doublet design network} \\ 0 & \text{otherwise, or if the extra control point appears on an edge marked "no doublet edge matching"} \end{cases} \tag{H.2.10}$$

H.2.3 Degenerate Boundary Conditions

If a control point lies in a plane of symmetry, then for each symmetry condition a degenerate boundary condition may be imposed by PAN AIR. The form and type of the various degenerate boundary conditions is given in figure H.4a, for configurations with one plane of symmetry and in figure H.4b for configurations with two planes of symmetry. In addition to giving the actual form of the degenerate boundary conditions, these figures also give the symmetry type, in the sense defined in section H.1.3. The reason this is necessary is that when a control point lies in a plane of symmetry, one must construct two boundary condition hierarchies, one for symmetric and another for antisymmetric type boundary conditions (cf. the boundary condition selection procedure described in section (H.2.2)).

To be specific consider the case of a composite network lying in a plane of symmetry, the whole configuration having just one plane of symmetry. We suppose that the user specified boundary conditions are:

bc_1: $\sigma = b_1$ (symmetric type)

bc_2: $\vec{W}_A \cdot \hat{n} = 0$ (antisymmetric type)

The formulation of boundary value problems for symmetry conditions* $\hat{\phi}^S$ and $\hat{\phi}^A$ then leads to the following hierarchies. (We ignore here any matching or closure boundary conditions.) The formulation procedure that leads to these hierarchies is discussed in appendix K.3.

---

* The symmetric and antisymmetric parts of the potential, $\hat{\phi}^S$ and $\hat{\phi}^A$, are defined by equation (K.3.22). When we treat the formulation of the integral equation for $\hat{\phi}^S$ (resp. $\hat{\phi}^A$) we say that we are dealing with the $\hat{\phi}^S$ (resp. $\hat{\phi}^A$) symmetry condition. These concepts extend to the case of two planes of symmetry in the obvious way. See eqn. (K.4.22) for $\hat{\phi}^{SS}$, etc.

	b.c. hierarchy for b.c.'s of symmetric type	b.c. hierarchy for b.c.'s of antisymmetric type
$\hat{\phi}^S$	o symmetric part of bc_1: $\hat{\sigma}^S = b_1$	o $\hat{\mu}^S = 0$ (degenerate) o symmetric part of bc_2: $0 = 0$
$\hat{\phi}^A$	b.c. hierarchy for <u>b.c.'s of symmetric type</u> o $\hat{\sigma}^A = 0$ (degenerate) o antisymmetric part of bc_1: $0 = 0$	b.c. hierarchy for <u>b.c.'s of antisymmetric type</u> o antisymmetric part of bc_2: $(\vec{W}_A^A \cdot \hat{n}) = 0$:

Thus, setting up the two hierarchies definitely avoids the imposition of a trivial condition of the form (0 = r.h.s.), which would in turn generate an identically zero row in the AIC matrix. If one did not set up the two hierarchies, the usual selection process would lead to the boundary conditions:

$$\hat{\phi}^S: \ \hat{\mu}^S = 0, \ 0 = 0 \qquad \hat{\phi}^A: \ \hat{\sigma}^A = 0, \qquad (\vec{W}_A^A \cdot \hat{n}) = 0$$

These selections, which include the singular boundary condition 0 = 0, are to be contrasted with the boundary conditions actually selected:

$$\hat{\phi}^S: \ \hat{\sigma}^S = b_1, \ \hat{\mu}^S = 0; \qquad \hat{\phi}^A: \ \hat{\sigma}^A = 0, \ (\vec{W}_A^A \cdot \hat{n}) = 0$$

This example also serves to illustrate the distinction between <u>symmetry condition</u>, which is a property of $\hat{\phi}^S$ and $\hat{\phi}^A$, and the <u>symmetry type</u> of a boundary condition. Thus, in this case, the symmetric part of the potential $\hat{\phi}^S$ has both a symmetric ($\hat{\sigma}^S = b_1$) and an antisymmetric ($\hat{\mu}^S = 0$) boundary condition imposed upon it.

H.2.4 <u>Doublet Matching, Velocity Jump Matching and Source Matching Boundary Conditions</u>

Each abutment (cf. appendix F) in the configuration will have associated with it a doublet matching boundary condition of the form (cf. eqn. (F.5.1))

$$\Sigma \ s_i \ \mu_i = 0 \tag{H.2.11a}$$

Here, the sum ranges over those networks involved in the abutment and μ_i is

the doublet strength on the i-th network. The coefficients $s_i = \pm 1$ or 0 are obtained by comparing the orientation of the abutment with the intrinsic orientation of the edge on the i-th network:

$$s_i = \begin{cases} +1 & \text{if the edge on the i-th network is aligned with the abutment's orientation} \\ -1 & \text{if the edge on the i-th network is opposed to the abutment's orientation} \\ 0 & \text{if the edge on the i-th network is marked "no doublet edge matching."} \end{cases}$$

In general, this matching condition may be assigned to any network involved in the abutment for which the doublet edge type is neither "null" nor "no doublet edge matching." The procedure by which a network receives a matching boundary condition is treated in detail in appendices F.4 and F.5. In appendix F.4, we have described the procedure by which a network is selected to receive the doublet matching condition along the interior of the abutment. Having made the selection, condition (H.2.11a) is imposed at each edge midpoint control point of the selected network. In appendix F.5 we have described the procedure by which matching condition assignments are performed at an abutment intersection. One finds, in general, that when n abutments come together at an abutment intersection (n-1) of the doublet matching conditions are assigned to appropriate corner control points.

Velocity jump matching conditions may be imposed along a network edge abutting the leading edge of a DW1 wake network. These boundary conditions have the form:

$$\vec{t} \cdot \left\{ \sum s_i \, \Delta \vec{v}_i \right\} = 0 \qquad \text{(H.2.11b)}$$

where s_i are the same as for the doublet matching conditions, t is a vector pointing downstream along the wake and the velocity jump $\Delta\vec{v}_i$ on the i-th network of the abutment is given by the Helmholtz relation (cf. eqns. (B.3.29-31)),

$$\Delta \vec{v}_i = \sigma \, \hat{n}/(\hat{n}.\vec{v}) + \nabla_t \mu \qquad \text{(H.2.12a)}$$

$$\nabla_t \mu = (\hat{n} \times \nabla \mu) \times \vec{v}/(\hat{n}.\vec{v}) \qquad \text{(H.2.12b)}$$

The velocity jump condition (H.2.11b), which is also called the vorticity matching condition, helps impose the Kutta condition in the neighborhood of the abutment (cf. appendix B). This condition is imposed only on the interior of an abutment and only on some network other than the network that performs doublet matching for the abutment. Because of this restriction, no conflict can occur between doublet matching and velocity jump matching. For this reason, there is no problem with assigning velocity jump matching the same position as doublet matching in any boundary condition hierarchies that we construct.

When $\vec{t}$ is chosen to point downstream along a wake, parallel to the compressibility axis, the condition (H.2.11b) implies the matching of upper and lower surface pressure coefficients (linear C_p rule) for both a thick and a thin trailing edge. We illustrate these facts with two examples.

Consider first the thin trailing edge configuration illustrated by figure H.5a. Assuming $\vec{t}$ to be parallel to the compressibility axis $\hat{c}_o$, we find that (H.2.11b) implies

$$\hat{c}_o \cdot \Delta \vec{v}_{wake} - \hat{c}_o \cdot \Delta \vec{v}_{wing} = 0$$

Now on the wing surface,

$$\Delta \vec{v}_{wing} = (\nabla\phi)_u - (\nabla\phi)_L$$

while on the wake surface,

$$\Delta \vec{v}_{wake} = [\sigma\, \hat{n}/(\hat{n}.\vec{v}) + \nabla_t\, \mu]_{wake}$$

Since $\sigma = 0$ on the wake, we find

$$\hat{c}_o \cdot \Delta \vec{v}_{wake} = \hat{c}_o \cdot \nabla_t\, \mu = c_o \cdot [(\hat{n} \times \nabla\, \mu)x\vec{v}]/(\hat{n}.\vec{v})$$

$$= \hat{c}_o \cdot [\nabla\mu - \hat{n}\, (\vec{v},\ \nabla\, \mu)/(\hat{n},\vec{v})]$$

$$= \hat{c}_o \cdot \nabla\, \mu$$

since $\hat{c}_o.\hat{n} = 0$. But because the doublet splines are constructed so that μ will be constant in the streamwise direction along the wake, $\hat{c}_o \cdot \nabla\, \mu = \vec{t}.\nabla\mu = 0$. This implies $\hat{c}_o \cdot \Delta \vec{v}_{wake} = 0$. Consequently we find

$$0 = \hat{c}_o \cdot \Delta \vec{v}_{wing} = \hat{c}_o \cdot (\nabla\phi)_u - \hat{c}_o \cdot (\nabla\phi)_L$$

$$= -\frac{1}{2} C_{p,U}^{lin} + \frac{1}{2} C_{p,L}^{lin}$$

since the formula for linear pressure coefficient is just

$$C_p^{lin} = -2\, \hat{c}_o \cdot \nabla\, \phi$$

This gives us the result we require, that upper and lower surface linear pressure coefficients match.

The case of a thick trailing edge is handled essentially the same way. Consider the case of figure H.5b. The matching condition (H.2.11b) becomes, in light of the Helmholtz relation, (eqn. H.2.12)

$$\vec{t} \cdot \left\{ \begin{array}{l} (+1)\ [\sigma_u\, \hat{n}_u/(\hat{n}_u,\ \vec{v}_u) + \nabla_t\, \mu_u] \\ (-1)\ [\sigma_L\, \hat{n}_L/(\hat{n}_L,\ \vec{v}_L) + \nabla_t\, \mu_L] \\ (-1)\ [\qquad \nabla_t\, \mu_w \qquad\qquad] \end{array} \right\} = 0$$

Again, because of the construction of the wake splines, (constant streamwise), we have

$$\vec{t} \cdot \nabla_t \mu_w = \hat{c}_o \cdot \nabla_t \mu_w = 0$$

Because of the stagnation condition $\phi = 0$ in the interior of the airfoil, we have

$$\sigma_u \hat{n}_u/(\hat{n}_u, \vec{v}_u) + \nabla_t \mu_u = (\nabla \phi)_u$$

$$\sigma_L \hat{n}_L/(\hat{n}_L, \vec{v}_L) + \nabla_t \mu_L = (\nabla \phi)_L$$

Since $\vec{t}$ points in the downstream direction $\hat{c}_o$, we observe that $(\vec{t} \cdot \nabla) = (\hat{c}_o \cdot \nabla)$

Putting all these results together, we obtain

$$(+1)\ \hat{c}_o \cdot (\nabla \phi)_u + (-1)\ \hat{c}_o \cdot (\nabla \phi)_L = 0$$

which clearly implies,

$$C_{p,U}^{lin} = C_{p,L}^{lin}$$

as we wished to prove.

Source matching conditions, which are much less important than doublet matching conditions, may be imposed along an abutment and have the form

$$\Sigma\ s_i\ \sigma_i = 0 \qquad \text{(H.2.13)}$$

This expression is interpretted very much the same as (H.2.11a) with the understanding that σ_i denotes the source strength on the i-th network. Since source matching can only be imposed along a source matching edge of a design network, relatively few abutments have these conditions imposed. Usually, only one of the network edges involved in an abutment is a source matching edge, so that it is clear which network should receive the source matching condition. If two or more edges in an abutment are designated source matching edges, then a selection process is performed that is quite similar to the process performed for doublet matching.

It is pertinent to remark that source matching along an abutment involving three or more edges is highly questionable in light of the definition of σ as the jump in the normal component of the mass flux $\vec{w}$. In fact, source matching makes sense only along those abutments at which just two networks join smoothly with a continuous surface normal. Considerations of this sort lead to the further conclusion that the only abutment intersection at which one can reasonably expect to impose source matching conditions are those of the form illustrated by figure H.6, for which the graph is either a ring or a partial ring. (See section F.5 for a full discussion of the construction of the graph associated with an abutment intersection.) Selecting matching assignments for graphs/abutment intersections of this form is quite a simple task and is

accomplished very much the same way as doublet matching is accomplished.

The procedures outlined above work quite well as long as the abutment along which matching is to be enforced lies away from any plane of symmetry. If an abutment lies on a plane of symmetry, special procedures (fully described in appendix F) must be followed in order to obtain correct matching condition assignments. If a network lying in a plane of symmetry should be assigned a matching boundary condition, then it is important that we know the symmetry type (in the sense of section H.1.3) of the matching condition. This is necessary in order that the matching condition be entered into the correct hierarchy. The symmetry types of the various matching conditions are given:

(i) Doublet matching is of antisymmetric type, and may only be imposed on an abutment lying on a plane of symmetry for symmetry conditions $\hat{\phi}^{ij}$ antisymmetric with respect to that plane of symmetry.

(ii) When velocity jump matching is imposed along an abutment lying on a plane of symmetry, a symmetry type will be defined for it only if the vector $\vec{t}$ (in equation (H.2.11b)) is either parallel to or perpendicular to n, the plane of symmetry normal. If $\vec{t}$ is parallel to $\hat{n}$, $\Delta\vec{v}$ matching will have symmetric type; if $\vec{t}$ is perpendicular to $\hat{n}$, (very much more the usual case) $\Delta\vec{v}$ matching will have antisymmetric type. If neither of these conditions holds the basic problem cannot be decoupled into symmetric and antisymmetric parts, and a fatal error results.

(iii) Source matching is of symmetric type, and may only be imposed on an abutment lying on a plane of symmetry for symmetry conditions $\hat{\phi}^{ij}$ symmetric with respect to that plane of symmetry.

H.2.5 Closure Boundary Conditions

Closure boundary conditions arise when one particular edge of a source or a doublet design network (SD1, SD2, DD1, DFW) is designated as a "closure edge" by the program user. Then, for each edge midpoint control point on the closure edge, the boundary condition

$$\iint_C (a_A \vec{w}_A \cdot \hat{n} + a_D \sigma)\, dS = b \qquad \text{(H.2.14)}$$

is imposed, where C is the row or column of panels headed by that control point, as illustrated in figure H.7. The coefficients a_A, a_D, and b are user-supplied, and once again can be redundantly defined in terms of upper, lower, average, and difference terms. We will explain (H.2.14) by means of a simple example.

In figure H.8, we illustrate a thick wing on the upper surface of which we desire a specified pressure distribution (see Appendix C for a discussion of the design process). Now, after solving the potential flow problem and relofting the surface, we obtain a relofted surface, whose trailing edge may or may not coincide with the unchanged trailing edge of the lower surface. The closure boundary condition can be used to insure that the trailing edges

coincide after relofting, that is, that the airfoil "closes."

But now, suppose the boundary condition

$$\int_A^B \vec{w}_u \cdot \hat{n}\, dl = 0 \qquad \text{(H.2.15)}$$

is satisfied, where A and B are shown in figure H.8. Then clearly a mass flux streamline originating on the wing upper surface at A will end up at B. It can not end up "above" B, since then a streamline starting slightly below A would end up slightly above B, and thus the integral of the mass flux through the surface would be non-zero (see figure H.9).

Now, a wing is a 3-dimensional object, and thus, in order to insure that any streamline originating at the leading edge of the design network will arrive at the trailing edge of the design network, equation (H.2.15) must be imposed on a dense set of integration contours originating at the leading edge, and following the wing surface in a streamwise direction to the trailing edge. Then the relofted surface, which is required to be impermeable, must necessarily be the surface defined by the streamlines originating at the leading edge and ending at the trailing edge. So, the imposition of (H.2.15) on a dense set of integration lines would insure that the trailing edge of the relofted surface agrees with the trailing edge of the design network.

Now, a panel method being a discretization method, we do not impose (H.2.15) at a dense set of lines, but instead on a set of narrow two-dimensional surfaces aligned streamwise, namely, rows or columns of panels. Thus we impose the boundary condition

$$\iint_C \vec{W}_U \cdot \hat{n}\, dS = 0 \qquad \text{(H.2.16)}$$

Now, $$\vec{W}_U = \vec{V}_\infty + \vec{w}_U \qquad \text{(H.2.17)}$$

$$\vec{w}_U \cdot \hat{n} = \vec{w}_A \cdot \hat{n} + 1/2\, \sigma \qquad \text{(H.2.18)}$$

and $$\vec{w}_L = 0 \qquad \text{(H.2.19)}$$

because of the perturbation stagnation boundary conditions ($\phi_L = 0$). Thus (H.2.16) can be written

$$\iint_C (\sigma + \vec{V}_\infty \cdot \hat{n})\, dS = 0 \qquad \text{(H.2.20)}$$

or

$$\iint_C \sigma\, dS = b = -\iint_C \vec{V}_\infty \cdot \hat{n}\, dS \qquad \text{(H.2.21)}$$

which is of the form (H.2.14), with $a_D = 1$, $a_A = 0$. The more general form of (H.2.14) is available for program users solving non-standard problems.

In order that there not be an excessive number of internally generated boundary conditions, the user is required to specify whether closure overrides a source matching or a doublet matching boundary condition. Thus, if the user specifies that closure override doublet matching on a particular network edge, then none of the edge midpoint control points on that network's edge will be used for doublet matching. Notice however that this override feature has no effect on corner control points, since closure boundary conditions are not imposed at such points. Consequently, this override requirement does not introduce any extra complication into the treatment of abutment intersections. (Remark: There is some danger that specifying that closure override doublet matching could result in doublet matching not being imposed on some abutment, a potentially disastrous event. Usually, however there will be some network available to accept the abutment's matching condition.)

If a design network happens to lie in a plane of symmetry, then its closure boundary condition cannot have the general form (H.2.14). Rather it must have either the form

antisymmetric type, overrides doublet matching

$$\iint_C a_A \vec{w}_A \cdot \hat{n} \, dS = b \qquad \text{(H.2.22)}$$

or else the form

symmetric type, overrides source matching

$$\iint_C a_D \, \sigma \, dS = b \qquad \text{(H.2.23)}$$

If the closure condition has the first form, (H.2.22), then it must override the doublet matching condition. If on the other hand it has the second form, (H.2.23), then it must override the source matching condition.

This completes our discussion of closure boundary conditions at this time. In section K.1.3 we describe the manner in which equation (H.2.14) is transformed into a linear equation involving the singularity parameters.

H.2.6 User Boundary Condition Hierarchy

In this section we describe the hierarchical ranking of the user specified boundary conditions. As observed in section H.2.2, the reason this ranking is necessary is that there are sometimes more boundary conditions available at a control point than are actually needed. When this happens, a hierarchical list of all available boundary conditions is constructed and the required number of boundary conditions is selected from the top of the list.

In PAN AIR, the hierarchical ranking of user boundary conditions was motivated by the following considerations:

(a) potential and doublet strength are quadratically varying, while source strength and velocity are linearly varying; therefore the former should be specified rather than the latter, since quadratic functions are not amenable to extrapolation, but need to be "pinned down" at network edges.

(b) tangential velocity boundary conditions are less stable than normal velocity ones, therefore the latter should be specified, given a choice, and

(c) there are fewer source parameters than doublet parameters on a network, in general, so specifying source strength (especially on network edges) risks overspecification and a singular AIC matrix.

Based on these considerations, six categories of user boundary conditions are identified by a hierarchy ranking as indicated by figure H.10. In the second part of figure H.10 we present a logical chart of the 6 boundary condition categories that clearly indicates two facts: (i) the categories are mutually exclusive and (ii) every nontrivial boundary condition falls into some category. This chart also indicates that category 1 and 4 boundary conditions should not be specified on a "null doublet" network while category 6 boundary conditions should not be specified on a "null-source" network. If these considerations are violated, it is very likely that a singular AIC matrix will result.

If a control point lies in a plane of symmetry, we must further categorize the user boundary conditions according to symmetry type, in the sense of section H.1.3. In figure H.11, we present an augmented version of figure H.10 that indicates the symmetry types of the various terms of the general boundary condition equation (H.0.1) together with the extra restrictions imposed when a control point lies in a plane of symmetry. Again, it is easy to see that the boundary condition categories are disjoint and complete provided the given boundary conditions are of purely symmetric or antisymmetric in type. We emphasize again here that the user must provide symmetric boundary conditions for a source network and antisymmetric boundary conditions for a doublet network, whenever the network lies in a plane of symmetry. The justification of these restrictions is given near the end of appendix K.3.

In concluding this discussion, we remark that the definitions and ranking of the boundary condition categories cannot be rigorously justified. Rather, the boundary condition hierarchy is a heuristic construct, based upon example and the general considerations outlined at the beginning of this section.

H.2.7 The Complete Boundary Condition Hierarchy

We are now in a position to describe the construction of the complete boundary condition hierarchy. In describing this construction, we will treat in a case by case fashion the 8 cases indicated by figure (H.1). In addition, for each case we will show that all of the internally generated boundary conditions selected by PAN AIR are actually imposed.

Interior Control Point, away from any plane of symmetry

In this instance, PAN AIR will not produce any internally generated boundary conditions so that the boundary condition hierarchy contains just the user specified boundary conditions, ranked in the order described in section H.2.6.

Edge Control Point, away from any plane of symmetry

The internally generated boundary conditions that can be imposed along an edge include doublet matching, closure and source matching*. However, because the program requires that the user specify for closure to override either source or doublet matching, there will never be more than two internally generated boundary conditions. The various hierarchies that can arise when closure is imposed are indicated below

Composite Network, Closure Overrides μ-matching	Composite Network, Closure Overrides σ-matching	Source Alone, Closure Overrides σ-matching	Doublet Alone, Closure Overrides μ-matching
Closure	[μ matching]	Closure	Closure
[σ matching]	Closure	user b.c.'s	user b.c.'s
user b.c.'s	user b.c.'s		

(H.2.24)

Symbols appearing in brackets indicate that a boundary condition of this form may or may not appear. The number of required boundary conditions, N_{NTBC}, is selected from the top of the appropriate boundary condition hierarchy. Note that user boundary conditions are entered into the hierarchy in the order described in section H.2.6 and illustrated by figures H.10 and H.11.

If closure is not a consideration along the edge, the various hierarchies that are possible are as follows:

Composite Network	Source Alone	Doublet Alone
[μ matching]	[σ matching]	[μ matching]
[σ matching]	user b.c.'s	user b.c.'s
user b.c.'s		

(H.2.25)

Corner Control Point, away from any plane of symmetry

Here, the boundary condition hierarchies that can arise are the same as for an edge control point at which closure is not imposed (cf. (H.2.25) above).

* PAN AIR can also generate a velocity jump matching condition at an edge control point. Such a condition is entered into any boundary condition hierarchy in the same position that a doublet matching condition would be entered. Because it plays the same role in a boundary condition hierarchy as that played by doublet matching, an explicit discussion of the velocity jump matching condition is unnecessary.

Edge Control Point, on a plane of symmetry

When a control point lies on a plane of symmetry, the boundary condition hierarchy must be constructed separately for each symmetry condition (e.g. $\hat{\phi}^S$, $\hat{\phi}^A$ etc.). Aside from this extra little complication, these control points are no different from edge control points away from a plane of symmetry, the possible hierarchies being given by (H.2.24) and (H.2.25). Of course it will generally happen that a different hierarchy is constructed for each symmetry condition. As a simple example, consider an edge control point on a doublet alone network. It is entirely possible that the two hierarchies shown below would be constructed:

$\hat{\phi}^S$ hierarchy	$\hat{\phi}^A$ hierarchy
user b.c.'s	μ matching user b.c.'s

Here, doublet matching would never be imposed on $\hat{\phi}^S$ since doublet matching is automatically satisfied for any abutment lying on an active plane of symmetry. (Remark: Notice that a single hierarchy is constructed for each symmetry condition. When we treat control points lying in a plane of symmetry, we will have, for each symmetry condition $\hat{\phi}^S$ or $\hat{\phi}^A$, both an [S] and an [A] hierarchy.)

Corner Control Point, on a plane of symmetry

The boundary condition hierarchies that can arise for a control point on a plane of symmetry are the same as for a corner control point away from any plane of symmetry, and are given by (H.2.25). Of course, a separate hierarchy must be constructed for each symmetry condition.

We now address the issue of a control point lying in a plane of symmetry. Our actual discussion will treat only the case of one plane of symmetry, so that only two symmetry conditions, $\hat{\phi}^S$ and $\hat{\phi}^A$, need be considered. The extension of our procedures to a situation with two planes of symmetry is fairly straightforward in principle, but intricate in implementation. In order to illustrate the basic principle, consider the case of a control point lying in the second plane of symmetry. In this case, we assign boundary conditions to symmetry conditions $\hat{\phi}^{SS}$ and $\hat{\phi}^{AS}$ in essentially the same way as we assign boundary conditions to $\hat{\phi}^S$ for problems with just one plane of symmetry. Similarly, $\hat{\phi}^{SA}$ and $\hat{\phi}^{AA}$ are to be handled very much the same as $\hat{\phi}^A$ is handled for problems with one plane of symmetry.

In the discussions that follow, we distinguish the symmetric and antisymmetric user specified boundary conditions by the notations bc_S and bc_A. The symmetric part of bc_S is denoted bc_S^S while the antisymmetric part of bc_A is denoted bc_A^A. One can also form bc_S^A and bc_A^S, with the obvious definitions. However, boundary conditions of this form are singular boundary conditions in the sense that they generate a zero row in the AIC matrix.

Finally we remark that when a control point lies in a plane of symmetry, two hierarchies are constructed for each symmetry condition, one with symmetry type [S] from which N^S_{NTBC} conditions are selected, and another of symmetry type [A] from which N^A_{NTBC} conditions are selected.

Interior Control Point, in a plane of symmetry

Here, the only possible internally generated boundary conditions are just those degenerate ones summarized by figure H.4, neither matching nor closure being imposed at the interior of a network. Consequently we obtain the following boundary condition hierarchies:

$\hat{\phi}^S$ hierarchies, interior control point in a plane of symmetry

Composite Network		Doublet Alone	Source Alone
[S]	[A]	[A]	[S]
bc^S_S	$\hat{\mu}^S=0$	$\hat{\mu}^S=0$	bc^S_S
	$\cdots\cancel{bc}^S_A\cdots$	$\cdots\cancel{bc}^S_A\cdots$	

(H.2.26)

$\hat{\phi}^A$ hierarchies, interior control point in a plane of symmetry

Composite Network		Doublet Alone	Source Alone
[S]	[A]	[A]	[S]
$\hat{\sigma}^A=0$	bc^A_A	bc^A_A	$\hat{\sigma}^A=0$
$\cdots\cancel{bc}^A_S\cdots$			$\cdots\cancel{bc}^A_S\cdots$

(H.2.27)

Notice that the singular boundary conditions bc^A_S and bc^S_A are always outranked by an appropriate degenerate boundary condition.

Edge control point, in a plane of symmetry

Here we have the possibility that closure may be imposed along the edge. Since closure may take either of the two forms (H.2.22) or (H.2.23), we must address both possibilities. In addition, we must treat the case in which no closure condition is imposed along the edge. For the cases in which closure is present, the various possible hierarchies are summarized by fig. H.12. If closure is not present, the possible hierarchies are given by fig. H.13.

Corner control point, in a plane of symmetry

In this case, the only possible internally generated boundary conditions are the degenerate ones summarized by figure H.4 and source and doublet matching. The hierarchies that can arise are the same as for an edge control point when closure is absent and are summarized in fig. H.13.

A careful perusal of (H.2.26), (H.2.27) and figures (H.12) and (H.13) leads to the observation that when a control point lies in a plane of symmetry, no boundary condition hierarchy contains more than one internally generated boundary condition. Consequently, an internally generated boundary condition will always be imposed provided an AIC row exists for the associated control point and symmetry type.

H.3 Onset Flows

Equation (H.0.1) is the most general possible equation in ϕ and its derivatives, but it is often inconvenient for the user to evaluate the scalar b on the right hand side of (H.0.1). The most common example arises from the boundary condition

$$\vec{W}_U \cdot \hat{n} = 0 \tag{H.3.1}$$

where $\vec{W}$ is total mass flux. Since

$$\vec{W} = \vec{w} + \vec{V}_\infty \tag{H.3.2}$$

equation (H.3.1) becomes

$$\vec{w}_U \cdot \hat{n} = - \vec{V}_\infty \cdot n = b \tag{H.3.3}$$

The scalar b could, of course, be computed by the user at every control point, but much labor is saved by having the program do so.

Similarly, consider the tangential velocity boundary condition

$$\vec{t}_U \cdot \vec{V}_U = \beta \qquad \text{(where } \beta \text{ is user-specified)}, \tag{H.3.4}$$

which becomes

$$\vec{t}_U \cdot \vec{v}_U = \beta - V_\infty \cdot \vec{t}_U \tag{H.3.5}$$

Finally, suppose a program user wishes to define total internal stagnation, as opposed to perturbation stagnation. The boundary conditions to be imposed should therefore indirectly (that is by specifying potential) specify

$$\vec{W}_L = 0 \tag{H.3.6}$$

Thus, we specify

$$\bar{\Phi}_L = 0 \tag{H.3.7}$$

where $\bar{\Phi}$ is defined by

$$\vec{W} = \tilde{\nabla} \bar{\Phi} \tag{H.3.8}$$

on the surface, as illustrated in figure H.14.

Note that $\bar{\Phi} \neq \Phi$, where $\vec{V} = \nabla\Phi$

Now, we prove that up to a constant, (H.3.8) requires that

$$\bar{\Phi}(x) = \frac{1}{s\beta^2} [\vec{V}_\infty , \vec{x}] + \phi(\vec{x}) \tag{H.3.9}$$

We now prove (H.3.9). We use reference coordinates. By (5.2.4)

$$\tilde{\nabla}_i [\vec{V}_\infty, \vec{x}] = \sum_j [B_o]_{ij} \frac{\partial}{\partial x_j} [\vec{V}_\infty, \vec{x}] \tag{H.3.10a}$$

= (by (E.2.4))

$$\sum_{j,k,m} [B_o]_{ij} \frac{\partial}{\partial x_j} (\{\vec{V}_\infty\}_k [C_o]_{km} \vec{x}_m) \tag{H.3.10b}$$

Noting that $\vec{V}_\infty$ and $[C_o]$ are independent of x_j, while

$$\frac{\partial}{\partial x_j} (x_m) = \delta_{jm} \tag{H.3.11a}$$

(the Kronecker delta), we have

$$\tilde{\nabla}_i [\vec{V}_\infty, \vec{x}] =$$

$$\sum_{j,k,m} [B_o]_{ij} \{V_\infty\}_k [C_o]_{km} \delta_{jm} =$$

$$[B_o]_{ij} [C_o]_{kj} \{V_\infty\}_k \tag{H.3.11b}$$

Now, applying (E.2.9) to B_o and C_o, and noting by (E.3.9) that C_o is its own transpose,

$$\tilde{\nabla} [\vec{V}_\infty, \vec{x}] = s\beta^2 \vec{V}_\infty \tag{H.3.12a}$$

Thus,

$$\tilde{\nabla} \left(\frac{1}{s\beta^2} [\vec{V}_\infty, x] + \phi (\vec{x}) \right) = V_\infty + \tilde{\nabla}\phi = \vec{W} \tag{H.3.12b}$$

which implies (H.3.9).

So, the boundary condition (H.3.7) is equivalent to

$$\phi_L (x) = \frac{-1}{s\beta^2} [\vec{V}_\infty, \vec{x}] \tag{H.3.13}$$

The right hand side quantities of equations (H.3.3), (H.3.5), and (H.3.13) are automatically computed in PAN AIR for user convenience. But, in fact, PAN AIR offers more general right hand side options which have a rather empirical

justification for existence. These options arise from the introduction of an "onset flow" $\vec{U}_0$ with the assumption

$$\vec{W} = \vec{U}_0 + \vec{w} \tag{H.3.15}$$

Now, there is nothing empirical about (H.3.15) unless we make the assumption

$$\vec{U}_0 \neq \vec{V} \tag{H.3.16}$$

where $\vec{V}_\infty$ is the uniform freestream, aligned with the compressibility direction $\hat{c}_0$.

Even so, at Mach zero, the boundary condition

$$\vec{W}\cdot\hat{n} = 0 \tag{H.3.17}$$

combined with (H.3.15), where $\vec{U}_0$ is a uniform vector field $\vec{U}_\infty$ which is not parallel to $\vec{V}_\infty$ (see figure H.15) is still theoretically valid, since the Prandtl-Glauert equation reduces to Laplace's equation, and therefore has no preferred direction.

Now, at non-zero Mach number, it is still possible for the small perturbation assumptions to be satisfied if U_0 is very close to $\vec{V}_\infty$ everywere. The most common application of this is to simulate flow conditions at multiple angles of attack which only differ slightly by varying the uniform onset flow without varying the compressibility direction $\hat{c}_0$. The advantage is that as long as $\vec{V}_\infty = \hat{c}_0$ is not varied, the same AIC matrix may be used each time, thus saving on computation time.

If the perturbation to the freestream defined by the onset flow is small, it need not be uniform. Consider the case of a propeller slipstream (see figure H.16). The action of the propellers causes an increased flow which does not arise from the solution of Prandtl-Glauert equation. Thus the appropriate boundary condition to impose is (H.3.17) where

$$\vec{W} = \vec{V}_\infty + \Delta\vec{U}_i + \vec{w} \tag{H.3.18}$$

and $\Delta\vec{U}_i$ is the "local incremental onset flow", in this case the incremental flow due to the action of the propellers. Once again, we can put $\vec{W}$ in the form (H.3.15) by setting

$$\vec{U}_0 = \vec{V}_\infty + \Delta\vec{U}_i \tag{H.3.19}$$

As a third example, we consider a case in which the onset flow is not a small perturbation of the freestream, but is so in the neighborhood of the configuration. Consider the case of an airplane undergoing a small rolling motion of magnitude $|\vec{\omega}|$ in a "right handed" rotation about an axis with direction $\vec{\omega}$ through a point P_0 (see figure H.17).

Computation of the magnitude $|\vec{\omega}|$ from a particular roll rate (in radians per unit time) is discussed in section 7 of the User's Manual. This is an unsteady phenomenon, but we simulate it (calling the flow "quasi-steady") by defining an onset flow

$$\vec{U}_0\,(P) = \vec{U}_\infty + \vec{\omega} \times (\vec{P} - \vec{P}_0) \tag{H.3.20}$$

where P is the control point, and imposing the boundary condition.

$$\vec{w}\cdot\hat{n} = -\vec{U}_0\cdot\hat{n} \tag{H.3.21}$$

Note that U_0 is unbounded as $|\vec{P} - \vec{P}_0|$ becomes large, and thus a rotational onset flow is never a "small perturbation" in all of space, no matter how small the rotation rate. Thus no theoretical justification for the use of rotational onset flows exists, and so rotational onset flows must be used with extreme caution. The use of a rotational onset flow is generally valid, however, if the perturbation it induces is small in the neighborhood of the configuration, and may be used to estimate aerodynamic derivatives due to steady roll, pitch, and yaw rates.

PAN AIR provides for all these right hand side boundary condition options by permitting an arbitrary linear combination of the options described. Thus, in general, the user may define an arbitrary onset flow at a control point P by

$$\vec{U}_0\ (P) = \vec{U}_\infty + \quad \Delta\vec{U}_i(P) + \vec{\omega} \times (\vec{P} - \vec{P}_0) \tag{H.3.22}$$

where the user defines $\vec{U}_\infty$, $\Delta\ \vec{U}_i$, $\vec{\omega}$, and P_0. The vector $\vec{U}_\infty$ is defined by a magnitude $|\vec{U}_\infty|$, an angle of attack α and angle of sideslip β, such that (compare with (E.3.1))

$$\vec{U}_\infty = |\vec{U}_\infty| \begin{Bmatrix} \cos\alpha\cos\beta \\ -\sin\beta \\ \sin\alpha\cos\beta \end{Bmatrix} \tag{H.2.23}$$

The vector $\vec{\Delta U}(P)$ is specified by the user on a control point by control point basis either as a vector in reference coordinates, or by specifying a magnitude U_l, and angles α_l, and β_l (l stands for local) such that

$$U_l = \vec{U}_\infty + \vec{U}_i = U_l \begin{Bmatrix} \cos\alpha_l\cos\beta_l \\ -\sin\beta_l \\ \sin\alpha_l\cos\beta_l \end{Bmatrix} \tag{H.3.24}$$

Now, the general right hand side expression which may be defined by a user for a boundary condition is

$$b(P) = b_0 - b_n\,\vec{U}_0\cdot\hat{n} - \vec{t}_T\cdot\vec{U}_0 \quad - \frac{b_\phi}{s_\beta^2}\ [\vec{U}_\infty\ ,\ \vec{P}] \tag{H.3.25}$$

where b_0, b_n, $\vec{t}_T$ and b_ϕ are user-defined quantities. We mention in passing that various default options are available to define the standard

combinations which occur. These options are described in the PAN AIR User's Manual.

This concludes our discussion of boundary conditions for the present. In appendix K, we present a detailed description of how boundary conditions are transformed into AIC constraints. In particular, the many complications caused by symmetry considerations are thoroughly discussed.

	Interior	Edge [Abutment interiors]	Corner [Abutment intersections]	
Away from P-O-S	(no internally generated boundary conditions)	μ match | $\Delta\vec{V}$ match closure σ match	μ match σ match	All Symmetry Conditions Identical
On P-O-S		μ match | $\Delta\vec{V}$ match closure σ match	μ match σ match	Each Symmetry Condition Handled Separately
In P-O-S	$\hat{\phi}^S$: Deg. μ[A] $\hat{\phi}^A$: Deg. σ[S]	$\hat{\phi}^S$: Deg. μ[A] $\iint a_D\sigma = b$[S] σ match[S] $\hat{\phi}^A$: Deg. σ[S] $\iint w_A \cdot \hat{n} = b$[A] μ match[A]	$\hat{\phi}^S$: Deg. μ[A] σ match[S] $\hat{\phi}^A$: Deg. σ[S] μ match[A]	

Remark 1 For each case, the DQG boundary conditions that may occur for that case are listed. For control points lying in a plane of symmetry, the symmetry type (in the sense of sec. H.1.3) for these boundary conditions is given in brackets (e.g. [S] or [A])

Remark 2 For control points lying on or in a plane of symmetry, selection must be done separately for each symmetry condition ($\hat{\phi}^S$ or $\hat{\phi}^A$)

Remark 3 No more than two DQG boundary conditions will ever be requested since closure must always override either source matching or doublet matching

Remark 4 Deg.→Degenerate boundary condition of the form $\hat{\mu}^S=0$ or $\hat{\sigma}^A=0$. See figure H.4 and appendix K.3 for more detail.

Figure H.1 - Summary of the separate cases that must be handled during boundary condition selection

a) Source analysis

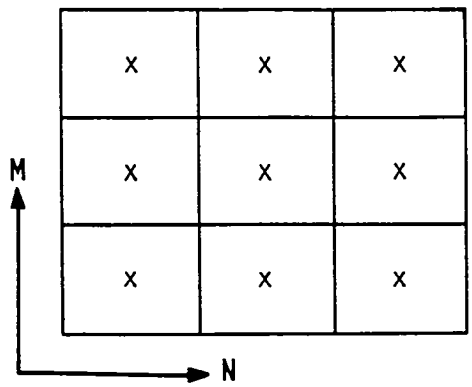

b) Source design/1

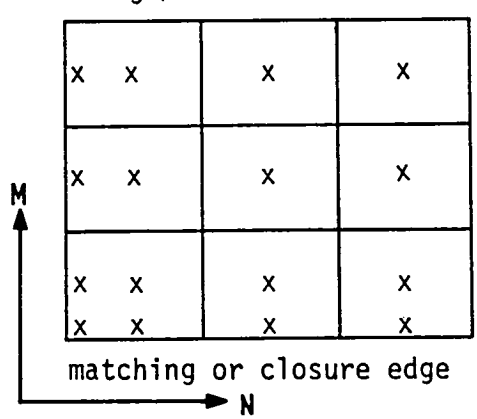

(Arrows show default directions of increasing row index M and column index N)

c) Source design/2

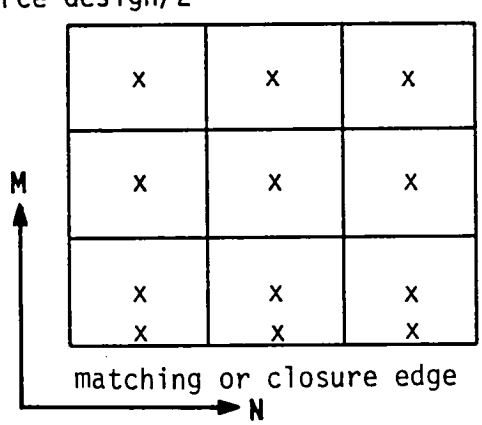

Figure H.2 - Boundary condition locations for source networks

a. Doublet analysis /Doublet forward weighted

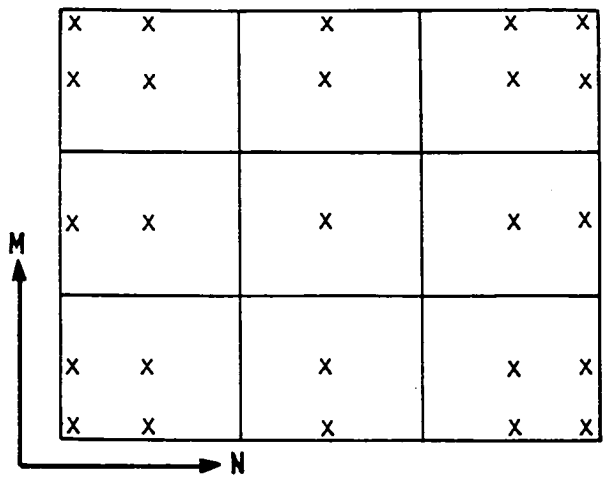

b. Doublet wake 1

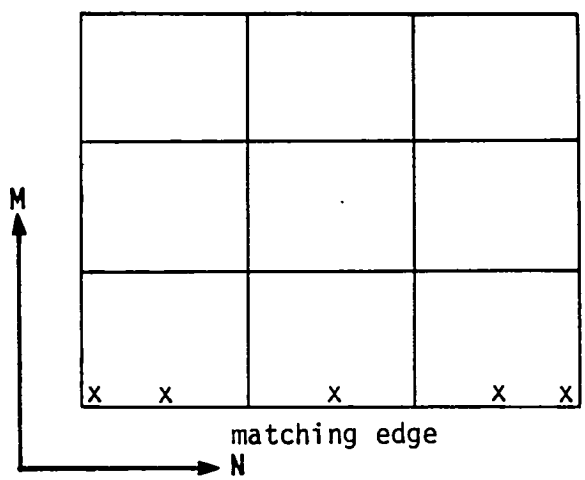

(Arrow show default directions of increasing row index M and column index N)

c. Doublet wake 2

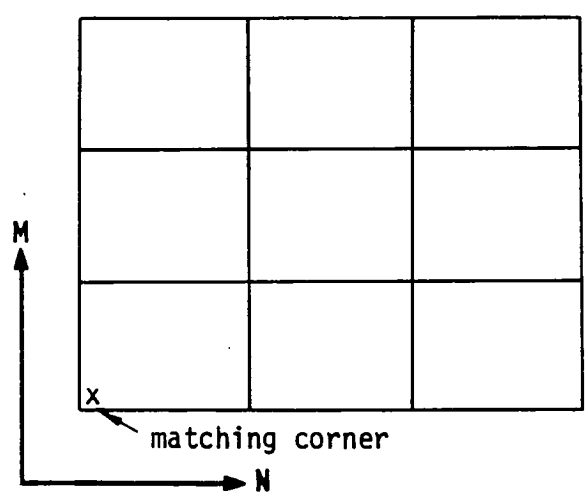

Figure H.3 - Boundary condition locations for doublet networks

d. Doublet analysis network with smooth abutment

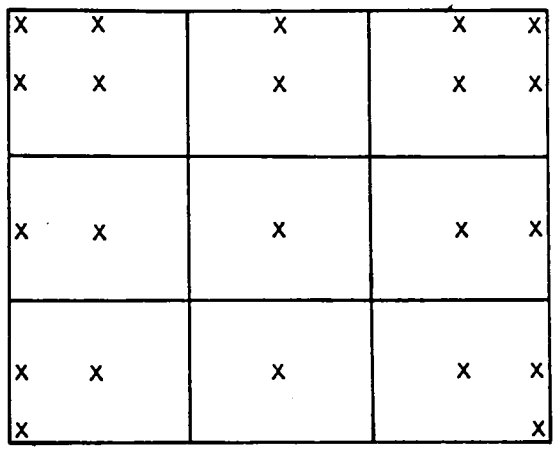

smooth abutment

e. Doublet design

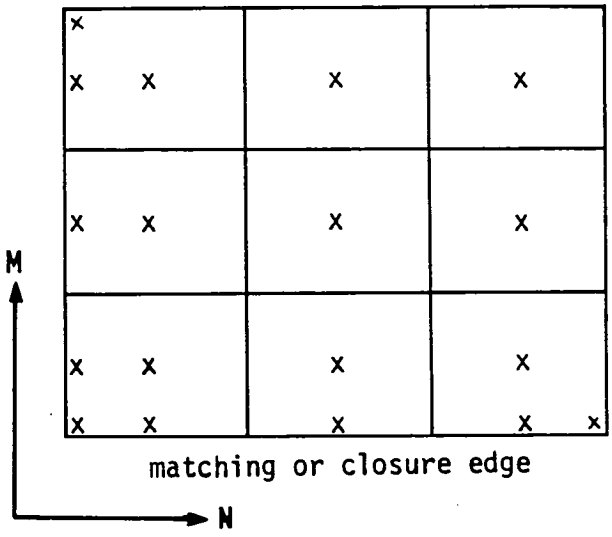

matching or closure edge

Figure H.3 - Concluded

Symmetry Condition:	$\hat{\phi}^S$	$\hat{\phi}^A$
Degenerate Boundary Condition	$\hat{\mu}^S = 0$	$\hat{\sigma}^A = 0$
Symmetry type of the degenerate boundary condition (cf. sec. (H.1.3))	antisymmetric	symmetric

Figure H.4a - Degenerate boundary conditions for configurations with one plane of symmetry

Control point lies in <u>first</u> plane of symmetry

Symmetry Condition:	$\hat{\phi}^{SS}$	$\hat{\phi}^{AS}$	$\hat{\phi}^{AA}$	$\hat{\phi}^{SA}$
Degenerate Boundary Condition	$\hat{\mu}^{SS} = 0$	$\hat{\sigma}^{AS} = 0$	$\hat{\sigma}^{AA} = 0$	$\hat{\mu}^{SA} = 0$
Symmetry Type	antisymmetric	symmetric	symmetric	antisymmetric

Control point lies in <u>second</u> plane of symmetry

Symmetry Condition:	$\hat{\phi}^{SS}$	$\hat{\phi}^{AS}$	$\hat{\phi}^{AA}$	$\hat{\phi}^{SA}$
Degenerate Boundary Condition	$\hat{\mu}^{SS} = 0$	$\hat{\mu}^{AS} = 0$	$\hat{\sigma}^{AA} = 0$	$\hat{\sigma}^{SA} = 0$
Symmetry Type	antisymmetric	antisymmetric	symmetric	symmetric

Figure H.4b - Degenerate boundary conditions for configurations with two planes of symmetry

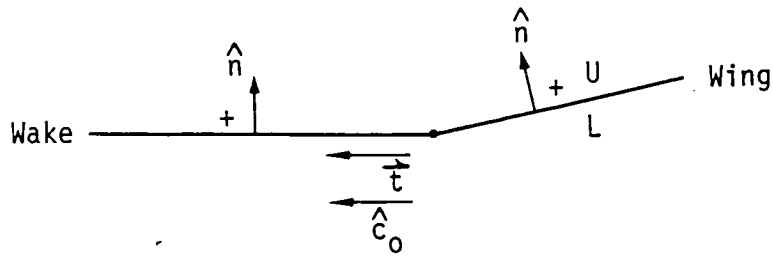

Figure H.5a - The velocity jump matching condition at a thin trailing edge (Vorticity matching)

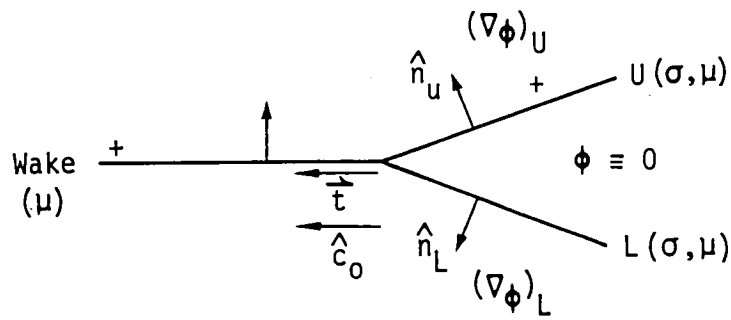

Figure H.5b - The velocity jump matching condition at a thick trailing edge (Vorticity matching)

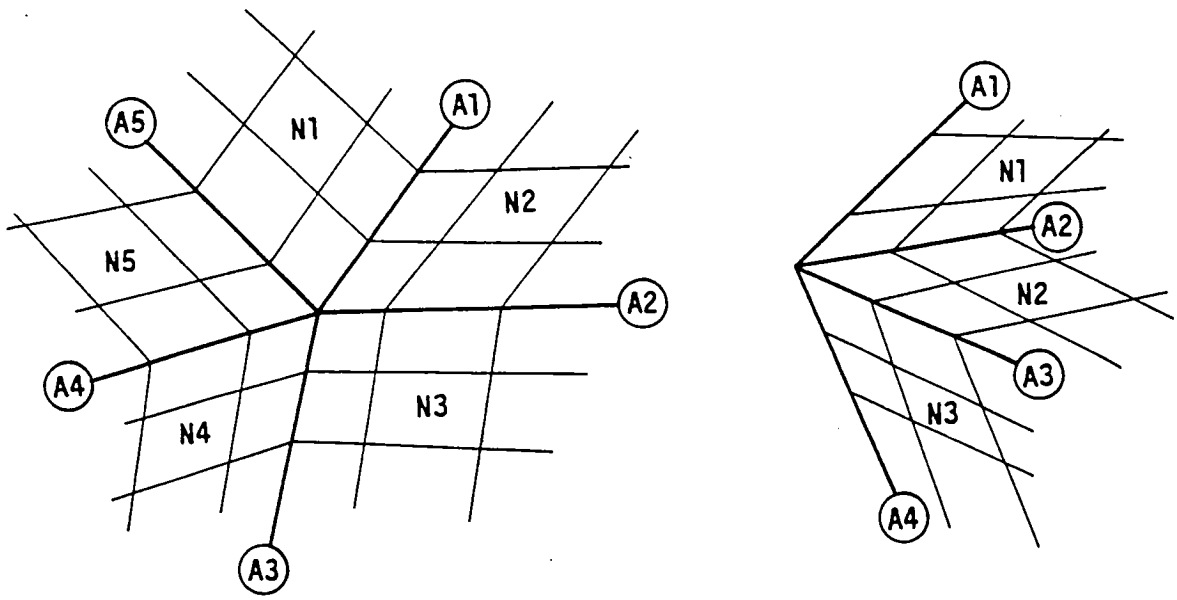

Abutment Intersection Configurations

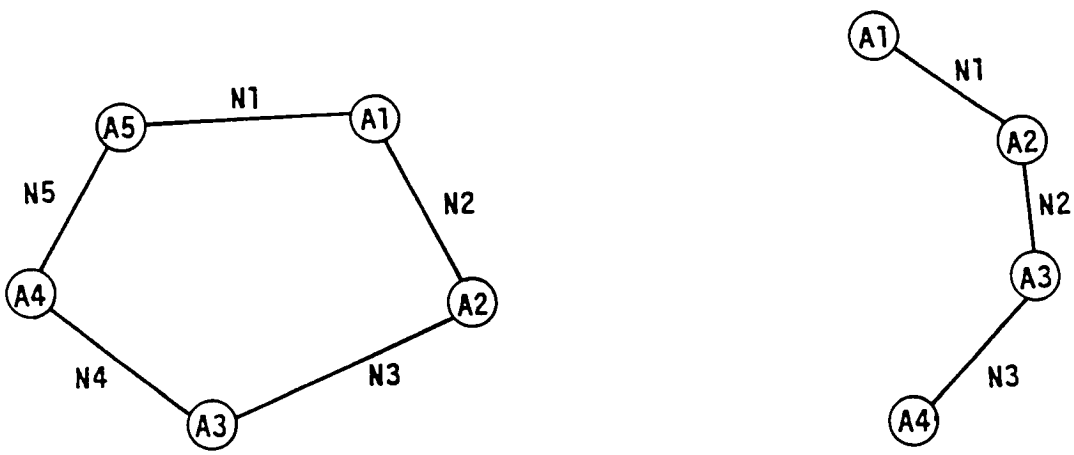

Associated Graphs (cf. appendix F.5)

Figure H.6 - Types of abutment intersections at which source matching is a reasonable boundary condition
Notation: A_k = Abutment k
N_j = Network j

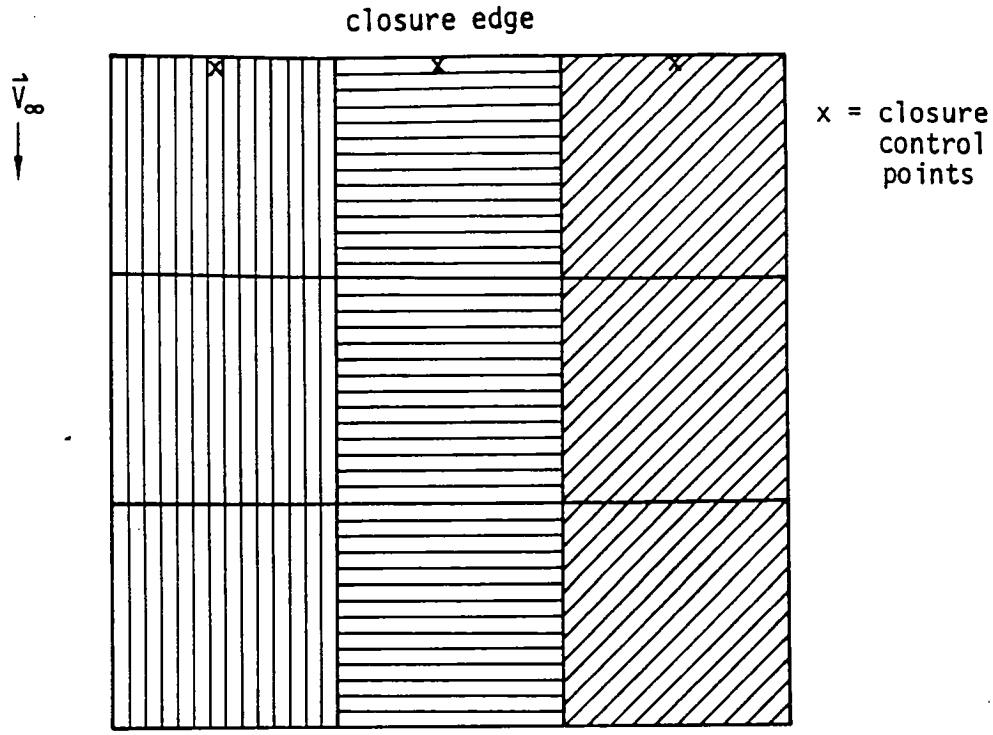

Figure H.7 - Columns of panels illustrated by cross-hatching

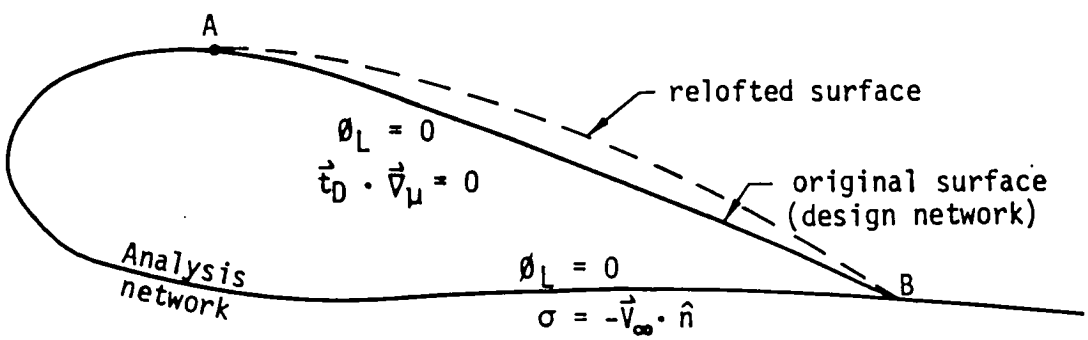

Figure H.8 - Design of upper surface of thick wing

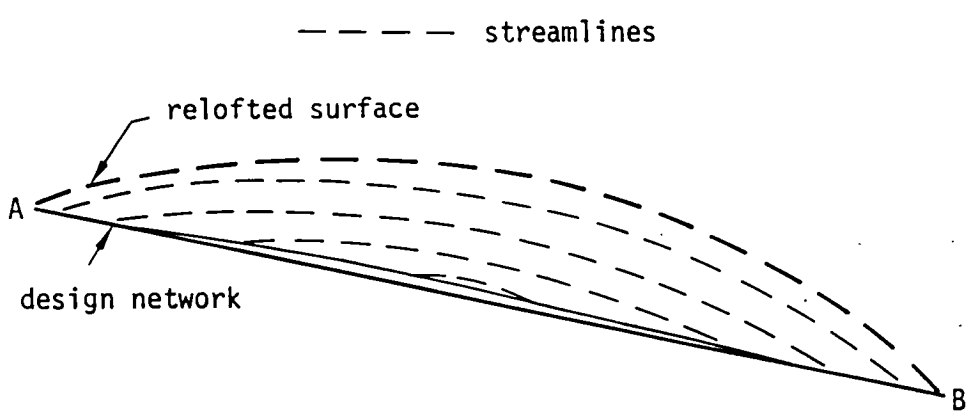

Figure H.9 - Pattern of streamlines on imposition of a closure boundary condition

Boundary Condition Category/ Hierarchy Ranking	Coefficient Restriction	Example
1	$c_D \neq 0$, all others $= 0$	$\mu = b$
2	$c_A \neq 0$, $a_A = \vec{t}_A = 0$	$\phi_A = b$
3	$a_A \neq 0$, $\vec{t}_A = 0$	$\vec{w}_A \cdot \hat{n} = b$
4	$\vec{t}_D \neq 0$, $a_A = c_A = \vec{t}_A = a_D = 0$	$\vec{t}_D \cdot \nabla\mu = b$
5	$\vec{t}_A \neq 0$	$\vec{t}_A \cdot \vec{v}_A = b$
6	$a_D \neq 0$, $a_A = c_A = \vec{t}_A = 0$	$\sigma = b$

Boundary Condition Category/ Hierarchy Ranking	c_D (μ)	t_D (∇_μ)	a_D (σ)	c_A (ϕ)	a_A (w_n)	t_A (v)
1	✓	0	0	0	0	0
4	?	✓	0	0	0	0
6	?	?	✓	0	0	0
2	?	?	?	✓	0	0
3	?	?	?	?	✓	0
5	?	?	?	?	?	✓

0 indicates the item must be zero

✓ indicates the item must be nonzero

? indicates the item is allowed to be zero or nonzero

Figure H.10 - User boundary condition hierarchy

Boundary Condition Category/ Hierarchy Ranking		c_D (μ) [A]	$\vec{t}_D$ (∇_μ) [A]	a_D (σ) [S]	c_A (ϕ) [S]	a_A (w_n) [A]	$\vec{t}_A$ ($\vec{v}$) [S]
1	[A]	✓	0	0	0	0	0
4	[A]	?	✓	0	0	0	0
6	[S]	0	0	✓	0	0	0
2	[S]	0	0	?	✓	0	0
3	[A]	?	?	0	0	✓	0
5	[S]	0	0	?	?	0	✓

BC Category/ Hierarchy Ranking	a_D (σ)	c_A (ϕ)	$\vec{t}_A$ ($\vec{v}$)
6	✓	0	0
2	?	✓	0
5	?	?	✓

Symmetric Boundary Condition Categories

BC Category/ Hierarchy Ranking	c_D (μ)	$\vec{t}_D$ (∇_μ)	a_A (w_n)
1	✓	0	0
4	?	✓	0
3	?	?	✓

Antisymmetric Boundary Condition Categories

0 indicates the item must be zero

? indicates the item is allowed to be zero or nonzero

✓ indicates the item must be nonzero

[S] indicates a term or boundary condition of symmetric type

[A] indicates a term or boundary condition of antisymmetric type

Figure H.11 - User boundary condition hierarchy for control points lying in a plane of symmetry

(a) Case: Closure condition of the form (H.2.22)
Note - this closure condition is of type [A], and must override doublet matching along the edge.
The network must have a non-null doublet type

$\hat{\phi}^S$ hierarchies

Composite Network		Doublet alone
[S]	[A]	[A]
[σ match]	$\hat{\mu}^S = 0$	$\hat{\mu}^S = 0$
bc_S^S	$-be_A^S-$	$-be_A^S-$

$\hat{\phi}^A$ hierarchies

Composite Network		Doublet alone
[S]	[A]	[A]
$\hat{\sigma}^A = 0$		closure
$-be_S^A-$	bc_A^A	bc_A^A

Figure H.12 - Possible boundary condition hierarchies for an edge control point in a plane of symmetry, closure is present

(b) Case: Closure condition of the form (H.2.23)
Note - this closure condition is of type $[S]$, and must override source matching along the edge.
The network must have a non-null source type

$\hat{\phi}^S$ hierarchies

Composite Network		Source alone
$[S]$	$[A]$	$[S]$
closure	$\hat{\mu}^S = 0$	closure
bc_S^S	$-be_{\bar{A}}^S-$	bc_S^S

$\hat{\phi}^A$ hierarchies

Composite Network		Source alone
$[S]$	$[A]$	$[S]$
$\hat{\sigma}^A = 0$	$[\mu \text{ match}]$	$\hat{\sigma}^A = 0$
$-be_{\bar{S}}^A-$	bc_A^A	$-be_{\bar{S}}^A-$

Figure H.12 - Continued

$\hat{\phi}^S$ hierarchies

Composite Network		Source alone	Doublet alone
[S]	[A]	[S]	[A]
[σ match]	$\hat{\mu}^S = 0$	[σ match]	$\hat{\mu}^S = 0$
bc_S^S	$-be_{\bar{A}}^S-$	bc_S^S	$-be_{\bar{A}}^S-$

$\hat{\phi}^A$ hierarchies

Composite Network		Source alone	Doublet alone
[S]	[A]	[S]	[A]
$\hat{\sigma}^A = 0$	[μ match]	$\hat{\sigma}^A = 0$	[μ match]
$-be_{\bar{S}}^A-$	bc_A^A	$-be_{\bar{S}}^A-$	bc_A^A

Figure H.13 - Boundary condition hierarchies for edge and corner control points in a plane of symmetry (no closure)

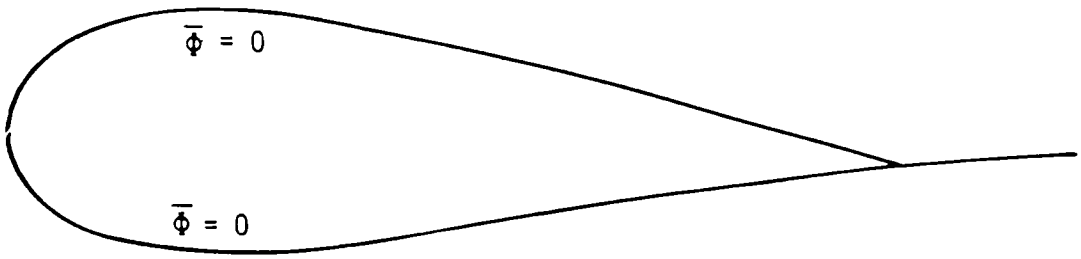

Figure H.14 - Total internal stagnation

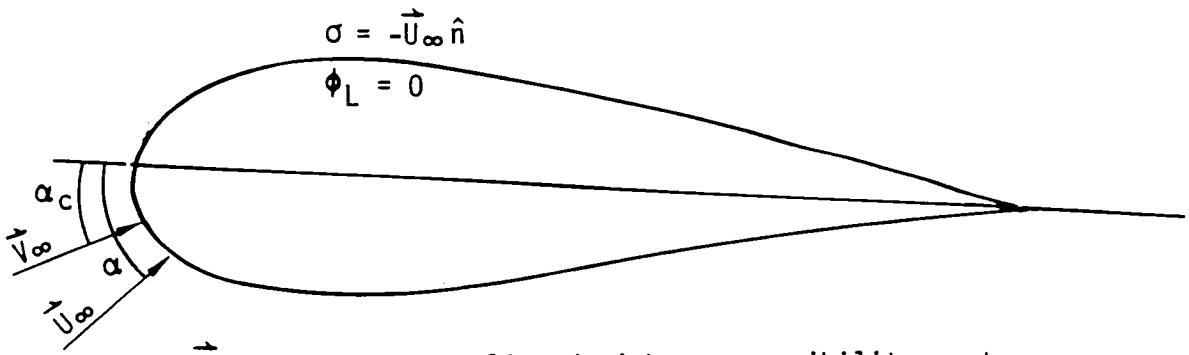

$\vec{V}_\infty$ = freestream aligned with compressibility vector

$\vec{U}_\infty$ = uniform onset flow

Figure H.15 - Onset flow, not parallel to compressibility direction

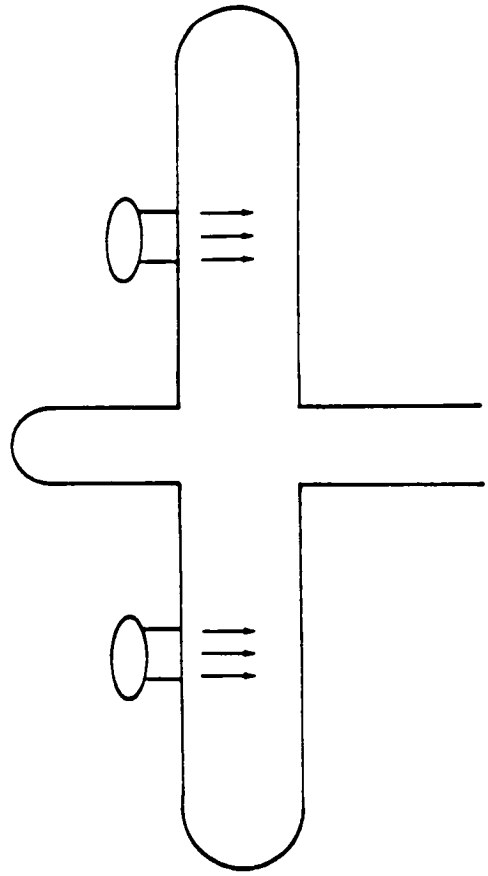

Figure H.16 - Propeller slipstream

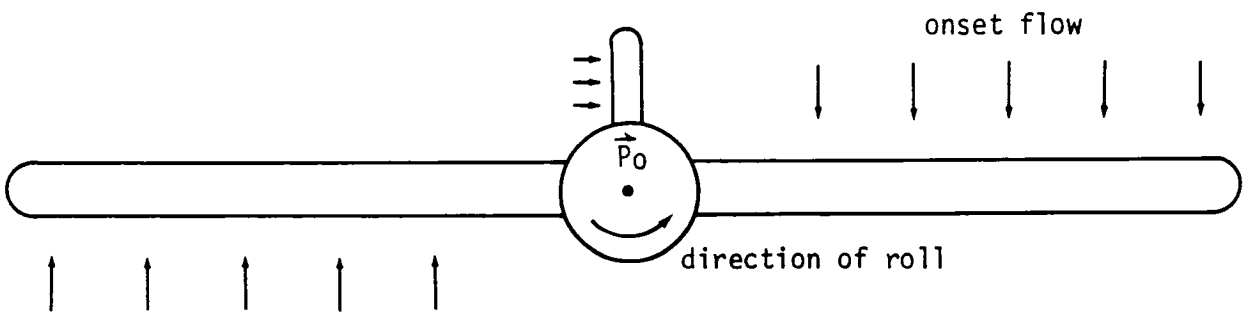

Figure H.17 - Airplane undergoing small rolling motion

I.0 Singularity Splines

Singularity splines define the source and doublet distributions on the entire configuration in terms of the source and doublet singularity parameters. These distributions are defined by a collection of matrices. First, the source and doublet distributions on a subpanel (recall from section 5.5 that a panel is partitioned into eight subpanels) are each defined by a "subpanel spline matrix" (denoted, respectively, $SPSPL^S$ and $SPSPL^D$) in terms of five "panel source parameters" and nine "panel doublet parameters." Thus there are eight of each of these matrices associated with each panel.

Next, the panel source and doublet parameters are defined by "outer spline matrices" (denoted, respectively, by B^S and B^D) in terms of singularity parameters located in the neighborhood of the panel. Each panel has associated with it a continuous doublet spline matrix, a continuous source spline matrix and, possibly, a discontinuous source spline matrix.

The subpanel spline matrices are defined by equation (5.5.7). That is, $[SPSPL^S]^{3x5}$ relates the three coefficients σ_0, σ_ξ, σ_η (which define a linear source distribution on the subpanel) to the five panel source parameters (that is, the source strengths at the five points on the panel illustrated in figure I.1a). Similarly, $[SPSPL^D]^{6x9}$ relates the six coefficients $\mu_0, \ldots, \mu_{\eta\eta}$ (which define a quadratic doublet distribution on the subpanel) to the nine panel doublet parameters (whose locations are illustrated in figure I.1b).

The outer spline matrices are defined by equation (5.5.8). That is, $[B^S]$ defines the five panel source parameters in terms of the neighboring source singularity parameters (generally nine in number), while $[B^D]$ defines the panel doublet parameters in terms of the neighboring doublet parameters (generally 21 in number).

The subpanel and outer spline matrices are used in the influence coefficient calculations. The subpanel spline matrices are first used in order to compute "panel influence coefficient" (PIC) matrices (see sections 4.4.2 and J.1), and the PIC matrices are multiplied by the outer spline matrices to obtain potential and velocity influence coefficient matrices ([ØIC] and [VIC]) which give the perturbation potential and velocity at a point, in terms of all singularity parameters, due to all the panels in the configuration (see sections 4.2.3 and 5.9.1).

In section I.1 we discuss the construction of outer spline matrices. While their construction is simple in principle, based on a least square procedure, in practice it is quite involved because there are many special cases. In particular, a special "edge spline" is used near network edges, which, in conjunction with the doublet matching boundary conditions discussed in Appendix F, results in precise matching of doublet strength along network edges. In section I.2 we describe the construction of subpanel spline matrices.

In section I.3 we discuss full panel and half panel spline matrices. These matrices define source and doublet distributions specified by single polynomials over the whole panel or half the panel, respectively, also in terms of the panel singularity parameters. The distributions are rough approximations to the 8 subpanel distributions defined by the subpanel splines. They are used in "intermediate field" influence coefficient calculation.

Next, in section I.4, we discuss "far field moments", matrices describing integrals of the singularity strength over a panel in terms of the panel singularity parameters. The matrices are used in far field influence coefficient calculation. Finally, in section I.5, we discuss the theory of the least squares procedure.

We now briefly discuss the reasoning behind the subpanel and outer spline construction techniques. First (cf. section C.3), we require the spline to be stable: the disturbance in the singularity distribution caused by a perturbation of a boundary condition should die off quickly.

Second, the source spline should be linearly accurate and the doublet spline quadratically accurate. That is, if the source parameters are defined by a linear function, the source distribution defined by the spline matrices should be exactly that linear function. An analogous property should hold for the doublet splines. The justification for using a linear source and quadratic doublet distribution is given in section B.5.

Third, the spline must be local in nature. That is, the singularity distribution on a panel must depend on a reasonably small number of singularity parameters. This is due to the storage problems which would occur otherwise. That is, too much core and disk storage would otherwise be required for each panel.

Fourth, the doublet strength should be continuous (see section B.4). It would be preferable to have continuously differentiable doublet strength, continuous source strength and smooth geometry as well, since these conditions would permit a further integration by parts of the influence coefficient integrals, reducing their singularity. Unfortunately, these goals are not achievable without an unacceptable increase in the cost of evaluation of influence coefficient integrals. Moreover, while it is a fairly straightforward matter to achieve a continuous source distribution, it has been found that without smooth geometry, continuous source splines induce significant errors in the total source strength on a network, seriously degrading the accuracy of the aerodynamic influence coefficient matrix.

Finally, the entries of the PIC matrices, which are defined as sums of integrals, should be computable in closed form. That is, numerical integration should not be required for the evaluation of the integrals. The reason for this requirement is one of simplicity. The integrands in (5.6.9-10) are far too singular to be integrated numerically as they stand. It might be possible to partition the integral into a regular part, integrable numerically, and singular part, integrable in closed form, but such a method has not yet been developed.

It is the avoidance of numerical integration, in combination with the maintenance of geometric continuity, that causes much of the complexity of the spline construction. Geometric continuity between panels can be maintained either by breaking up a panel into flat subpanels, or by defining a single curved panel. The integrals over the curved panel are not computable in closed form in supersonic flow, however.

Once one has decided to use flat subpanels, a minimum of five planar regions (those of figure 5.2) is mandated to achieve geometric continuity while avoiding any kink in the surface near a panel center control point. The use of eight subpanels has been chosen because it offers a convenient method of defining a continuous doublet distribution, while not requiring polynomials of degree greater than two. An explicit polynomial distribution has been chosen rather than a parametric distribution because the integration in parametric coordinates can not be performed in closed form.

I.1 Outer Splines

There are two basic methods that are used for the construction of outer splines, corresponding to the cases in which the resulting singularity distribution is required to be continuous, or is not. In PAN AIR, a continuous outer spline is constructed for the doublet distribution while both types of outer spline are constructed for the source distribution. The discontinuous source spline is used in the computation of influence coefficients and the evaluation of boundary conditions while the continuous source spline is used just in the post processing modules. (It was originally intended that the continuous source spline be used for all purposes. However its inability to conserve total source strength led to the introduction of discontinuous source splines in the solution portion of the code. Because the post-processing modules had built into them the assumption that source strength is single valued, the continuous source splines were retained for these essentially less demanding functions.)

The construction of continuous outer splines is a two step process. In the first step, row vectors SP^S and SP^D (called "spline vectors") are formulated for grid points as illustrated in Figure I.1c for some typical cases. These row vectors define the source or doublet strength at each enriched grid point in the network as a linear combination of surrounding singularity parameter values. In the second step, matrices $[B^S]$ and $[B^D]$ are constructed for each panel, giving the source or doublet strength at the appropriate grid points on the panel (panel singularity values) as linear combinations of values of singularity parameters in the neighborhood of the panel.

Thus the matrices $[B^S]$ have five rows while the $[B^D]$ have nine rows, since the source strength is defined at five points on a panel (the panel source parameter locations) by row vectors SP^S, while the doublet strength is defined at nine points by row vectors SP^D (see Figure I.1). The number of columns in a matrix B is variable: it equals the total number of distinct singularity parameters on which the panel source or doublet parameters depend. The matrices B are assembled from the required row vectors SP in a fairly straightforward manner described in the maintenance manual (see the preface of SUBROUTINE VECUNM of the DQG module). Briefly, first row vectors SP are computed for every grid point in the configuration (except that row vectors SP^S are not needed for panel source parameter locations) and stored on disk. Then, when the spline quantities for a single panel are being computed, the five (or nine) row vectors for each of the panel source (or doublet) singularity parameter are fetched from the disk. These row vectors are then amalgamated into a single matrix B^S (or B^D) by VECUNM.

In this section the discussion of continuous outer spline computation will simply describe the computation of individual row vectors SP^S or SP^D. The basic principle is simple. For source splines, the source strength at a grid point is fit in a linearly accurate manner to as few surrounding source parameters as possible while for doublet splines we do the same in a quadratically accurate manner. But while the basic principle is simple, implementation is complex because of a myriad of special cases which do not fit the general rules.

The construction of a discontinuous source outer spline matrix is also performed in two steps. First, a linear function of the form $\sigma_0+\sigma_\xi \xi+\sigma_\eta \eta$ is obtained by performing a least squares fitting procedure that formally uses the values of the global source parameters in the neighborhood of the panel. (Here, the variables ξ and η are local coordinates on the mean panel.) Second, this linear function is evaluated at the five panel source parameter locations, each evaluation generating a row of the source spline matrix, B^S.

I.1.1 Source Splines for Analysis Networks

I.1.1.1 Source Spline Vectors for Continuous Splines

Computing the row vector describing the source strength at the center of a panel in an analysis network is particularly simple, since a source singularity parameter is located there. Thus the source strength is just the singularity parameter value; that is,

$$\sigma g = \lambda_k^S = \lfloor 1 \rfloor \lambda_k^S \tag{I.1.1a}$$

$$\text{or} \quad \lfloor SP^S \rfloor = \lfloor 1 \rfloor \tag{I.1.1b}$$

the row vector of length 1 with unit value.

I.1.1.2 Neighboring Singularity Parameters

Next, to find the source strength at a panel corner, we perform a "bilinear fit" (a process to be described below) to the four surrounding source parameter values. In Figure I.2, we show the variety of cases which may occur in the course of determining the four neighboring source parameter locations. In the "standard" case (A), the four source parameters are the obvious adjacent ones. In cases (B) and (C), the network edge precludes the existence of some of the obvious choices, and neighboring parameters must be obtained by reaching toward the interior of the network. The logic used for points B or C, however, when extended to D, results in a large number of neighboring source parameters. To keep storage to a minimum, we choose (in a fairly arbitrary manner) from this set of points, those points which are as far as possible in index from the uncollapsed edges of the network.

I.1.1.3 Computation of a Local Coordinate System

Next we compute the source strength at a panel corner in terms of the four surrounding singularity parameter values, once we have in fact located these four parameters. The first step is to form a local coordinate system whose (ξ, η) plane is the one in which the source strength is to vary linearly.

The four singularity parameter locations determine (generally non-orthogonal) basis vectors $\vec{v}_\xi$ and $\vec{v}_\eta$, connecting pairs of panel edge midpoints, for this coordinate system as follows. Let P_0 be the grid point at which we wish to find the source strength. Then for any point P on the network, we want to be able to determine coordinates $\xi(P)$, $\eta(P)$, $\zeta(P)$, such that

$$(\vec{P} - \vec{P}_0) = \xi(P)\,\vec{v}_\xi + \eta(P)\,\vec{v}_\eta + \zeta(P)\,\vec{v}_\zeta \tag{I.1.2}$$

The (ξ, η, ζ) coordinates used here (in section I.1) are not related to the X' coordinate system (also denoted (ξ, η, ζ) at times) used in Appendix E and section I.2. Here, $\vec{v}_\zeta$ is a vector perpendicular to the plane spanned by $\vec{v}_\xi$ and $\vec{v}_\eta$. Such a vector is, of course, a multiple of $\vec{v}_\xi \times \vec{v}_\eta$, but a simple dimensional argument shows that if $\vec{v}_\zeta$ is to be independent of the scale of coordinates (that is, if $\vec{v}_\zeta$ is to be doubled when every point coordinate in the network is doubled), we must have

$$\vec{v}_\zeta = \frac{\vec{v}_\xi \times \vec{v}_\eta}{\left|\vec{v}_\xi \times \vec{v}_\eta\right|^{1/2}} \tag{I.1.3}$$

Now, to find the functions which define ξ, η, and ζ, let us first take the cross product of (I.1.2) with $\vec{v}_\xi$ on the left, and then the dot product with $\vec{v}_\zeta$. Next, we take the cross product with $\vec{v}_\eta$ on the right, and then take the dot product with $\vec{v}_\zeta$. Since

$$\begin{aligned}
\vec{v}_\xi \times \vec{v}_\xi &= 0 = \vec{v}_\eta \times \vec{v}_\eta \\
\vec{v}_\xi \cdot \vec{v}_\zeta &= 0 = \vec{v}_\eta \cdot \vec{v}_\zeta \\
(\vec{v}_\xi \times \vec{v}_\zeta) \cdot v_\zeta &= 0 = (\vec{v}_\zeta \times \vec{v}_\eta) \cdot \vec{v}_\zeta
\end{aligned} \tag{I.1.4}$$

we obtain

$$\begin{aligned}
\vec{v}_\xi \times (\vec{P} - \vec{P}_0) &= \eta(P)\,(\vec{v}_\xi \times \vec{v}_\eta) \\
(\vec{P} - \vec{P}_0) \times \vec{v}_\eta &= \xi(P)\,(\vec{v}_\xi \times \vec{v}_\eta) \\
(\vec{P} - \vec{P}_0) \cdot \vec{v}_\zeta &= \zeta(P)\,(\vec{v}_\zeta \cdot \vec{v}_\zeta)
\end{aligned} \tag{I.1.5}$$

Dotting the first two equations with $\vec{v}_\zeta$, we have

$$\vec{v}_\xi \times (\vec{P} - \vec{P}_0) \cdot \vec{v}_\zeta = \eta(P)\,(\vec{v}_\xi \times \vec{v}_\eta) \cdot \vec{v}_\zeta = \eta(P)\left|\vec{v}_\xi \times \vec{v}_\eta\right|^{3/2} \tag{I.1.6}$$

Thus,

$$\xi(P) = \frac{(\vec{P} - \vec{P}_0) \times \vec{v}_\eta \cdot \vec{v}_\zeta}{\left|\vec{v}_\xi \times \vec{v}_\eta\right|^{3/2}} \qquad \zeta(P) = \frac{(\vec{P} - \vec{P}_0) \cdot \vec{v}_\zeta}{\left|\vec{v}_\xi \times \vec{v}_\eta\right|} \tag{I.1.7}$$

I.1.1.4 The Bilinear Fit at Panel Corner Points

Now, let $P_1,\ldots,P_4$ be the four source parameter locations for any of the cases illustrated in figure I.2, and let $\lambda_i^S = \sigma(P_i)$ denote these source singularity parameters. Then these four values of source strength define a "bilinear" function in ξ and η, that is, a function

$$\sigma(\xi, \eta) = \sigma_0 + \sigma_1\xi + \sigma_2\eta + \sigma_3\xi\eta \tag{I.1.8}$$

(where the symbol σ_0 as used in section I.1 has a different meaning than in section 5 or the remainder of Appendix I), which takes on exactly these four values. The function $\sigma(\xi, \eta)$ is defined by the fitting condition

$$\begin{Bmatrix} \lambda_1^S \\ \lambda_2^S \\ \lambda_3^S \\ \lambda_4^S \end{Bmatrix} = \begin{bmatrix} 1 & \xi(P_1) & \eta(P_1) & \xi(P_1)\eta(P_1) \\ \hdashline 1 & \xi(P_4) & \eta(P_4) & \xi(P_4)\eta(P_4) \end{bmatrix} \begin{Bmatrix} \sigma_0 \\ \sigma_1 \\ \sigma_2 \\ \sigma_3 \end{Bmatrix}$$

$$= [BL] \begin{Bmatrix} \sigma_0 \\ \sigma_1 \\ \sigma_2 \\ \sigma_3 \end{Bmatrix} \tag{I.1.9}$$

and thus

$$\begin{Bmatrix} \sigma_0 \\ \sigma_1 \\ \sigma_2 \\ \sigma_3 \end{Bmatrix} = [BL]^{-1} \begin{Bmatrix} \lambda_1^S \\ \lambda_2^S \\ \lambda_2^S \\ \lambda_4^S \end{Bmatrix} \tag{I.1.10}$$

The points $P_1,\ldots,P_4$ are not coplanar in general, and thus computing $\sigma(\xi,\eta)$ by (I.1.10) in terms of surrounding source parameters, ignores the ζ-component of the parameter locations; in other words, we project the parameter locations to the plane defined by $\vec{v}_\xi$ and $\vec{v}_\eta$. This is justifiable

in view of the fact that a reasonable number of panels should be used in defining a geometric surface, and thus the distortions due to curvature can be neglected locally.

Now, by (I.1.7), $\xi(P_0) = \eta(P_0) = 0$, and thus by (I.1.8),

$$\sigma(P_0) = \sigma_0 \tag{I.1.11}$$

Thus by (I.1.10),

$$\sigma(P_0) = \sigma_0 = \lfloor 1 \quad 0 \quad 0 \quad 0 \rfloor [BL]^{-1} \begin{Bmatrix} \lambda_1^S \\ \vdots \\ \lambda_4^S \end{Bmatrix} \tag{I.1.12}$$

Setting

$$\lfloor SP^S \rfloor = \lfloor 1 \quad 0 \quad 0 \quad 0 \rfloor [BL]^{-1} \tag{I.1.13}$$

we see that

$$\sigma(P_0) = \lfloor SP^S \rfloor \begin{Bmatrix} \lambda_1^S \\ \vdots \\ \lambda_4^S \end{Bmatrix} \tag{I.1.14}$$

Note that $\lfloor SP^S \rfloor$ is just the first row of $[BL]^{-1}$. Now, by (I.1.14), SP^S is just the row vector we seek; namely, it gives the value of source strength at the point P_0 as a linear combination of four neighboring singularity parameters. A spline vector may similarly be constructed for every panel corner point in the network, whereupon matrices B^S may be computed for each panel as discussed at the beginning of section I.1.

This concludes the discussion of continuous source spline construction for source analysis networks. Two special cases, networks with only one row or column, and networks with only one panel, are discussed in the maintenance document (see section 4-I.4 and SUBROUTINE ONDFIT of the DQG module).

I.1.1.5 Discontinuous Source Analysis Splines

The construction of a panel's discontinuous source analysis spline, required for computation of influence coefficients, is achieved by solving for coefficients σ_0, σ_ξ, σ_η of the weighted linear least squares problem

$$\min_{\sigma_0, \sigma_\xi, \sigma_\eta} G$$

where the quadratic form G is defined by

$$G = \sum_{i=1}^{n} [w_i(\sigma_0 + \sigma_\xi \xi_i + \sigma_\eta \eta_i - \lambda_i^S)]^2$$

Here, w_i denotes a weight and λ_i^S is a global source parameter at some point $\vec{p}_i$ in the neighborhood of the panel. The coordinates (ξ_i, η_i) are obtained by performing a length preserving projection of $\vec{p}_i$ onto the panel's mean plane followed by a transformation of this projected point into the mean plane coordinate system. Passing over for the present the selection of w_i and λ_i^S, we observe that the minimization problem we have posed has a solution of the form

$$\begin{Bmatrix} \sigma_0 \\ \sigma_\xi \\ \sigma_\eta \end{Bmatrix} = \begin{bmatrix} & & \\ & A^+ & \\ & & \end{bmatrix} \begin{Bmatrix} \lambda_1^S \\ \lambda_2^S \\ \vdots \\ \lambda_n^S \end{Bmatrix}$$

Here, we have used the conventional notation A+ to denote a matrix pseudo-inverse. Now, letting $(\hat{\xi}_k, \hat{\eta}_k)$, $k = 1,\ldots,5$ denote mean plane coordinates of the projection* of the five panel source parameter locations onto the mean plane, we may evaluate the five panel source parameters by

$$\sigma_k = \sigma_0 + \sigma_\xi \hat{\xi}_k + \sigma_\eta \hat{\eta}_k$$

This evaluation process induces an expression for σ_k in terms of λ_i^S, providing a definition for $[B^S]$, the source outer spline,

$$\begin{Bmatrix} \sigma_1 \\ \sigma_2 \\ \vdots \\ \sigma_5 \end{Bmatrix} = \begin{bmatrix} 1 & \hat{\xi}_1 & \hat{\eta}_1 \\ 1 & \hat{\xi}_2 & \hat{\eta}_2 \\ & \vdots & \\ 1 & \hat{\xi}_5 & \hat{\eta}_5 \end{bmatrix} \begin{bmatrix} & & \\ & A^+ & \\ & & \end{bmatrix} \begin{Bmatrix} \lambda_1^S \\ \lambda_2^S \\ \vdots \\ \lambda_n^S \end{Bmatrix}$$

$$= [B^S] \vec{\lambda}$$

* This projection is performed in scaled coordinates.

We now return to the problem of selection of weights and global source parameters to be used in the fitting process. In Figure I.3 we illustrate the variety of cases which may arise when identifying the neighboring source parameters to be used in spline construction. For any given panel, the parameters λ_i^S are selected as indicated. The weights w_i are chosen as follows:

$$w_i = \begin{cases} 1 & \text{if } \lambda_i^S \text{ does not lie on the panel for which } B^S \text{ is being computed} \\ 10000 & \text{if } \lambda_i^S \text{ lies on the panel} \end{cases}$$

The choice of a very large weight for the panel's own source parameter is crucial in that it is this condition that causes total source strength for the panel to be correct to sufficient accuracy.

The foregoing procedure will fail to provide enough data points if the network in which the panel lies has only one row or column of panels. When this happens, points $\vec{p}_i$ are selected as indicated in Figure I.4. The value of λ_i^S used for points $\vec{p}_i$ that are not global source parameter points is just the value of source strength at the panel center.

I.1.2 Doublet Spline Vectors for Analysis Networks, Doublet Forward Weighted Splines

Doublet spline vectors SP^D are more complex to compute for a variety of reasons. First, the requirement of quadratic accuracy forces the doublet strength at a grid point to depend on a greater number of singularity parameters than the source strength. Second, to insure doublet continuity across network edges on non-smooth abutments (along which boundary conditions specifying the matching of doublet strength are imposed), we require that the doublet strength at any point on a network edge depend only on the singularity parameters located on the network edge. The example of a thin wing with a curved planform illustrates the need for this requirement (cf. Figure I.5). The doublet strength is zero at the singularity parameter locations on the free network edge. If the doublet strength at a panel corner point on the edge depended on singularity parameters in the interior, it could not be zero, independent of conditions in the network interior, as we wish it to be. But by insisting that it only depend on edge parameters, we insure that it is zero.

A third cause of increased complexity in determining doublet spline row vectors is the introduction of "smooth abutments." These are abutments consisting of portions of two distinct network edges, along which splines rather than boundary conditions are used to enforce continuity of doublet strength.

For grid points which do not lie on a network edge, obtaining the row vector SP^D which describes the doublet strength at each grid point in terms of surrounding singularity parameters is a two step process. First, the set of surrounding singularity parameters is determined. Second, the doublet strength at the grid point is determined in a quadratically accurate manner in terms of the neighboring singularity parameters.

Doublet forward weighted (DFW) spline vectors are calculated in the same manner as the doublet analysis spline vectors. The only difference being weighting factors used in the least squares fit. A description of the different weighting scheme is given in section I.1.2.4.

I.1.2.1 The Quadratic Least Squares Fit for Panel Corners or Panel Edge Midpoints

This quadratically accurate procedure is somewhat more complex than the bilinear fit employed for source splines. While there is generally a bilinear function which exactly fits values at four points (unless three of the four lie on a line, which is unlikely if they are panel centers), a quadratic function is less well behaved. There is a unique quadratic through six points, unless these points all lie on two lines. With very regular paneling, however, it is quite likely that six center points chosen as neighbors of a grid point will, in fact, lie on two lines. Thus, the procedure we choose for the quadratic fit is a "least squares" procedure.

That is, we choose an excessive number of neighboring singularity parameters, and find the quadratic function which takes on the values of the closest singularity parameters exactly, while taking on the the values of the remaining singularity parameters in a "least squares" sense. The row vector SP^D for the grid point is determined by the value the fitting function takes on at the grid point, expressed as a linear combination of the neighboring singularity parameter values.

We now describe this least squares procedure more precisely. Let $(\lambda_i^D,\ i = 1,\ldots,k)$ be the singularity parameters (in the neighborhood of the selected grid point) to which we fit the quadratic function exactly. Let $(\lambda_i^D,\ i = k+1,\ldots,k+m)$ be the remaining neighboring singularity parameters. Let λ_i^D be located at $(\xi_i,\ \eta_i,\ \zeta_i)$, where the computation of these coordinates will be discussed shortly. Once again, however, this is not the local $(\xi,\ \eta,\ \zeta)$ coordinate system denoted X' in Appendix E.

Let A be the matrix

$$A = \begin{bmatrix} 1 & \xi_1 & \eta_1 & 1/2\ \xi_1^2 & \xi_1\ \eta_1 & 1/2\ \eta_1^2 \\ \hdashline 1 & \xi_k & \eta_k & 1/2\ \xi_k^2 & \xi_k\ \eta_k & 1/2\ \eta_k^2 \end{bmatrix} \tag{I.1.15}$$

This is the matrix for which any function

$$f(\xi,\ \eta) = f_1 + f_2\xi + f_3\ \eta + 1/2\ f_4\ \xi^2 + f_5\ \xi\eta + 1/2\ f_6\ \eta^2 \tag{I.1.16}$$

taking on the values

$$f(\xi_i, \eta_i) = \lambda_i^D \qquad i = 1, \ldots, k \tag{I.1.17}$$

satisfies

$$[A]^{k\times 6} \begin{Bmatrix} f_1 \\ f_2 \\ \vdots \\ f_6 \end{Bmatrix} = \begin{Bmatrix} \lambda_1^D \\ \lambda_2^D \\ \vdots \\ \lambda_k^D \end{Bmatrix} \tag{I.1.18}$$

Now, whenever $k < 6$, as it will be in the current applications, equation (I.1.18) does not fully specify the coefficients of f. The coefficients are completely specified by requiring the minimization of

$$I = \sum_{i=k+1}^{k+m} w_i^2 \; [f(\xi_i, \eta_i) - \lambda_i^D]^2 \tag{I.1.19}$$

where w_i is a "weight", to be discussed shortly, which depends on the relative locations of the singularity parameter and the grid point.

If we write

$$[A_1]^{m\times 6} = \begin{bmatrix} 1 & \xi_{k+1} & \eta_{k+1} & 1/2\,\xi_{k+1}^2 & \xi_{k+1}\eta_{k+1} & 1/2\eta_{k+1}^2 \\ & & & & & \\ 1 & \xi_{k+m} & \eta_{k+m} & 1/2\,\xi_{k+m}^2 & \xi_{k+m}\eta_{k+m} & 1/2\eta_{k+m}^2 \end{bmatrix} \tag{I.1.20}$$

equation (I.1.19) becomes

$$I = \sum_{i=k+1}^{k+m} w_i^2 \left(\sum_{s=1}^{6} (A'_{i-k,s}) f_s - \lambda_i^D \right)^2 \tag{I.1.21}$$

The method by which we minimize (I.1.21), subject to the exact conditions (I.1.18), is called a "constrained least squares" procedure, and is discussed in section I.5. The result of performing this procedure is a (6 x (k+m)) matrix LSQ such that

$$\begin{Bmatrix} f_1 \\ \vdots \\ f_6 \end{Bmatrix} = [LSQ] \begin{Bmatrix} \lambda_1^D \\ \cdot \\ \cdot \\ \cdot \\ \lambda_{k+m}^D \end{Bmatrix} \tag{I.1.22}$$

Now, we will construct our (ξ, η, ζ) coordinate system such that at the grid point P_0 we have

$$\begin{aligned} \xi(P_0) &= 0 \\ \eta(P_0) &= 0 \end{aligned} \tag{I.1.23}$$

Thus,

$$f(P_0) = f_1 = \lfloor LSQ_{1,\cdot} \rfloor \begin{Bmatrix} \lambda_1^D \\ \vdots \\ \lambda_{k+m}^D \end{Bmatrix} \tag{I.1.24}$$

But we required the row vector SP^D to define the value at P_0 of the quadratic function f which satisfied (I.1.18) while minimizing (I.1.21), and thus

$$\lfloor SP^D \rfloor = \lfloor LSQ_{1,\cdot} \rfloor \tag{I.1.25}$$

that is, SP^D is the first row vector of the matrix LSQ defined by the constrained least squares procedure.

In describing the construction of SP^D for a grid point in a network interior, we have deferred the discussion of three items. These are the determination of the set of neighboring singularity parameters, their (ξ, η, ζ) coordinates, and the corresponding weights w_i. We will discuss them in order as follows.

I.1.2.2 Neighboring Points for Least Squares Fit

Figure I.6a illustrates the location of neighboring singularity parameters for grid points which do not lie near a network edge. Note that, since a singularity parameter is located at each panel center, the spline vector SP^D for a panel center point is (like the spline vector SP^S) a vector of length 1 with a unit entry.

Now, if the grid point (panel corner or edge midpoint) lies near (but not on) a network edge, the set of neighbors must include singularity parameters on the network edge. Actually, we fit a quadratic function to neighboring grid points, where these grid point need only be singularity parameter locations when they are in the interior of the network. The value of doublet

strength at those grid points which lie on the network edge depends in turn on a small number of singularity parameters located on the network edge. This is a procedure which is defined in detail in the maintenance document (see section 4-I).

Figure I.6b illustrates the neighboring points we use for the quadratic fit to obtain a spline vector for a grid point which lies near (but not on) a network edge which does not belong to a smooth abutment. Recall that only one singularity parameter is located on a collapsed edge of a network.

Figure I.6c illustrates the set of neighboring points when the grid point in question lies near a smooth abutment. In this case, we see that the set of "neighboring points" may lie in two distinct networks. This is because the singularity parameters on the network edges on the smooth abutment (though not at the corner points at the ends of the abutment) have been removed for reasons of economy. The neighboring points in the same network as the point P_0 are chosen in the usual manner (see Figure I.6a) while those in the adjacent network are chosen as illustrated. The precise method by which the latter points are picked is described in the maintenance document (section 4-I.2.1.2).

I.1.2.3 Construction of a Local Coordinate System

Next we discuss the construction of a (ξ, η, ζ) coordinate system. This system is similar but not identical to that of section I.1.1.3, and totally distinct from the X' coordinate system X' of Appendix E or section I.2.2.5. First, we construct basis vectors $\vec{v}_\xi$ and $\vec{v}_\eta$ as illustrated in Figure I.7 That is, $\vec{v}_\xi$ and $\vec{v}_\eta$ span pairs of enriched grid points adjacent to the base point P_0. Next, we define $\vec{v}$ by (I.1.3). Then, analogously to (I.1.17), we define

$$\vec{\xi}(P) = \frac{(\vec{P} - \vec{P}_0) \times \vec{v}_\eta \cdot \vec{v}_\zeta}{|\vec{v}_\xi \times \vec{v}_\eta|^{3/2}} \qquad \eta(P) = \frac{\vec{v}_\xi \times (\vec{P} - \vec{P}_0) \cdot \vec{v}_\zeta}{|\vec{v}_\xi \times \vec{v}_\eta|^{3/2}} \qquad \vec{\xi}(P) = \frac{(\vec{P} - \vec{P}_0) \cdot \vec{v}_\zeta}{|\vec{v}_\xi \times \vec{v}_\eta|} \tag{I.1.26}$$

The bars indicate that these are preliminary coordinate values which will be adjusted to account for surface curvature. Consider a cylindrical surface, as illustrated in Figure I.8 If we use the coordinates ξ and η above, we are essentially projecting the surface down to the tangent plane at the point P_0. When the surface is highly curved, this makes the points A and D appear to be closer to P_0 than they really are, since we are dealing with their projected images A' and D'. The points B' and C' are also closer to the grid point than B and C, but not in the same proportion.

We rectify this by scaling the ξ and η coordinates of a point according to its height above the tangent plane. We define a scaling factor

$$A(P) = \frac{\left[\bar{\xi}(P)^2 + \bar{\eta}(P)^2 + \bar{\zeta}(P)^2\right]}{\bar{\xi}(P)^2 + \bar{\eta}(P)^2} \tag{I.1.27}$$

Then we define

$$\xi(P) = A(P)\,\vec{\xi}(P)$$

$$\eta(P) = A(P)\,\vec{\eta}(P) \qquad \text{(I.1.28)}$$

This coordinate scaling assures that the contribution of distant points is more accurately measured. Note that the denominator of A(P) is non-zero provided $P \neq P_0$.

I.1.2.4 Weights for the Least Squares Fit

Next we consider the weights w_i for the least squares procedure. In order to provide stability, we would like to fit more closely to nearby singularity parameters than further ones. This is done in part by fitting the quadratic function exactly to the nearest parameters, as illustrated by Figure I.6.

A second consideration in determining weights is the desire to give heavier weights in supersonic flow to points which are upstream of the grid point than to those which are downstream. This weighting has been found experimentally to reduce instabilities which arise at high Mach numbers. In recognition of these requirements, we set $w_i = w(P)$ where

$$w(P) = \frac{1 + kM_\infty(1 - \hat{c}_0 \cdot (\vec{P} - \vec{P}_0)/\,|\vec{P} - \vec{P}_0|)}{(1 + 2\,kM_\infty)} \qquad \text{(I.1.29)}$$

The constant k is set to zero in subsonic flow in view of the lack of a preferred upstream direction. That is, the compressibility direction c_0 may be replaced by $-\hat{c}_0$ without changing the solution to the equation. In supersonic flow, k has been chosen by experiment, and has order of magnitude 1.

Since the dot product of unit vectors lies between -1 and 1, the numerator of (I.1.29) lies between 1 and $(1 + 2k\,M_\infty)$. Thus the ratio of weight (neglecting the effect of distance) at a directly upstream point to that at a directly downstream point is $1 + 2k\,M_\infty$. For $M_\infty = 3$, and $k = 1$ (the provisional choice for k), this ratio is 7.

The weights for the doublet forward weighted splines are obtained from equation I.1.29 by setting $k = 1$ and $M_\infty = 2$. Thus, the simple expedient of changing the weights in a least squares fit transforms a doublet analysis spline into a doublet design spline (DFW).

I.1.2.5 Edge Splines for Non-Smooth Abutments

Finally we consider grid points (panel corner points or edge midpoints) lying on a network edge. A network edge is divided into distinct portions belonging to different abutments. A doublet parameter is located at the grid points which form the endpoints of the portion of the edge belonging to the abutment (if such an endpoint is not a network corner point, the doublet parameter is an "extra" singularity parameter (see figure 5.13)). Doublet

parameters are also located at the panel edge midpoints unless the abutment is a smooth one, in which case the parameters are removed (doublet parameters located at abutment endpoints are retained for simplicity).

We discuss first the case of a non-smooth abutment. In that case, the value of doublet strength at a grid point depends only on singularity parameters located on the network edge.

Consider the abutment illustrated in Figure I.9a, with one network edge panelled more finely than the other and with a panel corner on the more finely paneled network located wherever the more coarsely paneled network edge has a panel corner. The goal is to find a splining method such that the imposition of doublet matching boundary conditions of some or all of the control points on the edge results in the exact matching of doublet strength on the whole edge.

Experimentation with least-squares-type splines shows that they cannot satisfy the above considerations. Let us consider, on the other hand, a differentiable spline. Let the edge be divided into n intervals, as illustrated in Figure I.9b. It is reasonable to ask how many differentiable functions exist, defined by a single quadratic on each of the n intervals. Now, there are 3n linearly independent quadratic functions altogether (since a quadratic function on an interval has 3 coefficients), and requiring continuity at $P_2,\ldots,P_{n-1}$ yields (n-1) constraints on the set of functions, while requiring continuity of derivative at these points provides (n-1) additional constraints. Thus, there are (n+2) linearly independent piecewise quadratic functions with continuous derivatives.

But this is equal to the number of control points on the edge, and so there is a unique differentiable function which takes on a prescribed set of (n + 2) values at the midpoints of the intervals and the endpoints of the edge.

We can apply this result to the situation illustrated by Figure I.9a The doublet distribution on the edge 1 will consist of some differentiable function defined by a single quadratic on each interval of edge 1. If we now impose doublet matching boundary conditions at the control points of edge 2, we obtain on edge 2 the unique differentiable doublet distribution defined as a single quadratic on each interval of edge 2, which agrees with the doublet distribution on edge 1 at the specified points. But, since every interval of edge 2 is a subset of a corresponding interval on edge 1, the doublet distribution on edge 1 satisfies the above criterion too. So, since the distribution is unique, the doublet distributions on edge 1 and edge 2 are identical.

Summarizing, we have shown that if edges 1 and 2 form an abutment, and the paneling on edge 2 is a "refinement" of the paneling on edge 1 (that is, every corner point of edge 1 is also a corner point on edge 2, though edge 2 may have additional corner points), then the imposition of doublet matching at the control points of edge 2 results in exact matching of doublet strength along the entire abutment. Generalizing, if several network edges meet in an abutment, and one edge is a refinement of each of the other edges, then the imposition of doublet matching boundary conditions on that edge forces the alternating sum of the doublet strengths to zero:

$$\sum s_i \mu_i = 0 \qquad (I.1.30)$$

where $s_i = \pm 1$.

Unfortunately, the differentiable edge spline, while leading to doublet continuity under a greater variety of circumstances, does not permit forward weighting in supersonic flow. As a result, the differentiable edge spline is insufficiently stable and cannot be used in Pan Air. This fact was determined fairly late in the development of Pan Air, and thus a discussion of the differentiable edge spline has been included in this document.

The spline which is actually implemented in Pan Air is a one dimension quadratic least squares fit. Consider, for instance, a network edge as illustrated in figure I.9b. The points $P_1, \ldots, P_{n+1}$, and M_i, $i=1,\ldots,n$, are singularity parameter locations, and the doublet strength there is defined to be equal to the value of the singularity located there. Thus the doublet spline vector SP^D for each of these points is a unit vector of length one, as it is for panel center points in a doublet analysis network.

Next, the doublet strength at the points P_i, $i=2,\ldots,n-1$, is obtained by a constrained least squares analgous to that described in section I.1.2.1, but in one dimension. That is, the quadratic function $f(t)$ (t a variable defining distance along the network edge) is found such that

$$f(M_k) = \mu(M_k) = \lambda_k^D \qquad k = i, i+1 \tag{I.1.31a}$$

and

$$f(M_r) = \mu(M_r) = \lambda_r^D \qquad r = i-1,\ i+2 \tag{I.1.31b}$$

in a least squares sense.

Then the row vector SP^D which defines $\mu(P_i)$ in terms of the singularity parameters (λ_k^D, $k= i-1,\ldots, i+2$), is such that

$$\mu(P_i) = f(P_i) \tag{I.1.31c}$$

We now discuss the differentiable edge spline which is not implemented in Pan Air. First we must compute the spline matrices which correspond to this differentiable piecewise quadratic distribution. It can be shown numerically that such a function, if it has a non-zero value at one panel center, and is zero at all other panel centers and the endpoints of the edge, is never identically zero. Rather, it behaves as illustrated in Figure I.10; oscillating with an amplitude which diminishes rapidly but never reaches zero. Thus, the spline is stable under doublet specification boundary conditions; however, it is not local, since the doublet strength on an interval depends weakly on the doublet strength at a panel center far away.

In order to avoid storing lengthy spline vectors, we must redefine our doublet parameters to make the spline local. That is, a doublet parameter on a network edge will not have as its value the doublet strength at its location. For this purpose, consider the interval $[-1, 1]$ on which we define the quadratic function

$$\mu(x) = a + bx + cx^2 \tag{I.1.32a}$$

Now,

$$\mu(-1) = a - b + c$$

$$\mu(1) = a + b + c \tag{I.1.32b}$$

$$\frac{d\mu}{dx}(-1) = b - 2c$$

$$\frac{d\mu}{dx}(1) = b + 2c \tag{I.1.33}$$

Thus,

$$\mu(-1) + \frac{d\mu}{dx}(-1) = a - c = \mu(1) - \frac{d\mu}{dx}(1) \tag{I.1.34}$$

Generalizing (I.1.34) to the interval $[P_i, P_{i+1}]$ in Figure I.9b, we have

$$\mu(P_i) + 1/2 \;\; \mu(P_i) \;\; (P_{i+1} - P_i)$$
$$= \mu(P_{i+1}) + 1/2 \;\; \mu(P_{i+1}) \;\; (P_i - P_{i+1}) \tag{I.1.35}$$

We thus define

$$\lambda_i^D = \mu(P_i) + 1/2\, \vec{\nabla}\mu(P_i) \cdot (\vec{P}_{i+1} - \vec{P}_i) \qquad i = 1,\ldots,n \tag{I.1.36}$$

$$\lambda_i^D = \mu(P_i), \qquad i = 0,\ n+1 \tag{I.1.37}$$

Now, by (I.1.35)

$$\lambda_{i-1}^D = \mu(P_i) + 1/2\, \vec{\nabla}\mu(P_i) \cdot (\vec{P}_{i-1} - \vec{P}_i) \qquad i = 2,\ldots,\ n+1 \tag{I.1.38}$$

Combining (I.1.40) and (I.1.42), and noting that $\vec{\nabla}\mu$ is continuous, we have

$$(P_i - P_{i-1})\,\lambda_i^D + (P_{i+1} - P_i)\,\lambda_{i-1}^D =$$

$$(P_i - P_{i-1})\,\mu(P_i) + 1/2\,\frac{d\mu}{dx}(P_i)\,(P_{i+1} - P_i)\,(P_i - P_{i-1}) \qquad \text{(I.1.39)}$$

$$+ (P_{i+1} - P_i)\,\mu(P_i) + 1/2\,\frac{d\mu}{dx}(P_i)\,(P_i - P_{i-1})\,(P_{i+1} - P_i)$$

Thus,

$$\mu(P_i) = \frac{|\vec{P}_i - \vec{P}_{i-1}|}{|\vec{P}_i - \vec{P}_{i-1}| + |\vec{P}_{i+1} - \vec{P}_i|}\,\lambda_i^D$$

$$+ \frac{|\vec{P}_{i+1} - \vec{P}_i|}{|\vec{P}_i - \vec{P}_{i-1}| + |\vec{P}_{i+1} - \vec{P}_i|}\,\lambda_{i-1}^D \qquad \text{(I.1.40)}$$

This defines the spline vector for P_i as computed with the differentiable edge spline, which is not implemented in Pan Air.

Now, we wish to evaluate $\mu(M_i)$, $i=1,\ldots,n$. Again consider a function $\mu(x)$ on $[-1, 1]$ defined by (I.1.31).

Then

$$\mu(-1) = a - b + c$$

$$\mu(1) = a + b + c$$

$$\mu(-1) + \frac{du}{dx}(-1) = a - c \qquad \text{(I.1.41)}$$

So,

$$\mu(o) = a =$$

$$1/4\,\mu(-1) + 1/4\,\mu(1) + 1/2\,[\mu(-1) + \frac{du}{dx}(-1)] \qquad \text{(I.1.42)}$$

Applying this to Figure I.9b, we see

$$\mu(M_i) = 1/4\,\mu(P_i) + 1/4\,\mu(u_{i+1}) + 1/2\,\lambda_i^D$$

$$i = 1,\ldots,n \qquad \text{(I.1.43)}$$

This defines the spline vector for M_i.

Equations (I.1.37), (I.1.41), and (I.1.43) together describe μ at grid points which lie on a network edge belonging to a non-smooth abutment as linear combinations of neighboring singularity parameters on the edge. We again point out that this procedure is not implemented in Pan Air.

I.1.2.6 Edge Splines for Smooth Abutments

We now describe the computation of spline vectors for grid points lying on smooth abutments. Once again, to obtain matching of doublet strength we require that one network be paneled as a refinement of the other, as in the example of Figure I.9a. Then, spline vectors for grid points on the more coarsely paneled edge are computed first, followed by spline vectors for grid points on the more finely paneled edge.

Spline vectors for grid points on the coarser edge are also computed by a constrained least squares procedure, even though again the "neighboring points" lie in two networks. Figure I.11a shows some representative examples which illustrate the procedure for choosing the set of neighboring points. The method is described precisely in the Maintenance Document (see Appendix I of section 4).

Now, continuity of doublet stength along a smooth abutment is insured by requiring the doublet strength at a grid point on the more finely paneled network to be identical (as a linear combination of surrounding singularity parameters) to that at the "corresponding" point on the coarsely paneled network. We determine the corresponding point by "parametrizing" the abutment, that is, assigning to each grid point a real number t, $0 < t < 1$, which specifies the proportion of the total abutment length that the grid point is distant from the starting point of the abutment. This procedure is discussed in more detail in the maintenance document (see SUBROUTINE PRMEDG of the DQG module).

Figure I.11b illustrates the parametrization of an abutment. Now, some grid point P'_i on the fine network will have parameter value t'_i, where

$$t_j < t'_i < t_{j+1} \tag{I.1.44}$$

for some integer j, that is, the corresponding point on the coarse network is not a grid point. But, μ must vary quadratically on the panel edge, so we can obtain $\mu(P'_i)$ as a linear combination of $\mu(P_j)$, $\mu(P_{j+1})$, and $\mu(P_{j+2})$.

Now, it follows from (I.1.31-32) that on an interval [-1, 1],

$$\begin{aligned} \mu(x) &= a + bx + cx^2 = \\ &\mu(0) + (1/2\mu(1) + 1/2\,\mu(-1))x \\ &+ [1/2\,\mu(1) + 1/2\,\mu(-1) - \mu(0)]x^2 \end{aligned} \tag{I.1.45}$$

We can apply this to the interval in Figure I.11c by making the transformation

$$x' = \frac{t - t_j}{t_{j+2} - t_j} \tag{I.1.46}$$

$$x = 2x' - 1$$

$$= \frac{2t - t_{j+2} - t_j}{t_{j+2} - t_j} \tag{I.1.47}$$

Equation (I.1.46) maps the interval in Figure I.11c to [0, 1], which in turn is mapped to [-1, 1] by (I.1.47).

Substituting (I.1.47) in (I.1.45), we obtain

$$\mu(t) = \mu(P_{j+1}) + [1/2\ \mu(P_{j+2}) - 1/2\ \mu(P_j)]\ \frac{2t - t_{j+2} - t_j}{t_{j+2} - t_j}$$

$$+ [1/2\ \mu(P_{j+2}) + 1/2\ \mu(P_j) - \mu(P_{j+1})] \left[\frac{2t - t_{j+2} - t_j}{t_{j+2} - t_j}\right]^2 \tag{I.1.48}$$

Setting $t = t'_i$, we have $\mu(P_i)$ as a linear combination of $\mu(P_j)$, $\mu(P_{j+1})$, and $\mu(P_{j+2})$:

$$\mu(P'_i) = (-1/2 + 1/2\ \tau^2)\ \mu(P_j)$$
$$+ (1 - \tau^2)\ \mu(P_{j+1}) + (1/2 + 1/2\ \tau^2)\ \mu(P_{j+2}) \tag{I.1.49}$$

where $$\tau = \frac{2\ t'_i - t_{j+2} - t_j}{t_{j+2} - t_j} \tag{I.1.50}$$

This concludes our discussion of spline vector construction for doublet analysis networks. We have now discussed the computation of doublet spline vectors for all enriched grid points in a doublet analysis network. In practice, these vectors are all computed and stored on a disk. Then, within a loop over panels, the spline vectors corresponding to the nine panel defining points are retrieved from the disk, and merged into an outer spline matrix B^D by VECUNM.

I.1.3 Doublet Spline Vectors for Wake Networks

Singularity parameter locations for doublet wake networks are illustrated in Figure D.3. In addition, if the edge of the wake I networks on which singularity parameters are located forms part of more than one abutment, an extra singularity parameter is located at the abutment endpoints lying in the interior of the edge.

The purpose of a doublet wake 1 network is to model a wake surface on which the doublet strength is constant in the streamwise direction. Thus, spline vectors for grid points are constructed as follows. First, spline vectors are constructed for each grid point on the edge containing singularity parameters, just as though the edge were part of a non-smooth abutment of an analysis network (it should be noted in passing that smooth abutments are only permitted between analysis networks). Then, the spline vector constructed for a particular grid point on the edge is also used for every grid point lying in the column or row of points emanating in an indicially perpendicular direction from the edge. This produces a doublet strength which is constant in one indicial direction, as desired. In general this direction is the direction of increasing row index, though this program default may be overridden by the user. See section 7, record N12, of the User's Manual.

Doublet wake 2 networks are used to define a constant strength doublet sheet, whose strength is the value of the one singularity parameter in the network. Thus, the identical spline vector is constructed for every grid point on the network; namely the row vector of length one with unit entry.

I.1.4 Source Splines for Design Networks

I.1.4.1 Source Design 1

Only one type of source outer spline, a continuous one, is used for source design 1 networks. Singularity locations for source design networks are given by Figure D.1. Since a source parameter is located at every panel corner, the spline vectors for these grid points are just unit vectors of length 1. Spline vectors for panel centers are also straightforward to compute:

$$SP^S = \lfloor 1/4 \quad 1/4 \quad 1/4 \quad 1/4 \rfloor \tag{I.1.51}$$

That is, the source strength at a panel center is defined as the average of the source strengths at all the panel corners.

I.1.4.2 Source Design 2, Discontinuous Source Splines

For source design 2 networks source parameters are located at those edge midpoints on edges parallel to the matching edge. To reduce the complexities of splines PAN AIR imposes two restrictions on source design 2 networks: They may not have collapsed edges and they may not have just one column or one row of panels.

The discontinuous source spline for a source design 2 network, used for influence coefficient computation and boundary condition evaluation, is computed by means of a three stage process. First, spline vectors are computed for the panel centers and for those panel edge midpoints that are not source parameter locations. (See figure D.1c for an illustration of the source parameter location on a source design 2 network.) Second, the five source values on the panel, (the panel center and four edge midpoint values) are fitted to obtain a source distribution function of the form $\sigma_0 + \sigma_\xi \xi + \sigma_\eta \eta$.

Third, this distribution is evaluated at the five panel source parameter locations.

This process can be summarized by the equation

$$\begin{Bmatrix} \hat{\sigma}_1 \\ \hat{\sigma}_2 \\ \hat{\sigma}_3 \\ \hat{\sigma}_4 \\ \hat{\sigma}_5 \end{Bmatrix} = \begin{bmatrix} 1 & \hat{\xi}_1 & \hat{\eta}_1 \\ 1 & \hat{\xi}_2 & \hat{\eta}_2 \\ 1 & \hat{\xi}_3 & \hat{\eta}_3 \\ 1 & \hat{\xi}_4 & \hat{\eta}_4 \\ 1 & 0 & 0 \end{bmatrix} \begin{bmatrix} A^+ \\ (3\text{x}5) \end{bmatrix} \begin{bmatrix} 1 & 0 & 0 & 0 & 0 & 0 \\ * & * & * & * & 0 & 0 \\ 0 & 1 & 0 & 0 & 0 & 0 \\ * & * & 0 & 0 & * & * \\ \frac{1}{2} & \frac{1}{2} & 0 & 0 & 0 & 0 \end{bmatrix} \begin{Bmatrix} \lambda_1 \\ \lambda_2 \\ \lambda_3 \\ \lambda_4 \\ \lambda_5 \\ \lambda_6 \end{Bmatrix}$$

Here, each stage of the process is represented by a matrix.

The first stage of this process requires further explanation. First the source strength at the panel center is taken to be the average of the two global source parameters that lie on the boundary of the panel. Next, the extra panel edge midpoint source strengths are obtained by means of a bilinear fit of neighboring global source parameter data, as illustrated in figure I.12. The bilinear fit performed here is essentially the same as the bilinear fit described in sections I.1.1.3 and I.1.1.4 in connection with continuous source analysis splines.

I.1.4.3 Source Design 2, Continuous Source Splines

The continuous source spline for a source design 2 network, used by PAN AIR's post processing modules for pressure, force and moment calculations, is generated by computing spline vectors for the panel center and corners. Taking the source strength at the panel center to be the average of the panel's two global source parameters, we have

$$SP^S = \lfloor 1/2 \quad 1/2 \rfloor$$

The panel corner spline vectors are obtained by means of the usual sort of bilinear fit using global source parameter data as indicated by figure I.13.

I.1.5 Doublet Splines for Design Networks

Figure D.2 shows the location of singularity parameters on a doublet design network. For grid points in the interior of the network, spline vectors are computed by fitting to neighboring points, as illustrated in Figure I.14a For grid points on the "matching edges" (which have singularity parameters located at the panel edge midpoints), the doublet analysis edge spline of section I.1.2.5 is used.

The only unusual aspect of doublet design splines is the edge spline for non-matching edges. The doublet parameters are located at panel corners along these edges (rather than panel edge midpoints) for stability, since the boundary conditions in the vicinity of non-matching edges tend to be doublet gradient boundary conditions. For nonmatching edges, as for matching edges, a differentiable edge spline and a least squares edge spline are available, though once again the least squares spline is implemented in Pan Air. The least squares spline is similar to that for matching edges, except that now it is at panel edge midpoints that the doublet strength is defined by least squaring to the four surrounding edge doublet parameters, while at panel corners the doublet strength is defined by a unit spline vector.

We now discuss the construction of the differentiable edge spline. Let λ_i^D be the value of the doublet parameter located as a panel corner P_i as illustrated in Figure I.14b We define a row vector $\lfloor \gamma_i \rfloor$, $0 \leq i \leq n$ (n the number of panel corners on the network edge) of length n as follows. We define γ_0 and γ_n to be row vectors with the entries 1 in the first entry and the nth entry, respectively, and otherwise zero. For $1 < i < n - 1$, we obtain γ_i by performing a one-dimensional least squares fit to the 4 (or 3, if i=1 or n-1) neighboring singularity parameters on the edge.

Thus, at each edge midpoint, and at the endpoints of the edge, a row vector γ_i is defined. This is analagous to the situation for the differentiable doublet analysis edge spline. We now obtain μ at corner points and edge midpoints by using the doublet analysis edge spline, but in terms of the γ_i rather than the singularity parameters.

For example, we have, analagously to (I.1.40),

$$\mu(P_5) = \frac{|\vec{P}_6 - \vec{P}_5|}{|\vec{P}_6 - \vec{P}_5| + |\vec{P}_5 - \vec{P}_4|} \lfloor \gamma_4 \rfloor \{\lambda_i^D\} + \frac{|\vec{P}_5 - \vec{P}_4|}{|\vec{P}_6 - \vec{P}_5| + |\vec{P}_5 - \vec{P}_4|} \lfloor \gamma_5 \rfloor \{\lambda_i^D\} \tag{I.1.52}$$

This concludes our discussion of spline vector construction. Details of the construction are contained in the Maintenance Document (section 4-I.2.3). We note that the "RESERVE" spline discussed there is in fact the least squares edge spline implemented in Pan Air.

I.2 Subpanel Splines

The subpanel spline matrices define the coefficients of the source and doublet distributions on a subpanel in terms of the panel singularity parameters. The panel singularity parameters consist of the source strengths at five points, σ_1, σ_2, σ_3, σ_4, σ_9 and doublet strengths at nine points μ_1, μ_2, $\ldots\mu_9$, the numbering of the various points on the panel being illustrated by figure I.15. The relation of these panel singularity parameters to the global singularity parameters has been treated in depth in section I.1. In this section we show how the panel parameters define the source and doublet distributions on the panel. Specifically, we will describe the construction of matrices $SPSPL_k^S$ and $SPSPL_k^D$ such that the singularity distributions restricted to subpanel T_k are given by the expressions

$$\sigma \Big|_{T_k} = (1, \xi, \eta)\, [SPSPL_k^S] \begin{Bmatrix} \sigma_1 \\ \sigma_2 \\ \sigma_3 \\ \sigma_4 \\ \sigma_9 \end{Bmatrix} \tag{I.2.1}$$

$$\mu \Big|_{T_k} = (1, \xi, \eta, \xi^2/2, \xi\eta, \eta^2/2)\, [SPSPL_k^D] \begin{Bmatrix} \mu_1 \\ \mu_2 \\ \vdots \\ \mu_9 \end{Bmatrix} \tag{I.2.2}$$

where (ξ,η) are local coordinates on the subpanel T_k (cf. appendix E).

I.2.1 Basis Functions for Interpolation on Triangles

We lay some groundwork for our discussion by describing the construction of the basis functions for polynomial interpolation on a triangle.

Consider triangle T for which the coordinates of the corners Q_i are denoted (ξ_i, η_i), $i = 1,2,3$. Any linear function f defined on this triangle is completely specified by its values $f(Q_i)$ at the three corners, and can be expressed in terms of these values by the formula

$$f(Q) = f(Q_1)\, L_1(Q) + f(Q_2)\, L_2(Q) + f(Q_3)\, L_3(Q) \tag{I.2.3}$$

where $L_i(Q)$ denotes a linear function of (ξ,η) taking on the value 1 at $Q = Q_i$ and zero at the other two corners. If, for a given index i, we define j and k by the condition that (i,j,k) be a positive permutation of the integers (1,2,3), (cf. figure I.16), then $L_i(Q)$ can be explicitly defined by the expression

$$L_i(Q) = \det\begin{bmatrix} \xi & \eta & 1 \\ \xi_j & \eta_j & 1 \\ \xi_k & \eta_k & 1 \end{bmatrix} \Big/ \det\begin{bmatrix} \xi_i & \eta_i & 1 \\ \xi_j & \eta_j & 1 \\ \xi_k & \eta_k & 1 \end{bmatrix} \qquad \text{(I.2.4)}$$

$$= \left[\det\begin{pmatrix} \xi_j & \eta_j \\ \xi_k & \eta_k \end{pmatrix} + \xi \det\begin{pmatrix} \eta_j & 1 \\ \eta_k & 1 \end{pmatrix} + \eta \det\begin{pmatrix} 1 & \xi_j \\ 1 & \xi_k \end{pmatrix}\right] \Big/ \det\begin{bmatrix} 1 & \xi_i & \eta_i \\ 1 & \xi_j & \eta_j \\ 1 & \xi_k & \eta_k \end{bmatrix}$$

$$= a_i + b_i\xi + c_i\eta$$

with the obvious definitions to be given for the coefficients a_i b_i c_i. It is an easy matter to check that these functions are linear in ξ and η and further, that they satisfy the interpolation conditions (cf. figure I.17),

$$L_i(Q_i) = 1 \qquad L_i(Q_j) = L_i(Q_k) = 0 \qquad \text{(I.2.5)}$$

The linear basis functions $L_i(Q)$ can be used to construct quadratic basis function $B_i(Q)$ and $B_i'(Q)$ that are used to represent quadratic functions defined on T. To see how this is done, let Q_i' denote the midpoint of the edge lying opposite the corner point Q_i (cf. figure I.18). Then any quadratic function g(Q) defined on T can be expressed in terms of the corner values $g(Q_i)$ and the midpoint values $g(Q_i')$ by the formula

$$g(Q) = \sum_{i=1}^{3} [g(Q_i)\, B_i(Q) + g(Q_i')\, B_i'(Q)] \qquad \text{(I.2.6)}$$

Here the quadratic basis functions B_i and B_i' are defined in terms of the functions L_i by

$$B_i = (2\, L_i - 1)\, L_i \qquad \text{(I.2.7a)}$$

$$B_i' = 4\, L_j L_k \qquad (i,j,k) = \text{positive permutation of } (1,2,3) \qquad \text{(I.2.7b)}$$

In order to verify the validity of (I.2.6) it is necessary to establish the interpolation conditions

$$B_i(Q_i) = 1 \qquad B_i(Q_j) = 0 \qquad B_i(Q_k) = 0 \qquad B_i(Q_l') = 0 \tag{I.2.8a}$$

$$B_i'(Q_i') = 1 \qquad B_i'(Q_j') = 0 \qquad B_i'(Q_k') = 0 \qquad B_i'(Q_l) = 0 \tag{I.2.8b}$$

These conditions in turn follow easily from the interpolation conditions (I.2.5) together with the observations that

$$L_i(Q_i') = 0 \qquad L_i(Q_j') = L_i(Q_k') = 1/2 \tag{I.2.9}$$

The verification is straightforward and is left to the reader.

We conclude our discussion of interpolation on triangles by constructing a cubic polynomial on T interpolating data at seven points, Q_i, Q_i' and the triangle midpoint M,

$$M = \frac{1}{3}(Q_1 + Q_2 + Q_3) \tag{I.2.10}$$

While this problem does not have a unique solution, the solution we present has certain virtues of symmetry. Given values of a function h(Q) at these seven points, we first construct a quadratic function $h_2(Q)$ defined by

$$h_2(Q) = \sum_{i=1}^{3} [h(Q_i)\, B_i(Q) + h(Q_i')B_i'(Q)] \tag{I.2.11}$$

and then patch it up to obtain the required cubic polynomial on T by defining

$$h_3(Q) = h_2(Q) + (h(M) - h_2(M))\, C(Q) \tag{I.2.12}$$

where C(Q) is a cubic polynomial in (ξ, η) defined by

$$C(Q) = 27\, L_1(Q)\, L_2(Q)\, L_3(Q). \tag{I.2.13}$$

It is a straightforward matter to verify that

$$C(M) = 1 \qquad C(Q_i) = 0, \qquad C(Q_i') = 0. \tag{I.2.14}$$

We find as a consequence that:

$$h_3(Q_i) = h_2(Q_i) + (h(M) - h_2(M))\, C(Q_i)$$

$$= h(Q_i) + (h(M)) - h_2(M)) \cdot 0 = h(Q_i)$$

$$h_3(Q_i') = h_2(Q_i') + (h(M) - h_2(M))\, C(Q_i')$$

$$= h(Q_i') + (h(M) - h_2(M)) \cdot 0 = h(Q_i')$$

$$h_3(M) = h_2(M) + (h(M) - h_2(M))\, C(M) = h(M)$$

thus verifying that $h_3(Q)$ satisfies the required conditions.

I.2.2 Source Subpanel Splines

Given the results of the previous section concerning interpolation on a triangle, it should be clear that all that is needed to define a linear source distribution on the triangular subpanel T_k is to relate the values of σ at the corners of T_k to the panel's source parameters. An examination of figure (I.15) immediately shows that the only subpanel corners at which we still need to define the source strength are panel points 5, 6, 7 and 8. These values are defined in terms of the panel source parameters by performing linear interpolation along each edge of the panel using the values of σ at the panel corners. This procedure leads to the definitions

$$\begin{aligned} \sigma_5 &= \frac{1}{2}(\sigma_1 + \sigma_2) \\ \sigma_6 &= \frac{1}{2}(\sigma_2 + \sigma_3) \\ \sigma_7 &= \frac{1}{2}(\sigma_3 + \sigma_4) \\ \sigma_8 &= \frac{1}{2}(\sigma_4 + \sigma_1) \end{aligned} \qquad (I.2.15)$$

Given these relations we have defined σ at every subpanel corner in terms of $\sigma_1 \ \sigma_2 \ \sigma_3 \ \sigma_4 \ \sigma_9$ and consequently, by virtue of equations (I.2.3) and (I.2.4), we have defined the distribution of σ on each subpanel.

To illustrate the actual construction of the subpanel spline matrix $SPSPL_k^S$, we consider the special case of subpanel 3. Referring again to figure I.15, we observe that the corners of subpanel 3 are P_3, P_7 and P_6. Making the identifications

$P_3 = Q_1$, local coordinates $(\xi_1 \ \eta_1)$

$P_7 = Q_2$, local coordinates $(\xi_2 \ \eta_2)$

$P_6 = Q_3$, local coordinates $(\xi_3 \ \eta_3)$

and writing out the basis function $L_i(Q)$ in the form (cf. (I.2.4))

$$L_i(Q) = a_i + b_i\xi + c_i\eta = (1, \xi, \eta) \begin{bmatrix} a_i \\ b_i \\ c_i \end{bmatrix} \qquad (I.2.16)$$

we observe that $\sigma(Q)$ is given by

$$
\begin{aligned}
\sigma(Q) &= \sigma(Q_1)\, L_1(Q) + \sigma(Q_2)\, L_2(Q) + \sigma(Q_3)\, L_3(Q) \\
&= \sigma(P_3)\, L_1(Q) + \sigma(P_7)\, L_2(Q) + \sigma(P_6)\, L_3(Q) \\
&= \sigma_3\, L_1(Q) + \tfrac{1}{2}(\sigma_3 + \sigma_4)\, L_2(Q) + \tfrac{1}{2}(\sigma_2 + \sigma_3)\, L_3(Q) \\
&= \left(0,\ \tfrac{1}{2} L_2(Q),\ L_1(Q) + \tfrac{1}{2}\left(L_2(Q) + L_3(Q)\right),\ \tfrac{1}{2} L_2(Q),\ 0\right) \begin{Bmatrix} \sigma_1 \\ \sigma_2 \\ \sigma_3 \\ \sigma_4 \\ \sigma_9 \end{Bmatrix}
\end{aligned}
\tag{I.2.17}
$$

$$
\sigma(Q) = (1, \xi, \eta) \begin{bmatrix} 0 & \frac{1}{2} a_3 & a_1 + \frac{1}{2}(a_2 + a_3) & \frac{1}{2} a_2 & 0 \\ 0 & \frac{1}{2} b_3 & b_1 + \frac{1}{2}(b_2 + b_3) & \frac{1}{2} b_2 & 0 \\ 0 & \frac{1}{2} c_3 & c_1 + \frac{1}{2}(c_2 + c_3) & \frac{1}{2} c_2 & 0 \end{bmatrix} \begin{Bmatrix} \sigma_1 \\ \sigma_2 \\ \sigma_3 \\ \sigma_4 \\ \sigma_9 \end{Bmatrix}
\tag{I.2.18}
$$

The source subpanel spline matrix $[SPSPL_3^S]$ is then identified with the matrix appearing in the right hand side of this expression.

I.2.3 Doublet Subpanel Splines

We now discuss the construction of the doublet subpanel splines matrix $[SPSPL_k^D]$ (cf. equation (I.2.2)) that relates the coefficients of a subpanel's quadratic doublet distribution to the panel's panel doublet parameters, (μ_i, i=1,2,...9). In view of the results of section I.2.1 concerning quadratic interpolation on a triangle, it should be clear that all that is needed to completely specify the quadratic doublet distribution μ on

subpanel T_k is to give its values at the corners and the edge midpoints of T_k (cf. equation (I.2.6) with the substitution $g \to \mu$). The relation of coefficients $\mu_o\ \mu_\xi\ \mu_\eta\ \cdots\ \mu_{\eta\eta}$ to the six doublet values $\mu(Q_i)$, $\mu(Q_i')$ is given explicitly by the following equation which is obtained by combining (I.2.6) and (I.2.7) with the representation for $L_i(Q)$ given by (I.2.4):

$$\begin{Bmatrix} \mu_o \\ \mu_\xi \\ \mu_\eta \\ \mu_{\xi\xi} \\ \mu_{\xi\eta} \\ \mu_{\eta\eta} \end{Bmatrix} = [B] \begin{Bmatrix} \mu(Q_1) \\ \mu(Q_2) \\ \mu(Q_3) \\ \mu(Q_1') \\ \mu(Q_2') \\ \mu(Q_3') \end{Bmatrix} \tag{I.2.19}$$

Here the matrix [B] is given by

$$[B] = \begin{bmatrix} 2a_1^2-a_1 & 2a_2^2-a_2 & 2a_3^2-a_3 & 4a_2a_3 & 4a_3a_1 & 4a_1a_2 \\ 4a_1b_1-b_1 & 4a_2b_2-b_2 & 4a_3b_3-b_3 & 4(a_2b_3+a_3b_2) & 4(a_3b_1+a_1b_3) & 4(a_1b_2+a_2b_1) \\ 4a_1c_1-c_1 & 4a_2c_2-c_2 & 4a_3c_3-c_3 & 4(a_2c_3+a_3c_2) & 4(a_3c_1+a_1c_3) & 4(a_1c_2+a_2c_1) \\ 4b_1^2 & 4b_2^2 & 4b_3^2 & 8b_2b_3 & 8b_3b_1 & 8b_1b_2 \\ 4b_1c_1 & 4b_2c_2 & 4b_3c_3 & 4(b_2c_3+b_3c_2) & 4(b_3c_1+b_1c_3) & 4(b_1c_2+b_2c_1) \\ 4c_1^2 & 4c_2^2 & 4c_3^2 & 8c_2c_3 & 8c_3c_1 & 8c_1c_2 \end{bmatrix} \tag{I.2.20}$$

The relation of the six doublet values $\mu(Q_i)$, $\mu(Q_i')$ to the nine doublet parameters involves the consideration of a number of special cases and is sometimes quite complicated. In figure I.19 we have drawn a typical panel with all of its subpanel corners Q_i denoted by •, and subpanel edge midpoints Q_i' denoted by the various symbols o, □, x . The problem of defining $\mu(Q_i)$, $\mu(Q_i')$ then reduced to the problem of defining μ at these 25 points on the panel. The definition of μ at these points takes up the remainder of this section, the discussion being divided into the following parts:

(i) considerations of continuity, leading to the definition of μ at points marked with o and □ ,

(ii) the definition of the "κ quantity" associated with a subpanel edge,

(iii) the computation of the four nontrivial κ quantities κ_{85}, κ_{56}, κ_{67} and κ_{78} leading to the definition of μ at the points marked with x.

Of course it should be fairly clear from an examination of figure I.19 that the subpanel corner points marked with • are also the location of the panel doublet parameters. Thus the definition of μ at these nine points is an

entirely trivial matter.

I.2.3.1 Considerations of Continuity

PAN AIR imposes the condition that doublet strength be continuous from panel to panel as well as continuous within a panel in order that the line vortex term be dropped from the expression for perturbation velocity. We now consider what consequences this requirement imposes upon the doublet distribution along edge 1 (consisting of points P_1, P_5, P_2) of the panel diagrammed in figure I.19.

First, observe that continuity at the points P_1, P_5 and P_2 requires that the doublet outer spline matrix B^D give the same value for μ at these points whether they are considered as lying on the panel diagrammed or on its neighbor below. This requirement is satisfied by the actual construction process of B^D (see section I.1) in which doublet values at fine grid points (points marked • in figure I.19) are related to global doublet parameters without consideration of which panel they are associated with. Now if continuity of μ at points P_1, P_5, P_2 is to imply the continuity of μ all along the edge, then the distribution of μ along the edge must be determined by its values at these three points. An edge distribution of μ satisfying this requirement is provided by a quadratic distribution of μ along the edge. If edge 1 is parameterized by a variable $t \in [-1, 1]$ with the correspondences

$$t = -1 \leftrightarrow P_1$$

$$t = 0 \leftrightarrow P_5$$

$$t = +1 \leftrightarrow P_2$$

than a suitable quadratic distribution is provided by the expression

$$\mu \Big|_{\text{edge } 1} = \mu_1[t(t-1)/2] + \mu_5[1-t^2] + \mu_2[t(t+1)/2] \qquad \text{(I.2.21)}$$

By setting $t = -1/2$ (resp. $1/2$) in this expression, we can compute μ at the subpanel edge midpoint $(Q_1 + Q_5)/2$ (resp. $(Q_5 + Q_2)/2$). We obtain

$$\mu_{15} = \mu((Q_1+Q_5)/2) = \mu_1(3/8) + \mu_5(3/4) + \mu_2(-1/8) \qquad \text{(I.2.22a)}$$

$$\mu_{52} = \mu((Q_5+Q_2)/2) = \mu_1(-1/8) + \mu_5(3/4) + \mu_2(3/8) \qquad \text{(I.2.22b)}$$

By repeating this process for the other edges, we can define the doublet strength at all the points marked with (o) in figure I.19.

Similar considerations of the requirement that μ be continuous from the top half to the bottom half of the panel lead us to define μ along the line (P_8, P_9, P_6) by a similar quadratic expression,

$$\mu \Big|_{(P_8,P_9,P_6)} = \mu_8[t(t-1)/2] + \mu_9[1-t^2] + \mu_6[t(t+1)/2] \tag{I.2.23}$$

As before we can compute μ at the subpanel edge midpoints along the line (P_8, P_9, P_6). We obtain,

$$\mu_{89} = \mu((P_8 + P_9)/2) = \mu_8(3/8) + \mu_9(3/4) + \mu_6(-1/8) \tag{I.2.24a}$$

$$\mu_{96} = \mu((P_9 + P_6)/2) = \mu_8(-1/8) + \mu_9(3/4) + \mu_6(3/8) \tag{I.2.24b}$$

By repeating this process on the line (P_5, P_9, P_7), we can define the doublet strength at all the points marked with (□) in figure I.19.

I.2.3.2 The Definition of "Kappa" Quantities

We begin our discussion of the computation of μ at the points marked x in figure I.19 by defining a quantity κ_{AB} associated with a quadratic function μ defined on a line AB:

$$\kappa_{AB} = \mu(\vec{A}) + (1/2)\,\nabla\mu(\vec{A}) \cdot (\vec{B}-\vec{A}) \tag{I.2.25}$$

If the line AB is parameterized by a variable $t\varepsilon[-1,1]$ by the expression

$$\vec{P}(t) = [(1-t)/2]\,\vec{A} + [(1+t)/2]\vec{B} \tag{I.2.26}$$

then the quadratic function $\mu(P(t))$ is given by

$$\mu(\vec{P}(t)) = \mu(\vec{A})\,[t(t-1)/2] + \mu(\vec{M})\,[1-t^2] + \mu(\vec{B})\,[t(t+1)/2] \tag{I.2.27}$$

where $\vec{M}$ denotes the midpoint, $(\vec{A}+\vec{B})/2$. Note that

$$\frac{d}{dt}\,\mu(\vec{P}(t)) = \nabla\mu(\vec{P}(t)) \cdot (d\vec{P}/dt) = \nabla\mu(\vec{P}(t)) \cdot (\vec{B}-\vec{A})/2 \tag{I.2.28}$$

Setting t=-1, we find that, since $\vec{P}(-1) = \vec{A}$,

$$(1/2)\,\nabla\mu(A) \cdot (\vec{B}-\vec{A}) = \frac{d}{dt}\,\mu(\vec{P}(t))\Big|_{t=-1}$$

$$= -\frac{3}{2}\,\mu(\vec{A}) + 2\,\mu(\vec{M}) - \frac{1}{2}\,\mu(\vec{B}) \tag{I.2.29}$$

Substituting this result into (I.2.25) we obtain

$$\kappa_{AB} = 2\,\mu(\vec{M}) - \frac{1}{2}\,(\mu(\vec{A}) + \mu(\vec{B})) \tag{I.2.30}$$

An entirely similar calculation shows that

$$\kappa_{BA} = \mu(\vec{B}) + (1/2)\,\nabla\mu(\vec{B}) \cdot (\vec{A}-\vec{B}) = \kappa_{AB} \tag{I.2.31}$$

Notice that if κ_{AB}, $\mu(\vec{A})$ and $\mu(\vec{B})$ are all known, then $\mu(\vec{M})$ is immediately given by

$$\mu(\vec{M}) = \frac{1}{2}\left[\kappa_{AB} + \frac{1}{2}\mu(\vec{A}) + \frac{1}{2}\mu(\vec{B})\right] \tag{I.2.32}$$

Since all that remains to be computed are the values of μ at the four points marked x in figure I.15, we only need to compute the values of κ associated with the line segments P_8P_5, P_5P_6, P_6P_7, P_7P_8. In describing this computation, we will treat in detail the calculation of one of these quantities (κ_{85}) and then simply quote the results for the other three.

I.2.3.3 Computation of the Nontrivial Kappa Quantities

The computation of the kappa quantities is most easily described if we introduce a skewed coordinate system for the mean panel. This coordinate system is essentially similar to the skewed coordinate systems described in section I.1. We define this coordinate system as follows.

Let $\vec{P}_s$, $\vec{P}_t$ and $\vec{P}_{st}$ be defined by

$$\vec{P}_s = \frac{1}{4}(\vec{P}_4 + \vec{P}_1 - \vec{P}_2 - \vec{P}_3) \tag{I.2.33}$$

$$\vec{P}_t = \frac{1}{4}(\vec{P}_1 + \vec{P}_2 - \vec{P}_3 - \vec{P}_4) \tag{I.2.34}$$

$$\vec{P}_{st} = \frac{1}{4}(\vec{P}_1 - \vec{P}_2 + \vec{P}_3 - \vec{P}_4) \tag{I.2.35}$$

and let $\vec{N}$ be the cross product of $\vec{P}_s$ and $\vec{P}_t$:

$$\vec{N} = \vec{P}_s \times \vec{P}_t \tag{I.2.36}$$

Note that the panel center $\vec{P}_9$ satisfies

$$\vec{P}_9 = \frac{1}{4}(\vec{P}_1 + \vec{P}_2 + \vec{P}_3 + \vec{P}_4) \tag{I.2.37}$$

We define the skewed coordinates $\vec{P}'$ of a point $\vec{P}$ by the equation

$$\vec{P}' = \left[\frac{\vec{P}_t \times \vec{N}}{|\vec{N}|^2} \;\vdots\; \frac{\vec{N} \times \vec{P}_s}{|\vec{N}|^2} \;\vdots\; \frac{\vec{N}}{|\vec{N}|^{3/2}}\right]^T (\vec{P} - \vec{P}_9) \tag{I.2.38}$$

Since $\vec{P}_1 = \vec{P}_9 + \vec{P}_s + \vec{P}_t + \vec{P}_{st}$, we find that

$$\vec{P}'_1 = \begin{bmatrix} 1 + c_1 \\ 1 + c_2 \\ c_3 \end{bmatrix} \tag{I.2.39}$$

where skewness parameters c_1, c_2, c_3 are defined

$$c_1 = \vec{P}_t \times \vec{N} \cdot \vec{P}_{st} / |\vec{N}|^2 \tag{I.2.40a}$$

$$c_2 = \vec{N} \times \vec{P}_s \cdot \vec{P}_{st} / |\vec{N}|^2 \tag{I.2.40b}$$

$$c_3 = \vec{N} \cdot \vec{P}_{st} / |\vec{N}|^{3/2} \tag{I.2.40c}$$

In an entirely similar fashion we find

$$\vec{P}'_2 = \begin{bmatrix} -1 - c_1 \\ 1 - c_2 \\ -c_3 \end{bmatrix}, \quad \vec{P}'_3 = \begin{bmatrix} -1 + c_1 \\ -1 + c_2 \\ c_3 \end{bmatrix}, \quad \vec{P}'_4 = \begin{bmatrix} 1 - c_1 \\ -1 - c_2 \\ -c_3 \end{bmatrix} \tag{I.2.39}$$

Relations of the form $\vec{P}_5 = \vec{P}_9 + \vec{P}_t$ lead to the results

$$\vec{P}'_5 = \begin{bmatrix} 0 \\ 1 \\ 0 \end{bmatrix}$$

$$\vec{P}'_6 = \begin{bmatrix} -1 \\ 0 \\ 0 \end{bmatrix}$$

$$\vec{P}'_7 = \begin{bmatrix} 0 \\ -1 \\ 0 \end{bmatrix} \tag{I.2.40}$$

$$\vec{P}'_8 = \begin{bmatrix} 1 \\ 0 \\ 0 \end{bmatrix}$$

Figure I.20 is a diagram of the panel in this local coordinate system as it appears viewed from above.

Projecting the panel onto the s-t plane, we are now ready to describe the computation of κ_{58}. First we observe that $\nabla'\mu$ can be computed at point $\vec{P}'_5$ provided we know the two directional derivatives:

$$(\vec{P}_1' - \vec{P}_2') \cdot \nabla'\mu(P_5') = 2(1+c_1, c_2) \cdot \nabla'\mu(\vec{P}_5')$$

$$(\vec{P}_5' - \vec{P}_7') \cdot \nabla'\mu(P_5') = 2(0, 1) \cdot \nabla'\mu(P_5') \tag{I.2.41}$$

Each of these quantities is easily computed using the fact that μ is a quadratic along the lines $(P_1' \; P_5' \; P_2')$ and $(P_7' \; P_9' \; P_5')$. We obtain

$$(P_1' - P_2') \cdot \nabla'\mu(P_5') = \mu_1 - \mu_2 \tag{I.2.42}$$

$$(P_5' - P_7') \cdot \nabla'\mu(P_5') = 3\mu_5 - 4\mu_9 + \mu_7$$

Solving the equation

$$2 \begin{bmatrix} 1+c_1 & c_2 \\ 0 & 1 \end{bmatrix} \nabla'\mu(P_5') = \begin{bmatrix} \mu_1-\mu_2 \\ 3\mu_5-4\mu_9+\mu_7 \end{bmatrix} \tag{I.2.43}$$

for $\nabla'\mu(P_5')$ we obtain

$$\nabla'\mu(P_5') = \begin{bmatrix} \frac{1}{(1+c_1)} \left[\frac{1}{2}\mu_1 - \frac{1}{2}\mu_2 - c_2(\frac{3}{2}\mu_5 - 2\mu_9 + \frac{1}{2}\mu_7) \right] \\ \frac{3}{2}\mu_5 - 2\mu_9 + \frac{1}{2}\mu_7 \end{bmatrix} \tag{I.2.44}$$

Forming $\bar{\kappa}_{58}$ using the definition

$$\bar{\kappa}_{58} = \mu_5 + \frac{1}{2}(\vec{P}_8' - \vec{P}_5') \cdot \nabla'\mu\,(P_5')$$

$$= \mu_5 + \frac{1}{2}(1, -1) \quad \nabla'\mu\,(P_5') \tag{I.2.45}$$

we obtain

$$\bar{\kappa}_{58} = \mu_5 + \frac{1}{4(1+c_1)}(\mu_1-\mu_2) - \frac{(1+c_2+c_1)}{2(1+c_1)}(\frac{3}{2}\mu_5-2\mu_9+\frac{1}{2}\mu_7)$$

$$= \frac{1}{4(1+c_1)} \Big\{ \mu_1-\mu_2 + \mu_5\,(1-3c_2+c_1)$$

$$+ \mu_9\, 4(1+c_1+c_2) - \mu_7(1+c_1+c_2) \Big\} \tag{I.2.46}$$

A similar calculation based upon the directional derivative formulae

$$(\vec{P}_1' - \vec{P}_4') \cdot \nabla'\mu\,(P_8') = 2\,(c_1,\ 1 + c_2) \quad \nabla'\mu\,(P_8')$$

$$= \mu_1 - \mu_4$$

$$(\vec{P}_8' - \vec{P}_6') \cdot \nabla'\mu\,(P_8') = 2\,(1,\ 0) \quad \nabla'\mu\,(P_8')$$

$$= 3\mu_8 - 4\mu_9 + \mu_6 \tag{I.2.47}$$

leads to the formula for $\nabla'\mu(P_8')$

$$\nabla'\mu(P_8') = \begin{bmatrix} \frac{3}{2}\mu_8 - \mu_9 + \frac{1}{2}\mu_6 \\ \frac{1}{1+c_2}\left[\frac{1}{2}\mu_1 - \frac{1}{2}\mu_4 - c_1\left(\frac{3}{2}\mu_8 - 2\mu_9 + \frac{1}{2}\mu_6\right)\right] \end{bmatrix} \tag{I.2.48}$$

Defining the quantity $\bar{\kappa}_{85}$ by

$$\bar{\kappa}_{85} = \mu_8 + \frac{1}{2}(\vec{P}_5' - \vec{P}_8') \cdot \nabla'\mu\,(P_8')$$

$$= \mu_8 + \frac{1}{2}(-1,\ 1) \quad \nabla'\mu(P_8') \tag{I.2.49}$$

we obtain after some manipulation

$$\bar{\kappa}_{85} = \frac{1}{4(1+c_2)}\Big\{\mu_1 - \mu_4 + (1 - 3c_1 + c_2)\,\mu_8$$

$$\mu_9\,4(1 + c_1 + c_2) - \mu_6\,(1 + c_1 + c_2)\Big\} \tag{I.2.50}$$

Now, clearly, the definition we use for κ_{58} should be some weighted average of the two values we have calculated. Further, if $(1+c_1)$ or $(1+c_2)$ is zero, one of the values of κ_{58} goes to infinity, indicating the impossibility of providing a continuous doublet gradient on that occasion (this situation occurs whenever the panel is triangular). Thus, our weighted average should be such that zero weight is given to an infinite value of κ_{58}. The simplest such weighted average is given below:

$$\kappa_{58} = \frac{1 + c_1}{2 + c_1 + c_2}\,\bar{\kappa}_{58} + \frac{1 + c_2}{2 + c_1 + c_2}\,\bar{\kappa}_{85} \tag{I.2.51}$$

Upon substituting (I.2.46) and (I.2.50) into (I.2.51), we obtain the formula for κ_{58}.

$$\kappa_{58} = \frac{1}{4(2+c_1+c_2)} \Big\{ 2\,\mu_1 + (1-3c_2+c_1)\mu_5 - \mu_2$$

$$(1-3c_1+c_2)\mu_8 + 8(1+c_1+c_2)\mu_9 - (1+c_1+c_2)\mu_6$$

$$-\mu_4 - (1+c_1+c_2)\mu_7 + 0\,\mu_3 \Big\} \tag{I.2.52}$$

Similar formulae for the other three values of are given by

$$\kappa_{56} = \frac{1}{4(2+c_1-c_2)} \Big\{ 2\,\mu_2 + (1-3c_1-c_2)\,\mu_6 - \mu_3$$

$$(1+3c_2+c_1)\,\mu_5 + 8(1+c_1-c_2)\,\mu_9 - (1+c_1-c_2)\,\mu_7$$

$$-\,\mu_1 - (1+c_1-c_2)\,\mu_8 + 0\,\mu_4 \Big\} \tag{I.2.53}$$

$$\kappa_{67} = \frac{1}{4(2-c_1-c_2)} \Big\{ 2\,\mu_3 + (1+3c_2-c_1)\,\mu_7 - \mu_4$$

$$(1+3c_1-c_2)\,\mu_6 + 8(1-c_1-c_2)\,\mu_9 - (1-c_1-c_2)\,\mu_8$$

$$-\mu_2 - (1-c_1-c_2)\mu_5 + 0\mu_1 \Big\} \tag{I.2.54}$$

$$\kappa_{78} = \frac{1}{4(2-c_1+c_2)} \Big\{ 2\,\mu_4 + (1+3c_1+c_2)\,\mu_8 - \mu_1$$

$$(1-c_1-3c_2)\,\mu_7 + 8(1-c_1+c_2)\,\mu_9 - (1-c_1+c_2)\,\mu_5$$

$$-\mu_3 - (1-c_1+c_2)\mu_6 + 0\mu_2 \Big\} \tag{I.2.55}$$

I.3 Full Panel and Half Panel Splines

Measuring the influence of a panel consisting of eight separate subpanels is quite costly in terms of computing effort. Consequently, this procedure is used just for those panels lying very near to a control point. For panels lying somewhat further away from a control point, two "intermediate field" procedures are available for estimating the influence of a panel. In the simplest of these procedures, the "quasi-far field" method, the panel is replaced by its mean plane projection, the source distribution is approximated by a single linear function and the doublet distribution is approximated by a single quadratic function defined on the mean panel surface. Somewhat more complicated than this is the "quasi-near field" approach, which divides the panel into two triangular half panels, approximating the source distribution with a linear function and the doublet distribution with a cubic function on each half panel. It is important to realize that while the more complicated quasi near field procedure does maintain continuity of doublet strength, the quasi far field procedure does not. Thus, in supersonic flow, the quasi far field procedure is never used unless the panel lies well inside the control point's domain of dependence, (i.e., the Mach cone emanating upstream from the control point). The quasi-far field's replacement of the exact doublet distribution with a discontinuous approximation is safe, then, provided the panel lies well inside the domain of dependence. For, when this condition holds, small changes in the doublet distribution produce small changes in the values of ϕ and $\vec{v}$ at the control point. This last fact follows from the well-boundedness of (1/R) and $\nabla(1/R)$ at points sufficiently far away from the boundary of the Mach cone.

I.3.1 Full Panel Spline Matrices

The full panel spline matrices, denoted $PSPL^S$ and $PSPL^D$ are used in the evaluation of far field (cf. appendix J.9) as well as quasi-far field panel influence coefficients. These spline matrices give the coefficients of a linear source distribution $\sigma(\xi,\eta)$ and a quadratic distribution $\mu(\xi,\eta)$ in terms of the panel's singularity parameters, that is, the 5 panel source parameters and 9 panel doublet parameters that help define $\sigma(Q)$ and $\mu(Q)$ on the panel. Thus we have σ and μ approximated by

$$\sigma(\xi,\eta) \cong \sigma_0 + \sigma_\xi \xi + \sigma_\eta \eta \tag{I.3.1}$$

$$\mu(\xi,\eta) \cong \mu_0 + \mu_\xi \xi + \mu_\eta \eta + \frac{1}{2}\mu_{\xi\xi} \xi^2 + \mu_{\xi\eta} \xi\eta + \frac{1}{2}\mu_{\eta\eta} \eta^2 \tag{I.3.2}$$

where the polynomial coefficients are given by

$$\begin{Bmatrix} \sigma_0 \\ \sigma_\xi \\ \sigma_\eta \end{Bmatrix} = [PSPL^S] \begin{Bmatrix} \sigma_1 \\ \sigma_2 \\ \sigma_3 \\ \sigma_4 \\ \sigma_9 \end{Bmatrix} \tag{I.3.3}$$

$$\begin{Bmatrix} \mu_0 \\ \mu_\xi \\ \mu_\eta \\ \mu_\xi \\ \mu_{\xi\eta} \\ \mu_{\eta\eta} \end{Bmatrix} = [PSPL^D] \begin{Bmatrix} \mu_1 \\ \mu_2 \\ \cdot \\ \cdot \\ \cdot \\ \cdot \\ \mu_8 \\ \mu_9 \end{Bmatrix} \tag{I.3.4}$$

The (ξ,η) coordinates used in these equations are the first two components of the average panel local coordinate system defined by equation (E.0.1), using the panel center as the origin and taking $\hat{n}$ to be the normal to the average plane. In what follows we will use the notation (ξ_i, η_i), i=1, ... , 9 to denote the local coordinates for the nine standard points on the panel at which panel doublet parameters are located.

The source panel spline matrix $PSPL^S$ is constructed by a constrained least squares procedure in which we enforce the constraint

$$\sigma(\xi_9, \eta_9) = \sigma_9 \tag{I.3.5}$$

while minimizing with respect to σ_0, σ_ξ and σ_η the expression

$$\sum_{i=1}^{4} [\sigma_0 + \sigma_\xi \xi_i + \sigma_\eta \eta_i - \sigma_i]^2 \tag{I.3.6}$$

Since the panel center is the origin of the local coordinate system, (ξ_9, η_9) = (0, 0) and equation (I.3.5) implies that

$$\sigma_9 = \sigma(\xi_9, \eta_9) = \sigma\ (0,0) = \sigma_0 \tag{I.3.7}$$

Thus $\sigma_0 = \sigma_9$ and the problem of minimizing the expression (I.3.6) can be reformulated as:

$$\min_{\sigma_\xi,\ \sigma_\eta} \sum_{i=1}^{4} [\sigma_\xi\ \xi_i + \sigma_\eta\ \eta_i - (\sigma_i - \sigma_9)]^2 \tag{I.3.8}$$

The normal equations for this problem read

$$\begin{bmatrix} \sum_{i=1}^{4} \xi_i^2 & \sum_{i=1}^{4} \xi_i\ \eta_i \\ \sum_{i=1}^{4} \xi_i\ \eta_i & \sum_{i=1}^{4} \eta_i^2 \end{bmatrix} \begin{Bmatrix} \sigma_\xi \\ \sigma_\eta \end{Bmatrix} = \begin{Bmatrix} \sum_{i=1}^{4} \xi_i\ \sigma_i - \sigma_9 \sum_{i=1}^{4} \xi_i \\ \sum_{i=1}^{4} \eta_i\ \sigma_i - \sigma_9 \sum_{i=1}^{4} \eta_i \end{Bmatrix} \tag{I.3.9}$$

Because the panel center $\vec{P}_9 = \frac{1}{4}(\vec{P}_1 + \vec{P}_2 + \vec{P}_3 + \vec{P}_4)$ is the origin of the local coordinate system, we have that $\sum_{i=1}^{4} \xi_i = \sum_{i=1}^{4} \eta_i = 0$. Using this fact to simplify the right hand side of (I.3.9), we may write the following expression for $PSPL^S$.

$$[PSPL^S] = \left[\begin{array}{c|cc} 1 & 0 & 0 \\ \hline 0 & \multicolumn{2}{c}{C^{-1}} \\ 0 & & \end{array}\right] \begin{bmatrix} 0 & 0 & 0 & 0 & 1 \\ \xi_1 & \xi_2 & \xi_3 & \xi_4 & 0 \\ \eta_1 & \eta_2 & \eta_3 & \eta_4 & 0 \end{bmatrix} \tag{I.3.10}$$

where C is the coefficient matrix of (I.3.9):

$$C = \begin{bmatrix} \sum_{i=1}^{4} \xi_i^2 & \sum_{i=1}^{4} \xi_i\ \eta_i \\ \sum_{i=1}^{4} \xi_i\ \eta_i & \sum_{i=1}^{4} \eta_i^2 \end{bmatrix} \tag{I.3.11}$$

The construction of the doublet panel spline matrix $PSPL^D$ is accomplished by rather different means. In order to explain the process, it is necessary to introduce the <u>isoparametric representation of a panel</u>.

The isoparametric representation of a panel consists of a mapping $\vec{q}(s,t)$ from the standard square I:

$$I = \{(s,t) \mid -1 \leq s,t \leq 1\}$$
$$= [-1,1] \times [-1,1] \qquad (I.3.12)$$

onto the approximate panel H. The mapping $\vec{q}(s,t)$ that defines the approximate panel H is constructed by performing bilinear interpolation on I using the data (cf. figure I.21)

$$\vec{q}(1,1) = \vec{P}_1$$
$$\vec{q}(-1,1) = \vec{P}_2$$
$$\vec{q}(-1,-1) = \vec{P}_3$$
$$\vec{q}(1,-1) = \vec{P}_4 \qquad (I.3.13)$$

The resulting mapping is given explicitly by

$$\vec{q}(s,t) = \frac{(1+s)(1+t)}{4}\vec{P}_1 + \frac{(1-s)(1+t)}{4}\vec{P}_2$$
$$+ \frac{(1-s)(1-t)}{4}\vec{P}_3 + \frac{(1+s)(1-t)}{4}\vec{P}_4 \qquad (I.3.14)$$

Writing this as a polynomial in (s,t) yields

$$\vec{q}(s,t) = \vec{q}_o + \vec{q}_s\, s + \vec{q}_t\, t + \vec{q}_{st}\, st \qquad (I.3.15)$$

where the coefficients are given by

$$\begin{bmatrix} \vec{q}_o \\ \vec{q}_s \\ \vec{q}_t \\ \vec{q}_{st} \end{bmatrix} = \frac{1}{4} \begin{bmatrix} 1 & 1 & 1 & 1 \\ 1 & -1 & -1 & 1 \\ 1 & 1 & -1 & -1 \\ 1 & -1 & 1 & -1 \end{bmatrix} \begin{bmatrix} \vec{P}_1 \\ \vec{P}_2 \\ \vec{P}_3 \\ \vec{P}_4 \end{bmatrix} \qquad (I.3.16)$$

Note that $\vec{q}_o = \vec{P}_9$, the panel center. The parameter space I and the mapping $\vec{q}(s,t)$ up to the approximate panel H are illustrated by fig. I.21.

The approximate panel H lies quite close to the actual panel and has precisely the same boundary. In point of fact, the approximate panel H was actually considered for use as the standard panel in PAN AIR. It was discarded however on the grounds that its use makes it impossible to evaluate panel influence integrals in closed form. Since these integrals are in fact nonconvergent finite part integrals in the case of supersonic flow, closed form evaluation is quite essential. In spite of this drawback, the approximate panel H frequently does provide a useful theoretical framework for constructing approximate doublet distributions.

The most natural choice of a doublet distribution on H is provided by performing biquadratic interpolation on I using doublet data associated with corresponding points on H. This process results in the doublet distribution on I given by

$$\tilde{\mu}(s,t) = \left(\frac{s(s+1)}{2},\ 1-s^2,\ \frac{s(s-1)}{2}\right)\begin{bmatrix} \mu_1 & \mu_8 & \mu_4 \\ \mu_5 & \mu_9 & \mu_7 \\ \mu_2 & \mu_6 & \mu_3 \end{bmatrix}\begin{bmatrix} t(t+1)/2 \\ 1-t^2 \\ t(t-1)/2 \end{bmatrix} \tag{I.3.17}$$

In order to transform this expression into a doublet distribution on H, we use the mapping $\vec{q}(s,t)$ from I to H to give us

$$\mu(\vec{q}(s,t)) = \tilde{\mu}(s,t) \tag{I.3.18}$$

This distribution agrees exactly with the PAN AIR doublet distribution on the boundary of the panel and on the lines $(\vec{P}_6, \vec{P}_9, \vec{P}_8)$, $(\vec{P}_5, \vec{P}_9, \vec{P}_7)$.

Now the panel doublet spline $PSPL^D$ is to be used to compute a doublet distribution on the mean panel. This distribution is defined by

$$\mu_M(\vec{q}'_M(s,t)) = \tilde{\mu}(s,t) \tag{I.3.19}$$

where $\vec{q}'_M(s,t)$ denotes the usual sort of mapping from I to the mean panel H_M, expressed in mean panel local coordinates. The approximate doublet distribution used for quasi far field computations is now obtained by computing a second order Taylor series for the function μ_M defined by (I.3.19). This computation requires that we compute $\mu_M(0,0)$ and various partial derivatives of μ_M at $(\xi,\eta) = (0,0)$.

In order to compute these derivatives, we need first to express the mapping $\vec{q}'_M(s,t)$ in the following form:

$$\vec{q}'_M(s,t) = \begin{bmatrix} s\,\xi_s + t\,\xi_t + st\,\xi_{st} \\ s\,\eta_s + t\,\eta_t + st\,\eta_{st} \\ 0 \end{bmatrix} = \begin{bmatrix} \xi(s,t) \\ \eta(s,t) \\ 0 \end{bmatrix} \tag{I.3.20}$$

Here, the third component is identically zero because $\vec{q}'_M(s,t)$ is a mapping for the mean panel. We will also need an expression giving the function $\tilde{\mu}(s,t)$ as a linear combination of the panel doublet parameters μ_i. This expression, which is derived from equation (I.3.17) by identifying the coefficients of μ_i as basis functions $\phi_i(s,t)$, has the form

$$\tilde{\mu}(s,t) = \sum_{i=1}^{9} \mu_i \, \phi_i(s,t) \tag{I.3.21}$$

The functions $\phi_i(s,t)$ are defined in the obvious way; for example, by comparing (I.3.21) to (I.3.17) we readily see that

$$\phi_5(s,t) = (1-s^2)\,[t(t+1)/2] \tag{I.3.22}$$

Combining (I.3.19), (I.3.20) and (I.3.21) we write

$$\mu_M(\xi(s,t), \eta(s,t)) = \sum_{i=1}^{9} \mu_i \, \phi_i(s,t) \tag{I.3.23}$$

Setting s=t=0, we obtain

$$\mu_M(0,0) = \sum_{i=1}^{9} \mu_i \, \phi_i(0,0) = \mu_9 \, \phi_9(0,0) = \mu_9 \tag{I.3.24}$$

Differentiating (I.3.23) with respect to (s,t) and setting s=t=0, we obtain the following implicit relation for $(\partial/\partial\xi, \partial/\partial\eta)\,\mu_M \mid_o$

$$(\partial\mu_M/\partial\xi\,,\ \partial\mu_M/\partial\eta)_o \begin{bmatrix} \xi_s & \xi_t \\ \eta_s & \eta_t \end{bmatrix} = \sum_{i=1}^{9} \mu_i \left(\frac{\partial\phi_i}{\partial s}, \frac{\partial\phi_i}{\partial t}\right)_{s=t=0} \tag{I.3.25}$$

If we denote by J the Jacobian matrix appearing on the left,

$$J = \begin{bmatrix} \xi_s & \xi_t \\ \eta_s & \eta_t \end{bmatrix} \tag{I.3.26}$$

we obtain the following relation for the gradient of μ_M:

$$\begin{bmatrix} \partial\mu_M/\partial\xi \\ \partial\mu_M/\partial\eta \end{bmatrix}_o = \sum_{i=1}^{9} \mu_i \; J^{-T} \begin{bmatrix} \partial\phi_i/\partial s \\ \partial\phi_i/\partial t \end{bmatrix}_o \tag{I.3.27}$$

If we differentiate (I.3.23) with respect to (s,t) twice and set s=t=0, we obtain

$$\begin{bmatrix} \xi_s & \eta_s \\ \xi_t & \eta_t \end{bmatrix} \begin{bmatrix} \partial^2\mu_M/\partial\xi^2 & \partial^2\mu_M/\partial\xi\,\partial\eta \\ \partial^2\mu_M/\partial\xi\,\partial\eta & \partial^2\mu_M/\partial\eta^2 \end{bmatrix}_o \begin{bmatrix} \xi_s & \xi_t \\ \eta_s & \eta_t \end{bmatrix}$$

$$+ \ \partial\mu_M/\partial\xi \begin{bmatrix} \xi_{ss} & \xi_{st} \\ \xi_{st} & \xi_{tt} \end{bmatrix} + \partial\mu_M/\partial\eta \begin{bmatrix} \eta_{ss} & \eta_{st} \\ \eta_{st} & \eta_{tt} \end{bmatrix}$$

$$= \sum_{i=1}^{9} \mu_i \begin{bmatrix} \partial^2\phi_i/\partial s^2 & \partial^2\phi_i/\partial s\,\partial t \\ \partial^2\phi_i/\partial s\,\partial t & \partial^2\phi_i/\partial t^2 \end{bmatrix} \qquad \text{(I.3.28)}$$

Since $\partial^2\xi/\partial s^2 = \partial^2\xi/\partial t^2 = 0$, and similarly for $\eta(s,t)$, we may rearrange and simplify this expression to obtain

$$\begin{bmatrix} \partial^2\mu_M/\partial\xi^2 & \partial^2\mu_M/\partial\xi\,\partial\eta \\ \partial^2\mu_M/\partial\xi\,\partial\eta & \partial^2\mu_M/\partial\eta^2 \end{bmatrix} = -\left(\frac{\partial\mu_M}{\partial\xi}\,\xi_{st} + \frac{\partial\mu_M}{\partial\eta}\,\eta_{st}\right) J^{-T} \begin{bmatrix} 0 & 1 \\ 1 & 0 \end{bmatrix} J^{-1}$$

$$+ \sum_{i=1}^{9} \mu_i\, J^{-T} \begin{bmatrix} \phi_{i,st} & \phi_{i,st} \\ \phi_{i,st} & \phi_{i,tt} \end{bmatrix} J^{-1} \qquad \text{(I.3.29)}$$

Now the doublet panel spline matrix $[PSPL^D]$ expresses the various coefficients $\mu_M(0,0)$, $\partial\mu_M/\partial\xi$, ... $\partial\mu_M/\partial\eta^2$ as linear combinations of the panel doublet parameters. Combining equations (I.3.24), (I.3.27) and (I.3.29), we can explicitly write out a formula for the i-th column of $PSPL^D$:

$$\left\{ PSPL_i^D \right\} = \left\{ \begin{array}{c} \phi_i(0,0) \\ \cdots\cdots\cdots\cdots \\ J^{-T} \begin{bmatrix} \partial\phi_i/\partial s \\ \partial\phi_i/\partial t \end{bmatrix}_o \\ \cdots\cdots\cdots\cdots \\ -\left((\xi_{st}, \eta_{st}) J^{-T} \begin{bmatrix} \partial\phi_i/\partial s \\ \partial\phi_i/\partial t \end{bmatrix}_o \right) \begin{bmatrix} S_{11} \\ S_{12} \\ S_{22} \end{bmatrix} + \begin{bmatrix} (\hat{A}_i)_{11} \\ (\hat{A}_i)_{12} \\ (\hat{A}_i)_{22} \end{bmatrix} \end{array} \right\} \qquad \text{(I.3.30)}$$

Here, 2x2 matrices S and A_i are defined by

$$S = J^{-T} \begin{bmatrix} 0 & 1 \\ 1 & 0 \end{bmatrix} J^{-1} \tag{I.3.31}$$

$$A_i = J^{-T} \begin{bmatrix} \partial^2\phi_i/\partial s^2 & \partial^2\phi_i/\partial s\, \partial t \\ \partial^2\phi_i/\partial s\, \partial t & \partial^2\phi_i/\partial t^2 \end{bmatrix}_0 J^{-1} \tag{I.3.32}$$

I.3.2 Half Panel Spline Matrices

Although the quasi-near field procedure for computing the influence of a panel is somewhat more complicated than the quasi-far field procedure, the half panel spline matrices $[HPSPL^S]$, $[HPSPL^D]$ associated with the quasi-near field procedure are somewhat easier to compute than were $[PSPL^S]$ and $[PSPL^D]$. We begin our discussion of their computation by stating clearly what they do.

Given a quadrilateral panel with corner points $(\vec{P}_1, \vec{P}_2, \vec{P}_3, \vec{P}_4)$, we begin by dividing it into two triangular subpanels. If the distance from $\vec{P}_1$ to $\vec{P}_3$ is less than the distance from $\vec{P}_2$ to $\vec{P}_4$, we perform the division (see fig. I.22a)

$$d(\vec{P}_1, \vec{P}_3) < d(\vec{P}_2, \vec{P}_4) \quad : \quad T_2 = (\vec{P}_2, \vec{P}_3, \vec{P}_1)$$
$$T_4 = (\vec{P}_4, \vec{P}_1, \vec{P}_3) \tag{I.3.33}$$

while if the opposite condition holds, we perform the division (see fig. I.18b)

$$d(\vec{P}_2, \vec{P}_4) \leq d(\vec{P}_1, \vec{P}_3) \quad : \quad T_1 = (\vec{P}_1, \vec{P}_2, \vec{P}_4)$$
$$T_3 = (\vec{P}_3, \vec{P}_4, \vec{P}_2) \tag{I.3.34}$$

Having divided the panel into two triangles, we address the problem of computing the coefficients for a linear source and a cubic doublet distribution on each triangular subpanel.

If we denote these distributions by $\sigma(\xi,\eta)$ and $\mu(\xi,\eta)$ respectively, the variables (ξ,η) being local coordinates associated with the triangular half panel under consideration, then our task is to compute half panel spline matrices such that

$$\begin{Bmatrix} \sigma_0 \\ \sigma_\xi \\ \sigma_\eta \end{Bmatrix} = [HPSPL^S] \begin{Bmatrix} \sigma_1 \\ \sigma_2 \\ \sigma_3 \\ \sigma_4 \\ \sigma_9 \end{Bmatrix} \tag{I.3.35}$$

$$\begin{Bmatrix} \mu \\ \mu_\xi \\ \vdots \\ \mu_{\eta\eta} \\ \mu_{\eta\eta\eta} \end{Bmatrix} = [HPSPL^D] \begin{Bmatrix} \mu_1 \\ \mu_2 \\ \vdots \\ \mu_8 \\ \mu_9 \end{Bmatrix} \tag{I.3.36}$$

with functions $\sigma(\xi,\eta)$ and $\mu(\xi,\eta)$ then being given by

$$\sigma(\xi,\eta) = \sigma_0 + \sigma_\xi \xi + \sigma_\eta \eta \tag{I.3.37}$$

$$\begin{aligned} \mu(\xi,\eta) &= \mu_0 + \mu_\xi \xi + \mu_\eta \eta \\ &+ \frac{1}{2} \mu_{\xi\xi} \xi^2 + \mu_{\xi\eta} \xi\eta + \frac{1}{2} \mu_{\eta\eta} \eta^2 \\ &+ \frac{1}{6} \mu_{\xi\xi\xi} \xi^3 + \frac{1}{2} \mu_{\xi\eta} \xi^2\eta + \frac{1}{2} \mu_{\xi\eta\eta} \xi\eta^2 + \frac{1}{6} \mu_{\eta\eta\eta} \eta^3 \end{aligned} \tag{I.3.38}$$

The computation of the source half panel splines is especially easy. To illustrate the procedure, let the triangular half panel under consideration be T_4 of (I.3.33), $(\vec{P}_4, \vec{P}_1, \vec{P}_3)$. Using the formula (I.2.3) for linear interpolation on these points, together with the identification of points

$$\begin{aligned} \vec{P}_4 &= \vec{Q}_1, \quad \text{local coordinates } (\xi_1, \eta_1) \\ \vec{P}_1 &= \vec{Q}_2, \quad \text{local coordinates } (\xi_2, \eta_2) \\ \vec{P}_3 &= \vec{Q}_3, \quad \text{local coordinates } (\xi_3, \eta_3) \end{aligned} \tag{I.3.39}$$

then the source distribution on triangle $(\vec{P}_4, \vec{P}_1, \vec{P}_3)$ is given by

$$\sigma(\xi,\eta) = \sigma_4 L_1(Q) + \sigma_1 L_2(Q) + \sigma_3 L_3(Q)$$

Using the explicit formula for $L_i(Q)$ given by (I.2.4), $(L_i = a_i + b_i\xi + c_i \eta)$, the function $\sigma(\xi,\eta)$ can be written out,

$$\sigma(\xi,\eta) = \lfloor 1, \xi, \eta \rfloor \begin{bmatrix} a_2 & 0 & a_3 & a_1 & 0 \\ b_2 & 0 & b_3 & b_1 & 0 \\ c_2 & 0 & c_3 & c_1 & 0 \end{bmatrix} \begin{Bmatrix} \sigma_1 \\ \sigma_3 \\ \sigma_3 \\ \sigma_4 \\ \sigma_9 \end{Bmatrix} \tag{I.3.41}$$

The matrix appearing on the right hand side of (I.3.41) is the source half panel spline matrix for triangle $(\vec{P}_4, \vec{P}_1, \vec{P}_3)$:

$$T_4 = (\vec{P}_4, \vec{P}_1, \vec{P}_3) \quad : \quad [HPSPL_4^S] = \begin{bmatrix} a_2 & 0 & a_3 & a_1 & 0 \\ b_2 & 0 & b_3 & b_1 & 0 \\ c_2 & 0 & c_3 & c_1 & 0 \end{bmatrix} \tag{I.3.42}$$

The procedure to be followed for any other triangular half panel should now be apparent from this example.

Turning now to the problem of computing the doublet half panel splines, we again consider the special case of triangle $T_4 = (\vec{P}_4, \vec{P}_1, \vec{P}_3)$. Referring to figure I.22a, observe that if the value of μ were known at the seven points $(\vec{P}_4, \vec{P}_1, \vec{P}_3, \vec{M}_2, \vec{P}_7, \vec{P}_8, \vec{C}_4)$, then a cubic distribution of doublet strength could be readily constructed using the interpolation formula given by equations (I.2.11) and (I.2.12). Now of these seven points, five are locations of panel doublet parameters and two ($\vec{M}_2$ and $\vec{C}_4$) are not. Thus, if we can manage to express $\mu(\vec{M}_2)$ and $\mu(\vec{C}_4)$ in terms of the panel doublet parameters by expressions of the form

$$\mu(\vec{M}_2) = \sum_{i=1}^{9} m_{2,i}\, \mu_i \tag{I.3.43}$$

$$\mu(\vec{C}_4) = \sum_{i=1}^{9} c_{4,i}\, \mu_i \tag{I.3.44}$$

then we will immediately be able to write down an expression for $\mu(Q)$ on $T_4 = (\vec{P}_4, \vec{P}_1, \vec{P}_2)$ as a linear combination of $\{\mu_i\}_{i=1}^{9}$. This is done as follows. Combining equations (I.2.11) and (I.2.12) while making the identifications

$$\vec{P}_4 = \vec{Q}_1 \qquad \vec{M}_2 = \vec{Q}_1'$$
$$\vec{P}_1 = \vec{Q}_2 \qquad \vec{P}_7 = \vec{Q}_2' \qquad \vec{C}_4 = \vec{M}$$
$$\vec{P}_3 = \vec{Q}_3 \qquad \vec{P}_8 = \vec{Q}_3' \tag{I.3.45}$$

we obtain after some manipulation

$$\begin{aligned}\mu(\vec{Q}) = &\sum_{i=1}^{3} \mu(\vec{Q}_i)\,[B_i(\vec{Q}) - B_i(\vec{M})\,C(\vec{Q})] \\ &+ \sum_{i=1}^{3} \mu(\vec{Q}_i')\,[B_i'(\vec{Q}) - B_i'(\vec{M})\,C(\vec{Q})] \\ &+ \mu(\vec{M})\,C(\vec{Q})\end{aligned} \tag{I.3.46}$$

that is,

$$\begin{aligned}\mu(\vec{Q}) = &\ \mu_4\,[B_1(\vec{Q}) - B_1(\vec{M})\,C(\vec{Q})] \\ &+ \mu_1\,[B_2(\vec{Q}) - B_2(\vec{M})\,C(\vec{Q})] \\ &+ \mu_3\,[B_3(\vec{Q}) - B_3(\vec{M})\,C(\vec{Q})] \\ &+ \left(\sum_{i=1}^{9} m_{2,i}\,\mu_i\right)[B_1'(\vec{Q}) - B_1'(\vec{M})\,C(\vec{Q})] \\ &+ \mu_7\,[B_2'(\vec{Q}) - B_2'(\vec{M})\,C(\vec{Q})] \\ &+ \mu_8\,[B_3'(\vec{Q}) - B_3'(\vec{M})\,C(\vec{Q})] \\ &+ \left(\sum_{i=1}^{9} c_{4,i}\,\mu_i\right) C(\vec{Q})\end{aligned} \tag{I.3.47}$$

This last equation yields an expression for the doublet half panel spline matrix as follows. Let [G] be a matrix containing the polynomial coefficients of the basis functions B_i, B_i', C. We express this fact algebraically by the equation

$$\begin{aligned}&\lfloor B_1, B_2, B_3, B_1', B_2', B_3', C \rfloor = \\ &\quad = \lfloor 1, \xi, \eta, \frac{\ }{2}^2, \xi\eta, \ldots \frac{\xi\eta^2}{2}, \frac{\eta^3}{6} \rfloor [G]^{10\times 7}\end{aligned} \tag{I.3.48}$$

Now using the facts that

$$B_i(\vec{M}) = -1/9 \tag{I.3.49}$$

$$B_i'(\vec{M}) = 4/9 \tag{I.3.50}$$

we can write $\mu(Q)$ as given by (I.3.47) in the form

$$\mu(Q) = \left\lfloor 1, \xi, \eta, \ldots \frac{\eta^3}{6} \right\rfloor [G]^{10x7} [T]^{7x7} [K]^{7x9} \begin{Bmatrix} \mu_1 \\ \mu_2 \\ \vdots \\ \mu_9 \end{Bmatrix} \tag{I.3.51}$$

where [T] accounts for the stray multiples of C(Q) appearing in (I.3.47):

$$[T]^{7x7} = \begin{bmatrix} 1 & & & & & & \\ & 1 & & & & & \\ & & 1 & & & & \\ & & & 1 & & & \\ & & & & 1 & & \\ & & & & & 1 & \\ \frac{1}{9} & \frac{1}{9} & \frac{1}{9} & -\frac{4}{9} & -\frac{4}{9} & -\frac{4}{9} & 1 \end{bmatrix} \tag{I.3.52}$$

and [K] expresses the seven required values of μ in terms of $\{\mu_i\}_{i=1}^{9}$

$$[K]^{7x9} = \begin{bmatrix} & & \vec{e}_4^T & \\ & & \vec{e}_1^T & \\ & & e_3^T & \\ m_{2,1} & m_{2,2} & \cdots & m_{2,9} \\ & & \vec{e}_7^T & \\ & & \vec{e}_8^T & \\ c_{4,1} & c_{4,2} & \cdots & c_{4,9} \end{bmatrix} \tag{I.3.53}$$

Here, the notation $\vec{e}_k$ denotes the k-th natural unit vector in R^9. The doublet half panel spline matrix for the triangle $T_4 = (\vec{P}_4, \vec{P}_1, \vec{P}_3)$ is now given by

$$[HPSPL_4^D]^{10x9} = [G]^{10x7} [T]^{7x7} [K]^{7x9} \tag{I.3.54}$$

that is, it is just the matrix sandwiched between the two vectors in equation (I.3.51).

All that remains to be done now, is to describe the computation of the coefficients $\{m_{2,i}\}$ and $\{c_{4,1}\}$ appearing in equations (I.3.43) and (I.3.44). These coefficients are computed with the help of the isoparametric representation of a panel (cf. equation (I.3.14)) together with the doublet distribution $\mu(s,t)$ on the canonical square I given by equation (I.3.17) or (I.3.21). We describe the procedure for computing $\{m_{2,i}\}$, the procedure for computing $\{c_{4,i}\}$ being essentially the same.

Now the computation of $\{m_{2,i}\}$ is essentially equivalent to the problem of computing $\mu(\vec{M}_2)$ or, since $\vec{M}_2$ may not actually lie on the panel, of computing $\mu(\vec{M}_2^+)$ where $\vec{M}_2^+$ is the point on the panel lying closest to $\vec{M}_2$. If, instead of finding $\vec{M}_2^+$, we find the point $\vec{M}_2^*$ on the approximate panel H that is closest to $\vec{M}_2$:

$$\vec{M}_2^* = \vec{q}(s^*, t^*) \tag{I.3.55}$$

then we may estimate $\mu(\vec{M}_2)$ as $\tilde{\mu}(s^*, t^*)$. Here (s^*, t^*) are the s-t coordinates of the point $\vec{M}_2^* \varepsilon H$ that solves the minimization problem

$$\begin{aligned} |\vec{M}_2 - \vec{M}_2^*| &= \min_{Q \varepsilon H} |\vec{M}_2 - \vec{Q}| \\ &= \min_{(s,t) \varepsilon I} |\vec{M}_2 - \vec{q}(s,t)| \end{aligned} \tag{I.3.56}$$

Given these coordinates (s^*, t^*) for the point $\vec{M}^* \varepsilon H$ nearest to $\vec{M}_2$, we take $\mu(\vec{M}_2) = \mu(\vec{M}_2^*)$. Combining this choice with equation (I.3.18) and (I.3.21) yields:

$$\begin{aligned} \mu(\vec{M}_2) = \mu(\vec{M}_2^*) = \mu(\vec{q}(s^*, t^*)) &= \tilde{\mu}(s^*, t^*) \\ &= \sum_{i=1}^{9} \mu_i \phi_i (s^*, t^*) \end{aligned} \tag{I.3.57}$$

Comparing this last result to equation (I.3.43) leads immediately to the formula for the coefficients $m_{2,I}$:

$$m_{2,i} = \phi_i(s^*, t^*) \ . \tag{I.3.58}$$

It should now be clear how the coefficients $c_{4,i}$ are computed: One simply finds the s-t coordinates of the point $\vec{C}_4^* \in H$ nearest to $\vec{C}_4$ and then performs the evaluation

$$c_{4,i} = \phi_i(s^*, t^*) \quad \text{where} \quad \vec{C}_4^* = \vec{q}(s^*, t^*) \ . \tag{I.3.59}$$

I.4 Panel Moment Matrices

A number of panel moment matrices are computed in PAN AIR for use in the far field evaluation of panel influence coefficients (see section J.9) and for certain post-processing functions (see section O.2). In this section we define these panel moments and describe their computation. Far field moments are treated in section I.4.1, post-processing moments are treated in section I.4.2 and finally, in section I.4.3, the computation of the basic flat panel moments is described. These basic flat panel moments are defined by the expression

$$C_{ij} = \iint_{\Sigma} \xi^i \eta^j \, d\xi \, d\eta \qquad 0 \leq i+j \leq N \tag{I.4.1}$$

Here, (ξ,η) are local coordinates on the surface of a flat panel Σ. We will find it convenient in our discussion of far field and post-processing moments to assume that flat panel moments of the form (I.4.1) can be readily computed, given the corner points of Σ in local coordinates.

I.4.1 Far Field Moments

The panel moments used in the evaluation of far field panel influences are now described. We begin by noting that the far field PIC procedure estimates a panel influence by implementing the following approximations:

(i) The panel is replaced by its mean panel.

(ii) Singularity distributions σ and μ are replaced by their quasi-far field approximations (see section I.3.2).

(iii) The kernel functions $(1/R)$ and $\nabla(1/R)$ are replaced by Taylor series approximations of degree 0 (monopole), 1 (dipole) or 2 (quadrupole).

The analysis of these approximations is carried out in detail in appendix J.9. At this point we are merely concerned with describing the computation of the far field moments that are defined by that analysis.

Toward this end, let the mean panel expressed in its local coordinates (ξ,η) be denoted by Σ_m. We define a collection of basis functions $\phi_\alpha(\xi,\eta)$, defined on Σ_m, as follows

$$\phi_\alpha : \; [1, \xi, \eta, \xi^2/2, \xi\eta, \eta^2/2, \xi^3/6, \xi^2\eta/2, \xi\eta^2/2, \eta^3/6] \tag{I.4.2}$$

Thus, for example $\phi_8(\xi,\eta) = \xi^2\eta/2$. Using the alternate notation for ξ and η:

$$\rho_1 = \xi \tag{I.4.3}$$

$$\rho_2 = \eta$$

we define the far field moments as follows (for motivation of these definitions, examine the coefficients appearing in equations (J.9.42-43)):

$$H_{\alpha\beta} = \frac{s}{\kappa} \iint_{\Sigma_m} \phi_\alpha \, \phi_\beta \, d\xi \, d\eta \qquad \begin{array}{l} 1 \leq \alpha \leq 10 \\ 1 \leq \beta \leq 6 \end{array} \tag{I.4.4}$$

$$\bar{H}_{i\alpha\beta} = \frac{s}{\kappa} \iint_{\Sigma_m} \rho_i \, \phi_\alpha \, \phi_\beta \, d\xi \, d\eta \qquad \begin{array}{l} 1 \leq i \leq 2 \\ 1 \leq \alpha \leq 6 \\ 1 \leq \beta \leq 3 \end{array} \tag{I.4.5}$$

In writing down these definitions, we have used the usual symbols s and κ to denote the following:

$$s = \begin{cases} +1 & \text{subsonic flow, } M_\infty < 1 \\ -1 & \text{supersonic flow, } M_\infty > 1 \end{cases} \tag{I.4.6}$$

$$\kappa = \begin{cases} 4\pi & \text{subsonic flow, } M_\infty < 1 \\ 2\pi & \text{supersonic flow, } M_\infty > 1 \end{cases} \tag{I.4.7}$$

A quick examination of the definitions (I.4.4-5) together with a look at the definitions of ϕ_α, (I.4.2) and ρ_i, (I.4.3) shows that the integrals in equations (I.4.4-5) are all of the form

$$\iint_{\Sigma_m} (\text{constant}) \quad \xi^i \, \eta^j \, d\xi \, d\eta \, , \qquad 0 \leq i+j \leq 5$$

These, of course, are just integrals of the form C_{ij} (see equation (I.4.1)) which we will discuss in section I.4.3.

I.4.2 Post Processing Panel Moments

A number of the post processing options in PAN AIR require the evaluation of panel integrals of the following form:

$$\iint_{\text{panel}} f \; dS$$

$$\iint_{\text{panel}} \hat{n} \; f \; dS$$

$$\iint_{\text{panel}} (\vec{Q} - \vec{P}_g) \; f \; dS$$

$$\iint_{\text{panel}} (\vec{Q} - \vec{P}_g) \times \hat{n} \; f \; dS$$

Here, f is a function specified at the nine panel doublet parameter locations and extended to the whole panel with the doublet inner splines. The vector $\hat{n}$ is the panel's unit normal, $\vec{P}_9$ is the panel center and $\vec{Q}$ is a position vector on the surface of the panel. If we denote by $\vec{f}$ the vector of the nine specified values of f our goal is to compute matrices having the following properties

$$\frac{s\beta^2}{\kappa} \iint_{\text{panel}} f \; dS = \lfloor FFM_0^D \rfloor^{1x9} \vec{f} \tag{I.4.8}$$

$$\frac{s\beta^2}{\kappa} \iint_{\text{panel}} \hat{n} \; f \; dS = [FFM_1^D]^{3x9} \vec{f} \tag{I.4.9}$$

$$\iint_{\text{panel}} (\vec{Q} - \vec{P}_9) \; f \; dS = [NCPM_1]^{3x9} \vec{f} \tag{I.4.10}$$

$$\iint_{\text{panel}} (\vec{Q} - \vec{P}_9) \times \hat{n} \; f \; dS = [NCPM_2]^{3x9} \vec{f} \tag{I.4.11}$$

We begin our discussion of the computation of these matrices by addressing the computation of FFM_1^D, as this allows us to introduce most of the notation we will need to handle the others.

We start the analysis of $[FFM_1^D]$ by breaking up the integral appearing on the left hand side of (I.4.9) into integrals over the 8 triangular subpanels, T_k:

$$\frac{s\beta^2}{\kappa} \iint_{\text{panel}} f \; \hat{n} dS = \sum_{k=1}^{8} \frac{s\beta^2}{\kappa} \iint_{T_k} f \; \hat{n} \; dS \tag{I.4.12}$$

Now on each triangular subpanel, the function f is given by a formula analogous to equation (I.2.2):

$$f \Big|_{T_k} = (1, \xi, \eta, \frac{\xi^2}{2}, \xi\eta, \frac{\eta^2}{2}) \; [SPSPL_k^D] \; \vec{f}$$

$$= \vec{\phi}^T \; [SPSPL_k^D] \; \vec{f} \tag{I.4.13}$$

where we have introduced the notation $\vec{\phi}^T$ for the row vector of basis functions on T_k:

$$\vec{\phi}^T = (1, \xi, \eta, \xi^2/2, \xi\eta, \eta^2/2) \tag{I.4.14}$$

Now a slight modification of equation (E.1.28) enables us to write $(\hat{n}dS)$ in terms of $\hat{n}'dS' = \hat{n}'d\xi\, d\eta$. This expression reads

$$\hat{n}\, dS \Big|_{T_k} = (1/\det(A))\; A_k^T\, \hat{n}'\, dS'$$

$$= (1/\beta^2)\; A_k^T \begin{bmatrix} 0 \\ 0 \\ 1 \end{bmatrix} d\xi\, d\eta \tag{I.4.15}$$

Substituting (I.4.13) and (I.4.15) into (I.4.12) yields then

$$\frac{s\beta^2}{\kappa} \iint_{\text{panel}} f\; \hat{n}\; dS = \sum_{k=1}^{8} \left(\frac{s}{\kappa}\right) A_k^T \begin{bmatrix} 0 \\ 0 \\ 1 \end{bmatrix} \iint_{T_k} \vec{\phi}^T\, [SPSPL_k^D]\, \vec{f}\, d\xi\, d\eta \tag{I.4.16}$$

Identifying the coefficient of $\vec{f}$ in this expression as the matrix $[FFM_1^D]$, we obtain after some simplification

$$[FFM^D] = \frac{s}{\kappa} \sum_{k=1}^{8} A_k^T \begin{bmatrix} 0 \\ 0 \\ 1 \end{bmatrix} \iint_{T_k} \vec{\phi}^T\, d\xi\, d\eta \quad [SPSPL_k^D] \tag{I.4.17}$$

In order to carry out a similar procedure for equation (I.4.8), we must introduce the area Jacobian J_k for the reference to local coordinate transformation on subpanel T_k. This quantity is given by equation (E.3.109). Applying that formula to the case under consideration, we have

$$J_k = dS/dS' = 1/[\beta\; |\{\hat{n}_k, \hat{n}_k\}|^{1/2}] \tag{I.4.18}$$

Using this quantity to transform area integrals over T_k from reference to local coordinates, we obtain for the left hand side member of (I.4.8):

$$\frac{s\beta^2}{\kappa} \iint_{\text{panel}} f\; dS = \sum_{i=1}^{8} \frac{s\beta^2}{\kappa} \iint_{T_k} (\vec{\phi}^T\, [SPSPL_k^D]\, \vec{f})\, (J_k\, d\xi\, d\eta)$$

$$= \sum_{k=1}^{8} \frac{s\beta^2}{\kappa} J_k \left(\iint_{T_k} \vec{\phi}^T\, d\xi\, d\eta \right) [SPSPL_k^D]\, \vec{f} \tag{I.4.19}$$

Clearly, the row vector $\llcorner FFM_0^D \lrcorner$ must be given by

$$\llcorner FFM_0^D \lrcorner = \frac{s\beta^2}{\kappa} \sum_{k=1}^{8} J_k \iint_{T_k} \vec{\phi}^T \, d\xi \, d\eta \quad [SPSPL_k^D] \tag{I.4.20}$$

The computation of $[NCPM_1]$, associated with equation (I.4.10) proceeds in a similar fashion. Here however we must introduce some more specific notation to describe the transformation from the reference coordinate system to subpanel T_k's local coordinate system. Letting $\vec{P}_{o,k}$ denote the origin of this coordinate system in reference coordinates, the local coordinates $\vec{Q}'$ of a point Q are given

$$\vec{Q}' = A_k (\vec{Q} - \vec{P}_{o,k}) \tag{I.4.21}$$

Note that $\vec{Q}-\vec{P}_9$ can be expressed

$$\vec{Q} - \vec{P}_9 = \vec{Q} - \vec{P}_{o,k} + \vec{P}_{o,k} - \vec{P}_9$$

$$= A_k^{-1} (\vec{Q}' - \vec{P}'_{9,k}) \tag{I.4.22}$$

where

$$\vec{P}'_{9,k} = A_k (\vec{P}_9 - \vec{P}_{o,k}) \tag{I.4.23}$$

Transforming the various pieces of equation (I.4.10) into panel local coordinates, we obtain

$$\iint_{panel} (\vec{Q}-\vec{P}_9) \, \vec{f} \, dS = \left\{ \sum_{k=1}^{8} J_k A_k^{-1} \iint_{T_k} (\vec{Q}'-\vec{P}'_{9,k}) \, \vec{\phi}^T \, [SPSPL_k^D] \, d\xi \, d\eta \right\} \vec{f} \tag{I.4.24}$$

The expression in curly brackets on the right is the matrix $[NCPM_1]$:

$$[NCPM_1] = \sum_{k=1}^{8} J_k A_k^{-1} \left[\iint_{T_k} (\vec{Q}'-\vec{P}_{9,k}) \, \phi^T \, d\xi \, d\eta \right] [SPSPL_k^D] \tag{I.4.25}$$

Note that the integrals are readily reducible to the form of the C_{ij} integrals, (I.4.1):

$$\iint_{T_k} \vec{Q}' \, \phi_\alpha \, d\xi \, d\eta = \iint_{T_k} \begin{bmatrix} \xi \\ \eta \\ 0 \end{bmatrix} \phi_\alpha \, d\xi \, d\eta$$

$$\iint_{T_k} \vec{P}'_{9,k} \, \phi_\alpha \, d\xi \, d\eta = \vec{P}'_{9,k} \iint_{T_k} \phi_\alpha \, d\xi \, d\eta$$

We conclude our discussion by evaluating (I.4.11) to express the matrix $[NCPM_2]$ in elementary terms. Proceeding as before, we find

$$\iint_{\text{panel}} (\vec{Q}-\vec{P}_9) \times \hat{n} \, f \, dS$$

$$= \sum_{k=1}^{8} \frac{1}{\beta^2} \iint_{T_k} \left(A_k^{-1} (\vec{Q}'-\vec{P}'_{9,k}) \times A_k^T \begin{bmatrix} 0 \\ 0 \\ 1 \end{bmatrix} \right) \vec{\phi}^T \, [SPSPL_k^D] \, \vec{f} \, d\xi \, d\eta$$

$$= - \sum_{k=1}^{8} \frac{1}{\beta^2} A_k^T \begin{bmatrix} 0 \\ 0 \\ 1 \end{bmatrix} \times A_k^{-1} \left[\iint_{T_k} (\vec{Q}'-\vec{P}'_{9,k}) \, \vec{\phi}^T \, d\xi \, d\eta \right] [SPSPL_k^D] \, \vec{f} \qquad (I.4.26)$$

Identifying the coefficient matrix as $[NCPM_2]$, we have

$$[NCPM_2] = - \sum_{k=1}^{8} \frac{1}{\beta^2} A_k^T \begin{bmatrix} 0 \\ 0 \\ 1 \end{bmatrix} \times A_k^{-1} \left[\iint_{T_k} (\vec{Q}'-\vec{P}'_{9,k}) \, \vec{\phi}^T \, d\xi \, d\eta \right] [SPSPL_k^D] \qquad (I.4.27)$$

I.4.3 Evaluation of Elementary Flat Panel Moments

The evaluation of the elementary flat panel moments C_{ij} defined by equation (I.4.1) is now addressed. We begin by applying Gauss' theorem in the plane to obtain,

$$C_{ij} = \iint_{\Sigma} \xi^i \, \eta^j \, d\xi \, d\eta = \frac{1}{(i+1)} \iint_{\Sigma} \frac{\partial}{\partial \xi} (\xi^{i+1} \, \eta^j) \, d\xi \, d\eta$$

$$= \frac{1}{(i+1)} \int_{\partial \Sigma} \hat{n}_\xi \, \xi^{i+1} \, \eta^j \, ds \qquad (I.4.28)$$

Breaking the boundary integral up into a sum of integrals over the individual edges E_k of $\partial \Sigma$, we obtain

$$C_{ij} = \frac{1}{i+1} \sum_k \int_{E_k} \hat{n}_\xi \; \xi^{i+1} \eta^j \, ds \tag{I.4.29}$$

Let edge E_k be parameterized by a variable $\tau \in [0,1]$ so that along the edge, ξ and η are given by

$$\begin{aligned} \xi &= \xi_k + (\Delta \xi_k)\tau \\ \eta &= \eta_k + (\Delta\eta_k)\tau \qquad 0 \le \tau \le 1 \end{aligned} \tag{I.4.30}$$

Note that the unit tangent $\hat{t}$, the unit normal $\hat{n}$ and the element of arclength ds are given by

$$\hat{t} = \begin{bmatrix} \Delta\xi_k \\ \Delta\eta_k \end{bmatrix} [\Delta\xi_k^2 + \Delta\eta_k^2]^{1/2} \tag{I.4.31}$$

$$\hat{n} = \begin{bmatrix} \Delta\eta_k \\ -\Delta\xi_k \end{bmatrix} [\Delta\xi_k^2 + \Delta\eta_k^2]^{1/2} \tag{I.4.32}$$

$$ds = [\Delta\xi_k^2 + \Delta\eta_k^2]^{1/2} \, d\tau \tag{I.4.33}$$

Combining the first component of (I.4.32) with (I.4.33) gives for n_ξ ds:

$$n_\xi \, ds = \Delta\eta_k \, d\tau \tag{I.4.34}$$

Substituting this into (I.4.29) yields for C_{ij}

$$C_{ij} = \sum_k \frac{\Delta\eta_k}{i+1} \int_0^1 \xi^{i+1} \eta^j \, d\tau \tag{I.4.35}$$

Evidently we need to be able to compute edge integrals of the form

$$G_{ij}^{(k)} = \int_{\text{edge } E_k}^{1} \xi^i \eta^j \, d\tau \tag{I.4.36}$$

Once this has been done, we will be able to compute C_{ij} from

$$C_{ij} = \sum_k \frac{\Delta\eta_k}{i+1} G^{(k)}_{i+1,j} \tag{I.4.37}$$

Turning now to the problem of computing the integrals $G^{(k)}_{ij}$, we suppress the superscript k and write

$$G_{ij} = \int_0^1 \xi^i \eta^j \, d\tau \qquad 0 \leq i+j \leq N+1 \tag{I.4.38}$$

with $\xi(\tau)$ and $\eta(\tau)$ given by

$$\begin{aligned} \xi &= \xi_o + (\Delta\xi)\tau \\ \eta &= \eta_o + (\Delta\eta)\tau \end{aligned} \tag{I.4.39}$$

The entries of G can be computed quite effectively by a simple recursive procedure. We begin by defining some auxiliary integrals H_{ij}:

$$H_{ij} = \int_0^1 \tau^i \eta^j \, d\tau \qquad 0 \leq i+j \leq N+1 \tag{I.4.40}$$

These are easy to compute. The entries of column j=0 are trivial:

$$H_{io} = 1/(i+1) \tag{I.4.41}$$

and the entries of subsequent columns can be computed by the recursion

$$\begin{aligned} H_{ij} &= \int_0^1 \tau^i \eta^{j-1} (\eta_o + \Delta\eta . \tau) \, d\tau \\ &= \eta_o H_{i,j-1} + \Delta\eta H_{i+1,j-1} \qquad 0 \leq i \leq N+1-j \end{aligned} \tag{I.4.42}$$

The integrals H_{ij} can then be transformed into the integrals G_{ij} by performing a similar procedure for each column of the array H. The recursion formula reads

$$\begin{aligned} \int_0^1 \xi^k \tau^{i-k} \eta^j \, d\tau &= \int_0^1 \xi^{k-1} (\xi_o + (\Delta\xi)\tau) \tau^{i-k} \eta^j \, d\tau \\ &= \xi_o \left(\int_0^1 \xi^{k-1} \tau^{i-k} \eta^j \, d\tau \right) + \Delta\xi \left(\int_0^1 \xi^{k-1} \tau^{i-k+1} \eta^j \, d\tau \right) \end{aligned} \tag{I.4.43}$$

A simple Algol-like procedure implementing these ideas is outlined below. The only feature of especial interest is the fact that the recursion in the third segment is run backward so that the procedure can be performed in place.

Algorithm for evaluating edge integrals G_{ij} (cf. equation (I.4.38))

```
<Initialization:  Equation (I.4.41)>

for i = 0(1) N+1 do

      G_io = 1/(i+1)

end i

<Recursion for η:  Equation (I.4.42)>

for j = 1(1) N+1 do

     for i = 0(1) N+1-j do

          G_ij = η_o G_i,j-1 + Δη G_i+1,j-1

     end i

end j

<Double recursion for ξ :  Equation (I.4.43)>

for j = 0(1) N do

     for k = 1(1) N+1-j

          for i = N+1-j (-1) k <Recursion is run backward>

              G_ij ← ξ_o G_i-1,j + Δξ  G_ij
          end i

     end k

end j
```

I.5 Constrained Least Squares

I.5.1 Definition of the Problem

In this section we discuss the solution to the following rather general problem, called the constrained least squares problem. Let A be a jxn matrix, $0 < j < n$, of rank j. Let A' be a kxn matrix, $j + k \geq n$. Let $\vec{b}$, $\vec{b}'$, and $\vec{w}$ be vectors of length j, k, and k, respectively. Then we wish to find the nx(j+k) matrix LSQ such that the vector $\vec{x}$ satisfying

$$[A]^{jxn}\ \vec{x}^{nx1} = \vec{b} \tag{I.5.1}$$

while minimizing

$$J = \sum_{i=1}^{k} w_i^2 \left(\sum_{s=1}^{n} A_{is}'\ x_s - b'_i \right)^2 \tag{I.5.2}$$

is given by

$$\vec{x} = [LSQ]^{nx(j+k)} \left\{ \frac{\vec{b}}{\vec{b}'} \right\} \tag{I.5.3}$$

I.5.2 Elimination of the Weights

Now, first we simplify (I.5.2) by noting that if we define a (kxk) matrix [W]:

$$[W]_{ij} = \delta_{ij}\ w_i \tag{I.5.4}$$

then

$$J = \sum_{i=1}^{k} \left(\sum_{s=1}^{n} w_i\ A_{is}'\ x_s - w_i\ b_i' \right)^2$$

$$= \sum_{i=1}^{k} \left[\sum_{j=1}^{k} \left(\sum_{s=1}^{n} W_{ij}\ A'_{js}\ x_s - W_{ij}\ b_j' \right) \right]^2$$

$$= \sum_{i=1}^{k} \left(\sum_{s=1}^{n} \bar{A}_{is}\ x_s - b_i \right)^2 \tag{I.5.5}$$

where

$$[\bar{A}] = [W]\ [A']$$

$$b = [W]\ b' \tag{I.5.6}$$

I.5.3 The Case of No Exact Constraints

First, we will consider the minimization of J in (I.5.5) in the special case when j=0; that is, when there are no exact constraints on x of the form (I.5.1). Now, the quantity J is a quadratic function in the variables (x_s), and since it is a non-negative function, we see that it is minimized for that vector x for which all first derivatives of the expression with respect to the x_s 's are zero. That is, minimization of (I.5.5) is equivalent to the requirement

$$\frac{\partial}{\partial x_l} \sum_{i=1}^{k} \left(\sum_{s=1}^{n} \bar{A}_{is} x_s - b_i \right)^2 = 0 \qquad (I.5.7)$$

$$l = 1,\ldots,n$$

Now,

$$\frac{\partial}{\partial x_l} \sum_{i=1}^{k} \left(\sum_{s=1}^{n} \bar{A}_{is} x_s - b_i \right)^2 =$$

$$\sum_{i=1}^{k} 2\left(\sum_{s=1}^{n} \bar{A}_{is} x_s - b_i \right) \frac{\partial}{\partial x_l} \sum_{s=1}^{n} \bar{A}_{is} x_s = \qquad (I.5.8)$$

$$2 \sum_{i=1}^{k} \left(\sum_{s=1}^{n} \bar{A}_{is} x_s - b_i \right) \bar{A}_{il} = \qquad (I.5.9)$$

$$2 \sum_{i=1}^{k} \bar{A}_{il} (A\vec{x} - \vec{b})_i = 2(\bar{A}^T \bar{A} \vec{x} - \bar{A}^T \vec{b})_l = 0 \qquad (I.5.10)$$

Since (I.5.10) holds for each value of l, l = 1,...,n, we have

$$[\bar{A}^T \bar{A}]\vec{x} = [\bar{A}^T] \vec{b} \qquad (I.5.11)$$

or

$$\vec{x} = [[\bar{A}^T \bar{A}]^{-1} \bar{A}^T] \vec{b} \qquad (I.5.12)$$

Comparing to (I.5.3) and (I.5.6), and recalling j=0, we get

$$[LSQ] = [A'^T W^T WA']^{-1} [A'^T W^T] [W] \qquad (I.5.13)$$

Within the PAN AIR code, equation (I.5.11) is solved without actually forming $[\bar{A}^T \bar{A}]$ and inverting it. The method actually used there, which involves factorization of $[\bar{A}^T \bar{A}]$ into a product of lower triangular and upper triangular matrices, is more efficient and more precise than the method indicated by (I.5.13).

I.5.4 Reduction of the General Case

Next, let us assume $j > 0$, so that there are non-trivial exact constraints of the form (I.5.1). Since A has rank j, its columns can be rearranged (that is, "pivoting" performed) so that the first j columns of the revised matrix A^* are linearly independent, and thus

$$[A^*] = [A_{11}{}^{j\times j} \mid A_{12}{}^{j\times(n-j)}] \qquad (I.5.14)$$

Here, the relationship between A* and A is that

$$[A^*]^{j\times n} = [A]^{j\times n} [P]^{n\times n} \qquad (I.5.15a)$$

where [P] is a product of matrices which are the identity except for one non-zero off-diagonal term (for any real number a, adding a times column i to column j is performed by multiplying on the right by the matrix with 1's on the diagonal, the value a in the (i,j) position, and 0's elsewhere; its inverse has -a in the (i,j) position).

That is, a typical matrix P is

$$P = \begin{bmatrix} 1 & & & 0 \\ 0 & 1 & & \\ 0 & 0 & 1 & \\ 0 & a & 0 & 1 \end{bmatrix} \qquad (I.5.15b)$$

$$P^{-1} = \begin{bmatrix} 1 & & & 0 \\ 0 & 1 & & \\ 0 & 0 & 1 & \\ 0 & -a & 0 & 1 \end{bmatrix} \qquad (I.5.15c)$$

So, (I.5.1) becomes

$$[A]\vec{x} = [A^*] [P]^{-1}\vec{x} = [A_{11} \mid A_{12}]^{j\times n} (P^{-1} \vec{x})^{n\times 1} = \vec{b} \qquad (I.5.16)$$

Writing

$$P^{-1}\vec{x} = \begin{Bmatrix} \vec{x}_1{}^{j\times 1} \\ \vec{x}_2{}^{(n-j)\times 1} \end{Bmatrix} \qquad \text{I.5.17)}$$

we have

$$[A_{11}\ A_{12}] \begin{Bmatrix} \vec{x}_1 \\ \vec{x}_2 \end{Bmatrix} = \vec{b} \qquad \text{(I.5.18)}$$

while we also want to minimize

$$\left| [A_{21}\ A_{22}] \begin{Bmatrix} \vec{x}_1 \\ \vec{x}_2 \end{Bmatrix} - \vec{b}' \right|^2 \qquad \text{(I.5.19)}$$

where

$$[A_{21}^{k\times j}\ \ A_{22}^{k\times(n-j)}] = [A]^{k\times n}\,[P^{-1}]^{n\times n} \qquad \text{(I.5.20)}$$

Now, since the j columns of A_{11} are independent, A_{11} is invertible, and thus, by (I.5.18),

$$[A_{11}]\ x_1 = -[A_{12}]\ x_2 + b \qquad \text{(I.5.21)}$$

or

$$\vec{x}_1{}^{(j\times 1)} = [A_{11}{}^{-1}]\ j\times j - [A_{12}]\ j\times(n-j)\ \ \vec{x}_2{}^{(n-j)\times 1} + \vec{b}(j\times 1) \qquad \text{(I.5.22)}$$

Substituting (I.5.22) into (I.5.19), we want to minimize

$$\left|[A_{21}]\ \vec{x}_1 + [A_{22}]\ \vec{x}_2 - \vec{b}'\right|^2 =$$

$$\left| \begin{matrix} -[A_{21}]^{k\times j}\ [A_{11}^{-1}]^{j\times j}\ [A_{12}]^{j\times(n-j)}\ \ \vec{x}_2{}^{(n-j)\times 1} \\ +[A_{21}]^{k\times j}\ [A_{11}^{-1}]^{j\times j}\ \ \vec{b}(j\times 1) - \vec{b}'(k\times 1) + [A_{22}]\vec{x}_2 \end{matrix} \right|^2 \qquad \text{(I.5.23)}$$

But this is just a least squares problem with no exact constraints, that is, it requires the minimization of

$$\left|[A^{\circ}]\ \vec{x}_2 - \vec{b}_0\right|^2 \qquad \text{(I.5.24)}$$

where

$$[A^{o}]^{kx(n-j)} = -[A_{21}]^{kxj} [A_{11}^{-1}]^{jxj} [A_{12}]^{jx(n-j)} + [A_{22}] \tag{I.5.25}$$

and

$$\vec{b}_{o}^{\,kx1} = -[A_{21}]^{(kxj)} [A_{11}^{-1}]^{jxj} \vec{b}^{(jx1)} + \vec{b}'^{(kx1)} \tag{I.5.26}$$

This minimization procedure is described by equations (I.5.5-12), and results in a matrix LSQ^{o} such that

$$\vec{x}_2 \; (n-j)x1 = [LSQ^{o}]^{(n-j)xk} \vec{b}_{o}^{(kx1)} \tag{I.5.27}$$

Combining (I.5.22), (I.5.26), and (I.5.27), we have obtained $\vec{x}_1$ and $\vec{x}_2$, and as linear combinations of entries of $\vec{b}$ and $\vec{b}'$. Thus, we have shown in principle how the constrained least square problem is solved. Considerations of efficiency cause complexities which will not be discussed here.

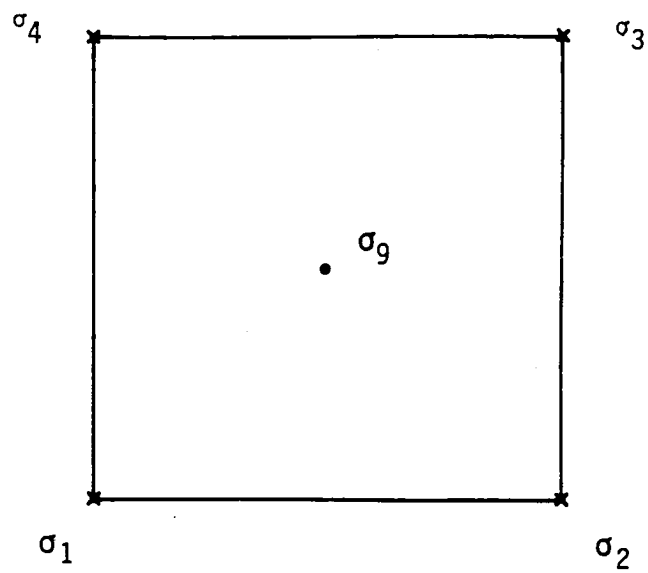

Figure I.1a - Panel source parameter locations

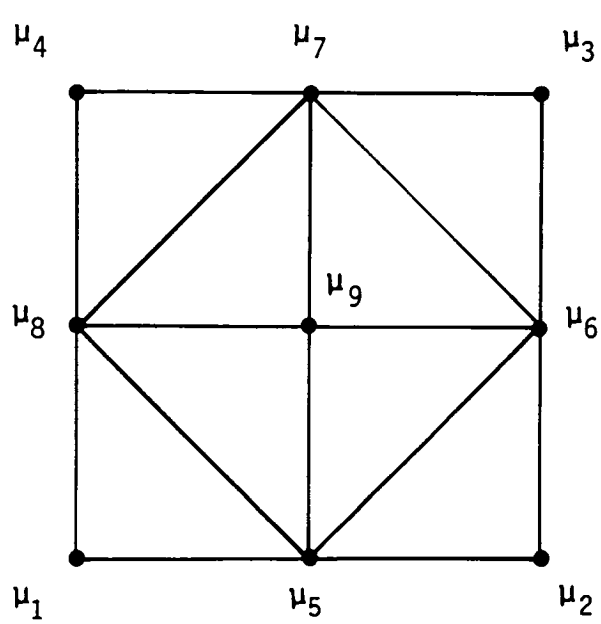

Figure I.1b - Panel doublet parameter locations

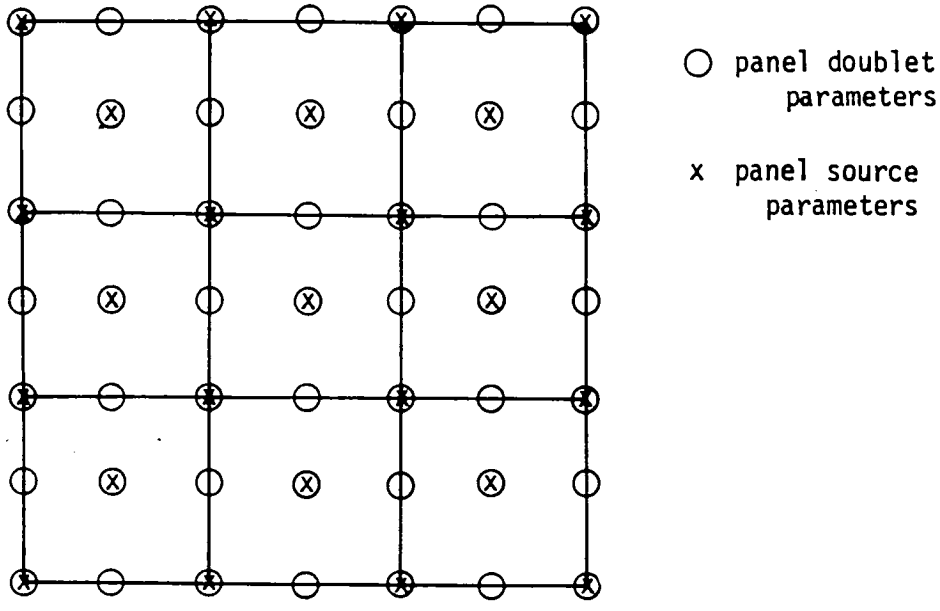

Figure I.1c - Panel singularity parameter locations for a nine-panel network

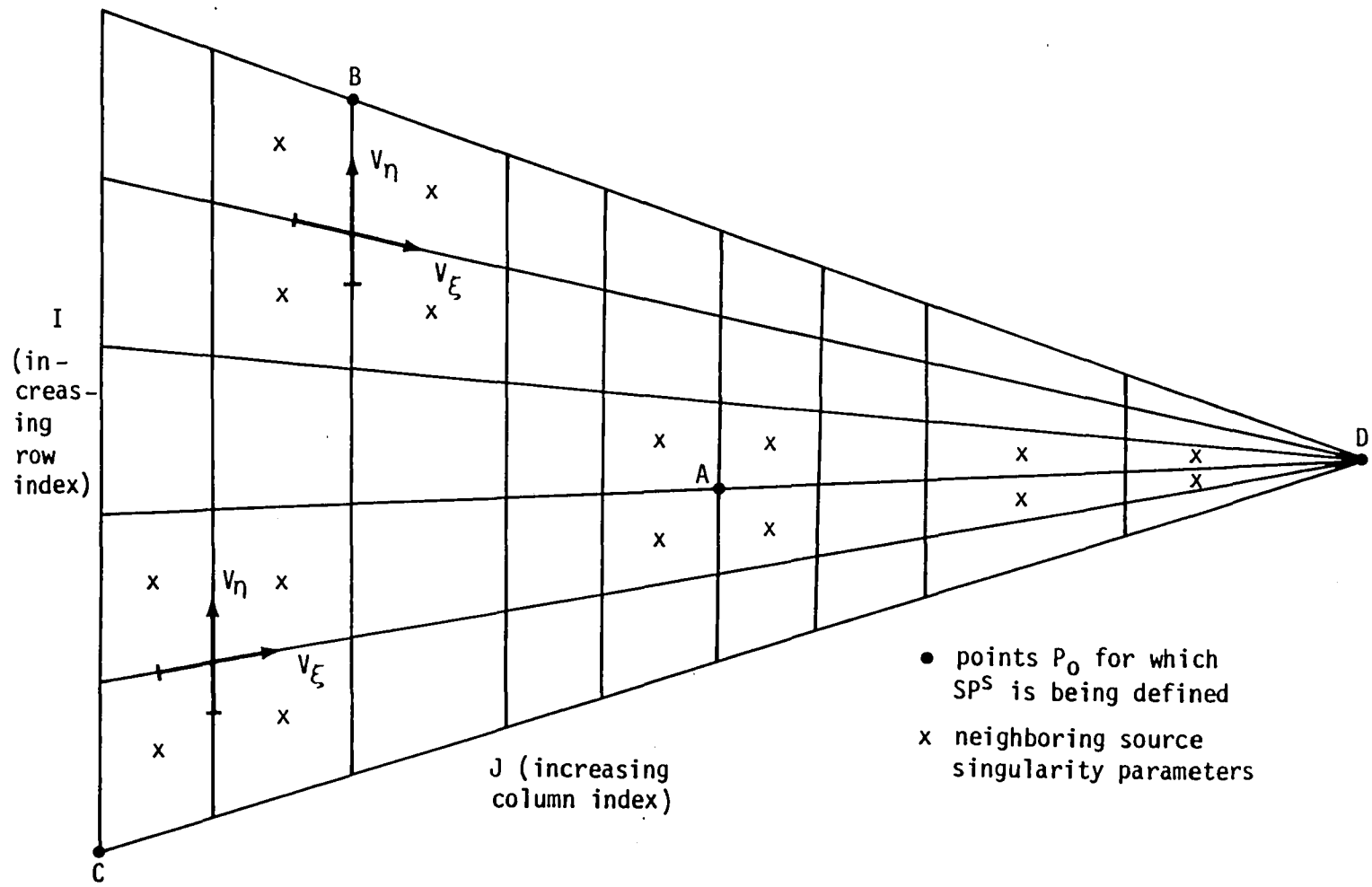

Figure I.2 - Neighboring source parameters for analysis network

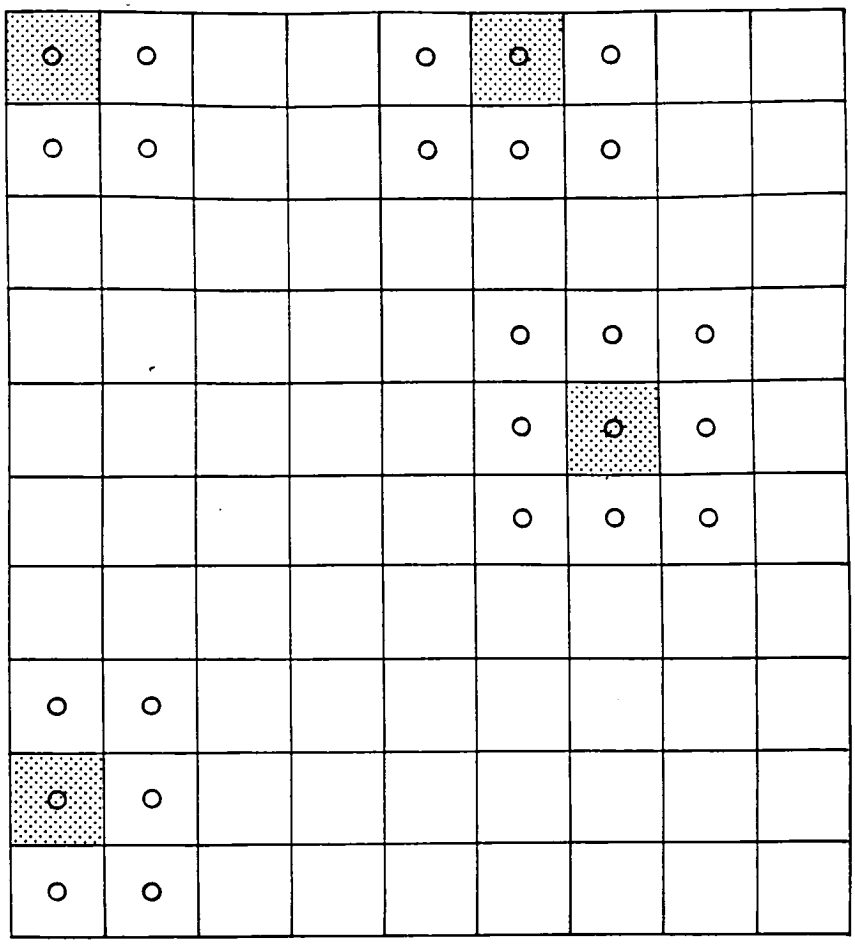

Panel for which spline is computed

Neighbors for least squares fit

Figure I.3 Location of global source parameters used in the construction of the discontinuous source analysis spline.

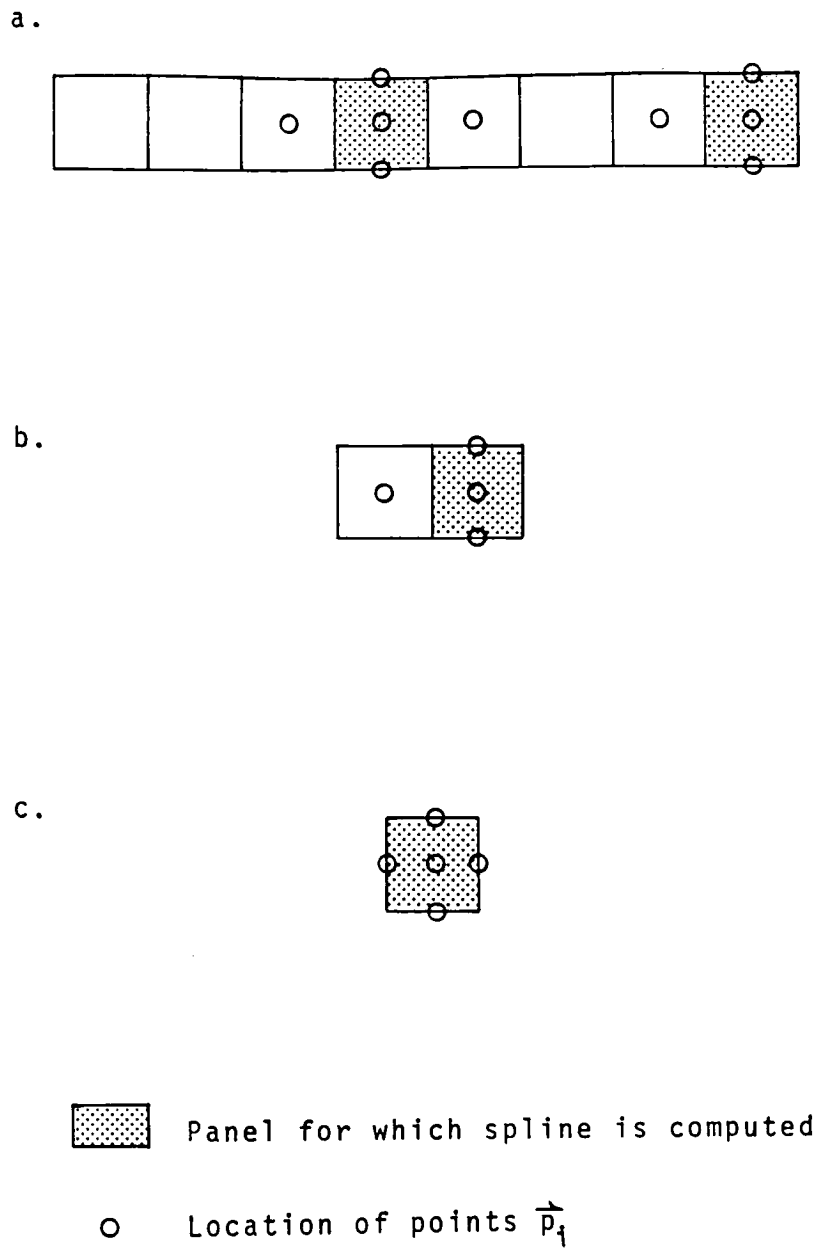

Figure I.4 Location of source parameter points for the special case construction of discontinuous source analysis splines

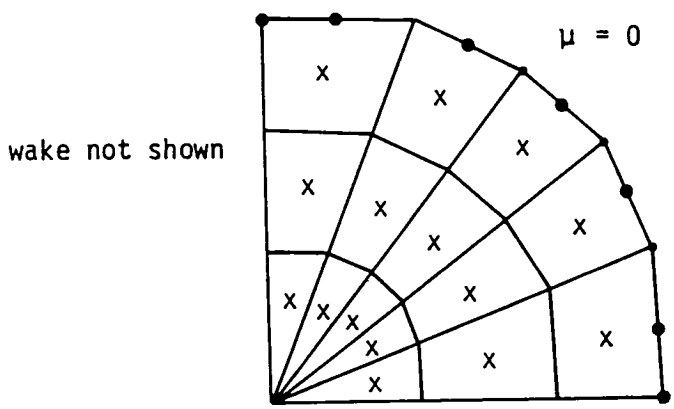

- ● doublet parameters on free edge ($\mu = 0$)
- x doublet parameters in network interior ($\mu \neq 0$)

Figure I.5 - Thin wing with curved planform

X points P_0 for which SP^D is being defined

● neighboring singularity parameters for exact fit

○ neighboring singularity parameters for weighted least squares fit

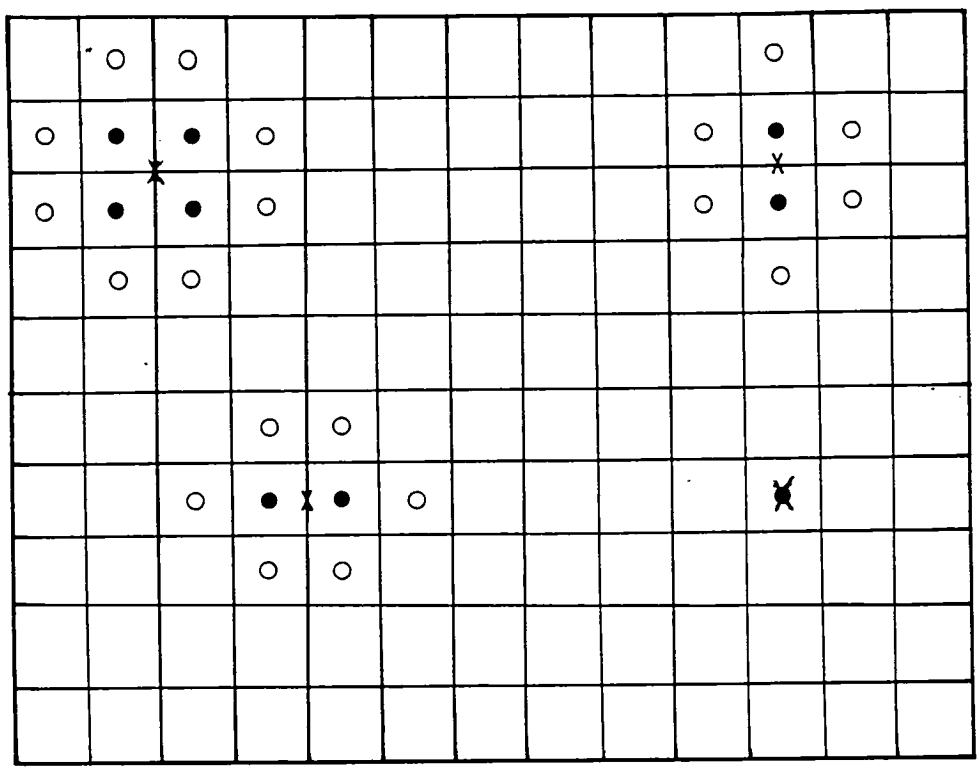

Figure I.6a - Neighboring points for least squares fit (P_0 away from network edge)

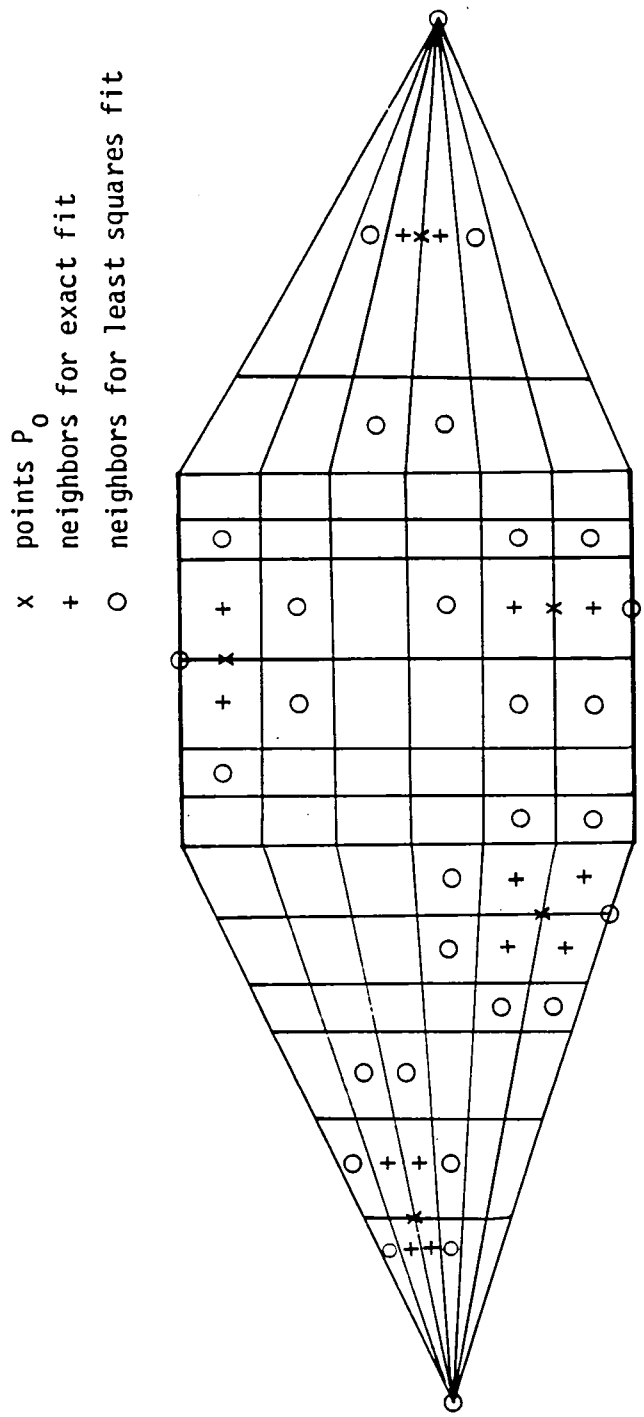

Figure I.6b - Neighboring points for least squares fit (P_0 near network edge)

x points P_o

• neighboring singularity parameters for exact fit

o neighboring singularity parameters for least squares fit

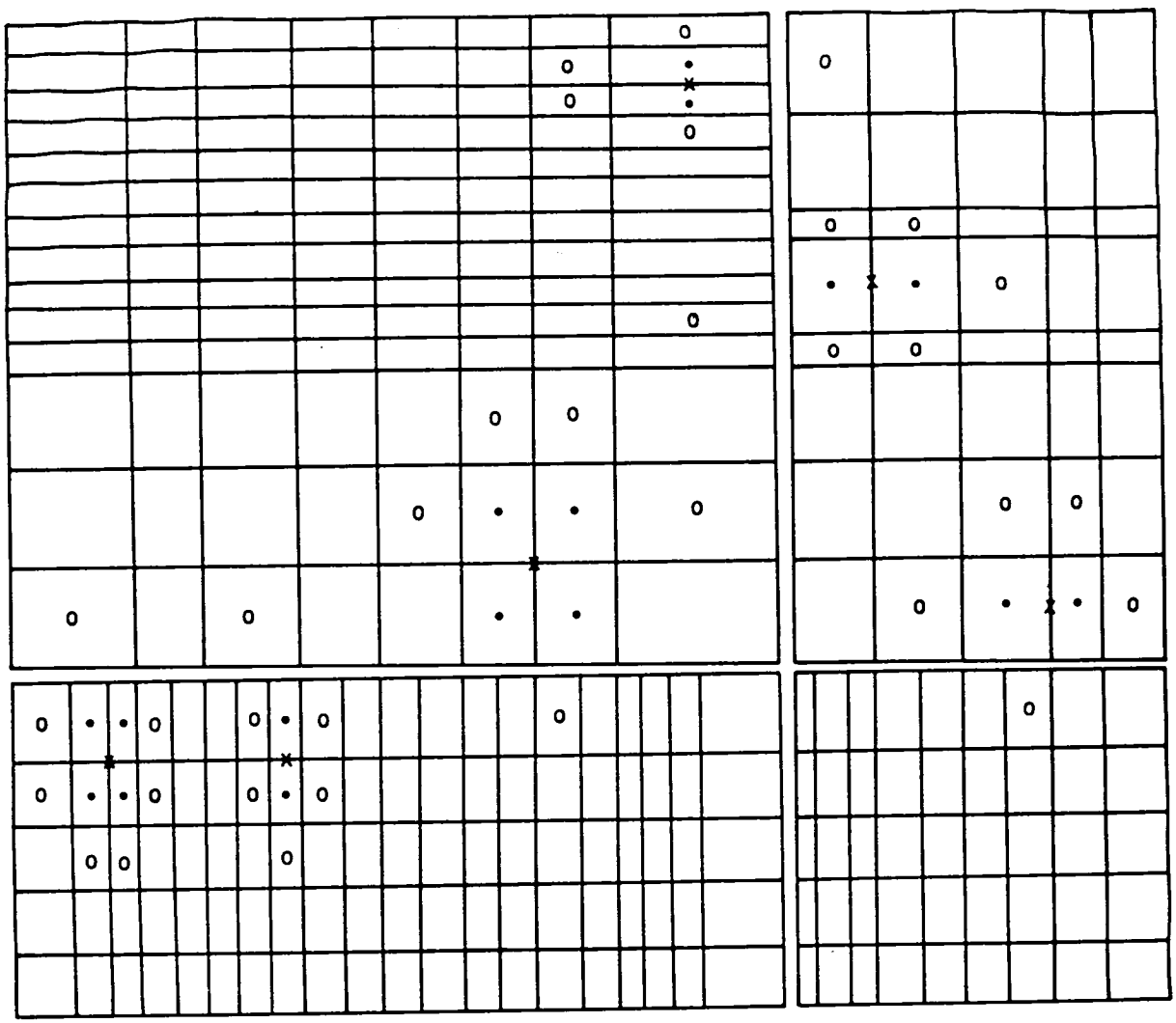

Figure I.6c - Neighboring points for least squares fit
(P_o near a smooth abutment)

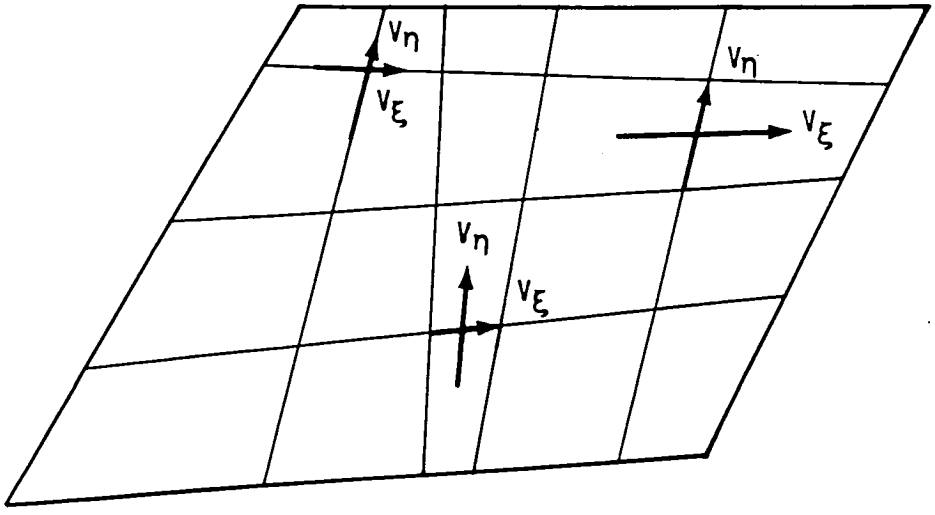

Figure I.7 - Basis Vectors for local Coordinate System for Spline Vector Construction

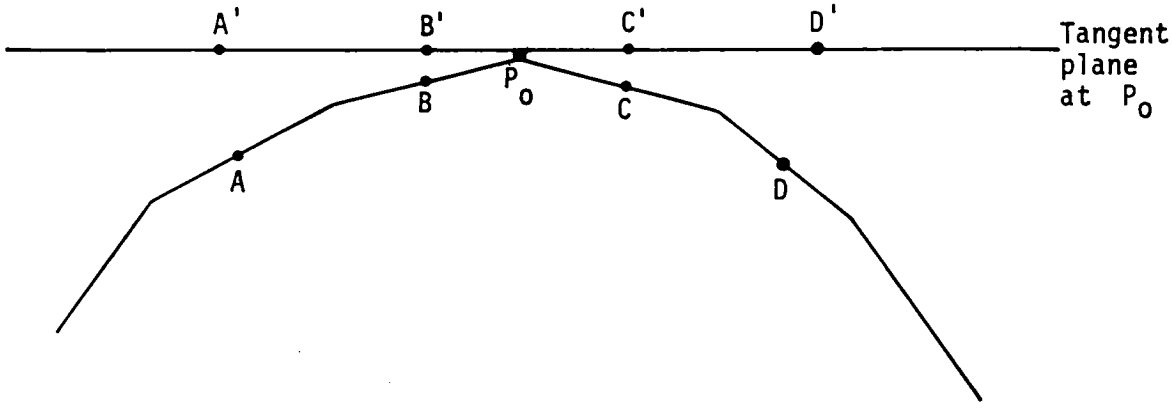

Figure I.8 - Projections to Tangent Plane of Points on Curved Surface

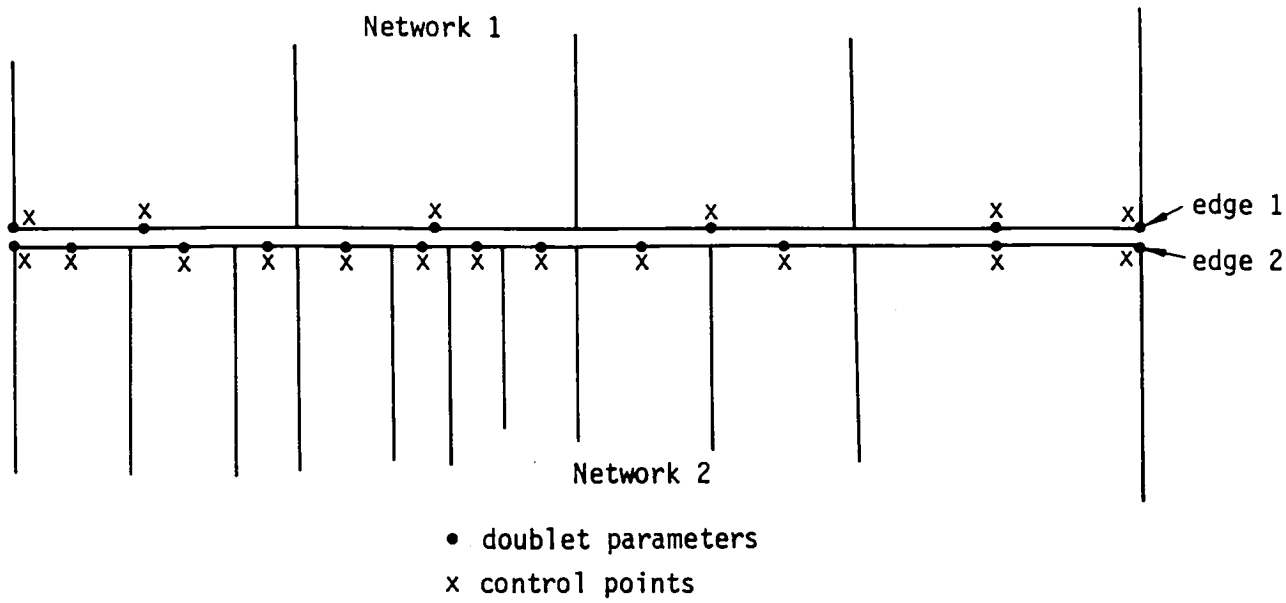

Figure I.9a - Unequal spacing in a non-smooth abutment
(second edge is a refinement of the first)

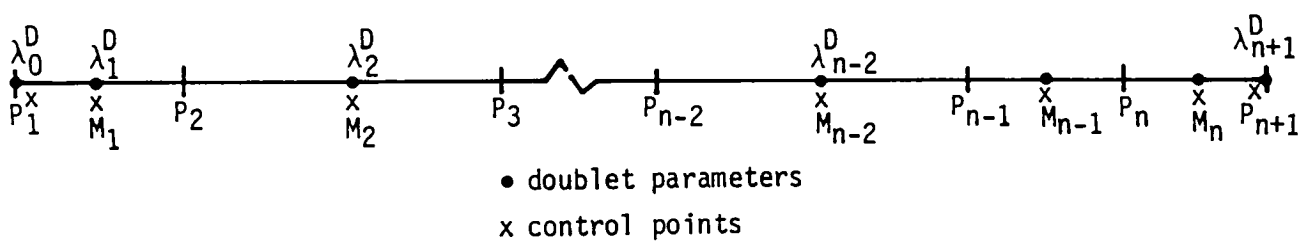

Figure I.9b - Identification of points on a network edge

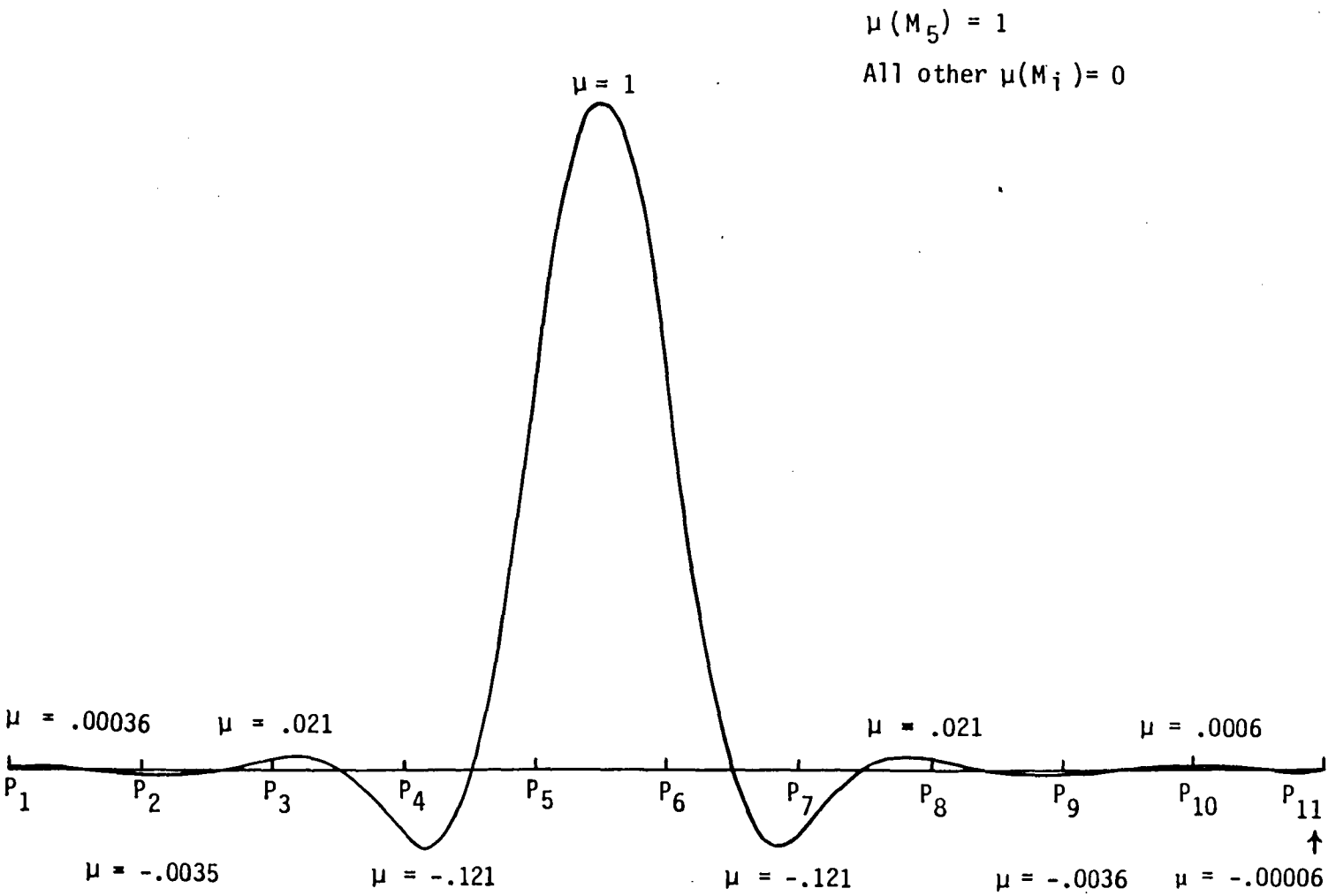

Figure I.10 - Differentiable 2-D quadratic spline

neighbors for grid points on smooth abutments

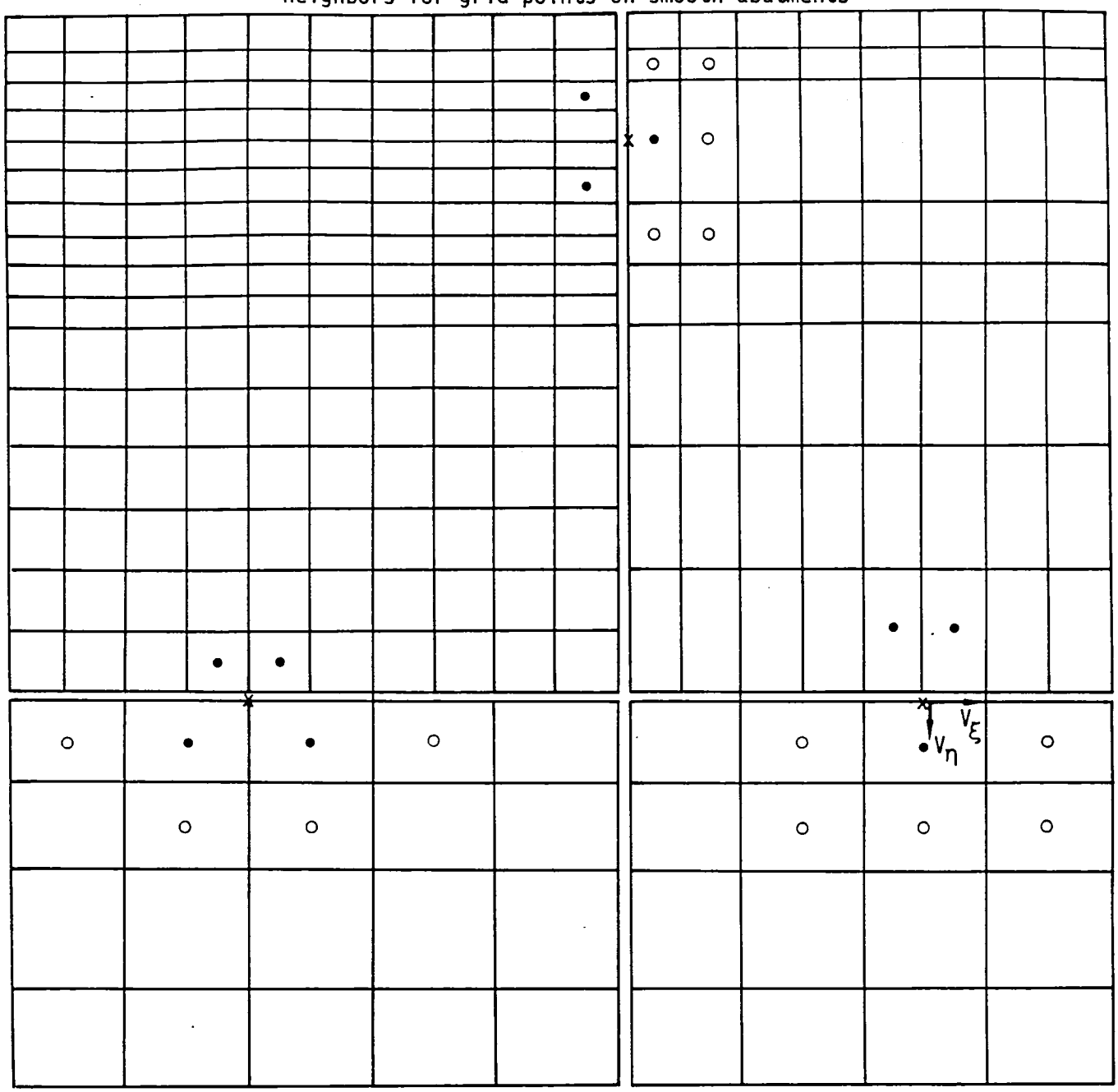

x point P_o

● exact fit

o least squares fit

Figure I.11a - Neighboring singularity parameters for points P_o on a smooth abutment

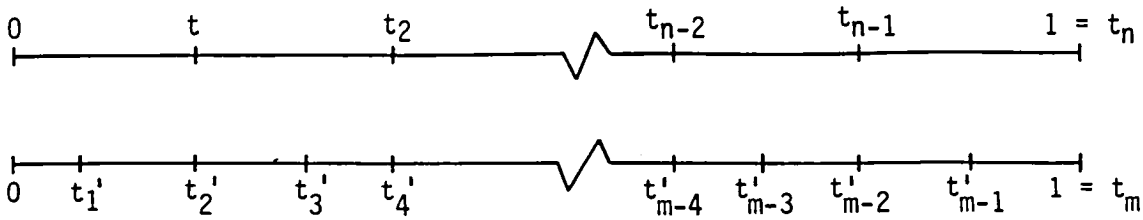

Figure I.11b - Parameterization of an abutment

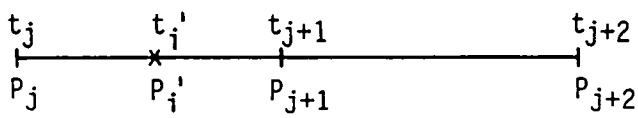

Figure I.11c - Panel edge on coarse network

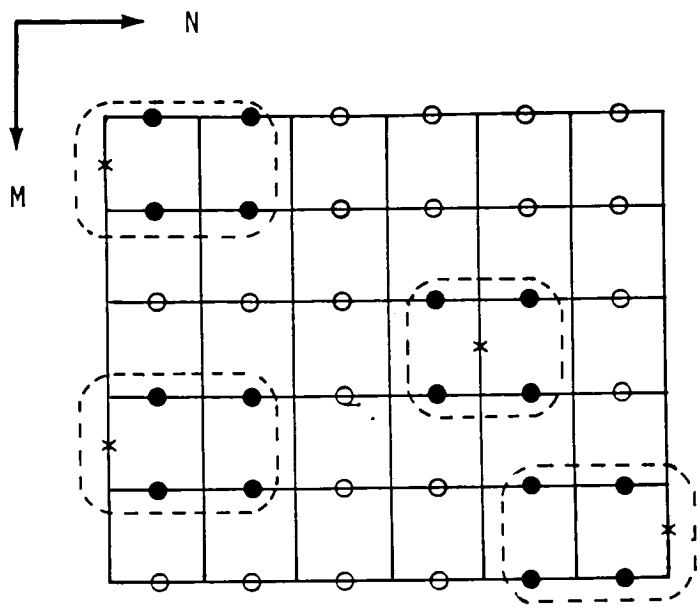

× Edge midpoint source strengths to be computed by bilinear fit

○ Global source parameters

● Global source parameters used in bilinear fits

Figure I.12 - Computation of panel edge midpoint source strengths for discontinuous SD2 source splines

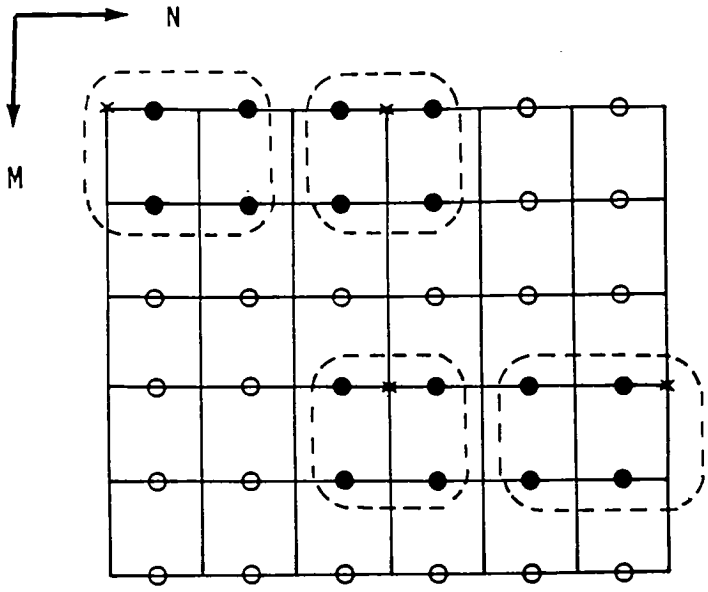

× Corner points for which spline vectors are to be computed

○ Global source parameters

● Global source parameters used in bilinear fits

Figure I.13 - Computation of panel corner spline vectors for continuous SD2 source splines

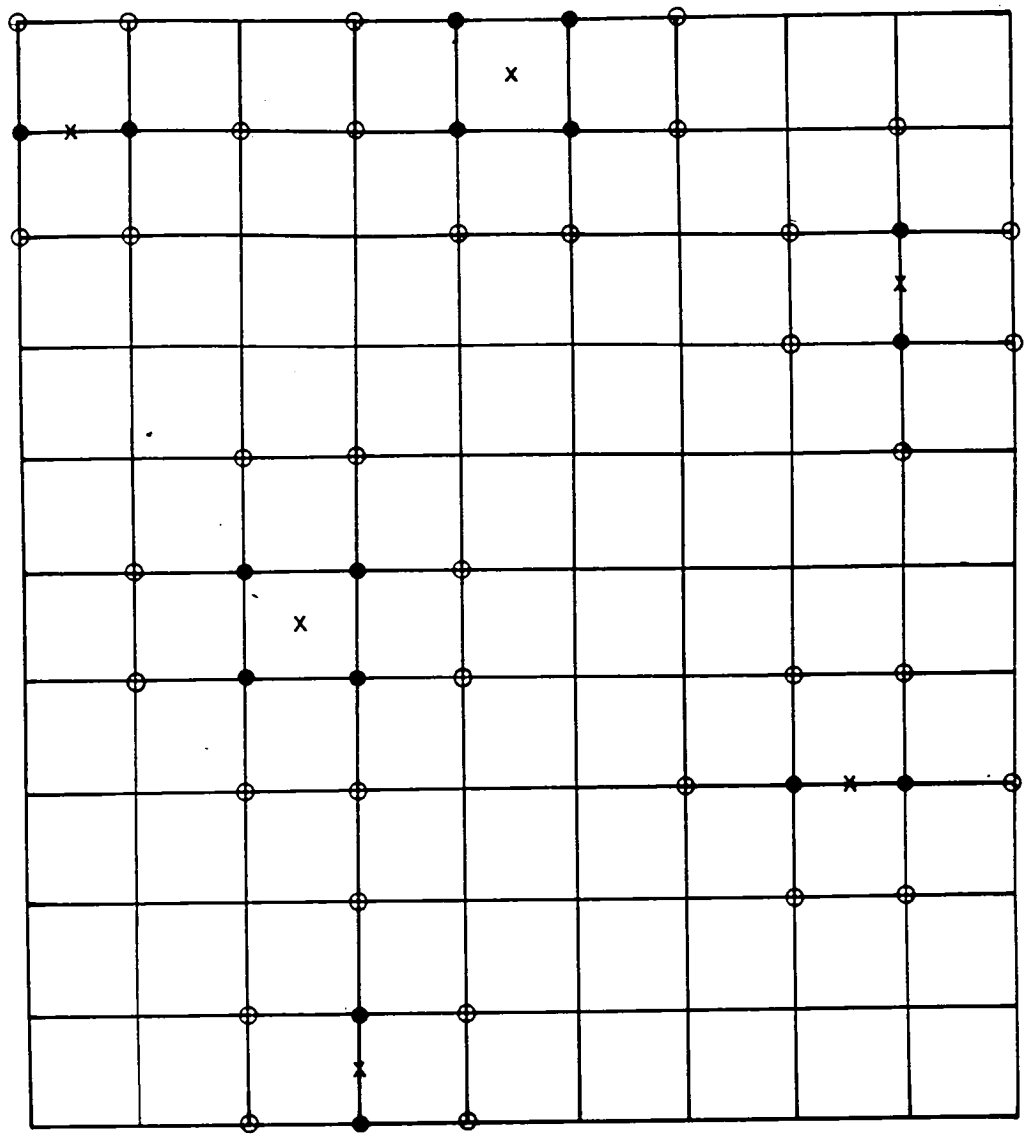

x grid point P_o
● neighboring points, exact fit
o neighboring points, least squares fit

Figure I.14a - Neighboring point for least squares fit (P_o on a doublet design network)

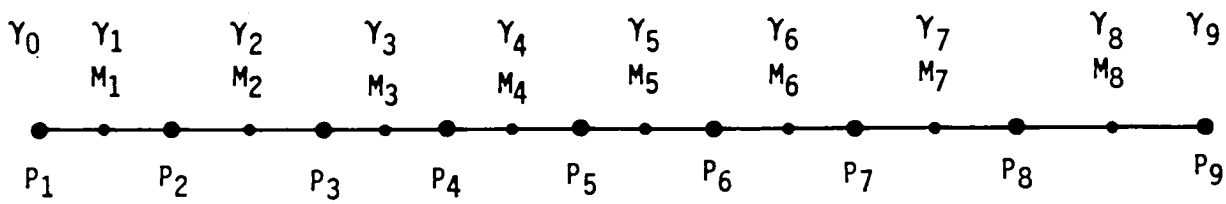

Figure I.14b - Edge of a doublet design network

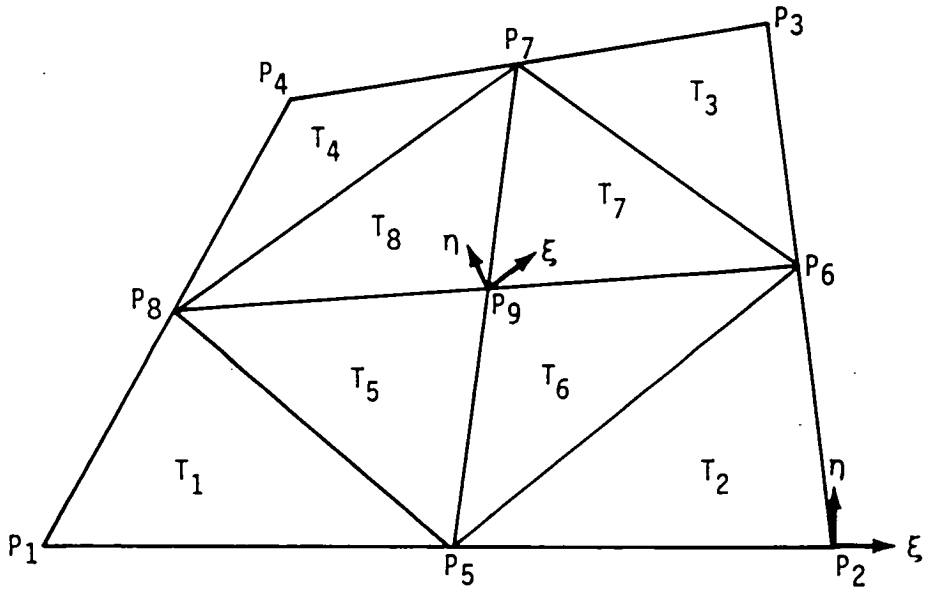

- points P_1 and P_3 lie above average plane
- P_2 and P_4 lie below plane
- P_5 through P_9 lie in a plane

Figure I.15 - Panel defining points and subpanel local coordinate systems

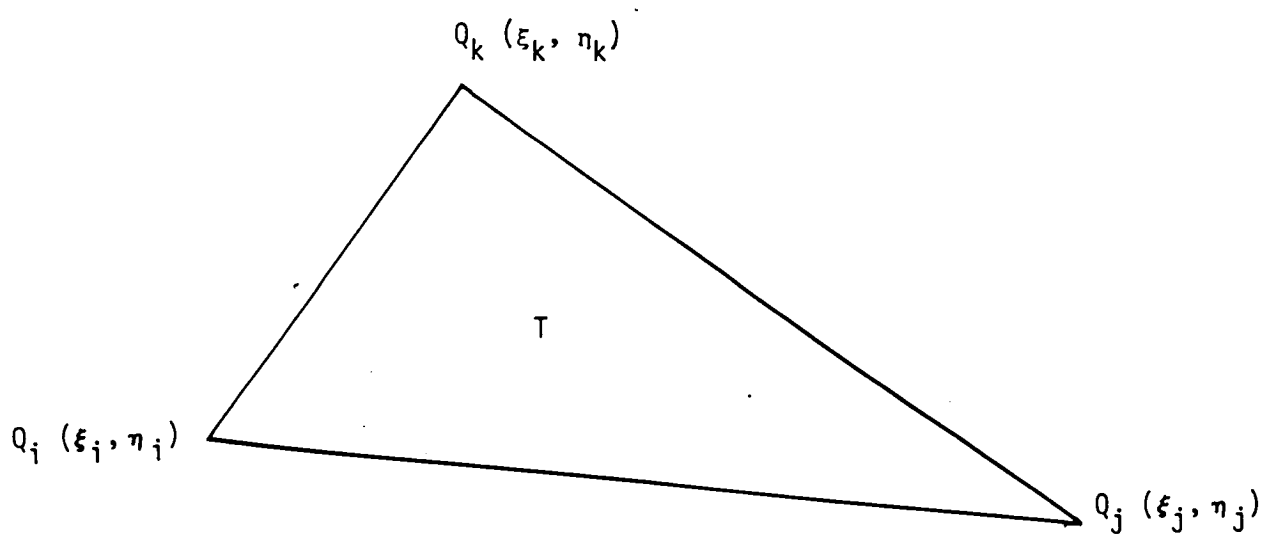

Figure I.16 - Definition of Q_j and Q_k, given Q_i

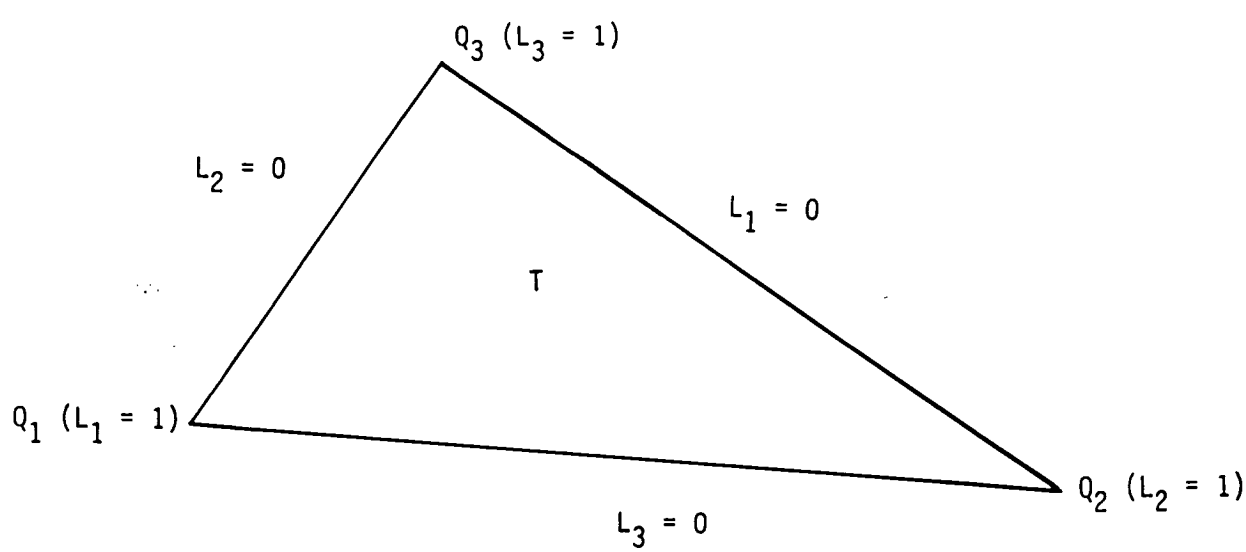

Figure I.17 - Interpolation Conditions that Define Basis Functions L_i

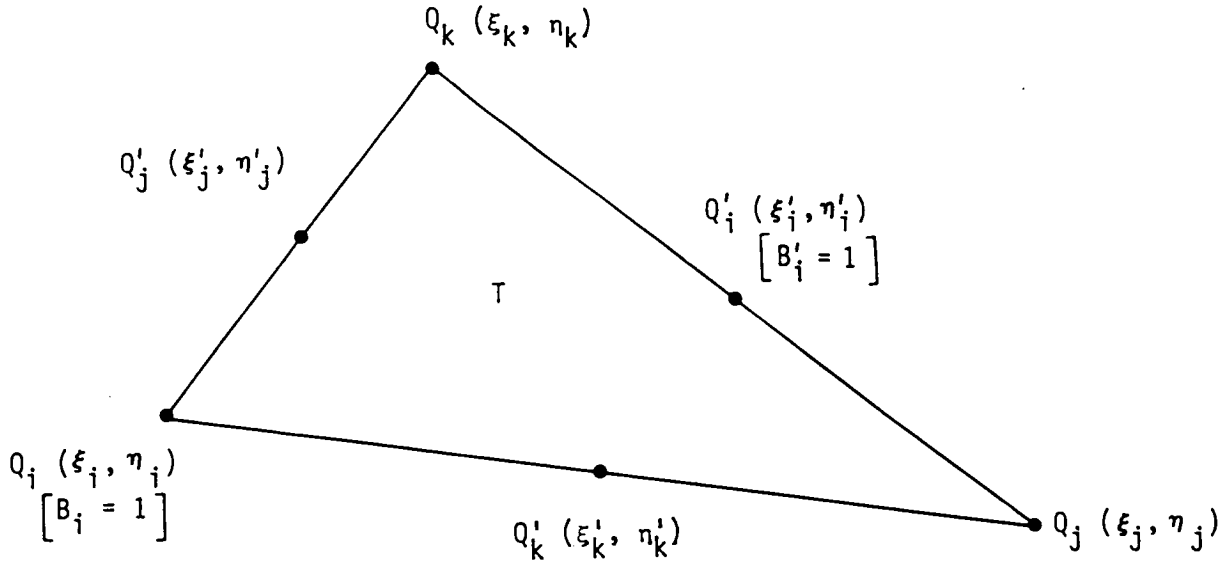

Figure I.18 - Definition of Quadratic Basis Functions B_i (Q), B'_i (Q)

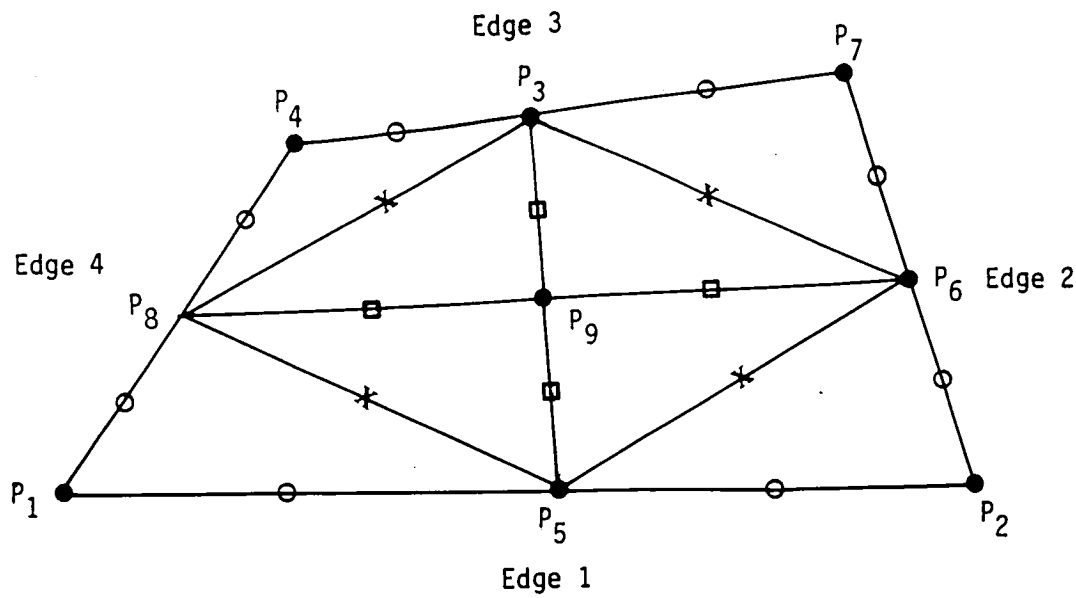

Figure I.19 - Panel with points requiring definition of μ marked with symbols ●,O,□,X

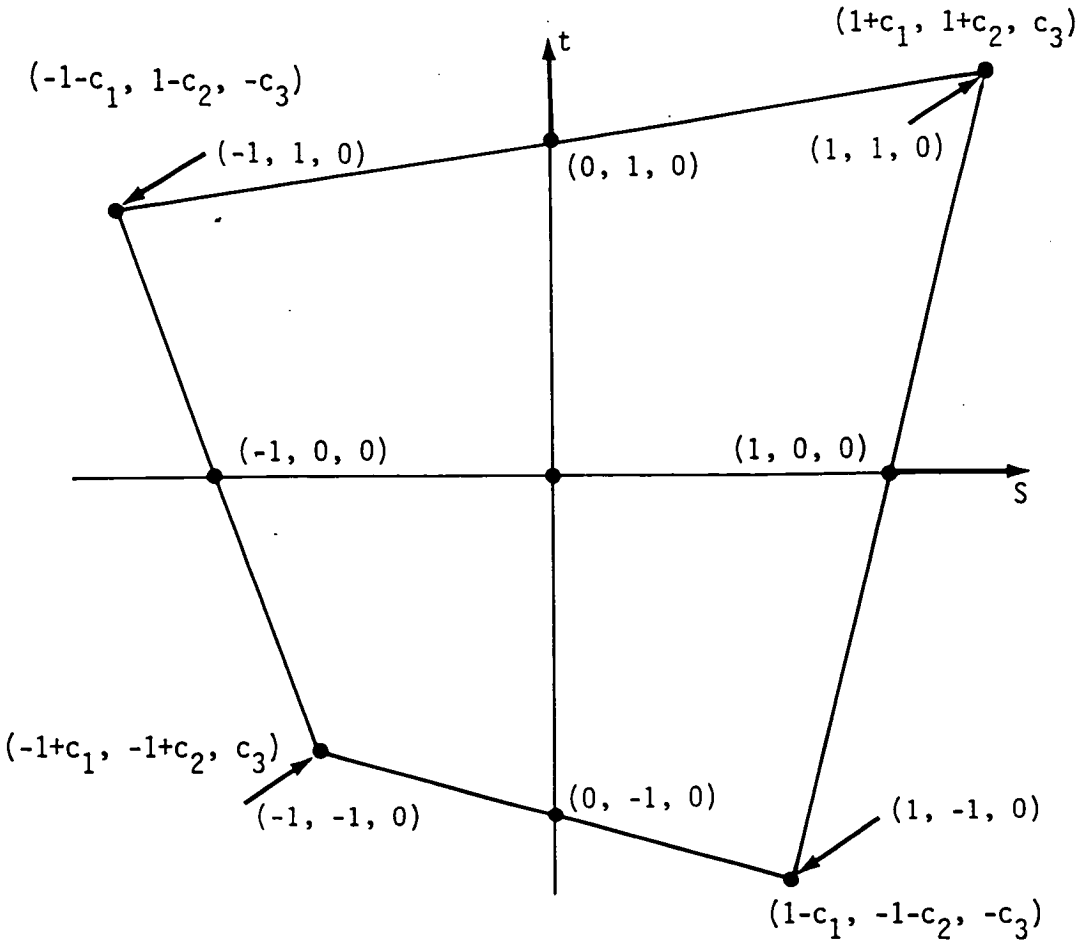

Figure I.20 - A Panel in Skewed Coordinates Viewed from Above

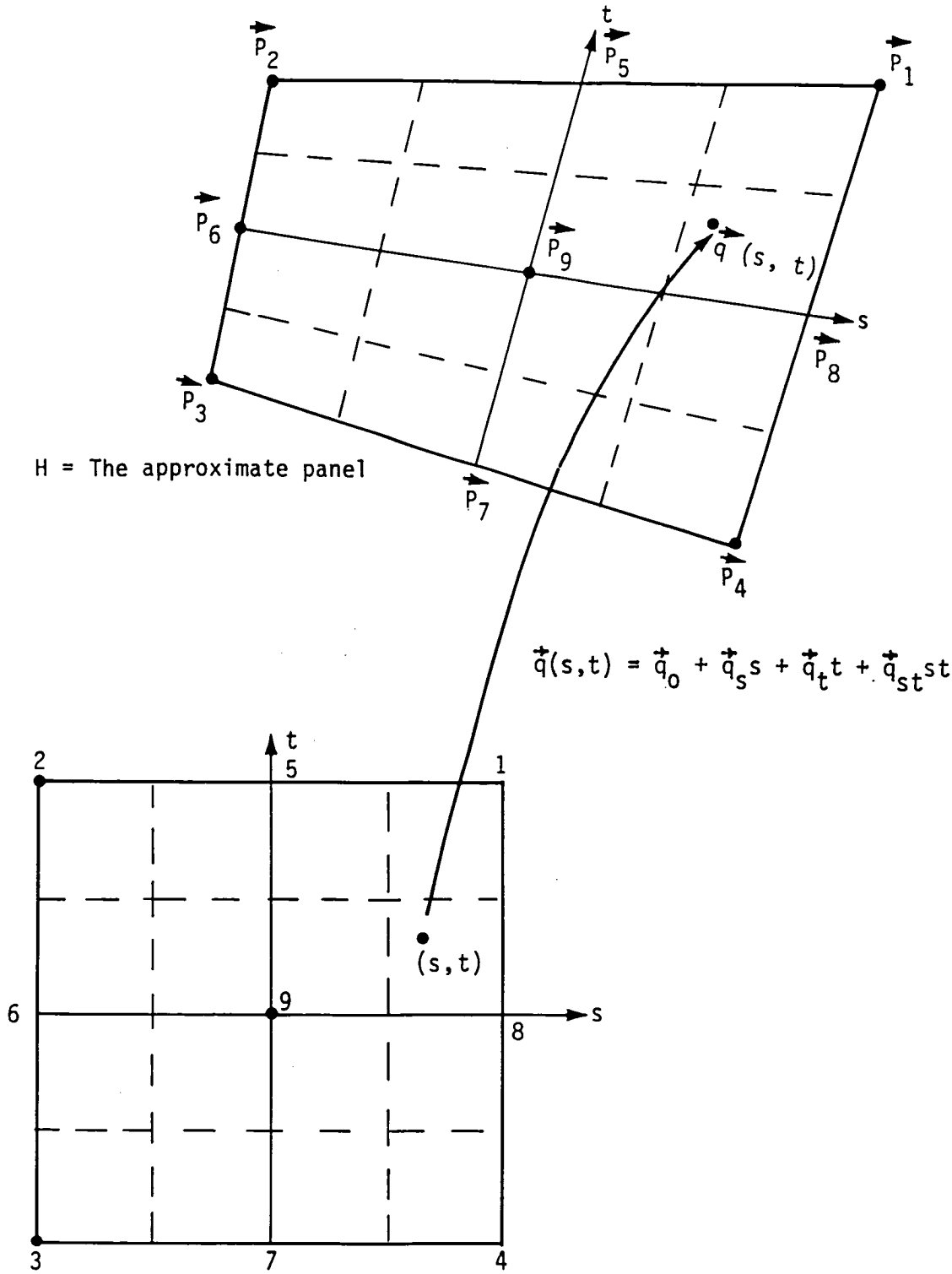

Figure I.21 - The isoparametric representation of a panel

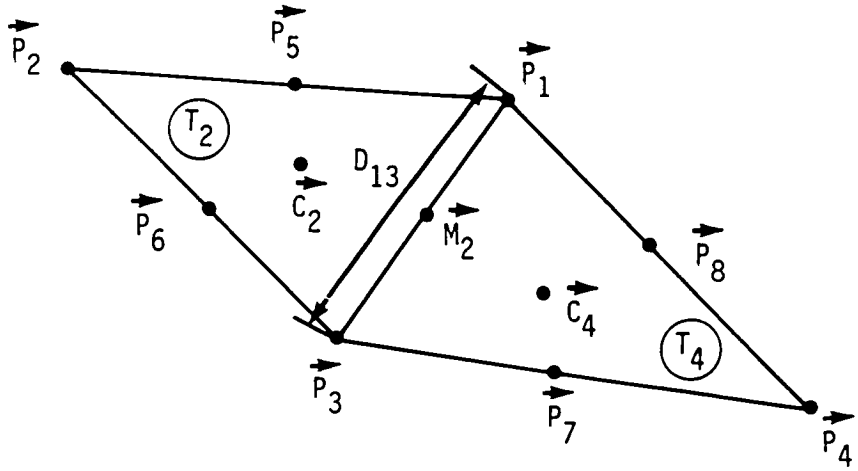

$$D_{13} = d\,(\vec{P}_1, \vec{P}_3) < D_{24} = d\,(\vec{P}_2, \vec{P}_4)$$

Figure I.22a - Division of a panel into T_2 and T_4 when $d\,(\vec{P}_1, \vec{P}_3) < d\,(\vec{P}_2, \vec{P}_4)$

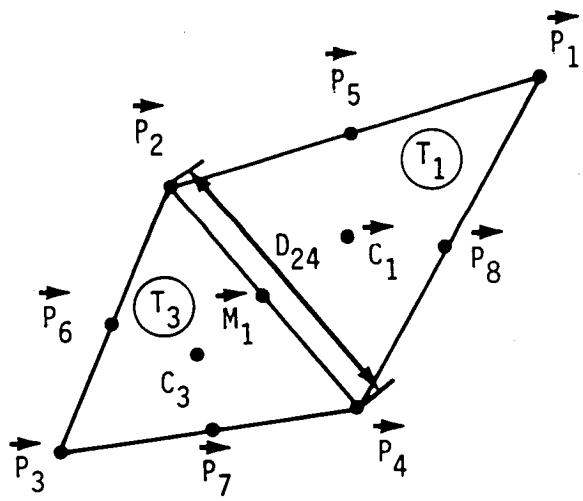

$$D_{24} = d\,(\vec{P}_2, \vec{P}_4) < D_{13} = d\,(\vec{P}_1, \vec{P}_3)$$

Figure I.22b - Division of a panel into T_1 and T_3 when $d\,(\vec{P}_2, \vec{P}_4) < d\,(\vec{P}_1, \vec{P}_3)$

J.0 Panel Influence Coefficient Calculation

J.1 Introduction and Notation

In this appendix we discuss the construction of a panel influence coefficient matrix (PIC). Two such matrices (one corresponding to the source distribution on the panel, the other to the doublet distribution) are defined for every pair of panel and control point. Thus, for this entire appendix, we will assume we are dealing with a single panel and a single control point. We will see that as the location of the control point with respect to the panel changes, the method used to compute the PIC matrices may vary.

The multiplicity of methods is necessary for efficiency: the "near field" method, which is always accurate, is too expensive always to be used, while the less expensive intermediate and far field methods are not always accurate. In this appendix, we will discuss the various methods and when to use each, and will examine the behavior of the entries of the PIC matrices in certain limiting circumstances.

J.1.1 Definitions

Given a panel Σ and a control point P, we define matrices PIC^S and PIC^D as follows. Let $\sigma_1, \ldots, \sigma_4, \sigma_9$ be the five panel source parameters, $\mu_1, \ldots, \mu_9$ the nine panel doublet parameters. Let ϕ_S and $\vec{v}_S$ be the perturbation potential and velocity which the source distribution on the panel defined by $\sigma_1, \ldots, \sigma_9$ induce at the control point, that is, (see (B.0.1) and (B.3.9))

$$\phi_S = -\frac{1}{\kappa} \iint_{\Sigma \cap D_P} \sigma(Q)\left(\frac{1}{R}\right) dS \tag{J.1.1}$$

$$\vec{v}_S = -\frac{1}{\kappa} \iint_{\Sigma \cap D_P} \sigma(Q)\, \vec{\nabla}_P \left(\frac{1}{R}\right) dS \tag{J.1.2}$$

Then we define PIC^S by the equation

$$\begin{Bmatrix} \phi_S \\ V_S \end{Bmatrix} = [PIC^S]^{4\times 5} \begin{Bmatrix} \sigma_1 \\ \vdots \\ \sigma_4 \\ \sigma_9 \end{Bmatrix} \tag{J.1.3}$$

Next, let ϕ_D be the perturbation potential, and $\vec{v}_D$ the regular part of the perturbation velocity, which the doublet distribution on the panel defined by $\mu_1, \ldots, \mu_9$ induce at the control point. That is (again, see (B.0.1) and (B.3.9)),

$$\phi_D = \frac{1}{\kappa} \iint_{\Sigma \cap D_p} [\mu(Q)\ \hat{n} \cdot \tilde{\nabla}(\tfrac{1}{R})] dS \tag{J.1.4}$$

$$\vec{v}_D = \frac{1}{\kappa} \iint_{\Sigma \cap D_p} (\hat{n} \times \vec{\nabla}_Q\ \mu) \times \tilde{\nabla}(\tfrac{1}{R})\ dS \tag{J.1.5}$$

Then we define $[PIC^D]$ by the equation

$$\begin{Bmatrix} \phi_D \\ - - - \\ \vec{v}_D \end{Bmatrix} = [PIC^D]^{4x9} \begin{Bmatrix} \mu 1 \\ \vdots \\ \mu 9 \end{Bmatrix} \tag{J.1.6}$$

In the actual operation of the program, fewer than 4 rows of the PIC matrices may be computed for reasons of efficiency. This subject is discussed in the Maintenance Document (see section 5-D and the preface of SUBROUTINE CONBLK of the MAG module); in this appendix, we will always consider the full (4-row) matrix.

Finally, let $\vec{v}^{\,*}_{D,i}$ be the line vortex component of the velocity that the doublet distribution defined by $\mu_1, \ldots, \mu_9$, restricted to the ith edge of the panel, induces at the control point. That is,

$$\vec{v}^{\,*}_{D,i} = \frac{1}{\kappa} \int_{\substack{\text{ith edge of} \\ D_p}} \mu\ \tilde{\nabla}_Q(\tfrac{1}{R}) \times \vec{dl} \tag{J.1.7}$$

Then we define matrices $[LINV_i]$ by

$$\vec{v}^{\,*}_{D,i} = [LINV_i]^{3x9} \begin{Bmatrix} \mu 1 \\ \vdots \\ \mu 9 \end{Bmatrix} \tag{J.1.8}$$

The computation of the matrix $[LINV_i]$ is not available in version 3.0 of Pan Air.

J.1.2 Summary

J.1.2.1 Near Field Versus Far Field

The first step in computation of the PIC matrices is to determine which

method should be used to compute them. In the near field method, the integration required to evaluate the PIC matrices is performed analytically over each of the eight subpanels. The resultant PIC matrices satisfy (J.1.3) and (J.1.6) "exactly" that is, with no error other than that due to roundoff in arithmetic calculations.

The near field method involves considerable computation, however, and thus its use is reserved for the cases where the other methods are inaccurate. Generally speaking, the farther (using a compressible distance metric) the control point lies from the panel, the more accurate the intermediate field and far field methods become. The algorithms summarized below, and described in detail in section J.2, are purely empirical, and thus subject to modification in time.

The first step is to determine if the panel center is in the domain of dependence of the control point. A far field PIC is never computed unless this holds, in which case we require in addition that the distance from the panel center to the control point is at least five times the panel radius, where all distances are measured by means of a compressible inner product.

If the far field test fails, an intermediate field test, described in section J.2, is performed. If the test is successful, an intermediate field PIC is computed. In computing such a PIC, the 8-segment panel and the singularity distribution on it are approximated, while the influences defined by these approximations are determined analytically.

J.1.2.2 The Domain of Dependence

In supersonic flow, the domain of dependence of a control point P is limited to the forward Mach cone from P, as illustrated in figure J.1. The panel Σ illustrated there is outside D_P, and thus has zero influence on P.

For subinclined panels, we will see in section J.3 that Σ lies outside D_P whenever all four edges do. For superinclined panels, this does not hold, as illustrated in figure J.2. The test performed on a superinclined panel to determine if it intersects D_P is also described in section J.3.

J.1.2.3 Near Field and Intermediate Field PIC Calculation

The principal step in computing a near field PIC matrix is the computation, for each subpanel, of "sub-panel integral" matrices $SPINT_i^S$ and $SPINT_i^D$ such that

$$\begin{Bmatrix} \phi_S \\ \partial\phi_S/\partial\xi' \\ \partial\phi_S/\partial\eta' \\ \partial\phi_S/\partial\zeta' \end{Bmatrix} = [SPINT^S] \begin{Bmatrix} \sigma_0 \\ \sigma_\xi \\ \sigma_\eta \end{Bmatrix} \qquad (J.1.9)$$

$$\begin{Bmatrix} \phi_D \\ \partial\phi_D/\partial\xi' \\ \partial\phi_D/\partial\eta' \\ \partial\phi_D/\partial\zeta' \end{Bmatrix} = [SPINT^D] \begin{Bmatrix} \mu_0 \\ \mu_\xi \\ \cdot \\ \cdot \\ \cdot \\ \mu_{\eta\eta} \end{Bmatrix} \tag{J.1.10}$$

where ϕ_S and ϕ_D are the perturbation potentials induced respectively by the linear source distribution defined by σ_0, σ_ξ, and σ_η, and the quadratic doublet distribution defined by $\mu_0, \ldots, \mu_{\eta\eta}$.

Equations (J.1.9) and (J.1.10) define a perturbation velocity in local (ξ', η', ζ') coordinates. It is easy to show (cf., equation E.1.11) that

$$\begin{Bmatrix} \partial\phi/\partial x_0 \\ \partial\phi/\partial y_0 \\ \partial\phi/\partial z_0 \end{Bmatrix} = [A_0{}^T] \begin{Bmatrix} \partial\phi/\partial\xi' \\ \partial\phi/\partial\eta' \\ \partial\phi/\partial\zeta' \end{Bmatrix} \tag{J.1.11}$$

where A_0 is the matrix sending reference coordinates to local coordinates:

$$[A_0] \begin{Bmatrix} x_0 \\ y_0 \\ z_0 \end{Bmatrix} = \begin{Bmatrix} \xi' \\ \eta' \\ \zeta' \end{Bmatrix} \tag{J.1.12}$$

Finally, recall the definitions of subpanel splines from section I.2.

$$\begin{Bmatrix} \sigma_0 \\ \sigma_\xi \\ \sigma_\eta \end{Bmatrix} = [SPSPL^S] \begin{Bmatrix} \sigma_1 \\ \cdot \\ \cdot \\ \cdot \\ \sigma_4 \\ \sigma_9 \end{Bmatrix} \tag{J.1.13}$$

$$\begin{Bmatrix} \mu_0 \\ \cdot \\ \cdot \\ \cdot \\ \mu_{\eta\eta} \end{Bmatrix} = [SPSPL^D] \begin{Bmatrix} \mu_1 \\ \cdot \\ \cdot \\ \cdot \\ \mu_9 \end{Bmatrix} \tag{J.1.14}$$

Then, we may combine (J.1.3), (J.1.9), (J.1.11), and (J.1.13) to obtain

$$[PIC^S]^{4x5} = \sum_{i=1}^{8} [\tilde{A}_i]^{4x4} [SPINT_i^S]^{4x3} [SPSPL_i^S]^{3x5} \qquad (J.1.15)$$

where the subscript i refers to the ith subpanel, and

$$[\tilde{A}_i] = \begin{bmatrix} 1 & 0 & 0 & 0 \\ 0 & & & \\ 0 & & A_i^T & \\ 0 & & & \end{bmatrix} \qquad (J.1.16a)$$

Similarly, for the 2-region intermediate field method, we have a corresponding equation

$$[PIC^S]^{4x5} = \sum_{i=1}^{2} [\tilde{A}_i]^{4x4} [HPINT_i^S]^{4x6} [HPSPL_i^S]^{6x5} \qquad (J.1.16b)$$

where i ranges over two "half panels," the half panel integral matrix $HPINT^S$ defines the influence of the half panel on the control point, and the half panel spline matrix $HPSPL^S$, defined in section I.3, gives a quadratic source distribution in terms of the five panel source parameters.

Finally, the one region intermediate field procedure approximates the panel by its projection to an average plane. In this procedure,

$$[PIC^S]^{4x5} = [\tilde{A}]^{4x4} [PINT^S]^{4x3} [PSPL^S]^{3x5} \qquad (J.1.17)$$

where $PINT^S$ ("panel integral") defines the influence of the projected panel on the control point, and $[PSPL^S]$ defines a source distribution on the projected panel in terms of the panel singularity parameters.

Equations corresponding to (J.1.15-17) hold for the doublet distribution as well. Thus the computation of PIC matrices by near field or intermediate field methods has been discussed, except for the computation of the subpanel, half panel, and panel integral matrices.

This is a rather complex subject and is discussed in full detail in section J.6. In that section the influence $[S_0]$ of a quadratic source distribution over a polygonal region and the influence $[D_0]$ of a cubic doublet distribution over a polygonal region are computed in terms of certain fundamental integrals we call "edge functions" and "panel functions". These edge and panel functions are computed in section J.7, though the formulas

derived there do not consider numerical instabilities which may occur during the compuation. These numerical instabilities are avoided by means of rationalization formulas discussed in section J.8.

J.1.2.4 Far Field PIC's

Recall from (B.0.1) that the denominator in the fundamental integral is 1/R, where in compressibility coordinates

$$R^2 = (\xi - x)^2 + s\beta^2(\eta - y)^2 + s\beta^2(\zeta - z)^2 \tag{J.1.18}$$

where the control point $\vec{P} = (x,y,z)$, and the point of integration $\vec{Q} = (\xi, \eta, \zeta)$.

Recalling from section E.2 the inner product

$$[\vec{x},\vec{y}] = \vec{x}^T [C_0] \vec{y} \tag{J.1.19}$$

where in compressibility coordinates,

$$[C_0] = \begin{bmatrix} 1 & & \\ & s\beta^2 & \\ & & s\beta^2 \end{bmatrix} \tag{J.1.20}$$

we see that

$$R^2 = [\vec{P} - \vec{Q}, \vec{P} - \vec{Q}] \tag{J.1.21}$$

Letting Q_0 be the panel center,

$$\vec{\Delta Q} = \vec{Q_0} - \vec{Q}$$
$$\vec{R_0} = \vec{P} - \vec{Q_0} \tag{J.1.22a}$$

we have

$$R^2 = [\vec{R_0} + \vec{\Delta Q}, \vec{R_0} + \vec{\Delta Q}] \tag{J.1.22b}$$

Now, the expression R^{-N}, N = 1 or 3, occurs in the fundamental integrals, and the basis for the far field method is the equation

$$R^{-N} = [\vec{R_0} + \vec{\Delta Q}, \vec{R_0} + \vec{\Delta Q}]^{-N/2}$$
$$= ([\vec{R_0}, \vec{R_0}] + 2[\vec{R_0}, \vec{\Delta Q}] + [\vec{\Delta Q}, \vec{\Delta Q}])^{-N/2} \tag{J.1.23}$$

$$= [\vec{R_0}, \vec{R_0}]^{-N/2} \left(1 + 2\frac{[\vec{R_0}, \vec{\Delta Q}]}{[\vec{R_0}, \vec{R_0}]} + \frac{[\vec{\Delta Q}, \vec{\Delta Q}]}{[\vec{R_0}, \vec{R_0}]}\right)^{-N/2} \tag{J.1.24}$$

The factor $[\vec{R}_0, \vec{R}_0]^{-N/2}$ is independent of Q and may thus be taken out of the integral, while the remaining factor may be expressed by a power series in ΔQ for which we ignore any terms of cubic or higher order.

We will show in section J.9 that the integrations (J.1.1) and (J.1.2) can then be performed as a sum of multiplication of matrices, one whose entries are computed from R_0, and one whose entries are integrals of powers of ΔQ, which, since they are independent of P, may be performed in advance (and thus need not be repeated for each control point).

J.1.3 Integration Techniques

The computation of the entries of the subpanel integral matrices [SPINT] (cf., J.1.9-10) involves considerable detail (see sections J.4 through J.6). At this time, however, we will give a brief outline of the process described in those sections.

In sections J.4 and J.5 we establish, respectively, special cylindrical and hyperbolic coordinate system, the former for use in subsonic flow or with superinclined panels, the latter for use with subinclined panels in supersonic flow. The coordinate systems have two advantages. First, the kernel 1/R of the integrals (J.1.1-2) has a very simple form (cf., J.6.59). Second, the limits of integration may also be expressed conveniently (cf., (J.4.62) and (J.5.107)). In section J.6, we first express the entries of a subpanel integral matrix in terms of fundamental integrals (a, $\vec{a}$, etc., cf., (J.6.152) and (J.6.164)). We then use the results of sections J.4 and J.5 to evaluate these integrals.

It is worth noting, however, that there exist other ways of computing the entries of the subpanel integral matrices. While all these methods are equivalent in that, if correct, they yield the same real numbers for the influence of a particular subpanel on a particular control point, they may have quite different structures. We now briefly summarize three alternate methods.

One such method (for zero Mach number) is described in Appendix D.2 of reference J.1. There, the entries of the subpanel integral matrices are given in terms of fundamental integrals, some of which are singular even when the control point is away from the panel. It can be shown that the singular integrals always cancel, however, and thus the entries of the subpanel integral matrix are finite.

A second approach is given in Appendix D.5 of reference J.1. Here, an additional integration by parts is performed, with the result that the entries of the subpanel integral matrices are computed exclusively as combinations of non-singular integrals. Of all published methods for PIC computation, this one most closely resembles that of section J.6. The fundamental integrals are also similar, with H(1,1,3) in reference J.1 being a multiple of the integral a (cf., (J.6.165)). In fact, the computation of H(1,1,3), which uses cylindrical coordinates as well, closely parallels the computation of a.

A third approach to PIC computation is contained in Reference 4.9 (Ehlers, et.al.). There, rectilinear coordinates are used in evaluation of the integrals. The resulting formulas appear totally different from those of

section J.6 because the entries of the subpanel integral matrices are expressed in terms of different (and also non-singular) fundamental integrals. The verification that the entries of the subpanel integral matrices as computed in reference 4.9 are in fact identical to the entries as computed in section J.6 is a major one.

J.1.4 Notation

The discussion of PIC computation is lengthy, and many terms are defined and then not used again until much later. The most frequently used terms are listed in figure J.3 for convenient reference. All vectors and matrices are in reference coordinates unless otherwise specified, except that those marked with a prime are in local coordinates unless otherwise specified.

J.2 Distance Algorithm

In this section we discuss the algorithms we use to determine whether to compute a far field, a one region intermediate field, a two region intermediate field, or a near field PIC. First, we consider the requirements for performing a far field PIC.

J.2.1 The Far Field Criterion

Consider equation (J.1.24). In order to ignore cubic terms in $\vec{\Delta Q}$, we must have

$$[\vec{R}_0, \vec{\Delta Q}] \ll [\vec{R}_0, \vec{R}_0] \tag{J.2.1}$$

To determine a condition on R_0 for which (J.2.1) holds, we digress into the realm of linear algebra.

Let $(\ ,\ )_P$ be a positive definite inner product (not necessarily the standard Euclidean inner product); that is,

$$(\vec{X}, \vec{X})_P > 0 \tag{J.2.2}$$

if x is non-zero. Let

$$|\vec{X}|_P = (\vec{X},\vec{X})_P \tag{J.2.3}$$

Then we have the triangle inequality (see, for instance, page 11 of reference J.2):

$$|\vec{X}|_P + |\vec{Y}|_P \geq |\vec{X} + \vec{Y}|_P \tag{J.2.4}$$

Squaring (J.2.4),

$$(\vec{X},\vec{X})_P + 2(\vec{X},\vec{Y})_P + (\vec{Y},\vec{Y})_P \leq (\vec{X},\vec{X})_P + 2|\vec{X}|_P\,|\vec{Y}|_P + (\vec{Y},\vec{Y})_P \tag{J.2.5}$$

or

$$(\vec{X},\vec{Y})_P \leq |\vec{X}|_P\ |\vec{Y}|_P \tag{J.2.6}$$

a relation called the Cauchy-Schwartz inequality.

We generalize (J.2.6) for the specific positive definite inner product

$$[\vec{X},\vec{Y}]_P = \vec{X}^T\,[C_0]\,\vec{Y} \tag{J.2.7}$$

where C_0 is the positive definite matrix

$$C_0 = \beta^2 I + (1 - \beta^2)\,\hat{c}_0\,\hat{c}_0^T \tag{J.2.8}$$

Then one can show (though we will not do so) that

$$[\vec{X}, \vec{Y}] \leq |\vec{X}|_P\ |\vec{Y}|_P = \sqrt{(\vec{X}^T\,C_0\,\vec{X})\ (\vec{Y}^T\,C_0\,\vec{Y})} \tag{J.2.9}$$

Substituting $\vec{R}_0$ for $\vec{X}$ and $\Delta\vec{Q}$ or $\vec{R}_0$ for $\vec{Y}$, we get

$$[\vec{R}_0, \Delta\vec{Q}] \leq |\vec{R}_0|_P \; |\Delta\vec{Q}|_P \tag{J.2.10}$$

and

$$[\vec{R}_0, \vec{R}_0] \leq |\vec{R}_0|_P \tag{J.2.11}$$

Then consider the requirement

$$|\vec{R}_0|_P \;\; |\Delta\vec{Q}|_P \;\; << \;\; [\vec{R}_0, \vec{R}_0] \tag{J.2.12}$$

If (J.2.12) holds, we obtain

$$[\vec{R}_0, \Delta\vec{Q}] \leq |\vec{R}_0|_P \;\; |\Delta\vec{Q}|_P << [\vec{R}_0, \vec{R}_0] \tag{J.2.13}$$

Thus, imposing (J.2.12), or the equivalent condition

$$|\Delta\vec{Q}|_P \;\; << \;\; \frac{[\vec{R}_0, \vec{R}_0]}{|R_0|_P} \tag{J.2.14}$$

we insure that the condition (J.2.1) holds and we may perform a far field PIC computation.

Now, the condition (J.2.14) must hold for all points Q on the panel, that is, defining the "compressible panel radius"

$$CR(\Sigma) = \max_{Q \text{ in } \Sigma} |\vec{Q} - \vec{Q}_0|_P \tag{J.2.15}$$

we must have

$$k \; CR(\Sigma) = \frac{[\vec{R}_0, \vec{R}_0]}{|R_0|_P} \tag{J.2.16}$$

where k is a "large" number.

Now, as the panel radius gets smaller and smaller compared to the "distance" from the control point to the panel center, we may neglect first the quadratic terms and finally neglect even the linear terms in ΔQ in the expansion (J.1.24). The corresponding far field computations are called dipole and monopole computations respectively, with the retention of quadratic terms in ΔQ (but not higher ones) called the quadrupole computation.

In practice, we perform a monopole computation if the factor k in (J.2.16) exceeds 24, a dipole computation for $8 < k \leq 24$, a quadrupole computation for $5 < k \leq 8$, and a one region intermediate field computation if $2 < k \leq 5$. These are empirical results not justifiable by a rigorous error analysis.

J.2.2 The Intermediate Field Criterion

As noted above, we perform a one-region intermediate field PIC computation when the constant k in (J.2.16) exceeds 2. We now discuss the circumstances under which we perform a two region intermediate field calculation, and if so, which pair of half panels we use.

Consider the panel approximations illustrated in figure J.4. The outer edges of the approximate panel coincide with the outer edges of the true panel; therefore our approximation preserves surface continuity. Furthermore, the doublet strength on the half panels, computed in section I.3, is identical to that of the exact panel on the panel edges; therefore doublet continuity is preserved. Thus we may perform a two region intermediate field PIC computation even though the control point is fairly close to the panel.

We require two criteria to hold before permitting a two region intermediate field computation. The first is that the constant k in (J.2.16) exceeds 1.2. Essentially, this means the "distance" from the control point to the panel center must exceed 1.2 panel radii; in particular, the control point does not lie on the panel.

To define the second criterion, let us recall some definitions from appendix I. We construct a special panel-wide local coordinate system similar to that constructed in section I.1, but we use different notation to avoid confusion with the coordinates (ξ, η, ζ) which occur in this appendix.

Let

$$\vec{W}_1 = \vec{P}_8 - \vec{P}_9$$
$$\vec{W}_2 = \vec{P}_5 - \vec{P}_9 \qquad \text{(J.2.17)}$$

Now, analogously to (I.1.3), let

$$W_3 = \frac{\vec{W}_1 \times \vec{W}_2}{|\vec{W}_1 \times \vec{W}_2|^{1/2}} \qquad \text{(J.2.18)}$$

Next, for any control point P, analogously to (I.1.7), let

$$\lambda_1(P) = \frac{((\vec{P} - \vec{P}_9) \times \vec{W}_2) \cdot \vec{W}_3}{|\vec{W}_1 \times \vec{W}_2|^{3/2}}$$

$$\lambda_2(P) = \frac{(\vec{W}_1 \times (\vec{P} - \vec{P}_9)) \cdot \vec{W}_3}{|\vec{W}_1 \times \vec{W}_2|^{3/2}}$$

$$\lambda_3(P) = \frac{(\vec{P} - \vec{P}_9) \cdot \vec{W}_3}{|\vec{W}_1 \times \vec{W}_2|} \qquad \text{(J.2.19)}$$

Also, recall from section P.2 the "skewness parameters"

$$C_{11} = \frac{((\vec{P}_1 - \vec{P}_9) \times \vec{W}_2) \cdot \hat{n}}{(W_1 \times W_2) \quad n} - 1$$

$$C_{21} = \frac{(\vec{W}_1 \times (\vec{P}_1 - \vec{P}_9)) \cdot \hat{n}}{(\vec{W}_1 \times \vec{W}_2) \cdot \hat{n}} - 1 \qquad \text{(J.2.20)}$$

These parameters are zero if the panel is a parallelogram.

Now, we perform a two region intermediate field PIC if

$$\sum_{i=1}^{3} \lambda_i(P)^2 \geq (1 + |C_{11}|)^2 + (1 + |C_{12}|)^2 \qquad \text{(J.2.21)}$$

For a square panel, this permits a two region intermediate field PIC to be performed unless the control point lies in the sphere, about the panel center, whose radius is the panel radius (see figure J.5). For skewed panels, the presence of C_{11} and C_{12} in (J.2.21) insures that the control point is further from the panel.

Finally, the choice of diagonal along which the panel is sliced into two half panels is chosen as follows: the value i, $1 \leq i \leq 4$, for which

$[\vec{P} - \vec{P}_i, \vec{P} - \vec{P}_i]$ is minimized, is computed.

Then, the panel is split in two along the diagonal which does not lie on P_i, that is, the diagonal with endpoints $P_{(i+1) \pmod 4}$ and $P_{(i+3) \pmod 4}$. An example of splitting a panel is shown in figure J.6. Note there that since

P_1 lies closest to P in hyperbolic distance, the panel Σ is split along the diagonal connecting P_2 and P_4.

In closing this section, we note that whenever we fail to compute a far field or intermediate field PIC, we compute a near field PIC. In the course of this computation, we may determine that the panel has no influence on the control point if the flow is supersonic, a subject we will discuss in the next section.

J.3 Supersonic Influence Test

In order to compute the influence of a subpanel on a control point P in supersonic flow, one must know

(a) whether the subpanel intersects D_P,

(b) if so, which of its edges intersect D_P, and

(c) which of its corners lie in D_P.

Rather than compute this data one subpanel at a time, the program takes several short cuts, which, if results are successful, give much or all of this data for a minimum of computation. First, a simple test is performed to check if the panel lies outside D_P (this test does not find all panels lying outside D_P, but does eliminate many of them). Second, a test which identifies panels lying wholly within D_P is performed. Finally, for panels which are identified neither as lying outside D_P or wholly within D_P, the influence test must be performed one subpanel at a time.

J.3.1 Definition of D_P

Given a control point P, we define D_P as the points Q, lying in the upstream pointing Mach cone from P. The condition that Q lie upstream from P is given by

$$(\vec{P} - \vec{Q}) \cdot \hat{c}_0 \geq 0 \tag{J.3.1}$$

The condition that $\vec{Q}$ lie in either the upstream or downstream Mach cone from $\vec{P}$ is given by

$$[\vec{P} - \vec{Q}, \vec{P} - \vec{Q}] \geq 0 \tag{J.3.2}$$

A point Q satisfying both (J.3.1) and (J.3.2) lies in D_P.

J.3.2 A Zero Influence Test

In this section, we determine the minimum distance $d(\vec{Q}, \partial D_P)$ from a point Q to the boundary ∂D_P of the domain of independence of P. We use this as follows. Let $R(\Sigma)$ be the true radius (as opposed to compressible radius) of the panel:

$$R(\Sigma) = \max_{1 \leq i \leq 4} |P_9 - P_i| \tag{J.3.3}$$

Then if P_9 does not lie in D_P, and

$$d(P_9, \partial D_P) > R(\Sigma) \tag{J.3.4}$$

no point on Σ can lie in D_P, and thus Σ is wholly outside D_P and so its influence on P is zero.

The computation of $d(Q, \partial D_P)$ is performed in the following manner. This distance is most easily computed in a coordinate system $\tilde{X}$ centered at the control point P, aligned with the compressibility vector $\hat{c}_0$ and oriented such that Q-P lies in the $\tilde{x}$-$\tilde{y}$ plane with positive $\tilde{y}$ coordinate, where the $\tilde{y}$ axis is orthogonal to $\hat{c}_0$, as illustrated in figure J.7.

Now, in this coordinate system, the Mach cone is defined by the lines

$$\tilde{y} = \pm \frac{\tilde{x}}{\beta} \tag{J.3.5}$$

since points on that line satisfy

$$\tilde{x}^2 + s\beta^2 \tilde{y}^2 = 0 \tag{J.3.6}$$

The line perpendicular to that defined by (J.3.5), passing through the origin, is

$$\tilde{y} = \beta\tilde{x} \tag{J.3.7}$$

and thus the line through Q perpendicular to the Mach line closer to Q is

$$\tilde{y} - \tilde{y}_0 = \beta(\tilde{x} - \tilde{x}_0) \tag{J.3.8}$$

Thus the point on ∂D_P lying closest to Q is the point $(\tilde{x},\tilde{y})$ lying on the lines

$$\tilde{y} - \tilde{y}_0 = \beta(\tilde{x} - \tilde{x}_0) \tag{J.3.9}$$

$$\tilde{y} = \frac{-\tilde{x}}{\beta}$$

Substituting (J.3.10) in (J.3.9),

$$-\frac{\tilde{x}}{\beta} + \tilde{y}_0 = \beta(\tilde{x} - \tilde{x}_0) \tag{J.3.11}$$

or

$$\tilde{x} = \frac{\beta\,\tilde{x}_0 - \tilde{y}_0}{\beta + 1/\beta} \tag{J.3.12}$$

and so

$$\tilde{y} = \frac{-\tilde{x}}{\beta} = \frac{-\beta\,\tilde{x}_0 + \tilde{y}_0}{\beta^2 + 1} \tag{J.3.13}$$

Then,

$$d(Q, \partial D_P) = \sqrt{(\tilde{x} - \tilde{x}_0)^2 + (\tilde{y} - \tilde{y}_0)^2} \tag{J.3.14}$$

So, $d(Q, \partial D_P)^2 =$

$$\left(\frac{\beta\tilde{x}_0 - \tilde{y}_0}{\beta + 1/\beta} - \tilde{x}_0\right)^2 + \left(\frac{-\beta\tilde{x}_0 + \tilde{y}_0}{\beta^2 + 1} - \tilde{y}_0\right)^2 \tag{J.3.15}$$

$$= \frac{1}{(\beta^2 + 1)} [\beta^2 \tilde{x}_0 - \beta \tilde{y}_0 - (\beta^2 + 1) \tilde{x}_0]^2 + \frac{1}{(\beta^2 + 1)^2} (-\beta \tilde{x}_0 - \beta^2 \tilde{y}_0)^2 \tag{J.3.16}$$

$$= \frac{1}{(\beta^2 + 1)^2} (-\tilde{x}_0 - \beta \tilde{y}_0)^2 + \frac{1}{(\beta^2 + 1)^2} (-\beta \tilde{x}_0 - \beta^2 \tilde{y}_0)^2 \tag{J.3.17}$$

$$= \frac{1 + \beta^2}{(\beta^2 + 1)^2} \tilde{x}_0^2 + \frac{2 (1 + \beta^2) (\tilde{x}_0 + \beta \tilde{y}_0)^2}{(\beta^2 + 1)^2}$$

$$+ \frac{(1 + \beta^2) (\beta^2 \tilde{y}_0)^2}{(\beta^2 + 1)^2} \tag{J.3.18}$$

$$= \frac{(\tilde{x}_0 + \beta \tilde{y}_0)^2}{1 + \beta^2} \tag{J.3.19}$$

So, $d(Q, \partial D_P) =$

$$\frac{\tilde{x}_0 + \beta \tilde{y}_0}{1 + \beta^2} \tag{J.3.20}$$

This formula holds as long as the nearest point on ∂D_P to Q is found by dropping a perpendicular to the Mach line, that is whenever (see figure J.7)

$$\tilde{y}_0 > \beta \tilde{x}_0 \tag{J.3.21}$$

Otherwise, the nearest point on D_P to Q is P, that is,

$$d(Q, \partial D_P) = |\vec{P} - \vec{Q}| \tag{J.3.22}$$

Finally, we compute $\tilde{x}_0$ and $\tilde{y}_0$ as follows. First, since the x-axis is aligned with $\hat{c}_0$,

$$\tilde{x}_0 = (\vec{Q} - \vec{P}) \cdot \hat{c}_0 \tag{J.3.23}$$

Next, since there is no coordinate scaling, we want

$$\tilde{x}_0^2 + \tilde{y}_0^2 = |\vec{Q} - \vec{P}|^2 \tag{J.3.24}$$

or

$$\tilde{y}_0 = \sqrt{|\vec{Q} - \vec{P}|^2 - \tilde{x}_0^2} \tag{J.3.25}$$

Then, summarizing, $d(Q, \partial D_P)$ is computed as

$$\begin{aligned} d(Q, \partial D_P)^2 &= (\tilde{x}_0 + \beta\, \tilde{y}_0)^2/(1 + \beta^2) & \tilde{y}_0 &\geq \beta\, \tilde{x}_0 \\ d(Q, \partial D_P)^2 &= |\vec{Q} - \vec{P}|^2 & \tilde{y}_0 &< \beta\, \tilde{x}_0 \end{aligned} \tag{J.3.26}$$

J.3.3 Panels Wholly within the Mach Cone

Just as a panel whose center lies further from ∂D_P than the panel radius has no influence on the control point if its center lies outside D_P, it analagously lies wholly within D_P if its center does. That is, if P_0 lies in D_P, and

$$d(P_9, \partial D_P) > R(\Sigma) \tag{J.3.27}$$

then Σ lies within D_P.

J.3.4 The Influence Test for a Subpanel

Finally, let us assume that the panel passes none of the simple tests described above. For each subpanel (or half panel or projected panel, in the case of intermediate field computations) we must determine which corners lie in D_P, which edges intersect D_P, and whether the region as a whole intersects D_P.

The corners of a subpanel are tested one at a time to see if they satisfy (J.3.1) and (J.3.2). If all corners do, then the entire subpanel lies in D_P. This follows from the fact that D_P is a "convex" region. A convex region is one such that the line segment joining any two points in the region also lies in the region. Thus if all vertices of a subpanel lie in D_P, then any point on an edge lies in D_P. Thus, since any point in the interior of the subpanel lies on some line segment joining points on edges, every point on the subpanel lies in D_P. Next, if one vertex of an edge lies in D_P and another does not, it is clear that both the edge and the subpanel lie partially within D_P.

J.3.4.1 The Point of Closest Approach

Let us assume neither vertex of an edge lies in D_P. Then we determine whether the edge intersects D_P as follows.

First, suppose the edge is a "subsonic edge." That is, let $\hat{t}_0$ be a unit vector parallel to the edge. Then defining

$$\tau = [\hat{t}_0, \hat{t}_0] \tag{J.3.28}$$

we call the edge subsonic if $\tau > 0$, supersonic if $\tau < 0$, and sonic if $\tau = 0$ (see figure J.8). A subsonic edge is inclined to the compressibility direction at less than the Mach angle; thus every point on the edge is in the domain of dependence of the most downstream point. So, if the most upstream point lies outside D_P, the entire edge does. In particular, if both vertices of a subsonic edge lie outside D_P, the entire edge does.

For a supersonic edge, this property does not hold, as illustrated in figure J.8. Thus, for a supersonic edge whose vertices lie outside D_P, we must check if the "point of closest approach" on the edge lies in D_P. If not, then the entire edge lies outside D_P.

What we mean by the point of closest approach is that point R_* on the line containing the edge which lies closest to the line through P parallel to the compressibility direction $\hat{c}_0$, as illustrated in figure J.9. We find R_* as follows. Let

$$\vec{\Delta R} = \vec{R}^+ - \vec{R}^- \tag{J.3.29}$$

where $\vec{R}^+$ and $\vec{R}^-$ are the vertices of the edge.

Now, let us write

$$\vec{R} = \alpha\vec{R}^- + (1 - \alpha)\,\vec{R}^+ = \vec{R}^+ - \alpha\vec{\Delta R} \tag{J.3.30}$$

for an arbitrary point on the line.

Then, the projection of R to the line parallel to $\hat{c}_0$ containing P is

$$\vec{P} + \hat{c}_0\,\hat{c}_0^T\,(\vec{R} - \vec{P}) \tag{J.3.31}$$

and so the square of the distance from R to that line is

$$d^2 = |\vec{R} - \vec{P} - \hat{c}_0\,\hat{c}_0^T\,(\vec{R} - \vec{P})|^2 \tag{J.3.32}$$

$$= (\vec{R} - \vec{P})\cdot(\vec{R} - \vec{P}) - (\hat{c}_0\cdot(\vec{R} - \vec{P}))^2 \tag{J.3.33}$$

$$= \text{(by (J.3.30))}$$

$$(\vec{R}^+ - \alpha\vec{\Delta R} - \vec{P})\,(\vec{R}^+ - \alpha\vec{\Delta R} - \vec{P}) - (\hat{c}_0\cdot(\vec{R}^+ - \alpha\vec{\Delta R} - \vec{P}))^2 \tag{J.3.34}$$

Now, d^2 is minimized by setting

$$\frac{d}{d\alpha}(d^2) = 0 = 2(\vec{R}^+ - \alpha\Delta\vec{R} - \vec{P})\cdot(-\Delta\vec{R})$$

$$-2\,(\hat{c}_0\cdot(\vec{R}^+ - \alpha\Delta\vec{R} - \vec{P}))\,(-\hat{c}_0\cdot\Delta\vec{R}) \qquad \text{(J.3.35)}$$

$$= [2(\Delta\vec{R}\cdot\Delta\vec{R}) - 2\,(\hat{c}_0\cdot\Delta\vec{R})^2\,\alpha$$

$$-2\,(\vec{R}^+ - \vec{P})\cdot\Delta\vec{R} + 2(\hat{c}_0\,(\vec{R}^+ - \vec{P}))\cdot(\hat{c}_0\cdot\Delta\vec{R}) \qquad \text{(J.3.36)}$$

So, d^2 is minimized for

$$\alpha = \alpha^* = \frac{(\vec{R} - \vec{P})\cdot\Delta\vec{R} - (\hat{c}_0\cdot(\vec{R} - \vec{P}))(\hat{c}_0\cdot\Delta\vec{R})}{(\Delta\vec{R}\cdot\Delta\vec{R}) - (\hat{c}_0\cdot\Delta\vec{R})^2} \qquad \text{(J.3.37)}$$

Thus, the point R_* on the line containing the edge which is the point of closest approach is

$$\vec{R}_* = \alpha_*\,\vec{R} + (1 - \alpha_*)\,\vec{R} \qquad \text{(J.3.38)}$$

Thus if R^+ and R^- both lie outside D_p, we compute α_*. If $0 < \alpha_* < 1$, the point of closest approach lies in the interior of the edge, and we thus test if R_* lies in D_p. If it does not, the entire edge lies outside D_p.

For reasons of efficiency, the program actually computes

$$\alpha_* = \frac{(\hat{c}_0 \times \Delta\vec{R})\,.\,(\hat{c}_0 \times (\vec{R}^+ - \vec{P}))}{|\hat{c}_0 \times \Delta\vec{R}|^2} \qquad \text{(J.3.39)}$$

The equivalence of (J.3.37) and (J.3.39) is easily seen in compressibility coordinates, where

$$\hat{c}_0 = \begin{Bmatrix} 1 \\ 0 \\ 0 \end{Bmatrix} \qquad \text{(J.3.40)}$$

Then,

$$\hat{c}_0\cdot\Delta\vec{R} = (\Delta\vec{R})_x \qquad \text{(J.3.41)}$$

and so the denominator of (J.3.37) is

$$(\Delta\vec{R})_y{}^2 + (\Delta\vec{R})_z{}^2 \qquad \text{(J.3.42)}$$

On the other hand

$$\hat{c}_0 \times \Delta\hat{R} = \begin{Bmatrix} 0 \\ -\Delta R_z \\ \Delta R_y \end{Bmatrix} \tag{J.3.43}$$

and so the expression (J.3.42) defines the denominator of (J.3.39).

Next,

$$(\hat{c}_0 \times \Delta\vec{R})\cdot(\hat{c}_0 \times (\vec{R}^+ - \vec{P})) =$$

$$\begin{Bmatrix} 0 \\ -\Delta R_z \\ \Delta R_y \end{Bmatrix} \bullet \begin{Bmatrix} 0 \\ -(\vec{R}^+ - \vec{P})_z \\ (\vec{R}^+ - \vec{P})_y \end{Bmatrix} = \tag{J.3.44}$$

$$\Delta R_y\ (\vec{R}^+ - \vec{P})_y + \Delta R_z\ (\vec{R}^+ - \vec{P})_z \tag{J.3.45}$$

$$= \Delta\vec{R}\cdot(\vec{R}^+ - \vec{P}) - (\hat{c}_0 \cdot \Delta\vec{R})\ (\hat{c}_0 \cdot (\vec{R}^+ - \vec{P})) \tag{J.3.46}$$

and thus the numerators of (J.3.37) and (J.3.39) are equal.

J.3.4.2 The Winding Number Test

Finally, let us assume that none of the edges of the subpanel intersect D_p. Then if the panel is subinclined, we can see from figure J.10 that the entire panel lies outside D_p, while for supersonic panels this does not hold.

Thus in this case we compute the point P_*, on the plane containing the subpanel, which is the intersection of the line through P parallel to c_0 with the plane of subpanel. It is clear that if P_* lies in the interior of the subpanel, the subpanel intersects D_p, while if it lies in the exterior of the subpanel, the subpanel lies wholly outside D_p.

Now, we can write

$$\vec{P}_* = \vec{P} + \beta\ \hat{c}_0 \tag{J.3.47}$$

and since P_* lies on the subpanel,

$$(\vec{P}_* - \vec{P}_i) \cdot \hat{n}_0 = 0 \tag{J.3.48}$$

where $\hat{n}_0$ is the subpanel normal and $\vec{P}_i$ is a vertex. Substituting (J.3.48) in (J.3.47),

$$(\vec{P}_* - \vec{P}_i) \cdot \hat{n}_0 + \beta(\hat{c}_0 \cdot \hat{n}_0) = 0 \tag{J.3.49}$$

or

$$\beta = \frac{(\vec{P}_i - \vec{P}) \cdot \hat{n}_0}{\hat{c}_0 \cdot \hat{n}_0} \tag{J.3.50}$$

Now, if P_* lies in the subpanel, the angles formed by P_i, P_*, and $P_{i(\text{mod } 3) + 1}$ are all of the same sign. That is, P_* is inside the subpanel if and only if

$$((\vec{P}_i - \vec{P}_*) \times (\vec{P}_{i(\text{mod } 3)+1} - \vec{P}_*)) \cdot \hat{n}_0 \tag{J.3.51}$$

has the same sign for i = 1,2,3.

J.3.4.3 Half Panels and Projected Panels

Everything we have said about subpanels holds equally well for half panels, since they are also triangular regions. It also holds equally well for projected panels, used in the one region intermediate field computation, provided the projected panel is convex. When the panel is not convex, there is a small risk that the influence will be calculated erroneously. For this reason, the program checks for non-convex panels and warns the user of their existence.

J.4 Cylindrical Coordinates

When the integrals (J.1.1), (J.1.2), (J.1.4) and (J.1.5) are transformed to local coordinates, they become integrals of the general form

$$\iint_{\Sigma' \cap D_p} \begin{Bmatrix} \sigma(\xi', \eta') \\ \mu(\xi', \eta') \end{Bmatrix} f(R')\, d\xi'\, d\eta' \tag{J.4.1}$$

where (see section E.3)

$$R'^2 = r(\xi' - x')^2 + s(\eta' - y')^2 + rs\,(\zeta' - z')^2 \tag{J.4.2}$$

When rs = 1 (this covers both the case of subsonic flow and of superinclined panels), these integrals are very naturally evaluated using cylindrical coordinates. In section J.4, we derive basic results which are necessary to perform these integrations. The case of rs = -1 (subinclined panels in supersonic flow) is best handled by hyperbolic coordinates discussed in section J.5.

J.4.1 Fundamental Results

Recall from section E.3 that in the local coordinate system, the flow is in the x' direction for subsonic flow and in the ±z' direction for superinclined panels. Thus D_p is all space for subsonic flow, and (writing P = (x',y',z') in local coordinates)

$$D_p = (\xi', \eta', \zeta') \quad (\zeta' - z')^2 - (\ ' - x')^2 - (\eta' - y')^2 > 0$$

$$\text{and} \quad (\zeta' - z')\ \text{sign}\ (\hat{c}_0 \cdot \hat{n}_0) \leq 0 \tag{J.4.3}$$

(where $\hat{n}_0$ is the subpanel normal) for superinclined panels. We can rewrite (J.4.3) as

$$D_p = \left\{ (\xi', \eta', \zeta') \middle| \sqrt{(\xi' - x')^2 + (\eta' - Y')^2} < -\ \text{sign}\ (\hat{c}_0 \cdot \hat{n}_0)(\zeta' - z') \right\} \tag{J.4.4}$$

Because both the function R' and the domain of dependence D_p exhibit circular symmetry with respect to the point (x', y'), we will find it convenient to use cylindrical coordinates centered at (x', y') to perform the required integrations. In addition, because the boundary of the panel image Σ' is composed of straight lines (the edges), local coordinate systems having axes perpendicular and parallel to the edges also arise naturally.

We should note here that our results will hold for any planar region which is convex. This, of course, includes subpanels and half panels, though not necessarily projected panels (see section J.3.4.3).

J.4.2 The Mach Disk

Since ζ' is a constant on the surface of integration Σ' (see section E.3), the region of integration $\Sigma' \cap D_p$ may equally well be taken to be $\Sigma' \cap C_h$ where C_h the "Mach disk" is defined by

$$C_h = \left\{ (\zeta', \eta') \,\middle|\, (\zeta' - x')^2 + (\eta' - y')^2 \leq \bar{h} \right\} \tag{J.4.5}$$

where

$$\bar{h} = \begin{cases} +\infty \text{ if } s = 1 \\ \\ \text{sign } (\hat{n}_0 \cdot \hat{c}_0) h \text{ if } s = -1 \end{cases} \tag{J.4.6}$$

where

$$\bar{h} = z' - \zeta' \tag{J.4.7}$$

The region of integration $\Sigma' \cap C_h$ for a typical panel image Σ' is shown in Figure J.12. Note that since both Σ' and C_h are convex, so is $\Sigma' \cap C_h$.

A careful examination of figure J.12 reveals that the boundary of $\Sigma' \cap C_h$ denoted $\partial(\Sigma' \cap C_h)$ is composed of both curved and straight line segments. Furthermore $\partial(\Sigma' \cap C_h)$ has sharp corners in two possible instances,

(i) Whenever a corner of Σ' lies <u>inside</u> C_h.

(ii) Whenever an edge Σ' intersects the boundary of C_h.

We will develop a scheme for numbering the <u>edges</u>, E_k, <u>corner points</u> $\rho_k^{\pm}$, and <u>phases of corner points</u> $\phi_k^{\pm}$ of the region $\Sigma' \cap C_h$. At the outset of this discussion, we distinguish three separate cases

(a) $\Sigma' \cap C_h$ is empty

(b) $\Sigma' \cap C_h = C_h$ (that is, $C_h \subset \Sigma'$)

(c) $\Sigma' \cap C_h$ is a proper subset of C_h

Case (a) is of absolutely no consequence since $\Sigma' \cap C_h$ is null and all integrals over it are zero.

J.4.3 The Case of the Mach Disk Lying within the Panel

Case (b) is handled in the following fashion (see fig. J.13). In the first place, no edges are defined when $\Sigma' \cap C_h = C_h$. Next, some point (ξ', η') lying on the boundary of C_h is chosen at random and $\vec{\rho} = (s_1, t_1)$ is defined by

$$\vec{\rho} = (\xi' - x', \eta' - y') \tag{J.4.8}$$

Next, $\vec{\rho}_1^{\pm}$, $\vec{\rho}_2^{-}$, $\phi_1^{\pm}$, ϕ_2^{-} are defined by

$$\vec{\rho}_1^{-} = \vec{\rho}_1^{+} = \vec{\rho}_2^{-} = \vec{\rho}$$

$$\phi_1^{-} = \phi_1^{+} = ph\ (s_1, t_1)$$

$$\phi_2^{-} = \phi_1^{+} + 2\pi \tag{J.4.9}$$

Here, ph is the "phase function" in two real variables

$$ph(x,y) = \arg\ (x + iy) \tag{J.4.10}$$

where arg is the complex argument function. Precisely, for any two real numbers x and y, one of them non-zero, the equations

$$-\pi < ph\ (x,y) \leq \pi$$

$$\cos\ (ph\ (x,y)) = x\ /\ \sqrt{\{\ x^2 + y^2\ \}}$$

$$\sin\ (ph\ (x,y)) = y\ /\ \sqrt{\{\ x^2 + y^2\ \}} \tag{J.4.11}$$

uniquely define ph(x,y). It should be noted in passing that ph(x,y) equals the FORTRAN function ATAN2(y,x).

With these definitions, it is clear that the integral J defined by

$$J = \frac{d\xi'\ d\eta'}{\sqrt{h^2 - (\xi' - x')^2 - (\eta' - y')^2}} \tag{J.4.13}$$

may equally well be computed by the expression

$$J = \left[\int_{\phi_1^-}^{\phi_1^+} d\phi + \int_{\phi_1^+}^{\phi_2^-} d\phi \right] \int_0^{|h|} \frac{\rho d\rho}{\sqrt{h^2 - \rho^2}}$$

(where $C_h \subset \Sigma'$) and $\rho = |\vec{\rho}|$), since

$$\rho d\rho d\phi = d\xi'\ d\eta' \tag{J.4.14}$$

J.4.4 Arbitrary Intersection of the Mach Disk with the Panel

We now take up the difficult and interesting case (c), when $\Sigma' \cap C_h \neq C_h$. For this discussion, the reader is referred back to Fig. J.12. Starting with any <u>edge</u> of Σ' that has some points lying inside C_h, we denote this edge E_1 and <u>begin</u> proceeding around the boundary of $\Sigma' \cap C_h$ in a

counterclockwise (positive) fashion. As we traverse $\partial(\Sigma' \cap C_h)$, we will move along straight and possibly curved pieces of boundary. The straight pieces of boundary are named $E_1, E_2, \ldots, E_n$ as they are encountered. Here, n is the number of edges of Σ' that have some points lying inside C_h (see Fig. J.14).

J.4.4.1 Corner Points

Having described the edge naming convention, the corner points $\rho_k^{\pm}$ are defined by

$$\vec{\rho}_k^{-} = (\xi', \eta') \Big|_{\substack{\text{lower edge} \\ \text{of } E_k}} -(x', y') \tag{J.4.15}$$

The components of $\vec{\rho}_k^{\pm}$ are denoted $(s_k^{\pm}, t_k^{\pm})$ as follows

$$(s_k^{\pm}, t_k^{\pm}) = \vec{\rho}_k^{\pm} \tag{J.4.16}$$

Also, the special corner point $\vec{\rho}_{n+1}^{-}$ is defined

$$\vec{\rho}^{-}_{n+1} = \vec{\rho}^{-}_{1} \tag{J.4.17}$$

J.4.4.2 The Phase Function

Finally, the phases of the corner points, $\phi_k^{\pm}$, are defined recursively by

$$\phi_1^{-} = \mathrm{ph}\,(s_1^{-}, t_1^{-})$$

$$\phi_k^{+} = \phi_k^{-} + \int_{\rho_k^{-}}^{\rho_k^{+}} d\phi \tag{J.4.18}$$

Great care must be taken here because of the problem of "phase wrap." That is, the phase function is discontinuous on a closed path in the x'-y' plane which does not contain the origin. Thus in the former case (that of the second or third illustration in figure J.14) ϕ_n^{+} is almost 2π greater than ϕ_1, while in the latter case the increment of 2π does not occur.

Next we compute

$$d\phi = \frac{\partial\phi}{\partial s} ds + \frac{\partial\phi}{\partial t} dt \tag{J.4.19}$$

Now, since, up to an additive constant,

$$\phi = ph(s,t) = \arg(s+it)$$

$$= \text{Im} \log(s+it) \tag{J.4.20}$$

(where Im is the imaginary part), we have

$$\frac{\partial\phi}{\partial s} = \text{Im} \frac{\partial}{\partial s} \log (s+it) = \text{Im} \left(\frac{1}{s+it}\right)$$

$$= \text{Im} \left(\frac{s-it}{s^2+t^2}\right) = \frac{-t}{s^2+t^2} \tag{J.4.21}$$

Similarly,

$$\frac{\partial\phi}{\partial t} = \text{Im} \left(\frac{i}{s+it}\right) = \text{Im} \left(\frac{is -t}{s^2+t^2}\right) = \frac{s}{s^2+t^2} \tag{J.4.22}$$

Combining these results, we have

$$d\phi = \frac{sdt - tds}{s^2+t^2} =$$

(by definition of $\vec{\rho}$)

$$\frac{(\vec{\rho} \times \vec{d\rho})}{\rho^2} \tag{J.4.23}$$

The integrals in (J.4.18) are straightforward to evaluate. Since (see figure J.15) the angle ϕ between $\vec{\rho}_k^-$ and $\vec{\rho}_k^+$ satisfies

$$(\vec{\rho}_k^- \times \vec{\rho}_k^+)_z = \rho_k^- \rho_k^+ \sin \phi$$

$$\vec{\rho}_k^- \cdot \vec{\rho}_k^+ = \rho_k^- \rho_k^+ \cos \phi \tag{J.4.24a}$$

we have (by J.4.11)

$$\phi = \int_{\rho^+_k}^{\rho^-_{k+1}} d\phi = ph(\vec{\rho}^-_k \cdot \vec{\rho}^+_{k+1}, (\vec{\rho}^-_k \times \vec{\rho}^+_k)_z) \tag{J.4.24b}$$

Now, geometric reasoning shows that in this case,

$$(\vec{\rho}^-_k \times \vec{\rho}^+_k)_z > 0 \tag{J.4.25}$$

and thus $0 \leq \phi \leq \pi$.

On the other hand, the angle ϕ' betweeen $\vec{\rho}^+_k$ and $\vec{\rho}^-_{k+1}$ may exceed π (see figure J.15), and must be correctly evaluated in view of phase wrap, and thus

$$\phi' = \int_{\rho^+_k}^{\rho^-_{k+1}} d\phi = \hat{ph}(\vec{\rho}^+_k \cdot \vec{\rho}^-_{k+1}, (\vec{\rho}^+_k \times \vec{\rho}^-_{k+1})_z) \tag{J.4.26}$$

where $\hat{ph}$ is defined by

$$\hat{ph}\,(x,y) = ph\,(x,y) + 2\pi n$$

$$0 \leq \hat{ph}\,(x,y) < 2\pi$$

$$n = 0 \text{ or } 1 \tag{J.4.27}$$

With phases $\phi^{\pm}_k$ defined in this fashion, the phase of a point ρ on the boundary of $\Sigma' \cap C_h$, defined by

$$\phi(\vec{\rho}) = \phi^-_1 + \int_{\rho^-_1}^{\rho} d\phi = \phi^-_1 + ph(\vec{\rho}_1 \cdot \vec{\rho}, (\vec{\rho}_1 \times \vec{\rho})_z) \tag{J.4.28}$$

is a continuous function for all points on the boundary satisfying

$$\phi(\rho^{\pm}_k) = \phi^{\pm}_k \qquad k = 1,\ldots,n \tag{J.4.29}$$

Because of phase wrap, it may happen that $\phi^-_{n+1} \neq \phi^-_1$ but rather $\phi^-_{n+1} = \phi^-_1 + 2\pi$. If this happens, it indicates that the center of our coordinate system (x',y') lies inside Σ'. Defining the <u>center indicator</u> C_Θ by

$$C_\Theta = \begin{cases} 1 \text{ if } (x', y') \in \Sigma' \\ 0 \text{ otherwise} \end{cases} \tag{J.4.30}$$

we observe that

$$\phi^-_{n+1} = \phi^-_1 + 2\pi\, C_\Theta \tag{J.4.31}$$

J.4.4.3 Edges and the Mach Disk

The discussion given above provides a very precise definition of the phases $\phi_k^\pm$ once the corner points are known; however, the determination of the edges E_k and the corner points $\rho_k^\pm$ will require some more detail which we now provide.

An edge E_k of the region $\Sigma' \cap C_h$ must be either part of, or all of an edge E of Σ'. Thus given an edge E of Σ', we seek to answer the question of when an edge E of Σ' is also an edge E_k of $\Sigma' \cap C_h$. Toward answering this question, we assume that the upper or lower endpoints of the edge E are given by (see figure J.15)

Edge E's lower endpoint = $(x',y') + \vec{\rho}-$

Edge E's upper endpoint = $(x',y') + \vec{\rho}+$ (J.4.32)

Thus $\vec{\rho}-(\vec{\rho}+)$ describes the vector from (x',y') to the lower (upper) end point of E. (The upper and lower endpoints of E may be assumed known because they are essential to the definition of Σ'). The components of $\vec{\rho}\pm$ are denoted $(s\pm,t\pm)$, i.e.,

$$(s\pm,\ t\pm) = \vec{\rho}\pm \tag{J.4.33}$$

It should be noted that the designations "lower" and "upper" are designations associated with the orientation of Σ'; as one traverses $\partial\Sigma'$ in a postive (counterclockwise) fashion, one moves along edges from their lower to their upper end.

J.4.4.4 Edge Tangents and Normals

Next, we define the <u>edge tangent</u> t by

$$\vec{t} = n(\vec{\rho}+ - \vec{\rho}-) \tag{J.4.34}$$

where n denotes the normalization operation

$$n(\vec{x}) = \frac{\vec{x}}{|\vec{x}|} \tag{J.4.35}$$

In component notation, $\vec{t}$ may be written

$$\vec{t} = (t_\xi, t_\eta) \tag{J.4.36}$$

We use this representation to define the <u>edge</u> <u>outer</u> normal $\vec{n}$ by

$$\vec{n} = (t_\eta, -t_\xi) = (n_\xi, n_\eta) \tag{J.4.37}$$

Clearly, $\vec{n}$ and $\vec{t}$ so defined satisfy the conditions

<u>Normalization Conditions</u> $\quad |\vec{t}| = (t_\xi^2 + t_\eta^2)^{1/2} = 1$

$$\vec{n} = (n_\xi^2 + n_\eta^2)^{1/2} = 1 \tag{J.4.38}$$

<u>Orthogonality</u> $\quad \vec{n} \cdot \vec{t} = n_\xi t_\xi + n_\eta t_\eta = 0 \qquad$ (J.4.39)

<u>Cross Product</u> $\quad (\vec{n} \times \vec{t})_\zeta = n_\xi t_\eta - n_\eta t_\xi = 1 \qquad$ (J.4.40)

As a consequence of (J.4.38-40), the vector pair $(\vec{n},\vec{t})$ (in that order) comprises a right handed basis for (u,v) space as shown in Fig. J.16.

The (s,t) system illustrated there has been previously introduced and is given by

$$\vec{\rho} = (s,t) = (\xi' - x', \eta' - y') \tag{J.4.41}$$

The coordinate functions u,v are defined by

$$u = \vec{n} \cdot \vec{\rho}$$
$$v = \vec{t} \cdot \vec{\rho} \tag{J.4.42}$$

or

$$\begin{Bmatrix} u \\ v \end{Bmatrix} = \begin{bmatrix} t_\eta & -t_\xi \\ t_\xi & t_\eta \end{bmatrix} \begin{Bmatrix} s \\ t \end{Bmatrix} = [A] \begin{Bmatrix} s \\ t \end{Bmatrix} \tag{J.4.43}$$

Since A is orthogonal,

$$A^{-1} = A^T$$

and so

$$\vec{\rho} = \begin{Bmatrix} s \\ t \end{Bmatrix} = A^T \begin{Bmatrix} u \\ v \end{Bmatrix} = \begin{bmatrix} t_\eta & t_\xi \\ -t_\xi & t_\eta \end{bmatrix} \begin{Bmatrix} u \\ v \end{Bmatrix} = u \begin{Bmatrix} t_\eta \\ -t_\xi \end{Bmatrix} + v \begin{Bmatrix} t_\xi \\ t_\eta \end{Bmatrix} \tag{J.4.44}$$

or

$$\vec{\rho} = u\vec{n} + v\vec{t} \tag{J.4.45}$$

For points lying on the edge E, we note that

$$\vec{\rho}|_E = \vec{\rho}_- + s\,\vec{t} \tag{J.4.46}$$

where s denotes arc length along E. Taking the dot product of (J.4.46) with n and taking account of (J.4.39), we find

$$\vec{n}\cdot\vec{\rho}|_E = \vec{n}\cdot\vec{\rho}_- \tag{J.4.47}$$

that is, the expression $\vec{n}\cdot\vec{\rho}$ is a constant along the edge E; this observation motivates the definition of a, the <u>edge distance</u>

$$a = \vec{n}\cdot\vec{\rho}|_E = \vec{n}\cdot\vec{\rho}_- = \vec{n}\cdot\vec{\rho}^+ \tag{J.4.48}$$

We may now express the vectors $\vec{\rho}^{\pm}$ in the new coordinate system as follows. Using (J.4.45) we have

$$\vec{\rho}^{\pm} = (\vec{n}\cdot\vec{\rho}^{\pm})\,\vec{n} + (\vec{t}\cdot\vec{\rho}^{\pm})\,\vec{t} \tag{J.4.49}$$

Now, defining $v^{\pm}$ by

$$v^{\pm} = \vec{\rho}^{\pm}\cdot\vec{t} \tag{J.4.50}$$

we find by (J.4.48) that (as illustrated in figure J.16)

$$\vec{\rho}^{\pm} = a\vec{n} + v^{\pm}\,\vec{t} \tag{J.4.51}$$

Equation (J.4.51) describes the <u>endpoints</u> of the edge E; for points interior to the edge E we have

$$\vec{\rho}|_E = a\vec{n} + v\vec{t} \tag{J.4.52}$$

where

$$v = \vec{\rho}\cdot\vec{t}$$

The representation (J.4.52) now provides us with the information necessary to answer the question posed earlier (when is an edge E of Σ' also an edge of $\Sigma' \cap C_h$). To see how this is done, we refer to figure J.17. First we note that what we are really trying to determine is if any points interior to E are also interior to C_h. In particular, if either $\vec{\rho}_-$ or $\vec{\rho}^+$ lies inside C_h the answer is <u>YES</u>. On the other hand, for all points $\vec{\rho}$ in C_h, $|\vec{\rho}| \leq h$. Since the smallest that $|\vec{\rho}|_E$ can become is $|a|$ (see equation (J.4.52)), we see that if $|a| > h$ then the answer is <u>NO</u>. Now if $|\vec{\rho}^+| > h$, $|\vec{\rho}_-| > h$ and $|a| \leq h$, we must still determine whether or not E passes through C_h without either of its endpoints actually lying inside. This will happen provided $v_- \leq 0 \leq v^+$. Otherwise, E will not pass through C_h. Thus we have determined in all circumstances whether E intersects C_h. These can be summarized by the following algorithm.

Algorithm: (Does an edge E have any points in C_h)

$$|a| > \vec{h} \implies \text{NO}$$

$$|a| < \bar{h} :$$

$$|\vec{\rho^+}| < \bar{h} \text{ or } |\vec{\rho^-}| < \bar{h} \implies \text{YES}$$

$$|\vec{\rho^+}| \geq \bar{h} \text{ and } |\vec{\rho^-}| \geq \bar{h}$$

$$0 \text{ in } [v-, v+] \implies \text{YES}$$

$$0 \text{ not in } [v-, v+] \Rightarrow \text{NO}$$

Once we have made the determination that an edge E has points inside C_h, we must assign it a number k (for E_k) and define the end points $\rho_k^{\pm}$ for E_k.

If we define the critical value of v_c by

$$v_c = \sqrt{h^2 - a^2} \tag{J.4.54}$$

then $\vec{\rho_k^{\pm}}$ are determined by the procedure

$$\vec{\rho_k^-} = \vec{\rho^-} \text{ if } |\vec{\rho^-}| < \bar{h}$$

$$= \vec{an} - v_c \vec{t} \text{ if } |\vec{\rho^-}| \geq \bar{h}$$

$$\vec{\rho_k^+} = \vec{\rho^+} \text{ if } |\vec{\rho^+}| < \bar{h}$$

$$= \vec{an} + \vec{v_c t} \text{ if } |\rho^+| \geq h \tag{J.4.55}$$

J.4.4.5 The Function $P(\phi)$

We have now given complete procedures for the specification of E_k, $\rho_k^{\pm}$, $\phi_k^{\pm}$. Before we can evaluate the integrals (J.4.1), we must define a function $P(\phi)$ (see Figure J.18) that describes the upper limit of integration from (x',y') to the boundary of $\Sigma' \cap C_h$. $P(\phi)$ is defined as follows:

$$P(\phi) = \begin{cases} |h\Gamma| & \text{if } \phi_k^{\pm} < \phi < \phi_{k+1}^{-} \\ P_k(\phi) & \text{if } \phi_k^{-} \leq \phi \leq \phi^{+}{}_k \end{cases} \tag{J.4.56}$$

where on each edge E_k, $P_k(\phi)$, is the distance from (x',y') to E_k

$$P_k(\phi) = \sqrt{a^2{}_k + v_k(\phi)^2} \tag{J.4.57}$$

In equation (J.4.57), $v_k(\phi)$ denotes the local edge coordinate v, evaluated on the edge E_k and expressed as a function of ϕ. Although we will never use it explicitly, we record it here for the sake of completeness

$$v_k(\phi) = a_k \tan(\phi - \phi_k' + ph(a_k, v_{\bar{k}})) \tag{J.4.58}$$

With all these definitions available, it is now a fairly simple matter to write down the integrals (J.4.1) using polar coordinates. For the sake of concreteness, we evaluate the integral J

$$J = \iint_{\Sigma' \cap C_h} \frac{d\xi' \, d\eta'}{\sqrt{h^2 - (\xi' - x')^2 - (\eta' - y')^2}} \tag{J.4.59}$$

Converting to polar coordinates centered at (x',y'), we have

$$d\xi' \, d\eta' = \rho d\rho d\phi \tag{J.4.60}$$

$$(\xi' - x')^2 + (\eta' - y')^2 = \rho^2 \tag{J.4.61}$$

so that (see Figure J.19 for limits of integration)

$$J = \iint_{\Sigma' \cap C_h} \frac{\rho d\rho d\phi}{\sqrt{h^2 - \rho^2}}$$

$$= \sum_{k=1}^{n} \left(\int_{\phi_k^-}^{\phi_k^+} d\phi \int_0^{P_k(\phi)} \frac{\rho d\rho}{\sqrt{h^2 - \rho^2}} + \int_{\phi_k^+}^{\phi_{\bar{k}+1}} d\phi \int_0^{|h|} \frac{\rho d\rho}{\sqrt{h^2 - \rho^2}} \right) \tag{J.4.62}$$

Evaluating the inner integrals in (J.4.62), we note

$$\int_0^P \frac{\rho d\rho}{\sqrt{h^2 - \rho^2}} = -\sqrt{h^2 - \rho^2} \Big|_0^{P_k} = -\sqrt{h^2 - \rho^2} + |h| \tag{J.4.63}$$

so that

$$J = \sum_{k=1}^{n} \left(\int_{\phi_k^-}^{\phi_k^+} d\phi \left(|h| - \sqrt{h^2 - P_k(\phi)^2} \right) + \int_{\phi_k^+}^{\phi_{k+1}^-} |h| d\phi \right)$$

$$= h \sum_{k=1}^{n} \left(\int_{\phi_k}^{\phi_k^+} d\phi + \int_{\phi_k^+}^{\phi_{k+1}^-} d\phi \right) - \sum_{k=1}^{h} \int_{\phi_k^-}^{\phi_k^+} d\phi \; h^2 P_k(\phi)^2$$

$$= |h| \left(\phi_{n+1}^- - \phi_1^-\right) - \sum_{k=1}^{n} \int_{\phi_k^-}^{\phi_k^+} d\phi \sqrt{h^2 - P_k(\phi)^2} \qquad (J.4.64)$$

Now equation (J.4.23) for $d\phi$ may be combined with the representation (J.4.45) for ρ to yield

$$\rho^2 \, d\phi = (\vec{\rho} \times \vec{d\rho})_\zeta =$$

$$(\vec{un} + \vec{vt}) \times (\vec{n}\, du + \vec{t} dv)$$

$$= udv - vdu \qquad (J.4.65)$$

Now if we agree to restrict $\vec{\rho}$ to the edge E_k, we find u = const. $= a_k$, $du = 0$, and for $d\phi$,

$$d\phi = \frac{udv}{\rho^2} = \frac{a_k \, dv}{a_k^2 + v^2} \qquad (J.4.66)$$

Substituting this into (J.4.64) and noting that when $\phi = \phi_k^\pm$, $v = v_k^\pm$, (at the points $\rho_k^\pm$) we obtain

$$J = |h| \, 2\pi \, C_\bullet - \sum_{k=1}^{n} \int_{v_k^-}^{v_k^+} \frac{a_k \, dv}{a_k^2 + v^2} \sqrt{h^2 - a_k^2 - v^2} \qquad (J.4.67)$$

where we have used $P_k(\phi)^2 = a_k^2 + v^2$ on edge E_k. The integral on the right may be evaluated by elementary means to yield

$$J = 2\pi \, C_\bullet |h| - \sum_{k=1}^{n} \left[h \, ph \left(a_k R_k(v), hv\right) + a_k \, ph(v, R_k(v)) \right]_{v_k^-}^{v_k^+} \qquad (J.4.68)$$

where

$$R_k\ (v) = \sqrt{h^2 - a_k - v^2}$$

This integral is verified in section J.7.1.4, where it is identified as "I(X)."

J.5 Hyperbolic Coordinates

Having examined the geometry of the circle in such gruesome detail we now do the same for the hyperbola. The motivation for this exercise stems from a desire to develop effective tools to deal with integrals of the following form arising from application of the transformations described in section (E.3) for subinclined panels:

$$\iint_{\Sigma' \cap D_p} \begin{Bmatrix} \sigma(\xi, \eta) \\ \mu(\xi, \eta) \end{Bmatrix} f(R)\, d\xi'\, d\eta' \tag{J.5.1}$$

where

$$R = (\xi' - x')^2 - (\eta' - y')^2 - (\zeta' - z')^2$$

$$D_p = \{P' = (\xi', \eta', \zeta') \mid (\xi' - x') \leq -(\eta' - y')^2 + (\zeta' - z')^2\} \tag{J.5.2}$$

and Σ' is some convex region lying in the (ξ', η') plane with oriented normal $\vec{n}' = (0,0,1)$. The points in Σ' are described by (ξ', η', ζ') in the coordinate system X', with ζ' constant.

J.5.1 Fundamental Results

As before, D_p denotes the domain of dependence described in the panel local coordinate system X'.

Because the geometry of the hyperbola is much less intuitive than that of the circle, our discussion will have to rely rather heavily upon algebraic arguments. We will, however, try to parallel the discussion of section (J.4) as closely as possible.

We begin our discussion of (J.5.1) with a trivial change of variables. Variables s and t are defined by (see Fig. J.20)

$$s = \xi' - x'$$

$$t = \eta' - y' \tag{J.5.4}$$

and the constant h is defined by

$$h = z' - \zeta' \tag{J.5.5}$$

Using these new variables, the integral (J.5.1) can be written

$$\iint_{\Sigma' \cap H_h} \begin{Bmatrix} \sigma(x' + s, y' + t) \\ \mu(x' + s, y' + t) \end{Bmatrix} f(R)\, ds\, dt \tag{J.5.6}$$

where the panel Σ' is of course translated, and H_h denotes the hyperbolic region

$$H_h = \left\{(s,t) \,\middle|\, s \leq -\sqrt{t^2 + h^2}\right\} \tag{J.5.7}$$

Using the new variables, the distance function R is

$$R = \sqrt{s^2 - t^2 - h^2} \tag{J.5.8}$$

Having made this transformation of variables, we now remark that both the function R and the region H_h exhibit hyperbolic symmetry with respect to the origin (of the s-t coordinate system). By this we mean that if s,t are defined by

$$\begin{Bmatrix} \tilde{s} \\ \tilde{t} \end{Bmatrix} = [A] \begin{Bmatrix} s \\ t \end{Bmatrix} \tag{J.5.9a}$$

where

$$A = \begin{bmatrix} a & b \\ b & a \end{bmatrix} \tag{J.5.9b}$$

and

$$a^2 - b^2 = 1$$

$$a > 0 \tag{J.5.9c}$$

and $\tilde{H}_h$, $\tilde{R}$ by

$$\tilde{H}_h = \left\{(\tilde{s},\tilde{t}) \,\middle|\, \tilde{s} \leq -\sqrt{\tilde{t}^2 + h^2}\right\}$$

$$\tilde{R} = \sqrt{\tilde{s}^2 - \tilde{t}^2 - h^2} \tag{J.5.10}$$

then

$$\tilde{R} = R$$

and

$$AH_h = \tilde{H}_h \tag{J.5.11}$$

that is to say, both the function R and the region H_h are invariant in form with respect to transformations of the type (J.5.9). We will use this fact very heavily in the treatment of the integrals (J.5.1).

A careful examination of the region of integration $\Sigma' \cap H_h$ (see fig. J.20) reveals that its boundary is composed of both straight and curved segments. If the boundary of $\Sigma' \cap H_h$ is traversed in a positive (counterclockwise) fashion, the straight segments of boundary are named E_1, $E_2 \ldots$, E_n (see fig. J.21), in the order they are encountered. Here, n is the numbers of edges of Σ' having some points lying inside H_h; the position of the lower end of edge E_k is denoted $\vec{p}_k$ while the upper end is denoted a^+_k. The s-t coordinates of $\vec{p}^+_k$ are denoted $(s^\pm_k, t^\pm_k)$, that is

$$\vec{\rho}_k^- = (s_k^-, t_k^-) = \text{lower end of edge } E_k$$

$$\vec{\rho}_k^+ = (s_k^+, t_k^+) = \text{upper end of edge } E_k \qquad \text{(J.5.12)}$$

Next, we introduce the hyperbolic coordinate system for the region $\{(s,t) \mid s < -|t|\}$ of the s-t plane. For a point $\vec{\rho} = (s,t)$ lying in this region, hyperbolic phase ϕ and hyperbolic radius ρ are defined by the requirement that

$$\vec{\rho} = \begin{Bmatrix} s \\ t \end{Bmatrix} = \begin{Bmatrix} -\rho \cosh \phi \\ -\rho \sinh \phi \end{Bmatrix} \qquad \text{(J.5.13)}$$

Here,

$$\cosh x = (e^x + e^{-x})/2$$

$$\sinh x = (e^x - e^{-x})/2 \qquad \text{(J.5.14)}$$

We define

$$\rho = \sqrt{s^2 - t^2} \qquad \text{(J.5.15)}$$

and defining

$$\tanh x = \frac{\sinh x}{\cosh x} \qquad \text{(J.5.16)}$$

and

$$\tanh^{-1} x = y \text{ such that } \tanh y = x \qquad \text{(J.15.17a)}$$

we obtain

$$\phi = \tanh^{-1} (t/s) \qquad \text{(J.5.17b)}$$

Solving (J.5.17),

$$\frac{e^{\phi} - e^{-\phi}}{e^{\phi} + e^{-\phi}} = \frac{t}{s} \qquad \text{(J.5.18)}$$

or $$s(e^{\phi} - e^{-\phi}) = t(e^{\phi} + e^{-\phi}) \qquad \text{(J.5.19)}$$

or $$(s - t)e^{\phi} = (s + t)e^{-\phi} \qquad \text{(J.5.20)}$$

or $$e^{2\phi} = \frac{s+t}{s-t} \tag{J.5.21}$$

or $$\phi = 1/2 \log\left(\frac{s+t}{s-t}\right) \tag{J.5.22}$$

In particular, the hyperbolic phase of the points $\vec{\rho}_k^{\pm}$ is denoted $\phi_k^{\pm}$:

$$\phi_k^{\pm} = 1/2 \log\left(\frac{s_k^{\pm} + t_k^{\pm}}{s_k^{\pm} - t_k^{\pm}}\right) \tag{J.5.23}$$

It is well to notice that not nearly as much care is required in the definition of hyperbolic phase as was required in the definition of circular phase in sec. J.4. The reason for this simplicity is that phase wrap simply does not occur when one is dealing with hyperbolic phase.

Having defined the <u>edges</u> E_k, <u>corner points</u> $\rho_k^{\pm}$, and <u>corner phases</u> $\phi_k^{\pm}$ of the region $\Sigma' \cap H_h$ we now delve more deeply into the problem of determining which edges E of Σ' are also edges of $\Sigma' \cap H_h$. Thus, given an oriented edge E with lower end point $\rho-$ and upper end point $\rho+$, we seek to determine if E has any points lying inside H_h; if it does, E, or part of E will be an edge E_k of $\Sigma' \cap H_h$. In addition, we will also want to determine the point (or points) at which E enters or exits the region H_h.

In order to answer these questions precisely, we need to define a number of new concepts. These include:

(i) A pseudo inner product $< \ , \ >$

(ii) The edge tangent $\vec{t}$

(iii) The edge normal $\vec{n}$, and conormal $\vec{\nu}$

(iv) The edge distance a, and edge variable v, and

(v) Differential arc length, ds, along an edge.

The pseudo inner product on two vectors, denoted $< \ , \ >$ is defined by the expression

$$< a, b > = -a_\xi b_\xi + a_\eta b_\eta \tag{J.5.24}$$

For points $\vec{\rho}$ lying inside H_h, we have

$$< \vec{\rho}, \vec{\rho} > = -s^2 + t^2 \leq -h^2 \tag{J.5.25}$$

an inequality that follows directly from the specification (J.5.7) of H_h. This inequality, combined with the condition that s be negative, provides a very useful characterization of those points lying inside H_h:

$$\rho \in H_h \text{ if and only if } s < 0 \text{ and } <\vec{\rho}, \vec{\rho}> \leq -h^2 \tag{J.5.26}$$

The usefulness of this inner product stems from the fact that it is invariant with respect to hyperbolic transformations of the form (J.5.9). Thus, if $\vec{x}$ and $\vec{y}$ are vectors of length two, and $\tilde{x}$ and $\tilde{y}$ are defined by

$$\tilde{x} = A\vec{x} \qquad A = \begin{bmatrix} a & b \\ b & a \end{bmatrix}, \qquad a > 0$$
$$\tilde{y} = A\vec{y} \qquad\qquad\qquad\qquad a^2 - b^2 = 1 \tag{J.5.27}$$

then

$$< \vec{x}, \vec{y} > \; = \; < \tilde{x}, \tilde{y} > \tag{J.5.28}$$

The edge tangent $\vec{t}$ to an edge E, with lower end point $\vec{\rho}-$ and upper end point $\vec{\rho}+$, is defined by the expression

$$t = (t_\xi, t_\eta) = \frac{\vec{\rho}+ - \vec{\rho}-}{< \vec{\rho}+ - \vec{\rho}-, \vec{\rho}+ - \vec{\rho}- >} \tag{J.5.29}$$

We have chosen the normalization for $\vec{t}$ given by (J.5.29) because this particular normalization is invariant with respect to hyperbolic transformations of the form (J.5.9). With $\vec{t}$ defined by (J.5.29), we can give the corresponding edge tangent T' in the coordinate system X'; we have,

$$\vec{T} = \begin{Bmatrix} t_\xi \\ t_\eta \\ 0 \end{Bmatrix} \tag{J.5.30}$$

Recall from (J.3.28) the definition of subsonic and supersonic edges. The inner product [,], defined by

$$[\vec{x}, \vec{y}] = \vec{x}^T[C_0]\vec{y} \tag{J.5.31}$$

in reference coordinates, is given in X' coordinates by

$$[\vec{x}', \vec{y}'] = \vec{x}'[C']\vec{y}' \tag{J.5.32}$$

where, from section E.3,

$$[C'] = \begin{bmatrix} r & & \\ & s & \\ & & rs \end{bmatrix} \tag{J.5.33}$$

Note that in this section, we have r = 1 and s= -1 (subinclined panel in supersonic flow). Thus, E is a subsonic edge if any only if

$$[\vec{T}', \vec{T}'] > 0 \tag{J.5.34}$$

if and only if

$$t_\xi^2 - t_\eta^2 > 0 \tag{J.5.35}$$

if and only if

$$[< \vec{t}, \vec{t} >] < 0 \tag{J.5.36}$$

Similarly, E is a supersonic edge when

$$[< \vec{t}, \vec{t} >] > 0 \tag{J.5.37}$$

Note that (J.5.29) is undefined for sonic edges. We will not treat them explicitly in this section; later we will deal with them by a limiting process.

Since the definition (J.5.29) of $\vec{t}$ ensures that

$$|< \vec{t}, \vec{t} >| = 1$$

we obtain the normalization conditions on t

$$\text{(subsonic edges)} \quad < \vec{t}, \vec{t} > = -t_\xi^2 + t_\eta^2 = -1 \tag{J.5.38}$$

$$\text{(supersonic edges)} \quad < \vec{t}, \vec{t} > = +1 \tag{J.5.39}$$

Next, the edge normal $\vec{n}$ and conormal $\vec{\nu}$ are defined by

$$\vec{n} = \begin{Bmatrix} n_\xi \\ n_\eta \end{Bmatrix} = \begin{Bmatrix} t_\eta \\ -t_\xi \end{Bmatrix} \tag{J.5.40}$$

$$\vec{\nu} = \begin{Bmatrix} -n_\xi \\ n_\eta \end{Bmatrix} = \begin{Bmatrix} -t_\eta \\ -t_\xi \end{Bmatrix} \tag{J.5.41}$$

It is well to note that $\vec{n}$ as defined by (J.5.40) is an <u>outward</u> edge normal to edge E. That $\vec{n}$ is normal (i.e. perpendicular) to edge E follows from the computation

$$\vec{n} \cdot \vec{t} = t_\eta t_\xi + (-t_\xi t_\eta) = 0 \tag{J.5.42}$$

and that it points outward follows from the computation (see figure 5.22)

$$(\vec{n} \times \vec{t})_\zeta = n_\xi t_\eta - n_\eta t_\xi = t_\eta^2 + t_\xi^2 > 0 \tag{J.5.43}$$

Note that $\vec{n} \times \vec{t}$ points out of the page (its ζ component is positive). Finally we note that for any vector $\vec{p}$, the following relationship holds by virtue of the definition (J.5.41) of $\vec{\nu}$.

$$\vec{\rho} \cdot \vec{n} = \langle \vec{\rho}, \vec{\nu} \rangle \tag{J.5.44}$$

The edge distance a and the edge variable v are defined by

$$a = \vec{n} \cdot \vec{\rho} = \langle \vec{\nu}, \vec{\rho} \rangle \tag{J.5.45}$$

$$v = \langle \vec{t}, \vec{\rho} \rangle \tag{J.5.46}$$

where $\vec{\rho}$ is any point on the edge E (see figure J.16 or J.18). The number a, of course, is independent of which point along the edge E is used to compute it.

Note that the vectors $\vec{\nu}$ and $\vec{t}$ are linearly independent (i.e., nonparallel). This fact follows from the computation

$$(\vec{\nu} \times \vec{t})_\zeta = \nu_\xi t_\eta - \nu_\eta t_\xi = -t_\eta^2 + t_\xi^2 = \pm 1 \tag{J.5.47}$$

by (J.5.38-39). Thus, the position vector $\vec{\rho}$ can be expressed as a linear combination of $\vec{\nu}$ and $\vec{t}$

$$\vec{\rho} = r_1 \vec{\nu} + r_2 \vec{t} \tag{J.5.48}$$

Using the normalization conditions

$$\langle \vec{t}, \vec{t} \rangle = -(t_\xi^2 - t_\eta^2) \tag{J.5.49a}$$

$$\langle \vec{\nu}, \vec{\nu} \rangle = -\nu_\xi^2 + \nu_\eta = -t_\eta + t_\xi^2 \tag{J.5.49b}$$

and the orthogonality condition

$$\langle \vec{\nu}, \vec{t} \rangle = \vec{n} \cdot \vec{t} = 0 \tag{J.5.49c}$$

we can solve for r_1 and r_2 in terms of a and v. Taking the pseudo inner product of (J.5.48) with ν gives

$$a = \langle \vec{\rho}, \vec{\nu} \rangle = r_1 \langle \vec{\nu}, \vec{\nu} \rangle = r_1(t_\xi^2 - t_\eta^2) \tag{J.5.50a}$$

while doing the same thing with t yields

$$\nu = \langle \vec{\rho}, \vec{t} \rangle = r_2 \langle \vec{t}, \vec{t} \rangle = -r_2(t_\xi^2 - t^2_\eta) \tag{J.5.50b}$$

Substituting these expressions back into (J.5.48) and taking account of the fact that $t_\xi^2 - t^2_\eta = \pm 1$ we obtain

$$\vec{\rho} = (t_\xi^2 - t_\eta^2)(a \vec{\nu} - v \vec{t}) \tag{J.5.51a}$$

or, using (J.5.38-39)

$$\vec{\rho} = a \vec{\nu} - v \vec{t} \qquad \text{(subsonic edge)} \tag{J.5.51b}$$

$$\vec{\rho} = -a \vec{\nu} + v \vec{t} \qquad \text{(supersonic edge)} \tag{J.5.51c}$$

Equations (J.5.50-51) now enable us to relate the differential of the edge variable, dv, to the differential arc length, ds. Differential arc length ds is defined by

$$ds = \frac{\vec{t} \cdot \vec{d}_\rho}{|\vec{t}|} \tag{J.5.52}$$

Using (J.5.50-51) we then find

$$\begin{aligned} ds &= -|\vec{t}|\, dv && \text{(subsonic edge)} \\ &= |\vec{t}|\, dv && \text{(supersonic edge)} \end{aligned} \tag{J.5.53}$$

Thus, v decreases along subsonic edges and increases along supersonic edges.

With the machinery developed above, we are now in a position to determine which edges E intersect the region H_h. In doing this, we will treat the cases of subsonic and supersonic edges separately. First, we treat the subsonic edge.

J.5.2 Subsonic Edges

For E a subsonic edge with tangent $\vec{t}$ defined by (J.5.29), we define an edge coordinate transformation of the type (J.5.9)

$$\tilde{\rho} = \begin{Bmatrix} \tilde{s} \\ \tilde{t} \end{Bmatrix} = A \begin{Bmatrix} s \\ t \end{Bmatrix} = A\vec{\rho} \tag{J.5.54}$$

where

$$A = \begin{bmatrix} t_\xi & -t_\eta \\ -t_\eta & t_\xi \end{bmatrix} s_\xi \tag{J.5.55}$$

The matrix A defined by (J.5.55) maps the region H_h into itself and preserves the pseudo-inner product < , > . The coordinate functions $\tilde{s}$, $\tilde{t}$ may be easily expressed using the pseudo inner product as follows

$$\begin{aligned} \tilde{s} &= s_\xi\,(t_\xi\,\rho_\xi - t_\eta\,\rho_\eta) = -s_\xi < \vec{t}, \vec{\rho} > \\ \tilde{t} &= s_\xi\,(-t_\eta\,\rho_\xi + t_\xi\,\rho_\eta) = -s_\xi\,(\vec{n}, \vec{\rho}) = -s_\xi < \vec{v}, \vec{\rho} > \end{aligned} \tag{J.5.56}$$

Thus, for points $\vec{\rho}$ lying on the edge E, the $\tilde{s}$ and $\tilde{t}$ coordinates are given

$$\begin{aligned} \tilde{s} &= -v s_\xi \\ \tilde{t} &= -a\, s_\xi = \text{cons.} \end{aligned} \tag{J.5.57}$$

so that the image of E under A, denoted E, is a line parallel to the s axis, as shown in figure J.23.

Note that for the edge E in figure J.23,

$$s_\xi = 1$$

$$a = (\vec{\rho}, \vec{n}) < 0 \qquad (J.5.58)$$

and thus

$$\tilde{t} = -a > 0 \qquad (J.5.59)$$

A careful examination of Figure J.23 reveals that it is a fairly easy matter to determine if an edge image E has any points lying inside $H_h = \{(\tilde{s}, \tilde{t}) \mid \tilde{s} < (t^2 + h^2)^{1/2}\}$. Since E is parallel to the s axis and since such lines can intersect the boundary of H_h at most once, E will have points lying inside H_h if and only if one of the image end points, $\vec{\rho}-$ or $\vec{\rho}+$, lies inside H_h. Furthermore, the point $\tilde{\rho}_c$ at which the edge E either enters or exits H_h is given.

$$\tilde{\rho}_c = \begin{Bmatrix} \tilde{s}_c \\ \tilde{t}_c \end{Bmatrix} = \begin{Bmatrix} -\sqrt{h^2 + a^2} \\ -\ s_\xi a \end{Bmatrix} \qquad (J.5.60)$$

The point $\tilde{\rho}_c$ will be a point of exit if $s_\xi = +1$ and a point of entry if $s_\xi = -1$.

Now since the transformation A is invertible, the above remarks about the image edge E can yield similar statements about the original edge E. In doing this, we must relate the position vector $\vec{\rho}$ to its image coordinates. This is done by combining (J.5.57) into (J.5.51a) to obtain

$$\vec{\rho} = a\,\vec{v} - v\,\vec{t} = s_\xi\,(-\tilde{t}\,\vec{v} + \tilde{s}\,\vec{t}) \qquad (J.5.61)$$

With this connection established we can now state an algorithm for determining if a subsonic edge E intersects the region H_h.

<u>ALGORITHM:</u> Does a subsonic edge E with lower and upper endpoints $\vec{\rho}^-$ and $\vec{\rho}^+$ intersect H_h. If it does, compute $\vec{\rho}_k^-$ and $\vec{\rho}_k^+$ appropriately.

Assume $-t_\xi^2 + t_\eta^2 = -1$ (subsonic)

$$\rho- \notin H_h \text{ and } \rho+ \notin H_h \Longrightarrow \text{NO}$$

$$\rho- \in H_h \text{ or } \rho+ \in H_h \Longrightarrow \text{YES} \qquad (J.5.62)$$

<u>Case s = +1</u> (Edge E leaves H)

$$\vec{\rho}_k^+ = \vec{\rho}_c$$

$$\vec{\rho}_k^- = \vec{\rho}^- \qquad (J.5.63)$$

Case $s = -1$ (Edge E enters H_h)

$$\vec{\rho}_k^{+} = \vec{\rho}^{+}$$

$$\vec{\rho}_k^{-} = \vec{\rho}_c \tag{J.5.64}$$

where, using (J.5.60) and (J.5.61),

$$\vec{\rho}_c = s_\xi \left(-\tilde{t}_c \vec{v} + \tilde{s}_c \vec{t}\right)$$

$$= a \vec{v} - s \vec{t} \sqrt{h^2 + a^2} \tag{J.5.65}$$

We complete our discussion of subsonic edges by developing the relation between the differential of the edge variable, dv, and the differential of hyperbolic phase, $d\phi$.

We define the angle of hyperbolic rotation X by

$$X = \tanh^{-1}\left(\frac{t_\eta}{t_\xi}\right) = \text{phh}\left(|t_\xi|, s_\xi t_\eta\right) \tag{J.5.66}$$

where "hyperbolic phase" phh is defined by (see J.5.22-23))

$$\text{phh}(x,y) = \tanh^{-1}\left(\frac{y}{x}\right) = \frac{1}{2} \log\left(\frac{x+y}{x-y}\right) \tag{J.5.67}$$

Then, the matrix A defined by (J.5.55) is given by

$$A = \begin{bmatrix} \cosh X & -\sinh X \\ -\sinh X & \cosh X \end{bmatrix} \tag{J.5.68}$$

Substituting this expression and the expression (J.5.13) for $\vec{\rho}$ into (J.5.54) yields for $\tilde{\rho}$: $\tilde{\rho} =$

$$\begin{bmatrix} \cosh X & -\sinh X \\ -\sinh X & \cosh X \end{bmatrix} \begin{Bmatrix} -\rho \cosh \phi \\ -\rho \sinh \phi \end{Bmatrix} = \begin{Bmatrix} -\rho \cosh(\phi - X) \\ -\rho \sinh(\phi - X) \end{Bmatrix} \tag{J.5.69}$$

Now, for points lying on the edge E, equation (J.5.57) gives the values for the s-t coordinates, combining this result with (J.5.69) yields

$$\tilde{\rho} = \begin{Bmatrix} \tilde{s} \\ \tilde{t} \end{Bmatrix} = \begin{Bmatrix} -s_\xi v \\ -s_\xi a \end{Bmatrix} = \begin{Bmatrix} -\rho \cosh(\phi - X) \\ -\rho \sinh(\phi - X) \end{Bmatrix} \tag{J.5.70}$$

Solving equation (J.5.70) for ϕ and ρ now gives

$$\rho = \sqrt{v^2 - a^2}$$

$$\phi = \tanh^{-1}(a/v) + X \qquad \text{(J.5.71)}$$

We can differentiate the second of these quantities to obtain $d\phi$. First, we develop two differentiation formulas which will be of use.

The first of these is

$$\frac{d}{dt}\, ph\,(x(t), y(t)) =$$

$$\frac{d}{dt} \tan^{-1}\left(\frac{y(t)}{x(t)}\right) = \qquad \text{(J.5.72)}$$

(after some algebra)

$$\frac{x\frac{dy}{dt} - y\frac{dx}{dt}}{x^2 + y^2} \qquad \text{(J.5.73)}$$

The second of these is

$$\frac{d}{dt}\, phh\,(x(t), y(t)) =$$

$$\frac{d}{dt}\,\frac{1}{2}\log\left(\frac{x+y}{x-y}\right) \qquad \text{(J.5.74)}$$

$$= \frac{1}{2}\left(\frac{x-y}{x+y}\right)\frac{d}{dt}\left(\frac{x+y}{x-y}\right) \qquad \text{(J.5.75)}$$

$$= \frac{x\frac{dy}{dt} - y\frac{dx}{dt}}{x^2 - y^2} \qquad \text{(J.5.76)}$$

Applying (J.5.76) to (J.5.71), and noting that a is a constant,

$$\frac{d\phi}{dv} = \frac{-a\frac{dv}{dv}}{v^2 - a^2} \qquad \text{(J.5.77)}$$

and thus

$$d\phi = \frac{a}{a^2 - v^2}\, dv \tag{J.5.78}$$

A quantity that will be useful in our computation of the integrals (J.5.1) is the value of v along an edge E_k. Taking the ratio of the two equations contained in (J.5.70) yields

$$v = v_k(\phi) = \frac{a}{\tanh\,(\phi - \chi)} = \tag{J.5.79}$$

(by definition)

$$a \coth\,(\phi - \chi)$$

This completes our study of subsonic edges. We now turn to the treatment of supersonic edges.

J.5.3 Supersonic Edges

For E a supersonic edge with tangent $\vec{t}$ defined by (J.5.29), we define an edge coordinate transformation of the type (J.5.9)

$$\tilde{\rho} = \begin{Bmatrix} \tilde{s} \\ \tilde{t} \end{Bmatrix} = A \begin{Bmatrix} s \\ t \end{Bmatrix} = A\vec{\rho} \tag{J.5.80}$$

where

$$A = s_\eta \begin{bmatrix} t_\eta & -t_\xi \\ -t_\xi & t_\eta \end{bmatrix} \tag{J.5.81}$$

$$s_\eta = \text{sign}\,(t_\eta)$$

That the matrix A so defined is a hyperbolic transformation of the form (J.5.9) follows from the normalization condition for $\vec{t}$, (J.5.39), $t_\eta^2 - t_\xi^2 = 1$.

For a given point $\vec{\rho}$, it is a trivial matter to compute the corresponding $\tilde{s}$-$\tilde{t}$ coordinate functions. Doing this, and using the pseudo-inner product, we find

$$\tilde{s} = s_\eta(t_\eta \rho_\xi - t_\xi \rho_\eta) = s_\eta \vec{n} \cdot \vec{\rho} = s_\eta \langle \vec{v}, \vec{\rho} \rangle$$

$$\tilde{t} = s_\eta(-t_\xi \rho_\xi + t_\eta \rho_\eta) = s_\eta \langle \vec{t}, \vec{\rho} \rangle \qquad \text{(J.5.82)}$$

Taking account of the definitions of a and v (J.5.45-46) we then find that, for points $\vec{\rho}$ on E,

$$\tilde{s} = s_\eta a = \text{cons.}$$

$$\tilde{t} = s_\eta v \qquad \text{(J.5.83)}$$

Thus $\tilde{E}$, the image of E, is a line parallel to the t-axis as shown in fig. J.24.

Note that for the edge illustrated there,

$$s_\eta = -1$$

$$a = \vec{\rho} \cdot \vec{n} > 0 \qquad \text{(J.5.84)}$$

and thus

$$\tilde{s} = s_\eta a < 0 \qquad \text{(J.8.85)}$$

A careful examination of fig. J.24 reveals that the image edge E can have points lying inside H_h even when neither endpoint, $\vec{\rho}^+$ nor $\vec{\rho}^-$ lies inside H_h. In particular, this can happen when the $\tilde{s}$ coordinate of the line E satisfies $\tilde{s} \leq -|h|$ and the t coordinate function has opposite signs when it is evaluated at the two endpoints of E. In light of equation (J.5.83) this criterion can be written

$\tilde{E} \cap \tilde{H}_h$ is not empty if

$$\tilde{s} = \sigma_\eta a < -|h| \text{ and } \tilde{t}_- \tilde{t}_+ = v_- v_+ < 0$$

where $v_\pm$ are defined

$$v_\pm = \langle \vec{t}, \vec{\rho}^\pm \rangle \qquad \text{(J.5.87)}$$

Having determined whether or not $\tilde{E}$ intersects $\tilde{H}_h$, we now seek to determine the point of entry or exit of the edge E. Any such entry or exit point must lie on the boundary of $\tilde{H}_h$, that is its $\tilde{s}$-$\tilde{t}$ coordinates must satisfy

$$\tilde{s}^2 - \tilde{t}^2 = h^2 \qquad \text{(J.5.88)}$$

Invoking the conditions (J.5.83) for points on $\tilde{E}$, this implies

$$a^2 - v^2 = h^2$$

or

$$|v| = v_c = \sqrt{a^2 - h^2} \qquad \text{(J.5.89)}$$

where the above equation defines v_c, the critical value of the edge variable. Since the variable v increases along supersonic edges, (by virtue of (J.5.53) we have in general

$$v_- < v_+ \tag{J.5.90}$$

Now if an edge $\tilde{E}$ that intersects $\tilde{H}_h$ is such that $\tilde{\rho}^- \notin \tilde{H}_h$, then we must have

$$v_- < -v_c \tag{J.5.91}$$

and the v-coordinate of point of entry equal to -v .

Similarly, if $\tilde{E} \cap \tilde{H}_h \neq 0$ but $\tilde{\rho}^+ \notin \tilde{H}_h$, we have

$$v_+ > v_c \tag{J.5.92}$$

and the v-coordinate of point of exit equal to v_c.

As in the case of subsonic edges, we may transform these observations about supersonic edges back into the s-t coordinate system by using the identity (J.5.51)

$$\vec{\rho} = -a\,\vec{v} + v\,\vec{t} = -s_\eta\,\tilde{s}\,\vec{v} + s_\eta\,\tilde{t}\,\vec{t} \tag{J.5.93}$$

We summarize our observations with the following algorithm.

<u>ALGORITHM:</u> Does a supersonic edge E with lower and upper endpoints

$\vec{\rho}^-$ and $\vec{\rho}^+$ intersect H_h. If it does, compute $\vec{\rho}_k^-$ and

$\vec{\rho}_k^+$ appropriately.

Assume $\quad -t_\xi^2 + t_\eta^2 = +1.$

<u>Determination if $E \cap H \neq 0$</u>

$\vec{\rho}^- \in H_h$ or $\vec{\rho}^+ \in H_h$ $\Longrightarrow$ YES

$\vec{\rho}^- \in H_h$ and $\vec{\rho}^+ \in H_h$

$s_\eta\, a < -|h|$ and $v_-\, v_+ \leq 0$ $\Longrightarrow$ YES

otherwise: NO

Determination of Endpoints: If the result of the above performance is YES, do the following

if $\vec{\rho}^- \in H_h$	then	$\vec{\rho}_k^- = \vec{\rho}^-$	
	else	$\vec{\rho}_k^- = -a\vec{v} - v_c\vec{t}$	
if $\vec{\rho}^+ \in H_h$	then	$\vec{\rho}_k^+ = \vec{\rho}^+$	
	else	$\vec{\rho}_k^+ = -a\vec{v} + v_c\vec{t}$	

We complete our discussion of supersonic edges by deriving the relationship between $d\phi$ and dv. Proceeding as before, we now define X by

$$X = \tanh^{-1}\left(\frac{t_\xi}{t_\eta}\right) = \mathrm{phh}(|t_\eta|, s_\eta t_\xi) \tag{J.5.94}$$

With this definition of X, the matrix A of (J.5.81) can be written

$$A = \begin{bmatrix} \cosh & -\sinh \\ -\sinh & \cosh \end{bmatrix} \tag{J.5.95}$$

Proceeding as before, we obtain the following relation analagous to (J.5.70).

$$\tilde{\rho} = \begin{Bmatrix} \tilde{s} \\ \tilde{t} \end{Bmatrix} = \begin{Bmatrix} s_\eta\ a \\ s_\eta\ v \end{Bmatrix} = \begin{Bmatrix} -\rho\ \cos(\phi - X) \\ -\rho\ \sinh(\phi - X) \end{Bmatrix} \tag{J.5.96}$$

Solving for ρ and ϕ then yields

$$\rho = \sqrt{a^2 - v^2}$$

$$\phi = \tanh^{-1}(v/a) + X \tag{J.5.97}$$

Differentiating the second of these equations yields (by (J.5.74-76))

$$d\phi = \frac{a\,dv}{a^2 - v^2} \tag{J.5.98}$$

a relation identical to (J.5.78). Finally, we note that along the edge E_k, v is given as a function of hyperbolic phase by

$$v = v_k(\phi) = a_k \tanh(\phi - X) \tag{J.5.99}$$

This completes our study of supersonic edges.

J.5.4 Computation of the Integrals

We conclude our discussion of the geometry of the hyperbola by using our plethora of newly defined quantities to evaluate the integral J

$$J = \iint_{\Sigma' \cap H_h} \frac{ds\ dt}{R} \tag{J.5.100}$$

A suitably intricate region of integration, $\Sigma' \cap H_h$, is diagrammed in figures J.25a and J.25b. In these figures, the cross-hatched regions make positive contributions to the integral while shaded regions make negative contributions. In Figures J.25 this corresponds to the fact that $d\phi > 0$ along edges 1,2,3 and 4 while $d\phi < 0$ on edge 5.

Transforming the integral (J.5.100) to hyperbolic polar coordinates (cf. (J.5.13)), we see that the Jacobian $\partial(s,t)/\partial(\rho, \phi)$ of the transformation is given by

$$\frac{\partial(s, t)}{\partial(\rho, \phi)} = \begin{bmatrix} -\cosh \phi & -\rho \sinh \phi \\ -\sinh \phi & -\rho \cosh \phi \end{bmatrix} \tag{J.5.101}$$

The determinant of this jacobian is easily computed

$$\det \left(\frac{\partial(s, t)}{\partial (\rho, \phi)}\right) = \rho \tag{J.5.102}$$

since

$$\cosh^2 \phi - \sinh^2 \phi = 1 \tag{J.5.103}$$

so that the element of area is given by

$$ds\ dt = \rho\ d\rho\ d\phi \tag{J.5.104}$$

The function R, given by (J.5.8), may be represented in polar coordinates by

$$R = \sqrt{\rho^2 - h^2} \tag{J.5.105}$$

Substituting (J.5.104-105) into (J.5.100) yields for J

$$J = \iint_{\Sigma' \cap H_h} \frac{\rho\ d\rho\ d\phi}{\rho^2 - h^2} \tag{J.5.106}$$

Now using the definitions given above it is easy to see that J can be evaluated as follows

$$J = \sum_{k=1}^{n} \int_{\phi_k^-}^{\phi_k^+} d\phi \int_{o}^{P_k(\phi)} \frac{\rho \, d\rho}{\sqrt{\rho^2 - h^2}} \tag{J.5.107}$$

where, using (J.5.71) and (J.5.97), $P_k(\phi)$ is given by

$$P_k(\phi) = \begin{cases} \sqrt{v_k(\phi)^2 - a_k^2} & \text{subsonic edges} \\ \sqrt{a_k^2 - v_k(\phi)^2} & \text{supersonic edges} \end{cases}$$

and, from (J.5.79) and (J.5.99), $V_k(\phi)$ is given by

$$V_k(\phi) = \begin{cases} a_k \coth(\phi - \chi) & \text{subsonic edges} \\ a_k \tanh(\phi - \chi) & \text{supersonic edges} \end{cases} \tag{J.5.108}$$

Performing the inner integral in (J.5.107) yields for J

$$J = \sum_{k=1}^{n} \int_{\phi_k^-}^{\phi_k^+} d\phi \sqrt{P_k(\phi)^2 - h^2} \tag{J.5.110}$$

Transforming each of the integrals in (J.5.110) into an edge integral with respect to the edge variable v, we have

$$d\phi = \frac{a\,dv}{a^2 - v^2} \tag{J.5.111}$$

and

$$J = \sum_{k=1}^{n} \int_{v_k^-}^{v_k^+} \frac{a_k \, dv}{a_k^2 - v^2} R_k(v) \tag{J.5.112}$$

where $R_k(v)$ is defined

$$R_k\ (v) = \sqrt{\rho_k^2 - h^2} = \begin{cases} \sqrt{v^2 - a^2 - h^2} & \text{(subsonic edges)} \\ \sqrt{a^2 - v^2 - h^2} & \text{(supersonic edges)} \end{cases} \tag{J.5.113}$$

and $v_k^{\pm}$ are defined by the obvious relations

$$v_k^{\pm} = \langle \vec{\rho}_k^{\pm}, \vec{t}_k \rangle \tag{J.5.114}$$

Now the integral $\int aRdv/(a^2 - v^2)$ can be evaluated by elementary means. Doing this, one obtains (see the integrals J(X) in section J.7.1)

$$\int \frac{R_k\ a_k\ dv}{a_k^2 - v^2} = -h\ ph(a_k\ R_k,\ h_v) - a_k\ \tanh^{-1}(R_k/v) \qquad \text{(subsonic case)}$$

$$= -h\ ph(a_k\ R_k,\ hv) - a_k\ ph(v,\ R_k) \qquad \text{(supersonic case)} \tag{J.5.115}$$

Thus, using hyperbolic coordinates, it is a fairly easy matter to evaluate the integrals of type (J.5.1).

J.6 The Panel Integral Matrices

In this section, we calculate matrices $[S_0]$ and $[D_0]$ which define the perturbation potential and velocity induced at a control point by a quadraticly varying source strength or a cubicly varying doublet strength on a convex, planar, polygonal region . These are (4x6) and (4x10) matrices respectively, defined by the equations

$$\begin{Bmatrix} \phi_S' \\ \vec{v}_S' \end{Bmatrix} = [S_0] \begin{Bmatrix} \sigma_0 \\ \sigma_\xi \\ \vdots \\ \sigma_{\eta\eta} \end{Bmatrix} \tag{J.6.1}$$

and

$$\begin{Bmatrix} \phi_D' \\ \vec{v}_D' \end{Bmatrix} = [D_0] \begin{Bmatrix} \mu_0 \\ \mu_\xi \\ \vdots \\ \mu_{\eta\eta\eta} \end{Bmatrix} \tag{J.6.2}$$

Here, the perturbation velocity $\vec{v}_S'$ induced by the source strength and the regular part of $\vec{v}_D^{*\prime}$ of the perturbation velocity induced by the doublet strength are expressed in a local (ξ', η', ζ') coordinate system (see section E.3) with the property that Σ lies in the plane $\zeta' = 0$, and the compressible distance R from the control point P to the point of integration Q is written

$$R^2 = [P-Q\ ,\ P-Q] = r(\xi'-x')^2 + s(\eta'-y')^2 + rs(\zeta'-z')^2 \tag{J.6.3}$$

There in local coordinates

$$\vec{P} = (x', y', z')$$
$$\vec{Q} = (\xi', \eta', \zeta') \tag{J.6.4}$$

Now, the values of $\vec{v}_S'$, $\vec{v}_D'$, and R are independent of the origin of the local coordinate system. The coefficients $\sigma_0, \sigma_{\eta\eta}, \ldots, \mu_0, \ldots, \mu_{\eta\eta\eta}$ of the source and doublet polynomials are not, however (after all, σ_0 and μ_0 are the source and doublet strengths at the origin). We define S and D to be the matrices for which (J.6.1) and (J.6.2) hold if the origin of the (ξ', η', ζ') coordinate system is the point $(x',y',0)$, that is, the projection of P to the plane containing Σ . This control point - dependent coordinate system origin is useful for computation of the panel integral matrix. In section J.6.6 we compute the matrices S_0 and D_0 which result from shifting the origin back to the standard one which is independent of the control point location.

J.6.1 Preliminaries

J.6.1.1 Transformation Rules

Consider the reference to local transformation,

$$A: \quad X_0 \longrightarrow X' \tag{J.6.5}$$

We now review the transformation properties of various quantities (see section E.3). We have

$$\vec{R}' = [A]\,\vec{R}$$

where

$$\vec{R} = \vec{P} - \vec{Q} \tag{J.6.6}$$

$$\vec{n}' = [A^{-T}]\,\vec{n}_0 \tag{J.6.7}$$

where

$$\vec{n}' = \begin{Bmatrix} 0 \\ 0 \\ 1 \end{Bmatrix}$$

$$\vec{n}'\,dS' = (\det A)\,[A^{-T}]\,\hat{n}\,dS$$

$$\text{and } dS' = \frac{1}{J}\,dS \tag{J.6.8}$$

where

$$dS' = d\xi' d\eta' \tag{J.6.9}$$

and J is the area Jacobian (the ratio of area in reference coordinates to area in local coordinates). Next,

$$[B'] = s\beta^2 \begin{bmatrix} r & & \\ & s & \\ & & rs \end{bmatrix} = A\,B_0\,A^T \tag{J.6.10}$$

$$[C'] = \begin{bmatrix} r & & \\ & s & \\ & & rs \end{bmatrix} = A^{-T}\,C_0\,A^{-1} \tag{J.6.11}$$

$$\tilde{\nabla}' = B'\vec{\nabla} = [B'] \begin{Bmatrix} \partial/\partial x' \\ \partial/\partial y' \\ \partial/\partial z' \end{Bmatrix} = A\tilde{\nabla} \tag{J.6.12}$$

We also define $\vec{\nabla}_Q'$ and $\tilde{\nabla}_Q'$ as gradient operators with respect to the location of the integration point Q whose local coordinates are (ξ', η', ζ'). We define

$$\vec{G}' = \tilde{\nabla}_Q'\left(\frac{1}{R}\right) = [A]\,\vec{G}_o \tag{J.6.13a}$$

where

$$\vec{G}_o = \tilde{\nabla}_Q\left(\frac{1}{R}\right) \tag{J.6.13b}$$

J.6.1.2 Transformation of the Integrals

Now, recall from (B.0.1) that

$$\phi_S = -\frac{1}{\kappa} \iint_{\Sigma' \cap D_p} \frac{\sigma(Q)}{R}\, ds \tag{J.6.14a}$$

$$= -\frac{J}{\kappa} \iint_{\Sigma' \cap D_p} \frac{\sigma(\xi', \eta')}{R}\, dS' \tag{J.6.14b}$$

$$= J\,\phi_S' \tag{J.6.14c}$$

where

$$\phi_S' = -\frac{1}{\kappa} \iint_{\Sigma' \cap D_p} \frac{\sigma(\xi', \eta')}{R}\, d\xi'\, d\eta' \tag{J.6.14d}$$

Next,

$$\phi_D = \frac{1}{\kappa} \iint_{\Sigma' \cap D_p} \mu\, \hat{n} \cdot \tilde{\nabla}\left(\frac{1}{R}\right) dS \tag{J.6.15a}$$

$$= \frac{1}{\kappa \det A} \iint_{\Sigma' \cap D_p} \mu(\xi', \eta') \left\{A^T \vec{n}'\right\} \cdot \tilde{\nabla}_Q \left(\frac{1}{R}\right) d\xi'\, d\eta' \tag{J.6.15b}$$

$$= \frac{1}{\kappa \det A} \iint_{\Sigma' \cap D_p} \mu(\xi', \eta')\, (\vec{n} \cdot \vec{G})\, d\xi'\, d\eta' \tag{J.6.15c}$$

Now, by (E.3.90)

$$\det A = \beta^2 \tag{J.6.16a}$$

and so, letting

$$\vec{H}' = \frac{1}{\beta^2} \vec{G}' \tag{J.6.16b}$$

we have

$$\phi_D = \frac{1}{\kappa} \iint_{\Sigma' \cap D_p} \mu(\xi', \eta') \, \vec{n}' \cdot \vec{H}' \, d\xi' d\eta' \tag{J.6.16c}$$

Note that

$$\frac{1}{\beta^2} [B'] = s [C'] \tag{J.6.17}$$

and so we can also write

$$\vec{H}' = s[C'] \, \vec{\nabla}'_Q \left(\frac{1}{R}\right) \tag{J.6.18}$$

Next, applying (B.3.9),

$$\vec{v}_s = \vec{\nabla}_P \, \phi_s = [A^T] \vec{\nabla}_{P'} \, \phi_s = J[A^T] \, \vec{v}_s' \tag{J.6.20}$$

where

$$\vec{v}_s' = \vec{\nabla}_{P'} \, \phi_s' =$$

$$- \frac{1}{\kappa} \iint_{\Sigma' \cap D_p} \sigma(\xi', \eta') \, \vec{\nabla}_{P'} \left(\frac{1}{R}\right) d\xi' d\eta' \tag{J.6.21}$$

$$= \frac{1}{\kappa} \iint_{\Sigma' \cap D_p} \sigma(\xi', \eta') \, \vec{\nabla}_{Q'} \left(\frac{1}{R}\right) d\xi' d\eta' \tag{J.6.22}$$

Finally,

$$\vec{v}_{D^*}' = \frac{1}{\kappa} \iint_{\Sigma' \cap D_p} (\hat{n} \times \vec{\nabla}_Q \, \mu) \times \vec{\nabla}_Q \left(\frac{1}{R}\right) dS \tag{J.6.23}$$

Applying the transformation rule for cross products (E.1.12) to

$$\vec{v}_D{}^{*\prime} = \frac{1}{\kappa} \iint_{\Sigma' \cap D_p} \left[\left(\frac{1}{\beta^2} [A^T]\, \vec{n}'\, dS'\right) \times \left(A^T \vec{\nabla}'_Q\, \mu\right)\right] \times \left(A^{-1}\, \vec{G}'\right) \tag{J.6.24}$$

we obtain

$$\vec{v}_D{}^{*\prime} = \frac{1}{\kappa} \det (A^T) \iint_{\Sigma' \cap D_p} \left(A^{-1}\left(\frac{1}{\beta^2}\, \vec{n}'\, dS' \times \vec{\nabla}_Q'\, \mu\right)\right) \times (A^{-1}\, G') \tag{J.6.25}$$

$$= -\frac{1}{\kappa} [A^T] \iint_{\Sigma' \cap D_p} (\vec{\nabla}'_Q \times \vec{n}') \times \frac{\vec{G}'}{\beta^2}\, ds' \tag{J.6.26}$$

$$= [A^T]\, \vec{v}_D{}'^{*} \tag{J.6.27}$$

where

$$\vec{v}_D{}'^{*} = -\frac{1}{\kappa} \iint_{\Sigma' \cap D_p} (\vec{\nabla}'_Q\, \mu \times \hat{n}') \times \vec{H}'\, dS' \tag{J.6.28}$$

J.6.1.3 Singularity Strength Coefficients

In Section J.6, we compute the quantities ϕ_S', ϕ_D', $\vec{v}_S'$ and $\vec{v}_D^*$, in terms of the coefficients describing the source and doublet strength on the panel. We now introduce some notation to describe the variation in singularity strength.

Let

$$\vec{\sigma} = \begin{Bmatrix} \sigma_\xi \\ \sigma_\eta \end{Bmatrix} \tag{J.6.29}$$

$$\vec{\mu} = \begin{Bmatrix} \mu_\xi \\ \mu_\eta \end{Bmatrix} \tag{J.6.30}$$

$$[\Sigma] = \begin{bmatrix} \sigma_\xi & \sigma_{\xi\eta} \\ \sigma_{\xi\eta} & \sigma_{\eta\eta} \end{bmatrix} \tag{J.6.31}$$

$$[M] = \begin{bmatrix} \mu_\xi & \mu_{\xi\eta} \\ \mu_{\xi\eta} & \mu_{\eta\eta} \end{bmatrix} \tag{J.6.32}$$

and let $\mathcal{M}$ be the 2x2x2 tensor

$$\mathcal{M}_{\cdot,\cdot,1} = \begin{bmatrix} \mu_{\xi\xi\xi} & \mu_{\xi\xi\eta} \\ \mu_{\xi\xi\eta} & \mu_{\xi\eta\eta} \end{bmatrix} \tag{J.6.33}$$

$$\mathcal{M}_{\cdot,\cdot,2} = \begin{bmatrix} \mu_{\xi\xi\eta} & \mu_{\xi\eta\eta} \\ \mu_{\xi\eta\eta} & \mu_{\eta\eta\eta} \end{bmatrix} \tag{J.6.34}$$

Then,

$$\sigma(\xi', \eta') = \sigma_0 + \vec{\sigma}^T \vec{\rho} + 1/2\ [\Sigma] : [\vec{\rho}\ \vec{\rho}^T] \tag{J.6.35}$$

where

$$\vec{\rho} = \begin{Bmatrix} \xi' \\ \eta' \end{Bmatrix} \tag{J.6.36}$$

and where for matrices A and B

$$[A] : [B] = \sum_{ij} A_{ij} B_{ij} \tag{J.6.37}$$

Similarly

$$\mu(\xi', \eta') = \mu_0 + \vec{\mu}^T \vec{\rho} + 1/2\ [M]: [\vec{\rho}\ \vec{\rho}^T]$$

$$+ 1/6 \sum_{i,j,k} \mathcal{M}_{ijk}\ \rho_i\ \rho_j\ \rho_k \tag{J.6.38}$$

J.6.1.4 Uniform Formulas for Local Variables

Recall from sections J.4 and J.5 that we introduced certain expressions depending on an edge E_h. These are the radius vector

$$\vec{\rho} = \begin{Bmatrix} \xi' - x' \\ \\ \eta' - y' \end{Bmatrix} \tag{J.6.39}$$

(this is consistent with Section J.6.1.3 if the local coordinate system is centered at the control point) with "magnitude" ρ satisfying

$$\rho^2 = (\xi' - x')^2 + rs(\eta' - y')^2 \tag{J.6.40}$$

the height h above the panel

$$h = z' - \zeta' \tag{J.6.41}$$

the edge tangent

$$\vec{T}_k = \vec{\rho}_k^{\,+} - \vec{\rho}_k^{\,-} \tag{J.6.42}$$

where $\vec{\rho}_k^{\,\pm}$ are the endpoints of $E_k \cap D_p$, the normalized edge tangent

$$\vec{t}_k = \begin{Bmatrix} t_\xi \\ t_\eta \end{Bmatrix} = \vec{T}_k / \left| \langle \vec{T}_k, \vec{T}_k \rangle \right|^{1/2} = \hat{t}_k / \tau \tag{J.6.43}$$

where $\hat{t}_k$ is a unit edge tangent, and for vectors a,b we define $\langle \vec{a}, \vec{b} \rangle$ by

$$\langle \vec{a}, \vec{b} \rangle = rs\, a_\xi\, b_\xi + a_\eta\, b_\eta \tag{J.6.44}$$

the edge normal

$$\vec{n}_k = \begin{Bmatrix} t_\eta \\ -t_\xi \end{Bmatrix} \tag{J.6.45}$$

the edge distance

$$a_k = \vec{n}_k \cdot \vec{\rho}_k^{\,\pm} \tag{J.6.46}$$

and the distance along the edge

$$v_k = \langle \vec{t}_k, \vec{\rho} \rangle \tag{J.6.47}$$

In addition, we define the edge type indicator

$$q_k = \text{sign}\,[t_k, t_k] = rt_\xi^2 + st_\eta^2 = s\,\langle \vec{t}_k, \vec{t}_k \rangle \tag{J.6.48}$$

which is 1 for subsonic edges, -1 for supersonic edges, the edge conormal

$$\nu_k = [G]\vec{n}_k \tag{J.6.49}$$

where

$$[G] = \begin{bmatrix} rs & \\ & 1 \end{bmatrix} \tag{J.6.50}$$

and the edge cotangent

$$\vec{\tau}_k = [G]\vec{t}_k \tag{J.6.51}$$

In terms of these definitions we have, combining (J.4.51), (J.5.50), (J.5.51), and (J.6.49),

$$\vec{\rho}_k = q_k\, r\, a_k\, \nu_k + a_k\, s\, v_k\, \vec{t}_k \tag{J.6.52}$$

From (J.6.44) and (J.6.49) we have

$$\langle\vec{v}_k, \vec{v}_k\rangle = rs\, t_\eta^2 + t_\xi^2 = rs\langle\vec{t}_k, \vec{t}_k\rangle \tag{J.6.53}$$

From (J.4.46) and (J.5.53) we obtain the differential of arc length

$$ds = sq\,|\vec{t}_k|\, dv \tag{J.6.54}$$

Next,

$$\begin{aligned}\langle\vec{v}_k, \vec{v}_k\rangle &= \langle\vec{n}_k, \vec{n}_k\rangle = t_\xi^2 + rst_\eta^2 \\ &= rs\langle\vec{t}_k, \vec{t}_k\rangle = rssq = rq\end{aligned} \tag{J.6.55}$$

Further,

$$\langle\vec{v}_k, \vec{t}_k\rangle = \left\langle \begin{pmatrix} rs & t_\eta \\ -t_\xi & \end{pmatrix}, \begin{pmatrix} t_\xi \\ t_\eta \end{pmatrix} \right\rangle = 0 \tag{J.6.56}$$

Thus, by (J.6.52)

$$\begin{aligned}\langle\vec{\rho}_k, \vec{\rho}_k\rangle &= a^2_k \langle\vec{v}_k, \vec{v}_k\rangle + v^2_k \langle\vec{t}_k, \vec{t}_k\rangle \\ &= rq_k\, a^2_k + sq_k\, v^2_k\end{aligned} \tag{J.6.57}$$

So,

$$\rho^2_k = rs\langle\vec{\rho}_k, \vec{\rho}_k\rangle = sq_k\, a^2_k + rq_k\, v^2_k \tag{J.6.58}$$

Finally,

$$\begin{aligned}r^2 &= r(\xi', x')^2 + s(\eta' - y')^2 + rs(\zeta' - z')^2 \\ &= r\rho^2 + rsh^2 = \\ &\quad rsq_k\, a^2_k + q_k\, v^2_k + rsh^2\end{aligned} \tag{J.6.59}$$

The above results will be used extensively in the following sections.

J.6.1.5 Differentiation Formulas

Now we introduce

$$\psi = \frac{1}{R} \tag{J.6.60}$$

Many of our formulas will be terms of ψ; an interested reader may compute the equations which would result if $1/R$ were replaced by a different expression such as the Helmholtz kernel $e^{i\omega R}/R$.

We now derive some integration and differentiation formulas concerning ψ which will be useful. First,

$$\frac{\partial\psi}{\partial\zeta'} = \frac{\partial}{\partial R}\frac{\partial R}{\partial\zeta'} = \tag{J.6.61}$$

(by (J.6.41) and (J.6.59))

$$\frac{\partial}{\partial R}\left(\frac{-rsh}{R}\right) \tag{J.6.62}$$

Similarly,

$$\frac{\partial\psi}{\partial\rho} = \frac{\partial\psi}{\partial R}\frac{\partial R}{\partial\rho} \tag{J.6.63}$$

By (J.6.59),

$$2RdR = 2r\rho\, d\rho \tag{J.6.64}$$

and so

$$\frac{\partial\psi}{\partial\rho} = \frac{r\rho}{R}\frac{\partial\psi}{\partial R} \tag{J.6.65}$$

Thus,

$$\frac{\partial\psi}{\partial\zeta'} = \frac{-sh}{\rho}\frac{\partial\psi}{\partial\rho} \tag{J.6.66}$$

Next, defining

$$\tilde{\nabla}'_{2,Q} = [G]\begin{Bmatrix} \partial/\partial\xi' \\ \\ \partial/\partial\eta' \end{Bmatrix} \tag{J.6.67}$$

(J.6.39-40) yield

$$\tilde{\nabla}'_{2,Q}(\rho^2) = 2rs\vec{\rho} \tag{J.6.68}$$

or

$$\tilde{\nabla}'_{2,Q}\ (\rho) = \frac{rs\vec{\rho}}{\rho} \tag{J.6.69}$$

Thus,

$$\tilde{\nabla}'_{2,Q}\ (\psi) = \frac{rs\vec{\rho}}{\rho}\ \partial\psi/\partial\rho \tag{J.6.70a}$$

and

$$\rho\ \frac{\partial\psi}{\partial\zeta'} = \frac{-sh\vec{\rho}}{\rho}\ \frac{\partial\psi}{\partial\rho} = -rh\ \tilde{\nabla}'_{2,Q}\ \psi \tag{J.6.70b}$$

Finally, let us introduce

$$X(R) = \int_0^R \bar{R}\ \psi(\bar{R})\ d\bar{R} \tag{J.6.71}$$

Then

$$\frac{\partial X}{\partial\rho} = \frac{\partial X}{\partial R}\ \frac{\partial R}{\partial\rho} = R\ \left(\frac{r\rho}{R}\right) = r\rho\psi \tag{J.6.72}$$

This concludes our derivation of preliminary integral formulas.

J.6.2 Source Potential and Velocity

In this section we compute the matrix S defining ϕ'_s and v'_s in terms of certain fundamental expressions.

J.6.2.1 Source Potential

From (J.6.18),

$$\phi'_s = \frac{-1}{\kappa} \iint_{\Sigma'\cap D_p} \sigma(\xi', \eta')\ d\xi'\ d\eta' \tag{J.6.73}$$

= (by (J.6.35))

$$-\frac{1}{\kappa}\left(\iint \sigma_0\ dS' + \iint \vec{\sigma}^T\vec{\rho}\ dS' + \frac{1}{2}\iint [\Sigma] : [\vec{\rho}\ \vec{\rho}^T]\ dS'\right) \tag{J.6.74}$$

Here we have used the fact that the coordinate system is centered on the projection of the control point to the panel, and thus

$$\begin{Bmatrix} \xi' - x' \\ \\ \eta' - y' \end{Bmatrix} = \vec{\rho} \tag{J.6.75}$$

So,

$$\phi_s' = \sigma_0 \left(-\frac{1}{K} \iint \psi dS'\right) + \vec{\sigma}^T \left\{-\frac{1}{K} \iint \vec{\rho}\, \psi \, dS'\right\} + 1/2\, [\Sigma]: \left[-\frac{1}{K} \iint \vec{\rho}\, \vec{\rho}^T \, \psi dS'\right] \tag{J.6.76}$$

Using (J.6.69) and (J.6.72),

$$\iint_{\Sigma'} \vec{\rho}\psi \, ds' = \iint_{\Sigma'} \frac{\vec{\rho}}{\rho} (\rho\psi) dS'$$

$$= \iint_{\Sigma'} (rs\, \tilde{\nabla}_{2,Q'}\, \rho) \left(\frac{r\partial X}{\partial \rho}\right) = \tag{J.6.77}$$

$$s \iint_{\Sigma'} \tilde{\nabla}_{2,Q'} \, dS' = s \int_{\partial\Sigma'} \frac{\vec{\nu}}{|\vec{\nu}|} X \, ds \tag{J.6.78}$$

Equation (J.6.78) is obtained by using the two-dimensional version of Gauss' theorem; if f is any function on a planar region ,

$$\iint_{\Sigma} \vec{\nabla} f \, dS = \int_{\partial\Sigma'} \frac{\vec{n}}{|\vec{n}|} f \, ds \tag{J.6.79}$$

Applying [G] to (J.6.79), and noting that

$$|\vec{\nu}| = |\vec{n}| \tag{J.6.80}$$

we obtain

$$\int_{\Sigma} \tilde{\nabla}_{2'} f \, dS = \int_{\partial\Sigma'} \frac{\vec{\nu}}{|\vec{\nu}|} f \, ds \tag{J.6.81}$$

Finally, using (J.6.69) and (J.6.72),

$$\tilde{\nabla}_2' X = \frac{\partial X}{\partial \rho} \vec{\nabla}_2' \rho = s\psi \rho \tag{J.6.82}$$

and thus

$$\iint_{\Sigma'} \vec{\rho}\, \vec{\rho}^T \psi \, dS' = s \iint_{\Sigma'} \vec{\rho}\, \tilde{\nabla}_{2'}^T X \, ds \tag{J.6.83}$$

Combining (J.6.76-78) and (J.6.83), we obtain

$$\phi_s' = \sigma_0\left(-\frac{1}{\kappa}\iint \psi dS'\right)$$

$$+ \vec{\sigma}^T\left(-\frac{s}{\kappa}\int_{\partial\Sigma'} \vec{\nu}X \frac{ds}{|\nu|}\right) \tag{J.6.84}$$

$$+ [\Sigma]: \left[-\frac{s}{2\kappa}\iint_{\Sigma'} \vec{\rho} \quad \tilde{\nabla}_2'^{\,T} X \quad dS'\right]$$

J.6.2.2 Tangential Source Velocity

Now, from (J.6.22) and (J.6.35)

$$\vec{v}_s' = \frac{1}{\kappa}\iint_{\Sigma'} \sigma(\xi', \eta') \vec{\nabla}_Q'\psi \quad dS' \tag{J.6.85}$$

where

$$\vec{\nabla}'_Q = \begin{Bmatrix} \partial/\partial\xi' \\ \partial/\partial\eta' \\ \partial/\partial\zeta' \end{Bmatrix} = \begin{Bmatrix} \vec{\nabla}_{2,Q}' \\ \partial/\partial\zeta' \end{Bmatrix} \tag{J.6.86}$$

So,

$$v_{s,\xi,\eta}' = \iint_{\Sigma'} \sigma\vec{\nabla}_{2,Q}'\psi \quad dS' \tag{J.6.87}$$

Applying (J.6.35)

$$v'_{s,\xi,\eta} = \frac{\sigma_0}{\kappa}\iint_{\Sigma'} \vec{\nabla}_{2,Q}'\psi \quad dS' +$$

$$\frac{1}{\kappa}\left[\iint_{\Sigma'} (\vec{\nabla}_{2,Q}'\psi)\,\vec{\rho}^T dS'\,\vec{\sigma} + \right.$$

$$\sum_{i,j} \frac{1}{2\kappa}\left(\iint_{\Sigma'} \rho_i\,\rho_j(\vec{\nabla}_{2,Q}')_k\psi \quad dS'\right)[\Sigma]_{ij} \tag{J.6.88}$$

Now, applying (J.6.79)

$$\iint_{\Sigma'} \vec{\nabla}_{2,Q}'\psi\, dS = \int_{\partial\Sigma'} \vec{n}\psi \frac{ds}{|\vec{n}|} \tag{J.6.89}$$

To compute the second term of (J.6.86), we extend (J.6.79) to a product fg of functions to obtain

$$\iint_{\Sigma'} \vec{\nabla}(fg)\, dS = \iint_{\Sigma'} (f\vec{\nabla}g + g\vec{\nabla}f)dS$$

$$= \int_{\partial\Sigma'} fg \frac{\vec{n}}{|\vec{n}|} ds \tag{J.6.91}$$

We thus obtain the general two dimensional integration by parts formula

$$\iint_{\Sigma'} f\, \vec{\nabla} g\, dS = \int_{\partial\Sigma'} fg \frac{\vec{n}}{|\vec{n}|} ds - \iint_{\Sigma'} g\vec{\nabla} f\, dS \tag{J.6.92}$$

For later use, note that applying the definitions of $\vec{\nabla}_2, \tilde{\nabla}_2$, $\vec{\rho}$, and [G] (equations (J.6.67), (J.6.36), and (J.6.50))

$$\iint_{\Sigma'} f\, \tilde{\nabla}_2\, g\, dS = \int_{\partial\Sigma'} fg \frac{\vec{\nu}}{|\vec{\nu}|} ds - \iint_{\Sigma'} g\, \tilde{\nabla} f\, dS \tag{J.6.93}$$

Now, applying (J.6.92)

$$\iint_{\Sigma'} \nabla'_{2,Q}\, \phi\, \vec{\rho}^T dS' =$$

$$\int_{\partial\Sigma'} \psi \frac{\vec{n}}{|\vec{n}|} \vec{\rho}^T ds - \iint_{\Sigma'} \psi[I]\, dS' \tag{J.6.94}$$

since

$$\vec{\nabla}'_{2,Q}\, \vec{\rho}^T = \begin{bmatrix} 1 & 0 \\ 0 & 1 \end{bmatrix} = I \tag{J.6.95}$$

Substituting (J.6.89) and (J.6.94) in (J.6.88),

$$\vec{v}'_{s,\xi',\eta'} = \frac{1}{\kappa}\left(\int_{\partial\Sigma'} \vec{n}\, \psi \frac{ds}{|\vec{n}|}\right)\sigma_0$$

$$+ \frac{1}{\kappa}\left[\int_{\partial\Sigma'} \vec{n}\, \vec{\rho}^T \frac{\psi}{|\vec{n}|} ds\right]\vec{\sigma} - \frac{1}{\kappa}\left(\iint_{\Sigma'} \psi\, dS'\right)\vec{\sigma}$$

$$+ \sum_{i,j} \frac{1}{2\kappa}\left(\iint_{\Sigma'} \rho_i\, \rho_j\, \vec{\nabla}'^2_Q \psi\right) dS'\ [\Sigma]_{ij} \tag{J.6.96}$$

J.6.2.3 Normal Source Velocity

Finally

$$\vec{v}'_{s,\zeta'} = \frac{1}{\kappa} \iint_{\Sigma'} \sigma \frac{\partial\psi}{\partial\zeta'} dS' = \tag{J.6.97}$$

(using J.6.66)

$$\frac{-sh}{\kappa} \iint_{\Sigma'} \sigma \frac{1}{\rho} \frac{\partial\psi}{\partial\rho} ds' = \tag{J.6.98}$$

(by J.6.35)

$$\left(\frac{-sh}{\kappa} \iint_{\Sigma'} \frac{1}{\rho} \frac{\partial\psi}{\partial\rho} dS'\right) \sigma_0 - \left\lfloor \frac{sh}{\kappa} \iint_{\Sigma'} \frac{\vec{\rho}^T}{\rho} \frac{\partial\psi}{\partial\rho} dS' \right\rfloor \vec{\sigma}$$

$$- \frac{1}{2} \left[\frac{sh}{\kappa} \iint_{\Sigma'} \frac{\vec{\rho}\vec{\rho}^T}{\rho} \frac{\partial\psi}{\partial\rho} dS' \right] : [\Sigma] \tag{J.6.99}$$

Now, by (J.6.70), (J.6.79) and multiplication by $[G]$,

$$\iint_{\Sigma'} \frac{\vec{\rho}}{\rho} \frac{\partial\psi}{\partial\rho} dS' = \int_{\partial\Sigma'} rs\, \tilde{\nabla}_{2,Q'}\psi \; ds$$

$$= rs \int_{\partial\Sigma'} \psi \frac{\vec{\nu}}{|\vec{\nu}|} ds \tag{J.6.100}$$

Next, by (J.6.70)

$$\iint_{\Sigma'} [\rho\, \vec{\rho}^T] \frac{1}{\rho} \frac{\partial\psi}{\partial\rho} dS' = rs \iint_{\Sigma'} (\tilde{\nabla}'_{2,Q}) \vec{\rho}^T dS' \tag{J.6.101}$$

= (using the integration by parts formula (J.6.93))

$$rs \int_{\partial\Sigma'} \frac{\vec{\nu}}{|\vec{\nu}|} \vec{\rho}^T ds - rs \iint_{\Sigma'} \tilde{\nabla}'_{2,Q} \vec{\rho}^T dS' \tag{J.6.102}$$

$$= rs \int_{\partial\Sigma'} \frac{\vec{\nu}}{|\vec{\nu}|} \vec{\rho}^T ds - rs \iint_{\Sigma'} \psi\, [G]\, dS' \tag{J.6.103}$$

since

$$\tilde{\nabla}_{2,Q'} \vec{\rho}^T = \begin{Bmatrix} rs\, \partial/\partial\xi' \\ \partial/\partial\eta' \end{Bmatrix} \left\lfloor \xi' \quad \eta' \right\rfloor \tag{J.6.104}$$

$$= \begin{bmatrix} rs & 0 \\ 0 & 1 \end{bmatrix} = [G] \tag{J.6.105}$$

Combining (J.6.99-104), we have

$$\vec{v}'_{s,\zeta} = \left(\frac{-sh}{\kappa} \iint_{\Sigma'} \frac{1}{\rho} \frac{\partial\psi}{\partial\rho} \, dS' \right) \sigma_0$$

$$- \frac{rh}{\kappa} \int_{\partial\Sigma'} \psi \, \vec{\nu}^T \frac{ds}{|\vec{\nu}|} \vec{\sigma}$$

$$+ \left[\frac{-1}{2} \frac{rh}{\kappa} \int_{\partial\Sigma'} \psi \, \vec{\nu}\vec{\rho}^T \frac{ds}{|\vec{\nu}|} \right] : [\Sigma]$$

$$+ \left(\frac{1}{2} \frac{rh}{\kappa} \iint_{\Sigma'} \psi \, dS' \right) [G] : [\Sigma] \qquad \text{(J.6.106)}$$

J.6.3 Doublet Potential and Velocity

J.6.3.1 Doublet Potential

From (J.6.10) and (J.6.18)

$$\phi_{D'} = \frac{s}{\kappa} \iint_{\Sigma'} \mu \vec{n}'^T \, [C'] \vec{\nabla}'_Q \psi \, dS' \qquad \text{(J.6.107)}$$

= (applying (J.6.7) and (J.6.11))

$$\frac{r}{\kappa} \iint_{\Sigma'} \mu \frac{\partial\psi}{\partial\zeta'} \, dS' \qquad \text{(J.6.108)}$$

= (applying (J.6.66))

$$\frac{-rsh}{\kappa} \iint_{\Sigma'} \mu \frac{1}{\rho} \frac{\partial\psi}{\partial\rho} \, dS' = \qquad \text{(J.6.109)}$$

$$\frac{-rsh}{\kappa} \left(\iint_{\Sigma'} \frac{1}{\rho} \frac{\partial\psi}{\partial\rho} \, dS' \right) \mu_0$$

$$\frac{-rsh}{\kappa} \left\llcorner \iint_{\Sigma'} \frac{\vec{\rho}}{\rho}^T \frac{\partial\psi}{\partial\rho} \, dS' \right\lrcorner \vec{\mu}$$

$$\frac{-rsh}{2\kappa} \left[\iint_{\Sigma'} \frac{\vec{\rho}\vec{\rho}^T}{\rho} \frac{\partial\psi}{\partial\rho} \, dS' \right] : [M]$$

$$\frac{-rsh}{6\kappa} \sum_{ijk} \left\{ \iint_{\Sigma'} \rho_i \, \rho_j \, \rho_k \frac{1}{\rho} \frac{\partial\psi}{\partial\rho} \, dS' \right\} \mathcal{M}_{ijk} \qquad \text{(J.6.110)}$$

The first three integrals are identical to those arising in the evaluation of $\vec{v}_{S,\zeta}$, and thus we need only consider the fourth integral.

Now, using (J.6.70)

$$\iint_{\Sigma'} \rho_i \, \rho_j \, \rho_k \, \frac{1}{\rho} \, \frac{\partial\psi}{\partial\rho} \, dS' =$$

$$rs \iint_{\Sigma'} \rho_i \, \rho_j \, (\tilde{\nabla}'_{2,Q})_k \, \psi \, dS' \tag{J.6.111}$$

Now, substituting equations (J.6.100), (J.6.103), and (J.6.111) in (J.6.11), we obtain

$$\phi_D = \frac{-rsh}{\kappa} \left(\iint_{\Sigma'} \frac{1}{\rho} \, \frac{\partial\psi}{\partial\rho} \, dS' \right) \mu_0$$

$$- \left[\frac{h}{\kappa} \int_{\partial\Sigma'} \frac{\vec{v}^T}{|\vec{v}|} \, ds \right] \vec{\mu}$$

$$\frac{h}{2\kappa} \left[\int_{\partial\Sigma'} \psi \, \frac{\vec{v}}{|\vec{v}|} \vec{\rho}^T ds \right] : [M]$$

$$+ \frac{h}{2\kappa} \left(\iint_{\Sigma'} \psi \, dS' \right) \; [G] : [M]$$

$$\frac{h}{6\kappa} \sum_{i,j,k} \left(\iint_{\Sigma'} \rho_i \rho_j \, (\tilde{\nabla}_{2,Q})_k \, \psi dS' \right) \mathcal{M}_{ijk} \tag{J.6.114}$$

J.6.3.2 Tangential Doublet Velocity

Combining (J.6.7), (J.6.18), and (J.6.28), we have

$$\vec{v}_D^{*'} = -\frac{1}{\kappa} \iint_{\Sigma'} \left\{ \begin{pmatrix} \partial\mu/\partial\xi' \\ \partial\mu/\partial\eta' \\ \partial\mu/\partial\zeta' \end{pmatrix} \times \begin{pmatrix} 0 \\ 0 \\ 1 \end{pmatrix} \right\} \times \begin{pmatrix} rs \; \partial\psi/\partial\xi' \\ \partial\psi/\partial\eta' \\ \partial\psi/\partial\zeta' \end{pmatrix} dS'$$

$$= -\frac{1}{\kappa} \iint_{\Sigma'} \begin{Bmatrix} \partial\mu/\partial\eta' \\ -\partial\mu/\partial\xi' \\ 0 \end{Bmatrix} \times \begin{Bmatrix} rs \; \partial\psi/\partial\xi' \\ \partial\psi/\partial\eta' \\ r\partial\psi/\partial\zeta' \end{Bmatrix} dS' \tag{J.6.115}$$

$$= -\frac{1}{\kappa} \iint_{\Sigma'} \begin{pmatrix} -r(\partial\mu/\partial\xi')(\partial\psi/\partial\zeta') \\ -r(\partial\mu/\partial\eta')(\partial\psi/\partial\zeta') \\ (\partial\mu/\partial\eta')(\partial\psi/\partial\eta') \\ + rs \; (\partial\mu/\partial\zeta')(\partial \; /\partial\zeta') \end{pmatrix} dS'$$

$$= - \left\{ \begin{array}{l} \frac{-r}{\kappa} \iint_{\Sigma'} \vec{\nabla}'_{2\mu} \frac{\partial\psi}{\partial\zeta'} \, dS' \\ \frac{1}{\kappa} \iint_{\Sigma'} \vec{\nabla}'_{2,Q\mu} \cdot \tilde{\nabla}'_{2,Q} \psi \, dS' \end{array} \right\} \tag{J.6.116}$$

In particular

$$\vec{v}_D'^{*} = \frac{r}{\kappa} \iint_{\Sigma'} (\vec{\nabla}_{2,Q\mu}) \frac{\partial\psi}{\partial\zeta'} \, dS' \tag{J.6.117}$$

Applying (J.6.38) and (J.6.66)

$$\vec{v}_{D,\xi,\eta}'^{*} = \frac{-rsh}{\kappa} \iint_{\Sigma'} \frac{1}{\rho} \frac{\partial\psi}{\partial\rho} \cdot$$

$$\left\{ \vec{\nabla}'_{2,Q} \mu_Q + [\nabla'_{2,Q}\vec{\rho}^T]\vec{\mu} + \frac{1}{2} \vec{\nabla}'_{2,Q} ([\vec{\rho}\vec{\rho}^T]:[M]) \right.$$

$$\left. + \frac{1}{6}\vec{\nabla}'_{2,Q} \left(\sum_{i,j,k} \rho_i\rho_j\rho_k \mathcal{M}_{ijk} \right) \right\} dS' \tag{J.6.118}$$

= (applying (J.6.90))

$$- \frac{rsh}{\kappa} \left(\iint_{\Sigma'} \frac{1}{\rho} \frac{\partial\psi}{\partial\rho} dS' \right)\vec{\mu} - \frac{rsh}{\kappa} \iint_{\Sigma'} \frac{1}{\rho} \frac{\partial\psi}{\partial\rho} [M] \vec{\rho} \, dS'$$

$$- \frac{rsh}{6\kappa} \sum_{i,j} \left(\iint_{\Sigma'} \frac{1}{\rho} \frac{\partial}{\partial\rho} \rho_i\rho_j \, dS' \right) \left(\mathcal{M}_{.,i,j} + \mathcal{M}_{i,.,j} + \mathcal{M}_{i,j,.} \right) \tag{J.6.119}$$

Inspection of (J.6.33) and (J.6.34) shows that

$$\mathcal{M}_{1,i.j} = \mathcal{M}_{i,1,j} = \mathcal{M}_{i,j,1} \tag{J.6.120}$$

and similarly for $\mathcal{M}_{2,i,j}$, and thus

$$\mathcal{M}_{.,i,j} + \mathcal{M}_{i,.,j} + \mathcal{M}_{i,j,.} = 3\mathcal{M}_{.,i,j} \tag{J.6.121}$$

Now, substituting (J.6.100), (J.6.103), and (J.6.121) in (J.6.119), we obtain

$$\vec{v}^{\,*}_{D,\xi',\eta'} = -\frac{rsh}{\kappa} \iint_{\Sigma'} \frac{1}{\rho} \frac{\partial\psi}{\partial\rho} dS' \, \vec{\mu}$$

$$- \frac{h}{\kappa} [M] \int_{\partial\Sigma'} \frac{\vec{v}}{|\vec{v}|} ds - \frac{h}{2\kappa} \sum_{i,j} \int_{\partial\Sigma'} [\frac{\vec{v}}{|\vec{v}|} \vec{\rho}^T]_{i,j} \, ds \left\{ \mathcal{M}_{.,i,j} \right\}$$

$$+ \frac{h}{2\kappa} \left(\iint_{\Sigma'} \psi \, dS' \right) \sum_{i,j} [G]_{ij} \left\{ \mathcal{M}_{.,i,j} \right\} \tag{J.6.122}$$

J.6.3.3 Normal Doublet Velocity

By (J.6.116),

$$\vec{v}^{\,*}_{D,\zeta'} = \frac{1}{\kappa} \iint_{\Sigma'} (\vec{\nabla}'_{2,Q} \, \mu) \cdot (\tilde{\nabla}'_{2,Q} \psi) dS' \tag{J.6.123}$$

Applying (J.6.38) and (J.6.70)

$$\vec{v}^{\,*}_{D,\zeta'} = -\frac{1}{\kappa} \sum_{i,j} \iint_{\Sigma'} \vec{\nabla}'_{2,Q,j} \, (\rho_i \vec{\mu}_i) \frac{rs\rho_j}{\rho} \frac{\partial\psi}{\partial\rho} dS'$$

$$- \frac{1}{2\kappa} \sum_{i,j,k} \iint_{\Sigma'} \vec{\nabla}'_{2,Q,k} (\rho_i \rho_j) [M_{ij}] \frac{rs\rho_k}{\rho} \frac{\partial\psi}{\partial\rho} dS'$$

$$- \frac{1}{6} \sum_{ijkl} \iint_{\Sigma'} \tilde{\nabla}'_{2,Q,l} \, (\rho_i \rho_j \rho_k) \, (\mathcal{M}_{ijk}) \frac{rs\rho_l}{\rho} \frac{\partial\psi}{\partial\rho} dS' \tag{J.6.124}$$

Applying (J.2.90)

$$\vec{v}^{\,*}_{D,\zeta'} = \frac{rs}{\kappa} \sum_i \left(\iint_{\Sigma'} \frac{\rho_i}{\rho} \frac{\partial\psi}{\partial\rho} dS' \right) \mu_i$$

$$- \frac{rs}{2\kappa} \sum_{ijk} \iint_{\Sigma'} (\delta_{ik}\rho_j\rho_k + \delta_{ij}\rho_i\rho_k) \frac{1}{\rho} \frac{\partial\psi}{\partial\rho} dS' \, [M]_{ij}$$

$$- \frac{rs}{6} \sum_{ijkl} \iint_{\Sigma'} dS' \, (\delta_{il}\rho_j\rho_k + \delta_{jl}\rho_i\rho_k + \delta_{kl}\rho_i\rho_j) \, \mathcal{M}_{ijk} \frac{\rho_l}{\rho} \frac{\partial\psi}{\partial\rho} \tag{J.6.125}$$

Using the definition of the delta function,

$$\vec{v}^{\,\prime *}_{D,\zeta} = -\frac{rs}{\kappa} \sum_i \left(\iint_{\Sigma'} \frac{\rho_i}{\rho} \frac{\partial \psi}{\partial \rho} dS' \right) \mu_i$$

$$-\frac{rs}{\kappa} \sum_{ij} \iint_{\Sigma'} \rho_i \rho_j \frac{1}{\rho} \frac{\partial \psi}{\partial \rho} dS' \, [M]_{ij}$$

$$-\frac{rs}{2\kappa} \sum_{ijk} \iint_{\Sigma'} \rho_i \rho_j \rho_k \frac{1}{\rho} \frac{\partial \psi}{\partial \rho} dS' \, \mathcal{M}_{ijk} \qquad \text{(J.6.126)}$$

Substituting (J.6.70) into (J.6.126),

$$v^{\prime *}_{D,\zeta} = -\frac{1}{\kappa} \sum_i \iint_{\Sigma'} \left\{ \vec{\nabla}'_{2,Q} \right\}_i \psi \, dS' \, \vec{\mu}_i$$

$$-\frac{1}{\kappa} \sum_{ij} \iint_{\Sigma'} \rho_i \, (\vec{\nabla}'_{2,Q})_j \, \psi \, dS' \, [M]_{ij}$$

$$-\frac{1}{2\kappa} \sum_{ijk} \iint_{\Sigma'} \rho_i \rho_j \, (\nabla'_{2,Q})_k \, dS' \, (\mathcal{M})_{ijk} \qquad \text{(J.6.127)}$$

Applying (J.6.81), (J.6.93), and (J.6.104-105),

$$v^{\prime *}_{D,z} = -\frac{1}{\kappa} \int_{\partial\Sigma'} \frac{\vec{v}^T}{|\vec{v}|} \psi \, dS' \, \vec{\mu}$$

$$-\frac{1}{\kappa} \left[\int_{\partial\Sigma'} \vec{\rho}\vec{v}^T \frac{ds}{|\vec{v}|} \right] : [M]$$

$$+\frac{1}{\kappa} \iint_{\Sigma'} \psi \, dS' \, [G] : [M]$$

$$-\frac{1}{2\kappa} \sum_{i,j,k} \iint_{\Sigma'} \rho_i \rho_j \, (\vec{\nabla}'_{2,Q})_k \, \psi \, dS' \, (\mathcal{M})_{ijk} \qquad \text{(J.6.128)}$$

J.6.4 Reduction to Fundamental Integrals

In this section, we will see that the entries of the matrices S and D, describing source and doublet potential and velocity, are all combinations of a small number of fundamental integrals.

J.6.4.1 Definition of the Integrals

We define the integrals as follows.

$$a = -\frac{sh}{\kappa} \iint_{\Sigma'} \frac{1}{\rho} \frac{\partial\psi}{\partial\rho} \, dS' \tag{J.6.129}$$

$$b = -\frac{1}{\kappa} \iint_{\Sigma'} \psi \, dS' \tag{J.6.130}$$

$$\vec{a} = \frac{1}{\kappa} \int_{\partial\Sigma'} \frac{\vec{n}}{|\vec{n}|} \psi ds \tag{J.6.131}$$

$$\vec{b} = -\frac{s}{\kappa} \int_{\partial\Sigma'} \vec{\nu} \times \frac{ds}{|\vec{\nu}|} \tag{J.6.132}$$

$$[B] = \frac{1}{\kappa} \int_{\partial\Sigma'} \frac{\vec{n}\vec{\rho}^T}{|\vec{n}|} \psi \, ds - \frac{1}{\kappa} \left(\iint_{\Sigma'} \psi dS' \right) [I] \tag{J.6.133}$$

where I is the identity matrix.

$$[F] = \frac{s}{\kappa} \iint_{\Sigma'} \vec{\rho} \vec{\nabla}'^{T}_{2,Q} \, \psi \, dS' \tag{J.6.134}$$

Finally, let H be the 2x2x2 tensor

$$H_{ijk} = \frac{1}{\kappa} \iint_{\Sigma'} \rho_i \rho_j \, (\vec{\nabla}'_{2,Q})_k \psi \, dS' \tag{J.6.135}$$

J.6.4.2 Source Potential and Velocity

Applying the above to (J.6.84), we see

$$\phi_{S'} = b\sigma_0 + \vec{b}^T\vec{\sigma} - 1/2 \, [F] : [\Sigma] \tag{J.6.136}$$

From (J.6.96) we get

$$\vec{v}'_{S,\xi',n'} = \sigma_0 \, \vec{a} + [B]\vec{\sigma} + \frac{1}{2} \sum_{ij} \left[\sum_l G_{.,l} \, H_{ijl} \right] \Sigma_{ij} \tag{J.6.137}$$

since

$$[G] \tilde{\nabla}'_{2,Q} = \vec{\nabla}'_{2,Q} \tag{J.6.138}$$

Finally, (J.6.106) yields

$$\vec{v}'_{S,\zeta} = a\,\sigma_0 - rh\,(Ga)^T\,\vec{\sigma}$$

$$-\frac{rh}{2}\,[GB] : [\Sigma] \qquad \text{(J.6.139)}$$

With a few simple definitions, we can write down the matrix [S] such that

$$\begin{Bmatrix} \phi_S' \\ \vec{v}'_{s,\xi',\eta'} \\ v'_{s,\zeta} \end{Bmatrix} = [S] \begin{Bmatrix} \sigma_0 \\ \sigma_\xi \\ \sigma_\eta \\ \sigma_{\xi\xi} \\ \sigma_{\xi\eta} \\ \sigma_{\eta\eta} \end{Bmatrix} \qquad \text{(J.6.140)}$$

First, for a (2x2) matrix [A], let $\llcorner A \lrcorner_3$ be the row vector of length 3:

$$\llcorner A \lrcorner_3 = \llcorner A_{11} \quad (A_{12} + A_{21}) \quad A_{22} \lrcorner \qquad \text{(J.6.141)}$$

For a (2x2x2) tensor $\{T\}$, let $\llcorner T \lrcorner_4$ be the row vector of length 4:

$$\llcorner T \lrcorner_4 = \llcorner T_{111}\ (T_{112} + T_{121} + T_{211})\ (T_{122} + T_{212} + T_{221})\ T_{222} \lrcorner \qquad \text{(J.6.142)}$$

and let $[T_k]$ (k = 1 or 2) be the 2x2 matrix

$$[T_k]_{ij} = (T)_{ijk} \qquad \text{(J.6.143)}$$

We easily see that if [A] is a 2x2 matrix,

$$[A] : [\Sigma] = \llcorner A \lrcorner_3 \begin{Bmatrix} \sigma_{\xi\xi} \\ \sigma_{\xi\eta} \\ \sigma_{\eta\eta} \end{Bmatrix} \qquad \text{(J.6.144)}$$

Thus, from (J.6.136)

$$\phi'_S = b\sigma_0 + \vec{b}^T\vec{\sigma} - \frac{1}{2}\,\llcorner F \lrcorner_3 \begin{Bmatrix} \sigma_{\xi\xi} \\ \sigma_{\xi\eta} \\ \sigma_{\eta\eta} \end{Bmatrix} \qquad \text{(J.6.145)}$$

and by (J.6.139)

$$\vec{v}'_{s,\zeta'} = a\sigma_0 - rh[G]\,\vec{a}^T\vec{\sigma}$$

$$-\frac{rh}{2}\,\llcorner GB \lrcorner_3 \begin{Bmatrix} \sigma_{\xi\xi} \\ \sigma_{\xi\eta} \\ \sigma_{\eta\eta} \end{Bmatrix} \qquad \text{(J.6.146)}$$

Finally, we note that

$$\sum_{l} G_{1l} \; H_{ijl} = rs[H_1] \tag{J.6.147}$$

while

$$\sum_{l} G_{2l} \; H_{ijl} = \; [H_2] \tag{J.6.148}$$

Thus,

$$\sum_{ijl} G_{1l} \, H_{ijl} \;\; \Sigma_{ij} = rs \llcorner H_1 \lrcorner \; 3 \quad \begin{Bmatrix} \sigma_{\xi\xi} \\ \sigma_{\xi\eta} \\ \sigma_{\eta\eta} \end{Bmatrix} \tag{J.6.149}$$

while

$$\sum_{ij} G_{2l} \, H_{ijl} \;\; ij = \llcorner H_2 \lrcorner \; 3 \quad \begin{Bmatrix} \sigma_{\xi\xi} \\ \sigma_{\xi\eta} \\ \sigma_{\eta\eta} \end{Bmatrix} \tag{J.6.150}$$

Applying (J.6.149-150)

$$\begin{Bmatrix} \vec{v}'_{s,\xi'} \\ \vec{v}'_{s,\eta'} \end{Bmatrix} = \sigma_0 \vec{a} + [B] \, \vec{\sigma}$$

$$+ \frac{1}{2} \begin{bmatrix} rs \llcorner H_1 \lrcorner \; 3 \\ \llcorner H_2 \lrcorner \; 3 \end{bmatrix}^{2x3} \begin{Bmatrix} \sigma_{\xi\xi} \\ \sigma_{\xi\eta} \\ \sigma_{\eta\eta} \end{Bmatrix} \tag{J.6.151}$$

Substituting (J.6.145-146) and (J.6.151) into (J.6.140),

$$[S] = \begin{array}{c} \\ 1 \\ 2 \\ \\ 1 \end{array} \begin{array}{c} \begin{array}{ccc} 1 & 2 & 3 \end{array} \\ \left[\begin{array}{c|c|c} b & \vec{b}^T & -1/2 \llcorner F \lrcorner \; 3 \\ \hline \vec{a} & B & \frac{rs}{2} \llcorner H_1 \lrcorner \; 3 \\ \hline & & \frac{1}{2} \llcorner H_2 \lrcorner \; 3 \\ \hline a & -hr(G\vec{a})^T & \frac{-rh}{2} \llcorner GB \lrcorner \; 3 \end{array}\right] \end{array} \tag{J.6.152}$$

J.6.4.3 Doublet Potential and Velocity

Applying (J.6.129-135) to (J.6.114), we see that

$$\phi_D = ra\,\mu_0 - h\,(G\vec{a})^T\,\vec{\mu} - \frac{h}{2}\,[GB] : [M]$$

$$-\frac{h}{6}\sum_{ijk} H_{ijk}\mathcal{M}_{ijk} \qquad \text{(J.6.153)}$$

Next, from (J.6.122), we obtain

$$\vec{v}^{\,*}_{D,\xi',\eta'} = ra\,\vec{\mu} - h[M]\,(G\vec{a}) - \frac{h}{2}\sum_{ij}[GB]_{ij}\mathcal{M}_{.,i,j} \qquad \text{(J.6.154)}$$

Finally, from (J.6.128),

$$\vec{v}'^{\,*}_{D,\zeta'} = -\,(Ga)^T\,\vec{\mu} - [GB] : [M]$$

$$-\frac{1}{2}\sum_{i,j,k} H_{ijk}\mathcal{M}_{ijk} \qquad \text{(J.6.155)}$$

Now, recalling the definition (J.6.33-34) of $\mathcal{M}$, we see that if T is a 2x2x2 tensor,

$$\sum_{ijk} T_{ijk}\mathcal{M}_{ijk} = \llcorner T \lrcorner_4 \quad \bullet \quad \begin{Bmatrix} \mu_{\xi\xi\xi} \\ \mu_{\xi\xi\eta} \\ \mu_{\xi\eta\eta} \\ \mu_{\eta\eta\eta} \end{Bmatrix} \qquad \text{(J.6.156)}$$

where $\llcorner T \lrcorner_4$ is defined by (J.6.142).

Now, applying (J.6.156) and the doublet equivalent of (J.6.144) to (J.6.153), we have

$$\phi'_D = ra\mu_0 - h\,(G\vec{a})^T\,\vec{\mu}$$

$$-\frac{h}{2}\,\llcorner GB \lrcorner_3 \begin{Bmatrix} \mu_{\xi\xi} \\ \mu_{\xi\eta} \\ \mu_{\eta\eta} \end{Bmatrix} \quad \frac{h}{6}\,\llcorner H \lrcorner_4 \begin{Bmatrix} \mu_{\xi\xi\xi} \\ \mu_{\xi\xi\eta} \\ \mu_{\xi\eta\eta} \\ \mu_{\eta\eta\eta} \end{Bmatrix} \qquad \text{(J.6.157)}$$

Next, expanding (J.6.154) into two equations,

$$\vec{v}'^{*}_{D,\xi'} = ra\ \mu_{\xi} - h \sum_{j} M_{ij}\ (Ga)_j$$

$$- \frac{h}{2} \sum_{ij} [GB]_{ij}\, \mathcal{M}_{1,i,j} \qquad (J.6.158)$$

= (using the definitions (J.6.32-34) of M and $\mathcal{M}$)

$$ra\ \mu_{\xi} - h(G\vec{a})^T \begin{Bmatrix} \mu_{\xi\xi} \\ \mu_{\xi\eta} \end{Bmatrix} - \frac{h}{2} \llcorner GB \lrcorner_3 \begin{Bmatrix} \mu_{\xi\xi\xi} \\ \mu_{\xi\xi\eta} \\ \mu_{\xi\eta\eta} \end{Bmatrix} \qquad (J.6.159)$$

Similarly,

$$\vec{v}'_{D,\eta'} = ra\ \mu_{\eta} - h \sum_{j} M_{2j}\ (G\vec{a})_j - \frac{h}{2} \sum_{ij} [GB]_{ij}\mathcal{M}_{2ij} \qquad (J.6.160)$$

$$= ra\ \mu_{\eta} - h\ (G\vec{a})^T \begin{Bmatrix} \mu_{\xi\eta} \\ \mu_{\eta\eta} \end{Bmatrix} - \frac{h}{2} \llcorner GB \lrcorner_3 \begin{Bmatrix} \mu_{\xi\xi\eta} \\ \mu_{\xi\eta\eta} \\ \mu_{\eta\eta\eta} \end{Bmatrix} \qquad (J.6.161)$$

Finally, applying (J.6.156) and the doublet equivalent of (J.6.144) to (J.6.155),

$$\vec{v}'^{*}_{D,\zeta'} = - (G\vec{a})^T\vec{\mu} - \llcorner GB \lrcorner_3 \begin{Bmatrix} \mu_{\xi\xi} \\ \mu_{\xi\eta} \\ \mu_{\eta\eta} \end{Bmatrix}$$

$$- \frac{1}{2} \llcorner H \lrcorner_4 \begin{Bmatrix} \mu_{\xi\xi\xi} \\ \mu_{\xi\xi\eta} \\ \mu_{\xi\eta\eta} \\ \mu_{\eta\eta\eta} \end{Bmatrix} \qquad (J.6.162)$$

So, we can now write down the matrix [D] such that

$$\begin{Bmatrix} \phi_{D'} \\ \vec{v}'_{\xi',\eta'} \\ v_{D,'\zeta'} \end{Bmatrix} = [D] \begin{Bmatrix} \mu_0 \\ \mu_{\xi} \\ \mu_{\eta} \\ \cdot \\ \cdot \\ \cdot \\ \mu_{\eta\eta\eta} \end{Bmatrix} \qquad (J.6.163)$$

From (J.6.157), (J.6.159), (J.6.161), and (J.6.162), we have $[D]^{4\times 10} =$

$$
\begin{array}{c}
\\ 1 \\ 2 \\ 1
\end{array}
\begin{array}{c}
\begin{array}{cccc} 1 & 2 & 3 & 4 \end{array} \\
\left[\begin{array}{c|c|cc|cc}
ra & -h\,(G\vec{a})^T & -\frac{h}{2}\,\llcorner GB\lrcorner_3 & & -\frac{h}{6}\,\llcorner H\lrcorner_4 & \\
\hline
0 & ra[I] & -h\,(G\vec{a})^T & 0 & -\frac{h}{2}\,\llcorner GB\lrcorner_3 & 0 \\
 & & 0 & -h(G\vec{a})^T & 0 & -\frac{h}{2}\,\llcorner GB\lrcorner_3 \\
\hline
0 & -\,(G\vec{a})^T & -\llcorner GB\lrcorner_3 & & -\frac{1}{2}\,\llcorner H\lrcorner_4 &
\end{array}\right]
\end{array}
\tag{J.6.164}
$$

J.6.5 The Fundamental Integrals in Terms of Panel and Edge Functions

The seven fundamental integrals which define the entries of the matrices [S] and [D] can themselves be reduced to simpler expressions. The only integrals involved in these expression are a single "panel function" and one "edge function" for each edge of the region.

J.6.5.1 Computation of a.

By (J.6.129),

$$a = -\frac{sh}{\kappa} \iint_{\Sigma'} \frac{1}{\rho} \frac{\partial\psi}{\partial\rho}\, dS' \tag{J.6.165}$$

Thus, for subsonic flow and superinclined panels

$$a = -\frac{sh}{\kappa} \sum_{\text{edges}} \int_{\phi_k}^{\phi_k^+} d\phi \int_0^{P_k(\phi)} \frac{\rho d\rho}{\rho} \frac{\partial\psi}{\partial\rho} \tag{J.6.166}$$

by (J.4.56-57) and (J.4.60).

Note that this integral is always finite unless the control point lies on the panel edge.

Now,

$$\int_0^{P_k(\phi)} \frac{\partial\psi}{\partial\rho}\, d\rho = \psi(P_k(\phi)) - \psi(0)$$

$$= \psi(P_k(\phi)) - \frac{1}{|h|} \qquad \text{(J.6.167)}$$

Thus,

$$a = -\frac{sh}{\kappa} \sum_{\text{edges}} \int_{\phi_k^-}^{\phi_k^+} \psi\, d\phi$$

$$- \frac{sh}{\kappa} \left(- \frac{2\pi}{|h|} C_\odot\right) \qquad \text{(J.6.168)}$$

where $C_\odot$ is defined by (J.4.30).

For subinclined panels,

$$a = -\frac{sh}{\kappa} \iint_{\Sigma'} \frac{1}{\rho} \frac{\partial\psi}{\partial\rho}\, dS' \quad = \text{(cf.(J.5.104))}$$

$$- \frac{sh}{\kappa} \sum_k \int_{\phi_k^-}^{\phi_k^+} d\phi \int_{|h|}^{P_k(\phi)} \frac{\partial\psi}{\partial\rho}\, d\rho \qquad \text{(J.6.169)}$$

Unlike the integral J.6.166, we will see shortly that this integral is in fact infinite. We have

$$a = -\frac{sh}{\kappa} \left[\sum_k \lim_{\varepsilon\to 0^+} \int_{\phi_k^-}^{\phi_k^+} d\phi \left[\left(\psi - \frac{1}{\varepsilon}\right)\right]_{\sqrt{h^2+\varepsilon^2}}^{P_k(\phi)}\right. \qquad \text{(J.6.170a)}$$

$$= -\frac{sh}{\kappa} \sum_{k=1}^{K} \int_{\phi_k^-}^{\phi_k^+} d\phi - \lim_{\varepsilon\to 0} \int_{\phi_k^-}^{\phi_k^+} \frac{1}{\varepsilon}\, d\phi \qquad \text{(J.6.170b)}$$

We now evaluate the first term of this integral, which is the "finite part". We discard the second term, or "infinite part", for reasons discussed in section J.6.7. Thus, setting $C_\odot = 0$ for subinclined panels, we always have

$$a = -\frac{sh}{\kappa} \left[\sum_k \int_{\phi_k^-}^{\phi_k^+} d\phi - \frac{2\pi}{|h|} C_\odot\right] \qquad \text{(J.6.171)}$$

Setting

$$J_k(\psi) = \int_{\phi_k^-}^{\phi_k^+} d\phi \tag{J.6.172}$$

and $$J = \sum_k hJ_k(\psi) - 2\pi \operatorname{sign}(h)\, C_\odot \tag{J.6.173}$$

we have

$$a = -\frac{s}{\kappa} J \tag{J.6.174}$$

The function J is called the panel function.

J.6.5.2 Computation of b.

By (J.6.130),

$$b = \frac{-1}{\kappa} \iint_{\Sigma'} dS' \tag{J.6.175}$$

Thus

$$b = -\frac{1}{\kappa} \sum_k \int_{\phi_k^-}^{\phi_k^+} d\phi \int_{|h|}^{P_k(\phi)} \psi \rho d\phi \tag{J.6.176}$$

Now, by (J.6.72)

$$\int \rho\psi \, d\rho = rX = rR \tag{J.6.177}$$

and thus for subsonic flow or superinclined panels

$$b = -\frac{r}{\kappa} \sum_k \int_{\phi_k^-}^{\phi_k^+} d\phi \, (R - |h|) \tag{J.6.178}$$

$$= \frac{-r}{\kappa} \left[\sum_k \int_{\phi_k^-}^{\phi_k^+} R d\phi - 2\pi |h| \, C_\odot \right] \tag{J.6.179}$$

since $R = |h|$ when $\rho = 0$ and thus

$$\int_{|h|}^{P_k(\phi)} \rho d\rho = r(R-|h|) \tag{J.6.180}$$

For subinclined panels, $R = 0$ when $\rho = |h|$, and thus

$$b = \frac{-r}{\kappa} \sum_k \int_{\phi_k^-}^{\phi_k^+} R d\phi \tag{J.6.181}$$

Thus b is defined in all cases by (J.6.179) by setting $C_\odot = 0$ for subinclined panels.

J.6.5.3 Computation of $\vec{a}$.

By (J.6.131),

$$\vec{a} = -\frac{1}{\kappa} \int_{\partial\Sigma'} \frac{\vec{n}}{|n|} ds \tag{J.6.182}$$

Applying (J.6.54), and noting from (J.6.45) that $|\vec{t}| = |\vec{n}|$, we have

$$\vec{a} = \frac{1}{\kappa} \sum_k \int_{edge} \vec{n}\, sq\psi\, dv = \frac{s}{\kappa} \sum_k \vec{n}_k\, q_k \int_{v_k^-}^{v_k^+} \psi\, dv \tag{J.6.183}$$

Defining

$$I_k = \int_{v_k^-}^{v_k^+} \psi\, dv \tag{J.6.184}$$

we have

$$\vec{a} = \frac{s}{\kappa} \sum_k \vec{n}_k\, q_k\, I_k \tag{J.6.185}$$

J.6.5.4 Computation of $\vec{b}$.

By (J.6.132),

$$\vec{b} = \frac{-s}{\kappa} \int_{\partial\Sigma'} \vec{v} X \frac{ds}{|\vec{v}|} = \frac{-1}{\kappa} \sum_k \vec{v}_k\, q_k \int_{V_k^-}^{v_k^+} R dv \tag{J.6.186}$$

= (by (J.6.54))

$$\frac{-s}{\kappa} \int_{\partial\Sigma'} \vec{v} sqx dv = \frac{-1}{\kappa} \sum_k \vec{v}_k \, q_k \int_{v_k^-}^{v_k^+} R dv \tag{J.6.189}$$

Integrating by parts,

$$\int R dv = Rv - \int v \frac{\partial R}{\partial v} dv \tag{J.6.190}$$

where (by J.6.59)

$$2R \frac{\partial R}{\partial v} = 2qv \tag{J.6.191}$$

Thus

$$\int_{v_k^-}^{v_k^+} R dv = [Rv] \Big|_{v_k^-}^{v_k^+} - \int_{v_k^-}^{v_k^+} \frac{q}{R} v^2 dv \tag{J.6.192}$$

= (once again applying (J.6.59))

$$[Rv] \Big|_{v_k^-}^{v_k^+} - \int_{v_k^-}^{v_k^+} \frac{R^2 - rsq_k a_k^2 - rsh^2}{R} dv \tag{J.6.193}$$

Collecting terms,

$$2 \int_{v_k^-}^{v_k^+} R dv = [Rv] \Big|_{v_k^-}^{v_k^+} + \int_{v_k^-}^{v_k^+} \frac{rsq_k \, a_k^2 + rsh^2}{R} dv \tag{J.6.194}$$

Substituting (J.6.184) and (J.6.194) in (J.6.189)

$$b = \frac{-1}{2\kappa} \sum_k \vec{v}_k \, q_k \, \Delta(Rv) - \frac{rs}{2\kappa} \sum_k \vec{v}_k \, (a_k^2 + q_k h^2) \, I_k \tag{J.6.195}$$

where, for any quantity f, we define

$$\Delta f = f(v_k^+) - f(v_k^-) \tag{J.6.196}$$

J.6.5.5 Computation of B

By (J.6.130) and (J.6.133),

$$[B] = b \, [I] + \frac{1}{\kappa} \int_{\partial\Sigma'} \frac{\vec{n} \, \vec{p}^T}{|n|} \psi \, ds \tag{J.6.197}$$

Applying (J.6.52) and (J.6.54)

$$[B] = b[I] + \frac{1}{\kappa}\sum_k \int_{v_k^-}^{v_k^+} \vec{n}_k \psi (q_k r a_k \vec{v}_k^T + q_k s v \ \vec{t}_k^T)\ q_k\ s\ dv \tag{J.6.198}$$

By (J.6.191),

$$\frac{\partial R}{\partial v} = q\ v \psi \tag{J.6.199}$$

and thus

$$[B] = b[I] + \frac{rs}{\kappa}\sum_k n_k\ a_k\ \vec{v}_k^T \int_{v_k^-}^{v_k^+} \psi dv + \frac{1}{\kappa}\sum_k q_k\ \vec{n}_k\ \vec{t}_k^T\ \Delta R \tag{J.6.200}$$

= (using (J.6.184))

$$b[I] + \frac{rs}{\kappa}\sum_k \vec{n}_k\ a_k\ \vec{v}_k^T\ I_k + \frac{1}{\kappa}\sum_k q_k\ \vec{n}_k\ \vec{t}_k^T\ \Delta R \tag{J.6.201}$$

J.6.5.6 Computation of F

By (J.6.134),

$$[F] = \frac{s}{\kappa}\iint_{\Sigma'} \vec{\rho}\ \vec{\nabla}_{2,Q}'^T\ X\ \ ds' \tag{J.6.202}$$

= (using J.6.93)

$$\frac{s}{\kappa}\int_{\partial\Sigma'} \vec{\rho}\ \frac{\vec{v}^T}{|\vec{v}|} X ds - \frac{s}{\kappa}\iint_{\Sigma'} X\ \vec{\nabla}_{2,Q}'\ \ \vec{\rho}^T\ dS' \tag{J.6.203}$$

= (applying (J.6.52) and (J.6.54))

$$\frac{s}{\kappa}\sum_k \int_{v_k^-}^{v_k^+} (q_k\ r\ a_k\ \vec{v}_k + q_k\ s v_k\ \vec{t}_k)\ \vec{v}_k^T\ X\ s\ q_k\ dv - \frac{s}{\kappa}\left(\iint_{\Sigma'} X\ dS'\right)[G] \tag{J.6.204}$$

We first compute $\iint_{\Sigma'} X\ dS'$.

We compute the integral using either circular cylindrical or hyperbolic cylindrical coordinates. In the derivation that follows, we assume that $|h| > 0$ so that we need not concern ourselves with the problem that hyperbolic phase becomes unbound on the lines $(\xi' - x') = \pm(\eta' - y')$. The upper

limit of integration with respect to ρ is $P_k(\phi)$; the lower limit is 0, $|h|$ or 0 in accordance with whether $s = +1$, $rs = -1$, or $r = -1$. We write then,

$$\iint X\, dS' = \sum_k \int_{\phi_k^-}^{\phi_k^+} d\phi \left. \frac{rR^3}{3} \right|_{\rho = 0 \text{ or } |h|}^{P(\phi)} \tag{J.6.205}$$

$$= \sum_k \int_{\phi_k^-}^{\phi_k^+} d\phi \left. \frac{rR^3}{3} \right|_{\rho = 0 \text{ or } |h|}^{P(\phi)} \tag{J.6.206}$$

$$= \frac{r}{3} \sum_k \int_{\phi_k^-}^{\phi_k^+} d\phi \left\{ \begin{matrix} R^3 - |h|^3 \\ \text{or} \\ R^3 \end{matrix} \right\} \tag{J.6.207}$$

Now the sum over k in equation (J.6.207) is over all segments of the boundary of Σ, $\partial\Sigma$, both straight and curved segments. On curved segments $R = 0$ so that we may write

$$\iint X\, dS' = \frac{r}{3} \sum_{\text{edges } k} \int_{\phi_k^-}^{\phi_k^+} R^3\, d\phi - |h|^3 \cdot 2\pi\, C_\odot \tag{J.6.208}$$

We now examine integrals of the form $\int R^3\, d\phi$. Transforming this integral into an integral with respect to v, the intrinsic edge variable, we find (using (J.4.66), (J.5.78), and (J.5.98)) that

$$\int_{\phi^-}^{\phi^+} R^3\, d\phi = \int_{v^-}^{v^+} \frac{adv}{a^2 + rsv^2} R^3 = \int_{v^-}^{v^+} \frac{adv}{a^2 + rsv^2} R\, [qrs\, (a^2 + rsv^2) + rsh^2] \tag{J.6.209}$$

$$= aqrs \int_{v^-}^{v^+} Rdv + rsh^2 \int_{v^-}^{v^+} \frac{adv}{a^2 + rsv^2} R =$$

$$aqrs \int_{v^-}^{v^+} Rdv + rsh^2 \left[aqrs \int_{v^-}^{v^+} \frac{dv}{R} + rsh^2 \int_{v^-}^{v^+} \frac{adv}{(a^2 + rsv^2)R} \right] \tag{J.6.210}$$

Defining

$$g^2 = ra^2 + rqh^2, \text{ and } \int Rdv = I\,(X) = \frac{1}{2}\,[Rv + sqg^2\, I\,(\Psi)] \tag{J.6.211}$$

where $\int \frac{dv}{R} = I\ (\psi)$ (see J.6.194) (J.6.212)

and $\int \frac{adv}{(a^2 + rsv^2)R} = \frac{d\rho}{R} = J(\psi)$ (J.6.213)

we find that

$$\int_{\phi^-}^{\phi^+} R^3 d\phi = [aqrs\ I\ (X) + (aqrs)\ rsh^2\ I(\psi) + h^4\ J\ (\psi)] \tag{J.6.214}$$

Substituting this expression into (J.6.208) and recalling the definition (J.6.173) of the panel function J we find

$$\iint X\ ds = \frac{r}{3}\ (h^3\ J + \sum_k\ aqrs) \tag{J.6.215}$$

Recalling the computed values (J.6.179) and (J.6.181) of b, the integral $\iint X dS$ can be written

$$\iint X\ dS = \frac{r}{3}\ (h^2\ (\frac{-\kappa b}{s}) + rs\ \Sigma\ aq\ I\ (X) \Big|_{v^-}^{v^+}) \tag{J.6.216}$$

or $$\iint X\ dS = \frac{-rs}{3}\ h^2 \kappa\ b + \frac{s}{3}\ aq\ I(X) \Big|_{v^-}^{v^+} \tag{J.6.217}$$

Applying (J.6.212) and (J.6.194)

$$I(X) \Big|_{v^-}^{v^+} = \int_{v^-}^{v^+} Rdv = \frac{1}{2}\ \Delta(Rv) + \frac{1}{2} \int_{v^-}^{v^+} \frac{rsqa^2 + rsh^2}{R}\ dv \tag{J.6.218a}$$

$$= \frac{1}{2}\ \Delta(Rv) + \frac{1}{2}\ (rsqa^2 + rsh^2)\ I(\psi) \Big|_{v^-}^{v^+} \tag{J.6.218b}$$

by (J.6.212).

Recalling the definition (J.6.184) of I_k we have

$$dS' = \frac{-rs}{3}\ h^3\ b + \frac{s}{6} \sum_k\ a_k\ q_k\ \Delta(Rv) + \frac{s}{6} \sum_k\ a_k\ q_k\ (rs\ q_k\ a_k^2 + rsh^2) I_k \tag{J.6.219}$$

We now consider the other terms in (J.6.204).

We have

$$\int_{v_k^-}^{v_k^+} v \times dv = \int_{v_k^-}^{v_k^+} Rvdv = \tag{J.6.220}$$

(by (J.6.191))

$$\int R(qR \frac{\partial R}{\partial v})\, dv = q \int R^2 \frac{\partial R}{\partial v}\, dv = \frac{q}{3} \Delta\, (R^3) \tag{J.6.221}$$

Substituting (J.6.194), (J.6.219), and (J.6.221) in (J.6.204)

$$[F] = \frac{s}{2\kappa} \sum_k q_k\, ra_k\, \vec{v}_k\, \vec{v}_k^T\, sq_k \left\{ \Delta(Rv) + (rsq_k\, a_k^2 + rsh^2)\, I_k \right\}$$

$$+ \frac{s}{k} \sum_k q_k \vec{t}_k\, \vec{v}_k^{\,T}\, q_k\, (\frac{q}{3} \Delta\, (R^3)) - \frac{s}{\kappa} [G]\, (\frac{-rs}{3} h^2 \kappa\, b + \frac{1}{6} \sum_k s\, a_k\, q_k\, \Delta\, (Rv)$$

$$+ \frac{1}{6} \sum_k a_k q_k\, (rq_k\, a_k^{\,2} + rh^2)\, I_k) \tag{J.6.222}$$

J.6.5.7 Computation of H.

Recalling the definition (J.6.135)

$$H_{ijk} = \frac{1}{\kappa} \iint_{\Sigma'} \rho_i\, \rho_j\, (\tilde{\nabla}'_{2,Q})_k \psi\, ds' \tag{J.6.223}$$

we apply (J.6.93) to obtain

$$H_{ijl} = \frac{1}{\kappa} \int_{\partial\Sigma'} \rho_i\, \rho_j\, \frac{\vec{v}_l}{|\vec{v}|}\, \psi\, ds - \frac{1}{\kappa} \iint_{\Sigma'} \psi\, (\tilde{\nabla}'_{2,Q})_l\, (\rho_i\, \rho_j)\, dS' \tag{J.6.224}$$

Now,

$$(\tilde{\nabla}'_{2,Q})_l\, (\rho_i\, \rho_j) = \rho_i\, [G]_{lj} + [G]_{li}\, \rho_j \tag{J.6.225}$$

Combining (J.6.77-78) with (J.6.132), we see

$$\vec{b} = \frac{-1}{\kappa} \iint_{\Sigma'} \rho\, \psi\, dS' \tag{J.6.226}$$

and thus

$$- \frac{1}{\kappa} \iint_{\Sigma'} \psi \, (\tilde{\nabla}'_{2,Q})_k \, (\rho_i \, \rho_j) \, dS' =$$

$$- \frac{1}{\kappa} \iint_{\Sigma'} \psi \, (\rho_i \, [G]_{kj} + [G]_{ki} \, \rho_j) \, dS'$$

$$= [G]_{kj} \, \vec{b}_i + [G]_{ki} \, \vec{b}_j \qquad (J.6.227)$$

We now consider the first term of (J.6.224).

By (J.6.52) and (J.6.54)

$$\int_{\partial\Sigma'} \rho_i \, \rho_j \, \frac{\vec{\nu}_l}{|\vec{\nu}|} \, \psi \, ds =$$

$$\int_{\partial\Sigma'} (qra\nu_i + qsvt_i) \, (qra\nu_j + qsvt_j) \, \nu_l \, sq \, \psi \, dv \qquad (J.6.228)$$

$$= \sum_k a_k^2 \, (\vec{\nu}_k)_i \, (\vec{\nu}_k)_j \, (\vec{\nu}_k)_l \, sq_k \int_{v_k^-}^{v_k^+} \psi \, dv$$

$$+ \sum_k rsa_k \, (\vec{\nu}_k)_i \, (\vec{t}_k)_j \, (\vec{\nu}_k)_l \, sq \int_{v_{\bar{k}}}^{v_k^+} \psi \, dv$$

$$+ (\vec{t}_k)_i \, (\vec{t}_k)_j \, (\vec{\nu}_k)_l \, sq \int_{v_k^-}^{v_k^+} \psi \, v^2 \, dv \qquad (J.6.229)$$

Now by (J.6.191)

$$\frac{\partial R}{\partial v} = \frac{qv}{R} = qv\psi \qquad (J.6.230)$$

Thus

$$\int_{v_k^-}^{v_k^+} \psi \, v \, dv = q_k \, \Delta R \qquad (J.6.231)$$

and

$$\int_{v_k^-}^{v_k^+} \psi\, v^2\, dv = \int_{v_k^-}^{v_k^+} q_k \frac{\partial R}{\partial v}\, v\, dv \tag{J.6.232}$$

= (applying (J.6.194))

$$q_k\, \Delta(vR) - \frac{1}{2} q_k\, \Delta(vR) - \frac{q_k}{2} \int_{v_k^-}^{v_k^+} \frac{rsq_k\, a_k^2 + rsh^2}{R}\, dv \tag{J.6.233}$$

$$= \frac{1}{2} q_k\, \Delta(vR) - \frac{q_k}{2} (rsq_k\, a_k^2 + rsh^2)\, I_k \tag{J.6.234}$$

where we have used the definition (J.6.184) of I_k. Applying the latter definition, along with (J.6.231) and (J.6.234) to (J.6.229), we define

$$\bar{H}_{ijl} = \frac{1}{\kappa} \int_{\partial\Sigma'} \rho_i \rho_j \frac{\nu_l}{|\vec{v}|} \psi\, ds =$$

$$\frac{s}{\kappa} \sum_k a_k^2 (\vec{v}_k)_i (\vec{v}_k)_j (\vec{v}_k)_l\, q_k\, I_k$$

$$+ \frac{r}{\kappa} \sum_k a_k (\vec{v}_k)_i (\vec{t}_k)_j (\vec{v}_k)_l\, \Delta R$$

$$+ \frac{s}{2\kappa} \sum_k (\vec{t}_k)_i (\vec{t}_k)_j (\vec{v}_k)_l \begin{pmatrix} \Delta(vR) - \\ (rsq_k\, a_k^2 + rsh^2)\, I_k \end{pmatrix} \tag{J.6.235}$$

Substituting (J.6.227) and (J.6.235) in (J.6.224)

$$H_{ijk} = \bar{H}_{ijk} + [G]_{kj}\, \vec{b}_i + [G]_{ki}\, \vec{b}_j \tag{J.6.236}$$

This concludes the reduction of fundamental integrals to the edge and panel functions.

J.6.6 The Origin Shift

The computation of the entries of the matrices [S] and [D] has been based on the assumption that the local (ξ', η') coordinate system is centered on the projection (x', y') of the control point to the plane of the panel. In practice, however, we require the matrices $[S_0]$ and $[D_0]$ corresponding to a (ξ_0', η_0') coordinate system centered on a fixed point (0, 0) on the panel.

That is, S and D were defined in terms of coefficients σ_0, σ_ξ, $\cdots$, $\sigma_{\eta\eta}$, μ_0, μ_ξ, $\cdots$, $\mu_{\eta\eta}$ defining a source distribution and doublet distribution

$$\sigma(\xi_0', \eta_0') = \sigma_0 + \cdots + \frac{1}{2}\sigma_{\eta\eta}(\eta_0' - y')^2$$

$$\mu(\ _0', \eta_0') = \mu_0 + \mu_\xi(\xi_0' - x') + \cdots + \frac{1}{6}\mu_{\eta\eta\eta}(\eta_0' - y')^3 \qquad \text{(J.6.237)}$$

The matrices S_0 and D_0 are defined in terms of coefficients $\sigma_0{}^0$, $\cdots$, $\sigma_{\eta\eta}{}^0$, $\mu_0{}^0$, $\cdots$, $\mu_{\eta\eta\eta}^0$ defining the same source and doublet distributions by

$$\sigma(\xi_0', \eta_0') = \sigma_0{}^0 + \sigma_\xi{}^0\,\xi_0' + \cdots + \frac{1}{2}\sigma_{\eta\eta}{}^0\ \ \eta_0'^2$$

$$\mu(\xi_0', \eta_0') = \mu_0{}^0 + \mu_\xi{}^0\,\xi_0' + \cdots + \frac{1}{6}\mu_{\eta\eta\eta}^0\ \ \eta_0'^3 \qquad \text{(J.6.238)}$$

Then, while [S] and [D] are defined by (J.6.1-2), $[S_0]$ and $[D_0]$ are defined by

$$\begin{Bmatrix} \phi_S' \\ \vec{v}_S' \end{Bmatrix} = [S_0] \begin{Bmatrix} \sigma_0{}^0 \\ \cdot \\ \cdot \\ \sigma_{\eta\eta}{}^0 \end{Bmatrix} \qquad \text{(J.6.239)}$$

$$\begin{Bmatrix} \phi_D' \\ \vec{v}_D{}'^* \end{Bmatrix} = [D_0] \begin{Bmatrix} \mu_0{}^0 \\ \cdot \\ \cdot \\ \mu_{\eta\eta\eta}^0 \end{Bmatrix} \qquad \text{(J.6.240)}$$

To obtain $[S_0]$ and $[D_0]$ from [S] and [D], we must compute the matrices $[T_S]^{6x6}$ and $[T_D]^{10x10}$ such that

$$\begin{Bmatrix} \sigma_0 \\ \cdot \\ \cdot \\ \cdot \\ \sigma_{\eta\eta} \end{Bmatrix} = [T_S] \begin{Bmatrix} \sigma_0{}^0 \\ \cdot \\ \cdot \\ \cdot \\ \sigma_{\eta\eta}^0 \end{Bmatrix} \qquad \text{(J.6.241)}$$

$$\begin{Bmatrix} \mu_0 \\ \cdot \\ \cdot \\ \cdot \\ \mu_{\eta\eta\eta} \end{Bmatrix} = [T_D] \begin{Bmatrix} \mu_0{}^0 \\ \cdot \\ \cdot \\ \cdot \\ \mu_{\eta\eta\eta}^0 \end{Bmatrix} \qquad \text{(J.6.242)}$$

for then, combining (J.6.1-2) with (J.6.239-242), we have

$$[S_o] = [S]\,[T_S] \tag{J.6.243}$$

$$[D_o] = [D]\,[T_o] \tag{J.6.244}$$

Thus we need to compute $[T_S]$ and $[T_D]$, or, in particular T_D, since $[T_S]$ is just the upper left (6x6) corner of $[T_D]$. So, we rewrite the second equation in (J.6.238) as

$$\begin{aligned}\mu(\xi_o', \eta_o') = {} & \mu_o{}^o + \mu_\xi{}^o\,(\xi_o' - x' + x') + \mu_\eta{}^o\,(\eta_o' - y' + y') \\ & + \frac{1}{2}\,\mu_{\xi\xi}{}^o\,(\xi_o' - x' + x')^2 + \cdots \\ & + \frac{1}{6}\,\mu_{\eta\eta\eta}^o\,(\eta_o' - y' + y')^3\end{aligned} \tag{J.6.245}$$

Now, we equate the coefficients of $(\xi_o' - x')^i\,(\eta_o' - y')^j$, $i + j \leq 3$, in (J.6.237) and (J.6.245) to obtain

$$\begin{Bmatrix} i = 0 \\ j = 0 \end{Bmatrix} \quad \mu_o = \mu_o{}^o + \mu_\xi{}^o\,x' + \mu_\eta{}^o y' + \frac{1}{2}\,\mu_{\xi\xi}^o\,x'^2 + \cdots + \frac{1}{6}\,\mu_{\eta\eta\eta}^o\,y'^3 \tag{J.6.246a}$$

$$\begin{Bmatrix} i = 1 \\ j = 0 \end{Bmatrix} \quad \begin{aligned}\mu_\xi = {} & \mu_\xi{}^o + \mu_{\xi\xi}{}^o\,x' + \mu_{\xi\eta}{}^o\,y' + \frac{1}{2}\,\mu_{\xi\xi\xi}^o\,x'^2 \\ & + \mu_{\xi\xi\eta}^o\,x'y' + \frac{1}{2}\,\mu_{\xi\eta\eta}^o\,y'^2\end{aligned} \tag{J.6.246b}$$

$$\begin{Bmatrix} i = 0 \\ j = 1 \end{Bmatrix} \quad \begin{aligned}\mu_\eta = {} & \mu_\eta{}^o + \mu_{\xi\eta}{}^o\,x' + \mu_{\eta\eta}{}^o\,y' + \frac{1}{2}\,\mu_{\xi\xi\eta}^o\,x'^2 \\ & + \mu_{\xi\eta\eta}^o\,x'y' + \frac{1}{2}\,\mu_{\eta\eta\eta}^o\,y'^2\end{aligned} \tag{J.6.246c}$$

$$\begin{Bmatrix} i = 2 \\ j = 0 \end{Bmatrix} \quad \mu_{\xi\xi} = \mu_{\xi\xi}{}^o + \mu_{\xi\xi\xi}{}^o\,x' + \mu_{\xi\xi\eta}^o\,y' \tag{J.6.246d}$$

$$\begin{Bmatrix} i = 1 \\ j = 1 \end{Bmatrix} \quad \mu_{\xi\eta} = \mu_{\xi\eta}{}^o + \mu_{\xi\xi\eta}^o\,X' + \mu_{\xi\eta\eta}^o\,Y' \tag{J.6.246e}$$

$$\begin{Bmatrix} i = 0 \\ j = 2 \end{Bmatrix} \quad \mu_{\eta\eta} = \mu_{\eta\eta}{}^o + \mu_{\xi\eta\eta}^o\,X' + \mu_{\eta\eta\eta}^o\,Y' \tag{J.6.246f}$$

$$i + j = 3 \qquad \begin{aligned} \mu_{\xi\xi\xi} &= \mu^0_{\xi\xi\xi} \\ \mu_{\xi\xi\eta} &= \mu^0_{\xi\xi\eta} \\ \mu_{\xi\eta\eta} &= \mu^0_{\xi\eta\eta} \\ \mu_{\eta\eta\eta} &= \mu^0_{\eta\eta\eta} \end{aligned} \tag{J.6.246g}$$

Comparing (J.6.242) with (J.6.246), we see that the latter equation defines the entries of T_D :

$$[T_D] =$$

$$\left[\begin{array}{c|cc|ccc|cccc}
1 & x' & y' & \frac{1}{2}x'^2 & x'y' & \frac{1}{2}y'^2 & \frac{1}{6}x'^3 & \frac{1}{2}x'^2y' & \frac{1}{2}x'y'^2 & \frac{1}{6}y'^3 \\
\hline
0 & 1 & 0 & x' & y' & 0 & \frac{1}{2}x'^2 & x'y' & \frac{1}{2}y'^2 & 0 \\
 & 0 & 1 & 0 & x' & y' & 0 & \frac{1}{2}x'^2 & x'y' & \frac{1}{2}y'^2 \\
\hline
0 & & & 1 & 0 & 0 & x' & y' & 0 & 0 \\
 & 0 & & 0 & 1 & 0 & 0 & x' & y' & 0 \\
 & & & 0 & 0 & 1 & 0 & 0 & x' & y' \\
\hline
 & & & & & & 1 & 0 & 0 & 0 \\
 & & & & & & 0 & 1 & 0 & 0 \\
0 & 0 & & & 0 & & 0 & 0 & 1 & 0 \\
 & & & & & & 0 & 0 & 0 & 1
\end{array}\right]. \tag{J.6.247}$$

Introducing

$$\vec{d} = \begin{Bmatrix} x' \\ y' \end{Bmatrix} \tag{J.6.248}$$

and recalling the notation (J.6.141-142) which defines row vectors from tensors, and defining D as the 2x2x2 tensor

$$D_{ijk} = d_i \, d_j \, d_k \tag{J.6.249}$$

we have

$$T_D = \begin{array}{c} \\ 1 \\ \\ 2 \\ \\ 3 \\ \\ 4 \end{array} \begin{array}{c} \begin{array}{cccc} 1 & 2 & 3 & 4 \end{array} \\ \left[\begin{array}{c|c|c|c} 1 & \vec{d}^T & \frac{1}{2}\lfloor \vec{d}\,\vec{d}^T \rfloor_3 & \frac{1}{6}\lfloor D \rfloor_4 \\ \hline 0 & I & \begin{array}{cc} \vec{d}^T & 0 \\ 0 & \vec{d}^T \end{array} & \begin{array}{cc} \frac{1}{2}\lfloor dd^T \rfloor_3 & 0 \\ 0 & \frac{1}{2}\lfloor \vec{d}\vec{d}^T \rfloor_3 \end{array} \\ \hline 0 & 0 & I & \begin{array}{ccc} \vec{d}^T & 0 & 0 \\ 0 & \vec{d}^T & 0 \\ 0 & 0 & \vec{d}^T \end{array} \\ \hline 0 & 0 & 0 & I \end{array}\right] \end{array}$$

(J.6.250)

Similarly, T_S is just the quadratic portion of T :

$$T_S = \left[\begin{array}{c|c|c} 1 & d & \frac{1}{2}\lfloor \vec{d}\vec{d}^T \rfloor_3 \\ \hline 0 & I & \begin{array}{cc} \vec{d}^T & 0 \\ 0 & \vec{d}^T \end{array} \\ \hline 0 & 0 & I \end{array}\right]$$

(J.6.251)

Combining (J.6.152), (J.6.243) and (J.6.251) we get $[S_o]$ =

$$
\left[\begin{array}{c|c|c}
b & \vec{b}^T + b\vec{d}^T & \frac{1}{2} b \lfloor \vec{d}\vec{d}^T \rfloor_3 + \lfloor \vec{b}\vec{d}^T \rfloor_3 - \frac{1}{2} \lfloor F \rfloor_3 \\
\hline
\vec{a} & a\vec{d}^T + B & \begin{array}{l} \frac{1}{2} \vec{a}_1 \lfloor \vec{d}\vec{d}^T \rfloor_3 + \lfloor B_{1,\cdot} \vec{d}^T \rfloor_3 + rs \lfloor H_1 \rfloor_3 \\ \\ \frac{1}{2} \vec{a}_2 \lfloor \vec{d}\vec{d}^T \rfloor_3 + \lfloor B_{2,\cdot} \vec{d}^T \rfloor_3 + \lfloor H_2 \rfloor_3 \end{array} \\
\hline
a & a\vec{d}^T - hr\,(G\vec{a})^T & \begin{array}{l} \frac{1}{2} a \lfloor \vec{d}\vec{d}^T \rfloor_3 - hr \lfloor [G]\,[a\vec{d}^T] \rfloor_3 \\ \\ -\frac{rh}{2} \lfloor GB \rfloor_3 \end{array}
\end{array}\right]
\qquad (J.6.252)
$$

Combining (J.6.164), (J.6.244) and (J.6.247), $[D_o]$ =

$$
\left[\begin{array}{c|c|c|c}
ra & ra\vec{d}^T - h\,(G\vec{a})^T & \begin{array}{l} ra \lfloor \vec{d}\vec{d}^T \rfloor_3 - \\ h \lfloor [G]\,[\vec{a}\vec{d}^T] \rfloor_3 \\ -\frac{h}{2} \lfloor GB \rfloor_3 \end{array} & \begin{array}{l} ra \lfloor D \rfloor_4 - \frac{h}{2} \lfloor (G\vec{a})_i\, d_j d_k \rfloor_4 \\ -\frac{h}{2} \lfloor [GB]_{ij} d_k \rfloor_4 - \frac{h}{6} \lfloor H \rfloor_4 \end{array} \\
\hline
0 & ra\,I & \begin{array}{c|c} ra\vec{d}^T - \vec{h}\,(G\vec{a})^T & 0 \\ \hline 0 & ra\vec{d}^T - h\,(G\vec{a})^T \end{array} & \begin{array}{c|c} ra \lfloor \vec{d}\vec{d}^T \rfloor_3 & 0 \\ h \lfloor (Ga)\,\vec{d}^T \rfloor_3 - \frac{h}{2} \lfloor GB \rfloor_3 & \\ \hline 0 & ra \lfloor \vec{d}\vec{d}^T \rfloor_3 \\ & -h \lfloor (G\vec{a})\,\vec{d}^T \rfloor_3 - \frac{h}{2} \lfloor GB \rfloor_3 \end{array} \\
\hline
0 & -(Ga)^T & \begin{array}{l} -\lfloor [G]\,[\vec{a}\vec{d}^T] \rfloor_3 \\ -\lfloor GB \rfloor_3 \end{array} & \begin{array}{l} -\frac{1}{2} \lfloor (G\vec{a})_i\, d_j\, d_k \rfloor_4 \\ -\lfloor [GB]_{ij}\, d_k \rfloor_4 - \frac{1}{2} \lfloor H \rfloor_4 \end{array}
\end{array}\right]
$$

(J.6.253)

J.6.7 Finite Parts of Integrals

In section J.6.5.1 we evaluated the integral

$$a = \frac{-sh}{\kappa} \iint_{\Sigma' \cap Dp} \frac{1}{\rho} \frac{\partial \psi}{\partial \rho} \, dS' \tag{J.6.254}$$

for Σ' a subinclined panel. In doing so, we discarded a term, leaving the justification for discarding that term to this section.

We will show in section J.6.7.4 that the term we discard is in fact zero if we only consider the "finite part" of the integral (J.6.254). The finite part of an integral is a concept we define in section J.6.7.1, and for which we cite certain well-known properties in section J.6.7.2. Next, in section J.6.7.3, we review the manipulations of integrals we have performed prior to Appendix J and conclude that they are still valid if we consider only the finite parts of various integrals. We then note in section J.6.7.4 that we really want to compute only the finite part of (J.6.254), and thus we properly discarded the extra term which appeared in section J.6.5.1.

J.6.7.1 Definition of a Finite Part

Let f be a function on a surface S (though our definition will have an obvious extension to functions on a line or in a volume of space) of finite area. Let S_ε be the set of points in S which are distance greater than ε from any point on S at which f is infinite, where $\varepsilon > 0$. Then we define

$$\overset{*}{\iint_S} f \, dS = \lim_{\varepsilon \to 0} \iint_{S_\varepsilon} f \, dS \tag{J.6.255}$$

and we call the integral on the left side of (J.6.255) the finite part of the integral of f over S. We call

$$\iint_S f \, dS - \overset{*}{\iint_S} f \, dS \tag{J.6.256}$$

the infinite part of the integral whenever it is non-zero.

J.6.7.2 Properties of a Finite Part

Several important properties of ordinary integrals of bounded functions also hold for finite parts of integrals. First, the standard integration by parts theorems in several variables (the divergence theorem, Stokes' Theorem, Green's Theorem) hold for finite parts of integrals.

Second, differentiation with respect to a parameter on which f depends may be moved under the integral. That is, if f is a function of t,

$$\frac{\partial}{\partial t} \overset{*}{\iint_S} f \, dS = \iint_S \frac{\partial f}{\partial t} \, dS \tag{J.6.257}$$

These results are discussed in the paper of Robinson (reference J.3).

J.6.7.3 Finite Parts and the Integral Equation

In section B.0, we quoted the fundamental integral equation (B.0.1),

$$\phi = \frac{1}{\kappa} \overset{*}{\iint_{S \cap Dp}} -\frac{\sigma}{R} + \mu \hat{n} \cdot \tilde{\nabla} \left(\frac{1}{R}\right) dS \qquad \text{(J.6.258)}$$

But thereafter, we treated this integral as though it were an ordinary integral rather than a finite part integral. In particular, we applied Stokes' Theorem and took the gradient operator under the integral equation to obtain (B.3.31)

$$\vec{v}(P) = \frac{1}{\kappa} \overset{*}{\iint_{S \cap Dp}} \left[-\sigma \vec{\nabla}_p \left(\frac{1}{R}\right) + (\hat{n} \times \vec{\nabla}_Q \mu) \times \tilde{\nabla}\left(\frac{1}{R}\right)\right] dS$$

$$+ \frac{1}{\kappa} \overset{*}{\iint_{S \cap Dp}} \mu \tilde{\nabla}_Q \left(\frac{1}{R}\right) \times \vec{dl} \qquad \text{(J.6.259)}$$

The derivation of (J.6.259) from (J.6.258) is only justifiable, however, in light of the results we quote in section J.6.7.2.

J.6.7.4 Finite Parts and PIC Computation

Now, in appendix J, we have consistently ignored the fact that we really were interested only in the finite parts of the integrals which defined. Until section J.6.5.1, where we attempted actually to evaluate such an integral, this caused no problem. In that section, however, we obtained an infinite term because we failed to evaluate only the finite part of the integral (J.6.254). That is, we should compute

$$a = \overset{*}{\iint_{\Sigma' \cap Dp}} \frac{1}{\rho} \frac{\partial \psi}{\partial \rho} dS'$$

$$= -\frac{sh}{\kappa} \lim_{\varepsilon \to 0} \iint_{\Sigma'_\varepsilon} \frac{1}{\rho} \frac{\partial \psi}{\partial \rho} dS' \qquad \text{(J.6.260)}$$

where Σ'_ε is a polygonal region, entirely within Dp, which approaches Σ'nDp as ε goes to zero (cf., figure J.26)

Then, if Σ'_ε has K_ε edges, by (J.6.169-170), we have

$$a = \lim_{\varepsilon \to 0} \frac{-sh}{\kappa} \sum_{k=1}^{K_\varepsilon} \int_{\phi_k^-}^{\phi_k^+} \psi \, d\phi - \int_{\phi_k^-}^{\phi_k^+} \frac{1}{\varepsilon} \, d\phi \tag{J.6.261}$$

$$= \lim_{\varepsilon \to 0} \frac{1}{\kappa} \sum_{k=1}^{K_\varepsilon} \int_{\phi_k^-}^{\phi_k^+} \psi \, d\phi$$

$$- \lim_{\varepsilon \to 0} \frac{1}{\varepsilon} \sum_{k=1}^{K_\varepsilon} \int_{\phi_k^-}^{\phi_k^+} d\phi \tag{J.6.262}$$

But it follows from section J.5 (cf. (J.5.22), along with figure J.20, which shows that $(s+t)/(s-t) > 0$) that ϕ is a smooth function on Dp, and bounded on Σ'_ε. In particular, ϕ is single-valued. Thus by the fundamental theorem of calculus

$$\sum_{k=1}^{K_\varepsilon} \int_{\phi_k^-}^{\phi_k^+} d\phi = \int_{\partial\Sigma'_\varepsilon} d\phi = 0 \tag{J.6.263}$$

and thus the second term of (J.6.262) is zero, and thus should be neglected, as we do in section J.6.5.1.

J.6.7.5 Summary of Finite Part Integrals

We now briefly summarize the role of finite parts of integrals in influence coefficient computation. First, we state the fundamental integral equation (B.0.1), which involves the finite part of a surface integral, and whose validity we do not prove, but is discussed in Ward (reference 1.5) and in more detail in Ehlers, et. al. (reference 4.9). Second, we derive (B.3.31) from (B.0.1), a derivation which is only valid because of the properties (whose validity we also do not prove) of finite parts of integrals cited in section J.6.7.2. Third, for reasons of clarity, we leave the finite parts symbol off many integrals in appendix J. Fourth, we see that a term which appears in section J.6.5.1 must be discarded, since we only require the finite part of the integral which is being evaluated. In section J.7 we will see that the remaining term in this expression can be evaluated in closed form.

J.7 Edge and Panel Functions

In section J.7.1, we compute the edge function

$$I_k(\psi) - \int_{v_k^-}^{v_k^+} \psi \, dv \tag{J.7.1}$$

and the function

$$J_k(\psi) = \int_{\phi_k^-}^{\phi_k^+} \psi \, d\phi \tag{J.7.2}$$

where the panel function J is given by (cf. (J.6.173))

$$J = \sum_k h \, J_k(\psi) - 2\pi \, \text{sign}(h) \, C_\theta \tag{J.7.3}$$

We also compute integrals I(X) and J(X) used in sections J.4 - J.6 (cf.(J.4.68), (J.5.115), (J.6.212))

$$I_k(X) = \int_{v_k^-}^{v_k^+} R_k \, dv \tag{J.7.4}$$

$$J_k(X) = \int_{v_k^-}^{v_k^+} \frac{Ra_k}{\rho_k^2} \, dv = \int_{\phi_k^-}^{\phi_k^+} R \, d\phi \tag{J.7.5}$$

J.7.1 Expressions for Edge and Panel Functions

J.7.1.1 Subsonic Flow

Since the flow is subsonic, $r = s = q_k = 1$, and (J.6.58-59) become

$$\rho_k^2 = a_k^2 + v_k^2 \tag{J.7.6}$$

$$R^2 = a_k^2 + v_k^2 + h^2 \tag{J.7.7}$$

By (J.4.66) we have

$$J_k(\psi) = \int_{v_k^-}^{v_k^+} \frac{a_k}{a_k^2 + v_k^2} \, dv$$

$$= \int_{v_k^-}^{v_k^+} R_k(a_k^2 + v_k^2)\, dv \qquad (J.7.8)$$

We now exhibit without derivation the functions which are the indefinite integrals $I(\psi)$, $J(\psi)$, $I(X)$, $J(X)$. The integrations can be verified by differentiating the functions with respect to v, while noting (J.7.6-7). The differentiations are tedious but straightforward.

We find

$$I(\psi) = \int \frac{dv}{R} = \frac{1}{2} \log\left(\frac{R+v}{R-v}\right) \qquad (J.7.9)$$

$$J(\psi) = \int \frac{a}{R(a^2+v^2)}\, dv = \frac{1}{h}\, ph\ (hv, aR) \qquad (J.7.10)$$

$$I(X) = \int R dv = \frac{1}{2}\left(vR + (a^2 + h^2) I(\psi)\right) \qquad (J.7.11)$$

$$J(X) = \int \frac{a\ R\ dv}{a^2 + v^2} = h^2\ J(\psi) + aI(\psi) \qquad (J.7.12)$$

Clearly

$$I_k(\psi) = I\ (\psi)\ (R_k^+, v_k^+) - I\ (\psi)\ (R_k^-, v_k^-) \qquad (J.7.13)$$

Similarly, evaluation at both endpoints of the intersection of the panel edge and the domain of dependence gives us the remaining definite integrals.

J.7.1.2 Subsonic Edges of Subinclined Panels in Supersonic FLow

Now (J.6.58-59) become

$$\rho^2 = v^2 - a^2 \qquad (J.7.14)$$

$$R^2 = v^2 - a^2 - h^2 \qquad (J.7.15)$$

since $s = -1$, $r = +1$, $q = +1$. Also, we have

$$J_k(\psi) = \int_{V_k^-}^{v_k^+} \frac{a_k R}{a_k^2 - v^2}\, dv \qquad (J.7.16)$$

The indefinite integrals now become

$$I(\psi) = \int \frac{dv}{R} = \frac{1}{2} \log\left(\frac{v+r}{v-r}\right) \tag{J.7.17}$$

$$J(\psi) = \int \frac{adv}{(a^2 - v^2)R} = -\frac{1}{h} \text{ ph } (hv, aR) \tag{J.7.18}$$

$$I(X) = \int Rdv = \frac{1}{2}(vR - (a^2 + h^2) I(\psi)) \tag{J.7.19}$$

$$J(X) = \int \frac{aR\ dv}{a^2 - v^2} = - h^2 J(\psi) - aI(\psi) \tag{J.7.20}$$

J.7.1.3 Supersonic Edges of Subinclined Panels

Now $r = +1$, $s = -1 = q$, so

$$\rho^2 = a^2 - v^2 \tag{J.7.21}$$

$$R^2 = a^2 - h^2 - v^2 \tag{J.7.22}$$

and

$$J_k (\psi) = \int_{V_k^-}^{V_k^+} \frac{a_k R dv}{a_k^2 - v^2} \tag{J.7.23}$$

The indefinite integrals become

$$I(\psi) = \int \frac{dv}{R} = -\text{ph } (v,R) \tag{J.7.24}$$

$$J(\psi) = \int \frac{adv}{(a^2 - v^2)R} = -\frac{1}{h} \text{ ph } (hv,aR) \tag{J.7.25}$$

$$I(X) = \int Rdv = \frac{1}{2} (vR + (a^2 - h^2) I(\psi)) \tag{J.7.26}$$

$$J(X) = \int \frac{aRdv}{a^2 - v^2} = - h^2 J(\psi) + aI(\psi) \tag{J.7.27}$$

J.7.1.4 Superinclined Panels

Now $r = s = q = -1$, and

$$\rho^2 = a^2 + v^2 \tag{J.7.28}$$

$$R^2 = h^2 - a^2 - v^2 \tag{J.7.29}$$

and

$$J_k(\psi) = \int_{v_k^-}^{v_k^+} \frac{a_k dv}{(a_k^2 + v^2)R} \tag{J.7.30}$$

The indefinite integrals become

$$I(\psi) = \int \frac{dv}{R} = -ph(hv,R) \tag{J.7.31}$$

$$J(\psi) = \int \frac{adv}{R(a^2 + v^2)} = -\frac{1}{h}\, ph(hv,aR) \tag{J.7.32}$$

$$I(\chi) = \int Rdv = \frac{1}{2}\,(vR - (a^2 - h^2)\; I(\psi)) \tag{J.7.33}$$

$$J(\chi) = \int \frac{aR\; dv}{a^2 + v^2} = h^2\; J(\psi) - aI(\psi) \tag{J.7.34}$$

J.7.1.5 Uniform Formulas

We unify the results of section J.7.1 for $I_k(\psi)$ and $J_k(\psi)$. We obtain

$$I_k(\psi) = \begin{cases} \frac{1}{2}\log\left(\frac{R+v}{R-v}\right)\Big|_-^+ & s = 1 \\ \frac{1}{2}\log\left(\frac{v+R}{v-R}\right)\Big|_-^+ & s = -1,\; q = 1 \\ -ph\;(hv,R) & q = -1 \end{cases} \tag{J.7.35}$$

$$J_k(\psi) = -\frac{1}{h}\, ph(hv,aR)\Big|_-^+ \tag{J.7.36}$$

where evaluation occurs at the two endpoints of the intersection of the edge and the domain of dependence.

J.7.2 Computation of Edge and Panel Function Arguments in Reference Coordinates

In this section, we compute h, v, a, and

$$g = \sqrt{rsq\; a^2 + rsh^2} \tag{J.7.37}$$

in reference coordinates. These quantities are computed in reference coordinates in PAN AIR to minimize numerical error.

J.7.2.1 Computation of h

By (J.6.41)

$$h = z' - \zeta' = \begin{Bmatrix} 0 \\ 0 \\ 1 \end{Bmatrix} \cdot \quad A \quad (P - Q_0) \tag{J.7.38}$$

where Q_0 is any point on the panel, such as the panel center, and A is the reference to local transformation.

Thus

$$h = \lfloor 0 \; 0 \; 1 \rfloor \quad [A] \quad (\vec{P} - \vec{Q}_0) \tag{J.7.39}$$

$$= \sum_{j=1}^{3} A_{3j} \quad (\vec{P} - \vec{Q}_0)_j \tag{J.7.40}$$

Applying (E.0.1)

$$h = \frac{\beta}{\{\hat{n}_0, \hat{n}_0\}} \; \hat{n}_0 \cdot (\vec{P} - \vec{Q}_0) \tag{J.7.41}$$

J.7.2.2 Computation of v

By (J.6.47)

$$v = \langle \vec{t}_k, \vec{\rho} \rangle = \vec{t}_k^{\,T} [G] \vec{\rho} \tag{J.7.42}$$

where G, $\vec{t}_k$, and $\vec{\rho}$ are defined in section J.6.1.4. Now, define a 3-vector

$$\vec{t}' = \begin{Bmatrix} \vec{t}_k \\ -- \\ 0 \end{Bmatrix} \tag{J.7.43}$$

Next, we note from (E.3.24) that

$$\begin{bmatrix} r & s_{rs} \end{bmatrix} = [A^{-T}] \; C_0 \; [A^{-1}] \tag{J.7.44}$$

So,

$$v = \vec{t}_k^{\,T} \begin{bmatrix} rs & 0 \\ 0 & 1 \end{bmatrix} \vec{\rho}$$

$$= t'^T \begin{bmatrix} rs & & \\ & 1 & \\ & & s \end{bmatrix} \begin{Bmatrix} \vec{\rho} \\ 0 \end{Bmatrix} \qquad (J.7.45)$$

$$= s\vec{t}'^T \begin{bmatrix} r & & \\ & s & \\ & & rs \end{bmatrix} A \; (\vec{Q} - \vec{P}) \qquad (J.7.46)$$

$$= s\vec{t}' \; [A^{-T}] \; C_0 \; (\vec{Q} - \vec{P}) \qquad (J.7.47)$$

$$= s \; [A^{-1} \vec{t}', \; \vec{Q} - \vec{P}] \qquad (J.7.48)$$

$$= s \; |A^{-1} \vec{t}'| \; [\vec{t}_0, \; \vec{Q} - \vec{P}] \qquad (J.7.49)$$

where $\vec{t}_0$ is the unit edge tangent, $\vec{P}$ is the field point, and $\vec{Q}$ lies on the edge.

Noting (J.6.42-43), we see that

$$\vec{t}' = \frac{A\vec{t}}{|\langle A\vec{t}, \; A\vec{t}\rangle|^{\frac{1}{2}}} \qquad (J.7.50)$$

where $\vec{t}$ is any tangent vector in reference coordinates. Thus we define

$$\tau = \frac{1}{|A^{-1} \vec{t}'|} = |\langle A\vec{t}_0, \; A\vec{t}_0\rangle|^{\frac{1}{2}}$$

$$= \left|\vec{t}_0^{\,T} A^T \begin{bmatrix} G & 0 \\ 0 & 0 \\ 0 & 0 \end{bmatrix} A\hat{t}_0\right|^{\frac{1}{2}} = |\vec{t}_0^{\,T} \, C \, \vec{t}_0|^{\frac{1}{2}}$$

$$= |[\hat{t}_0, \; \hat{t}_0]|^{\frac{1}{2}} \qquad (J.7.51)$$

where we have chosen a unit tangent vector $\hat{t}_0$.

Then

$$v = \frac{s}{\tau} [\hat{t}_0, \; \vec{Q} - \vec{P}] \qquad (J.7.52)$$

J.7.2.3 Computation of a

The edge distance a_k is (cf (J.6.46))

$$a_k = \vec{n}_k \cdot \vec{\rho}_k \tag{J.7.53}$$

where

$$\vec{n} = \begin{Bmatrix} t_\eta \\ -t_\xi \end{Bmatrix} \tag{J.7.54}$$

Note that

$$\vec{t}' \times \vec{n}' = \begin{Bmatrix} t_\xi \\ t_\eta \\ o \end{Bmatrix} \times \begin{Bmatrix} 0 \\ 0 \\ 1 \end{Bmatrix} = \begin{Bmatrix} t_\eta \\ -t_\xi \\ 0 \end{Bmatrix} \tag{J.7.55}$$

Thus

$$a = \left(\vec{t}' \times \begin{Bmatrix} 0 \\ 0 \\ 1 \end{Bmatrix}\right) \cdot (\vec{Q}' - \vec{P}') \tag{J.7.56}$$

$$= \begin{Bmatrix} 0 \\ 0 \\ 1 \end{Bmatrix} \cdot \left\{((\vec{Q}' - \vec{P}') \times \vec{t}')\right\}$$

$$= \begin{Bmatrix} 0 \\ 0 \\ 1 \end{Bmatrix} \cdot \left\{A(Q - P) \times \frac{A\,\hat{t}_o}{\tau}\right\} \tag{J.7.57}$$

$$= \text{(cf. (E.1.12))} \quad \begin{Bmatrix} 0 \\ 0 \\ 1 \end{Bmatrix} \cdot \frac{\det A}{\tau} A^{-T} \left\{((\vec{Q} - \vec{P}) \times \hat{t}_o)\right\} \tag{J.7.58}$$

$$= \frac{\det A}{\tau} \quad (A^{-1}_{\cdot,3}) \cdot ((\vec{Q} - \vec{P}) \times \hat{t}_o) \tag{J.7.59}$$

= (cf (E.3.59))

$$\frac{\det A}{\tau} \quad \frac{r}{\beta\,|\{n_o, n_o\}|^{\frac{1}{2}}} \quad B_o\,\hat{n}_o \cdot ((\vec{Q} - \vec{P}) \times \hat{t}_o) \tag{J.7.60}$$

Finally, applying (E.3.90) to obtain det A,

$$a = \frac{r \ \beta}{\tau \left| \{n_o, n_o\} \right|^{\frac{1}{2}}} \quad \{ \hat{n}_o, (\vec{Q} - \vec{P}) \times \hat{t}_o \} \tag{J.7.61}$$

J.7.2.4 Computation of g

Applying (J.6.59)

$$g^2 = sq \ (R^2 - qv^2) \tag{J.7.62}$$

$$= sq \ ([\vec{Q} - \vec{P}, \vec{Q} - \vec{P}] - \frac{q}{\tau^2} [\hat{t}_o, \vec{Q} - \vec{P}]^2) \tag{J.7.63}$$

Now we use the following identity, which we prove shortly. For arbitrary vectors a and b, and a matrix C,

$$(\vec{a} \times \vec{b})^T \ [C^{-1}] \ (\vec{a} \times \vec{b}) = \det (C^{-1})((\vec{a}^T \ C\vec{a}) \ (\vec{b}^T \ C\vec{b}) - (\vec{a}^T \ C\vec{b})^2) \tag{J.7.64}$$

We apply (J.7.64) to (J.7.63) with

$$\vec{a} = \vec{Q} - \vec{P}$$

$$\vec{b} = \frac{\hat{t}_o}{\tau} = \vec{t}$$

$$[C] = [C_o] \tag{J.7.65}$$

Since (cf. E.2.9))

$$C_o^{-1} = \frac{1}{s\beta^2} \ B_o \tag{J.7.66}$$

we get (by J.7.64)

$$\frac{1}{s\beta^2}\left\{(\vec{Q} - \vec{P}) \times \vec{t}, (\vec{Q} - \vec{P}) \times \vec{t}\right\} =$$

$$\frac{1}{\beta^4} \ ([\vec{Q} - \vec{P}, \vec{Q} - \vec{P}] \ [\vec{t},\vec{t}] - [\vec{Q} - \vec{P}, \vec{t}])^2 \tag{J.7.67}$$

= (cf. (J.7.51))

$$\frac{s}{\beta^4} \ g^2 \tag{J.7.68}$$

Here we use the fact (cf. (J.7.51))

$$[\hat{t}_o, \hat{t}_o] = q \ \tau^2 \tag{J.7.69}$$

Thus

$$g^2 = \beta^2 \left\{ (\vec{Q} - \vec{P}) \times \frac{\hat{t}_o}{\tau} , (\vec{Q} - \vec{P}) \times \frac{\hat{t}_o}{\tau} \right\} \tag{J.7.70}$$

We now need only to prove (J.7.64)

We prove in general, for vectors, $\vec{a}, \vec{b}, \vec{c}, \vec{d}$, and a matrix C:

$$(\vec{a} \times \vec{b})^T C (\vec{c} \times \vec{d}) =$$

$$(\det C) [(\vec{a}^T C^{-1} \vec{c}) (\vec{b}^T C^{-1} \vec{d}) - (\vec{a}^T C^{-1} \vec{d}) (\vec{b}^T C^{-1} \vec{c})] \tag{J.7.71}$$

Now, by (E.1.23)

$$[C] (\vec{c} \times \vec{d}) = (\det C) (C^{-1} \vec{c}) \times (C^{-1} \vec{d}) \tag{J.7.72}$$

Thus

$$(\vec{a} \times \vec{b})^T [C] (\vec{c} \times \vec{d}) =$$

$$(\det C) (\vec{a} \times \vec{b}) \cdot (C^{-1} \vec{c} \times C^{-1} \vec{d}) \tag{J.7.73}$$

Now, using the notation of section B.3, for vectors $\vec{a}, \vec{b}, \vec{e}, \vec{f}$,

$$(\vec{a} \times \vec{b}) \cdot (e \times f) = \sum_{ijmn} (\varepsilon_{ijk} a_i b_j) (\varepsilon_{mnk} e_m f_n) \tag{J.7.74}$$

Now, recalling (B.3.31):

$$(\vec{a} \times \vec{b}) \times \vec{c} = -(\vec{b} \cdot \vec{c}) \vec{a} + (\vec{a} \cdot \vec{c}) \vec{b} \tag{J.7.75}$$

we convert to ε notation and obtain

$$((\vec{a} \times \vec{b}) \times \vec{c})_k =$$

$$\sum_{ijmn} \varepsilon_{ijk} (\varepsilon_{mni} a_m b_n) c_j = \tag{J.7.76}$$

$$- (\vec{b} \cdot \vec{c}) a_k + (\vec{a} \cdot \vec{c}) b_k =$$

$$- \sum_n (b_n c_n) a_k + \sum_m a_m c_m b_k = \tag{J.7.77}$$

$$- \sum_{jnm} \delta_{jn} \delta_{km} a_m b_n c_j + \sum_{jmn} \delta_{jm} \delta_{kn} a_m b_n c_j \tag{J.7.78}$$

where δ is the Kronecker delta (zero unless the two subscripts are equal, in which case it equals one).

Now, noting that $\varepsilon_{ijk} = \varepsilon_{jki}$, (J.7.76-78) yield

$$\sum_i \varepsilon_{jki}\varepsilon_{mni} = \delta_{jm}\delta_{kn} - \delta_{jn}\delta_{km} \tag{J.7.79}$$

Applying (J.7.79) to (J.7.74)

$$(\vec{a} \times \vec{b}) \cdot (\vec{e} \times \vec{f}) = \sum_{ijmn} \varepsilon_{ijk}\, \varepsilon_{mnk}\, a_i b_j e_m f_n \tag{J.7.80}$$

$$= \sum_{ijmn} (\delta_{im}\delta_{jn} - \delta_{in}\delta_{jm})\, a_i\, b_j\, e_m\, f_n$$

$$= (\vec{a} \cdot \vec{e})\,(\vec{b} \cdot \vec{f}) - (\vec{a} \cdot \vec{f})\,(\vec{b} \cdot \vec{e}) \tag{J.7.81}$$

Substituting (J.7.80-81) into (J.7.73)

$$(\vec{a} \times \vec{b})^T\, C\, (\vec{c} \times \vec{d}) =$$

$$(\det C) \begin{pmatrix} (\vec{a}^T C^{-1}\vec{c})\,(\vec{b}^T C^{-1}\vec{d}) \\ -(\vec{a}^T C^{-1}\vec{d})\,(\vec{b}^T C^{-1}\vec{c}) \end{pmatrix} \tag{J.7.82}$$

which is (J.7.64) with C^{-1} replacing C.

J.8 Rationalization Formulas

The computation of the edge and panel functions has been described in section J.7. These formulas are not always computationally stable. In this section we describe the actual formulas we use to compute the edge and panel functions.

J.8.1 Edge Functions

In this section we will discuss the computation of the quantites

$$\hat{I} = \frac{q}{\tau} \; I(\psi) \Big|_{v^-}^{v^+} \tag{J.8.1}$$

$$\Delta\vec{R} = \vec{R}\Big|_{\vec{r}_+} - \vec{R}\Big|_{\vec{r}_-} \tag{J.8.2}$$

$$\hat{K} = \frac{1}{\tau^2} \; \left(q\Delta R - \frac{1}{2}(v_+ + v_-) \; I(\psi)\Big|_{v^-}^{v^+}\right) \tag{J.8.3}$$

where

$$\tau = |[\hat{t}_o, \hat{t}_o]|^{\frac{1}{2}} \tag{J.8.4}$$

$$q = \text{sign}\,[\hat{t}_o, \hat{t}_o] \tag{J.8.5}$$

$$I(\psi) = \begin{cases} \frac{1}{2} \log\left(\frac{v+R}{v-R}\right) & q = +1 \\ -ph(V,R) & q = -1 \end{cases} \tag{J.8.6}$$

$$\vec{r} = \vec{p} - \vec{Q} \tag{J.8.7}$$

$$R = [\vec{r}, \vec{r}]^{\frac{1}{2}} \tag{J.8.8}$$

and r_+, v_+ denote the values of r and v at the upper and lower end points of $E \cap D_p$, where E is the edge in question. We use a Δ to denote the difference of a value at the endpoints, and a bar to denote the average.

The procedure used to evaluate these edge functions is as follows.

In section J.8.1.1, we will discuss edges for which

$$\tau^2 > 10^{-4} \tag{J.8.9}$$

We will call these non-sonic edges, and will distinguish four cases. We will first consider the case where at most one endpoint of the edge lies in the interior of D_p, dividing this into the regular case of a supersonic edge or $R \leq .95v$, and a special case of a subsonic edge and $R > .95v$. We will also consider the case of both endpoints lying within the interior of D_p. This is divided into a regular case and a special case in which v changes sign ($v_- < 0 < v_+$) and $g^2 \ll 1$.

In section J.8.1.2 we will discuss nearly sonic edges, for which

$$10^{-10} \leq \tau^2 \leq 10^{-4} \tag{J.8.10}$$

Here the regular case is

$$q = 1$$

or

$$\text{sign}\,(R_+R_- + v_+v_-) = 1 \tag{J.8.11}$$

In section J.8.13, we will consider essentially sonic edges, for which

$$\tau^2 < 10^{-10} \tag{J.8.12}$$

J.8.1.1 Non-Sonic Edges

We will calculate

$$\hat{I} = \frac{q}{\tau}\left(I(\psi)\big|_{v_+} - I(\psi)\big|_{v_-}\right) \tag{J.8.13}$$

and

$$\vec{\Delta R} = \vec{R}\big|_{r_+} - \vec{R}\big|_{r_-} \tag{J.8.14}$$

When an edge intersects the Mach cone, it is possible to compute these functions without actually evaluating the point of intersection. We have

$$R\big|_{\text{Mach cone}} = 0 \tag{J.8.15}$$

(subsonic)

$$\left.\begin{aligned} I(\psi)\big|_{v_+,\text{Mach cone}} &= 0 \\ I(\psi)\big|_{v_-,\ \text{M.C.}} &= 0 \end{aligned}\right\} \quad q = +1 \tag{J.8.16}$$

(supersonic)

$$\left.\begin{aligned} I(\psi)\big|_{v_+,\ \text{M.C.}} &= 0 \\ I(\psi)\big|_{v_-,\ \text{M.C.}} &= 0 \end{aligned}\right\} \quad q = -1 \tag{J.8.17}$$

Thus, when only one endpoint of the edge E lies inside the Mach cone, (we are now treating the case of supersonic flow), we need compute only one elementary transcendental function. For a subsonic edge, we would then compute

$$I(\psi) = \frac{1}{2} \log \frac{v+R}{v-R} \qquad (q = +1) \tag{J.8.18}$$

while for a supersonic edge we would have

$$I(\psi)\Big|_v = -ph(v,R) \qquad (q = -1) \tag{J.8.19}$$

If we recall equation (J.7.62) we obtain

$$R^2 = qv^2 + sqg^2 = \begin{cases} v^2 - g^2 & (q = +1,\ s = -1) \\ g^2 - v^2 & (q = -1,\ s = -1) \end{cases} \tag{J.8.20}$$

we see that some difficulties may arise in the evaluation of $I(\psi)\big|_v$ for subsonic edges when g^2 is very small, for then $R \approx v$ and the log function in equation (J.8.18) blows up. Thus, for the very special case in which (a) one end of $E \cap D_p$ lies on the Mach cone (E subsonic) and (b) g^2 is very small, the following procedure should be used

$$I(\psi)\Big|_v = \frac{1}{2} \log \frac{v+R}{v-R}$$

$$= \log (v+R) - \frac{1}{2} \log(g^2) \qquad (v > 0)$$

$$= \frac{1}{2} \log(g^2) - \log (R + v) \qquad (v < 0) \tag{J.8.21}$$

$$= \text{sign}(v)\ (\log(|v| + R) - \frac{1}{2} \log g^2 \tag{J.8.22}$$

where g should be computed by the relation (see Section J.7.2.4)

$$g^2 = \frac{\beta^2}{\tau^2} \{\vec{r}_o \times \hat{t}_o\ ,\ \vec{r}_o \times \hat{t}_o\} \tag{J.8.23}$$

The initial test for small g can be made by asking whether $R > .95|v|$. If this test is satisfied, g^2 is small and the special procedure outlined by equation (J.8.22) should be used.

This completes the discussion of what must be done when one endpoint of $E \cap D_p$ lies on the Mach cone. We now turn our attention to the case in which both endpoints lie inside the Mach cone. We begin this discussion by deriving some expressions for $I(\psi)\Big|_{v_-}^{v_+}$ that are generally valid; that is, they do not depend upon the assumption that both endpoints of $E \cap D_p$ lie inside the Mach cone.

Using equation (J.8.6), we have, for subsonic edges

$$I(\psi)\Big|_{v_-}^{v_+} = \frac{1}{2}\log\frac{v+R}{v-R}\Big|_{v_-}^{v_+} \tag{J.8.24a}$$

$$= \frac{1}{2}\log\frac{(v_+v_- - R_+R_-) + (R_+v_- - v_-R_+)}{(v_+v_- - R_+R_-) - (R_+v_- - R_-v_+)}$$

$$= \frac{1}{2}\log\frac{1+z}{1-z} \tag{J.8.24b}$$

where z is defined by

$$z = \frac{R_+v_- - R_-v_+}{v_+v_- - R_-R_+} \tag{J.8.25}$$

The definition (J.8.25) for z may be arranged somewhat by using equation (J.8.20) to obtain

$$R^2 = v^2 + sg^2 \tag{J.8.26}$$

Then

$$z = \frac{R_+v_- - R_-v_+}{v_+v_- - R_-R_+}\;\frac{R_+v_- + R_-v_+}{R_+v_- + R_-v_+} \tag{J.8.27a}$$

$$= \frac{R_+^2v_-^2 - R_-^2v_+^2}{R_+v_+(v_-^2 - R_-^2) + R_-v_-(v_+^2 - R_+^2)} \tag{J.8.27b}$$

$$= \frac{v_+^2 - v_-^2}{R_+v_+ + R_-v_-} \tag{J.8.27c}$$

In a precisly analogous fashion, we have for supersonic edges

$$I(\psi)\Big|_{v_-}^{v_+} = -ph(v,R)\Big|_{v_-}^{v_+} = -\left[\frac{\pi}{2} - ph(R,v)\right]_{v_-}^{v_+} \tag{J.8.28}$$

$$= ph(R_+,v_+) - ph(R_-,v_-)$$

$$= ph(R_+R_- + v_+v_-,\; v_+R_- - v_-R_+) \tag{J.8.29}$$

$$= ph(\sigma,\; \sigma\tilde{z}) \tag{J.8.30}$$

where in this case we define σ and $\tilde{z}$ by

$$\sigma = \text{sign}\ (R_+R_- + v_+v_-) \tag{J.8.31}$$

$$\tilde{z} = \frac{v_+R_- - v_-R_+}{R_+R_- + v_+v_-} \tag{J.8.32}$$

As before, the definition of $\tilde{z}$ may be rearranged somewhat with the help of equation (J.8.20). Doing this, we find

$$\tilde{z} = \tilde{z}\ \frac{R_+v_- + R_-v_+}{R_+v_- + R_-v_+} = \tag{J.8.33}$$

$$= \frac{v_+^2 - v_-^2}{R_+v_+ + R_-v_-} = z \tag{J.8.34}$$

Thus, $\tilde{z} = z$ and we can drop the tilde. Summarizing, we have found,

$$I(\psi)\Big|_{v_-}^{v_+} = \begin{cases} \frac{1}{2}\log\frac{1+z}{1-z} & q = +1 \\ \text{ph}(\sigma,\ \sigma z) & q = -1 \end{cases} \tag{J.8.35}$$

where

$$z = \frac{v_+^2 - v_-^2}{R_+v_+ + R_-v_-} = \frac{(v_+ - v_-)(v_+ + v_-)}{R_+v_+ + R_-v_-}$$

$$\sigma = \text{sign}(R_+R_- + v_+v_-) \tag{J.8.36}$$

Equation (J.8.35) will permit stable and accurate evaluation of $I(\psi)\Big|_{v_-}^{v_+}$ in all instances with the exception that when g^2 is small, $q = +1$, and v changes sign along the edge, some additional care must be taken. We now describe the procedure to be used in this case.

Since v changes sign along the edge, the flow must be subsonic. Consequently, equation (J.8.20) gives us

$$R^2 = v^2 + g^2 \tag{J.8.37}$$

Next, we note that the function $I(\psi)$ may be written

$$I(\psi) = \frac{1}{2}\log\frac{v+R}{v-R} = \frac{1}{2}\log\left(-\frac{R+v}{R-v}\right) + \frac{i}{2} \tag{J.8.38}$$

Concentrating on the function $\frac{1}{2}\log\frac{R+v}{R-v}$, we find

$$\frac{1}{2}\log\frac{R+v}{R-v} = \log g - \log(R-v) \tag{J.8.39}$$

Evaluating $I(\psi)$ at the two limits and noting that since $v_-v_+ < 0$, we must have $v_- < 0 < v_+$, we get

$$\begin{aligned} I(\psi)\Big|_{v_-}^{v_+} &= \left(\frac{1}{2}\log\frac{R+v}{R-v}\right)_{v_+} - \left(\frac{1}{2}\log\frac{R+v}{R-v}\right)_{v_-} \\ &= (\log(R_+ + v_+) - \log g) - (\log g - \log(R_- - v_-)) \\ &= \log((R_+ + v_+)(R_- + v_-)) - 2\log g \end{aligned} \tag{J.8.40}$$

or

$$I(\psi)\Big|_{v_-}^{v_+} = \log\frac{(R_+ + v_+)(R_- v_-)}{g^2} \qquad \begin{matrix} s = 1,\ q = 1 \\ v_- < 0 < v_+ \end{matrix} \tag{J.8.41}$$

With g^2 computed from equation (J.8.23), equation (J.8.41) may be used for the evaluation of $I(\psi)\Big|_{v_-}^{v_+}$ whenever g is small, $q = +1$, and v changes sign along the edge.

This completes our discussion of non-sonic edges.

J.8.1.2 Nearly Sonic Edges

The very fact that we are discussing nearly sonic edges ensures us that the flow itself is supersonic, that is, $s = -1$. Thus, equation (J.8.20) gives us

$$R^2 = \begin{cases} v^2 - g^2 & q = +1 \\ g^2 - v^2 & q = -1 \end{cases} \tag{J.8.42}$$

Also, we know that on subsonic edges, v cannot change sign. Note also that in the evaluation procedure for AIC's for nearly sonic edges, the expression ΔR is not needed. However, as we will shortly see, it will be necessary to compute $\vec{r}_\pm$ for nearly sonic edges (recall that $\vec{r}_\pm$ are the values of $\vec{P}-\vec{Q}$ at the first and last points of $E \cap D_p$).

The basic idea of the evaluation procedure for nearly sonic edges is to use equation (J.8.35) for $I(\psi)\Big|_{v_-}^{v_+}$ and at the same time notice two facts: (a) z will almost always be quite small and (b) on supersonic edges, we will almost always have $\sigma = +1$. The first of these two observations follows from the calculation

$$z = \frac{(v_+ - v_-)(v_+ + v_-)}{R_+v_+ + R_-v_-} = \frac{(\Delta v)\bar{v}}{\overline{(Rv)}} = \frac{qs\Delta s_0\bar{\hat{v}}}{\overline{(Rv)}} \qquad (J.8.43)$$

where the definition of $\hat{v}$, $\hat{v} = \tau v$, and (cf.(J.6.54))

$$\Delta v = \tau qs(\Delta s_0) \qquad (J.8.44)$$

have been used. Because of the presence of the coefficient τ in equation (J.8.43), we may expect that z is of order τ, and consequently that it is small. The second of these two observations follows from the fact that if σ is to be equal to -1, v must change sign along the edge. Consequently, the edge and control point must be arranged as shown in figure J.27, where the angle $\delta \approx \tau^2/2$ is very small. (Recall that an edge is said to be nearly sonic only if $\tau < .01$. This implies $\delta < .00005$) Invoking our two assumptions, and expanding equation (J.8.35) in a maclaurin series, we obtain

$$I(\psi)\Big|_{v_-}^{v_+} = \begin{cases} \sum_{j=0}^{\infty} \dfrac{z^{2j+1}}{2j+1} & q = +1 \\ \sum_{j=0}^{\infty} (-1)^j \dfrac{z^{2j+1}}{2j+1} & q = -1, \sigma = +1, \ |z| < 1 \end{cases}$$

$$I(\psi)\Big|_{v_-}^{v_+} = z \sum_{j=0}^{\infty} \frac{(qz^2)^j}{2j+1} \qquad \begin{matrix} q = -1 \\ \sigma = +1 \\ |z| < 1 \end{matrix} \qquad (J.8.45)$$

We may now use this expression to obtain stable and accurate expressions for I, K. We begin by defining the function $\phi_q(z)$ such that

$$I(\psi)\Big|_{v_-}^{v_+} = z\,(1 + z^2\phi_q(z)) \qquad (J.8.46)$$

Evidently, for $|z| < 1$ and $\sigma = +1$, ϕ_q has the expansion

$$\phi_q(z) = q \sum_{j=1}^{\infty} \frac{(qz^2)^{j-1}}{2j+1} \qquad (J.8.47)$$

Substituting the expression (J.8.46) into (J.8.1) and (J.8.3) yields the results for $\hat{I}$, $\hat{K}$

$$\hat{I} = \frac{qz}{\tau}\,(1 + z^2\,\phi_q(z)) \tag{J.8.48}$$

$$\hat{K} = \left(\frac{1}{\tau^2}\,(q\,\Delta R - \bar{v}z)\right) - \left(\frac{\bar{v}}{\tau^2}\,z^3\right)\,\phi_q(z) \tag{J.8.49}$$

We now show how to evaluate the three expressions

$$\frac{q^z}{\tau}\,,\ \frac{1}{2}\ (q\Delta R - \bar{v}z),\ \frac{\bar{v}\ z^3}{\tau^2} \tag{J.8.50}$$

First,

$$\frac{qz}{\tau} = \frac{(\Delta R)^2}{\tau(2Rv)} = \frac{R\Delta R}{\tau(\overline{Rv})} = \frac{\bar{R}\Delta R}{\overline{R\ v}} \tag{J.8.51}$$

Now

$$\overline{Rv} - \bar{R}\ \bar{v} = \frac{1}{2}\,(R_+v_+ + R_-v_-) - \frac{1}{4}\,(R_+ + R_-)(v_+v_-)$$

$$= \frac{1}{4}\,\Delta R\Delta v \tag{J.8.52}$$

Thus

$$\frac{qz}{\tau} = \frac{\bar{R}\Delta R}{\tau(\bar{R}\bar{v} + \frac{1}{4}\,\Delta R\Delta v)} =$$

$$\frac{\Delta R}{\bar{\hat{v}} + \frac{1}{4}\,(sq\,\tau^2\,\Delta s_0)\Delta R/\bar{R}} \tag{J.8.53}$$

since

$$sq\,\tau^2\,\Delta s_0 = \Delta\hat{v} \tag{J.8.54}$$

Next,

$$(1/\tau)\ (q\Delta R - \bar{v}z) = (1/\tau^2)(q\Delta R - \bar{v}\,\frac{\Delta(v^2)}{2\overline{Rv}}\ ) = \tag{J.8.55}$$

$$\frac{q}{\tau^2(2\overline{Rv})}\,[2\overline{Rv}\ \Delta R - \bar{v}\Delta(R^2)] = \frac{q}{\tau^2(2\overline{Rv})}\,[2\overline{Rv}\ \Delta R - 2\bar{v}\bar{R}\ \Delta R] \tag{J.8.56}$$

$$= \frac{q}{\tau^2 \cdot 2\overline{Rv}} \left[2\Delta R \cdot \frac{1}{4} \Delta R \Delta v\right] .$$

$$= \frac{1}{4} \left(\frac{q\Delta v}{\tau}\right) \frac{(\Delta R)^2}{\tau \overline{Rv}} \tag{J.8.57}$$

$$= \frac{1}{4} s \, \Delta s_o \frac{(\Delta R)^2}{\overline{Rv}} = \frac{1}{4} \frac{R(\Delta R)^3}{\overline{R\hat{v}} \, \hat{\bar{v}}}$$

$$= \frac{1}{4} \left(\frac{qz}{\tau}\right) \frac{(\Delta R)^2}{\hat{\bar{v}}} \tag{J.8.58}$$

Finally,

$$\frac{vz^3}{\tau^2} = q \tau \bar{v} \left(\frac{qz}{\tau}\right)^3 \tag{J.8.59}$$

where (qz/τ) is given by (J.8.53). In deriving these equations, we have used (J.8.54) and the definition of $\hat{v}$.

To summarize our procedure then, $\hat{I}$ and $\hat{K}$ are to be evaluated using equations (J.8.48-49) for all subsonic edges and for supersonic edges when $\sigma = +1$. When $|z| < .3$, say, the series (J.8.47) should be used to evaluate ϕ_q; however for larger $|z|$, one should use

$$\phi_q(z) = \frac{\frac{1}{2} \log \frac{1+z}{1-z} - z}{z^3} \qquad \begin{array}{l} q = +1 \\ |z| > .3 \end{array} \tag{J.8.60a}$$

$$\phi_q(z) = \frac{ph(1,z) - z}{z^3} \qquad \begin{array}{l} q = -1 \\ |z| > .3 \end{array} \tag{J.8.60b}$$

where now, Fortran library routines should be used for the evaluations. The expression z should be computed by

$$z = \tau \frac{qs\Delta s_o \, \bar{\hat{v}}}{\overline{R\hat{v}}} \tag{J.8.61}$$

We know in particular that this approach works for supersonic edges even when $|z| > 1$ provide only that $\sigma = +1$. This is because, as long as $\sigma = +1$,

$$I(\psi)\Big|_{v_-}^{v_+} = ph(1,z) = z(1+z^2 \, \phi_q(z)) \tag{J.8.62}$$

Consequently, we are done except for the case of supersonic, nearly sonic edges for which

$$\sigma = \text{sign}(R_+R_- + v_+v_-) = -1 \tag{J.8.63}$$

In this case, both $\hat{I}$ and $\hat{K}$ are quite close to an actual singularity of strength $(1/\tau)$. Consequently, we will only show how the quantities $\tau\hat{I}$, $\tau\hat{K}$ can be stably evaluated. The first of these is trivial. Using (J.8.1) and (J.8.35),

$$\tau\hat{I} = q\ I(\psi)\Big|_{v_-}^{v_+} = -ph(-1,\ -z) \tag{J.8.64}$$

where z may again be computed from (J.8.61). For $\tau\hat{K}$, we have, using (J.8.2) and (J.8.35),

$$\tau\hat{K} = q\ \left(\frac{\Delta R}{\tau}\right) - \frac{\bar{v}}{\tau}\ ph(-1,\ -z) \tag{J.8.65}$$

We now conclude our discussion with a prescription of what is to be done in and case of edges that can only be regarded as truly sonic, $\tau^2 \leq 10^{-10}$.

J.8.1.3 Essentially Sonic Edges

In this case, the only reasonable thing to do is to evaluate the limits, as $\tau \to 0$ of the functions $\hat{I}$, ΔR, $\hat{K}$. ΔR is trivial to compute, but both $\hat{I}$ and $\hat{K}$ require great care. We begin with equations (J.8.48-49) and evaluate the following expressions in the limit as $\tau \to 0$:

$$\frac{qz}{\tau},\ \frac{1}{\tau^2}(q\Delta R - vz),\ \frac{vz^3}{2},\ z,\ \phi_q(z) \tag{J.8.66}$$

First, equation (J.8.53) gives us

$$\lim_{\tau\to 0} \frac{qz}{\tau} = \frac{\Delta R}{\hat{v}} \tag{J.8.67}$$

Next, from (J.8.58)

and

$$\lim_{\tau\to 0} \overline{R\hat{v}} = \bar{R}\ \bar{\hat{v}} \tag{J.8.68}$$

we obtain

$$\lim_{\tau \to 0} \frac{1}{\tau^2}(q\Delta R - \bar{v}z) = \frac{s\Delta s_o}{4} \frac{(\Delta R)^2}{\bar{R}\,\bar{\hat{v}}} = \frac{1}{4} \frac{(\Delta R)^3}{(\bar{\hat{v}})^2} \tag{J.8.69}$$

Again, equation (J.8.59) combined with (J.8.67) yields

$$\lim_{\tau \to 0} \frac{\bar{v}z^3}{\tau^2} = q\,\bar{\hat{v}}\,(\Delta R/\,\bar{\hat{v}})^3 \tag{J.8.70}$$

Finally, equation (J.8.67) implies that $\lim_{\tau \to 0} z = 0$ so that

$$\lim_{\tau \to 0} \phi_q(z) = \phi_q(o) = q/3 \tag{J.8.71}$$

Combining all these results, we find

$$\hat{I}\big|_{\tau=0} = \lim_{\tau \to 0} \frac{qz}{\tau} = \Delta R/\bar{\hat{v}} \tag{J.8.72}$$

and

$$\hat{K}\big|_{\tau=0} = \lim_{\tau \to 0} \left(\frac{1}{\tau^2}(q\Delta R - vz) - \frac{v}{\tau^2}\,\phi_q(z)\right)$$

$$= \frac{s\Delta s_o}{4} \frac{(\Delta R)^2}{\bar{R}\,\bar{\hat{v}}} - q\,\bar{\hat{v}}\,\left(\frac{\Delta R}{\bar{\hat{v}}}\right)^3 \frac{q}{3} \tag{J.8.73}$$

Now

$$(s\Delta s_o)(\bar{\hat{v}}) = \frac{q\Delta v}{\tau}\,\tau\bar{v} =$$

$$\frac{q}{2}\Delta(v^2) = \frac{1}{2}\,\Delta R^2 = \bar{R}\Delta R \tag{J.8.74}$$

so that

$$\hat{K}\big|_{\tau=0} = \frac{1}{4}\,\frac{\bar{R}\Delta R}{\bar{\hat{v}}}\,\frac{(\Delta R)^2}{} - \frac{\bar{\hat{v}}}{3}\left(\frac{\Delta R}{\bar{\hat{v}}}\right)^3$$

$$= \frac{1}{12}\,\frac{(\Delta R)^3}{(\bar{\hat{v}})^2} \tag{J.8.75}$$

J.8.2 Panel Function Computation

The panel function J is defined by

$$J = -\text{sign}(h)\ J'$$

$$J' = 2\pi C_{\bullet} + \sum_{\text{edges}} ph(|h|\ v,\ a_k R)\Big|_{v_k^-}^{v_k^+} \tag{J.8.76}$$

where $C_{\bullet} =$

$$\begin{cases} 1 \text{ if } (x', y') \in \Sigma' \cap D_p' \text{ and } rs = +1 \\ 0 \text{ otherwise} \end{cases} \tag{J.8.77}$$

In section J.8.2.1 we compute a "standard rationalization" which is valid even for a panel with sonic edges. In section J.8.2.2 we consider the special case

$$g^2 << 1 \tag{J.8.78}$$

In section J.8.2.3 we consider a point on the panel.

J.8.2.1 The Standard Rationalization

Defining $h' = |h|$ (J.8.79)

we have

$$J' = \Sigma ph(h'v_k^+,\ a_k R^+) - (\pi \text{ sign } a_k - ph(-h'v_k',\ a_k R^-))$$

$$+ 2\pi C_{\bullet} =$$

$$\Sigma\,(ph(h'v_k^+,\ a_k R_k^+) + ph(-h'v_k^-,\ a_k R_k^-)) - \pi\,\Sigma \text{sign } a_k - 2\pi C_{\bullet}$$

$$= \sum_{k \text{ corners}} (ph(h'v_k^+,\ a_k R_k^+) + ph(-h'\bar{v}_{k+1},\ a_{k+1}\bar{R}_{k+1})) - \pi\,\Sigma \text{sign } a_k$$

$$+ 2\pi C_{\bullet} \tag{J.8.80}$$

We now define

$$Q_k = ph(h'v_k^+,\ a_k R_k^+) + ph(-h'\bar{v}_{k+1},\ a_{k+1}\bar{R}_{k+1}) \tag{J.8.81}$$

Then, using the sum of angles formulas,

$$\cos Q_k = \frac{1}{R_k R_{k+1}} (-h^2 v_k^+ v_{k+1}^- - a_k a_{k+1} R^2)$$

$$\sin Q_k = \frac{1}{R_k R_{k+1}} \quad (h'R(a_{k+1} v_k^+ - a_k v_{k+1}^-)) \tag{J.8.82}$$

We then define

$$Q_k = ph(-h^2 v_k^+ v_{k+1}^- - a_k a_{k+1} R^2,\ h'R(a_{k+1} v_k^+ - a_k v_{k+1}^-)) \tag{J.8.83}$$

We now investigate the sign of $a_{k+1}\ v_k^+ - a_k\ v_{k+1}^-$. First, by definition, (cf. Section J.6.1.4)

$$a = \xi t_\eta - \eta t_\xi$$

$$v = rs\xi t_\xi + \eta\ t_\eta$$

$$\vec{t}_k = (t_\xi,\ t_\eta) \quad , \quad \vec{t}_{k+1} = (\bar{t}_\xi,\ \bar{t}_\eta) \tag{J.8.84}$$

Thus

$$a_{k+1} v_k^+ - a_k v_{k+1}^- = (\xi t_\eta - \eta t_\xi)(rs\xi t_\xi + \eta t_\eta) \tag{J.8.85}$$

$$= \xi^2(rs\ \bar{t}_\eta t\ - rs\ t_\eta \bar{t}_\xi) + \ \eta(-rs\bar{t}_\xi t_\xi + \bar{t}_\eta t_\eta + rst_\xi \bar{t}_\xi - t_\eta \bar{t}_\eta)$$
$$+ \eta^2(-\bar{t}_\xi t_\eta + t_\xi \bar{t}_\eta) \tag{J.8.86}$$

$$= (rs\xi^2 + \eta^2)\ (t_\xi \bar{t}_\eta - \bar{t}_\xi t_\eta)$$

$$= rs\rho^2(\vec{t}_k \times \vec{t}_{k+1})_\zeta \tag{J.8.87}$$

Now since the region is convex,

$$(\vec{t}_k \times \vec{t}_{k+1})_\zeta \ > 0 \tag{J.8.88}$$

Thus

$$\text{sign}(a_{k+1}\ v_k^+ - a_k\ v_{k+1}^-) = rs \tag{J.8.89}$$

We first consider the case of rs = 1.

Careful consideration of the range of Q_k, Q_k and a_k shows

$$J' = \Sigma \bar{Q}_k \ - 2\pi - \pi \text{ sign } a_k \ + 2\pi C_\theta$$

$$= \Sigma \bar{Q}_k - \sum_k \pi + 2\pi + K \tag{J.8.90}$$

where $m_k = 1$ if $a_k < 0$ and $a_{k+1} < 0$, zero otherwise, and

$$K = \sum_k \pi - 2\pi - \sum_k 2\pi m_k - \sum_k \pi \text{ sign } a_k + 2\pi C_\theta \tag{J.8.91}$$

Let

$$\tau_k = 1 \quad \text{if} \quad a_k > 0$$

$$\tau_k = 0 \quad \text{if} \quad a_k < 0 \tag{J.8.92}$$

Then

$$\text{sign } a_k = 2\tau_k - 1$$

$$m_k = (1-\tau_k)(1-\tau_{k+1})$$

$$C_\theta = \pi\tau_k \tag{J.8.93}$$

and

$$K = \sum_k [\pi - 2\pi(1 - \tau_k)(1 - \tau_{k+1}) - \pi(2\tau_k - 1)] + 2\pi(C_\theta - 1)$$

$$= \sum_k 2\pi(1-\tau_k)\, \tau_{k+1} + 2\pi(C_\theta - 1) \tag{J.8.94}$$

or

$$\frac{K}{2\pi} = \sum_k (1 - \tau_k)\, \tau_{k+1} + \pi\tau_k - 1 \tag{J.8.95}$$

It follows by a careful analysis from the convexity of the polygonal region that $K = 0$.

Next, we assume $rs = -1$.
By definition, $C_\theta = 0$.

Defining $l_k = 1$ if $a_k > 0$ and $a_{k+1} > 0$, it follows that

$$Q_k = \bar{Q}_k + 2\pi l_k \tag{J.8.96}$$

Thus

$$J' = \Sigma\bar{Q}_k + 2\pi l_k - \pi \text{ sign } a_k$$

$$= (\bar{Q}_k + \pi) - 2\pi + K \tag{J.8.97}$$

So,

$$K = 2\pi - \Sigma\pi + \Sigma 2\pi\, l_k - \pi\ \Sigma \text{sign } a_k \tag{J.8.98}$$

or

$$\frac{K}{2\pi} = 1 - \Sigma\frac{1}{2} + \Sigma\tau_k\,\tau_{k+1} - \frac{1}{2}\Sigma(2\tau_k - 1)$$

$$= 1 + \Sigma\tau_k(\tau_{k+1} - 1) = 0 \qquad \text{(J.8.99)}$$

Thus in general

$$J' = \sum_{\text{corners}} \bar{Q}_k + rs(2\pi - \sum_{\text{edges}} \pi) \qquad \text{(J.8.100)}$$

Now, $\bar{Q}_k =$

$$ph(-h^2 v_k^+ v_{k+1}^- - a_k a_{k+1} R^2,\ h' Rrs\rho^2\ (\vec{t}_k \times \vec{t}_{k+1})_\zeta) \qquad \text{(J.8.101)}$$

So,

$J = -\text{sign}(h)\ J' =$

$$-\ \text{sign}(h) rs\,(\,2\pi - \sum_E \pi + \sum_C ph(-h^2 v_k^+ v_{k+1}^- - a_k a_{k+1} R^2,\ |h|\ R\rho^2 (t_k \times t_{k+1})_\zeta)) \qquad \text{(J.8.102)}$$

We now define

$$X_k = -h^2\ v_k^+ v_{k+1}^- - a_k a_{k+1} R^2$$

$$Y_k = |h|\, R\rho^2 (\vec{t}_k \times \vec{t}_{k+1})_\zeta \qquad \text{(J.8.103)}$$

Then

$$X_k = -h^2 v_k^+ v_{k+1}^- - a_k a_{k+1}(rsh^2 + r\rho^2) \qquad \text{(J.8.104)}$$

Now,

$$v_k^+ v_{k+1}^- + rs\ a_k a_{k+1} = (rs\xi t_\xi + \eta t_\eta)(rs\xi \bar{t}_\xi + \eta \bar{t}_\eta)$$

$$+ rs(\xi t_\eta - \eta t_\xi)(\xi \bar{t}_\eta - \eta \bar{t}_\xi) \qquad \text{(J.8.105)}$$

$$= \xi^2(t_\xi \bar{t}_\xi + rst_\eta \bar{t}_\eta) + \xi^2(t_\eta \bar{t}_\eta + rst_\xi \bar{t}_\xi)$$

$$+ rs\ \xi\eta(t_\eta \bar{t}_\xi + \bar{t}_\eta t_\xi - t_\xi \bar{t}_\eta - \bar{t}_\xi t_\eta) \qquad \text{(J.8.106)}$$

$$= \rho^2(t_\xi \bar{t}_\xi + rst_\eta \bar{t}_\eta) = \rho^2 rs \langle \vec{t}_k, \vec{t}_{k+1} \rangle \tag{J.8.107}$$

So,

$$X_k = -h^2\rho^2 rs \langle \vec{t}_k, \vec{t}_{k+1} \rangle - a_k a_{k+1} r\rho^2 \tag{J.8.108}$$

Thus

$$J = -\mathrm{sign}(h) rs(2\pi - \sum_E \pi + \sum_C ph(X_{k,k+1}, Y_{k,k+1})) \tag{J.8.109}$$

where

$$X_{k,k+1} = -h^2 rs \langle \vec{t}_k, \vec{t}_{k+1} \rangle - ra_k a_{k+1}$$
$$Y_{k,k+1} = R\ h\ \ (\vec{t}_k \times \vec{t}_{k+1})_\zeta \tag{J.8.110}$$

Using the results of Sections J.7.2.1 and J.7.2.2 we find for X_{k+1}

$$X_{k,k+1} = -\left(\frac{\beta(\hat{n}_o \cdot (\vec{x}_o - \vec{\xi}_o))}{|\{\hat{n}_o, \hat{n}_o\}|^{1/2}}\right)^2 r\,[t_k, t_{k+1}]$$

$$-r\left(\frac{\beta}{|\{\hat{n}_o, \hat{n}_o\}|^{1/2}}\right)^2 \{n_o, (\vec{\xi}_o - \vec{x}_o) \times \vec{t}_{o,k}\} \quad \{\hat{n}_o, \{(\vec{\xi}_o - \vec{x}_o) \times \vec{t}_{o,k+1}\} \tag{J.8.111}$$

$$= \frac{-\beta^2}{n_o, n_o} [(\hat{n}_o, \vec{x}_o - \vec{\xi}_o)^2 [\vec{t}_{o,k}, \vec{t}_{o,k+1}]$$

$$+ \{\hat{n}_o, (\vec{\xi}_o - \vec{x}_o) \times \vec{t}_{o,k}\} \quad \{\hat{n}_o, (\vec{\xi}_o - \vec{x}_o) \times \vec{t}_{o,k+1}\}$$

$$= \frac{-\beta^2}{\{\hat{n}_o, \hat{n}_o\}} G_o \tag{J.8.112}$$

We will now simplify the expression G_o (J.8.112). Employing the identity (J.7.64) with

$$\vec{a} = \vec{c} = \hat{n}_o\ ,\ \vec{b} = (\vec{\xi}_o - \vec{x}_o) \times \vec{t}_k$$
$$\vec{d} = (\vec{\xi}_o - \vec{x}_o) \times \vec{t}_{k+1}$$
$$C^{-1} = B_o \tag{J.8.113}$$

we find

$$G_o = (\hat{n}_o, \vec{x}_o - \vec{\xi}_o)^2 \, [\vec{t}_{o,k}, \vec{t}_{o,k+1}]$$
$$+ (\hat{n}_o^T B_o \hat{n}_o) \, ((\vec{\xi}_o - \vec{x}_o) \times \vec{t}_{o,k})^T \, B_o \, ((\vec{\xi}_o - \vec{x}_o) \times \vec{t}_{o,k+1})$$
$$- (\hat{n}_o \times ((\vec{\xi}_o - \vec{x}_o) \times \vec{t}_{o,k}))^T \, \frac{B_o^{-1}}{\det B_o^{-1}} \, (\hat{n}_o \times ((\vec{\xi}_o - \vec{x}_o) \times \vec{t}_{o,k+1})) \tag{J.8.114}$$

Now (cf. (B.3.31))

$$\hat{n}_o \times ((\vec{\xi}_o - \vec{x}_o) \times \vec{t}_{o,k}) = (\vec{\xi}_o - \vec{x}_o) \, (\hat{n}_o, \vec{t}_{o,k}) - \vec{t}_{o,k} \, (\hat{n}_o, \vec{\xi}_o - \vec{x}_o)$$
$$= (\vec{x}_o - \vec{\xi}_o, \hat{n}_o) \, \vec{t}_{o,k} \tag{J.8.115}$$

Similarly

$$\hat{n}_o \times ((\vec{\xi}_o - \vec{x}_o) \times \vec{t}_{o,k+1} = (\vec{x}_o - \vec{\xi}_o, \hat{n}_o) \, \vec{t}_{o,k} \tag{J.8.116}$$

Using the results (cf. Appendix E)

$$C_o B_o = s\beta^2 I$$
$$\det B_o = \beta^2 \tag{J.8.117}$$

we find

$$\frac{B_o^{-1}}{\det B_o^{-1}} = C_o \tag{J.8.118}$$

Consequently, we find for G_o

$$G_o = (\hat{n}_o, \vec{x}_o - \xi_o)^2 \, [\vec{t}_{o,k}, \vec{t}_{o,k+1}]$$
$$+ \{\hat{n}_o, \hat{n}_o\} \, ((\vec{\xi}_o - \vec{x}_o) \times \vec{t}_{o,k})^T \, B_o \, ((\vec{\xi}_o - \vec{x}_o) \times \vec{t}_{o,k+1})$$
$$- (\hat{n}_o, \vec{x}_o - \vec{\xi}_o) \, (\vec{t}_{o,k}^T \, C \, \vec{t}_{o,k+1}) \, (\hat{n}_o, \vec{x}_o - \vec{\xi}_o) \tag{J.8.119}$$

The first and last terms cancel and we are left with

$$G_o = \{\vec{n}_o, \vec{n}_o\} \, ((\vec{\xi}_o - \vec{x}_o) \times \vec{t}_{o,k})^T \, B_o \, ((\vec{\xi}_o - \vec{x}_o) \times \vec{t}_{o,k+1}) \tag{J.8.120}$$

Substituting this result into equation (J.8.108) we find

$$X_{k,k+1} = -r\beta^2 \, ((\vec{\xi}_o - \vec{x}_o) \times \vec{t}_{o,k})^T \, B_o \, ((\vec{\xi}_o - \vec{x}_o) \times \vec{t}_{o,k+1}) \tag{J.8.121}$$

Turning now to $Y_{k,k+1}$, we find

$$Y_{k,k+1} = R\,|h(t_k \times t_{k+1})| \tag{J.8.122}$$

The expression inside the absolute value sign can be written

$$\begin{aligned} h(\vec{t}_k \times \vec{t}_{k+1}) &= (z' - \zeta')(\vec{t}_k \times \vec{t}_{k+1}) \\ &= (\vec{x}' - \vec{\xi}') \cdot (\vec{t}_k \times \vec{t}_{k+1}) \end{aligned} \tag{J.8.123}$$

Transforming this expression into the reference coordinate system we find

$$\begin{aligned} h(\vec{t}_k \times \vec{t}_{k+1}) &= (A(\vec{x}_o - \vec{\xi}_o)) \cdot (A\vec{t}_{o,k} \times A\vec{t}_{o,k+1}) \\ &= (\vec{x}_o - \vec{\xi}_o)^T\ A^T(\det A)\ A^{-T}\ (\vec{t}_{o,k} \times \vec{t}_{o,k+1}) = \\ &\beta^2\ (\vec{x}_o - \vec{\xi}_o) \cdot (\vec{t}_{o,k} \times \vec{t}_{o,k+1}) \end{aligned} \tag{J.8.124}$$

Thus for $Y_{k,k+1}$ we have

$$Y_{k,k+1} = \beta^2 R\ |(\vec{x}_o - \vec{\xi}_o) \cdot (\vec{t}_{o,k} \times \vec{t}_{o,k+1})| \tag{J.8.125}$$

Upon comparing equations (J.8.121) and (J.8.125) we see that the factor $\beta^2/\tau_k\,\tau_{k+1}$ can be extracted from each of them and that we can write

$$ph(X_{k,k+1}, Y_{k,k+1}) = ph(\bar{X}_{k,k+1}, \bar{Y}_{k,k+1}) \tag{J.8.126}$$

where

$$\begin{aligned} \bar{X}_{k,k+1} &= -\{(\vec{\xi}_o - \vec{x}_o) \times \hat{t}_{o,k},\ (\vec{\xi}_o - \vec{x}_o) \times \hat{t}_{o,k+1}\} \\ \bar{Y}_{k,k+1} &= R\ |(\hat{\xi}_o - \vec{x}_o,\ \hat{t}_{o,k} \times \hat{t}_{o,k+1})| \end{aligned} \tag{J.8.127}$$

Thus we obtain the standard rationalization

$$J = -\mathrm{sign}(h)\ rs(2\pi - \sum_{\text{edges}} \pi + \sum_{\text{corners}} ph(\bar{X}_{k,k+1}, \bar{Y}_{k,k+1})) \tag{J.8.128}$$

J.8.2.2 A Special Rationalization

In equation (J.8.128) the summation extends over the straight edges of Σ' and over the corners of Σ' internal to Dp'. When $h \to 0$, the form (J.8.128) may not be sufficiently stable for accurate evaluation if on any edge $a_k \approx 0$. The precise situation in which resolvable difficulties can arise is when $g_k^2 = r(q_k h^2 + a_k^2) \approx 0$ and the panel is subinclined

($r = +1$). Although it can happen that $g_k^2 \approx 0$ for some edge on a superinclined panel (see figure J.28) the difficulties associated with evaluating the panel function for this configuration are quite unavoidable and the standard rationalization must be regarded as optimal. To illustrate this difficulty, we point out that for the configuration shown, the value of $|h|$ decreases down to the inner circle.

Having identified the situation $g^2 \approx 0$ as a source of difficulty, we now show how this problem may be resolved (when it is resolvable). Thus we define the procedure to be used for evaluating J'.

First, if $r = -1$

or $r = 1,\ s = -1$ and $g_k^2 \geq 10^{-4} \max(a_k^2 + h^2,\ D_\Sigma{}^2)$

on all subsonic or nearly sonic edges

or $r = 1,\ s = +1$, and $g_k^2 \geq 10^{-4}\ D_\Sigma{}^2$ (J.8.129)

(where D_Σ is the panel diameter) we use the standard rationalization.

Otherwise, we calculate J' by

$$J' = 2\pi C_\Theta + \sum_{\text{edges}} Q_k \tag{J.8.130}$$

where (cf.(J.8.81)

$$Q_k = ph(|h|\ v,\ aR)\Big|_{v_k^-}^{v_k^+}$$

We now describve stable methods for computing C_Θ and Q_k.

Since either the flow is subsonic or $C_\Theta = 0$, the most direct way of getting C_Θ is by the formula

$$C_\Theta = \begin{cases} 1 \text{ if } \{\hat{n},\ (\vec{Q}_k - \vec{P}_k) \times \vec{t}_k\} > 0 \text{ for all } k \\ 0 \text{ otherwise} \end{cases} \tag{J.8.133}$$

The topological justification of the procedure defined above stems from the following observation. As one traverses the boundary of a convex polygonal region, proceeding in a positive fashion, any point inside the region always lies to the left of the extension of the edge. Thus the edge distance a_k is always positive.

We now provide a detailed prescription for the computation of Q_k. This description will consist of two parts.

(i) Evaluation of $ph(|h|v, aR)$ when $R = 0$ together with the evaluation of Q_k on edges that intersect the Mach cone, and

(ii) Evaluation of Q_k when both end points of edge k lie inside the domain of dependence Dp.

It is a fairly straightforward matter to show that the value of v at the point at which an edge enters the domain of dependence satisfies the inequality

$$v_k^- \Big|_{R=0} < 0 \tag{J.8.134}$$

Similarly, when an edge leaves Dp, v_k^+ satisfies the inequality

$$v_k^+ \Big|_{R=0} > 0 \tag{J.8.135}$$

These inequalities can in fact be verified by a careful study of the special cases in figure J.29.

As a consequence of these observations, we see that

$$ph(|h|\ v_k^-,\ a_k\ R)\Big|_{R=0} = \text{sign}(a_k)\pi \tag{J.8.136}$$

and

$$ph\ (|h|\ v_k^+,\ a_k R)\Big|_{R=0} = 0 \tag{J.8.137}$$

If just the lower endpoint of the edge intersects D_p, Q_k is given by

$$Q_k = ph(|h|\ v_k^+,\ a_k\ R_k^+) - \pi\ \text{sign}\ a_k \tag{J.8.138}$$

If just the upper endpoint intersects D_p we have

$$Q_k = -ph(|h|\ v_k^-,\ a_k R_k^-) \tag{J.8.139}$$

Finally if both endpoints intersect D_p

$$Q_k = -\pi\ \text{sign}\ a_k \tag{J.8.140}$$

We now develop a rationalization for Q_k when $R_k^+ \neq 0$, $R_k^- \neq 0$. Evaluating (J.8.128) we have

$$Q_k = ph(|h|\ v,\ a_k\ R)\Big|_{v_k^-}^{v_k^+} =$$

$$ph(|h|\ v_k^+,\ a_k\ R_k^+) - ph(|h|\ v_k^-,\ a_k\ R_k^-)$$

$$= \bar{Q}_k + 2\pi n \qquad n \text{ an integer} \tag{J.8.141}$$

where $\bar{Q}_k$ is defined by

$$\bar{Q}_k = ph(h^2 v_k^+ v_k^- + a_k^2 R_k^+ R_k^-,\ |h|\ a_k(R_k^+ v_k^- - R_k^- v_k^+)) \tag{J.8.142}$$

In order that we might determine n, we investigate the sign of $R_k^+ v_k^- - R_k^- v_k^+$.

$$R_k^+ v_k^- - R_k^- v_k^+ = R_k^+ R_k^- \left(\frac{v_k^-}{R_k^-} - \frac{v_k^+}{R_k^+}\right) = -R_k^+ R_k^- \int_{v_k^-}^{v_k^+} d\left(\frac{v}{R}\right) \tag{J.8.143}$$

Now $R^2 = sqg^2 + qv^2$, hence,

$$d\left(\frac{v}{R}\right) = \frac{1}{R} - \frac{qv^2}{R^3} = \frac{sqg^2}{R^3} \tag{J.8.144}$$

Consequently

$$\text{sign}(R_k^+ v_k^- - R_k^- v_k^+) = -sq_k \tag{J.8.145}$$

Thus

$$-sq_k\ \text{sign}(a_k)\ Q_k \quad \varepsilon \quad (o,\pi) \tag{J.8.146}$$

Now an inspection of equation (J.8.138) shows that $Q_k\ \varepsilon(0,\pi)$. Consequently we see that no phase wrap is possible, and that n = 0 and

$$Q_k = \bar{Q}_k \tag{J.8.147}$$

Multiplying both arguments of Q_k by $(R_k^+ v_k^- + R_k^- v_k^+)$, we find that

$$Q_k = \bar{Q}_k = ph(X,Y) \tag{J.8.148}$$

$$\sigma X = R_k^+ v_k^+ (h^2 v_k^{-2} + a_k^2 R_k^{-2}) + R_k^- v_k^- (h^2 v_k^{+2} + a_k^2 R_k^{+2})$$

$$Y = |h|\ a_k\ \mathrm{sign}(R_k^+ v_k^- + R_k^- v_k^+)(sqg^2)(v_k^{-2} v_k^{+2}) \qquad \text{(J.8.149)}$$

Now,

$$\begin{aligned} \mathrm{sign}(R^+ v^- + R^- v^+) &= -sq\ \mathrm{sign}((R^+ v^-)^2 - (R^- v^+)^2) \\ &= -sq(sq)\ \mathrm{sign}(v^{-2} - v^{+2}) \\ &= \mathrm{sign}(v^{+2} - v^{-2}) \\ &= \mathrm{sign}(v^+ + v^-) \end{aligned} \qquad \text{(J.8.150)}$$

Consequently, Y is given by

$$Y = -a_k\ |h|\ g^2\ |\Delta(R^2)| \qquad \text{(J.8.151)}$$

Next, we examine X. First, note that

$$\begin{aligned} h^2 v^2 + a^2 R^2 &= (h^2 + qa^2)(v^2 + rsa^2) = rqg^2(v^2 + rsh^2) \\ &= rg^2(qv^2 + rsq) = rg^2(R^2 - rsh^2) \end{aligned} \qquad \text{(J.8.152)}$$

Consequently $\sigma X =$

$$(R_k^+ v_k^+ (R_k^{-2} - rsh^2) + R_k^- v_k^- (R_k^{+2} - rsh^2))\ rg^2 \qquad \text{(J.8.153)}$$

Comparing (J.8.152) and (J.8.153) we see that they contain a common factor of g^2. We remove this common factor to obtain the rationalized expression for Q_k

$$Q_k = -ph(\sigma[R_k^+\ v_k^+ (R_k^{-2} - rsh^2) + R_k^-\ v_k^- (R_k^{+2} - rsh^2)],\ \tau a_k |h| |\Delta(R^2)|\ ) \qquad \text{(J.8.154)}$$

This is the basic formula we use to compute Q_k for subsequent substitution into equation (J.8.130) for J'. The arguments for the expression (J.8.154) may be computed in the obvious fashion using the relations found in Section (J.7.2).

We can now evaluate J' if $|h| = 0$. In doing this, we use the following formula for J' (cf. J.8.109-110)

$$J' = rs\ (2\pi - \sum_E \pi + \sum_C ph(-h^2 rs\ \langle \vec{t}_k, \vec{t}_{k+1} \rangle - ra_k a_{k+1},\ |h|\ R_k^+ \vec{t}_k \cdot \vec{t}_{k+1})) \qquad \text{(J.8.155)}$$

Setting $|h| = 0$ we find

$$J'\Big|_{h=0} = rs(2\pi - \sum_E \pi + \sum_C ph(-ra_k a_{k+1}, 0^+)) \tag{J.8.156}$$

Since $a_k > 0$ for all k, we then obtain

$$J'\Big|_{h=0} = rs(2\pi - \sum_E \pi + \frac{(1+r)}{2} \sum_C \pi) \tag{J.8.157}$$

We can now examine the three special cases described by Figure J.30. First, consider $s = 1$. Then $r = +1$ and the number of corners in the domain of dependence equals the number of edges (=n, say). Thus

$$\sum_E \pi = n\pi, \sum_C \pi = n\pi$$

and

$$J'\Big|_{h=0} = 2\pi \tag{J.8.158}$$

Next, suppose $rs = -1$. Then $r = +1$, $s = -1$ and the number of straight edges of D' exceeds the number of interior corners by 1. Hence

$$\sum_E \pi = (m + 1)\pi$$

$$\sum_C \pi = m\pi \tag{J.8.159}$$

and

$$J'\Big|_{h=0} = -\pi \tag{J.8.160}$$

Finally, suppose $r = -1$. Here, $r = -1$, $s = -1$ and D' has no straight edges or corners. Hence

$$J'\Big|_{h=0} = 2\pi \tag{J.8.161}$$

Summarizing, for a field point lying on the panel

$$J'\Big|_{h=0} = \begin{cases} 2\pi rs & \text{if } rs = 1 \\ \pi rs & \text{if } rs = -1 \end{cases} \tag{J.8.162}$$

In general we write

$$J'\Big|_{h=0} = \frac{\pi}{2}(rs + 3) \tag{J.8.163}$$

Of additional interest is the jump in J and the average value of J. In order that we might define the jump in J we must define it by

$$[J] = \lim_{\epsilon \to 0^+} [J(\vec{P} + \epsilon\hat{n}) - J(\vec{P} - \epsilon\hat{n})] \tag{J.8.164}$$

The average value, $(J)_{Av}$, is the average of these two quantities. First let $s = 1$. Here

$$[J] = -2\pi - (2\pi) = -4\pi$$

$$(J)_{Av} = \frac{1}{2}(-2\pi + 2\pi) = 0 \tag{J.8.165}$$

Next, consider $rs = -1$. Here

$$[J] = 2\pi$$

$$(J)_{Av} = 0 \tag{J.8.166}$$

Finally let $r = -1$. Here we must proceed very carefully. First we must recall that a panel may influence a point only when

$$\text{sign}(h)\ \text{sign}(\hat{n},\hat{c}_0) = 1 \tag{J.8.167}$$

Next, we must compute the sign of h for field points lying just above the panel $(\vec{P} + \epsilon\hat{n})$ and for points just below the panel. Now

$$\text{sign}(h(\vec{P} \pm \epsilon\hat{n})) = \pm 1 \tag{J.8.168}$$

Thus,

$$[J] = 2\pi\ \text{sign}(\hat{n},\hat{c}_0)$$

$$(J)_{Av} = \pi\ \text{sign}(\hat{n},\hat{c}_0) \tag{J.8.169}$$

J.9 Far Field PIC's

As noted earlier in appendix I.4, the far field estimation of a panel influence is calculated by implementing the following approximations:

(i) The panel is replaced by its mean panel

(ii) Singularity distributions σ and μ are replaced by their quasi far field approximations (see section I.3.1)

(iii) The kernel functions (1/R) and $\nabla(1/R)$ are replaced by Taylor series approximations of degree 0 (monpole), 1 (dipole) or 2 (quadrupole).

In this section we carry out the analysis of these approximations as they relate to the computation of the integrals defined by equations (J.1.1), (J.1.2), (J.1.4), (J.1.5).

We begin this analysis by noting that the far field evaluation procedure is used only when the panel Σ (and its mean plane approximation Σ_m) is completely contained within the domain of dependence, D_p. In fact, all points of Σ are required to be some distance away from the boundary of D_p. As a consequence, we find that for all cases of interest,

$$\Sigma \cap D_p = \Sigma \qquad \text{(far field evaluation condition)}$$

$$\Sigma_m \cap D_p = \Sigma_m \tag{J.9.1}$$

The local coordinate system associated with the mean panel is defined by the panel center $\vec{P}_9$, and the mean panel normal $\hat{n}_m$, which determines the reference to local transformation matrix A_m by means of equation (E.0.1). This transformation gives the local coordinates $\vec{Q}'$ of a point $\vec{Q}$ by the formula

$$\vec{Q}' = A_m (\vec{Q} - \vec{P}_9) \tag{J.9.2}$$

The area Jacobian J_m for this transformation is given by (E.3.109), (with appropriate modifications) by

$$J_m = 1/[\beta \mid \{\hat{n}_m, \hat{n}_m\} \mid^{1/2}] \tag{J.9.3}$$

Using the basis functions ϕ_α defined by

$$[\phi_\alpha] = [1, \xi, \eta, \xi^2/2, \xi\eta, \eta^2/2] \tag{J.9.4}$$

we write the mean panel singularity approximations (I.3.1) and (I.3.2) in the form

$$\sigma = \sum_{\alpha=1}^{3} \sigma_\alpha \phi_\alpha (\xi, \eta) \tag{J.9.5}$$

$$\mu = \sum_{\beta=1}^{6} \mu_\beta \phi_\beta (\xi, \eta) \tag{J.9.6}$$

If we now substitute all these results into the defining relations for ϕ_s, $\vec{v}_s$ given by (J.1.1-2), replacing integrals over Σ with integrals over Σ_m we obtain the following approximations

$$\phi_s \cong -\frac{1}{\kappa} \iint_{\Sigma_m} \left(\sum_{\alpha=1}^{3} \sigma_\alpha \phi_\alpha \right) \left(\frac{1}{R}\right) (J_m \, d\xi \, d\eta) \tag{J.9.7}$$

$$\vec{v}_s \cong \frac{1}{\kappa} \iint_{\Sigma_m} \left(\sum_{\alpha=1}^{3} \sigma_\alpha \phi_\alpha \right) \left(\nabla_Q \frac{1}{R}\right) (J_m \, d\xi \, d\eta) \tag{J.9.8}$$

The corresponding transformations for ϕ_D, $\vec{v}_D$ requires the use of the identity (cf. (E.1.28))

$$\hat{n}' \, dS' = \beta^2 A^{-T} \hat{n}_m \, dS, \qquad \hat{n}_m \, dS = \frac{1}{\beta^2} A^T \hat{n}' \, dS' \tag{J.9.9}$$

and the identity

$$\tilde{\nabla} = B \nabla = B A^T \nabla' \tag{J.9.10}$$

The crucial calculation for the treatment of ϕ_D reads

$$n_m \, dS \cdot \tilde{\nabla} = \frac{1}{\beta^2} (A^T \hat{n}' \, dS') \cdot B A^T \nabla'$$

$$= \frac{1}{\beta^2} \hat{n}' \, dS \cdot (A B A^T) \nabla' = s \, \hat{n}' dS' \cdot D \nabla' \tag{J.9.11}$$

where $D = \text{diag}(r, s, rs)$ (see equation (E.3.31)). In deriving the last result we have used the identity (E.3.106), modified for the present context, that

$$A B A^T = s\beta^2 D \tag{J.9.12}$$

Substituting (J.9.11) into the definition of ϕ_D, (J.1.4), and taking account of our earlier observations yields:

$$\phi_D \cong \frac{s}{\kappa} \iint_{\Sigma_m} \left(\sum_{\beta=1}^{6} \mu_\beta \phi_\beta \right) (\hat{n}' \, dS' \cdot D \nabla' \frac{1}{R}) \tag{J.9.13}$$

The crucial calculation for the treatment of $\vec{v}_D$ reads

$$(\hat{n}_m \, dS \times \nabla\mu) \times \tilde{\nabla} f = (\frac{1}{\beta^2} A^T \hat{n}' \, dS' \times A^T \nabla'\mu) \times B \, A^T \nabla' f$$

$$= \frac{1}{\beta^2} A^T [(\hat{n}' \, dS' \times \nabla'\mu) \times A \, B \, A^T \nabla' f]$$

$$= s \, A^T [(\hat{n}' \, dS' \times \nabla'\mu) \times D \, \nabla' f] \qquad \text{(J.9.14)}$$

Here we have used twice the standard identity for the transformation of a cross product (cf. equation (E.1.12)):

$$G\vec{x} \times G\vec{y} = \det(G) \, G^{-T} (\vec{x} \times \vec{y})$$

as well as the result (J.9.12). Substituting (J.9.14) into (J.1.5) as usual we obtain for $\vec{v}_D$:

$$\vec{v}_D = \frac{s}{\kappa} A^T \iint_{\Sigma_m} (\hat{n}' \, dS' \times \nabla'\mu) \times D \, \nabla' (\frac{1}{R}) \qquad \text{(J.9.15)}$$

Having implemented the first two approximations set forth in our list at the beginning of this section, we now simplify our expression a bit and identify some common integrals before proceeding further. We begin this simplification process by examining in somewhat greater detail the form of our integrals in the local coordinate system for Σ_m.

In panel local coordinates, the metric matrix C' is defined by equation (E.2.18) to be

$$C' = A^{-T} \, C \, A^{-1}$$

By taking the inverse of equation (E.3.31) and recognizing that the matrix D is its own inverse, we conclude that

$$C' = (C')^{-1} = D = \begin{bmatrix} r & & \\ & s & \\ & & rs \end{bmatrix} \qquad \text{(J.9.16)}$$

Letting $\vec{P}'$ denote the local coordinate representation of the control point $\vec{P}$,

$$\vec{P}' = A_m (\vec{P} - \vec{P}_9) \qquad \text{(J.9.17)}$$

we find that the kernel function (1/R) has the following representation in local coordinates

$$1/R = 1/\,[\vec{Q}' - \vec{P}', \vec{Q}' - \vec{P}']^{1/2}$$

$$= 1/\,[(\vec{Q}' - \vec{P}')^T C' (\vec{Q}' - \vec{P}')]^{1/2} \qquad \text{(J.9.18)}$$

Introducing the following notation for the components of $\vec{Q}'$ and $\vec{P}'$,

$$\vec{Q}' = \begin{bmatrix} \xi \\ \eta \\ \zeta \end{bmatrix} \qquad \text{(J.9.19)}$$

$$\vec{P}' = \begin{bmatrix} x \\ y \\ z \end{bmatrix} \qquad \text{(J.9.20)}$$

we obtain for the kernel

$$(1/R) = 1/\,[\, r\,(\xi - x)^2 + s\,(\eta - y)^2 + rs\,(\zeta - z)^2\,]^{1/2} \qquad \text{(J.9.21)}$$

Rather than compute $\nabla'(1/R)$, we prefer to work with the quantity $D\ \nabla'\ (1/R)$. On the mean panel Σ_m, $\zeta = 0$ and we obtain

$$D\ \nabla'\ (1/R)\Big|_{\zeta=0} = \begin{bmatrix} x - \xi \\ y - \eta \\ z \end{bmatrix} / R^3 \qquad \text{(J.9.22)}$$

We now write out the formulas for ϕ_s and $\vec{v}_s$ that we require:

$$\phi_s = -\frac{J_m}{\kappa} \sum_{\alpha=1}^{3} \sigma_\alpha \iint_{\Sigma_m} \phi_\alpha \frac{d\xi\, dn}{R} \qquad \text{(J.9.23)}$$

$$\vec{v}_s = \frac{J_m}{\kappa} A^T D \sum_{\alpha=1}^{3} \sigma_\alpha \iint_{\Sigma_m} \phi_\alpha \frac{1}{R^3} \begin{bmatrix} x - \xi \\ y - \eta \\ z \end{bmatrix} d\xi\, d\eta \qquad \text{(J.9.24)}$$

The formula for $\vec{v}_s$ follows from (J.9.8) by using (J.9.22) together with the result

$$\nabla = A^T \nabla' = A^T D\ (D\ \nabla')$$

Upon examining these equations we are led to define the integrals Ψ_a and $\vec{W}_\alpha$ by

$$\Psi_\alpha = \frac{s}{\kappa} \iint_{\Sigma_m} \phi_\alpha \frac{1}{R}\, d\xi\, dn \qquad \text{(J.9.25)}$$

$$\vec{W}_\alpha = \begin{bmatrix} W_{1,\alpha} \\ W_{2,\alpha} \\ W_{3,\alpha} \end{bmatrix} = \frac{s}{\kappa} \iint_{\Sigma_m} \phi_\alpha \begin{bmatrix} x - \xi \\ y - \eta \\ z \end{bmatrix} \frac{1}{R^3} \, d\xi \, d\eta \tag{J.9.26}$$

The reason for including the factor (s/κ) will become apparent when we consider the case of the doublet influence coefficients. Using the quantities Ψ_α and $\vec{W}_\alpha$, we can rewrite ϕ_s and $\vec{v}_s$ as

$$\phi_s = -sJ_m \sum_{\alpha=1}^{3} \sigma_\alpha \Psi_\alpha \tag{J.9.27}$$

$$\vec{v}_s = sJ_m A^T D \sum_{\alpha=1}^{3} \sigma_\alpha \vec{W}_\alpha \tag{J.9.28}$$

The corresponding equation for ϕ_D is obtained by using the fact that

$$\hat{n}' = \begin{bmatrix} 0 \\ 0 \\ 1 \end{bmatrix} \tag{J.9.29}$$

and substituting (J.9.22) into (J.9.13) to obtain

$$\phi_D \simeq \frac{s}{\kappa} \iint_{\Sigma_m} \sum_{\beta=1}^{6} \mu_\beta \phi_\beta \frac{z}{R^3} \, d\xi \, d\eta$$

$$= \sum_{\beta=1}^{6} \mu_\beta W_{3,\beta} \tag{J.9.30}$$

The required equation for $\vec{v}_D$ is obtained by first recognizing that the integrand in equation (J.9.15) can be written

$$(\hat{n}' \times \nabla'\mu) \times D \nabla' (1/R) = \begin{bmatrix} \mu_\xi \, z/R^3 \\ \mu_\eta \, z/R^3 \\ -\mu_\xi \, (x-\xi)/R^3 - \mu_\eta \, (y-\eta)/R^3 \end{bmatrix} \tag{J.9.31}$$

Differentiating the relation (J.9.6) for μ yields

$$\mu_\xi = \mu_2 \phi_1 + \mu_4 \phi_2 + \mu_5 \phi_3 = \sum_{\alpha=1}^{3} \mu_{x,\alpha} \phi_\alpha \tag{J.9.32}$$

$$\mu_\eta = \mu_3 \phi_1 + \mu_5 \phi_2 + \mu_6 \phi_3 = \sum_{\alpha=1}^{3} \mu_{y,\alpha} \phi_\alpha \tag{J.9.33}$$

with the obvious definitions for $\mu_{x,\alpha}$ and $\mu_{y,\alpha}$. Substituting these expressions into (J.9.31) and the result of that back into (J.9.15) yields after some manipulation and taking account of the definition of $\vec{W}_\alpha$,

$$\vec{v}_D = A^T \sum_{\alpha=1}^{3} \begin{bmatrix} \mu_{x,\alpha} & W_{3,\alpha} & \\ \mu_{y,\alpha} & W_{3,\alpha} & \\ -\mu_{x,\alpha} & W_{1,\alpha} & -\mu_{y,\alpha} \; W_{2,\alpha} \end{bmatrix} \tag{J.9.34}$$

We have now reduced the problem of computing the approximate influence coefficients for ϕ_s, $\vec{v}_s$, ϕ_D and $\vec{v}_D$ down to the evaluation of the integrals Ψ_α and $\vec{W}_\alpha$ defined by (J.9.25) and (J.9.26). We will now focus our attention on the computation of these quantities bringing into play our final approximation technique, the Taylor expansion of the kernel functions about the panel center.

Letting R_o denoted the value of R at the panel center, the origin of the local coordinate system, we observe (cf. J.9.21)

$$R_o = [rx^2 + sy^2 + rsz^2]^{1/2} \tag{J.9.35}$$

We may expand (1/R) in a Taylor series about the point $\vec{Q}' = 0$ and obtain on the surface of Σ_m ($\zeta = 0$):

$$\begin{aligned} (1/R) \approx\ & (1/R_o) \\ & + (rx/R_o^3) + \eta\,(sy/R_o^3) \\ & + \frac{\xi^2}{2}\left(\frac{3x^2}{R_o^5} - \frac{r}{R_o^3}\right) + \xi\eta\left(\frac{3rsxy}{R_o^5}\right) + \frac{\eta^2}{2}\left(\frac{3y^2}{R_o^5} - \frac{s}{R_o^3}\right) \end{aligned} \tag{J.9.36}$$

PAGE J.9-7 MISSING FROM ORIGINAL DOCUMENT.

PAGE J.9-8 MISSING FROM ORIGINAL DOCUMENT.

Using these we can write for W_α:

$$\vec{W}_\alpha = \begin{bmatrix} xH_\alpha - \bar{H}_{1\alpha} \\ yH_\alpha - \bar{H}_{2\alpha} \\ zH_\alpha \end{bmatrix} \tag{J.9.48}$$

Consequently we obtain for our various panel influences

$$\phi_S = -sJ_m \sum_{\alpha=1}^{3} \sigma_\alpha \Psi_\alpha \tag{J.9.49}$$

$$\vec{v}_s = sJ_m A^T D \sum_{\alpha=1}^{3} \sigma_\alpha \begin{bmatrix} xH_\alpha - \bar{H}_{1\alpha} \\ yH_\alpha - \bar{H}_{2\alpha} \\ zH_\alpha \end{bmatrix} \tag{J.9.50}$$

$$\phi_D = \sum_{\beta=1}^{6} \mu_\beta zH_\beta \tag{J.9.51}$$

$$\vec{v}_D = A^T \sum_{\alpha=1}^{3} \mu_{x,\alpha} \begin{bmatrix} zH_\alpha \\ 0 \\ \bar{H}_{1\alpha} - xH_\alpha \end{bmatrix} + \mu_{y,\alpha} \begin{bmatrix} 0 \\ zH_\alpha \\ \bar{H}_{2\alpha} - yH_\alpha \end{bmatrix} \tag{J.9.52}$$

J.10 Line Vortex PIC's

The line vortex term of the velocity is given by (cf.(B.3.55))

$$\vec{v}_D{}^* = \frac{1}{\kappa} \int_{\partial S \cap D_p} \mu \; \tilde{\nabla}(\frac{1}{R}) \times \vec{dl} \tag{J.10.1}$$

Differentiating in compressibility coordinates yields

$$\tilde{\nabla}(\frac{1}{R}) = -s\beta^2 \quad (\vec{Q} - \vec{P}) \; /R^3 \tag{J.10.2}$$

and thus

$$\vec{v}_D{}^* = \frac{-s\beta^2}{\kappa} \int_{\partial S \cap D_p} \frac{\mu}{R^3} \; (\vec{Q}_o - \vec{P}_o) \quad \times \; \vec{dl} \tag{J.10.3}$$

In general, the doublet strength is assumed to be continuous everywhere, and thus the line vortex contribution to the velocity cancels and may be ignored. In addition, evaluation of this integral is not possible in supersonic flow without additional assumptions.

In subsonic flow, however, the inclusion of a "line vortex" corresponding to a discontinuity in doublet strength may be meaningful (see Appendix B). The option is not available in version 1.0 of Pan Air, but the theory is included here as background material. In this section, we compute the 3x3 matrix which gives $\vec{v}_D^*$ in terms of μ_-, μ_o, and μ_+, the values of doublet strength at the initial point, center point, and endpoint of a line segment, such as a panel edge.

J.10.1 Computation of $\vec{v}_D^*$

Now along a straight segment of $\partial\Sigma_o$, we have

$$\vec{dx}_o = \hat{t}_o \; ds_o \tag{J.10.4}$$

where $\hat{t}_o$ denotes the unit edge tangent in reference coordinates and ds_o denotes the element of arc length. Also, as one moves along such an edge, the point of integration Q_o varies according to the rule

$$\vec{Q}_o = \vec{Q}_o{}^{(o)} + \hat{t}_o \; s \tag{J.10.5}$$

Thus

$$\tilde{\nabla}(\frac{1}{R}) \times \vec{dx}_o = -s\beta^2 \iint (\vec{Q}_o{}^{(o)} - \vec{P}_o) \times \hat{t}_o \quad \frac{ds_o}{R^3} \tag{J.10.6}$$

Substituting this into equation (J.10.3) we obtain the line vortex velocity due to a straight segment of edge E

$$\vec{v}_D{}^* = \frac{-s\beta^2}{\kappa} \quad (Q_o(o) - P_o) \times \hat{t}_o) \int_E \frac{\mu \, ds_o}{R^3} \tag{J.10.7}$$

This equation motivates us to define the integral

$$\omega = \int_E \frac{\mu \, ds_o}{R^3} \tag{J.10.8}$$

so that $\vec{v}_D{}^*$ is given by

$$\vec{v}_D{}^* = \frac{-s\beta^2}{\kappa} \quad ((\vec{Q}_o(o) - \vec{P}_o) \times \hat{t}_o) \quad \omega \tag{J.10.9}$$

Thus $\vec{v}_D{}^*$ is a constant vector times the integral ω. We evaluate ω by applying a coordinate transformation from the reference system X_o to a local coordinate system X' such that in X', the element of arc length along the edge image is $ds'\big|_{edge} = sqdx'$. Our new coordinate system is defined by the transformations

$$X_o \xrightarrow{\Gamma} X \xrightarrow{E} \bar{X} \xrightarrow{A} X' \tag{J.10.10}$$

The transformation Γ is discussed in Appendix E. The coordinates X are compressibility coordinates, while E is a scaling transformation,

$$E = \begin{bmatrix} 1 & & \\ & \beta & \\ & & \beta \end{bmatrix} \tag{J.10.11}$$

We define

$$A = \frac{1}{|(\bar{t},\bar{t})|^{1/2}} \begin{bmatrix} s\bar{t}_x & \alpha & 0 \\ -s\alpha & s\bar{t}_x & 0 \\ 0 & 0 & q \end{bmatrix} \begin{bmatrix} 1 & 0 & 0 \\ 0 & \bar{t}_y/\alpha & \bar{t}_z/\alpha \\ 0 & -\bar{t}_z/\alpha & \bar{t}_y/\alpha \end{bmatrix} \tag{J.10.12}$$

where

$$\bar{t} = E \; \Gamma \; \vec{t}_o$$

$$\alpha^2 = \bar{t}x^2 + \bar{t}y^2$$

$$q = \text{sign}\,[\bar{t}, \bar{t}] \tag{J.10.13}$$

Before proceeding further, we note in passing that when t_o is chosen to have the normalization

$$[\hat{t}_o, \hat{t}_o] = q = \pm 1 \tag{J.10.14}$$

then $\vec{t}$, $\bar{t}$, and $\vec{t}'$, defined by

$$\vec{t} = \Gamma \vec{t}_0$$

$$\bar{t} = E\,\vec{t}$$

$$\vec{t}' = \bar{A}\,\bar{t} \tag{J.10.15}$$

retain this normalization

$$[\vec{t}, \vec{t}]_x = [\bar{t}, \bar{t}]_{\bar{x}} = [\vec{t}', \vec{t}']_{x'} = q \tag{J.10.16}$$

Because of this nice property, we will assume that $\vec{t}_0$ has the normalization (J.10.14). We can now prove the two identities

$$ds_0 = |\vec{t}_0|\, ds' \tag{J.10.17}$$

$$ds' = sq\, dx' \tag{J.10.18}$$

The first identity is proved by the calculation

$$(ds')^2 = (\hat{t}'\, ds') \cdot (\hat{t}'\, ds') = (\vec{dx}') \cdot (\vec{dx}')$$

$$= (\bar{A}\bar{E}\ \Gamma\ \vec{dx}_0) \cdot (\bar{A}\bar{E}\ \Gamma\ \vec{dx}_0) = \tag{J.10.19}$$

$$(\bar{A}\bar{E}\ \Gamma\ \hat{t}_0\, ds_0) \cdot (\bar{A}\bar{E}\ \Gamma\ \hat{t}_0\, ds_0) =$$

$$(ds_0)^2\, |\bar{A}\bar{E}\ \Gamma\ \hat{t}_0|^2 \tag{J.10.20}$$

Now since $\hat{t}_0 = \vec{t}_0/|\vec{t}_0|$, we find

$$(ds')^2 = (ds_0)^2\ |\bar{A}\bar{E}\ \Gamma\ \vec{t}_0|^2/|\vec{t}_0|^2$$

$$= (ds_0)^2\ |\vec{t}'|^2/|\vec{t}_0|^2 \tag{J.10.21}$$

where we have used equation (J.10.15) to notice that

$$\vec{t}' = \bar{A}\bar{E}\ \Gamma\ \vec{t}_0 = \bar{A}\,\bar{t} \tag{J.10.22}$$

The quantity $\bar{A}\,\bar{t}$ is readily computed:

$$\bar{A}\,\bar{t} = \frac{1}{|[\bar{t}, \bar{t}]|^{1/2}} \begin{Bmatrix} s\bar{t}_x{}^2 + \bar{t}_y{}^2 + \bar{t}_z{}^2 \\ 0 \\ 0 \end{Bmatrix} = sq\sqrt{|[\bar{t}, \bar{t}]|} \begin{Bmatrix} 1 \\ 0 \\ 0 \end{Bmatrix} \tag{J.10.23}$$

Invoking the normalization condition (J.10.16) we then find that

$$\vec{t}' = \bar{A}\,\bar{t} = sq \begin{Bmatrix} 1 \\ 0 \\ 0 \end{Bmatrix} \quad , \quad |\bar{A}\,\bar{t}| = 1 \tag{J.10.24}$$

Using this in equations (J.10.21-22) then yields the required identity

$$|\vec{t}_o|\, ds' = ds_o \tag{J.10.25}$$

The second identity (J.10.18) can be proved by noticing that

$$\hat{t}' = \frac{\vec{t}'}{|t'|} = \vec{t}' = sq \begin{Bmatrix} 1 \\ 0 \\ 0 \end{Bmatrix} \tag{J.10.26}$$

The identity $d\vec{x}' = \hat{t}'\, ds'$ then provides the desired result as follows

$$\begin{Bmatrix} dx' \\ dy' \\ dz' \end{Bmatrix} = d\vec{x}' = \hat{t}'\, ds' = \begin{Bmatrix} sq \\ 0 \\ 0 \end{Bmatrix} ds' \tag{J.10.27}$$

It should be noted that the ratio of arc elements, $|\vec{t}_o|$ (cf.(J.10.17), is closely related to the quantity τ defined by

$$\tau^2 = |[\hat{t}_o, \hat{t}_o]| \tag{J.10.28}$$

To see this relationship note that

$$\vec{t}_o = \frac{\hat{t}_o}{|[\hat{t}_o, \hat{t}_o]|^{1/2}} = \frac{\hat{t}_o}{\tau} \tag{J.10.29}$$

Taking norms and remembering that $|\hat{t}_o| = 1$, we find

$$|\vec{t}_o| = \frac{1}{\tau} \tag{J.10 30}$$

The next piece of information we will need is the form of the function R in the coordinate system X'. Using the fact that in $\bar{X}$, R^2 is given by

$$R2 = (\xi - x)^2 + s(\eta - y)^2 + s(\zeta - z)^2 \tag{J.10.31}$$

one may then use the definition (J.10.12) of A to compute R^2 in X'. One quickly finds that

$$R^2 = q(\xi' - x')^2 + sq(\eta' - y')^2 + s(\zeta' - z')^2 \tag{J.10.32}$$

If we now define the edge variable v and the edge parameter g by

$$v = \xi' - x' \tag{J.10.33}$$

$$sqg^2 = sq(\eta' - y')^2 + s(\zeta' - z')^2 \tag{J.10.34}$$

one quickly obtains the necessary expression for R^2

$$R^2 = qv^2 + sq\ g^2 \tag{J.10.35}$$

We may now write the integral ω in the concise form

$$\omega = \int_E \mu \frac{|\vec{t}_0|\ ds'}{R^3} = \frac{sq}{\tau} \int_E \frac{\mu\ dv}{\sqrt{qv^2 + sqg^2}^{\,3}} \tag{J.10.36}$$

Now on a given edge E, μ is assumed to be a quadratic function, completely determined by its values at the lower and upper endpoints v_- and v_+ and at the midpoint $v_0 = 1/2\ (v_- + v_+)$. The corresponding values of μ are denoted μ_-, μ_+, μ_0. As a function of v, μ may be written

$$\mu = \mu(v) = \mu_-\ f_-\ (v) + \mu_0\ f_0\ (v) + \mu_+\ f_+\ (v)$$

$$= \lfloor \mu_-\ \mu_0\ \mu_+ \rfloor \begin{Bmatrix} f_- \\ f_0 \\ f_+ \end{Bmatrix} \tag{J.10.37}$$

where the functions f are defined

$$f_-\ (v) = \frac{(v - v_0)(v - v_+)}{(v_- - v_0)(v_- - v_+)}$$

$$f_0\ (v) = \frac{(v - v_-)(v - v_+)}{(v_0 - v_-)(v_0 - v_+)}$$

$$f_+\ (v) = \frac{(v - v_-)(v - v_0)}{(v_+ - v_-)(v_+ - v_0)} \tag{J.10.38}$$

If we introduce the basis functions $\phi_0\ (v)$, $\phi_1\ (v)$, $\phi_2\ (v)$ by the definitions

$$\Delta v = v_+ - v_- \tag{J.10.39}$$

$$\phi_0\ (v) = 1$$

$$\phi_1(v) = \frac{v - v_o}{\frac{1}{2}\Delta v}$$

$$\phi_2(v) = \frac{(v - v_o)^2}{\frac{1}{4}(\Delta v)^2} - 1 \qquad \text{(J.10.40)}$$

we see that the f functions can be written

$$\begin{Bmatrix} f_- \\ f_o \\ f_+ \end{Bmatrix} = \begin{bmatrix} \frac{1}{2} & -\frac{1}{2} & \frac{1}{2} \\ 0 & 0 & -1 \\ 0 & \frac{1}{2} & \frac{1}{2} \end{bmatrix} \begin{Bmatrix} \phi_o \\ \phi_1 \\ \phi_2 \end{Bmatrix} \qquad \text{(J.10.41)}$$

Substituting (J.10.40) into (J.10.36) and thence into (J.10.35) we obtain for ω

$$\omega = \lfloor \mu_- \mu_o \mu_+ \rfloor \begin{bmatrix} \frac{1}{2} & -\frac{1}{2} & \frac{1}{2} \\ 0 & 0 & -1 \\ \frac{1}{2} & \frac{1}{2} & \frac{1}{2} \end{bmatrix} \frac{sq}{\tau} \int_E \begin{Bmatrix} \phi_o \\ \phi_1 \\ \phi_2 \end{Bmatrix} \frac{dv}{R^3}$$

$$= \lfloor \mu_- \mu_o \mu_+ \rfloor \begin{bmatrix} \frac{1}{2} & -\frac{1}{2} & \frac{1}{2} \\ 0 & 0 & -1 \\ \frac{1}{2} & \frac{1}{2} & \frac{1}{2} \end{bmatrix} \begin{Bmatrix} \omega_o \\ \omega_1 \\ \omega_2 \end{Bmatrix} \qquad \text{(J.10.42)}$$

where ω_i are defined by

$$\omega_i = \frac{sq}{\tau} \int_E \frac{\phi_i dv}{R^3} \qquad \text{(J.10.43)}$$

The functions ω_i can be computed by repeated integration by parts. In doing this, we treat the general case of a quadratic basis function ϕ. We consider then

$$\omega(\phi) = \frac{sq}{\tau} \int \frac{\phi \, dv}{\sqrt{qv^2 + sqg^2}^{\,3}} \qquad \text{(J.10.44)}$$

$$U = \phi \qquad dV = \frac{dv}{\sqrt{qv^2 + sqg^2}^{\,3}}$$

$$dU = \phi'(v)\, dv \qquad V = \frac{v}{sqg^2 R} \qquad \text{(J.10.45)}$$

Thus

$$\omega(\phi) = \frac{sq}{\tau}\left[\frac{\phi v}{sqg^2R} - \frac{1}{sqg^2}\int \frac{\phi' v}{R}\, dv\right]_{v_-}^{v_+} \tag{J.10.46}$$

Again integrating by parts, let

$$U = \phi'(v) \qquad dV = \frac{v\, dv}{R}$$

$$dU = \phi'(v)\, dv \qquad V = qR \tag{J.10.47}$$

Thus,

$$\omega(\phi) = \frac{sq}{sqg^2}\left[\frac{\phi v}{R} - \phi' qR + q\phi'' \int R dv\right]_{v_-}^{v_+} \tag{J.10.48}$$

Now, note that

$$\frac{d}{dv}(vR) = R + \frac{qv^2}{R} - R + \frac{R^2 - sqg^2}{R}$$

$$= 2R - \frac{sqg^2}{R} \tag{J.10.49}$$

Consequently

$$\int R dv = \frac{1}{2}\left[vR + sqg^2 \int dv/R\right] \tag{J.10.50}$$

and we obtain for $\omega(\phi)$.

$$\omega(\phi) = \frac{sq}{sqg^2}\left[\frac{\phi v}{R} - \phi' qR + \frac{q\phi''}{2}\left(vR + sqg^2 I(\psi)\right)\right]_{v_-}^{v_+} \tag{J.10.51}$$

where, of course, $I(\psi)$ is given by

$$I(\psi) = \int \frac{dv}{R} = \begin{cases} \frac{1}{2}\log\frac{v + R}{v - R} & q = +1 \\ -ph(v,R) & q = -1 \end{cases} \tag{J.10.52}$$

We now apply the formula (J.10.50) to the evaluation of ω_i, i = 0, 1, 2.

First $$\omega_o = \frac{sq}{sqg^2}\ \frac{v}{R}\Big|_{v_-}^{v_+} = \frac{sq/\tau}{sqg^2}\left(\frac{v_+}{R} - \frac{v_-}{R}\right)$$

$$= \frac{sq/\tau}{sqg^2}\ \frac{R_-v_+ - R_+v_-}{R_+R_-}\ \frac{R_-v_+ + R_+v_-}{R_-v_+ + R_+v_-} \qquad (J.10.53)$$

$$= \frac{sq/\tau}{sqg^2}\ \frac{sqg^2(v_+^2 - v_-^2)}{R_+R_-(R_-v_+ + R_+v_-} \qquad (J.10.54)$$

$$= \frac{sq}{\tau}\ \frac{2\Delta v\ v_o}{R_+R_-(R_-v_+ + R_+v_-)} \qquad (J.10.55)$$

where

$$v_o = \frac{1}{2}(v_- + v_+) \qquad (J.10.56)$$

In perofrming this evaluation, we have taken special care that the possibility that $g^2 \approx 0$ not cause any difficulty.

Next, we consider ω_1, which corresponds to

$$\phi_1(v_-) = -1$$

$$\phi_1(v_+) = +1$$

$$\phi_1' = -2/\Delta v \qquad (J.10.57)$$

Using equation (J.10.50) we find

$$\omega_1 = \frac{sq}{sqg^2}\left[\frac{v_+}{R_+} + \frac{v_-}{R_-} - \frac{2q}{\Delta v}(R_+ - R_-)\right] \qquad (J.10.58)$$

After considerable manipulation, one then finds

$$\omega_1 = -\frac{1}{2}\left[\Delta\left(\frac{1}{R}\right)\right]^2\ \frac{s}{\tau\overline{(v/R)}} \qquad (J.10.59)$$

where the overscore denotes the average value of the quantity at the lower and upper endpoints. Finally we compute ω_2, which corresponds to

$$\phi_2(v_+) = \phi_2(v_-) = 0$$

$$\phi_2'(v_+) = -\phi_2'(v_-) = \frac{4}{\Delta v}$$

$$\phi_2'' = \frac{8}{(\Delta v)^2} \qquad (J.10.60)$$

Applying equation (J.10.50), we find

$$\omega_2 = \frac{sq}{(sqg^2)} \left[- \frac{4q}{\Delta v} (R_+ + R_-) + \frac{4q}{(\Delta v)^2} (\Delta(vR) + sqg^2 \Delta I)\right]$$

$$= \frac{4s}{\tau sqg^2(\Delta v)^2} \left[-\Delta v(R_+ + R_-) + \Delta(vR) + sqg^2 \Delta I\right] \qquad (J.10.61)$$

Now

$$- \Delta v(R_+ + R_-) + \Delta(vR) = \bar{v}\Delta R + \bar{R}\Delta v - 2\Delta v\bar{R}$$

$$= \bar{v}\Delta R - \Delta v\bar{R} = v_-R_+ - v_+r_- \qquad (J.10.62)$$

$$= \frac{sqg^2(v_-^2 - v_+^2)}{v_-R_+ + v_+R_-} \qquad (J.10.63)$$

Consequently

$$\omega_2 = \frac{4s}{(\Delta v)^2} \left[\Delta I - \frac{\Delta(v^2)}{v_-R_+ + v_+R_-}\right] \qquad (J.10.64)$$

This may be written

$$\omega_2 = \frac{4s}{\Delta v} \left[\frac{\Delta I}{\Delta v} - \frac{\bar{v}}{R_+R_- - (\overline{v/R})}\right] \qquad (J.10.65)$$

As in the case of ω_0 and ω_1, we have found a form that is perfectly well behaved in the limit $g^2 \approx 0$. Of course, the expression ΔI must be calculated in a stable manner. This problem has already been considered in Section J.8.1.

J.11 Singular Behavior of Integrals

In this section we will examine the behavior of the perturbation potential and velocity induced by a discontinuous source strength, a discontinuous doublet strength, or a discontinuous doublet gradient. It can be seen that no generality is lost by examining the potential and velocity induced by various non-zero source and doublet distributions on the triangular region in figure J.31.

We will consider the cases of discontinuous singluarity strength or gradient across edges in subsonic flow, and subsonic, supersonic, or nearly sonic edges in supersonic flow. The case of $\varepsilon = 0$, $M_\infty = 0$ will be of sufficient generality in subsonic flow. For supersonic flow, the cases of subsonic and supersonic edges may be treated by considering edge 3, and ε a small positive or negative real number. Finally, the compressibility direction may always be taken to be the x-direction, except when considering the case of a superinclined panel. Thus with the exception of this last case, the reference to local transformation (cf.(E.0.1)) is the identity.

In the sections which follow, we will first compute the potential and velocity induced by the three discontinuities in singularity strength or gradient in terms of edge and panel functions. We will then evaluate the computed expressions for each of the flow regimes. We will borrow heavily from the notation of Section J.6, especially J.6.1.4 and J.6.5.

J.11.1 Discontinuous Source Strength

The source strength may be discontinuous across a panel edge in such a fashion that the discontinuity retains the same magnitude along the entire edge, in which case the tangential derivative of source strength is continuous. On the other hand, the magnitude may vary, in which case the tangential derivative is discontinuous. The two representative cases are the constant source strength

$$\sigma_1(x,y) = 1 \tag{J.11.1}$$

and the linearly varying strength

$$\sigma_2(x,y) = x - y \tag{J.11.2}$$

We will now consider the potential and velocity induced by σ_1 and σ_2.

We recall the definition of $[S_o]$

$$\begin{Bmatrix} \phi_s \\ \vec{v}_s \end{Bmatrix} = [S_o]^{4x6} \begin{Bmatrix} \sigma_o \\ \sigma_x \\ \sigma_y \\ \cdot \\ \cdot \\ \cdot \\ \sigma_{yy} \end{Bmatrix} \tag{J.11.3}$$

and note that therefore

$$\begin{Bmatrix} \phi_s \\ \vec{v}_s \end{Bmatrix}_{\substack{\text{due to} \\ \sigma_1}} = [S_o]^{4x6} \begin{Bmatrix} 1 \\ 0 \\ 0 \\ 0 \\ 0 \\ 0 \end{Bmatrix} \tag{J.11.4}$$

$$\begin{Bmatrix} \phi_s \\ \vec{v}_s \end{Bmatrix}_{\substack{\text{due to} \\ \sigma_2}} = [S_o] \begin{Bmatrix} 0 \\ 1 \\ -1 \\ 0 \\ 0 \\ 0 \end{Bmatrix} \tag{J.11.5}$$

Applying (J.6.25), we have

$$\begin{Bmatrix} \phi_s \\ \vec{v}_s \end{Bmatrix}_1 = \begin{Bmatrix} b \\ \vec{a} \\ a \end{Bmatrix} \tag{J.11.6}$$

and

$$\begin{Bmatrix} \phi_s \\ \vec{v}_s \end{Bmatrix}_2 = \begin{Bmatrix} \vec{b}_1 + b\vec{d}_1 - \vec{b}_2 - b\vec{d}_2 \\ \vec{a}_1\vec{d}_1 + B_{11} - \vec{a}_1\vec{d}_2 - B_{12} \\ \vec{a}_2\vec{d}_1 + B_{21} - \vec{a}_2\vec{d}_2 - B_{22} \\ \vec{a}\vec{d}_1 - hr\,(G\vec{a})_1 - \vec{a}\vec{d}_2 + hr\,(G\vec{a})_2 \end{Bmatrix} \tag{J.11.7}$$

where a, b, $\vec{a}$, $\vec{b}$, and B are the fundamental integrals of Section J.6.5, and

$$\vec{d} = \vec{P}_o' = \begin{Bmatrix} x_o' \\ y_o' \end{Bmatrix} \tag{J.11.8}$$

the local coordinate value of the field point.

We first consider the potential and velocity induced by the source distribution σ_1.

We have (cf. J.6.179)

$$b = \frac{-r}{\kappa} \left(\sum_k \int_{\phi_k^-}^{\phi_k^+} R d\phi - 2\pi |h| \; C_\odot \right) \tag{J.11.9}$$

= (cf(J.7.5))

$$\frac{-r}{\kappa} \sum_k J_k(X) \tag{J.11.10}$$

= (cf(J.7.3), (J.7.12), (J.7.27), (J.7.34))

$$\frac{-sh}{\kappa} J - \frac{s}{\kappa} \Sigma a_k q_k I_k \tag{J.11.11}$$

where (cf(J.7.3))

$$J = \sum_k h \; J_k(\psi) - 2\pi \; \mathrm{sign}(h) \; C_\odot \tag{J.11.12}$$

is the panel function and I_k is the edge function. I_k and J_k are defined by (J.7.1) and (J.7.2) respectively.

Next, we have (cf(J.6.174))

$$a = \frac{-s}{\kappa} J \tag{J.11.13}$$

and (cf(J.6.185))

$$\vec{a} = \frac{s}{\kappa} \sum_k \vec{n}_k q_k I_k \tag{J.11.14}$$

Thus we have

$$\phi_{s,1} = b = \frac{-sh}{\kappa} J - \frac{s}{\kappa} \Sigma a_k q_k I_k \tag{J.11.15}$$

$$(\vec{v}_{s,1})_{x,y} = \vec{a} = \frac{s}{\kappa} \Sigma \vec{n}_k q_k I_k \tag{J.11.16}$$

$$(v_{s,1})_z = a = \frac{-s}{\kappa} J \tag{J.11.17}$$

Next we consider the potential and velocity induced by the second source distribution. We have (cf(J.6.195))

$$\vec{b} = \frac{-1}{2\kappa} \sum_k \vec{v}_k q_k \, \Delta(Rv) - \frac{rs}{\kappa} \sum_k \vec{v}_k (a_k^2 + q_k h^2) \, I_k \tag{J.11.18}$$

Thus

$$\phi_{s,2} = \vec{b}_1 - \vec{b}_2 + b(\vec{d}_1 - \vec{d}_2) =$$

$$- \frac{1}{2\kappa} \sum_k (\vec{v}_{k,1} - \vec{v}_{k,2}) \, q_k \, \Delta(Rv) - \frac{rs}{2\kappa} \sum_k (\vec{v}_{k,1} - \vec{v}_{k,2}) \, (a_k^2 + q_k h^2) \, I_k$$

$$+ \phi_{s,1} \, (x_o' - y_o') \tag{J.11.19}$$

Next, by (J.6.201)

$$[B] = b \, I + \frac{rs}{\kappa} \sum_k \vec{n}_k a_k \vec{v}_k^T \, I_k + \frac{1}{\kappa} \sum_k q_k \vec{n}_k \vec{t}_k^T \Delta R \tag{J.11.20}$$

Thus

$$\vec{v}_{s,2,x} = \vec{a}_1(\vec{d}_1 - \vec{d}_2) + B_{11} - B_{12} =$$

$$\vec{v}_{s,1,x} \, (x_o' - y_o') + \phi_{s,1} +$$

$$\frac{rs}{\kappa} \sum_k \vec{n}_{k,1} \, a_k (\vec{v}_{k,2} - \vec{v}_{k,1}) \, I_k +$$

$$\frac{1}{\kappa} \sum_k q_k \, \vec{n}_{k,1} (\vec{t}_{k,1} - \vec{t}_{k,2}) \, \Delta R \tag{J.11.22}$$

Similarly,

$$\vec{v}_{s,2,y} = \vec{a}_2(\vec{d}_1 - \vec{d}_2) + B_{21} - B_{22} \tag{J.11.23}$$

$$= \vec{v}_{s,1,y}(x_o' - y_o') - \phi_{s,1}$$

$$+ \frac{rs}{\kappa} \sum_k \vec{n}_{k,2} \, a_k (\vec{v}_{k,1} - \vec{v}_{k,2}) \, I_k$$

$$+ \frac{1}{\kappa} \sum_k q_k \vec{n}_{k,2} (\vec{t}_{k,1} - \vec{t}_{k,2}) \, \Delta R \tag{J.11.24}$$

Finally,

$$\vec{v}_{s,2,z} = a(\vec{d}_1 - \vec{d}_2) - hr((G\vec{a})_1 - (G\vec{a})_2) \tag{J.11.25}$$

Now,

$$G\vec{n} = \vec{v} \tag{J.11.26}$$

and so

$$\vec{v}_{s,2,z} = \vec{v}_{s,1,z}(x_o' - y_o') - \frac{hrs}{\kappa} \sum_k (\vec{n}_{k,1} - \vec{n}_{k,2})\, q_k I_k \tag{J.11.27}$$

J.11.2 Discontinuous Doublet Strength

A complete discussion of the potential and velocity induced by a discontinuous doublet strength would require consideration of a varying doublet distribution as well as a constant one, in parallel with the discussion on discontinuous source strength. This process would be lengthy, however, and not contribute any additional insight, and so will be neglected. We thus consider a panel with constant doublet strength $\mu = 1$ only.

J.11.2.1 Doublet Potential

We have

$$\phi_D = [D_o]_{1,.}^{1x10} \begin{Bmatrix} \mu_o \\ \cdot \\ \cdot \\ \cdot \\ \mu_{nn} \end{Bmatrix} \tag{J.11.28}$$

where D_o is given by (J.6.253), and $\mu_o = 1$, while all other coefficients are zero.

Thus

$$\phi_D = ra = \frac{-rs}{\kappa} J \tag{J.11.29}$$

$$= \frac{-rs}{\kappa} \left(\sum_k h\, J(\psi) - 2\pi\, \mathrm{sign}(h)\, C_\odot\right) \tag{J.11.30}$$

J.11.2.2 Doublet Velocity

To compute the velocity indeuced by a discontinuous doublet strength, we must use the results of Section J.10. We consider (J.10.41) in light of the fact that $\mu = 1$ on the entire panel. Thus

$$\mu_1 = \mu_o = \mu_+ = 1$$

and

$$\omega = \lfloor 1 \quad 0 \quad 0 \rfloor \begin{Bmatrix} \omega_0 \\ \omega_1 \\ \omega_2 \end{Bmatrix} = \omega_0 \tag{J.11.31}$$

$$\tag{J.11.32}$$

Combining (J.10.9) and (J.11.32)

$$\vec{v}^*_{D,edge} = \frac{-s\beta^2}{\kappa} \quad ((\vec{Q}_0 - \vec{P}_0) \times \vec{t}_0) \quad \vec{\omega}_0 \tag{J.11.33}$$

where Q_0 is any point on the edge. From (J.10.52),

$$\omega_0 = \frac{1}{\tau g^2} \left(\frac{v_+}{R_+} - \frac{v_-}{R_-}\right) \tag{J.11.34}$$

and thus

$$\vec{v}^*_{D,edge} = \frac{-s\beta^2}{\tau\kappa g^2} \left(\frac{v_+}{R_+} - \frac{v_-}{R_-}\right) \quad (\vec{Q}_0 - \vec{P}_0) \quad \times \vec{t}_0 \tag{J.11.35}$$

J.11.3 Discontinuities in Doublet Gradient

Since a discontinuity in the tangential derivative of doublet gradient produces a doublet discontinuity of the type we are neglecting to consider, we need only consider a discontinuity in the normal derivative of the doublet gradient across a panel edge. It is clearly not possible to find a panel with a quadratic doublet distribution which has zero doublet strength on its perimeter without being identically the zero distribution. Thus we look at the effect of a discontinuous doublet gradient across a single edge of the panel. We must later consider the possibility that some of the singular behavior of the induced potential or velocity is artificial, resulting from the isolation of a single edge. That is, the contribution from a neighboring panel may cancel the contribution from this panel edge.

We thus assume that the coordinate system is translated so that it lies on the kth edge of our triangular region, k = 1, 2, 3, and that the doublet strength on the panel is given by

$$\mu_k\ (Q) = \vec{Q} \cdot \hat{n}_k$$

where

$$\hat{n}_k = \tau \vec{n}_k \tag{J.11.36}$$

and $\vec{n}_k$ is the outward pointing edge normal, normalized by (J.6.43) and (J.6.45). Thus $\mu = 0$ on the kth edge, while the normal derivatrive of μ jumps by 1 on the edge.

Thus, applying (J.6.240) and (J.6.253), the potential and velocity induced by μ_k is

$$\begin{Bmatrix} \phi_D \\ \\ v_D \end{Bmatrix}_k = \begin{array}{c} \\ 1 \\ 2 \\ \\ 1 \end{array} \begin{array}{c} \begin{array}{cc} 1 & 2 \end{array} \\ \left[\begin{array}{c|c} ra & ra\vec{d}^T - h\,(G\vec{a})^T \\ \hline 0 & ra\,I \\ \hline 0 & -(G\vec{a})^T \end{array}\right] \end{array} \cdot \begin{Bmatrix} 0 \\ \hline \\ \vec{n}_k \end{Bmatrix} \tag{J.11.37}$$

We now recall that reference and local coordinates are identical. Thus (cf(J.6.39) and (J.6.46))

$$a_k = -\vec{d} \cdot \vec{n}_k = -\frac{1}{\tau}\,\vec{d} \cdot \vec{n}_k \tag{J.11.38}$$

and (cf(J.6.44), (J.6.49-50), and (J.6.55))

$$(G\,\vec{n}_k) \cdot \vec{n}_k = \vec{v}_k \cdot \vec{n}_k = q_k r_\tau \tag{J.11.39}$$

Thus,

$$\begin{aligned} \phi &= ra\,\vec{d}^T\,\vec{n}_k - h\,(G\vec{a})^T\,\vec{n}_k \\ &= -ra\,\tau a_k - h\,(G\vec{a})^T\,\vec{n}_k \end{aligned} \tag{J.11.40}$$

Thus, by (J.11.13-14), and (J.11.39) the contribution due to the kth edge is

$$\phi_k = \frac{rsh\tau}{\kappa}\,J_k a_k - \frac{rsh\tau}{\kappa}\,I_k \tag{J.11.41}$$

Next,

$$\vec{v} = \begin{Bmatrix} ra\,\hat{n}_k \\ -(\vec{Ga})^T\,\vec{n}_k \end{Bmatrix} \tag{J.11.42}$$

Thus

$$\vec{v}_{k,x,y} = \frac{-rs}{\kappa}\,J_k\,\vec{n}_k \tag{J.11.43}$$

while

$$\vec{v}_{k,z} = \frac{-rs}{\kappa}\,I_k \tag{J.11.44}$$

This concludes our reduction to fundamental integrals of the potential and velocity due to discontinuous singularity strength or gradient. We now consider the behavior of the panel function J.

J.11.4 Singularities of the Panel Function

The panel function J is defined by (J.11.12) where (cf Section J.7)

$$J_k(\psi) = \frac{-1}{h}\, ph(hr, aR)\Big|_{-}^{+} \tag{J.11.45}$$

We also have (cf.J.8.105-106)

$$J = -\mathrm{sign}(h) rs \;\; 2\pi - \sum_{\text{edges}} \pi + \sum_{\text{corners}} ph(X_{k,k+1},\, Y_{k,k+1}) \tag{J.11.46}$$

where

$$X_{k,k+1} = -h^2 rs \;\; \langle \hat{t}_k,\, \hat{t}_{k+1} \rangle \;\; - r a_k a_{k+1}$$

$$Y_{k,k+1} = R\,|h| \;\; |\hat{t}_k \times \hat{t}_{k+1}| \tag{J.11.47}$$

J.11.4.1 The Plane h = 0

We see that a possible region of discontinuity for J is the plane h = 0. On this plane,

$$X_{k,k+1} = -r a_k a_{k+1}$$

$$Y_{k,k+1} = 0 \tag{J.11.48}$$

Thus J is not readily defined on the h = 0 plane whenever a = 0 for some edge, that is, whenever the field point lies on the line containing the edge. In addition, on all Mach lines downstreasm from the panel corners, the number of edges or number of corners in D_p may change, and thus J may experience a jump. In figure J.32, we illustrate potential lines of discontinuity for the expression

$$J_+ = \lim_{h \to 0_+} J = -rs(2\pi - \sum_E \pi + \sum_C ph(-r a_k a_{k+1},\, 0^+)) \tag{J.11.49}$$

These lines include some which are upstream of the panel and thus apply only in subsonic flow.

We now claim that J_+ has a constant value on the exterior of the panel and a (perhaps different) constant value on the interior of the panel. This assertion may be proved by careful examination of the behavior of J_+ in the vicinity of a Mach line or a panel edge extension. In any region which does not contain such a line, the number of corners and edges in D_p is a constant, while in addition $a_k a_{k+1}$ never changes sign, and thus J_+ is a constant.

Now, careful examination of figure J.32 makes it clear how J_+ changes when an extension of a panel edge (though not part of the panel edge) is crossed. If the panel is superinclined it has no influence on the field point since $h = 0$. If the flow is subsonic, a_k changes sign, for some edge E_k, while all the a_i, $i = k$, have unchanged sign. Thus $a_{k-1}a_k$ and $a_k a_{k+1}$ both change sign, and so two of the phase functions change in value, one from zero to π, the other from π to zero. Thus J_+ remains unchanged.

Next, when the extension of the edge E_k of a subinclined panel in supersonic flow is crossed, then either both the (k-1) and kth corners lie in D_p or neither does. In the former case, the value of J_+ remains unchanged for the same reasons as in subsonic flow. In the latter case, none of terms of J changes, since the summation over corners includes only those in D_p.

Next we consider the behavior of J_+ as Mach lines are crossed. Here we need only consider subinclined panel in supersonic flow, since for superinclined panels the Mach cones from panel corners intersect the $h = 0$ plane only at the corner itself. Careful consideration of figure J.33 yields the following conclusions.

First, suppose sign $(a_k a_{k+1}) = +1$. Then as the field point P moves such that the kth corner moves into D_p, the number of edges intersecting D_p increases by one. On the other hand, if sign $(a_k a_{k+1}) = -1$, then as the kth corner moves into D_p, the number of edges intersecting D_p increases by zero (if the panel already intersected D_p) or by two (if the panel did not previously intersect D_p).

Thus in the first case, as the corner enters D_p, the sum in (J.11.49) over edges decreases by π while the sum over corners increases by π, and so J remains constant. In the second case (Figure J.33b) the sum over edges is unchanged, but $-ra_k a_{k+1} > 0$, and so the sum over corners is changed by

$$ph(1, 0^+) = 0 \qquad \text{(J.11.50)}$$

In the third case, J_+ is zero when the corner is outside D_p since by convexity, the entire panel is outside D_p (note that (J.11.49) is not valid when the entire panel is outside D_p). Now, when the corner enters D_p, J_+ becomes

$$J_+ = -rs(2\pi - \sum_E \pi + \sum_{1\ \text{corner}} ph(1,0)) = 0 \qquad \text{(J.11.51)}$$

Thus in all cases, J_+ remains constant across Mach lines, even if the point P_0 lies on the panel. In addition, J_+ remain constant across panel extensions. Thus in supersonic flow, $J_+ = 0$ whenever P_0 is outside the panel, since it is zero for a point P_0 for which the panel lies outside

D_p. On the other hand, if P_0 lies inside the panel, $a_k a_{k+1}$ is always positive, and so in both supersonic or subsonic flow we have

$$J_+ = -2\pi rs \tag{J.11.52}$$

by choosing P_0 such that the same number of edges and corners lie in D_p.

Finally, considering a point P_0 outside the panel in subsonic flow, we see that as P_0 crosses from being inside the panel to outside, sign $(a_k a_{k+1})$ changes from +1 to −1 for exactly two corners, and so $-rsJ_+$ decreases by 2π from its value inside the panel of 2π.

Summarizing,

$$\begin{aligned} J_+ &= -2\pi rs && P_0 \text{ inside panel} \\ J_+ &= 0 && P_0 \text{ outside panel} \end{aligned} \tag{J.11.53}$$

We may go through the same arguments for J_-,

$$\begin{aligned} J_- &= \lim_{h \to 0^-} J = rs(2\pi - \sum_E \pi + \sum_C ph(-ra_k a_{k+1}, 0^+) \\ &= -J_+ \end{aligned} \tag{J.11.54}$$

But now, the panel lies outside D_p for a superinclined panel, and thus

$$\begin{aligned} J_- &= 2\pi rs && r = +1, \text{ or} \\ & && P_0 \text{ inside panel} \\ J_- &= 0 && r = -1, \text{ or} \\ & && P_0 \text{ outside panel} \end{aligned} \tag{J.11.55}$$

We thus see that J is continuous on the h = 0 plane except on the panel itself, where J experiences a discontinuity

$$J_+ - J_- = \pi(r + 3)s \tag{J.11.56}$$

J.11.4.2 Discontinuities Due to $C_\bullet$

Let us recall our original definition of J (cf(J.11.12) and (J.11.45))

$$J = \sum_k hJ_k(\psi) - 2\pi \operatorname{sign}(h)\, C_\bullet \tag{J.11.57a}$$

where

$$J_k(\psi) = \frac{-1}{h}\, ph(hv, aR)\Big|_{-}^{+} \qquad (J.11.57b)$$

We now wish to investigate whether the discontinuity in $C_\bullet$ reflects a true discontinuity in J. To do so, we consider the formulation (J.11.46-47) of J. Note that we need only consider subsonic flow and superinclined panels. We also assume h = 0, and that we are not directly above a corner of the panel. Thus $v_- < 0 < v_+$.

Now consider Figure J.34. If the point P_0 is moved so that it lies above the panel, crossing edge 1, then a_1 changes sign, while h, $v_1 \overset{+}{-}$, and $R_1 \overset{+}{-}$ remain essentially unchanged. If $R_1 \overset{+}{-} > 0$, we have

$$ph(hv_1 \overset{+}{-}, a_1R_1) = ph(\mathrm{sign}(hv\overset{+}{-}), 0\overset{+}{-}) \qquad (J.11.58)$$

If we first consider the case of h = 0, $a_1 > 0$ we have

$$ph(hv_1, a_1R_1)\Big|_{-}^{+} = ph(1,0^+) - ph(-1,0^+) = -\pi \qquad (J.11.59)$$

If h = 0, $a_1 < 0$, we have

$$ph(hv_1, a_1R_1)\Big|_{-}^{+} = ph(1,0^-) - ph(-1,0^-) = \pi \qquad (J.11.60)$$

Thus as P_0 moves from being not above the panel (a > 0) to being above it (a < 0),

$$ph(hv, a_1R_1)\Big|_{-}^{+}$$

jumps by 2π. In general, by considering h < 0, we find

$$J_1(\psi)_{outer} - J_1(\psi)_{inner} = 2\pi\ \mathrm{sign}(h) \qquad (J.11.61)$$

On the other hand, when we consider any other edge, we find that the small change in point location has no effect on $J_k(\ )$. That is,

$$J_k(\psi)_{outer} - J_k(\psi)_{inner} = 0$$

$$\text{if } k \neq 1 \qquad (J.11.62)$$

If we combine (J.11.56) with (J.11.61-62), we find

$$J_{outer} - J_{inner} = 0 \qquad (J.11.63)$$

Thus under the assumptions $v_\pm \neq 0$, R > 0, the function J has no discontinuity where $C_\bullet$ does.

These are not regions of discontinuity either, however. The lines $v_{\pm} = 0$ cannot be regions where a jump of 2π occurs, since jumps in a function can only occur across a surface. The problem of $R = 0$ may be handles by redefining J_k:

$$J_k(\psi) = \lim_{R \to R^+} ph(hv^+, a_k R)$$

$$- \lim_{R \to R^-} ph(hv^-, a_k R) \qquad (J.11.64)$$

Summarizing, we find that the discontinuity in C_θ is exactly matched by a corresponding discontinuity in $J_k(\psi)$.

J.11.4.3 Discontinuities in $J_k(\psi)$

We note that the function

$$f(x,y) = ph(x,y) \qquad (J.11.65)$$

may be discontinuous if

$$x < 0 \quad \text{and} \quad y \approx 0$$

or

$$x \approx 0 \quad \text{and} \quad y \approx 0 \qquad (J.11.66)$$

We have already noted that if $h \neq 0$, a discontinuity in $J_k(\psi)$ due to a_k changing sign is matched by a corresponding discontinuity in C_θ, provided that P_0 lies directly above the panel. We now consider the case where a_k changes sign, while P_0 is not directly above the panel. Then defining

$$\Delta J_k = (J_k \mid a_{k>0}) - (J_k \mid a_{k<0}) \qquad (J.11.67)$$

$$\Delta J_k = ph(hv^+, 0^+) - ph(hv^-, 0^+)$$

$$- (ph(hv^+, 0^-) - ph(hv^-, 0^-)) \qquad (J.11.68)$$

$$= ph(hv^+, 0^+) - ph(hv^+, 0^-)$$

$$- (ph(hv^-, 0^+) - ph(hv^-, 0^-)) \qquad (J.11.69)$$

Defining

$$s^{\pm} = 0 \quad \text{if} \quad hv^{\pm} > 0$$

$$= 1 \quad \text{if} \quad hv^{\pm} < 0 \tag{J.11.70}$$

$$\Delta J_k = 2\pi s^+ - 2\pi s^- \tag{J.11.71}$$

since

$$ph(-1,0^+) - ph(-1,0^-) = 2\pi \tag{J.11.72}$$

But, looking at the point P_0' in figures J.34 and J.35, with subsonic flow in figure J.34, we see that if a_k changes sign and P_0 does not lie directly above the panel, then v^+ and v^- have the same sign. Thus $s^+ = s^-$, and so

$$\Delta J_k = 0 \tag{J.11.73}$$

So, we conclude that if $a \approx 0$, $h = 0$, then J is a continuous function.

Thus we can assume that aR has constant sign (since $R \geq 0$) as P_0 moves slightly, though perhaps with changing magnitude. Since we need only consider the case

$$\begin{aligned} v^+ &\approx 0 \\ R &\approx 0 \\ |a| &> 0 \\ |h| &> 0 \end{aligned} \tag{J.11.74}$$

Now, by (J.6.59),

$$R^2 = rsqa^2 + qv^2 + rsh^2 \geq 0 \tag{J.11.75}$$

Thus (J.11.74) can only be satisfied if

$$rsqa^2 + rsh^2 \approx 0 \tag{J.11.76}$$

that is, if

$$\text{sign}(rsq) = \text{sign}(rs) \tag{J.11.77}$$

But this is equivalent to

$$q = -1 \tag{J.11.78}$$

Thus we need only look at a supersonic edge, as illustrated in figure J.36. For P_0 as located there,

$$J_k = ph(hv^+, aR^+) - ph(hv^-, aR^-)$$

$$= ph(hv^+, aR^+) - ph(hv^-, 0) \qquad (J.11.79)$$

$$= ph(hv^+, aR^+) - \pi s^- \qquad (J.11.80)$$

But as P_0 is moved slightly, aR may range over small numbers of constant sign, while hv^+ ranges over small number of constant sign. More precisely, for any real number $\varepsilon > 0$, and any real number x, $-\pi < x < \pi$, there exists a point P such that

$$|\vec{P} - \vec{P_0}| < \varepsilon$$

and

$$ph(hv^+(P), aR^+(P)) = x \qquad (J.11.81)$$

This, by definition, means that the phase function is discontinuous at P_0. Since s^- is a constant which is not dependent on the precise location of P_0, the function J_k is in fact discontinuous at P_0.

Finally, let us consider the behavior of the phase function in the neighborhood of P_0'. Then if the edge intersects D_p,

$$-hJ_k = ph(hv, aR)\Big|_-^+$$

$$= \lim_{R \to 0^+} (ph(hv^+, aR) - ph(hv^-, aR)) \qquad (J.11.82)$$

Since

$$v^- < 0 < v^+ \qquad (J.11.83)$$

we have (considering the four separate cases for sign h and sign a)

$$-hJ_k = -\pi \text{ sign}(h) \text{ sign}(a) \qquad (J.11.84)$$

On the other hand, if the edge does not intersect D_p, J_k is zero.

J.11.4.4 Summary of Panel Function Behavior

We now summarize the results we have obtained concerning the panel function. We find that J experiences a simple jump discontinuity of magnitude

$$J_+ - J_- = \pi(r+3)\ s \qquad (J.11.85)$$

across the panel. In addition, J experiences a jump

$$J_+ - J_- = -\pi \text{ sign}(h) \text{ sign}(a_k) \tag{J.11.86}$$

across a portion of the boundary "Mach wedge" emanating downstream from any supersonic edge. We illustrate such a Mach wedge in cross-section in figure J.37a, where the plane of the paper is a plane downstream from the edge and perpendicular to the flow direction. If the panel is subinclined, it is a plane of constant a_k, while if superinclined, it is a plane of constant h. In figure J.37b, we illustrate a Mach wedge in three dimensions.

Finally, there are certain lines in space along which J takes infinitely many values over a range of 2π as a point on the line is approached from different directions. These lines are the panel edges and the lines emanating from a supersonic panel edge along which $v = 0$ and $R = 0$ (see figure J.37a).

J.11.5 Singularities of the Edge Function

By (J.7.35)

$$I_k(\psi) = \frac{1}{2} \log \left. \frac{R + v}{R - v} \right|_-^+ \quad \text{if } q_k = +1$$

$$= -ph(v,R)\Big|_-^+ \quad \text{if } q_k = -1 \tag{J.11.87}$$

J.11.5.1 Supersonic Edges

We first consider the behavior of the edge function for a supersonic edge. Defining

$$I_k^{\pm} = -ph(v^{\pm}, R^{\pm}) \tag{J.11.88}$$

we see that $I_k^{\pm}$ is continuous if $v^{\pm} = 0$, since if $v^{\pm} < 0$ and $R^{\pm} = 0$,

$$I_k^{\pm} = -\lim_{R \to 0^+} ph(v^{\pm}, R) = -ph(-1,0) = -\pi \tag{J.11.89}$$

But by (J.6.59), for supersonic edges,

$$R^2 = r(a^2 - h^2) - v^2 \tag{J.11.90}$$

Thus

$$R \approx v \approx 0$$

$$|a| \approx |h| \qquad (J.11.91)$$

We therefore see that I_k is discontinuous along the lines defined by the intersection of the Mach cones with the planes $v_{\pm} = 0$ (cf. figure J.37), the same lines along which J_k is discontinuous.

Even when P_0 approaches the panel edge (except at its endpoints), I_k is continuous provided the limit is taken such that the edge intersects D_p. For then

$$v^{\pm} = \pm |\varepsilon| \qquad \varepsilon \approx 0$$

$$R^{\pm} = 0 \qquad (J.11.92)$$

Thus $I_k =$

$$-ph(v,R)\Big|_{-}^{+} = -ph(|\varepsilon|, 0^+) + ph(-|\varepsilon|, 0^+)$$

$$= \pi \qquad (J,11.93)$$

regardless of the direction from which the point approaches the edge, unless the edge is approached so that it does not lie in D_p, in which case the limit is zero.

J.11.5.2 Subsonic Edges

By (J.11.87) we see that I_k is continuous unless

$$|R^{\pm}| = |v^{\pm}|$$

$$\text{or} \quad R^{\pm 2} - v^{\pm 2} = 0 \qquad (J.11.94)$$

By (J.6.59) we have, since $r = q = 1$,

$$R^2 = v2 + s(a2 + h^2) \qquad (J.11.95)$$

Thus I_k may be singular when

$$|R^{\pm 2} - v^{\pm 2}| = |s(a^2 + h^2)| = g^2 = 0 \qquad (J.11.96)$$

that is, whenever the field point P_0 lies on the line containing the panel edge. Now, if P_0 lies on an extension of the edge, v^+ and v^- have the

same sign, and are non-zero. Applying the rationalization (J.8.35-36)

$$I_k = \frac{1}{2} \log \left(\frac{1 + z}{1 - z}\right) \tag{J.11.97}$$

$$Z = \frac{(v_+ - v_-)(v_+ + v_-)}{R_+v_+ + R_-v_-}$$

$$\approx \frac{v_+^2 - v_-^2}{(v_+^2 + v_-^2)\ \mathrm{sign}(v_+)} \tag{J.11.98}$$

we see that $|z| < 1$. Thus I_k is a continuous function in this case.

Next, suppose P_0 lies very near the panel edge. If the flow is supersonic, this means $R^- = 0$, and thus by (J.8.27)

$$z = \frac{v_+^2 - v_-^2}{R_+v_+} \tag{J.11.99}$$

As long as the point is away from the edge, $v_+ < R_+$, $v_\pm^2 > 0$, and so $|z| < 1$, making I_k continuous. But as P_0 approaches the edge, v_+ approaches R_+ , v_- approaches zero, and so $|z|$ approaches 1. Thus I_k becomes infinite as the point approaches the panel edge.

For subsonic flow, if P_0 approaches the panel edge, v changes sign along the edge and we thus use the rationalization (J.8.40-41))

$$I_k = \log \frac{(R_+ + v_+)(R_- + |v_-|)}{g^2} \tag{J.11.100}$$

The denominator is non-zero, and thus we see that is both subsonic and supersonic flow, the edge function I_k becomes logarithmically infinite when the field point approaches the edge.

J.11.5.3 Subsonic Nearly Sonic Edges

The same arguments used for subsonic edges show that the only potential singularity occurs when $v = R$, that is, when the point P_0 is on the line extending the subsonic edge. This situation is illustrated in figure J.38.

Defining a unit edge tangent

$$\hat{t}_0 = \frac{\vec{Q}_+ - \vec{Q}_-}{|\vec{Q}_+ + \vec{Q}_-|} \tag{J.11.101}$$

we see that

$$R_\pm^2 = [\vec{Q}_\pm - \vec{P}_0, \vec{Q}_\pm - \vec{P}_0]$$

$$= |\vec{Q}_\pm - \vec{P}_0|^2 \, [\hat{t}_0, \hat{t}_0] = \tau^2 \, |\vec{Q}_\pm - \vec{P}_0|^2 \qquad \text{(J.11.102)}$$

while

$$v_\pm = [t_0, Q_\pm - P_0] = \quad Q_\pm - P_0 \quad = R_\pm \qquad \text{(J.11.103)}$$

Applying (J.11.97-98)

$$I_k = \frac{1}{2} \log \left(\frac{1 + z}{1 - z}\right) \qquad \text{(J.11.104)}$$

where

$$z = \frac{|\vec{Q}_+ - \vec{P}_0|^2 - |\vec{Q}_- - \vec{P}_0|^2}{|Q_+ - P_0|^2 + |Q_- - P_0|^2} = \frac{(s_0 + \Delta s)^2 - s_0^2}{(s_0 + \Delta s)^2 + s_0^2} \qquad \text{(J.11.105)}$$

where we have used the notation of figure J.38.

So,

$$|z| = \left| \frac{2s_0\Delta s + \Delta s^2}{2s_0^2 + 2s_0\Delta s + \Delta s^2} \right| < 1 \qquad \text{(J.11.106)}$$

whenever $s_0 > 0$. But as s_0 approaches zero, z approaches 1. In fact

$$\lim_{s_0 \to 0} I_k = \frac{1}{2} \lim_{s_0 \to 0} \log \frac{1 + z}{1 - z}$$

$$= \frac{1}{2} \lim_{s_0 \to 0} \log \left(\frac{2}{1 - \dfrac{2s_0\Delta s + \Delta s^2}{2s_0^2 + 2s_0\Delta s + \Delta s^2}} \right) \qquad \text{(J.11.107)}$$

$$= \frac{1}{2} \lim_{s_0 \to 0} \log \frac{2(2s_0^2 + 2s_0\Delta s_0 + \Delta s^2)}{2s_0^2} \qquad \text{(J.11.108)}$$

$$= \frac{1}{2} \lim_{s_0 \to 0} \log \frac{\Delta s^2}{s_0^2} \qquad \text{(J.11.109)}$$

Thus as P approaches the endpoint of the edge, I_k becomes logarithmically infinite. Otherwise, however, I_k is continuous.

J.11.5.4 Supersonic Nearly Sonic Edges

We have seen that $v = R$ only when the point P_0 lies on the line containing the edge. But a supersonic edge has the property that no point on the edge lies in the domain of dependence of any point on the line containing the edge. Thus, if $v = R$, the edge does not influence P_0. Thus I_k is continuous everywhere except along the edge itself.

J.11.5.5 Essentially Sonic Edges

Combining (J.8.13) and (J.8.72), we see that for essentially sonic edges

$$I_k(\psi) = \lim_{\tau \to 0} q\tau\hat{I} = \lim_{\tau \to 0} \frac{q\tau\Delta R}{\hat{v}} \tag{J.11.110}$$

Now,

$$\frac{\tau}{\hat{v}} = \frac{1}{\dfrac{\hat{v}_+ + \hat{v}_-}{2\tau}} = \frac{2}{v_+ + v_-} \tag{J.11.111}$$

But v can not change sign for an essentially sonic edge, in fact, both v_+ and v_- will be very large numbers (of order $1/\tau$) of the same sign, unless P_0 lies very near to the edge itself. We thus find that I_k is not only continuous, but of order τ, everywhere except at the edge.

J.11.6 Singularities in Subsonic Flow

In this section, we consider the effect of a continuous source strength, doublet strength, or doublet gradient on the potential or velocity in subsonic flow. We illustrate the distances h,v,a,g and R for subsonic flow in Figure J.39.

J.11.6.1 Discontinuous Source Strength

We see by (J.11.15) that the potential due to a panel with source strength 1 is

$$\phi_{s,1} = \frac{-sh}{\kappa} J - \frac{s}{\kappa} \Sigma a_k q_k I_k \tag{J.11.112}$$

But by Section J.11.4.4, J is continuous in subsonic flow except for a jump by 4π across the panel. Thus hJ is continuous everywhere in subsonic flow except near the panel edge, where

$$I_k = \log \left(\frac{\text{constant}}{g^2}\right) \tag{J.11.113}$$

$$= \text{constant} - 2 \log |g|$$

But $\quad g^2 = a^2 + h^2$

or $\quad |g| \geq |a|$ (J.11.114)

and thus $a_k I_k$ is continuous and bounded everywhere. We thus see that in subsonic flow the potential due to a constant strength source panel is continuous everywhere.

Next we consider the velocity due to the constant source distribution. By (J.11.6)

$$\vec{v}_s = \begin{Bmatrix} \vec{a} \\ -- \\ a \end{Bmatrix} \tag{J.11.115}$$

where

$$\vec{a} = \frac{1}{\kappa} \Sigma \vec{n}_k I_k$$

$$a = \frac{-s}{\kappa} J \tag{J.11.116}$$

We thus see that the component of the source velocity perpendicular to the edge becomes logarithmically infinite as we approach the panel edge.

That is,

$$\vec{v}_{s,x,y} = \text{bounded terms} - \vec{n}_k \log(g) \tag{J.11.117}$$

as P_o approaches the kth panel edge.

In addition, the z-component of velocity jumps as the panel is crossed, which is to be expected in light of the definition of source strength as the jump in normal mass flux (or normal velocity at Mach zero).

We will leave consideration of the varying source distribution (cf.(J.11.5)) to the reader. We do note, however, that no new discontinuities or singularities appear.

J.11.6.2 Discontinuous Doublet Strength

By (J.11.29) the potential induced by a constant strength doublet panel in subsonic flow is

$$\phi_D = ra = \frac{1}{\kappa} J \tag{J.11.118}$$

This function is continuous in subsonic flow except for a jump across the panel, which is to be expected since the doublet strength is defined as the jump in potential.

Next, the line vortex term of the doublet velocity is given by (cf.(J.11.35))

$$\vec{v}^{*}_{D,edge} = \frac{-\beta^2}{g^2}\left(\frac{v_+}{R} - \frac{v_-}{R}\right) \quad (\vec{Q}_o - \vec{P}_o) \times \hat{t}_o \tag{J.11.119}$$

Thus in subsonic flow this velocity is continuous whenever $g = 0$. Applying the rationalization (J.10.54) for the case $g \approx 0$,

$$v^{*}_{D,edge} = \frac{-\beta^2}{\kappa\tau} \; \frac{\Delta v(v_+ + v_-)}{R_+R_-(R_-v_+ + R_+v_-} \quad (\vec{Q}_o - \vec{P}_o) \times \hat{t}_o \tag{J.11.120}$$

we see that if

$$R_-v_+ + R_+v_- \neq 0 \tag{J.11.121}$$

the velocity is again well-behaved, since (J.11.120) cannot occur whenever R_+ or R_- is zero. But if $g = 0$

$$\begin{aligned} R_-^2 &= v_-^2 \\ R_+^2 &= v_+^2 \end{aligned} \tag{J.11.122}$$

and so

$$\begin{aligned} R_-v_+ + R_+v_- = 0 \quad &\Longrightarrow \\ R_+ &= v_+ \\ -R_- &= v_- \end{aligned} \tag{J.11.123}$$

That is, v_+ and v_- have opposite sign unless one of them is zero. Thus, the point P_o lies on the panel edge. So, the velocity is well-behaved for all points which do not lie on the panel edge.

We now consider the limiting value of the velocity as P_o approaches the panel edge. By (J.11.122)

$$\frac{v_+}{R_+} - \frac{v_-}{R_-} = 2 \tag{J.11.124}$$

except perhaps at the endpoints of the edge. Further, it is easy to see that

$$\left| (\vec{Q}_o - \vec{P}_o) \times \hat{t}_o \right| = g \tag{J.11.125}$$

and thus

$$\lim_{P_0 \to \text{edge}} \vec{v}_D^* = \frac{2\beta^2}{\kappa g} \tag{J.11.126}$$

That is, the velocity has a magnitude proportional to the inverse of the distance from the point to the edge.

J.11.6.3 Discontinuous Doublet Gradient

We have seen that the potential due to a discontinuity in the normal component of doublet gradient is (cf(J.11.41))

$$\phi_k = \frac{-rsh\tau\, a_k}{\kappa} J_k + \frac{rsh\tau}{\kappa} I_k \tag{J.11.127}$$

Examination of section J.11.4 shows that the panel function contribution to the potential is continuous except on the panel surface. On the other hand, (J.11.100) describes the edge function behavior in subsonic flow. We thus see that the potential becomes infinite in the neighborhood of a panel edge, and is proportional to the logarithm of the distance from the edge.

J.11.7 Discontinuous Source Strength in Supersonic Flow

J.11.7.1 Source Potential

We recall from (J.11.15) that the potential due to a constant source panel is

$$\phi_s = \frac{-sh}{\kappa} J - \frac{s}{\kappa} \Sigma a_k q_k I_k \tag{J.11.128}$$

An examination of the results of Sections J.11.4 and J.11.5 show that hJ and are continuous with several exceptions. One exception for J is that if the kth edge is supersonic, and $a = h$, $R_\pm = v_\pm = 0$, J_k may take on any value (cf. Section J.11.4.3). Also, if $R_+ = 0 = R_-$, $h = a$, then J_k undergoes a jump across the "Mach wedge" located there. On the other hand (cf. Section J.11.5.1) I has discontinuiutes at the same locations. Consideration of (J.11.82) and (J.11.88) shows that if $h = a$

$$-h\, J_k = -\text{sign}(h)\ \text{sign}(a)\ I_k \tag{J.11.129}$$

Thus

$$\frac{-sh}{\kappa} (hJ_k) + \frac{sa_k}{\kappa} I_k = 0 \tag{J.11.130}$$

when $|h| = |a|$. So, while J_k and I_k are discontinuous away from the panel, the sum ϕ_S is continuous everywhere except on the panel.

J.11.7.2 Source Velocity

By (J.11.16-17)

$$\vec{v}_S = \left\{ \begin{array}{c} \frac{s}{\kappa} \sum_k \vec{n}_k q_k I_k \\ \hline \frac{-s}{\kappa} J \end{array} \right\} \qquad \text{(J.11.131)}$$

Thus the z-component of the velocity is always finite, though it is discontinuous on the panel and on the Mach wedges emanating from supersonic edges. On the other hand, by Section J.11.5, the tangential component of becomes logarithmically infinite as the point P_0 approaches a subsonic or sonic edge and is discontinuous as P_0 approaches a supersonic edge.

Now, for nearly sonic edges, I_k remains bounded but non-zero. Since $\vec{n}_k = \hat{n}_k/\tau$ is of order $1/\tau$, the velocity in a very small region (that is, along the extension of the edge) is of order $1/\tau$. This is not a singularity since for any particular nearly sonic edge the resulting velocity is bounded.

Finally, for essentially sonic edges, the edge function is of order τ everywhere except at the edge, and thus the source velocity remains bounded.

J.11.8 Discontinuous Doublet Strength in Supersonic Flow

By (J.11.29-30), the potential due to a panel with unit doublet strength is

$$\phi_D = \frac{-rs}{\kappa} J \qquad \text{(J.11.132)}$$

Thus the singularities of the doublet potential are exactly those of the panel function. That is (cf Section J.11.4.4) the potential has a jump across the panel, snd across the Mach wedge emanating from any supersonic edge, and is discontinuous with multiple limiting values at panel edges and the lines $R_{\pm} = v_{\pm} = 0$.

Next, we consider the doublet velocity. By (J.11.35)

$$\vec{v}_D^* = \frac{-s\beta^2}{g^2} \left(\frac{v_+}{R_+} - \frac{v_-}{R_-}\right) \quad (\vec{Q}_o - \vec{P}_o) \times \hat{t}_o \tag{J.11.133}$$

We state here without proof that a "finite part" of the doublet velocity line vortex term may be computed as

$$\vec{v}_{D,\text{finite}}^* = \frac{-s\beta^2}{g^2} \quad (\vec{Q}_o - \vec{p}_o) \times \hat{t}_o \cdot$$

$$\left(\sum_{\substack{\text{edge vertices} \\ \text{in } D_p}} \frac{v}{R} \text{ sign(vertex)} \right) \tag{J.11.134}$$

Using (J.11.134), it is straightforward to show that $\vec{v}$ is bounded over any region of space which does not include the Mach cone emanationg downstream from the vertices of the edge. In the vicinity of these cones, $\vec{v}$ is of order (1/R).

J.11.9 Discontinuous Doublet Gradient in Supersonic Flow

By (J.11.41), a discontinuous doublet gradient along an edge yields a potential

$$\phi_k = \frac{hrs}{\kappa} \tau a_k J_k \; \frac{-rsh}{\kappa} \tau I_k \tag{J.11.135}$$

It can easily be seen that this function is continuous along panel edges, since h and a_k are zero there. In addition, the discontinuities of J_k and I_k on the surface $|h| = |a|$ cancel (cf(J.11.129)). Thus the potential due to a discontinuity in doublet gradient is continuous away from the panel.

Next (cf(J.11.43)),

$$\vec{v}_{k,x,y} = \frac{-rs}{\kappa} J_k \vec{n}_k \tag{J.11.136}$$

and so is discontinuous on the Mach wedge emanating from a supersonic panel edge. Finally (cf(J.11.44))

$$\vec{v}_{k,z} = \frac{-rs}{\kappa} \tau I_k \tag{J.11.137}$$

and so the normal velocity is logarithmically infinite in the neighborhood of subsonic edges, and discontinuous on the Mach wedge emanating from a supersonic edge.

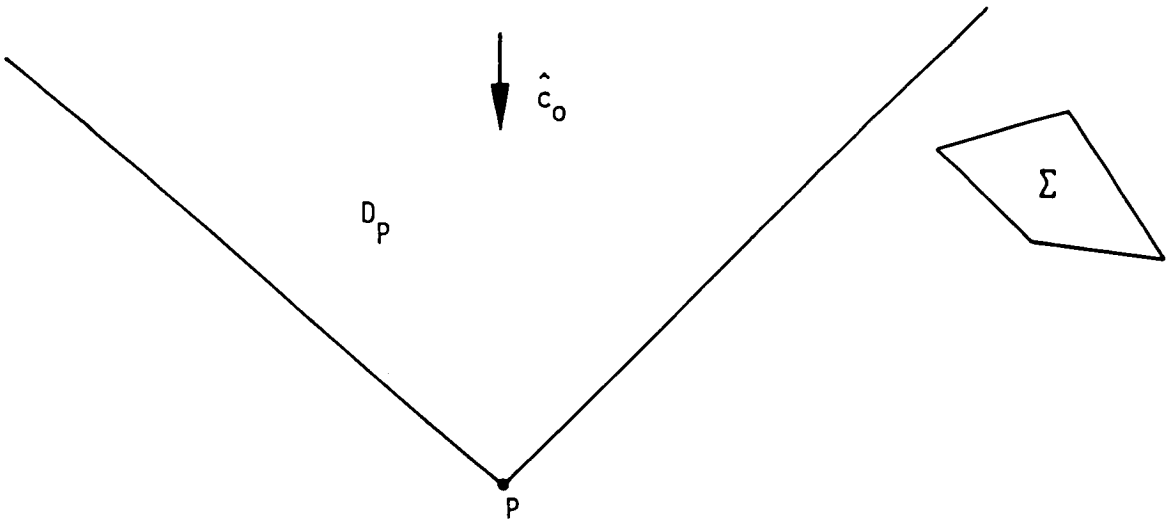

Figure J.1 - Domain of dependence

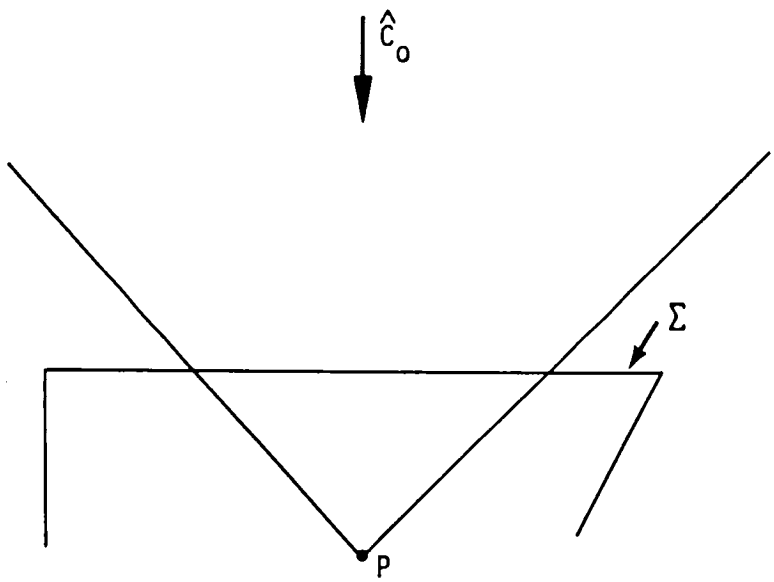

Figure J.2 - Superinclined panel partially within D_P without corners in D_P

Notation

$\hat{c}_o$	unit compressibilty vector
$[C_o]$	metric matrix $C_o = sB^2 I + (1-sB^2)\,\hat{c}_o\,\hat{c}_o^T$
$[\tilde{C}_o]$	positive definite metric matrix $\tilde{C}_o = \beta^2 I + (1-\beta^2)\,\hat{c}_o\,\hat{c}_o^T$
D_P	domain of dependence
$[B_o]$	dual metric matrix $B_o = I + (s\beta^2-1)\,\hat{c}_o\,\hat{c}_o^T$
P	control point or field point
Q	point or panel, point of integration
Q_o	panel center
Q_i, $i=1,\ldots,9$	panel defining points
$[\ ,\ ]$	compressible inner product, corresponding to $[C_o]$
$\{\ ,\ \}$	dual inner product, corresponding to $[B_o]$
$\vec{R}$	$\vec{Q} - \vec{P}$
$\hat{n}_o$	subpanel unit normal vector
$\hat{t}_o$	unit edge tangent
A_o	reference to local transformation
A_i	reference to local transformation for i^{th} region

Figure J.3 - Notation used frequently in Appendix J

a. Panel

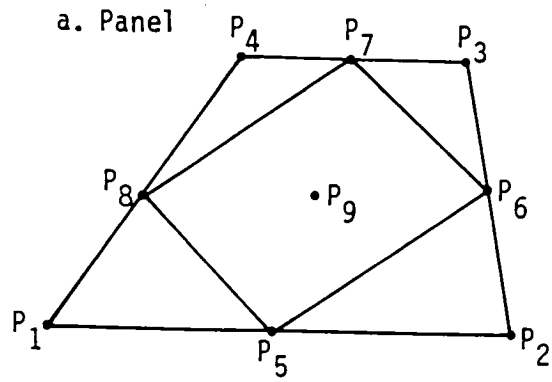

b. Two half panels

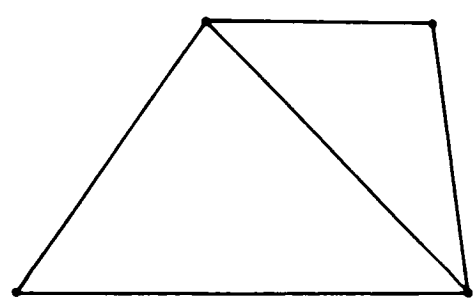

c. Two half panels

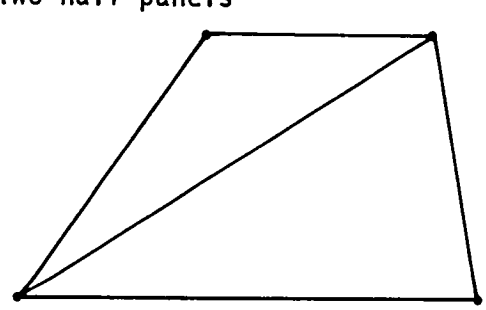

Figure J.4 - Two region approximations to panel

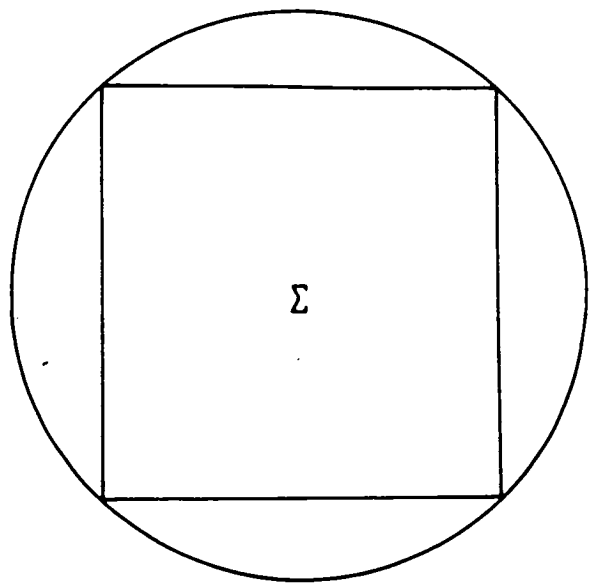

Figure J.5 - Region in which intermediate field PIC is not performed

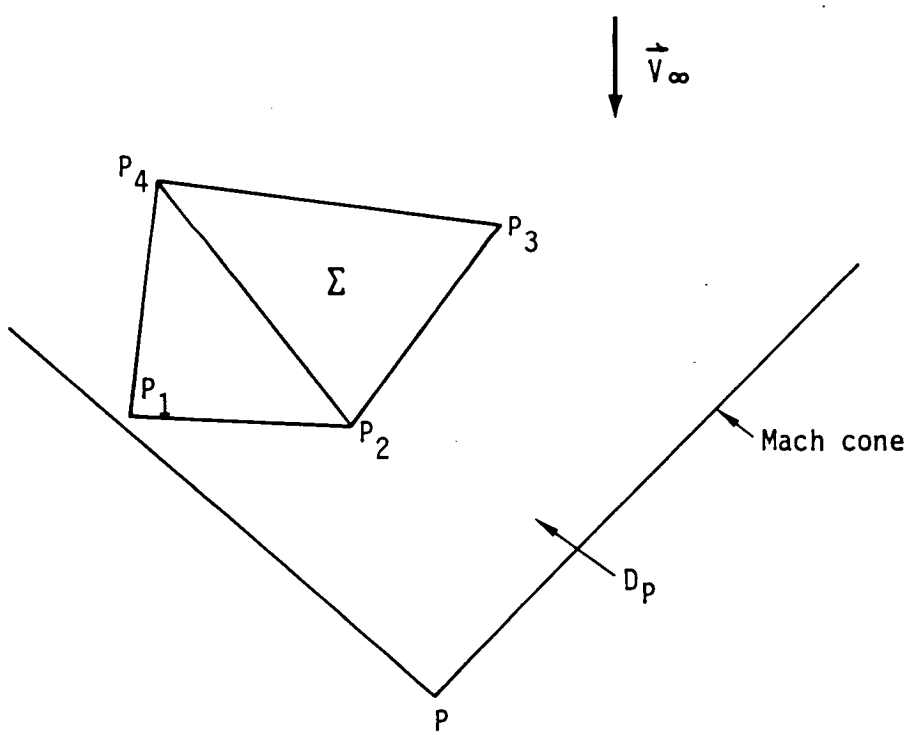

Figure J.6 - Splitting a panel into half panels

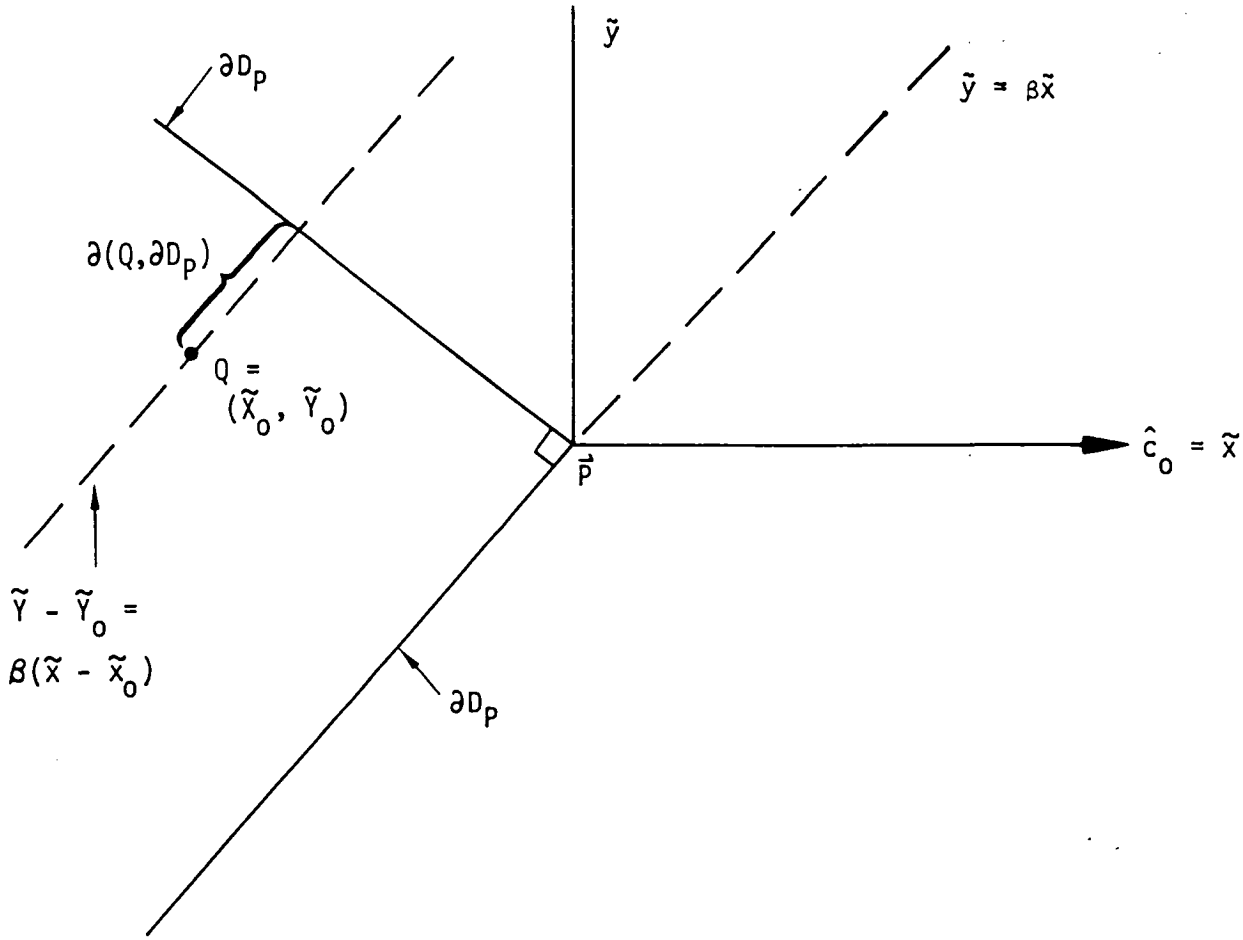

Figure J.7 $(\tilde{X},\tilde{Y})$ coordinate system

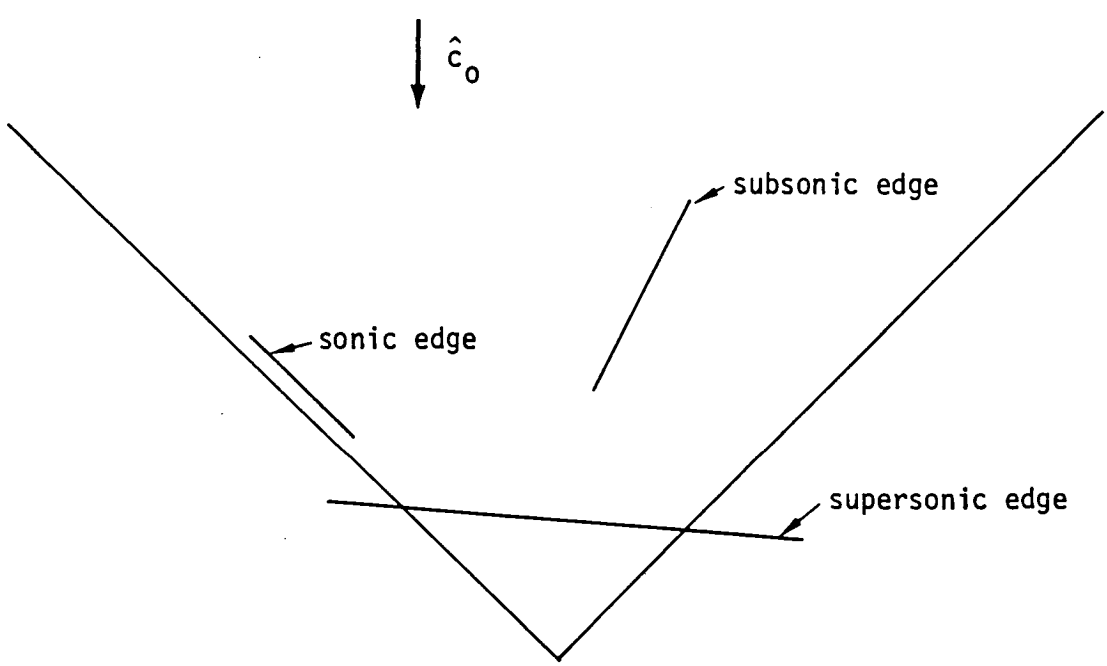

Figure J.8 - Subsonic and supersonic edges

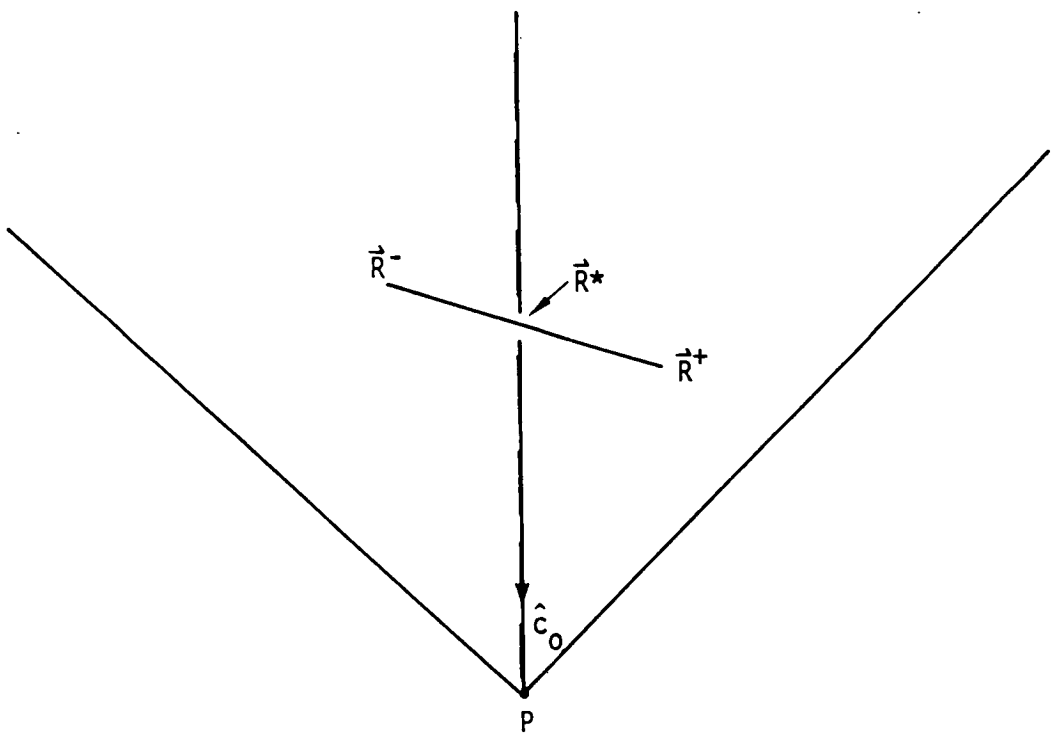

Figure J.9 - Point of closest approach

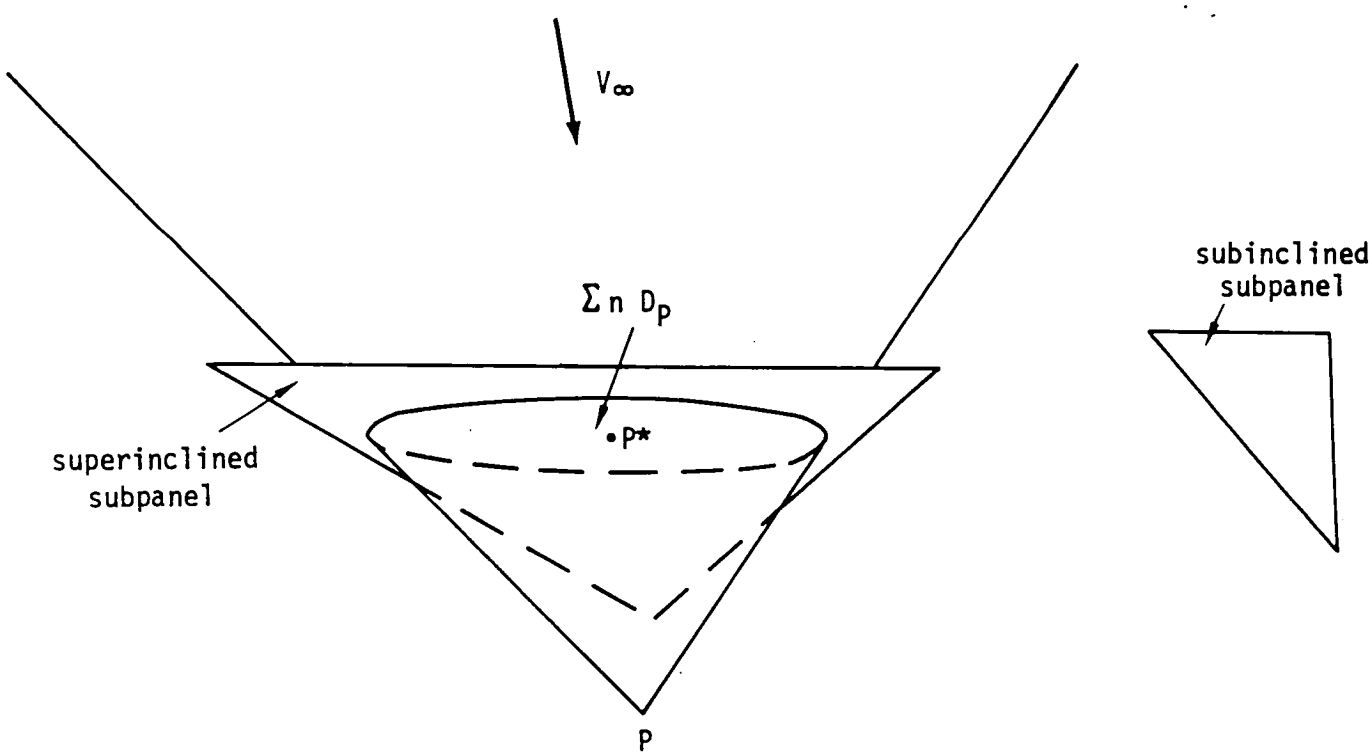

Figure J.10 - Subinclined and superinclined panel

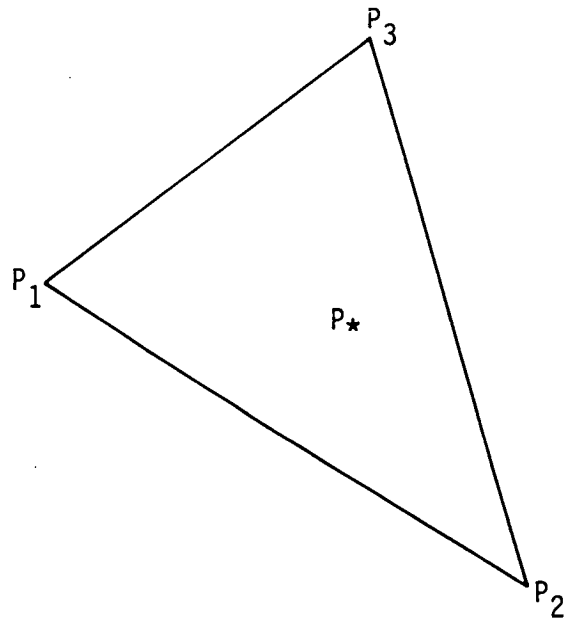

Figure J.11 - P_* lies in the interior of the subpanel

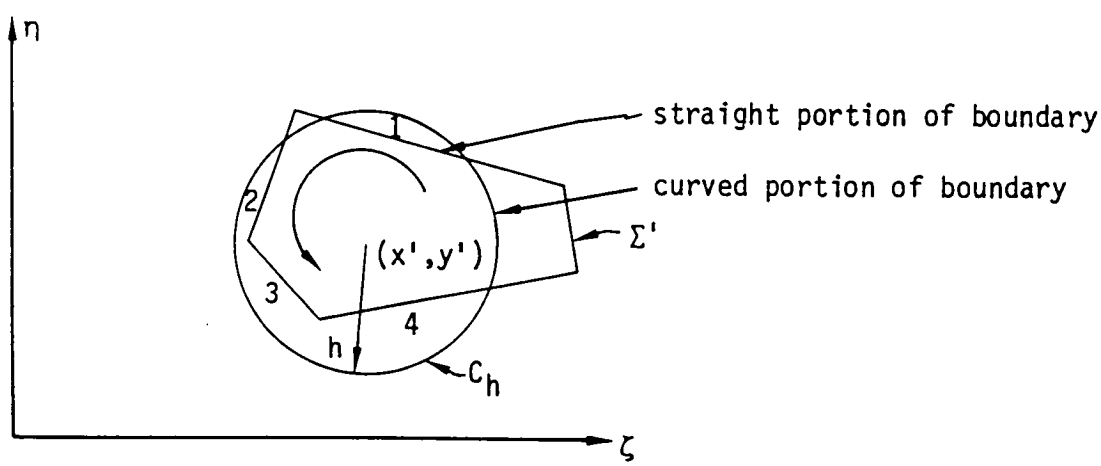

Figure J.12 - Region of integration, $\Sigma' \cap C_h$ for a typical subpanel

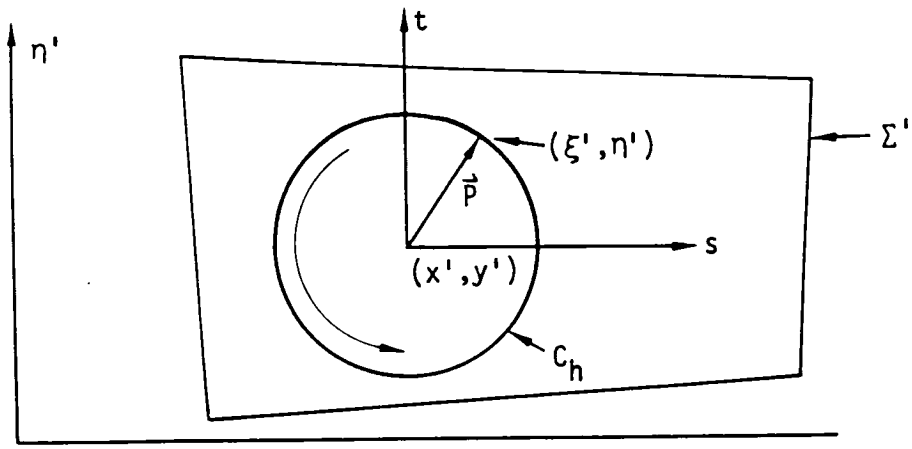

Figure J.13 - $P_k^{\pm}$, $Q_k^{\pm}$ when $C_h \subset \Sigma'$

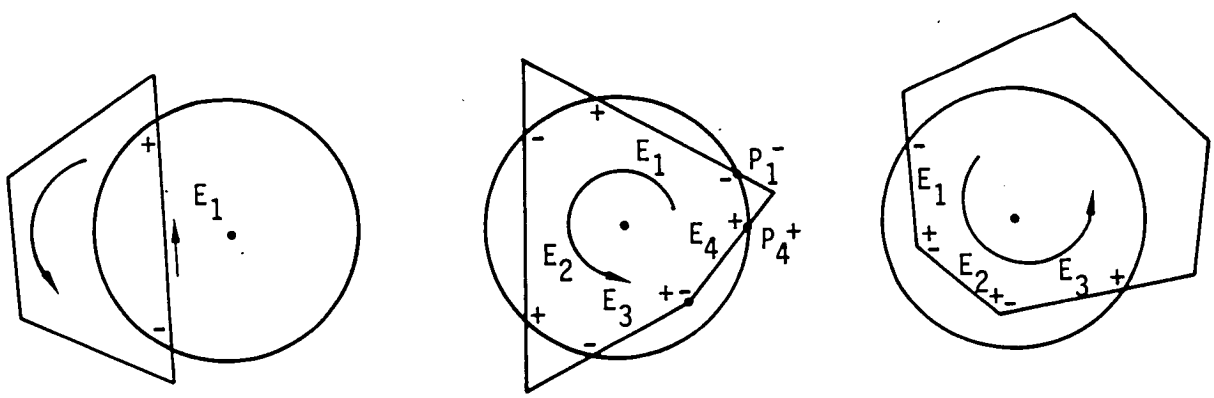

Figure J.14 - Edge numbering for various panel configurations

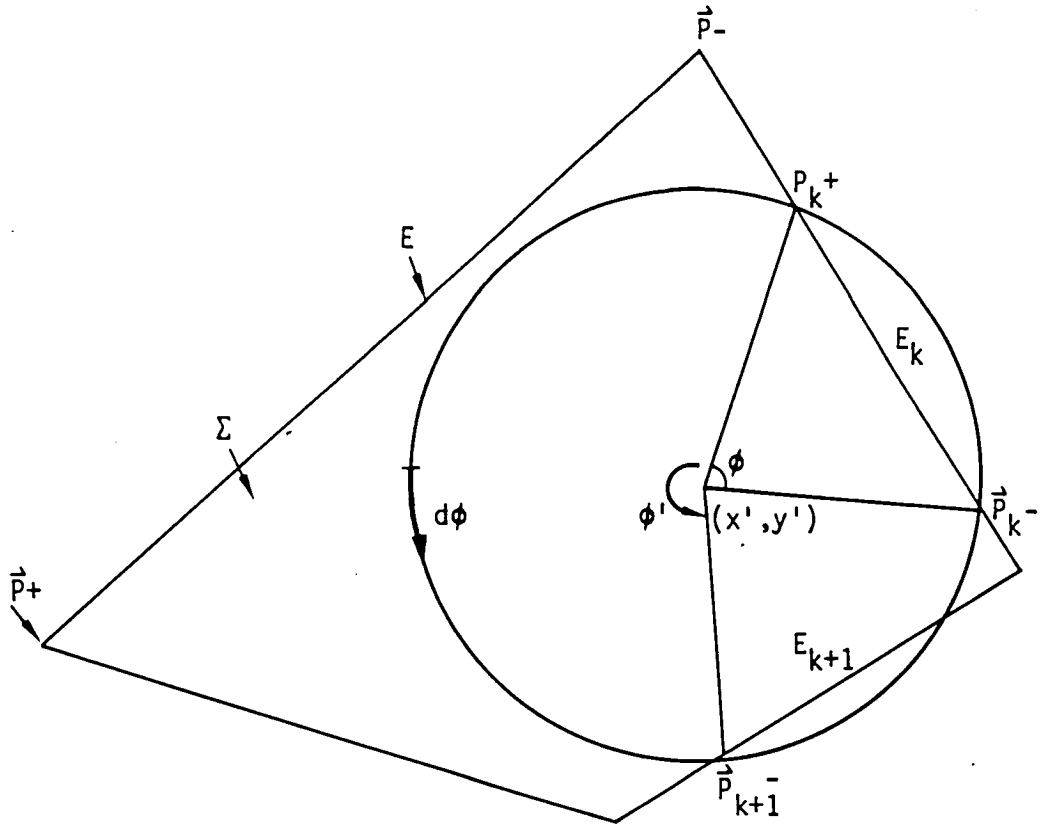

Figure J.15 - Phase angle ϕ' exceeds π

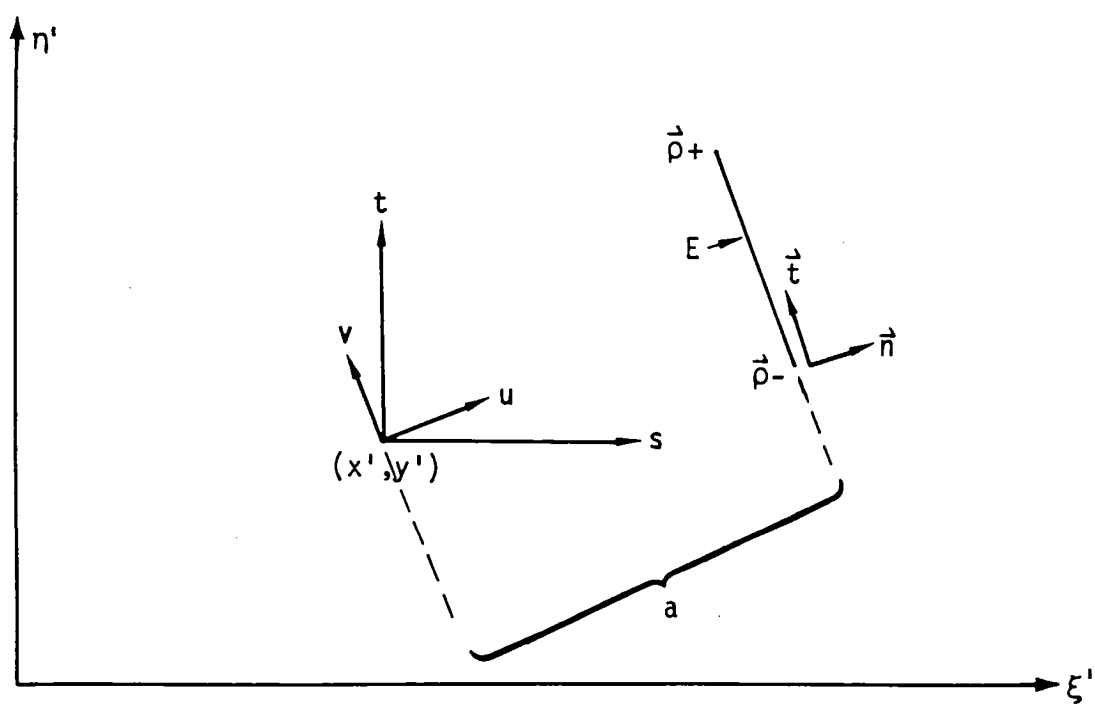

Figure J.16 - Coordinate systems in the (ξ',η') plane

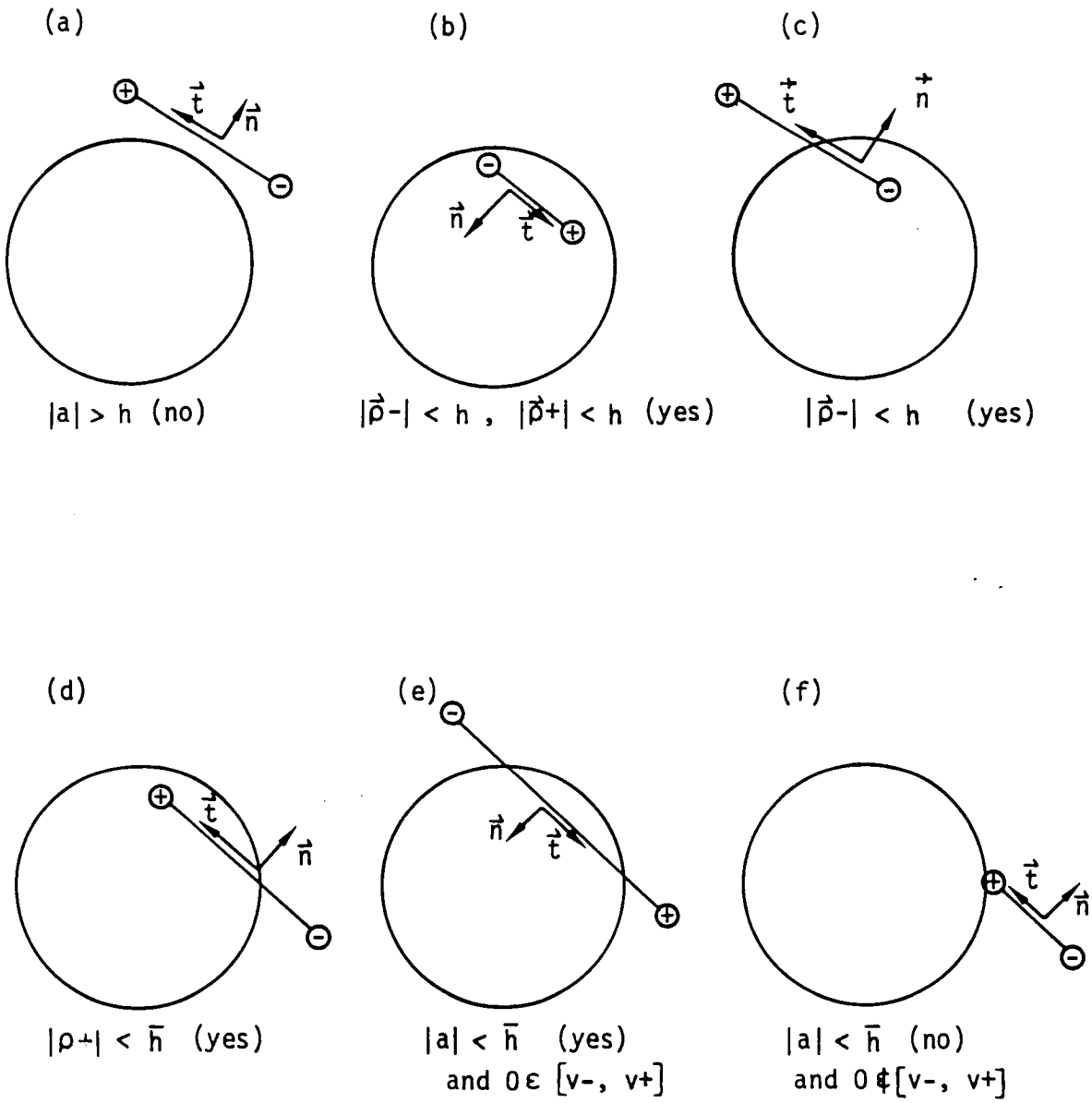

Figure J.17 - Determining if an edge of Σ' is an edge of $\Sigma' \cap C_h$

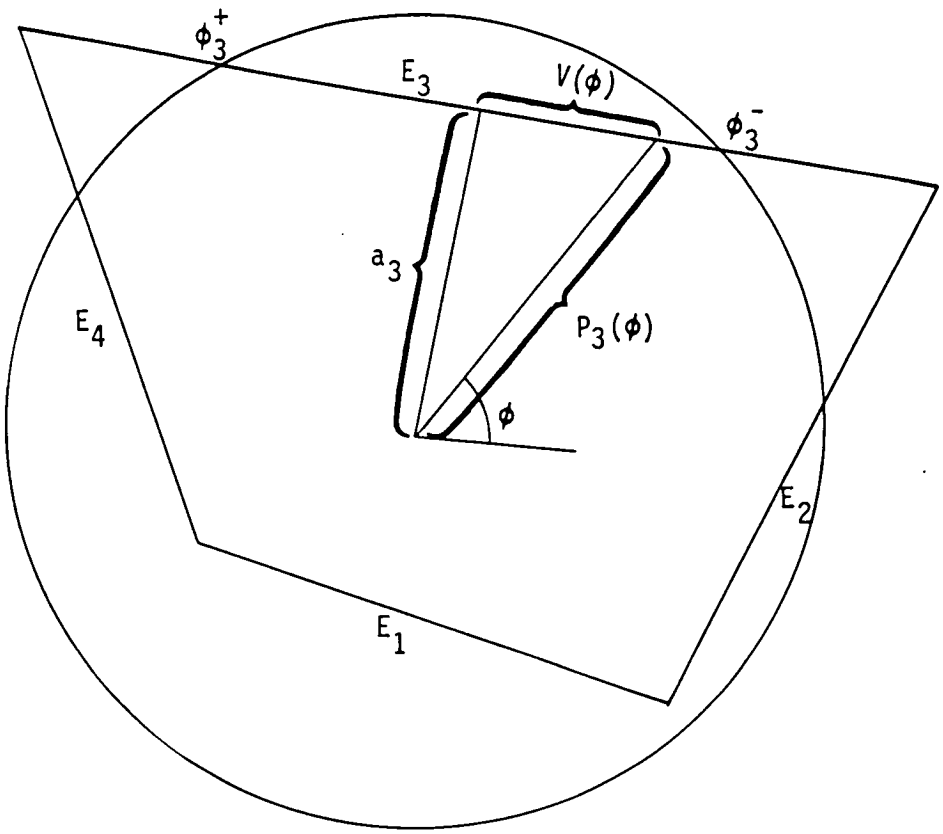

Figure J.18 - Definition of $P(\phi)$, the upper limit of integration for ρ

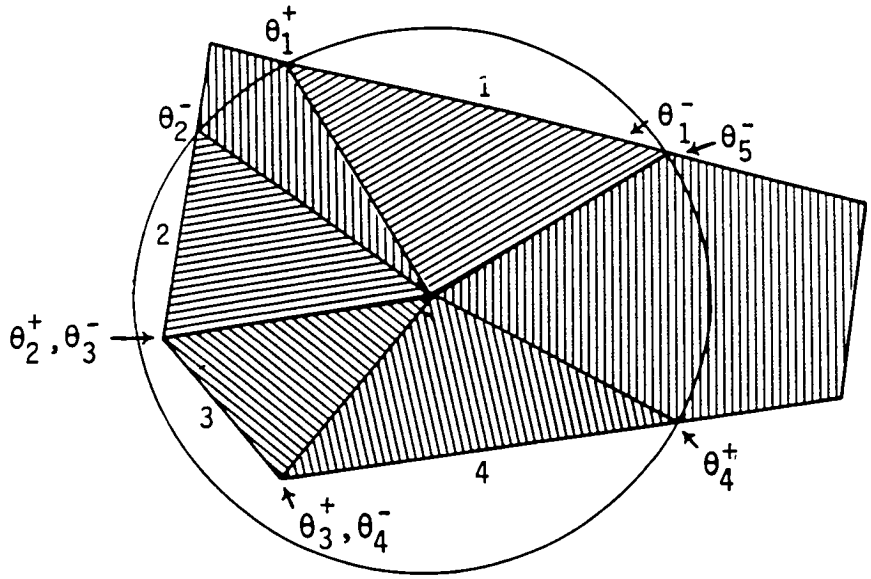

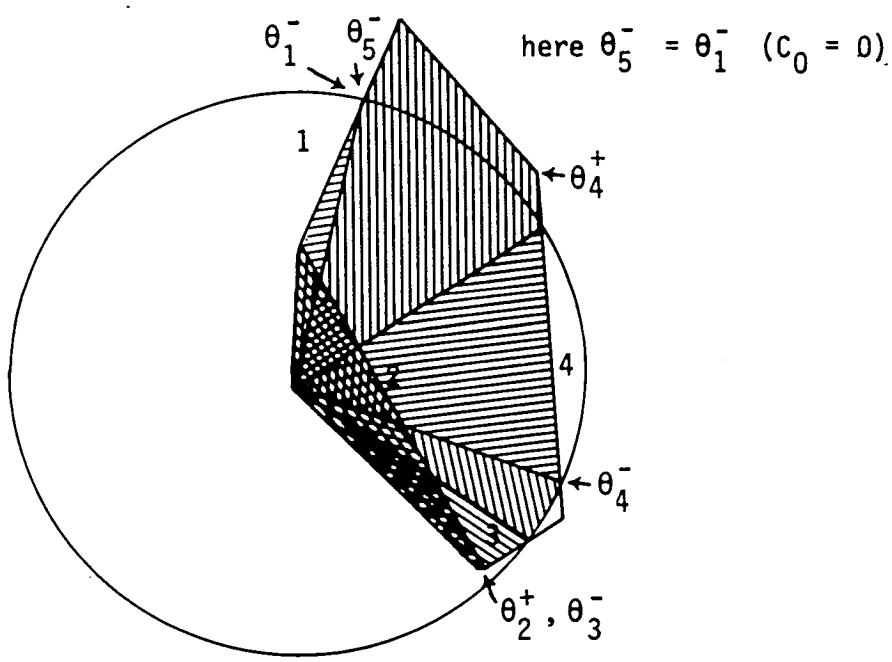

Figure J.19 - Region of integration for superinclined panel

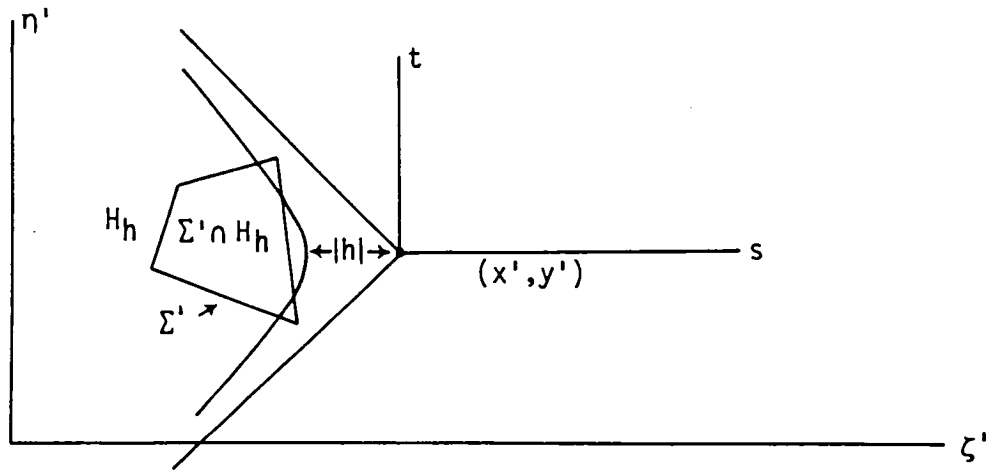

Figure J.20 - Transformation to (s,t) variables and region of integration

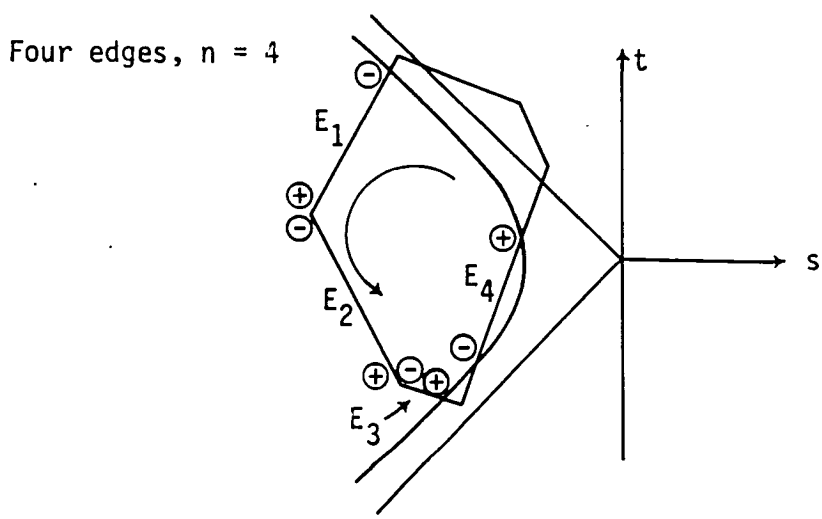

Figure J.21 - Numbering of edges of $\Sigma' \cap H_h$

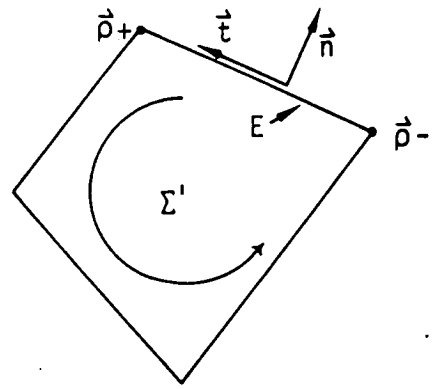

Figure J.22 - A region Σ' with edge E, oriented tangent $\vec{t}$ and outward edge normal $\vec{n}$.

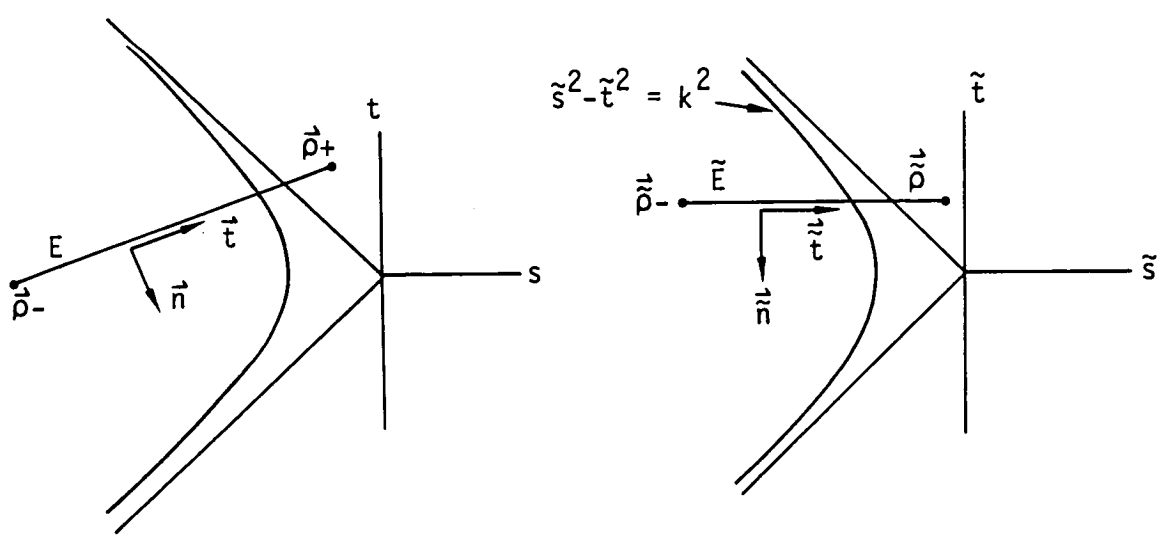

Figure J.23 - An edge E and its image $\tilde{E}$ in the $\tilde{s}$ - $\tilde{t}$ coordinate system (subsonic edge)

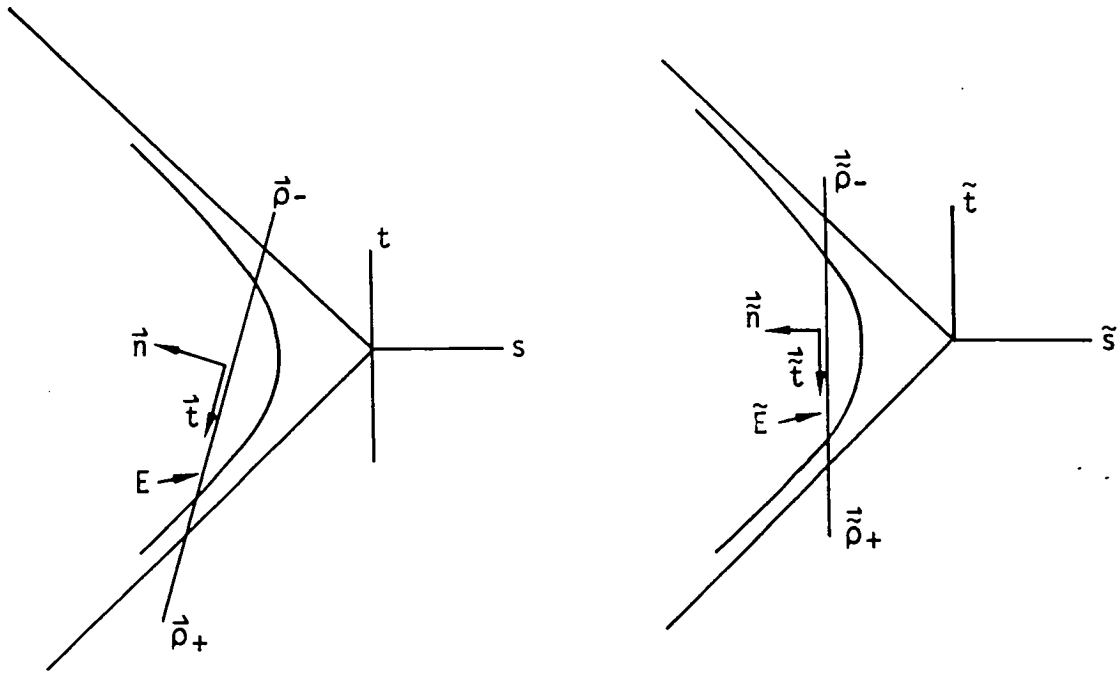

Figure J.24 - An edge E and its image $\tilde{E}$ in the $\tilde{s}$-$\tilde{t}$ coordinate system (supersonic edge)

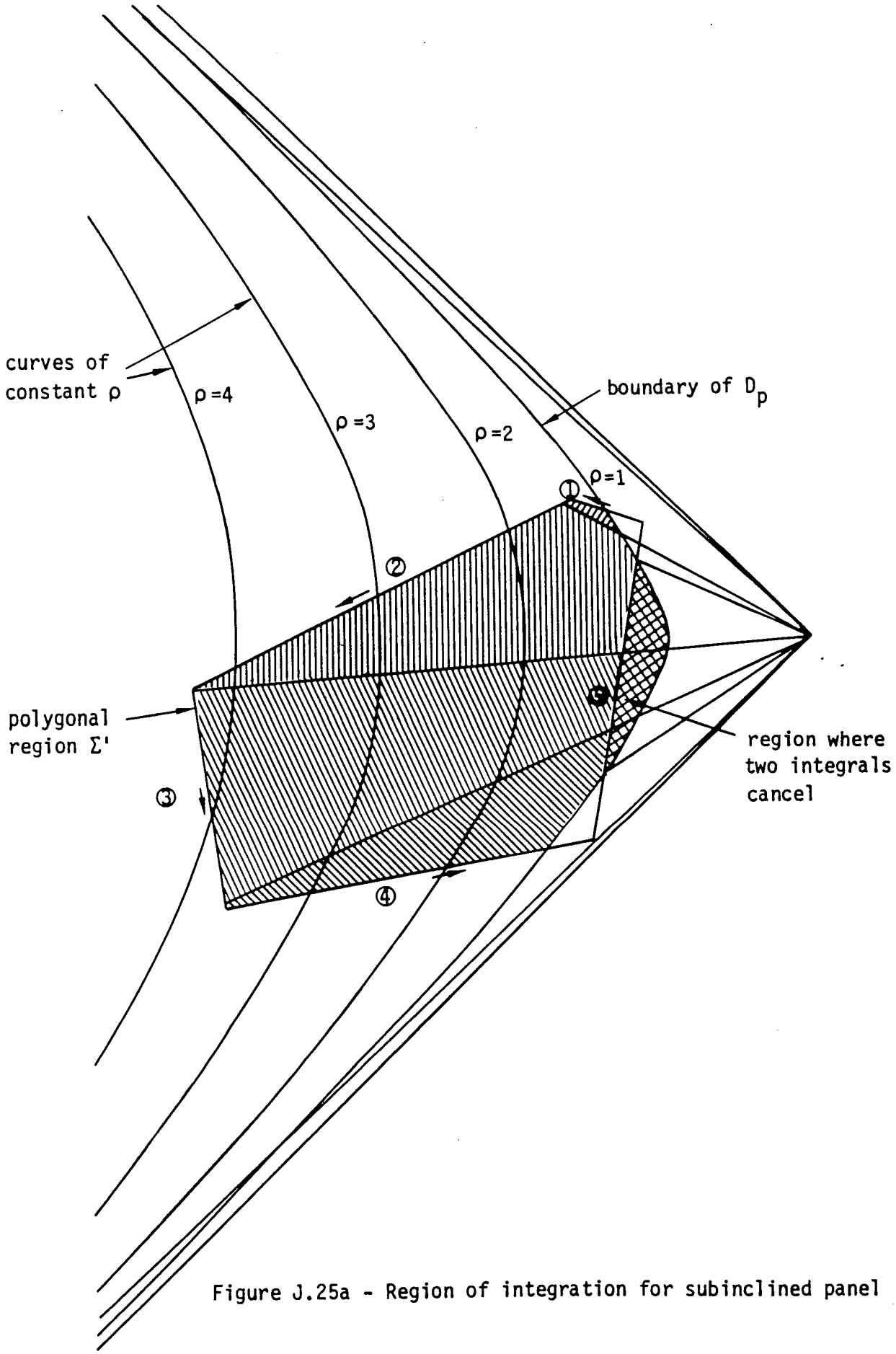

Figure J.25a - Region of integration for subinclined panel

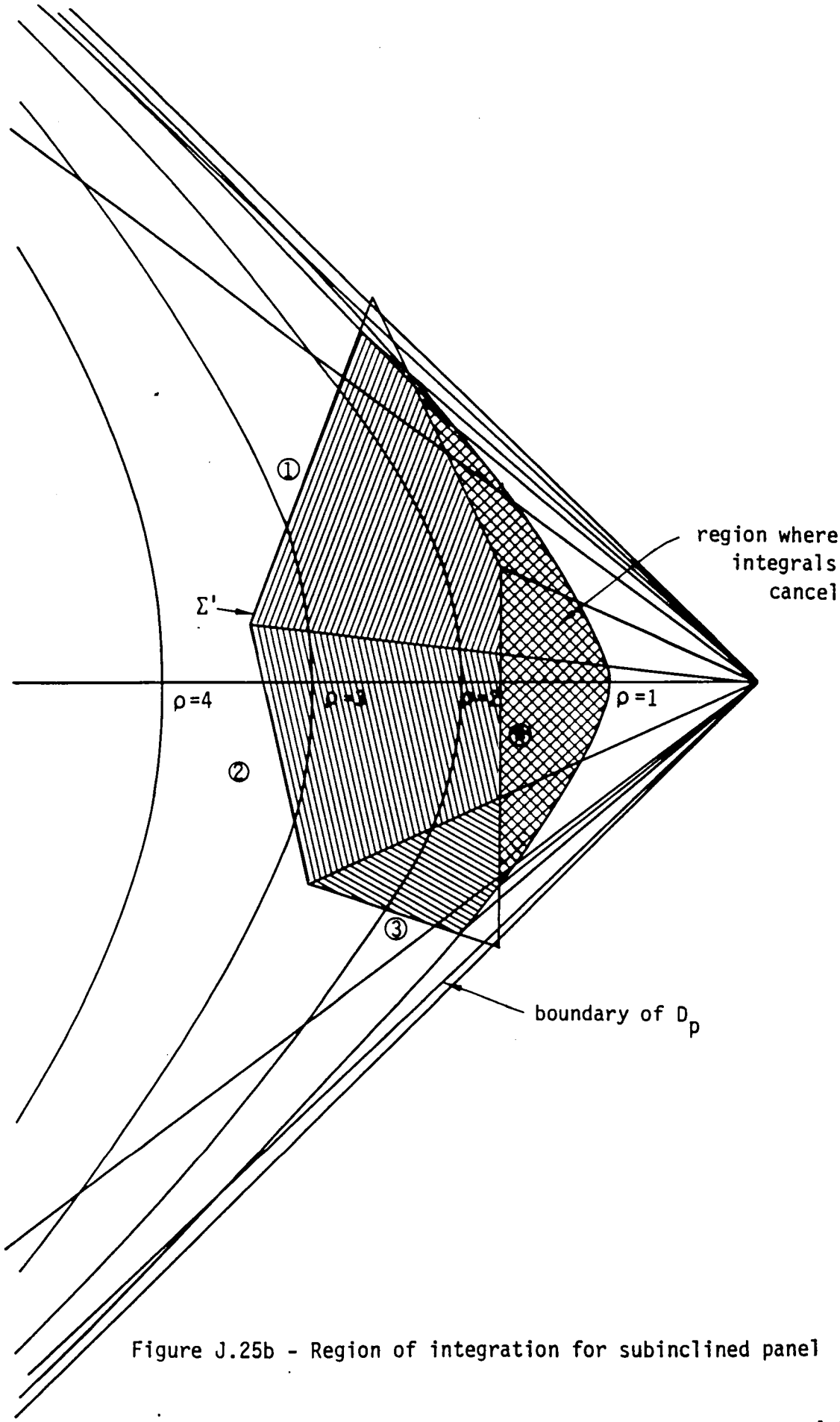

Figure J.25b - Region of integration for subinclined panel

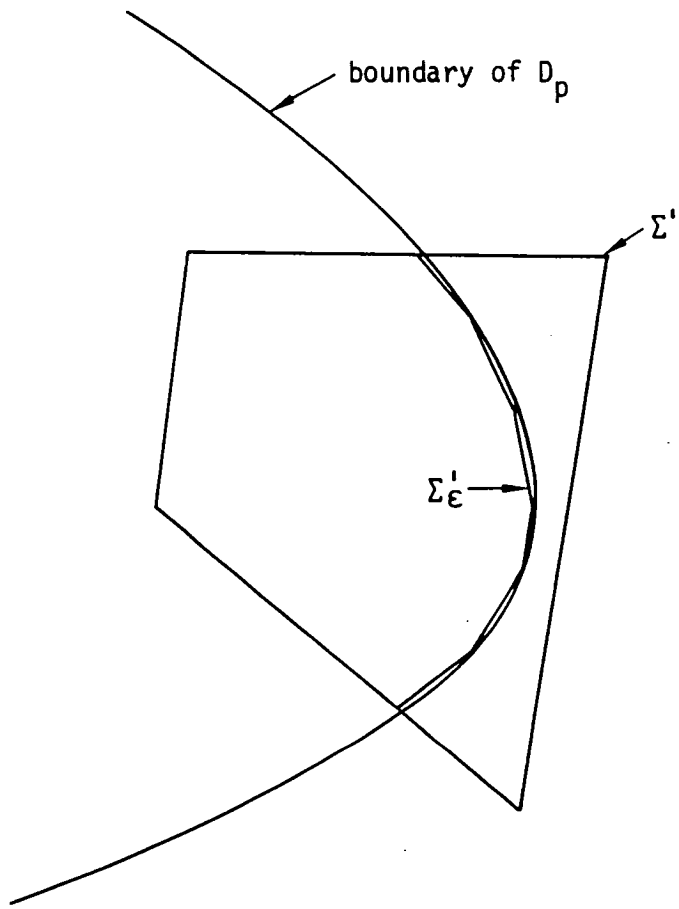

Figure J.26 - Polygon Σ'_ε approximating $\Sigma' \cap D_p$

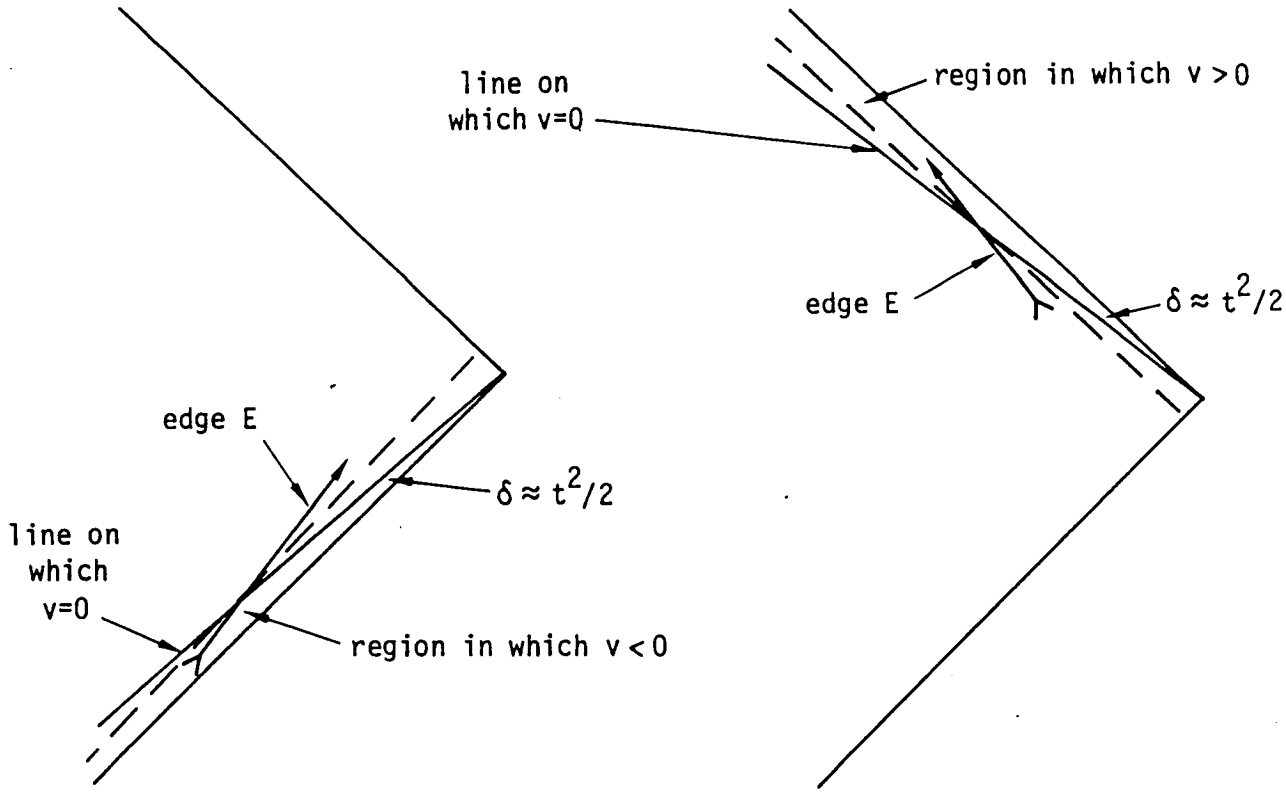

Figure J.27 - Illustration of supersonic, nearly sonic edges on which v changes sign

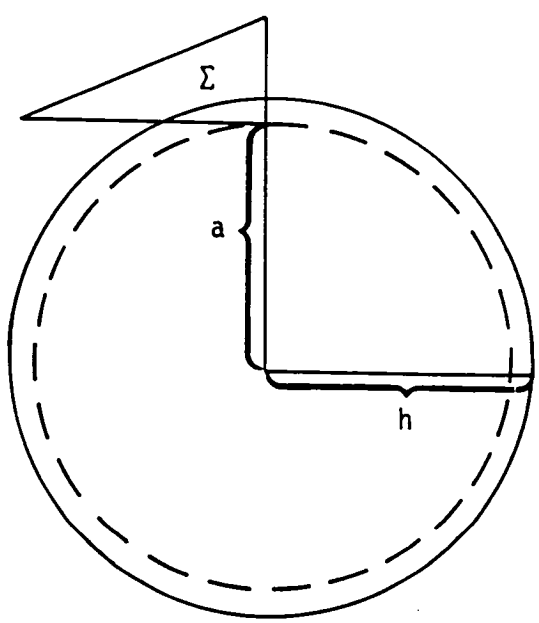

Figure J.28 - An example of a superinclined panel with $g^2 = h^2 - a^2 \approx 0$

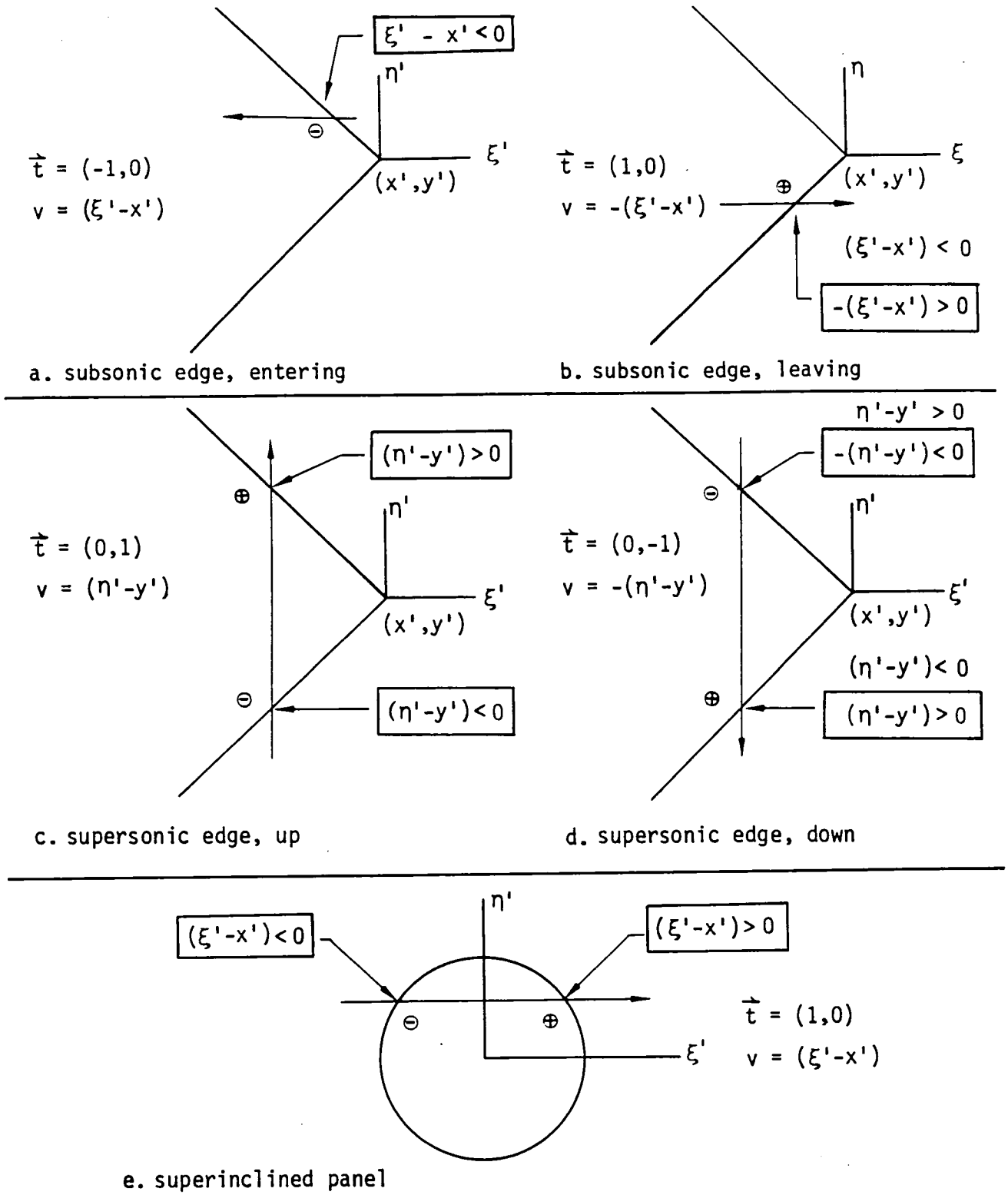

Figure J.29 - Evaluating v on the boundary of D_p : the various special cases

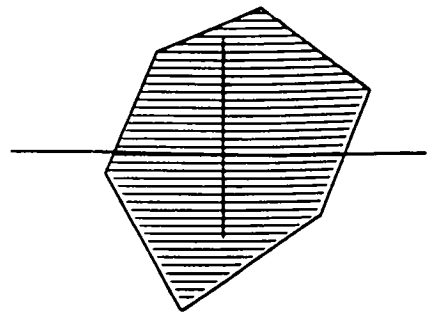

$C_\Theta = 1 \qquad J'\big|_{|h|=0} = 2\pi$

a. s = +1

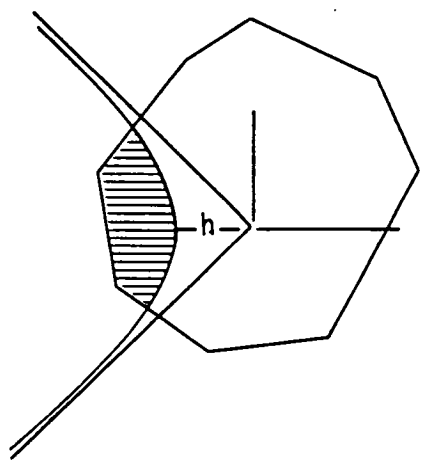

$C_\Theta = 0 \qquad J'\big|_{|h|=0} = \pi$

b. rs = -1

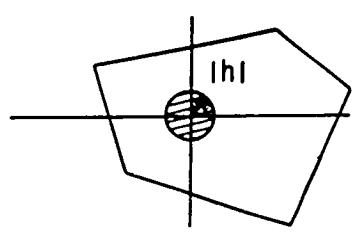

$C_\Theta = 1 \qquad J'\big|_{|h|=0} = 2\pi$

c. r = -1

Figure J.30 - The value of J' for some special configurations

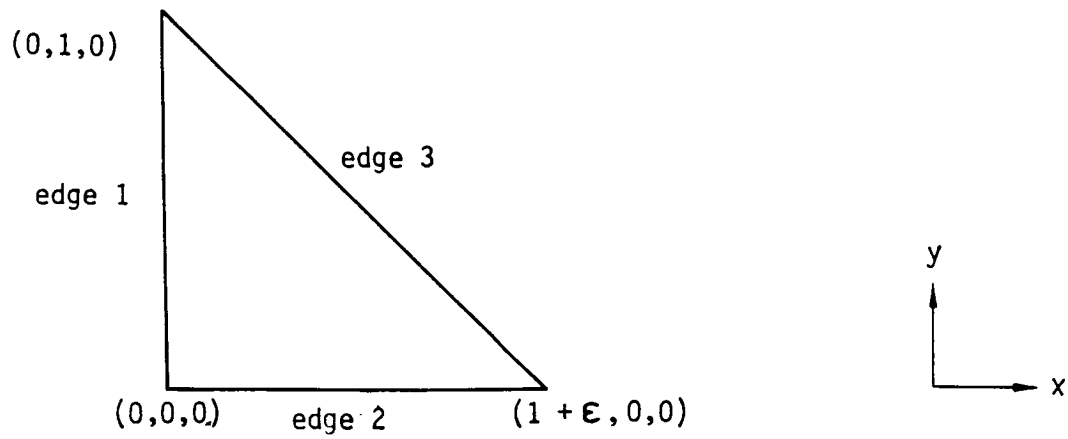

Figure J.31 - Region with nearly sonic edge

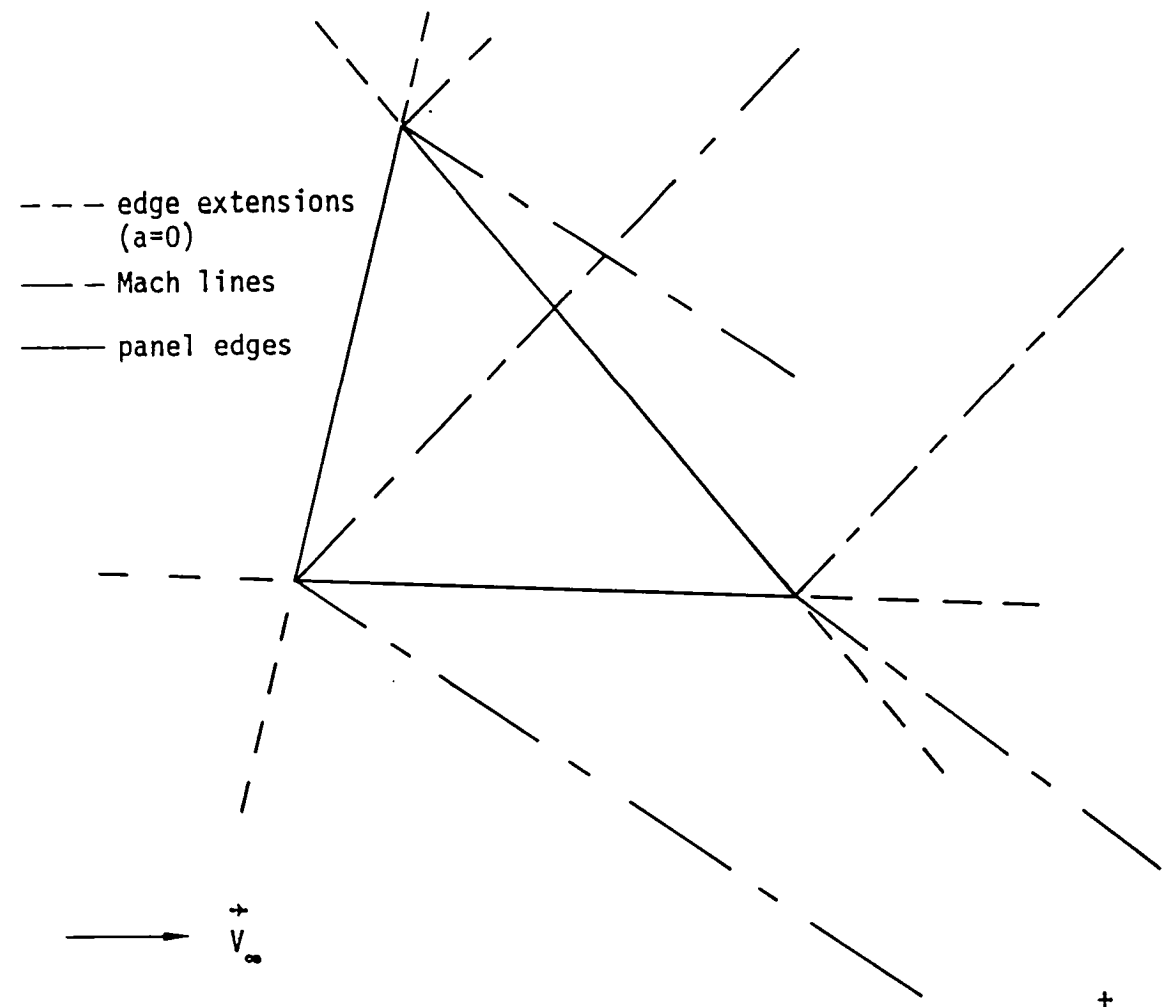

Figure J.32 - Potential lines of discontinuity in J^+

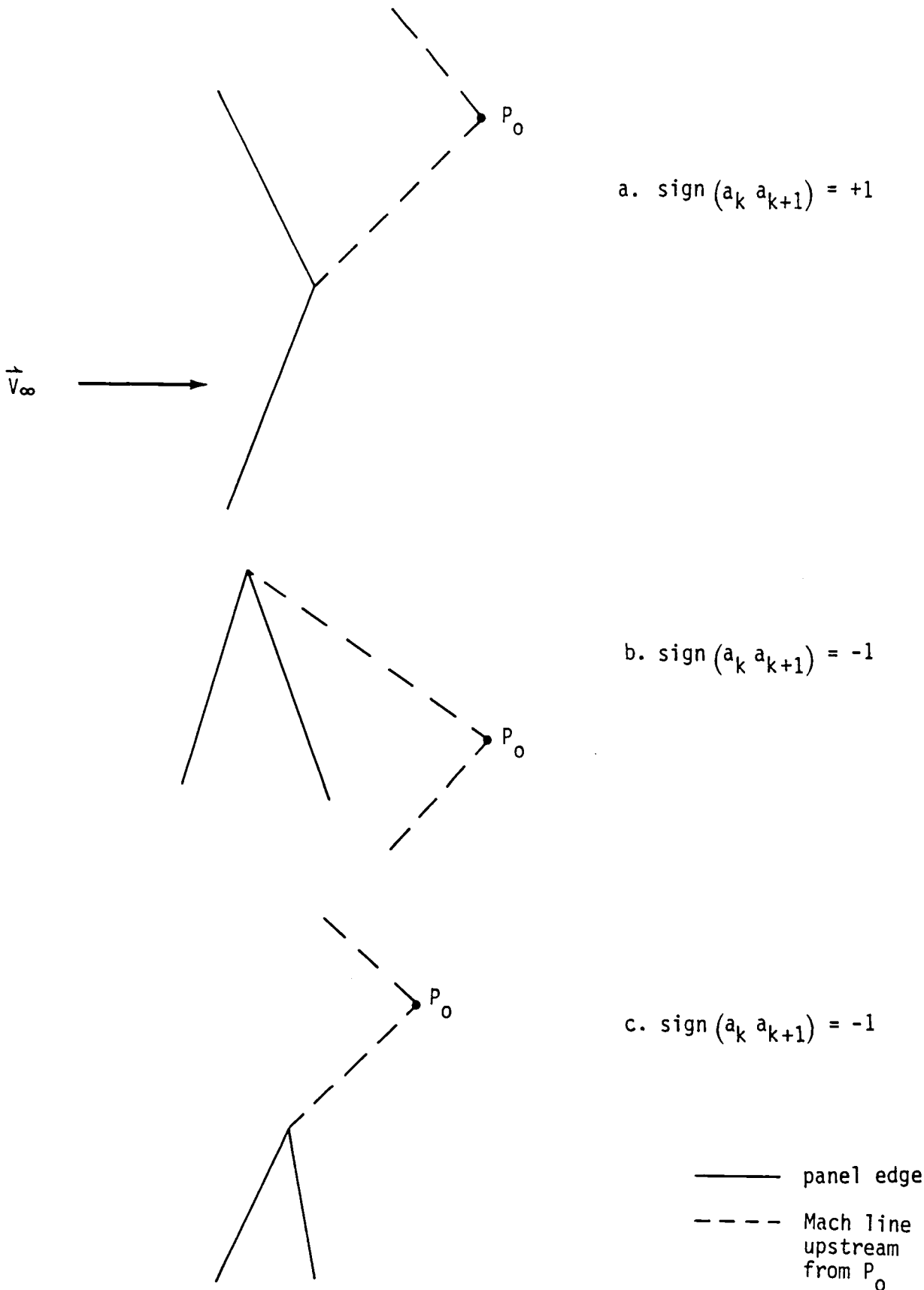

Figure J.33 - Panel corners on Mach lines

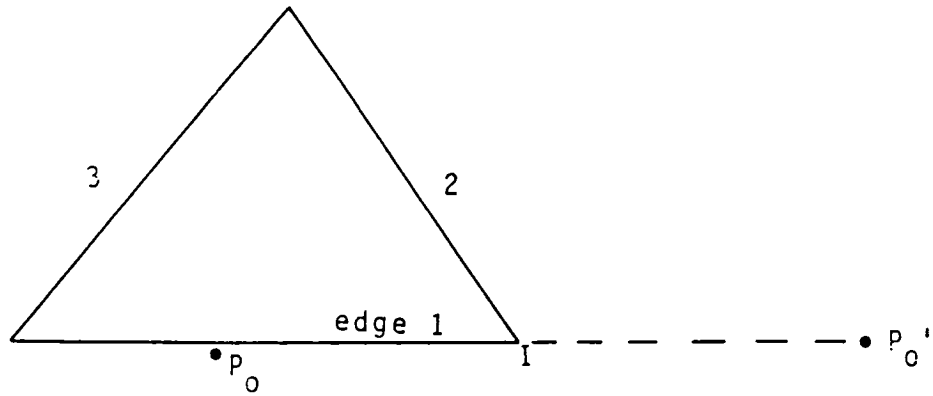

Figure J.34 - A point lies on the extension of an edge (subsonic flow)

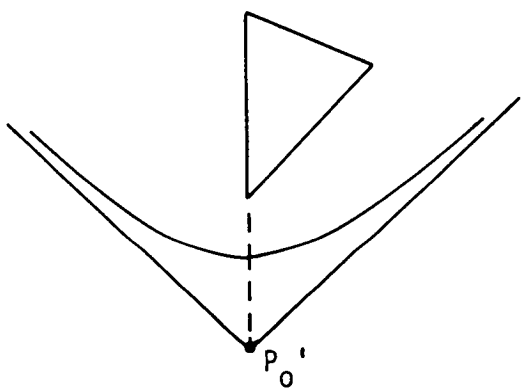

a. subinclined panel

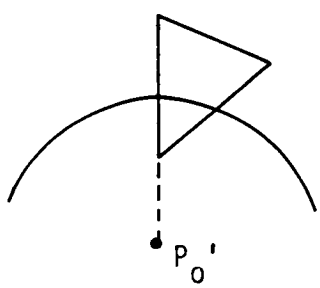

b. superinclined panel

Figure J.35 - A point lies on the extension of an edge (supersonic flow)

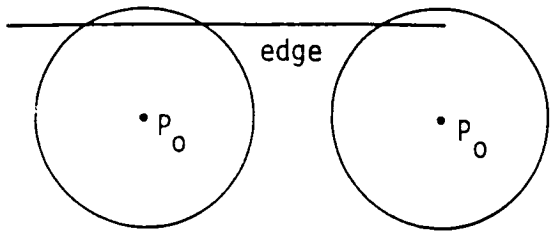

$V^+ = 0$ $\quad$ $V^- < 0$

$R^+ \approx 0$ $\quad$ $R^- = 0$

$|h| > 0$

$|a| > 0$

Figure J.36 - Edge barely intersects D_p

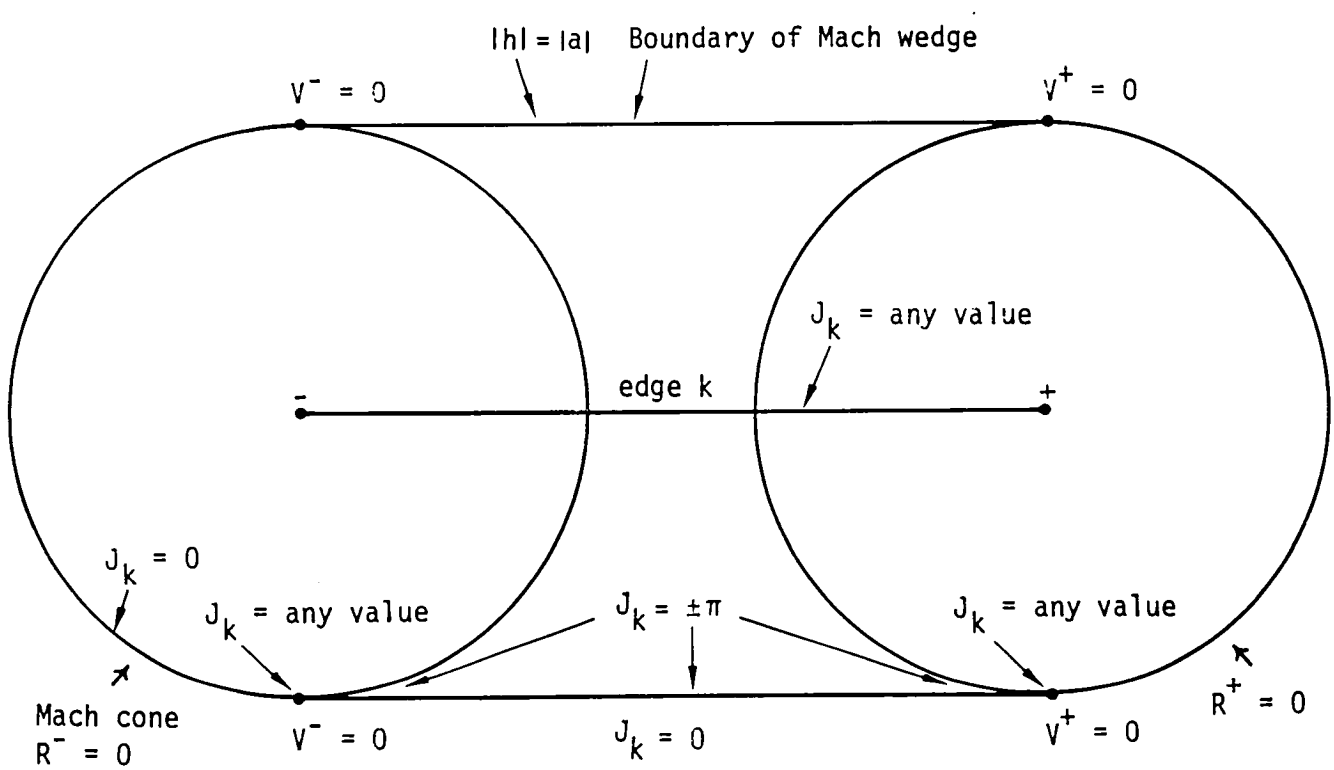

Figure J.37a - The Mach wedge in cross-section

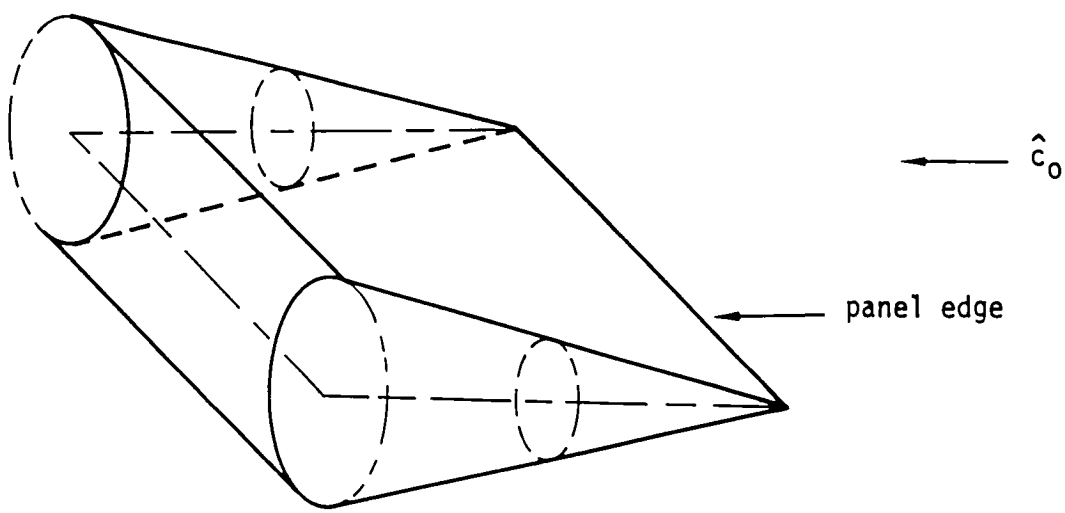

Figure J.37b - Mach wedge behind supersonic panel edge

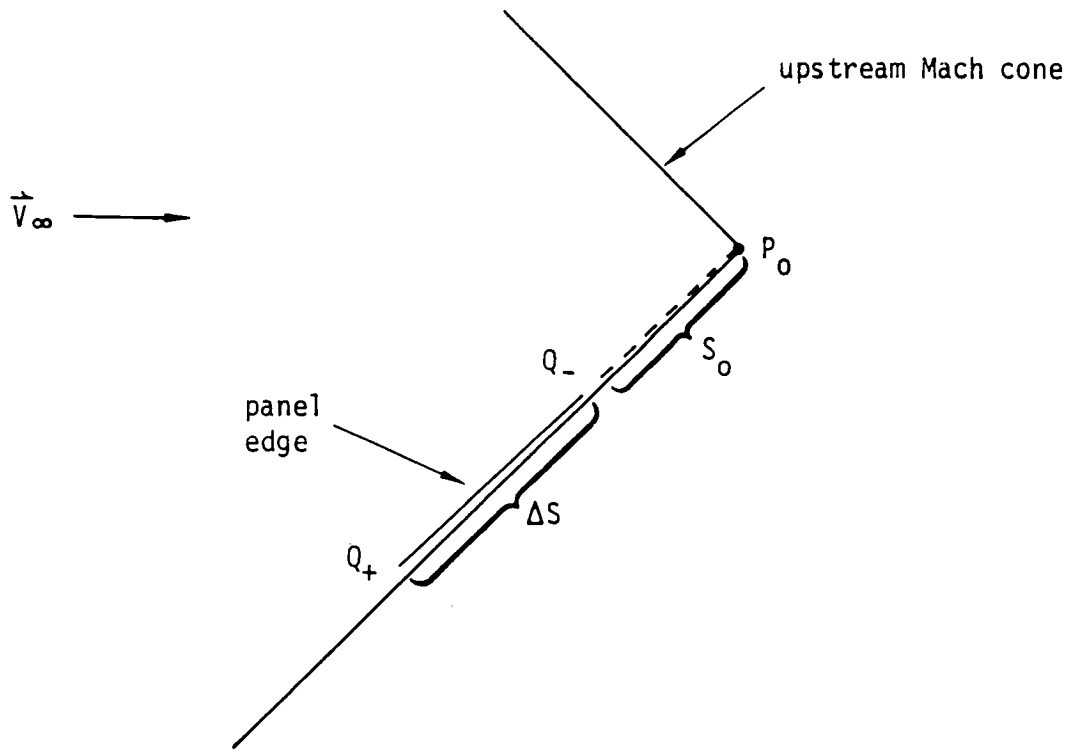

Figure J.38 - Subsonic nearly sonic edge

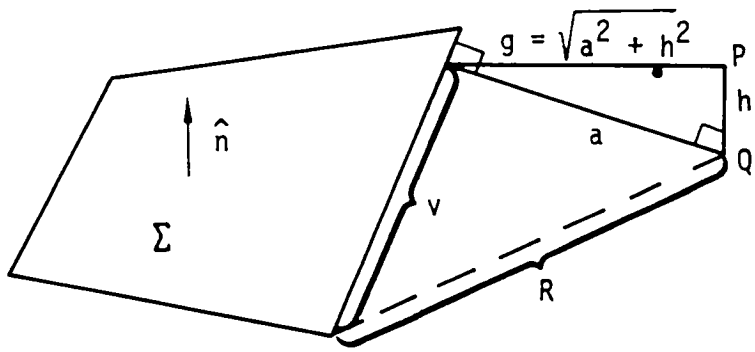

Note: $\vec{P} - \vec{Q}$ is perpendicular to the plane of Σ

Figure J.39 - The distances h, v, a, g, and R in subsonic flow

K.0 AIC Matrix Assembly

The process by which a boundary condition is transformed into a row of an AIC matrix was discussed briefly in section 5.7.1. Here, we discuss those details of the AIC assembly process omitted from section 5.7.1. Initially, we will study this process when no symmetry exists in the problem. Having done this, we will then study the problem formulation in the presence of first one, and then two planes of symmetry. When we do treat the symmetry cases, we will first pose the problem as though it had no planes of symmetry, and then use the symmetry side conditions to formulate a boundary value problem for each of the various symmetric and antisymmetric parts of the perturbation potential, ϕ. For example, when one plane of symmetry is present, we will obtain a boundary value problem for each of the two potential functions, $\hat{\phi}^S$ the symmetric part of the ϕ and $\hat{\phi}^A$ the antisymmetric part of ϕ. When one plane of symmetry is present, PAN AIR obtains and solves matrix equations for $\hat{\phi}^S$ and $\hat{\phi}^A$. This approach of formulating a separate boundary value problem for each symmetry condition turns out to be quite fruitful when we address the problem of enforcing doublet matching at abutments and abutment intersections. In particular, when an abutment or abutment intersection lies on a plane of symmetry, doublet matching will usually be performed differently for each symmetry condition.

Having given the overall plan of the analysis, the individual sections of this appendix are now briefly summarized.

In section K.1, the generation of rows of the AIC matrix is discussed under the assumption that no planes of symmetry are present in the configuration. In particular, the construction of a row of the AIC matrix is described in detail for three forms of boundary conditions: (i) general boundary conditions of the form (5.6.1) (including singularity specification boundary conditions), (ii) matching boundary conditions of the type discussed in detail in appendix F and in appendix (H.2.4), and (iii) closure boundary conditions of the form (5.7.3).

Next, the concepts of symmetry are introduced in section K.2 where the constraints on the admissable planes of symmetry are derived.

For the case of one plane of symmetry, section K.3 then defines the symmetrized potential functions $\hat{\phi}^S$ and $\hat{\phi}^A$, investigates their properties and the form that general boundary conditions take when imposed on these functions. Using the ideas developed in this section, the same analysis is repeated for configurations with two planes of symmetry in section K.4.

Much of the analysis of sections K.3 and K.4 is then combined, refined and summarized in section K.5. In this section, explicit detailed instructions are provided for the evaluation of potential and velocity influence coefficients when symmetry is present.

In section K.6 the generation of rows of the AIC matrices for the various symmetry conditions is described in terms of the symmetrized influence coefficients described in section K.5. As in section K.1, we describe the construction of an AIC row for general, matching and closure boundary conditions.

Finally, in section K.7, the implementation of the IC update capability in the construction of the AIC matrix is discussed. This capability permits a user to change the geometry of a portion of a configuration and then analyze the modified configuration without recomputing the entire influence coefficient matrix.

K.1 Generation of AIC's in the Absence of Symmetry

K.1.1 Transformation of a General Boundary Condition into an AIC Row (No Symmetry)

We now describe the process by which a general boundary condition of the form (5.6.1) is transformed into an equation which can then be entered as a single row into the AIC matrix. Recalling the boundary condition equation (5.6.1), imposed at a point $\vec{p}$, we write,

$$[\, a_A \, \vec{w}_A \cdot \hat{n} + c_A \, \phi_A + \vec{t}_A \cdot \vec{v}_A + a_D \, \sigma + c_D \, \mu + \vec{t}_D \cdot \nabla\mu \,]_{\vec{p}} = b \qquad (K.1.1)$$

where the coefficients a_A, c_A, $\vec{t}_A$, a_D, c_D, $\vec{t}_D$, b are assumed to be known. A single equation to be imposed upon the global singularity parameters λ_I is obtained by combining the basis function representations of σ and μ (cf. (3.3.1) and (3.3.2))

$$\sigma(\vec{p}) = \sum_{I=1}^{N} s_I(\vec{p}) \, \lambda_I \qquad (K.1.2)$$

$$\mu(\vec{p}) = \sum_{I=1}^{N} m_I(\vec{p}) \, \lambda_I \qquad (K.1.3)$$

together with the integral representations of $\phi(\vec{p})$ and $\vec{v}(\vec{p})$ (cf. (5.2.8) and (B.3.9) with the line vortex term removed)

$$\phi(\vec{p}) = (1/\kappa) \iint_{S \cap D_p} [-\sigma(\vec{q})/R + \mu(\vec{q}) \, \hat{n}(\vec{q}) \cdot \tilde{\nabla}_q(1/R)] \, dS_q \qquad (K.1.4)$$

$$\vec{v}(\vec{p}) = (1/\kappa) \iint_{S \cap D_p} \sigma(\vec{q}) \, \nabla_q \, (1/R) \, dS_q \qquad (K.1.5)$$

$$+ (1/\kappa) \iint_{S \cap D_p} [(\hat{n} \, dS_q) \times \nabla\mu] \times \tilde{\nabla}_q(1/R)$$

and then substituting these representations into equation (K.1.1). There results from this process the aerodynamic influence equation

$$\sum_{I=1}^{N} AIC_I \; \lambda_I = b \qquad (K.1.6)$$

where

$$AIC_I = a_A \, \vec{w}_{A,I} \cdot \hat{n} + c_A \, \phi_{A,I} + \vec{t}_A \cdot \vec{v}_{A,I} \qquad (K.1.7)$$
$$+ a_D \, s_I(\vec{p}) + c_D \, m_I(\vec{p}) + \vec{t}_D \cdot \nabla_p m_I(\vec{p})$$

and,

$\phi_{A,I}(\vec{p})$ = average potential induced at $\vec{p}$ by a source distribution $s_I(\vec{q})$ and a doublet distribution $m_I(\vec{q})$ (K.1.8)

$\vec{v}_{A,I}(\vec{p})$ = average velocity induced at $\vec{p}$ by a source distribution $s_I(\vec{q})$ and a doublet distribution $m_I(\vec{q})$ (K.1.9)

$\vec{w}_{A,I}(\vec{p})$ = $B_o \vec{v}_{A,I}(\vec{p})$ (cf. equation (5.4.10)). (K.1.10)

Thus, $\phi_{A,I}(\vec{p})$ is obtained by performing the substitutions $\sigma(\vec{q}) \rightarrow s_I(\vec{q})$, $\mu(\vec{q}) \rightarrow m_I(\vec{q})$ in equation (K.1.4) while $\vec{v}_{A,I}(\vec{p})$ is obtained by performing these same substitutions in equation (K.1.5). The evaluation of integrals of the form (K.1.4) and (K.1.5) when $\sigma(\vec{q})$ and $\mu(\vec{q})$ are polynomial functions of the local coordinates on S has already been treated in exhaustive detail in appendix J. Since $s_I(\vec{q})$ and $m_I(\vec{q})$ are explicitly known functions of this type, the evaluation of $\phi_{A,I}(\vec{p})$ and $\vec{v}_{A,I}(\vec{p})$ clearly presents no difficulty.

Turning now to the terms $s_i(\vec{p})$, $m_i(\vec{p})$ and $\vec{t}_D \cdot \nabla m_i(\vec{p})$ appearing on the second line of equation (K.1.7), we readily see that

$$s_I(\vec{p}) = \lfloor 1, \xi', \eta' \rfloor^{1x3} \; [SPSPL^S]^{3x5} \left\{ B_I^S \right\}^{5x1} \qquad (K.1.11)$$

$$m_I(\vec{p}) = \lfloor 1, \xi', \eta', \xi'^2/2, \xi'\eta', \eta'^2/2 \rfloor^{1x6} \; [SPSPL^D]^{6x9} \left\{ B_I^D \right\}^{9x1} \qquad (K.1.12)$$

where:

$(\xi' \; \eta')$ are the local coordinates of the control point $\vec{p}$ on the subpanel in which it lies

$[SPSPL^S]$ is the source subpanel spline matrix for the panel in which $\vec{p}$ lies

$\left\{ B_I^S \right\}$ is the column of the source outer spline matrix B^S corresponding to λ_I. (Zero, if no such column exists)

$[SPSPL^D]$ is the doublet subpanel spline matrix for the panel in which $\vec{p}$ lies

$\left\{ B_I^D \right\}$ is the column of the doublet outer spline matrix B^D corresponding to λ_I. (Zero, if no such column exists)

The evaluation of $\vec{t}_D \cdot \nabla m_I(\vec{p})$ presents somewhat more difficulty. First of all, since the function $m_I(\vec{p})$ is only defined for points $\vec{p}$ in the singularity surface S, we must first be sure that this expression is well defined.

To see that this is so for $\vec{p} \in S$, recall that for an arbitrary function $f(\vec{p})$, the directional derivative $(\vec{t}_D \cdot \nabla f)_{\vec{p}}$ satisfies the relation

$$(\vec{t}_D \cdot \nabla f)_{\vec{p}} = [(d/d\tau)\, f(\vec{c}(\tau))]_{\tau = 0} \tag{K.1.13}$$

whenever $\vec{c}(\tau)$ is some curve lying in S and satisfying

$$\vec{c}(o) = \vec{p} \tag{K.1.14a}$$

$$(d\vec{c}/d\tau)_o = \vec{t}_D \tag{K.1.14b}$$

Thus, for $\vec{t}_D \cdot \nabla m_I(p)$ to be well defined, we merely need to observe that the function $m_I(\vec{c}(\tau))$ is well defined by virtue of the fact that $\vec{c}(\tau)$ lies on S, on which m_I is well defined. In order to obtain an explicit formula for $\vec{t}_D \cdot \nabla m_I(\vec{p})$ we must now introduce the local coordinate system for the panel in which $\vec{p}$ lies (cf. equation (5.2.23) with the origin shift $\vec{q}_o$ included):

$$\vec{q}\,' = A(\vec{q} - \vec{q}_o)$$

For points $\vec{q}$ lying on the subpanel, $\vec{q}\,'$ has the form $(\xi', \eta', o)^T$. Thus, since $\vec{c}(\tau)$ lies on the subpanel for τ in some neighborhood of $\tau = 0$, we have

$$A(\vec{c}(\tau) - \vec{q}_o) = \begin{bmatrix} \xi(\tau) \\ \eta(\tau) \\ 0 \end{bmatrix}$$

Moreover, given the local coordinates of a point $\vec{p}$, m_I is given by equation (K.1.12); thus

$$m_I(\vec{c}(\tau)) = \lfloor 1 \quad \xi(\tau) \quad \eta(\tau) \quad \xi^2(\tau)/2 \quad \xi(\tau)\eta(\tau) \quad \eta^2(\tau)/2 \rfloor^{1\times 6} \times [SPSPL^D]^{6\times 9} \left\{ B_I^D \right\}^{9\times 1}$$

Differentiating this and evaluating at $\tau=0$, we find

$$[\frac{d}{d\tau} m_I(\vec{c}(\tau))]_0 = [(\frac{d\xi}{d\tau})_0, (\frac{d\eta}{d\tau})_0, 0] \begin{bmatrix} 0 & 1 & 0 & \xi(0) & \eta(0) & 0 \\ 0 & 0 & 1 & 0 & \xi(0) & \eta(0) \\ 0 & 0 & 0 & 0 & 0 & 0 \end{bmatrix} \times [SPSPL^D]^{6\times 9} \left\{ B_I^D \right\}^{9\times 1}$$

Now $(\xi(0), \eta(0), 0)$ and $(d/d\tau)\,(\xi(\tau), \eta(\tau), 0)_o$ can be readily evaluated:

$$\begin{bmatrix} \xi\,(0) \\ \eta\,(0) \\ 0 \end{bmatrix} = A(\vec{c}(0) - \vec{q}_o) = A\,(\vec{p} - \vec{q}_o) = \begin{bmatrix} \xi' \\ \eta' \\ 0 \end{bmatrix}$$

while

$$\begin{bmatrix} d\xi/d\tau \\ d\eta/d\tau \\ 0 \end{bmatrix}_0 = (d/d\tau)\ [\ A(\vec{c}(\tau)-\vec{q}_0)\ ] = A(d\vec{c}/d\tau)_0 = A\ \vec{t}_D$$

Consequently we find,

$$\frac{d}{d\tau}\ m_I\ (\vec{c}(\tau))_0 = \vec{t}_D \cdot \nabla m_I(\vec{p}) =$$

$$= \vec{t}_D{}^T\ A^T \begin{bmatrix} 0 & 1 & 0 & \xi' & \eta' & 0 \\ 0 & 0 & 1 & 0 & \xi' & \eta' \\ 0 & 0 & 0 & 0 & 0 & 0 \end{bmatrix} [SPSPL^D]\ \left\{B_I^D\right\} \tag{K.1.15}$$

as asserted in equation (5.7.1).

K.1.2 Transformation of a Matching Boundary Condition into an AIC Row (No Symmetry)

In the absence of a plane of symmetry, the conversion of a doublet matching boundary condition (cf. equation (F.5.1) or (H.2.11a))

$$\sum_k\ s_k\ \mu_k = 0 \tag{K.1.16}$$

into a row of aerodynamic influence coefficients is straightforward in light of the explicit representation of μ provided by equations (K.1.3) and (K.1.12). To see this suppose that μ_k is the evaluation of $\mu(\vec{q})$ at point $\vec{p}_k$, and that (ξ'_k, η'_k) are the local coordinates of $\vec{p}$ in the panel in which it lies. Combining (K.1.3) and (K.1.12) we then obtain

$$\mu_k = \mu(\vec{p}_k) = \sum_{I=1}^{N} \lfloor 1\ \xi'_k\ \ \eta'_k\ \ \xi'^2_k/2\ \ \ \xi'_k\eta'_k\ \ \eta'^2_k/2 \rfloor\ [SPSPL_k^D]\ \left\{B_{k,I}^D\right\}\ \lambda_I. \tag{K.1.17}$$

Here, $[SPSPL_k^D]$ is the doublet subpanel spline matrix for the subpanel in which $\vec{p}_k$ lies while $\left\{B_{k,I}^D\right\}$ is the column corresponding to λ_I in the doublet outer spline matrix of $\vec{p}_k$'s panel. Combining (K.1.16) with (K.1.17) leads to an equation

$$\sum_{I=1}^{N}\ AIC_I\ \ \lambda_I = 0 \tag{K.1.18}$$

where

$$AIC_I = \sum_k s_k \lfloor 1 \;\; \xi'_k \;\; \eta'_k \;\; \xi'^2_k/2 \;\; \xi'_k \eta'_k \;\; \eta'^2_k/2 \rfloor [SPSPL^D_k] \left\{ B^D_{k,I} \right\} \tag{K.1.19}$$

(Remark: The actual determination of the form of the matching conditions, i.e., the values of s_k and $\vec{p}_k$, is fully discussed in appendix F).

The conversion of a source matching condition into an AIC row is performed in essentially the same way. Here, the representation of σ provided by equations (K.1.2) and (K.1.11) allows us to transform the source matching condition (cf. equation (H.2.13)) into an AIC equation of the form (K.1.18). The result reads,

$$\sum_k s_k \sigma_k = \sum_I AIC_I \lambda_I = 0 \tag{K.1.20}$$

where the matrix entries AIC_I are given by

$$AIC_I = \sum_k s_k \lfloor 1, \xi'_k \;\; \eta'_k \rfloor [SPSPL^S_k] \left\{ B^S_{k,I} \right\} \tag{K.1.21}$$

The conversion of the velocity jump matching condition into an AIC row is slightly more complicated. Combining the basic matching condition (H.2.11b) with the formulas for the velocity jumps $\Delta\vec{v}_k$ given by the Helmholtz relation (see equation (H.2.12)), we obtain after some manipulation,

$$\begin{aligned} 0 &= \sum_k s_k \vec{t} \cdot \Delta\vec{v}_k \\ &= \sum_k s_k \left\{ \sigma(\vec{t}.\hat{n})/(\hat{n}.\vec{v}) + ((\vec{v}x\vec{t})x\hat{n}).\nabla\mu/(\hat{n}.\vec{v}) \right\}_k \end{aligned} \tag{K.1.22}$$

Upon using the representations (K.1.2) and (K.1.3) for σ and μ, together with the evaluation formulae (K.1.11) for $s_I(\vec{p}_k)$ and (K.1.15) for the tangential derivative of $m_I(\vec{p})$, this becomes an AIC equation of the form (K.1.18) with the AIC row entries given by the formula

$$\begin{aligned} AIC_I = &\sum_k s_k(\vec{t}.\hat{n}_k)/(\hat{n}_k.\vec{v}_k) \lfloor 1 \; \xi'_k \; \eta'_k \rfloor [SPSPL^S_k] \left\{ B^S_{k,I} \right\} \\ &+ \sum_k \frac{s_k}{(\hat{n}_k \cdot \vec{v}_k)} [A_k((\vec{v}_k x\vec{t})x\hat{n}_k)]^T \begin{bmatrix} 0 & 1 & 0 & \xi_k' & \eta'_k & 0 \\ 0 & 0 & 1 & 0 & \xi'_k & \eta'_k \\ 0 & 0 & 0 & 0 & 0 & 0 \end{bmatrix} [SPSPL^D_k] \left\{ B^D_{k,I} \right\} \end{aligned} \tag{K.1.23}$$

K.1.3 Transformation of a Closure Boundary Condition into an AIC Row (No Symmetry)

The closure boundary condition (see equation (5.7.3) or (H.2.14)) may be imposed in place of a source or doublet matching boundary condition at the control points on a matching edge of a source or doublet design network. The boundary condition is

$$\iint_{\substack{\text{column}\\ \text{or row}}} (a_A \vec{w}_A \cdot \hat{n} + a_D \sigma)\, dS = b \qquad \text{(K.1.24)}$$

where the column or row of panels is that one which is headed by the edge control point.

The row vector which defines the above integral in terms of the singularity parameters is computed by approximating the average normal mass flux and source strength on a panel by their values at the panel center. That is, we estimate

$$\iint (a_A \vec{w}_A \cdot \hat{n} + a_D \sigma)\, dS = \sum_{\text{panels}} A_k \left(a_A \vec{w}_A \cdot \hat{n} \Big|_{\vec{p}_k} + a_D \sigma \Big|_{\vec{p}_k}\right) =$$

$$= \sum_{\text{panels}} A_k \left\{ a_A \hat{n}_k^T B_o [VIC_k] + a_D \lfloor 1, \xi_k', \eta_k' \rfloor [SPSPL_k^S] [B_k^S] \right\} \vec{\lambda} \qquad \text{(K.1.25)}$$

Here A_k is the area of the k-th panel, VIC_k is the VIC matrix for $\vec{p}_k$, the center control point of the panel (see below for a complete definition), (ξ_k', η_k') are the local coordinates of $\vec{p}_k$, $[SPSPL^S]$ the source subpanel spline matrix for the subpanel in which $\vec{p}_k$ lies, and B_k^S the 5xN matrix (N the total number of singularity parameters) which is the extension of the panel's outer spline matrix from 9 columns to N columns. Thus the row of the AIC matrix corresponding to the closure boundary condition is given by the row vector multiplying $\vec{\lambda}$ on the right side of (K.1.25). The 3xN VIC matrix VIC_k is defined in terms of the velocity influence coefficients of equation (K.1.9) by

$$[VIC_k] = [\vec{v}_{A,I}(\vec{p}_k)\ ;\ I = 1, \ldots, N] \qquad \text{(K.1.26)}$$

K.2 Symmetry

Having discussed the process of AIC construction in the absence of considerations of symmetry, we must now address the problem of AIC construction when symmetry is present. Much of our discussion will consist of careful definitions of symmetric and antisymmetric parts of the perturbation potential, ϕ. Once these definitions have been carefully laid out and the appropriate representation formulae obtained (i.e., formulae analogous to (K.1.4) and (K.1.5) for the various symmetry conditions of ϕ), it will be a relatively straightforward matter to derive the form of boundary conditions when symmetry is present. In the process of analyzing what is to be done when symmetry is present, we will find that the most intricate technical questions arise from the treatment of boundary conditions on the plane of symmetry. Because PAN AIR performs control point recession, the only control points that actually lie on a plane of symmetry are those that lie <u>in</u> a plane of symmetry in the sense defined in section (H.1.2).

K.2.1 Admissible Planes of Symmetry

The basic principle of symmetry is that for each point $\vec{p}$ on the configuration of networks and panels, there is also an image point $\vec{p}'$ lying on the configuration of networks and panels. The point $\vec{p}'$ is the reflection of $\vec{p}$ in some plane containing the point $\vec{p}_0$ and having normal $\hat{n}$ (cf. figure K.1)

$$\vec{p}' - \vec{p}_0 = (I - 2\,\hat{n}\,\hat{n}^T)\,(\vec{p} - \vec{p}_0) \tag{K.2.1}$$

that is,

$$\vec{p}' = \vec{p} - 2\,\hat{n}\,(\hat{n},\, \vec{p} - \vec{p}_0) \tag{K.2.2}$$

If we assume that the plane of reflection defined by $\vec{p}_0$ and $\hat{n}$ contains the origin of the coordinate system (i.e., $(\hat{n},\, 0 - \vec{p}_0) = 0$), then we obtain

$$\vec{p}' = \vec{p} - 2\hat{n}(\hat{n},\vec{p}) = (I - 2\,\hat{n}\,\hat{n}^T)\vec{p} \tag{K.2.3}$$

If this reflection in a plane of symmetry is to be of any use, the compressible length of a vector must be invariant with respect to reflection. Thus, we require that

$$[\vec{p}',\, \vec{p}'] = [p,\, p] \tag{K.2.4}$$

where [.,.] denotes the compressible inner product of section (E.2). Defining the reflection matrix [R] by

$$[R] = I - 2\,\hat{n}\,\hat{n}^T \tag{K.2.5}$$

notice that [R] satisfies

$$[R] = [R]^T = [R]^{-1} \tag{K.2.6}$$

and that $\vec{p}'$ is given terms of $\vec{p}$ and [R] by

$$\vec{p}' = [R]\,\vec{p} \tag{K.2.7}$$

Now the invariance condition (K.2.4) can be written

$$\vec{p}^T\,[C_o]\,\vec{p} = [\vec{p},\vec{p}] = [\vec{p}',\vec{p}'] =$$

$$= \vec{p}^T\,[R]^T\,[C_o]\,[R]\,\vec{p}$$

If this condition is to hold for all vectors $\vec{p}$, we must require that

$$[C_o] = [R]^T\,[C_o]\,[R]$$

or equivalently, since $[R]\,[R]^T = [R]^T\,[R] = I$,

$$[R]\,[C_o] = [C_o]\,[R].$$

Substituting the definition of [R], equation (K.2.5), into this yields

$$[R]\,[C_o] = (I - 2\,\hat{n}\,\hat{n}^T)\,[C_o] = [C_o] - (2\,\hat{n}\,\hat{n}^T)\,[C_o]$$

$$= [C_o]\,[R] = [C_o]\,(I - 2\,\hat{n}\,\hat{n}^T) = [C_o] - [C_o]\,(2\,\hat{n}\,\hat{n}^T)$$

Thus, we find

$$\hat{n}\,\hat{n}^T\,[C_o] = [C_o]\,\hat{n}\,\hat{n}^T$$

Substituting formula (E.3.9) for $[C_o]$ then yields, in a similar manner, the identity

$$(1-s\beta^2)\,(\hat{n},\hat{c}_o)\,[\hat{n}\,\hat{c}_o^T - \hat{c}_o\,\hat{n}^T] = 0$$

This relation will hold and $\hat{n}$ will be admissable as a normal to a plane of symmetry provided one of the following three conditions is satisfied:

(i) $1 - s\beta^2 = 0 \iff M_\infty = 0$ (incompressible flow) (K.2.8a)

or (ii) $(\hat{n}, \hat{c}_o) = 0$ ($\hat{n}$ is perpendicular to $\hat{c}_o$) (K.2.8b)

or (iii) $[\hat{n}\,\hat{c}_o^T - \hat{c}_o\,\hat{n}^T] = 0 \iff \hat{n} = \pm\,\hat{c}_o \iff (\hat{n},\hat{c}_o) = \pm\,1$ (K.2.8c)

Having obtained a characterization for the normal to a single plane of symmetry, we next characterize a pair of vectors $\hat{n}_1$, $\hat{n}_2$ that are taken to be normals to two planes of symmetry. Defining $[R_1]$ and $[R_2]$ by

$$[R_i] = I - 2\,\hat{n}_i\,\hat{n}_i^{\,T} \qquad i = 1,2 \tag{K.2.9}$$

it is easy to see that both $\hat{n}_1$ and $\hat{n}_2$ must satisfy one of the restrictions (K.2.8) if the compressible length of a vector is to be invariant with respect to reflection in each plane of symmetry. In addition to these conditions, we also require that the reflection of $\vec{p}$ in both planes yield a unique point,

independent of the order in which the two reflections are performed. Thus, for arbitrary $\vec{p}$ we require that (see figure K.2 for a geometric interpretation),

$$[R_1]\,[R_2]\,\vec{p} = [R_2]\,[R_1]\,\vec{p}$$

which implies

$$[R_1]\,[R_2] = [R_2]\,[R_1].$$

Substituting the definitions (K.2.9) into this expression yields, after some manipulation, the condition

$$(\hat{n}_1, \hat{n}_2)\,[\hat{n}_1\,\hat{n}_2^T - \hat{n}_2\,\hat{n}_1^T] = 0$$

which holds provided

(i) $(\hat{n}_1, \hat{n}_2) = 0$ ($\hat{n}_1$ and $\hat{n}_2$ are orthogonal)

or (ii) $\hat{n}_1 = \pm\,\hat{n}_2 \iff (\hat{n}_1, \hat{n}_2) = \pm 1.$

The second of these conditions corresponds to two identical planes of symmetry; consequently we ignore it. Summarizing our results then, $\hat{n}_1$ and $\hat{n}_2$ are admissable normals for a pair of planes of symmetry provided

(i) $(\hat{n}_1, \hat{n}_2) = 0$ (K.2.10a)

and (ii) either $M_\infty = 0$ or $(\hat{n}_i, \hat{c}_0) = 0, \pm 1$ (K.2.10b)

In practice, the program requires that somewhat more stringent conditions be satisfied, regardless of Mach number. These conditions are:

$$\left.\begin{array}{ll} \text{(i)} & (\hat{n}_1, \hat{n}_2) = 0 \\ \text{(ii)} & (\hat{n}_i, \hat{c}_0) = 0 \quad i = 1,2 \end{array}\right\} \text{Two planes of symmetry} \qquad \begin{array}{r}\text{(K.2.11a)}\\ \text{(K.2.11b)}\end{array}$$

Similarly, for just one plane of symmetry the program requires that $\hat{n}$ satisfy

$$(\hat{n}, \hat{c}_0) = 0 \qquad \text{(one plane of symmetry)} \qquad \text{(K.2.12)}$$

In what follows, we will assume that whichever of these conditions is appropriate, is in fact satisfied.

Reflecting a moment on the significance of the restrictions (K.2.11) and (K.2.12), we see that if there are two planes of symmetry, they must be perpendicular to one another and that the compressibility axis must be perpendicular to any plane of symmetry normal. This second restriction implies that when PAN AIR is used to compute a potential flow solution for a symmetric configuration with nonzero sideslip in the onset flow, the compressibility axis will not be aligned with the onset flow. Thus, an additional approximation is implicitly performed in the treatment of nonsymmetric flows about symmetric configurations. Note however that for incompressible flows ($M_\infty = 0$), no approximation is made.

K.3 Problem Formulation for One Plane of Symmetry

In figure K.3 we illustrate a configuration with a single plane of symmetry with normal $\hat{n}_1$. The singularity surface S on which sources and doublets are defined is decomposed into three parts: S+, the principal image, lying in the interior of the region $C^+ = \{\vec{p} \mid (\vec{p}, \hat{n}_1) > 0\}$; S^-, the reflected image of S+ lying in the interior of the region $C^- = \{\vec{p} \mid (\vec{p}, \hat{n}_1) < 0\}$; and S_1 that part of S lying on the plane of symmetry $C_1 = \{\vec{p} \mid (\vec{p}, \hat{n}_1) = 0\}$. The singularity distributions on S+ (S^-) are denoted σ^+, μ^+ (σ^-, μ^-). In contrast to this, the source and doublet distributions on S_1 are denoted $\hat{\sigma}_1^S$ and $\hat{\mu}_1^A$ respectively. The reasons for these conventions are that the potentials induced by $\hat{\sigma}_1^S$ and $\hat{\mu}_1^A$, given by

$$\phi_{1,\sigma}(\vec{p}) = -(1/\kappa) \iint_{S_1 \cap D_p} \hat{\sigma}_1^S(q)/R \; dS_q \tag{K.3.1}$$

$$\phi_{1,\mu}(\vec{p}) = (1/\kappa) \iint_{S_1 \cap D_p} \hat{\mu}_1^A(\vec{q}) \; \hat{n}(\vec{q}) \cdot \tilde{\nabla}_q (1/R) \, dS_q \tag{K.3.2}$$

are respectively symmetric and antisymmetric functions in the sense that

$$\phi_{1,\sigma}(R_1\vec{p}) = \phi_{1,\sigma}(\vec{p}) \tag{K.3.3}$$

$$\phi_{1,\mu}(R_1\vec{p}) = -\phi_{1,\mu}(\vec{p}) \tag{K.3.4}$$

We will prove the two identities (K.3.3) and (K.3.4) in the course of our discussion.

The perturbation potential induced by all of the singularity distributions $\sigma^\pm$, $\mu^\pm$, $\hat{\sigma}_1^S$ and $\hat{\mu}_1^A$ is given by the formula

$$\begin{aligned}
\phi(\vec{p}) = & \sum_{i \in \{+1,-1\}} - (1/\kappa) \iint_{S^i \cap D_p} \sigma^i(\vec{q}) \, (1/R(\vec{p},\vec{q})) \, dS_q \\
& + \sum_{i \in \{+1,-1\}} (1/\kappa) \iint_{S^i \cap D_p} \mu^i(\vec{q}) \, \hat{n}(\vec{q}) \cdot \tilde{\nabla}_q (1/R(\vec{p},\vec{q}) \, dS_q \\
& - (1/\kappa) \iint_{S_1 \cap D_p} \hat{\sigma}_1^S(\vec{q}) \, (1/R(\vec{p},\vec{q})) \, dS_q \\
& + (1/\kappa) \iint_{S_1 \cap D_p} \hat{\mu}_1^A(\vec{q}) \, \hat{n}(\vec{q}) \cdot \tilde{\nabla}_q (1/R(\vec{p},\vec{q})) \, dS_q
\end{aligned} \tag{K.3.5}$$

Notice that we use the set $\{+1, -1\}$ as an index set for the summation. This will be the usual index set in all the expressions that follow, so that we will frequently write ($\sum_i$) with the implicit convention that i is to take on the values +1, -1. Notice also that $\sigma^{(+1)}$ and σ^+ refer to the same function - because the index set is just $\{+1, -1\}$, it is only necessary to specify the sign of a particular superscript.

Our next task will be to introduce the definitions that will enable us to express the integrals in equation (K.3.5) as integrals over the regions S^+ and S_1. First, we define R^i, the reflection matrix that maps S^i into S^+.

$$R^+ = I$$
$$R^- = I - 2\,\hat{n}_1\hat{n}_1^T \qquad \text{(K.3.6)}$$

Next, observe that the functions σ^i, μ^i are defined only for points $\vec{q} \in S^i$. Thus we define $\bar{\sigma}^i(\vec{q})$, $\vec{q} \in S^+$ by

$$\bar{\sigma}^i(\vec{q}) = \sigma^i(R^i\vec{q}) \qquad \vec{q} \in S^+ \qquad \text{(K.3.7)}$$

Notice as well that the unit normal in S^i is related to the unit normal in S^+ by the relation,

$$\hat{n}\,(R^i\vec{q}) = R^i\,\hat{n}\,(\vec{q}) \qquad \vec{q} \in S^+ \qquad \text{(K.3.8)}$$

Next observe that the invariance relation for the compressible inner product gives us

$$R^2\,(\vec{p}, R^i\vec{q}) = [\vec{p} - R^i\,\vec{q}, \vec{p} - R^i\,\vec{q}] = [R^i\,(R^i\vec{p} - \vec{q}), R^i\,(R^i\,\vec{p} - \vec{q})]$$
$$= [R^i\,\vec{p} - \vec{q}, R^i\,\vec{p} - \vec{q}] = R^2\,(R^i\,\vec{p}, \vec{q}) \qquad \text{(K.3.9)}$$

Using these relations, one has

$$\sigma^i\,(\vec{q}) = \bar{\sigma}^i\,(R^i\vec{q}) \qquad \text{(K.3.10)}$$

$$R(\vec{p},\vec{q}) = R(R^i\vec{p}, R^i\vec{q}) \qquad (\vec{q} \in S^i,\ R^i\,\vec{q} \in S^+) \qquad \text{(K.3.11)}$$

$$dS(\vec{q}) = dS(R^i\vec{q}) \qquad \text{(K.3.12)}$$

$$\mu^i(\vec{q}) = \bar{\mu}^i\,(R^i\vec{q}) \qquad \text{(K.3.13)}$$

$$\hat{n}(\vec{q}) \cdot \tilde{\nabla}_q\,(1/R) = \hat{n}(R^i\vec{q}) \cdot R^i(-s\beta^2)(\vec{q}-\vec{p})/R^3(\vec{p},\vec{q})$$

$$= \hat{n}(R^i\vec{q})\cdot(-s\beta^2)(R^i\vec{q} - R^i\vec{p})/R^3(R^i\vec{p},\ R^i\vec{q})$$

$$= [\hat{n}(\vec{u}).\ \tilde{\nabla}_u\ (1/R(\vec{v},\vec{u})]\ \Big|\ (\vec{v} = R^i\ \vec{p}),\ (\vec{u} = R^i\ \vec{q})$$

(K.3.14)

Thus the expression (K.3.5) may be rewritten

$$\phi(\vec{p}) = \sum_i\ -(1/\kappa)\iint_{S+\cap D_p} \bar{\sigma}^i(\vec{q})\ (1/R(R^i\vec{p},\vec{q}))\ dS_q$$

$$+\ \sum_i\ (1/\kappa)\iint_{S+\cap D_p} \bar{\mu}^i(\vec{q})\ \hat{n}(\vec{q})\ .\ \tilde{\nabla}_q\ (1/R(R^i\vec{p},\vec{q}))\ dS_q$$

$$-\ (1/\kappa)\iint_{S_1\cap D_p} \hat{\sigma}_1^S\ (\vec{q})\ (1/R(\vec{p},\vec{q}))\ dS_q$$

$$+\ (1/\kappa)\iint_{S_1\cap D_p} \hat{\mu}_1^A\ (\vec{q})\ \ \hat{n}(\vec{q})\cdot\tilde{\nabla}\ (1/R(\vec{p},\vec{q}))\ dS_q$$

(K.3.15)

If we define operators $\Phi_\sigma(\vec{p},\sigma)$, $\Phi_\mu(\vec{p},\mu)$, $\Phi_{1,\sigma}(\vec{p},\sigma)$ and $\Phi_{1,\mu}(\vec{p},\mu)$ by the relations:

$$\Phi_\sigma(\vec{p},\sigma) = -(1/\kappa)\iint_{S^+\cap D_p} \sigma(\vec{q})\ \ 1/R(\vec{p},\vec{q})\ dS_q \qquad \text{(K.3.16)}$$

$$\Phi_\mu\ (\vec{p},\mu) = (1/\kappa)\iint_{S^+\cap D_p} \mu(\vec{q})\ \ \hat{n}(\vec{q})\ \cdot\ \tilde{\nabla}_q\ (1/R(\vec{p},\vec{q}))\ dS_q \qquad \text{(K.3.17)}$$

$$\Phi_{1,\sigma}\ (\vec{p},\sigma) = -(1/\kappa)\iint_{S_1\cap D_p} \sigma(\vec{q})\ \ 1/R(\vec{p},\vec{q})\ dS_q \qquad \text{(K.3.18)}$$

$$\Phi_{1,\mu}\ (\vec{p},\mu) = (1/\kappa)\iint_{S_1\cap D_p} \mu(\vec{q})\ \hat{n}(\vec{q})\ \cdot\ \nabla_q(1/R(\vec{p},\vec{q}))\ dS_q \qquad \text{(K.3.19)}$$

then $\phi(\vec{p})$ can be written in shorthand form as

$$\phi(\vec{p}) = \sum_i \{\Phi_\sigma (R^i\vec{p}, \bar{\sigma}^i) + \Phi_\mu (R^i \vec{p}, \bar{\mu}^i)\}$$

$$+ \Phi_{1,\sigma} (\vec{p}, \hat{\sigma}_1{}^S) + \Phi_{1,\mu} (\vec{p}, \hat{\mu}_1{}^A) \qquad (K.3.20)$$

We now have the machinery necessary to define the symmetric and antisymmetric part of ϕ. Letting H^{ij} be the 2x2 matrix

$$\begin{bmatrix} H^{++} & H^{+-} \\ H^{-+} & H^{--} \end{bmatrix} = \begin{bmatrix} 1 & 1 \\ 1 & -1 \end{bmatrix} \qquad (K.3.21)$$

we define $\hat{\phi}^i(\vec{p})$ by

$$\hat{\phi}^i(\vec{p}) = \sum_j H^{ij} \phi (R^j\vec{p}). \qquad (K.3.22)$$

With functions $\hat{\phi}^i$ so defined, we remark that $\hat{\phi}^+$ is called the symmetric part of ϕ and is frequently denoted $\hat{\phi}^S$, while $\hat{\phi}^-$ is called the antisymmetric part of ϕ and is frequently denoted $\hat{\phi}^A$. The symmetry relations satisfied by $\hat{\phi}^i$ may be compactly summarized by the expression

$$\hat{\phi}^i (R^j\vec{p}) = H^{ij} \hat{\phi}^i(\vec{p}) \qquad \text{(no summation)} \qquad (K.3.23)$$

The proof of (K.3.23) depends upon two easily proved facts:

$$R^i R^j = R^{(i.j)} \qquad (K.3.24)$$

$$H^{i(j.k)} = H^{ij} H^{ik} \qquad (K.3.25)$$

Using these facts we write

$$\phi^i (R^j \vec{p}) = \sum_l H^{il} \phi(R^l(R^j\vec{p})) = \sum_l H^{il} \phi(R^{l.j}\vec{p})$$

Let $k = l.j$; then as l range over $\{+1, -1\}$, so does k, independent of the value of j. Notice also since $j^2 = 1$, $l = j.k$. Thus changing the index of summation to k we find

$$\hat{\phi}^i (R^j \vec{p}) = \sum_k H^{i(j.k)} \phi(R^k\vec{p}) = \sum_k H^{ij} H^{ik} \phi(R^k\vec{p})$$

$$= H^{ij} \sum_k H^{ik} \phi(R^k\vec{p}) = H^{ij} \hat{\phi}^i (\vec{p})$$

This proves the assertion of equation (K.3.23).

If functions $\hat{\sigma}^i$ and $\hat{\mu}^i$ are defined by

$$\hat{\sigma}^i(\vec{p}) = \sum_j H^{ij}\, \bar{\sigma}^j(\vec{p}) = \sum_j H^{ij}\, \sigma^j(R^j\vec{p}) \qquad (\vec{p} \in S^+) \tag{K.3.26}$$

$$\hat{\mu}^i(\vec{p}) = \sum_j H^{ij}\, \bar{\mu}^j(\vec{p}) = \sum_j H^{ij}\, \mu^j(R^j\vec{p}) \tag{K.3.27}$$

then we will show that equation (K.3.20) implies the following analogous representation

$$\hat{\phi}^i(\vec{p}) = \sum_j H^{ij}\, \Phi_\sigma\, (R^j\vec{p}, \hat{\sigma}^i) + H^{ij}\, \Phi_\mu\, (R^j\vec{p}, \hat{\mu}^i)$$

$$+ 2\, \delta^{i+}\, \Phi_{1,\sigma}(\vec{p}, \hat{\sigma}_1{}^S) + 2\, \delta^{i-}\, \Phi_{1,\mu}\, (\vec{p}, \hat{\mu}_1{}^A) \tag{K.3.28}$$

Here, δ^{ij} denotes the usual sort of Kronecker delta, $\delta^{ij} = 1$ if $i=j$ and 0 otherwise. The proof of this assertion follows directly from the following facts:

$$\sum_{j,k} H^{ij}\, \Phi_\sigma\, (R^j R^k\, \vec{p}, \bar{\sigma}^k) = \sum_l H^{il}\, \Phi_\sigma\, (R^l\vec{p}, \hat{\sigma}^i) \tag{K.3.29}$$

$$\sum_{j,k} H^{ij}\, \Phi_\mu\, (R^j R^k\, \vec{p}, \bar{\mu}^k) = \sum_l H^{il}\, \Phi_\mu\, (R^l\vec{p}, \hat{\mu}^i) \tag{K.3.30}$$

$$\sum_j H^{ij}\, \Phi_{1,\sigma}\, (R^j\vec{p}, \hat{\sigma}_1{}^S) = 2\, \delta^{i+}\, \Phi_{1,\sigma}\, (\vec{p}, \hat{\sigma}_1{}^S) \tag{K.3.31}$$

$$\sum_j H^{ij}\, \Phi_{1,\mu}\, (R^j\vec{p}, \hat{\mu}_1{}^A) = 2\, \delta^{i-}\, \Phi_{1,\mu}\, (\vec{p}, \hat{\mu}_1{}^A) \tag{K.3.32}$$

which we now prove. Equation (K.3.29) is established by the following argument.

$$\sum_{j,k} H^{ij}\, \Phi_\sigma\, (R^j\, R^k\vec{p}, \bar{\sigma}^k) = \sum_{l,k} H^{i(l.k)}\, \Phi_\sigma\, (R^l\vec{p}, \bar{\sigma}^k)$$

$$= \sum_l H^{il} \sum_k H^{ik}\, \Phi_\sigma\, (R^l\vec{p}, \bar{\sigma}^k)$$

$$= \sum_l H^{il}\, \Phi_\sigma\, (R^l\vec{p}, \sum_k H^{ik}\, \bar{\sigma}^k)$$

$$= \sum_{l} H^{il} \Phi_{\sigma} (R^{l}\vec{p}, \hat{\sigma}^{i})$$

Equation (K.3.30) is established in an identical fashion. Equations (K.3.31) and (K.3.32) follow fairly readily from the standard symmetry relations

$$\Phi_{1,\sigma}(R_1\vec{p},\sigma) = \Phi_{1,\sigma}(\vec{p},\sigma) \tag{K.3.33}$$

$$\Phi_{1,\mu}(R_1\vec{p},\mu) = -\Phi_{1,\mu}(\vec{p},\mu) \tag{K.3.34}$$

which we now prove. For the first we have, using the definition (K.3.18),

$$\Phi_{1,\sigma}(R_1\vec{p},\sigma) = -(1/\kappa) \iint_{S_1 \cap D_p} \sigma(\vec{q}) \quad 1/R(R_1\vec{p},\vec{q}) \, dS_q \tag{K.3.35}$$

Now by the invariance condition (K.2.4) applied to R_1 we have

$$R^2(R_1\vec{p},\vec{q}) = [R_1\vec{p} - \vec{q}, R_1\vec{p} - \vec{q}] = [\vec{p} - R_1\vec{q}, \vec{p} - R_1 \vec{q}]$$

$$= R^2(\vec{p}, R_1\vec{q})$$

For $\vec{q} \in S_1$, $R_1\vec{q} = \vec{q}$ so that we obtain

$$R^2(R_1\vec{p},\vec{q}) = R^2(\vec{p},\vec{q}) \quad (\vec{q} \in S_1) \tag{K.3.36}$$

Substituting this into the expression (K.3.35), we find

$$\Phi_{1,\sigma}(R_1\vec{p},\sigma) = -(1/\kappa) \iint_{S_1 \cap D_p} \sigma(\vec{q}) \quad 1/R(\vec{p},\vec{q}) \, dS_q$$

$$= \Phi_{1,\sigma}(\vec{p},\sigma)$$

and we are done. Turning now to equation (K.3.34) we find, using the definition (K.3.19)

$$\Phi_{1,\mu}(R_1\vec{p}) = (1/\kappa) \iint_{S_1 \cap D_p} \mu(\vec{q}) \, \hat{n}(q)^T \quad \tilde{\nabla}_q(1/R(R_1\vec{p},\vec{q})) \, dS_q$$

Now, for $\vec{q} \in S_1$

$$\tilde{\nabla}_q \, (1/R(R_1\vec{p},\vec{q})) = -s\beta^2 \, \frac{\vec{q} - R_1\vec{p}}{R^3(R_1\vec{p},\vec{q})}$$

$$= -s\beta^2 \, R_1(\vec{q}-\vec{p})/R^3(\vec{p},\vec{q})$$

$$= R_1 \quad \tilde{\nabla}_q(1/R(\vec{p},\vec{q})) \tag{K.3.37}$$

Now for networks lying in the plane of symmetry, $\hat{n}(\vec{q}) = \alpha\hat{n}_1$, $\alpha = \pm 1$, so that

$$\hat{n}(\vec{q})^T R_1 = \alpha\, \hat{n}_1^T R_1 = \alpha\, \hat{n}_1^T (I - 2\, \hat{n}_1\, \hat{n}_1^T) = -\alpha\, \hat{n}_1^T$$

$$= -\, \hat{n}(\vec{q})^T \qquad (\vec{q} \in S_1) \qquad \text{(K.3.38)}$$

Using all these observations, we find

$$\Phi_{1,\mu}\,(R_1\vec{p},\mu) = (1/\kappa) \iint_{S_1 \cap D_p} \mu(\vec{q})\, \hat{n}(\vec{q})^T R_1 \quad \tilde{\nabla}_q\, (1/R(\vec{p},\vec{q}))\, dS_q$$

$$= (1/\kappa) \iint_{S_1 \cap D_p} \mu(\vec{q})\, (\underset{\substack{\uparrow \\ \text{(note the minus sign)}}}{-}\hat{n}(\vec{q})^T)\, \tilde{\nabla}_q\, (1/R(\vec{p},\vec{q}))\, dS_q$$

and we are done.

We have derived all of the representation and symmetry results that we require for the potential and must now state and prove the implied representation and symmetry results for $\vec{v}(\vec{p}) = \nabla_p\, \phi(\vec{p})$

With the understanding the line vortex velocity singularities are always to be removed, one finds after some manipulation that $\vec{v}(\vec{p})$ is given

$$\vec{v}(\vec{p}) = \nabla_p\, \phi(\vec{p}) = \sum_i R^i[\vec{V}_\sigma(R^i\vec{p},\, \hat{\sigma}^i) + \vec{V}_\mu(R^i\vec{p},\, \hat{\mu}^i)]$$

$$+ \vec{V}_{1,\sigma}\,(\vec{p},\hat{\sigma}_1^S) + \vec{V}_{1,\mu}(\vec{p},\hat{\mu}_1^A) \qquad \text{(K.3.39)}$$

where the operators $\vec{V}_\sigma$, $\vec{V}_\mu$, $\vec{V}_{1,\sigma}$, $\vec{V}_{1,\mu}$ are defined

$$\vec{V}_\sigma(\vec{p},\sigma) = -(1/\kappa) \iint_{S^+ \cap D_p} \sigma(\vec{q})\ \nabla_p(1/R(\vec{p},\vec{q}))\, dS_q \qquad \text{(K.3.40)}$$

$$\vec{V}_\mu(\vec{p},\mu) = (1/\kappa) \iint_{S^+ \cap D_p} (\hat{n}(\vec{q})dS_q \times \nabla_q\, \mu) \times \tilde{\nabla}_q(1/R(\vec{p},\vec{q})) \qquad \text{(K.3.41)}$$

$$\vec{V}_{1,\sigma}(\vec{p},\sigma) = -(1/\kappa) \iint_{S_1 \cap D_p} \sigma(\vec{q})\ \nabla_p(1/R(\vec{p},\vec{q}))\, dS \qquad \text{(K.3.42)}$$

$$\vec{V}_{1,\mu}(\vec{p},\sigma) = (1/\kappa) \iint_{S_1 \cap D_p} (\hat{n}(\vec{q})dS_q \times \nabla_q\mu) \times \tilde{\nabla}_q(1/R(\vec{p},\vec{q})) \qquad \text{(K.3.43)}$$

Notice that $\vec{V}_\mu$ and $\vec{V}_{1,\mu}$ are not defined as the gradients of Φ_μ and $\Phi_{1,\mu}$ in that the line vortex singularity has been removed. Nevertheless for all practical purposes, $\vec{V}_\mu$ and $\vec{V}_{1,\mu}$ behave like the gradients of Φ_μ and $\Phi_{1,\mu}$. Formal differentiation of the definition (K.3.22) for $\hat{\phi}^i$ leads to the following definition for $\hat{v}^i(\vec{p})$:

$$\hat{v}^i(\vec{p}) = \sum_j H^{ij} R^j \vec{v}(R^j\vec{p}) \tag{K.3.44}$$

The symmetry relation analogous to (K.3.23) is given

$$\hat{v}^i(R^j\vec{p}) = H^{ij}R^j\hat{v}^i(\vec{p}) \qquad \text{(no summation)} \tag{K.3.45}$$

and is proved just as easily -

$$\hat{v}^i(R^j\vec{p}) = \sum_l H^{il}R^l\vec{v}(R^lR^jp) = \sum_k H^{i(j.k)}R^{(j.k)}\vec{v}(R^k\vec{p})$$

$$= H^{ij}R^j \sum_k H^{ik}R^k\vec{v}(R^k\vec{p}) = H^{ij}R^j\hat{v}^i(\vec{p})$$

The representation result analogous to (K.3.28) is given

$$\hat{v}^i(p) = \sum_j H^{ij}R^j[\vec{V}_\sigma(R^j\vec{p},\hat{\sigma}^i) + \vec{V}_\mu(R^j\vec{p},\hat{\mu}^i)]$$

$$+ 2\,\delta^{i+}\,\vec{V}_{1,\sigma}(\vec{p},\hat{\sigma}_1{}^S) + 2\,\delta^{i-}\vec{V}_{1,\mu}(\vec{p},\hat{\mu}_1{}^A) \tag{K.3.46}$$

The first two parts of this identity are generated in the obvious way from the corresponding terms in equation (K.3.39) while the last two parts follow from the symmetry relations

$$\vec{V}_{1,\sigma}(R_1\vec{p},\sigma) = R_1\,\vec{V}_{1,\sigma}\,(\vec{p},\sigma) \tag{K.3.47}$$

$$\vec{V}_{1,\mu}\,(R_1\vec{p},\mu) = -R_1\,\vec{V}_{1,\mu}\,(\vec{p},\mu) \tag{K.3.48}$$

The proof of (K.3.47) is trivial in view of the symmetry relation for $\Phi_{1,\sigma}$, (K.3.33) and the definition of $\vec{V}_{1,\sigma}$, (K.3.42). The proof of (K.3.48) offers somewhat greater challenges; using (K.3.37) we find,

$$V_{1,\mu}(R_1\vec{p},\mu) = (1/\kappa)\iint_{S_1\cap D_p} (\hat{n}(\vec{q})dS_q \times \nabla\mu) \times \tilde{\nabla}_q\,(1/R(R_1\vec{p},\vec{q}))$$

$$= (1/\kappa)\iint_{S_1\cap D_p} (\hat{n}(\vec{q})dS_q \times \nabla\mu) \times R_1\;\tilde{\nabla}_q\,(1/R(\vec{p},\vec{q}))$$

$$= (1/\kappa)(\det R_1)\, R_1^{-T} \iint_{S_1 \cap D_p} [R_1(\hat{n}(\vec{q})dS_q \times \nabla\mu)] \times \tilde{\nabla}_q\, (1/R(\vec{p},\vec{q}))$$

Now $R_1^{-T} = R_1$, $\det R_1 = -1$ and on the surface S_1 lying on the plane of symmetry,

$$R_1(\hat{n} \times \nabla\mu) = (I - 2\,\hat{n}_1\,\hat{n}_1^T)\,\hat{n} \times \nabla\mu$$

$$= \hat{n} \times \nabla\mu - 2\,\hat{n}_1\,(\hat{n}_1 \cdot \hat{n} \times \nabla\mu)$$

$$= \hat{n} \times \nabla\mu$$

since for points $\vec{q} \in S_1$, $\hat{n}(\vec{q}) = \pm\hat{n}_1$. Consequently

$$\vec{V}_{1,\mu}(R_1\vec{p},\mu) = (1/\kappa)\,(-1)\,R_1 \iint_{S_1 \cap D_p} (\hat{n}(\vec{q})dS_q \times \nabla\mu) \times \tilde{\nabla}_q(1/R(\vec{p},\vec{q}))$$

and we are done.

We have now derived all of the machinery necessary to perform the symmetrization of boundary conditions. In symmetrizing the boundary conditions, we treat first the case of a control point <u>not</u> lying in the plane of symmetry and then the case of a control point lying <u>in</u> the plane of symmetry. (Note: A control point $\vec{p}$ is said to lie <u>in the</u> plane of symmetry provided (i) $R_1\,\vec{p} = \vec{p}$ <u>and</u> (ii) $\hat{n}(\vec{p}) = \pm\hat{n}_1$. See appendix (H.1.2) for a detailed discussion of control point classification.)

<u>Symmetrization for $\vec{p} \in S^+$</u>

Let $\vec{p} \in S^+$ be a control point not lying in the plane of symmetry; then $R_1\,\vec{p} \in S^-$ is the image of $\vec{p}$ in the plane of symmetry. Using the notation developed earlier in this section, we can write the boundary conditions at $\vec{p}$ and $R_1\vec{p}$ with a single formula:

$$\underline{bc}^j: \quad (a_A\hat{n}^T(\vec{p})B_o + \vec{t}_A^{\,T})\, R^j(\vec{v}(R^j\vec{p}))_A + c_A(\phi(R^j\vec{p}))_A$$

$$+ a_A\,\sigma^j(R^j\vec{p}) + c_D\,\mu^j(R^j\vec{p}) + \vec{t}_D^{\,T}R^j\,\nabla_v\,\mu^j(\vec{v})\Big|_{\vec{v} = R^j\vec{p}} = b^j \tag{K.3.49}$$

Notice that we require the scalar coefficients of the boundary condition to be identical for both the control point $\vec{p}$ and its image $R_1\vec{p}$ while the vector coefficients are reflected by R_1. Multiplying equation (K.3.49) by H^{ij}, summing over j and taking account of the definitions (K.3.22) of $\hat{\phi}^i$, (K.3.44) of $\hat{v}^i$ together with relations (K.3.26) and (K.3.27) for $\hat{\sigma}^i$ and $\hat{\mu}^i$, yields, after some manipulation,

$$bc^i: \quad (a_A\, \hat{n}^T(\vec{p})B_o + \vec{t}_A{}^T)(\hat{v}^i(\vec{p}))_A + c_A(\hat{\phi}^i(\vec{p}))_A$$

$$+ a_A\, \hat{\sigma}^i(\vec{p}) + c_D\, \hat{\mu}^i(\vec{p}) + \vec{t}_D{}^T\, \nabla_p\, \hat{\mu}^i(\vec{p}) = \sum_j H^{ij}\, b^j \qquad \text{(K.3.50)}$$

Symmetrization for $\vec{p} \in S_1$, $\hat{n}(\vec{p})$ parallel to $\hat{n}_1$

When a control point lies in a plane of symmetry, very special care must be used in order to achieve the desired symmetrization. Part of the problem is caused by the fact that we do not really have enough boundary conditions to fully determine the source and doublet parameters associated with both $\hat{\phi}^S$ and $\hat{\phi}^A$. Thus, the user specified boundary conditions must be supplemented by special, program supplied, degenerate boundary conditions. We begin our treatment of symmetrization for control points in the plane of symmetry by deriving the form of these special degenerate boundary conditions.

Let $\vec{p} \in S_1$ be a control point lying in the plane of symmetry and let $\hat{n}$ be the normal to S_1 at $\vec{p}$ where $\hat{n} = \pm\hat{n}_1$. Let $\hat{\phi}^S$ and $\hat{\phi}^A$ be respectively the symmetric and antisymmetric part of ϕ as defined above. Then the following jump conditions hold for $\hat{\phi}^S$ and $\hat{\phi}^A$.

$$[\![\ \hat{\phi}^S(\vec{p})\ ]\!] = \lim_{\varepsilon \to 0} [\hat{\phi}^S(\vec{p} + \varepsilon\hat{n}) - \hat{\phi}^S(\vec{p} - \varepsilon\hat{n})] = 0 \qquad \text{(K.3.51)}$$

$$[\![\ \partial\, \hat{\phi}^A/\partial\hat{n}\ ]\!] = \lim_{\varepsilon \to 0} [\hat{n} \cdot \nabla\, \hat{\phi}^A\, (\vec{p} + \varepsilon\hat{n}) - \hat{n} \cdot \nabla\, \hat{\phi}^A(\vec{p} - \varepsilon\hat{n})] = 0 \qquad \text{(K.3.52)}$$

The first of these relations follows from the argument,

$$\hat{\phi}^S(\vec{p} + \varepsilon\, \hat{n}) = \hat{\phi}^S\, (R_1(\vec{p} + \varepsilon\hat{n})) = \hat{\phi}^S\, (R_1\vec{p} + \varepsilon\, R_1\, \hat{n})$$

$$= \phi^S\, (\vec{p} + \varepsilon(-\hat{n}))$$

In this sequence of equalities, the first equality follows from the general symmetry condition (K.3.23) with $i = +1$, $j = -1$ while the third equality follows from the facts $R_1\vec{p} = \vec{p}$ ($\vec{p} \in S_1$) and $R_1\hat{n} = -\hat{n}$ ($\hat{n} = \pm\hat{n}_1$).

Relation (K.3.52) is proved by first noticing that the relation (K.3.23) with $i = -1$, $j = -1$, implies,

$$\hat{\phi}^A\, (R_1\vec{q}) = -\hat{\phi}^A(\vec{q}).$$

Applying ∇_q to this, we obtain,

$$R_1\ \nabla\, \hat{\phi}^A(R_1\vec{q}) = -\, \nabla\, \hat{\phi}^A\, (\vec{q})$$

Letting $\vec{q} = \vec{p} + \varepsilon\hat{n}$, we see as before that $R_1\vec{q} = \vec{p} - \varepsilon\hat{n}$ so that

$$R_1 \quad \nabla \hat{\phi}^A(\vec{p} - \varepsilon\hat{n}) = - \nabla\hat{\phi}^A(\vec{p} + \varepsilon\hat{n})$$

Multiplying by $\hat{n}^T$ and recalling that $\hat{n}^T R_1 = -\hat{n}^T$, we get

$$-\hat{n}^T \ \nabla\hat{\phi}^A \ (\vec{p} - \varepsilon\hat{n}) = -\hat{n}^T \ \nabla\hat{\phi}^A \ (\vec{p} + \varepsilon\hat{n})$$

Equation (K.3.52) now follows immediately.

As a consequence of these jump conditions, we are led to the conclusion that the doublet strength associated with $\hat{\phi}^S$ and the source strength associated with $\hat{\phi}^A$ are both zero for points $\vec{p} \ \varepsilon \ S_1$. Thus, we write

$$\hat{\mu}_1{}^S(\vec{p}) = 0 \qquad (\vec{p} \ \varepsilon \ S_1) \tag{K.3.53}$$

$$\hat{\sigma}_1{}^A(\vec{p}) = 0 \qquad (\vec{p} \ \varepsilon \ S_1) \tag{K.3.54}$$

These then are the degenerate boundary conditions to be imposed on, respectively, the symmetric and antisymmetric problems.

Turning now to the symmetrization of a regular aerodynamic boundary condition imposed at $\vec{p} \ \varepsilon \ S_1$, we use the relations

$$\phi(\vec{p}) = \frac{1}{2} \ (\hat{\phi}^S(\vec{p}) + \hat{\phi}^A(\vec{p})), \tag{K.3.55}$$

$$\vec{v}(\vec{p}) = \frac{1}{2} \ (\hat{v}^S(\vec{p}) + \hat{v}^A(\vec{p})) \tag{K.3.56}$$

(which follow directly from the definitions (K.3.22) and (K.3.44)) to obtain

$$\begin{aligned}(a_A\hat{n}^T B_o + \vec{t}_A^T)(\tfrac{1}{2})(\hat{v}^S(\vec{p}) + \hat{v}^A(\vec{p}))_A + c_A(\tfrac{1}{2})(\hat{\phi}^S(\vec{p}) + \hat{\phi}^A(\vec{p}))_A \\ + a_A \ \hat{\sigma}_1{}^S(\vec{p}) + c_D \ \hat{\mu}_1{}^A(\vec{p}) + \vec{t}_D{}^T \ \nabla \hat{\mu}_1^A \qquad = b\end{aligned} \tag{K.3.57}$$

where we have used the fact that the source and doublet distributions on S_1 are denoted $\hat{\sigma}_1{}^S$ and $\hat{\mu}_1{}^A$. Considerable simplification is obtained by recognizing the following average value formulae

$$(\hat{\phi}^A(\vec{p}))_A = 0 \tag{K.3.58}$$

$$(\vec{t}_A{}^T \ \hat{v}^A(\vec{p}))_A = 0 \tag{K.3.59}$$

$$(\hat{n}^T \ B_o \ \hat{v}^S(\vec{p}))_A = 0 \tag{K.3.60}$$

Of these formulae, the first is an obvious consequence of the asymmetry of $\hat{\phi}^A$, the second is an easy consequence of the symmetry relation (K.3.45) and the identity $R_1 \vec{t}_A = \vec{t}_A$, and the third is a consequence of (K.3.45) together with the identities $B_0\hat{n} = \hat{n}$ (since $\hat{n} = \pm\hat{n}_1$ and $(\hat{n}_1, \hat{c}_0) = 0$), $R_1\hat{n} = -\hat{n}$. Using the relations (K.3.58), (K.3.59), (K.3.60), the boundary condition (K.3.57) becomes,

$$\frac{1}{2} a_A \hat{n}^T B_0(\hat{v}^A(\vec{p}))_A + c_D \hat{\mu}_1^A(\vec{p}) + \vec{t}_D^T \nabla \hat{\mu}_1^A$$

$$+ \frac{1}{2} \vec{t}_A^T (\hat{v}^S(\vec{p}))_A + \frac{1}{2} c_A(\hat{\phi}^S(\vec{p}))_A + a_D \hat{\sigma}_1^S(\vec{p}) = b \qquad \text{(K.3.61)}$$

A notable feature of this equation is the fact that the coefficient (1/2) appears in three of the terms, that is, those terms that are computed from IC integrals. [This minor nuisance could be avoided if we were to change the definition (K.3.22) to

$$\hat{\phi}^i(\vec{p}) = (\tfrac{1}{2}) \sum_j H^{ij} \phi(R^j\vec{p})$$

and similarly for (K.3.44). However, we choose to leave things as they are.]

Without further additional assumptions, it is impossible to do any more about symmetrizing a boundary condition in a plane of symmetry. However, a careful examination of (K.3.61) reveals that if either $(a_A, c_D, \vec{t}_D) = 0$ or $(a_D, c_A, \vec{t}_A) = 0$, then equation (K.3.61) becomes a condition on just the symmetric or just the antisymmetric part of ϕ. Thus we are led to the definitions:

<u>Symmetric boundary condition.</u> A boundary condition on a plane of symmetry is said to be a symmetric boundary condition if $(a_A, c_D, \vec{t}_D) = 0$. From (K.3.61) we observe that a symmetric boundary condition imposes upon $\hat{\phi}^S$ the condition

$$\frac{1}{2} \vec{t}_A^T(\hat{v}^S(p))_A + \frac{1}{2} c_A(\hat{\phi}^S(\vec{p}))_A + a_D \hat{\sigma}_1^S(\vec{p}) = b \qquad \text{(K.3.62)}$$

The associated boundary condition (of symmetric type) to be imposed upon $\hat{\phi}^A$ is the degenerate boundary condition (cf.(K.3.54))

$$\hat{\sigma}_1^A(\vec{p}) = 0$$

<u>Antisymmetric boundary condition.</u> A boundary condition on a plane of symmetry is said to be an antisymmetric boundary condition if $(a_D, c_A, \vec{t}_A) = 0$. From (K.3.61) we observe that an antisymmetric boundary condition imposes upon $\hat{\phi}^A$ the condition

$$\frac{1}{2} a_A \hat{n}^T B_0 (\hat{v}^A(\vec{p}))_A + c_D \hat{\mu}_1^A(\vec{p}) + \vec{t}_D^T \nabla \hat{\mu}_1^A = b \qquad \text{(K.3.63)}$$

The associated boundary condition (of antisymmetric type) to be imposed upon $\hat{\phi}^S$ is the degenerate boundary condition (cf. (K.3.53))

$$\hat{\mu}_1^{\,S}(\vec{p}) = 0$$

We find, then, that the boundary value problem for $\hat{\phi}^S$ can be fully decoupled from the boundary value problem for $\hat{\phi}^A$ only if the user specifies a symmetric boundary condition on a source network and an antisymmetric boundary condition on a doublet network for any network lying in the plane of symmetry. This condition should be regarded as the natural extension of the condition that boundary conditions on opposite sides of the plane of symmetry be connected with one another as indicated by (K.3.49).

Having performed the analysis to this level of detail, we can now make fairly precise statements about the efficiency gains that can be achieved when a plane of geometric symmetry is present.

First, even if no special conditions are imposed upon the boundary conditions, the cost of computing influence coefficients can be cut in half. This efficiency gain is achieved because it is not necessary to compute the influences of any image panels on the control points, a fact which is clearly indicated by equation (K.3.20). [Note: The evaluation of influence coefficients associated with $\Phi_\sigma(\vec{p},\hat{\sigma}^-)$ requires no extra effort over the evaluation $\Phi_\sigma(\vec{p}, \hat{\sigma}^+)$].

Second, if special symmetry conditions are imposed on the form of the boundary conditions (equation (K.3.49) and the symmetric/antisymmetric properties on the plane of symmetry), then it is possible to reduce the matrix solution cost by a factor of 4 by solving two AIC matrices of size N rather than one AIC matrix of size 2N.

Third, if there is partial geometric symmetry together with partial boundary condition symmetry, some efficiency gains are possible provided one is willing to develop quite complex influence coefficient generation and linear equation codes.

In the PAN AIR program, the decision has been made to implement geometric symmetry for only that case which yields the greatest efficiency gains, that is the case in which the boundary conditions satisfy the symmetry constraints (K.3.49) away from the plane of symmetry and (K.3.62), (K.3.63) in the plane of symmetry. Thus, when it is appropriate, we obtain the efficiency gains described in the second of the three situations described above.

K.4 Problem Formulation for Two Planes of Symmetry

In this section, we extend the results of the previous section to the case in which the configuration has two planes of geometric symmetry. In figure K.4 we illustrate such a configuration where the unit normals to the planes of symmetry are denote $\hat{n}_1$ and $\hat{n}_2$ and these normals satisfy the usual conditions (cf. equation (K.2.11))

$$\hat{n}_1 \cdot \hat{n}_2 = \hat{n}_1 \cdot \hat{c}_0 = \hat{n}_2 \cdot \hat{c}_0 = 0$$

The singularity surface S on which sources and doublets are defined is decomposed in eight parts as follows

$$S^{ij}: \quad S^{++} = S \cap C^{++}, \quad C^{++} = \{ \vec{p} \mid (\vec{p},\hat{n}_1) > 0, (\vec{p},\hat{n}_2) > 0 \} \tag{K.4.1}$$

$$S^{-+} = S \cap C^{-+}, \quad C^{-+} = \{ \vec{p} \mid (\vec{p},\hat{n}_1) < 0, (\vec{p},\hat{n}_2) > 0 \}$$

$$S^{+-} = S \cap C^{+-}, \quad C^{+-} = \{ \vec{p} \mid (\vec{p},\hat{n}_1) > 0, (\vec{p},\hat{n}_2) < 0 \}$$

$$S^{--} = S \cap C^{--}, \quad C^{--} = \{ \vec{p} \mid (\vec{p},\hat{n}_1) < 0, (\vec{p},\hat{n}_2) < 0 \}$$

$$S_1{}^j: \quad S_1{}^+ = S \cap C_1{}^+, \quad C_1{}^+ = \{ \vec{p} \mid (\vec{p},\hat{n}_1) = 0, (\vec{p},\hat{n}_2) > 0 \} \tag{K.4.2}$$

$$S_1{}^- = S \cap C_1{}^-, \quad C_1{}^- = \{ \vec{p} \mid (\vec{p},\hat{n}_1) = 0, (\vec{p},\hat{n}_2) < 0 \}$$

$$S_2{}^i: \quad S_2{}^+ = S \cap C_2{}^+, \quad C_2{}^+ = \{ \vec{p} \mid (\vec{p},\hat{n}_1) > 0, (\vec{p},\hat{n}_2) = 0 \} \tag{K.4.3}$$

$$S_2{}^- = S \cap C_2{}^-, \quad C_2{}^- = \{ \vec{p} \mid (\vec{p},\hat{n}_1) < 0, (\vec{p},\hat{n}_2) = 0 \}$$

Allowing the symmetry superscripts i,j to range over the index set {+1, -1}, we denote the singularity distributions on S^{ij} by σ^{ij}, μ^{ij}, on $S_1{}^j$ by $\tilde{\sigma}_1{}^{Sj}$, $\tilde{\mu}_1{}^{Aj}$ and on S_2^i by $\tilde{\sigma}_2^{iS}$, $\tilde{\mu}_2^{iA}$. The tilde written above the singularity distributions on the planes of symmetry is intended to indicate that these functions are already partially symmetrized. The perturbation potential induced by these singularity distributions is given by the formula (compare with (K.3.5)),

$$\phi(\vec{p}) = (1/\kappa) \sum_{i,j} \iint_{S^{ij} \cap D_p} [-\sigma^{ij}(\vec{q})/R(\vec{p},\vec{q}) + \mu^{ij}(\vec{q})\, \hat{n} \cdot \tilde{\nabla}_q (1/R(\vec{p},\vec{q}))]\, dS_q$$

$$+ (1/\kappa) \sum_{j} \iint_{S_1{}^j \cap D_p} [-\tilde{\sigma}_1^{Sj}(\vec{q})/R(\vec{p},\vec{q}) + \tilde{\mu}_1^{Aj}(q)\, \hat{n} \cdot \tilde{\nabla}_q\, (1/R(\vec{p},\vec{q}))]\, dS_q$$

(continued on following page)

$$+ (1/\kappa) \sum_i \iint_{S_2{}^i \cap D_p} [-\tilde{\sigma}^{iS}(\vec{q})/R(\vec{p},\vec{q}) + \tilde{\mu}_1^{iA}(\vec{q})\ \hat{n} \cdot \tilde{\nabla}_q\ (1/R(\vec{p},\vec{q}))]\ dS_q \tag{K.4.4}$$

Proceeding as before, we now define a family of reflection matrices R^{ij} that allow us to express all of the integrals appearing in (K.4.4) as integrals over the principal images of the various singluarity surfaces, S^{++}, $S_1{}^+$ and $S_2{}^+$.

$$R^{++} = I$$

$$R^{-+} = R_1 = I - 2\hat{n}_1\ \hat{n}_1{}^T$$

$$R^{+-} = R_2 = I - 2\ \hat{n}_2\ \hat{n}_2{}^T$$

$$R^{--} = R_1\ R_2 \tag{K.4.5}$$

These reflections have the properties that

$$(R^{ij}) = (R^{ij})^T = (R^{ij})^{-1} \tag{K.4.6}$$

$$R^{ij}\ R^{kl} = R^{(i.k)\ (j.l)} \tag{K.4.7}$$

and also that

$$\begin{aligned} \vec{q} \in C^{++} &\rightarrow R^{ij}\vec{q} \in C^{ij} \\ \vec{q} \in C^{ij} &\rightarrow R^{ij}\vec{q} \in C^{++} \end{aligned} \tag{K.4.8}$$

Using these reflectors, we define some auxiliary singularity distributions on the principal image of the configuration by

$$\left.\begin{aligned} \sigma^{ij}(\vec{q}) &= \bar{\sigma}^{ij}(R^{ij}\vec{q}) \quad (K.4.9) \\ \mu^{ij}(\vec{q}) &= \bar{\mu}^{ij}(R^{ij}\vec{q}) \quad (K.4.10) \end{aligned}\right\} \quad \vec{q} \in S^{ij}$$

$$\left.\begin{aligned} \tilde{\sigma}_1^{Sj}(\vec{q}) &= \tilde{\bar{\sigma}}_1^{Sj}(R^{+j}\vec{q}) \quad (K.4.11) \\ \tilde{\mu}_1^{Aj}(\vec{q}) &= \tilde{\bar{\mu}}_1^{Aj}(R^{+j}\vec{q}) \quad (K.4.12) \end{aligned}\right\} \quad \vec{q} \in S_1{}^j$$

$$\left.\begin{aligned} \tilde{\sigma}_2{}^{iS}(\vec{q}) &= \tilde{\bar{\sigma}}_2{}^{iS}(R^{i+}\vec{q}) \quad (K.4.13) \\ \tilde{\mu}_2{}^{iA}(\vec{q}) &= \tilde{\bar{\mu}}_2{}^{iA}(R^{i+}\vec{q}) \quad (K.4.14) \end{aligned}\right\} \quad \vec{q} \in S_2{}^i$$

These auxiliary singularity distributions, together with the following integral operators (compare with equations (K.3.16) - (K.3.19)),

$$\Phi_\sigma(\vec{p},\sigma) = -(1/\kappa) \iint_{S^{++} \cap D_p} \sigma(\vec{q})/R(\vec{p},\vec{q})\, dS_q \tag{K.4.15}$$

$$\Phi_\mu(\vec{p},\mu) = (1/\kappa) \iint_{S^{++} \cap D_p} \mu(\vec{q})\, \hat{n}(\vec{q}) \cdot \tilde{\nabla}_q (1/R(\vec{p},\vec{q}))\, dS_q \tag{K.4.16}$$

$$\Phi_{1,\sigma}(\vec{p},\sigma) = -(1/\kappa) \iint_{S_1^+ \cap D_p} \sigma(\vec{q})/R(\vec{p},\vec{q})\, dS_q \tag{K.4.17}$$

$$\Phi_{1,\mu}(\vec{p},\mu) = (1/\kappa) \iint_{S_1^+ \cap D_p} \mu(\vec{q})\, \hat{n}(\vec{q}) \cdot \tilde{\nabla}_q (1/R(\vec{p},\vec{q}))\, dS_q \tag{K.4.18}$$

$$\Phi_{2,\sigma}(\vec{p},\sigma) = -(1/\kappa) \iint_{S_2^+ \cap D_p} \sigma(\vec{q})/R(\vec{p},\vec{q})\, dS_q \tag{K.4.19}$$

$$\Phi_{2,\mu}(\vec{p},\mu) = (1/\kappa) \iint_{S_2^+ \cap D_p} \mu(\vec{q})\, \hat{n}(\vec{q}) \cdot \tilde{\nabla}_q (1/R(\vec{p},\vec{q}))\, dS_q \tag{K.4.20}$$

allow us to write $\phi(\vec{p})$ in the shorthand form

$$\begin{aligned}\phi(\vec{p}) = &\sum_{i,j} [\Phi_\sigma(R^{ij}\vec{p}, \bar{\sigma}^{ij}) + \Phi_\mu(R^{ij}\vec{p}, \bar{\mu}^{ij})] \\ &+ \sum_j [\Phi_{1,\sigma}(R^{+j}\vec{p}, \tilde{\sigma}_1^{Sj}) + \Phi_{1,\mu}(R^{+j}\vec{p}, \tilde{\mu}_1^{Aj})] \\ &+ \sum_i [\Phi_{2,\sigma}(R^{i+}\vec{p}, \tilde{\sigma}_2^{iS}) + \Phi_{2,\mu}(R^{i+}\vec{p}, \tilde{\mu}_2^{iA})]\end{aligned} \tag{K.4.21}$$

Our next definition will be of the various symmetric and antisymmetric parts of ϕ. Using the 2x2 matrix $[H^{ij}] = \begin{bmatrix} 1 & 1 \\ 1 & -1 \end{bmatrix}$ as before, we define $\hat{\phi}^{ij}$ by

$$\hat{\phi}^{ij}(\vec{p}) = \sum_{k,l} H^{ik} H^{jl} \phi(R^{kl}\vec{p}) \tag{K.4.22}$$

The four functions $\hat{\phi}^{ij}$ possess the following symmetry properties and alternative names:

	1st pos	2nd pos	alias
$\hat{\phi}^{++}$	symmetric	symmetric	$\hat{\phi}^{SS}$
$\hat{\phi}^{-+}$	antisymmetric	symmetric	$\hat{\phi}^{AS}$
$\hat{\phi}^{+-}$	symmetric	antisymmetric	$\hat{\phi}^{SA}$
$\hat{\phi}^{--}$	antisymmetric	antisymmetric	$\hat{\phi}^{AA}$

These symmetry conditions may be stated concisely as

$$\hat{\phi}^{ij}(R^{kl}\vec{p}) = H^{ik}\, H^{jl}\, \hat{\phi}^{ij}(\vec{p}) \qquad \text{(no summation)} \qquad (K.4.23)$$

The proof of (K.4.23) follows quite readily from the definition of $\hat{\phi}^{ij}$ by using the identities (K.3.25) and (K.4.7). The calculation goes as follows

$$\hat{\phi}^{ij}(R^{kl}\vec{p}) = \sum_{m,n} H^{im}\, H^{jn}\, \phi\, (R^{mn}\, R^{kl}\, \vec{p})$$

$$= \sum_{m,n} H^{im}\, H^{jn}\, \phi\, (R^{(m.k)(n.l)}\vec{p})$$

$$= \sum_{p,q} H^{i(p.k)}\, H^{j(q.l)}\, \phi\, (R^{pq}\vec{p})$$

$$= H^{ik}\, H^{jl} \sum_{p,q} H^{ip}\, H^{jq}\, \phi\, (R^{pq}\vec{p})$$

$$= H^{ik}\, H^{jl}\, \hat{\phi}^{ij}(\vec{p})$$

The representation (K.4.21) induces an analogous representation for $\hat{\phi}^{ij}$. In order to state this representation, we need to define symmetrized singularity distributions as follows.

$$\hat{\sigma}^{ij}(\vec{p}) = \sum_{k,l} H^{ik}\, H^{jl}\, \bar{\sigma}^{kl}(\vec{p}) = \sum_{k,l} H^{ik}\, H^{jl}\, \sigma^{kl}\, (R^{kl}\vec{p}) \qquad (K.4.24)$$

$$\hat{\mu}^{ij}(\vec{p}) = \sum_{k,l} H^{ik}\, H^{jl}\, \bar{\mu}^{kl}(\vec{p}) = \sum_{k,l} H^{ik}\, H^{jl}\, \mu^{kl}\, (R^{kl}\vec{p}) \qquad (K.4.25)$$

$$\hat{\sigma}_1^{Sj}(\vec{p}) = \sum_l H^{jl}\, \tilde{\sigma}_1^{Sl}(\vec{p}) = \sum_l H^{jl}\, \tilde{\sigma}_1^{Sl}\,(R^{+l}\vec{p}) \tag{K.4.26}$$

$$\hat{\mu}_1^{Aj}(\vec{p}) = \sum_l H^{jl}\, \tilde{\mu}_1^{Al}(\vec{p}) = \sum_l H^{jl}\, \tilde{\mu}_1^{Al}\,(R^{+l}\vec{p}) \tag{K.4.27}$$

$$\hat{\sigma}_2^{iS}(\vec{p}) = \sum_k H^{ik}\, \tilde{\sigma}^{kS}(\vec{p}) = \sum_k H^{ik}\, \tilde{\sigma}_2^{kS}\,(R^{k+}\vec{p}) \tag{K.4.28}$$

$$\hat{\mu}_2^{iA}(\vec{p}) = \sum_k H^{ik}\, \tilde{\mu}_2^{kA}(\vec{p}) = \sum_k H^{ik}\, \tilde{\mu}_2^{kA}\,(R^{k+}\vec{p}) \tag{K.4.29}$$

The required representation of $\hat{\phi}^{ij}$ is then given (compare with equation (K.3.28)),

$$\begin{aligned}\hat{\phi}^{ij}(\vec{p}) = {} & \sum_{k,l} H^{ik} H^{jl} [\Phi_\sigma(R^{kl}\vec{p}, \hat{\sigma}^{ij}) + \Phi_\mu(R^{kl}\vec{p}, \hat{\mu}^{ij})] \\ & + 2\delta^{i+} \sum_l H^{jl}\, \Phi_{1,\sigma}(R^{+l}\vec{p}, \hat{\sigma}_1^{Sj}) + 2\,\delta^{i-} \sum_l H^{jl}\, \Phi_{1,\mu}(R^{+l}\vec{p}, \hat{\mu}_1^{Aj}) \\ & + 2\delta^{j+} \sum_k H^{ik}\, \Phi_{2,\sigma}(R^{k+}\vec{p}, \hat{\sigma}_2^{iS}) + 2\delta^{i-} \sum_k H^{ik}\, \Phi_{2,\mu}(R^{k+}\vec{p}, \hat{\mu}_2^{iA})\end{aligned} \tag{K.4.30}$$

For the most part, the proof of this representation is a straightforward computation. To illustrate the method of proof, we simply prove the identity corresponding to the fourth term on the right:

$$\sum_{k,l,q} H^{ik} H^{jl}\, \Phi_{1,\mu}(R^{+q} R^{kl}\, \vec{p}, \tilde{\mu}_1^{Aq}) = 2\delta^{i-} \sum_l H^{jl}\, \Phi_{1,\mu}(R^{+l}\vec{p}, \hat{\mu}_1^{Aj})$$

Since $R^{+q} R^{kl} = R^{k(q.l)}$, the expression on the left is equal to:

$$\begin{aligned}\text{L.H.S.} &= \sum_{k,n,q} H^{ik} H^{j(n.q)}\, \Phi_{1,\mu}(R^{kn}\vec{p}, \tilde{\mu}_1^{Aq}) \\ &= \sum_{k,n} H^{ik} H^{jn}\, \Phi_{1,\mu}(R^{kn}\vec{p}, \sum_q H^{jq}\, \tilde{\mu}_1^{Aq}) \\ &= \sum_n H^{jn} (\sum_k H^{ik}\, \Phi_{1,\mu}(R^{kn}\vec{p}, \hat{\mu}_1^{Aj}))\end{aligned}$$

Now $\Phi_{1,\mu}$ is antisymmetric in the first plane of symmetry, that is,

$$\Phi_{1,\mu}\,(R^{-n}\vec{p},\mu) = -\,\Phi_{1,\mu}\,(R^{+n}\vec{p},\,\mu) \tag{K.4.31}$$

Consequently, we have

$$\sum_k \; H^{ik}\,\Phi_{1,\mu}\,(R^{kn}p,\hat{\mu}_1{}^{Aj}) = \begin{cases} 0 & i = +1 \\ 2\,\Phi_{1,\mu}\,(R^{+n}\vec{p},\,\hat{\mu}_1{}^{Aj}) & i = -1 \end{cases}$$

Thus the left hand side is equal to:

$$\text{L.H.S.} = \sum_n \; H^{jn}\,(2\delta^{i-})\,\Phi_{1,\mu}\,(R^{+n}\vec{p},\,\hat{\mu}_1{}^{Aj})$$

and we are done. The validation of the remaining parts of the identity requires the use of the symmetry relations

$$\Phi_{1,\sigma}\,(R^{-n}\vec{p},\,\sigma) = +\,\Phi_{1,\sigma}\,(R^{+n}\vec{p},\,\sigma) \tag{K.4.32}$$

$$\Phi_{2,\mu}\,(R^{m-}\vec{p},\mu) = -\,\Phi_{2,\mu}\,(R^{m+}\vec{p},\,\mu) \tag{K.4.33}$$

$$\Phi_{2,\sigma}\,(R^{m-}\vec{p},\sigma) = \;\;\Phi_{2,\sigma}\,(R^{m+}\vec{p},\,\sigma) \tag{K.4.34}$$

Just as we found in the case of one plane of symmetry, all of the relations we have found so far have counterpart relations for velocities. The first of these relations, the representation of $\vec{v}(\vec{p})$ in terms of singularity distributions $\bar{\sigma}^{ij}$, $\bar{\mu}^{ij}$, $\tilde{\tilde{\sigma}}_1{}^{Sj}$, $\tilde{\tilde{\mu}}_1{}^{Aj}$, $\tilde{\tilde{\sigma}}_2{}^{iS}$, $\tilde{\tilde{\mu}}_2{}^{iA}$ is given

$$\begin{aligned}\vec{v}(\vec{p}) = &\sum_{i,j} R^{ij}\,[\vec{V}_\sigma(R^{ij}\vec{p},\,\bar{\sigma}^{ij}) + \vec{V}_\mu(R^{ij}\vec{p},\,\bar{\mu}^{ij})] \\ &+ \sum_j \; R^{+j}\,[\vec{V}_{1,\sigma}\,(R^{+j}\vec{p},\,\tilde{\tilde{\sigma}}_1{}^{Sj}) + \vec{V}_{1,\mu}\,(R^{+j}\vec{p},\,\tilde{\tilde{\mu}}_1{}^{Aj})] \\ &+ \sum_i \; R^{i+}\,[\vec{V}_{2,\sigma}\,(R^{i+}p,\,\tilde{\tilde{\sigma}}_2{}^{iS}) + \vec{V}_{2,\mu}\,(R^{i+}\vec{p},\,\tilde{\tilde{\mu}}_2{}^{iA})]\end{aligned} \tag{K.4.35}$$

where operators $\vec{V}_\sigma$, $\vec{V}_\mu$ etc. are defined by

$$(\vec{V}_\sigma,\,\vec{V}_{1,\sigma},\,\vec{V}_{2,\sigma})\,(\vec{p},\sigma) = -(1/\kappa) \iint_{(S^{++},\,S_1^+,\,S_2^+)\,\cap\,D_p} \sigma(\vec{q})\;\;\nabla_p\,(1/R(\vec{p},\vec{q}))dS_q \tag{K.4.36}$$

$$(\vec{V}_\mu, \vec{V}_{1,\mu}\ \vec{V}_{2,\mu})(\vec{p},\mu) = (1/\kappa) \iint_{(S^{++},S_1^+,\ S_2^+)\ \cap\ D_p} (\hat{n}(\vec{q})dS_q \times \nabla\mu) \times \tilde{\nabla}_q\ (1/R(\vec{p},\vec{q})) \tag{K.4.37}$$

The symmetrized velocities, $\hat{v}^{ij}(\vec{p})$, defined by

$$\hat{v}^{ij}(\vec{p}) = \sum_{k,l} H^{ik}\ H^{jl}\ R^{kl}\ \vec{v}(R^{kl}\vec{p}) \tag{K.4.38}$$

satisfy the symmetry relations

$$\hat{v}^{ij}\ (R^{kl}\vec{p}) = H^{ik}\ H^{jl}\ R^{kl}\ \hat{v}\ (R^{kl}\vec{p}) \tag{K.4.39}$$

The representation formula for $\hat{v}^{ij}$ that corresponds to the representation (K.4.30) for $\hat{\phi}^{ij}$ is given by the formula

$$\begin{aligned}\hat{v}^{ij}(\vec{p}) = &\sum_{k,l} H^{ik}\ H^{jl}\ R^{kl}\ [\vec{V}_\sigma\ (R^{kl}\vec{p},\ \hat{\sigma}^{ij}) + \vec{V}_\mu\ (R^{kl}\vec{p},\ \hat{\mu}^{ij})] \\ &+ \sum_l H^{jl}\ R^{+l}\ [2\delta^{i+}\ \vec{V}_{1,\sigma}(R^{+l}\vec{p},\ \hat{\sigma}_1{}^{Sj}) + 2\delta^{i-}\ \vec{V}_{1,\mu}\ (R^{+l}\vec{p},\ \hat{\mu}_1{}^{Aj})] \\ &+ \sum_k H^{ik}\ R^{k+}\ [2\delta^{j+}\ \vec{V}_{2,\sigma}\ (R^{k+}\vec{p},\ \hat{\sigma}_1{}^{iS}) + 2\delta^{j-}\ \vec{V}_{2,\mu}\ (R^{k+}\vec{p},\ \hat{\mu}_2{}^{iA})]\end{aligned} \tag{K.4.40}$$

The proof of this representation formula is a fairly straightforward matter, given the symmetry formulae for $\vec{V}_{1,\sigma}$, $\vec{V}_{1,\mu}$, $\vec{V}_{2,\sigma}$, $\vec{V}_{2,\mu}$:

$$\vec{V}_{1,\sigma}\ (R_1\vec{p},\ \sigma) = R_1\ \vec{V}_{1,\sigma}\ (\vec{p},\sigma) \tag{K.4.41}$$

$$\vec{V}_{1,\mu}\ (R_1\vec{p},\mu) = -R_1\ \vec{V}_{1,\mu}\ (\vec{p},\mu) \tag{K.4.42}$$

$$\vec{V}_{2,\sigma}\ (R_2\vec{p},\sigma) = R_2\ \vec{V}_{2,\sigma}\ (\vec{p},\sigma) \tag{K.4.43}$$

$$\vec{V}_{2,\mu}\ (R_2\vec{p},\mu) = -R_2\ \vec{V}_{2,\mu}\ (\vec{p},\mu) \tag{K.4.44}$$

<u>Symmetrization for $\vec{p} \in S^{++}$</u>

Let $\vec{p} \in S^{++}$ be a control point not lying in any plane of symmetry. The four images of $\vec{p}$ are given by $R^{ij}\vec{p}$ and the boundary conditions at these points are required to have the form

$$\underline{bc^{kl}} \quad (a_A\, \hat{n}^T(\vec{p})B_o + \vec{t}_A^{\,T})\, R^{kl}\, (\vec{v}(R^{kl}\vec{p}))_A + c_A\, (\phi\, (R^{kl}\vec{p}))_A$$

$$+ \quad a_A\, \sigma^{kl}(R^{kl}\vec{p}) + c_D\, \mu^{kl}\, (R^{kl}\vec{p}) + \vec{t}_D^{\,T}\, R^{kl}\, \nabla_u\, \mu^{kl}\, (\vec{u})\Big|_{R^{kl}p} = b^{kl} \tag{K.4.45}$$

As before, the scalar coefficients are independent of image while the vector coefficients for the various images are related to the vector coefficients for the principal image by way of the reflection transformations R^{ij}. Multiplying equation (K.4.45) by $H^{ik}\, H^{jl}$ and summing over k and l, yields, after the appropriate simplifications are made,

$$\underline{bc^{ij}} \quad (a_A\, \hat{n}^T(p)B_o + \vec{t}_A^{\,T})\, (\hat{v}^{ij}(\vec{p}))_A + c_A\, (\hat{\phi}^{ij}(\vec{p}))_A$$

$$+ a_A\, \hat{\sigma}^{ij}(\vec{p}) + c_D\, \hat{\mu}^{ij}(\vec{p}) + t_D^{\,T}\, \nabla\hat{\mu}^{ij} = \sum_{k,l} H^{ik}\, H^{jl}\, b^{kl} \tag{K.4.46}$$

<u>Symmetrization for $\vec{p} \in S_1^{\,+}$, $\hat{n}(\vec{p})$ parallel to $\hat{n}_1$</u>

Just as we found in the case of one plane of symmetry, special degenerate boundary conditions must be imposed in order for the problem to be solvable. For a control point $\vec{p}$ lying in the first plane of symmetry, these conditions are

$$\hat{\sigma}_1^{\,AS} = \hat{\sigma}_1^{\,AA} = 0 \tag{K.4.47}$$

$$\hat{\mu}_1^{\,SS} = \hat{\mu}_1^{\,SA} = 0 \tag{K.4.48}$$

For a control point $\vec{p} \in S_1^{\,+}$, the boundary conditions at $\vec{p}$ and at its image point $R^{+-}\,\vec{p}$ can be written together as

$$\underline{bc_1^{\,1}} \quad (a_A\, n^T(\vec{p})B_0 + \vec{t}_A^{\,T})\, R^{+1}\, (\vec{v}(R^{+1}\vec{p}))_A + c_A\, (\phi(R^{+1}\vec{p}))_A$$

$$+ a_D\, \tilde{\sigma}_1^{\,S1}\, (R^{+1}\vec{p}) + c_D\, \tilde{\mu}_1^{\,A1}\, (R^{+1}\vec{p}) + \vec{t}_D^{\,T}\, R^{+1}\nabla\, \tilde{\mu}_1^{\,A1}\Big|_{R^{+1}\vec{p}} = b^1 \tag{K.4.49}$$

Because this equation represents only two boundary conditions it is not possible to fully symmetrize it. However, we can multiply by H^{jl} and sum over l to obtain a partial symmetrization. Using equations (K.4.26) and (K.4.27) to simplify the terms involving the singularity distributions, we obtain

$$(a_A\ \hat{n}^T(\vec{p})B_o + \vec{t}_A{}^T)\ (\sum_l H^{jl}\ R^{+l}\ \vec{v}\ (R^{+l}\vec{p}))_A$$

$$+\quad c_A\ (\sum_l H^{jl}\ \phi\ (R^{+l}\vec{p}))_A$$

$$+\ a_D\ \hat{\sigma}_1{}^{Sj} + c_D\ \hat{\mu}_1{}^{Aj} + \vec{t}_D{}^T \cdot \nabla\hat{\mu}_1{}^{Aj} = \sum_l H^{jl}\ b^l \qquad \text{(K.4.50)}$$

Now if we multiply (K.4.22) by H^{im} and sum over i, we obtain (note: $\sum_i H^{im}\ H^{ik} = 2\ \delta^{mk}$),

$$\sum_i H^{im}\ \hat{\phi}^{ij} = 2\ \sum_l H^{jl}\ \phi\ (R^{ml}\vec{p})$$

Setting m = +1, we obtain

$$\hat{\phi}^{Sj} + \hat{\phi}^{Aj} = 2\ \sum_l H^{jl}\ \phi\ (R^{+l}\vec{p}) \qquad \text{(K.4.51)}$$

In a similar fashion, multiplying (K.4.38) by H^{im} and summing over i, yields, for m = +1,

$$\hat{v}^{Sj} + \hat{v}^{Aj} = 2\ \sum_l H^{jl}\ R^{+l}\ \vec{v}\ (R^{+l}\vec{p}) \qquad \text{(K.4.52)}$$

Thus, we obtain for the partially symmetrized boundary condition

$$(a_A\ \hat{n}^T(\vec{p})\ B_o + \vec{t}_A{}^T)\ \tfrac{1}{2}\ (\hat{v}^{Sj}(\vec{p}) + \hat{v}^{Aj}(\vec{p}))_A + c_A\ (\tfrac{1}{2})\ (\hat{\phi}^{Sj}(\vec{p}) + \hat{\phi}^{Aj}(\vec{p}))_A$$

$$+\ a_A\ \hat{\sigma}_1{}^{Sj} + c_A\ \hat{\mu}_1{}^{Aj} + \vec{t}_D\ \nabla\hat{\mu}_1{}^{Aj} = \sum_l H^{jl}\ b^l. \qquad \text{(K.4.53)}$$

The symmetry properties of $\hat{\phi}^{ij}$ and $\hat{v}^{ij}$ provide the following simplifications (compare with (K.3.58), (K.3.59), (K.3.60)):

$$(\hat{\phi}^{Aj}(\vec{p}))_A = 0 \qquad \text{(K.4.54)}$$

$$(\vec{t}_A{}^T\ \hat{v}^{Aj}(\vec{p}))_A = 0 \qquad \text{(K.4.55)}$$

$$(\hat{n}^T\ B_o\ \hat{v}^{Sj}(\vec{p}))_A = 0 \qquad \text{(K.4.56)}$$

Thus we obtain finally

$$\frac{1}{2} a_A \hat{n}^T B_o (\hat{v}^{Aj}(\vec{p}))_A + c_D \hat{\mu}_1^{Aj}(\vec{p}) + \vec{t}_D^{\,T} \nabla \hat{\mu}_1^{Aj}$$

$$+ \frac{1}{2} t_A^T (\hat{v}^{Sj}(p))_A + \frac{1}{2} c_A (\hat{\phi}^{Sj}(\vec{p}))_A + a_D \hat{\sigma}^{Sj}(\vec{p}) = \sum_l H^{jl} b^l \tag{K.4.57}$$

Here again, we find it necessary to insist that a boundary condition be either purely symmetric, on a source network, or purely antisymmetric, on a doublet network. Thus, given a purely symmetric boundary condition, the constraints that should be imposed on the various $\hat{\phi}^{ij}$'s are given:

<u>Symmetric boundary conditions in first plane of symmetry</u>

SS and SA: $$\frac{1}{2} \vec{t}_A^{\,T} (\hat{v}^{Sj}(\vec{p}))_A + \frac{1}{2} c_A (\hat{\phi}^{Sj}(\vec{p}))_A + a_D \hat{\sigma}_1^{Sj}(\vec{p}) = \sum_l H^{jl} b^l \tag{K.4.58}$$

AS and AA: $$\hat{\sigma}_1^{Aj} = 0 \tag{K.4.59}$$

For a purely antisymmetric boundary condition, the constraints have the form:

<u>Antisymmetric boundary conditions in first plane of symmetry</u>

AS and AA: $$a_A \frac{1}{2} \hat{n}^T B_o (\hat{v}^{Aj}(\vec{p}))_A + c_D \hat{\mu}_1^{Aj}(\vec{p}) + \vec{t}_D^{\,T} \nabla \hat{\mu}_1^{Aj} = \sum_l H^{jl} b^l \tag{K.4.60}$$

SS and SA: $$\hat{\mu}_1^{Sj} = 0 \tag{K.4.61}$$

K.5 Evaluation of ΦIC's and VIC's when Symmetry is Present

We now consider the evaluation of potential and velocity influence coefficients when symmetry is present. Our goal is to provide representations of the form

$$\hat{\phi}^{ij}(\vec{p}) = \sum_{I=1}^{N} \Phi IC_I^{ij} \; \hat{\lambda}_I^{ij} = \llcorner \Phi IC^{ij} \lrcorner \; \{\hat{\lambda}^{ij}\} \tag{K.5.1}$$

$$\hat{v}^{ij}(\vec{p}) = \sum_{I=1}^{N} \overrightarrow{VIC}_I^{ij} \; \hat{\lambda}_I^{ij} = [VIC^{ij}] \; \{\hat{\lambda}^{ij}\} \tag{K.5.2}$$

for the various symmetric parts of ϕ and v, where $\hat{\lambda}^{ij}$ denotes the vector of singularity parameters associated with the (i,j) symmetry condition. An additional goal will be to provide procedures for the evaluation of ΦIC's and VIC's that involve a minimum amount of special case logic. Toward this latter goal, we initiate our investigations by developing somewhat more symmetric formulae for the quantities $\hat{\phi}^i$, $\hat{v}^i$, ϕ^{ij} and $\hat{v}^{ij}$ than the formulae (K.3.28), (K.3.46) (K.4.30), (K.4.40).

K.5.1 One Plane of Symmetry

It turns out that when the problem has one plane of symmetry, $\hat{\phi}^i$ and $\hat{v}^i$ as given by (K.3.28) and (K.3.46) can also be expressed by the somewhat more symmetrical formulae

$$\begin{aligned}\hat{\phi}^i(\vec{p}) = &\sum_j [H^{ij} \; \Phi_\sigma (R^j\vec{p}, \hat{\sigma}^i) + H^{ij} \; \Phi_\mu (R^j\vec{p}, \hat{\mu}^i)] \\ &+ \sum_j [H^{ij} \; \Phi_{1,\sigma} (R^j\vec{p}, \hat{\sigma}_1{}^i) + H^{ij} \; \Phi_{1,\mu} (R^j\vec{p}, \hat{\mu}_1{}^i)]\end{aligned} \tag{K.5.3}$$

$$\begin{aligned}\hat{v}^i(\vec{p}) = &\sum_j H^{ij} \, R^j \, [\vec{V}_\sigma (R^j\vec{p}, \hat{\sigma}^i) + V_\mu (R^j p, \hat{\mu}^i)] \\ &+ \sum_j H^{ij} \, R^j \, [\vec{V}_{1,\sigma} (R^j\vec{p}, \hat{\sigma}_1{}^i) + \vec{V}_{1,\mu} (R^j\vec{p}, \hat{\mu}_1{}^i)]\end{aligned} \tag{K.5.4}$$

The proof of these formulae is fairly straightforward once one notices that the degenerate boundary conditions (K.3.53) and (K.3.54) which state that $\hat{\mu}_1^S = \hat{\sigma}_1^A = 0$ imply that

$$\delta^{i+} \; \hat{\sigma}_1{}^S = \hat{\sigma}_1{}^i \tag{K.5.5}$$

$$\delta^{i-} \; \hat{\mu}_1{}^A = \hat{\mu}_1{}^i \tag{K.5.6}$$

Consequently we find (working backward) that

$$\text{(i)} \quad \sum_j H^{ij} \; \Phi_{1,\sigma}(R^j\vec{p}, \hat{\sigma}_1^i) = \sum_j H^{ij} \; \Phi_{1,\sigma}(R^j\vec{p}, \delta^{i+} \hat{\sigma}_1^S)$$

$$= \delta^{i+} [2 \; \Phi_{1,\sigma} (\vec{p}, \hat{\sigma}_1{}^S)] \qquad \text{(K.5.7)}$$

(using equation (K.3.31))

$$\text{(ii)} \quad \sum_j H^{ij} \; \Phi_{1,\mu} (R^j\vec{p}, \hat{\mu}_1{}^i) = \sum_j H^{ij} \; \Phi_{1,\mu} (R^j\vec{p}, \delta^{i-} \hat{\mu}_1{}^A)$$

$$= \delta^{i-} [2 \; \Phi_{1,\mu} (\vec{p}, \hat{\mu}_1{}^A)] \qquad \text{(K.5.8)}$$

(using equation (K.3.32))

$$\text{(iii)} \quad \sum_j H^{ij} R^j \vec{V}_{1,\sigma} (R^j\vec{p}, \hat{\sigma}_1{}^i) = \delta^{i+} \sum_j H^{ij} R^j \vec{V}_{1,\sigma} (R^j\vec{p}, \hat{\sigma}_1{}^S)]$$

$$= \delta^{i+} [\vec{V}_{1,\sigma} (\vec{p}, \hat{\sigma}_1{}^S) + R_1 \vec{V}_{1,\sigma} (R_1\vec{p},\hat{\sigma}_1{}^S)]$$

$$= \delta^{i+} (2) V_{1,\sigma} (\vec{p},\hat{\sigma}_1{}^S) \qquad \text{(K.5.9)}$$

(using equation (K.3.47))

$$\text{(iv)} \quad \sum_j H^{ij} R^j \vec{V}_{1,\mu} (R^j\vec{p},\hat{\mu}_1{}^i) = \delta^{i-} \sum_j H^{ij} R^j \vec{V}_{1,\mu} (R^j \vec{p},\hat{\mu}_1{}^A)$$

$$= \delta^{i-} [\vec{V}_{1,\mu} (\vec{p},\hat{\mu}_1{}^A) - R_1 \vec{V}_{1,\mu} (R_1\vec{p}, \hat{\mu}_1{}^A)]$$

$$= \delta^{i-} (2) V_{1,\mu}(\vec{p}, \hat{\mu}_1{}^A) \qquad \text{(K.5.10)}$$

(using equation (K.3.48))

Recall that from their definitions, $\hat{\sigma}^i$ and $\hat{\mu}^i$ are defined only for $\vec{p} \in S^+$. If we now choose to extend their definition to points $\vec{p} \in S_1$ by the obvious specifications

$$\hat{\sigma}^i \Big|_{S_1} = \hat{\sigma}_1{}^i \qquad \text{(K.5.11)}$$

$$\hat{\mu}^i \Big|_{S_1} = \hat{\mu}_1{}^i \tag{K.5.12}$$

and then define operators $\Phi_\sigma{}^*$, $\Phi_\mu{}^*$, $\vec{V}_\sigma{}^*$, $\vec{V}_\mu{}^*$ by

$$\Phi_\sigma{}^* (\vec{p},\sigma) = \Phi_\sigma(\vec{p},\sigma) + \Phi_{1,\sigma}(\vec{p},\sigma) \tag{K.5.13}$$

$$\Phi_\mu{}^* (\vec{p},\mu) = \Phi_\mu(\vec{p},\mu) + \Phi_{1,\mu}(\vec{p},\mu) \tag{K.5.14}$$

$$\vec{V}_\sigma{}^*(\vec{p},\sigma) = \vec{V}_\sigma(\vec{p},\sigma) + \vec{V}_{1,\sigma}(\vec{p},\sigma) \tag{K.5.15}$$

$$\vec{V}_\mu{}^* (\vec{p},\mu) = \vec{V}_\mu (\vec{p},\mu) + \vec{V}_{1,\mu} (\vec{p},\mu) \tag{K.5.16}$$

then we are simply left with the compact formulae

$$\hat{\phi}^i(\vec{p}) = \sum_j H^{ij} [\Phi_\sigma{}^* (R^j\vec{p}, \sigma^i) + \Phi_\mu{}^* (R^j\vec{p}, \hat{\mu}^i)] \tag{K.5.17}$$

$$\hat{v}^i(\vec{p}) = \sum_j H^{ij} R^j [\vec{V}_\sigma{}^* (R^j\vec{p}, \hat{\sigma}^i) + \vec{V}_\mu{}^* (R^j\vec{p},\hat{\mu}^i)] \tag{K.5.18}$$

We can now describe the computation of potential and velocity influence coefficients. Recalling the representations (K.1.2) and (K.1.3) for σ and μ in the absence of symmetry, we observe that $\hat{\sigma}^i$ and $\hat{\mu}^i$ have the representation in terms of spline basis functions and singularity parameters,

$$\hat{\sigma}^i (\vec{q}) = \sum_{I=1}^{N} s_I (\vec{q}) \hat{\lambda}_I{}^i \tag{K.5.19}$$

$$\hat{\mu}^i (\vec{q}) = \sum_{I=1}^{N} m_I(\vec{q}) \hat{\lambda}_I{}^i \tag{K.5.20}$$

Upon substituting these representations into the formulae for $\hat{\phi}^i$ and $\hat{v}^i$ we obtain

$$\hat{\phi}^i(\vec{p}) = \sum_{I=1}^{N} \Phi IC_I{}^i \hat{\lambda}_I{}^i = \llcorner \Phi IC^i \lrcorner \{\hat{\lambda}^i\} \tag{K.5.21}$$

$$\hat{v}^i(\vec{p}) = \sum_{I=1}^{N} \overrightarrow{VIC}_I{}^i \hat{\lambda}_I{}^i = [VIC^i] \{\hat{\lambda}^i\} \tag{K.5.22}$$

where

$$\Phi IC_I^{\,i} = \sum_j H^{ij} \left[\Phi_\sigma^{\,*} (R^j\vec{p}, s_I) + \Phi_\mu^{\,*} (R^j\vec{p}, m_I)\right] \qquad (K.5.23)$$

$$\overrightarrow{VIC}_I^{\,i} = \sum_j H^{ij} R^j \left[\vec{V}_\sigma^{\,*} (R^j\vec{p}, s_I) + \vec{V}_\mu^{\,*} (R^j\vec{p}, m_I)\right] \qquad (K.5.24)$$

Having derived these formulae for potential and velocity influence coefficients, we are still not finished. Rather, we must investigate in some detail the correct interpretation of these expressions when the evaluation point $\vec{p}$ lies on S^+ or S_1. The case of $\vec{p} \in S_1$ is especially difficult because of the fact that a network that is recognized as lying in a plane of symmetry may in fact lie some small distance away. The proper interpretation of the formula (K.5.23) and (K.5.24) which we now describe will consist of specific instructions for the evaluation of the integrals that arise.

First we treat the case in which $\vec{p}$ lies in S^+, away from the plane of symmetry. If we write the integral operator Φ_σ^* as a sum of integrals over the constituent panels Q of S_1 and S^+, then we have

$$\Phi_\sigma^{\,*} (\vec{p},s) = \sum_{Q \in S_1 \cup S^+} \Phi_\sigma^{\,Q} (\vec{p},s) , \qquad (K.5.25)$$

where $\Phi_\sigma^{\,Q}$ has the obvious definition

$$\Phi_\sigma^{\,Q} (\vec{p},s) = -(1/\kappa) \iint_{Q \cap D_p} s(\vec{q}) \quad 1/R(\vec{p},\vec{q})\, dS_q \qquad (K.5.26)$$

Clearly, the integral operators $\Phi_\mu^{\,*}$, $\vec{V}_\sigma^{\,*}$, and $\vec{V}_\mu^{\,*}$ have precisely analogous decompositions involving panel integral operators $\Phi_\mu^{\,Q}$, $\vec{V}_\sigma^{\,Q}$ and $\vec{V}_\mu^{\,Q}$. Given these decompositions, the interpretation of the influence coefficient expressions is now summarized.

<u>Algorithm A^+: Evaluation of $\Phi_\sigma^{\,Q} (R^j\vec{p}, s)$, etc., when $\vec{p} \in S^+$</u>

$j = +1$, $R^+ = I$: $\Phi_\sigma^{\,Q} (\vec{p},s)$

<u>$\vec{p} \in Q$</u>

Use the average value of $\Phi_\sigma^{\,Q}(\vec{p},s)$ for points $\vec{p}$ above and below Q.

<u>$\vec{p} \notin Q$</u>

Proceed naively: $\Phi_\sigma^{\,Q} (\vec{r},s)$ is regular (has no jumps) for $\vec{r}$ in a neighborhood of $\vec{p}$. (By "proceeding naively," we mean that no special care is required to evaluate the PIC's in order to avoid ambiguities associated with jumps in the PIC integrals across the singularity surface.)

$j = -1,\ R^- = R_1 :\quad \Phi_\sigma^Q\ (R_1\vec{p},\ s)$

Proceed naively: $\Phi_\sigma^Q\ (\vec{r},s)$ is regular (has no jumps) for $\vec{r}$ in a neighborhood of $R_1\vec{p}$. Thus we evaluate $\Phi_\sigma^Q\ (R_1\vec{p},s)$

Thus, when $\vec{p} \in S^+$, the only special care required is that average value integrals (above and below the panel Q) be used whenever the control point $\vec{p}$ lies directly on Q. This is done because the general form of a boundary condition, (K.1.1), specifically imposes a condition on the average values of potential, velocity and mass flux, ϕ_A, $\vec{v}_A$ and $\vec{w}_A$. With this interpretation of what is to be done with integrals over the panel in which $\vec{p}$ lies, equations (K.5.23) and (K.5.24) provide a precisely accurate description of the actual IC computations performed by PAN AIR for the case $\vec{p} \in S^+$.

The case in which $\vec{p}$ lies in S_1, that portion of the configuration on the plane of symmetry, is somewhat more difficult. The rules we actually use for the evaluation of influence coefficients are motivated by two requirements:

(i) The evaluation procedure must be consistent with the program control structures implicit in a "naive" interpretation of equations (K.5.23) and (K.5.24)

(ii) The evaluation should yield influence coefficients that possess the basic symmetry properties for $\vec{p} \in S_1$

a) $\hat{\phi}^A\ (\vec{p}) = 0$

b) $(I - \hat{n}_1\hat{n}_1^T)\hat{v}^A(\vec{p}) = 0$ (K.5.27)

c) $\hat{n}_1 \cdot \hat{v}^S\ (\vec{p}) = 0$

(compare these with equations (K.3.58), (K.3.59), (K.3.60))

The actual rules for the interpretation of (K.5.23) and (K.5.24) are now given in terms of instructions for the evaluation of Φ_σ^Q.

Algorithm A_1: Evaluation of $\Phi_\sigma^Q\ (R^j\vec{p},\ s)$ etc., when $\vec{p} \in S_1$

$j = +1,\ R^+ = I:\ \Phi_\sigma^Q\ (\vec{p},s)$

$\vec{p} \in Q$

Use the average value of $\Phi_\sigma^Q(\vec{p},s)$ for points $\vec{p}$ above and below Q.

$\vec{p} \notin Q$

Proceed naively

$j = -1,\ R^- = R_1$: $\Phi_\sigma^Q\ (R_1\vec{p},s)$

$\vec{p} \in Q$

Use the average value of $\Phi_\sigma^Q\ (\vec{p},s)$ for points $\vec{p}$ above and below Q. Note that we use $\vec{p}$ and not $R_1\ \vec{p}$.

$\vec{p} \notin Q$

Use $\Phi_\sigma^Q(\vec{p},s)$

Thus, we proceed much the same as we proceded before except that the control point $\vec{p}$ is never actually reflected in the plane of symmetry, even if it does not lie exactly on the plane of symmetry. It is also important to note that the same influence coefficients are generated for j = +1 and j = -1. Consequently we find that when $\vec{p} \in S_1$

$$\Phi IC_I^S = \sum_j H^{+j}\ [\ \Phi_\sigma^*(\vec{p},s_I) + \Phi_\mu^*(\vec{p},m_I)\ ]$$

$$= 2\ [\ \Phi_\sigma^*\ (\vec{p},s_I) + \Phi_\mu^*\ (\vec{p},m_I)\ ] \qquad \text{(K.5.28)}$$

$$\Phi IC_I^A = 0 \qquad \text{(K.5.29)}$$

$$\overrightarrow{VIC}_I^S = (I + R_1)\ [\vec{V}_\sigma^*(\vec{p},s_I) + \vec{V}_\mu^*\ (\vec{p},m_I)]$$

$$= 2\ (I - \hat{n}_1\hat{n}_1^T)\ [\vec{V}_\sigma^*(\vec{p},s_I) + \vec{V}_\mu^*\ (\vec{p},m_I)] \qquad \text{(K.5.30)}$$

$$\overrightarrow{VIC}_I^A = 2\ \hat{n}_1\hat{n}_1^T\ [\vec{V}_\sigma^*\ (\vec{p},s_I) + \vec{V}_\mu^*\ (\vec{p},m_I)] \qquad \text{(K.5.31)}$$

These results verify that the influence coefficients exhibit the basic symmetry properties of equation (K.5.27).

It is interesting to compare the formulae (K.5.28) through (K.5.31) with what one would obtain from a straightforward application of equations (K.3.28) and (K.3.46). This comparison is summarized in figure K.5. The differences between the two methods are of three types: (i) some extra integrals over S_1 appear in the expansions of equations (K.5.28) - (K.5.31), (ii) some of the integrals over S^+ are different (e.g., $\Phi_\sigma\ (\vec{p},s_I)$ replaces $\Phi_\sigma(R_1\vec{p},\ s_I)$ and (iii) there are some very definite differences in form for the remaining integrals over S_1.

The first type of differences are of no consequence in view of the restrictions on $\hat{\lambda}_I^i$ implied by the degenerate boundary conditions, $\hat{\sigma}_1^A = 0$, $\hat{\mu}_1^S = 0$. These restrictions read:

$$s_I\Big|_{S_1} \neq 0 \quad \longrightarrow \quad \hat{\lambda}_I^A = 0 \qquad (\hat{\sigma}_1^A = 0) \tag{K.5.32}$$

$$m_I\Big|_{S_1} \neq 0 \quad \longrightarrow \quad \hat{\lambda}_I^S = 0 \qquad (\hat{\mu}_1^S = 0) \tag{K.5.33}$$

The terms appearing in figure (K.5) which can be neglected because of these considerations have been lightly crossed out with an arrow ($\longrightarrow$).

The differences of the second type have the forms

$$\Phi_\sigma(\vec{p},s_I) - \Phi_\sigma(R_1\vec{p},s_I)$$

$$\Phi_\mu(\vec{p},m_I) - \Phi_\mu(R_1\vec{p},m_I)$$

$$R_1[\vec{V}_\sigma(\vec{p},s_I) - \vec{V}_\sigma(R_1\vec{p},s_I)]$$

$$R_1[\vec{V}_\mu(\vec{p},m_I) - \vec{V}_\mu(R_1\vec{p},m_I)]$$

These differences will all be negligible by virtue of the fact that $\Phi_\sigma(\vec{p},s_I)$, $\Phi_\mu(\vec{p},m_I)$, etc. are continuous function of $\vec{p}$ for $\vec{p}$ in the neighborhood of the plane of symmetry. This continuity, coupled with the bound

$$|\vec{p} - R_1\vec{p}| \leq 2 \text{ (geometric tolerance distance)}$$

ensures that all the differences of the second type are small.

The third type of differences have the forms

$$-2\,\hat{n}_1\hat{n}_1^T\,\vec{V}_{1,\sigma}(\vec{p},s_I)$$

$$-2\,(I - \hat{n}_1\hat{n}_1^T)\,\vec{V}_{1,\mu}(\vec{p},m_I)$$

These differences will be identically zero provided both S_1 and $\vec{p}$ lie exactly on the plane of symmetry. If S_1 deviates slightly from the plane of symmetry, these differences will still be small provided $\vec{p}$ lies on S_1 and average value integrals are systematically used.

Thus the method of calculating IC's described in this section can be expected to yield very similar results to the method of section K.3. We choose to use the algorithm A_1 because it permits much simpler program structure and at the same time it enforces the symmetry conditions (K.5.27).

K.5.2 Two planes of Symmetry

In this section, we devise influence coefficient evaluation procedures for the case of two planes of symmetry. We begin this task by transforming equations (K.4.30) and (K.4.40) for $\hat{\phi}^{ij}$, $\hat{v}^{ij}$ into the following symmetrical forms:

$$\hat{\phi}^{ij} = \sum_{k,l} H^{ik} H^{jl} [\Phi_\sigma(R^{kl}\vec{p}, \hat{\sigma}^{ij}) + \Phi_\mu(R^{kl}\vec{p}, \hat{\mu}^{ij})$$

$$+ \Phi_{1,\sigma}(R^{kl}\vec{p}, \hat{\sigma}_1{}^{ij}) + \Phi_{1,\mu}(R^{kl}\vec{p}, \hat{\mu}_1{}^{ij})$$

$$+ \Phi_{2,\sigma}(R^{kl}\vec{p}, \hat{\sigma}_2{}^{ij}) + \Phi_{2,\mu}(R^{kl}\vec{p}, \hat{\mu}_2{}^{ij})] \tag{K.5.34}$$

$$\hat{v}^{ij} = \sum_{k,l} H^{ik} H^{jl} R^{kl} [\vec{V}_\sigma(R^{kl}\vec{p}, \hat{\sigma}^{ij}) + \vec{V}_\mu(R^{kl}\vec{p}, \hat{\mu}^{ij})$$

$$+ \vec{V}_{1,\sigma}(R^{kl}\vec{p}, \hat{\sigma}_1{}^{ij}) + \vec{V}_{1,\mu}(R^{kl}\vec{p}, \hat{\mu}_1{}^{ij})$$

$$+ \vec{V}_{2,\sigma}(R^{kl}\vec{p}, \hat{\sigma}_2{}^{ij}) + \vec{V}_{2,\mu}(R^{kl}\vec{p}, \hat{\mu}_2{}^{ij})] \tag{K.5.35}$$

The proof of equation (K.5.34) depends upon identities of the form

$$\sum_{k,l} H^{ik} H^{jl} \Phi_{1,\sigma}(R^{kl}\vec{p}, \hat{\sigma}_1{}^{ij}) = 2\,\delta^{i+} \sum_{l} H^{jl} \Phi_{1,\sigma}(R^{+l}\vec{p}, \hat{\sigma}_1{}^{Sj})$$

$$\sum_{k,l} H^{ik} H^{jl} \Phi_{1,\mu}(R^{kl}\vec{p}, \hat{\mu}_1{}^{ij}) = 2\,\delta^{i-} \sum_{l} H^{jl} \Phi_{1,\mu}(R^{+l}\vec{p}, \hat{\mu}_1{}^{Aj}) \tag{K.5.37}$$

which follow easily from the observations

$$\hat{\sigma}_1{}^{ij} = \delta^{i+} \hat{\sigma}_1{}^{Sj}; \quad \hat{\mu}_1{}^{ij} = \delta^{i-} \hat{\mu}_1{}^{Aj}$$

$$\hat{\sigma}_2{}^{ij} = \delta^{j+} \hat{\sigma}_2{}^{iS}; \quad \hat{\mu}_2{}^{ij} = \delta^{j-} \hat{\mu}_2{}^{iA} \tag{K.5.37}$$

together with symmetry relations

$$\Phi_{1,\sigma}(R^{-1}\vec{p},\sigma) = \Phi_{1,\sigma}(R^{+1}\vec{p},\sigma)$$

$$\Phi_{1,\mu}(R^{-1}\vec{p},\mu) = -\Phi_{1,\mu}(R^{+1}\vec{p},\mu)$$

$$\Phi_{2,\sigma}(R^{k-}\vec{p},\sigma) = \Phi_{2,\sigma}(R^{k+}\vec{p},\sigma)$$

$$\Phi_{2,\mu}(R^{k-}\vec{p},\mu) = -\Phi_{2,\mu}(R^{k+}\vec{p},\mu)$$

Equation (K.5.35) is proved in very much the same way as the formula (K.5.4) for $\hat{v}^i$, using the relations (K.5.37) together with the symmetry relations (K.4.41) - (K.4.44) for the operators $\vec{V}_{\alpha,\sigma}$, $\vec{V}_{\alpha,\mu}$

Our expressions for $\hat{\phi}^{ij}$, $\hat{v}^{ij}$ can be compressed even further if we extend the definitions of $\hat{\sigma}^{ij}$ and $\hat{\mu}^{ij}$ in the obvious sort of way:

$$\hat{\sigma}^{ij}\Big|_{S_\alpha} = \hat{\sigma}_\alpha^{ij} \qquad \hat{\mu}^{ij}\Big|_{S_\alpha} = \hat{\mu}_\alpha^{ij} \tag{K.5.38}$$

If we then define Φ_σ^*, Φ_μ^* etc by

$$\Phi_\sigma^* = \Phi_\sigma + \Phi_{1,\sigma} + \Phi_{2,\sigma}$$

$$\Phi_\mu^* = \Phi_\mu + \Phi_{1,\mu} + \Phi_{2,\mu}$$

$$\vec{V}_\sigma^* = \vec{V}_\sigma + \vec{V}_{1,\sigma} + \vec{V}_{2,\sigma}$$

$$\vec{V}_\mu^* = \vec{V}_\mu + \vec{V}_{1,\mu} + \vec{V}_{2,\mu}$$

we obtain finally

$$\hat{\phi}^{ij} = \sum_{k,l} H^{ik} H^{jl} [\Phi_\sigma^*(R^{kl}\vec{p}, \hat{\sigma}^{ij}) + \Phi_\mu^*(R^{kl}\vec{p}, \hat{\mu}^{ij})] \tag{K.5.39}$$

$$\hat{v}^{ij} = \sum_{k,l} H^{ik} H^{jl} R^{kl} [\vec{V}_\sigma^*(R^{kl}\vec{p}, \hat{\sigma}^{ij}) + \vec{V}_\mu^*(R^{kl}\vec{p}, \hat{\mu}^{ij})] \tag{K.5.40}$$

As before, much care must be exercised in the evaluation of these expressions. Three separate cases must be treated: (i) $\vec{p} \in S^{++}$, (ii) $\vec{p} \in S_1^{+}$ and (iii) $\vec{p} \in S_2^{+}$.

The first case, $\vec{p} \in S^{++}$, in which $\vec{p}$ lies away from either plane of symmetry is fairly straightforward. The only special care that must be taken is in the evaluation of panel integrals of the form $\Phi_\sigma^Q(R^{kl}\vec{p},\sigma)$, $\Phi_\mu^Q(R^{kl}\vec{p},\mu)$, etc., when $\vec{p} \in Q$ and $k = l = +1$. (We are using here the natural decomposition of Φ_σ^* into panel integrals, viz., $\Phi_\sigma^* = \sum_{Q \in S^{++} \cup S_1^+ \cup S_2^+} \Phi_\sigma^Q$.) For this particular case, care must be taken that the <u>average</u> value of the panel integrals Φ_σ^Q, Φ_μ^Q, $\vec{V}_\sigma^Q$ and $\vec{V}_\mu^Q$ be computed.

The second case, $\vec{p} \in S_1^+$, in which $\vec{p}$ lies on the first plane of symmetry is handled essentially the same as the case of one plane of symmetry. Our description of it, however will be somewhat different. First, observe that if S_1 truly lies on the first plane of symmetry and $\vec{p} \in S_1$, then $R^{kl}\vec{p} = R^{+l}\vec{p}$. Using this relation in (K.5.39) and (K.5.40) we find,

$(\vec{p} \in S_1^{+})$

$$\hat{\phi}^{ij}(\vec{p}) = \sum_{k,l} H^{ik} H^{jl} [\Phi_\sigma^*(R^{+l}\vec{p}, \hat{\sigma}^{ij}) + \Phi_\mu^*(R^{+l}\vec{p}, \hat{\mu}^{ij})] \tag{K.5.41}$$

$$\hat{v}^{ij}(\vec{p}) = \sum_{k,l} H^{ik} H^{jl} R^{kl} [\vec{V}_\sigma^*(R^{+l}\vec{p}, \hat{\sigma}^{ij}) + \vec{V}_\mu^*(R^{+l}\vec{p}, \hat{\mu}^{ij})] \tag{K.5.42}$$

Here again the evaluation of $\Phi_\sigma^Q(R^{+l}\vec{p}, \sigma)$, $\Phi_\mu^Q(R^{+l}\vec{p}, \mu)$, etc., must be handled carefully when $\vec{p} \in Q$ and $l = +1$. Thus when $\vec{p} \in Q \subset S_1$, average value integrals must be used for both the principal image condition ($k = +1$, $l = +1$) and its reflection in the first plane of symmetry ($k = -1$, $l = +1$). When equations (K.5.41) and (K.5.42) are used in this way to generate IC's when $\vec{p} \in S_1$, the following important symmetry properties are preserved even if S_1 does not lie precisely on the first plane of symmetry:

a) $\hat{\phi}^{Aj}(\vec{p}) = 0$

b) $(I - \hat{n}_1\hat{n}_1^T)\,\hat{v}^{Aj}(\vec{p}) = 0 \qquad \vec{p} \in S_1$

c) $\hat{n}_1^T\,\hat{v}^{Sj}(\vec{p}) = 0 \qquad$ (K.5.43)

The third case, $\vec{p} \in S_2^+$, in which $\vec{p}$ lies on the second plane of symmetry is virtually identical to the second case. The point $\vec{p}$ satisfies the relation $R^{kl}\,\vec{p} = R^{k+}\,\vec{p}$ and the expressions for $\hat{\phi}^{ij}$ and $\hat{v}^{ij}$ read

$(\vec{p} \in S_2^+)$

$$\hat{\phi}^{ij}(\vec{p}) = \sum_{k,l} H^{ik} H^{jl} \left[\Phi_\sigma^* (R^{k+}\vec{p}, \hat{\sigma}^{ij}) + \Phi_\mu^* (R^{k+}\vec{p}, \hat{\mu}^{ij}) \right] \qquad (K.5.44)$$

$$\hat{v}^{ij}(\vec{p}) = \sum_{k,l} H^{ik} H^{jl} R^{kl} \left[\vec{V}_\sigma^* (R^{k+}\vec{p}, \hat{\sigma}^{ij}) + \vec{V}_\mu^* (R^{k+}\vec{p}, \hat{\mu}^{ij}) \right] \qquad (K.5.45)$$

Summarizing our treatment of the case of two planes of symmetry, we observe that influence coefficients are computed as follows:

Case $\vec{p} \in S^{++}$: Use (K.5.39), (K.5.40),

Case $\vec{p} \in S_1^+$: Use (K.5.41), (K.5.42),

Case $\vec{p} \in S_2^+$: Use (K.5.44), (K.5.45).

K.6 Generation of AIC's when Symmetry is Present

In this section we discuss the construction of rows of the AIC matrix when symmetry is present. Given the influence coefficients whose computation was described in the previous section, the construction of AIC's in the presence of symmetry is very much the same as in the absence of symmetry. The only essential difference occurs when a control $\vec{p}$ lies in a plane of symmetry. When this happens, the contributions of the <u>integral influence coefficients</u> (e.g. ΦIC_I^i, VIC_I^i) to an AIC row must be multiplied by (1/2) before the corresponding contributions are included in an AIC row. This factor of (1/2) appears clearly in equation (K.3.61), the general form of a boundary condition on a plane of symmetry. As we noted when equation (K.3.61) was first derived, these anomalous factors of (1/2) appear because the symmetric and antisymmetric parts of ϕ are defined by

$$\hat{\phi}^i = \sum_j H^{ij} \phi (R^j \vec{p})$$

rather than

$$\hat{\phi}^i = \frac{1}{2} \sum_j H^{ij} \phi (R^j \vec{p})$$

Of course if one were to change the technique of symmetrization to this second form, one would have to investigate very carefully its impact on the form of matching conditions at a plane of symmetry as well as the interpretation of singularity distributions on the plane of symmetry.

The actual discussion of AIC construction will consist of four parts. These include -

- General Boundary Conditions
- Matching Boundary Conditions
- Closure Boundary Conditions
- Degenerate Boundary Conditions

In the discussions that follow, we will freely use the symbols ΦIC_I, VIC_I, ΦIC_I^i, VIC_I^i, etc., to refer to the potential and velocity influence coefficients associated with a particular basis function, s_I or m_I.* Formulae for these influence coefficients are summarized on the following page. These expressions reflect all of the special precautions required to ensure that the various symmetrized potentials and velocities have the correct properties when evaluated on the plane of symmetry.

* For any given singularity parameter λ_I, only one of the functions s_I, m_I will be not identically zero.

Summary of IC formulae

No plane of symmetry

$$\Phi IC_I = \Phi_\sigma(\vec{p},s_I) + \Phi_\mu(\vec{p},m_I)$$

$$\overrightarrow{VIC}_I = \vec{V}_\sigma(\vec{p},s_I) + \vec{V}_\mu(\vec{p},m_I)$$

1 plane of symmetry

$\vec{p} \in S^+$

$$\Phi IC_I^i = \sum_k H^{ik}\,[\Phi_\sigma^*(R^k\vec{p},s_I) + \Phi_\mu^*(R^k\vec{p},m_I)]$$

$$\overrightarrow{VIC}_I^i = \sum_k H^{ik}\,R^k\,[\vec{V}_\sigma^*(R^k\vec{p},s_I) + \vec{V}_\mu^*(R^k\vec{p},m_I)]$$

$\vec{p} \in S_1$

$$\Phi IC_I^i = \sum_k H^{ik}\,[\Phi_\sigma^*(\vec{p},s_I) + \Phi_\mu^*(\vec{p},m_I)]$$

$$\overrightarrow{VIC}_I^i = \sum_k H^{ik}\,R^k\,[\vec{V}_\sigma^*(\vec{p},s_I) + V_\mu^*(\vec{p},m_I)]$$

2 Planes of Symmetry

$\vec{p} \in S^{++}$

$$\Phi IC_I^{ij} = \sum_{k,l} H^{ik}\,H^{jl}\,[\Phi_\sigma^*(R^{kl}\vec{p},s_I) + \Phi_\mu^*(R^{kl}\vec{p},m_I)]$$

$$\overrightarrow{VIC}_I^{ij} = \sum_{k,l} H^{ik}\,H^{jl}\,R^{kl}\,[\vec{V}_\sigma^*(R^{kl}\vec{p},s_I) + \vec{V}_\mu^*(R^{kl}\vec{p},m_I)]$$

$\vec{p} \in S_1^{\,+}$

$$\Phi IC_I^{ij} = \sum_{k,l} H^{ik}\,H^{jl}\,[\Phi_\sigma^*(R^{+l}\vec{p},s_I) + \Phi_\mu^*(R^{+l}\vec{p},m_I)]$$

$$\overrightarrow{VIC}_I^{ij} = \sum_{k,l} H^{ik}\,H^{jl}\,R^{kl}\,[\vec{V}_\sigma^*(R^{+l}\vec{p},s_I) + \vec{V}_\mu^*(R^{+l}\vec{p},m_I)]$$

$\vec{p} \in S_2^{\,+}$

$$\Phi IC_I^{ij} = \sum_{k,l} H^{ik}\,H^{jl}\,[\Phi_\sigma^*(R^{k+}\vec{p},s_I) + \Phi_\mu^*(R^{k+}\vec{p},m_I)]$$

$$\overrightarrow{VIC}_I^{ij} = \sum_{k,l} H^{ik}\,H^{jl}\,R^{kl}\,[\vec{V}_\sigma^*(R^{k+}\vec{p},s_I) + \vec{V}_\mu^*(R^{k+}\vec{p},m_I)]$$

K.6.1 General Boundary Conditions

When one plane of symmetry is present and the control point $\vec{p}$ lies away from the plane of symmetry, the general symmetrized boundary condition (K.3.50) induces the symmetrized AIC equations

$$\sum_{I=1}^{N} AIC_I^i \, \hat{\lambda}_I^i = \sum_j H^{ij} b^j \tag{K.6.1}$$

where AIC_I^i are given

$$AIC_I^i = (a_A \hat{n}^T B_o + \vec{t}_A^{\,T}) \overrightarrow{VIC}_I^i + c_A \Phi IC_I^i + a_D s_I(\vec{p}) + c_D m_I(\vec{p}) + \vec{t}_D \cdot \nabla_p m_I(\vec{p}) \qquad (p \in S^+) \tag{K.6.2}$$

If the control point $\vec{p}$ lies in the plane of symmetry, then a general boundary condition will induce an AIC equation only if the symmetry type of boundary condition and AIC equation agree. For example, the symmetric boundary condition (cf. (H.1.20))

$$\vec{t}_A \cdot \vec{v}_A(\vec{p}) + c_A \phi_A(\vec{p}) + a_D \hat{\sigma}_1^S(\vec{p}) = b \tag{K.6.3}$$

is equivalent to the symmetrized boundary condition (cf. (K.3.62))

$$(1/2)\, \vec{t}_A^{\,T} (\hat{v}^S(\vec{p}))_A + (1/2)\, c_A \hat{\phi}^S(\vec{p}) + a_D \hat{\sigma}_1^S(\vec{p}) = b \tag{K.6.4}$$

which in turn induces the AIC equation for $\hat{\phi}^S$,

$$\sum_{I=1}^{N} AIC_I^S \, \hat{\lambda}_I^S = b \tag{K.6.5}$$

where AIC_I^S is given by

$$AIC_I^S = (1/2)\, \vec{t}_A^{\,T} \overrightarrow{VIC}_I^S + (1/2)\, c_A \Phi IC_I^S + a_D s_I(\vec{p}) \tag{K.6.6}$$

On the other hand, an antisymmetric boundary condition (cf. (H.1.19))

$$a_A \hat{n}^T B_o (\vec{v}(\vec{p}))_A + c_D \hat{\mu}_1^A(\vec{p}) + \vec{t}_D \cdot \nabla \hat{\mu}_1^A = b \tag{K.6.7}$$

is equivalent to the symmetrized boundary condition (cf. (K.3.63))

$$(1/2)\, a_A \hat{n}^T B_o (\hat{v}^A(p))_A + c_D \hat{\mu}_1^A(\vec{p}) + \vec{t}_D \cdot \nabla \hat{\mu}_1^A = b \tag{K.6.8}$$

which induces the AIC equation for $\hat{\phi}^A$,

$$\sum_{I=1}^{N} AIC_I^A \, \hat{\lambda}_1^A = b \tag{K.6.9}$$

where

$$AIC_I^A = (1/2)\ a_A\ \hat{n}^T\ B_o\ \overrightarrow{VIC}_I^A + c_D\ m_I\ (\vec{p}) + \vec{t}_D \cdot \nabla\ m_I(\vec{p}) \tag{K.6.10}$$

When two planes of symmetry are present, equation (K.4.46) provides us with the symmetrization of a general boundary condition away from either plane of symmetry. Using it, one obtains the symmetrized AIC equations

$$\sum_{I=1}^{N} AIC_I^{ij}\ \hat{\lambda}_I^{ij} = \sum_{k,l} H^{ik}\ H^{jl}\ b^{kl} \tag{K.6.11}$$

where

$$AIC_I^{ij} = (a_A\ \hat{n}^T\ B_o + \vec{t}_A{}^T)\ \overrightarrow{VIC}_I^{ij} + c_A\ \Phi IC_I^{ij}$$

$$+ a_D\ s_I(\vec{p}) + c_D\ m_I(\vec{p}) + \vec{t}_D\ \cdot\ \nabla_p\ m_I(\vec{p}) \tag{K.6.12}$$

If a control point $\vec{p}$ lies in the first plane of symmetry, then symmetric boundary conditions at $\vec{p}$ and at $R_2\vec{p}$ can be written concisely as

$$a_D\ \tilde{\sigma}_1^{Sl}\ (R^{+l}\vec{p}) + c_A\ (\phi(R^{+l}\vec{p}))_A + \vec{t}_A\ .\ (\vec{v}(R^{+l}\vec{p}))_A = b^l \tag{K.6.13}$$

These conditions can be symmetrized to give (cf. K.4.58)

$$a_D\ \hat{\sigma}_1^{Sj}\ (\vec{p}) + (1/2)\ c_A\ (\hat{\phi}^{Sj}(\vec{p}))_A + (1/2)\vec{t}_A\ .\ (\hat{v}^{Sj}(\vec{p}))_A = \sum_l H^{jl}\ b^l \tag{K.6.14}$$

which in turn yields the two AIC equations

$$\sum_{I=1}^{N} AIC_I^{Sj}\ \hat{\lambda}_I^{Sj} = \sum_l H^{jl}\ b^l \tag{K.6.15}$$

where

$$AIC_I^{Sj} = a_D\ s_I\ (\vec{p}) + (1/2)c_A\ \Phi IC_I^{Sj} + (1/2)\vec{t}_A\ .\ \overrightarrow{VIC}_I^{Sj} \tag{K.6.16}$$

Similarly, an antisymmetric boundary condition on the first plane of symmetry yields the AIC equations (cf. K.4.60)

$$\sum_{I=1}^{N} AIC_I^{Aj}\ \hat{\lambda}_I^{Aj} = \sum_l H^{jl}\ b^l \tag{K.6.17}$$

where

$$AIC_I^{Aj} = (1/2)a_A\ \hat{n}^T\ B_o\ \overrightarrow{VIC}_I^{Aj} + c_D\ m_I(\vec{p}) + \vec{t}_D\ .\nabla\ m_I \tag{K.6.18}$$

The treatment of control points lying in the second plane of symmetry is essentially the same.

K.6.2 Matching Boundary Conditions

In this section, we examine the imposition of matching conditions when a configuration possesses some symmetry. Our discussion will concentrate on doublet matching, source matching being handled in an essentially similar fashion. Notice however that the concept of source matching along an abutment involving more than two networks is not really sound, since even the idea of a continuous surface normal is ill-defined in the neighborhood of such an abutment(*). For this reason, we prefer to deal with the concept of doublet matching, which has a thoroughly sound theoretical basis.

Our discussion will consist of two major parts. First, we will investigate the forms that doublet matching takes when symmetry is present. In the second part, we will show how these matching conditions induce AIC constraint relations.

K.6.2.1 The Form of Doublet Matching Conditions

If an abutment lies away from any plane of symmetry, doublet matching along the abutment and its images can be expressed by (cf. eqn. (H.2.11a) or (F.5.1))

$$\sum_k \quad s_k \, \mu_k^i \, (R^i \vec{p}) = 0 \qquad\qquad i \in \{+1,-1\}$$

if the configuration has one plane of symmetry, and by

$$\sum_k \quad s_k \, \mu_k^{ij} \, (R^{ij} \vec{p}) = 0 \qquad\qquad i,j \in \{+1,-1\}$$

if the configuration has two planes of symmetry. These conditions can be symmetrized in the obvious fashion to yield the symmetrized matching conditions,

one plane of symmetry $$\sum_k \quad s_k \, \hat{\mu}_k^i \, (\vec{p}) = 0 \qquad \text{(K.6.19a)}$$

two planes of symmetry $$\sum_k \quad s_k \, \hat{\mu}_k^{ij} \, (\vec{p}) = 0 \qquad \text{(K.6.19b)}$$

Here $\hat{\mu}_k^i(\vec{p})$ denotes the evaluation of $\hat{\mu}^i(\vec{p})$ on the k-th network of the abutment, $\hat{\mu}^i$ being defined by (cf. (K.3.27)) $\hat{\mu}^i(\vec{p}) = \sum_j H^{ij} \, \mu^j(R^j\vec{p})$.

(*) Recall that source strength is defined, for incompressible flow, by $\sigma = (\hat{n}\cdot\vec{v})^+ - (\hat{n}\cdot\vec{v})^-$. If $\vec{v}$ is continuous, σ will not likely be continuous unless $\hat{n}$ is continuous. In any event, the whole issue of source matching is not of much consequence since it can only arise when (a) one uses design networks and (b) one specifies that closure override doublet matching (not recommended).

If an abutment lies on a plane of symmetry, four separate cases, illustrated by figure K.6, must be analyzed. These are

(a) there is just one plane of symmetry

(b) the abutment lies on the first of two planes of symmetry

(c) the abutment lies on the second of two planes of symmetry

(d) the abutment lies on the intersection of two planes of symmetry

We study each of these cases in turn.

In fig. K.6a, we illustrate the case of just one plane of symmetry. Six networks are involved in the abutment, N_a and N_d in the plane of symmetry and N_b^+, N_b^-, N_c^+, N_c^-, the images of N_b and N_c. In line with our convention of denoting the doublet strength on S_1 by $\hat{\mu}_1^A$, we denote the doublet strengths on networks N_a and N_d by $\hat{\mu}_{1,a}^A$ and $\hat{\mu}_{1,d}^A$. The doublet matching condition for this abutment is, clearly,

$$\hat{\mu}_{1,a}^A - \mu_b^+ + \mu_c^+ - \hat{\mu}_{1,d}^A - \mu_c^- + \mu_b^- = 0$$

Rearranging, we write

$$\hat{\mu}_{1,a}^A - (\mu_b^+ - \mu_b^-) + (\mu_c^+ - \mu_c^-) - \hat{\mu}_{1,d}^A = 0$$

Recognizing $(\mu_b^+ - \mu_b^-)$ as $\hat{\mu}_b^A$ and $(\mu_c^+ - \mu_c^-)$ as $\hat{\mu}_c^A$, this yields

$$\hat{\mu}_{1,a}^A - \hat{\mu}_b^A + \hat{\mu}_c^A - \hat{\mu}_{1,d}^A = 0 \qquad \text{(K.6.20)}$$

a matching condition involving just the antisymmetric doublet strengths. There are no symmetric doublet matching conditions at a plane of symmetry. This can be clearly seen in fig. K.7 for which one can see that the doublet matching condition reduces to the trivial condition, 0 = 0.

In fig. K.6b, we illustrate the case of an abutment lying on the first plane of symmetry when two planes of symmetry are present in the problem. The doublet matching conditions on the abutment and its image read

$$\tilde{\mu}_{1,a}^{A+} + \mu_b^{++} - \mu_c^{++} + \mu_c^{-+} - \mu_b^{-+} = 0$$

$$\tilde{\mu}_{1,a}^{A-} + \mu_b^{+-} - \mu_c^{+-} + \mu_c^{--} - \mu_b^{--} = 0$$

Adding and subtracting these two conditions, and taking account of the relations $\hat{\mu}_{1,a}^{AS} = \tilde{\mu}_{1,a}^{A+} + \tilde{\mu}_{1,a}^{A-}$, $\hat{\mu}_{1,a}^{AA} = \tilde{\mu}_{1,a}^{A+} - \tilde{\mu}_{1,a}^{A-}$, we obtain

$$\hat{\mu}^{AS}_{1,a} + \hat{\mu}^{AS}_{b} - \hat{\mu}^{AS}_{c} = 0$$

$$\hat{\mu}^{AA}_{1,a} + \hat{\mu}^{AA}_{b} - \hat{\mu}^{AA}_{c} = 0 \qquad \text{(K.6.21)}$$

Notice that when the abutment lies in the first plane of symmetry, both of the doublet matching conditions are antisymmetric with respect to the first plane of symmetry.

The case of an abutment lying in the second plane of symmetry, illustrated by fig. K.6c, is handled in essentially the same way as the previous case. The resulting doublet matching conditions,

$$\hat{\mu}^{SA}_{2,a} + \hat{\mu}^{SA}_{b} + \hat{\mu}^{SA}_{c} = 0$$

$$\hat{\mu}^{AA}_{2,a} + \hat{\mu}^{AA}_{b} + \hat{\mu}^{AA}_{c} = 0 \qquad \text{(K.6.22)}$$

are both antisymmetric with respect to the second plane of symmetry.

When an abutment lies on the intersection of both planes of symmetry, as illustrated by fig. K.6d, there is only one doublet matching condition. Referring to fig. K.6d, it is easy to see that for this example the matching condition reads

$$\tilde{\mu}^{A+}_{1,a} - \tilde{\mu}^{A-}_{1,a} + \mu_b^{++} - \mu_b^{+-} + \mu_b^{--} - \mu_b^{-+} + \tilde{\mu}^{+A}_{2,c} - \tilde{\mu}^{-A}_{2,c} = 0$$

Recognizing the various antisymmetric/antisymmetric parts, this simplifies to read

$$\hat{\mu}^{AA}_{1,a} + \hat{\mu}^{AA}_{b} + \hat{\mu}^{AA}_{2,c} = 0 \qquad \text{(K.6.23)}$$

Notice that this condition is antisymmetric with respect to both planes of symmetry.

A careful perusal of equation (K.6.20), (K.6.21), (K.6.22) and (K.6.23) leads to the following general conclusions.

(i) if an abutment lies on a plane of symmetry, the matching conditions imposed for that abutment are antisymmetric with respect to the plane of symmetry

(ii) the doublet matching conditions have the same form as the doublet matching conditions for just the principal image of the configuration, $S^{+} \cup S_1$ when one plane of symmetry is present and $S^{++} \cup S_1^{+} \cup S_2^{+}$ when two are present.

Consequently we find that equations (K.6.19) capture the correct form of the doublet matching conditions even when the abutment lies on a plane of symmetry.

K.6.2.2 The Imposition of Doublet Matching Conditions

We now study the imposition of the doublet matching conditions, (K.6.19). In order to simplify the discussion, we treat only the case of one plane of symmetry where the matching conditions are given by (K.6.19a).

We begin by observing that the basic problem to be addressed is the problem of expressing $\hat{\mu}_k^i(\vec{p})$ in terms of the global singularity parameters $\hat{\lambda}_I^i$. Here, $\hat{\mu}_k^i$ denotes the restriction of $\hat{\mu}^i$ to N_k, the k-th network of the abutment. Following the notation of section (K.1.1), we observe that

$$\hat{\mu}_k{}^i(\vec{p}) = \sum_{I=1}^{N} m_I(\vec{p})\Big|_{N_k} \hat{\lambda}_I{}^i \tag{K.6.24}$$

Here, $m_I\big|_{N_k}$ denotes the restriction of the global basis function m_I to the network N_k. It may be written

$$m_I(p)\big|_{N_k} = \lfloor 1 \quad \xi' \quad \eta' \quad \xi'^2/2 \quad \xi'\eta' \quad \eta'^2/2 \rfloor \, [SPSPL_k^D] \, \{B_{k,I}^D\} \tag{K.6.25}$$

where

(ξ',η') are the local coordinates of the matching point $\vec{p}$ in the subpanel in which it lies,

$[SPSPL_k^D]$ is the doublet subpanel spline for the subpanel in which $\vec{p}$ lies, in network N_k

$\{B_{k,I}^D\}$ is the column of the doublet outer spline matrix $[B_k^D]$ corresponding to λ_I and associated with the panel of N_k in which $\vec{p}$ lies.

With this understanding of how one computes $m_I\big|_{N_k}$, it is easy to see that a matching condition of the form (K.6.19a) induces AIC constraint relations of the form

$$\sum_{I=1}^{N} AIC_I \; \hat{\lambda}_I^i = 0 \tag{K.6.26}$$

where

$$AIC_I = \sum_k s_k \, m_I(\vec{p})\big|_{N_k} \tag{K.6.27}$$

K.6.2.3 Source Matching (Design Cases Only)

When symmetry is present, the enforcement of the symmetrized source matching conditions is handled in essentially the same way as the doublet matching conditions discussed in the previous section. Away from any planes of symmetry the symmetrized matching conditions read (compare with equations (K.6.19))

One plane of symmetry $$\sum_k s_k \hat{\sigma}_k^i(\vec{p}) = 0 \qquad \text{(K.6.28a)}$$

Two planes of symmetry $$\sum_k s_k \hat{\sigma}_k^{ij}(\vec{p}) = 0 \qquad \text{(K.6.28b)}$$

If the source matching abutment lies on a plane of symmetry, the source matching conditions are still of this form, but are imposed only on symmetrized potentials $\hat{\phi}^i$ (or $\hat{\phi}^{ij}$) that are symmetric with respect to the plane of symmetry containing the abutment. If the source matching condition is to be imposed at a control point lying in the plane of symmetry, it must replace the user boundary condition of symmetric type (in the sense of section (H.1.3)).

In any event, the source matching boundary conditions can be transformed into AIC constraint relations of the form (K.6.26) with numbers AIC_I given by the same formula, equation (K.1.21) that we obtained for the case of no symmetry at all. The only modification that is required in our interpretation of equation (K.1.21) is that the summation over k be restricted to networks lying in the principal image of the configuration.

K.6.2.4 Velocity Jump Matching

The symmetrization of the velocity jump matching conditions is now described. In order to simplify the discussion, we restrict outselves to configurations with just one plane of symmetry. The extension of the results to configurations with two planes of symmetry is straightforward.

When the abutment lies away from any plane of symmetry, we obtain the usual results (compare with equation (K.1.22))

$$\sum_k s_k \left\{ \hat{\sigma}^i (\vec{t}.\hat{n})/(\hat{n}.\vec{v}) + ((\vec{v}x\vec{t})x\hat{n}).\nabla\hat{\mu}^i/(\hat{n}.\vec{v}) \right\}_k = 0 \qquad \text{(K.6.29)}$$

This relation can now be transformed into an AIC equation for each symmetry condition in the usual way with equation (K.1.23) giving the formula for the AIC row entries for all symmetry conditions.

When the abutment lies on a plane of symmetry, the situation is significantly more complicated than anything we have treated up to this point. Consider figure K.8, which gives an edge-on view of an abutment lying on a plane of symmetry. For this situation the expression $\Sigma s_k \Delta\vec{v}_k$ can be written, using the notation of figure K.8,

$$\Sigma s_k \Delta\vec{v}_k = (+1)\ [\sigma^+\ \hat{n}^+/(\hat{n},\vec{v})_+ + \nabla_t\mu^+]$$

$$(-1)\ [\sigma^-\ \hat{n}^-/(\hat{n},\vec{v})_- + \nabla_t\mu^-]$$

$$(-1)\ [\hat{\sigma}_1^S\ n_1/(\hat{n},\vec{v})_1 + \nabla_t\hat{\mu}_1^A]$$

(K.6.30)

Using the relations (K.3.26) and (K.3.27) relating σ^j, μ^j to $\hat{\sigma}^j$, $\hat{\mu}^j$, we obtain

$$\sigma^+ \Big|_{\vec{p}^+} = \frac{1}{2}\ (\hat{\sigma}^S + \hat{\sigma}^A)\Big|_{\vec{p}^+} \qquad \text{(K.6.31a)}$$

$$\sigma^- \Big|_{\vec{p}^-} = \frac{1}{2}\ (\hat{\sigma}^S - \hat{\sigma}^A)\Big|_{R_1\vec{p}^-} \qquad \text{(K.6.31b)}$$

$$\mu^+ \Big|_{\vec{p}} = \frac{1}{2}\ (\hat{\mu}^S + \hat{\mu}^A)\Big|_{\vec{p}} \qquad \text{(K.6.32a)}$$

$$\mu^- \Big|_{\vec{p}} = \frac{1}{2}\ (\hat{\mu}^S - \hat{\mu}^A)\Big|_{R_1\vec{p}} \qquad \text{(K.6.32b)}$$

Applying ∇_t to these last two equations and recognizing that ∇_t behaves just like the regular gradient operator, we obtain

$$\nabla_t\ \mu^+\Big|_{\vec{p}^+} = \frac{1}{2}\ (\ \nabla_t\ \hat{\mu}^S + \nabla_t\ \hat{\mu}^A)\Big|_{\vec{p}^+} \qquad \text{(K.6.33a)}$$

$$\nabla_t\ \mu^-\Big|_{p^-} = \frac{1}{2}\ R_1\ (\ \nabla_t\ \hat{\mu}^S - \nabla_t\ \hat{\mu}^A)\Big|_{R_1\vec{p}^-} \qquad \text{(K.6.33b)}$$

Substituting relations (K.6.31) and (K.6.33) into (K.6.30) and recognizing that the evaluation point $\vec{p}$ of equation (K.6.30) satisfies $R_1\vec{p} = \vec{p}$, and that $\hat{n}^+ = R_1\ \hat{n}^-$, we obtain

$$\Sigma\ s_k\ \Delta\ \vec{v}_k = (+1)\ \frac{1}{2}\ (I - R_1)\ [\hat{\sigma}^S\ \hat{n}^+/(\hat{n}.\vec{v})_+ + \nabla_t\ \hat{\mu}^S]$$

$$(-1)\ \frac{1}{2}\ (I - R_1)\ [\hat{\sigma}_1^S\ \hat{n}_1/(\hat{n},\vec{v})_1]$$

$$(+1)\ \frac{1}{2}\ (I + R_1)\ [\hat{\sigma}^A\ \hat{n}^+/(\hat{n},\vec{v})_+ + \nabla_t\ \hat{\mu}^A]$$

$$(-1)\ \frac{1}{2}\ (I + R_1)\ [\ \nabla_t\ \hat{\mu}_1^A]$$

(K.6.34)

Now the reflector matrix R_1 satisfies the relations

$$\frac{1}{2}(I - R_1) = \hat{n}_1 \hat{n}_1^T \quad = \text{projection in direction of } \hat{n}_1$$

$$\frac{1}{2}(I + R_1) = I - \hat{n}_1 \hat{n}_1^T = \text{projection orthogonal to } \hat{n}_1$$

Using these relations, we can write the following decomposition of $\Sigma s_k \Delta\vec{v}_k$ into symmetric and antisymmetric parts,

$$\Sigma s_k \Delta\vec{v}_k = (\Sigma s_k \Delta\vec{v}_k)^S + (\Sigma s_k \Delta\vec{v}_k)^A \tag{K.6.35}$$

where we define

$$(\Sigma s_k \Delta\vec{v}_k)^S = (\hat{n}_1 \hat{n}_1^T) \left\{ (+1)\,[\hat{\sigma}^S \hat{n}^+/(\hat{n},\vec{v})_+ + \nabla_t \hat{\mu}^S] \right.$$

$$\left. (-1)\,[\hat{\sigma}_1^S \hat{n}_1/(\hat{n},\vec{v})_1] \right\}$$

$$(\Sigma s_k \Delta\vec{v}_k)^A = (I - \hat{n}_1 \hat{n}_1^T) \left\{ (+1)\,[\hat{\sigma}^A \hat{n}^+/(\hat{n},\vec{v})_+ + \nabla_t \hat{\mu}^A] \right.$$

$$\left. (-1)\,[\nabla_t \hat{\mu}_1^A] \right\} \tag{K.6.36}$$

Now in section (K.4) we found that it is necessary that boundary conditions on the plane of symmetry be either purely symmetric or purely antisymmetric in order for the symmetric and antisymmetric problems to decouple. In terms of the velocity jump matching condition

$$\vec{t} \cdot \Sigma s_k \Delta\vec{v}_k = 0$$

this clearly requires that either

$$\text{(i)} \quad \vec{t} \cdot \hat{n}_1 \hat{n}_1^T = 0$$

or

$$\text{(ii)} \quad \vec{t} \cdot (I - \hat{n}_1 \hat{n}_1^T) = 0$$

In the first instance we obtain the antisymmetric matching condition:

$$\vec{t} \cdot \hat{n}_1 = 0 : \qquad \vec{t} \cdot \left\{ (+1)\,[\hat{\sigma}^A \hat{n}^+/(\hat{n},\vec{v})_+ + \nabla_t \hat{\mu}^A] \right.$$

$$\left. (-1)\,[\nabla_t \hat{\mu}_1^A] \right\} = 0 \tag{K.6.37a}$$

while in the second instance we obtain the symmetric matching condition

$\vec{t} \cdot (I - \hat{n}_1 \hat{n}_1^T) = 0$:

$$\vec{t} \cdot \left\{ (+1) \, [\hat{\sigma}^S \, \hat{n}^+ / (\hat{n}, \vec{v})_+ + \nabla_t \hat{\mu}^S] \right.$$

$$\left. (-1) \, [\hat{\sigma}_1^S \, \hat{n}_1 / (\hat{n}, \vec{v})_1] \right\} = 0 \qquad \text{(K.6.37b)}$$

The first of these conditions represents the usual case in which the network lying in the plane of symmetry is a wake network, as illustrated in figure K.8. The form of the symmetrized matching conditions (K.6.37) is the same as the usual form (K.6.29) with the following restrictions

(i) the sum over k in equation (K.6.29) must be interpretted as being just a sum over those networks in the principal image of the configuration, $S^+ \cup S_1$

(ii) the symmetrized singularity distributions in the plane of symmetry satisfy the usual degenerate boundary conditions, $\hat{\sigma}_1^A = 0$, $\hat{\mu}_1^S = 0$.

K.6.3 Closure Boundary Conditions

We now study the generation of a closure AIC equation for those problems possessing symmetry. Two basic cases must be treated, (i) the case in which the control point lies away from any plane of symmetry and (ii) the case in which the control point lies in a plane of symmetry. For the second case, two subcases exist, corresponding to the situations in which the closure condition is of symmetric type or of antisymmetric type. In the discussion that follows, we describe in detail only those problems having one plane of symmetry. The extension to problems with two planes of symmetry is fairly obvious and its treatment is summarized with only cursory discussion.

When a closure control point lies away from the plane of symmetry, the closure boundary condition at $\vec{p}$ and at the image point $R^- \vec{p}$ may be concisely summarized by (compare with (K.1.24))

$$\iint_{\substack{\text{column or row of} \\ \text{panels in image } S^+}} [a_A \, \hat{n}^T R^j B_o \vec{v} \, (R^j \vec{q}) + a_D \, \sigma^j (R^j \vec{q})] \, dS_q = b^j \qquad \text{(K.6.38)}$$

Notice that we perform our integration on the principal image S^+, so that the integration space is the same for both boundary conditions. Multiplying this by H^{ij} and summing over j yields

$$\iint_{\substack{\text{column or row of} \\ \text{panels in image } S^+}} [a_A \, \hat{n}^T B_o \hat{v}^i (\vec{q}) + a_D \, \hat{\sigma}^i (\vec{q})] dS_q = \sum_j H^{ij} b^j \qquad \text{(K.6.39)}$$

To obtain this result, we have used the definition (K.3.26) of $\hat{\sigma}^i$ and the definition (K.3.44) of $\hat{v}^i$, together with the fact $R^j B_o = B_o R^j$.

Proceeding now as in section K.1.3, we approximate the integral on the left by evaluating the integrands at the panel centers of the particular row or column, multiplying these values by the panel area, and forming the sum. One obtains the approximate equation

$$\sum_k A_k \left[a_A(\vec{p}_k)\ (\hat{n}^T B_o \hat{v}^i)\Big|_{\vec{p}_k} + a_D(\vec{p}_k)\ \hat{\sigma}^i(\vec{p}_k)\right] = \sum_j H^{ij} b^j \tag{K.6.40}$$

This immediately provides the AIC constraint equations

$$\sum_{I=1}^{N} AIC_I^i\ \hat{\lambda}_I^i = \sum_j H^{ij} b^j \tag{K.6.41}$$

where

$$AIC_I^i = \sum_k A_k \left[a_A(\vec{p}_k)\ (\hat{n}^T B_o\ \overrightarrow{VIC}_I^i)\Big|_{p_k} + a_D(\vec{p}_k) s_I(\vec{p}_k)\right] \tag{K.6.42}$$

If a closure control point lies <u>in</u> the plane of symmetry, it must lie on a network that itself lies in the plane of symmetry. When this happens, the closure condition may have either the form

symmetric closure condition

$$\iint_{\substack{\text{column or}\\ \text{row in } S_1}} a_D\ \hat{\sigma}_1^A(\vec{q})\ dS_q = b \tag{K.6.43}$$

or else the form

antisymmetric closure condition

$$\iint_{\substack{\text{column or}\\ \text{row in } S_1}} a_A\ \hat{n}^T\ B_o\ \vec{v}(\vec{q})\ dS_q = b \tag{K.6.44}$$

A symmetric closure condition of the form (K.6.43) clearly provides the symmetric AIC constraint equation

$$\sum_{I=1}^{N} AIC_I^S\ \lambda_I^S = b \tag{K.6.45}$$

where

$$AIC_I^S = \sum_k A_k\ a_D(\vec{p}_k)\ s_I\ (\vec{p}_k) \tag{K.6.46}$$

The antisymmetric closure condition, (K.6.44), is a bit trickier and requires the use of the general identity (cf. eqn. (K.3.56))

$$\vec{v}(\vec{q}) = \frac{1}{2}\ (\hat{v}^S(\vec{q}) + \hat{v}^A(\vec{q}))$$

together with the observation that for $\vec{q} \in S_1$, $\hat{n}^T B_o \hat{v}^S (\vec{q}) = 0$ (cf. eqn. (K.3.60)). These two observations imply that (K.6.44) is equivalent to

$$\iint_{\substack{\text{column or} \\ \text{row in } S_1}} a_A \hat{n}^T B_o (\tfrac{1}{2}) \hat{v}^A (\vec{q}) \, dS_q = b \tag{K.6.47}$$

This clearly provides the antisymmetric AIC constraint equation

$$\sum_{I=1}^{N} AIC_I^A \hat{\lambda}_I^A = b \tag{K.6.48}$$

where

$$AIC_I^A = \sum_k A_k a_A(\vec{p}_k) (\hat{n}^T B_o(\tfrac{1}{2}) \overrightarrow{VIC}_I^A)\Big|_{\vec{p}_k} \tag{K.6.49}$$

Notice the appearance of the factor of (1/2) as a coefficient of the integral influence coefficient $\overrightarrow{VIC}_I^A$.

We now turn to the case of two planes of symmetry. If the closure control point lies away from both planes of symmetry, then the four image closure conditions

$$\iint_{\substack{\text{column or row of} \\ \text{panels in image } S^{++}}} [a_A \hat{n}^T R^{kl} B_o \vec{v} (R^{kl}\vec{q}) + a_D \sigma^{kl}(R^{kl}\vec{q})] \, dS_q = b^{kl} \tag{K.6.50}$$

yield, upon symmetrization, the four AIC constrain equations

$$\sum_{I=1}^{N} AIC_I^{ij} \hat{\lambda}_I^{ij} = \sum_{k,l} H^{ik} H^{jl} b^{kl} \tag{K.6.51}$$

where AIC_I^{ij} are given by

$$AIC_I^{ij} = \sum_{\text{panels } k} A_k [a_A(\vec{p}_k) (\hat{n}^T B_o \overrightarrow{VIC}_I^{ij})\Big|_{\vec{p}_k} + a_D(\vec{p}_k) s_I(\vec{p}_k)] \tag{K.6.52}$$

If a closure control point $\vec{p}$ lies in the first plane of symmetry, then the closure boundary conditions at $\vec{p}$ and its image $R^{+-}\vec{p}$ will have either the symmetric forms

$$\iint_{\substack{\text{column or row of} \\ \text{panels in } S_1^+}} a_D \, \bar{\sigma}_1^{S1} \, (R^{+1}\vec{q}) \, dS_q = b^1 \tag{K.6.53}$$

or the antisymmetric forms

$$\iint_{\substack{\text{column or row of} \\ \text{panels in } S_1^+}} a_A \, \hat{n}^T \, R^{+1} \, B_o \, \vec{v} \, (R^{+1}\vec{q}) \, dS_q = b^1 \tag{K.6.54}$$

The pair of equations (K.6.53) induces the pair of AIC constraint equations,

$$\sum_{I=1}^{N} AIC_I^{Sj} \; \hat{\lambda}_I^{Sj} = \sum_{1} H^{j1} \, b^1 \tag{K.6.55}$$

where the AIC's are given by

$$AIC_I^{Sj} = \sum_{k} A_k \, a_D(\vec{p}_k) \, s_I \, (\vec{p}_k) \tag{K.6.56}$$

The pair of equations (K.6.54), on the other hand, induces the pair of AIC constraint equations,

$$\sum_{I=1}^{N} AIC_I^{Aj} \; \hat{\lambda}_I^{Aj} = \sum_{1} H^{j1} \, b^1 \tag{K.6.57}$$

where the AIC's are given by

$$AIC_I^{Aj} = \frac{1}{2} \sum_{k} A_k \, a_A \, (\vec{p}_k) \quad \hat{n}^T \, B_o \, \overrightarrow{VIC}_I^{Aj} \Big|_{\vec{p}_k} \tag{K.6.58}$$

Notice that here, as in the case of one plane of symmetry, that the integral influence coefficients are modified by a factor of (1/2).

K.6.4 Degenerate Boundary Conditions

In this section, we discuss the AIC constraint equations induced by degenerate boundary conditions.

Recall from sections (K.3) and (K.4) that when a control point lies in a plane of symmetry it may receive some degenerate boundary conditions. These conditions, which have the various forms

(Degenerate Source Condition in a Plane of Symmetry) $\hat{\sigma}_1^{A} = 0$ (K.6.59a)

(Degenerate Source Conditions in first Plane of Symmetry) $\hat{\sigma}_1^{AS} = 0$, $\hat{\sigma}_1^{AA} = 0$ (K.6.59b)

(Degenerate Source Conditions in Second Plane of Symmetry) $\hat{\sigma}_2^{SA} = 0$, $\hat{\sigma}_2^{AA} = 0$ (K.6.59c)

(Degenerate Doublet Condition in a Plane of Symmetry) $\hat{\mu}_1^{S} = 0$ (K.6.59d)

(Degenerate Doublet Conditions in First Plane of Symmetry) $\hat{\mu}_1^{SS} = 0$, $\hat{\mu}_1^{SA} = 0$ (K.6.59e)

(Degenerate Doublet Conditions in Second Plane of Symmetry) $\hat{\mu}_2^{SS} = 0$, $\hat{\mu}_2^{AS} = 0$ (K.6.59f)

The implementation of these conditions is fairly obvious, given the representation formulae for source and doublet distributions,

$$\hat{\sigma}^{i}(p) = \sum_{I=1}^{N} s_I(\vec{p}) \; \hat{\lambda}_I^{\,i} \tag{K.6.60a}$$

$$\hat{\sigma}^{ij}(p) = \sum_{I=1}^{N} s_I(\vec{p}) \; \hat{\lambda}_I^{\,ij} \tag{K.6.60b}$$

$$\hat{\mu}^{i}(p) = \sum_{I=1}^{N} m_I(\vec{p}) \; \hat{\lambda}_I^{\,i} \tag{K.6.61a}$$

$$\hat{\mu}^{ij}(p) = \sum_{I=1}^{N} m_I(\vec{p}) \; \hat{\lambda}_I^{\,ij} \tag{K.6.61b}$$

In fact, for most control points $\vec{p}$ at which these conditions are to be imposed, only one of the basis functions s_I or m_I will be nonzero. Thus the conditions $\hat{\sigma}_1^{A}(p) = 0$ or $\hat{\mu}_1^{S}(p) = 0$ will usually reduce to either

$$s_K(\vec{p}) \quad \hat{\lambda}_K^{\,A} = 0 \tag{K.6.62}$$

or

$$m_K(\vec{p}) \quad \hat{\lambda}_K^{\,S} = 0 \tag{K.6.63}$$

When this happens, one has the choice of characterizing the boundary condition as a "singularity specification" boundary condition, in which case it induces a row in the AIC matrix, or as a "known singularity" boundary condition which does not induce a row in the AIC matrix. To determine the characterization, we must employ the general principal that the AIC matrix must have the same size for all symmetry conditions. In practice, this means that we must examine the boundary condition which the degenerate boundary condition replaces. If the boundary condition that gets replaced is a "null" or "known singularity" boundary condition, the corresponding degenerate boundary condition must be either "null" or "known singularity." If, on the other hand, the boundary condition that gets replaced is "general," "singularity specification," "closure" or "matching," the corresponding degenerate boundary condition must be a "singularity specification."

K.7 The IC Update Capability

The purpose of the influence coefficient update capability is to permit a program user to make changes in the geometry (or, occasionally, the left hand side of the boundary condition equation (5.6.1) of a portion of a configuration), and to solve the resulting potential flow problem more economically by making use of the previous solution.

The program user specifies certain networks as "updatable," that is, subject to future modification, when specifying the original potential flow problem. The program then identifies each control point and each singularity parameter as either "updatable" or "non-updatable," and resequences them so that the updatable ones occur last. The resulting AIC matrix can then be partitioned

$$[AIC] = \left[\begin{array}{c|c} AIC_{NU} & AIC_{U,1} \\ \hline AIC_{U,2} & AIC_{U,3} \end{array}\right] \qquad (K.7.1)$$

When the modified flow problem is solved, the matrix AIC_{NU} remains unchanged, and need not be recomputed. Only the matrices $AIC_{U,i}$ $i = 1, 2, 3$, defining the influence of the updatable portion of the configuration, and the influence on the updatable portion, need to be computed. Thus, if r is the fraction of the configuration which is non-updatable, a proportion of the AIC computation of size r^2 is saved.

The imposition of doublet matching causes the specification of updatable control points and singularity parameters to be non-trivial. Clearly every control point and singularity parameter on an updatable network is itself updatable. In addition, though, control points on an edge of a non-updatable network which abuts an updatable network must be made updatable. This arises from the possibility that the abutment in question may change by the addition, deletion, or change in panel density, of the updatable network. As a result, the boundary conditions on the edge of the non-updatable network may change from matching to a standard aerodynamic boundary condition (5.6.1) or vice versa.

In addition, the modification of the updatable network may cause the definition or deletion of extra singularity parameters on the edge of the non-updatable network (see figure K.9). Thus the edge spline on this edge may change, and so the singularity parameters on this edge must be specified as updatable.

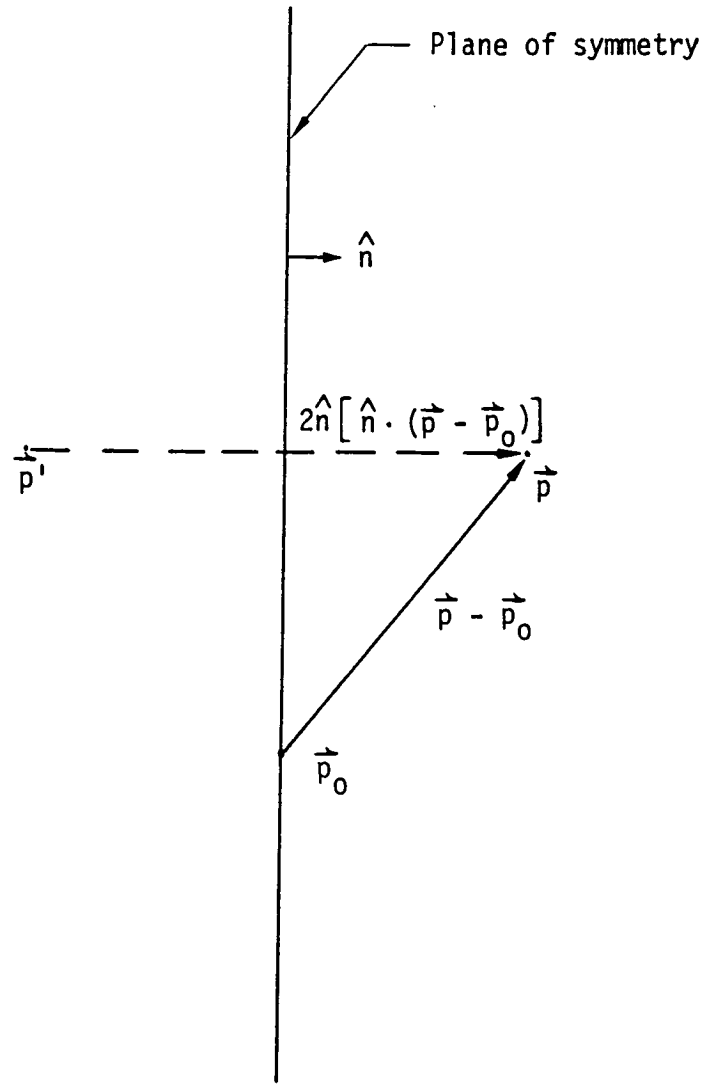

$$\vec{p}' = \vec{p} - 2\hat{n}\left[\hat{n}.(\vec{p}-\vec{p}_o)\right]$$

Figure K.1 - Reflection of point ($\vec{p}$) in a plane of symmetry

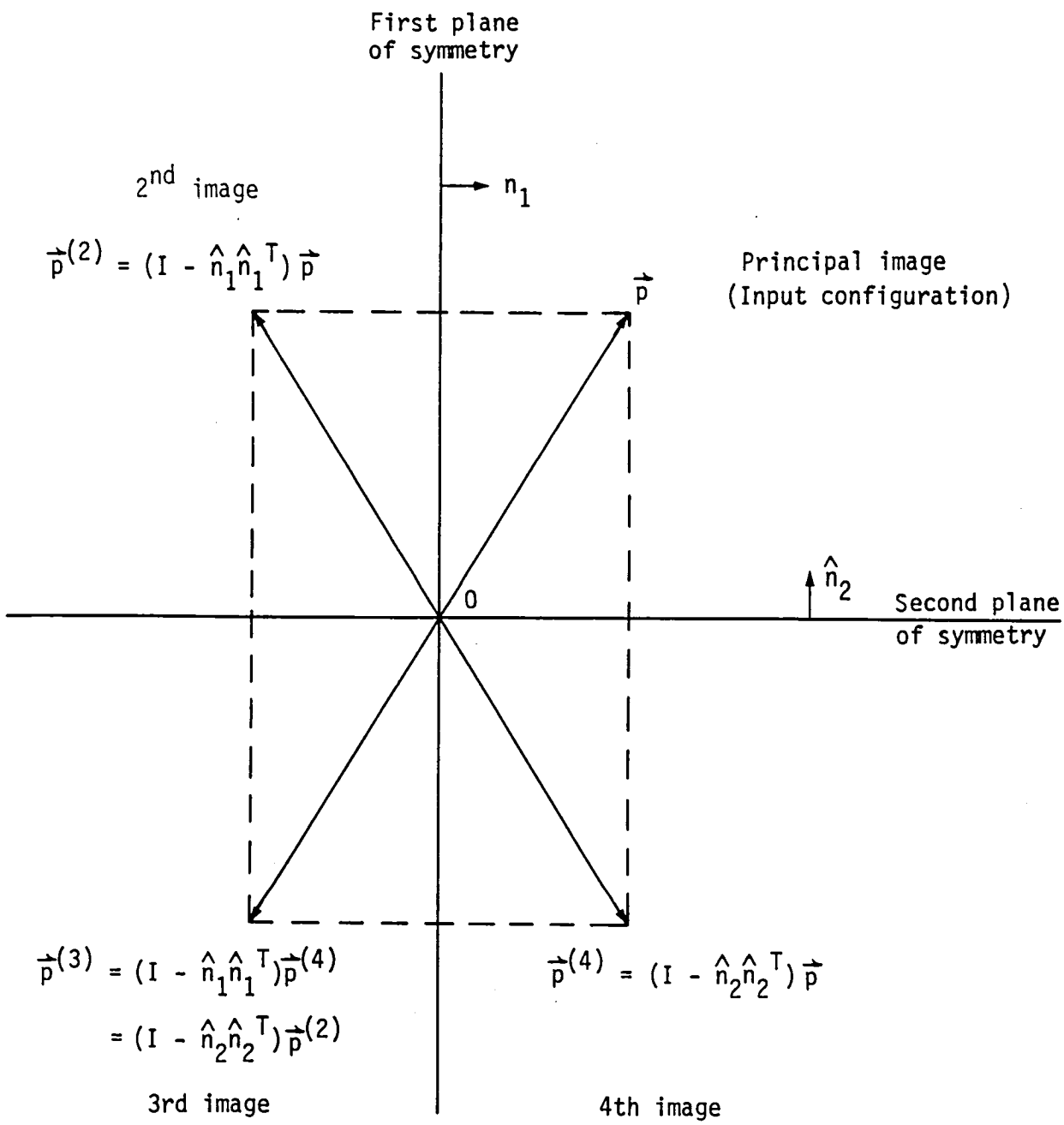

Figure K.2 - Reflections of a point $\vec{p}$ in 2 planes of symmetry
(Asummes $\vec{p}_o.\hat{n}_1 = \vec{p}_o.\hat{n}_2 = 0$)

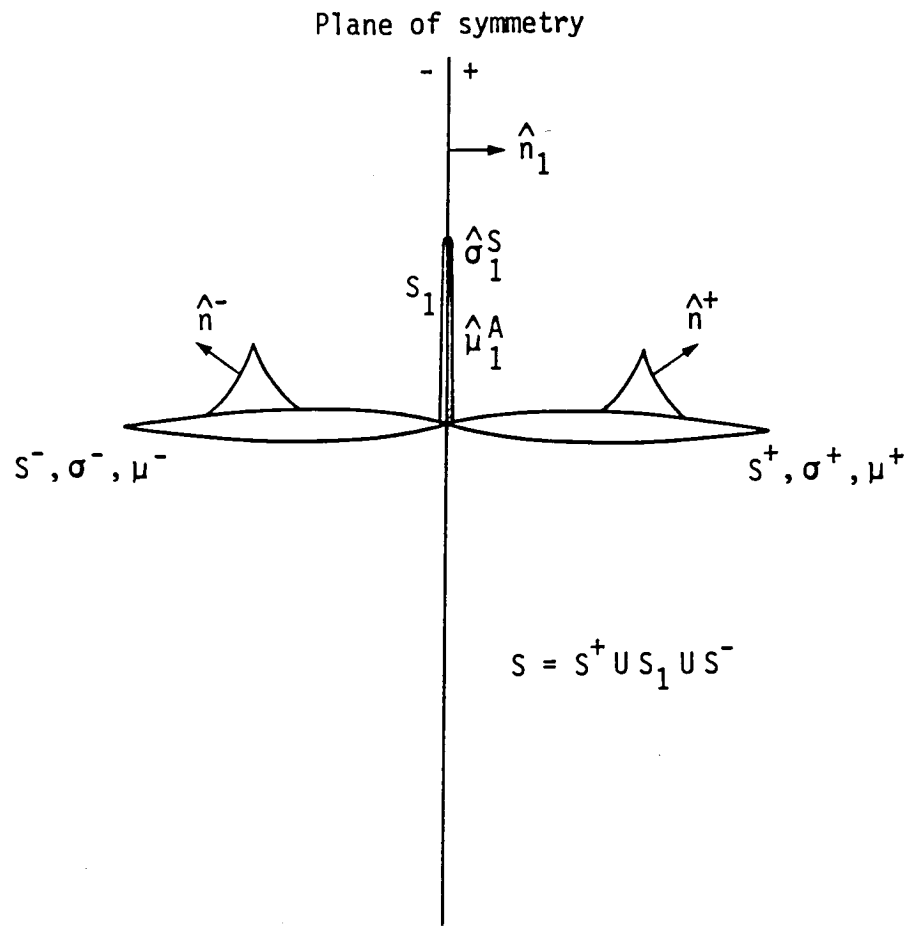

Figure K.3 - A configuration with one plane of geometric symmetry

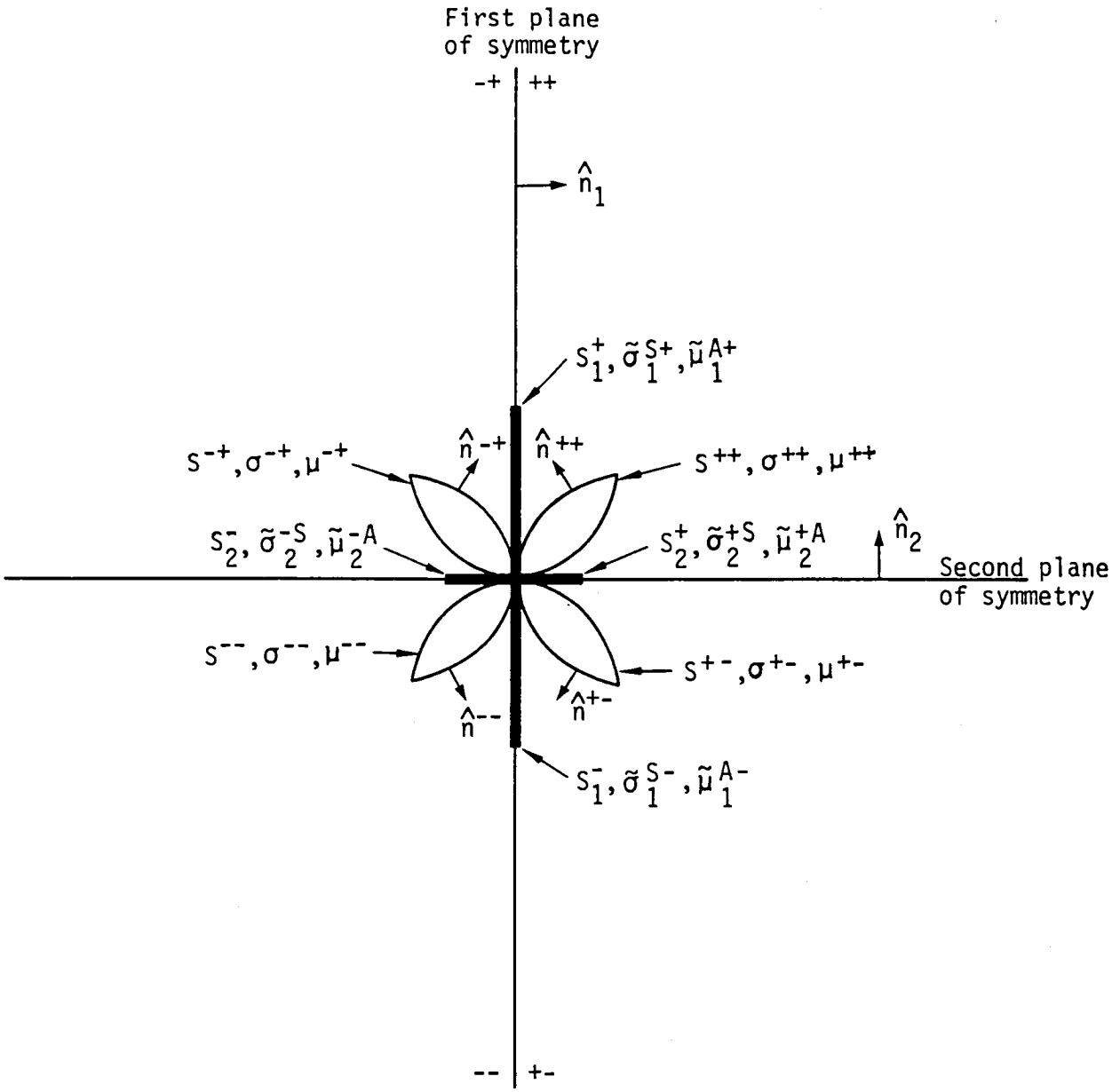

Figure K.4 - A configuration with two planes of geometric symmetry

$\underline{\underline{\Phi IC_I^S}}$

(K.3.28) $\Phi_\sigma(\vec{p},s_I) + \Phi_\sigma(R_1\vec{p},s_I) + \Phi_\mu(\vec{p},m_I) + \Phi_\mu(R_1\vec{p},m_I) + 2\Phi_{1,\sigma}(\vec{p},S_I)$

(K.5.28) $2\Phi_\sigma(\vec{p},s_I) \qquad + 2\Phi_\mu(\vec{p},m_I) \qquad + 2\Phi_{1,\sigma}(\vec{p},S_I) + \cancel{2\Phi_{1,\mu}(\vec{p},m_I)}$

$\underline{\underline{\Phi IC_I^A}}$

(K.3.28) $\Phi_\sigma(\vec{p},s_I) - \Phi_\sigma(R_1\vec{p},s_I) + \Phi_\mu(\vec{p},m_I) - \Phi_\mu(R_1\vec{p},m_I) + 2\Phi_{1,\mu}(\vec{p},m_I)$

(K.5.29) 0

$\underline{\underline{\overrightarrow{VIC_I^S}}}$

(K.3.46) $\vec{V}_\sigma(\vec{p},s_I) + R_1\vec{V}_\sigma(R_1\vec{p},s_I) + \vec{V}_\mu(\vec{p},m_I) + R_1\vec{V}_\mu(R_1\vec{p},m_I) + 2\vec{V}_{1,\sigma}(\vec{p},s_I)$

(K.5.30) $\vec{V}_\sigma(\vec{p},s_I) + R_1\vec{V}_\sigma(\vec{p},s_I) + \vec{V}_\mu(\vec{p},m_I) + R_1\vec{V}_\mu(\vec{p},m_I) + 2(I-\hat{n}_1\hat{n}_1^T)\,\vec{V}_{1,\sigma}(\vec{p},s_I) + \cancel{2(I-\hat{n}_1\hat{n}_1^T)\,\vec{V}_{1,\mu}(\vec{p},m_I)}$

$\underline{\underline{\overrightarrow{VIC_I^A}}}$

(K.3.46) $\vec{V}_\sigma(\vec{p},S_I) - R_1\vec{V}_\sigma(R_1\vec{p},S_I) + \vec{V}_\mu(\vec{p},m_I) - R_1\vec{V}_\mu(R_1\vec{p},m_I) + 2\vec{V}_{1,\mu}(\vec{p},m_I)$

(K.5.31) $\vec{V}_\sigma(\vec{p},S_I) - R_1\vec{V}_\sigma(\vec{p},S_I) + \vec{V}_\mu(\vec{p},m_I) - R_1\vec{V}_\mu(\vec{p},m_I) + \cancel{2\hat{n}_1\hat{n}_1^T\,\vec{V}_{1,\sigma}(\vec{p},S_I)} + 2\hat{n}_1\hat{n}_1^T\,\vec{V}_{1,\mu}(\vec{p},m_I)$

Figure K.5 - Comparison of AIC formula obtained using (K.3.28), (K.3.46) with (K.5.28-31) when $\vec{p} \in S_1$

(a)

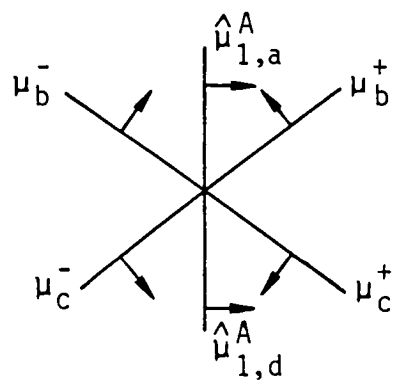

$$\hat{\mu}^{A}_{1,a} - (\mu^{+}_{b} - \mu^{-}_{b}) + (\mu^{+}_{c} - \mu^{-}_{c}) - \hat{\mu}^{A}_{1,d} = 0$$

or

$$\hat{\mu}^{A}_{1,a} - \hat{\mu}^{A}_{b} + \hat{\mu}^{A}_{c} - \hat{\mu}^{A}_{1,d} = 0$$

(b)

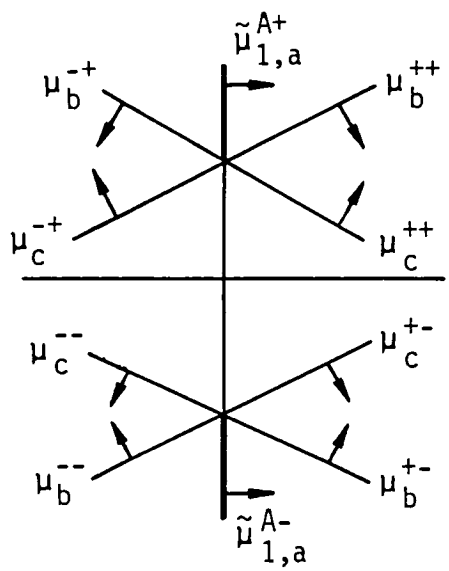

$$\tilde{\mu}^{Aj}_{1,a} + (\mu^{+j}_{b} - \mu^{-j}_{b}) - (\mu^{+j}_{c} - \mu^{-j}_{c}) = 0$$

Symmetrizing with $H^{j\ell}$,

$$\hat{\mu}^{A\ell}_{1,a} + \hat{\mu}^{A\ell}_{b} - \hat{\mu}^{A\ell}_{c} = 0$$

(c)

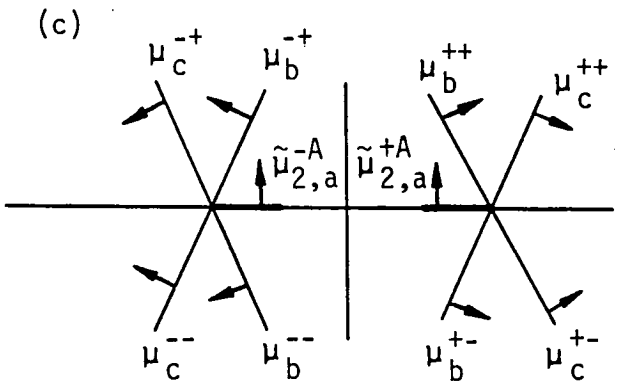

$$\tilde{\mu}^{iA}_{2,1} + (\mu^{i+}_{b} - \mu^{i-}_{b}) + (\mu^{i+}_{c} - \mu^{i-}_{c}) = 0$$

Symmetrizing with H^{ki}

$$\hat{\mu}^{kA}_{2,a} + \hat{\mu}^{kA}_{b} + \hat{\mu}^{kA}_{c} = 0$$

Figure K.6 - Four cases of an abutment lying on a plane of symmetry

(d)

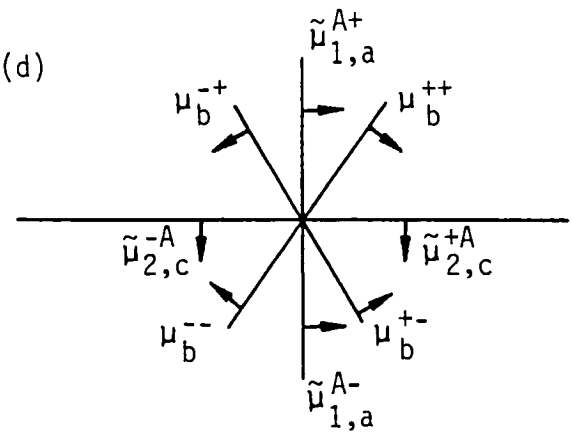

$$\tilde{\mu}_{1,a}^{A+} - \tilde{\mu}_{1,a}^{A-}$$

$$+(\mu_b^{++} - \mu_b^{+-} + \mu_{bb}^{--} - \mu_b^{-+})$$

$$+(\tilde{\mu}_{2,c}^{+A} - \tilde{\mu}_{2,c}^{-A}) = 0$$

Simplifying,

$$\hat{\mu}_{1,a}^{AA} + \hat{\mu}_b^{AA} + \hat{\mu}_{2,c}^{AA} = 0$$

Figure K.6 - Continued

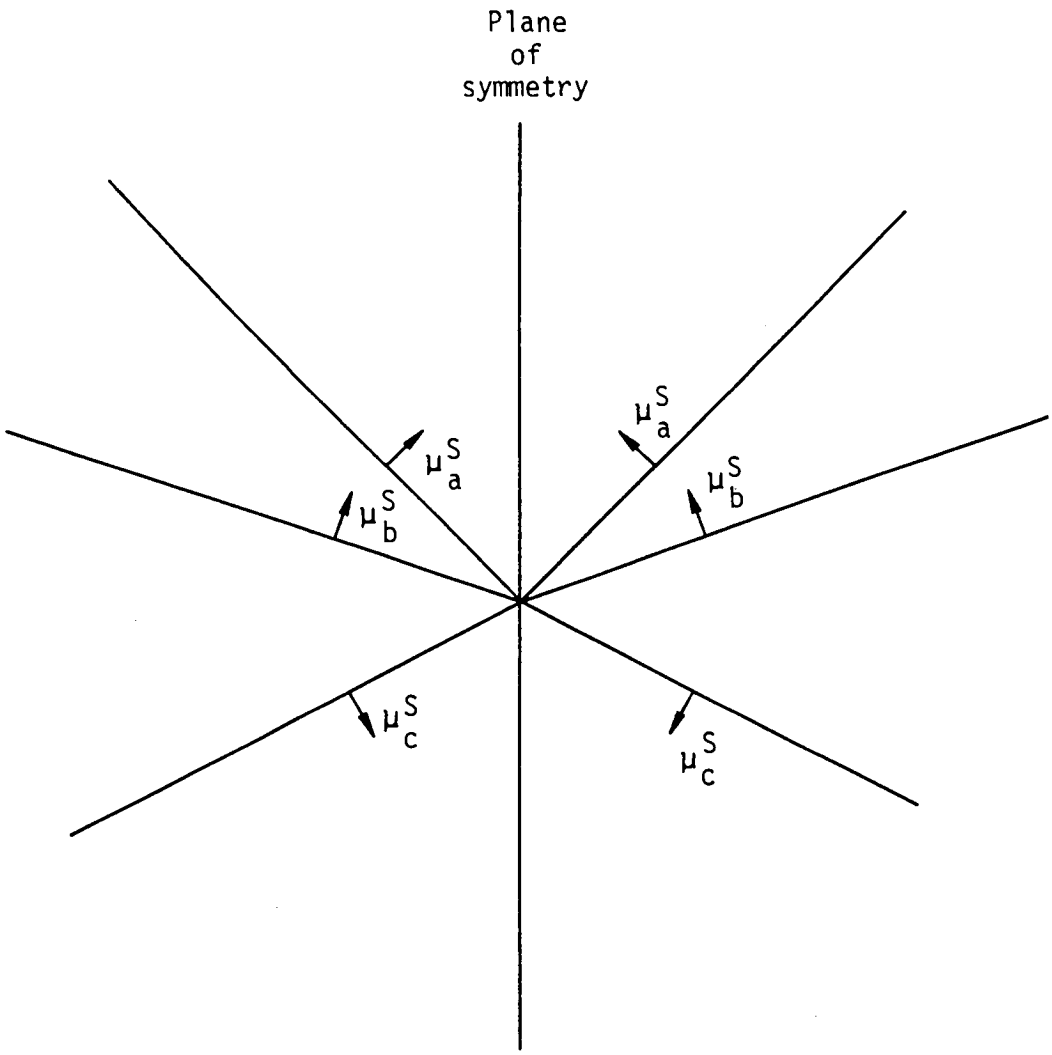

Doublet matching: $-\mu_a^S - \mu_b^S + \mu_c^S - \mu_c^S + \mu_b^S + \mu_a^S = 0$

Figure K.7 - Doublet matching for $\hat{\phi}^S$ at a plane of symmetry

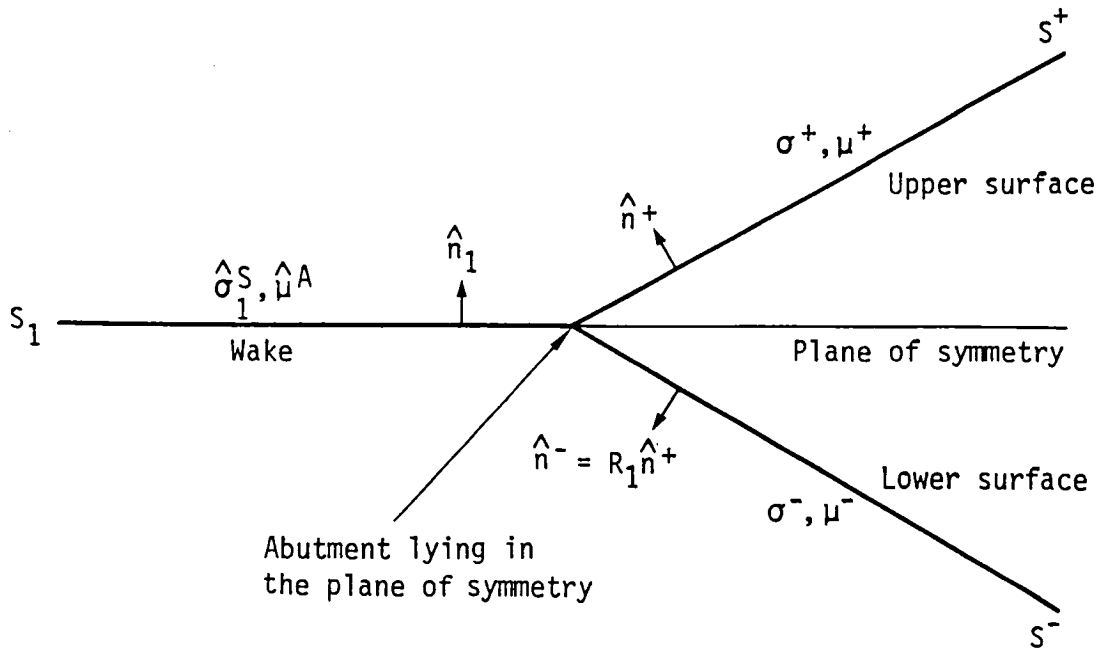

Antisymmetric Matching:

$$(+1)\left[\hat{\sigma}^A \hat{n}^+ / (\hat{n},\vec{\nu})_+ + \nabla_t \hat{\mu}^A\right]$$

$$(-1)\left[\nabla_t \hat{\mu}_1^A\right] = 0$$

Symmetric Matching:

$$(+1)\left[\hat{\sigma}^S \hat{n}^+ / (\hat{n},\vec{\nu})_+ + \nabla_t \hat{\mu}^S\right]$$

$$(-1)\left[\hat{\sigma}_1^S \hat{n}_1 / (\hat{n},\vec{\nu})_1\right] = 0$$

Figure K.8 - Velocity jump matching on a network lying on a plane of symmetry

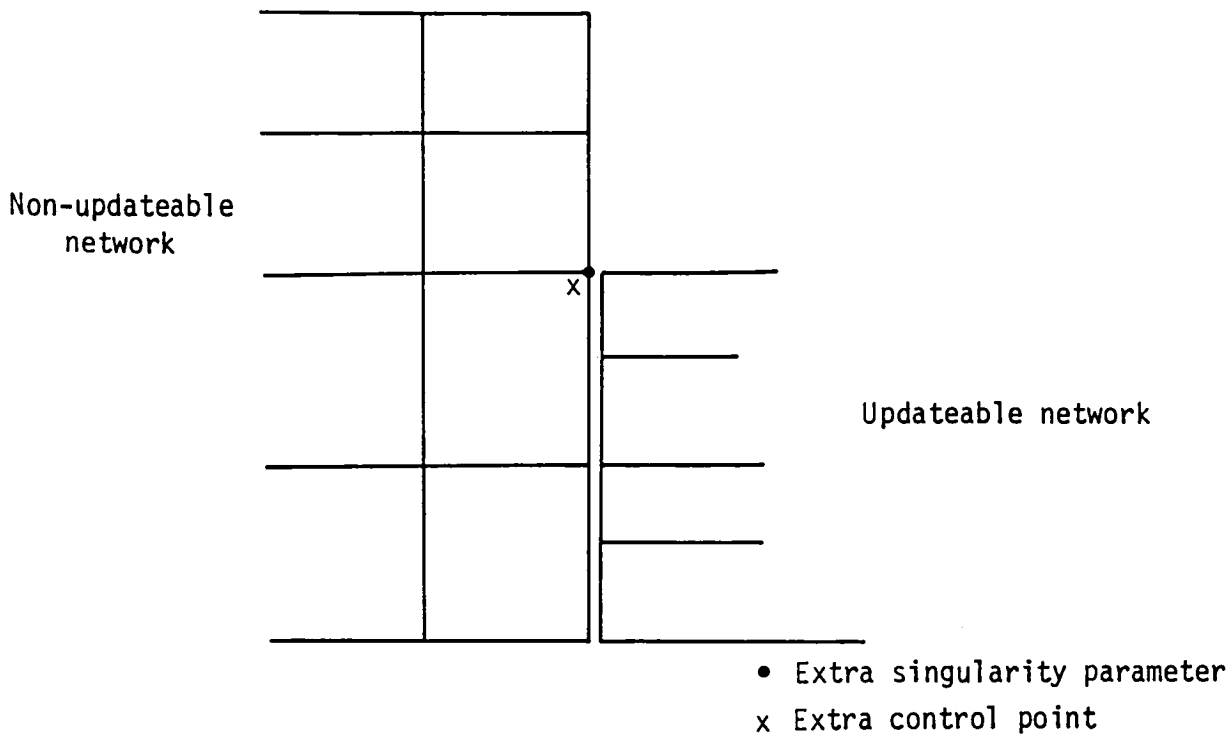

Figure K.9 - Extra singularity parameter and control point dependent on existence of updateable network

L.0 The Constraint Matrix

In this section we describe the theory underlying the activities of the programs RMS and RHS in the PAN AIR system. The basic function of this pair of programs is to organize and execute the calculation of the symmetrized singularity vectors $\hat{\lambda}_\alpha^{ij}$ that satisfy AIC constraint equations of the form (we assume two planes of symmetry)

$$[AIC^{ij}]\ \{\hat{\lambda}_\alpha^{ij}\} = \{\hat{b}_\alpha^{ij}\} \tag{L.0.1}$$

In this equation the pair of indices (i,j) corresponds to one of four possible symmetry conditions (cf. the definition of $\hat{\phi}^{ij}$ in appendix K.4) while the index α is a solution index. That is, α is associated with a particular choice of onset flow. The four major topics associated with the treatment of equation (L.0.1) are listed below:

(1) The calculation of the matrix $[AIC^{ij}]$. This calculation process must deal with the complexities introduced by considerations of symmetry, by configuration updatability and by the distinction between "known" and "unknown" singularity parameters.

(2) The calculation of the constraint vectors $\{\hat{b}_\alpha^{ij}\}$.

(3) The solution of the linear system of equations, (L.0.1).

(4) The desymmetrization of the vectors $\hat{\lambda}_\alpha^{ij}$ to obtain the singularity vectors $\vec{\lambda}_\alpha^{ij}$ associated with symmetry image (i,j) and the onset flow with index α.

Of these four topics, the first has been treated in Section 5.7 and in much more detail, in appendix K. In particular, the details of symmetry were discussed in sections K.2 through K.6 while configuration updatability was discussed in section K.7. The exploitation of the computational efficiencies associated with the distinction between known and unknown singularity parameters was discussed in section 5.7. See especially equation (5.7.12). The remaining three topics are discussed in the following three subsections of this appendix.

L.1 Calculation of Constraint Vectors

In Section H.3 we have discussed in detail the automatic options for the calculation of the onset flow. In general, the onset flow defines all of the non-zero entries of the constraint vector $\hat{b}_\alpha^{ij}$. In the case where there is no configuration symmetry and only one onset flow (solution) is specified, an entry of the constraint vector has the form (cf. eqn. (H.3.25))

$$\beta = b(\vec{p}) = b_o - b_n \vec{U}_o.\hat{n} - b_T \vec{U}_o.\vec{t}_T - \frac{b_p}{s\beta^2}[\vec{U}_\infty,\vec{p}] \qquad (L.1.1)$$

where b_o, b_n, b_T, $\hat{t}_T$ and b_p are user specified, $\vec{U}_\infty$ is the uniform onset flow and $\vec{U}_o$ is the total onset flow

$$\vec{U}_o = \vec{U}_o(\vec{p}) = \vec{U}_\infty + \Delta\vec{U}(\vec{p}) + \vec{\omega} \times (\vec{p}-\vec{p}_o) \qquad (L.1.2)$$

with $\Delta\vec{U}$, $\vec{\omega}$ and $\vec{p}_o$ also being specified by the user. For a configuration that has configuration symmetry as well as multiple onset flows, we need to define β_α^{ij}, the entry in the constraint vector associated with onset flow α and control point image $\vec{p}^{ij}$. Using the notation of appendix K.2 and K.3 for R^{ij} we write

$$\beta_\alpha^{ij} = b_\alpha^{ij}(\vec{p}^{ij}) = b_{o,\alpha} - b_n \vec{U}_{o,\alpha}^{ij}(\vec{p}^{ij}).R^{ij}\hat{n} - b_T \vec{U}_{o,\alpha}^{ij}(\vec{p}^{ij}).R^{ij}\vec{t}_T - \frac{b_p}{s\beta^2}[\vec{U}_{\infty,\alpha}, \vec{p}^{ij}] \qquad (L.1.3)$$

where $b_{o,\alpha}$, b_n, b_T, $\vec{t}_T$ and b_p are user specified as before, $\vec{U}_{\infty,\alpha}$ is the uniform onset flow for solution α and $\vec{U}_{o,\alpha}^{ij}$ is given by

$$\vec{U}_{o,\alpha}^{ij}(\vec{p}^{ij}) = \vec{U}_{\infty,\alpha} + \Delta\vec{U}_\alpha^{ij}(\vec{p}^{ij}) + \vec{\omega}_\alpha \times (\vec{p}^{ij} - \vec{p}_o) \qquad (L.1.4)$$

Here again, $\vec{U}_{\infty,\alpha}$, $\Delta\vec{U}_\alpha^{ij}$ and $\vec{\omega}_\alpha$ are user specified. Having computed β_α^{ij}, the corresponding entry $\hat{\beta}_\alpha^{ij}$ of the constraint vector $\hat{b}_\alpha^{ij}$ is computed according to the rules developed in sections K.3 and K.6. For a control point that does not lie in any plane of symmetry we have (cf. equation (K.6.11) with appropriate modifications)

$$\hat{\beta}_{\alpha}^{ij} = \sum_{k=\mp 1} \sum_{\ell=\mp 1} H^{ik} H^{j\ell} \beta_{\alpha}^{k\ell} \qquad \text{(L.1.5)}$$

For control points lying in a plane of symmetry the situation is more complicated and is summarized by the two tables below. Notice that for a control point lying in the first (resp. second) plane of symmetry, the false image quantities $\beta_{\alpha}^{-\ell}$ (resp. β_{α}^{k-}) are neither needed nor used.

Symmetry Condition (i,j)	Boundary Condition of Symmetric Type [S]	Boundary Condition of Antisymmetric Type [A]
(+1,+1) (S,S)	$\sum_{\ell} H^{+\ell}\beta_{\alpha}^{+\ell}$	0
(-1,+1) (A,S)	0	$\sum_{\ell} H^{+\ell} \beta_{\alpha}^{+\ell}$
(-1,-1) (A,A)	0	$\sum_{\ell} H^{-\ell} \beta_{\alpha}^{+\ell}$
(+1,-1) (S,A)	$\sum_{\ell} H^{-\ell} \beta_{\alpha}^{+\ell}$	0

Table L-1: Control point lies in 1st plane of symmetry: Evaluation of $\hat{\beta}_{\alpha}^{ij}$

Symmetry Condition (i,j)	Boundery Condition of Symmetry type [S]	Boundary Condition of Antisymmetric Type [A]
(+1,+1) (S,S)	$\sum_k H^{+k} \beta_\alpha^{k+}$	0
(-1,+1) (A,S)	$\sum_k H^{-k} \beta_\alpha^{k+}$	0
(-1,-1) (A,A)	0	$\sum_k H^{-k} \beta_\alpha^{k+}$
(+1,-1) (S,A)	0	$\sum_k H^{+k} \beta_\alpha^{k+}$

Table L-2: Control point lies in 2nd plane of symmetry: Evaluation of $\hat{\beta}_\alpha^{ij}$

For configurations with just one plane of symmetry the corresponding table is substantially simpler and is given as follows:

Symmetry Condition (i)	Boundary Condition of Symmetric Type [S]	Boundary Condition of Antisymmetric Type [A]
(+1)(S)	β_α^{+}	0
(-1)(A)	0	β_α^{+}

Table L-3: Control point lies in a plane of symmetry: Calculation of $\hat{\beta}_\alpha^{i}$ when there is one plane of symmetry

The zeros appearing in all of these three tables are just the zero values that appear on the right hand side of a degenerate boundary condition.

L.2 The Solution of a Linear System of Equations

The process by which PAN AIR solves a linear system of equations of the form (L.0.1) will be more clearly explained if we suppress the indices (i,j) and α and consider the standard linear system of the form

$$A \vec{x} = \vec{b} \tag{L.2.1}$$

where A is an NxN AIC matrix, $\vec{x}$ is a singularity vector and $\vec{b}$ is a constraint vector. Now since most problems of aerodynamic interest result in the matrix A being too large to fit in the main memory of the computer, it was found necessary to develop an out of core linear equation solver for PAN AIR. The basic operation of this solver proceeds as follows.

First the matrix A is divided up into rectangular blocks as follows:

$$A = \begin{bmatrix} A_{11} & A_{12} & \cdot & \cdot & \cdot & A_{1n} \\ A_{21} & A_{22} & \cdot & \cdot & \cdot & A_{2n} \\ \cdot & \cdot & & & & \cdot \\ \cdot & \cdot & & & & \cdot \\ \cdot & \cdot & & & & \cdot \\ A_{n1} & A_{n2} & \cdot & \cdot & \cdot & A_{nn} \end{bmatrix} \tag{L.2.2}$$

where the rectangular components of A are of the form

$$\text{block } (i,j) \text{ of } A = A_{ij} = p_i \times p_j \text{ matrix} \tag{L.2.3}$$

Here the matrix partition dimensions $\{p_i\}_{i=1}^{n}$ satisfy

$$\sum_{i=1}^{n} p_i = N, \text{ the dimension of } A \tag{L.2.4}$$

Having partitioned A as shown by (L.2.2), one can conceptually describe the operation of the PAN AIR solver as performing a sequence of transformations of the form listed below with the result that matrix $A^{(nn)}$ is lower triangular. (The calculation of the transformation matrices T_{ij} is described below in detail by equations (L.2.13-18).)

$$
\left.\begin{array}{l}
A^{(1,1)} = A\,T_{1,1} \\[2ex]
A^{(1,2)} = A^{(1,1)}T_{1,2} \\
\quad\vdots \\
A^{(1,n)} = A^{(1,n-1)}T_{1,n}
\end{array}\right\}
\quad \begin{array}{l}\text{transformations } T_{1,j} \\ j = 1, \ldots n\end{array}
$$

- - - - - - - - - - - - - - -

$$
\left.\begin{array}{l}
A^{(2,2)} = A^{(1,n)}T_{2,2} \\[2ex]
A^{(2,3)} = A^{(2,2)}T_{2,3} \\
\quad\vdots \\
A^{(2,n)} = A^{(2,n-1)}T_{2,n}
\end{array}\right\}
\quad \text{transformations } T_{2,j}
$$

- - - - - - - - - - - - - - -

$\vdots \quad \vdots$

- - - - - - - - - - - - - - -

$$
\left.\begin{array}{l}
A^{(n-1,n-1)} = A^{(n-2,n)}T_{n-1,n-1} \\[2ex]
A^{(n-1,n)} = A^{(n-1,n-1)}T_{n-1,n}
\end{array}\right\}
\quad \text{transformations } T_{n-1,j}
$$

- - - - - - - - - - - - - - -

$$
\left.\begin{array}{l}
A^{(n,n)} = A^{(n-1,n)}T_{n,n}
\end{array}\right\}
\quad T_{n,n}
$$

(L.2.5)

It is worth emphasizing here that the transformations T_{ij} are NxN matrices, and not submatrices of any larger matrix T. If we aggregate the relations of (L.2.5) together and denote the lower triangular matrix $A^{(n,n)}$ by L, we obtain

$$L = A(T_{11}\ T_{12} \ldots T_{1n})(T_{22}\ T_{23} \ldots T_{2n})\ldots(T_{n-1,n-1}\ T_{n-1,n})(T_{nn})$$

(L.2.6)

We note in passing that the intermediate matrix $A^{(i,j)}$ has the partially upper triangular structure:

$$A^{(i,j)} = \begin{array}{c} \left[\begin{array}{cccccccccccc} L & 0 & & . & & . & & . & & . & & 0 \\ X & L & 0 & & & & & & & & & \\ X & X & L & 0 & . & . & . & 0 & & . & & 0 \\ . & & & & & & & & & & & \\ . & & & & & & & & & & & \\ X & X & X & . & . & . & L & 0 & 0 & 0 & 0 & 0 \\ X & X & X & . & . & . & X & L & 0 & 0 & X & X \\ X & X & X & . & . & . & X & X & X & X & X & X \\ . & . & . & & & & . & . & . & & & . \\ . & . & . & & & & . & . & . & & & . \\ . & . & . & & & & . & . & . & & & . \\ X & X & X & . & . & . & X & X & X & \underbrace{X}_{\uparrow} & \underbrace{X}_{\uparrow} & X \end{array}\right] \begin{array}{l} \\ \\ \\ \\ \\ \\ \}\leftarrow \text{row block } i \\ \\ \\ \\ \\ \\ \end{array} \\ \text{column block } j \quad j+1 \end{array} \tag{L.2.7}$$

The operation

$$A^{(i,j+1)} = A^{(i,j)}\, T_{i,j+1} \tag{L.2.8}$$

will then serve to introduce zeros into block (i,j+1) of $A^{(i,j+1)}$. An alternative and convenient way of viewing the sequence of transformations (L.2.5) is expressed with the help of the replacement symbol (←) by the pidgin Algol,

```
for i = 1, 2, ... n
    for j = i, i+1, ... n
        A ← A T_ij [A . T_ij replaces A]
    end j
end i
```

(L.2.9)

Before proceeding further with the discussion of the operations of (L.2.5) we briefly describe how the transformation process expressed by (L.2.6) allows us to solve (L.2.1). Letting $\vec{y}$ satisfy,

$$L\,\vec{y} = \vec{b} \tag{L.2.10}$$

observe that $\vec{x}$ defined by

$$\vec{x} = (T_{11}\ T_{12} \ldots T_{1n})(T_{22} \ldots T_{2n}) \ldots (T_{n-1,n-1}\ T_{n-1,n})(T_{nn})\vec{y} \tag{L.2.11}$$

satisfies

$$A\vec{x} = A[(T_{11}\ldots T_{nn})\vec{y}] = [A(T_{11}\ldots T_{nn})]\vec{y} = L\,\vec{y} = \vec{b} \tag{L.2.12}$$

Returning now to the process described by (L.2.9), we observe that T_{ij} must introduce zeros into block (i,j) of the working array A. (Notice that here and throughout the rest of this section we use the notation A to denote the current contents of a working array. This working array is further partitioned as indicated by (L.2.2)). The transformation T_{ij} consists of a product of interchanges and elementary transformations of the form

$$T_{ij} = (P_1U_1)(P_2U_2)\ \ldots\ (P_{p_i}\ U_{p_i}). \tag{L.2.13}$$

The pivot matrix P_k is either the identity matrix or else it is used to interchange column k in the i-th block of columns with column q_k in the jth block of columns, where q_k is defined by the condition

$$[\text{case } (i=j)]\ \ |\ (A_{ii})_{k,q_k}\ | = \max_{k\le\ell\le p_i}\ |\ (A_{ii})_{k,\ell}\ | \tag{L.2.14a}$$

$$[\text{case } (i\neq j)]\ \ |\ (A_{ij})_{k,q_k}\ | = \max_{1\le\ell\le p_j}\ |\ (A_{ij})_{k,\ell}\ | \tag{L.2.14b}$$

The matrix U_k is an elementary column transformation designed to introduce zeros into row k of block (i,j) of A. It is given as follows

<u>Case i=j</u>

$$U_k\ (\text{for } T_{ii}) = \begin{array}{c} \\ \\ \\ \\ \\ (i) \\ \\ \\ \end{array} \begin{array}{c} (i) \\ \begin{bmatrix} I & & & & & & & \\ & I & & & & & & \\ & & \cdot & & & & & \\ & & & \cdot & & & & \\ & & & & I & & & \\ & & & & & V_k & & \\ & & & & & & I & \\ & & & & & & & \cdot \\ & & & & & & & & I \end{bmatrix} \end{array}$$

where

$$V_k = \begin{bmatrix} 1 & & & & & & & \\ & \ddots & & & & & & \\ & & \ddots & & & & & \\ & & & 1 & m_{k+1} & m_{k+2} & \cdots & m_{p_i} \\ & & & & 1 & & & \\ & & & & & \ddots & & \\ & & & & & & \ddots & \\ & & & & & & & 1 \end{bmatrix} \quad \leftarrow \text{row } k$$

$$m_\ell = -(A_{ii})_{k,\ell}/(A_{ii})_{k,k} \qquad \ell = k+1, \ldots, p_i$$

<u>Case $i \neq j$</u>

$$U_k \text{ (for } T_{ij}) = \begin{array}{c} \\ \\ \\ (i) \\ \\ \\ (j) \\ \\ \\ \end{array} \begin{array}{c} \begin{array}{cc} (i) & (j) \end{array} \\ \begin{bmatrix} I & & & & & & \\ & \ddots & & & & & \\ & & I & V_k & & & \\ & & & \ddots & & & \\ & & & & I & & \\ & & & & & \ddots & \\ & & & & & & I \end{bmatrix} \end{array}$$

where

$$V_k = \begin{bmatrix} & 0 & & \\ v_{k,1} & v_{k,2} & \cdots & v_{k,p_j} \\ & 0 & & \end{bmatrix} \quad \leftarrow \text{row } k$$

$$v_{k,\ell} = -(A_{ij})_{k\ell}/(A_{ii})_{kk} \qquad \ell = 1, \ldots p_j \tag{L.2.16}$$

The selection of the pivot matrices P_k deserves further comment. In order to best maintain numerical stability it would be desirable to choose P_k according to the classical pivoting strategy

$$P_k = \begin{cases} I & \text{if } |(A_{ii})_{kk}| > |(A_{ij})_{k,q_k}| \\ \text{interchange of column } k \text{ of column block } i \text{ with column } q_k \text{ of column block } j \text{ if the inequality does not hold} \end{cases} \tag{L.2.17}$$

In the case that $i \neq j$, such a stringent pivoting strategy is not necessary and could significantly increase the I-O costs associated with the solution process. In order to keep the I-O costs down while still preserving numerical stability, the following "threshold pivoting strategy" is used when $(i \neq j)$:

$$P_k = \begin{cases} I & \text{if } |(A_{ii})_{kk}| > \mu\, |(A_{ij})_{k,q_k}| \\ \text{interchange of column } k \text{ of column block } i \text{ with column } q_k \text{ of column block } j \text{ if the inequality does not hold} \end{cases} \tag{L.2.18}$$

In PAN AIR the parameter μ that controls pivoting has been set equal to (.2).

Now while the foregoing discussion is an accurate presentation of the mathematics underlying PAN AIR's out-of-core solution package, it is somewhat incomplete in that the question of algorithmic organization has not been fully addressed. We now remedy that deficiency.

In the algorithm to be given presently we use the notation

$$(A_{ki}, A_{kj})\ T_{ij} \ : \ [\text{Apply } T_{ij} \text{ in row block } k] \tag{L.2.19}$$

to indicate that the effect of transformation T_{ij} upon block row k is to be computed. This is a natural notation since T_{ij} acts on block column (i) and block column (j). In a similar spirit we use the notation

$$(A_{ki})\ T_{ii} \ : \ [\text{Apply } T_{ii} \text{ to block row } k] \tag{L.2.20}$$

to indicate that T_{ii} is to be applied in block row k to the subarray A_{ki}. Given this statement of notation, we can now state the reduction algorithm.

Algorithm: Out-of-Core Factorization of A

for k = 1, 2, ... n do

<Part A: Perform Crout Style eliminations>

Perform the following indicated transformations (for k=1, do nothing)

$\{(A_{ki},A_{kk})T_{ik}\}_{i=1}^{k-1}$ $\{(A_{ki}, A_{k,k+1})T_{i,k+1}\}_{i=1}^{k-1}$ ... $\{(A_{ki},A_{kn})T_{in}\}_{i=1}^{k-1}$

$\{(A_{k+1,i},A_{k+1,k})T_{ik}\}_{i=1}^{k-1}$

$\vdots$

$\{(A_{k+2,i},A_{k+2,k})T_{ik}\}_{i=1}^{k-1}$

$\vdots$

$\{(A_{n,i},A_{n,k})T_{ik}\}_{i=1}^{k-1}$

<Part B: Generate New Factors, Apply T_{kk}>

Form T_{kj}, j=k,k+1,...,n while performing the following transformations

$(A_{kk})T_{kk}$ $(A_{k,k},A_{k,k+1})T_{k,k+1}$ ... $(A_{k,k},A_{k,n})T_{k,n}$

Apply T_{kk} in block column k

$(A_{k+1,k})T_{kk}$

$(A_{k+2,k})T_{kk}$

$\vdots$

$(A_{n,k})T_{kk}$

end k

A few remarks are in order concerning this algorithm. When in part A we perform a set of transformations of the form

$$\{(A_{ki}, A_{kq})T_{iq}\}_{i=1}^{k-1} \tag{L.2.21}$$

the algorithm proceeds as follows

Read A_{kq}

for i = 1,..., k-1 do

Read A_{ki}

Read T_{iq}

Perform $(A_{ki}, A_{kq})T_{iq}$

Conditional write A_{ki}

[If T_{iq} involves any interblock interchanges, the array A_{ki} has been modified and must be rewritten]

end i

write A_{kq}

This particular organization is very effective at minimizing disk I-O. In a similar fashion, the sequence of operations

$$\{(A_{pi}, A_{pk})T_{ik}\}_{i=1}^{k-1} \tag{L.2.22}$$

is implemented via the following sequence of operations:

Read A_{pk}

for i = 1,...,k-1 do

Read A_{pi}

Read T_{ik}

Perform $(A_{pi}, A_{pk})T_{ik}$

Conditional write A_{pi}

end i

Write A_{pk}

The volume of I-O performed by this algorithm when it is carefully coded satisfies the following bounds, where we assume that all n partition dimensions p_i are equal size: ($p_i = b$).

$$\frac{2}{3}\, n\, (n^2+6n+2)b^2 \;\le\; \begin{bmatrix}\text{number of words of}\\ \text{disk input-output}\end{bmatrix} \;\le\; n(n^2+\frac{7}{2}\, n+\frac{1}{2})b^2 \qquad \text{(L.2.23)}$$

Since the total dimension of the matrix A is given by

$$\dim(A) = N = n \,.\, b$$

we see that A has $N^2 = n^2b^2$ elements. Thus, the total I-O volume lies roughly between 2n/3 and n times the volume of I-O required to read the matrix A. It should be noted the lower bound in (L.2.23) is attained if <u>no</u> interblock pivotting is performed (as would happen if we set $\mu = 0$ in (L.2.18)) while the upper bound is attained if interblock pivotting is performed by every transformation T_{ij}, $i \neq j$.

The skeptical reader may perhaps doubt that this out-of-core factorization algorithm actually generates and applies the transformations T_{ij} in such an order that the mathematical development presented earlier is correctly realized. To help convince such suspicious individuals I have provided in figure L.1 a complete list of all the transformation processes, in the order they are performed, for the case n=5. In figure L.2 is provided a diagram indicating the precise stage of the algorithm at which T_{ij} is applied to an appropriate pair of arrays (A_{ki}, A_{kj}). The careful reader will study these figures, meditate a while, and, after a day or two of quiet obsession, will convince himself that the algorithm really does work. I leave it at that: a complete proof of the algorithm's correctness is beyond my endurance, and probably beyond the endurance of the reader as well.

L.3 Desymmetrization of Singularity Parameters

In this section we describe and comment upon the process of desymmetrizing the singularity parameters $\{\hat{\lambda}_\alpha^{ij}\}$ that are obtained by solving equation (L.0.1). Suppressing, for the purpose of this discussion, the solution index α, we rewrite equation (L.0.1) for the case of just one plane of symmetry as

$$[AIC^i]\ \{\hat{\lambda}^i\} = \{\hat{b}^i\} \tag{L.3.1}$$

Denoting the J-th entry of $\{\hat{\lambda}^i\}$ by $\hat{\lambda}_J^i$ we observe from equations (K.3.26) and (K.3.27) that this symmetrized singularity parameter must be related to the corresponding principal image singularity parameter λ_J^+ and the reflected image singularity parameter λ_J^- by the relation

$$\hat{\lambda}_J^i = \sum_k H^{ik}\ \lambda_J^k \tag{L.3.2}$$

This relation is trivial to invert (see equation (K.3.21), the definition of H^{ik}). Doing this, we find

$$\lambda_J^i = (\tfrac{1}{2}) \sum_k H^{ik}\ \hat{\lambda}_J^k \tag{L.3.3}$$

Now it is clear that the singularity vectors $\{\lambda_J^+\}$ and $\{\lambda_J^-\}$ must determine respectively singularity distributions on S^+ (the principal image) and S^- (the reflected image) of the configuration.

These distributions are given explicitly by the formulas (compare with equations (3.3.1-2))

$$\sigma^+(\vec{p}) = \sum_{J=1}^{N} \lambda_J^+\ s_J(\vec{p}) \qquad \vec{p} \in S^+ \tag{L.3.4a}$$

$$\sigma^-(\vec{p}) = \sum_{J=1}^{N} \lambda_J^-\ s_J(R_1\vec{p}) \qquad \vec{p} \in S^- \tag{L.3.4b}$$

$$\mu^+(\vec{p}) = \sum_{J=1}^{N} \lambda_J^+\ m_J(\vec{p}) \qquad \vec{p} \in S^+ \tag{L.3.5a}$$

$$\mu^-(\vec{p}) = \sum_{J=1}^{N} \lambda_J^-\ m_J(R_1\vec{p}) \qquad \vec{p} \in S^- \tag{L.3.5b}$$

What is not immediately clear is how the singularity distributions are determined on S_1, that part of the configuration lying on the plane of symmetry. While it is clear that equations (L.3.4a) and (L.3.4b) can be evaluated at points $\vec{p} \in S_1$, it turns out that when this is done, we obtain (1/2) of the correct values for the singularity strengths.

To demonstrate this result, we begin by recalling the development of section K.3 that states that for networks lying on the plane of symmetry,

$$\sigma \text{ (restricted to the plane of symmetry)} = \hat{\sigma}_1^S \tag{L.3.6}$$

$$\mu \text{ (restricted to the plane of symmetry)} = \hat{\mu}_1^A \tag{L.3.7}$$

and (cf. equations (K.3.53) and (K.3.54))

$$\hat{\sigma}_1^{\ A} = 0 \tag{L.3.8}$$

$$\hat{\mu}_1^{\ S} = 0 \tag{L.3.9}$$

Consequently we find that when J is an index of a source parameter lying on S_1 we obtain from equation (L.3.3) the result,

$$\begin{aligned} \text{source parameter } \lambda_J^+ \text{ on } S_1 &= (\tfrac{1}{2}) \sum H^{+k} \hat{\lambda}_J^k \\ &= (\tfrac{1}{2}) \left[\hat{\lambda}_J^S + \hat{\lambda}_J^A\right] \\ &= (\tfrac{1}{2}) \hat{\lambda}_J^S \qquad \text{(using (L.3.8))} \\ &= (\tfrac{1}{2}) \hat{\sigma}_1^S (\vec{r}_J) \end{aligned} \tag{L.3.10}$$

where $\vec{r}_J$ is the location of $\hat{\lambda}_J^+$ on S_1. A very similar calculation shows that for <u>doublet</u> parameters lying on S_1, we obtain (using (L.3.9)) the result -

$$\text{doublet parameter } \lambda_J^+ \text{ on } S_1 = (\tfrac{1}{2}) \hat{\mu}_1^A (\vec{r}_J) \tag{L.3.11}$$

A close inspection of equations (L.3.10) and (L.3.11) together with equations (L.3.6-7) shows that the functions $\sigma^{+}(\vec{p})$ and $\mu^{+}(\vec{p})$ (defined by (L.3.4-5)) will yield (1/2) of the correct value of the source and doublet strength when evaluated at $\vec{p} \in S_1$. This is the general result we seek that tells us how to interpret the result of the desymmetrizing relation (L.3.3).

The case of two planes of symmetry is not much more difficult. In place of the relation (L.3.2) we have (compare with (K.4.22))

$$\hat{\lambda}_I^{ij} = \sum_k \sum_\ell H^{ik} H^{jl} \lambda_J^{kl} \tag{L.3.12}$$

As before, this is trivial to invert. This time we obtain,

$$\lambda_J^{ij} = (\tfrac{1}{4}) \sum_k \sum_\ell H^{ik} H^{jl} \hat{\lambda}_J^{kl} \tag{L.3.13}$$

Defining the singularity distributions $\sigma^{ij}(\vec{p})$, $\mu^{ij}(\vec{p})$ for the various symmetry images by the equations

$$\sigma^{ij}(\vec{p}) = \sum_{J=1}^{N} \lambda_J^{ij} s_J (R^{ij} \vec{p}) \qquad \vec{p} \in S^{ij} \tag{L.3.14}$$

$$\mu^{ij}(\vec{p}) = \sum_{J=1}^{N} \lambda_J^{ij} m_J (R^{ij} \vec{p}) \qquad \vec{p} \in S^{ij} \tag{L.3.15}$$

we are again confronted with the problem of interpretting these relations for points lying on the planes of symmetry. By means of the same sort of argument as we used in the case of one plane of symmetry, we obtain the following results

$$\sigma^{+j}(\vec{p}) = \frac{1}{2}\sigma \text{ (evaluated at } \vec{p} \in S_1{}^j)$$

$$\mu^{+j}(\vec{p}) = \frac{1}{2}\mu \text{ (evaluated at } \vec{p} \in S_1{}^j)$$

$$\sigma^{i+}(\vec{p}) = \frac{1}{2}\sigma \text{ (evaluated at } \vec{p} \in S_2{}^i)$$

$$\mu^{i+}(\vec{p}) = \frac{1}{2}\mu \text{ (evaluated at } \vec{p} \in S_2{}^i) \tag{L.3.16}$$

As a general rule, then, we find that for networks lying on a plane of symmetry, the values of the singularity distributions obtained by using the functions

$$\sigma^{+}, \mu^{+}$$

or

$$\sigma^{+j}, \mu^{+j}, \sigma^{i+}, \mu^{i+}$$

should be doubled in order to obtain the singularity strengths on such networks. This action is in fact performed by PAN AIR.

A1: k=1, part A: no-op

B1: k=1, part B: Form T_{ij}, j=1(1)5; then apply T_{11} in column 1

$(A_{11})T_{11}$ $(A_{11},A_{12})T_{12}$ $(A_{11},A_{13})T_{13}$ $(A_{11},A_{14})T_{14}$ $(A_{11},A_{15})T_{15}$

$(A_{21})T_{11}$

$(A_{31})T_{11}$

$(A_{41})T_{11}$

$(A_{51})T_{11}$

A2: k=2, part A: Perform elimination in block row 2, block column 2

$(A_{21},A_{22})T_{12}$ $(A_{21},A_{23})T_{13}$ $(A_{21},A_{24})T_{14}$ $(A_{21},A_{25})T_{15}$

$(A_{31},A_{32})T_{12}$

$(A_{41},A_{42})T_{12}$

$(A_{51},A_{52})T_{12}$

B2: k=2, part B: Form T_{2j} j = 2(1)5; then apply T_{22} in column 2

$(A_{22})T_{22}$ $(A_{22},A_{23})T_{23}$ $(A_{22},A_{24})T_{24}$ $(A_{22},A_{25})T_{25}$

$(A_{32})T_{22}$

$(A_{42})T_{22}$

$(A_{52})T_{22}$

A3: k=3, part A: Perform elimination in block row 3, block column 3

$$\begin{Bmatrix}(A_{31},A_{33})T_{13}\\(A_{32},A_{33})T_{23}\end{Bmatrix}\begin{Bmatrix}(A_{31},A_{34})T_{14}\\(A_{32},A_{34})T_{24}\end{Bmatrix}\begin{Bmatrix}(A_{31},A_{35})T_{15}\\(A_{32},A_{35})T_{25}\end{Bmatrix}$$

$$\begin{Bmatrix}(A_{41},A_{43})T_{13}\\(A_{42},A_{43})T_{23}\end{Bmatrix}$$

$$\begin{Bmatrix}(A_{51},A_{53})T_{13}\\(A_{52},A_{53})T_{23}\end{Bmatrix}$$

Figure L.1 Order of Transformation Application for the case n=5 (page 1 of 2)

B3:k=3, part B: Form T_{3j}, j=3(1)5; then apply T_{33} in column 3

$$(A_{33})T_{33} \qquad (A_{33},A_{34})T_{34} \qquad (A_{33},A_{35})T_{35}$$

$$(A_{43})T_{33}$$

$$(A_{53})T_{33}$$

A4:k=4, part A: Perform elimination in block column 4, block row 4

$$\begin{Bmatrix} (A_{41},A_{44})T_{14} \\ (A_{42},A_{44})T_{24} \\ (A_{43},A_{44})T_{34} \end{Bmatrix} \begin{Bmatrix} (A_{41},A_{45})T_{15} \\ (A_{42},A_{45})T_{25} \\ (A_{43},A_{45})T_{35} \end{Bmatrix}$$

$$\begin{Bmatrix} (A_{51},A_{54})T_{14} \\ (A_{52},A_{54})T_{24} \\ (A_{53},A_{54})T_{34} \end{Bmatrix}$$

B4:k=4, part B: Form T_{44}, T_{45}; then apply T_{44} in column 4

$$(A_{44})T_{44} \qquad (A_{44},A_{45})T_{45}$$

$$(A_{54})T_{44}$$

A5:k=5, part A: Perform elimination on A_{55}

$$\begin{Bmatrix} (A_{51},A_{55})T_{15} \\ (A_{52},A_{55})T_{25} \\ (A_{53},A_{55})T_{35} \\ (A_{54},A_{55})T_{45} \end{Bmatrix}$$

B5:k=5, part B: Form T_{55}

$$(A_{55})T_{55}$$

Figure L.1 Order of Transformation Application for the case n=5 (Page 2 of 2)

T_{11}	T_{12}	T_{13}	T_{14}	T_{15}
R.... B1	AP... B1	A.P.. B1	A..P. B1	W...P B1
P.... B1	CP... A2	C.P.. A2	C..P. A2	C...P A2
P.... B1	CP... A2	C.R.. A3	C..R. A3	C...R A3
P.... B1	CP... A2	C.R.. A3	C..R. A4	C...R A4
P.... B1	CP... A2	C.R.. A3	C..R. A4	C...R A5

T_{22}	T_{23}	T_{24}	T_{25}
.....	.....	.....	.....
.R... B2	.AP.. B2	.A.P. B2	.W..P B2
.P... B2	.CW.. A3	.C.W. A3	.C..W A3
.P... B2	.CW.. A3	.C.A. A4	.C..A A4
.P... B2	.WW.. A3	.C.A. A4	.C..A A5

T_{33}	T_{34}	T_{35}
.....	.....	.....
.....	.....	.....
..R.. B3	..AP. B3	..W.P B3
..P.. B3	..CW. A4	..C.W A4
..P.. B3	..CW. A4	..C.A A5

T_{44}	T_{45}
.....	.....
.....	.....
.....	.....
...R. B4	...WP B4
...P. B4	...CW A5

T_{55}
.....
.....
.....
.....
....P B5

Symbols

R = item read
W = item written
A = item is available in memory
P = item is both read and written
C = item is read, and written if interblock transfers have occurred

This indicates that the operation $(A_{53},A_{54})T_{34}$ is performed during stage A4 of the algorithm. At the end of this step, A_{54} is written out and A_{53} is written out if any inter-block transfers have happened.

Figure L.2 Diagram Describing the Application of T_{ij} to Various Subarrays of the Working Array $A = [A_{ij} ; i,j = 1(1)5]$

M.0 Computation of the Minimal Data Set

It is desirable that the solution of the potential flow problem (that is, the combination of the Prandtl-Glauert equation with a set of boundary conditions) be distilled into the smallest possible amount of data, yet still be readily convertible to data of aerodynamic interest. This smallest amount of data is called the minimal data set, and consists of the average potential and normal component of mass flux, source strength, and doublet strength at each control point and each grid point on the configuration. Each of these items exists for each solution, that is, for each column $\vec{\lambda}_i$ of the solution matrix $[\Lambda]$ (cf. (L.0.1)). In our discussion here, we will assume we are dealing with only one solution, even though the program deals with blocks of solutions.

Under certain circumstances, an additional vector is added to the minimal data set. This vector is the average velocity, as computed from the velocity influence coefficient matrix. This occurs when the standard spline method of velocity computation (called the "boundary condition method" for simplicity; see section B.4.1 of the User's Manual), which computes the velocity from the potential and normal mass flux, is of insufficient accuracy for the purposes of the program user.

M.1 Recovery of the Singularity Parameters

The recovery of the singularity parameters for the various symmetry images of the configuration (i.e., S^{++}, S^{-+}, S^{+-} and S^{--}) has been treated in detail in section L.3. In this section we merely restate those results using the notation and terminology used by MDG and the post processing modules of PAN AIR.

In MDG, the various symmetry conditions are denoted by the names listed in the tables below.

Case: 1 plane of symmetry

$\hat{\phi}^S$ = 1st symmetry condition, $S^+ = S^{(1)}$ = 1st image

$\hat{\phi}^A$ = 2nd symmetry condition, $S^- = S^{(2)}$ = 2nd image

Case: 2 planes of symmetry

$\hat{\phi}^{SS}$ = 1st symmetry condition $S^{++} = S^{(1)}$ = 1st image

$\hat{\phi}^{AS}$ = 2nd symmetry condition $S^{-+} = S^{(2)}$ = 2nd image

$\hat{\phi}^{AA}$ = 3rd symmetry condition $S^{--} = S^{(3)}$ = 3rd image

$\hat{\phi}^{SA}$ = 4th symmetry condition $S^{+-} = S^{(4)}$ = 4th image

Having listed these correspondences, we can give the singularity parameter vectors $\vec{\lambda}^{(k)}$ for the two (or possibly four) images of the configuration. In terms of quantities λ_J^i and λ_J^{ij} defined in section L.3. We have:

Case: 1 plane of symmetry

1st image $\vec{\lambda} = \vec{\lambda}^{(1)} = [\lambda_J^+] = \frac{1}{2}(\hat{\lambda}^S + \hat{\lambda}^A)$

2nd image $\vec{\lambda} = \vec{\lambda}^{(2)} = [\lambda_J^-] = \frac{1}{2}(\hat{\lambda}^S + \hat{\lambda}^A)$

Case: 2 planes of symmetry

1st image $\vec{\lambda} = \vec{\lambda}^{(1)} = [\lambda_J^{++}] = \frac{1}{4}(\hat{\lambda}^{SS} + \hat{\lambda}^{AS} + \hat{\lambda}^{AA} + \hat{\lambda}^{SA})$

2nd image $\vec{\lambda} = \vec{\lambda}^{(2)} = [\lambda_J^{-+}] = \frac{1}{4}(\hat{\lambda}^{SS} - \hat{\lambda}^{AS} - \hat{\lambda}^{AA} + \hat{\lambda}^{SA})$

3rd image $\vec{\lambda} = \vec{\lambda}^{(3)} = [\lambda_J^{--}] = \frac{1}{4}(\hat{\lambda}^{SS} - \hat{\lambda}^{AS} + \hat{\lambda}^{AA} - \hat{\lambda}^{SA})$

4th image $\vec{\lambda} = \vec{\lambda}^{(4)} = [\lambda_J^{+-}] = \frac{1}{4}(\hat{\lambda}^{SS} + \hat{\lambda}^{AS} - \hat{\lambda}^{AA} - \hat{\lambda}^{SA})$

Given the vectors $\vec{\lambda}^{(k)}$, the singularity strengths can be directly evaluated on the various images of the configuration. This process is completely straightforward unless a network lies on a plane of symmetry. The following tables summarize the treatment of that situation for the various cases that arise. Notice that the straightforward procedure generates (1/2) of the singularity strengths for networks lying on a plane of symmetry. This result is more fully explained in appendix L.3.

Notation

P_1 (P_2) = first (second) plane of symmetry

N_1 (N_2) = a network lying on the first (second) plane of symmetry

N_1^+ (N_2^+) = same as N_1 (N_2). (Principal images).

N_1^- (N_2^-) = the reflection N_1 (N_2) in the second (first) plane of symmetry. (Reflected images).

Case: 1 plane of symmetry

N_1 : Use $\vec{\lambda}^{(1)}$, obtain $\sigma/2$ and $\mu/2$

Case: 2 planes of symmetry

N_1^+ : Use $\vec{\lambda}^{(1)}$, obtain $\sigma/2$ and $\mu/2$

N_1^- : Use $\vec{\lambda}^{(4)}$, obtain $\sigma/2$ and $\mu/2$

N_2^+ : Use $\vec{\lambda}^{(1)}$, obtain $\sigma/2$ and $\mu/2$

N_2^- : Use $\vec{\lambda}^{(2)}$, obtain $\sigma/2$ and $\mu/2$

M.2 Singularity Strength Calculation

Obtaining the source and doublet strength at a control point or grid point P, with local coordinates (ξ', η'), from the vector of singularity parameters, has in fact already been described. If the source and doublet subpanel spline and outer spline matrices for the subpanel and panel on which the control point lies are $SPSPL^S$, $SPSPL^D$, B^S, and B^D respectively, then by (5.6.2) and (K.3.11)

$$\sigma(P) = \lfloor 1 \quad \xi' \quad \eta' \rfloor \, [SPSPL^S] \, [B^S] \begin{Bmatrix} \lambda_1^S \\ \cdot \\ \cdot \\ \cdot \\ \lambda_9^S \end{Bmatrix} \tag{M.2.1}$$

and

$$\mu(P) = \lfloor 1 \quad \xi' \quad \eta' \quad 1/2\,\xi'^2 \quad \xi'\eta' \quad 1/2\,\eta'^2 \rfloor \, [SPSPL^D] \, [B^D] \begin{Bmatrix} \lambda_1^D \\ \cdot \\ \cdot \\ \cdot \\ \lambda_{21}^D \end{Bmatrix} \tag{M.2.2}$$

Here, λ_i^S and λ_i^D are the source and doublet parameters in the neighborhood of the panel, and are entries of $\vec{\lambda}$.

M.3 Computation of Potential and Normal Mass Flux

Three approaches to the computation of potential and normal mass flux at control points are described in section 5.9. One is the multiplication of the influence coefficient matrices by the vector of singularity parameters (cf. (5.9.1)). The second makes use of the boundary conditions to obtain ϕ_A from μ and $\vec{w}_A \cdot \hat{n}$ from σ. For instance, suppose the boundary conditions

$$\phi_L = 0 \tag{M.3.1}$$

$$\sigma = -\vec{V}_\infty \cdot \hat{n} \tag{M.3.2}$$

are imposed.

The specification of (M.3.1) insures perturbation stagnation in the configuration interior. Thus

$$\phi_L = 0 \tag{M.3.3}$$

So,

$$\vec{\nabla}\phi_L \cdot \tilde{n} = \vec{w}_L \cdot \hat{n} = 0 \tag{M.3.4}$$

Combining (M.3.2) and (M.3.4),

$$\vec{w}_A \cdot \hat{n} = 1/2\ (\vec{w}_u \cdot \hat{n} + \vec{w}_L \cdot \hat{n}) = 1/2\ \vec{w}_u \cdot \hat{n}$$

$$= 1/2\ (\vec{w}_u \cdot \hat{n} - \vec{w}_L \cdot \hat{n}) = 1/2\ \sigma \tag{M.3.5}$$

Similarly,

$$\phi_A = 1/2\ \mu \tag{M.3.6}$$

Thus both average normal mass flux and average potential may be obtained directly from the singularity strength.

We note that (M.3.6) follows directly from (M.3.1), while (M.3.5) only holds when both (M.3.1) and (M.3.2) are imposed. The average normal mass flux can however be computed directly from the boundary conditions in other circumstances as well. For instance, if the boundary condition

$$\vec{w}_u \cdot \hat{n} = b \tag{M.3.7}$$

is imposed, then it follows from the definitions of source strength and average normal mass flux that

$$\vec{w}_A \cdot \hat{n} = 1/2\ (\vec{w}_u \cdot \hat{n} + \vec{w}_L \cdot \hat{n}) = \vec{w}_u \cdot \hat{n} - 1/2\ (\vec{w}_u \cdot \hat{n} - \vec{w}_L \cdot \hat{n})$$

$$= b - 1/2\ \sigma \tag{M.3.8}$$

Once average potential and normal mass flux have been computed at control points, they may be computed at grid points by a splining method virtually identical to the method used to construct the doublet spline vector SP^D which defines the doublet strength at a grid point as a linear combination of

surrounding doublet parameters. The spline vector SP^D consists of a row of an outer spline matrix B^D (cf., section I.1). That is, if P is one of the nine "panel defining points", then the spline vector SP^D corresponding to P is defined by

$$\mu\ (P) = \lfloor SP^D \rfloor^{1xk} \begin{Bmatrix} \lambda_1^D \\ \vdots \\ \lambda_k^D \end{Bmatrix} \qquad k \leq 12 \tag{M.3.9}$$

where the λ_i^D are the doublet parameters located in the neighborhood of the grid point.

Similarly, a "potential spline" row vector $\lfloor SP^P \rfloor$ is computed such that

$$\lfloor \phi_A\ (P) \quad \vec{w}_A(P) \cdot \hat{n} \rfloor = \lfloor SP^P \quad (1xk) \rfloor \begin{bmatrix} \phi_1 & (\vec{w}_A \cdot \hat{n})_1 \\ \vdots & \vdots \\ \phi_k & (\vec{w}_A \cdot \hat{n})_k \end{bmatrix}^{kx2} \tag{M.3.10}$$

where ϕ_i and $(\vec{w}_A \cdot \hat{n})_i$ are average potential and normal mass flux at the neighboring control points, rather than singularity parameter locations. The row vector SP^P is computed by the same least squares method as the row vector SP^D, but the choice of the set of surrounding control points is slightly different from the choice of surrounding singularity parameters, as illustrated in figure M.1.

In particular, the potential at grid points on a network edge depends on control points in the interior of the network. An "edge spline" can not be used because the edge control points are receded from the network edge, while singularity parameters are not.

Whenever the program computes the velocity at control points by the influence coefficient method, the same potential spline vectors may be used to define an average velocity vector at each grid point P by

$$\{\vec{v}_A\ (P)\}^T = \lfloor SP^P \rfloor\ (1xk) \cdot \begin{Bmatrix} \{\vec{v}_{A,1}\}^T \\ \vdots \\ \{\vec{v}_{A,k}\}^T \end{Bmatrix}^{(kx3)} \tag{M.3.11}$$

where $\vec{v}_{A,i}$ is the average velocity, computed by the influence coefficient method, at the ith control point in the neighborhood of P.

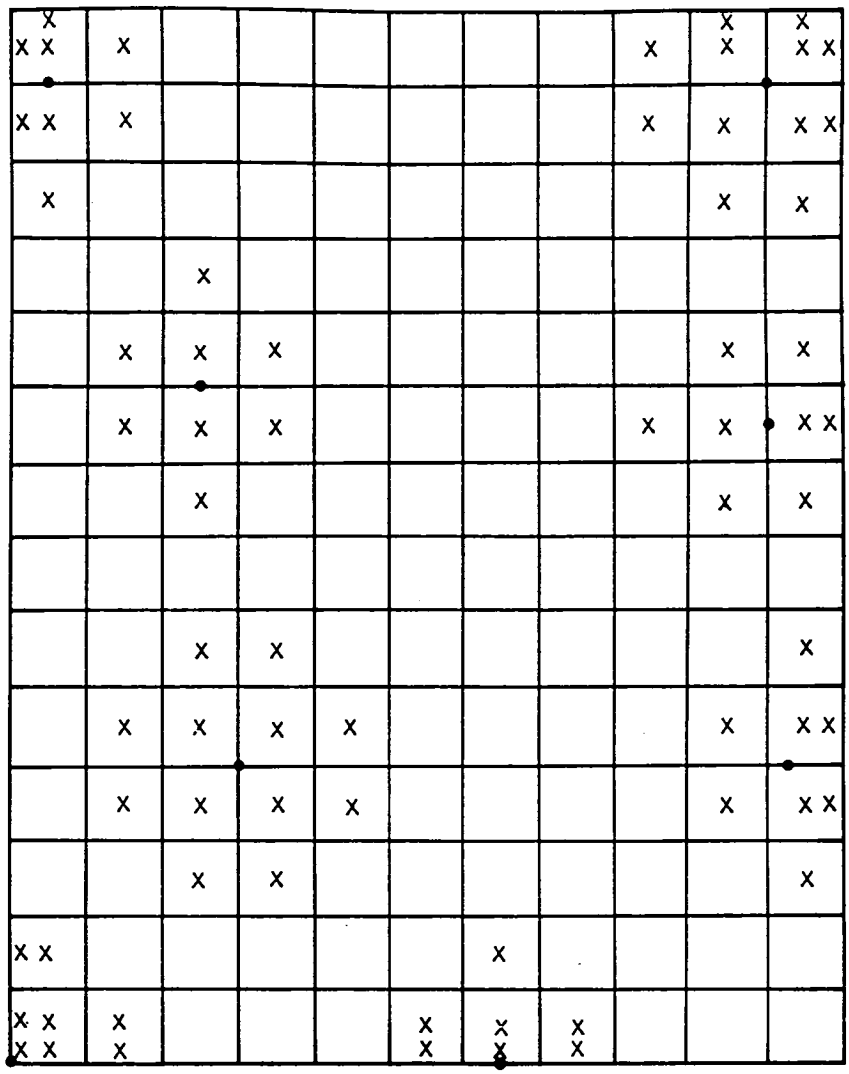

• grid point

x neighboring control points

Figure M.1 - Neighboring control points for potential spline computation

N.0 Surface and Wake Flow Properties

With the construction of the minimal data set, the potential flow solution is complete. The items in the minimial data set, however, are not generally of great aerodynamic interest. Of more interest are the velocity and pressure at points in the configuration. In section N.1, the computation of velocity from the elements of the minimal data set is discussed. In section N.2 the computation of pressure from velocity is discussed. In section N.3, two semi-empirical velocity correction formulas are discussed. These are of use where the magnitude of the total velocity is significantly less than freestream. In section N.4, the effect of a non-uniform onset flow on pressure coefficient formulas is considered. Finally, in section N.5, we define the additional quantities computed by PAN AIR at points on the configuration surface.

N.1 Velocity Computation

The splining method defines a distribution of potential on the configuration surface, with this distribution being defined by a single quadratic function on each subpanel. This distribution, when differentiated, defines the tangential component of the velocity. On the other hand, the normal mass flux, equal to the conormal component of the velocity, is also known. From these two components, we may reconstruct the entire velocity vector.

First, assume the distribution of potential on a subpanel is given by

$$\phi = \phi_S \; (\xi' , \eta') \tag{N.1.1}$$

where (ξ',η') are the subpanel local coordinates, and the subscript emphasizes that this is a distribution on the configuration surface.

Now, applying (K.3.15)

$$\begin{Bmatrix} \partial\phi_S/\partial x_0 \\ \partial\phi_S/\partial x_0 \\ \partial\phi_S/\partial z_0 \end{Bmatrix} = \vec{\nabla}\phi_S = [A^T] \begin{Bmatrix} \partial\phi_S/\partial\xi' \\ \partial\phi_S/\partial\eta' \\ \partial\phi_S/\partial\zeta' \end{Bmatrix}$$

$$= [A^T] \begin{Bmatrix} \partial\phi_S/\partial\xi' \\ \partial\phi_S/\partial\eta' \\ 0 \end{Bmatrix} \tag{N.1.2}$$

where A (cf., equations (E.0.1) and (E.1.1)) sends reference coordinates to local coordinates.

Next, the tangential component of the velocity $\vec{v}$ is clearly equal to that of $\vec{\nabla}\phi$; that is; for any tangent vector $\vec{t}$,

$$\vec{t} \cdot \vec{v} = \vec{t} \cdot \vec{\nabla}\phi_S \tag{N.1.3}$$

On the other hand,

$$\tilde{n} \cdot \vec{v} = \vec{w} \cdot \hat{n} \tag{N.1.4}$$

where $\tilde{n}$ is the conormal to the surface.

Since any two linearly independent tangent vectors, along with $\tilde{n}$, form a set of three independent vectors, there is a unique vector $\vec{v}$ which satisifes

(N.1.4), and also (N.1.3) for all tangent vectors $\vec{t}$. Now, consider the expression

$$\vec{v}_o = (\vec{\nabla}\,\phi)_T - \frac{\tilde{n}\cdot(\vec{\nabla}\,\phi)_T}{\tilde{n}\cdot\hat{n}}\,\hat{n} + \frac{\vec{w}\cdot\hat{n}}{\tilde{n}\cdot\hat{n}}\,\hat{n} \tag{N.1.5}$$

where $(\vec{\nabla}\,\phi)_T$ is the tangential component of the gradient of the potential.

We see that for any tangent vector $\vec{t}$,

$$\vec{t}\cdot\vec{v}_o = \vec{t}\cdot(\vec{\nabla}\,\phi)_T \tag{N.1.6}$$

and that

$$\tilde{n}\cdot\vec{v}_o = \vec{w}\cdot\hat{n} \tag{N.1.7}$$

Thus, $\vec{v}_o$ satisfies (N.1.3-4) and so

$$\vec{v} = \vec{v}_o \tag{N.1.8}$$

Equations (N.1.5) and (N.1.8) apply equally well to average and difference velocity. That is, applying (N.1.2),

$$V_A = [A^T]\;\vec{\nabla}'\,\phi_A - \frac{\tilde{n}\cdot\{A^T\;\vec{\nabla}'\phi_A\}}{\hat{n}\cdot\tilde{n}}\,\hat{n} + \frac{\vec{w}_A\cdot\hat{n}}{\hat{n}\cdot\tilde{n}}\,\hat{n} \tag{N.1.8a}$$

$$V_D = [A^T]\,\vec{\nabla}'\mu - \frac{\tilde{n}\cdot\{A^T\,\vec{\nabla}'\,\mu\}}{\hat{n}\cdot\tilde{n}}\,\hat{n} + \frac{\sigma}{\hat{n}\cdot\tilde{n}}\,\hat{n} \tag{N.1.8b}$$

where

$$\vec{\nabla}' = \begin{Bmatrix} \partial/\partial\xi' \\ \partial/\partial n' \\ 0 \end{Bmatrix} \tag{N.1.9}$$

We note from (E.3.70) that $\tilde{n}$ is a multiple of $A^{-1}\begin{Bmatrix} 0 \\ 0 \\ 1 \end{Bmatrix}$

Thus

$$\tilde{n}\cdot(A^T\,\vec{\nabla}') = (A\tilde{n})\cdot\vec{\nabla}'$$

$$= \begin{Bmatrix} 0 \\ 0 \\ \alpha \end{Bmatrix} \cdot \begin{Bmatrix} \partial/\partial x'_1 \\ \partial/\partial x'_2 \\ 0 \end{Bmatrix} = 0 \tag{N.1.10}$$

where α is some real number.
Substituting (N.1.10) in (N.1.9)

$$\vec{v}_A = A^T(\vec{\nabla}'\phi_A) + \frac{\vec{w}_A \cdot \hat{n}}{\tilde{n}\cdot\hat{n}}\,\hat{n} \tag{N.1.11a}$$

$$\vec{v}_D = A^T(\vec{\nabla}'\mu) + \frac{\sigma}{\tilde{n}\cdot\hat{n}}\,\hat{n} \tag{N.1.11b}$$

We have thus decomposed the average and difference velocity at a surface point into tangential and normal components. In addition, we see that they can be computed from the "minimal data set" consisting of ϕ_A, w_A n, σ, and μ.

Finally, upper surface and lower surface velocities may be computed from average and difference quantities:

$$\begin{aligned} \vec{v}_U &= \vec{v}_A + 1/2\ \vec{v}_D \\ \vec{v}_L &= \vec{v}_A - 1/2\ \vec{v}_D \end{aligned} \tag{N.1.12}$$

N.2 Pressure Formulas

In this section, we assume the existence of a uniform freestream velocity $\vec{V}_\infty$, aligned with the x-direction of the compressibility coordinate system, and a perturbation velocity at a point P:

$$\vec{v}(P) = \begin{pmatrix} u \\ v \\ w \end{pmatrix} \tag{N.2.1}$$

In this section, we derive the pressure coefficient C_p at P under a variety of simplifying assumptions, thus obtaining a collection of pressure coefficient formulas.

The assumption that the freestream and compressibility directions are identical is a necessary one in order to derive the results of this section (except when the Mach number is zero). In practice, however, Pan Air does not require these directions to be identical. If the user chooses the "uniform onset flow method" of pressure computation, then all the equations of this section are applied with $\vec{V}_\infty$ replaces by the uniform onset flow $\vec{U}_\infty$ defined in Appendix H, and with the compressibility coordinate system replaced by a "wind-axis system" whose x-axis is parallel to $\vec{U}_\infty$.

In addition, Pan Air makes available a "total onset flow" method of pressure computation. This will be discussed in section N.4.

N.2.1 Preliminary Results

First, let us define the pressure coefficient as

$$C_p = \frac{p - p_\infty}{1/2\ \rho_\infty \cdot |\vec{V}_\infty|^2} \tag{N.2.2}$$

where p is pressure and ρ is density. In order to compute C_p from velocity, we need some basic results which hold for "one-dimensional" flows from Liepmann and Roshko (Ref. 1.4). A precise definition of one-dimensional flows is given there on p. 39. A tube of streamlines in a uniform fluid flow in three dimensional space, perturbed by an object of finite size, is such a flow.

The results we use are:

(a) Bernoulli's equation (2.18b in Liepmann and Roshko)

$$\frac{|\vec{V}|^2}{2} + \int \frac{dP}{\rho} = \text{constant} \tag{N.2.3}$$

where the path of integration is a streamline, and $\vec{V}$ is velocity at a point,

(b) The integrated form of Bernoulli's equation for a perfect gas (see p. 55 of Liepmann and Roshko):

$$\frac{\gamma}{\gamma - 1} \frac{P}{\rho} + 1/2 \, |\vec{V}|^2 = \frac{\gamma}{\gamma - 1} \frac{P_\infty}{\rho_\infty} + 1/2 \, |\vec{V}_\infty|^2 \qquad (N.2.4)$$

where γ is the ratio of specific heats (7/5 for a diatomic gas), and

(c) an expression for the local speed of sound (equation 2.23)

$$a^2 = \frac{\gamma P}{\rho} \qquad (N.2.5)$$

We also define the local Mach number

$$M = \frac{|\vec{V}|}{a} \qquad (N.2.6)$$

Finally, for isentropic flow in a perfect gas (cf., Liepmann and Roshko, 2.21a)

$$\frac{P}{P_\infty} = \left(\frac{\rho}{\rho_\infty}\right)^\gamma \qquad (N.2.7)$$

N.2.2 Constant Density Flow

If the density ρ may be assumed to be a constant ρ_∞ (for instance, for an incompressible fluid or at zero Mach number), then (N.2.3) reduces to

$$\frac{|\vec{V}|^2}{2} + \frac{P}{\rho_\infty} = \frac{|\vec{V}_\infty|^2}{2} + \frac{P_\infty}{\rho_\infty} \qquad (N.2.8)$$

Solving for P,

$$P = 1/2 \, \rho_\infty \left(|\vec{V}_\infty|^2 - |\vec{V}|^2 \right) + P_\infty \qquad (N.2.9)$$

and so, by (N.2.2),

$$Cp = 1 - \frac{|\vec{V}|^2}{|\vec{V}_\infty|^2} . \qquad (N.2.10)$$

N.2.3 Compressible Flow

We first apply (N.2.7) to (N.2.4) in order to eliminate ρ from the equation. It follows from (N.2.7) that

$$\rho^{-1} = \rho_\infty^{-1} \left(\frac{P}{P_\infty}\right)^{\frac{-1}{\gamma}} \tag{N.2.11}$$

Thus

$$\frac{\gamma}{\gamma-1} \left(\frac{P}{\rho}\right) = \frac{\gamma}{\gamma-1} \left(\frac{P_\infty}{\rho_\infty}\right) \left(\frac{P}{P_\infty}\right)^{\frac{\gamma-1}{\gamma}} \tag{N.2.12}$$

and so (N.2.4) becomes

$$1/2 \, |\vec{V}|^2 + \frac{\gamma}{\gamma-1} \left(\frac{P}{P_\infty}\right)^{\frac{\gamma-1}{2}} \left(\frac{P_\infty}{\rho_\infty}\right) = \frac{\gamma}{\gamma-1} \left(\frac{P_\infty}{\rho_\infty}\right) + 1/2 \, |\vec{V}_\infty|^2 \tag{N.2.13}$$

Next, we apply (N.2.5-6) to the freestream to obtain

$$a_\infty^2 = \frac{\gamma P_\infty}{\rho_\infty} = \frac{|\vec{V}_\infty|^2}{M_\infty^2} \tag{N.2.14}$$

Thus

$$1/2 \, \rho_\infty |\vec{V}_\infty|^2 = \frac{\gamma M_\infty^2 P_\infty}{2} \tag{N.2.15}$$

Substituting this into (N.2.2),

$$C_p = \frac{2}{\gamma M_\infty^2 P_\infty} (P - P_\infty) = \frac{2}{\gamma M_\infty^2} \left(\frac{P}{P_\infty} - 1\right) \tag{N.2.16}$$

The quantity P/P_∞ may be calculated by rearranging (N.2.13):

$$\left(\frac{P}{P_\infty}\right)^{\frac{\gamma-1}{\gamma}} = 1 - 1/2 \left(|\vec{V}|^2 - |\vec{V}_\infty|^2 \right) \frac{(\gamma-1)}{\gamma} \frac{\rho_\infty}{P_\infty} \qquad \text{(N.2.17)}$$

= (substituting (N.2.15))

$$1 - \frac{\gamma-1}{2} M_\infty^2 \frac{|\vec{V}|^2 - |\vec{V}_\infty|^2}{|\vec{V}_\infty|^2} \qquad \text{(N.2.18)}$$

Thus

$$\frac{P}{P_\infty} = \left[1 - \left(\frac{|\vec{V}|^2}{|\vec{V}_\infty|^2} - 1\right) \cdot \left(\frac{\gamma-1}{2}\right) \cdot M_\infty^2\right]^{\frac{\gamma}{\gamma-1}} \qquad \text{(N.2.19)}$$

Substituting this expression in (N.2.16),

$$C_p = \frac{2}{\gamma M_\infty^2} \left[1 + \frac{\gamma-1}{2} \left(1 - \frac{|\vec{V}|^2}{|\vec{V}_\infty|^2}\right) M_\infty^2\right]^{\frac{\gamma}{\gamma-1}} - 1 \qquad \text{(N.2.20)}$$

This is often called the isentropic pressure coefficient formula. In section N.2.5, we will consider certain simplifying assumptions, and the behavior of the pressure coefficient formula under these assumptions.

N.2.4 Limitations of the Formula

Under certain circumstances the velocity computed by the potential flow solution is so unrealistic that the resulting pressure coefficient is meaningless. One such case is a velocity for which the corresponding pressure coefficient is more negative than the "vacuum pressure." A second case is that of a local flow exceeding the speed of sound while the freestream flow is subsonic.

N.2.4.1 The Vacuum Pressure Coefficient

The isentropic pressure coefficient may only be evaluated if the expression in (N.2.20) which is raised to the power $\gamma/(\gamma-1)$ is non-negative. Thus the isentropic pressure coefficient reaches its minimum, or vacuum, value when this expression equals zero. So, we write

$$C_{P,vac} = \frac{-2}{\gamma M_\infty^2} \tag{N.2.21}$$

The velocity V_m for which $C_{P,vac}$ is attained is therefore given by

$$1 + \frac{\gamma-1}{2} \cdot \left(1 - \frac{|\vec{V}_m|^2}{|\vec{V}_\infty|^2}\right) M_\infty^2 = 0 \tag{N.2.22}$$

Solving,

$$\frac{|\vec{V}_m|^2}{|\vec{V}_\infty|^2} = 1 + \frac{2}{(\gamma-1) M_\infty^2} \tag{N.2.23}$$

Thus the speed

$$V_m = |\vec{V}_\infty| \left[1 + \frac{2}{(\gamma-1)M_\infty^2}\right]^{1/2} \tag{N.2.24}$$

is called the maximum speed, since for any speed in excess of V_m the vacuum pressure is exceeded.

N.2.4.2 The Critical Speed

In subsonic flow, if the magnitude of the velocity exceeds the local speed of sound, the Prandtl-Glauert equation is clearly invalid. Thus a program user may be interested to know if the "critical speed," that is, the local speed of sound, has been exceeded.

To compute the local speed of sound, we substitute (N.2.11) in (N.2.5) to

obtain

$$a^2 = \gamma P \rho_\infty^{-1} \cdot \left(\frac{P}{P_\infty}\right)^{\frac{-1}{\gamma}} \tag{N.2.25}$$

$$= \gamma \left(\frac{P}{P_\infty}\right)^{\frac{\gamma-1}{\gamma}} \frac{P_\infty}{\rho_\infty} \tag{N.2.26}$$

= (applying (N.2.5))

$$\left(\frac{P}{P_\infty}\right)^{\frac{\gamma-1}{\gamma}} \cdot a_\infty{}^2 \tag{N.2.27}$$

Thus by (N.2.19)

$$\frac{a^2}{a_\infty{}^2} = 1 - \left(\frac{\gamma-1}{2}\right) M_\infty^2 \left(\frac{|\vec{V}|^2}{|\vec{V}_\infty|^2} - 1\right) \tag{N.2.28}$$

So,

$$\text{So} \quad \frac{|\vec{V}|^2}{a^2} = \frac{|\vec{V}|^2}{|\vec{V}_\infty|^2} \cdot \frac{|\vec{V}_\infty|^2}{a_\infty{}^2} \cdot \frac{a_\infty{}^2}{a^2} =$$

$$\frac{|\vec{V}|^2 \; M_\infty^2}{\left[1 + \frac{\gamma-1}{2} \cdot M_\infty^2 \left(1 - \frac{|\vec{V}|^2}{|\vec{V}_\infty|^2}\right)\right] |\vec{V}_\infty|^2} \tag{N.2.29}$$

Defining the local Mach number

$$M_1 = \frac{|\vec{V}|}{a} \tag{N.2.30}$$

we see that the speed attains its critical value V_c if the local Mach number is 1, or if

$$(V_c)^2 M_\infty{}^2 = [1 + \frac{\gamma-1}{2} \cdot M_\infty^2 \quad (1 - \frac{(V_c)^2}{|\vec{V}_\infty|^2})] \; |\vec{V}_\infty|^2 \tag{N.2.31}$$

Solving,

$$\frac{(V_c)^2}{|\vec{V}_\infty|^2} = \frac{\gamma-1}{\gamma+1} + \frac{2}{(\gamma+1)M_\infty^2} \tag{N.2.32}$$

Applying (N.2.24),

$$V_c = (\frac{\gamma-1}{\gamma+1})^{1/2} \cdot V_m \tag{N.2.33}$$

The Pan Air user may request the program to compute the critical and maximum speeds, and the corresponding pressure coefficients.

N.2.4.3 Pressure Coefficient at the Critical Speed

Substituting (N.2.32) in (N.2.20) yields, after some algebraic manipulation, the value of the isentropic pressure coefficient at the critical speed. It is

$$C_{p,c} = \frac{2}{\gamma M^2} \left[\frac{2}{\gamma+1} + \frac{\gamma-1}{\gamma+1} \cdot M_\infty^2 \right]^{\frac{\gamma}{\gamma-1}} - 1 \tag{N.2.34}$$

N.2.5 The Isentropic Formula under Simplifying Assumptions

For complete generality, we have avoided the assumption that $|\vec{V}_\infty| = 1$. Thus we can write, in compressibility coordinates,

$$\vec{V}_\infty = \begin{pmatrix} |\vec{V}_\infty| \\ 0 \\ 0 \end{pmatrix} \tag{N.2.35}$$

$$\vec{V} = \begin{pmatrix} |\vec{V}_\infty| + u \\ v \\ w \end{pmatrix} \tag{N.2.36}$$

Thus cp is a function of u, v, and w, the components of the perturbation velocity. We now look at (N.2.20) under a variety of small perturbation assumptions.

N.2.5.1 Second Order Theory

First, let us make the assumption that cubic and higher order terms in u, v, and w may be ignored. This is called second order theory.

According to the binomial theorem,

$$(1 + \varepsilon)^{\frac{\gamma}{\gamma-1}} = 1 + \frac{\gamma}{\gamma-1} \cdot \varepsilon + 1/2 \left(\frac{\gamma}{\gamma-1}\right) \cdot \varepsilon^2$$

$$+ \text{ cubic and higher terms in } \varepsilon \qquad \text{(N.2.37)}$$

We will substitute (N.2.37) in (N.2.20) with

$$\varepsilon = \frac{\gamma-1}{2} \cdot \left(1 - \frac{|\vec{V}|^2}{|\vec{V}_\infty|^2}\right) M_\infty^2 \qquad \text{(N.2.38)}$$

$$= \frac{\gamma-1}{2} \frac{\left(1 - (|\vec{V}_\infty| + u)^2 + v^2 + w^2\right)}{|V_\infty|^2} M_\infty^2 \qquad \text{(N.2.39)}$$

$$= \frac{\gamma-1}{2} \cdot M_\infty^2 \cdot \left(\frac{-2u}{|\vec{V}_\infty|} - \frac{u^2 + v^2 + w^2}{|\vec{V}_\infty|^2}\right) \qquad \text{(N.2.40)}$$

We see that, neglecting cubic and higher order terms

$$\varepsilon^2 = \frac{(\gamma-1)^2 M_\infty^4 u^2}{|\vec{V}_\infty|^2} \qquad \text{(N.2.41)}$$

and

$$(1+\varepsilon)^{\frac{\gamma}{\gamma-1}} = 1 + \frac{\gamma}{2} M_\infty^2 \left(\frac{-2u}{|V_\infty|} - \frac{(1-M_\infty^2)u^2 + v^2\ w^2)}{|V_\infty|^2}\right) \tag{N.2.42}$$

So, neglecting cubic and higher order terms in (N.2.20),

$$C_p = \frac{2}{\gamma M^2}\left((1+\varepsilon)^{\frac{\gamma}{\gamma-1}} - 1\right) = \frac{-2u}{|\vec{V}_\infty|} - \frac{(1-M_\infty^2)u^2 + v^2 + w^2}{|\vec{V}_\infty|^2} \tag{N.2.43}$$

$$= \text{(alternatively)} \quad 1 - \frac{|\vec{V}|^2}{|\vec{V}_\infty|^2} + M_\infty^2 \frac{u^2}{|\vec{V}_\infty|^2} \tag{N.2.44}$$

This is the second order pressure coefficient formula.

Now we consider the evaluation of a number of other quantities under the assumption of neglect of cubic and higher terms. First, we see that (N.2.28) remains unchanged under the assumption, and so (N.2.29) still holds. That is, the local Mach number is still

$$M_l = \frac{\vec{V}}{|\vec{V}_\infty|} \quad \frac{M_\infty}{\left[1 + \left(\frac{\gamma-1}{2}\right) M_\infty^2 \left(1 - \frac{|\vec{V}|^2}{|\vec{V}_\infty|^2}\right)\right]^{1/2}} \tag{N.2.45}$$

Similarly, equation (N.2.24) for the maximum speed V_m and equation (N.2.33) for the critical speed still hold. To obtain $cp_{,c}$, the pressure coefficient at the critical speed, it does not suffice to substitute (N.2.32) in (N.2.44). In addition, a second order expression for $u^2/|\vec{V}_\infty|^2$ at the sonic speed must be computed.

Noting that $\frac{|\vec{V}|^2}{|\vec{V}_\infty|^2} = 1 + \frac{2u}{|\vec{V}_\infty|}$

$$+ \text{ second order terms} \tag{N.2.46}$$

and substituting in (N.2.32), we see that at the critical speed

$$1 + \frac{2u}{|\vec{V}_\infty|} + \text{higher terms} = \frac{\gamma-1}{\gamma+1} + \frac{2}{(\gamma+1)M_\infty^2} \tag{N.2.47}$$

Thus to second order

$$\frac{u^2}{|\vec{V}_\infty|^2} = 1/4 \left[\frac{\gamma-1}{\gamma+1} + \frac{2}{(\gamma+1)\, M_\infty^2} - 1\right]^2 \tag{N.2.48}$$

at the critical speed. Substituting (N.2.32) and (N.2.48) in (N.2.44) we obtain a second order expression for the critical pressure coefficient

$$C_{p,c} = 1 - \frac{\gamma-1}{\gamma+1} - \frac{2}{(\gamma+1)\, M^2} + \frac{1}{(\gamma+1)^2} \left[M_\infty{}^2 - 2 + \frac{1}{M_\infty^2}\right] \tag{N.2.49}$$

$$= \frac{1}{(\gamma^2+1)} \left(2\gamma + M_\infty^2 - \frac{(2\gamma+1)}{M_\infty^2}\right) \tag{N.2.50}$$

N.2.5.2 The Second Order Theory under Additional Assumptions

It may under certain circumstances be of interest to calculate the pressure coefficient under the additional assumption that the freestream Mach number is nearly zero, and thus terms with coefficient M may be neglected. Combining this and the second order assumption yields the "reduced second order" pressure formula (cf., (N.2.44))

$$C_p = 1 - \frac{|\vec{V}|^2}{|\vec{V}_\infty|^2} \tag{N.2.51}$$

Note that this is equivalent to the constant density or incompressible pressure formula (N.2.10). Further, if the Mach number is zero, they are both equivalent to the second order pressure formula. Finally, the reader may verify that, in the limit as Mach number approaches zero, the isentropic pressure formula (N.2.20) becomes equivalent to (N.2.51) also.

Another possible simplifying assumption is that the configuration is sufficiently slender that quadratic expressions in u may be ignored. This results in the slender body pressure formula:

$$C_p = \frac{-2u}{|\vec{V}_\infty|} - \frac{v^2 + w^2}{|\vec{V}_\infty|^2} \tag{N.2.52}$$

Finally, one may neglect all quadratic expressions in components of the perturbation, and thus obtain the linear pressure formula

$$C_p = \frac{-2u}{|\vec{V}_\infty|} \tag{N.2.53}$$

The local Mach number, the critical speed, and the pressure coefficient at the critical speed may be computed under each of these simplifying assumptions. The validity of these expressions is questionable, since the existence of a point at which the local Mach number equals 1 is evidence that the particular assumption is not valid.

N.3 Velocity Corrections

The empirical observation on which the two velocity corrections are based is that the linearized mass flux computed by a panel method under some circumstances more accurately represents the true mass flux than the computed velocity represents the true velocity. Thus a corrected velocity $\vec{V}'$ may be calculated from the computed mass flux by the equations below.

$$\frac{\rho}{\rho_\infty} V'_x = W_x \tag{N.3.1a}$$

$$V'_y = W_y \tag{N.3.1b}$$

$$V'_z = W_z \tag{N.3.1c}$$

or by

$$\frac{\rho}{\rho_\infty} \vec{V}' = \vec{W} \tag{N.3.2}$$

That is, to arrive at the first velocity correction formula,the exact relation for isentropic flow

$$\frac{\rho}{\rho_\infty} \vec{V} = \vec{W} \tag{N.3.3}$$

is applied to obtain a corrected value of the freestream or x-component of velocity. To arrive at the second velocity correction formula, equation (N.3.3) is used to obtain a corrected velocity vector which is a multiple of the mass flux vector.

N.3.1 The First Velocity Correction

This velocity correction is only applied, and in fact is only well-defined if the local flow is slower than freestream, that is, if

$$u = \frac{\vec{V} \cdot \vec{V}_\infty}{|\vec{V}_\infty|} < 0 \tag{N.3.4}$$

In that case, (N.3.1) is applied.

Now, substituting (N.2.7) in (N.2.19) we see that

$$\frac{\rho}{\rho_\infty} = \left[1 + \left(\frac{\gamma-1}{2}\right) M_\infty^2 \left(1 - \frac{|\vec{V}|^2}{|\vec{V}_\infty|^2}\right)\right]^{\frac{1}{\gamma-1}} \tag{N.3.5}$$

Thus (N.3.1a) becomes

$$W_x = \left[1 + \left(\frac{\gamma-1}{2}\right) M_\infty^2 \cdot \left(1 - \frac{|\vec{V}'|^2}{|\vec{V}_\infty|^2}\right)\right]^{\frac{1}{\gamma-1}} V'_x \tag{N.3.6}$$

It follows easily from (N.3.6) that W_x is a monotonic function of V_x. That is, as V_x increases, so does W_x. Thus a simple iterative method (Newton's method) is available for numerically computing V'_x as a function of W_x while V'_y and V'_z are obtained from (N.3.1).

N.3.2 The Second Velocity Correction

Under the second correction, the corrected velocity is some multiple of the mass flux. This correction is divided into two cases.

In the first case, we assume the local flow is again slower than freestream; that is, that (N.3.4) holds. Then (N.3.2) is applied, but using the linear density relationship

$$\frac{\rho}{\rho_\infty} = 1 + (s\beta^2 - 1) \frac{\vec{V} \cdot \vec{V}_\infty}{|\vec{V}_\infty|^2} \tag{N.3.7}$$

To see that (N.3.7) follows from (N.3.5) to first order, we apply the binomial theorem to (N.3.5), to obtain

$$\frac{\rho}{\rho_\infty} = 1 - \frac{M_\infty^2}{2} \left(\frac{\vec{V}^2}{|\vec{V}_\infty|^2} - 1\right) + \text{higher terms}$$

$$= 1 - \frac{M_\infty^2}{2} \left(\frac{2\,\vec{V} \cdot \vec{V}_\infty}{|\vec{V}_\infty|^2}\right) + \text{higher terms} \tag{N.3.8}$$

and then (N.3.7) follows from the definition $s\beta^2 = 1 - M_\infty^2$.

Thus for slower than freestream flow, the correction which is applied is

$$\vec{V}' = \frac{\vec{W}}{1 + (s\beta^2 - 1)\dfrac{\vec{V} \cdot \vec{V}_\infty}{|\vec{V}_\infty|^2}} \tag{N.3.9}$$

In the second case, the local flow is faster than freestream. That is

$$u = \frac{\vec{V} \cdot \vec{V}_\infty}{|\vec{V}_\infty|^2} > 0 \tag{N.3.10}$$

Under these circumstances, the magnitude of the velocity is left unchanged, while its direction is changed so that it is proportional to the mass flux. That is

$$\vec{V}' = \frac{|\vec{V}|}{|\vec{W}|}\,\vec{W} \tag{N.3.11}$$

where $\vec{V}$ is the uncorrected velocity computed by the program. This concludes our discussion of the velocity corrections.

N.4 Onset Flow Calculations

We now consider the effect of a non-uniform onset flow on the pressure formulas. That is, we assume that the velocity is

$$\vec{V} = \vec{v} + \vec{U}_\infty + \Delta\vec{V} \tag{N.4.1}$$

where ΔV is the "incremental onset flow" and includes both rotational onset flow and a local incremental onset flow. In the notation of appendix H,

$$\Delta\vec{V} = \vec{U}_0 - \vec{U}_\infty \tag{N.4.2}$$

Our final equations will be based on a number of simplifying assumptions, which will be discussed as they come up. The first assumption is that

$$\vec{U}_\infty = \vec{V}_\infty \tag{N.4.2b}$$

That is, the uniform onset flow must be aligned with the compressibility direction for our formulas to hold. For the remainder of this section, we will assume that (N.4.2b) holds. When the pressures are computed by the program, however, the vector $\vec{U}_\infty$ is used in place of $\vec{V}_\infty$ whether or not (N.4.2b) holds. Thus if the program user violates (N.4.2b), the resulting presssures may not be correct, nor does any correct method for computing the effect of the incremental onset flow on the pressures exist. A user may violate (N.4.2b) by setting $\alpha \neq \alpha_C$, $\beta \neq \beta_C$ (see section (B.2.2) of the User's Manual for definitions of these quantities).

N.4.1 Bernoulli's Equation

We now need to revise Bernoulli's equation (N.2.4) to account for the incremental onset flow $\Delta\vec{V}$. Both (N.2.3) and its integrated form (N.2.4) state that the total energy per unit mass (kinetic energy in the form $1/2\ |\vec{V}_\infty|^2$ plus potential energy $\gamma p/((\gamma - 1)\rho)$ is constant at any point on a streamline. Thus to correct (N.2.4) to account for the incremental onset flow we must add to the right hand side the energy per unit mass ΔE added to the system by the incremental onset flow:

$$\frac{\gamma}{\gamma-1} \cdot \frac{p}{\rho} + 1/2\ |\vec{V}|^2 = \frac{\gamma}{\gamma-1} \cdot \frac{p_\infty}{\rho_\infty} + 1/2\ |\vec{V}_\infty|^2 + \Delta E \tag{N.4.3}$$

Now, this added energy speeds up the fluid at infinity. Writing $\Delta\vec{V}_\infty$ for the incremental onset flow along the streamline infinitely far from the configuration, we have

$$1/2\ |\vec{V}_\infty|^2 + \Delta E = 1/2\ |\vec{V}_\infty + \Delta\vec{V}|^2 \tag{N.4.4}$$

Thus

$$\Delta E = \vec{V}_\infty \cdot \Delta\vec{V}_\infty + 1/2|\Delta\vec{V}_\infty|^2 \qquad (N.4.5)$$

At present there is no mechanism for the program user to specify either ΔE or , equivalently, $\Delta\vec{V}$. For many problems involving onset flow, it will be quite reasonable to make the assumption

$$\Delta\vec{V}_\infty \approx \Delta\vec{V} \qquad (N.4.6)$$

This is especially true if the control point at which the incremental onset flow is defined lies far from the source of the added energy. An example would be the analysis of an airplane flying in the onset flow generated by a second airplane. On the other hand, (N.4.6) would be highly inaccurate for a control point on an airplane wing directly behind the propeller.

Nevertheless, at present, the program assumes that (N.4.6) holds. That is, it computes ΔE by

$$2 \cdot \Delta E = 2\vec{V}_\infty \cdot \Delta\vec{V} + |\Delta\vec{V}|^2 \qquad (N.4.7)$$

We may now recompute all the equations in section N.2 using (N.4.3) in place of (N.2.4). Following the algebra of section N.2, (N.2.17) becomes

$$\left(\frac{P}{P_\infty}\right)^{\frac{\gamma-1}{\gamma}} = 1 - 1/2\left(|\vec{V}|^2 - |\vec{V}_\infty|^2 - 2\Delta E\right)\left(\frac{\gamma-1}{\gamma}\right)\cdot\frac{\rho_\infty}{P_\infty} \qquad (N.4.8)$$

N.4.2 Pressure Formulas

Similarly (N.2.20) becomes

$$C_p\text{, isentropic} = \frac{2}{\gamma M_\infty^2} \cdot \left[1 + \frac{\gamma-1}{2}\left(1 - \frac{|\vec{V}|^2 - 2\,\Delta E}{|\vec{V}_\infty|^2}\right)M_\infty^2\right]^{\frac{\gamma}{\gamma-1}} - 1 \qquad (N.4.9)$$

The vacuum pressure is still given by

$$C_{p,vac} = \frac{-2}{\gamma M_\infty^2} \qquad (N.4.10)$$

but now (N.2.22) becomes

$$1 + \frac{\gamma-1}{2}\left(1 - \frac{(V_m)^2 - 2\Delta E}{|\vec{V}_\infty|^2}\right) M_\infty^2 = 0 \qquad \text{(N.4.11)}$$

and (N.2.24) becomes

$$V_m = |\vec{V}_\infty| \left[1 + \frac{2}{(\gamma-1)M_\infty^2} + \frac{2\Delta E}{|\vec{V}_\infty|^2}\right]^{1/2} \qquad \text{(N.4.12)}$$

Next, (N.2.29) becomes

$$M_1{}^2 = \frac{|\vec{V}|^2}{a^2} = \frac{|\vec{V}|^2}{|\vec{V}_\infty|^2} \frac{M_\infty{}^2}{1 + \left(\frac{\gamma-1}{2}\right)M_\infty{}^2\left(1 - \frac{|\vec{V}|^2 - 2\Delta E}{|\vec{V}_\infty|^2}\right)} \qquad \text{(N.4.13)}$$

Setting $M_1 = 1$, the critical velocity becomes

$$\frac{V_c}{|\vec{V}_\infty|^2} = \frac{\gamma-1}{\gamma+1} + \frac{2}{(\gamma+1)M_\infty{}^2} + \frac{\gamma-1}{\gamma+1}\left(\frac{2\ E}{|\vec{V}_\infty|^2}\right) \qquad \text{(N.4.14)}$$

or (from (N.4.12))

$$V_c = \left(\frac{\gamma-1}{\gamma+1}\right) V_m \qquad \text{(N.4.15)}$$

Now, substituting (N.4.14) into (N.4.9),

$$C_{p,c} = \frac{2}{\gamma M_\infty{}^2}\left[\frac{2}{\gamma+1} + \frac{\gamma-1}{\gamma+1} M_\infty^2 \left(1 + \frac{2\ \Delta\ E}{|\vec{V}_\infty|^2}\right)\right]^{\frac{\gamma}{\gamma-1}} - 1 \qquad \text{(N.4.16)}$$

N.4.3 Simplifying Assumptions

Next, we may apply second order theory to (N.4.9), and thus we obtain

$$C_{p,2nd\ order} = 1 - \frac{|\vec{V}|^2}{|\vec{V}_\infty|^2} + \frac{2\,\Delta E}{|\vec{V}_\infty|^2} + M_\infty^2 \frac{(u + \Delta U)^2}{|\vec{V}_\infty|^2} \tag{N.4.17a}$$

where ΔU is the x-component of $\Delta\vec{V}$.

Applying equation (N.4.5-6), we then obtain

$$C_{p,2nd} = 1 - \frac{|\vec{V}|^2}{|V_\infty|^2} + \frac{2\Delta U}{|\vec{V}_\infty|} + \frac{|\Delta\vec{V}|^2}{|\vec{V}_\infty|^2} + M_\infty^2 \cdot \frac{u^2}{|\vec{V}_\infty|^2} \tag{N.4.17b}$$

Note from equation (N.4.5) that ΔE is the sum of a first order and a second order quantity. Thus if $2\Delta E$ is user-specified, it is no longer clear how to evaluate a second order expression for the pressure coefficient. One possible solution may be to use the user-specified value of $2\Delta E$ only for the computation of the isentropic pressure coefficient formula. We will not address this problem at the present time; rather, we will assume that (N.4.6) holds.

Now, to obtain a second order expression for $C_{p,c}$, we first note that by (N.4.1)

$$|\vec{V}|^2 = |\vec{v}|^2 + |\vec{V}_\infty|^2 + |\Delta\vec{V}|^2 + 2\vec{v}\cdot\Delta\vec{V} + 2\vec{v}\cdot\vec{V}_\infty + 2\,\Delta\vec{V}\cdot\vec{V}_\infty \tag{N.4.18}$$

Thus $|\vec{V}|^2 =$

$$\frac{|\vec{V}|^2}{|\vec{V}_\infty|^2} + \frac{2u}{|\vec{V}_\infty|} + 2\Delta E + \text{second order terms} \tag{N.4.19}$$

Substituting into (N.4.14) we see that at the critical speed

$$1 + \frac{2u}{|\vec{V}_\infty|} + \frac{2\,\Delta E}{|\vec{V}_\infty|^2} = \frac{\gamma-1}{\gamma+1} + \frac{2}{(\gamma+1)M^2} + \frac{\gamma-1}{\gamma+1}\left(\frac{2\Delta E}{|\vec{V}_\infty|^2}\right) \tag{N.4.20}$$

$$+ \text{ second order terms}$$

or

$$\frac{2u}{|\vec{V}_\infty|^2} = \frac{2}{(\gamma+1)}\left(1 + \frac{2\Delta E}{|\vec{V}_\infty|^2}\right) + \frac{2}{(\gamma+1)M_\infty^2} \tag{N.4.21}$$

$$+ \text{ 2nd order terms}$$

or

$$\frac{u^2}{|\vec{V}_\infty|^2} = \frac{1}{(\gamma+1)^2}\left(1 + \frac{2\Delta E}{|\vec{V}_\infty|^2} - \frac{1}{M_\infty^2}\right)^2 \tag{N.4.22}$$

at the critical speed, to second order.

Substituting (N.4.14) and (N.4.22) into (N.4.17)

$$C_{p,c,\text{2nd order}} = \frac{1}{(\gamma+1)^2} \cdot 2(\gamma + M_\infty^2) \cdot \left(1 + \frac{2\Delta E}{|\vec{V}_\infty|^2} - M_\infty{}^2 - \frac{(2\gamma+1))}{M^2}\right. \tag{N.4.23}$$

Further simplifying assumptions may be applied to (N.4.17). The "reduced second order" or small Mach number assumption yields

$$C_p = 1 - \frac{|\vec{V}|^2 - 2\Delta E}{|\vec{V}_\infty|^2} \tag{N.4.24}$$

We note from (N.4.18) that

$$1 - \frac{|\vec{V}|^2 - 2\Delta E}{|\vec{V}_\infty|^2} = \frac{-2u}{|\vec{V}_\infty|} - \frac{2\vec{v}\cdot\Delta V}{|\vec{V}_\infty|^2} + |\vec{v}|^2 \tag{N.4.25}$$

and thus the slender body assumption, applied to (N.4.17b), yields

$$C_p = \frac{-2u}{|\vec{V}_\infty|} - \frac{2(v\Delta v + w\Delta w) + v^2 + w^2}{|\vec{V}_\infty|^2} \tag{N.4.26}$$

where we again make use of (N.4.5-6), and Δv and Δw are y and z-components of $\vec{\Delta V}$.

Finally, the linear assumption yields

$$C_p = \frac{-2u}{|\vec{V}_\infty|} \tag{N.4.27}$$

N.4.4 Velocity Corrections

In the presence of an onset flow, (N.3.6) becomes

$$W_x = \left[1 + \frac{(\gamma-1)}{2}M^2 \left(1 - \frac{|\vec{V}'|^2}{|\vec{V}_\infty|^2} + \frac{2\Delta E}{|\vec{V}_\infty|^2}\right)\right]^{\frac{1}{\gamma-1}} V'_x \qquad \text{(N.4.28)}$$

and is used to solve for V'_x to obtain the first velocity correction. Also, (N.3.8) becomes

$$\frac{\rho}{\rho_\infty} = 1 + \frac{M_\infty^2}{2}\left(1 - \frac{|\vec{V}|^2}{|\vec{V}_\infty|^2} + \frac{2\Delta E}{|\vec{V}_\infty|^2}\right) + \text{higher terms} \qquad \text{(N.4.29)}$$

Applying (N.4.19),

$$\frac{\rho}{\rho_\infty} = 1 - M^2 \cdot \frac{u}{|\vec{V}_\infty|} + \text{higher terms} \qquad \text{(N.4.30)}$$

and thus (N.3.7) still holds. Thus equations (N.3.9) and (N.3.11), which define the second velocity correction, remain valid in the presence of an incremental onset flow.

This concludes our discussion of the computation of pressure coefficients in the presence of an onset flow.

It should always be remembered, however, that the presence of an onset flow violates the basic assumptions from which the Prandtl-Glauert equation was derived. In addition, the inability of the user to specify $2 \cdot \Delta E$ means that even if the potential flow solution represents the true flow well, the effect of the onset flow on the pressure may be incorrectly calculated.

N.5 Associated Data

The PAN AIR program user has a large number of options available to instruct the program in calculating flow properties at a point on the configuration surface. We discuss here the effect that certain of these options have. Some options, such as choosing a value for γ other than 7/5, are implemented in such an obvious manner that they require no discussion. Some options, such as the choice of velocity corrections, have already been discussed in detail.

One user option is a reference speed U_r for pressure calculations. This speed is then used in place of $|\vec{V}_\infty|$ whenever that quantity occurs in pressure computation formulas. This speed must be specified in the rare case that $|\vec{V}_\infty|$ is zero, that is, when there is no freestream. Otherwise the appearance of $|\vec{V}_\infty|$ in the denominator of various expressions will cause the program to terminate. The value the user chooses for U_r depends very heavily on the physics of the problem, and will not be discussed in this document.

Another user option is the "computation option for pressures." The user may choose to compute pressure using the uniform onset flow $\vec{U}_\infty$, in which case, the formulas of the previous sections are applied with $\vec{U}_\infty$ substituted for $\vec{V}_\infty$. Second, he may choose to compute pressures using the compressibility vector, in which case $\vec{V}_\infty$ is replaced by $U_r\, c_0$ where U_r is the reference speed for pressure calculation defined above. In both of these cases, the incremental onset flow is assumed to be zero, that is, the vector $\Delta\vec{V}$ is set to zero for all the equations in section N.4. Finally, if the user requests that the local onset flow be used to calculate pressures, then $\vec{V}_\infty$ is replaced by $\vec{U}_\infty$ and $\Delta\vec{V}$ is included in all equations in section N.4. No guidelines are given to the user on the appropriate option to use, since under practically all circumstances, the uniform onset flow option, which is the default, is appropriate.

Next, the user may request the computation of the angle between the surface vorticity $\vec{\gamma}$ and the velocity $\vec{V}$, where $\vec{\gamma}$ is defined by

$$\vec{\gamma} = \hat{n} \times \vec{\nabla}\mu \qquad \text{(N.5.1)}$$

(see section 5.6 following equation (5.6.11)). The program also prints the components of $\vec{\nabla}\mu$ in reference coordinates.

0.0 Forces and Moments

In this appendix we describe the computation of forces and moments in the PAN AIR system. In section 0.1 we comment briefly on the defining equations. In section 0.2 we describe the method by which PAN AIR performs the required integration. In section 0.3, we discuss edge forces, which must be calculated separately because the true potential flow solution for velocity at a subsonic edge of a thin configuration is infinite, while that calculated by a panel method is finite. In section 0.4 we compute the properties of force and moment vectors under a coordinate transformation.

0.1 Basic Formulas

A force is defined as a time rate of change of momentum. Ward (reference 1.5, equation 4.6.3) shows that for potential flow, equation (5.9.9) holds. PAN AIR actually computes a coefficient of force defined analagously to the pressure coefficient (cf., (N.2.2)):

$$\vec{c_F} = -\frac{1}{S_R} \iint \left[\frac{\vec{V}(\rho \vec{V} \cdot \hat{n})}{1/2\, \rho_\infty\, |V_\infty|^2} + C_p\, \hat{n} \right] dS \qquad (0.1.1)$$

where S_R is a user-specified "reference area" available for normalization of the force coefficient.

Applying the relation (N.3.3) between velocity and mass flux, we have, for either the upper or lower surface of a network,

$$\vec{c_F} = -\frac{1}{S_R} \iint \left[\frac{2\vec{V}(\vec{W} \cdot \hat{n})}{|\vec{V_\infty}|^2} + C_p\, \hat{n} \right] dS \qquad (0.1.2)$$

We note that the first term, called the "momentum transfer" term, is zero for impermeable surfaces. This term makes a contribution to the force on the surface, however, when the normal mass flux is non-zero. Note that the net force on a network of panels is the difference between upper and lower surface forces. Thus the net force on a fully permeable nacelle face is zero, though both the upper and lower surface forces are non-zero. The momentum transfer term is only computed in Pan Air when requested by the user.

The coefficient of moment $\vec{c_M}$ is similarly derived from (5.9.10) and is defined by

$$\vec{c_M} = -\frac{1}{L_R} \iint \left[\{ \vec{Q} - \vec{R_0} \} \times \vec{V} \left(\frac{2\vec{W} \cdot \hat{n}}{|\vec{V_\infty}|^2} \right) + C_p \{ \vec{Q} - \vec{R_0} \} \times \hat{n} \right] dS \qquad (0.1.3)$$

Here L_R is a user-specified reference length, Q is a point of integration and R_0 is the point about which the moment is calculated. Once again the first term is the momentum transfer term. If the surface is impermeable, this term makes no contribution to the angular force exerted by the fluid on the body.

0.2 Integration Procedure

The integrand in (0.1.2) may be evaluated from the velocity (see Appendix N). The velocity, in turn, may be computed at any point on the configuration by the splining methods (see section N.1). In fact, a velocity distribution may be computed on each subpanel, and so it is theoretically possible to integrate this distribution exactly over the entire configuration to obtain the resulting force distribution. In fact, the integrals are precomputed (in the DQG module) for an arbitrary piecewise quadratic pressure distribution, so that the integral over a panel may be obtained by the CDP module during post-processing by matrix multiplications.

This procedure makes use of the far field moments already required for far field influence coefficient calculation. Recall from section I.4.2 the row vector FFM_0^D and the matrix FFM_1^D defined by

$$\frac{s\beta^2}{\kappa} \iint_\Sigma \mu \, dS = \lfloor FFM_0^D \rfloor \begin{Bmatrix} \mu_1 \\ \vdots \\ \mu_9 \end{Bmatrix} \tag{0.2.1}$$

$$\frac{s\beta^2}{\kappa} \iint_\Sigma \hat{\mu} \, \hat{n} \, dS = [FFM_1^D]^{3x9} \begin{Bmatrix} \mu_1 \\ \vdots \\ \mu_9 \end{Bmatrix} \tag{0.2.2}$$

But now, if we assume that the pressure varies in a piecewise quadratic manner (as μ does) on each panel we may apply (0.2.2). This is actually a fairly reasonable assumption. Since we approximate the doublet strength by a quadratic function and the source strength by a linear function, (N.1.11b) shows that the velocity is of linear accuracy. Thus by (N.2.43) and (N.2.51-53), the second order, reduced second order, slender body, and linear pressure coefficient formulas can be adequately represented by quadratically varying fuctions. Further, the small perturbation assumptions on which the Prandtl-Glauert equation is based insure that differences between the isentropic and the second order formula should be negligeable anyway.

So, we may compute the pressure coefficient $C_{p,q}$ at the nine panel defining points, and obtain

$$\frac{s\beta^2}{\kappa} \iint_\Sigma C_p \, \hat{n} \, dS = [FFM_1^D] \, \vec{C}_p \tag{0.2.3}$$

where $\vec{C}_p$ is the vector of length 9 whose qth entry is $C_{p,q}$.

Similarly, since the velocity on a panel is of linear accuracy, $\vec{V}$ $(\vec{W}\cdot\hat{n})$ also may be described by a piecewise quadratic, and so, writing $\{\vec{V}_q\}_i$ for the ith entry of $\vec{V}_q$, the 3x1 column vector giving the velocity at the qth

panel defining point, the first term in (0.1.2) may be computed by,

$$\frac{s\beta^2}{\kappa} \iint_{\Sigma} \{\vec{V}\}_i \; (2\vec{W}\cdot\hat{n})dS \;=\; \lfloor FFM_0^D \rfloor \begin{Bmatrix} \{\vec{V}_1\}_i \cdot (\vec{W}\cdot\hat{n})_1 \\ \vdots \\ \{\vec{V}_9\}_i \cdot (\vec{W}\cdot\hat{n})_9 \end{Bmatrix}$$

$$= \; 2[VWN]_{i,\cdot} \; \lfloor FFM_0^D \rfloor \qquad (0.2.4)$$

where VWN is the 3x9 matrix whose i,q entry is the ith component of V_q times the normal mass flux at the qth defining point.

Thus, equation (0.1.2) becomes

$$S_R \; \{\vec{C}_F\}_i \;=\; \frac{-\kappa}{s\beta^2} \sum_{\text{all panels}} \sum_{q=1}^{9} \left\{ \frac{2}{|\vec{V}_\infty|^2} \; [VWN]_{iq} \; \lfloor FFM_0^D \rfloor_q \right.$$

$$\left. + \; [FFM_1^D]_{iq} \; C_{p,q} \right\} \qquad (0.2.5)$$

Next we consider the calculation of the moment coefficient. Assume that we have computed the 3x9 matrix $NCPM_1$ ("normal cross-product moment") defined by

$$\iint_{\Sigma} (\vec{Q} - \vec{P}_9) \; \mu \; dS \;=\; [NCPM_1] \; \vec{\mu} \qquad (0.2.6)$$

where P_9 is the panel center.

This matrix is precomputed in the same manner as the remaining far field moments. Similarly, let us define a 3x9 matrix $[NCPM_2]$ by

$$\iint_{\Sigma} \mu \; (\vec{Q} - \vec{P}_9) \times \hat{n} \; dS \;=\; [NCPM_2] \; \vec{\mu} \qquad (0.2.7)$$

The computation of $NCMP_1$ and $NCMP_2$ is described shortly. We may then compute (0.1.3) using the above two matrices.

First, we easily see that $\iint_{\Sigma} [C_p \; (\vec{Q} - \vec{R}_0) \times \hat{n}] \; dS \;=$

$$\iint_{\Sigma} c_p \; (\vec{Q} - \vec{P}_9) \times \hat{n} \; dS + (\vec{P}_9 - \vec{R}_0) \times \iint_{\Sigma} C_p \; \hat{n} \; dS \qquad (0.2.8)$$

$$= \; [NCPM_2] \; \vec{c}_p \; + \; (\vec{P}_9 - \vec{R}_0) \times \frac{\kappa}{s\beta^2} \; [FFM_1^D] \; \vec{C}_p \qquad (0.2.9)$$

Next we recall from appendix E the permutation symbol

$$\epsilon_{ijk}: \quad 1 \le i,j,k \le 3$$

$$\epsilon_{ijk} = \begin{cases} = 1 \text{ if } i,j,k \text{ are distinct and cyclic} \\ = -1 \text{ if } i,j,k \text{ are distinct and in reverse cyclic order} \\ = 0 \text{ otherwise} \end{cases} \tag{0.2.10}$$

which has the property that for vectors $\vec{v}$ and $\vec{w}$,

$$(\vec{v} \times \vec{w})_k = \sum_{i,j} \epsilon_{ijk} v_i w_j \tag{0.2.11}$$

Thus $\iint [(\vec{Q} - \vec{R}_o) \times \vec{V} (\vec{W}\cdot\hat{n})] \, dS =$

$$\sum_{i,j} (\vec{Q} - \vec{R}_o)_i V_j (\vec{W}\cdot\hat{n}) \epsilon_{ijk} \, dS +$$

$$[(\vec{P}_9 - \vec{R}_o) \times \iint \vec{V} (\vec{W}\cdot\hat{n}) \, dS]_k \tag{0.2.12}$$

Then $\iint [(\vec{Q} - \vec{R}_o) \times \vec{V} (\vec{W}\cdot\hat{n})]_k \, dS =$

$$\sum_{i,j,q} [NCPM_2]_{iq} [VWN]_{jq} \epsilon_{ijk}$$

$$+ \sum_{i,j,q} (\vec{P}_9 - \vec{R}_o)_i \frac{\kappa}{s\beta^2} [VWN]_{jq} \lfloor FFM_0^D \rfloor_q \epsilon_{ijk} \tag{0.2.13}$$

Combining (0.1.3), (0.2.9), and (0.2.13),

$$L_R \vec{C}_M = \sum_{\text{panels}} -[NCMP_2] \vec{C}_p - (\vec{P}_9 - \vec{R}_o) \times \left\{ \frac{\kappa}{s\beta^2} [FFM_1^D] \vec{C}_p \right\}$$

$$- \frac{2}{|\vec{V}_\infty|^2} \sum_{q=1}^{9} \left\{ [NCMP_1]_{.,q} + \frac{\kappa}{s\beta^2} (\vec{P}_q - \vec{R}_o) \lfloor FFM_0^D \rfloor_q \right\} \times [VWN]_{.,q} \tag{0.2.14}$$

This completes our discussion of the integration of (0.1.3); the computation of the matrices $[NCMP_i]$ has been discussed in detail in section I.4.2, equations (I.4.21) through (I.4.27).

0.3 Leading and Side Edge Force

0.3.1 Linearized Three-Dimensional Theory

Consider a flat plate at an angle of attack, as illustrated in figure 0.1. It is known that such a configuration experiences zero drag in subsonic two-dimensional potential flow, where drag is the component of force in the freestream or x-direction. Yet the surface normal has an x-component and the surface is impermeable, and thus equation (0.1.1) indicates non-zero drag.

The resolution of this contradiction is found in the existence of a leading edge force resulting from an infinite leading edge velocity (see Ashley and Landahl, Ref. 5.3, section 5.3, or, for more detail, Hancock and Garner, Ref. 5.2, part II). This leading edge force exactly cancels out the drag computed by integrating the pressure over the configuration surface. Since the surface is impermeable, the momentum transfer term gives no contribution to the force on the surface.

A formula for the edge force magnitude per unit distance (on a three dimensional wing) is given in Hancock and Garner (ref. 5.2). This formula, valid for all subsonic edges (there is no edge force on a supersonic edge) gives edge force per unit length by

$$dS/dy_n = (\pi/8)\, \beta_n \left[\lim_{x_n \to 0} (\mu/\sqrt{x_n}) \right]^2 \tag{0.3.1}$$

where, S is the edge force, y_n measures distance along the edge, x_n measures distance perpendicular to the edge and in the plane of the surface, μ is the doublet strength on the surface and β_n is given by

$$\beta_n^2 = 1 - M_n^2 \tag{0.3.2}$$

where M_n is the Mach number in the direction of the edge force. Thus, $M_n = M_\infty \cos \Lambda$ where Λ is the sweepback angle as shown in figure 0.2. The edge force direction is away from the edge and perpendicular to both the edge and the surface normal, also as shown in figure 0.2.

0.3.2 Application in PAN AIR

To apply equation (0.3.1) in PAN AIR, we must first consider the evaluation of the limit. First note that it is known that if z_n is a polynomial in x_n and y_n, then the exact value of $\mu/\sqrt{x_n}$ can be uniformly approximated by a polynomial. Given this fact, it is tempting to estimate the limit by evaluating $\mu/\sqrt{x_n}$ at the first and second panels from the edge and extrapolating these values to $x_n = 0$. However, because PAN AIR represents μ itself as a quadratic polynomial in x_n and y_n, the expression $\mu_{PA}/\sqrt{x_n}$ (we denote the doublet distribution computed by PAN AIR as μ_{PA}) will not converge uniformly to $\mu/\sqrt{x_n}$ in the neighborhood of the edge. Consequently, if we denote the computed and exact values of μ at the center of the first panel by $\mu_{1,PA}$ and $\mu_{1,exact}$, then $\mu_{1,PA}/\mu_{1,exact}$ will not converge to 1 as the

number of panels is increased. Similarly, $\mu_{2,PA}/\mu_{2,exact}$ does not converge to 1. These ratios will, however, converge to finite values, the specific values depending upon the solution details, especially the panel spacing and density. For example, different limit ratios are obtained for uniform spacing than for cosine spacing. Also, since a potential flow field near an edge is mathematically similar to two-dimensional flow about a flat plate, the convergence properties for three-dimensional cambered surfaces will be similar to those for three dimensional flat plates. Thus, we assume that the limiting behavior of $\mu_{1,PA}/\mu_{1,exact}$ for a three-dimensional cambered surface will closely resemble the behavior of $\mu_{1,PA}/\mu_{1,exact}$ for a 2-D flat plate as the number of chordwise panels is increased.

In light of these considerations, the following method is proposed as one that (i) will yield reasonably accurate results without an excessive number of panels and (ii) will converge to exact results as the number of panels is increased, provided certain panel spacing rules are followed. Referring to figure 0.3, define Y_1, Y_2 by

$$Y_i = \mu/\sqrt{x_n}\,\Big|_{x_{n,i}} \qquad i = 1,2 \tag{0.3.3}$$

where $x_{n,i}$ denote the values of x_n at the first and second panel center away from the edge (see figure 0.3 for definition). These two evaluations now immediately provide an extrapolated value of $\mu/\sqrt{x_n}$ at $x_n = 0$:

$$G = (Y_1\, x_{n,2} - Y_2\, x_{n,1})/(x_{n,2} - x_{n,1}) \tag{0.3.4}$$

If $\mu/\sqrt{x_n}$ converged uniformly to its limit value we could approximate

$$\lim_{x_n \to 0} \mu/\sqrt{x_n} \cong G$$

In fact, using equation (0.3.1) we write

$$dS/dy_n = (\pi/8)\,\beta_n\, G^2\, f \tag{0.3.5}$$

where the correction factor f (which is O(1)) is determined from program/theory comparisons for a series of two-dimensional flat plate problems. The correction factor f depends on the number of panels and the panel spacing method. The total leading edge force is computed from the formula

$$S = \int_{y_{n,1}}^{y_{n,2}} (dS/dy_n)\, dy_n \tag{0.3.6}$$

where the integral is evaluated by the midpoint rule using the formula (0.3.5) to provide values for (dS/dy_n).

Correction factors for three types of panel spacing and various panel counts are given in figure 0.4. Correction factors for untabulated values of NPAN, the panel count, are obtained by interpolation, where f is regarded as a function of (1/NPAN). Correction factors have not been computed for any other types of panel spacing, and results obtained by PAN AIR for such types of panel spacing may be neither accurate nor convergent.

The correct use and interpretation of figure 0.4 requires that one know precisely what is meant by "cosine spacing" and "semi-cosine spacing." Let t be a nondimensional coordinate defined such that the value t=0 coincides with the edge on which the edge force acts and t = 1 coincides with the opposite edge. Then the panel corner points for cosine spacing are located at the t-stations given by

$$\text{(cosine-spacing)} \quad t_i = (1/2)[1 - \cos((i-1)\pi/\text{NPAN})] \quad i=1,\ldots,\text{NPAN}+1 \tag{0.3.7}$$

while for semi-cosine spacing these x stations are given by

$$\text{(semi-cosine spacing)} \quad t_i = 1 - \cos[(i-1)\pi/(2\cdot\text{NPAN})] \quad i=1,\ldots,\text{NPAN}+1 \tag{0.3.8}$$

0.3.3 Edge Force Verification

A leading edge suction distribution has been computed by PAN AIR using the technique described above for a 60° delta wing in incompressible flow. This distribution is compared in figure 0.5 to the result derived in Medan, (ref. 0.1). Notice that the quantity $(dS/dy_\eta)/[(1-\eta)^{.28154}\alpha^2]$ is plotted against η where η represents "spanwise fraction," the fractional transverse distance from the centerline to the outboard tip and α is angle of attack. This scaling of the leading edge suction distribution is based upon the theoretical results derived in (ref. 0.1). In fact, as η approaches 1, dS/dy_η itself tends to zero so that the differences between results shown in figure 0.5 are not significant when scaled and integrated to obtain overall forces. Note also that PAN AIR results appear to converge to the theoretical values except for the panels closest to the tip. In fact, the PAN AIR computed suction force on the tip panel will never converge no matter how densely the wing is panelled. This is another manifestation of nonuniform convergence arising from the fact that PAN AIR constrains the doublet distribution to be a quadratic function of the surface coordinates. Nevertheless, overall forces and moments do converge as panel density increases.

Drag values predicted for a supersonic delta wing are compared in figure 0.6 to the theoretical results presented in figure A,14m of Jones and Cohen (ref. F.1). The PAN AIR results lie very close to the theoretical curve. Since edge suction is a significant contributor to drag, this close comparison provides some verification of the validity of PAN AIR's method of computing edge suction forces.

0.4 Coordinate Transformations

In this section we examine the behavior of force and moment vectors under an orthogonal transformation of coordinates

$$\Gamma : \begin{Bmatrix} x \\ y \\ z \end{Bmatrix} \longrightarrow \begin{Bmatrix} x' \\ y' \\ z' \end{Bmatrix} \tag{0.4.1}$$

This is necessary because the program permits force and moment computation in a multiplicity of axis systems. These axis systems are defined in section B.2.1 of the User's Manual.

We know from appendix E that velocity and normal vectors are dual vectors w transforming according to

$$\vec{w} = \Gamma^T \vec{w}' \tag{0.4.2}$$

But since we assume Γ is orthogonal, its inverse is its transpose, and so

$$\vec{w}' = \Gamma \vec{w} \tag{0.4.3}$$

Further, if $\vec{w}$ is a vector rather than a dual vector, it also obeys (0.4.3), according to appendix E, because det $\Gamma = 1$. In fact, because Γ is orthogonal, vectors and dual vectors behave identically in all cases, and so we make no further distinction between them.

Applying (0.4.3) in (0.1.1) we obtain

$$\vec{c}'_F = \Gamma \vec{c}_F \tag{0.4.4}$$

since

$$\{\rho \Gamma V\}. \hat{n} = \rho \vec{V}^T \Gamma^T \Gamma \hat{n} = \rho \vec{V} \cdot \hat{n} \tag{0.4.5}$$

and Γ, being a matrix of constants, may be taken out of the integral (0.1.1).

Next, we consider the transformation of the moment coefficient. Let us assume we have computed the moment vector $\vec{c}_M$ about the origin in reference coordinates. That is,

$$\vec{C}_M = -\frac{1}{L_R S_R} \iint [\vec{Q} \times \vec{V}\left(\frac{2\vec{W} \cdot \hat{n}}{|\vec{V}_\infty|^2} \right) + C_p \vec{Q} \times \hat{n}] dS \tag{0.4.6}$$

We now wish to compute the moment coefficient $\vec{C}_M$ in the primed coordinate system about a point R_0. That is, $\vec{C}'_M$ is defined by (0.1.3) with $\vec{Q}$, $\vec{R}_0$, $\vec{V}$, $\vec{W}$, and $\hat{n}$ replaced by primed counterparts.

So,

$$\vec{C}'_M = -\frac{1}{L_R S_R}\left[\{\Gamma\vec{Q} - \Gamma\vec{R}_0\}\times\Gamma\vec{V}\left(2\frac{\Gamma\vec{W}\cdot\Gamma\hat{n}}{|\vec{V}_\infty|^2}\right) + C_p\{\Gamma\vec{Q} - \Gamma\vec{R}_0\}\times\Gamma\hat{n}\right]dS \tag{0.4.7}$$

But for vectors $\vec{w}_1$ and $\vec{w}_2$, we have (cf. (E.1.12-13)):

$$\Gamma\vec{w}_1 \times \Gamma\vec{w}_2 = \Gamma\{\vec{w}_1 \times \vec{w}_2\} \tag{0.4.8}$$

Thus

$$\vec{C}'_M = -\frac{1}{L_R S_R}\left[\Gamma\{\vec{Q}\times\vec{V}\}\left(\frac{2\vec{W}\cdot\hat{n}}{|\vec{V}_\infty|^2}\right) + C_p\,\Gamma\{\vec{Q}\times\hat{n}\}\right]dS$$

$$+\frac{1}{L_R S_R}\left[\Gamma\{\vec{R}_0\times\vec{V}\}\left(\frac{2\vec{W}\cdot\hat{n}}{|\vec{V}_\infty|^2}\right) + C_p\,\Gamma\{\vec{R}_0\times\hat{n}\}\right]dS \tag{0.4.9}$$

Noting that both Γ and R_0 may be removed from the integral,

$$\vec{C}'_M = \Gamma\vec{C}_M + \frac{1}{L_R S_R}\,\Gamma\{R_0 \times \iint\left[\vec{V}\left(\frac{2\vec{W}\cdot\hat{n}}{|\vec{V}_\infty|^2}\right) + C_p\,\hat{n}\right]dS \tag{0.4.10}$$

So, substituting (0.1.2) in (0.4.10),

$$\vec{C}'_M = \Gamma\vec{C}_M - \frac{1}{L_R}\,\Gamma\{\vec{R}_0 \times \vec{C}_F\} \tag{0.4.11}$$

Thus moment vectors transform like force vectors, except with an extra term which results from a shift in the point about which the moment is calculated.

An addition minor complication is cause by the use of separate scaling factors for different components of the moment coefficient vector. The effect of separate scaling factors on (0.4.11) can easily be computed and is given by the code in SUBROUTINE TRNSFM of the CDP module.

0.5 Added Mass Coefficients

The inertial properties of a submerged body moving in a fluid are affected by the motion of the fluid surrounding the body. These properties, which become quite significant when the mass of the displaced fluid is commensurate with the mass of the body, are concisely summarized by a collection of tensors called "added mass coefficients." In this section we will define the added mass coefficients, describe their computation and derive some of their transformation properties.

0.5.1 Formulation of Added Mass Coefficients

Consider an impermeable body B with boundary surface S moving through a fluid. We suppose that the fluid has constant density ρ and that the fluid motion is itself irrotational. Thus, a velocity potential exists and satisfies Laplace's equation. At the instant of observation, the motion of the fluid is observed from an axis system fixed in the undisturbed fluid and momentarily coincident with a body fixed axis system. The velocity of any point $\vec{p}$ on the body's surface is given by

$$\vec{u} + \vec{\omega} \times (\vec{p} - \vec{p}_0)$$

where $\vec{u}$ specifies the body's translational velocity and $\vec{\omega}$ specifies its rotational velocity about a center of rotation $\vec{p}_0$. The harmonic velocity potential for the fluid's instantaneous velocity is now uniquely determined by the impermeable surface boundary condition

$$\partial\phi/\partial n = (\vec{u} + \vec{\omega} \times (\vec{p}-\vec{p}_0)) \cdot \hat{n} \quad \text{on} \quad S \tag{0.5.1}$$

An equivalent form of (0.5.1) using the implied summation notation is

$$\partial\phi/\partial n = u_i n_i + \omega_i (\vec{r} \times \hat{n})_i \quad ; \quad \vec{r} = \vec{p} - \vec{p}_0 \tag{0.5.2}$$

where we introduce the shorthand $\vec{r}$ for the vector from the center of rotation to a point on the body surface. Evidently, ϕ can be written in the form

$$\phi = u_i \phi_i + \omega_i \psi_i \tag{0.5.3}$$

where ϕ_i and ψ_i are harmonic velocity potentials satisfying the boundary conditions

$$\begin{aligned} \partial\phi_i/\partial n &= n_i \\ \partial\psi_i/\partial n &= (\vec{r} \times \hat{n})_i \qquad \text{on } S \end{aligned} \tag{0.5.4}$$

The potentials introduced in (0.5.3) are associated with motion along an axis in the case of ϕ_i, and with rotation about an axis in the case of ψ_i.

The expression for added mass coefficients is obtained by computing T, the kinetic energy of the fluid induced by the motion of the body. Summarizing the development given in ref. 0.2, T is given by

$$T = (\rho/2) \iiint_{R^3-B} (\nabla\phi)^2 \, dV$$

$$= -(\rho/2) \iint_S \phi \, (\partial\phi/\partial n) \, dS \qquad (0.5.5)$$

Substituting (0.5.3) into (0.5.5) yields for T

$$T = (1/2) \, u_i \, M_{ij} \, u_j + (1/2) \, \omega_i \Sigma_{ij} \, u_j$$
$$+ (1/2) \, u_i \, S_{ij} \, \omega_j + (1/2) \, \omega_i \, I_{ij} \, \omega_j \qquad (0.5.6)$$

where we define the various added mass coefficients by the expressions

$$M_{ij} = -\rho \iint_S \phi_i \, (\partial\phi_j/\partial n) \, dS$$

$$S_{ij} = -\rho \iint_S \phi_i \, (\partial\psi_j/\partial n) \, dS$$

$$\Sigma_{ij} = -\rho \iint_S \psi_i \, (\partial\phi_j/\partial n) \, dS$$

$$I_{ij} = -\rho \iint_S \psi_i \, (\partial\psi_j/\partial n) \, dS \qquad (0.5.7)$$

The coefficients M_{ij} are called inertia coefficients while I_{ij} are called moment of inertia coefficients; S_{ij} and Σ_{ij} are called mixed coefficients. Green's second identity implies that M and I are symmetric and further, that

$$S_{ij} = \Sigma_{ji} \qquad (0.5.8)$$

Thus, the full 6x6 added mass coefficient matrix given by

$$A = \left[\begin{array}{c|c} M & S \\ \hline \Sigma & I \end{array}\right] \qquad (0.5.9)$$

is symmetric.

0.5.2 Integration Procedures

Because the method by which PAN AIR solves for ϕ_i and ψ_i ensures internal stagnation ($\phi_i = \psi_i = 0$ interior to B), the integrals appearing in equation (0.5.7) can be expressed quite simply in terms of the fundamental singularity distributions. Letting μ_i, $\tilde{\mu}_i$ denote respectively the doublet distributions associated with ϕ_i, ψ_i and using the boundary conditions (0.5.4), we obtain

$$M_{ij} = -\rho \iint_S \mu_i \, n_j \, dS$$

$$S_{ij} = -\rho \iint_S \mu_i \, (\vec{r} \times \hat{n})_j \, dS$$

$$\Sigma_{ij} = -\rho \iint_S \tilde{\mu}_i \, n_j \, dS$$

$$I_{ij} = -\rho \iint_S \tilde{\mu}_i \, (\vec{r} \times \hat{n})_j \, dS \qquad (0.5.10)$$

Clearly these integrals can be evaluated by techniques similar to those described in section 0.2 by using the moment matrices $[FFM_1^D]$ and $[NCPM_2]$.

It is important to note that the added mass coefficients given by equation (0.5.10) are not precisely the results computed and printed by PAN AIR. Rather, scaled quantities $\hat{M}_{ij}$, $\hat{S}_{ij}$, $\hat{\Sigma}_{ij}$ and $\hat{I}_{ij}$ are printed. These are defined by

$$\hat{M}_{ij} = M_{ij}/(\tfrac{1}{2} \rho \, SL)$$

$$\hat{S}_{ij} = S_{ij}/(\tfrac{1}{2} \rho \, SL^2)$$

$$\hat{\Sigma}_{ij} = \Sigma_{ij}/(\tfrac{1}{2} \rho \, SL^2)$$

$$I_{ij} = I_{ij}/(\tfrac{1}{2} \rho \, SL^3) \qquad (0.5.11)$$

where S is a user specified reference area and L a user specified reference length. Notice that if one takes $S = L = \rho = 1$, one finds that $\hat{M}_{ij} = 2 \, M_{ij}$, $\hat{S}_{ij} = 2 \, S_{ij}$, etc.

0.5.3 Orthogonal Transformation

Added mass coefficients computed in a body axis system which has been subjected to an orthogonal transformation Γ can be defined in terms of added mass coefficients in a reference coordinate system. Using primes to denote quantities in the transformed system, the boundary conditions can be written as

$$(\partial \phi_i'/\partial n') = (\Gamma \hat{n})_i \qquad (0.5.12)$$

$$(\partial \psi_i'/\partial n') = [\Gamma (\vec{r} \times \hat{n})]_i \quad \text{on } S$$

Equation (0.4.8) was applied to the second part of (0.5.12). For (0.5.12) to be satisfied, it must happen that

$$\phi'_i = \Gamma_{ij}\,\phi_j$$
$$\psi'_i = \Gamma_{ij}\,\psi_j \qquad (0.5.13)$$

Substituting (0.5.12) and (0.5.13) into a primed form of (0.5.7) will show that

$$M'_{ij} = \Gamma_{ik}\,M_{kl}\,\Gamma_{jl} \qquad (0.5.14)$$

The other coefficients transform identically.

0.5.4 Translation

Added mass coefficients computed about an arbitrary moment reference point $\vec{r}_o$ can be defined in terms of coefficients computed about the origin. The technique is similar to that of section 0.5.2. The boundary conditions become

$$\partial\phi'_i/\partial n' = n_i$$
$$\partial\psi'_i/\,n' = (\vec{r} \times \hat{n})_i - (\vec{r}_o \times \hat{n})_i \qquad (0.5.15)$$

To satisfy these boundary conditions, the potentials in the translated system must take the form

$$\phi'_i = \phi_i$$
$$\psi'_i = \psi_i - \varepsilon_{ijk}\,r_{o,j}\,\phi_k \qquad (0.5.16)$$

where ε_{ijk} denotes the usual permutation symbol, (cf. eqn. B.3.21 and ff.). Substitution of (0.5.15) and (0.5.16) into a primed form of (0.5.7) gives

$$M'_{ij} = M_{ij}$$
$$S'_{ij} = S_{ij} - \varepsilon_{ikl}\,r_{o,k}\,M_{lj}$$
$$\Sigma'_{ij} = \Sigma_{ij} - \varepsilon_{ikl}\,r_{o,k}\,M_{lj}$$
$$I_{ij} = I_{ij} - \varepsilon_{ilm}\,r_{o,l}\,S_{mj} - \varepsilon_{jlm}\,r_{o,l}\,\Sigma_{im} + \varepsilon_{inp}\,\varepsilon_{jlm}\,r_{o,n}\,r_{o,l}\,M_{pm} \qquad (0.5.17)$$

0.5.5 Symmetric Configuration

If the surface S consists of a surface S' and its mirror image S", the added mass coefficients on S" can be defined in terms of those on S'. Suppose the plane of symmetry passes through $\vec{r}_s$ and has a unit normal $\hat{\nu}$. A point $\vec{p}'$ on S' and its image point $\vec{p}''$ on S" are related by

$$p''_i = R_{ij}\, p'_j + x_{o,j} \tag{0.5.18}$$

where $R_{ij} = \delta_{ij} - 2\,\nu_i\,\nu_j$

and $x_{o,j} = r_{s,j} - R_{jk}\, r_{s,k}$

The point $\vec{x}_o$ is the image point of the origin and R is the reflection matrix.

With primes and double primes denoting entities related to S' and S" respectively, the boundary conditions become

$$\partial\phi''_i/\partial n'' = R_{ij}\, n'_j$$

$$\partial\psi''_i/\partial n'' = -R_{ij}\,(\vec{r}' \times \hat{n}')_j + R_{ij}\,(\vec{x}_o \times \hat{n}')_j \tag{0.5.19}$$

where $\vec{r}'$ is the vector from $\vec{p}_o$, the center of rotation, to $\vec{p}'$.

$$\vec{r}' = \vec{p}' - \vec{p}_o$$

The second part of (0.5.19) required applications of (0.1.12) and (0.5.18). To satisfy (0.5.19), the potentials take the form

$$\phi''_i = R_{ij}\,\phi'_j$$

$$\psi''_i = -R_{ij}\,\psi'_j + R_{ij}\,\epsilon_{jkl}\,x_{o,k}\,\phi'_l \tag{0.5.20}$$

Applying (0.5.19) and (0.5.20) to a form of (0.5.7) yields

$$M''_{ij} = R_{ik}\,M'_{kn}\,R_{jn}$$

$$S''_{ij} = \epsilon_{jlm}\,x_{o,l}\,M_{im} - R_{ik}\,S_{kq}\,R_{jq}$$

$$\Sigma''_{ij} = -R_{ik}\Sigma'_{kl}\,R_{jl} + \epsilon_{ipq}\,x_{o,p}\,M''_{qj}$$

$$I''_{ij} = R_{ik}\,I'_{kq}\,R_{jq} + \epsilon_{ikn}\,x_{o,k}\,S''_{n,j} \tag{0.5.21}$$

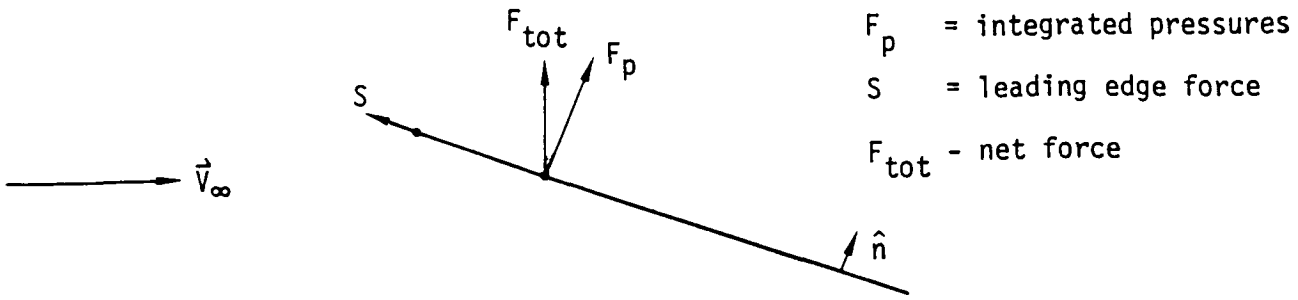

Figure 0.1 - Effect of leading edge force

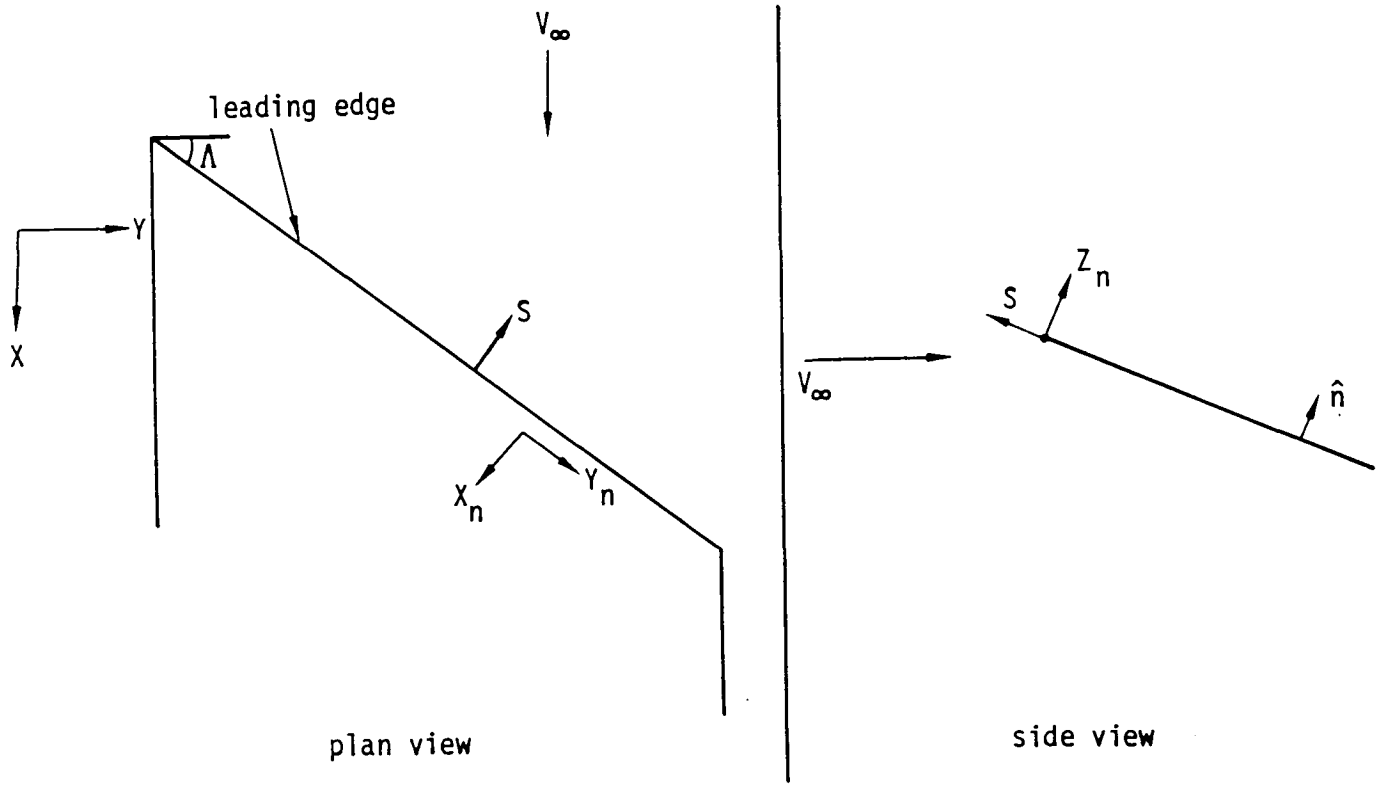

Figure 0.2 - Leading edge force on a three-dimensional thin wing

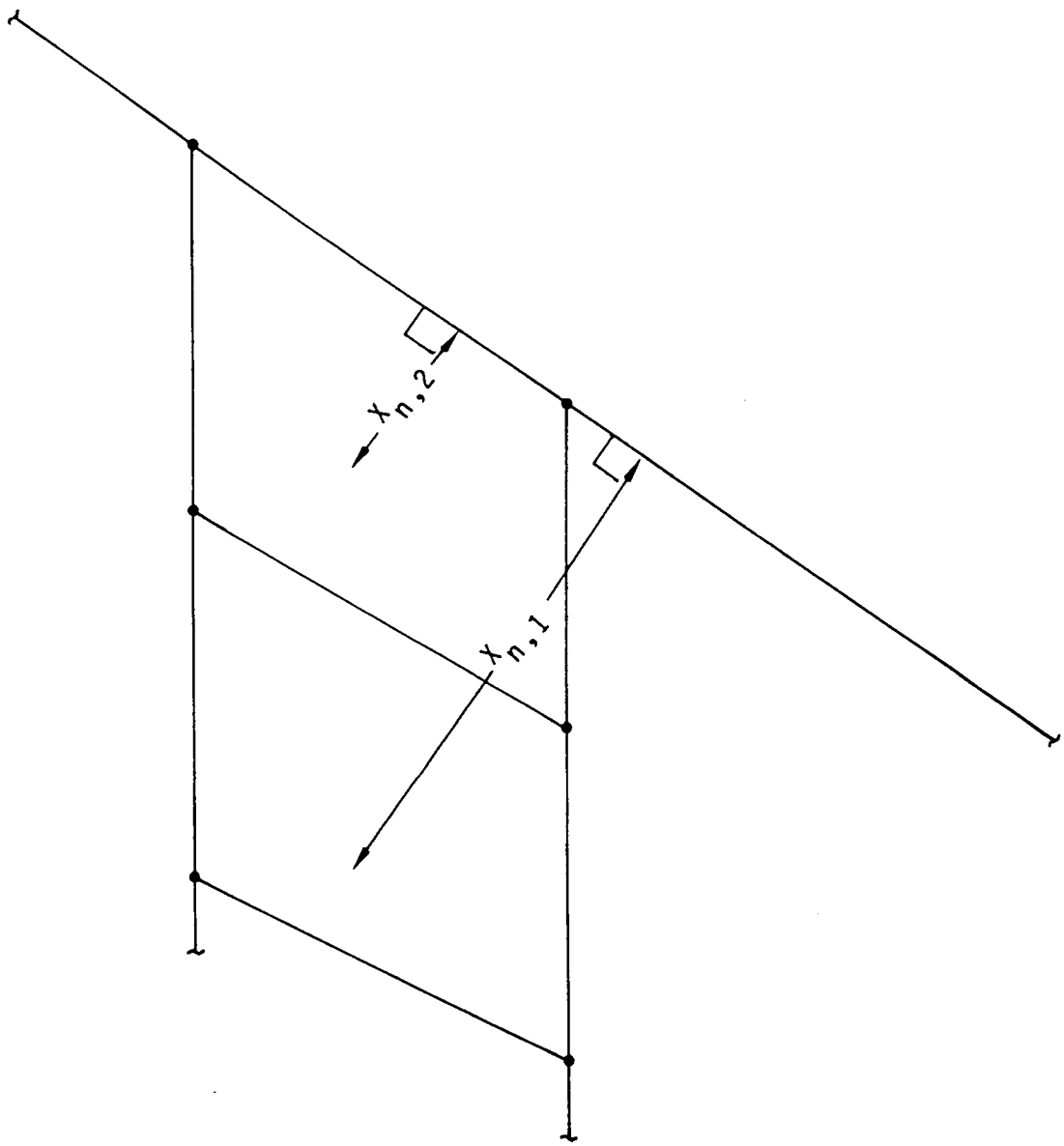

Figure 0.3 - Definition of $X_{n,1}$ and $X_{n,2}$

	Correction Factors f (Derived Using PAN AIR Version 1.0)		
NPAN	Uniform	Cosine	Semi-Cosine
2	1.1579008	1.1579008	1.4059546
3	1.3289155	1.4039062	1.4977210
4	1.3462617	1.4766240	1.5680541
5	1.3513135	1.5336144	1.5985113
7	1.3544339	1.5852960	1.6212810
10	1.3557162	1.6149452	1.6323902
14	1.3562257	1.6294277	1.6359293
20	1.3564644	1.6373295	1.6407743
40	1.3566063	1.6431274	1.6435113
60	1.3566336	N.A.	1.6442279
80	1.3566417	N.A.	1.6444954

NPAN = Number of panel rows or number of panel columns, depending on which edge the edge forces are calculated for.

Figure 0.4 - Edge force correction factors

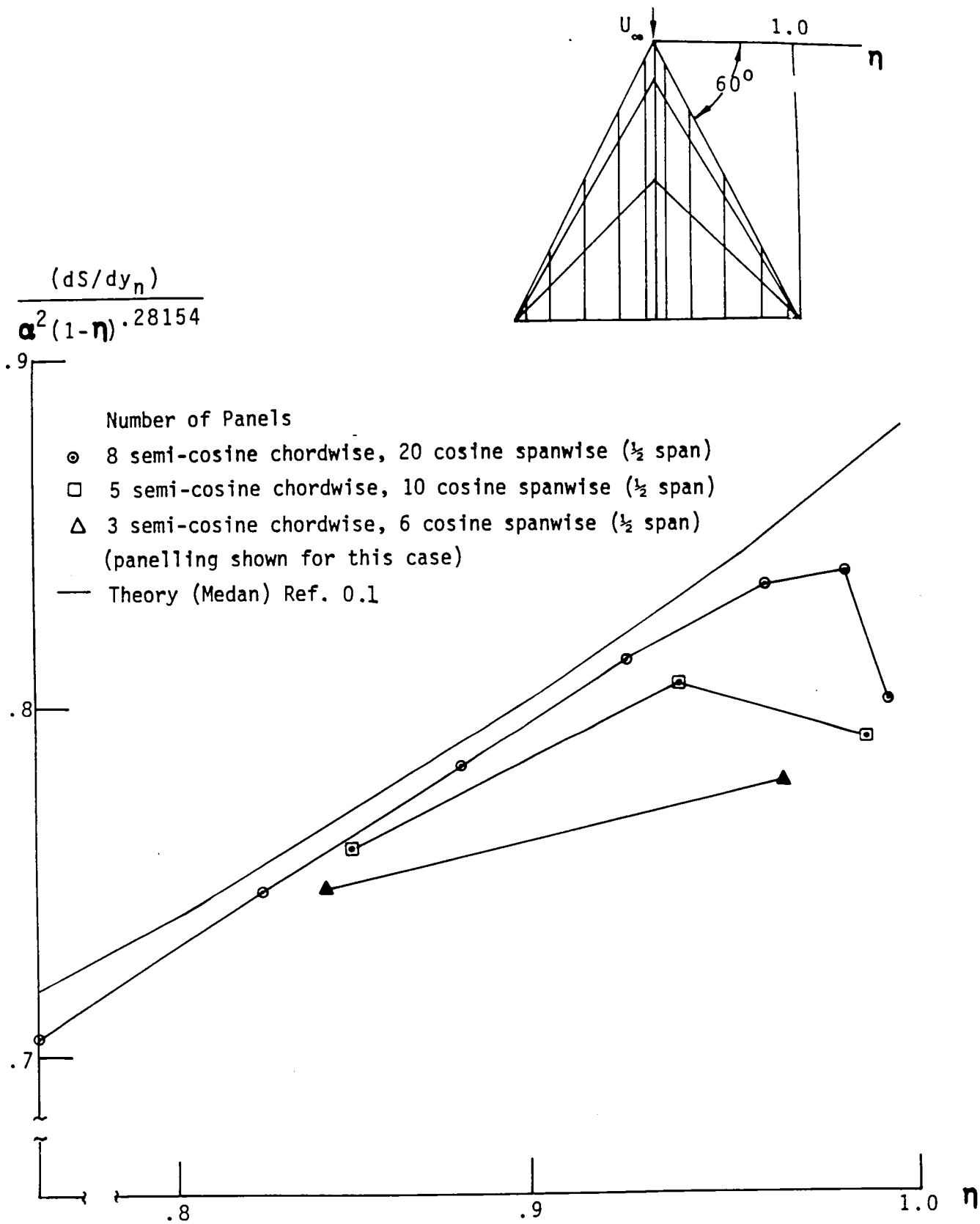

Figure 0.5 - Comparison of leading edge suction predicted by PAN AIR with theoretical results.

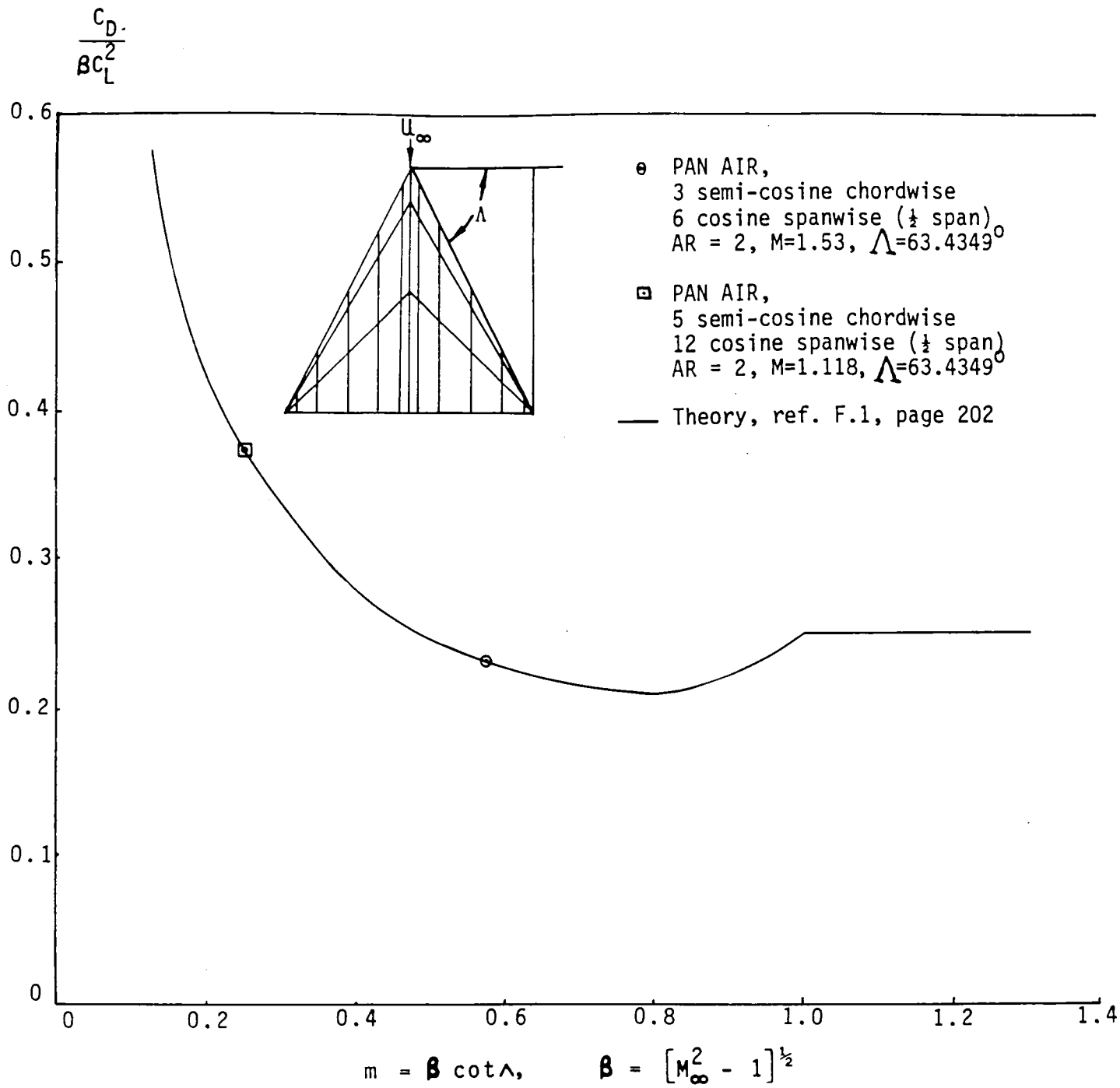

Figure 0.6 - Comparison of drag predicted by PAN AIR with theory for a delta wing in supersonic flow

P.0 Flow Properties at Off-Body Points and Streamline Calculation

Once the potential flow problem has been solved, the program user frequently has the need to evaluate the potential and velocity field at points away from the configuration, to aid in flow field visualization. In this appendix we will outline the processes by which flow properties are calculated at off-body points and then describe the calculation of streamlines. The basic idea underlying both of these procedures is that, once the potential flow problem has been solved, both the source and doublet distribution are known on the full singularity surface S. Then, by virtue of the representation formulas for potential ϕ (equation (3.2.7)) and perturbation velocity $\vec{v}$ (equation (B.3.9)) it becomes possible to evaluate ϕ and $\vec{v}$ at any point in the flow field. This evaluation of ϕ and $\vec{v}$ at an off-body point is central to the evaluation of off-body flow properties as well as streamline calculation. For off-body flow properties, the connection is straightforward: given ϕ and $\vec{v}$ one simply applies the procedures of appendix N to obtain the various pressure coefficients and corrected velocities. In the case of streamline calculation, the perturbation velocity $\vec{v}$ is combined with the onset flow to obtain a total velocity ($\vec{V}$) or mass flux ($\vec{W}$) vector field which is then integrated to trace the streamlines. This process is described more fully in section P.2.

P.1 Evaluation of Potential and Velocity at Off-Body Points

Once the potential flow problem has been solved and the global singularity parameters $\{\lambda_i\}_{i=1}^{N}$ are evaluated, the source strength σ and doublet strength μ are given everywhere on the singularity surface S by (cf. equations (3.3.1-2))

$$\sigma(\vec{q}) = \sum_{I=1}^{N} \lambda_I \, s_I \, (\vec{q}) \tag{P.1.1}$$

$$\mu(\vec{q}) = \sum_{I=1}^{N} \lambda_I \, m_I \, (\vec{q}) \tag{P.1.1}$$

Here, $\vec{q}$ denotes an arbitrary source point on S.

When no symmetry planes are present, we may combine these relations with the representation formulas (3.2.7) and (B.3.9) and obtain for $\phi(\vec{p})$ and $\vec{v}(\vec{p})$:

$$\phi(\vec{p}) = -\frac{1}{\kappa} \iint^{*}_{S \cap D_p} \left(\frac{\sigma}{R} - \mu \, \hat{n} \cdot \tilde{\nabla}_q \frac{1}{R}\right) dS_q \tag{P.1.3}$$

$$\vec{v}(\vec{p}) = \frac{1}{\kappa} \iint^{*}_{S \cap D_p} \sigma \; \nabla_q\left(\frac{1}{R}\right) dS_Q + \frac{1}{\kappa} \iint^{*}_{S \cap D_p} (\hat{n} \times \nabla_q \mu) \times \tilde{\nabla}_q \left(\frac{1}{R}\right) dS_q \tag{P.1.4}$$

Note that we have dropped the line vortex term from $\vec{v}$.

The evaluation of these formulae is now achieved by dividing S up into panels and evaluating individual panel contributions in the fashion described in detail in appendices J and K. The resulting evaluation procedure may be summarized, using the notation of appendix K.6 (cf. page K.6-2):

$$\phi(\vec{p}) = \sum_{I=1}^{N} \Phi IC_I \, \lambda_I$$

$$= \sum_{I=1}^{N} [\, \Phi_\sigma(\vec{p}, s_I) + \Phi_\mu(\vec{p}, m_I)] \, \lambda_I \tag{P.1.5}$$

$$\vec{v}(\vec{p}) = \sum_{I=1}^{N} \overrightarrow{VIC}_I \, \lambda_I$$

$$= \sum_{I=1}^{N} [\vec{V}_\sigma(\vec{p}, s_I) + \vec{V}_\mu(\vec{p}, m_I)] \, \lambda_I \qquad \text{(P.1.6)}$$

Here, the various operators Φ_σ, Φ_μ etc. have the obvious definitions:

$$\Phi_\sigma(\vec{p}, s_I) = -\frac{1}{\kappa} \iint^{*}_{S \cap D_p} s_I(\vec{q})/R(\vec{p},\vec{q}) \, dS_q \qquad \text{(P.1.7)}$$

$$\Phi_\mu(\vec{p},m_I) = \frac{1}{\kappa} \iint^{*}_{S \cap D_p} m_I(\vec{q}) \, \hat{n} \cdot \tilde{\nabla}_q(1/R(\vec{p},\vec{q})) \, dS_q \qquad \text{(P.1.8)}$$

$$\vec{V}_\sigma(\vec{p},s_I) = \frac{1}{\kappa} \iint^{*}_{S \cap D_p} s_I(\vec{q}) \, \nabla_q(1/R(\vec{p},\vec{q})) \, dS_q \qquad \text{(P.1.9)}$$

$$\vec{V}_\mu(\vec{p},m_I) = \frac{1}{\kappa} \iint^{*}_{S \cap D_p} (\hat{n} \times \nabla_q m_I) \times \tilde{\nabla}_q(1/R(\vec{p},\vec{q})) \, dS_q \qquad \text{(P.1.10)}$$

Up to this point, the evaluation of ϕ and $\vec{v}$ has offered few surprises. The situation becomes somewhat more complicated when we introduce the concept of symmetry. Fortunately many of the complicated details have already been worked out and presented in appendix K. Throughout the remainder of this section we assume that the reader has a good familiarity with the results of appendix K.

We begin our present study of symmetry by recalling the definition of $\hat{\phi}^i$, equation (K.3.22). Inverting this definition, we obtain

$$\phi(\vec{R}^i\vec{p}) = \frac{1}{2} \sum_j H^{ij} \, \hat{\phi}^j \, (\vec{p}) \qquad \text{(P.1.11)}$$

Setting $i = +1$ and noting that $H^{+j} = 1$ and $R^+ = I$ (cf. (K.3.6) and (K.3.21)) we find $\phi(\vec{p})$ given by

$$\phi(\vec{p}) = \frac{1}{2} (\hat{\phi}^S(\vec{p}) + \hat{\phi}^A(\vec{p})) \qquad \text{(P.1.12)}$$

Now $\hat{\phi}^S(\vec{p})$ and $\hat{\phi}^A(\vec{p})$ are given by equation (K.5.17) combined with the representations (K.5.19-20) for $\hat{\sigma}^i$, $\hat{\mu}^i$:

$$\hat{\phi}^i = \sum_I \sum_j H^{ij} [\Phi^*_\sigma (R^j\vec{p},s_I) + \Phi^*_\mu(R^j\vec{p},m_I)] \lambda^i_I \qquad \text{(P.1.13)}$$

Substituting this result into (P.1.12) we obtain

$$\phi(\vec{p}) = \frac{1}{2} \sum_I \sum_i \sum_j H^{ij} [\Phi^*_\sigma(R^j\vec{p},s_I) + \Phi^*_\mu(R^j\vec{p},m_I)] \hat{\lambda}^i_I \qquad \text{(P.1.14)}$$

Introducing the following notation (and definition) for desymmetrized singularity parameters λ^j_I :

$$\lambda^j_I = \frac{1}{2} \sum_i H^{ij} \hat{\lambda}^i_I \qquad \text{(P.1.15)}$$

we obtain for $\phi(\vec{p})$ the equation

$$\phi(\vec{p}) = \sum_I \sum_j [\Phi^*_\sigma(R^j\vec{p},s_I) + \Phi^*_\mu(R^j\vec{p},m_I)] \lambda^j_I \qquad \text{(P.1.16)}$$

The corresponding formula for $\vec{v}(\vec{p})$ is obtained by formally applying ∇_p to the above result and using the operator equations

$$\nabla_r \Phi^*_\sigma (\vec{r},s) = \vec{V}^*_\sigma (\vec{r},s)$$

$$\nabla_r \Phi^*_\mu (\vec{r},m) = \vec{V}^*_\mu (\vec{r},m)$$

One obtains

$$\vec{v}(\vec{p}) = \sum_I \sum_j R^j[\vec{V}^*_\sigma(R^j\vec{p},s_I) + \vec{V}^*_\mu(R^j\vec{p},m_I)] \lambda^j_I \qquad \text{(P.1.17)}$$

As before the various operator integrals are computed by accumulating individual panel contributions as described in appendix J.

Having treated the case of one plane of symmetry, the handling of two planes of symmetry is easy. One obtains for $\phi(\vec{p})$:

$$\vec{\phi}(\vec{p}) = \sum_I \sum_j \sum_l [\Phi^*_\sigma(R^{jl}\vec{p},s_I) + \Phi^*_\mu(R^{jl}\vec{p},m_I)] \lambda^{jl}_I \qquad \text{(P.1.18)}$$

Here, λ^{jl}_I are desymmetrized global singularity parameters:

NASA
National Aeronautics and Space Administration

Report Documentation Page

1. Report No. NASA CR-3251 (Revision 1)	2. Government Accession No.	3. Recipient's Catalog No.
4. Title and Subtitle PAN AIR - A Computer Program for Predicting Subsonic or Supersonic Linear Potential Flows about Arbitrary Configurations Using a Higher Order Panel Method Volume I - Theory Document (Version 3.0)		5. Report Date March 1990
		6. Performing Organization Code
7. Author(s) Michael A. Epton and Alfred E. Magnus		8. Performing Organization Report No.
		10. Work Unit No.
9. Performing Organization Name and Address Boeing Military Airplane Company P. O. Box 3707 Seattle, Washington 98124		11. Contract or Grant No. NAS2-12036
12. Sponsoring Agency Name and Address National Aeronautics and Space Administration, Washington, DC 20546-0001; AFWAL and ASD, Wright-Patterson AFB, Ohio 45433; NCSC, Panama City, Florida 32407		13. Type of Report and Period Covered Contractor Report October 1984 - September 1987
		14. Sponsoring Agency Code

15. Supplementary Notes

Points of Contact: Larry L. Erickson, Ralph L. Carmichael, Alan D. Levin, Ames Research Center, MS 227-2, Moffett Field, CA 94035-1000 (415) 604-5856 or FTS 464-5856

16. Abstract

An outline of the derivation of the differential equation governing linear subsonic and supersonic potential flow is given. The use of Green's Theorem to obtain an integral equation over the boundary surface is discussed. The engineering techniques incorporated in the PAN AIR (Panel Aerodynamics) program (a discretization method which solves the integral equation for arbitrary first order boundary conditions) are then discussed in detail.

Items discussed include the construction of the compressibility transformation, splining techniques, imposition of the boundary conditions, influence coefficient computation (including the concept of the finite part of an integral), computation of pressure coefficients, and computation of forces and moments.

Principal revisions to version 3.0 are (1) appendices H and K more fully describe the AIC construction, (2) appendix L now provides a complete description of the AIC solution process, (3) appendix P is new and discusses the theory for the new FDP module (which calculates streamlines and offbody points), and (4) numerous small corrections and revisions reflecting the MAG module rewrite.

17. Key Words (Suggested by Author(s)) Aerodynamics, Linear potential flow, Panel methods, Prandtl-Glauert equation, Spines, Influence coefficients, Discretization		18. Distribution Statement ~~FEDD Distribution~~ Subject Category - 02	
19. Security Classif. (of this report) Unclassified	20. Security Classif. (of this page) Unclassified	21. No. of Pages 876	22. Price A41

NASA FORM 1626 OCT 86

For sale by the National Technical Information Service, Springfield, Virginia 22161

☆ U.S. GOVERNMENT PRINTING OFFICE: 1990---728-385